Best
Available
Copy

FTD-TT- 63-852

AD609452

TRANSLATION

GASDYNAMICS OF ENGINES

By

A. I. Borisenko

#65-60474

864 P

COPY 3 of 3 pages

HARD COPY $.11.65

MICROFICHE $.3.75

FOREIGN TECHNOLOGY DIVISION

AIR FORCE SYSTEMS COMMAND

WRIGHT-PATTERSON AIR FORCE BASE

OHIO

DDC

RECEIVED

JAN 4 1965

DDC-IRA B

ARCHIVE COPY

CLEARINGHOUSE FOR FEDERAL SCIENTIFIC AND TECHNICAL INFORMATION CFSTI
DOCUMENT MANAGEMENT BRANCH 410.11

LIMITATIONS IN REPRODUCTION QUALITY

65-60474

ACCESSION # AD 609452

☑ 1. LEGIBILITY OF THIS DOCUMENT IS IN PART UNSATISFACTORY. REPRODUCTION HAS BEEN MADE FROM THE BEST AVAILABLE COPY.

☐ 2. ORIGINAL DOCUMENT CONTAINS COLOR OTHER THAN BLACK AND WHITE AND IS AVAILABLE IN LIMITED SUPPLY. AFTER PRESENT STOCK IS EXHAUSTED, IT WILL BE AVAILABLE IN BLACK-AND-WHITE ONLY.

☐ 3. THE REPRODUCIBLE QUALITY OF THIS DOCUMENT IS NOT ADEQUATE FOR PUBLIC SALE. AVAILABLE TO CUSTOMERS OF THE DEFENSE DOCUMENTATION CENTER ONLY.

☐ 4. DOCUMENT AVAILABLE FROM CLEARINGHOUSE ON LOAN ONLY (TECHNICAL TRANSLATIONS).

PROCESSOR: JMC

TSL-107-12/64

UNEDITED ROUGH DRAFT TRANSLATION

GASDYNAMICS OF ENGINES

BY: A. I. Borisenko

English Pages: 852

THIS TRANSLATION IS A RENDITION OF THE ORIGINAL FOREIGN TEXT WITHOUT ANY ANALYTICAL OR EDITORIAL COMMENT. STATEMENTS OR THEORIES ADVOCATED OR IMPLIED ARE THOSE OF THE SOURCE AND DO NOT NECESSARILY REFLECT THE POSITION OR OPINION OF THE FOREIGN TECHNOLOGY DIVISION.

PREPARED BY:

TRANSLATION DIVISION
FOREIGN TECHNOLOGY DIVISION
WP-AFB, OHIO.

A. I. Borisenko

GAZOVAYA DINAMIKA DVIGATELEY

Gosudarstvennoye
Nauchno-Tekhnicheskoye Izdatel'stvo
Oborongiz
Moskva 1962

pages 3 - 793

FTD-TT-63-852/1+2

BLANK PAGE

TABLE OF CONTENTS

Preface 2

Introduction 5

0.1. Topic of Gasdynamics 5
Classification of Forces. The Principle of Reactive Motion. Aim and Task of the Course.

0.2. Physical Properties of Liquids and Gases . . . 8
Structure of Liquids and Gases. Liquid and Gas as Continuous Media. The Deformation Rate as a Criterion for Classifying Bodies. Viscosity. Pressure in Liquids (gases). Thus, in a Sufficiently Small Region of a Fluid at Rest the Pressure is the Same for Any Area Taken Inside the Region. Inviscid Liquids and Gases. Perfect and Real Gases. Compressibility. Propagation of Small Disturbances. Subsonic and Supersonic Gas Flows. The Model of the Atmosphere. References.

Chapter 1. Kinematics of Liquid and Gas 26

1.1. Velocity and Acceleration of Particles 26
The Velocity Field. Methods of Investigating the Motion of a Fluid. The Euler Method. Streamlines and Trajectories. The Choice of the Coordinate System. The Acceleration Field.

1.2. Decomposition of the General Motion into the Simplest Ones 32
Linear Variation of Speed in the Vicinity of a Point. Deformation of a Plane Element. General Case of Deformation of a Parallelepiped.

1.3. Potential and Turbulent Motions 37
Connectedness of a Region. The Velocity Potential. Vortex Motion. Circulation of Speed and the Connection Between Circulation and Vorticity. Stokes' Theorem. Many-Valued Potential. Invariance of the Vorticity of a Vortex Tube. Streamlines in the Case of Vortex Motion. References.

Chapter 2. Fundamental Laws 47

2.1. The Mass Conservation Law. Continuity Equation in Euler Variables 47
Continuity Equation for Fixed Mass. Continuity Equation for the Reference Volume. Continuity

Equation in Differential Form.
2.2. Momentum Conservation Law. Equation of Motion 49
Equation of Motion in Terms of Stress. Symmetry of the Tangential Stresses. Tangential Stresses. The Relation Between the Normal Stresses and the Deformation Rates. Pressure at a Point. The Equation of Motion. The Second Viscosity. Euler's Equation. The Equation of Motion in the Form Given by Gromeka. The Integrals of the Equation of Motion. The Velocity Potential as the Impulse of a Pressure Shock. Conservation of Circulation with Time. Lagrange's Theorem. Helmholtz's Theorem on the Conservation of Vortex Lines. Determination of Forces Acting on a Body from the State of Flow at the Boundaries.
2.3. The Energy Conservation Law. The Energy Equation 71
Energy, Work and Heat. Reversible and Irreversible Processes. Entropy. The Second Law of Thermodynamics. Isentropic and Adiabatic Processes. The Integral Form of the Energy Equation. Analysis of the Energy Equation. The Energy Equation for a Flow Element. Energy Exchange Between a Flowing Liquid and Solid Bodies in It.
2.4. The System of Aerohydromechanical Equations. Initial and Boundary Conditions 86
The System of Equations. Initial and Boundary Conditions.
2.5. Similarity Theory and Dimensional Analysis . . 88
The Concept of Dimensionality. The Utilization of Experiments in Aeromechanics. The Topic of the Similarity Theory. Physical Similarity. The Dimensionless Form of the Equations of Aeromechanics. Similarity Criteria as Characteristics of the Quantities of the Terms of Equations. Analysis of the Similarity Conditions. Dimensional Analysis. Basic Theorems of Dimensional Analysis.
2.6. Methods of Solving the Equations of Mechanics of a Viscous Incompressible Fluid 99
Exact Solutions to the Equations of Aerohydromechanics. Flow of a Viscous Fluid in a Tube. The Vortical Character of a Laminar Flow. The Drag Coefficient ζ. The Critical Re Number and Turbulence. The Two Regions of the Flow of a Viscous Fluid. The Thickness of the Laminar Boundary Layer. Stability of flow. The Motion of an Inviscid Fluid as a Limiting Case of Turbulent Motion with $Re \to \infty$. The Statistical Method of Investigating Turbulent Motion. Time Averaging. Averaging of the Equations of Hydromechanics. Turbulent Stresses. The Turbulence Characteristics.
2.7. Singularities in Gasdynamics 114
The System of Equations of Gasdynamics Potential Flow. The Boundary Conditions

The Propagation of Small Disturbances in One Direction. Plane Waves. The Cauchy Problem. The Appearance of Discontinuities. The Process of Compression Shock Formation. Conditions of Dynamic Consistency. The Hugoniot Curve. Impossibility of Rarefaction Shock. Propagation of Discontinuities. Thickness of a Shock Wave. References.

Chapter 3. Potential Flows of a Completely Incompressible Fluid 135

3.1. Plane Flows 135
Definitions. The Basic System of Equations. The Velocity Potential. The Stream Function. The Hydrodynamic Meaning of the Stream Function. Streamlines and Equipotential Lines. The Complex Potential. The Velocity in a Polar Coordinate System.

3.2. Addition of the Simplest Flow Regimes 142
Plane Parallel Flow. Sources and Sinks. The Plane Vortex. Singularities. The Core of a Vortex. The Superposition Method. A Plane Dipole. Flow About a Circular Cylinder. Pressure Distribution Along a Cylinder. Circulatory Flow About a Circulat Cylinder. Forces on a Circular Cylinder. The Flow About Bodies of Arbitrary Shape. Flow Near Plane Walls (Fictitious Singularities). Approximate Methods. Simulation of a Flow by Means of Analogy Considerations. Singularity Flow About a Circle

3.3. The Method of Conformal Mapping 161
The Geometrical Meaning of a Derivative. The Hydrodynamic Significance of Conformal Mapping Flow About a Corner. Flow About an Arbitrary Contour. Optimum Shape of a Plane Air Intake.

3.4. Forces and Moments of Forces Acting on the Body in a Plane Flow 173
The Chaplygin Formulas. The Zhukovskiy Formula for the Lift.

3.5. Wing Profile Theory. 180
Wing Profile. Aeridtbanuc Profile Characteristics. Mechanism of Viscous Fluid Flow about a Profile. Induced Drag of Wind of Finite Span The Infinite-Span Wing. Flow about an Arbitrarily Positioned Disc. Circulation About a Profile. The Lift and the First Axis. Moment and the Second Axis of the Profile. The Zhukovskiy Profile. A Plane Plate. The Symmetrical Profile. The Solid Zhukovskiy Profile. The Transformation of an Ellipse. Generalized Zhukovskiy Profiles. Rounding of the Profile at the Leading Edge. Comparison with Experiment. Chaplygin Profiles.

3.6. Solution of the Problem of the Flow About a Body by the Method of Continuously Distributed Singularities 200

Methods of Vortex Sheets. Vorticity of a Vortex. The Vortex System of a Wing Profile. Camber Line Equation. Speed Determination for the Points of the Camber Line. Speed on the Axis. Integral Equation of the Theory of Thin Profiles. Choice of a Suitable Vorticity Distribution in the Vortex Sheet. Velocity at the ($y = 0$). Connection with Profile Geometry. Lift. Moment. Approximate Relations. Circulation-Free Flow About a Symmetrical Profile. The Profile Equation. Velocity at the Points of the Profile. The Integral Equation. Vorticity of a Vortex Shield. Radii of Curvature of the Profile Edges. Example.

3.7. Jet Flow About a Body 217
The Form of Motion. A Plane Plate. Comparison with Experiment. Vortex Drag.

3.8. Spatial Flows 225
Source in Space. Flow About a Half-Body. The Dipole. Flow About a Sphere. Source-Sink Distribution Along the Axis of Rotation of a Body Determination of the Velocity Field of an Incompressible Fluid From the Given Source Distribution. Determination of the Velocity Field From the Given Vorticity. Velocity Field of an Arbitrarily Shaped Vortex Tube. The Rectilinear Vortex Line. References.

Chapter 4. Onedimensional Flows. Flows in Tubes and Channels 232

4.1. The Forms of Action 233
Thermal Influences. Mechanical Influences.

4.2. Gasdynamic Functions 234
Parameters of Decelerated Flow. Characteristic Velocities. Fundamental Gasdynamic Functions. Critical Parameters. The Mass Flow Function. The Impulse Function. Gasdynamic Functions of p/p_0. Approximate Relations.

4.3. Geometrical Influence and Flow Rate Influence 240
Geometrical Nozzle. Design of a Geometrical Nozzle. Outflow Nozzle. Example of Calculating a Geometrical Nozzle. Conditions of Isentropic Gas Flow Through The Nozzle. Formation of Normal Compression Shocks. The Kinematic Relation for a Normal Shock. Collection of Formulas for Normal Shock. The Pressure Recovery Coefficient.

4.4. Influence of Friction 250
Semiempirical Theory of Turbulency. The Theory of the Mixture Length. Experimental Data on the Friction in Tubes. The Law of the Seventh-Order Root. Generalization of the Law of the Seventh-Order Root. Logarithmic Law of Velocity Distribution (4.4.11). Viscous Boundary Layer. Roughness. Equation of Adiabatic Motion of a Viscous Gas in a Cylindrical Tube.

Change of Number M*. Determination of the Gas Parameters for Various Tube Cross Sections. The Position of the Compression Shock.
4.5. Thermal Influence 270
The System of Equations. Thermal Nozzle. Change of the Gas Parameters in a Cylindrical Tube. The Gas Parameters. Thermal Resistance. Fanneau Lines. Raleigh Lines. Compression Shock in the iS Graph. Mechanism of Combustion. Thermal Shocks. Gas Parameters in the Detonation. Steady Regime of Detonation. Absolute Velocities.
4.6. The Law of Reversal of Influence 286
Combined Influence. Evaporation and Condensation. Change of the Physical Properties. References.

Chapter 5. Plane Potential Motions of a Gas 293

5.1. Fundamental Equations 293
The Velocity Potential. The Stream Function.
5.2. Approximate Linearization of the Equation for Thin Bodies 296
Statement of the Problem. Linearized Equation for the Velocity Potential. The Pressure Coefficient. Subsonic and Supersonic Plane Flows.
5.3. Flow About a Wavy Surface 300
Boundary Conditions. Subsonic Flow. Supersonic Flow. Comparison of the Results. Transition Through Sonic Speed.
5.4. Linearized Subsonic Plane Flow 306
The Bases of the Method of Solution. Substitution of the Variables. Correspondence of the Boundary Conditions. The Coefficients of Pressure, Lift and Moment. Pressure Distribution Over a Given Body. Determination of the Shape of the Body for a Given Pressure Distribution. Improvement of the Solution to the Linearized Equation. The Critical Mach Number M.
5.5. The Linearized Plane Supersonic Flow 314
General Form of the Solution to a Linearized Equation. Range of Applicability of the Solution. Streamlines. The Pressure Distribution. Characteristics. Choice of the Sign of the Characteristics. Flow About the Outside of an Obtuse Angle. The Pressure Coefficient. Flow Inside an Obtuse Angle. Flow About a Curvilinear Wall.
5.6. A Plane Wing In A Supersonic Flow 319
The Plane Plate. The Lift Distribution. Circulation and Lift. Drag. Arbitrary Thin Profile. The Superposition Principle.
5.7. Reflection and Intersection of Waves 323
Reflection From a Plane Wall. Change of Pressure. The Velocity Hodograph. Extinction of a Wave. Reflection of a Wave From a Free Boundary. Intersection of Waves. A Nozzle Under Off-De-

sign Conditions. Regions of Dependence and Influence.
5.8. Characteristics 331
Mach lines as Characteristics. Velocity Variation Along the Characteristics. Equation of the Characteristics in the Velocity Hodograph Plane. Choice of the Constant in the Characteristics Equation. The Adiabatic Ellipse. Four Basic Problems on Potential Gas Flow Solved By the Method of Characteristics.
5.9. Finite Disturbances in a Supersonic Flow . . . 343
Classification of Discontinuities. Prandtl-Meyer Flow. Diagonal Compression Shocks. Conditions of Dynamic Consistency. The Hugoniot Curve. Practical Formulas For Calculating a Diagonal Compression Shock. The Hugoniot Curve. Flow About a Wedge.
5.10. The Method of Successive Approximations For Subsonic Flows 356
Expansion of the Velocity Potential in a Power Series of M_∞. Expansion of the Thickness Parameter into a Power Series.
5.11. The Hodograph Method 359
The Method of Exact Linearization. Chapygin Transformation. Subsidiary Flow. Approximate Solutions. The Pressure Coefficient. A Profile In a Subsonic Gas Flow.
5.12. Nearsonic Flows 371
Approximate Differential Equation of Nearsonic Flows. Similarity Rule for Nearsonic Flows. The Pressure Coefficient. Description of the Transition from Subsonic to Mixed Flow.
5.13. Hypersonic Flows 379
Approximate Differential Equation of Hypersonic Flows. The Force Coefficient. Example. Infinitely Large Number M_∞. References.

Chapter 6. The Boundary Layer 383

6.1. Equations of Motion In the Boundary Layer . . . 383
Prandtl's Equations. The Plane Plate. The Method of Successive Approximations. The Turbulent Boundary Layer. Integral Relations. The Impulse Equation. The Energy Equation. Separation of the Boundary Layer.
6.2. Correspondence Between the Internal and External Problems 398
Velocity Distribution. The Region of Transition From Laminar to Turbulent Flow. Example 1, 2, 3. Drag of a Rough Plate. Admissible Roughness. Influence of the Pressure Gradient. Boundary Layer on a Wing. Logarithmic Velocity Distribution.
6.3. Universal Method of Calculating the Boundary Layer on Curvilinear Surfaces 410
The Shape Factor. One-Parametric Family of Velocity Distributions. Determination of the

Polygonal Coefficients. Calculation of the Laminar Boundary Layer. The Separation Point of a Laminar Boundary Layer. Method for Calculating the Laminar Boundary Layer. Calculations of the Turbulent Boundary Layer. Transition of a Laminar to a Turbulent Boundary Layer on a Curvilinear Surface. Boundary Layer Equations for a Compressible Gas. A.A. Dorodnitsyn's Transformation.

6.4. Boundary Layer and Shock Waves 426
The Sound Barrier. Laminar Boundary Layer. The Turbulent Boundary Layer. Conditions of Separation.

6.5. Aerodynamic Heating 431
Aerodynamic (Kinetic) Heating. Similarity Criteria. Thickness of the Thermal Boundary Layer. Analogy Between Friction and Heat Exchange. The Turbulent Boundary Layer. Plane Plate. The Recovery Coefficient. Calculation of Heat Transfer. Boundary Layer Control. References.

Chapter 7. Wing of Finite Span 446

7.1. Wing of Finite Span in Incompressible Fluid . 446
Vortex Sheet Behind the Wing. Connection Between the Circulation on the Wing and the Vorticity in the Sheet. Fundamental Equation for a Finite Wing. Solution of the Basic Equation of the Finite Wing. The Forces on the Wing. The Moments of a Finite Wing. Calculation of the Wing Characteristics. Finite Wing in Subsonic Linearized Gas Flow.

7.2. Methods of Raising M_{kr} 459
Swept Wing. Streamlines of Swept Wing in Subsonic Flow. Advantages and Disadvantages of a Swept Wing. Wing of Small Aspect Ratio.

7.3. Wing of Finite Span in Supersonic Flow [7.5]. Region of Plane Flows. Supersonic and Subsonic Edges. Plane Flow for Wing with Positive Sweep. Approximate Formulas Thin Profile at Small Angle of Attack. Conical Flows. Comparison of Wings of Various Design Shapes. Comparison of Calculation with Experimental Data. References.

Chapter 8. Air Intakes, Nozzles, Jets 469

8.1. Thrust of Jet Engines 469
Rocket Motors and Air-Breathing Jet Engines. Solid Fuel Rocket Motor (RRDTT). Liquid Fuel Rocket Motors (ZhRD) Jet Engines (VRD). VRD with no Compressor. Jet Engine with a Compressor. The Turbo-Compressor VRD (TKVRD). Effective Thrust. Conventional Thrust and Additional Drag. The Mass Flow Coefficient φ. Thrust and Drag Distributions Over the Cowling Elements. Thrust of the Air Intake. The Thrust of the Air Intake. Drag of the Rear

Part. The Thrust of the Engine.
8.2. Air Intakes 489
Air Intake Parameters. Influence of Compressibility in a Subsonic Flow. Optimum Subsonic Air Intake. The Outer Contour of the Air Intake. The Inner Channel. Supersonic Air Intakes. Additional Drag. Single-Shock Air Intake. Multi-Shock Air Intakes. Optimum Compression Shock System. Air Intake Characteristics. Air Intake Control.
8.3. Cowlings 525
The Thin Cowling. Thick Optimum Cowling. The Thin Annular Profile.
8.4. Jet Nozzles 530
Subsonic Nozzles. Supersonic Nozzles. The Thrust of a Conical Nozzle. The Subsonic Part of the Nozzle. The Transient Section. The Supersonic Section. Optimum Nozzles. Allowance for the Boundary Layer.
8.5. The Flow in Curvilinear Channels 545
The Internal Problem. Velocity Distribution Transverse to a Plane Channel. Calculation of the Flow of an Incompressible Fluid in a Plane Channel. Allowance for Compressibility.
8.6. Jets 550
Fundamental Suppositions. The Structure of a Free Jet. The Weakly Heated Jet. The Propelling Jet.
8.7. The Ejector 558
Ejector Losses. Losses in the Ejector. The Ejection Equation. The Ejection Equation in Gasdynamic Functions. The Conditions at the Exit. The Length of the Mixing Chamber. References.

Chapter 9. Hydrodynamic Lattices 565

9.1. Fundamental Information of Profile Lattices . 565
Types of Turbines. Classification of Turbomachines According to Their Mechanisms. Absolute and Relative Motion. Axial-Flow Turbines. Radial-Flow Turbines. Active and Reactive Turbines. Second Form of the Euler Turbine Equation. The Reactivity Ratio. Geometrical and Kinematic Parameters of a Plane Linear Lattice. The Form of Motion of the Flow Through a Fixed Linear Lattice. Structure of the Flow in a Lattice of Profiles. Deflection of the Flow Through a Lattic of Profiles. Energy Exchange Between Moving Lattice and Flow. The Forces Acting on a Linear Lattice. The Lift and Drag Coefficients of a Profile in a Lattice. Conditions of Flow about a Lattice. Lattice Efficiency.
9.2. Potential Flow of Incompressible Fluid Through A Lattice of Thin Profiles 587
The Theory of the Lattice Wing Due to Chaplygin and Zhukovskiy. Lattice of Unstaggered Plane Plates. Lattice of Plane Plates

Arranged One After the Other. Staggered (Diagonal) Lattice. Lattice of Plates with Nonzero Angle of Attack. Purely Circulatory Flow Through a Lattice of Plane Plates. The General Case. Change of Angle of Attack. Deflection of the Flow. Lattice of Solid Zhukovskiy Profiles.

9.3. Solution of the Problem of a Profile Lattice by the Method of Vortex Sheets 605
Lattice of Thin Profiles. The Velocity Induced by the Vortex Sheets.
Sparse Lattice of Plane Plates. Dense Lattice of Plates. Flow About a Lattice of Discs. The Fundamental Equation. The Transverse Flow. The Longitudinal Flow. The Circulatory Flow. The Velocity Potential on the Circle. Lattice of Staggered Discs. The Complex Potential of a Flow Through a Lattice of Discs. Lattice of Approximately Circular Contours.

9.4. Mapping of a Lattice of Circles to a Lattice of Theoretical Profiles 627
The Mapping Function. The Equation of the Profile Contour. Shape of Camber Line and Thickness Curve. Velocity Distribution on the Profile Contour. The Pressure Coefficient. The Lift Coefficient in a Lattice. Deflection of Flow from a Lattice.

9.5. Construction of Profile Lattice 637
The Principal Streamline. The Channel Method. Teh Velocity Hodograph. The Trailing Edge. Construction of Streamlines. The Velocity Potential. Choice of the Velocity Hodograph. Mapping of the Hodograph Region on a Circle. The Construction of a Lattice.

9.6. Circular Lattice of Profiles 644
The Centrifugal Compressor (CC). Rotation of Circular Lattice. The Bernoulli Equation in the Relative Motion. Velocity Distribution in the Channels of a CC. The Critical Velocity in Relative Motion. Equation for the Compression Shock in Relative Motion. The Axial Vortex. The Axial Vortex in Elliptical and Triangular Cavities. Radial Channels. Determination of the Form of Motion of the Axial Vortex by the Method of Analogy.

9.7. Lattices of Profiles in Subsonic Gas Flow . . 667
The Influence of the Compressibility. Shock Stall and Choking Effect for a Lattice. The Lift of a Profile in a Lattice Placed in a Subsonic Flow. Numerical Calculation of the Gas Flow in a Lattice. Linearized Solution for Subsonic Flow.

9.8. Allowance for the Viscosity Effect 675
The Profile Drag Coefficient. Circulation About a Profile in a Lattice. The Influence of Viscosity on the Defelction of the Flow. The Loss Coefficient. The Influence of Roughness.

9.9. A Lattice of Profiles in a Supersonic Flow . . 688
Conditions of Supersonic Flow Through a Lattice of Profiles. Velocity Field Behind a Lattice of Profiles with a Supersonic Axial Component. Lattices Which Accelerate a Supersonic Flow with no Wave Drag. Lattices Which Decelerate a Supersonic Flow. The Forces on a Profile in the Lattice. Lift and Lattice Geometry. The Guiding Properties of a Supersonic Lattice of Profiles. References.

Chapter 10. Some Special Problems 705

10.1. Cavitation 705
Cavitation Effects. Cavitation in a Tube of Variable Cross Section. Cavitation-Induced Destruction of Metals. The Cavitation Number. Influence of the Air and Dust Content on the Appearance of Cavitation. Three Forms of Fluid Motion. The Process of Formation and Disappearance of a Single Cavitational Bubble. The Collapse of a Bubble. Cavitation Damage. Influence of Surface Tension and Viscosity. Cavitation on Hydrodynamic Profiles. References.
10.2. Atomization of a Fluid 726
Disintegration of a Jet. The Similarity Criteria. The Maximum Drop Diameter. The Drop Trajectory. Centrifugal Atomizers. The Spray Density of a Torch. References.
10.3. Motion of Rarefied Gases 743
Elements of Gas Dynamics. The Distribution Function of the Molecules. Boltzmann's Kinetic Equation. Interaction of the Gas Molecules With the Surfaces of Solids. The Adhesion Coefficient. The Accommodation Coefficient. The Energy Balance Equation. The Problems of Molecular Aerodynamics. The Plate. Body of Revolution. Sphere. Free Molecular Flow in a Tube. Convective Heat Exchange with a Free Molecular Flow. Flow with Slipping. Slip Flow in a Tube. References.
10.4. Magnetogasdynamics 779
The Electric Field. Conductors and Dielectrics The Ionized Gas. Ohm's Law. Joulean Heat. The Electrical Induction Vector (Displacement Vector). The Magnetic Field. The Lorentz Force. Induction. The Displacement Current. Lenz's Rule. Electric Volume Force. The Maxwell Equations. The Electromagnetic Field Energy. The Equations of Motion. Similarity Criteria in Magnetogasdynamics. Flow of an Electrically Conducting Gas in a Transverse Magnetic Field. Magnetohydrodynamics of a Two-Dimensional Flow. Acceleration of a Fluid in a Channel By Magnetic and Electric Fields. Boundary Layer Control. Control of Critical Heating. Flow of a Perfectly Conducting Gas about a Body from

the Interior of Which a Magnetic Field is Excited. References.

Appendices

1. Denotations of the Fundamental Quantities 819
2. Formulas of Vector Analysis 824
3. Physical Characteristics of Space Near the Earth. 826
4. Gasdynamic Functions 831
5. Table of Parameters for Normal Shock 835
6. Diagram of Characteristics (k = 1.4) 837
7. Parameters of Prandtl-Meyer Flow 838
8. Diagram of Oblique Compression Shocks 840
9. Velocities and Their Potentials on a Circle in Transverse (w_1, φ_1^*), Longitudinal (w_2, φ_2^*) and Circulatory (w_3) Flows Through a Lattice of Unit Circles as a Function of $\theta = \vartheta + \gamma$ 842
10. Auxiliary Tables and Graphs for Calculating Lattices of Two-Parametric Chaplygin Profile Families 843

BLANK PAGE

The book deals with the basic problems of the gasdynamics of aircraft engines, particularly gas turbines. The statements are preceded by a derivation and analysis of the equations of the mechanics of continuous media. One-dimensional and linearized plane flows are considered in detail. A theory is given of the isolated profile and the profile skeleton. Fundamental information on boundary layers is given; the theory of a wing of finite span is presented in brief. The inlet arrangements of a jet, the nozzles, are considered in detail. The physics of cavitation and spraying of liquids, the fundamentals of the mechanics of highly rarefied gases, and the elements of magneto-gasdynamics are discussed.

The book has been written for students at aviation colleges and faculties, students at power engineering faculties of institutes of machine building, and workers in design offices and turbine-building laboratories.

Reviewers: Department of the Theory of Aircraft at the Kazan' Aviation Institute, Doctor of Physico-Mathematical Sciences, G. Yu. Stepanov

Editor: Candidate of Physico-mathematical Sciences, I. Ye. Taparov

Editorial manager: Engineer S.D. Krasil'nikov

In memory of the teacher
Georgy Fedorovich Proskura
Engineer, Professor, Academician

PREFACE

The increase in speed and flight altitude and the thrust outward into cosmic space have put forward a series of problems for the solution of which the designers need a greater and more sophisticated knowledge of aerodynamics. This situation has been taken into consideration in that the educational plans of the higher technical schools are paying great attention to the training of future aircraft engine construction engineers in aerodynamics.

The various flying craft designs, the organic combination of power plant and supporting construction, the transition to new sources of energy, higher accuracy of calculations, the profiling of tunnels for sub- and supersonic stages of turboengines and the designing of an optimum jet nozzle requires broad theoretical training and a knowledge of the common methods of mechanics of continuous media which should also be the basis of a course on gasdynamics.

The present book was intended to serve as a textbook for a course on "Gasdynamics of Engines" but in the interim prior to publication the courses on hydraulics and gasdynamics were run together in educational plans to form a single course on "Applied hydro- and gasdynamics." Since the author was not able to take this change into account the old title of the course has been retained in the book, but large parts of it also take the syllabus of the new course into consideration.

Besides the problems raised in the syllabus of the course on "Gasdynamics of Engines" the book also deals with other problems which

go beyond the limits of this syllabus but which have a fundamental bearing on the training of an aircraft engine construction engineer; they are collected in Chapter 10 i.e., "Some special problems." We regret that due to the limited volume of this book the flow of gas accompanied by a chemical reaction has not been considered in it; furthermore, the very effective method of L.I. Sedov concerning the solution of the problem of flow about a spatial profile and profile skeleton by a subsonic flow of gas should have been dealt with in greater detail, and, finally, spatial flow in turboengines is incompletely considered.

The MKSA system of units is adopted in the book and specific quantities are referred to kilogram-mass. Many equations are thus liberated from these dimensional constants such as the gravitational constant, the equivalents of heat and work, etc., so that the physical meaning becomes apparent. Owing to these considerations the basic equations are derived in vector form.

The author expresses his deep gratitude to the teachers responsible to him in the Department of Gasdynamics and Jet Engines at the Khar'kov Aviation Institute for maintaining the over-all policy and the scheme of its structure in lecturing the course of gasdynamics. The author feels obliged to express his further gratitude to his pupil and friend, Docent I. Ye. Tarapov who did not fail to participate in discussing the plan and the contents both of the course as a whole and of the individual chapters and who took the pains with editing the book; his paper on the mechanics of rarefied gases has been used by the author in setting out the appropriate part of the book. The author also thanks the students of the Khar'kov Aviation Institute E.P. Zimin, B.N. Mel'nikov, I.P. Miroshnik, and Engineer G.T. Pozhidayeva who were a great help in selecting the material; in particular, the thesis of

E.P. Zimin was used in revising the part dealing with magnetogasdynamics.

Moreover, the author expresses his gratitude to Professor I.L. Povekha, to Docent B.S. Vinogradov, to G.S. Stepanov, Doctor of Physico-Mathematical Sciences and teacher at the Department of the Theory of Aircraft Engines at the Kazan' Aviation Institute, to Docent K.N. Davydov, Engineer, who became acquainted with the manuscript, and also to N.I. Akhiyezer, Corresponding Member of AS UkrSSR, to I.M. Kirkho, Corresponding Member of AS LatvSSR, to Professor A.D. Myshkis, to A.I. Bunimovich, Candidate of Physico-mathematical Sciences, to Engineer A.V. Vatazhin, to Docent V.N. Yershov, and to Docent Yu. V. Stepanov who read the proofs of some chapters of the manuscript. The comments made by the above comrades on the manuscript were gratefully accepted by the author and taken into account when editing the book.

The author

INTRODUCTION

0.1. TOPIC OF GASDYNAMICS

The topic of aeromechanics consists in investigating the motion of a gas and its interaction with bodies coming into contact with it. The mechanics of incompressible fluids is called hydromechanics. When attention is focused on the motion of a gas at high speeds, we are dealing with gasdynamics; in this case it is the compressibility of the gas that plays the main part.

The scope of gasdynamics has been considerably widened in recent times and its results have been applied to solving many problems which were previously assigned to physics and chemistry. Thus, for example, the motion of a gas is studied which is accompanied by the chemical reaction of the fuel burning, when the temperature may rise to such a degree that the molecules may dissociate and subsequently recombine on cooling, or the motion of a gas at high temperatures near the surface of a body moving at very high speed. The investigation of flight to great altitudes (in region where the air is greatly rarefied) requires that methods of the kinetic gas theory be applied and developed in gasdynamics. Gasdynamics is also applied to investigating the motion of ionized gases in astrophysical problems; at present very great attention is paid to studies in this field, namely to the motion of a conducting medium in the presence of electromagnetic fields.

Classification of forces. Forces acting on a mechanical system are divided into external and internal forces. If active and reaction

forces are applied to a body included in the system considered, these forces will be internal for the given system. If, however, the reaction force is applied to a body not belonging to the system, the active force will be external for the given system.

In aeromechanics as well as in the theory of elasticity, the "method of sections" is used for determining the internal forces, with the help of which the internal forces are transformed into external ones. At the same time the action of the remainder of the liquid is replaced by the resulting internal forces at the fluid section.

The forces may be subdivided into two classes according to the way in which they act: volume forces and surface forces. Volume forces are those which act on every volume element, regardless of whether there are other elements or not. They include the forces if inertia, gravity, electrical attraction, etc. The surface forces express the direct action of the environment on the surface particles of an isolated volume V of the system.

The principle of reactive motion. From the second law of mechanics it follows that any force acting on a body is equal to the change of the momentum of the body with time.

For producing the thrust in the case of propeller-driven airplanes the change of momentum is achieved through a small change in the speed of large masses; with jet-powered airplanes through a large change in the speed of relatively small masses.

The development of aviation is characterized by increasing speed, range and flight altitude; this evolution has been brought about by improving the aerodynamic forms of flying craft and by raising the power of the engines mounted on them.

The power demand of airplanes increases proportionally to the

cube of the flying speed. Since the estimated power of the propeller planes is independent of the speed an effective increase of speed may be reached only by increasing the power of the motor and, consequently, its size and weight. At a certain speed of flight the dimensions of the reciprocating engine become the greatest possible and a further increase of power demand leads to an increase of estimated power, which, at higher flying speeds, is moreover considerably reduced owing to the sharp drop of the propeller's efficiency. It was K.E. Tsiolkovskiy who foresaw this and as early as 1930 he said that the era of propeller planes would be followed by an era of jet planes.

The simplest reaction engine is the rocket engine whose thrust P is independent of the flying speed w; the thrust of a power plant with such an engine is N = Pw and increases linearly with increasing flying speed.

The most important property of the rocket engine consists in the fact that it may operate in space where there is no air. The rocket motor has been used for launching artificial satelites, the first of which was launched on October 4, 1957 in the Soviet Union. This type of engine has been used to produce on the basis of a multistage rocket the world's first Soviet artificial planet of the solar system and to carry 300 kg of terrestrial matter to the moon.

For flights in the atmosphere another type of reaction engines is used i.e., the air-reaction type (turbo-blower, ramjet, etc.) using atmospheric air as the oxidizer.

Aim and task of the course. The great variety of engines already existing has given rise to new problems connected with investigations into and calculations on their operation. Many aircraft engines have become an organic and inseparable part of the flying craft, determining its construction as a whole. Therefore the course on gasdynamics

of engines must not and should not contain ready made recipes which are always associated exclusively with a certain type of machine.

The present book is intended to impart an understanding of the basic processes and phenomena of gas flow and to construct accurately schemes for calculations on them. This becomes particularly important when the aspects of aircraft engine development are considered which might be based on new principles and effects, for example, magnetogasdynamic, ionic, etc. The only basis on which the study of these principles and effects can be built up is the basis of the general laws of the mechanics of continuous media, The title "Gasdynamics of Engines," however, circumscribes the choice of the area of problems subject to investigation.

0.2. PHYSICAL PROPERTIES OF LIQUIDS AND GASES

Structure of liquids and gases. As is well known, substantial bodies are subdivided into solids, liquids, and gases. In idealized models of crystalline solids in a state of stable equilibrium the atoms form nodes in the space called the crystal lattice and execute small vibrations about these nodes. In amorphous solids the atoms oscillate about randomly positioned centers.

In liquids the distances separating the molecules from each other are of the order of the dimensions of these molecules. The interaction of the molecules is therefore intense and the vibrations are also not so small.

In gases the distance between the molecules is considerably greater than their linear dimensions and the interactions of the molecules can be assumed to occur only through collisions.

Liquid and gas as continuous media. In aero-hydromechanics, when disregarding the molecular structure, gas and liquid are considered as continuous media in which there is no molecular motion and no

intermolecular space. All the physical characteristics of a continuous medium are uniformly distributed over their volume thus forming the respective fields.

Attributing to the medium the property of continuity means satisfying the following condition: in all problems the linear dimensions of the selected elementary volumes must be so small with respect to the characteristic linear dimensions* of the body (medium) that they may be considered as points; at the same time the volumes must be so large that they contain a sufficiently large number of molecules for the mean values of the physical quantities at the respective points to be determined statistically.

This condition is satisfied by liquids and not too rarefied gases.

Let us discuss how the value of a physical quantity is determined at some point of space in the continuous medium.

The concept of force tension is employed to characterize the force at a point. The tension or density of a volume force is defined as the limit of the ratio

$$\vec{f} = \lim_{\delta V \to 0} \frac{\delta \vec{P}}{\delta m} \left[\mathrm{m/sec^2}\right] \qquad (0.1)$$

where $\delta\vec{P}$ is a volume force acting on the unit mass δm, assuming that the volume $\delta V \to 0$, i.e., that it diminisnes to a point. Similarly, the tension of a surface force is

$$\vec{p} = \lim_{\delta A \to 0} \frac{\delta \vec{P}}{\delta A} \left[\mathrm{kg/m^2}\right] \qquad (0.2)$$

where $\delta\vec{P}$ is the force acting per unit area δA, where the area diminishes to a point with $\delta A \to 0$.

In both cases it is necessary to determine the meaning of the limiting transition taking the molecular structure of the substance into account. From the formal point of view the operation of the

limiting transition has no sense for a medium of discrete structure. Let us explain this through the example of determining the gas density at the point.

The mean density of the gas is determined as the ratio of its mass δm and the volume δV it occupies:

$$\rho_{sr} = \frac{\delta m}{\delta V} \left[\text{kg-sec}^2/\text{m}^4\right] \qquad (0.3)$$

We place the point considered inside the volume δV which will then be diminished to this point in order to determine the true value of the density in it:

$$\rho = \lim_{\delta V \to 0} \frac{\delta m}{\delta V}.$$

The dimensions of the molecules are considerably smaller than the intermolecular distances but their density is very high; this results from the fact that the density of nuclear matter amounts to about $1.16 \cdot 10^{16}$ kg/cm^3. Therefore, when the volume is reduced only at the expense of the intermolecular space, the mean density is increased. During the process of volume reduction the density oscillations are increased. Moreover, the molecules move and the mass even of a fixed volume varies with time. In the limiting case the value of the density may be either very large or zero depending on whether the point selected coincides with any molecule (nucleus) or falls in an empty intermolecular space.

Thus, the function $\rho_{sr} = \rho_{sr}(\delta V, t)$ in the coordinates ρ_{sr} and δV represents an area (Fig. 0.1, i.e., shaded area).

In the case of a concrete problem, if the accuracy for determining the density is given, density oscillations may be neglected up to a certain value of the volume δV_0. This will be also the continuity bound for the case considered. The density value at the point is then determined from the relation

$$\rho = \left(\frac{\Delta m}{\Delta V}\right)_{\Delta V \to \Delta V_0} \qquad (0.4)$$

The deformation rate as a criterion for classifying bodies.

A series of properties constituting according to the common view the particularities of only liquid and gaseous bodies apply also to solids and vice versa, i.e., solids can evaporate and diffuse, while fluids exhibit tensile strength, etc.

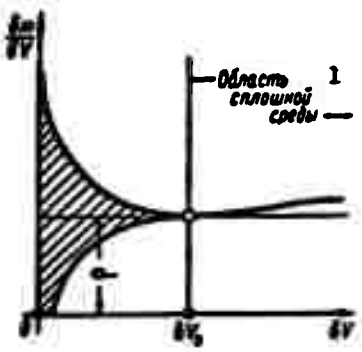


Fig. 0.1. To the definition of the concept of a continuous medium. 1) Region of continuous medium.

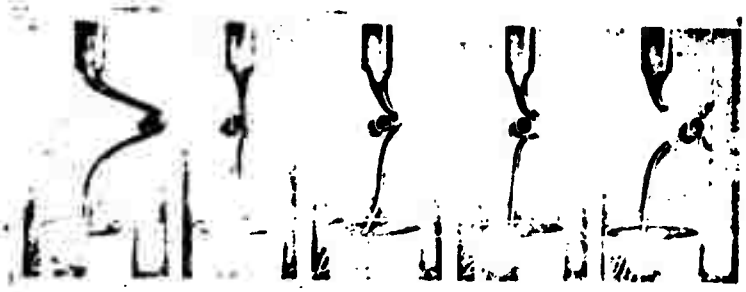
Sometimes, the ability of solids to maintain their shape is regarded as a characteristic property. It is, however, well known that a lump of tar which can be broken into pieces by an impact may also behave like a viscous liquid by flowing, although very slowly. A thin jet of oil [2] cut through by a circular rod displays plastic rupture when the speed of the rod destroying the jet is low; when the rod moves at high speed the destruction of the jet shows the character of brittle rupture similar to the destruction of glass (Fig. 0.2).

The difference in behavior of tar and the oil jet in the above case consists, as may be seen, in the deformation rate*. In the case of brittle rupture the deformation rate is high, and in the case of plastic rupture deformation occurs slowly.

Experiments shows that a certain stress must be applied to change the shape of an arbitrary body. This resistance to a change in shape is determined by laws that are different for solids and non-solids. Within the limits of small deformations of solids it may be assumed with sufficient accuracy that the stress in the solid is proportional

to the strain (Hooke's law).

GRAPHIC NOT REPRODUCIBLE



a b c d e

Fig. 0.2. Character of destruction of an oil jet, i.e., whether plastic or brittle depends on the deformation rate. a) In the case of a low rate the destruction is plastic in character; b, c, d, e) destruction becomes brittle when the rod moves at high speed (under experimental conditions, i.e., higher than 23 m/sec).

Considering, for example, small shearing deformations (Fig. 0.3), we may write

$$\tau = G\gamma \left[\text{kg/m}^2\right] \qquad (0.5)$$

where τ being the shear stress; G the elastic modulus of second kind, and γ the angular variation.

If we denote by $\delta\xi$ the displacement along the x-axis of the points of the plane at a distance δy, then

$$\gamma \approx \operatorname{tg}\gamma = \frac{\delta\xi}{\delta y}; \quad \tau = G\frac{\partial\xi}{\partial y}.$$

For nonsolid bodies, Newton's experimental law establishes that the tangential stresses characterizing the internal friction between the single layers of the fluid, are proportional to the velocity gradient with respect to the normal to these layers, and are independent of the magnitude of the velocity:

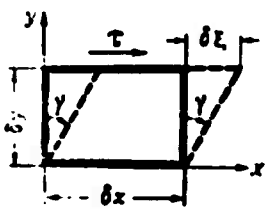


Fig. 0.3. Shear deformation.

$$\tau = \mu\frac{\partial w}{\partial y}. \qquad (0.6)$$

This property of the substance of offering resistance to slip of the fluid's particles, i.e., to changes only in shape but not in volume, is called viscosity. The proportion-

ality factor μ kg-sec/m^2 in Eq. (0.6) is called <u>coefficient of viscosity.</u>

Since the velocity is $w = \partial\xi/\partial t$,

$$\tau = \mu \frac{\partial}{\partial y}\frac{\partial \xi}{\partial t} = \mu \frac{\partial}{\partial t}\frac{\partial \xi}{\partial y} = \mu \frac{\partial \eta}{\partial t}. \qquad (0.7)$$

It follows from this that for nonsolid bodies the <u>tangential stresses are proportional to the deformation rate</u>, i.e., the smaller the deformation rate, the smaller the force causing the deformation in question. In the limiting case of an infinitesimal deformation rate any deformation can be caused by an arbitrarily small force.

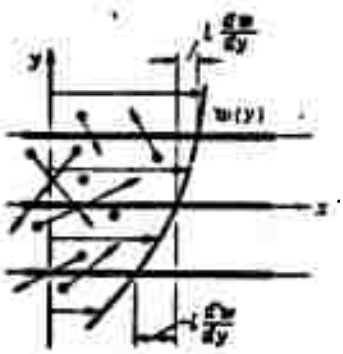


Fig. 0.4 For the definition of tangential stresses of friction.

Liquids and gases are therefore able to change their shape to any degree under the action of arbitrarily small foces.

<u>Viscosity</u>. Previously, viscosity was defined as the physical property of nonsolid bodies of offering resistance to a change in the shape of the body. The kinetic theory of matter makes it possible to describe the mechanism of viscosity and to estimate its magnitude. Furthermore it can be shown that the mechanism of internal friction in a liquid is different from that in a gas.

Let us consider the internal friction in a gas. We suppose for simplicity that the gas is moving parallel to the xz-plane (Fig. 0.4) in the direction of the x-axis, its velocity varying only in the y-direction. Let the velocity of the gas in xz-plane be <u>w</u>, then, at a distance above the xz-plane equal to the mean free path <u>l</u> of the molecules, the velocity (because <u>l</u> is small) will be equal to $w_1 = w + \underline{l}\, dw/d\underline{l}$, and at the same distance below the xz-plane, it will

be $w_2 = w - l\, dw/dl$. After a certain interval of time some of the molecules of the upper region will have pased to the lower one, and, since these molecules have greater momenta, they accelerate the motion of the lower layer of gas. Owing to the assumed equilibrium distribution of the gas molecules over the entire volume, after the same lapse of time the same quantity of molecules will have passed to the upper layer; but since these molecules have smaller momenta, they will also reduce the motion of the upper layer. Thus, the origin of the internal friction lies in the momentum exchange between the molecules of neighboring layers of the moving gas.

The mass of gas passing per unit time through some area δA in a direction perpendicular to the latter is equal to

$$\alpha n_0 c m \delta A = \alpha \rho c \delta A,$$

where α is a proportionality factor which, as is well known from physics, is determined by the velocity distribution function of the molecules; n_0 is the number of molecules per unit volume; c is the mean velocity of the thermal motion of the molecules and m is the mass of the molecules.

The momentum transferred by the molecules through the area δA in the xz-plane from above to below is equal to $\alpha\rho c w_1 \delta A$, and the momentum transferred from below to above is equal to $\alpha\rho c w_2 \delta A$. The difference of these momenta determines the internal friction force $\tau\delta A$ acting on this area. Therefore

$$\tau \delta A = (\alpha \rho c w_1 - \alpha \rho c w_2)\, \delta A = 2\alpha\rho c \frac{dw}{dy} l \delta A.$$

Comparing this expression with Formula (0.6) yields $\mu = 2\alpha\rho cl$, where 2α is a numerical coefficient. For the gas in a state of uniform equilibrium we have

$$2\alpha = 0{,}499 \text{ and } \mu = 0{,}499\rho cl. \qquad (0.8)$$

Similarly, by determining the energy exchanges between the molecules of gas layers of different temperatures, the coefficient of thermal conductivity (λ) kgm/m·sec·deg may be determined from the relation $dQ = \lambda \frac{dT}{dy}$

The kinetic gas theory yields the temperature dependence of the viscosity of a gas

$$\mu = \mu_0 \left(\frac{T}{T_0}\right)^{3/2} \frac{C + T_0}{C + T}. \qquad (0.9)$$

where μ_0 is the value of the viscosity coefficient at $T_0 = 273^\circ K$ and C is a constant (for air $C = 120^\circ K$).

As can be seen the viscosity of the gas increases with the temperature (Fig. 0.5).

For practical calculations the simpler relation

$$\mu = \mu_0 \left(\frac{T}{T_0}\right)^n \qquad (0.10)$$

is sometimes used (for air $n = 0.79$ gives good agreement with experiments).

In aeromechanics the kinematic coefficient of viscosity is frequently used:

$$\nu = \frac{\mu}{\rho} \ [m^2/sec] \qquad (0.11)$$

In contradistinction to gases, the viscosity of a liquid drops with increasing temperature, and, moreover, does so very noticeably (cf. Fig. 0.5). This proves that the mechanism of internal friction in liquids differs from that in gases; it may be assumed that the viscosity of liquids is caused by an association between groups of molecules, i.e., therefore the viscosity of liquids drops with increasing temperature.

Good agreement with experiment is achieved by the formula of A.I. Bachinskiy (1912) for the coefficient of viscosity of liquids

$$p = \frac{C}{v - \omega}.$$

where C and ω are constants and $v = 1/\rho$ is the specific volume.

For liquids we may assume

$$v = v_0(1 + a_1 T + a_2 T^2 + \ldots), \quad \frac{\rho}{\rho_0} = \frac{1}{1 + a_1 T + a_2 T^2 + \ldots}. \qquad (0.12)$$

Pressure in liquids (gases). During the motion of liquids (gases) the tension of the surface forces on any area consists of components normal (p) and tangential (τ) to the isolated area which determine the viscosity of the fluid.

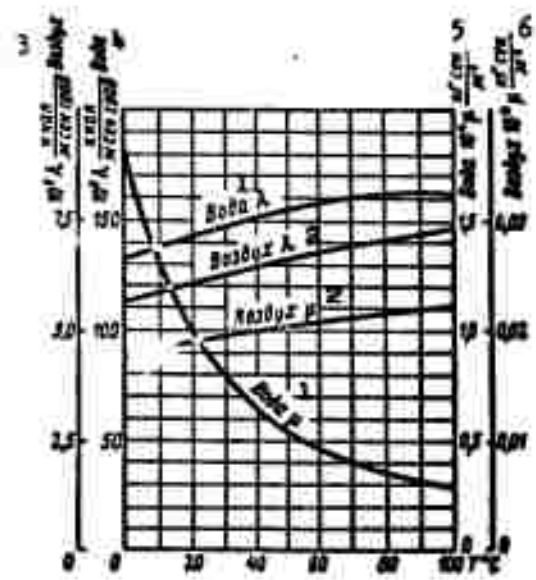


Fig. 0.5. Temperature dependence of viscosity coefficient μ and coefficient of thermal conductivity λ for air and water.
For air the μ and λ curves are similar since the heat and momentum transfer mechanisms are the same. 1) Water; 2) air; 3) kcal/m·sec·deg, air; 4) kcal/m·sec·deg, water; 5) water, $10^4\mu$ kg·sec/m^2; 6) $10^4\mu$ kg·sec/m^2.

When the fluid is at rest, i.e., $\vec{w} = 0$, the tangential stresses $\tau = \mu\frac{\partial w}{\partial n}$ are equal to zero and the tension of the surface forces will be directed along the normal.

Only when the experiments are performed with particular care to exclude any possibility of even the slightest slipping of particles

can the fluid sustain tensile stresses. It is therefore reasonable to assume that liquids and gases are not able to sustain tensile stresses, and that the normal stresses are always stresses of compression; these are called pressure.

Let us isolate in a fluid at rest an infinitesimal tetrahedron with its vertex at some arbitrary point (Fig. 0.6).

Let δA_x, δA_y and δA_z be the face areas of the tetrahedron, perpendicular to the respective axes x, y, z; p_x, p_y, p_z the pressure on these faces, p_n and δA_n the corresponding pressure and area of an inclined face, taken completely arbitrarily.

When $\vec{f} = \vec{i}f_x + \vec{j}f_y + \vec{k}f_z$ is the stress of the volume force at the point P, the equilibrium condition results in

$$\vec{i}p_x\delta A_x + \vec{j}p_y\delta A_y + \vec{k}p_z\delta A_z - \vec{n}p_n\delta A_n + \rho\vec{f}\delta V = 0,$$

where $\vec{n}$ is the unit vector of the outer normal of the inclined face.

Since the volume of the tetrahedron, δV, is a third-order small quantity the last term in this equation can be neglected. Projecting this equation onto the x-axis we obtain

$$p_x\delta A_x - \vec{i}\vec{n}p_n\delta A_n = 0.$$

The scalar product $\vec{i}\cdot\vec{n} = \cos(n, x)$, and since we have $\delta A_x = \delta A_n \cos(n, x)$, то $p_x = p_n$;

similarly, we obtain $p_y = p_n$, $p_z = p_n$. (0.13)

Thus, in a sufficiently small region of a fluid at rest the pressure is the same for any area taken inside the region.

In the general case of a moving viscous fluid the tension of the surface forces at each point depends on how the area in which the point considered lies is taken.

Inviscid liquids and gases. In a number of cases the tangential

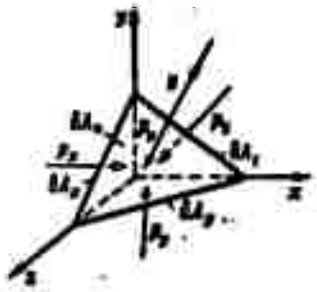


Fig. 0.6. In a liquid at rest the pressure is independent of the orientation of the area $p_x = p_y = p_z = p$.

stresses are considerably smaller than the normal ones and their effect may be neglected. Such a liquid (gas) which shows no viscosity will be called an inviscid liquid (inviscid gas).

Perfect and real gases. A gas is said to be perfect if it completely satisfies the Boyle-Mariotte and Gay-Lussac laws, or their common expression, the equation of state

$$p = \rho RT. \qquad (0.14)$$

Here R = 848 g/μG [kgm·m/kg·deg·sec^2] is the gas constant referred to the unit of mass (μG is the molecular weight).

For air R = 29.23 g = 287 [kg·m^2/kg·sec^2·deg].

In fact, the gases which we call real gases deviate from the characteristic equation; corrections are therefore frequently introduced into this equation for practical calculations. For real gases the semi-empirical Van der Waals relation

$$\left(p + \frac{a}{v^2}\right)(v - b) = RT. \qquad (0.15)$$

has become widely used as an equation of state; a and b are certain constants.

The higher the temperature and the lower the pressure the more closely a real gas approaches a perfect one.

Compressibility. The compressibility is conveniently characterized by means of the compression modulus which represents the ratio of pressure change δp and relative change of volume, δV/V, caused by this pressure change in the process considered:

$$K = -V\frac{\delta p}{\delta V}\ (\mathrm{kg/m^2}) \qquad (0.16)$$

Liquids offer enormous resistance to forces which tend to change their volume (for water K = 22,000 kg/cm^2, for oil K = 26,000 kg/cm^2), their compression modulus is almost independent of pressure and so liquids are considered as virtually incompressible.

With gases a change in volume can be achieved through very small pressure changes. In the case of isothermal compression we obtain

$$pdV = -Vdp,$$

from the equation of state, whence

$$K_T = -V\frac{dp}{dV} = p,$$

i.e., the compression modulus of gases in an isothermal process is equal to the pressure; at atmospheric pressure K = 1 kg/cm^2, i.e., it is 22,000 times smaller than for water. In the case of adiabatic compression ($pV^k = \text{const}$; $k = c_p : c_v$)

$$K_{ad} = -V\frac{dp}{dV} = kp = kK_T.$$

In a number of cases of gas motion the pressure changes are so small that the compressibility of the gas can be ignored; in this case the motions of gases and liquids are subject to one and the same law.

Propagation of small disturbances. From the fact that the compression (expansion) of a gas is accompanied by an increase (decrease) of pressure it follows that it exhibits the properties of an elastic body. A local compression of small intensity ($\frac{\delta p}{p} \ll 1, \frac{\delta \rho}{\rho} \ll 1$) will be propagated at a certain speed a in the medium in the form of a disturbance (change of state) which is called a wave. Sonic waves are of this kind; the propagation rate of any small disturbance is therefore equal to the sonic velocity.

The interface that separates the disturbed region from the undisturbed is called the wave front. In a homogeneous medium a wave

of small intensity is propagated at uniform speed in all directions and the wave front is a sphere; this is said to be a spherical wave.

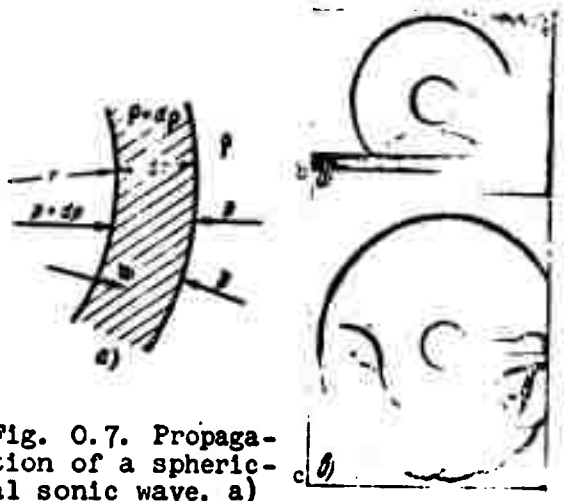


Fig. 0.7. Propagation of a spherical sonic wave. a) Diagram; b) photograph of reflection from a plane wall; c) penetration of a spherical sonic wave into a sphere with openings.

Let us consider two positions of a spherical wave (Fig. 0.7).

When the radius of wave front increases by dr during the time dt the sonic velocity is

$$a = \frac{dr}{dt}.$$

An increase dρ in the density of the wave occurs due to gas flowing into the disturbed region at a certain speed w. Denoting the mean value of the density in the wave by ρ', $\rho < \rho' < \rho + d\rho$, we may write the increase in the mass of the gas in the spatial region traversed by the wave as $\rho' \cdot 4\pi r^2 \cdot w\,dt$, which may also be written in the form $d\rho \cdot 4\pi r^2 dr$. Equating these expressions, $\rho' \cdot 4\pi r^2 \cdot w\,dt = d\rho \cdot 4\pi r^2 dr$, and noting that $\rho \approx \rho'$ we arrive at

$$d\rho = \rho w \frac{dt}{dr} = \frac{\rho w}{a}. \qquad (*)$$

On the other hand, the force impulse $dp \cdot 4\pi r^2 \cdot dt$, causing a gas mass $\rho'' \cdot 4\pi r^2 \cdot dr$ ($\rho < \rho'' < \rho + d\rho$) to flow in must be equal to its momentum change

$\rho' \cdot 4\pi r^2 \cdot dr \cdot w$, i.e.,

$$dp \cdot 4\pi r^2 \cdot dt = \rho' \cdot 4\pi r^2 \cdot dr \cdot w. \qquad (**)$$

Noting that $\rho'' \approx \rho$ and substituting ρw from (*) into (**) we find

$$a^2 = \frac{dp}{d\rho}. \qquad (0.17)$$

The most important property of all continuous media is the fact that a pressure increase at constant entropy always causes an increase in density, i.e., we always have

$$\frac{dp}{d\rho} > 0.$$

From Eq. (0.17) it follows that the rate of propagation of small disturbances depends on the law relating the pressure change with the density change, i.e., on the process of compression of the gas. As Laplace has shown, the propagation of sonic oscillations occurs so rapidly that no heat can be exchanged with the surrounding medium, i.e., the process is an adiabatic one, $p = \text{const}\ \rho^k$, and therefore

$$a = \sqrt{k\frac{p}{\rho}} = \sqrt{kRT}. \qquad (0.18)$$

Thus it proves that the sonic velocity for the given medium depends only on the temperature.

The sonic velocity can also be expressed in terms of the compression modulus

$$a = \sqrt{\frac{dp}{d\rho}} = \sqrt{\frac{dp}{dv^{-1}}} = \sqrt{-v^2\frac{dp}{dv}} = \sqrt{\frac{K}{\rho}}. \qquad (0.19)$$

In incompressible media the disturbances are promptly propagated ($a \to \infty$ so that $K = \infty$, $\rho = \text{const}$) in contradistinction to compressible media where the disturbance front propagates with a finite speed. In compressible media, therefore, an interface can exist that separates the disturbed from the remaining undisturbed medium. When passing through this interface, namely the wave front, all (or some) of the

physical quantities will be changed by a certain amount; it will be a discontinuity surface.

The propagation of waves is associated with the propagation of the state of the medium over its particles. The actual displacements of the particles are very small. The propagation of longitudinal disturbances may be represented by the mechanical model of a system of balls connected by springs like a train whose cars are joined by buffers (Fig. 0.8). When any one of the balls is pushed in the direction of another the disturbance is propagated along the whole train of balls. At the same time the displacement rate of these balls

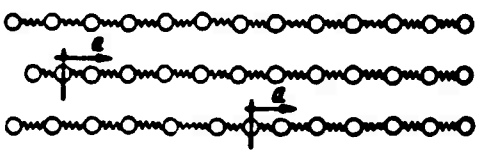


Fig. 0.8. Mechanical model of propagation of longitudinal disturbances.

will be small compared with the propagation rate of the disturbances, which is determined by the elasticity of the springs. The more rigid the spring (analogous to the compression modulus K), the more rapidly the disturbance will run.

The propagation of disturbances in fluids moving at a certain constant velocity w can be reduced to the case considered by introducing a coordinate system which is also moving with the same velocity w. Hence it results that the rate with respect to a fixed coordinate transfer at which the disturbance is propagated is a + w downstream and a − w upstream. When w ≥ a the disturbance is not propagated upstream at all. This fact involves very considerable changes in the behavior of fluids moving at speeds greater than that of sound.

Subsonic and supersonic gas flows. A qualitative difference between subsonic and supersonic flows is easily seen when a point sour

of disturbances, e.g., a small body A moving at the speed w in a quiescent gas, is considered. The disturbances propagate in the form of spherical waves at the sonic velocity a. When the speed at which the body moves is lower than that of sound, the motion of the body is accompanied by signals sent forward at a speed equal to the difference between sonic speed and the speed at which the body is moving (Fig. 0.9). In this case the disturbed region precedes the body and the flow changes its shape even before the gas particles come into contact with the body (cf. Fig. 0.9,a).

RAPHIC NOT
REPRODUCIBLE

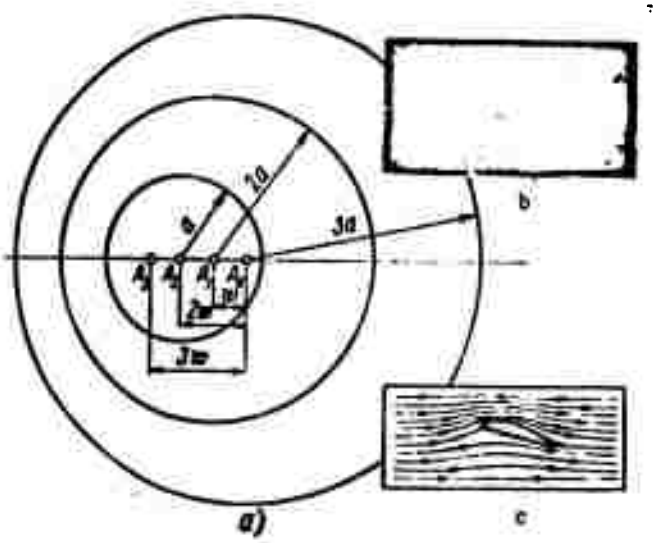


Fig. 0.9. When body A is moving at a speed w less than sonic speed a, the signals precede it. a) Spherical waves, 3 sec after the beginning of the motion; b) the shape of the flow changes before contact with the body; c) incompressible fluid streaming around a wing profile.

If, however, the speed is greater than sonic speed the disturbance source will precede the signals following it, and the spherical wave will be inside the cone enveloping the sphere (Fig. 0.10). This cone is called the disturbance cone (Mach cone).

The region outside the cone which is not disturbed by the body may be called "the zone of silence." The body "runs blindly against" the gas of this zone (cf. Fig. 0.10, b).

The disturbances in a supersonic flow are propagated along the lines that form the disturbance cone. They are called disturbance lines. As may be seen from Fig. 0.10 the angle between the disturbance lines and the direction of motion is determined by the equation

$$\sin\beta=\frac{a}{w}. \qquad (0.20)$$

In contradistinction to the subsonic flow where the disturbances are propagated in all directions in unbounded space, in the case of supersonic flow the disturbance occupy the region inside the disturbance cone, i.e., the transition to sonic speed is accompanied by a concentration of the disturbances.

GRAPHIC NOT REPRODUCIBLE

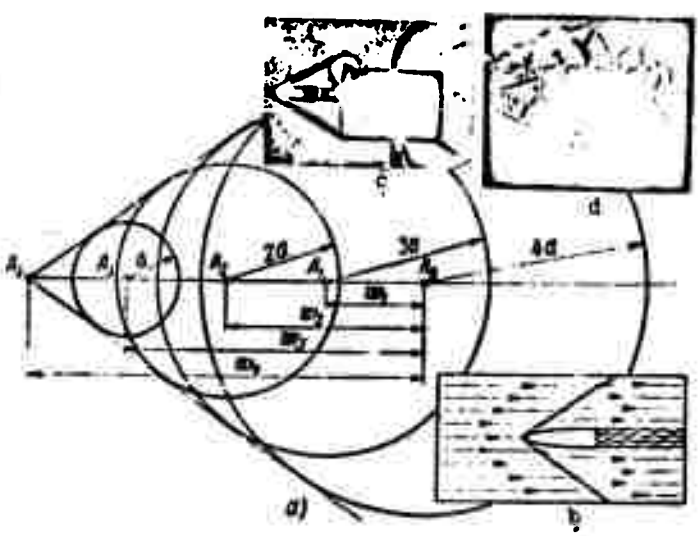


Fig. 0.10. When the body A moves at a speed w greater than sonic speed a, the signals (disturbances generated by the body) do not go beyond the disturbance cone (a). The supersonic flow does not change before it makes contact with the body (b). The bullet travels through a cylindrical tube (c), i.e., the compression shocks and the spherical waves are to be observed. The bullet travels through a series of short tubes (d).

The model of the atmosphere. In order to design a modern flying craft it is necessary to know the physical conditions at a sufficiently great distance from the earth. The conditions vary not only with the latitude and the season but also during the course of the day. To introduce uniformity, certain average quantities are used to character-

ize these conditions which are called atmosphere models. The model taken as a standard is called the standard atmosphere.

Observations made with the help of the first Soviet earth satellite gave rise to substantial modifications in the present ideas about the structure of the upper layers of the atmosphere. Up to now, however, the data for heights above 100 km have not yet been finally established and the characteristics given in Appendix 3 are only more or less probable ones.

Manuscript Page No.

[Footnotes]

9 For instance, when flow occurs around an arbitrary body, the length of this body may be taken as the characteristic linear dimension (scale of length) with which the linear dimension of the elementary particle is compared, e.g., the length of an edge if the particle is chosen in the form of a cube.

11 Remember that deformation is the change in shape or size of a body which is due to a change in the relative positions of of the body's particles caused by their displacements.

REFERENCES

1. Putilov, K.A., Kurs fiziki [Course in Physics], Fizmatgiz [State Publishing House for Physicomathematical Literature], 1959.

2. Kornfel'd, M., Uprugost' i prochnost' zhidostey [Elasticity and Toughness of Liquids], GTTI [State Technical and Theoretical Press], 1959.

Manuscript Page No.

[Transliterated Symbol]

19 ад = ad = adiabaticheskiy = adiabatic

Chapter 1

KINEMATICS OF LIQUID AND GAS

1.1. VELOCITY AND ACCELERATION OF PARTICLES

The velocity field. For determining the motion of a solid it is sufficient to know the motion of three of its points. The motion of a fluid may be taken as determined only in the case when the velocity of each of its points is known, i.e., when the whole velocity field* is known. This is connected with the fact that the distances between the points of a liquid are not constant. Since the velocity at a point may vary with time, the velocity field in the general case will be a function of time.

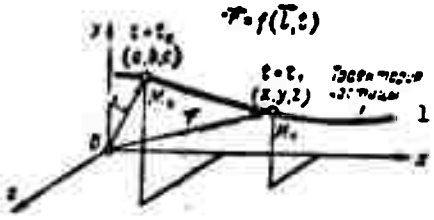


Fig. 1.1.1. Studying the motion by the Lagrange method, the whole path (trajectory) of each particle is determined. 1) Particle trajectory.

Methods of investigating the motion of a fluid. The motion of a fluid can be studied by determining the motion of each of its single particles; this is the Lagrange method. Another method also exists, however, this is the Euler method, which consists in determining the parameters of motion at all points of the flowing region.

The Lagrange method. To study the "fate" of each particle in a fluid, they must be distinguished. This can be accomplished by denoting the particle by its coordinates (a,b,c) at the initial instant of time ($t = t_0$). In an orthogonal coordinate system each particle will correspond to the vector $\vec{l} = \vec{ia} + \vec{jb} + \vec{kc}$ (Fig. 1.1.1). The coordinates a,

b, c are called the Lagrange variables. The motion is taken as determined if for each particle the changes with time of its radius vector $\vec{r}=\vec{i}x+\vec{j}y+\vec{k}z$ are known, i.e., if the vector

$$\left.\begin{array}{c}\vec{r}=\vec{r}(\vec{l}, t)\\ \text{or the set of equations}\\ x=x(a, b, c, t);\ y=y(a, b, c, t);\ z=z(a, b, c, t).\end{array}\right\} \qquad (1.1.1)$$

is known.

Equation (1.1.1) represents the set of trajectories of all the particles of the fluid; the time t is an independent variable and a, b, c are the parameters of the set.

The vector velocity $(\vec{w})$ of any particle at any instant of time is equal to

$$\left.\begin{array}{c}\vec{w}=\dfrac{\partial\vec{r}}{\partial t}\\ \text{or}\\ w_x=\dfrac{\partial x}{\partial t},\quad w_y=\dfrac{\partial y}{\partial t},\quad w_z=\dfrac{\partial z}{\partial t}.\end{array}\right\} \qquad (1.1.2)$$

The Euler method. The Lagrange method proves complicated for solving certain problems and it is frequently simpler to trace the variations occurring with the passage of time t at the points $\vec{r}(x, y, z)$ in space, i.e., to determine the function

$$\left.\begin{array}{c}\vec{w}=\vec{w}(\vec{r}, t)\\ \text{or}\\ w_x=w_x(x, y, z, t);\ w_y=w_y(x, y, z, t);\ w_z=w_z(x, y, z, t).\end{array}\right\} \qquad (1.1.3)$$

where x, y, z, t are what are called the Euler variables (Fig. 1.1.2).

To pass over from the Euler representation to the Lagrange representation it is necessary to solve the equation

$$\frac{d\vec{r}}{dt}=\vec{w}(\vec{r}, t)$$

or the set

$$\frac{dx}{dt}=w_x(x, y, z, t);\quad \frac{dy}{dt}=w_y(x, y, z, t);$$

$$\frac{dz}{dt}=w_z(x, y, z, t).$$

The solution x, y, z will contain three arbitrary integration constants which may be chosen as the coordinates a, b, c of the particles at the initial instant of time.

Streamlines and trajectories. When the motion of the fluid is given in Lagrange variables, the geometrical representation of the flow is given by the trajectories. In Euler variables the streamlines (Fig. 1.1.3) are used for the geometrical interpretation of the flow.

The streamline is a line such that at a given instant the velocity vector at every point of the line coincides with the tangent to the line. The only case in which the streamlines at different moments of time coincide with each other and, moreover, with the trajectories, is when all the parameters of the motion, including the velocity, do not depend explicitly on the time. This sort of motion is termed stabilized or steady. In the case of unsteady motion the streamlines constructed for different instants of time will not coincide, either with each other or with the trajectories. Since the tangent to a streamline coincides with the velocity vector, the streamline equation may be written in one of the following forms:

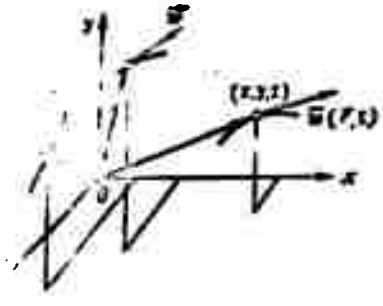


Fig. 1.1.2. Studying a motion by the Euler method determines the state of motion at each point of space at each instant of time.

$$\vec{dr}\times\vec{w}=0,\quad \begin{vmatrix} i & j & k \\ dx & dy & dz \\ w_x & w_y & w_z \end{vmatrix}=0 \qquad (1.1.4)$$

or

$$\frac{dx}{w_x}=\frac{dy}{w_y}=\frac{dz}{w_z}.$$

Note that the time t appearing in the expression for $\vec{w}=\vec{w}(\vec{r},t)$ must considered as a parameter whose value is given. Therefore, in spite of the formal analogy between Eqs. (1.1.3) and (1.1.4), in

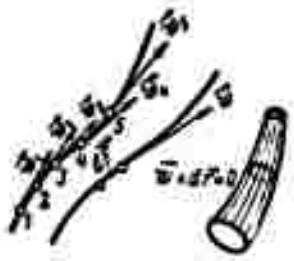


Fig. 1.1.3. Streamlines and stream tubes.

the coordinate form, they show in principle a difference which is that in the trajectory equation

$$\frac{dx}{v_x} = \frac{dy}{v_y} = \frac{dz}{v_z} = dt$$

the time appears as an independent variable and $\vec{r}(x, y, z, t)$ is determined as a function of it, whereas in the streamline equation

$$\frac{dx}{v_x} = \frac{dy}{v_y} = \frac{dz}{v_z}$$

the time t is considered as a parameter.

The stream tube is used as well as the streamline to represent the motion of a fluid graphically; this is a surface formed by the streamlines passing through all points of a closed contour (Fig. 1.1.3). In the case of an inviscid fluid in steady motion the stream tube behaves like a tube with solid walls. The fluid moving inside the tube is called flow element.

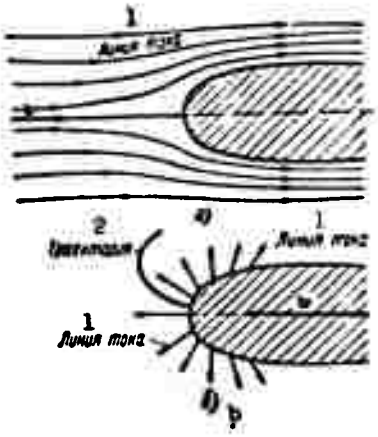


Fig. 1.1.4. Trajectories and streamlines about a body. a) Fluid streaming against a quiescent body; b) body moving in quiescent fluid. 1) Streamline; 2) trajectory.

The choice of the coordinate system to which the fluid's motion is referred is of considerable importance for constructing the geometrical pattern of the motion.

Let us consider, for example, the motion near a body moving at constant speed which is so long that the disturbance at its rear end can be neglected when considering, e.g., the nose of an airship (Fig. 1.1.4).

When the coordinate system is fixed to the body the motion of the liquid will be steady with respect to the observer. It will look

like a nonmoving body with a stream impinging against it at the same speed. The streamlines which also coincide with the trajectories will form a pattern like that shown in Fig. 1.1.4, a.

When, however, the coordinate system is connected with the flowing liquid, the motion in this system will be unsteady for the observer. The body will displace the particles of the fluid and will do so in such a way that the particles in front of it are pushed forward all the time and the particles near the sides of the body flow aside (cf. Fig. 1.1.4,b). Streamlines and particle trajectories will differ from each other.



Fig. 1.1.5. Flow of liquid around a moving plate. a) When taking the photograph the camera was kept at rest (as to the path followed by the plate one may follow the traces of its lateral edges); b) camera moved together with the plate.

It may be seen from this example that, provided the coordinate system is suitably chosen, any steady motion can be considered as an unsteady one. The converse conclusion will not always be correct, however; for example, in the case of a body that oscillates in the fluid it is impossible to choose a coordinate system in which this motion could be observed as a steady one.

Figure 1.1.5 shows a photograph of the flow around a moving plate taken by (a) a camera at rest and (b) a camera moved together with the plate.

The acceleration field. The acceleration of different particles at a fixed point in space has to be distinguished from the acceleration of a certain fixed moving particle of the liquid at different points in space. When the motion is investigated by Legendre's method the change with time of the vector velocity of a fixed particle

ORIGINAL NOT REPRODUCIBLE

at any point in space is characterized by a partial time derivative (here $\vec{l}=\vec{i}a+\vec{j}b+\vec{k}c$ is assumed constant):

$$\frac{d\vec{w}(\vec{l},t)}{dt}=\vec{i}\frac{\partial w_x}{\partial t}+\vec{j}\frac{\partial w_y}{\partial t}+\vec{k}\frac{\partial w_z}{\partial t}. \qquad (1.1.5)$$

When the motion is investigated by Euler's method, at a fixed point in space various particles may pass through and the total increase in particle velocity (Fig. 1.1.6) is made up of the local increase, defined as the local derivative, and of the velocity increment due to the spatial displacement of particles (transport - convection), defined as what is called the convective derivative.

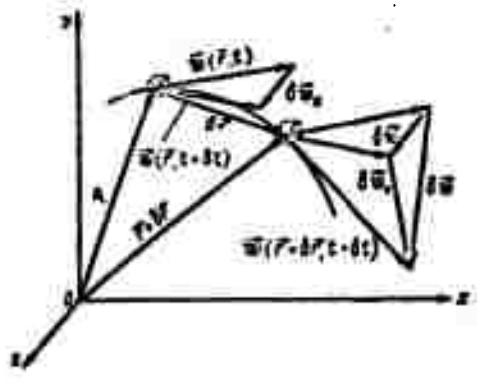


Fig. 1.1.6. Variation of speed when passing over from one point to another, over the distance $\delta\vec{r}$, during the time δt.

In fact, for the general case of the variation of a certain quantity F $(\vec{r}, t)$ of the fluid we have

$$\frac{dF}{dt}=\lim_{\delta t\to 0}\frac{F(\vec{r}+\delta\vec{r},t+\delta t)-F(\vec{r},t)}{\delta t}=\lim_{\delta t\to 0}\frac{F(\vec{r},t+\delta t)-F(\vec{r},t)}{\delta t}+$$

$$+\lim_{\delta t\to 0}\frac{F(\vec{r}+\delta\vec{r},t)-F(\vec{r},t)}{\delta t}=\frac{\partial F}{\partial t}+\vec{w}\cdot\vec{\nabla}F,$$

where

$$F(\vec{r}+\delta\vec{r},t)-F(\vec{r},t)=\frac{\partial F}{\partial x}\delta x+\frac{\partial F}{\partial y}\delta y+\frac{\partial F}{\partial z}\delta z=$$

$$=(\vec{i}\delta x+\vec{j}\delta y+\vec{k}\delta z)\left(\vec{i}\frac{\partial}{\partial x}+\vec{j}\frac{\partial}{\partial y}+\vec{k}\frac{\partial}{\partial z}\right)F=$$

$$=\delta\vec{r}\cdot\vec{\nabla}F \text{ and } \lim_{\delta t\to 0}\delta\vec{r}/\delta t=\vec{w};$$

and therefore, dividing by dt, we obtain for the convective derivative

$$\left(\frac{dF}{dt}\right)_k = \vec{w}\cdot\vec{\nabla}F = (\vec{w}\cdot\vec{\nabla})F. \qquad (1.1.6)$$

In the particular case of the speed $F = \vec{w}$ the total acceleration (total derivative) is determined as the sum of local and convective accelerations:

$$\frac{d\vec{w}}{dt} = \frac{\partial\vec{w}}{\partial t} + (\vec{w}\cdot\vec{\nabla})\vec{w} = \frac{\partial\vec{w}}{\partial t} + w_x\frac{\partial\vec{w}}{\partial x} + w_y\frac{\partial\vec{w}}{\partial y} + w_z\frac{\partial\vec{w}}{\partial z} \qquad (1.1.7)$$

or, in the form of projections onto the coordinate axes:

$$\left.\begin{aligned}
\frac{dw_x}{dt} &= \frac{\partial w_x}{\partial t} + w_x\frac{\partial w_x}{\partial x} + w_y\frac{\partial w_x}{\partial y} + w_z\frac{\partial w_x}{\partial z},\\
\frac{dw_y}{dt} &= \frac{\partial w_y}{\partial t} + w_x\frac{\partial w_y}{\partial x} + w_y\frac{\partial w_y}{\partial y} + w_z\frac{\partial w_y}{\partial z},\\
\frac{dw_z}{dt} &= \frac{\partial w_z}{\partial t} + w_x\frac{\partial w_z}{\partial x} + w_y\frac{\partial w_z}{\partial y} + w_z\frac{\partial w_z}{\partial z}.
\end{aligned}\right\} \qquad (1.1.8)$$

These three formulas may for brevity be written as one if the coordinates x, y, z are replaced by x_1, x_2, x_3, respectively. Then

$$\frac{dw_i}{dt} = \frac{\partial w_i}{\partial t} + \sum_{k=1}^{3} w_k\frac{\partial w_i}{\partial x_k} \qquad (i = 1, 2, 3). \qquad (1.1.9)$$

1.2. DECOMPOSITION OF THE GENERAL MOTION INTO THE SIMPLEST ONES

Linear variation of speed in the vicinity of a point. Let us consider the speed near the point $\vec{r}_0 = \vec{i}x_0 + \vec{j}y_0 + \vec{k}z_0$ for a fixed instant of time. The speed $\vec{w}$ of the fluid near the point $P_0(\vec{r}_0)$ is assumed to be a regular function of the point, i.e., assumed to be a power expansion. Then, for the neighboring points $P_0(\vec{r}_0 + \delta\vec{r})$ we have

$$\begin{aligned}
w_x &= w_{0x} + \left(\frac{\partial w_x}{\partial x}\right)_0\delta x + \left(\frac{\partial w_x}{\partial y}\right)_0\delta y + \left(\frac{\partial w_x}{\partial z}\right)_0\delta z + \\
&+ \frac{1}{2!}\left(\frac{\partial^2 w_x}{\partial x^2}\right)_0\delta x^2 + \ldots,\\
w_y &= w_{0y} + \left(\frac{\partial w_y}{\partial x}\right)_0\delta x + \left(\frac{\partial w_y}{\partial y}\right)_0\delta y + \left(\frac{\partial w_y}{\partial z}\right)_0\delta z + \\
&+ \frac{1}{2!}\left(\frac{\partial^2 w_y}{\partial x^2}\right)_0\delta x^2 + \ldots.\\
w_z &= w_{0z} + \left(\frac{\partial w_z}{\partial x}\right)_0\delta x + \left(\frac{\partial w_z}{\partial y}\right)_0\delta y + \left(\frac{\partial w_z}{\partial z}\right)_0\delta z + \\
&+ \frac{1}{2!}\left(\frac{\partial^2 w_z}{\partial x^2}\right)_0\delta x^2 + \ldots.
\end{aligned}$$

Taking the region around P_0 small enough for the small expansion terms of second and higher orders to be negligible, we obtain for the chosen region the velocity as a linear function of the distance. Then we may write [omitting the subscript zero at the derivatives, indicating that the derivative is calculated for the point $P_0(\vec{r}_0)$]:

$$\left.\begin{aligned} w_x &= w_{0x} + \frac{\partial w_x}{\partial x}\delta x + \frac{\partial w_x}{\partial y}\delta y + \frac{\partial w_x}{\partial z}\delta z, \\ w_y &= w_{0y} + \frac{\partial w_y}{\partial x}\delta x + \frac{\partial w_y}{\partial y}\delta y + \frac{\partial w_y}{\partial z}\delta z, \\ w_z &= w_{0z} + \frac{\partial w_z}{\partial x}\delta x + \frac{\partial w_z}{\partial y}\delta y + \frac{\partial w_z}{\partial z}\delta z \end{aligned}\right\} \qquad (1.2.1)$$

or

$$\vec{w} = \vec{w}_0 + (\delta\vec{r}\cdot\vec{\nabla})\vec{w},$$

where

$$\vec{\nabla} = \vec{i}\frac{\partial}{\partial x} + \vec{j}\frac{\partial}{\partial y} + \vec{k}\frac{\partial}{\partial z}$$

and

$$\delta\vec{r} = \vec{i}\delta x + \vec{j}\delta y + \vec{k}\delta z.$$

It can be seen that the change of speed near the point is in general determined by nine numerical values of partial derivatives with respect to the axes of the speed components calculated for the point $P_0(x_0, y_0, z_0)$:

$$\frac{\partial w_x}{\partial x}, \frac{\partial w_x}{\partial y}, \frac{\partial w_x}{\partial z}, \frac{\partial w_y}{\partial x}, \frac{\partial w_y}{\partial y}, \frac{\partial w_y}{\partial z}, \frac{\partial w_z}{\partial x}, \frac{\partial w_z}{\partial y}, \frac{\partial w_z}{\partial z}.$$

Deformation of a plane element. Let us assume that all particles of the fluid move parallel to the xy-plane so that $w_z = 0$ and the speeds in any direction perpendicular to the plane of motion are equal, i.e., $\frac{\partial w_x}{\partial z}=0, \frac{\partial w_y}{\partial z}=0$; a motion of this sort is called a plane motion. Separating a layer of unit thickness, we may consider instead of the prism with its generatrices parallel to the z-axis only its outlines. Let abcd (Fig. 1.2.1) be a plane fluid element lying in the xy-plane. The difference in the speeds of its points is a ter-

mined by the four derivatives $\frac{\partial w_x}{\partial x}, \frac{\partial w_x}{\partial y}, \frac{\partial w_y}{\partial x}, \frac{\partial w_y}{\partial y}$, which are for convenience written in a matrix (Table)*:

$$\begin{Bmatrix} \frac{\partial w_x}{\partial x} & \frac{\partial w_y}{\partial x} \\ \frac{\partial w_x}{\partial y} & \frac{\partial w_y}{\partial y} \end{Bmatrix}. \qquad (1.2.2)$$

If all matrix elements except $\partial w_x/\partial x$, are equal to zero this indicates that only the speed component in the x-direction is increased when moving along this axis (Fig, 1.2.2) and therefore the element is elongated at the rate $\frac{\partial w_x}{\partial x}\delta x$. The relative deformation of a unit length per unit time will then be

$$\varepsilon_{xx} = \frac{\partial w_x}{\partial x}.$$

If $\frac{\partial w_y}{\partial x} \neq 0$, and all other terms of the matrix are equal to zero only the velocity w_y varies (linearly) along the x-axis. At the same time a shear deformation occurs along the y-axis and also a <u>rotation</u> [illegible] a rotation of the diagonal element during shearing (Fig. 1.2.

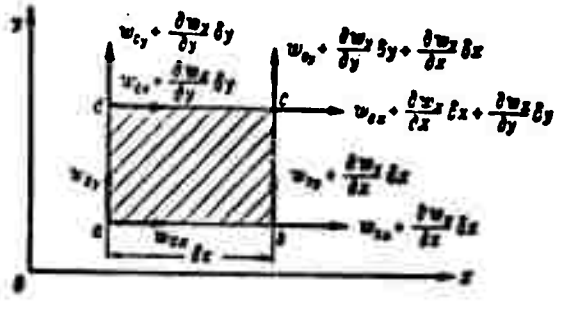


Fig. 1.2.1. Speeds at the corner points of a plane fluid element.

If only $\frac{\partial w_y}{\partial x} = \frac{\partial w_x}{\partial y} \neq 0$, the diagonal element will not be turned during shear deformation, i.e., we have a <u>pure shear deformation</u> in this case. If only $\frac{\partial w_y}{\partial x} = -\frac{\partial w_x}{\partial y} \neq 0$, we have <u>pure rotation</u>.

Regardless of the values of its terms, the matrix element as a whole may be displaced at a constant rate having the components w_{0x} and w_{0y}.

As can be seen from Fig. 1.2.4, the measure of the shear deformation per unit time, i.e., the measure of the rate of variation of the right angle, is the quantity

$$\varepsilon_{xy}=\frac{1}{2}\left(\frac{\partial w_y}{\partial x}+\frac{\partial w_x}{\partial y}\right).$$

and

the rotation of the plane element of shear is characterized by the value of its angular velocity (cf. Fig. 1.2.4):

$$\omega_z=\frac{1}{2}\left(\frac{\partial w_y}{\partial x}-\frac{\partial w_x}{\partial y}\right).$$

The matrix of the plane element can be represented as the sum of the three matrices

$$\begin{Vmatrix} \frac{\partial w_x}{\partial x} & \frac{\partial w_y}{\partial x} \\ \frac{\partial w_x}{\partial y} & \frac{\partial w_y}{\partial y} \end{Vmatrix}=\begin{Vmatrix} \frac{\partial w_x}{\partial x} & 0 \\ 0 & \frac{\partial w_y}{\partial y} \end{Vmatrix}+\begin{Vmatrix} 0 & \frac{1}{2}\left(\frac{\partial w_y}{\partial x}+\frac{\partial w_x}{\partial y}\right) \\ \frac{1}{2}\left(\frac{\partial w_x}{\partial y}+\frac{\partial w_y}{\partial x}\right) & 0 \end{Vmatrix}+$$

$$+\begin{Vmatrix} 0 & \frac{1}{2}\left(\frac{\partial w_y}{\partial x}-\frac{\partial w_x}{\partial y}\right) \\ \frac{1}{2}\left(\frac{\partial w_x}{\partial y}-\frac{\partial w_y}{\partial x}\right) & 0 \end{Vmatrix}=$$

$$=\begin{Vmatrix} \varepsilon_{xx} & 0 \\ 0 & \varepsilon_{yy} \end{Vmatrix}+\begin{Vmatrix} 0 & \varepsilon_{xy} \\ \varepsilon_{yx} & 0 \end{Vmatrix}+\begin{Vmatrix} 0 & \omega_z \\ -\omega_z & 0 \end{Vmatrix}; \quad (1.2.3)$$

the meaning of the composition of the matrix is evident.

The first matrix gives information on the elongation, the second on pure shear deformation and the third on pure rotation.

The second matrix, characterized by terms symmetric relative to the main diagonal and identical, is said to be symmetric, and the

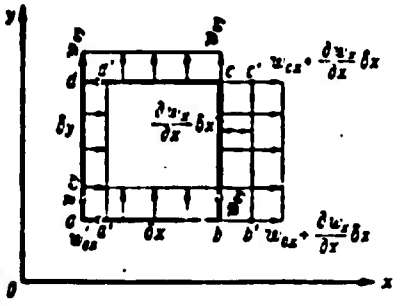


Fig. 1.2.2. Elongation of an element per unit time in the direction of the x-axis and displacement without deformation at the rate $\vec{w}(w_{0x}, w_{0y})$. The quantity $\frac{\partial w_x}{\partial x}$ characterizes the relative rate of stretching deformation in the direction of the x-axis.

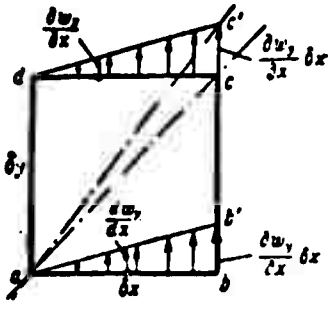
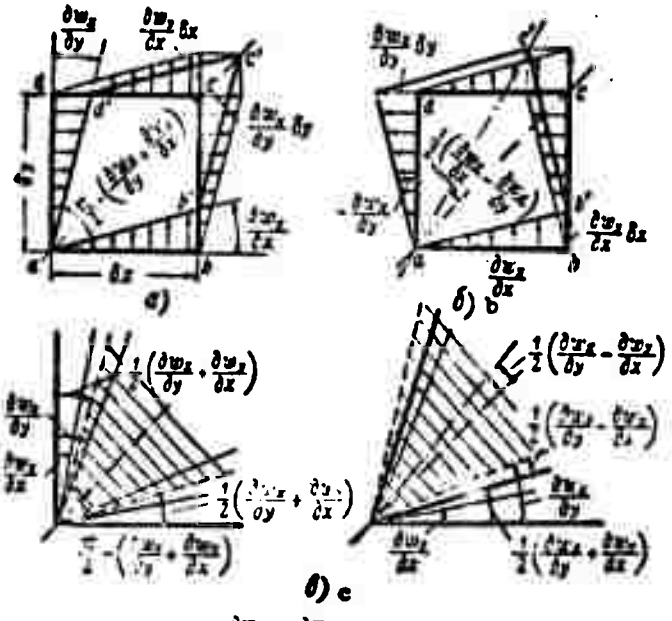


Fig. 1.2.3. Shear deformation and rotation of the element per unit time.

third matrix, whose terms symmetrical with respect to the main diagonal are equal in absolute magnitude but of opposite sign, is said to be antisymmetric (skew-symmetric).



. 1.2. . With pure shear, $\frac{\partial w_x}{\partial y} = \frac{\partial w_y}{\partial x}$ differ from zero, and the right ... reduced by $\left(\frac{\partial w_x}{\partial y} + \frac{\partial w_y}{\partial x}\right)(a)$. With pure rotation the whole element is turned through the angle $\frac{1}{2}\left(\frac{\partial w_y}{\partial x} - \frac{\partial w_x}{\partial y}\right)$ (b). General case of shear and rotation $\frac{\partial w_x}{\partial y} \neq \frac{\partial w_y}{\partial x}$ (c).

General case of deformation of a parallelepiped. Considering an elementary parallelepiped in the general spatial case, we obtain

$$\varepsilon_{xx} = \frac{\partial w_x}{\partial x}, \quad \varepsilon_{yy} = \frac{\partial w_y}{\partial y}, \quad \varepsilon_{zz} = \frac{\partial w_z}{\partial z}; \tag{1.2.4}$$

$$\left.\begin{aligned} \varepsilon_{xy} &= \frac{1}{2}\left(\frac{\partial w_y}{\partial x} + \frac{\partial w_x}{\partial y}\right) = \varepsilon_{yx}, \\ \varepsilon_{xz} = \frac{1}{2}\left(\frac{\partial w_z}{\partial x} + \frac{\partial w_x}{\partial z}\right) &= \varepsilon_{zx}, \ \varepsilon_{yz} = \frac{1}{2}\left(\frac{\partial w_z}{\partial y} + \frac{\partial w_y}{\partial z}\right) = \varepsilon_{zy}; \end{aligned}\right\} \tag{1.2.5}$$

$$\left.\begin{aligned} \omega_x &= \frac{1}{2}\left(\frac{\partial w_z}{\partial y} - \frac{\partial w_y}{\partial z}\right), \\ \omega_y = \frac{1}{2}\left(\frac{\partial w_x}{\partial z} - \frac{\partial w_z}{\partial x}\right), \quad \omega_z &= \frac{1}{2}\left(\frac{\partial w_y}{\partial x} - \frac{\partial w_x}{\partial y}\right) \end{aligned}\right\} \tag{1.2.6}$$

and the vector of angular velocity (cf. Appendix 2) is therefore

$$\vec{\omega} = \frac{1}{2}\operatorname{rot}\vec{w}.$$

In the general case of a spatial motion, the nonuniformity of the velocity field is determined by the numerical values of nine partial derivatives of the three velocity components (w_x, w_y, w_z) with respect to the three axes (x, y, z):

$$\begin{Bmatrix} \frac{\partial w_x}{\partial x} & \frac{\partial w_y}{\partial x} & \frac{\partial w_z}{\partial x} \\ \frac{\partial w_x}{\partial y} & \frac{\partial w_y}{\partial y} & \frac{\partial w_z}{\partial y} \\ \frac{\partial w_x}{\partial z} & \frac{\partial w_y}{\partial z} & \frac{\partial w_z}{\partial z} \end{Bmatrix} = \begin{Bmatrix} \varepsilon_{xx} & 0 & 0 \\ 0 & \varepsilon_{yy} & 0 \\ 0 & 0 & \varepsilon_{zz} \end{Bmatrix} + \\ + \begin{Bmatrix} 0 & \varepsilon_{xy} & \varepsilon_{xz} \\ \varepsilon_{yx} & 0 & \varepsilon_{yz} \\ \varepsilon_{zx} & \varepsilon_{zy} & 0 \end{Bmatrix} + \begin{Bmatrix} 0 & \omega_z & -\omega_y \\ -\omega_z & 0 & \omega_x \\ \omega_y & -\omega_x & 0 \end{Bmatrix} \qquad (1.2.7)$$

As in (1.2.3) the first matrix characterizes the stretching deformation of an element, the second the shear deformation and the third the rotation of the element. Therefore the speed of a sufficiently small particle is composed of a translatory speed, the deformation rate (stretching and shear) and the rotation. This theorem is named after Helmholtz.

In the coordinate system x_1, x_2, x_3 (1.2.7) can be immediately obtained as

$$w_i = w_{0i} + \sum_{k=1}^{3} \frac{\partial w_i}{\partial x_k} \delta x_k = w_{0i} + \frac{1}{2} \sum_{k=1}^{3} \left(\frac{\partial w_i}{\partial x_k} + \frac{\partial w_k}{\partial x_i} \right) \delta x_k + \\ + \frac{1}{2} \sum_{k=1}^{3} \left(\frac{\partial w_i}{\partial x_k} - \frac{\partial w_k}{\partial x_i} \right) \delta x_k. \qquad (1.2.8)$$

1.3. POTENTIAL AND TURBULENT MOTIONS

Connectedness of a region. When investigating the motion of a fluid it is frequently necessary to subdivide it into separate regions. A region in which some arbitrary closed line may be continuously constricted to a point without interfering with the boundaries of the region is called simply connected. Regions which are not simply connected are called multiply connected.

A multiply connected region can be rendered simply connected by incorporating additional boundaries which "forbid" those contours which cannot be contracted to a point. The connectedness of the re-

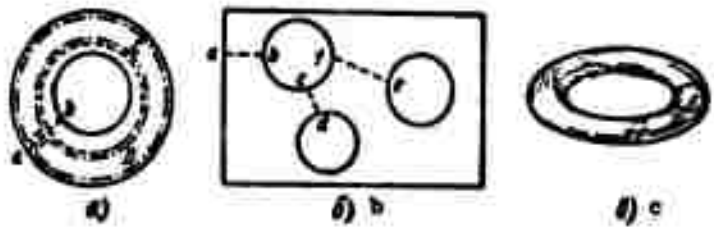


Fig. 1.3.1. The contour C inside the ring cannot be contracted to a point, the line ab "forbids" such a contour (a), i.e., this is a doubly connected region. A plane with three holes (b) is a quadruply connected region. The interior of a tore (c) is a doubly connected region.

gion is determined by the number of additional boundaries plus one. For example, the interior of a sphere, a cube, a circle on a plane, or the plane as a whole are all singly connected regions; the same is true of the space between two spheres. The interior of a plane ring, however, is doubly connected; to make it singly connected an additional boundary needs be added; this is the line ab joining the two circles (Fig. 1.3.1). A plane with three holes is fourfold connected; the interior of a tore can be made singly connected by introducing a dividing wall; it is doubly connected.

The velocity potential. Subdividing the general motion of the particles of a fluid into translational, vibrational, and rotational motions makes it possible to set up two most general classes of motion: the first is rotation-free and the vorticity (curl) is zero, the second includes rotation and the curl of the speed differs from zero.

If in a certain singly connected region of a fluid

$$\operatorname{curl}\vec{w}=\vec{i}\left(\frac{\partial w_z}{\partial y}-\frac{\partial w_y}{\partial z}\right)+\vec{j}\left(\frac{\partial w_x}{\partial z}-\frac{\partial w_z}{\partial x}\right)+$$
$$+\vec{k}\left(\frac{\partial w_y}{\partial x}-\frac{\partial w_x}{\partial y}\right)=0,$$

then in this region

$$\frac{\partial w_z}{\partial y}=\frac{\partial w_y}{\partial z};\quad \frac{\partial w_x}{\partial z}=\frac{\partial w_z}{\partial x};\quad \frac{\partial w_y}{\partial x}=\frac{\partial w_x}{\partial y}.$$

Hence follows the immediately verifiable statement that in a singly connected region there will exist a scalar coordinate function $\Phi(x,y,z)$ such that

or
$$\left.\begin{aligned} &w_x=\frac{\partial\Phi}{\partial x},\quad w_y=\frac{\partial\Phi}{\partial y},\quad w_z=\frac{\partial\Phi}{\partial z}\\ &\vec{w}=\operatorname{grad}\Phi=\vec{\nabla}\Phi. \end{aligned}\right\} \qquad (1.3.1)$$

Denoting the projection of the speed vector onto the direction characterized by the unit vector $\vec{l}$ by w_l we obtain

$$w_l=\vec{l}\cdot\vec{\nabla}\Phi=\frac{\partial\Phi}{\partial l}.$$

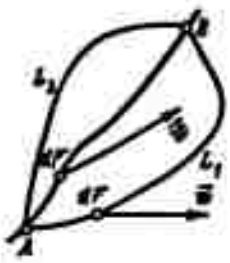


Fig. 1.3.2. For the definition of circulation.

This function Φ is called the velocity potential, and a motion for which curl $\vec{w}$ = 0 is a potential or vortex-free motion.

Consider a linear velocity integral along an open contour L from point A to point B (Fig. 1.3.2)

$$\int_{A(L)}^{B}\vec{w}\cdot d\vec{l}, \qquad (1.3.2)$$

which, in general, depends on the path of integration. In the case when this integral is independent of the path of integration and is completely determined only by the limits of integration A and B, we can show that

$$\int_{A(L_1)}^{B}\vec{w}\cdot d\vec{r}=\int_{A(L_2)}^{B}\vec{w}\cdot d\vec{r}=\Phi(B)-\Phi(A). \qquad (1.3.3)$$

In fact, fixing point M and calculating the integral $\int_M^P \vec{w}\cdot d\vec{r}$ for various points $P(\vec{r})$, we may attribute its value, denoted by $\Phi(\vec{r})$, to each of the points $P(\vec{r})$. We then obtain for points A and B the equation derived above.

Consequently, the integrand is a total differential of a certain function $\Phi(\vec{r})$:

$$\vec{w}\cdot d\vec{r} = w_x dx + w_y dy + w_z dz = -\frac{\partial \Phi}{\partial x}dx + \frac{\partial \Phi}{\partial y}dy + \frac{\partial \Phi}{\partial z}dz = d\vec{r}\cdot\vec{\nabla}\Phi$$

and in this case $\vec{w} = \vec{\nabla}\Phi$, i.e., the function $\Phi(\vec{r})$ is the <u>velocity potential</u>.

The physical meaning of the velocity potential will be explained in Part 2.2.

<u>Vortex motion</u>. When there exists in the space occupied by the fluid a region in which curl $\vec{w} \neq 0$, i.e., inside which the particles of the fluid are in rotation, then the motion inside this region is called vortex motion, Supposing that in these regions the angular velocity vector

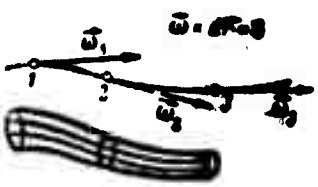


Fig. 1.3.3. Vortex line and vortex tube.

$$\vec{\omega} = \frac{1}{2}\operatorname{rot}\vec{w},$$

is uniformly distributed, one may speak of a vector field of vortices whose geometrical pattern is described by the <u>vortex lines</u>; these are lines whose tangents at any point and at a given instant of time coincide with the direction of the vortex vector (Fig. 1.3.3). By definition the differential vortex line equation reads

or

$$\left.\begin{aligned} \operatorname{rot}\vec{w}\times d\vec{r} &= 0 \\ \frac{dx}{\omega_x} = \frac{dy}{\omega_y} &= \frac{dz}{\omega_z}. \end{aligned}\right| \qquad (1.3.4)$$

When we consider in a vortex region an infinitely small simply

connected contour and lead vortex lines through all of its points, the surface obtained constitutes a vortex tube. The fluid inside the vortex tube is called vortex filament (vortex column).

Circulation of speed and the connection between circulation and vorticity. Stokes' theorem. The contour integral of the velocity taken along a closed curve C is called the circulation of speed, Γ:

$$\Gamma=\oint_C \vec{w}\cdot d\vec{r}. \qquad (1.3.5)$$

Let us consider a vortex tube whose cross section is for simplicity taken in the form of a parallelogram with the sides $\delta\vec{l}_1$ and $\delta\vec{l}_2$ (Fig. 1.3.4). When the speed at point A is equal to $\vec{w}$, for points a, b and c we shall have respectively:

$$\vec{w}+\frac{\partial\vec{w}}{\partial l_1}\delta l_1;\quad \vec{w}+\frac{\partial\vec{w}}{\partial l_1}\delta l_1+\frac{\partial\vec{w}}{\partial l_2}\delta l_2;\quad \vec{w}+\frac{\partial\vec{w}}{\partial l_2}\delta l_2.$$

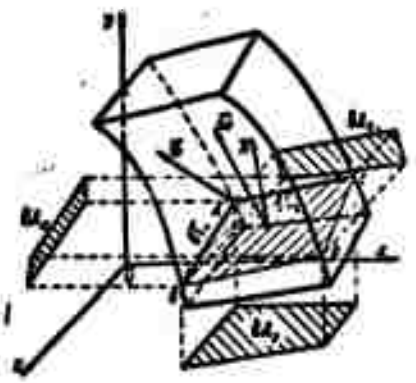


Fig. 1.3.4. Circulation with respect to the elementary contour Aabc is equal to twice the scalar product of the vector $\vec{w}$ of angular velocity and the vector $\vec{n}\delta A$ of the area of the element (flux of vortex vector).

Taking this into account, we calculate the circulation with respect to the contour Aabc, assuming that on each of the sides Aa, ab, bc, cA, the velocity is constant and equal to the average of its values at the ends of the sections:

$$\oint_{ABCDA} \vec{w}\cdot d\vec{r} = \left(\vec{w} + \frac{1}{2}\frac{\partial \vec{w}}{\partial l_1}\delta l_1\right)\cdot \delta\vec{l}_1 + \left(\vec{w} + \frac{\partial \vec{w}}{\partial l_1}\delta l_1 + \frac{1}{2}\frac{\partial \vec{w}}{\partial l_2}\delta l_2\right)\cdot \delta\vec{l}_2 -$$
$$-\left(\vec{w} + \frac{1}{2}\frac{\partial \vec{w}}{\partial l_1}\delta l_1 + \frac{\partial \vec{w}}{\partial l_2}\delta l_2\right)\cdot \delta\vec{l}_1 - \left(\vec{w} + \frac{1}{2}\frac{\partial \vec{w}}{\partial l_2}\delta l_2\right)\cdot \delta\vec{l}_2 =$$
$$= \frac{\partial \vec{w}}{\partial l_1}\delta l_1\cdot \delta\vec{l}_2 - \frac{\partial \vec{w}}{\partial l_2}\delta l_2\cdot \delta\vec{l}_1.$$

But

$$\frac{\partial \vec{w}}{\partial l_i}\delta l_i = \frac{\partial \vec{w}}{\partial x}\delta x_i + \frac{\partial \vec{w}}{\partial y}\delta y_i + \frac{\partial \vec{w}}{\partial z}\delta z_i \qquad (i=1, 2).$$

Therefore

$$\oint_{ABCDA} \vec{w}\cdot d\vec{r} = \frac{\partial \vec{w}}{\partial l_1}\delta l_1\cdot \delta\vec{l}_2 - \frac{\partial \vec{w}}{\partial l_2}\delta l_2\cdot \delta\vec{l}_1 =$$
$$= \left(\frac{\partial w_z}{\partial x} - \frac{\partial w_x}{\partial y}\right)(\delta x_1\delta y_2 - \delta x_2\delta y_1) +$$
$$+ \left(\frac{\partial w_x}{\partial z} - \frac{\partial w_z}{\partial x}\right)(\delta z_1\delta x_2 - \delta z_2\delta x_1) +$$
$$+ \left(\frac{\partial w_y}{\partial y} - \frac{\partial w_y}{\partial z}\right)(\delta y_1\delta z_2 - \delta y_2\delta z_1) =$$
$$= 2(\omega_x\delta A_x + \omega_y\delta A_y + \omega_z\delta A_z) = 2\vec{\omega}\cdot\delta\vec{A} = \vec{n}\cdot \operatorname{rot}\vec{w}\,\delta A.$$

Here

$$\delta\vec{A} = \vec{i}\delta A_x + \vec{j}\delta A_y + \vec{k}\delta A_z = \vec{\delta l}_1 \times \vec{\delta l}_2 = \begin{vmatrix} \vec{i} & \vec{j} & \vec{k} \\ \delta x_1 & \delta y_1 & \delta z_1 \\ \delta x_2 & \delta y_2 & \delta z_2 \end{vmatrix}.$$

Thus,

$$\Gamma = \oint_{ABCDA} \vec{w}\cdot d\vec{r} = \vec{n}\cdot \operatorname{rot}\vec{w}\,\delta A = 2\vec{n}\cdot\vec{\omega}\delta A.$$

The product $2\vec{\omega}\delta A$ is called the tension of the vortex tube or the velocity. If the vortex tube section is taken perpendicularly to the vector $\vec{\omega}$ of angular velocity then

$$\cos(\vec{n}, \vec{\omega}) = 1 \text{ and } \Gamma = 2\omega\delta A_n.$$

The circulation Γ with respect to some closed contour C is equal to the sum of circulations with respect to contours enclosing the regions into which the whole region may be subdivided, which are bounded by this contour C (Fig. 1.3.5):

$$\Gamma_1+\Gamma_2=\int_{adb}\vec{w}\cdot d\vec{r}+\int_{bc}\vec{w}\cdot d\vec{r}+\int_{ca}\vec{w}\cdot d\vec{r}+\int_{ab}\vec{w}\cdot d\vec{r}=$$
$$=\int_{adb}\vec{w}\cdot d\vec{r}+\int_{bca}\vec{w}\cdot d\vec{r}=\oint_C\vec{w}\cdot d\vec{r}=\Gamma.$$

Thus, when the whole region bounded by contour C is subdivided into an arbitraty number of small regions bounded by the contours δC_k (Fig. 1.3.6), then

$$\Gamma_C=\sum_k\delta\Gamma_{k\,(\delta C_k)}.$$

Considering an arbitrary region A in the fluid, bounded by the contour C, and subdividing it into unit regions (cf. Fig. 1.3.6), we obtain in the limit with an infinite number of divisions ($k\to\infty$) the Stokes theorem:

$$\Gamma=\oint_C\vec{w}\cdot d\vec{r}=\lim_{k\to\infty}\sum_i\int_{\delta C_i}d\Gamma=2\sum_i\int_{\delta A_i}\vec{\omega}\cdot d\vec{A}=\int_A\operatorname{rot}\vec{w}\cdot d\vec{A};$$
$$\oint_C\vec{w}\cdot d\vec{r}=\int_A\vec{n}\cdot\operatorname{rot}\vec{w}\,dA, \qquad (1.3.6)$$

where $\vec{n}$ is the outer normal, i.e., the circulation with respect to a closed contour is equal to the flux of the vortex vector through the surface bounded by this contour (let us agree to denote it as positive when the direction of the normal forms a right-handed system with the direction of circumvention). It is assumed here that this surface lies as a whole in the region occupied by the fluid.

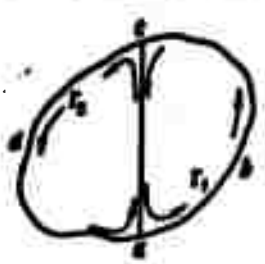


Fig. 1.3.5. Circulation with respect to the contour bcda is equal to the sum of circulations with respect to the contours abca and acda.

Many-valued potential. In the singly connected region of a vortex-free field, when curl $\vec{w}$ = 0 everywhere, the equation

$$\Gamma=\oint_C\vec{w}\cdot d\vec{r}=\oint_C w_x dx+w_y dy+w_z dz=0$$

will be valid, and, therefore, $\vec{w}\cdot d\vec{r}=d\Phi$, i.e., $\vec{w}=\vec{\nabla}\Phi$, where the potential $\Phi(\vec{r})$ is a single-valued function of the point.

When the contour is multiply connected,

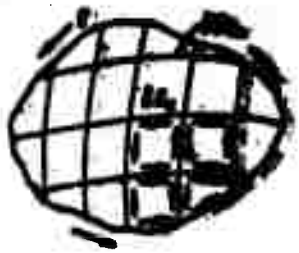


Fig. 1.3.6. The circulation with respect to the contour C is equal to the sum of circulations with respect to all contours δC_k.

the value of the potential Φ, after traveling along the contour C and returning to the starting point will, in general, be another one.

In fact, let us consider, for example, the region of one vortex tube (Fig. 1.3.7), which we shall regard as the inner boundary of a doubly connected region. The linear velocity integral between the points A and B will not depend on the paths L_1, L_2, ..., -- they do not form a closed contour that envelops the vortex tube, i.e.,

$$\int_{A(L_1)}^{B} \vec{w}\cdot d\vec{r} = \int_{A(L_2)}^{B} \vec{w}\cdot d\vec{r} = \ldots = \int_{A}^{B} d\Phi = \Phi(B) - \Phi(A),$$

where ϕ is the many-valued potential.

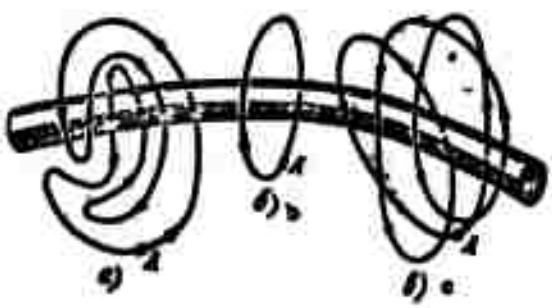


Fig. 1.3.7. Many-valuedness of the potential in the presence of vortices. a) Circumscription along a contour that envelops no vortices, i.e., circulation is equal to zero, the potential at point A after a circumvention will be $\varphi(A)$. b) circumscription of the vortex column along a closed contour that envelops the vortex once., i.e., the potential increases by the magnitude of the vortex circulation, i.e., it will be $\varphi(A) + \Gamma$; c) circumscription along a contour enveloping the vortex m times, i.e., the potential will be $\varphi(A) + m\Gamma$.

Its value depends on the path of integration along the contour enveloping the vortex. If, however, the contour envelops the vortex tube once, the potential, determined by $\int \vec{w}\cdot d\vec{r} = \int w_x dx + w_y dy + w_z dz$, will be $\Phi(A) + \Gamma$ when returning to point A, and if the tube is circumscribed m times it will become equal $\Phi(A) + m\Gamma$. In this case one speaks

about a many-valued potential.

Invariance of the vorticity of a vortex tube. Setting up the expression of the vortex divergence, div curl $\vec{w}$, we satisfy ourselves by direct verification that div $\vec{\omega} = 0$,

or

$$\frac{\partial \omega_x}{\partial x}+\frac{\partial \omega_y}{\partial y}+\frac{\partial \omega_z}{\partial z}=0.$$

Applying the Ostrogradskiy-Gauss* integral formula we obtain

$$\int_V \vec{\nabla}\cdot\vec{\omega}\,dV=\int_A \vec{n}\cdot\vec{\omega}\,dA=0. \qquad (1.3.7)$$

i.e., the vector flux through a closed surface is equal to zero.

Since the vortex vector flux through the lateral surfaces of the vortex tube is equal to zero ($\vec{n}\cdot\vec{\omega}=0$), the Helmholtz theorem follows: the vorticity of the vortex tube is constant along it. Therefore vortex tubes must be either infinitely long or closed in themselves or end at the fluid's surface.

Streamlines in the case of vortex motion. From the fact that the velocity circulation with respect to closed singly connected contours is vanishing it follows that the streamlines of motion with a single-valued potential need not be closed. Indeed, if they were closed, all elements of the linear integral of the velocity vector $\int_\xi \vec{w}\cdot d\vec{r}$ taken along a closed streamline would have one and the same sign and the circulation along this line could not become zero. Therefore, in a singly connected volume bounded at all sides by solid walls a vortex-free motion cannot exist, since the normal velocity component on the walls must be zero (the fluid cannot pass through a solid wall) and the streamlines will therefore be closed. Thus, the fluid is either at rest or in vortex motion.

If,however, we consider a fluid volume that lies outside one or more closed surfaces so that it may be regarded as an inner volume

bounded by this (or these) closed surface or surfaces sufficiently far off.

Manuscript Page No.

[Footnotes]

26 The field of some quantity (vector or scalar) is understood to be the totality of values of this quantity, uniquely defined in a certain region.

34 This table should not be confused with a determinant.

45 The formulas of vector analysis are collected in Appendix 2. As to the derivation of the formulas, see the special course, e.g., [1, 3].

REFERENCES

1.1. Loytsyanskiy, L.G., Mekhanika zhidkosti i gaza [Mechanics of Liquids and Gases], GTTI [State Technical and Theoretical Press], 1957.

1.2. Kochin, N.Ye., Kibel', I.A. and Roze, N.V., Teoreticheskaya gidromekhanika [Theoretical Fluid Mechanics], Vol. I, GTTI, 1958.

1.3. Borisenko, A.I. and Tarapov, I.Ye., Vektornyy analiz i nachala tenzornogo ischisleniya [Vector Analysis and the Origins of Tensor Calculus], KhGU [Khar'kov State University], Khar'kov, 1959.

Chapter 2

FUNDAMENTAL LAWS

2.1. THE MASS CONSERVATION LAW. CONTINUITY EQUATION IN EULER VARIABLES

Continuity equation for fixed mass. We isolate an arbitrary volume V in the fluid with a mass $\int_V \rho dV$, so that we can write the mass conservation law in the form of the equation

$$\frac{d}{dt}\int_V \rho dV = 0. \tag{2.1.1}$$

which expresses the fact that the mass of an arbitrary fluid volume remains unchanged with the course of time as if its shape were unchanged. This equation is known as the equation of nondiscontinuity, i.e., the equation of continuity.

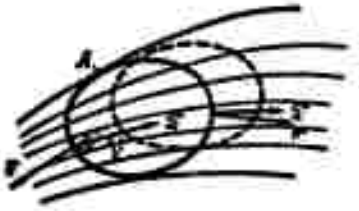


Fig. 2.1.1. For deriving the continuity equation we may consider either the outflow of mass through a fixed reference volume V during the time δt or a certain mass at the instants of time t and $t + \delta t$.

Let us note that this integral form of the equation is valid also in the case when quantities appearing in the integrand undergo a discontinuity inside the isolated volume. In this form, however, one does not obtain information on the behavior of quantities characterizing the motion at a point. This information may be obtained with the help of differential equations by applying the conservation laws to an infinitesimal volume.

Continuity equation for the reference volume. Equation (2.1.1) is written for a fixed mass of fluid whose volume may in general

vary with time. Applying the Euler representations the continuity equation may also be obtained by considering the fluid flux through a quiescent spatial region, which is called <u>reference volume</u>, while the surface bounding it is called the <u>reference surface</u> (Fig. 2.1.1).

Since the difference between the mass of the fluid flowing into the reference volume, and the mass flowing out of it during an infinitesimal time interval must be compensated by a change of fluid mass inside this volume (cf. Fig. 2.1.1), we have

$$\int_A \vec{n}\cdot(\rho\vec{w})\,dt\,dA = -\int_V \frac{\partial\rho}{\partial t}\,dt\,dA,$$

where $\vec{n}$ is the unit vector of the outer normal and V is the volume.

A is the surface boundary of the isolated volume. This equation valid if the interior of the region is free from sources and sinks of inflow (or outflow) of fluid.

Using the theorem of Ostrogradskiy-Gauss (Appendix 2) we obtain

$$\int_V \left(\operatorname{div}\rho\vec{w} + \frac{\partial\rho}{\partial t}\right)dV = 0. \qquad (2.1.2)$$

<u>Continuity equation in differential form.</u> When the density ρ, the speed $\vec{w}$, and their derivatives are continous, then, due to the arbitrariness of the volume V, the integrand of (2.1.2) must become zero. This yields the continuity equation in differential form:

$$\frac{\partial\rho}{\partial t} + \operatorname{div}\rho\vec{w} = 0. \qquad (2.1.3)$$

Transforming Eq. (2.1.3)

$$\frac{\partial\rho}{\partial t} + \operatorname{div}\rho\vec{w} = \frac{\partial\rho}{\partial t} + \vec{w}\operatorname{grad}\rho + \rho\operatorname{div}\vec{w} = \frac{d\rho}{dt} + \rho\operatorname{div}\vec{w},$$

we obtain

$$\frac{d\rho}{dt} + \rho\operatorname{div}\vec{w} = 0. \qquad (2.1.4)$$

For an incompressible fluid the density is constant and the continuity equation assumes the form

$$\operatorname{div}\vec{w} = \frac{\partial w_x}{\partial x} + \frac{\partial w_y}{\partial y} + \frac{\partial w_z}{\partial z} = 0. \qquad (2.1.5)$$

In this case the sum of the diagonal elements of the matrix (1.2.8) characterizing the expansion (compression) of the particles is equal to zero, and therefore the particle volume will remain unchanged during the motion of an incompressible fluid.

2.2. MOMENTUM CONSERVATION LAW. EQUATION OF MOTION

Equation of motion in terms of stress. By introducing forces of inertia into the consideration, the problem of the motion of a fluid may be formally transformed into the problem of its equilibrium; the equilibrium condition is the vanishing of the resultants and of the main moment of all foces acting on the isolated volume of the fluid (D'Alembert's principle)

$$\sum \vec{P}=0, \quad \sum(\vec{r}\times\vec{P})=0. \tag{2.2.1}$$

Let us isolate a certain arbitrary volume V in the moving fluid. Solid bodies should be present inside this volume: at rest, G_i; and

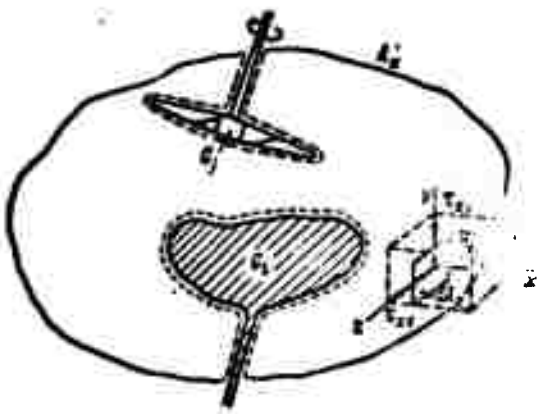


Fig. 2.2.1. For the derivation of the equation of motion. a) Decomposition of the stress vector p_x of the area δA_x with respect to the axes x, y, z.

in motion, G_j, e.g., turbomachines, carrying out the energy [illegible]. Heat transfer may also occur via the solid bodies. In the general case the surface A bounding the volume V will consist of [illegible]

ary surface A_k separating the volume considered from the remaining fluid, and the surfaces A_i and A_j of the bodies G_i and G_j.

The isolated volume V of the fluid bounded by the surface A will be subject to volume forces $\int_V \vec{f}\rho dV$ ($\vec{f}$ is the stress vector of the volume forces), to surface forces $\int_A \vec{p}_n dA$ ($\vec{p}_n$ is the stress vector of the surface forces for the area characterized by the unit vector $\vec{n}$), and to inertial forces $\int_V \frac{d\vec{w}}{dt}\rho dV$ ($\frac{d\vec{w}}{dt}$ is the acceleration vector).

The first equation of (2.2.1) may now be written in the form

$$\int_V \vec{f}\rho dV + \int_A \vec{p}_n dA - \int_V \frac{d\vec{w}}{dt}\rho dV = 0 \qquad (2.2.2)$$

which corresponds to

$$\int_V (\vec{r}\times\vec{f})\rho dV + \int_A (\vec{r}\times\vec{p}_n) dA - \int_V \left(\vec{r}\times\frac{d\vec{w}}{dt}\right)\rho dV = 0. \qquad (2.2.3)$$

In the space occupied by the moving fluid, let us choose a unit volume in the form of a parallelepiped (cf. Fig. 2.2.1). The stress vector of the surface forces acting on the area δA_x perpendicular to the axis x is equal to

$$\vec{p}_x = \vec{i}\sigma_x + \vec{j}\tau_{xy} + \vec{k}\tau_{xz}$$

Similarly,

$$\vec{p}_y = \vec{i}\tau_{yx} + \vec{j}\sigma_y + \vec{k}\tau_{yz}$$
$$\vec{p}_z = \vec{i}\tau_{zx} + \vec{j}\tau_{zy} + \vec{k}\sigma_z$$

Here, σ_x, σ_y, σ_z are the normal stresses on the areas A_x, A_y, A_z perpendicular to the axes x, y, z, respectively: τ denotes the tangential stresses; the first subscript indicates the area to which the stress is applied and the second indicates its direction.

Neglecting the infinitesimal terms of more than second order we determine the resultant of the surface forces (Fig. 2.2.2) acting on the parallelepiped considered:

$$\int_{\Delta A} \vec{p}_n\,dA = -\vec{p}_x\delta A_x + \left(\vec{p}_x + \frac{\partial \vec{p}_x}{\partial x}\delta x\right)\delta A_x -$$

$$-\vec{p}_y\delta A_y + \left(\vec{p}_y + \frac{\partial \vec{p}_y}{\partial y}\delta y\right)\delta A_y - \vec{p}_z\delta A_z + \left(\vec{p}_z + \frac{\partial \vec{p}_z}{\partial z}\delta z\right)\delta A_z = \vec{R}\delta V.$$

where $\vec{R}$ is the resultant of the surface forces per unit volume

$$\vec{R} = \frac{\partial \vec{p}_x}{\partial x} + \frac{\partial \vec{p}_y}{\partial y} + \frac{\partial \vec{p}_z}{\partial z}$$

or, as projections onto the axes,

$$R_x = \frac{\partial \sigma_x}{\partial x} + \frac{\partial \tau_{xy}}{\partial y} + \frac{\partial \tau_{xz}}{\partial z},$$

$$R_y = \frac{\partial \tau_{yx}}{\partial x} + \frac{\partial \sigma_y}{\partial y} + \frac{\partial \tau_{yz}}{\partial z},$$

$$R_z = \frac{\partial \tau_{zx}}{\partial x} + \frac{\partial \tau_{zy}}{\partial y} + \frac{\partial \sigma_z}{\partial z}.$$

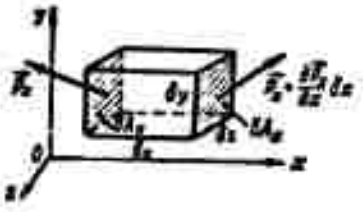


Fig. 2.2.2. For the determination of the resultant of the surface forces per unit volume.

Subdividing the isolated volume V into unit parallelepipeds and noting that at the faces separating neighboring parallelepipeds there will exist for each vector $\vec{p}_n$ a corresponding stress vector $-\vec{p}_n$, we may write

$$\int_{\Delta A} \vec{p}_n\,dA = \int_V \left(\frac{\partial \vec{p}_x}{\partial x} + \frac{\partial \vec{p}_y}{\partial y} + \frac{\partial \vec{p}_z}{\partial z}\right)dV.$$

Equation (2.2.2) can now be written in integral form

$$\int_V \left[\rho\left(\vec{f} - \frac{d\vec{w}}{dt}\right) + \frac{\partial \vec{p}_x}{\partial x} + \frac{\partial \vec{p}_y}{\partial y} + \frac{\partial \vec{p}_z}{\partial z}\right]dV = 0.$$

If all quantities are continuous, [illegible] to the arbitrariness of the volume the integrand will be equal to zero, hence the equation of motion of the continuous medium will read in terms of stress

$$\frac{d\vec{w}}{dt} = \vec{f} + \frac{1}{\rho}\left(\frac{\partial \vec{p}_x}{\partial x} + \frac{\partial \vec{p}_y}{\partial y} + \frac{\partial \vec{p}_z}{\partial z}\right).$$

Finally, heat supply does not [illegible] equation of motion directly though it affects the value of the parameter p, [illegible]

terizing the motion.

In projections onto the coordinate axes we have

$$\left.\begin{aligned}\frac{dw_x}{dt}&=f_x+\frac{1}{\rho}\left(\frac{\partial\sigma_x}{\partial x}+\frac{\partial\tau_{xy}}{\partial y}+\frac{\partial\tau_{xz}}{\partial z}\right),\\ \frac{dw_y}{dt}&=f_y+\frac{1}{\rho}\left(\frac{\partial\tau_{yx}}{\partial x}+\frac{\partial\sigma_y}{\partial y}+\frac{\partial\tau_{yz}}{\partial z}\right),\\ \frac{dw_z}{dt}&=f_z+\frac{1}{\rho}\left(\frac{\partial\tau_{zx}}{\partial x}+\frac{\partial\tau_{zy}}{\partial y}+\frac{\partial\sigma_z}{\partial z}\right).\end{aligned}\right\} \qquad (2.2.5)$$

Symmetry of the tangential stresses. The equation of motion contains four unknown vectors, $\vec{w}$, $\vec{p}_x$, $\vec{p}_y$, $\vec{p}_z$, and one scalar, ρ (or three unknown scalars). The vector Eq. (2.2.5) makes it possible to reduce the number of unknowns to three scalar quantities.

In fact, we transform Eq. (2.2.3) similarly

$$\int_V\left[\vec{r}\times\left(\vec{f}-\frac{d\vec{w}}{dt}\right)\right]dV+\int_V\left[\frac{\partial(\vec{r}\times\vec{p}_x)}{\partial x}+\frac{\partial(\vec{r}\times\vec{p}_y)}{\partial y}+\frac{\partial(\vec{r}\times\vec{p}_z)}{\partial z}\right]dV=$$

$$=\int_V\left\{\vec{r}\times\left[\vec{f}-\frac{d\vec{w}}{dt}+\frac{1}{\rho}\left(\frac{\partial\vec{p}_x}{\partial x}+\frac{\partial\vec{p}_y}{\partial y}+\frac{\partial\vec{p}_z}{\partial z}\right)\right]+[(\vec{i}\times\vec{p}_x)+(\vec{j}\times\vec{p}_y)+(\vec{k}\times\vec{p}_z)]\right\}dV=0.$$

By virtue of (2.2.4) the expression in the first parentheses following the integral is equal to zero and therefore

$$(\vec{i}\times\vec{p}_x)+(\vec{j}\times\vec{p}_y)+(\vec{k}\times\vec{p}_z)=0.$$

Subsequently projecting this equation onto the coordinate axes, we obtain the equation

$$\tau_{xy}=\tau_{yx},\quad \tau_{yz}=\tau_{zy},\quad \tau_{zx}=\tau_{xz}. \qquad (2.2.6)$$

Tangential stresses. Applying the relations between tangential stress and deformation rate

$$\tau=\mu\frac{\partial w}{\partial n}=\mu\frac{\partial\gamma}{\partial t}$$

to the unit cube (Fig. 2.2.3) and noting, for example, that

$$\frac{\partial\tau_{xy}}{\partial t}=\frac{\partial w_x}{\partial y}+\frac{\partial w_y}{\partial x},$$

we obtain

$$\left.\begin{aligned}\tau_{xy}&=\mu\left(\frac{\partial w_x}{\partial y}+\frac{\partial w_y}{\partial x}\right)=\tau_{yx},\\ \tau_{yz}&=\mu\left(\frac{\partial w_y}{\partial z}+\frac{\partial w_z}{\partial y}\right)=\tau_{zy},\\ \tau_{zx}&=\mu\left(\frac{\partial w_z}{\partial x}+\frac{\partial w_x}{\partial z}\right)=\tau_{xz}.\end{aligned}\right\} \qquad (2.2.7)$$

Equations (2.2.7) provide the interrelation between the tangential stresses and the deformation rates.

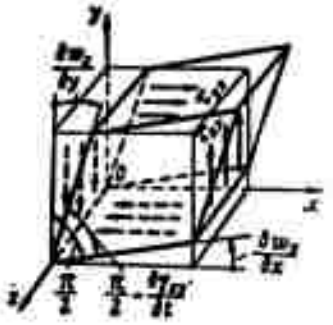


Fig. 2.2.3. Shear stresses on the faces of a cube.

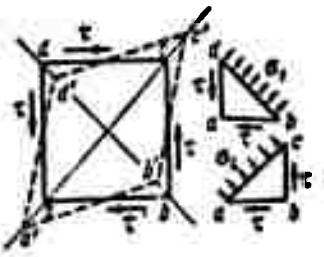


Fig. 2.2.4. Relation between the normal stresses σ_1 and σ_2 on the diagonal of the square subject to shear deformation, and the tangential stresses τ on its faces.

The relation between the normal stresses and the deformation rates. Let us consider the diagonal planes of a cube which is subjected to a very small shear deformation by the stresses τ. As can be seen from Fig. 2.2.4, one of these will undergo pure elongation and the other a compression under the influence of the stresses σ_1 and σ_2, respectively.

From the condition of equilibrium for the prism [illegible] and the prism abc, [illegible]

$$\sigma_1=\tau,\quad \sigma_2=-\tau$$

and, therefore

$$\sigma_1-\sigma_2=2\tau.$$

Let us find the relation between the diagonal ac and the shear of the diagonal bd (Fig. 2.2.5). Placing the x-axis along the long axis of the rhomb [illegible] the square is deformed, we obtain [illegible] axes x and y:

$$\varepsilon_x = \frac{ac' - ac}{ac} = \frac{ff'}{af} = \frac{ad\,\frac{1}{2}\sqrt{2}}{2ad\,\frac{\sqrt{2}}{2}} = \frac{1}{2}$$

and

$$-\varepsilon_y = \frac{bd - b'd'}{bd} = \frac{1}{2}.$$

If $\delta\xi$ and $\delta\eta$ denote the displacements in the directions of the x and y,

$$\omega_z = \frac{\partial \xi}{\partial t}; \quad \omega_1 = \frac{\partial \eta}{\partial x}$$

$$\sigma_x - \sigma_y = 2\mu \frac{\partial}{\partial t} \varepsilon_x - 2\mu \frac{\partial}{\partial t} \varepsilon_y =$$

$$= 2\mu \frac{\partial}{\partial t}\left(\frac{\partial \xi}{\partial x} - \frac{\partial \eta}{\partial y}\right) = 2\mu\left(\frac{\partial w_x}{\partial x} - \frac{\partial w_y}{\partial y}\right)$$

and we can find analogously

$$\sigma_y - \sigma_z = 2\mu\left(\frac{\partial w_y}{\partial x} - \frac{\partial w_z}{\partial z}\right).$$

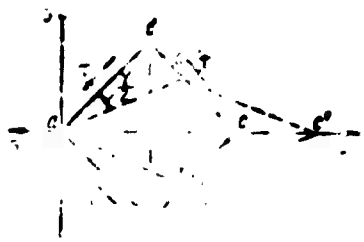


Fig. 2.2.1. Connection between shear deformation and stretching.

Moreover, by means of the identity

$$\sigma_z - \sigma_x = 2\mu\left(\frac{\partial w_z}{\partial x} - \frac{\partial w_x}{\partial z}\right),$$

we find by joining the three last equalities

$$3\sigma_x - (\sigma_x + \sigma_y + \sigma_z) = 2\mu 3 \frac{\partial w_x}{\partial x} - 2\mu\left(\frac{\partial w_x}{\partial x} + \frac{\partial w_y}{\partial y} + \frac{\partial w_z}{\partial z}\right) =$$

$$= 2\mu\left(3\frac{\partial w_x}{\partial x} - \operatorname{div}\vec{w}\right).$$

Pressure at a point. This quantity is determined as the negative arithmetical mean of the normal tensions on the three mutually perpendicular areas passing through this point:

$$p = -\frac{1}{3}(\sigma_x + \sigma_y + \sigma_z). \qquad (2.2.8)$$

Now

$$\left.\begin{aligned} \sigma_x &= -p + 2\mu\left(\frac{\partial w_x}{\partial x} - \frac{1}{3}\operatorname{div}\vec{w}\right) = -p + \tau_{xx}, \\ \sigma_y &= -p + 2\mu\left(\frac{\partial w_y}{\partial y} - \frac{1}{3}\operatorname{div}\vec{w}\right) = -p + \tau_{yy}, \\ \sigma_z &= -p + 2\mu\left(\frac{\partial w_z}{\partial z} - \frac{1}{3}\operatorname{div}\vec{w}\right) = -p + \tau_{zz}; \end{aligned}\right\} \qquad (2.2.9)$$

where τ_{xx}, τ_{yy}, τ_{zz} denote the components of the normal tension which depend on the viscosity.

Thus, we may write for R_x:

$$R_x = \frac{\partial}{\partial x}\left[-p + 2\mu\left(\frac{\partial w_x}{\partial x} - \frac{1}{3}\operatorname{div}\vec{w}\right)\right] + \frac{\partial}{\partial y}\mu\left(\frac{\partial w_x}{\partial y} + \frac{\partial w_y}{\partial x}\right) + \frac{\partial}{\partial z}\mu\left(\frac{\partial w_x}{\partial z} + \frac{\partial w_z}{\partial x}\right).$$

When μ = constant, we have

$$R_x = -\frac{\partial p}{\partial x} + \frac{1}{3}\mu\frac{\partial}{\partial x}\left(\frac{\partial w_x}{\partial x} + \frac{\partial w_y}{\partial y} + \frac{\partial w_z}{\partial z}\right) + \mu\left(\frac{\partial^2 w_x}{\partial x^2} + \frac{\partial^2 w_x}{\partial y^2} + \frac{\partial^2 w_x}{\partial z^2}\right) = -\frac{\partial p}{\partial x} + \frac{1}{3}\mu\frac{\partial}{\partial x}\operatorname{div}\vec{w} + \mu\Delta w_x.$$

The expressions for R_y and R_z read analogously.

When μ = const, the total force per unit volume is given by

$$\vec{R} = -\vec{\nabla}p + \frac{1}{3}\mu\vec{\nabla}(\vec{\nabla}\cdot\vec{w}) + \mu(\vec{\nabla}\cdot\vec{\nabla})\vec{w}.$$

The equation of motion. Introducing the value of $\vec{R}$ into the equation of motion (2.2.5) we obtain the fundamental equation of aerohydrodynamics:

$$\left.\begin{aligned} \frac{d\vec{w}}{dt} &= \frac{\partial\vec{w}}{\partial t} + (\vec{w}\cdot\vec{\nabla})\vec{w} = \vec{f} - \frac{1}{\rho}\vec{\nabla}p + \\ &+ \frac{\nu}{3}\vec{\nabla}(\vec{\nabla}\cdot\vec{w}) + \nu(\vec{\nabla}\cdot\vec{\nabla})\vec{w} \end{aligned}\right\}$$

or, in projections onto the axes of a cartesian coordinate system (2.2.10)

$$\left.\begin{aligned} \frac{dw_x}{dt} &= f_x - \frac{1}{\rho}\frac{\partial p}{\partial x} + \frac{\nu}{3}\frac{\partial}{\partial x}\left(\frac{\partial w_x}{\partial x} + \frac{\partial w_y}{\partial y} + \frac{\partial w_z}{\partial z}\right) + \\ &+ \nu\left(\frac{\partial^2 w_x}{\partial x^2} + \frac{\partial^2 w_x}{\partial y^2} + \frac{\partial^2 w_x}{\partial z^2}\right). \end{aligned}\right\}$$

$$\left.\begin{aligned}
\frac{dw_y}{dt} &= f_y - \frac{1}{\rho}\frac{\partial p}{\partial y} + \frac{\nu}{3}\frac{\partial}{\partial y}\left(\frac{\partial w_x}{\partial x} + \frac{\partial w_y}{\partial y} + \frac{\partial w_z}{\partial z}\right) + \\
&\quad + \nu\left(\frac{\partial^2 w_y}{\partial x^2} + \frac{\partial^2 w_y}{\partial y^2} + \frac{\partial^2 w_y}{\partial z^2}\right), \\
\frac{dw_z}{dt} &= f_z - \frac{1}{\rho}\frac{\partial p}{\partial z} + \frac{\nu}{3}\frac{\partial}{\partial z}\left(\frac{\partial w_x}{\partial x} + \frac{\partial w_y}{\partial y} + \frac{\partial w_z}{\partial z}\right) + \\
&\quad + \nu\left(\frac{\partial^2 w_z}{\partial x^2} + \frac{\partial^2 w_z}{\partial y^2} + \frac{\partial^2 w_z}{\partial z^2}\right).
\end{aligned}\right| \qquad (2.2.10)$$

In the system of the axes x_1, x_2, x_3

$$\frac{dw_i}{dt} = f_i - \frac{1}{\rho}\frac{\partial p}{\partial x_i} + \frac{\nu}{3}\frac{\partial}{\partial x_i}\operatorname{div}\vec{w} + \nu\Delta w_i.$$

second viscosity. Supposition (2.2.8) that $-p = \frac{1}{3}(\sigma_x + \sigma_y + \sigma_z)$.

[illegible] invariance condition [illegible] library of a [illegible] coordinate system (fundamental proper[illegible]), [illegible] by a more general invariant interrelation of normal pressure and tangential stresses, and the deformation rates connected with the [illegible]

$$[illegible] \frac{\sigma_x + \sigma_y + \sigma_z}{3} + \mu' \operatorname{div}\vec{w}.$$

[illegible]

$$\sigma_x = -p + \left(\mu' - \frac{2}{3}\mu\right)\operatorname{div}\vec{w} + 2\mu\frac{\partial w_x}{\partial x}$$

[illegible] of (2.2.8), [illegible] corresponding expressions for σ_y and σ_z. The [illegible] is called the coefficient of second viscosity.

In accordance with the discontinuity equation, $\operatorname{div}\vec{w} = -\frac{1}{\rho}\frac{d\rho}{dt}$ [illegible] characterizes the rate of density variation at the point. Introducing the second viscosity μ' therefore makes it possible to take the dependence of the pressure on the rate of density variation into account, i.e., the fact that when the density varies a certain time is needed for thermodynamic equilibrium to be established; this time is called relaxation time. The second viscosity becomes apparent only in those cases where the relaxation time is long compared with the time [illegible] density variation and where [illegible] establishment of equilibrium cannot [illegible] up with the variation in density.

Euler's equation. Assuming $\mu = 0$ in Eq. (2.2.10), we arrive at the equation of motion of an inviscid fluid, first obtained and discussed by Euler:

$$\frac{d\vec{w}}{dt} = \vec{f} - \frac{1}{\rho}\vec{\nabla}p. \qquad (2.2.11)$$

The equation of motion in the form given by Gromeka. Nothing that (cf. Appendix 2)

$$(\vec{w}\cdot\vec{\nabla})\vec{w} = \vec{\nabla}\frac{w^2}{2} - \vec{w}\times\operatorname{rot}\vec{w},$$

the equation of motion of an inviscid fluid may be written in a form given by I.S. Gromeka, Professor at the Kazan' University:

$$\frac{d\vec{w}}{dt} = \frac{\partial\vec{w}}{\partial t} + \vec{\nabla}\frac{w^2}{2} - \vec{w}\times\operatorname{rot}\vec{w} = \vec{f} - \frac{1}{\rho}\vec{\nabla}p. \qquad (2.2.12)$$

The advantage of this form of the equation of motion consists in that it explicitly contains the curl of speed.

The integrals of the equations of motion. When the motion has become steady and there exists a potential (U) of the volume forces $\vec{f} = -\vec{\nabla}U$, the Gromeka equation may be written in the form

$$\vec{\nabla}\frac{w^2}{2} + \vec{\nabla}U + \frac{1}{\rho}\vec{\nabla}p = \vec{w}\times\operatorname{rot}\vec{w}.$$

Multiplying this equation scalarly by the length $d\vec{r}$ and assuming the fluid to be barotropic*, we obtain

$$\frac{1}{\rho}\vec{\nabla}p\cdot d\vec{r} = \frac{dp}{\rho} = dP = \vec{\nabla}P\cdot d\vec{r},$$

where $P = \int\frac{dp}{\rho}$ denotes a function which may always be determined for a barotropic fluid if the form of the function $p = p(\rho)$ is known.

Here the Gromeka equation has the form

$$d\left(\frac{w^2}{2} + U + P\right) = (\vec{w}\times\operatorname{rot}\vec{w})\,d\vec{r}.$$

As can be seen, the integral of this equation is easily found if $(\vec{w}\times\operatorname{rot}\vec{w})\cdot d\vec{r} = 0$ on all paths of integration and has the form

$$\frac{w^2}{2} + U + P = \text{const}.$$

Let us consider the case when $(\vec{w} \times \operatorname{rot} \vec{w}) \cdot d\vec{r} = 0$. First of all this is possible if curl $\vec{w} = 0$ everywhere, i.e., if $\vec{w} = \nabla\Phi$. In this case too the unsteadiness of the motion is easily taken into account, noting that

$$\frac{\partial \vec{w}}{\partial t} \cdot d\vec{r} = \frac{\partial}{\partial t} \vec{\nabla}\Phi \cdot d\vec{r} \quad \vec{\nabla}\frac{\partial \Phi}{\partial t} \cdot d\vec{r} = d\frac{\partial \Phi}{\partial t}.$$

Hence the integral of the equation will be

$$\frac{\partial \Phi}{\partial t} + \frac{w^2}{2} + U + P = f(t). \qquad (2.2.14)$$

[illegible] an arbitrary function of the time t and is determined [illegible] initial conditions. Its integral has acquired the name [illegible] integral.

[illegible] element of a streamline then, by definition, $\vec{w} \times d\vec{r} = 0$. [illegible] by [illegible] the properties of the mixed product, $(\vec{w} \times \operatorname{curl} \vec{w}) \cdot d\vec{r} = (d\vec{r} \times \vec{w}) \cdot \operatorname{curl} \vec{w} = 0$ and Eq. (2.2.13) will hold along the streamline [illegible] called the Bernoulli integral.

[illegible] emphasized that, although they both are given by the same expression, there is a considerable difference between the Lamb integral for a steady motion and the Bernoulli integral. The former holds for any arbitrary path of integration in the region of potential motion and the constant of the equation is one and the same for all streamlines. The latter is valid only along one streamline and, generally speaking, the constant will have its own value for every streamline.

In the case of turbulent motion along a vortex line, the integral has likewise the form (2.2.13) if curl $\vec{w} \times d\vec{r} = 0$ or if the streamlines coincide with the vortex lines, i.e., if $\vec{w} \times \operatorname{curl} \vec{w} = 0$; in the latter case it is called the Gromeka integral.

The velocity potential as the impulse of a pressure shock. Let us consider the development of a motion out of the state of rest

under the action of a suddenly applied pressure (shock) during a short time interval δt. In this case the effects of friction and volume forces will be very small and can be neglected. Since the motion arises out of the state of rest, the convective term of acceleration, $(\vec{w}\cdot\vec{\nabla})\,\vec{w}$ will be considerably smaller than the local one, $\frac{\partial \vec{w}}{\partial t}$ and the equation of motion can be taken in the form

$$\frac{d\vec{w}}{dt} \approx \frac{\partial \vec{w}}{\partial t} = -\frac{1}{\rho}\vec{\nabla}p.$$

If for simplicity an incompressible fluid (ρ = const) is considered, integration yields the velocity

$$\vec{w} = -\frac{1}{\rho}\int_0^{\delta t}\vec{\nabla}p\,dt.$$

Since the convective term of acceleration is small, differentiation may be carried out under the integral sign and we obtain

$$\vec{w} = -\frac{1}{\rho}\vec{\nabla}\int_0^{\delta t} p\,dt = \vec{\nabla}\left(-\frac{1}{\rho}\int_0^{\delta t} p\,dt\right).$$

Thus, the velocity potential

$$\Phi = -\frac{1}{\rho}\int_0^{\delta t} p\,dt$$

may be considered as the impulse of the pressure shock.

Conservation of circulation with time. In connection with the important significance of vortex motion in aerodynamics we shall consider its fundamental properties. For this purpose we choose a closed contour in the fluid (Fig. 2.2.6) and determine the variation with time of the circulation, $\Gamma = \oint_C \vec{w}\cdot d\vec{r}$ with respect to this contour, assuming that the contour consists of one and the same aggregate of fluid particles. In this case the variation of the integral considered must be calculated by taking its total time derivative.

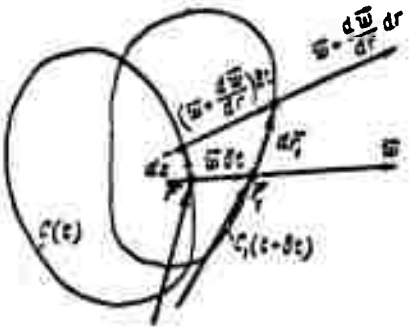


Fig. 2.2.6. The fluid particles forming the contour C over to contour C_1 during the time δt.

If C and C_1 are the positions of the contour assumed during the time δt, $\Gamma=\Gamma(t)=\int_C \vec{w}\cdot d\vec{r}$ and $\Gamma_1=\Gamma(t+\delta t)=\int_{C_1}\vec{w}\cdot d\vec{r}$. Noting that by virtue of the continuity of motion $\vec{r}_1=\vec{r}+\vec{w}\delta t$; $\vec{w}_1=\vec{w}+\frac{d\vec{w}}{dt}\delta t$, we may write

$$\Gamma_1=\int_{C_1}\left(\vec{w}+\frac{d\vec{w}}{dt}\delta t\right)\cdot(d\vec{r}+d\vec{w}_1\delta t)=\int_C\left(\vec{w}\cdot d\vec{r}+\vec{w}\cdot d\vec{w}\delta t+\frac{d\vec{w}}{dt}\cdot\vec{\delta r}\,\delta t\right).$$

Thus,

$$\frac{d}{dt}\int_C\vec{w}\cdot d\vec{r}=\frac{d\Gamma}{dt}=\lim_{\delta t\to 0}\frac{\Gamma(t+\delta t)-\Gamma(t)}{\delta t}=\int_C\vec{w}\cdot d\vec{w}+\int_C\frac{d\vec{w}}{dt}\cdot d\vec{r}.$$

When the speed varies continuously along the closed contour C were return to the starting point after circumscribing the contour of integration with the same value of the speed; therefore,

$$\oint_C\vec{w}\cdot\frac{d\vec{r}_1-d\vec{r}}{dt}=\oint_C\vec{w}\cdot\frac{d\vec{w}}{dt}dt=\oint_C\vec{w}\cdot d\vec{w}=0$$

and the expression for the derivative $\frac{d}{dt}\oint_C\vec{w}\cdot d\vec{r}$ is the same when calculated for a contour made up of one and the same aggregate of particles as well as for a quiescent contour imaginarily drawn in the fluid.

The Euler equation of motion for an inviscid fluid, when the volume forces have a potential, $\vec{f}=-\vec{\nabla}U$, and when the fluid is barotropic, i.e., $\frac{1}{\rho}\vec{\nabla}p=\vec{\nabla}P$; $P=P(p)$, gives $\frac{d\vec{w}}{dt}=-\vec{\nabla}(P+U)$.

Passing over from point A of a fluid line to point B of the same line we obtain

$$\frac{d}{dt}\int_A^B\vec{w}\cdot d\vec{r}=-[P+U]_A^B.$$

For a closed contour C when the points A and B coincide and when we assume that there are no speed discontinuity surfaces along the path C, we shall have

$$\frac{d}{dt}\oint_{\tilde{C}}\vec{w}\cdot d\vec{r}=0,\quad \oint_{\tilde{C}}\vec{w}\cdot d\vec{r}=\text{const.} \qquad (2.2.15)$$

i.e. if the volume forces have a potential and the inviscid fluid is barotropic, the velocity circulation with respect to an arbitraty closed contour which is not intersected by a speed discontinuity surface remains constant throughout the duration of the motion. This theorem was established by Thomson.

Lagrange's theorem. An inviscid barotropic fluid is assumed to be at rest at the initial instant of time. If motion sets in under the action of a potential field of forces, at all subsequent instants of time the motion will be a potential one. This results from the fact that at the initial instant of time the circulation with respect to some arbitrary fluid contour is equal to zero. From this follows the theorem of Lagrange: if in a field of volume forces having a potential the motion of a viscous barotropic fluid has a velocity potential at the initial instant of time, it will be a potential motion throughout the whole duration of the motion.

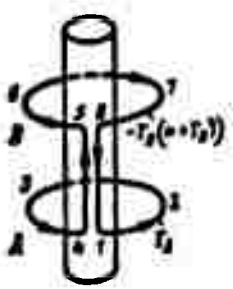


Fig. 2.2.7. The circulation along a vortex line is constant.

Helmholtz's theorem on the conservation of vortex lines. When an inviscid barotropic fluid is placed in a potential field of forces, the following may be stated for vortices in this fluid:

1) the intensity of a vortex tube remains constant throughout the whole duration of the motion.

The proof follows immediately from Thomson's theorem since the intensity of the vortex tube is determined by the circulation with respect to a contour circumscribing the vortex tube;

2) the intensity of the vortex tube is constant over its whole

length. Therefore the vortex tubes of a fluid must be either closed or end at the fluids boundaries. For the proof it is sufficient to take circumferential contours of two sections of the tube and make a cut along it that connects the circumferences of the sections (Fig. 2.2.7). Since the circulation with respect to the over-all contour 123456781, which does not envelop the tube, is equal to zero, and the cut 45,81 runs twice in contrary directions so that, taking the direction of the circumscription into account, we find that the circulations with respect to the two contours, Γ_A and Γ_B, are equal.

Determination of forces acting on a body from the state of flow at the boundaries. There are two methods for determining the reaction of a fluid to a body located in it. The first method requires a knowledge of the forces of pressure and friction at each point of the body's surface with respect to which their resultant and moment is to be found. The second method makes it possible to determine the action of the fluid when its state is known, namely the distribution of the tension of the forces (pressure and friction), the speed and the density, at a certain fictitious boundary of the region, the reference surface, enclosing the body considered.

To determine the forces acting on solid bodies G_i located in the flow of a liquid we consider the region V bounded by the surfaces A_i of these bodies and the reference surface A_k. Noting that by virtue of (2.2.10)

$$\int_{A_0+A_i} \vec{p}_n\, dA = \int_V \left[-\vec{\nabla} p + \frac{1}{3}\mu \vec{\nabla}(\vec{\nabla}\cdot\vec{w}) + \mu (\vec{\nabla}\cdot\vec{\nabla})\vec{w} \right] dV,$$

we write the equation of motion (2.2.2) in the form

$$\int_V \frac{d\vec{w}}{dt}\rho dV = \int_V \vec{f}\rho dV + \int_V \vec{\nabla}p dV + \int_V \rho\left[\frac{1}{3}\vec{\nabla}(\vec{\nabla}\cdot\vec{w}) + (\vec{\nabla}\cdot\vec{\nabla})\vec{w}\right]dV. \qquad (2.2.16)$$

Since the region V is fixed,

$$\int_V \frac{d\vec{w}}{dt}\rho dV = \int_V \left[\frac{\partial \vec{w}}{\partial t} + (\vec{w}\cdot\vec{\nabla})\vec{w}\right]\rho dV = \frac{\partial}{\partial t}\int_V \rho\vec{w}dV + \int_{A_0+A_1} \rho(\vec{w}\cdot\vec{n})\vec{w}dA = \frac{\partial}{\partial t}\int_V \rho\vec{w}dV + \int_{A_0} \rho(\vec{w}\cdot\vec{n})\vec{w}dA.$$

Here it was taken into consideration that $\int_{A_1} \rho(\vec{w}\cdot\vec{n})dA = 0$, since A_1 is a solid surface and the flux through it is zero. The left-hand side gives the total change of momentum of the fluid passing through the isolated region V.

The first term of the right-hand side of (2.2.16) represents the volume forces acting on the isolated volume

$$F = \int_V \rho\vec{f}dV.$$

Rewriting the second term in the form

$$-\int_V \vec{\nabla}p\,dV = -\int_{A_0+A_1} \vec{n}p\,dA = \sum_i \vec{P}_i - \int_{A_0} \vec{n}p\,dA,$$

where $\vec{n}$ is the outer normal to the surface A, we find that it is the sum of the pressure forces applied to the solid body and the pressure forces applied to the reference surface from the side of the surrounding fluid.

Let us now consider the third term of the right-hand side of (2.2.16). Applying the Ostrogradskiy-Gauss formula, we may obtain

$$\int_V \rho\left[\frac{1}{3}\vec{\nabla}(\vec{\nabla}\cdot\vec{w}) + (\vec{\nabla}\cdot\vec{\nabla})\vec{w}\right]dV = \int_{A_0+A_1} \mu\frac{1}{3}\vec{n}(\vec{\nabla}\cdot\vec{w})dA + \int_{A_0+A_1} \rho(\vec{n}\cdot\vec{\nabla})\vec{w}\,dA.$$

When the fluid is incompressible, $\vec{\nabla}\cdot\vec{w} = 0$, and with

$$(\vec{n}\cdot\vec{\nabla})\vec{w}=\left[\cos(n,x)\frac{\partial}{\partial x}+\cos(n,y)\frac{\partial}{\partial y}+\right.$$
$$\left.+\cos(n,z)\frac{\partial}{\partial z}\right]\vec{w}=\frac{\partial\vec{w}}{\partial n},$$

we may write

$$\int_{A_0+A_1}\mu(\vec{n}\cdot\vec{\nabla})\vec{w}\,dA=\int_{A_0}\mu\frac{\partial\vec{w}}{\partial n}dA+\sum_i\int_{A_i}\mu\frac{\partial\vec{w}}{\partial n}dA=$$
$$=\int_{A_0}\mu\frac{\partial\vec{w}}{\partial n}dA+\sum_i\vec{R}_{\mu i}.$$

...re $\vec{\Sigma}_{\mu i}$ denotes the tangential forces of friction on the surfaces ... solid bodies. In the case of a compressible fluid $\vec{\nabla w}\neq 0$ and ... $\vec{n}(\vec{\nabla}\cdot\vec{w})dA$ will differ from zero; this term characterizes the ...cous due to extension or compression of the fluid's volume.

If the reference surface is taken sufficiently far from the ...aries of the solid bodies where the friction effects may be neglected (as to this, we shall discuss it later on) then adding the viscous forces, we obtain

$$\frac{\partial}{\partial t}\int_V\rho\vec{w}\,dV+\int_{A_0}\rho\vec{w}_n\vec{w}\,dA=\vec{F}+\sum_i\vec{P}_i+\sum_i\vec{R}_{\mu i}-\int_{A_0}p\vec{n}\,dA. \qquad (2.2.17)$$

..., the total change of momentum is equal to the sum of all forces acting on the isolated volume. Notice that if another surface A_k is ...ken, all terms will change but so that $\Sigma_i\vec{P}_i$ and $\Sigma_i\vec{R}_{\mu i}$ remain un...anged.

Adding the forces of pressure, $\vec{P}_i$, and of friction, $\vec{R}_{\mu i}$, applied to the solid bodies G_i, we may also write

$$\sum_i(\vec{P}_i+\vec{R}_{\mu i})=\frac{\partial}{\partial t}\int_V\rho\vec{w}\,dV+\int_{A_0}[\vec{n}p+\rho(\vec{n}\cdot\vec{w})\vec{w}]\,dA-\vec{F}.$$

The expression $\vec{n}p+\rho(\vec{n}\cdot\vec{w})\vec{w}$ is called the flux of the vector of ...al impulse in the direction of $\vec{n}$, i.e., through a surface per...dicular to $\vec{n}$. If $\vec{n}$ coincides with the direction of the speed we ...ain a longitudinal component of the total impulse flux density

equal to $p + \rho w^2$; the transverse component (perpendicular to the speed $\vec{w}$) will be simply p.

Thus, in steady motion and when volume forces are absent, the resultant $\vec{R}$ of all forces applied to all solid bodies present in the fluid will be equal to the flux of the total impulse through the (fictitious) reference surface, namely

$$\vec{R}=\int_{A_0}[\vec{n}p+\rho(\vec{n}\cdot\vec{w})\vec{w}]\,dA.$$

Analogously, multiplying the equation of motion vectorially by the radius vector $\vec{r}$, we obtain the corresponding expression for the moment of forces which is equal to the change in angular momentum:

$$\frac{\partial}{\partial t}\int_V \rho(\vec{r}\times\vec{w})\,dV+\int_{A_0}\rho(\vec{r}\times\vec{w})\,w_n\,dA=\vec{r}_1\times\vec{F}+ \\ +\sum_i \vec{r}_i\times\vec{P}_i+\sum_i\vec{r}_0\times\vec{R}_{\mu i}-\int_{A_0}(\vec{r}\times\vec{n}p)\,dA. \qquad (2.2.18)$$

Example 1. Reaction of a liquid, flowing in a curvilinear channel (Fig. 2.2.8). Consider a reference surface as shown by Fig. 2.2.8 (the sections A_1 and A_2 are normal to the speeds $\vec{w}_1$ and $\vec{w}_2$, respectively) for which, neglecting friction and gravity forces and noting that $\vec{n}_1=\vec{w}_1/w_1$; $\vec{n}_2=\vec{w}_2/w_2$, we can write

$$(\rho_1 A_1 w_1\vec{w}_1-\rho_2 A_2 w_2\vec{w}_2)-\left(p_1\frac{\vec{w}_1}{w_1}A_1-p_2\frac{\vec{w}_2}{w_2}A_2\right)=\vec{P}.$$

Thus,

$$\vec{P}=(p_1+\rho_1 w_1^2)A_1\frac{\vec{w}_1}{w_1}-(p_2+\rho_2 w_2^2)A_2\frac{\vec{w}_2}{w_2}. \qquad (2.2.19)$$

Example 2. Pressure force on an inclined plate (Fig. 2.2.9). We shall assume the flow to be two-dimensional, and the fluid incompressible and weightless. The reference surface as shown in the figure is regarded as a semi-circle with its center at the point of intersection of the jet axis with the plate and the longitudinal plate diameter; the radius of the circle is taken so large that the branching of the

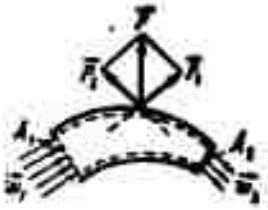


Fig. 2.2.8. A force $\vec{P}$ acting on the walls of a unit tube which is equal to the change in momentum per unit time of motion of liquid flowing through.



Fig. 2.2.9. Impact of the jet on the plate.

jet may be assumed to be complete. Since at the sites of intersection of the reference surface with the flow of the fluid the pressure is the same and equal to atmospheric pressure, p_a, the speed here will also be the same, namely w_a. Now we can write in accordance with (2.2.17)

$$\vec{P} = -\int_{A_{ин}} \vec{p}\,dA + \int_{A_0} \rho(\vec{w}\cdot\vec{n})\vec{w}\,dA.$$

The projection of this equation onto the directions perpendicular to and along the jet on the plate.

$$P = h_0 w_a^2 \sin\alpha, \quad 0 = \rho h_1 w_a^2 - \rho h_2 w_a^2 - \rho h w_a^2 \cos\alpha. \quad (2.2.20)$$

Hence

$$h_1 - h_2 = h\cos\alpha,$$

and, by virtue of the continuity equation,

$$h_1 + h_2 = h,$$
$$h_1 = \frac{1+\cos\alpha}{2}h; \quad h_2 = \frac{1-\cos\alpha}{2}h.$$

To determine the position of the pressure center (point of application of force) we use the theorem of moments. For point 0 we obtain

$$\rho h_1 w_a^2 \frac{h_1}{2} - \rho h_2 w_a^2 \frac{h_2}{2} = Pl,$$

whence

$$l = \frac{1}{\sin\alpha}\cdot\frac{h_1^2 - h_2^2}{2h} = \frac{h}{2}\operatorname{ctg}\alpha. \quad (2.2.21)$$

Example 3. Work of a moving blade. A horizontal jet of speed w assumed to hit a curvilinear vane moving horizontally at speed u. The relation between u and w is to be found for which the work of the jet in shifting the vane is maximum (Fig. 2.2.10).

The fluid's speed relative to the blade is $w - u$. The force will therefore be

$$P = -[\rho(w-u)A(w-u)\cos\beta - \rho(w-u)A(w-u)] = \rho(w-u)^2 A(1-\cos\beta). \qquad (2.2.22)$$

The work is

$$L = Pu = \rho(w-u)^2 A(1-\cos\beta)u = \rho A w^3(1-\cos\beta)\left(1-\frac{u}{w}\right)^2\frac{u}{w}.$$

For determining the maximum condition we put the derivative of L with respect to u/w equal to zero; this yields the equation $\left(1-\frac{u}{w}\right)\left(1-3\frac{u}{w}\right)=0$. The solution u/w = 1 corresponds to the minimum $L_{min} = 0$; the solution u/w = 1/3 gives the maximum $L_{max} = \frac{4}{27}\rho A w^3(1-\cos\beta)$.

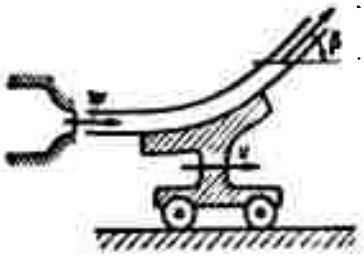


Fig. 2.2.10. Simplest hydraulic drive.

Example 4. Thrust of VRD (air reaction engine) (Fig. 2.2.11). We consider a reference surface surrounding the VRD in the form of a cylinder whose generatrices are parallel to the motor's x-axis, and whose end faces are perpendicular to it. The radius of the cylinder is taken so large that the generatrices may be assumed to be parallel to the streamlines. Due to the symmetry condition, the resultant of the pressure forces on the lateral surface will be zero and the thrust will be directed along the motor axis. Supposing that the parameters of the flow outside the jet emerging from the engine are equal over both sections of the cylinder, and taking the directions of the normals of the end faces into account, we may write

$$\vec{P} = \int_{A_0} [\vec{n}p + \rho(\vec{n}\cdot\vec{w})\vec{w}]\,dA = \vec{i}\int_{A_\infty}(p+\rho w^2)\,dA - \vec{i}\int_{A_u}(p_\infty + \rho_\infty w_\infty)\,dA.$$

We denote by A_∞ the area of the reference section of the stream tube through which the whole mass of air impinging on the motor is coming in, and by A_u the reference area of the stream tube thro...

which the combustion products are ejected, and we shall assume that the stream parameters with respect to a section of the jet ejected by the motor are the same. Then, bearing in mind the similarity of the flows through the end sections outside the jet passing through the engine, we obtain

$$\begin{aligned} P &= \left\{\int_{A_0}(p+\rho w^2)\,dA + \int_{A_1-A_0}(p+\rho w^2)\,dA\right\} - \\ &- \left\{\int_{A_\infty}(p+\rho w^2)\,dA + \int_{A_1-A_\infty}(p+\rho w^2)\,dA\right\} = \\ &= (p_0 A_0 + (m_0+m_1)w_0 + p_\infty(A_1-A_0)) - \\ &\quad - (p_\infty A_\infty + m_0 w_\infty + p_\infty(A_1-A_\infty)) = \\ &= (p_0-p_\infty)A_0 + m_0(w_0-w_\infty) + m_1 w_0. \end{aligned} \tag{2.2.23}$$

here m_v and m_g designate the mass of air and fuel consumed per [illegible] by the engine.

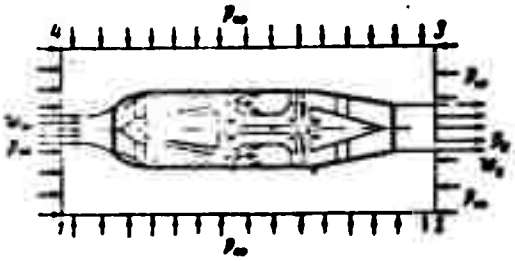


Fig. 2.2.11. Determination of thrust for air reaction engine.

The nozzle is so designed that $p_u = p_\infty$. The operating conditions of the nozzle under which this equality remains valid are called the design conditions. Neglecting the fuel mass m_g which amounts to 2 - 3% of the weight of the air passing through we obtain the following thrust formula for design conditions:

$$P = m_0(w_0 - w_\infty). \tag{2.2.24}$$

Example 5. Euler's turbine equation. A system of solid bodies (blades) is assumed to be inside the reference volume bounded lateral-

ly by the two surfaces of revolution A_n and A_v, and at its ends by the planes A_1 and A_2 perpendicular to the axis of rotation; part of the reference surface may consist of solid walls (Fig. 2.2.12). In order to eliminate the influence of hydrostatic pressure we shall assume that the center of gravity of the volume displaced by this system of solid bodies lies on the axis of rotation.

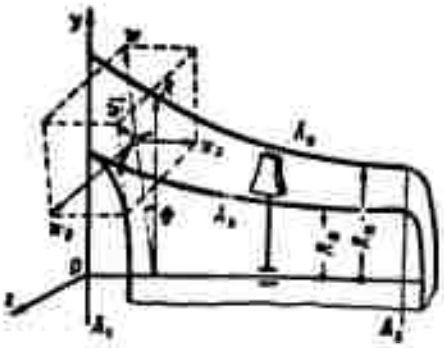


Fig. 2.2.12. For the derivation of Euler's turbine equation.

Since the vectors of pressure distributed over the lateral surface of the reference volume pass through the axis, the moment of pressure forces with respect to the axis is equal to zero. The pressure forces to the end walls are parallel to the axis and their moment with respect to the axis is also zero. Neglecting friction we may therefore write

$$M_x = (\vec{r} \times \sum \vec{P})_x = \int_{A_1} \rho (\vec{r} \times \vec{w})_x w_n \, dA + \int_{A_n} \rho (\vec{r} \times \vec{w})_x w_n \, dA + \\ + \int_{A_2} \rho (\vec{r} \times \vec{w})_x w_n \, dA + \int_{A_v} \rho (\vec{r} \times \vec{w})_x w_n \, dA. \qquad (2.2.25)$$

Passing over to a cylindrical coordinate system (R, ϑ, x) and decomposing the speed $\vec{w}$ into the axial w_x, the radial w_R and the circumferential w_ϑ components, we obtain

$$(\vec{r} \times \vec{w})_x = y w_z - z w_y = R w_\vartheta,$$

where

$$R = \sqrt{y^2 + z^2}.$$

At the first end section $w_n = -w_x$, at the second one $w_n = w_x$.

One the outer surface of revolution $w_n = w_R$ and on the inner one $w_n = -w_R$. Therefore

$$M_z = \int_{A_2} \rho R w_{u_2} w_{z_2} dA - \int_{A_1} \rho R w_{u_1} w_{z_1} dA + \int_{A_0} \rho R w_{u_0} w_{z_0} dA - \int_{A_0} \rho R w_{u_0} w_{z_0} dA. \quad (2.2.26)$$

This is the fundamental equation of the turbine theory: it is called the Euler equation.

For an axial turbine (Fig. 2.2.13, a and b) $w_R = 0$ and

$$M_z = \int_{A_2} \rho R w_{u_2} w_{z_2} dA - \int_{A_1} \rho R w_{u_1} w_{z_1} dA.$$

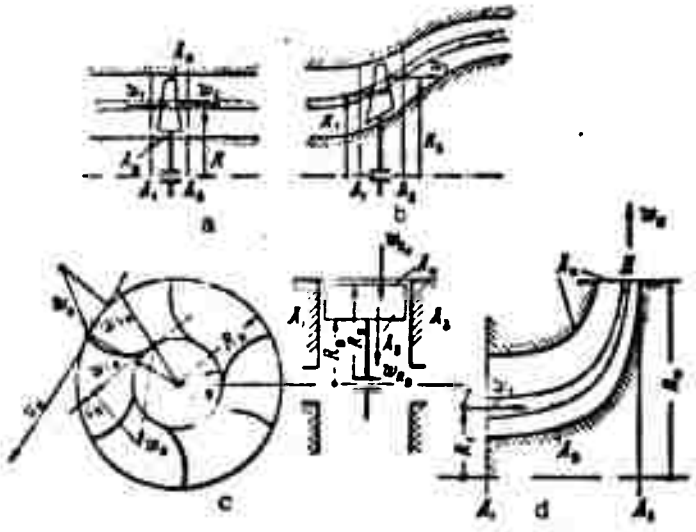


Fig. 2.2.13. Types of turbines. a) axial cylindrical; b) diagonal; c) radial centripetal; d) radial-axial (centrifugal compressor).

Considering a flow element in an annular stream tube of not very large thickness (so that R may be taken as constant) with a flow rate equal to m, we obtain

$$M_z = m[(Rw_u)_2 - (Rw_u)_1].$$

For a radial turbine, e.g., a centripetal one (cf. Fig. 2.2.13c), $w_z = 0$ and

$$M_z = \int_{A_0} \rho R w_{u_0} w_{R_0} dA - \int_{A_0} \rho R w_{u_0} w_{R_0} dA;$$

for the flow element (w_u = const.

$$M_z = m[(Rw_u)_2 - (Rw_u)_1]$$

For turbines of the radial-axial type in which the direction on the flow velocity varies from axial to radial as, for example, in a centrifugal compressor (cf. Fig. 2.2.13d)

$$M_z = \int_{A_2} \rho R w_u w_z \, dA - \int_{A_1} \rho R w_u w_z \, dA.$$

When we consider a flow element of the current I-II of sufficiently small thickness for R and w_z of section 1, and w_z and w_R of section 2 to be assumed constant, we obtain

$$M_z = m[(Rw_u)_2 - (Rw_u)_1].$$

It is easily seen that the form of the equations is one and the same for all types of turbines:

$$M_z = m[(Rw_u)_{\text{entrance}} - (Rw_u)_{\text{exit}}]. \qquad (2.2.27)$$

2.3. THE ENERGY CONSERVATION LAW. THE ENERGY EQUATION

The energy conservation law not only establishes the invariance of all energies for an arbitrary isolated mass of the fluid but also expresses the mutual convertibility of the various forms of motion of matter.

The necessity of introducing an energy equation results from the fact that the two equations, namely that of continuity (scalar) and that of motion (vector), contain three unknown quantities: a vector (velocity $\vec{w}$) and two scalars (pressure p and density ρ), so that in the case of a gas (compressible fluid) the number of quantities sought exceeds the number of equations by one. When the (scalar) energy equation is added to the system, another new unknown scalar quantity is added, namely the temperature T. The system of equations is completed by adding the partition equation, and the problem of aero-mechanics (with given initial and boundary conditions which will be discussed later on) becomes a definite one.

Energy, work and heat. Motion as a mode of existence of matter assumes qualitatively different forms. The energy may serve as a measure of the motion. Qualitatively divergent forms of motion correspond to the following different forms of energy: mechanical, thermal, electrical, chemical, etc. All these forms of energy have the property of mutual convertibility, during which the numerical amount of the measure of motion, i.e., of energy, remains unchanged. When the state of the system is changed the motion changes too and in the general case, accompanied by a conversion of one form of energy into another. We may, say that energy is a function of the state of the system. Its quantitative amount is independent of the manner) in which the system is led over from one state to another, i.e., the infinitesimal energy conversion dE is a total differential of a certain function so that the energy variation of the system due to the transition from state 1 to state 2 is determined by the difference of the values of this function in the initial and final states:

$$\int_1^2 dE = E(2) - E(1).$$

The transition of the system from one state to another is characterized quantitatively by the work. Work is the measure of change of form of motion and, therefore, it depends essentially on the manner of transition, i.e., on the process.

This indicates that the work element, dL, is not a total differential and the total work for the transition of the system from one state to another cannot be represented as a difference between the values of certain functions of these states.

In aeromechanics a large part is played by the processes of heat transfer.

The amount of heat supplied (the same as of work) depends es-

sentially on the process and therefore the heat element is not a total differential. In order to emphasize this, the heat element is frequently designated as δQ (and the work element as δL).

The first law of thermodynamics. In thermodynamics the energy of a system is usually divided into two: the external and the internal part. The external energy is the mechanical energy of the system; it consists of kinetic and potential energy and depends on the velocity and position of the system as a whole (or of its macroscopic parts). The internal energy is that part of the energy which depends on temperature, volume, etc., but not on the velocity and position of the system as a whole.

The energy conservation law may be formulated in the following manner: the energy increment per unit time of a certain nonisolated system is equal to the work of the external forces applied to the system plus the heat supplied to the system during the same time

$$\frac{dE}{dt}=\sum L_i+Q. \qquad (2.3.1)$$

In a coordinate system fixed to the center of gravity of the system, the energy E of the system will be equal to the internal energy ε, and the heat element supplied to the system is, therefore, equal to the increment of internal energy plus the work of the pressure forces:

$$dQ=d\varepsilon+p\,dv, \qquad (2.3.2)$$

where pdv is the work performed under the environment. As was shown the heat dQ supplied and the work pdv are here not differentials of some arbitrary function but very small quantities.

Note should be taken of the fact that all of the heat supplied to the system represents not only the heat taken by the body from the external source dQ_0 but also the heat dQ_f liberated in the body by dissipation, e.g., by the work of the internal forces of

friction.

Relationship (2.3.2) is called the first law of thermodynamics.

One of the basic concepts of thermodynamics is the concept of specific heat

$$c=\frac{dQ}{dT}\ [\text{kgm/kg}\cdot\text{deg}]$$

The specific heat is the amount of heat necessary to raise the temperature of a unit mass by one degree during the process considered.

When the volume remains constant in the process of heating the following is obtained from the first law (2.3.2):

$$c_v=\left(\frac{dQ}{dT}\right)_v=\frac{d\varepsilon}{dT};\quad d\varepsilon=c_v dT.$$

c_v is the specific heat at constant volume (per unit mass). It follows from this that $\varepsilon=\int c_v dT$ In the general case c_v varies with temperature. For simplicity, however, the specific heat c_v will be assumed in what follows to be independent of temperature: $\varepsilon = c_v T$.

Noting that $d(pv) = vdp + pdv$, we rewrite the first law in the form

$$dQ=d\varepsilon+p\,dv=c_v dT+d(pv)-v\,dp.$$

Since $pv = RT$, we have

$$dQ=(c_v+R)\,dT-v\,dp.$$

When heating occurs at constant pressure, then, denoting the specific heat at constant pressure by $c_p = (dQ/dT)_p$, we obtain for gases $R = c_p - c_v$.

The ratio of the specific heats, $k = c_p/c_v$, plays an essential part in thermodynamic calculations.

This ratio depends on the structure of the molecules and on the number of atoms forming them. Therefore k is sometimes said to be the number of atoms. According to the kinetic theory of gases $k = (n+2)/n$, where n is the number of degrees of freedom of the gas molecules. For air (diatomic gas) $k = 1.4$ and $c_p = 1000\ m^2/$

/sec^{2}deg (= 0.24 kcal/kg·deg). In fact k decreases somewhat with temperature, for diatomic molecules $k = 1.10 - 0.5 \cdot 10^{-4} t°C$ [2.6].

Reversible and irreversible processes. When the state of an isolated system is determined by constant nonvarying parameters the system is said to be in the state of thermodynamic equilibrium. All systems reach this state sooner or later.

As soon as parameters of the system start varying, the process of transition from the initial (primary) state to another state begins. When the parameters vary very slowly, a state of thermodynamic equilibrium will be set up and the system will gradually go over from one state to the other.

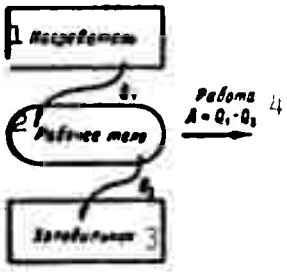


Fig. 2.3.1. Scheme of heat engine. 1) Heater; 2) working fluid; 3) cooler; 4) work.

An infinitely slow process of this kind is termed quasistatic.

Reversible is the term applied to a process that may proceed in the reverse direction such that the system passes through the same states as in the forward process but in the reverse sequence. A quasistatic process has the property of reversibility, for, in every stage of the process, the state is an equilibrium state and when the parameters vary in the reverse direction the body will pass through the same states but in the reverse order.

In nature all processes occur at a finite rate and are therefore irreversible.

In mutual conversions the quantitative association established by the first law of thermodynamics must be supplemented by the qualitative condition as to the direction of the conversion process.

It is known from experience that mechanical work can be con-

verted into heat, for example by friction. This process will occur "by itself." The process of heat transfer from a hot to a cold body, the expansion of a gas from a small volume to a large one, etc., likewise occur "by themselves."

By heating a gas which is able to expand we can convert heat into work; a reversal of this process needs, however, an input of work to compress the gas. When the gas is compressed at the same pressure as that at which it has been expanded, exactly the same amount of work is consumed to restore the gas to its initial state as gained when it expanded. As the result there is no conversion of heat to work.

When, however, the reverse process, namely the compression of the gas, occurs at a lower temperature, the compression work will be smaller. Thus, a machine for converting heat to work operating on the principle of a cyclic process must consist at least of three parts: the heater, the working fluid, and the cooler (Fig.

Entropy. This part of work which is irreversibly involved in a process is said to be "lost" for accomplishing efficient work. Thus the efficiency may be considered as a certain measure of the reversibility of a process. It is, however, not a function of state.

It would be convenient to introduce a parameter which, being a function of state, could at the same time characterize the process of change of state of the body and indicate whether this process is possible in nature (whether it may occur "by itself").

Let us consider the [illegible] of thermodynamics for an ideal gas.

or, since

$$\left.\begin{aligned} dQ &= c_v\,dT + p\,dv \\ p &= \rho RT \quad \text{и} \quad v = 1/\rho, \\ dQ &= c_v\,dT - RT\frac{d\rho}{\rho}. \end{aligned}\right\} \tag{2.3.3}$$

Hence it is seen that when the whole equation is divided by T the right-hand side is a total differential, $c_v\frac{dT}{T} - R\frac{d\rho}{\rho}$ and therefore, the left-hand side, dQ/T, will also be a total differential of some function of state S. This function of state whose differential is

$$dS = \frac{dQ}{T}, \tag{2.3.4}$$

is called entropy. The accuracy with which it is determined by Eq. (2.3.3) is within an arbitrary constant whose value can be chosen conventionally:

$$S = c_v \ln T - R\ln\rho + S_0 \tag{2.3.5}$$

The second law of thermodynamics. The second law of thermodynamics may be formulated as follows: heat cannot pass from a cold to a heated body. With the help of Carnot's cycle it can be shown that for an arbitrary cycle the entropy cannot diminish. Besides, this follows from the definition dS = dQ/T where dQ is, in general, the sum of heat supplied from an external source dQ_0 (> 0) and the heat supply due to energy dissipation in the system itself, dQ_f. Since dQ_f can never be negative, $dS \geq 0$; in the limiting case dQ = 0 and dS = 0.

In a reversible process $dQ_f = 0$ and $dQ_0 = T\,dS$; in an irreversible one, $dQ = T\,dS > dQ_0$.

From Relation (2.3.5) we obtain

$$\frac{S_2 - S_1}{c_v} = \ln\frac{T_2}{T_1}\left(\frac{\rho_1}{\rho_2}\right)^{k-1}$$

or, introducing $p = \rho RT$,

$$\frac{p_2}{p_1} = \left(\frac{\rho_2}{\rho_1}\right)^k e^{\frac{S_2 - S_1}{c_v}}. \tag{2.3.6}$$

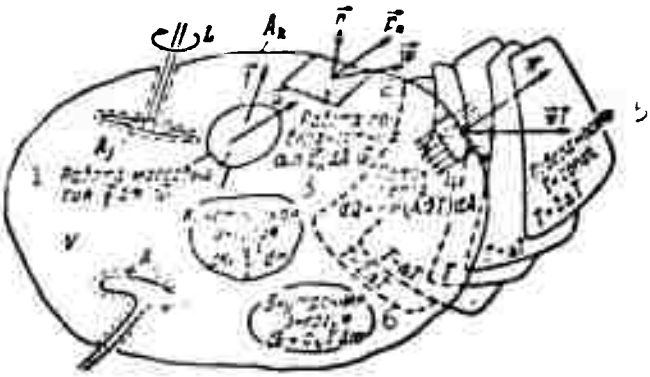
In the general case of a flow $S = S(x, y, z, t)$ and we may put

$$p = A(S)\rho^{k}. \qquad (2.3.6)$$

Isentropic and adiabatic processes. For an isentropic process in which the entropy remains unchanged, $S_2 - S_1 = 0$, Relation (2.3.6) assumes the form

$$\frac{p_2}{p_1} = \left(\frac{\rho_2}{\rho_1}\right)^{k}. \qquad (2.3.7)$$

An adiabatic process is characterized by the absence of heat exchange with the surroundings, i.e., $dQ_t = 0$.



. . . . The variation of internal energy $\int \rho\varepsilon dV$ and kinetic energy $\int \rho\frac{w^2}{2} dV$ per unit time is equal to the sum of work of the volume forces $\int \vec{f}\cdot\vec{w}\rho dV$ and the surface forces $\int \vec{p}_n\cdot\vec{w}\,dA$ plus the heat supply $\int \vec{n}\cdot\lambda\nabla T\,dA$ during the same time. 1) Work of mass forces; 2) work of surface forces; 3) kinetic energy; 4) heat flow; 5) surfaces; 6) internal energy.

Thus, every reversible isentropic process is an adiabatic process. not all adiabatic processes are isentropic; despite the fact that there is no heat exchange with the surroundings, T dS can be larger than zero, i.e., $dS \neq 0$.

The integral form of the energy equation. We apply the energy conservation law in its general form to some volume V of a fluid (Fig. 2.3.2), bounded by the surface A. Inside the isolated volume, solid stationary bodies G_i and moving bodies G_j (e.g., turbines)

are assumed to exist which effect the energy exchange with the fluid (as will be shown in what follows, unsteadiness of pressure is a necessary condition for energy exchange with continuous variation of the parameters in an inviscid fluid). The reference surface A will be assumed to consist of the fictitious surface A_k separating the isolated fluid from the remainder, and the surfaces A_i and A_j surrounding the stationary and moving bodies, G_i and G_j.

Expressing all quantities in mechanical units we can put the total energy of the isolated volume of the fluid equal to the sum of internal and kinetic energies:

$$\int_V \left(e + \frac{w^2}{2}\right) \rho \, dV.$$

The work of the mass forces is equal to $\int_V \rho \vec{f} \cdot \vec{w} \, dV$, and the work of the surface forces equal to $\int_A \vec{p}_n \cdot \vec{w} \, dA$.

According to Fourier's law, the heat flux density passing per unit time through the unit area of an isothermic surface will be equal to $\vec{q} = -\lambda \vec{\nabla} T$, where λ is the coefficient of thermal conductivity provided the temperature gradient is not too large, which is usually the case.

Then the amount of heat transferred through the surface A with the outer normal $\vec{n}$ is

$$Q = -\int_A \vec{n} \cdot \vec{q} \, dA.$$

By virtue of the mass conservation law $d(\rho dV)/dt = 0$, therefore

$$\frac{d}{dt} \int_V \left(e + \frac{w^2}{2}\right) \rho \, dV = \int_V \rho \frac{d}{dt} \left(c_v T + \frac{w^2}{2}\right) dV +$$

$$+ \int_V \left(c_v T + \frac{w^2}{2}\right) \frac{d}{dt} (\rho \, dV) = \int_V \rho \frac{d}{dt} \left(c_v T + \frac{w^2}{2}\right) dV$$

and the energy equation can be written in the form

$$\int_V \rho \frac{d}{dt} \left(e + \frac{w^2}{2}\right) dV = \int_V \vec{f} \cdot \vec{w} \rho \, dV + \int_A \vec{p}_n \cdot \vec{w} \, dA - \int_A \vec{n} \cdot \vec{q} \, dA. \qquad (2.1)$$

This equation is the mathematical formulation of the energy conservation law: the variation of total energy of the volume of the liquid or gas per unit time is equal to the sum of work of the mass and the surface forces at the surface bounding the isolated volume plus the heat supply during the same time.

The energy equation in differential form. Let us calculate $\int_A \vec{p}_n \cdot \vec{w}\, dA$; for this purpose we consider a unit parallelepiped with edges δx, δy, δz, parallel to the coordinate axes. Calculating the work of the surface forces we obtain

$$\int_A \vec{p}_n \cdot \vec{w}\, dA = -\vec{p}_x \cdot \vec{w}\,\delta A_x + \left(\vec{p}_x \cdot \vec{w} + \frac{\partial(\vec{p}_x \cdot \vec{w})}{\partial x}\delta x\right)\delta A_x + \ldots = -\left[\frac{\partial(\vec{p}_x \cdot \vec{w})}{\partial x} + \frac{\partial(\vec{p}_y \cdot \vec{w})}{\partial y} + \frac{\partial(\vec{p}_z \cdot \vec{w})}{\partial z}\right]\delta V.$$

Dividing the whole volume into unit volumes we find that for the entire surface A

$$\int_A \vec{p}_n \cdot \vec{w}\, dA = -\int_V \left[\frac{\partial(\vec{p}_x \cdot \vec{w})}{\partial x} + \frac{\partial(\vec{p}_y \cdot \vec{w})}{\partial y} + \frac{\partial(\vec{p}_z \cdot \vec{w})}{\partial z}\right] dV.$$

Applying the Ostrogradsky formula to transforming the second surface integral of Eq. (2.3.8) as well, we obtain the energy equation in the form

$$\int_V \rho \frac{d}{dt}\left(\varepsilon + \frac{w^2}{2}\right) = \int_V \left[\rho \vec{f} \cdot \vec{w} + \frac{\partial(\vec{p}_x \cdot \vec{w})}{\partial x} + \frac{\partial(\vec{p}_y \cdot \vec{w})}{\partial y} + \frac{\partial(\vec{p}_z \cdot \vec{w})}{\partial z}\right] dV - \int_V \vec{\nabla} \cdot \vec{q}\, dV. \qquad (2.3.9)$$

With continuous integrands Eq. (2.3.9) will become

$$\rho \frac{d}{dt}\left(\varepsilon + \frac{w^2}{2}\right) = \rho \vec{f} \cdot \vec{w} + \frac{\partial(\vec{p}_x \cdot \vec{w})}{\partial x} + \frac{\partial(\vec{p}_y \cdot \vec{w})}{\partial y} + \frac{\partial(\vec{p}_z \cdot \vec{w})}{\partial z} - \vec{\nabla} \cdot \vec{q}. \qquad (2.3.10)$$

Writing the scalar products in explicit form we obtain

$$\rho \frac{d}{dt}\left(\varepsilon + \frac{w^2}{2}\right) = \rho(f_x w_x + f_y w_y + f_z w_z) + \frac{\partial}{\partial x}(\sigma_x w_x + \tau_{yx} w_y + \tau_{zx} w_z) + \frac{\partial}{\partial y}(\tau_{xy} w_x + \sigma_y w_y + \tau_{zy} w_z) + \frac{\partial}{\partial z}(\tau_{xz} w_x + \tau_{yz} w_y + \sigma_z w_z) - \left(\frac{\partial q_x}{\partial x} + \frac{\partial q_y}{\partial y} + \frac{\partial q_z}{\partial z}\right). \qquad (2.3.10)$$

Analysis of the energy equation. We represent Eq. (2.3.9) in the form

$$\left\{\rho\frac{de}{dt}-\left[\left(\vec{p}_x\cdot\frac{\partial\vec{w}}{\partial x}+\vec{p}_y\cdot\frac{\partial\vec{w}}{\partial y}+\vec{p}_z\frac{\partial\vec{w}}{\partial z}-\vec{\nabla}\cdot q\right)\right\}+\right.$$
$$+\left\{\rho\frac{d}{dt}\frac{w^2}{2}-\left[\rho\vec{f}\cdot\vec{w}+\left(\frac{\partial\vec{p}_x}{\partial x}+\frac{\partial\vec{p}_y}{\partial y}+\frac{\partial\vec{p}_z}{\partial z}\right)\cdot\vec{w}\right]\right\}=0. \qquad (2.3.11)$$

Each of the terms in the braces is equal to zero. Indeed, multiplying the equation of motion (2.2.4) scalarly by $\vec{w}$ and taking into account that $\rho\frac{d}{dt}\frac{w^2}{2}=\rho\vec{w}\cdot\frac{d\vec{w}}{dt}$ we obtain the expression of the second brace:

$$\rho\frac{d}{dt}\frac{w^2}{2}-\rho\vec{f}\cdot\vec{w}-\left(\frac{\partial\vec{p}_x}{\partial x}+\frac{\partial\vec{p}_y}{\partial y}+\frac{\partial\vec{p}_z}{\partial z}\right)\cdot\vec{w}=0. \qquad (2.3.12)$$

The equation indicates that the kinetic energy varies only at the expense of the work done by the volume forces and the work of the surface forces above the element.

We represent the surface forces by their components due to viscosity, and by the pressure

$$\vec{p}_x=-\vec{i}p+\vec{p}_x';\quad \vec{p}_y=-\vec{j}p+\vec{p}_y';$$
$$\vec{p}_z=-\vec{k}p+\vec{p}_z'. \qquad (2.3.13)$$

Taking (2.3.13) and (2.2.8) into account we may then write

$$\vec{w}\cdot\left(\frac{\partial\vec{p}_x}{\partial x}+\frac{\partial\vec{p}_y}{\partial y}+\frac{\partial\vec{p}_z}{\partial z}\right)=-\vec{w}\cdot\vec{\nabla}p+\mu\vec{w}\cdot\left(\Delta\vec{w}+\frac{1}{3}\vec{\nabla}\vec{\nabla}\cdot\vec{w}\right)=$$
$$=-\vec{w}\cdot\vec{\nabla}p+\vec{w}\left(\frac{\partial\vec{p}_x}{\partial x}+\frac{\partial\vec{p}_y}{\partial y}+\frac{\partial\vec{p}_z}{\partial z}\right). \qquad (2.3.14)$$

The term $\vec{w}\cdot\vec{\nabla}p$ characterizes the work performed in displacing the element as a whole under the action of unbalanced hydromechanical pressure p (the "−" sign is associated with the fact that the pressure is directed into the volume), and the component $\mu\vec{w}\left(\Delta\vec{w}+\frac{1}{3}\vec{\nabla}\vec{\nabla}\cdot\vec{w}\right)$ characterize the increment of kinetic energy due to the entrainment of the fluid element as a whole by the forces of viscosity.

Thus, the second component enclosed by braces in (2.3.11) is the energy equation of an element moved as a whole; it does not take

the internal energy processes in the element into account.

The expression in the first braces of Eq. (2.3.11),

$$\rho\frac{di}{dt}-\left[\left(\vec{p}_x\cdot\frac{\partial\vec{w}}{\partial x}+\vec{p}_y\cdot\frac{\partial\vec{w}}{\partial y}+\vec{p}_z\frac{\partial\vec{w}}{\partial z}\right)-\vec{\nabla}\cdot\vec{q}\right]=0 \qquad (2.3.15)$$

takes the changes inside the moving element into account.

The derivatives $\partial\vec{w}/\partial x$, $\partial\vec{w}/\partial y$, $\partial\vec{w}/\partial z$ are the deformation rates [cf. (1.2.7)] and their product with the stresses of the surface forces characterize the work connected with the deformation of the element changing the volume and shape of the element (p. 13).

By virtue of (2.2.7) the second component is in fact

$$\vec{p}_x\cdot\frac{\partial\vec{w}}{\partial x}+\vec{p}_y\cdot\frac{\partial\vec{w}}{\partial y}+\vec{p}_z\cdot\frac{\partial\vec{w}}{\partial z}=-p\vec{\nabla}\cdot\vec{w}+$$

$$+\left(\vec{p}'_x\cdot\frac{\partial\vec{w}}{\partial x}+\vec{p}'_y\cdot\frac{\partial\vec{w}}{\partial y}+\vec{p}'_z\cdot\frac{\partial\vec{w}}{\partial z}\right)=-p\vec{\nabla}\cdot\vec{w}+$$

$$+\mu\left\{2\left[\left(\frac{\partial w_x}{\partial x}\right)^2+\left(\frac{\partial w_y}{\partial y}\right)^2+\left(\frac{\partial w_z}{\partial z}\right)^2\right]-\frac{2}{3}(\mathrm{div}\,\vec{w})^2+\right.$$

$$\left.+\left(\frac{\partial w_x}{\partial y}+\frac{\partial w_y}{\partial x}\right)^2+\left(\frac{\partial w_y}{\partial z}+\frac{\partial w_z}{\partial y}\right)^2+\left(\frac{\partial w_z}{\partial x}+\frac{\partial w_x}{\partial z}\right)^2\right\}=$$

$$=-p\vec{\nabla}\cdot\vec{w}+\mu D. \qquad (2.3.16)$$

Using the continuity equation, the first component $(-p\vec{\nabla}\cdot\vec{w})$ may be represented in the form $-\frac{p}{\rho}\frac{d\rho}{dt}$. The latter expression characterizes the work of deformation of the element under the action of pressure p, i.e., the work associated with the change in the volume element.

The second component (μD) characterizes the work done in deforming the element under the action of the viscosity forces; this work is connected with the change of shape of the element and represents the work of friction forces; it does not increase the kinetic energy but goes over into heat and is dissipated in the fluid itself. The function μD is called the scattering (dissipation) function.

Thus, Eq. (2.3.16) may be written in the form

$$\rho\frac{de}{dt}+p\vec{\nabla}\cdot\vec{w}=\rho\left(\frac{d}{dt}c_vT+p\frac{dv}{dt}\right)=\mu D+\vec{\nabla}\cdot\lambda\vec{\nabla}T. \qquad (2.3.17)$$

i.e., the heat supplied to the fluid and the heat set free owing to work performed by the forces of friction increases the internal energy and the expansion work.

For a perfect gas $d\varepsilon = c_v dT$, then

$$\frac{d\varepsilon}{dt} = c_v \frac{\partial T}{\partial t} + c_v\left(\frac{\partial T}{\partial x}\cdot\frac{dx}{dt} + \frac{\partial T}{\partial y}\frac{dy}{dt} + \frac{\partial T}{\partial z}\frac{dz}{dt}\right) = c_v\left(\frac{\partial T}{\partial t} + \vec{w}\cdot\vec{\nabla}T\right).$$

where $c_v\frac{\partial T}{\partial t}$ is the local increment of the internal energy associated with the local variation with time of the temperature field and $c_v\vec{w}\cdot\vec{\nabla}T$ is the convective increment of the internal energy associated with the transition of particles of the fluid from one point into another.

Equation (2.3.17) now assumes the form

$$\rho c_v\left(\frac{\partial T}{\partial t} + \vec{w}\cdot\vec{\nabla}T\right) + p\vec{\nabla}\cdot\vec{w} = \mu D + \vec{\nabla}\cdot\lambda\vec{\nabla}T. \qquad (2.3.18)$$

The energy equation for a flow element. We consider the linear motion of an inviscid ($\mu = 0$) compressible fluid along a stream tube with a cross section small enough for velocity, pressure and density to be constant over the cross section.

If there is no heat transfer, the motion considered will be adiabatic and the energy Eq. (2.3.17) assumes the form

$$c_v dT - \frac{p}{\rho^2}d\rho = c_v dT + p d\frac{1}{\rho} = 0 \qquad (2.3.19)$$

We form the scalar product of the equation of motion

$$\frac{d\vec{w}}{dt} = \vec{f} - \frac{1}{\rho}\vec{\nabla}p$$

and the streamline element $d\vec{r}$:

$$d\vec{r}\cdot\frac{d\vec{w}}{dt} = \vec{w}\cdot d\vec{w} = d\frac{w^2}{2} = \vec{f}\cdot d\vec{r} - \frac{dp}{\rho}. \qquad (2.3.20)$$

From the equation of state $p = \rho RT = \rho(c_p - c_v)T$ we have

$$c_v T + \frac{p}{\rho} = c_p T;$$

the quantity $i = c_p T$ is called the enthalpy (heat content).

$$i = c_p dT = c_v dT + \frac{dp}{\rho} + p d\frac{1}{\rho},$$

which, together with Eq. (2.3.19), gives

$$\frac{dp}{\rho} = c_p dT = d\left(c_v T + \frac{p}{\rho}\right).$$

Equation (2.3.20) therefore assumes the form

$$d\left(c_v T + \frac{p}{\rho} + \frac{w^2}{2}\right) = \vec{f} \cdot d\vec{r}; \qquad (2.3.21)$$

nd after integration we have

$$c_v T + \frac{p}{\rho} + \frac{w^2}{2}\Big|_1^2 = \int_1^2 \vec{f} \cdot d\vec{r}. \qquad (2.3.22)$$

The quantity $c_v T + \frac{p}{\rho} + \frac{w^2}{2} = c_p T + \frac{w^2}{2}$ is the <u>specific energy</u>; in a perfect ($p = \rho RT$) inviscid gas without heat transfer it varies only ... expense of the work done by the volume forces. If there are ... s forces, it follows from (2.3.21) that the specific energy ... constant. Then, noting that $c_v T = c_v \frac{p}{\rho R} = \frac{k}{k-1}\frac{p}{\rho}$,

$$\frac{k}{k-1}\frac{p}{\rho} + \frac{w^2}{2} = \text{const}. \qquad (2.3.23)$$

... the mass forces ... a potential, $\vec{f} = \vec{\nabla} U$, then $\int_1^2 \vec{f} \cdot d\vec{r} = U\Big|_1^2$ ... ead of (2.3.22) we may write

$$c_v T + \frac{p}{\rho} + \frac{w^2}{2} + U = \text{const}; \qquad (2.3.24)$$

... this case the <u>total specific energy</u> is said to <u>remain constant</u> ... <u>a streamline</u>.

<u>Energy transfer between a flowing liquid and solid bodies in it.</u>

... onsider for simplicity an adiabatic flow ($Q = 0$) of an inviscid ... id ($\mu = 0$) in a field of forces which have a potential $\vec{f} = -\vec{\nabla} U$, i.e., ... put $\vec{q} = 0$, $\vec{p}_n = -n\vec{p}$, $\vec{f} = -\vec{\nabla} U$ in the energy Eq. (2.3.8).

Assuming that the force potential is a function of a point only, ..., the local part $\frac{\partial U}{\partial t} = 0$, we may write

$$\vec{w} \cdot \vec{\nabla} U = w_x \frac{\partial U}{\partial x} + w_y \frac{\partial U}{\partial y} + w_z \frac{\partial U}{\partial z} = \frac{dU}{dt};$$

... therefore (2.3.8) will have the form

$$\int_V \rho \frac{d}{dt}\left(c_v T + \frac{w^2}{2} + U\right) dV = -\int_A \vec{n}p \cdot \vec{w}\, dA.$$

i.e., the change in the sum of internal, kinetic and potential energies inside the reference volume is equal to the work of the surface forces of pressure on the reference surface.

Applying the Ostrogradskiy-Gauss theorem we write the right-hand part in the form

$$\int_A \vec{n}p \cdot \vec{w}\, dA = \int_A \vec{n} \cdot p\vec{w}\, dA = \int_V \vec{\nabla} \cdot p\vec{w}\, dV.$$

Using the continuity equation $\vec{\nabla} \cdot \vec{w} = -\frac{1}{\rho}\frac{d\rho}{dt}$, we can write

$$\vec{\nabla} \cdot p\vec{w} = p\vec{\nabla} \cdot \vec{w} + \vec{w} \cdot \vec{\nabla} p = -\frac{p}{\rho}\frac{d\rho}{dt} + \vec{w} \cdot \vec{\nabla} p =$$

Now

$$= \rho \frac{d}{dt}\left(\frac{p}{\rho}\right) - \frac{dp}{dt} + \vec{w}\vec{\nabla} \cdot p = \rho \frac{d}{dt}\frac{p}{\rho} - \frac{\partial p}{\partial t}.$$

$$\int_A \vec{n}p \cdot \vec{w}\, dA = -\int_V \left[\rho \frac{d}{dt}\left(\frac{p}{\rho}\right) - \frac{\partial p}{\partial t}\right] dV.$$

Since $\frac{1}{\rho} = v$,

$$\frac{d}{dt}\left(\frac{p}{\rho}\right) = \frac{d}{dt}(pv) = p\frac{dv}{dt} + v\frac{dp}{dt}.$$

i.e., $\frac{d}{dt}(p/\rho)$ represents the sum of the power (work per unit time) consumed in deforming the volume (p dv/dt) and the power consumed in displacing the volume (v dp/dt) in the nonuniform pressure field.

Thus,

$$\int_V \rho \frac{d}{dt}\left(c_v T + \frac{p}{\rho} + \frac{w^2}{2} + U\right) dV = \int_V \frac{\partial p}{\partial t} dV. \qquad (2.3.25)$$

i.e., the variation per unit mass of the specific energy $+\frac{p}{\rho} + \frac{w^2}{2} + U$ is connected with the presence of regions in the volume in which the pressure will certainly vary with time. Since the non-moving bodies cannot cause the pressure to vary with time, it is also impossible that mechanical energy is exchanged between them and the fluid. Only when the pressure is variable with time can energy be exchanged inside the fluid. It is possible, for example, for this time-variable pressure field to be produced by turbomachines in the reference volume

As a rule the pressure variation occurs in a periodic manner and usually the motion is quasisteady in nature. For such a motion, having the period t_p,

$$\int_t^{t+t_p}\int_V \rho \frac{d}{dt}\left(c_v T+\frac{p}{\rho}+\frac{w^2}{2}+U\right)dV\,dt=\int_t^{t+t_p}\int_V \frac{\partial p}{\partial t}\,dV\,dt$$

and since $\int_t^{t+t_p}\frac{\partial p}{\partial t}\,dt=0$, то $\frac{d}{dt}\left\{\left[c_v T+\frac{p}{\rho}+\frac{w^2}{2}+U\right]_{\text{average}}\right\}=0.$

Consequently,

$$\left[c_v T+\frac{w^2}{2}+\frac{p}{\rho}+U\right]_{\text{average}}=\text{const.}$$

i.e., the total specific energy composed of the mean values of its components is a constant quantity.

THE SYSTEM OF AEROHYDROMECHANICAL EQUATIONS. INITIAL AND BOUNDARY CONDITIONS

The system of equations. We write the continuity Eq. (2.1.3), the equation of motion (2.2.8), the energy equation (2.3.18), and the equation of state in the form of a system (assuming μ = const and λ = const):

$$\left.\begin{aligned}
&\frac{\partial\rho}{\partial t}+\vec{w}\cdot\vec{\nabla}\rho+\rho\vec{\nabla}\cdot\vec{w}=0,\\
&\frac{\partial\vec{w}}{\partial t}+(\vec{w}\cdot\vec{\nabla})\vec{w}=\vec{f}-\frac{1}{\rho}\vec{\nabla}p+\frac{\nu}{3}\vec{\nabla}(\vec{\nabla}\cdot\vec{w})+\nu(\vec{\nabla}\cdot\vec{\nabla})\vec{w},\\
&\rho c_v\left(\frac{\partial T}{\partial t}+\vec{w}\cdot\vec{\nabla}T\right)+p\vec{\nabla}\cdot\vec{w}=\Phi D+\lambda\Delta T,\\
&p=\rho RT\ (\text{in the general case } p=p(\rho,T)).
\end{aligned}\right\}\qquad(2.4.1)$$

This system establishes in differential form the relation between the quantities characterizing the state of motion (p, $\vec{w}$, ρ, T). To determine these quantities as coordinate and time functions we have to integrate the differential equations obtained in partial derivatives with the given initial and boundary conditions. The number of equations of the system (one vector and three scalar equations) is equal to the number of the unknowns $\vec{w}$, p, ρ, T (one vector and three scalars).

Initial and boundary conditions. The problem of integrating differential equations is indefinite and, as a rule, it has an infinite multitude of solutions. Usually, however, additional conditions are given which make it possible to select a certain unique solution.

If the region in which the process considered occurs is bounded, the character of the interaction occurring at the boundaries of the region is completely defined in advance and, at the boundaries of the region, the function sought must satisfy a certain additional condition which is called the boundary condition; it (or its derivative) must assume at the boundary a certain definite value.

The course with time of physical processes requires what is called the initial condition to be satisfied, in order to have the function sought assume a completely definite and given value at a definite instant of time, which we shall call the initial one.

These additional conditions, the initial and the boundary conditions, make it possible to select among the infinite multitude of solutions a single one that corresponds to reality.

In the case of a steady motion the initial conditions drop out; for an unsteady motion they represent the values of speed $\vec{w}$, pressure p, temperature T, etc., at the initial instant of time and at each point of the space.

The boundary conditions may be given for a free surface or for solid boundaries. If an inviscid fluid is adjacent to an impermeable surface whose equation is $F(x, y, z) = 0$, the boundary condition consists in that over the whole surface the velocity has only a component tangential to it. Since the gradient of the function $F(x, y, z)$ coincides with the normal to the plane surface (in the given case to the surface of the body) we have $\vec{w} \cdot \vec{\nabla} F = 0$ or

$$w_x \frac{\partial F}{\partial x} + w_y \frac{\partial F}{\partial y} + w_z \frac{\partial F}{\partial z} = 0. \qquad (2.4.2)$$

When the boundary varies with time so that the surface function has the form $F(x, y, z, t) = 0$, the boundary condition will make the particle coordinates coincide with the coordinates of the surface, x, y, z, at the instant of time t and at the instant of time t + dt, when the coordinates will be x + dx, y + dy, z + dz, i.e., at this instant of time too the particle coordinates must satisfy the equation

$$F(x+dx,\ y+dy,\ z+dz,\ t+dt)=0.$$

If we restrict ourselves to the first terms of a Taylor series expansion we obtain

$$\frac{\partial F}{\partial x}dx+\frac{\partial F}{\partial y}dy+\frac{\partial F}{\partial z}dz+\frac{\partial F}{\partial t}dt=0.$$

Dividing by dt we obtain the boundary condition in the following form

$$w_x\frac{\partial F}{\partial x}+w_y\frac{\partial F}{\partial y}+w_z\frac{\partial F}{\partial z}+\frac{\partial F}{\partial t}=0. \qquad (2.4.3)$$

It is as a particular case, Eq. (2.4.2) is obtained for a fixed surface.

An example of a boundary condition given for a free surface is the equality of the pressure on it and the external pressure:

$$p(x, y, z, t)=p_e \qquad (2.4.4)$$

When investigating a heat-exchanging body placed in a flow, the boundary conditions can be, for example, the temperature distribution over the surface of the body or the heat flux through each point of the surface, or the temperature of the medium flowing around the body and the law governing the heat transfer between them.

2.5. SIMILARITY THEORY AND DIMENSIONAL ANALYSIS

The concept of dimensionality. Physical phenomena are mathematically described by means of relations holding between the quantities. This is, for example, the fact that the force F is proportional to the

mass m of a body and its acceleration j is expressed by the relation $F = \alpha mj$, α being the proportionality factor.

Physical quantities may be measured in various units: time - in seconds, minutes, hours; weight - in grams, kilograms, pounds, etc. The numerical value of the physical quantity depends on the choice of the measuring unit (scale). The system of measuring units must, therefore, be specified beforehand; it is finally convenient to choose it in such a way that the equations interrelating the quantities on the basis of the laws of nature become as simple as possible, for example, so that the proportionality factor α in the equation $F = \alpha mj$ becomes unity.

The measuring unit of a given physical quantity expressed in terms of the measuring units of the quantities upon which the system of units is based is called the dimension of the quantity. One and the same physical quantity may assume different dimensions in different systems of units.

The equations describing physical phenomena are subject to the rule that the dimensions of all components of the equation must be equal. At the same time dimensions may be arbitrarily attributed to all quantities entering the equation except one, which is called the derived quantity, in contradistinction to the others which are called the fundamental quantities.

The systems of measuring units adopted for the basic quantities are correspondingly called the fundamental systems. The dimensions of the derived quantities in each system are determined by the fundamental ones. The number of fundamental quantities and their choice is determined by concrete conditions.

In physics it is the CGS system of units that is used (fundamental quantities: length - centimeter, mass - gram, time - second;

in engineering it is the MKS system (length - meter, mass - kilogram, time - second) or the MKGS system (length - meter, force - kilogram, time - second).

The utilization of experiments in aeromechanics. With mathematical methods in their present state, the nonlinearity of the Eqs. (2.4.1), - the presence of terms like $\vec{\omega}\cdot\vec{\nabla}\rho$, $\vec{\omega}\cdot\vec{\nabla}T$ expressing the "entanglement" of fields, the presence of the convective term $(\vec{\omega}\cdot\vec{\nabla})\vec{\omega}$, the kinetic equation, and also the dependence of λ and μ on T, - does not allow of integrating the equations in their general form. This makes it necessary to simplify the equations in some way, such as discarding terms which are inessential for the given problem, replacing complex exact interrelations of quantities by approximate but simpler ones. Estimating the importance of the individual terms of the equation, the presuppositions, substitutions or the like, requires a knowledge of the relation between the quantities . . ., of the solution sought. The viscious circle thus obtained is broken in a certain measure by using experimental results and by building up empirical relations connecting the characteristics of state. From an analysis of these relations it is possible to derive suppositions for simplifying the equations. The correctness and accuracy by comparing the calculations with experiments.

The topic of the similarity theory. The equation set up as the result of analyzing the experimental data applies only to the concrete case for which it was derived.

One of the problems of the similarity theory and dimensional analysis is to establish the rules governing the generalization and extension of the results of experiments carried out under similar conditions to others, and also of determining the limits of applicability of these generalizations.

Regarded in a wider context, the similarity theory and dimensional analysis investigate the methods of applying the properties of invariance of mathematical and physical laws with respect to the choice of the system of units for describing the physical phenomena investigated.

Physical similarity. The term "similarity" is borrowed from geometry. Extending this concept to physical effects, we shall state: two physical effects are similar if the ratios of analogous physical quantities are the same at analogous instants of time and at all analogous points of space. In other words, in the general case physical phenomena are similar if each of them can be obtained from any other one by altering each of the quantities characterizing the effect by the same factor. This change can be effected, for example, by changing the fundamental quantities. Thus, in similar physical effects the change of the basic measuring units must transform the equations describing these effects together with the boundary conditions in such a way that they become equivalent. This is possible only in the case when each term of one equation is equal to the corresponding term of the other multiplied by a factor which is the same constant number for all terms of the equation. In particular, this will be the case if all quantities determining the physical [illegible] expressed in dimensionless form, i.e., if they refer each quantity to a certain predetermined value (scale) [illegible] characteristic of the given effect. These considerations form the basis of the theory of similarity.

The consideration of the conditions under which the dimensionless forms of the equations are analogous, together with the initial and boundary conditions, leads to the similarity criterion.

The dimensionless form of the equations of aeromechanics. As

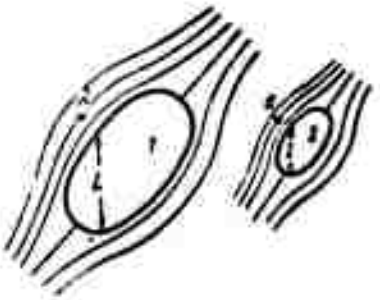


Fig. 2.5.1. Flow around ... tically similar ...odies.

the scale of variable quantities we take some arbitrary definite value of them at a selected instant of time and a selected point in space.

Assuming physically similar flows, ... denote (Fig. 2.5.1) nondimensial values in the same manner as dimensional ones, while the scale of the variable quantities is denoted by the subscript ... System (2.4.1) can then be represented in the following form ...ving in view that μ = const, c_v = const, and λ = const):

$$\frac{\rho_0}{t_0}\frac{\partial \rho}{\partial t}+\frac{\rho_0 w_0}{l_0}\nabla\cdot\rho\vec{w}=0;$$

$$\frac{\rho_0 w_0}{t_0}\rho\frac{\partial \vec{w}}{\partial t}+\frac{\rho_0 w_0^2}{l}\rho(\vec{w}\cdot\vec{\nabla})\vec{w}=\rho_0 f_0\rho\vec{f}-\frac{p_0}{l_0}\vec{\nabla}p+$$

$$+\frac{\mu_0 w_0}{l_0^2}\left(\vec{\nabla}\cdot\vec{\nabla}\vec{w}+\frac{1}{3}\vec{\nabla}\vec{\nabla}\cdot\vec{w}\right);$$

$$\frac{\rho_0 c_0 T_0}{t_0}\rho\frac{\partial T}{\partial t}+\frac{\rho_0 c_0 w_0 T_0}{l_0}\rho(\vec{w}\cdot\vec{\nabla})T+\frac{\lambda_0 T_0}{l_0^2}\vec{\nabla}\cdot\vec{q}+\frac{p_0 w_0}{l_0}p\vec{\nabla}\cdot\vec{w}=$$

$$=\frac{\mu_0 w_0^2}{l_0^2}\left\{2\left[\left(\frac{\partial w_x}{l_0}\right)^2+\dots\right]\right.;$$

$$\frac{p_0}{\rho_0 T_0}\cdot\frac{p}{\rho T}=R.$$

Transforming these equations and noting that $\frac{p_0}{\rho_0 T_0}=R$, we obtain

$$\left.\begin{aligned}
&\frac{l_0}{w_0 t_0}\frac{\partial \rho}{\partial t}+\vec{\nabla}\cdot\rho\vec{w}=0,\\
&\frac{l_0}{w_0 t_0}\rho\frac{\partial \vec{w}}{\partial t}+\rho(\vec{w}\cdot\vec{\nabla})\vec{w}=\frac{l_0 f_0}{w_0^2}\rho\vec{f}-\frac{p_0}{\rho_0 w_0^2}\vec{\nabla}p+\\
&+\frac{\mu_0}{l_0\rho_0 w_0}\left(\frac{1}{3}\vec{\nabla}\vec{\nabla}\cdot\vec{w}+\vec{\nabla}\cdot\vec{\nabla}\vec{w}\right),\\
&\frac{l_0}{w_0 t_0}\rho\frac{\partial T}{\partial t}+\rho(\vec{w}\cdot\vec{\nabla})T-\frac{\lambda_0}{l_0 c_0\rho_0 w_0}\vec{\nabla}\cdot\vec{q}+\frac{p_0}{l_0 c_0 T_0}p\vec{\nabla}\cdot\vec{w}=\\
&=\frac{\mu_0 w_0}{l_0\rho_0 c_0 T_0}\left\{2\left[\left(\frac{\partial w_x}{\partial x}\right)^2+\dots\right]\right.,\\
&p=\rho T.
\end{aligned}\right\}\qquad(2.5.1)$$

Similarity criteria. For complete similarity of motion the di-

mensionless forms of the equations must be analogous, i.e., the constant factors of the dimensionless terms must be equal. They are called criteria (numbers) of similarity:

$\frac{\omega_0 t_0}{l_0} = \mathrm{Sh}$ — the Strouhal number

$\frac{\omega_0^2}{f_0 l_0} = \mathrm{Fr}$ — the Froude number

$\frac{p_0}{\rho_0 \omega_0^2} = \mathrm{Eu}$ — the Euler number

$\frac{\rho_0 \omega_0 l_0}{\mu_0} = \mathrm{Re}$ — the Reynolds number

$\frac{c_{p0} \mu_0}{\lambda_0} = \mathrm{Pr}$ — the Prandtl number

$\frac{\omega_0}{a_0} = \mathrm{M}$ — the Maiyevskiy number*

Moreover the specific heat ratio, $k = \frac{c_p}{c_v}$, of the gas must be the same.

Introducing these numbers into Eq. (2.5.1) we obtain

$$\frac{1}{\mathrm{Sh}} \frac{\partial \rho}{\partial t} + \vec{\nabla} \cdot \rho \vec{w} = 0,$$

$$\frac{1}{\mathrm{Sh}} \rho \frac{\partial \vec{w}}{\partial t} + \rho (\vec{w} \cdot \vec{\nabla}) \vec{w} = \frac{1}{\mathrm{Fr}} \rho \vec{f} - \mathrm{Eu} \cdot \vec{\nabla} p + \frac{1}{\mathrm{Re}} \left(\frac{1}{3} \vec{\nabla} \vec{\nabla} \cdot \vec{w} + \vec{\nabla} \cdot \vec{\nabla} \vec{w} \right),$$

$$\frac{1}{\mathrm{Sh}} \rho \frac{\partial T}{\partial t} + \rho (\vec{w} \cdot \vec{\nabla}) T - \frac{k}{\mathrm{Pr} \cdot \mathrm{Re}} \vec{\nabla} \cdot \vec{q} + (k-1) p \vec{\nabla} \cdot \vec{w} =$$

$$= \frac{k(k-1)\mathrm{M}^2}{\mathrm{Re}} \left\{ 2 \left[\left(\frac{\partial w_x}{\partial x} \right)^2 + \cdots \right] \right\},$$

$$p = \rho T. \qquad (2.5.2)$$

Thus, motions are similar if their numbers Sh, Fr, M, Re, Pr, Eu and k are equal.

Similarity criteria as characteristics of the quantities of the terms of equations. From the demand that the dimensions of all components in the equation describing the physical phenomenon be equal it follows that any equation can be obtained in a dimensionless form by dividing all its terms by some arbitrarily chosen term of this equation. Introducing scales for the quantites entering the equation, each term of the equation can be written in the form of a product of two factors, one dimensional and the other dimensionless.

For example, assuming $\rho = \rho_0 \rho_1$, $\vec{w} = w_0 \vec{w}_1$, $x = l_0 x_1$, $y = l_0 y_1$, $z = l_0 z_1$ and $\vec{\nabla}_1 = \vec{i} \frac{\partial}{\partial x_1}$,

$+\vec{j}\frac{\partial}{\partial y_1}+\vec{k}\frac{\partial}{\partial z_1}$, we may put the convective term $\rho(\vec{w}\cdot\vec{\nabla})\vec{w}$ in the equation of motion equal to $\frac{\rho_0 w_0^2}{l_0}\left[\rho_1(\vec{w}_1\cdot\vec{\nabla}_1)\vec{w}_1\right]$, where $\frac{\rho_0 w_0^2}{l_0}$ is the dimensional characteristic of this term and $\rho_1(\vec{w}_1\cdot\vec{\nabla}_1)\vec{w}_1$ is the dimensionless one.

When the order of magnitude of the value of each dimensionless factor is taken to be unity, the value of each term of the equation will be characterized by the dimensional factor (coefficient). Therefore the similarity criteria, which are the ratios of the quantities characterizing the term of the equation to an arbitrary one of them, will indicate the order of each of them compared with the one of them taken as unity.

For example, the forces of friction are characterized by the

$$\frac{\mu w_0}{l_0^2}\left[(\vec{\nabla}_1\cdot\vec{\nabla}_1)\vec{w}_1+\frac{1}{3}\vec{\nabla}_1(\vec{\nabla}_1\cdot\vec{w}_1)\right].$$

The criterion $\mathbf{Re}=\frac{\rho_0 w_0^2}{l_0}:\frac{w_0\mu_0}{l_0^2}=\frac{\rho_0 w_0 l_0}{\mu_0}$ indicates the factor by which the acceleration of the forces of friction is smaller than the convective component of acceleration.

The number $\mathbf{Sh}=\frac{\rho_0 w_0^2}{l_0}:\frac{\rho_0 w_0}{t_0}=\frac{l_0}{w_0 t_0}$ indicates the factor by which the local acceleration component is smaller than the convective one. The meaning of the similarity numbers Eu, Fr is determined from the equation of motion by similar considerations.

Noting that the elastic forces per unit volume are proportional to κ_0/l_0, where K_0 is the compression modulus, we see that the number $M^2=(\rho_0 w_0^2/l_0):(K_0/l_0)=\frac{w_0^2}{K_0/\rho_0}=\frac{w_0^2}{a^2}$ indicates the factor by which the term characterizing the elastic forces is smaller than the convective component of acceleration.

In the same way, if the magnitudes of all terms of the energy equation are compared with the term $\rho(\vec{w}\cdot\vec{\nabla})c_v T$, characterizing the displacement of internal energy caused by transport (convection), the

energetic meaning of the similarity criteria can be established.

Analysis of the similarity conditions. Complete similarity requires that all similarity criteria be kept identical. In fact, there are special cases where some of the conditions may fall away (for example, in the case of a steady motion the number $Sh=\frac{wt}{l}$ falls away). In many cases, however, not all of the similarity conditions can be fulfilled. For example, when the same liquid flows around two bodies with the geometrical similarity $\frac{l_2}{l_1}=n$ the conditions

$$Sh=idem^1,\quad Re=idem \text{ и } M=idem,$$

must be satisfied, i.e., $\frac{w_1 t_1}{l_1}=\frac{w_2 t_2}{l_2}$; $\frac{\rho w_1 l_1}{\mu}=\frac{\rho w_2 l_2}{\mu}$; $\frac{w_1}{a}=\frac{w_2}{a}$,

which leads to the conditions

$$n w_1 t_1 = w_2 t_2;\quad w_1 = w_2 n \text{ and } w_1 = w_2.$$

which cannot be simultaneously satisfied.

In practice, therefore, the similarity conditions are only approximately fulfilled and, moreover, only those among them which are essential for the given concrete problem.

In most of the problems of aerohydromechanics the most important numbers are Sh, Re and M. When motions in which the volume forces play a decisive part are investigated, the Fr number becomes very important. An analysis of the energy transfer in a viscous gas of specific heat c_p realized by heat transfer characterized by the coefficient λ, indicated the necessity of keeping the number $Pr = c_p\mu/\lambda$ identical for similar flows.

Experiments show, however, that similarity is approximately accomplished over a large range of values of the similarity criteria. For example, the drag factor of badly streamlined bodies is virtually independent of Re; in these cases we speak about self-similar phenomena.

Dimensional analysis. The theory of similarity is closely related

to dimensional analysis, which makes it possible to set up a system of dimensionless numbers (criteria) characteristic of a given physical phenomenon by comparing the dimensions of the quantities which determine this phenomenon.

Basic theorems of dimensional analysis. There are two theorems constituting the basis of dimensional analysis. The first of them originates from the fact that the ratio of two numerical values of derived quantity must not depend on the choice of the scale of the fundamental quantities. For example, the ratio of two values of velocity is independent of whether they are expressed in cm/sec or m/sec. It can be shown [2.2] that this will be true if the dimensions of derived quantities have the form of a power monomial:

$$S = A_1^{\alpha} A_2^{\beta} \ldots, \qquad (2.5.3)$$

where $A_1 = [a_1]$, $A_2 = [a_2]$ are the dimensions of the fundamental quantities ... and $S = [s]$ is the dimension of the derived quantity s.

The second theorem ("π-theorem") is based on the fact that the mathematical formulation of physical laws does not depend on the choice of the system of measuring units and therefore any relation between dimensioned quantities can be reduced to a relation between dimensionless quantities.

Let the dimensioned quantity a be a function of the dimensioned quantities $a_1, a_2, \ldots, a_{k-1}, a_k, a_{k+1}, \ldots, a_n$:

$$a = f(a_1, a_2, \ldots, a_{k-1}, a_k, a_{k+1}, \ldots, a_n), \qquad (2.5.4)$$

among which $a_1, a_2, \ldots, a_k$ have independent dimensions, i.e., it is impossible to express the dimension of any of them as a power monomial of the dimensions of the other quantites, whereas the quantities $a_{k+1}, a_{k+2}, \ldots, a_n$ can be expressed in terms of the quantities $a_1, a_2, \ldots, a_k$.

For example, the dimensions of the length l, of the speed $w = l/t$,

and of the density ($kg\text{-}sec^2/m^4$) are independent but the dimensions of length $\underline{l}$, speed $\underline{w}$, and acceleration $\underline{l}/t^2$ are interrelated. Obviously, the number of quantities with independent dimensions must be smaller than or equal to the number of fundamental quantities.

Then, denoting by π with appropriate subscripts the dimensionless combinations of one of the dependent quantities with independent ones.

$$\pi = \frac{a}{a_1^{\alpha_1} \cdot a_2^{\alpha_2} \cdot \ldots \cdot a_k^{\alpha_k}}; \quad \pi_1 = \frac{a_{k+1}}{a_1^{\beta_1} \cdot a_2^{\beta_2} \cdot \ldots \cdot a_k^{\beta_k}}; \quad \ldots \pi_{n-k} = \frac{a_n}{a_1^{\gamma_1} \cdot a_2^{\gamma_2} \cdot \ldots \cdot a_k^{\gamma_k}}.$$

it can be shown that

$$\pi = \varphi(\pi_1, \pi_2, \ldots, \pi_{n-k}). \tag{2.5.5}$$

This fact, establishing the possibility of a transition from relations between dimensioned quantities to equivalent dimensionless relations serves as a basis for applying the theory of dimensions.

Example. Let us consider the determination of the force R acting on a body in the flow of a liquid.

First we assume that the motion of the liquid is slow enough for the inertial forces to be assumed to be negligibly small as compared with the forces of viscosity. In other words, the parameters to be determined will be the velocity $\underline{w}$, the linear dimension $\underline{l}$ of the body, and the viscosity μ of the liquid, and we can put

$$R = Cl^{\alpha} w^{\beta} \mu^{\gamma},$$

where C is a dimensionless coefficient that depends on the shape of the body and its position relative to the flow.

The dimensional formula will be

$$[R] = [l]^{\alpha} [w]^{\beta} [\mu]^{\gamma}$$

or

$$[кГ] = [м]^{\alpha} [м/сек]^{\beta} [кГ \cdot сек/м^2]^{\gamma}.$$

Hence we obtain immediately $\gamma = 1$, $\beta = 1$, $\alpha = 1$ and the relation

for the force

$$R = C_1 \mu l w = \frac{C_1}{Re} \frac{\rho w^2}{2} l^2 \quad \left(Re = \frac{wl}{\nu}\right).$$

When the forces of inertia are large with respect to all other forces we may assume

$$R = C_2 l^2 w^2 \rho^2$$

C_2 being a dimensionless factor for the shape of the body, or

$$\kappa\Gamma = (m)^{\alpha} (m/sec)^{\beta} (\kappa\Gamma \sec^2/m^4)^{\gamma}.$$

The solution yields $\gamma = 1$, $\beta = 2$, $\alpha = 2$ and $R = C_2 \frac{\rho w^2}{2} l^2$.

In the general case we may assume that the force R depends on the speed w of the flow, the linear body dimension l, the density ρ of the liquid, its viscosity μ, the compressibility K, the stress of the volume forces f, and the period t of the body's vibrations.

Writing this relation in the form of an equation

$$R = F(w, \rho, l, \mu, f, K, t)$$

and taking the quantities w, ρ, l as the basic system we set up the possible dimensionless combinations of each of the derived quantities with the basic ones:

$$\frac{R}{\rho w^2 l^2}, \frac{\mu}{\rho w l}, \frac{K}{\rho w^2}, \frac{f}{\rho w^2}, \frac{tw}{l}.$$

If we note that $K/\rho = a^2$, the third dimensionless combination may be represented as a^2/w^2, and, according to the "π-theorem," we can then write

$$\frac{R}{\rho w^2 l^2} = f\left(\frac{wl}{\nu}, \frac{w^2}{c^2}, \frac{w^2}{fl}, \frac{tw}{l}\right) = f(Re, Ma, Fr, Sh) = C$$

or

$$R = C \rho w^2 l^2,$$

where C is a coefficient that depends on the shape of the body, its position relative to the flow, and the numbers Re, M, Fr, Sh.

2.6. METHODS OF SOLVING THE EQUATIONS OF MECHANICS OF A VISCOUS INCOMPRESSIBLE FLUID

Exact solutions to the equations of aerohydromechanics (2.4.1) can be obtained only in the case of what is called laminar (stratified) motion when Newton's law on the linear relation between stresses and deformation rates, $\tau = \mu \frac{\partial w}{\partial n}$, is valid, where μ is a physical constant of the fluid; the derivation of the Navier - Stokes equation is based on this law. The number of exactly solved problems is greatly restricted due to the nonlinearity of the equations caused by the convective terms. The solution is simplified when the convective terms of the equations become zero either due to an appropriate statement of the problem or due to additional suppositions.

Flow of a viscous fluid in a tube. Let us consider by way of an example the steady flow of a viscous incompressible fluid in a circular-cylindrical tube of radius r_0. In this case ($w_y = w_z = 0$), it follows from the continuity equation $\partial w_x / \partial x = 0$ that, when mass forces are absent, the speed may vary only transversaly to the tube: $w_x = w = w(y, z)$.

The projection of the equation of motion onto the axes x, y, z

$$\left.\begin{aligned} \frac{\partial p}{\partial x} &= \mu\left(\frac{\partial^2 w}{\partial y^2} + \frac{\partial^2 w}{\partial z^2}\right), \\ \frac{\partial p}{\partial y} &= 0, \\ \frac{\partial p}{\partial z} &= 0 \end{aligned}\right\} \qquad (2.6.1)$$

shows that the pressure p can be a function only of x.

Since the right-hand part of the equation $\frac{\partial p}{\partial x} = \mu\left(\frac{\partial^2 w}{\partial y^2} + \frac{\partial^2 w}{\partial z^2}\right)$ can depend only on y and z, and the left-hand only on x, both parts must be equal to one and the same constant number:

$$\mu\left(\frac{\partial^2 w}{\partial y^2} + \frac{\partial^2 w}{\partial z^2}\right) = \left(\frac{dp}{dx}\right) = \text{const} = -\frac{p_1 - p_2}{l}, \qquad (2.6.2)$$

where $p_1 - p_2$ is the pressure drop over the length l of the tube.

For integrating we naturally pass over to a cylindrical coordinate system $x=x$, $r=\sqrt{y^2+z^2}$, $\theta=\operatorname{arctg}(y/z)$.

Calculating

$$\frac{\partial w}{\partial y}=\frac{\partial w}{\partial r}\cdot\frac{\partial r}{\partial y}=\frac{\partial w}{\partial r}\cdot\frac{y}{r};$$
$$\frac{\partial^2 w}{\partial y^2}=\frac{\partial^2 w}{\partial r^2}\cdot\frac{y^2}{r^2}+\frac{\partial w}{\partial r}\cdot\frac{r^2-y^2}{r^3};$$
$$\frac{\partial^2 w}{\partial z^2}=\frac{\partial^2 w}{\partial r^2}\cdot\frac{z^2}{r^2}+\frac{\partial w}{\partial r}\cdot\frac{r^2-z^2}{r^3}$$

and replacing the partial derivatives by the total ones, we obtain owing to the symmetry of w = w (r)

$$\mu\left(\frac{d^2w}{dr^2}+\frac{1}{r}\frac{dw}{dr}\right)=\frac{\mu}{r}\frac{d}{dr}\left(r\frac{dw}{dr}\right)=-\frac{p_1-p_2}{l}. \qquad (2.6.3)$$

Hence

$$r\frac{dw}{dr}=-\frac{1}{2\mu}\frac{p_1-p_2}{l}r^2+A$$

and

$$w=\frac{1}{4\mu}\frac{p_1-p_2}{l}r^2+A\ln r+B. \qquad (2.6.4)$$

The boundary conditions (finite speed over all the region and zero speed at the tube walls) give A = 0 and $B=\frac{1}{4\mu}\cdot\frac{\Delta p}{l}r_0^2$.

Thus

$$w=\frac{1}{4\mu}\frac{p_1-p_2}{l}(r_0^2-r^2). \qquad (2.6.5)$$

The flow rate per second is

$$V=\int_0^{r_0}2\pi r w\,dr=\frac{p_1-p_2}{8\mu l}\pi r_0^4. \qquad (2.6.6)$$

and the mean speed

$$w_m=\frac{V}{\pi r_0^2}=\frac{p_1-p_2}{8\mu l}r_0^2=\frac{w_{max}}{2}. \qquad (2.6.7)$$

where w_{max} being the maximum speed at the tube axis (r = 0).

From the equation $2\pi r l\tau=-(p_1-p_2)\pi r^2$, valid for any r it follows that the tangential stresses are linearly distributed with respect to the radius

$$\tau=\tau_0\frac{r}{r_0},$$

where τ_0 is the stress at the wall (for $r = r_0$).

The vortical character of a laminar flow. Laminar flow is often erroneously described as a vortex-free potential motion. In fact, in a laminar motion each particle is rotating; for example, calculating the components of angular velocity for a laminar motion in a circular tube we obtain

$$\omega_x = \frac{1}{2}\left(\frac{\partial w_z}{\partial y} - \frac{\partial w_y}{\partial z}\right) = 0;$$
$$\omega_y = \frac{1}{2}\left(\frac{\partial w_x}{\partial z} - \frac{\partial w_z}{\partial x}\right) = -w_{max}\frac{z}{r_0^2};$$
$$\omega_z = \frac{1}{2}\left(\frac{\partial w_y}{\partial x} - \frac{\partial w_x}{\partial y}\right) = -w_{max}\frac{y}{r_0^2}.$$

Thus, the angular velocity $\omega = \sqrt{\omega_x^2 + \omega_y^2 + \omega_z^2} = w_{max}\frac{r}{r_0^2}$ increases proportionally to the distance from the tube axis where it is equal to zero.

The drag coefficient for round tubes is determined by the relation

$$p_1 - p_2 = \zeta \frac{l}{r_0}\frac{\rho w_m^2}{2}. \qquad (2.6.8)$$

Comparing it with Eq. (2.6.7) we find

$$\zeta = \frac{16}{\frac{w_m r_0}{\nu}} = \frac{16}{Re}.$$

The critical Re number and turbulence. The value obtained for the coefficient is very well verified by experiment provided the Re number does not exceed a certain value called the critical value, $\frac{w_m D}{\nu} \approx 2000$, beyond which the laminar (stratified) form of motion is disturbed owing to stability losses during random disturbances. The flow, maintaining its average motion, becomes irregular and disordered. This form of flow is called turbulent flow.

The most recent experiments have shown that with special precautionary measures against initial disturbances it is possible to reach a critical number Re_{kr} which considerably exceeds the value

obtained under normal conditions, namely up to 50,000. We can therefore speak of two critical numbers Re_{kr}: a lower and fairly stable one below which no turbulence may occur for a given channel, and an upper one that depends on the experimental conditions.

Figure 2.6.1 shows a sketch of a device in which the transition from one form of motion to another can be observed. For a number $Re < Re_{kr}$ the colored stria passes through the tube in the form of a sharply drawn color thread. But as soon as the Re number surpasses the critical value the thread splits at certain sites and the entire fluid in the tube becomes colored (Fig. 2.6.2).



Fig. 2.6.1. Diagram of device for demonstrating the laminar and turbulent forms of motion. 1) Colored water; 2) water.

Figure 2.6.3 shows the resistance factor as a function of the Reynolds number $Re = \frac{Dw}{\nu}$

The two regions of the flow of a viscous fluid. Since exact solutions to the equation of motion of a viscous fluid can be obtained only in a very limited number of cases, basically the problem must be solved for one approximate statement or another.

Disregarding very slow motions, what are called "creeping" motions, we consider the case of the motion of a fluid at speeds which are low compared with that of sound when the compressibility of the air can be neglected. In this case the continuity equation and the equation of motion will read

$$\operatorname{div} \vec{w} = \frac{\partial w_x}{\partial x} + \frac{\partial w_y}{\partial y} + \frac{\partial w_z}{\partial z} = 0,$$

$$\frac{d\vec{w}}{dt} = \vec{f} - \frac{1}{\rho}\vec{\nabla} p + \nu \Delta \vec{w}.$$

As has been shown by N. Ye. Zhukovskiy, the system written

GRAPHIC NOT REPRODUCIBLE

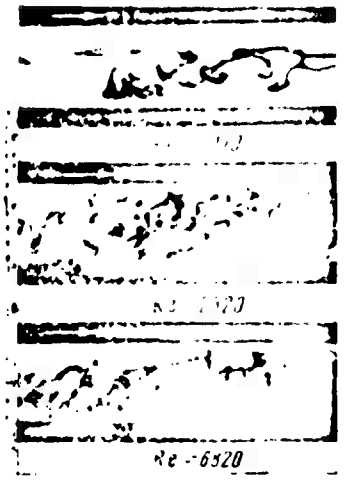


Fig. 2.6.2. Formation of turbulence in a tube.

down applies to a motion with potential speed, i.e., with $\vec{w} = \vec{\nabla}\Phi$ and, therefore,

$$\text{curl } \vec{w} = 0.$$

In fact, by virtue of $\text{div } \vec{w} = 0$, we have

$$\Delta\vec{w} = (\vec{\nabla}\cdot\vec{\nabla})\,\vec{w} = (\vec{\nabla}\cdot\vec{\nabla})\,\vec{\nabla}\Phi =$$
$$= \left(\frac{\partial^2}{\partial x^2} + \frac{\partial^2}{\partial y^2} + \frac{\partial^2}{\partial z^2}\right)\left(\vec{i}\frac{\partial}{\partial x} + \vec{j}\frac{\partial}{\partial y} + \vec{k}\frac{\partial}{\partial z}\right)\Phi =$$
$$= \vec{i}\frac{\partial}{\partial x}\Delta\Phi + \vec{j}\frac{\partial}{\partial y}\Delta\Phi + \vec{k}\frac{\partial}{\partial z}\Delta\Phi = \text{grad}\,\Delta\Phi = \text{grad div}\,\vec{w} = 0$$

The physical meaning of this is that, in the presence of a potential speed $\vec{w} = \vec{\nabla}\Phi$, the forces of viscosity are counterbalanced in every volume element. Therefore the term that takes the viscosity effect in the kinetic equation into account that falls away.

GRAPHIC NOT REPRODUCIBLE

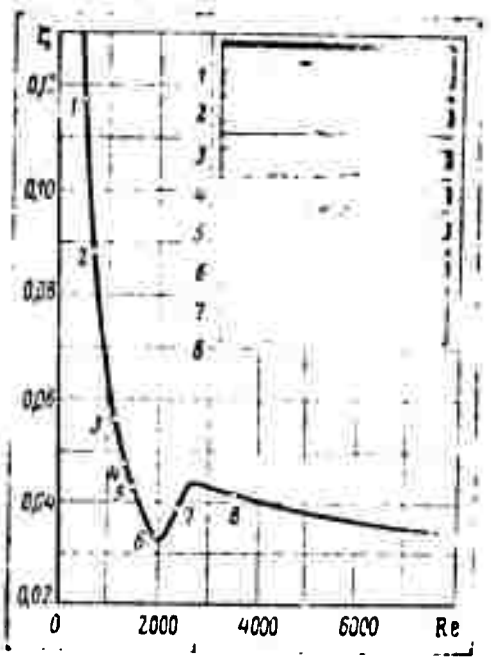


Fig. 2.6.3. Drag coefficient of motion of a fluid in a tube as a function of the Re number. The circles on the curve correspond to the given photographs of the form of motion.

In a potential motion, however, the boundary conditions cannot be satisfied in general; for a viscous fluid they consist in the demand that both the normal and the tangential speed components at the wall of the body must vanish:

$$w_n = \frac{\partial \Psi}{\partial n} = 0, \quad w_s = \frac{\partial \Phi}{\partial s} = 0. \tag{2.6.9}$$

The first condition $w_n = 0$ characterized the impermeability of the solid wall, which must necessarily consist of streamlines. The second condition indicates that the fluid layer directly adjacent to the wall must have the same speed as the wall itself. The fluid, so to speak, adheres to its boundary surfaces. This condition, first expressed by D.I. Mendeleyev and applied by N.Ye. Zhukovskiy, has been verified by many very accurate experiments.

The simultaneous observation of these boundary conditions leads to a constant value of the potential, Φ = const, i.e., to complete absence of motion, to a standstill. The impossibility of satisfying the boundary conditions in the presence of a velocity potential indicates the presence of vortex formation near the walls and near the boundaries of the body.

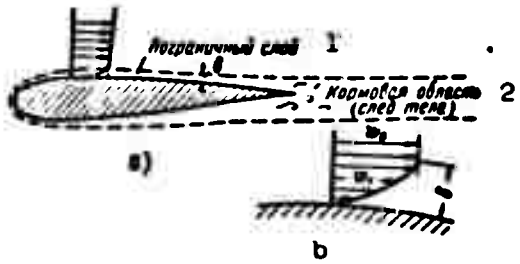


Fig. 2.6.4. When a viscous liquid flows around a body a boundary layer is formed on its boundaries (a); velocity profile in the boundary layer (b). 1) Boundary layer; 2) stern region (wake of body).

The flow of a viscous fluid streaming around a solid body can thus be subdivided into two regions: a continuously turbulent layer directly adjacent to the body where the viscosity appears, and the

remaining fluid outside the layer where the flow can be described sufficiently well by the equation for an inviscid fluid.

The thickness of the laminar boundary layer. Let us estimate the thickness of the layer in which the forces of viscosity play an appreciable part, i.e., where they are of the same order of magnitude as the forces of inertia. This layer is called the boundary layer. Let us consider the plane motion of an incompressible fluid at the boundary of a sufficiently long body (Fig. 2.6.4). When w_x is assumed to be of the order of magnitude of the undisturbed speed w of flow and x of the order of magnitude of the length l of the body, $\partial w_x/\partial x$ will be of the order of w/l. Denoting by δ the thickness of the boundary layer the ordinates y $(0 \leq y \leq \delta)$ can be taken as being of the order of δ; consequently, from the continuity equation $\partial w_x/\partial x = -\partial w_y/\partial y$ we arrive at

$$w\,l \sim w_y\,\delta,$$

whence we deduce that the transverse speed w_y is of the order of $\frac{\delta}{l}w$. Therefore, the convective term of acceleration is

$$(\vec{w}\cdot\vec{\nabla})\vec{w} = w_x\frac{\partial w_x}{\partial x} + w_y\frac{\partial w_x}{\partial y} \sim \frac{w^2}{l}.$$

The forces of viscosity ($\operatorname{div}\vec{\tau} = 0$) are characterized by the term $\mu\left(\frac{\partial^2 w_x}{\partial x^2} + \frac{\partial^2 w_x}{\partial y^2}\right)$. The first term $\mu\frac{\partial^2 w_x}{\partial x^2} \sim \mu\frac{w}{l^2}$, and the second $\mu\frac{\partial^2 w_x}{\partial y^2} \sim \mu\frac{w}{\delta^2}$; since the experiment shows that $\delta \ll l$, the first component can be neglected and the forces of viscosity can be assumed to be $\sim \mu\frac{w}{\delta^2}$. Since in the boundary layer all terms are of the same order of magnitude as the inertial ones, we have

$$\rho\frac{w^2}{l} \sim \mu\frac{w}{\delta^2}, \text{ whence } \frac{\delta}{l} \sim \frac{1}{\sqrt{Re}};$$

$$Re = \frac{wl}{\nu}. \qquad (2.6.10)$$

For a plane plate an approximate solution to the equation of laminar motion of an incompressible fluid yields a velocity distri-

bution that is in good agreement with experiment and from which $\delta = 5.5\frac{x}{\sqrt{Re_x}}$ can be derived (cf. Fig. 6.1.1). In this thin layer a sudden change of velocity occurs which induces the formation of very intense vortices. These vortices are carried along by the outer flow and penetrate into the outer region of flow and strongly affect the form of motion behind the body.

Stability of flow. Disturbances from various origins can be superimposed on a laminar flow, which, provided they do not reach the lower number Re_{kr} die out with time. However, as has been shown, when the lower value of Re_{kr} is surpassed, the disturbances, even those which have arisen at random, start growing and the flow becomes turbulent. The fact than when special precautions are taken against random disturbances the critical Re number can be considerably raised, shows that the appearance of turbulence is connected with a loss of stability of the laminar motion.

When solving a problem on the stability of the motion, the method of imposing small disturbances on the basic motion is usually applied. For. e.g. a liquid, it is assumed that the velocity is $w = w_0 + w'$, the pressure $p = p_0 + p'$, the density $\rho = \rho + \rho'$, etc., the zero subscripts referring to the basic motion (which is only coordinate-dependent) and the primes to the disturbances (depending on coordinates and time). These values of $\underline{w}$, p, ρ,... etc. are substituted in the fundamental equations. Neglecting terms of more than first order we obtain a linearized system of equations with respect to the disturbances w', p', ρ',... with coefficients depending only on the coordinates.

The general solution is usually sought as the sum of particular solutions of the form of $L = L_0(x, y, z)e^{\nu t}$, where L is the amplitude and ν the frequency of the disturbances. If the roots of the system of

algebraic equations obtained are complex for the frequency ν, i.e., if $\nu = \nu_1 + i\nu_2$, the problem as to the stability is solved by the sign of ν_2. When $\nu_2 > 0$ the disturbance will have a real factor $e^{-\nu_2 t}$ and the motion is stable. When $\nu_2 < 0$ the factor $e^{-\nu_2 t}$ grows boundlessly, i.e., the basic motion is unstable.

Applying this method to a flow between two parallel planes shows that stability depends on the shape of the normal velocity distribution. When it is convex, α, (Fig. 2.6.5), some minimum value $Re = Re_{\alpha kr}$ will exist and the disturbance will be intensified when this value is passed through. As $Re \to \infty$ both branches (a) of the curve determining the stability limits approach the abscissa ($\nu \to 0$). The presence of an inflection point in the normal velocity distribution (β) reduces $Re_{\beta kr}$ and as $Re \to \infty$ the two branches of the curve approach different limits, $\nu = 0$ and $\nu > 0$.

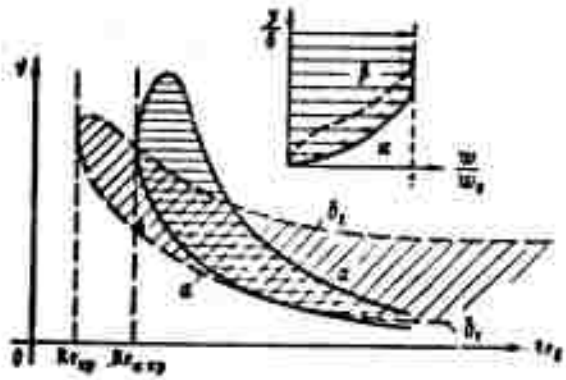


Fig. 2.6.5. The region of undamped frequencies is shaded. The existence of a laminar flow is connected with the attenuation of disturbances of arbitrary frequencies. The lower critical number Re_{kr} for convex normal velocity distribution (α) is larger than Re_{kr} for the normal velocity distribution with an inflection point (β).

We notice that in the boundary layer, in the case of a positive pressure gradient $dp/dx > 0$, the normal velocity distribution has an inflection point.

Figure 2.6.5 shows the region of undisturbed oscillations

(shaded) in the coordinates disturbance frequency (ν) versus Re number. It is obvious that the laminar flow will be everywhere to the left of the line tangential to this region and parallel to the frequency axis, so that for any $Re > Re_{kr}$ the random disturbances with undamped frequencies cause the flow to become turbulent. In the case of distributions without inflection points the frequency region for undamped oscillations decreases with increasing Re number.

The motion of an inviscid fluid as a limiting case of turbulent motion with $Re \to \infty$. It must be noticed that as the Re number increases turbulent flow approaches a flow of an inviscid fluid and the limiting case of zero viscosity ($\mu = 0$) corresponds formally to $Re \to \infty$. Experiments show that with a flow in a round tube the radial velocity distribution can be represented by a power function

$$w_x = w_{max}\left(1 - \frac{r}{r_0}\right)^q = w_{max}\left(\frac{y}{r_0}\right)^q.$$

With an increase in Re the exponent q diminishes (see Fig. 2.6.6) and the velocity profile in the tube evens out, tending in the limit case ($Re \to \infty$) to uniformity. In the case of turbulent flow the transition from layer to layer because of pulsations is achieved in large volumes (moles) of fluid, i.e., in addition to molecular momentum transfer there is also the so-called molar exchange which leads to an increase in internal friction, but at the same time smoothes out the velocities in the flow.

The statistical method of investigating turbulent motion. The entire chaos of the pulsation of both the magnitude and direction of the velocity at each point of the turbulent flow justifies the application of the statistical method for investigating this form of fluid motion.

We represent the true value of every parameter of the flow as the sum of the mean ($\bar{u}$) and the pulsating (u') values:

$$u=\tilde{u}+u'. \qquad (2.6.11)$$

Averaging can be carried out over space and time.

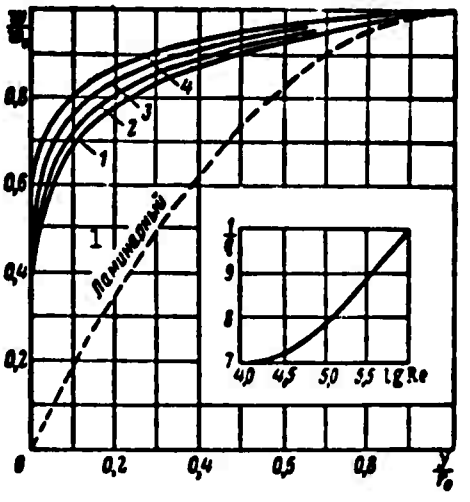


Fig. 2.6.6 With increasing Re number the velocity distribution in the tube flattens; it is [illegible] described by the equation $w = w_0(y/r)^q$, where $q = f(\mathrm{Re})$. 1) Laminar.

Time averaging. The quantity u is averaged over time (Fig. 2.6.7) in the following manner:

$$\tilde{u}(x, y, z, t)=\frac{1}{t_n}\int_{t-\frac{t_n}{2}}^{t+\frac{t_n}{2}} u(x, y, z, t)\,dt. \qquad (2.6.12)$$

where t_n is the averaging period, which must be large enough compared with the pulsation period to make the mean value $\tilde{u}'$ of pulsation, as a mean random quantity, vanish in this interval. But on the other hand, since the averaged function in the averaging period is a straight line parallel to the abscissa (time axis), the averaging period must be sufficiently small to indicate correctly the way in which the function $\tilde{u}$ varies with time. It can be shown that the

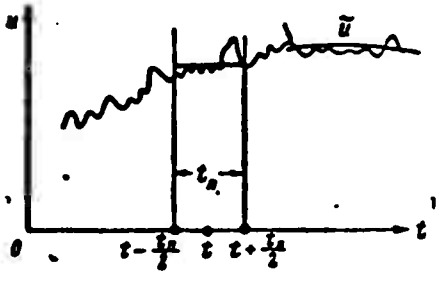


Fig. 2.6.7. Time averaging.

averaging always gives the same value of the averages quantities, $\tilde{\tilde{u}} = \tilde{u}$.

The properties of averaging are the following

$$\left.\begin{aligned} &\widetilde{s+v}=\tilde{s}+\tilde{v}, \\ &\widetilde{\frac{\partial u}{\partial t}}=\frac{\partial \tilde{u}}{\partial t};\ \widetilde{\frac{\partial u}{\partial s}}=\frac{\partial \tilde{u}}{\partial s}\ (s=x,\ y,\ z). \\ &\widetilde{uv}=\tilde{u}\tilde{v}. \end{aligned}\right\} \qquad (2.6.13)$$

If $\tilde{u} = \tilde{u}(t)$ the latter property is postulated.

Averaging of the equations of hydromechanics. We average the equation of motion (2.2.5) and the continuity equation (2.1.5) of a viscous incompressible fluid

$$\rho\frac{d\vec{w}}{dt}=\rho\vec{f}+\frac{\partial\vec{p}_x}{\partial x}+\frac{\partial\vec{p}_y}{\partial y}+\frac{\partial\vec{p}_z}{\partial z}.$$

$$\vec{\nabla}\cdot\vec{w}=0.$$

Since the speed and the other quantities vary not only in magnitude but also in direction, averaging is carried out with the projections of the equation of motion.

In accordance with (2.6.11) we put

$$w_x=\tilde{w}_x+w_x',\ w_y=\tilde{w}_y+w_y',$$

$$w_z=\tilde{w}_z+w_z'.$$

Noting that div $\vec{w} = 0$, we write

$$w_x\frac{\partial w_x}{\partial x}+w_y\frac{\partial w_x}{\partial y}+w_z\frac{\partial w_x}{\partial z}=\frac{\partial w_x^2}{\partial x}+\frac{\partial w_xw_y}{\partial y}+\frac{\partial w_xw_z}{\partial z}$$

and, by virtue of (2.6.13), we obtain

$$\overline{w_x\frac{\partial w_x}{\partial x}}+\overline{w_y\frac{\partial w_x}{\partial y}}+\overline{w_z\frac{\partial w_x}{\partial z}}=\overline{\frac{\partial}{\partial x}\left[\left(\tilde{w}_x+w_x'\right)\left(\tilde{w}_x+w_x'\right)\right]}+$$

$$+\overline{\frac{\partial}{\partial y}\left[\left(\tilde{w}_y+w_y'\right)\left(\tilde{w}_x+w_x'\right)\right]}+\overline{\frac{\partial}{\partial z}\left[\left(\tilde{w}_z+w_z'\right)\left(\tilde{w}_x+w_x'\right)\right]}=$$

$$=\frac{\partial}{\partial x}\left(\overline{\tilde{w}_x\tilde{w}_x}+\overline{\tilde{w}_xw_x'}+\overline{w_x'\tilde{w}_x}+\overline{w_x'w_x'}\right)+\frac{\partial}{\partial y}\left(\overline{\tilde{w}_x\tilde{w}_y}+\overline{\tilde{w}_xw_y'}+\right.$$

$$+\overline{w_x'w_y'}+\overline{w_x'\tilde{w}_y}\Big)+\frac{\partial}{\partial z}\Big(\overline{\tilde{w}_x\tilde{w}_z}+\overline{\tilde{w}_x w_z'}+\overline{w_x'\tilde{w}_z}+\overline{w_x'w_z'}\Big)=$$

$$-\frac{\partial}{\partial x}\Big(\tilde{w}_x\tilde{w}_x+\overline{\tilde{w}_x^2}\Big)+\frac{\partial}{\partial y}\Big(\tilde{w}_x\tilde{w}_y+\overline{w_x'w_y'}\Big)+\frac{\partial}{\partial z}\Big(\tilde{w}_x\tilde{w}_z+\overline{w_x'w_z'}\Big)=$$

$$-\tilde{w}_x\frac{\partial\tilde{w}_x}{\partial x}+\tilde{w}_x\frac{\partial\tilde{w}_y}{\partial y}+\tilde{w}_x\frac{\partial\tilde{w}_z}{\partial z}+\tilde{w}_x\frac{\partial\tilde{w}_x}{\partial x}+\tilde{w}_y\frac{\partial\tilde{w}_x}{\partial y}+\tilde{w}_z\frac{\partial\tilde{w}_x}{\partial z}+$$

$$+\frac{\partial}{\partial x}\overline{\tilde{w}_x^2}+\frac{\partial}{\partial y}\Big(\overline{w_x'w_y'}\Big)+\frac{\partial}{\partial z}\Big(\overline{w_x'w_z'}\Big).$$

Averaging the continuity equation gives

$$\frac{\partial w_x}{\partial x}+\frac{\partial w_y}{\partial y}+\frac{\partial w_z}{\partial z}=\frac{\partial\tilde{w}_x}{\partial x}+\frac{\partial\tilde{w}_y}{\partial y}+\frac{\partial\tilde{w}_z}{\partial z}=0 \qquad (2.6.14)$$

and the first trinomial of the equation previously written down vanishes; therefore

$$\frac{d\tilde{w}_x}{dt}=\frac{\partial\tilde{w}_x}{\partial t}+\tilde{w}_x\frac{\partial\tilde{w}_x}{\partial x}+\tilde{w}_y\frac{\partial\tilde{w}_x}{\partial y}+\tilde{w}_z\frac{\partial\tilde{w}_x}{\partial z}+\frac{\partial}{\partial x}\Big(\overline{w_x'w_x'}\Big)+$$
$$+\frac{\partial}{\partial y}\Big(\overline{w_x'w_y'}\Big)+\frac{\partial}{\partial z}\Big(\overline{w_x'w_z'}\Big).$$

Since

$$\vec{p}_x=\vec{i}\sigma_x+\vec{j}\tau_{xy}+\vec{k}\tau_{xz},\quad \sigma_x=-p+\tau_{xx},$$
$$p_y=\vec{i}\tau_{yx}+\vec{j}\sigma_y+\vec{k}\tau_{yz},\quad \sigma_y=-p+\tau_{yy},$$
$$p_z=\vec{i}\tau_{zx}+\vec{j}\tau_{zy}+\vec{k}\sigma_z,\quad \sigma_z=-p+\tau_{zz},$$
$$\tilde{\vec{p}}_x=\vec{i}\tilde{\sigma}_x+\vec{j}\tilde{\tau}_{xy}+\vec{k}\tilde{\tau}_{xz}.$$

we have for example

Here

$$\tilde{\sigma}_x=-\tilde{p}+2\mu\overline{\frac{\partial w_x'}{\partial x}}=-\tilde{p}+2\mu\frac{\partial\tilde{w}_x}{\partial x}=-\tilde{p}+\tilde{\tau}_{xx},$$

$$\tilde{\tau}_{xy}=\mu\Big(\overline{\frac{\partial w_x'}{\partial y}+\frac{\partial w_y'}{\partial x}}\Big)=\mu\Big(\frac{\partial\tilde{w}_x}{\partial y}+\frac{\partial\tilde{w}_y}{\partial x}\Big),$$

$$\tilde{\tau}_{xz}=\mu\Big(\overline{\frac{\partial w_x'}{\partial z}+\frac{\partial w_z'}{\partial x}}\Big)=\mu\Big(\frac{\partial\tilde{w}_x}{\partial z}+\frac{\partial\tilde{w}_z}{\partial x}\Big).$$

Thus, $\tilde{\vec{p}}_x$ is made up with respect to $\tilde{p}$ and $\tilde{w}$ as $\vec{p}_x$ with respect to the true p and $\underline{w}$.

Therefore for the projection of the kinetic equation onto the x-axis we obtain

$$\rho\left(\frac{\partial\tilde{w}_x}{\partial t}+\tilde{w}_x\frac{\partial\tilde{w}_x}{\partial x}+\tilde{w}_y\frac{\partial\tilde{w}_y}{\partial y}+\tilde{w}_z\frac{\partial\tilde{w}_x}{\partial z}\right)=\rho\tilde{f}_x+\frac{\partial\tilde{\sigma}_x}{\partial x}+\frac{\partial\tilde{\tau}_{yx}}{\partial y}+\frac{\partial\tilde{\tau}_{zx}}{\partial z}-$$

$$-\rho\left(\frac{\partial}{\partial x}\overline{\tilde{w}_x^2}+\frac{\partial}{\partial y}\overline{\tilde{w}_x\tilde{w}_y}+\frac{\partial}{\partial z}\overline{\tilde{w}_x\tilde{w}_z}\right)=\rho\tilde{f}_x-\frac{\partial\tilde{p}}{\partial x}+$$

$$+\frac{\partial}{\partial x}\left(\tilde{\tau}_{xx}-\rho\overline{\tilde{w}_x^2}\right)+\frac{\partial}{\partial y}\left(\tilde{\tau}_{yx}-\rho\overline{\tilde{w}_x\tilde{w}_y}\right)+\frac{\partial}{\partial z}\left(\tilde{\tau}_{zx}-\rho\overline{\tilde{w}_x\tilde{w}_z}\right) \qquad (2.6.15)$$

and analogous expressions for the projections on the y and z axes.

Turbulent stresses. By comparing the equations of motion (2.6.15) and (2.2.5) it can be seen that velocity pulsation leads to the appearance of additional (turbulent) stresses.

The stresses on an area perpendicular to the x-axis are equal to

$$\tau_{\text{турб}\,xx}=-\rho\overline{\tilde{w}_x^2};\quad \tau_{\text{турб}\,xy}=-\rho\overline{\tilde{w}_x\tilde{w}_y};\quad \tau_{\text{турб}\,xz}=-\rho\overline{\tilde{w}_x\tilde{w}_z}.$$

Setting up analogous expressions for the other axes, we can write down the matrix of the turbulent stresses:

$$\begin{vmatrix} -\rho\overline{\tilde{w}_x^2} & -\rho\overline{\tilde{w}_x\tilde{w}_y} & -\rho\overline{\tilde{w}_x\tilde{w}_z} \\ -\rho\overline{\tilde{w}_y\tilde{w}_x} & -\rho\overline{\tilde{w}_y^2} & -\rho\overline{\tilde{w}_y\tilde{w}_z} \\ -\rho\overline{\tilde{w}_z\tilde{w}_x} & -\rho\overline{\tilde{w}_z\tilde{w}_y} & -\rho\overline{\tilde{w}_z^2} \end{vmatrix} \qquad (2.6.16)$$

Decomposing the unknown magnitude of speed into an unknown averaged speed and an unknown pulsation rate increases the number of unknowns whereas the number of equations remains unchanged. As a result, the system of equations obtained is not closed. In order to solve it additional suppositions must be made as to the interrelation of the unknowns. These suppositions are often made on the basis of experimental data in what are called the semi-empirical theories of turbulence.

The turbulence characteristics are the quantities of pulsatory speeds, pulsation frequency and turbulence scale which are defined as shown in what follows.

The pulsatory speed w' (w'_x, w'_y, w'_z) is the difference between

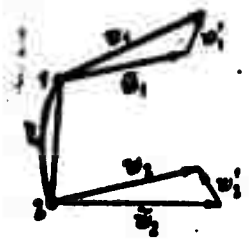


Fig. 2.6.8. The closer the points 1 and 2 are located, the closer the connection between the velocity pulsations at these points.

the true speed $\underline{w}$ and the averaged speed $\tilde{w}$. The amount of pulsation is estimated by using the root-mean-square value

$$\sqrt{\frac{1}{t_0}\int_0^{t_0}(w_{act}-\tilde{w})^2\,dt}.$$

The pulsation frequency is the number of pulsations per unit time.

Let us consider two points in a flow at a distance ξ apart. Let the pulsation velocities at these points be w_1' and w_2' (Fig. 2.6.8). Regardless of the random character of the pulsations, the quantities w_1' and w_2' will be interrelated to some degree, In fact, if the distance ξ is very small, particles of the fluid at points 1 and 2 in general participate in the motion, and the pulsations w_1' and w_2' will differ little from each other; in the limiting case of $\xi \to 0$, $w_1' - w_2'$.

As the distance ξ increases this interrelation will weaken and, theoretically at infinity, but in practice beyond a certain distance, it will vanish completely, i.e., the pulsation at point 1 becomes completely independent of the pulsation at point 2.

This kind of random dependence is determined by using the correlation coefficient:

$$K = \frac{\overline{w_1' w_2'}}{\sqrt{\overline{w_1'^2}}\sqrt{\overline{w_2'^2}}} \qquad (2.6.17)$$

With $\xi \to 0$ $w_1' - w_2'$; $\overline{w_1' w_2'} = \overline{w_1'^2} = \sqrt{\overline{w_1'^2}}\sqrt{\overline{w_2'^2}}$ & $K = 1$.

Without this dependence $\overline{w_1' w_2'} = \overline{w_1'}\,\overline{w_2'} = 0$ & $K = 0$.

The turbulence scale is the name given to the quantity $\underline{l}$ defined by the equation

$$l = \int_0^\infty K(\xi)\,d\xi$$

2.7. SINGULARITIES IN GASDYNAMICS

The system of equations of gasdynamics describing the flow of an inviscid ($\mu = 0$) and compressible ($\rho \neq$ const) and perfect ($p = \rho RT$) gas, when mass forces ($\vec{f} = 0$) and thermal conductivity ($\lambda = 0$) are neglected, can be given, owing to (2.4.1) and (2.3.6) in the form

$$\left.\begin{aligned} &\frac{\partial \rho}{\partial t} + \vec{\nabla}\cdot\rho\vec{w} = 0, && (-)\\ &\frac{\partial \vec{w}}{\partial t} + (\vec{w}\cdot\vec{\nabla})\vec{w} = -\frac{1}{\rho}\vec{\nabla}p, && (-)\\ &c_v\left[\frac{\partial T}{\partial t} + (\vec{w}\cdot\vec{\nabla})T\right] + p\vec{\nabla}\cdot\vec{w} = 0, && (-)\\ &p = A(S)\rho^{\gamma}. && (-) \end{aligned}\right\} \qquad (2.7.1)$$

In the case of reversible processes for continuous flows

$$\frac{dS}{dt} = \frac{\partial S}{\partial t} + (\vec{w}\cdot\vec{\nabla})S = 0. \qquad (2.7.2)$$

In fact, if $\lambda = \mu = 0$, by virtue of (2.3.17), $\rho\frac{d}{dt}c_vT + p\vec{\nabla}\cdot\vec{w} = 0$ and, since according to the continuity equation $\vec{\nabla}\cdot\vec{w} = -\frac{1}{\rho}\frac{d\rho}{dt}$, we have, in view of (2.3.3) and (2.3.4), $\frac{d}{dt}c_vT + p\frac{d}{dt}\frac{1}{\rho} = T\frac{dS}{dt} = 0$.

Equation (2.7.2) indicates that the entropy of each particle of the gas does not vary when it moves. For different particles the entropy can be different and in this case the entropy field will be non-uniform and unsteady.

Potential flow. In the case of a continuous steady vortex-free motion (curl $\vec{w} = 0$, everywhere) the entropy is constant at all points of the flow.

In fact, since

$$TdS = de + pd\left(\frac{1}{\rho}\right) \text{ and } i = e + \frac{p}{\rho},$$

we have

$$TdS = di + \frac{dp}{\rho} \text{ or } -\frac{\vec{\nabla}p}{\rho} = T\vec{\nabla}S - \vec{\nabla}i$$

and, instead of (2.7.1**), we shall have

$$\frac{d\vec{w}}{dt} = T\vec{\nabla}S - \vec{\nabla}i. \qquad (2.7.3)$$

Now, applying the Thomson theorem (2.2.15),

$$\frac{d\Gamma}{dt}=\oint_{l_t}\frac{d\vec{w}}{dt}\cdot d\vec{l}=\oint_{l_t}(T\vec{\nabla}S-\vec{\nabla}i)\cdot d\vec{l}=\oint_{l_t}T\vec{\nabla}S\cdot d\vec{l}.$$

since, by virtue of the continuity of enthalpy variation, $\oint_{l_t}\vec{\nabla}i\cdot d\vec{l}=0$.

According to the Stokes theorem (1.3.5), however,

$$\oint_{l_t}T\vec{\nabla}S\cdot d\vec{l}=\int_{A}\vec{n}\cdot\mathrm{rot}(T\vec{\nabla}S)\,dA.$$

Therefore

$$\frac{d\Gamma}{dt}=\int_{A}n\cdot\mathrm{rot}(T\cdot\vec{\nabla}S)\,dA.$$

Since the contour l and the surface A are arbitrary and since at any point of the flow* curl $\vec{w}$ = 0, we then have $\frac{d\Gamma}{dt}=0$.

Consequently

$$\mathrm{rot}(T\vec{\nabla}S)=\vec{\nabla}T\times\vec{\nabla}S=0.$$

Thus, the conditions for the existence of a vortex-free flow are: T = T(S) and $\vec{\nabla}T\parallel\vec{\nabla}S$; T and S depend on only one coordinate, i.e., the flow is one-dimensional and $\vec{\nabla}S$ = 0 or S = const, i.e., the flow is isentropic.

In the case Eq. (2.7.1***) is exactly satisfied and in Eq. (2.7.1****) A = const and $\frac{p}{\rho^{\varkappa}}=\text{const}$.

The boundary conditions in gasdynamics are usually given in the form:

1) speed, density and pressure at infinity:

$$\vec{w}|_{\infty}=\vec{w}_{\infty},\ \rho|_{\infty}=\rho_{\infty},\ p|_{\infty}=p_{\infty};$$

2) the normal speed component at the boundary of solid bodies (when the body is at rest):

$$\vec{w}\cdot\vec{n}|_{w_n}=0;$$

3) the pressure on a free surface

$$p|_{w_n=w_0}=p_0.$$

The propagation of small disturbances in one direction. In the introduction we have schematically determined the propagation rate of weak disturbances in a barotropic $p = p(\rho)$ compressible medium. A more exact solution to this problem can be obtained for a linear motion by solving the system of the equation of motion and the continuity equation:

$$\left.\begin{aligned} &\frac{\partial w}{\partial t}+w\frac{\partial w}{\partial x}=-\frac{1}{\rho}\frac{\partial p}{\partial \rho}=-\frac{1}{\rho}\frac{dp}{d\rho}\frac{\partial \rho}{\partial x},\\ &\frac{\partial \rho}{\partial t}+\rho\frac{\partial w}{\partial x}+w\frac{\partial \rho}{\partial x}=0. \end{aligned}\right\} \qquad (2.7.4)$$

We shall consider small disturbances when the density and pressure variations are very small and it can be assumed that $p = p_0 + p'$, $\rho = \rho_0 + \rho'$, where $|p'| \ll p_0$, $|\rho'| \ll \rho_0$, with p_0, ρ_0 denoting the density and pressure in an undisturbed gas. We also assume that the variation of the ratio $dp/d\rho$ is so small that this quantity can be replaced by some constant value, e.g., its value at infinity where the gas is at rest, i.e.,

$$\frac{dp}{d\rho}\approx\left(\frac{dp}{d\rho}\right)_0=\frac{p'}{\rho'}=a_0^2(>0). \qquad (2.7.5)$$

When the disturbances arise in a quiescent gas and moreover do so with such speed that no great change in parameters is possible via transport, the convective terms will be small compared with the local ones $\left(w\frac{\partial}{\partial x}\ll\frac{\partial}{\partial t}\right)$; here

$$\left.\begin{aligned} &\frac{\partial w}{\partial t}+a_0^2\frac{1}{\rho_0}\frac{\partial \rho'}{\partial x}=0,\\ &\frac{\partial \rho'}{\partial t}+\rho_0\frac{\partial w}{\partial x}=0. \end{aligned}\right\} \qquad (2.7.6)$$

Differentiating the first equation with respect to t and the second with respect to x in order to eliminate ρ', we obtain by substracting one from the other the second-order equation

$$\frac{\partial^2 w}{\partial t^2}=a_0^2\frac{\partial^2 w}{\partial x^2}.$$

The equations for determining ρ' and $p' = \rho' a_0^2$ are obtained analogously:

$$\frac{\partial^2 w'}{\partial t^2} = a_0^2 \frac{\partial^2 w'}{\partial x^2}, \quad \frac{\partial^2 p'}{\partial t^2} = a_0^2 \frac{\partial^2 p'}{\partial x^2}. \tag{2.7.7}$$

An equation of this type

$$\frac{\partial^2 f}{\partial t^2} = a_0^2 \frac{\partial^2 f}{\partial x^2} \quad (f = w, p', \rho', \ldots) \tag{2.7.8}$$

is called a wave equation. To solve it we substitute the variables

$$x_1 = x - a_0 t, \quad x_2 = x + a_0 t \tag{2.7.9}$$

and, using the rules for differentiating functions of functions

$$\frac{\partial}{\partial x} = \frac{\partial x_1}{\partial x} \cdot \frac{\partial}{\partial x_1} + \frac{\partial x_2}{\partial x} \cdot \frac{\partial}{\partial x_2} = \frac{\partial}{\partial x_1} + \frac{\partial}{\partial x_2},$$

$$\frac{\partial}{\partial t} = \frac{\partial x_1}{\partial t} \cdot \frac{\partial}{\partial x_1} + \frac{\partial x_2}{\partial t} \cdot \frac{\partial}{\partial x_2} = a_0 \left(- \frac{\partial}{\partial x_1} + \frac{\partial}{\partial x_2} \right),$$

$$\frac{\partial^2}{\partial x^2} = \frac{\partial^2}{\partial x_1^2} + 2 \frac{\partial^2}{\partial x_1 \partial x_2} + \frac{\partial^2}{\partial x_2^2},$$

$$\frac{\partial^2}{\partial t^2} = a_0^2 \left(\frac{\partial^2}{\partial x_1^2} - 2 \frac{\partial^2}{\partial x_1 \partial x_2} + \frac{\partial^2}{\partial x_2^2} \right),$$

we obtain

$$\frac{\partial^2 f(x_1, x_2)}{\partial x_1 \partial x_2} = 0.$$

The total integral of this equation is

$$f(x_1, x_2) = f_1(x_1) + f_2(x_2) = f_1(x - a_0 t) + f_2(x + a_0 t). \tag{2.7.10}$$

where f_1 and f_2 are arbitrary functions of $(x - a_0)$ and $(x + a_0 t)$ respectively, which must be defined in each concrete case from the initial conditions.

Let us trace the change of density ρ' with $f_2 = 0$, i.e., when

$$\rho' = f_1(x - a_0 t).$$

Regardless of the form of the function f the density will be the same for the instants of time t and for the sections x satisfying the relation

$$x - a_0 t = \text{const} \text{ or } x = t + a_0 t. \tag{2.7.11}$$

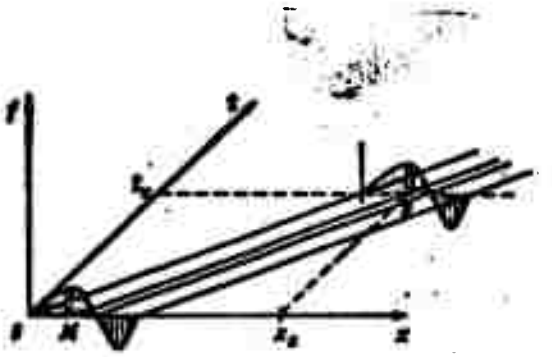


Fig. 2.7.1. The lines MP connect the time t with the sections x in which all disturbance parameters of the gas are equal.

Thus, if at the instant of time $t = 0$ the density in the section $x = \xi$ has a certain value, then after a time interval δt this value of the density will hold for the section $x = \xi + a_0\delta t$, and after the time interval $2\delta t$ it will hold for the section $x = \xi + 2a_0\delta t$, etc.

Let us represent the dependence $x = \xi + a_0 t$ and $x = \xi - a_0 t$ in a graph (2.7.1). The straight lines MP connect the instants of time t with the passage of the gas through those sections x in which all disturbance parameters of the gas will have the same values. It should be noticed that the straight lines MP are determined by two quantities: the section ξ on the x-axis and the tangent of the angle of inclination of the straight line MP to the x-axis $x(\frac{dx}{dt} = a_0)$ and is quite independent of the form of f_1 and f_2. These straight lines are called characteristics. For them the integral of Eq. (2.7.8) assumes constant values. The disturbances are therefore said to be propagated according to characteristics.

Plane waves. Let, for example, $f_1 = 0$ with $t = 0$ everywhere except for point M where $f_1(\xi) = A = \text{const}$ in the interval $\xi - \varepsilon < \xi < \xi + \varepsilon$. This value $f_1(x - a_0 t) = A = \text{const}$ will hold at the instant of time t for the section $x = \xi + a_0 t$. Thus, if the density distribution at the instant of time t (Fig. 2.7.2) is given by curve L_0 (whose shape

is determined by the form of function f_1), then the density distribution after the time interval δt will be represented by curve L_1 by shifting curve L_0 to the right by an amount of $a_0\delta t$ without deforming it. The initial curve itself is shifted without any distortion at a rate of

$$a_0 = \frac{dx}{dt} = \sqrt{\left(\frac{dp}{d\rho}\right)_0}.$$

In other words, the disturbance $f_1(x-a_0t)$ having a constant shape will be shifted in the positive direction of the x-axis at the rate a_0. Similarly, the second component $f_2(x + a_0t)$ represents a disturbance shifted in the negative direction of the x-axis at the same rate a_0. The disturbance $f(x-a_0t)$, propagated in the positive x-direction is called the direct (right) plane wave*, and the disturbance $f_2(x + a_0t)$ propagated in the negative x-direction is called <u>reverse (left) plane wave</u>.

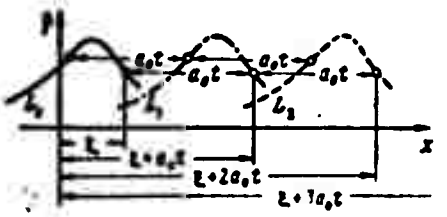


Fig. 2.7.2. The change of density distribution for a small (acoustic) disturbance. Curve L is shifted to the right at the rate a_0 and is not distorted.

<u>The Cauchy problem</u>. Solution (2.7.10) is general solution. To obtain a particular solution it is necessary to [illegible] initial conditions (the values of w and $\partial w/\partial t$ or ρ and $\partial\rho/\partial t$, etc. at the initial instant of time). The determination of the solution with given initial conditions constitutes the Cauchy problem.

Let it be given, for example, that at $t = 0$

$$w(x, t)|_{t=0} = f(x)$$

and

$$\frac{\partial w}{\partial t}\Big|_{t=0} = g(x).$$

Substituting here the solution found, (2.7.10), we obtain

$$\left.\begin{aligned} &f_1(x)+f_2(x)=f(x),\\ &-a_0f_1'(x)+a_0f_2'(x)=g(x).\end{aligned}\right\} \qquad (*)$$

Integrating the latter equation with respect to x we find, after dividing by a_0,

$$-f_1(x)+f_2(x)=\frac{1}{a_0}\int_0^x g(\xi)\,d\xi+C. \qquad (**)$$

Combining Eq. (*) and Eq. (**) we obtain

$$f_1(x)=\frac{1}{2}\left[f(x)-\frac{1}{a_0}\int_0^x g(\xi)\,d\xi-C\right].$$

$$f_2(x)=\frac{1}{2}\left[f(x)+\frac{1}{a_0}\int_0^x g(\xi)\,d\xi+C\right].$$

Now, if the form of the functions f_1 and f_2 is known, the integral of our equation can be written as

$$w(x,t)=f_1(x-a_0t)+f_2(x+a_0t)=$$
$$=\frac{1}{2}\left[f(x-a_0t)+f(x+a_0t)+\frac{1}{a_0}\int_{x-a_0t}^{x+a_0t} g(\xi)\,d\xi\right].$$

The appearance of discontinuities. In the case of weak disturbances we have $w = w(\rho)$. We assume that from $\rho = \rho(x,t)$ and $w = w(x,t)$ we can derive a relation $w = w(\rho)$ determining the speed w as a function of ρ in the general case as well, i.e., when the disturbances are not weak.

Then System (2.7.4) has the following form

$$\left.\begin{aligned} &\rho\frac{dw}{d\rho}\frac{\partial\rho}{\partial t}+\rho w\frac{dw}{d\rho}\frac{\partial\rho}{\partial x}=-\frac{dp}{d\rho}\frac{\partial\rho}{\partial x},\\ &\frac{\partial\rho}{\partial t}+w\frac{\partial\rho}{\partial x}+\rho\frac{dw}{d\rho}\frac{\partial\rho}{\partial x}=0.\end{aligned}\right\} \qquad (2.7.12)$$

Deriving $\frac{\partial\rho}{\partial t}+w\frac{\partial\rho}{\partial x}=-\rho\frac{dw}{d\rho}\frac{\partial\rho}{\partial x}$ from the last equation and substituting this value in the first one we find

$$\frac{dw}{d\rho}=\pm\frac{1}{\rho}\sqrt{\frac{dp}{d\rho}}. \qquad (2.7.13)$$

For definity we take the positive sign before the root and

so find the rate (u) of shift of the state for the instant of time considered and for the point $\underline{x}$ at which $\underline{p}$, ρ and $\underline{w}$ remain constant with time. Since $w = w(\rho)$ and $p = p(\rho)$ a solution for $\underline{w}$ and $\underline{p}$ will be found if we find a solution for the density ρ. The disturbances are propagated at finite velocity; therefore, if at the instant of time $t = t_0$ in the section $\underline{x}$ the density is equal to ρ_1 the density will have the same value ρ_1 in the section $x + \delta x$ at the next instant of time $t = t_0 + \delta t$ (Fig. 2.7.3). This leads to the concept of a propagation rate for the disturbance ($u = dx/dt$), the propagation rate of the state of a gas (e.g., compression) with respect to the particles.

For determining this rate we have the condition

$$\frac{d\rho}{dt} = \frac{\partial \rho}{\partial t} + \frac{\partial \rho}{\partial x}\frac{dx}{dt} = 0. \qquad (2.7.14)$$

After having substituted $\rho \frac{dw}{d\rho} = \pm \sqrt{\frac{dp}{d\rho}}$ in the second equation of (2.7.12) we obtain

$$\frac{\partial \rho}{\partial t} + \left(w \pm \sqrt{\frac{dp}{d\rho}}\right)\frac{\partial \rho}{\partial x} = 0;$$

and comparing this expression with (2.7.14) we find

$$u = \frac{dx}{dt} = w \pm \sqrt{\frac{dp}{d\rho}} = w \pm a$$

Here $\underline{a}$ denotes the <u>local sonic velocity</u> or, briefly, <u>the sonic velocity in a moving gas which would be if the gas were at rest</u>, having the pressure p and the density ρ (p_0, ρ_0). The local sonic velocity depends on the speed of the flow itself and varies from point to point together with the speed of the flow. In the case of an isentropic flow, $p = c\rho^k$ we have $a = \sqrt{k\frac{p}{\rho}} = \sqrt{k\kappa T}$, i.e., the local velocity increases proportional to the square root of the absolute temperature.

The integrals of the differential equations

$$\frac{dx}{dt} = w(x, t) \pm a(x, t)$$

determine the equations of the characteristics. In the general case they will be curvilinear and their meaning will be elucidated in what follows (cf. Part 5.8). If, in the case of weak disturbances, the propagation rate of the disturbance had one and the same value a_0, independent of the magnitude of the disturbance, then it is now equal to w + a, i.e., those sections in which the speed w (and also the density ρ and the pressure p) have larger values will move more rapidly; the velocity distribution curve will be deformed during this movement. In fact, let us determine the propagation rate u of disturbances, assuming that the motion is isentropic, i.e., $p = \text{const} \cdot \rho^k$ and $a^2 = dp/d\rho = \text{const}\ \rho^{k-1}$. Still taking for definiteness the (+) sign in Expression (2.7.13) for w*, we obtain

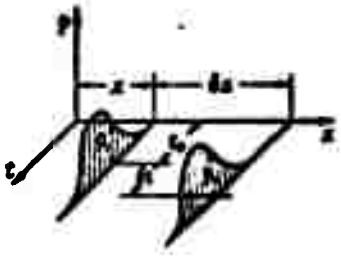


Fig. 2.7.3. Changes of a disturbance with the passage of time in the sections x and x + δx.

$$w = \int_{w=0}^{w} dw = \int_{p_0}^{p} \frac{1}{\rho} \sqrt{\frac{dp}{d\rho}}\, d\rho = \frac{2}{k-1}(a - a_0);$$

$$a = a_0 + \frac{k-1}{2} w.$$

Therefore, the propagation rate of the right wave is

$$u = w + a = w + a_0 + \frac{k-1}{2} w = a_0 + \frac{k+1}{2} w$$

or, introducing $\rho' = \rho - \rho_0$, the density increment in the wave

$$u = a_0 + \frac{k+1}{k-1}(a - a_0) = a_0 \left\{ 1 + \frac{k+1}{k-1} \left[\left(\frac{\rho}{\rho_0} \right)^{\frac{k-1}{2}} - 1 \right] \right\} \approx \frac{k+1}{2} \frac{\rho'}{\rho_0} a_0.$$

The right branch of the disturbance curve (Fig. 2.7.4) will become steeper and steeper and the left one, conversely, will become flat. At the moment when the right branch of the curve is normal to the

axis, the physical quantity considered displays a discontinuity. A further deformation of the curve cannot take place (see the dashed curve of Fig. 2.7.4,a), since it is physically impossible that in one and the same section there exist more than one value of speed (density or pressure).

The process of compression shock formation. This process can be visualized better if we consider the change of state of a quiescent gas in a cylindrical tube in which an accelerated piston is moving. We suppose that during some period of time taken as a unit the piston moves uniformly, that its velocity is increased instantaneously by a small amount, and that during the subsequent unit period of time it moves uniformly again. Then the velocity again instantaneously increases s[illegible]what and the piston once more moves uniformly, etc.

After the first impulse of acceleration (at t = 1) a pressure wave arises in the gas. Ne[illegible] the piston there will be a small mass a of gas at an elevated pressure moving to the right. At the instant of time t = 2 the piston receives the second impulse of acceleration. A second wave of higher pressure [illegible]ich affects the mass a at a time when the first pressure wave propagates further and raises the pressure of mass b, and then speed and pressure rise proceed to sections 3, 4,... etc. The pressure wave arising each time will be propagated at its (local) sonic velocity with respect to the gas. The closer the gas is to the piston the more it is compressed and the higher is its temperature, and, consequently, the higher is the local sonic velocity ($a = \sqrt{kRT}$).

Figure 2.7.4 shows the pressure distribution at the in[illegible]nts of time t = 0, 1, 2,... The position of the ordinate indicates the position of the piston .

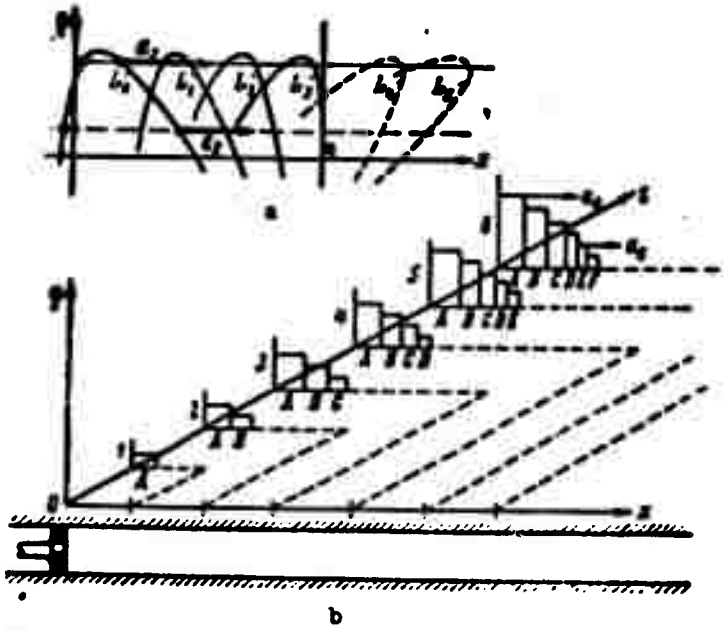


Fig. 2.7.4. Deformation of the density distribution curve and the formation of discontinuities (a). Mechanism of formation of jump-like discontinuities (b).

Conditions of dynamic consistency. The possible discontinuities of physical quantities, on both sides of the discontinuity surface, with which the motion does not contradict the fundamental laws of mass, momentum and energy conservation, are determined by the conditions of dynamic consistency. To determine these conditions it is necessary to apply the equations of mechanics to a finite volume containing a discontinuity surface, i.e., to consider the fundamental laws of energy conservation in integral form.

Let us consider a steady one-dimensional motion (for example, in an infinitely long cylindrical tube) with a section (AA) in which the pressure, speed, density, and temperature change jumpwise from the values p_1, w_1, ρ_1, T_1 to the values p_2, w_2, ρ_2, T_2 (Fig. 2.7.5). Let $\underline{u}$ be the rate of shift of the discontinuity. The difference $c = u - w$ is the rate of displacement of the discontinuity surface with

respect to the moving fluid and is known as the propagation of the discontinuity; when the speed w of the gas undergoes a discontinuity, the very same discontinuity will also exist for the speed c at which the discontinuity is propagated. With $u = 0$ the discontinuity is said to be stationary.

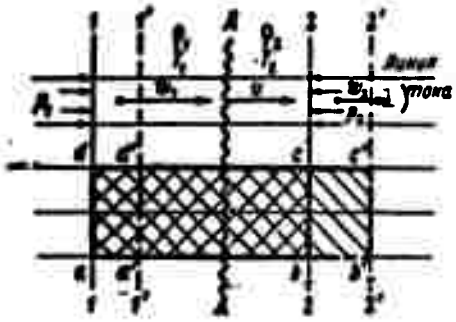


Fig. 2.7.5. For the determination of the conditions of dynamic consistency in the range of a direct compression shock (wavy line). 1) Streamline.

For the amount of the discontinuity (jump) b_2-b_1 of some quantity b, ($b = p, w, \ldots$), arising when a discontinuity section is passed through, we introduce the designation

$$b_2-b_1=[b].$$

Let us consider a volume bounded by streamlines and the sections 1–1 and 2–2, taken on both sides of a discontinuity plane sufficiently near to it (cf. Fig. 2.7.5). We shall consider the displacement of this volume with respect to the discontinuity plane during the time δt which is so small that the section 1–1 does not pass throught the discontinuity plane but reaches the position 1'–1'. For a steady motion, the mass of gas enclosed between the sections 1'–1' and 2–2 (containing the discontinuity plane) is common to the two positions of the mass considered. The conservation laws must therefore be valid for the mass of gas enclosed between the sections 1–1, 1'–1' and between 2–2, 2'–2'. Thus, the mass conservation law gives

$$\rho_1 A (w_1-u)\delta t=\rho_2 A (w_2-u)\delta t,$$

where A is the cross-sectional area of the flow. The mass j passing per unit time through a unit area of the flow cross section (mass flux density) is equal to

$$j = \rho_1(w_1 - u) = \rho_2(w_2 - u). \qquad (2.7.15)$$

Noting that the propagation rate of the discontinuity is c = u − w, we obtain

$$j = -\rho_1 c_1 = -\rho_2 c_2.$$

Since ρ_1 and ρ_2 cannot become less than zero, the signs of c_1 and c_2 must be the same; hence either the discontinuity surface precedes the moving gas (c_1, $c_2 > 0$) - and in this case the motion of the gas relative to the discontinuity surface is directed to the opposite side, - or else the discontinuity surface lags behind the moving gas (c_1, $c_2 < 0$).

From this follows the first condition of dynamic consistency:

$$[\rho c] = 0. \qquad (2.7.16)$$

The equality between the impulse of the forces and the change of momentum during the time δt yields the second condition of dynamic consistency; $(p_1 - p_2)A\,\delta t$ is the impulse of the forces acting on the mass of gas enclosed between the chosen sections during the time δt and is equal to the change in momentum of the mass of gas enclosed between the sections 2–2, 2'–2' and 1–1, 1'–1':

$$A\delta t(p_1 - p_2) = Aj\delta t[(w_2 - u) - (w_1 - u)],$$

whence

$$p_1 - p_2 = j(w_2 - w_1) = \rho_1 c_1(c_2 - c_1) = \rho_2 c_2(c_2 - c_1). \qquad (2.7.17)$$

follows. Noting that $j = -\rho_1 c_1 = -\rho_2 c_2$ and, consequently, $p_2 - p_1 = -j(w_2 - w_1)$. the second condition of dynamic consistency can be rewritten:

$$[p] = -j[w] \text{ or } [p + \rho c^2] = 0. \qquad (2.7.18)$$

The energy conservation law gives us the third condition (after reducing by JAδt):

$$c_p T_1 + \frac{(w_1 - u)^2}{2} = c_p T_2 + \frac{(w - u)^2}{2} \qquad (2.7.19)$$

or

$$\left[c_p T + \frac{(w - u)^2}{2}\right] = \left[c_p T + \frac{c^2}{2}\right] = 0. \qquad (2.7.20)$$

As the fourth additional condition we take the fact that the gas constant remains unchanged when passing through the discontinuity surface, i.e.,

$$\left[\frac{p}{\rho T}\right]=0. \tag{2.7.21}$$

Surfaces at which physical quantities change jumpwise when passing through are called surfaces of a strong discontinuity for these quantities.

Surfaces of fundamental significance in gasdynamics are those at which the derivative of some quantity with respect to some coordinate or to time changes jumpwise when passing through whereas the quantity itself varies continuously. These surfaces are termed surfaces of a weak discontinuity of this quantity.

The Hugoniot curve. In the previous section we determined the conditions for dynamic consistency:

$$\left.\begin{aligned} &\rho_1 c_1=\rho_2 c_2,\\ &p_1-p_2=\rho_1 c_1(c_2-c_1),\\ &c_p T_1+\frac{c_1^2}{2}=c_p T_2+\frac{c_2^2}{2},\\ &\frac{p_1}{\rho_1 T_1}=\frac{p_2}{\rho_2 T_2}=R. \end{aligned}\right| \tag{2.7.22}$$

Eliminating the temperature T from the third equation by means of the fourth, and taking $\frac{c_p}{R}=\frac{c_p}{c_p-c_v}=\frac{k}{k-1}$. into account, we obtain

$$c_p\frac{p_1}{\rho_1 R}+\frac{c_1^2}{2}=\frac{k}{k-1}\frac{p_1}{\rho_1}+\frac{c_1^2}{2}=\frac{k}{k-1}\frac{p_2}{\rho_2}+\frac{c_2^2}{2}$$

Substituting here the values for c_1 and c_2 determined from the first and second equations, we obtain a relation between pressure and density:

$$\frac{k}{k-1}\left(\frac{p_1}{\rho_1}-\frac{p_2}{\rho_2}\right)=\frac{c_2^2-c_1^2}{2}=\left(\frac{1}{\rho_2}+\frac{1}{\rho_1}\right)\frac{p_1-p_2}{2},$$

whence we have

$$\frac{p_2-p_1}{\rho_2-\rho_1}=k\frac{p_2+p_1}{\rho_2+\rho_1}. \tag{2.7.23}$$

This equation, called the shock adiabat (or Hugoniot curve) establishes the connection between pressure and density for the two sides of the discontinuity surface.

From Relation (2.7.23) we can obtain

$$\frac{p_2}{p_1}=\frac{\frac{k+1}{k-1}\frac{\rho_2}{\rho_1}-1}{\frac{k+1}{k-1}-\frac{\rho_2}{\rho_1}} \quad \text{and} \quad \frac{\rho_2}{\rho_1}=\frac{1+\frac{k+1}{k-1}\frac{p_2}{p_1}}{\frac{k+1}{k-1}+\frac{p_2}{p_1}}. \qquad (2.7.24)$$

Comparing this expression of p_2/p_1 with Expression (2.3.6), $\frac{p_2}{p_1}=\left(\frac{\rho_2}{\rho_1}\right)^k e^{\frac{s-s_0}{c_v}}$ for the general case of an adiabatic flow, we can ascertain ourselves that a motion with a discontinuity is associated with a change of entropy.

Plotting the dependence of the ratio ρ_2/ρ_1 on p_2/p_1 in logarithmic coordinates, we obtain (Fig. 2.7.6) for the isentropic curve $p_2/p_1 = (\rho_2/\rho_1)^k$ a straight line with the slope 1/k. To determine the shape of the Hugoniot curve H we take into account that $\rho_2/\rho_1 = 1$ for $p_2/p_1 = 1$, as for the isentropic curve.

Denoting p_2/p_1 by z we arrive at

$$\frac{d}{dz}\ln\left(\frac{\rho_2}{\rho_1}\right)=\frac{4k}{k^2(z+1)^2-(z-1)^2}.$$

In the range $z = 1 + \varepsilon$, ε being a small quantity, we have

$$\frac{d}{d\left(\frac{p_2}{p_1}\right)}\ln\left(\frac{\rho_2}{\rho_1}\right)=\frac{4k}{k^2(2+\varepsilon)^2-\varepsilon^2}\approx\frac{1}{k(1+\varepsilon)}.$$

With $\varepsilon \to 0$ the slope angle of the Hugoniot curve becomes exactly 1/k, i.e., the isentropic curve at the point ($p_2/p_1 = 1$, $\rho_2/\rho_1 = 1$) is a tangent to the Hugoniot curve.

When $\varepsilon < 0$, the slope of the tangent to the H-curve is smaller than the slope of the straight line P whereas when $\varepsilon > 0$ the slope of the tangent to the H-curve is greater. Noting that as $p_2/p_1 \to \infty$, $\rho_2/\rho_1 \to \frac{k+1}{k-1}$, it can be concluded that the H-curve will have the appearance shown in Fig. 2.7.6.

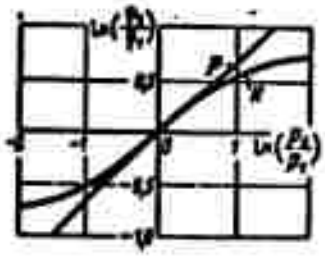


Fig. 2.7.6. Hugoniot curve H and isentropic curve P.

Impossibility of rarefaction shock.

Let us consider the case $w_1 > u$; it then follows from the mass conservation law that $w_2 > u$. In this case the discontinuity surface moves relative to the gas in the negative direction of the x-axis at a speed $c = u - w$. Then, if $\rho_1 > \rho_2$ (Fig. 2.7.7,a) the gas passes over from the region of higher density to the region of lower density, i.e., a rarefaction shock occurs. If however, $\rho_1 < \rho_2$ (cf. Fig. 2.7.7,b) the density suddenly increases on passing through the discontinuity surface and a compression shock occurs.

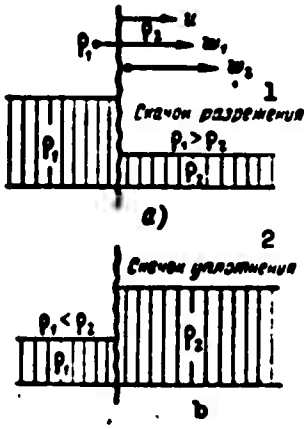


Fig. 2.7.7. A rarefaction shock (a) is impossible since its existence would be connected with a decrease in entropy. Only a compression shock (b) can occur. 1) Rarefaction shock; 2) compression shock.

Let us prove the impossibility of a rarefaction shock. For this purpose we notice that the entropy per unit mass is

$$\frac{S_2 - S_1}{c_v} = \ln\frac{p_2}{p_1} - k\ln\frac{\rho_2}{\rho_1}; \qquad (2.7.25)$$

for an isentropic curve $S_2 = S_1$.

By comparing the Hugoniot curve (H) and the isentropic curve (F) in Fig. 2.7.6, it can be seen that if $p_2/p_1 > 1$, then $\ln\left(\frac{\rho_2}{\rho_1}\right)_H < \ln\left(\frac{\rho_2}{\rho_1}\right)_s$, and if $p_2/p_1 < 1$, $\ln\left(\frac{\rho_2}{\rho_1}\right)_H > \ln\left(\frac{\rho_2}{\rho_1}\right)_s$.

Therefore, by virtue of (2.7.25), if $\frac{\rho_2}{\rho_1} > 1$, then $\ln\frac{\rho_2}{\rho_1} > 0$ and $\frac{S_2 - S_1}{c_v} > 0$, and if $\frac{\rho_2}{\rho_1} < 1$, then $\ln\frac{\rho_2}{\rho_1} < 0$ and $\frac{S_2 - S_1}{c_v} < 0$.

Owing to the second law of thermodynamics the entropy must decrease, i.e., $S_2 - S_1 > 0$, therefore the case $\frac{\rho_2}{\rho_1} < 1$ (and hence also $\frac{\rho_2}{\rho_1} < 1$) cannot occur; a rarefaction shock is impossible; in the

case of an adiabatic flow the discontinuity surface always represents a compression shock.

Similar conclusions can be drawn for $w_1 < u$ too, i.e., when the discontinuity surface overtakes the moving fluid. Therefore, when the gas passes through a discontinuity surface, the density (and also the pressure) can only increase.

Apart from the speed, pressure and density, the entropy also undergoes a discontinuity when passing through a discontinuity surface. To estimate the magnitude of this entropy difference (per unit mass and unit time) we consider a weak discontinuity, i.e., the case of $p_2 - p_1 = [p]$being a small quantity. Assuming $p_2 = (1 + \varepsilon)p_1$, where ε is a small quantity, we can write

$$\frac{S_2 - S_1}{c_v} = \ln\frac{p_2}{p_1} - k\ln\frac{\rho_2}{\rho_1} = \ln\frac{p_2}{p_1} - k\ln\frac{1 + \frac{k+1}{k-1}\frac{p_2}{p_1}}{\frac{k+1}{k-1} + \frac{p_2}{p_1}} =$$

$$= \ln(1+\varepsilon) - k\left[\ln\left(1 + \frac{k+1}{k-1} + \varepsilon\frac{k+1}{k-1}\right) - \ln\left(1 + \frac{k+1}{k-1} + \varepsilon\right)\right] =$$

$$= \varepsilon - \frac{\varepsilon^2}{2} + \frac{\varepsilon^3}{3} - \ldots - \varepsilon + \frac{\varepsilon^2}{2} - \frac{3(k^2+1)\varepsilon^3}{12k^2} + \ldots =$$

$$= \frac{k^2-1}{12k^2}\varepsilon^3 \ldots .$$

Thus,

$$\frac{S_2 - S_1}{c_v} = \frac{k^2-1}{12k^2}\left(\frac{p_2 - p_1}{p_1}\right)^3 + \ldots . \qquad (2.7.26)$$

i.e., the entropy jump is a second-order small quantity compared with the pressure jump. Since the increase in entropy, characterizing the irreversibility of the process, takes place in the present case with no viscosity and no heat conduction, this indicated an energy dissipation in the case of a disturbed flow, even in a perfect fluid.

Propagation of discontinuities. From the two first equations of dynamic consistency

$$\rho_1 c_1 = \rho_2 c_2 \text{ и } p_1 - p_2 = \rho_1 c_1 (c_2 - c_1)$$

it follows that

$$c_1 c_2 = \frac{p_1 - p_2}{\rho_1 - \rho_2},$$

whence we obtain for the propagation rate of the discontinuity

$$\left.\begin{aligned} c_1 &= u - w_1 = \pm \sqrt{\frac{\rho_2}{\rho_1}\frac{p_1 - p_2}{\rho_1 - \rho_2}}, \\ c_2 &= u - w_2 = \pm \sqrt{\frac{\rho_1}{\rho_2}\frac{p_1 - p_2}{\rho_1 - \rho_2}}. \end{aligned}\right| \qquad (2.7.27)$$

where the plus sign refers to the case $u > w_1$, $u > w_2$ when the discontinuity surface precedes the particles of the fluid, and the minus sign to the case where the fluid precedes the discontinuity. Using the equation of the Hugoniot curve, we obtain

$$\left.\begin{aligned} c_1^2 &= \frac{p_2}{\rho_2}\frac{p_1 - p_2}{\rho_1 - \rho_2} = \frac{p_1}{\rho_1}\frac{1 - \frac{p_2}{p_1}}{\frac{\rho_1}{\rho_2} - 1} = \frac{p_1}{\rho_1}\frac{1 - \frac{k+1}{k-1}\frac{p_2}{p_1}}{\frac{\rho_2}{\rho_1} - \frac{k+1}{k-1}} = \\ &= k\frac{p_1}{\rho_1}\frac{2\rho_2}{(k+1)\rho_1 - (k-1)\rho_2}, \\ c_2^2 &= \frac{p_1}{\rho_2}\frac{p_1 - p_2}{\rho_1 - \rho_2} = k\frac{p_2}{\rho_2}\frac{2\rho_1}{(k+1)\rho_2 - (k-1)\rho_1}. \end{aligned}\right| \qquad (2.7.28)$$

Relation (2.7.28) indicates that the propagation rate of a strong discontinuity always differs from the local sonic speed $a_1 = \sqrt{k\frac{p_1}{\rho_1}}$ or $a_2 = \sqrt{k\frac{p_2}{\rho_2}}$, where c_1 rapidly increases with increasing discontinuity ρ_2/ρ_1 beginning from $c_1 = a$ - without discontinuity ($\rho_2 = \rho_1$) to infinity (with $\frac{\rho_2}{\rho_1} = \frac{k+1}{k-1}$), when $c_1 > a_1$, then $c_2 < a_2$ and vice versa.

If $u = 0$ the speed w will, at least at one side of the strong discontinuity, exceed the local sonic speed.

For weak discontinuities we may assume $\rho_2 \approx \rho_1$ and $p_2 - p_1 \approx \frac{dp}{d\rho}(\rho_2 - \rho_1)$.

Therefore

$$u - w_2 = u - w_1 = \pm \sqrt{\frac{dp}{d\rho}} = a,$$

i.e., weak discontinuities are propagated at a speed equal to the local sonic speed.

local speed of sound.

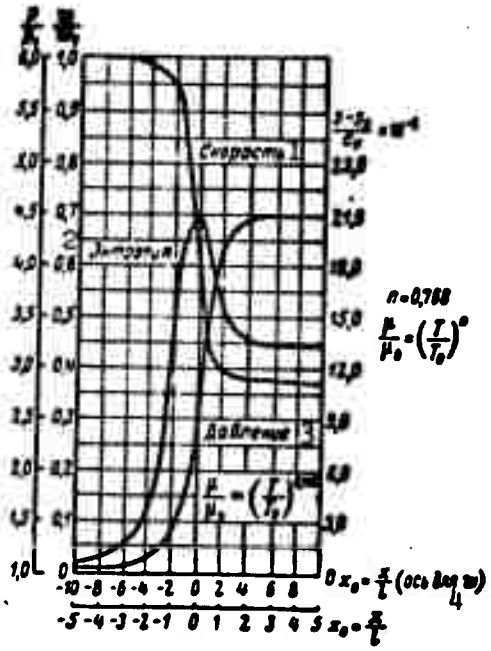


Fig. 2.7.8. Jump-like change of speed, pressure and entropy. 1) speed; 2) entropy; 3) pressure; 4) (axis for $\underline{w}$).

Thickness of a shock wave. Mathematically, a discontinuity is a simplified representation of a region in which physical quantities undergo a very sharp change. In a real viscous and heat conducting gas the thickness of a shock wave will differ from zero.

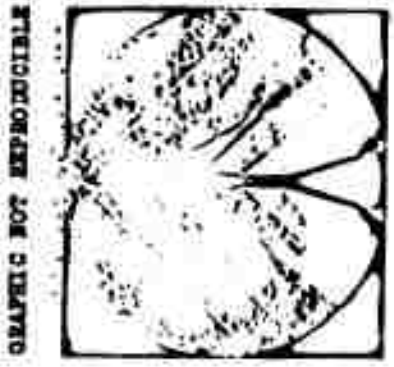


Fig. 2.7.9. Aircraft model in supersonic flow.

Figure 2.7.8 gives us a graph showing the change of the gas parameters in the shock wave. It can be seen from it that the entropy S at first increases sharply, then starts dropping. This entropy decrease does not violate the second law because the entropy of the system as a whole increases.

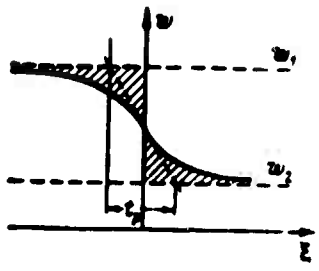


Fig. 2.7.10. For determining the shock wave thickness.

From the theoretical standpoint the region of change of the gas parameters propagates to infinity. In fact, as can be seen from Fig. 2.7.8, all changes occur in a very narrow region whose width, as to the order of magnitude, corresponds to the mean free path of a molecule. The exceedingly small thickness of a shock wave explains, for example, the sharp lines in the photograph of the supersonic flow (Fig. 2.7.9).

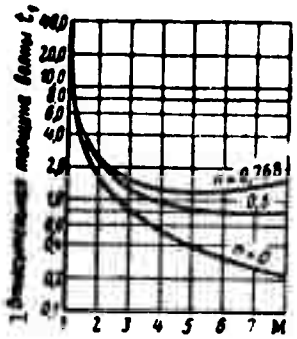


Fig. 2.7.11. Dependence of the relative thickness of a shock wave $t = t_p/\underline{l}$ ($\underline{l}$ - mean free path of molecules) on the Mach number M; n is the exponent from the formula $\mu/\mu_0 = (T/T_0)^n$. 1) Relative thickness of wave, t_1.

The concept of the shock wave thickness can be conditionally determined.

The wave thickness is understood by [illegible] as the distance between the points of intersection of the tangent to the velocity distribution at the inflection point of the velocity distribution with the asymptotic lines $w = w_1$ and $w = w_2$.

Fig. 2.7.11 indicates that the ratio between wave [illegible] and the mean free path of molecules drops sharply as the Mach number M increases.

It should also be noted that estimating the shock wave [illegible] thickness indicated the necessity of using the methods of kinetic [illegible] theory to investigate this problem in more detail.

Manuscript Page No.

[Footnotes]

57 Barotropic fluid is the name given to a fluid the density of which depends only on the pressure $\rho = \rho(p)$; thus, for example, an incompressible fluid (ρ = const), a gas during isothermic (T = const) and adiabatic ($p = c\rho^k$) changes of state is barotropic.

93 In foreign literature it is called Mach number.

95 idem (Latin) - the same.

101 If instead of (2.6.8) we determine $p_1 - p_2 = \zeta \frac{l}{D} \frac{\rho w_m^2}{2}$ and Re = $= w_m D/\nu$ then $\zeta = 64/\mathrm{Re}$. When reading special literature we have to pay attention to the characteristical parameters applied in defining the similarity criteria, in formulas, etc.

115 The region of the flow is assumed to be singly connected.

119 Plane wave is the term applied to a wave whose front is a plane.

122 It should be kept in mind that w is the speed of particle motion of the gas caused by the disturbance entering it.

REFERENCES

2.1. Loytsyanskiy, L.G., Mekhanika zhidkosti i gaza [Mechanics of Liquids and Gases], GTTI [State Technical and Theoretical Press], 1957.

2.2. Sedov, L.I., Metody podobiya i razmernosti v mekhanike [Similarity and Dimensional Analysis Methods in Mechanics], GTTI, 1954.

2.3. Slezkin, N.A., Dinamika vyazkoy neszhimayemoy zhidosti [Dynamics of the Viscous Incompressible Fluid], GTTI, 1955.

2.4. Kurant, G. and Fridrikhs, K., Sverkhzvukovyye techeniya i udarnyye volny [Supersonic Flow and Shock Waves], IL [Foreign Literature Press], 1950.

2.5. Shirokov, M.F., Fizicheskiye osnovy gazodinamiki [Physical Found-

ations of Gasdynamics], 1958.

2.6. Landau, L.D. and Lifshits, Ye.M., Mekhanika sploshnykh sred [Mechanics of Continuous Media], GTTI, 1955.

2.7. Zhukovskiy, V.S., Tekhnicheskaya termodinamika [Engineering Thermodynamics], GTTI, 1952.

Manuscript Page No.	[Transliterated Symbols]
68	в = v = vozdukh = air
68	г = g = goryucheye = fuel
69	н = n = niz = bottom
69	в = v = verkh = top
71	выход = vykhod = vykhod = outlet
71	вход = vkhod = vkhod = inlet
113	ист = ist = istinnaya = true
115	тв.т = tv.t = tverdoye telo = solid
115	св.пов = sv.pov svobodnaya poverkhnost' = free surface

BLANK PAGE

Chapter 3

POTENTIAL FLOWS OF A COMPLETELY INCOMPRESSIBLE FLUID

3.1. PLANE FLOWS

Definitions. When cylindrical bodies are placed in a transverse flow, the motion in the symmetry plane of a body will not depart from it, i.e., the particle trajectories will lie entirely in this plane. Here the motion will be two-dimensional*, i.e., plane (Fig. 3.1.1). But even in an arbitrary plane lying arbitrarily close to the symmetry plane, the motion will be three-dimensional and only in the case of an infinitely long cylindrical body will the motion in all planes parallel to the symmetry plane be the same as in the latter. Nevertheless, there are many problems in aeromechanics which are first solved for a plane flow and then corrected for the fact that the body's dimensions are finite in the perpendicular direction; this is done because it is considerably simpler to investigate plane motion than a three-dimensional motion, not only because there is one variable less but also since it is then possible to apply the highly developed apparatus of the theory of functions of a complex variable.

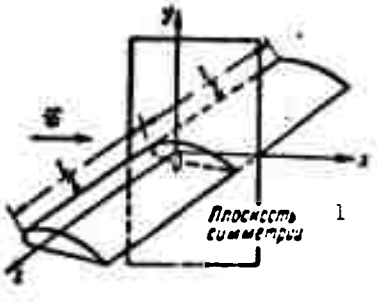


Fig. 3.1.1. When flow occurs around a symmetrical cylindrical body, the flow in the symmetry plane is two-dimensional. The velocity vector is assumed to lie in the symmetry plane. 1) Symmetry plane.

Let us denote as a plane flow one in which all particles move parallel to one plane (guide) and, at the same time, move uniformly

at all points lying on one perpendicular to this plane. Thus, both velocity components depend only on the coordinates of the point (x, y) in the guide of the plane (x0y) and are independent of the coordinate (z) normal to this plane.

The mathematical formulation of this fact reads:

$$w_x = w_x(x, y),\ w_y = w_y(x, y),\ w_z = 0,\ \frac{\partial}{\partial z} = 0. \qquad (3.1.1)$$

In order to maintain the dimensions of the quantities obtained, all calculations refer to a fluid layer bounded by two planes which are parallel to the guide of the plane and are separated by a distance equal to unity.

The basic system of equations of a plane flow of an incompressible inviscid fluid consists of the continuity equation with $\rho = \text{const}$:

$$\frac{\partial w_x}{\partial x} + \frac{\partial w_y}{\partial y} = 0 \qquad (3.1.2)$$

and the equation of motion for the projections onto the x and y axes:

$$\left.\begin{aligned} \frac{\partial w_x}{\partial t} + w_x\frac{\partial w_x}{\partial x} + w_y\frac{\partial w_x}{\partial y} &= f_x - \frac{1}{\rho}\frac{\partial p}{\partial x}, \\ \frac{\partial w_y}{\partial t} + w_x\frac{\partial w_y}{\partial x} + w_y\frac{\partial w_y}{\partial y} &= f_y - \frac{1}{\rho}\frac{\partial p}{\partial y}. \end{aligned}\right\} \qquad (3.1.3)$$

These three scalar equations serve to determine the three functions $w_x(x, y, t)$, $w_y(x, y, t)$, $p(x, y, t)$ with boundary conditions set up for plane flows in the same way as this has been done in the case of spatial flow (2.4.3). We notice that here the part of the surface of the solid body is played by a solid contour (guide of the cylindrical surface of the solid body).

As regards the equation of motion (3.1.3), we notice that, since the motion of an incompressible fluid is barotropic and when the volume forces f have a potential, it can be integrated in accordance with (2.2.13):

a) if curl $\vec{w} = 0$, or, for a plane flow, $\frac{\partial w_y}{\partial x} - \frac{\partial w_x}{\partial y} = 0$ and the

Lagrange integral for (3.1.3) has the form

$$\frac{\partial \Phi}{\partial t}+\frac{w_x^2+w_y^2}{2}+\frac{p}{\rho}+U=f(t). \qquad (3.1.4)$$

as this follows from (2.2.14);

b) for a steady motion $\left(\frac{\partial}{\partial t}=0\right)$ along the streamline, when the Bernoulli integral (2.2.13) reads

$$\frac{w_x^2+w_y^2}{2}+\frac{p}{\rho}+U=C(L). \qquad (3.1.5)$$

where C(L) is a constant that is in general different for different streamlines.

Thus, for plane vortex-free flows w_x and w_y are determined from the system

$$\frac{\partial w_x}{\partial x}+\frac{\partial w_y}{\partial y}=0, \quad \frac{\partial w_y}{\partial x}-\frac{\partial w_x}{\partial y}=0. \qquad (3.1.6)$$

and the pressure p is found from (3.1.4); in the case of a steady motion the constant C in this integral f(t) is the same for all streamlines.

The velocity potential. As has been shown, in the singly connected region of a vortex-free motion the value of the integral $\int_A^B \vec{w}\cdot d\vec{l}$ from point A to point B is independent of the path of integration; it is a point function and can be written (accurately to within an arbitrary constant)

$$\int_A^{B(x,y)} w_x dx+w_y dy=\int_A^{B(x,y)} d\Phi=\Phi(x, y).$$

Thus,

$$w_x=\frac{\partial \Phi}{\partial x}, \quad w_y=\frac{\partial \Phi}{\partial y}. \qquad (3.1.7)$$

The function $\Phi(x,y)$ is called the velocity potential.

Relations (3.1.7) are obtained from purely kinematic considerations and do not contain the density. They can therefore be applied likewise to vortex-free flows of both incompressible and compressible fluids.

For an incompressible fluid the continuity Eq. (3.1.2) with (3.1.7) yields

$$\frac{\partial^2\Phi}{\partial x^2}+\frac{\partial^2\Phi}{\partial y^2}=\Delta\Phi=0. \qquad (3.1.8)$$

A vortex-free motion of an incompressible fluid is completely determined by one scalar function, namely the velocity potential, which satisfies Eq. (3.1.8), which is called the Laplace equation.

On solid contours C, the boundary condition expressing the vanishing of the normal velocity component must be fulfilled:

$$w_n\Big|_C=\frac{\partial\Phi}{\partial n}\Big|_C=0. \qquad (3.1.9)$$

The stream function. Considering the differential equation of the streamlines of a plane flow

$$w_x:dx=w_y:dy$$

or

$$w_x dy-w_y dx=0 \qquad (3.1.10)$$

and the continuity Eq. (3.1.2)

$$\frac{\partial}{\partial x}(w_x)=\frac{\partial}{\partial y}(-w_y),$$

it can be shown that the left-hand side of Eq. (3.1.10) is the total differential of a certain function $\Psi(x,y)$:

$$w_x dy-w_y dx=d\Psi. \qquad (3.1.11)$$

Here, if dx and dy belong to the streamline, $d\Psi = 0$, i.e., the Ψ-function remains constant along an arbitrary streamline. Therefore the equation

$$\Psi(x, y)=C \qquad (3.1.12)$$

is the equation of the family of streamlines. The function $\Psi(x,y)$ is called the stream function.

Comparing Eq. (3.1.11) with the expression of the total differential $d\Psi=\frac{\partial\Psi}{\partial x}dx+\frac{\partial\Psi}{\partial y}dy$, we obtain

$$w_x = \frac{\partial \Psi}{\partial y}; \quad w_y = -\frac{\partial \Psi}{\partial x}. \tag{3.1.13}$$

Here

$$\operatorname{rot}_z \vec{w} = -\left(\frac{\partial^2 \Psi}{\partial x^2} + \frac{\partial^2 \Psi}{\partial y^2}\right) = -\Delta \Psi. \tag{3.1.14}$$

For a vortex-free flow curl $\vec{W} = 0$, $\Delta \Psi = 0$, i.e., the stream function as well as the velocity potential, satisfies the Laplace equation

$$\Delta \Psi = \frac{\partial^2 \Psi}{\partial x^2} + \frac{\partial^2 \Psi}{\partial y^2} = 0.$$

At solid walls the normal velocity component of the flow is equal to zero, so the walls must coincide with the streamlines. From this follows the boundary condition at the walls, Ψ = const.

<u>The hydrodynamic meanin of the streamfunction</u>. Let us consider the volume flow rate Q of fluid through a plane stream tube bounded by the streamlines AB and CD, on which the values of the stream function are Ψ_1 and Ψ_2, respectively (Fig. 3.1.2). This flow rate is equal to the contour integral $\int_{l_M}^{N} w_n \, dl = \int_{l_M}^{N} \vec{w} \cdot \vec{n} \, dl$ of the velocity vector flux $\vec{w} \cdot \vec{n}$ with respect to an arbitrary curve connecting two arbitrary points, M and N, on the lines AB and CD. Let $d\vec{l}$ be an element of the curve MN and $\vec{n}$ the normal to it, directed such that the vectors $\vec{n}$, $d\vec{l}$, indicationing the direction of integration, and $\vec{k}$, the unit vector of the z-axis, form a right-handed system. Then, noting that $\vec{n} \cdot dl = d\vec{l} \times \vec{k}$, we can write

$$\begin{aligned} Q = \int_M^N \vec{w} \cdot \vec{n} \, dl = \int_M^N \vec{w} \cdot (d\vec{l} \times \vec{k}) = \int_M^N (\vec{k} \times \vec{w}) \cdot d\vec{l} = \\ = \int_M^N w_x \, dy - w_y \, dx = \int_M^N d\Psi = \Psi_1 - \Psi_2. \end{aligned} \tag{3.1.15}$$

Thus, the flow rate through any contour between two arbitrary points in the flow is determined by the difference of the values of the stream function at these points.

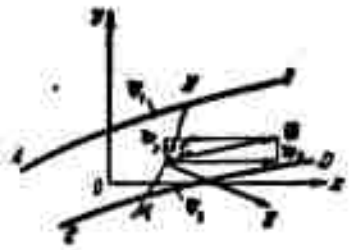


Fig. 3.1.2. The amount of fluid streaming through the line element is equal to the difference of the values of the stream functions $\Psi(N) - \Psi(M) = \psi_1 - \psi_2$ at the points M and N.

It should be noted that the concept about the stream function is valid only for two-dimensional flows, for example, as has been shown, for plane flows, and also for axisymmetric flows when considering the flow in the meridional plane.

Streamlines and equipotential lines. In the graphic representation of a plane flow, a decisive part is played by the equipotential lines whose equations are $\Phi(x,y) = \text{const}$, and especially by the streamlines determined by the condition $\Psi(x,y) = \text{const}$. Moreover these systems form an orthogonal net, i.e., the lines $\Phi = \text{const}$ are perpendicular to the lines $\psi = \text{const}$. In fact (Fig. 3.1.3), the gradient of the Φ-function is directed normally to the lines $\Phi = \text{const}$ and the gradient of the stream function is normal to the streamlines $\psi = \text{const}$; calculating $\vec{\nabla}\Phi \cdot \vec{\nabla}\Psi$ we obtain

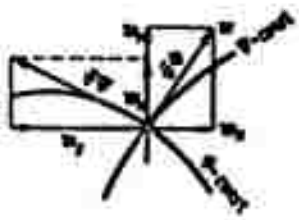


Fig. 3.1.3. The equipotential lines $\Phi = \text{const}$ are perpendicular to the streamlines $\Psi = \text{const}$.

$$\vec{\nabla}\Phi \cdot \vec{\nabla}\Psi = \left(\vec{i}\frac{\partial \Phi}{\partial x} + \vec{j}\frac{\partial \Phi}{\partial y}\right)\left(\vec{i}\frac{\partial \Psi}{\partial x} + \vec{j}\frac{\partial \Psi}{\partial y}\right) =$$

$$= \frac{\partial \Phi}{\partial x}\frac{\partial \Psi}{\partial x} + \frac{\partial \Phi}{\partial y}\frac{\partial \Psi}{\partial y} = -w_x w_y + w_x w_y = 0,$$

i.e., $\vec{\nabla}\Phi \perp \vec{\nabla}\Psi$, whence follows that the lines $\Phi = \text{const}$ intersect the lines $\Psi = \text{const}$ at right angles.

If dl is a streamline element and dn is an element of an equipotential line at some arbitrary point, the direction of the fluid's velocity at this point will coincide with the element dl and

$$w_l = \frac{\partial \Phi}{\partial l} = \frac{\partial \Psi}{\partial n}.$$

Hence, provided the increments of the functions Φ and Ψ are

equal, the sections Δl and Δn between two neighboring lines will be equal too. Such a net is called an isothermal net. The converse of this is also true, i.e., an arbitrary isothermal net can be regarded as the net of streamlines and equipotential lines.

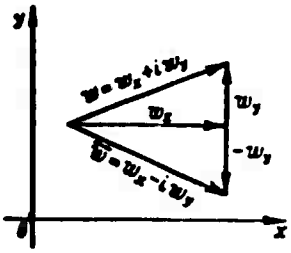


Fig. 3.1.4. The vector of the complex conjugate velocity $\bar{w}=w_x-iw_y$ is the mirror image of the velocity vector $w=w_x+iw_y$

The complex potential. From Relations (3.1.7) and (3.1.13) the Cauchy-Riemann conditions

$$\frac{\partial\Phi}{\partial x}=\frac{\partial\Psi}{\partial y},\quad \frac{\partial\Phi}{\partial y}=-\frac{\partial\Psi}{\partial x}. \qquad (3.1.16)$$

follow, expressing that the function

$$\chi(z)=\Phi(x,y)+i\Psi(x,y) \qquad (3.1.17)$$

is an analytic function of the complex variable $z = x + iy$. The function $\chi(z)$ whose real part is the velocity potential and whose imaginary part is the stream function, is called the complex potential (a characteristic function of the flow).

It can easily be seen that from the analysis condition of the function, i.e., from the fact that the derivative is independent of the path along which $\Delta x + i\Delta y$ tends to zero, it follows that

$$\frac{d\chi}{dz}=\frac{\partial\Phi}{\partial x}+i\frac{\partial\Psi}{\partial x}=-i\frac{\partial\Phi}{\partial y}+\frac{\partial\Psi}{\partial y}=w_x-iw_y=\bar{w}(z). \qquad (3.1.18)$$

The quantity $\bar{w}(z) = w_x - iw_y$, which plays a particularly important role in investigating the flow of an incompressible fluid, represents the mirror image of the velocity vector about the real axis w_x (Fig. 3.1.4) and is called the complex conjugate velocity.

The single complex $\chi(z) = \Phi + i\Psi$ of the one variable $z = x + iy$, consisting of the stream function $\Psi(x,y)$ and the velocity potential $\Phi(x,y)$, makes it possible to reduce the problem of the flow of a liquid to the determination of only one function, $\chi(z)$. This considerably facilitates and simplifies the solution of prob-

lems on the flow of a completely incompressible liquid by the methods of the theory of functions of a complex variable.

The velocity in a polar coordinate system. If we take into consideration that in the case of a potential motion $\vec{w}=\vec{\nabla}\Phi$ and $\frac{\partial\Phi}{\partial l}=\vec{\nabla}\Phi\vec{\tau}=w_l$, the radial and the tangential components will be

$$w_r=\frac{\partial\Phi}{\partial r},\quad w_\theta=\frac{1}{r}\frac{\partial\Phi}{\partial\theta}. \tag{3.1.19}$$

From the Cauchy-Riemann condition the expression

$$w_r=\frac{1}{r}\frac{\partial\Psi}{\partial\theta},\quad w_\theta=-\frac{\partial\Psi}{\partial r}. \tag{3.1.20}$$

follows.

3.2. ADDITION OF THE SIMPLEST FLOW REGIMES

Plane parallel flow. The simplest case of a plane flow is a parallel flow, in which the velocity is equal in its magnitude and direction at all points (Fig. 3.2.1). If $w_x=w_\infty\cos\alpha$, $w_y=w_\infty\sin\alpha$, we have

$$w_x-iw_y=w_\infty(\cos\alpha-i\sin\alpha)=w_\infty e^{-i\alpha}=\frac{d\chi}{dz}. \tag{3.2.1}$$

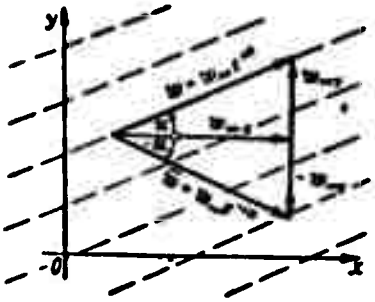


Fig. 3.2.1. Plane parallel flow at the angle α to the x-axis.

The complex potential, the velocity potential and the stream function will be

$$\chi(z)=\bar{w}_\infty z,\quad \Phi=xw_\infty\cos\alpha+yw_\infty\sin\alpha,\quad \Psi=yw_\infty\cos\alpha-xw_\infty\sin\alpha. \tag{3.2.2}$$

In most cases the x-axis is oriented along the velocity w_0, i.e., $\alpha = 0$, so that $\bar{w}_\infty=w_\infty$ and $\chi(z)=w_\infty z$; $\Phi=w_\infty x$; $\Psi=w_\infty y$.

Sources and sinks. A stream of a fluid flowing continuously and uniformly out of each point of an infinite straight line parallel to the z-axis at a rate of Q unit volumes per unit time per unit length [m^3/sec-m], is called a flow from a plane source. The straight line is called the plane source

and Q the flow rate of the source (Fig. 3.2.2). Because of symmetry the velocity is assumed to have components only in planes normal to the z-axis and to be equal to $Q/2\pi r$, where $2\pi r \cdot 1$ is the surface area enveloping the source and its potential will be a function of radius

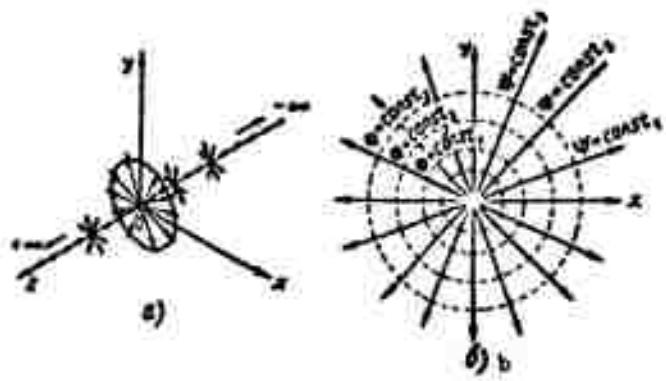


Fig. 3.2.2. A plane source (a) is produced by the steady and uniform outflow of a fluid from a point of the z-axis. Streamlines and equipotential lines for the source (b).

r only. Therefore,

$$w_r = \frac{d\Phi}{dr} = \frac{Q}{2\pi r},$$

whence

$$\Phi = \frac{Q}{2\pi} \ln r. \tag{3.2.3}$$

The equipotential lines are circles with their centers at the source, and the streamlines are the radii.

To determine the stream function we write

$$d\Psi = w_x dy - w_y dx = \frac{Q}{2\pi} \frac{x\,dy - y\,dx}{r^2} = \frac{Q}{2\pi} d\left(\operatorname{arc\,tg} \frac{y}{x}\right)$$

which yields

$$\Psi = \frac{Q}{2\pi} \operatorname{arc\,tg} \frac{y}{x} = \frac{Q}{2\pi} \theta \tag{3.2.4}$$

and

$$\left.\begin{aligned} \chi(z) &= \Phi + i\Psi = \frac{Q}{2\pi}(\ln r + i\theta) = \frac{Q}{2\pi} \ln re^{i\theta} = \frac{Q}{2\pi} \ln z, \\ \overline{w} &= w_x - iw_y = \frac{d\chi}{dz} = \frac{Q}{2\pi z} = \frac{Q}{2\pi r^2}(x - iy). \end{aligned}\right\} \tag{3.2.5}$$

The complex potential of a sink is obtained by changing the sign of the flow of a source, for which we have

$$\chi(z) = -\frac{Q}{2\pi}\ln(z). \qquad (3.2.6)$$

The plane vortex. Let us consider the plane steady motion of an incompressible fluid whose streamlines are circles (Fig. 3.2.3a).

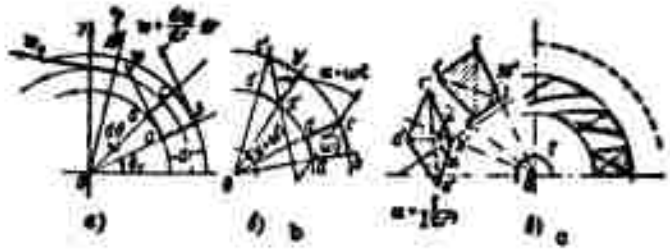


Fig. 3.2.3. Motion of particles along curvilinear trajectories (a). When the fluid is rotating like a solid body, a particle taken near an arbitraty point revolutes with the same angular velocity as the whole fluid; the motion everywhere is without exception a vortex motion with the same angular velocity (b). The fluid elements in the vortex field are subjected only to shear deformation, the motion is a potential one (c).

The simplest suppositions about the velocity distribution is that the velocity is proportional to the distance from the center, i.e., the fluid rotates like a solid body:

$$w_\theta = \omega r, \quad w_r = 0. \qquad (3.2.7)$$

Such a motion will not be a potential motion. In fact, calculating the circulation with respect to an infinitely small contour abcd (cf. Fig. 3.2.3a) taken at an arbitrary point, we obtain

$$\Gamma_{abcd} = \left(w + \frac{dw}{dr}dr\right)(r+dr)\,d\theta - w r\,d\theta = \left(w + r\frac{dw}{dr}\right)dr\,d\theta = \frac{1}{r}\frac{d(rw)}{dr}dA, \qquad (3.2.8)$$

where $dA = r\,d\theta\,dr$ the area bounded by the contour abcd. As we have taken $w = \omega r$ we have $\Gamma = 2\omega\,dA$, i.e., a particle rotates at any point with the same angular velocity as the whole fluid (cf. Fig. 3.2.3,b); at every point the motion is a vortex motion.

To answer the question whether a potential motion could exist whose streamlines were circles, we write the condition for absence of vortices at each point, or, what is the same, we put expression (3.2.8) equal to zero:

$$\frac{1}{r}\frac{d(rw)}{dr}=0.$$

Assuming $r \neq 0$ we obtain the condition

$$rw=\text{const}$$

or

$$w=C:r. \qquad (3.2.9)$$

The point $r = 0$ is a singularity; the motion near it must be studied separately.

To determine the constant we consider some arbitrary contour around the singularity, e.g., a circle. The circulation for it is $\Gamma=2\pi r\cdot w=2\pi r\frac{C}{r}=2\pi C$, i.e., it is independent of the radius and equals a constant quantity. Thus, the resultant motion

$$w_r=0, \quad w_\theta=w=\frac{\Gamma}{2\pi r} \qquad (3.2.10)$$

is everywhere a potential motion except at the singularity.

At the z-axis, i.e., where $r = 0$, all particles rotate; consequently, the z-axis forms an infinitely long straight vortex of intensity Γ. Let us stress once more that the velocity field produced by the rectilinear vortex has a potential which can be found from the system

$$w_r=\frac{\partial\Phi}{\partial r}=0, \quad w_\theta=\frac{1}{r}\frac{\partial\Phi}{\partial\theta}=\frac{\Gamma}{2\pi r},$$

whence immediately follows $\Phi=\Phi(\theta)$ and

$$\Phi=\frac{\Gamma}{2\pi}\theta=\frac{\Gamma}{2\pi}\operatorname{arctg}\frac{y}{x}. \qquad (3.2.11)$$

The equipotential lines are spokes emanating from the vortex. It can be seen that the velocity potential is a many-valued

function; with every circumscription of the origin (singular point) its value increases by $2\pi\Gamma$. To eliminate the many-valuedness, the angle ϑ is assumed to vary from 0 to 2π. Writing the equation that determines the stream function as

$$w_r = \frac{1}{r}\frac{\partial\psi}{\partial\vartheta} = 0; \quad w_\vartheta = -\frac{\partial\psi}{\partial r} = \frac{\Gamma}{2\pi r},$$

we find

$$\psi = -\frac{\Gamma}{2\pi}\ln r = -\frac{\Gamma}{2\pi}\ln\sqrt{x^2+y^2},$$

which yields the complex potential as

$$\chi(z) = \Phi + i\psi = \frac{\Gamma}{2\pi}\vartheta - i\frac{\Gamma}{2\pi}\ln r = \frac{-i\Gamma}{2\pi}(\ln r + i\vartheta) = \frac{\Gamma}{2\pi i}\ln z.$$

If the vortex is located at point a, the complex potential at point z will be

$$\chi(z) = \frac{\Gamma}{2\pi i}\ln(z-a) \qquad (3.2.12)$$

and the complex conjugate velocity is

$$\overline{w} = w_x - iw_y = \frac{\Gamma}{2\pi i(z-a)}. \qquad (3.2.13)$$

The potential motion discussed above is generated by a vortex. This is not in the least contradictory to the concept of potential motion without vortices. In fact, potential motion requires that the rotation of each particle of the fluid is equal to zero and this is satisfied everywhere (in the flow considered), with the only exception of the singular point r = 0 which has been excluded from consideration. It was this condition from which the motion was deduced.

Thus, the fluid elements in the flow considered are subjected only to shear deformation as this is shown in Fig. 3.2.3,c,for example, for the element abcd. The velocity at point b is equal to $\Gamma/2\pi r$, and at point C the velocity amounts to $\frac{\Gamma}{2\pi(r+\delta r)} \approx \frac{\Gamma}{2\pi r} - \frac{\Gamma\delta r}{2\pi r^2}$.

Therefore, the edge bc turns through the angle $-\frac{\dot{\Gamma}}{2\pi r^2}$ per unit time. During the same time the edge ba, moving along the circle of radius r at the speed $\Gamma:2\pi r$, turns through the angle $\Gamma:2\pi r^2$. The rate of change of the right angle, characterizing shear, will thus be $-\frac{\dot{\Gamma}}{2\pi r^2}-\frac{\Gamma}{2\pi r^2}=-\frac{\dot{\Gamma}}{\pi r^2}$; at the same time the bisector of the angle abc maintains its oritientation and the fluid element abcd does not rotate.

Singularities. Points on the flow plane at which a source or a vortex are located are singularities: the velocity at these points becomes infinite. Therefore flows which are generated by sources and vortices are sometimes called flows of singularities.

The core of a vortex. Since the velocity increases in inverse proportion to the radius, in accordance with the Bernoulli equation the pressure near the vortex axis should be zero or even negative, which is physically impossible. Experience (Fig. 3.2.4) shows that in a real fluid the velocity increases with decreasing radius only up to a certain limiting value after which it starts to drop linearly to reach zero at the vortex axis. Schemating the effect, it is possible to single out a vortex core which rotates like a solid body, with linear velocity distribution.

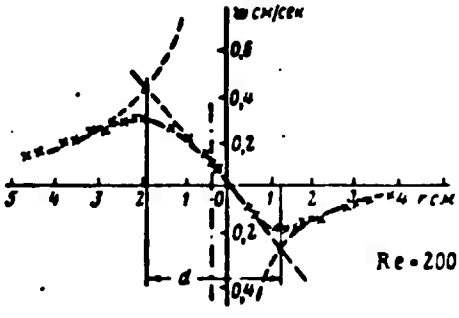


Fig. 3.2.4. Velocity field of a real vortex (experiment).

The superposition method. It follows from the linearity of the Laplace equation that if Φ_1 and Φ_2 are velocity potentials each of which satisfies the Laplace equation, their sum $\Phi = \Phi_1 + \Phi_2$ will also be a solution to this equation and is the velocity potential of a certain plane motion. In fact, if $\Delta\Phi_1 = 0$ and $\Delta\Phi_2 = 0$, we have

$$\frac{\partial^2\Phi}{\partial x^2}+\frac{\partial^2\Phi}{\partial y^2}=\frac{\partial^2}{\partial x^2}(\Phi_1+\Phi_2)+\frac{\partial^2}{\partial y^2}(\Phi_1+\Phi_2)=$$
$$=\frac{\partial^2\Phi_1}{\partial x^2}+\frac{\partial^2\Phi_1}{\partial y^2}+\frac{\partial^2\Phi_2}{\partial x^2}+\frac{\partial^2\Phi_2}{\partial y^2}=\Delta\Phi=0. \qquad (3.2.14)$$

Since the stream function of the potential motion exactly satisfies the Laplace equation, this conclusion holds for it too.

When velocity potentials or stream functions are added, their respective velocity fields add geometrically.

In fact,

$$\vec{w}=\vec{\nabla}\Phi=\vec{\nabla}\Phi_1+\vec{\nabla}\Phi_2=\vec{w}_1+\vec{w}_2.$$

Let us consider the streamlines of two arbitraty flows, ψ_1 = = const and ψ_2 = const, and determine the conditions under which the streamlines of the resultant flow come to coincide with the diagonals of a sufficiently fine net of the two families of the streamlines. If $\vec{w}_1$ and $\vec{w}_2$ are the velocity vectors of the first and second flows, respectively, the condition for the vector $\vec{w}$ = = $\vec{w}_1 + \vec{w}_2$ of the resultant flow to be directed along the diagonal of the parallelogram is the relation $\delta h_1/\delta h_2 = w_2/w_1$, where δh_1 and δh_2 are the normal distances between each pair of streamlines. This follows from the fact (Fig. 3.2.5) that the area of the elementary parallelogram Aabc is equal to $\delta h_1 w_1 \delta l = \delta h_2 w_2 \delta l$. For Ab to be directed along the diagonal of this parallelogram it is necessary that $w_1 : w_2 = Aa : Ac = \delta h_2 : \delta h_1$. Hence $w_1 \delta h_1 = w_2 \delta h_2 = \delta Q = \text{const}$ follows, i.e., the flow rate of the fluid between each pair of adjacent streamlines must be the same for both of the flows.

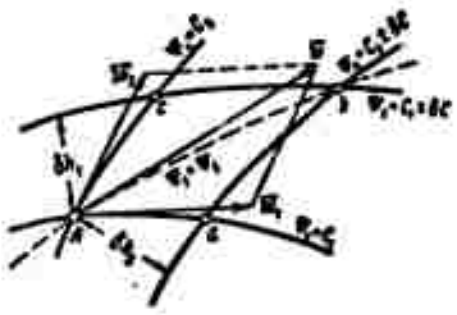


Fig. 3.2.5. For geometrical addition of two flows the flow rates between each pair of streamlines of both flows need be equal: $\delta C_1 = -\delta C_2$.

A plane dipole. This consists of a plane source and a sink with equal flow rates Q, when their separation 2l tends to zero and the flow rate to infinity, so that the product of the distance and the flow rate, M = 2Ql, (the dipole moment), remains constant. The direction from the sink to the source is called the dipole axis. The dipole flow plays a great part in classical hydromechanics. Its complex potential is obtained by the superposition method:

$$\chi(z) = \lim_{l\to 0} \frac{Q}{2\pi} \ln\frac{z+l}{z-l} = \lim_{l\to 0} \frac{Q\cdot 2l}{2\pi} \frac{\ln(z+l)-\ln(z-l)}{2l} = \\ = \frac{M}{2\pi}\frac{d}{dz}\ln z = \frac{M}{2\pi z}. \qquad (3.2.15)$$

The velocity potential and the stream function have the form

$$\Phi = \frac{Mx}{2\pi r^2} = \frac{M}{2\pi r}\cos\theta; \quad \Psi = -\frac{M}{2\pi r}\sin\theta. \qquad (3.2.16)$$

The streamline equation reads

$$-\frac{M}{2\pi(x^2+y^2)}y = C_1, \quad x^2+\left(y-\frac{C}{2}\right)^2 = \left(\frac{C}{2}\right)^2. \qquad (3.2.17)$$

i.e., the streamlines are circles of radius C/2, centered on the y-axis and touching the x-axis at the origin (Fig. 3.2.6).

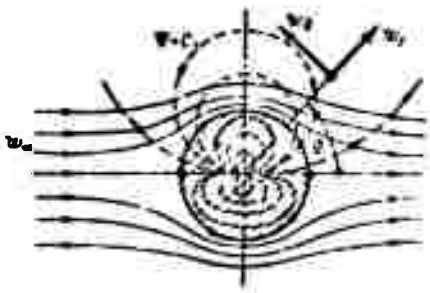


Fig. 3.2.6. The dipole with the moment M located in a parallel flow moving at the speed w_∞ deforms it in the same way as a solid circle of radius $r_0 = \sqrt{M/2\pi w_\infty}$ would. The streamlines of the dipole alone are given by the dashed lines in the upper part of the figure.

Taking into consideration that the equation of the equipotential lines, i.e., is obtained by substituting y by x in the streamline equations we arrive at the result that these lines will be circles which pass through the origin and have their centers on the x-axis.

Flow about a circular cylinder. Let us place a dipole in a flow parallel to the x-axis. The complex potential of the resultant flow will be

$$\chi(z)=w_\infty z+\frac{M}{2\pi}. \qquad (3.2.18)$$

The streamlines are determined by the equation

$$w_\infty y-\frac{M}{2\pi}\frac{y}{x^2+y^2}=C$$

or

$$y\left[w_\infty(x^2+y^2)-\frac{M}{2\pi}\right]=C(x^2+y^2).$$

They are third-order curves with the asymptotes $y = C/w_\infty$, with the exception of the case $C = 0$, for which the streamline equation $y\left[w_\infty(x^2+y^2)-\frac{M}{2\pi}\right]=0$ disintegrates into two equations

$$y=0\,(^*);\quad x^2+y^2=\frac{M}{2\pi w_\infty}=r_0^2\,(^*) \qquad (3.2.19)$$

i.e., the streamline consists of the x-axis and a circle centered in the origin, having the radius $r_0=\sqrt{\frac{M}{2\pi w_\infty}}$.

Thus, a flow element, coming from infinity along the x-axis, runs against the circle of radius r_0 and then flows above and below this circle, joins again and flows off along the axis to infinity (cf. Fig. 3.2.6). Since every streamline may be taken as a solid boundary, such a flow can be considered as the flow about a cylinder of radius $r_0=\sqrt{\frac{M}{2\pi w_\infty}}$. The dipole moment necessary to obtain the flow about a cylinder of given radius r_0 will be $M = 2\pi w_\infty r_0^2$.

Therefore, the function describing a flow parallel to the x-axis and flowing around a circular cylinder of radius r_0 at the given velocity w_∞, will be

$$\left.\begin{aligned}\chi(z)&=w_\infty\left(z+\frac{r_0^2}{z}\right).\\ \Phi&=w_\infty\left(r+\frac{r_0^2}{r}\right)\cos\theta,\\ \Psi&=w_\infty\left(r-\frac{r_0^2}{r}\right)\sin\theta.\end{aligned}\right\} \qquad (3.2.20)$$

In a polar coordinate system (r, θ)

$$\left.\begin{aligned} w_r &= \frac{\partial \Phi}{\partial r} = w_\infty \left(1 - \frac{r_0^2}{r^2}\right)\cos\vartheta, \\ w_\vartheta &= \frac{1}{r}\frac{\partial \Phi}{\partial \vartheta} = -w_\infty \left(1 + \frac{r_0^2}{r^2}\right)\sin\vartheta. \end{aligned}\right\} \qquad (3.2.21)$$

On the cylinder surface $r = r_0$ we have

$$w_r = 0, \quad w_\vartheta = -2w_\infty \sin\vartheta. \qquad (3.2.22)$$

The minus sign indicates that the direction of the velocity at the cylinder surface is opposite to the positive direction of angle reading.

Stagnation points on a solid body is the name given to the points at which the velocity becomes zero. In the case of the circle considered the stagnation points will lie on the x-axis at $\vartheta = 0$ and $\vartheta = \pi$.

Pressure distribution along a cylinder. To determine the pressure on the surface of the cylinder, we connect the point at infinity where the velocity is w_∞ and the pressure is p_∞ with the point on the cylinder surface where the pressure is p and the velocity is w, by the Lagrange equation:

$$p_\infty + \frac{\rho w_\infty^2}{2} = p + \frac{\rho w^2}{2}.$$

Determining the pressure coefficient by the relation $C_p = \frac{p - p_\infty}{\frac{1}{2}\rho w_\infty^2}$, we obtain for the cylinder

$$C_p = 1 - 4\sin^2\vartheta. \qquad (3.2.23)$$

Figure 3.2.7 gives the theoretical pressure distribution curve. It also gives the experimental curves as functions of the path l traveled by the cylinder from the beginning of the motion. As can be seen, in the forward region, the theoretical and the experimental curves lie close to each other throughout the duration of the motion. From an angle of about 120-130° on (50-60° from the forward stagnation point), however, the divergence becomes greater and greater and in the

rear region rarefaction arises instead of pressure. This is explained by the action of a vortex system formed in the boundary layer and concentrated in the wake region which strongly affects the motion pattern and the pressure distribution as well.

From the symmetry of the theoretical pressure distribution curve with respect to the x and y axes we can conclude that the resulting force acting on the cylinder is equal to zero because the sum of the projections of all pressure forces onto an arbitrary axis is zero. In fact, finally, the drag differs from zero; this can be seen from the asymmetry of the experimental pressure distribution curve.

Circulatory flow about a circular cylinder. The streamlines of a potential motion caused by a single vortex are circles. Each of them can be taken as a solid boundary. This makes it possible to superimpose the flow from a vortex onto the flow from a dipole in a parallel and so to obtain the circulatory flow about a cylinder of radius $r_0 = \sqrt{M : 2\pi w_\infty}$. For such a flow, the complex potential is

and correspondingly

$$\left.\begin{aligned} \chi(z) &= w_\infty\left(z+\frac{r_0^2}{z}\right)+\frac{\Gamma}{2\pi i}\ln z \\ \Phi &= w_\infty\left(r+\frac{r_0^2}{r}\right)\cos\vartheta+\frac{\Gamma}{2\pi}\vartheta, \\ \Psi &= w_\infty\left(r-\frac{r_0^2}{r}\right)\sin\vartheta-\frac{\Gamma}{2\pi}\ln r. \end{aligned}\right\} \qquad (3.2.24)$$

The radial and tangential velocity components at an arbitrary point of the stream will be

$$\left.\begin{aligned} w_r &= \frac{\partial\Phi}{\partial r} = w_\infty\left(1-\frac{r_0^2}{r^2}\right)\cos\vartheta, \\ w_\vartheta &= \frac{1}{r}\frac{\partial\Phi}{\partial\vartheta} = -w_\infty\left(1+\frac{r_0^2}{r^2}\right)\sin\vartheta+\frac{\Gamma}{2\pi r} \end{aligned}\right\} \qquad (3.2.25)$$

with $r = r_0$, i.e., at the cylinder surface,

$$w_r = 0, \quad w_\vartheta = -2w_\infty \sin\vartheta + \frac{\Gamma}{2\pi r_0}. \qquad (3.2.26)$$

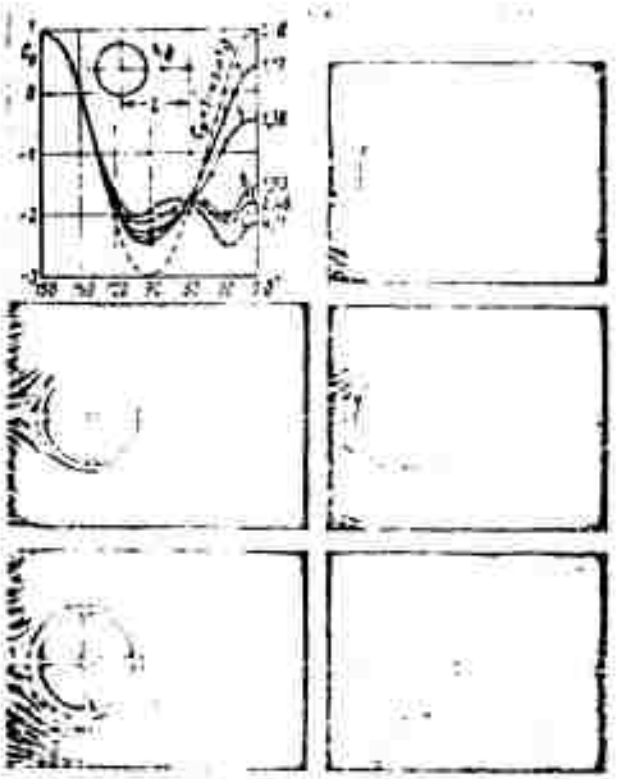


Fig. 3.2.7. Change of pressure distribution on a cylinder in dependence on the path $\frac{l}{d}$ traveled (in terms of diameter d); the figures on the pressure distribution curves correspond to the numbers of the motion picture frames.

The stagnation points will now be shifted [illegible] -axis. Their position is determined by the equation $w_\vartheta = 0$ that gives value of the angle ϑ_{kr} determined by the equation

$$\sin\vartheta_{kr} = \frac{\Gamma}{4\pi w_\infty r_0}. \qquad (3.2.27)$$

Since $\sin\vartheta = \sin(\pi - \vartheta)$, the stagnation points for $\Gamma < 4\pi w_\infty r_0$ will be symmetrical with respect to the y-axis. For $\Gamma = 4\pi w_\infty r_0$ the two stagnation points fuse to one $\left(\vartheta_{kr} = \frac{\pi}{2}\right)$. When $\Gamma > 4\pi w_\infty r_0$ part of the stream circulates about the cylinder and does not flow off together with the remaining fluid to infinity. The forms of motion [illegible]

cases discussed are given in Fig. 3.2.8.

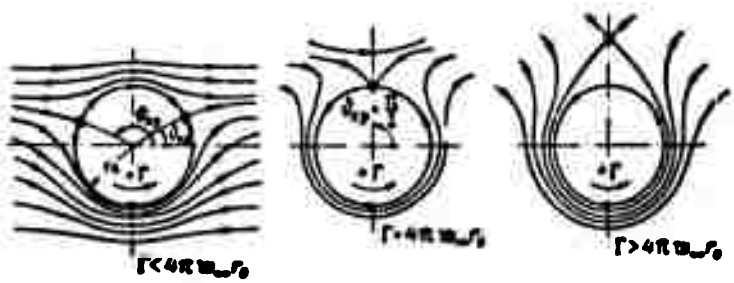


Fig. 3.2.8. Flow about a cylinder with circulation. The stagnation points are determined by the equation $\sin\vartheta_{kr} = \Gamma/4\pi w_\infty r_0$

Forces on a circular cylinder. The presence of a circulatory motion violates the symmetry of motion and the pressure distribution with respect to the x-axis. This leads to the appearance of non-vanishing resulting pressure forces of the fluid acting on the cylinder in the direction of the y-axis. Since the symmetry with respect to the y-axis is conserved, the reaction as to the x-axis will be zero, as before. In fact, determining the pressure at some arbitrary point of the cylinder surface from the Bernoulli equation, we have

$$p = p_\infty + \frac{\rho w_\infty^2}{2} - \frac{\rho}{2}\left(-2w_\infty \sin\vartheta + \frac{\Gamma}{2\pi r_0}\right)^2.$$

However, (Fig. 3.2.9), we also have

$$dX = -pr_0\cos\vartheta\, d\vartheta; \quad dY = -pr_0\sin\vartheta\, d\vartheta.$$

Integrating over the whole surface of the cylinder, we obtain

$$-X = \int_0^{2\pi} pr_0\cos\vartheta\, d\vartheta = r_0\left(p_\infty + \frac{\rho w_\infty^2}{2}\right)\int_0^{2\pi}\cos\vartheta\, d\vartheta - \\ - \frac{\rho r_0}{2}\int_0^{2\pi}\left(\frac{\Gamma}{2\pi r_0} - 2w_\infty\sin\vartheta\right)^2\cos\vartheta\, d\vartheta = 0 \qquad (3.2.28)$$

For the y-component of the reaction we obtain

$$-Y = \int_0^{2\pi} pr_0\cos\vartheta\, d\vartheta = r_0\left(p_\infty + \frac{\rho w_\infty^2}{2}\right)\int_0^{2\pi}\cos\vartheta\, d\vartheta - \\ - \frac{\rho r_0}{2}\int_0^{2\pi}\left(\frac{\Gamma}{2\pi r_0} - 2w_\infty\sin\vartheta\right)^2\sin\vartheta\, d\vartheta = \rho w_\infty\Gamma. \qquad (3.2.29)$$

Thus, when a parallel flow of velocity w_∞ and of circulation Γ streams round a cylinder, a force acts per unit length of the circular cylinder that is equal to the product of the density ρ, the velocity w_∞ and the circulation Γ; the direction of the force is obtained by turning the velocity vector 90° in the direction opposite to that of the circulation (Fig. 3.2.10). We shall show in what follows that this conclusion remains valid for a cylinder of any other cross section. This result is a special case of particular importance for the aeromechanical theorem of N. Ye. Zhukovskiy who first established the relation between circulation and lift.

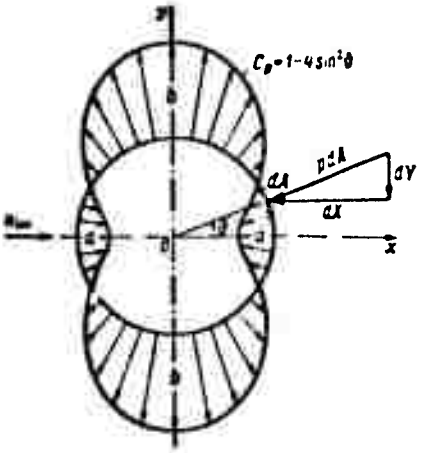


Fig. 3.2.9. Determination of the forces acting on the cylinder in a circulatory flow. a) Pressure region; b) rarefaction region

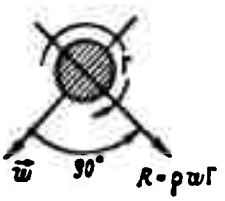


Fig. 3.2.10. Force vector R acting per unit length of the cylinder is equal to the modulus $\rho w \Gamma$ and coincides with the direction of the speed vector turned through 90° in the direction opposite to that of the circulation.

The flow about bodies of arbitrary shape.

The flow regime about bodies of various shapes can be built up by selecting the appropriate singularity distribution in such a way that one of the streamlines comes to coincide with the body contour. These singularities are termed adjacent. It should be noted, however, that in the case of a given shape the solution depends on the choice of this distribution being more or less fortunate.

Adjacent sources and sinks which are to distort a parallel stream in such a way as if it were deformed by the body considered, in the region of which they must be arranged, have to

satisfy the condition that the sum of the flow rates vanishes for closed bodies, namely

$$\sum_{i=1}^{n} Q_i = 0. \qquad (3.2.30)$$

A circulatory flow about a body can be obtained if not only sources, sinks (and dipoles), but also vortices are located inside the contour; the total vorticity of the adjacent vortices must be equal to the total circulation about the body.

Flow near plane walls (fictitious singularities). Let us first consider the form of flow from two sources with equal flow rates. It can be seen from Fig. 3.2.11 that the normal passing through the midpoint of the line section connecting the two sources will be a streamline; the velocity component normal to it is equal to zero. It is therefore possible to regard it as a solid wall and to suppose that one of the sources distorts the flow from the other source in the same way as a solid wall passing perpendicularly through the line section connecting the sources would.

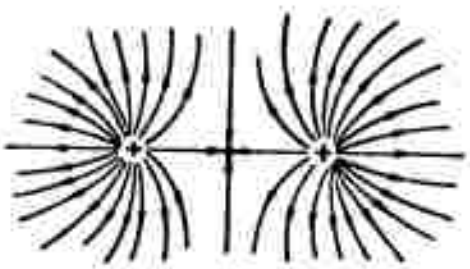


Fig. 3.2.11. In the flow from two equal sources the normal passing throught the midpoint of the straight line connecting the sources is a streamline.

To construct the flow pattern of a source near a solid plane wall, the wall should, therefore, be taken as the symmetry axis and a fictitious source should be placed at the symmetrical point. The flow produced be these two sources in the semi-plane of the true source will be the very same as that of the true source near the plane wall. The flow pattern of a vortex near a wall is constructed analogously.

This result can be generalized to any form and any number of

singularities to obtain the flow about bodies near a plane wall; this method is also called the method of the fictitious singularities.

Approximate methods. The net of streamlines and equipotential lines constitutes an isothermal net; when one streamline, namely the body contour, is known, it is therefore possible to construct the corresponding net which, in first approximation, yields the streamlines and equipotential line sections.

The net of streamlines and equipotential lines obtained is corrected by the method of successive approximations. It can be shown that if abcd is a small square of the net and if ψ_a, ψ_b, ψ_c, ψ_d, and ψ_m are the respective values of the stream function at the corners and the center m of the net square, we have

$$\psi_m = \frac{1}{4}(\psi_a + \psi_b + \psi_c + \psi_d) \qquad (3.2.31)$$

This relation can also be used for improving the net. The correction process is continued until there is virtually no difference between the results of successive calculations.

Simulation of a flow by means of analogy considerations. The tediousness of the calculations and the considerable errors in the region of the stagnation points are the main disadvantages of the calculation methods for constructing flow patterns of the given bodies. If we ignore physical simulation which consists in the physical nature of the effects being maintained and the experimental results obtained with the models being transformed to natural ones, of the calculation methods of similarity theory, when the flow is studied, then what we are considering is analog simulation using the analogy between the differential equations describing the model and the process to be represented.

The electrohydrodynamic analogy (EHDA) is based on the formal similarity of the equations of electric current and potential motion.

of an inviscid fluid; the EHDA is very often used for constructing plane flow patterns. Since both the electrical field and the electrical potential in a plate are characterized by a stream function ψ satisfying the Laplace equation, the potential field (field A) and the stream function (field B) can be analogous to each other. In system A the model contour is made up of an insulator, since it must represent the streamline. In system B the model contour must be the equipotential line and is made of a conductor. By the analogy of system B, it is possible to construct the streamline field about the body.

Since in system A a sufficiently small electrode corresponds to a point source (or sink), and in the analogous system B to a vortex (the streamlines, represented by equipotential lines, enclose the electrode as circles), in the system B the current carrying bounding bars can be considered as the total of the vortices. Consequently, this system permits of a model representation of a vortex field which is important in representing a circulatory contour flow about bodies. In this case we make use of the many-valuedness of the vortex potential. This is done by cutting apart the field in system B at a known electrical equipotential line and a potential jump corresponding to the given circulation is obtained

$$\Gamma = \varphi_2(a) - \varphi_1(a) = k\,[u_2(a) - u_1(a)]. \qquad (3.2.31)$$

Singularity flow about a circle. For the following considerations it is of importance to note that streamlines in the form of circles can be obtained not only in a parallel stream but also in a singularity field. Let us consider, for example, a sink at the coordinate origin and two sources of equal intensity Q at the points x = a and x = 1, satisfying the equation $a1 = r_0^2$ (Fig. 3.2.12). In this case the stream function will be

$$\Psi = \frac{Q}{2\pi}\left[-\operatorname{arc\,tg}\frac{y}{x} + \operatorname{arc\,tg}\frac{y}{x-a} + \operatorname{arc\,tg}\frac{y}{x-\left(\frac{r_0^2}{a}\right)}\right] =$$

$$= \frac{Q}{2\pi}\operatorname{arc\,tg}\frac{\frac{ay}{x^2+y^2-ax} + \frac{ay}{ax-r_0^2}}{1-(x^2-ax+y^2)\left(x-\frac{r_0^2}{a}\right)}. \qquad (3.2.32)$$

Obviously, if $x^2+y^2=r_0^2$, $\Psi=0$ and this streamline $\Psi = 0$ will be a circle. Some of the streamlines of the flow pattern obtained are given in Fig. 3.2.12.

In the general case, in order to maintain the streamline as a circle of radius r_0 in the flow of sources (sinks) and vortices outside it at the distance r_a from the center, like singularities must be placed inside the circle but at the distances

$$r_i = \frac{r_0^2}{r_a}. \qquad (3.2.33)$$

the sign of vortex circulation at the corresponding prongs being changed.

As may be seen, each of these singularities introduced can be considered as a mirror image of a given singularity reflected in the circle.

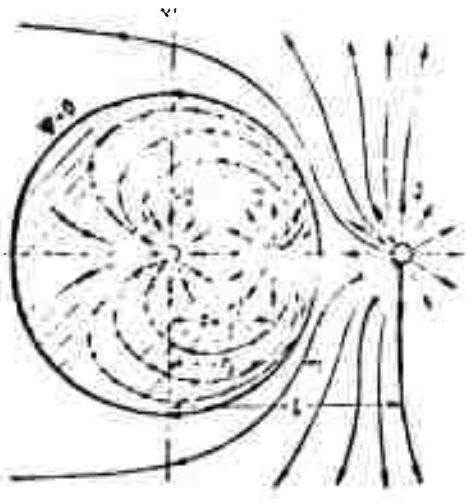


Fig. 3.2.12. A flow about a circle of radius r_0 from a plane source Q at point $x = \underline{1}$ can be obtained by introducing into the flow from this source a sink at the coordinate origin and a source of the same intensity, Q, on the x-axis at the point $r_0^2/\underline{1}$.

A parallel flow can be considered as a flow from a dipole located at infinity $r_a \to \infty$ and having an arbitrarily large dipole moment. The parallel flow about a circle considered above is thus equal to the flow about it from this dipole. For this reason a dipole is placed in the origin of the coordinates, $r_1 \to 0$, at a distance satisfying the condition $r_a r_1 = r_0^2$. To solve the problem of the values of the dipole moments the problem has to be considered in greater detail.

Let a source be placed at the point $x = a - \varepsilon$ and a sink of equal intensity at the point $x = a + \varepsilon$. To obtain circular streamlines it is necessary to place the same source and sink at the points $x = r_0^2/(a - \varepsilon)$ and $x = r_0^2/(a + \varepsilon)$, respectively. The complex potential will be

$$\chi(z) = \frac{Q}{2\pi}\left\{\ln[z-(a-\varepsilon)] - \ln[z-(a+\varepsilon)] + \right.$$
$$\left. + \ln\left(z - \frac{r_0^2}{a-\varepsilon}\right) - \ln\left(z - \frac{r_0^2}{a+\varepsilon}\right)\right\}. \qquad (3.2.34)$$

As $\varepsilon \to 0$ so that $2Q\varepsilon = M = \text{const}$, then, noticing that

$$1:(a \pm \varepsilon) \approx \frac{a \mp \varepsilon}{a^2},$$

we obtain

$$\chi(z) = \frac{M}{2\pi}\lim_{\varepsilon \to 0}\left\{\frac{\ln[(z-a)+\varepsilon] - \ln[(z-a)-\varepsilon]}{2\pi} + \right.$$
$$\left. + \frac{\ln\left[z - \frac{r_0^2}{a^2}(a-\varepsilon)\right] - \ln\left[z - \frac{r_0^2}{a^2}(a+\varepsilon)\right]}{2\pi}\right\} =$$
$$= \frac{M}{2\pi}\frac{d}{dz}\left\{\ln(z-a) + \frac{r_0^2}{a^2}\ln\left(z - \frac{r_0^2}{a}\right)\right\} =$$
$$= \frac{M}{2\pi}\left\{\frac{1}{z-a} + \frac{r_0^2}{a^2}\frac{1}{z-(r_0^2:a)}\right\}. \qquad (3.2.35)$$

i.e., the moment of the external dipole is larger than the moment of the dipole placed inside the circle by a factor of (r_0^2/a^2) and the dipole axes run in opposite directions.

3.3. THE METHOD OF CONFORMAL MAPPING

The geometrical meaning of a derivative. Let us consider the analytic function $\chi(z)=\Phi+i\Psi$ of the complex variable $z = x + iy$.

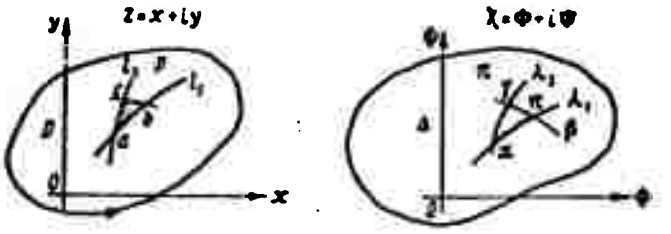


Fig. 3.3.1. In conformal mapping of infinitesimal figures they remain similar (extended or shrunk) at the respective points of the plane and are rotated.

If we choose some region D in the (x, y)-plane, the function $\chi(z)$ maps (transforms) it into region Δ of the plane $\chi = \Phi + i\Psi$. The properties of this transformation (Fig. 3.3.1) are very important for aerohydromechanics. Let a be some point on the curve l_1 in the region D in which the derivative $\chi'(z) = \sigma e^{i\omega} \neq 0$, and let α be the corresponding point in the region Δ on the curve λ_1 which is a model of curve l_1. Moreover, let p and π be corresponding variable points on the curves l_1 and λ_1.

We set up the derivative

$$\frac{d\chi}{dz}=\lim_{z\to z_1}\frac{\chi(z)-\chi(z_1)}{z-z_1}=\sigma e^{i\omega},$$

and obtain

$$|d\chi|=\sigma|dz|,\quad \arg d\chi=\arg dz+\omega. \tag{3.3.1}$$

i.e., the modulus of the derivative is equal to the linear scale of mapping and the argument of the derivative gives us the angle of turn of the linear element in the vicinity of the point $z = z_1$. Both σ and ω are independent of the choice of curve l_1; they are equal for all curves passing through the chosen point but differ at different points of the plane. Therefore the infinitely small

figure near the point considered is transformed to a similar figure turned through the angle ω, its linear parameters being enlarged by the factor σ. Such a transformation, in which the magnitudes and reading directions of the angles ara maintained, is termed conformal.

The hydrodynamic significance of conformal mapping. Let us consider an arbitrary flow in the z-plane

$$\chi(z)=\Phi(x,y)+i\Psi(x,y).$$

The streamlines and the equipotential lines constitute an orthogonal net of curves. If we now choose an arbitrary analytic function $\zeta=\xi+i\eta=F(z)$ take its independent variable as $z=f(\zeta)$, and substitute this value in $\chi(z)$, we obtain the new analytic function $\chi[f(\zeta)]=\Phi[x(\xi,\eta),y(\xi,\eta)]+i\Psi[x(\xi,\eta),y(\xi,\eta)]$. The lines Ψ = const and the lines Φ = const in the ζ-plane will also be orthogonal, i.e., this new function will represent the complex potential (stream function) of some new flow which is obtained by deforming and rotating the elements of the primary flow. In this case the function $f(\zeta)$ is said to perform conformal mapping of the flow in the z-plane to a flow in the ζ-plane. The flow about the given body can be obtained by choosing the transforming function properly.

Let us consider the physical conditions of correspondence for these flows. Since the indices of Φ and Ψ are equal at points which correspond to each other in the two flows, their differences for corresponding lines will also be equal, i.e., the flow rate (Fig. 3.3.2) of a fluid between two streamlines will be equal:

$$\Psi_2-\Psi_1=a_1d_1\cdot w_1=ad\cdot w.$$

In the limiting case, when the net is diminished without restriction, $a_1d_1 = \delta z$, $ad = \delta\zeta$, we obtain

$$\frac{w(\zeta)}{w(z)}=\left|\frac{dz}{d\zeta}\right|. \qquad (3.3.2)$$

where $w(\zeta)$ and $w(z)$ are the velocities at corresponding points of the planes ζ and z.

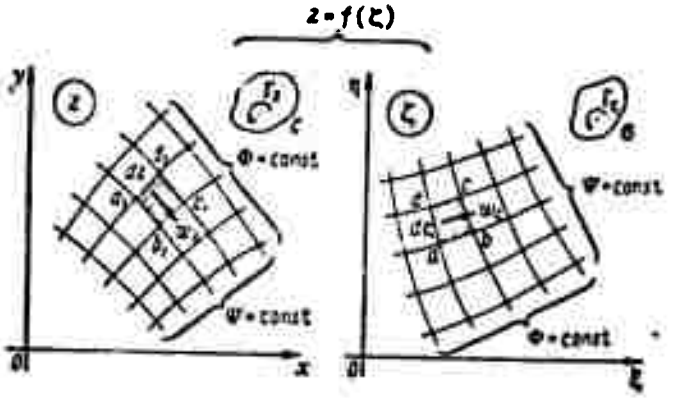


Fig. 3.3.2. In conformal mapping $w_z dz = w_\zeta d\zeta$ and therefore the vorticity remains unchanged

Let us consider an arbitrary closed contour C in the z-plane and the corresponding contour σ in the ζ-plane around a singular point, namely a vortex. We set up the expression for the circulation and obtain

$$\begin{aligned}\Gamma(z) &= -\oint_C \vec{w}\cdot d\vec{l} = -\oint_C (\vec{i}w_x + \vec{j}w_y)\cdot(\vec{i}\,dx + \vec{j}\,dy) = \\ &= -\mathrm{Re}\left\{\oint_C [(w_x dx + w_y dy) - i(w_x dy - w_y dx)]\right\} = \\ &= -\mathrm{Re}\oint_C (w_x - iw_y)(dx + i\,dy)\Big\} = \mathrm{Re}\left\{\oint_C \bar{w}\,dz\right\} = \\ &= \mathrm{Re}\left\{\oint_\sigma \frac{d\gamma}{dz}\,dz\right\} = \mathrm{Re}\left\{\oint_\sigma \frac{d\zeta}{d\zeta}\,d\zeta\right\} = \Gamma(\zeta),\end{aligned} \tag{3.3.3}$$

i.e., mapping leaves the vorticity unchanged.

Flow about a corner. Let us consider a flow parallel to the x-axis in the upper semiplane (the x-axis is this boundary), $\chi(z) = w_\infty z$ and study the transformation of this flow with the help of the function $\zeta = z^n$, $(n > 0)$ (Fig. 3.3.3). We put $z = re^{i\varphi}$, $\zeta = \rho e^{i\theta}$, then $re^{i\varphi} = \rho^{\frac{1}{n}} e^{i\frac{\theta}{n}}$, i.e.,

$$r=\sqrt[n]{\rho},\quad \alpha=\frac{\theta}{n}. \tag{3.3.4}$$

This transformation is conformal everywhere except at the point z = 0 where $\frac{d\zeta}{dz}=nz^{n-1}$, is equal to zero (n > 1) or to infinity (n < 1). (The case n = 1 is without interest since it does not influence the flow). The right-hand semiaxis x, i.e., the streamline a = 0, goes

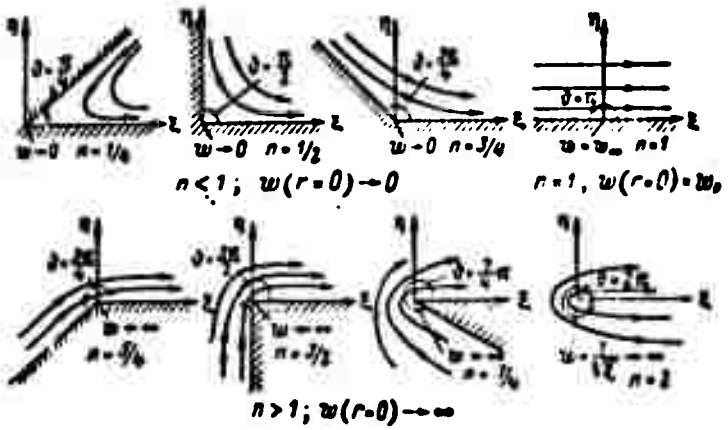


Fig. 3.3.3. With n < 1 the function $\zeta = z^n$ transforms the parallel flow w_∞ z in the upper semiplane z to a flow inside the corner on the ζ-plane, and for n > 1 it gives the flow outside the corner.

over to the right-hand semiaxis ξ for which α = 0. The left-hand semiaxis x, for which a = π, is transformed to a straight line forming the angle α = πn. Thus, the whole x-axis is transformed to the angle πn formed by the ξ-axis and the straight line of the angle πn. Hence n ≤ 2. Since the complex velocity on the ζ-plane is

$$\overline{w}=w_1-iw_2=\frac{dx}{dz}\frac{dz}{d\zeta}=w_\infty\frac{1}{n}z^{\frac{1}{n}-1},$$

it vanishes in the corner itself (ζ = 0, z = 0) when n < 1 (flow inside the corner), and when n > 1 it becomes infinite (flow outside the corner).

Assuming n = 2 ($\zeta = z^2$) we obtain the flow about the edge of a plane plate positioned on the positive semiaxis x. Let us note

that in this case, if $\zeta \to 0$, the velocity tends to infinity as $1/\zeta$. The flow patterns for various values of λ are shown in Fig. 3.3.3.

Flow about an arbitrary contour. The method of conformal mapping makes it possible to solve the problem of the flow about an arbitrary contour provided we know its conformal mapping to some other contour, the flow about which is known; for the latter a circle is usually chosen. Since in this case we are interested in both the region outside the given contour and that outside the circle, we consider the general form of the function performing the conformal mapping of the region outside this contour to the region outside the circle. However, sometimes the flow region outside the body is mapped to the region inside the circle in the τ-plane; this transition is performed by replacing ζ by $1/\tau$.

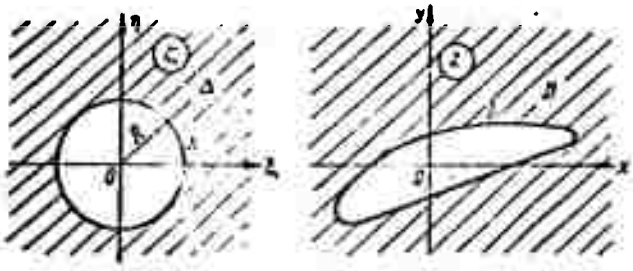


Fig. 3.3.4. Correspondence of the regions outside the circle and the contour L.

Let the ζ-plane be the plane of the circle K of radius r with its center at the origin and let region A outside the circle contains an infinitely distant point. The contour L of the region D is given on the z-plane; its infinitely distant point lies in the region outside the contour L (Fig. 3.3.4).

The unique mutual correspondence between these regions is formulated with the help of the analytic functions

$$z = f(\zeta); \quad \zeta = g(z).$$

We represent $z = f(\zeta)$ as a Loran series

$$z=\sum_{n=-\infty}^{\infty}a_n\zeta^n.$$

If we require that the points $z = \infty$ and $\zeta = \infty$ correspond to each other and that the derivative $dz/d\zeta$ is positive at infinity (i.e., that the velocity does not change its direction at infinity), we can show that the mapping function must have the form

$$z=a_1\zeta+a_0+\frac{a_{-1}}{\zeta}+\frac{a_{-2}}{\zeta^2}+\ldots \qquad (3.3.5)$$

or, with $a_1=b_{-1}$, $a_0=b_0$, $a_{-n}=b_n$,

$$z=b_{-1}\zeta+b_0+\frac{b_1}{\zeta}+\frac{b_2}{\zeta^2}+\ldots, \quad b_{-1}>0. \qquad (3.3.6)$$

Conversely,

$$\zeta=c_{-1}z+c_0+\frac{c_1}{z}+\frac{c_2}{z^2}+\ldots. \qquad (3.3.7)$$

The coefficients b_n and c_n are linked by relations, the first of which have the form

$$\begin{gathered}b_{-1}c_{-1}=1;\ \ b_{-1}c_0+b_0=0;\ \ b_{-1}c_{-1}c_1+b_1=0;\\ b_{-1}c_{-1}^2c_2-b_1c_1c_{-1}+b_2=0.\end{gathered} \qquad (3.3.8)$$

If the complex potential of the flow about the contour L being $\chi(z)=\Phi+i\Psi$, and the velocity at infinity $\overline{w}_\infty=\left.\frac{d\chi}{dz}\right|_{z=\infty}=w_\infty e^{i\alpha}$, then substituting $z = f(\zeta)$ in $\chi(z)$ yields the stream function $\chi(\zeta)=\chi[f(\zeta)]=\Phi_1+i\Psi_1$ in the ζ-plane, and the velocity at infinity is

$$\overline{w}_\infty=\left.\frac{d\chi(\zeta)}{d\zeta}\right|_{\zeta=\infty}=\left.\frac{d\chi}{dz}\cdot\frac{dz}{d\zeta}\right|_{\substack{\zeta=\infty\\ z=\infty}}=b_{-1}w_\infty e^{i\alpha},$$

i.e., the circle is placed in a flow whose velocity at infinity is larger by the factor b_{-1}.

Moreover, by convention we have $\chi(z)=\chi[\zeta(z)]$; $\Phi=\Phi_1$; $\Psi=\Psi_1$, for corresponding points on the planes z and ζ.

For the circle

$$\chi(\zeta)=w_\infty\zeta+\frac{w_\infty R^2}{\zeta}+\frac{\Gamma}{2\pi i}\ln\zeta. \qquad (3.3.9)$$

and for the contour, if $\zeta = g(z)$, the solution to the equation

$z = f(\zeta)$ is

$$\chi[g(\zeta)] = w_\infty g(z) + \frac{w_\infty R^2}{g(z)} + \frac{\Gamma}{2\pi i} \ln g(z) \qquad (3.3.10)$$

These expressions contain an arbitrary constant, Γ, determining the circulation with respect to the contour L, which has to be given for a smooth contour having no corner points (thus also for a circle).

A wing profile has a round leading edge and a sharp trailing edge. When a flow with an arbitrary circulation streams around the sharp edge, as in the case of a flow about a corner (cf. p. 163), the velocity will become infinitely large. N.Ye. Zhukovskiy and S.A. Chaplygin suggested determining the value of the circulation in such a way that the velocity at the trailing edge remains finite. This suggestion is called the Zhukovskiy-Chaplygin postulate or the condition of smooth flow around the trailing edge. This will be elucidated in what follows.

The hodograph method. In a number of cases the determination of the stream function $\chi(z)$ is simplified if it is possible to make some suppositions as to the nature of the velocity distribution of the

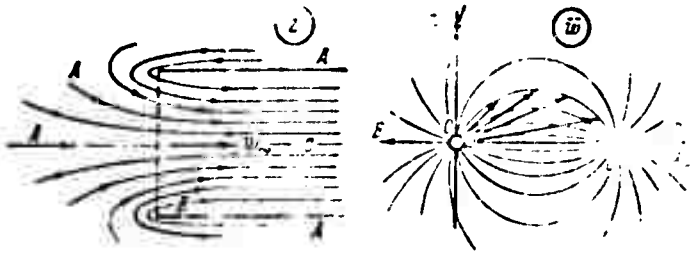


Fig. 3.3.5. Flow at the inlet and its hodograph.

flow considered. Thus, if $\overline{w} = d\chi/d\zeta$, it can be proved that χ will be also an analytic function, i.e., the mapping of the plane $\overline{w}$ to the plane χ will be conformal. Hence, if the relation between $\overline{w}$ and χ can be more or less simply established in the form $\overline{w} = f(\chi)$, the relation between χ and z is found by integrating;

$$z = \int \frac{dq}{\bar{w}} + \text{const} = \int \frac{dq}{f(q)} + \text{const.} \qquad (3.3.11)$$

This method of determining the stream function is called the hodograph method.

We consider as an example a fluid coming from infinity and flowing into the opening of a gap in which, at a sufficient distance from the inlet, the velocity has assumed a constant value $w_x = w_0$ (Fig. 3.3.5). Let us construct the velocity hodograph for this flow. Since inside the gap the velocity decreases with the distances as $1/r^2$ it will tend to zero at infinity; at the edges of the opening, as has been shown in the case of the flow about the edge of a plate (cf. Fig. 3.3.3) it is infinitely large. Therefore, the inifinity A in the plane of flow will correspond to the origin of the coordinates of the hodograph plane. The middle streamline AC will correspond to the straight line section between origin and point C, where $OC = w_0$, since the velocity in it increases from zero at infinity to $w_x = w_0$ without changing its direction.

The streamline for the lower boundary of the opening will begin (as all the streamlines of the z-plane) at infinity A, i.e., for the $\bar{w}$-plane at the origin of the coordinates, and, without changing its direction, it will increase to infinity at point B;here the velocity, reversing its direction, will start dropping to the value w_0. In the $\bar{w}$-plane this will be a straight line from zero to minus infinity on the left and then from plus infinity to the point C, where $w_x = w_0$. The other streamlines will begin at the origin and end at point C, their form resembling the flow from a source (at point O) to a sink (at point C).

We assume that there is in fact a source at point O and a sink at point C, and we investigate whether in this case the boundary

conditions are satisfied in the physical plane of flow. If they are, the solution found will be unique and therefore regular. The complex potential of this flow in the hodograph plane will be

$$\chi(\bar{w}) = C[\ln \bar{w} - \ln(\bar{w} - w_0)] = C \ln \frac{\bar{w}}{\bar{w} - w_0}.$$

whence

$$\frac{d\bar{w}}{dz} = -\frac{w_0 e^{\frac{\Phi}{C}}}{1 - e^{\frac{\Phi}{C}}} = \frac{w_0}{1 - e^{-\frac{\Phi}{C}}}.$$

When integrating this and ignoring the unimportant constant we find

$$z = \int \frac{d\bar{w}}{\bar{w}} = \int \frac{d\Phi}{w_0}\left(1 - e^{-\frac{\Phi}{C}}\right) = \frac{\Phi}{w_0} + \frac{C}{w_0} e^{-\frac{\Phi}{C}}. \qquad (3.3.12)$$

separating the real and imaginary parts we obtain

$$z = x + iy = \frac{1}{w_0}\left[\Phi + i\Psi + Ce^{-\frac{\Phi}{C}}\left(\cos\frac{\Psi}{C} - i\sin\frac{\Psi}{C}\right)\right].$$

$$x = \frac{1}{w_0}\left(\Phi + Ce^{-\frac{\Phi}{C}}\cos\frac{\Psi}{C}\right).$$

$$y = \frac{1}{w_0}\left(\Psi - Ce^{-\frac{\Phi}{C}}\sin\frac{\Psi}{C}\right).$$

We check whether the functions found satisfy the boundary condition that the walls must be [illegible]. For $\Psi = 0$ we have $w_0 y = 0$, i.e., the lower wall is a streamline. For the streamline $\Psi = 2\pi C$ we obtain the equation $y = 2\pi C/w_0$. This streamline must coincide with the upper wall of the opening, and so the constant C is determined by the condition $C = \frac{w_0 d}{2\pi}$.

The boundary conditions are thus satisfied. Since the solution is unique it is the only one. The central line will lie at $y = d/2$; its equation reads $\Psi = \pi C = \text{const}$. The explicit solution is easily found for the streamline $\Psi = \pi C/2$ as well, namely

$$w_0 y = \frac{\pi C}{2} + Ce^{-\frac{\Phi}{C}}; \quad w_0 x = \Phi.$$

i.e.,

$$x, y = \frac{aC}{2} + Ce^{-\frac{\pi x}{C}} = \frac{\pi w_0 d}{2 \cdot 2\pi} + \frac{w_0 d}{2\pi} e^{-\frac{\pi x \cdot 2\pi}{w_0 d}}$$

or

$$y = \frac{d}{4} + \frac{d}{2\pi} e^{-\frac{2\pi}{d} x}.$$

Optimum shape of a plane air intake. In the subsonic flow of an inviscid gas the thrust of an infinitely long air intake is independent of the shape of the outer contour CJKLM (Fig. 3.3.6) as will be shown in detail in Chapter 8. It is exactly equal to the drag of the inner contour (CDE), which depends only on the ratio between the speed w_k in the tube and the speed of the undisturbed flow, w_∞. The pressure distribution, however, depends on the shape of the air intake; when viscosity and compressibility of the gas and the strength of the air intake are taken into account, it is expeditious to construct it in such a way that the pressure on the outer surface is uniformly distributed. An air intake having such a form will be referred to as optimum.

Let us construct an exemplary velocity hodograph for a plane air intake whose inner tube is of constant width h, and let us assume that the pressure p and the speed w are constant on its outer contour (Fig. 3.3.6). We consider the streamline through the stagnation point C.

The velocity that is constant at infinity A is mapped in the hodograph by the line section $Oa = w_\infty$. When approaching point C, the velocity along the streamline will drop to zero at point C and deviate a little from the x-direction; let it be given by the curve abc. On the streamline branching at point C, the inner speed contour fairly quickly reaches the given finite value w_k somewhere at point D. The part of the streamline parallel to the x-axis transforms to

the section cd. The other streamlines inside the channel, AFG, etc., correspond to the dashed curves afd,... in the hodograph. The streamline from the branching point C on the outer contour CJKL will be the section cj of the w_x-axis of the hodograph on which the velocity reaches its maximum value w_m; the velocity vector then rotates through 180° keeping its magnitude constant - in the hodograph this will correspond to the semicircle jkl, and, beginning at a certain point L it will decrease, keeping the x-direction, until, at some point M, it becomes equal to the velocity w_∞ of the undisturbed flow at point A. The outer streamlines APQR outside the contour are given as dashed lines in the hodograph.

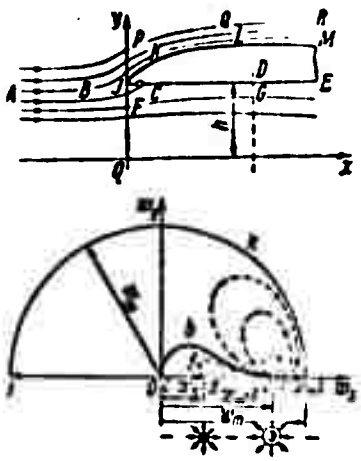


Fig. 3.3.6. Speed hodograph of a plane air intake. It can be considered as the flow from a source (intensity Q), a dipole at the point $w_\infty = 1$ with the moment M and a sink at point w_k (of the same intensity Q as the source).

Completing the hodograph to a full circle by reflecting it from the real axis, we may assume that the flow in the hodograph plane can be realized by a dipole and a source at point a and a sink at point d with an intensity equal to that of the source at point a.

For the circle of radius w_m to be a streamline it is necessary that at points reflected with respect to the circle, there exist a source and a sink of equal intensity and a dipole with a moment greater by a factor of w_m^2/w_∞ [cf. (3.2.35)].

Assuming $w_\infty = 1$ in (3.2.35) we obtain the complex potential in the form

$$\chi(w) = \frac{Q}{2\pi}[\ln(w-1)+\ln(w-w_m^2)]+$$
$$+\frac{M}{2\pi}\left(\frac{1}{w-1}-\frac{w_m^2}{w-w_m^2}\right)-\frac{Q}{2\pi}\left[\ln(w-w_k)+\ln\left(w-\frac{w_m^2}{w_k}\right)\right]= \qquad (3.3.13)$$

$$= \frac{Q}{2\pi} \ln \frac{(w-1)(w-w_m^2)}{(w-w_0)\left(w-\frac{w_m^2}{w_0}\right)} + \frac{M}{2\pi}\left(\frac{1}{w-1} - \frac{w_m^2}{w-w_m^2}\right). \qquad (3.3.13)$$

Introducing the denotation M/Q = κ and differentiating $\chi(w)$ with respect to $\underline{w}$ we obtain the velocity in the hodograph plane:

$$\frac{2\pi}{Q}\frac{df}{dw} = \frac{1}{w-1} - \frac{1}{w-w_0} + \frac{1}{w-w_m^2} - \frac{1}{w-\frac{w_m^2}{w_0}} +$$

$$+ \varkappa\left[\frac{1}{(w-1)^2} - \frac{w_m^2}{(w-w_m^2)^2}\right]. \qquad (3.3.14)$$

For determining the ratio M/Q we have the condition that the point w = 0 is a stagnation point. This yields

$$\varkappa = \frac{w_m^2\left(\frac{1}{w_0}-1\right)-(1-w_0)}{w_m^2-1}. \qquad (3.3.15)$$

Here

$$z = \int \frac{d\chi}{dw}\cdot\frac{dw}{w} + \text{const}$$

or

$$\frac{2\pi}{Q} z = (1+\varkappa)\ln(w-1) - \frac{1}{w_0}\ln(w-w_0) +$$

$$+ \frac{1-\varkappa}{w_m^2}(w-w_m^2) - \frac{w_0}{w_m^2}\ln\left(w-\frac{w_m^2}{w_0}\right) +$$

$$+ \frac{\varkappa}{w-1} - \frac{\varkappa}{w-w_m^2} + \text{const}. \qquad (3.3.16)$$

This equation is very inconvenient to apply in practice. Introducing the parameter $\underline{t}$ lying between the values $(t_1<t<t_2)$.

$$t_1 = \frac{(w_m^2+1)(w_m+w_0)^2}{(w_m^2+w_0^2)(w_m+1)}; \quad t_2 = \frac{(w_m^2+1)(w_m-w_0)^2}{(w_m^2+w_0^2)(w_m-1)^2}. \qquad (3.3.17)$$

the following approximate relations can be introduced [3, 2]

$$\frac{x}{h} = \frac{w_m^2+w_0^2}{2w_m^2}(t-\ln t-1);$$

$$\frac{y}{h} = \pm\frac{(w_m^2+w_0^2)(w_m^2-1)}{2w_m^2(w_m^2+1)}\left[\sqrt{(t-t_1)(t_2-t)} + \right.$$

$$+ (t_1+t_2)\operatorname{arc\,tg}\sqrt{\frac{t-t_1}{t_2-t}} -$$

$$\left. - 2\sqrt{t_1 t_2}\operatorname{arc\,tg}\sqrt{\frac{t_2(t-t_1)}{t_1(t_2-t_1)}}\right] \pm 1. \qquad (3.3.18)$$

To determine the length $\underline{l}$ of the curvilinear part of the outer surface (Fig. 3.3.7) with given w_k and w_m the following relation can be used:

$$\frac{l}{h} = \frac{w_m^2 + w_k^2}{2w_m^2}(\ell_2 - \ln \ell_2 - 1). \qquad (3.3.19)$$

The results of checking optimum plane air intakes show good agreement with the calculation (cf. Fig. 3.3.7). It should be noticed here that a very small radius of curvature of the intake edge leads to the appearance of a sharp peak in the pressure distribution at the intake when the velocity in the tube deviates from the calculated value (cf. curves a and b in Fig. 3.3.7). An especially sharp rarefaction peak arises if the velocity in the tube is smaller than the calculated value; in the case of a flow of a real fluid this will cause stall. The range of operation of an air intake can be extended by designing it with nonuniform pressure distribution at the input but with larger radius of curvature of the entry part.

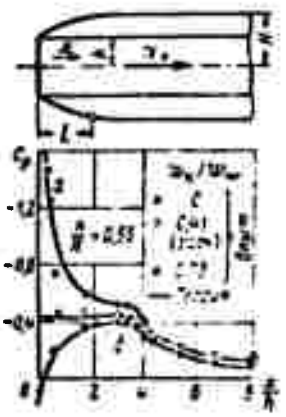


Fig. 3.3.7. Pressure distribution over the contour of the air intake as a function of x/h from experiment $w_k/w_\infty = 0$, 0.41, 0.73. The calculated ratio is $w_k/w_\infty = 0.40$.

3.4. FORCES AND MOMENTS OF FORCES ACTING ON THE BODY IN A PLANE FLOW

The Chaplygin formulas. Let us consider a steady flow of an incompressible fluid (not necessarily a potential flow) without volume forces, flowing without stall about the contour L. At each point of the streamline contour the pressure can be expressed in terms of the velocity with the help of the Bernoulli equation $p = H - \rho w^2/2$.

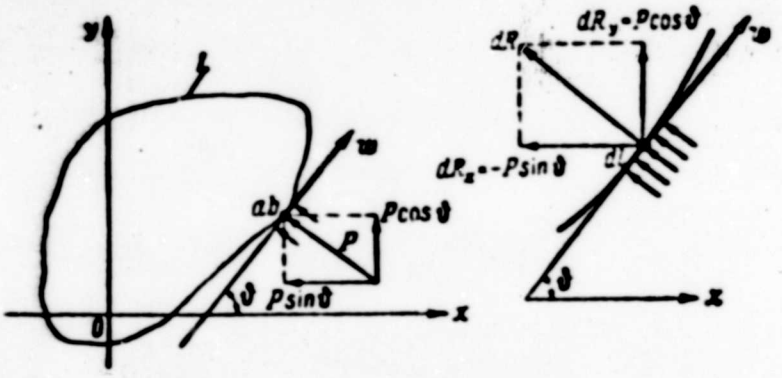


Fig. 3.4.1. For the determination of force interaction between a solid body and a flow.

The force components acting on the element with respect to the coordinate axes will be

$$dX = -p\sin\vartheta\, dl; \quad dY = p\cos\vartheta\, dl,$$

where dl is the contour element (Fig. 3.4.1). Integrating over the whole contour we can formulate the complex quantity of the force vector reflected in the real axis:

$$\overline{R} = X - iY = \oint_l (dX - i\,dY) = -\oint_l p(\sin\vartheta + i\cos\vartheta)\, dl =$$
$$= -i\oint_l p(\cos\vartheta - i\sin\vartheta)\, dl,$$

but

$$dz = e^{i\vartheta} dl; \quad d\bar{z} = e^{-i\vartheta} dl = (\cos\vartheta - i\sin\vartheta)\, dl,$$

and therefore

$$\overline{R} = X - iY = -i\oint_l p\, d\bar{z}.$$

Substituting the expression for p from the Bernoulli equation we obtain

$$\overline{R} = X - iY = -i\oint_l H d\bar{z} + i\oint_l \frac{\rho w^2}{2} d\bar{z} =$$
$$= \frac{i\rho}{2}\oint_l w^2 e^{-2i\vartheta} dz = \frac{i\rho}{2}\oint_l \overline{w}^2\, dz,$$

since

$$d\bar{z} = e^{-i\vartheta} dl = e^{-i\vartheta}\cdot e^{-i\vartheta}\cdot e^{i\vartheta} dl = e^{-2i\vartheta} dz.$$

This expression represents the first Chaplygin formula:

$$\bar{R}=X-iY=\frac{ip}{2}\oint_L\left(\frac{dz}{dz}\right)^2 dz. \qquad (3.4.1)$$

Further, calculating the moment of the forces acting on the contour L we obtain

$$\begin{aligned}M&=\oint_L x\,dY-y\,dX=\oint_L p(x\cos\vartheta+y\sin\vartheta)\,dl=\\&=\oint_L Hd\frac{x^2+y^2}{2}-\oint_L\frac{\rho w^2}{2}(x\,dx+y\,dy)=\\&=\operatorname{Re}\left(-\frac{\rho}{2}\oint_L w^2 z\,d\bar{z}\right)=\operatorname{Re}\left\{-\frac{\rho}{2}\oint_L\overline{w^2}z\,dz\right\}=\\&=\operatorname{Re}\left\{-\frac{\rho}{2}\oint_L\left(\frac{dz}{dz}\right)^2 z\,dz\right\}.\end{aligned} \qquad (3.4.2)$$

Let us remember that the sign of Re designates the real part of the expression following it. This formula is called the second Chaplygin formula.

The Zhukovskiy formula for the lift. Let a contour located in a flow be replaced by the totality of correspondingly arranged singularities in a parallel flow (Fig. 3.4.2): 1) n sources (sinks) at the points $a_1, a_2, \ldots, a_n$ with the intensities $Q_1, Q_2, \ldots Q_n$, satisfying the condition that the contour be closed, $\sum_{k=1}^{n} Q_k=0$; 2) m vortices at points $b_1, b_2, \ldots b_m$ with the vorticities $\Gamma_1, \Gamma_2, \ldots, \Gamma_m$ and $\Gamma=\sum_{k=1}^{m}\Gamma_k$.

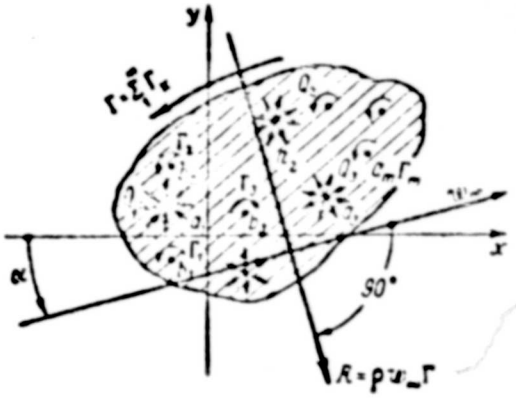


Fig. 3.4.2. The reaction of a fluid on a body is equal to the product of fluid density, circulation about the body and speed at infinity. The direction of reaction is obtained by turning the speed vector through 90° in the direction opposite to that of circulation.

The complex potential of the resulting flow will then be

$$\zeta(z)=\bar{w}_\infty z+\frac{1}{2\pi}\sum_{k=1}^{n}Q_k\ln(z-a_k)+$$

$$+\frac{1}{2\pi i}\sum_{k=1}^{m}\Gamma_k\ln(z-b_k) \qquad (3.4.3)$$

and the complex velocity

$$\overline{w}=\frac{d\chi}{dz}=\overline{w}_\infty+\frac{1}{2\pi}\sum_{k=1}^{n}\frac{Q_k}{z-a_k}+\frac{1}{2\pi i}\sum_{k=1}^{m}\frac{\Gamma_k}{z-b_k}. \tag{3.4.4}$$

where $\overline{w}_\infty=w_\infty e^{-i\alpha}$ is the complex velocity of the flow at infinity, enclosing the angle α with the x-semiaxis. Since $d\chi/dz$ is an analytic function in the whole region outside the contour considered, including the point $z = \infty$, the calculation of the integrals can be reduced to determining the residues of the integrand for the point $z = \infty$. But, as may be seen from Formula (3.4.4), in the vicinity of $z = \infty$ we have

$$\left.\begin{aligned}
\frac{d\chi}{dz}&=\overline{w}_\infty+\frac{A_1}{z}+\frac{A_2}{z^2}+\dots\\
\left(\frac{d\chi}{dz}\right)^2&=\overline{w}_\infty^2+\frac{2A_1\overline{w}_\infty}{z}+\frac{A_1^2+2A_2\overline{w}_\infty}{z^2}+\dots\\
z\left(\frac{d\chi}{dz}\right)^2&=\overline{w}_\infty^2 z+2A_1\overline{w}_\infty+\frac{A_1^2+2A_2\overline{w}_\infty}{z}+\dots
\end{aligned}\right\} \tag{3.4.5}$$

When calculating the coefficients A_1, A_2,... we take into account that in the vicinity of $z = \infty$

$$\left.\begin{aligned}
\frac{1}{z-a_k}&=\frac{1}{z}+\frac{a_k}{z^2}+\frac{a_k^2}{z^3}+\dots\\
\frac{1}{(z-a_k)^2}&=\frac{1}{z^2}+\frac{2a_k}{z^3}+\dots\\
A_1&=\frac{1}{2\pi}\sum_{k=1}^{n}Q_k+\frac{1}{2\pi i}\sum_{k=1}^{m}\Gamma_k=\frac{\Gamma}{2\pi i}\left(\Gamma-\sum_{k=1}^{m}\Gamma_k\right).\\
A_2&=\frac{1}{2\pi}\sum_{k=1}^{n}a_kQ_k+\frac{1}{2\pi i}\sum_{k=1}^{m}\Gamma_k b_k.
\end{aligned}\right\} \tag{3.4.6}$$

Thus,

$$\int_L\left(\frac{d\chi}{dz}\right)^2dz=2\pi i2A_1\overline{w}_\infty=2\Gamma\overline{w}_\infty;$$

$$\int_L z\left(\frac{d\chi}{dz}\right)^2dz=2\pi i\left(A_1^2+2A_2\overline{w}_\infty\right)=$$

$$=2\pi i\left[-\frac{\Gamma^2}{4\pi^2}+2\overline{w}_\infty\left(\frac{\sum_{k=1}^{n}a_kQ_k}{2\pi}+\frac{\sum_{k=1}^{m}\Gamma_kb_k}{2\pi i}\right)\right]$$

and, by virtue of (3.4.1) and (3.4.2), we have

$$\overline{R}=X-iY=i\rho\Gamma\overline{w}_\infty \tag{3.4.7}$$

$$M = \mathrm{Re}\left\{-i\rho\bar{w}_\infty \sum_{k=1}^{n} a_k Q_k - \rho\bar{w}_\infty \sum_{k=1}^{n} \Gamma_k b_k\right\}. \qquad (3.4.8)$$

Since

$$\bar{w}_\infty = we^{-i\alpha} = w_\infty(\cos\alpha - i\sin\alpha),$$

we have

$$X - iY = i\rho w_\infty \Gamma(\cos\alpha - i\sin\alpha) = \rho w_\infty \Gamma\sin\alpha + i\rho w_\infty \Gamma\cos\alpha. \qquad (3.4.9)$$

This formula is named after N.Ye. Zhukovskiy. It expresses that the pressure force $\vec{R}$ of a flow of speed w_∞ streaming about a contour with the circulation Γ is equal to the product of fluid density ρ, circulation Γ and flow speed w_∞; the direction of the force is obtained by rotating the velocity vector at infinity through 90° in direction opposite to that of the circulation (cf. Fig. 3.4.2).

The force directed perpendicularly to the velocity is called the lift, and the force in the direction of the velocity is called the drag. Thus, in the case of a plane flow of an inviscid incompressible fluid about a body the drag is equal to zero and a lift will arise only if a circulation exists about the body.

Drag. When a real viscous fluid actually flows around a body the latter is subject to the action of a drag. The influence of the viscosity manifests itself not only in the form of a direct action of tangential stresses but also in a change of the pressure distribution about the body caused by the change of the flow pattern under the action of the viscosity. This difference between the components of the total drag is best elucidated by the example of the flow about a plane plate. When the plate moves in a direction perpendicular to its plane, the total drag (Fig. 3.4.3) is due to normal stresses (pressure p). But when the plate is displaced in its plane the drag will arise only due to tangential stresses (friction τ).

Observation shows that when a fluid streams round a circular

THIC NOT
ODUCIBLE

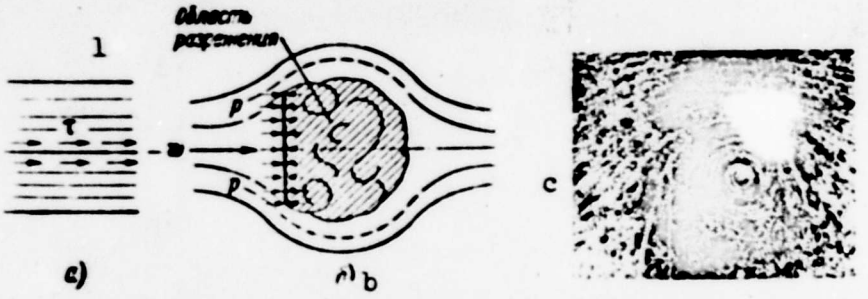


Fig. 3.4.3. The drag of a plane plate arises in case (b) mainly on the expense of the normal pressure and in case (a) on the expense of friction; (c) photograph of the flow about a sharp edge. 1) Rarefaction zone.

cylinder, its motion in the first instant of time after leaving the state of rest has a character that deviates little from potential flow (Fig. 3.2.7; $l/d = 1.17$). At this instant of time the pressure distribution is very similar to a distribution that would correspond to potential flow. The adhesion of the fluid to the body surface in its immediate proximity causes the formation of a boundary layer which represents an entirely turbulent region. The fluid particles inside the boundary layer lose kinetic energy in overcoming the friction and are no longer able to enter the region of higher pressure; what is more, they start moving in the opposite direction under the action of the increased pressure in the wake zone, thus giving rise to the formation of a vortex pair that changes the velocity field and hence the pressure distribution (later on, in Chapter 6, this effect will be discussed in greater detail (cf. Fig. 6.1.5)). As already indicated, Fig. 3.2.7 gives the pressure distributions for a cylinder with respect to the path it travels after the motion starts. As can be seen from these curves, the pressure distribution is changed mainly in the wake region. The vortices arising in this region change the form of motion (cf. Fig. 3.2.7); a rarefaction zone is formed behind the cylinder and the

asymmetry in the pressure distribution with respect to the y-axis causes a drag force to arise (from normal stresses!). This is how drag forces (pressure) appear on a plate positioned normally to the stream (cf. Fig. 3.4.3,b). In the first instant the motion is a potential one; then, at the plate edges where the speed is theoretically infinite, vortices arise under the action of the viscosity (cf. Fig. 3.4.3,c) which alter the form of motion, and behind the plate a vortex zone forms with lowered pressure and hence a drag force arises at the expense of the normal stresses.

Applying the law of momentum conservation, Newton obtained the formula for the drag of a body; it reads $X = CA\rho w^2$, where C is a coefficient taking the degree of elasticity of the impact into account and A is the area of the middle cross section. Thus, according to Newton's theory, the drag is independent of the shape of the body. This can be explained by the fact that Newton considered in his studies a hypothetical medium consisting of a very large number of very small substantial particles of definite mass which are not interrelated. When a body moves in such a medium, it collides with all the particles positioned along its path and exchanges momenta with them. Since the mass of fluid colliding per second with the body is equal to ρAw, then, assuming that a velocity w', proportional to the velocity $\underline{w}$ of the body, is imparted to them, we obtain the above expression for the drag of a body.

Newton's theory is not confirmed by experiment. The divergence can be explained by the fact that the particles postulated by Newton in his theory do not interact with each other and the forces acting on the body were taken as solely due to effects occurring on the front, the sides and back being disregarded. In fact, however, they are of great importance. This is because the mean free path i.

the molecules is small compared with the linear dimensions of the body and because a whole group of fluid particles comes into motion in the flow about a body. Owing to the particle interaction, the action of forces on the body cannot be determined by adding up the single actions as if parts of its surface could be separated from the body. As will be shown in Part 10.3, the drag model suggested by Newton corresponds to the motion of a body in a highly rarefied gas.

3.5. WING PROFILE THEORY

Wing profile. The profiles of wings and vanes used in aircraft and turbine construction usually have a form that is considerably elongated in the direction of motion. Their front edges (or leading edges) differ from the rear edges (or trailing edges). The wing shape is determined by taking the wing chord as the first axis (x) and the normal to it (usually at the leading edge or in the middle of the chord) as the second axis (y-axis). The wing chord is determined as the projection of the profile on a certain straight line

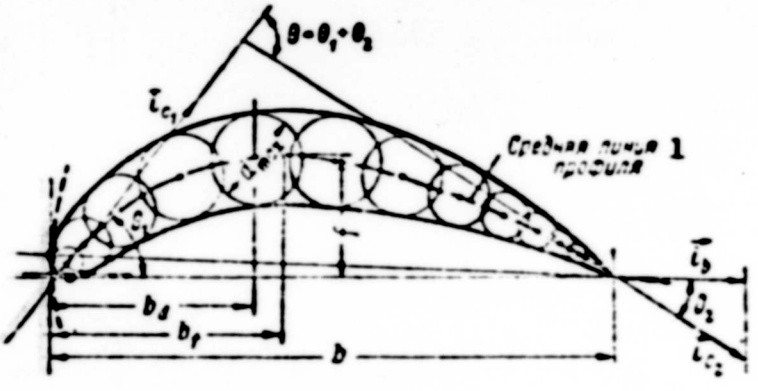


Fig. 3.5.1. The geometrical parameters of the profile. b – chord $\bar{d} = d/b$ – thickness/chord ratio $\bar{f} = f/b$ – maximum camber; $\bar{b}_d = b_d/b$ – position of maximum thickness; $\bar{b}_f = b_f/b$ – position of maximum camber; θ_1 and θ_2 are the angles of direction of the leading (trailing) edges; θ is the angle of bend of the profile. The chord position is conventional. 1) Camber line of profile.

along the profile, the position of which has to be exactly fixed

For example, the tangent to the lower contour is taken as this straight line, provided it can be drawn. Frequently this strraight line is drawn from the cusp of the trailing edge to the most distant point of the leading edge (Fig. 3.5.1). The position of the profile with respect to the direction of motion is determined by the geometrical angle of attack, i.e., by the angle between speed vector and wing chord. The line passing through the centers of the circles drawn in the profile is called the camber line. In Fig. 3.5.1 the profile chord is determined by the straight line joining the ends of the camber line.

The profiles are characterized by the maximum bend of the camber line, $\bar{f} = f/b$, and by the position of this maximum, $\bar{b}_f = b_f/b$. The profile thickness is determined by the maximum diameter d of a circle inscribed in the profile (thickness/chord ratio $\bar{d} = d/b$); it is often essential to know the position of the maximum thickness, $\bar{b}_d = b_d/b$. The curve plotted from the camber line of the profile in order to obtain a profile of finite thickness – what is called a body profile – is called the thickness curve. It also determines the angle ω between the tangents to the trailing edge.

Aerodynamic profile characteristics. When a wing moves in a fluid it is subjected to the fluid's reaction which usually consists of the lift Y (normal to the speed) and the drag X. Besides these, a force moment M acts on the wing. Usually these quantities are characterized by the dimensionless coefficients of lift, drag and moment defined by the relations

$$Y = C_y A \frac{\rho w^2}{2}, \quad X = C_x A \frac{\rho w^2}{2}, \quad M = C_m A \frac{\rho w^2}{2} b. \qquad (3.5.1)$$

Here A is the wing area in the diagram, $q = \rho w^2/2$ is the dynamic (speed-induced) load, b is the chord of the wing at any cross

section when the wing chord varies along the span.

In the case of a steady motion these coefficients mainly depend on the numbers Re = wb/ν and M = w/a.

The essential characteristic of a wing profile is its lift/drag ratio,

$$k = \frac{C_y}{C_x}, \qquad (3.5.2)$$

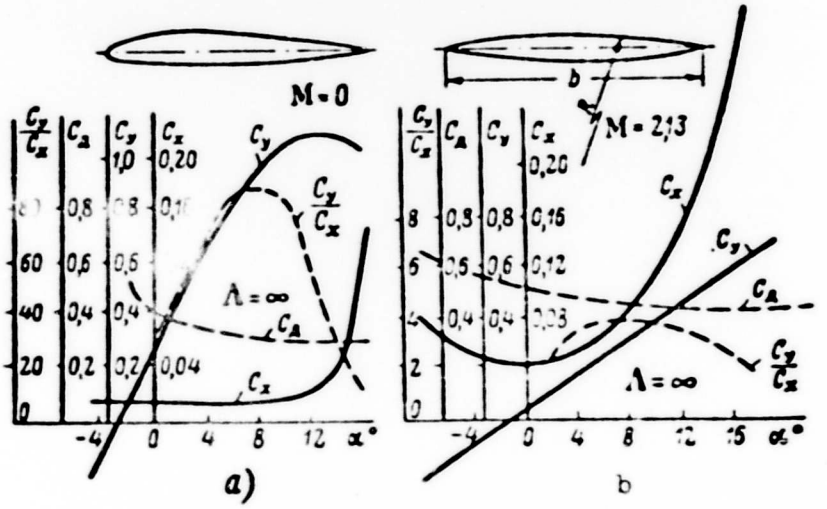
which is called the quality of the wing. The inverse quantity, $C_x/C_y = 1/k$ is called the gliding characteristic (or inverse quality). Fig. 3.5.2 shows typical characteristics for three profiles. The distinguishing features of the profiles for low speed of flight are the rounded leading edge and the sharp training edge. The profiles used for transsonic and supersonic speeds (Fig. 3.5.3) are characterized by sharp leading and trailing edges.

The quantities C_y, C_x and C_m are given in tables or graphs.

The graph that directly links C_x and C_y is called the polar L of first kind – on which we plot the angles of attack or the curve C_y as a function of the angles of attack, α. On the same graph usually $C_m = f(C_y)$ and the profile quality C_y/C_x are given.

Mechanism of viscous fluid flow about a profile. Using the example of a cylinder (cf. Fig. 3.2.7), it has been shown that at the initial instant when a solid body begins to move in a real fluid the flow is potential in character and free from circulation. If a wing profile is located in the fluid stream, then, when the angle of attack is large enough (exactly with $C_y > 0$), the forward stagnation point will lie on the lower surface near the leading edge and the rear stagnation point will be on the upper surface of the wing profile near the trailing edge (cf. Fig. 3.5.3,a). The sketch in Fig. 3.5.3 shows the streamlines drawn after the photograph

of a flow about a wing profile at the initial instant of motion. As has been shown (cf. Fig. 3.5.3), in the flow about a sharp corner the speed at the sharp edge of the profile S reaches very high values, which are, theoretically, infinitely high. If we choose at this instant a certain contour C enclosing the wing profile and formulate the expression for the circulation $\Gamma = \oint_C \vec{w} \cdot \vec{dl}$ with respect to this contour, then, as the motion is a potential one everywhere, the circulation vanishes.

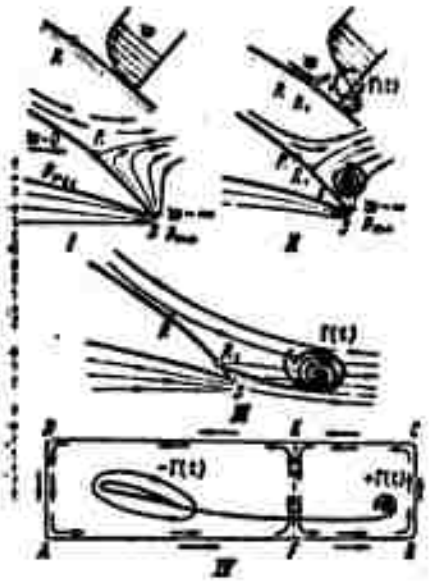


Fig, 3.5.2. Typical profile characteristics. a) For low speed of flow; b) for supersonic speed.

By virtue of the Bernouilli equation, the pressure at the point S will be minimum and since at the point R the speed is zero and therefore the pressure is highest, a pressure gradient will exist in the direction from R to S.

If a fluid streaming about a profile is inviscid, the kinetic energy of an arbitrary particle, and hence of those passing through near the point S will be high enough for such a particle to reach the point R. But owing to the presence of friction, however small it may be, the kinetic energy of the particles passing near S will be insufficient for them to enter the region of higher pressure and

to reach point R. Their motion becomes frozen, and, what is more, the fluid in this zone displays a reverse motion, which, owing to



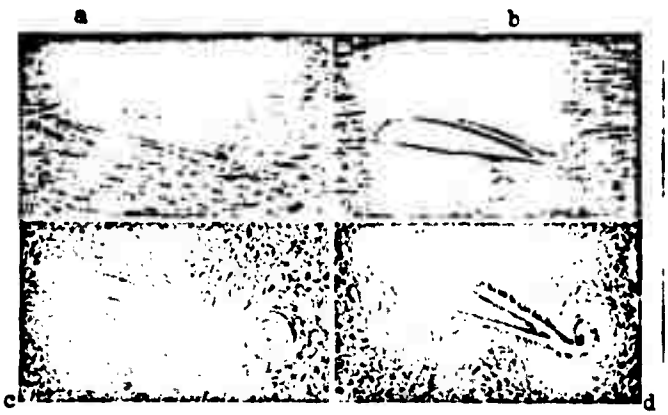


Fig. 3.5.3. Appearance of circulation about a wing. At the very beginning of the motion the flow is potential in character (photograph a and sketch I). Under the influence of viscosity and pressure difference (the pressure is higher at point R than at point S) a reverse motion arises in the boundary layer (sketch II), the initial vortex is formed)photograph b) and is carried downstream with the flow; photograph c shows the formation of the vortex in the case of a large angle of attack (the camera is at rest with respect to the undisturbed fluid); photograph d shows the motion when the wing was stopped right after the starting vortex had formed (photograph c) and the second strating vortex of opposite sign appeared. The process of growth of the starting vortices takes until (sketch III) the partition point R coincides with the trailing edge S. The starting vortex formed alters the velocity field about the wing in such a way that the circulation with respect to the contour enclosing the wing becomes different from zero, and, at any instant of time, equal to the circulation of the starting vortex, but with the opposite sign (sketch IV).

the great difference of pressures at R and S (cf. Fig. 3.5.3, II), leads to the formation of what is called the initial (starting) vortex whose strength will increase with time. Since this vortex is located in the fluid stream moving from S to R, a Zhukovskiy force will arise in it, directed away from the profile, under the action of which the vortex will be carried along by the main flow. Since the circulation with respect to a sufficiently large contour AFBCEDA would be equal to zero at the origin of motion, the formation of

the starting vortex must lead to a change of the velocity field on the wing that is equivalent to the application of a circulatory motion about the profile with a circulation equal in magnitude and opposite in sign to the circulation of the starting vortex; (cg. Fig. 3.5.3, IV). The intensity of the starting vortex increases as long as the speeds at the trailing edge from the upper and lower surfaces differ (Zhukovskiy-Chaplygin condition), i.e., until the point R where the flow parts coincides with the trailing edge S. In other words, the circulation about the wing must be so chosen that the infinitely large speed at the sharp trailing edge of the wing profile is eliminated. The vortex producing such a circulatory motion as the wing does and which, consequently, can replace the wing, is, according to N. Ye. Zhukovskiy, termed the adjacent vor[illegible].

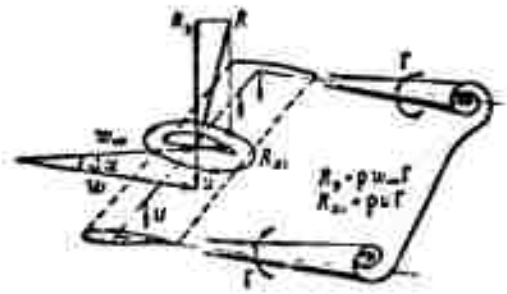


Fig. 3.5.4. Vortex system of a finite wing; the system of adjacent and free vortices produces at the wing the velocity u in the direction opposite to that in which the lift acts; the lift $R_y = \rho w_\infty \Gamma$ and an induced drag act in each wing cross section (per unit length of the wing span).

Induced drag of a wing of finite span. As early as 1913 S.A. Chaplygin considered a scheme in which an adjacent vortex of constant strength at the tips of a finite-span wing goes over into free vortices, which are carried along by the main flow and driven towards the rear. This is the simplest scheme of a wing of finite span (Fig. 3.5.4) and is termed П-shaped.

In fact, owing to the pressure compensation at the tips of the wing, the circulation with respect to the wing span varies from section to section and vortices with the strength $\delta\Gamma$ separate from each section of the wing and they form the vortex shroud behind the wing. This shroud is unstable and yet at a relatively short distance from the wing it disintegrates into a series of discrete vortices which are especially intense at the tips – the vortex "whiskers."

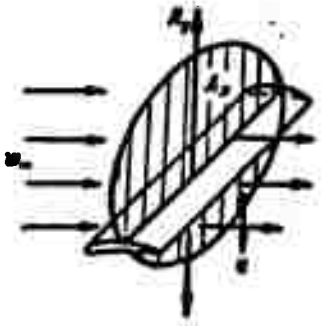


Fig. 3.5.5. To the mass $\rho w_\infty A_N$ passing per second through the section A_N the wing imparts the velocity $\underline{u}$ directed downwards which changes the momentum of this mass. The force R_y arises acting on the wing in upward direction.

The system of adjacent and free vortices, the theory of which has recently been developed in the papers of L. Prandtl produce at the wing the velocity $\underline{u}$ in the direction opposite to that in which the lift is acting. The interaction between vortices and the flow causes in accordance with Zhukovskiy's theory, a drag force to arise which is equal to $\rho u\Gamma$ per unit length and which is called the induced drag X_1.

An expression for the induced drag can be obtained also from purely mechanical considerations. Let us assume (Fig. 3.5.5) that the action of the wing on the air is limited by the mass of air passing through a certain area A_N perpendicular to the direction of motion. The mass of air passing through A_N per second receives from the wing a momentum directed downwards which is equal to the lift:

$$Y = \rho A_N w_\infty u.$$

The kinetic energy of this mass of fluid

$$E = \frac{mu^2}{2} = \frac{1}{2}\rho A_N w_\infty u^2$$

must be equal to the work of moving the wing, $X_i w_\infty$. Thus,

$$X_i = \frac{1'}{2}\rho A_N w^2 = \frac{\gamma^2}{2\rho w_\infty^2 A_N}; \quad C_{x_i} = \frac{C_y^2}{4}\frac{A_{wg}}{A_N};$$

In the theory of a wing of finite span it will be shown that when the load is so distributed over the span that the drag is minimum, the area A_N is the area of a circle constructed with the wing span $\underline{l}$ as the diameter ($A_N = \pi \underline{l}^2/4$),

$$C_{x_i} = \frac{A_{wg}}{\pi l^2} C_y^2 = \frac{1}{\pi \Lambda} C_y^2. \qquad (3.5.3)$$

The ratio $\Lambda = \underline{l}^2/A$ is called the aspect ratio.

The induced drag represented in a first-order plot of the coordinates C_x, C_y is, as can be seen from the latter relation, a second-order parabola (cf. Fig. 3.5.2,a). The additional motion of fluid arising about the finite wing and having a velocity directed normally to the velocity of the main flow leads to the actual angle (cf. Fig. 3.5.4)

$$\delta_i = \operatorname{arc\,tg} \frac{w}{w_\infty} \approx \frac{w}{w_\infty}. \qquad (3.5.4)$$

A more detailed analysis of the operation of a finite wing will be given later on, i.e., in Chapter 7. Right now we want to point out that even in an inviscid fluid a drag force arises, a force that is directed along the flow velocity. This induced drag force is proportional to the lift squared.

The infinite-span wing. When considering a cylindrical wing whose span reaches to infinity on both sides (i.e., $\Lambda = \infty$), the mass of the downwash will also tend to infinity (as the square of the span) and the speed of the mass of the downwash will tend to zero. The induced drag, proportional to $1/\Lambda$, will at the same time also tend to zero.

In the Π-shaped vortex system of a finite wing the circulation of the adjacent vortex for a cylindrical wing and the circulation

of the free trailing vortices at the tips are constant and identical. In the case of a wing of infinite span the distance between the free vortices of finite strength Γ generated at the wing tips becomes infinitely large, while at the same time the speed and the force of the induced drag due to these vortices vanish.

The case of the infinite cylindrical wing considered is a case of plane motion.

Flow about an arbitrarily positioned disk. To develop the theory of a body profile of arbitrary shape we start by considering a stream with the circulation Γ flowing about a circle of radius r_0 in the plane $\zeta=\xi+i\eta$ with the center at the point ζ_0. If the direction of the velocity w_∞ at infinity includes the angle α with the x-axis, then, transposing the center of the circle to the point ζ_0 and turning the plane through the angle α we obtain from Expression (3.2.23) the complex potential (the additive constant being disregarded)

$$\chi(\zeta)=w_\infty e^{-i\alpha}(\zeta-\zeta_0)+\frac{w_\infty e^{i\alpha}r_0^2}{\zeta-\zeta_0}+\frac{\Gamma}{2\pi}\ln(\zeta-\zeta_0). \qquad (3.5.5)$$

Here the clockwise direction of circulation is taken as the positive one. The complex velocity is

$$\frac{d\chi}{d\zeta}=w_1-iw_2=w_\infty e^{-i\alpha}-\frac{r_0^2 w_\infty e^{i\alpha}}{(\zeta-\zeta_0)^2}+\frac{\Gamma}{2\pi(\zeta-\zeta_0)}. \qquad (3.5.6)$$

Circulation about a profile. As has been already shown, a function $z = f(\zeta)$ can be set up that conformally transforms the region outside the circle – this circle is denoted as the generatrix – to the region outside some arbitrary contour L in the plane $z = x + iy$. Here, if we demand that the infinity points and the speeds at them should coincide, ($b_0 = 0$; $b_{-1} = 1$), the function must have the form of a series

$$z=\zeta+\frac{b_1}{\zeta}+\frac{b_2}{\zeta^2}+\ldots+\frac{b_n}{\zeta^n}+\ldots \qquad (3.5.7)$$

The characteristic stream function for the flow about the con-

tour L is found by substituting the value $\zeta = g(z)$ in (3.5.5) and will read $\chi(z) = \chi[g(z)]$, where $\zeta = g(z)$ is the solution to the equation $z = f(\zeta)$. The complex velocity in the z-plane is

$$\bar{w}_z = w_x - iw_y = \frac{d\chi}{dz} = \frac{d\chi}{d\zeta} \cdot \frac{d\zeta}{dz}. \qquad (3.5.8)$$

The determination of the circulation Γ for the general case of a cylindrical body is an indefinite problem as the magnitude of the circulation depends on the viscosity of the fluid and is connected with the formation of vortices on the body surface. For contours of small curvature and thickness having a sharp trailing edge with small angles of attack the magnitude of the circulation can be determined independently of the viscosity from the Zhukovskiy-Chaplygin condition.

The fact that the profile has a sharp trailing edge disturbs the conformal mapping at this point. In fact, the angle π at point σ on the circle corresponding to the trailing edge S of the profile will correspond to the angle $2\pi - \omega$ on the profile (Fig. 3.5.6). Therefore, the mapping function in the vicinity of this point must read

$$z - z_0 = (\zeta - \zeta_0)^{\frac{2\pi-\omega}{\omega}} \Phi(\zeta), \qquad (3.5.9)$$

where $\Phi(\zeta)$ is a function that is analytic at this point and different from zero. Since $\omega < \pi$, we have for this point

$$\left(\frac{dz}{d\zeta}\right)_{\sigma} = \left[\frac{2\pi-\omega}{\omega}(\zeta-\zeta_0)^{\frac{2\pi-\omega}{\omega}-1}\Phi(\zeta) + \Phi'(\zeta)(\zeta-\zeta_0)^{\frac{2\pi-\omega}{\omega}}\right]_{\zeta=\zeta_0} = 0.$$

Comparing this result with (3.5.8) we come to the conclusion that the Zhukovskiy-Chaplygin condition of finite speed at the trailing edge requires that $d\chi/d\zeta = 0$ at this point of the circle, i.e., that the rear separation point (stagnation point) of the circle is transformed to the trailing edge of the profile.

To determine the position of the stagnation points on the

circle we use Eq. (3.5.6). Let α_0 (Fig. 3.5.7) be the angle between the radius drawn from the center of the circle to the rear separation point of the stream and the ξ-axis, so that $\zeta_s = \zeta_0 + r_0 \exp(-i\alpha_0)$. Then from Expression (3.5.6)

$$\left.\frac{dx}{d\zeta}\right|_{\zeta=\zeta_s} = w_\infty e^{-i\alpha} - w_\infty e^{i(\alpha+2\alpha_0)} + \frac{\Gamma}{2\pi r_0} e^{i\alpha_0} = 0$$

we obtain

$$\Gamma = 4\pi r_0 w_\infty \sin(\alpha + \alpha_0). \qquad (3.5.10)$$

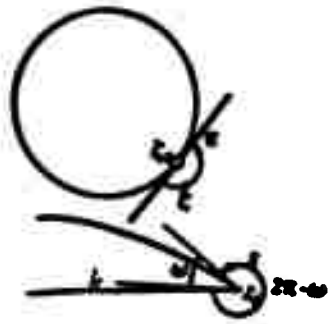


Fig. 3.5.6. Mapping in the trailing edge region; according to the Zhukovskiy-Chaplygin condition the trailing edge must be mapped to the separation point of the circle.

Assuming $\Gamma : 4\pi w_\infty r_0 < 1$ and denoting the angle between the radius vector OS and the direction of the velocity w_∞ by $\varphi = \alpha + \alpha_0$ we find the position of the forward stagnation point for the angle $\pi - \varphi = \pi - (\alpha + \alpha_0)$ (Fig. 3.5.7).

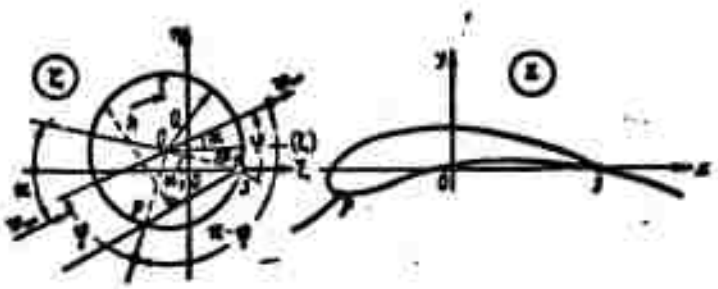


Fig. 3.5.7. Correspondence of the stagnation points on the circle and on the profile.

Thus, since (3.5.10) is fulfilled for the angle $\pi - (\alpha + \alpha_0)$, as well, the second point will lie on the circle in such a way that the chord joining the stagnation points on the circle will be parallel to the velocity at infinity.

The lift and the first axis. Substituting the expression

$$\Gamma = 4\pi w_\infty r_0 \sin(\alpha + \alpha_0)$$

in the Zhukovskiy formula for the lift we find (per unit length)

$$\Gamma = 4\pi\rho v_\infty r_0 \sin(\alpha + \alpha_0). \qquad (3.5.11)$$

In what follows it is more convenient to consider that the z-plane (wing profile) and the ζ-plane (generating circle) are superimposed in such a way that the x-axis coincides with the ξ-axis passing through the forward stagnation point, and the y-axis with the η-axis (Fig. 3.5.8).

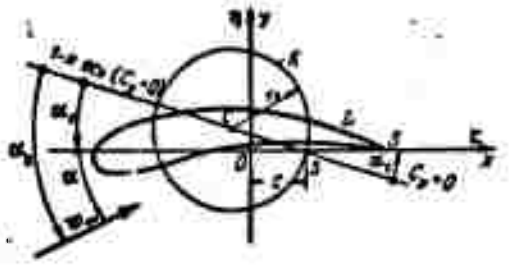


Fig. 3.5.8. Superposition of the z-plane (profile) and the ζ-plane (circle).

Taking the direction of reading the angles α and α_0 into account we notice that the lift becomes zero when the speed is directed along the radius joining the center of the circle with the backward stagnation point on the circle. This direction defines the first axis of the profile. The angle $\alpha + \alpha_0$, i.e., the angle enclosed by the speed direction and the first axis of the profile is called the aerodynamic angle of attack.

The aerodynamic properties of the profile are of course not determined by the geometrical angle of attack, α, which depends on the choice of the direction of the x-axis, but by the aerodynamic angle of attack $\alpha_a = \alpha + \alpha_0$ which is independent of the coordinate system.

Moment and the second axis of the profile. To determine the moment with respect to the coordinate origin the second Chaplygin formula (3.4.3) must be used. Noticing that b_1 in (3.5.7) has the

dimension of length squared and therefore supposing

$$b_1 = b^2 e^{2i\beta},$$

it can be shown that

$$M_C = -\frac{\rho v_\infty^2}{2} \operatorname{Re}\left(4\pi i b^2 e^{2i(\beta-\alpha)}\right) = 2\pi\rho v_\infty^2 b^2 \sin 2(\beta-\alpha). \qquad (3.5.12)$$

If the flow is directed at the angle $\alpha = \beta$, the moment with respect to the center of the transforming circle will be equal to zero, i.e., in this case the lift vector will pass through the center of the circle. The straight line passing through the generating circle and including the angle β with the ξ-axis is called the second axis of the profile.

The Zhukovskiy profile. If Series (3.5.7) is broken off after the first two terms and we put $b_1 = c^2$ where c is a real number, i.e., we take

$$z = \zeta + \frac{c^2}{\zeta}. \qquad (3.5.13)$$

then, depending on the position and the radius of the generating circle passing through point $\zeta = c$ contours will be obtained which have the form of a wing profile with a sharp trailing edge at the point $z = 2c$. Such profiles have been investigated by N.Ye. Zhukovskiy and are named after him.

Writing (3.5.13) in the form

$$z - 2c = \zeta + \frac{c^2}{\zeta} - 2c = (\zeta - c)^2 \cdot \frac{1}{\zeta},$$

and comparing it with (3.5.9), we find that the trailing edge angle, namely the angle between the tangents drawn at the trailing edge to the upper and the lower profile contours, is $\omega = 0$ for such profiles.

A plane plate. It is obtained when the center of the generating circle is taken in the coordinate origin (Fig. 3.5.9,a). Then

$$x + iy = \zeta + \frac{c^2}{\zeta} = ce^{i\theta} + \frac{c^2}{ce^{i\theta}} = 2c\cos\theta; \quad x = 2c\cos\theta; \quad y = 0.$$

Here $\alpha_0 = 0$, $c = r_0$, the chord of the plate is $b = 4c$ and,

owing to (3.5.11), we have

$$C_y = 2\pi \sin\alpha \approx 2\pi\alpha. \qquad (3.5.14)$$

The arc of the circle (Fig. 3.5.9). If we place the center of the generating circle at the point $\zeta_0 = ih$, we obtain the arc of the circle.

Writing (3.5.13) in the form

$$\frac{z-2c}{z+2c} = \left(\frac{\zeta-c}{\zeta+c}\right)^2. \qquad (3.5.15)$$

we obtain $\ln\frac{z-2c}{z+2c} = 2\ln\frac{\zeta-c}{\zeta+c}$ i.e.,

$$\arg\frac{z-2c}{z+2c} = 2\arg\frac{\zeta-c}{\zeta+c}.$$

If the point ζ runs over the upper arc of the initial circle from c to $-c$, $\arg\frac{\zeta-c}{\zeta+c}$ will be equal to the angle θ adjacent to the chord $(+c, -c)$. The chord $(+c, -c)$ is said to be seen from any point of the circle at the angle of θ. This angle will be the same for all points of the upper arc of the circle. Thus, passing around the upper arc of the initial circle in the ζ-plane will correspond to passing along a certain path on the z-plane, the chord of which is $(-2c, +2c)$; the angle at which this chord is seen from any point of the arc is 2θ.

For the lower part of the initial circle this angle will be equal to $\pi - \theta$. The corresponding angle on the z-plane will be $2(\pi - \theta)$; traveling round the lower part of the circle K will correspond to traveling in the opposite direction round the same arc of the circle in the z-plane. The circle K is thus transformed to an arc which must be run through twice. The maximum camber $\underline{f}$ of this arc is obtained by substituting $\zeta = i(r_0 + h)$ in (3.5.13) where $\underline{h}$ is the ordinate of the center of the circle:

$$if = i(r_0+h) + \frac{c^2}{i(r_0+h)} \approx 2ih;$$

$$C_y = \frac{2\pi\sin(\alpha+\alpha_0)}{\cos\beta} \approx 2\pi\alpha_0 = 2\pi\left(\alpha + \frac{2f}{b}\right). \qquad (3.5.16)$$

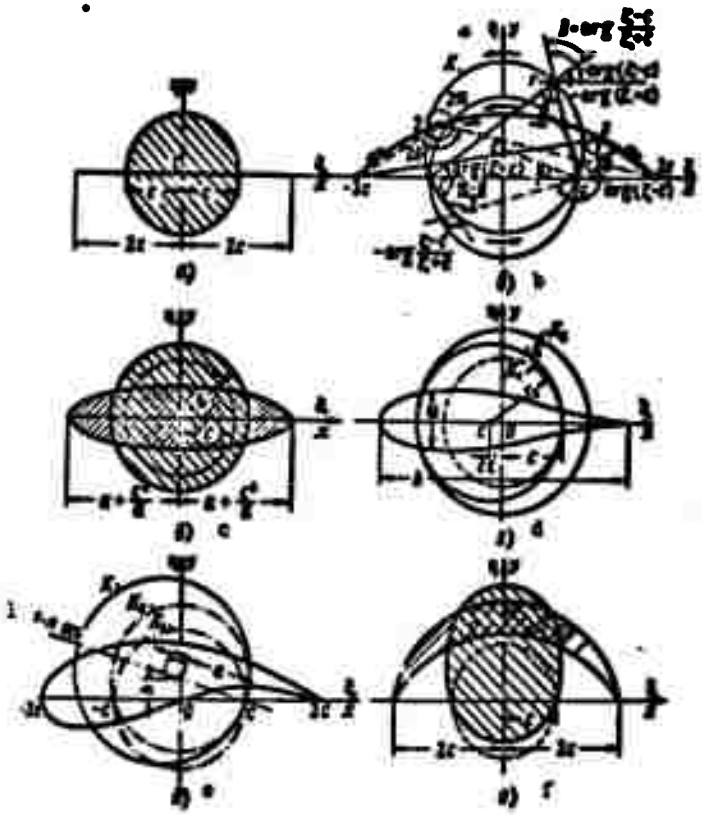


Fig. 3.5.9. Zhukovskiy profiles obtained by a transformation of the form $z=\zeta+\frac{a^2}{\zeta}$, change their shape in dependence on the position of the center and the size of the transforming circle. a) Plane plate with a midpoint coinciding with the coordinate origin and $r_0 = c$; b) arc of circle, its center shifted along the imaginary axis by f/2, $r_0=\sqrt{c^2+f^2/4}$; c) ellipse with the semiaxes $a + c^2/a$ and $a - c^2/a$, its center at the coordinate origin $r_0 = a$; d) symmetrical profile, its center shifted along the real axis - mapping of the ellipse (K_2 transformation) in the leading edge zone and of a plate (K_1 transformation) in the trailing edge zone; e) general case of a solid Zhukovskiy profile, its center shifted along both the imaginary axis (for camber) and the real axis (for thickness); f) a very strongly bent profile can be obtained if the circle is replaced by another closed curve, for example, an ellipse positioned as is shown in the figure. 1) First axis.

The symmetrical profile. To obtain profiles with rounded leading edges we first consider the transformation $z=\zeta+\frac{a^2}{\zeta}$ of a circle with the center at the coordinate origin and a radius a greater

than c:

$$z=x+iy=ae^{i\theta}+\frac{c^2}{ae^{i\theta}}=\left(a+\frac{c^2}{a}\right)\cos\theta+i\left(a-\frac{c^2}{a}\right)\sin\theta,$$

i.e., z described an ellipse (cf. Fig. 3.5.9,c) with the semi-axes $a + c^2/a$ and $a - c^2/a$.

Thus, if we take a circle of radius $r_0 = c(1 + \varepsilon)$ with the center on the real axis and passing through the points $\zeta = c$ and $\zeta=-a=-c(1+2\varepsilon)$ (cf. Fig. 3.5.9,d) and transform it to the z-plane, in the region of point $z = 2c$ we shall obtain an element of the plane plate and in the region of $z = -2c$ an element of the ellipse, and the whole circle K is transformed to a symmetrical profile. Hence, to obtain profiles with rounded leading edges, the center of the generating circle needs to be shifted so that, as before, this circle passes through the backward singular point and the forward one should lie within it. The equation of the generating circle is $\zeta=-c+(1+\varepsilon)ce^{i\theta}$; introducing this expression for ζ into the transformation Formula (3.5.13) and expanding it into a power series in ε we find

$$z=\zeta+\frac{c^2}{\zeta}=-c+(1+\varepsilon)ce^{i\theta}+\frac{c^2}{-c+(1+\varepsilon)ce^{i\theta}}=$$
$$=2c\cos\theta+c\varepsilon(\cos 2\theta-1)+ic\varepsilon(2\theta-\sin 2\theta)+\ldots$$

Here the chord of the wing is equal to $b=x(0)-x(\pi)\approx 4c$. (to within ε^2) and the greatest thickness of the profile, d, is determined from the equation

$$y_{max}=\frac{d}{2}=c\varepsilon(2\sin\theta-\sin 2\theta)_{max}.$$

Thus,

$$\frac{d}{b}=\frac{3\sqrt{3}\varepsilon}{4}\approx 1{,}3\varepsilon. \qquad (3.5.17)$$

The lift coefficient is

$$C_y=2\pi(1+\varepsilon)\sin\alpha\approx 2\pi\left(1+0{,}77\frac{d}{b}\right)\sin\alpha. \qquad (3.5.18)$$

The solid Zhukovskiy profile with rounded leading edge and

with a frame* in the form of circular arcs is obtained if the center of the generating circle is shifted in such a way that the point c comes to lie within it. To render the analysis more convenient the center of the circle is shifted by εa along the first axis, with $a=\sqrt{c^2+h^2}$ (cf. Fig. 3.5.9,e), i.e., the position of the center of the generating circle will be $\zeta_0=a(1+\varepsilon)e^{i\alpha_0}$ and its radius $r_0=a(1+\varepsilon)$; the lift will therefore be equal to

$$Y=4\pi\rho v_\infty^2 a(1+\varepsilon)\sin(\alpha+\alpha_0). \qquad (3.5.19)$$

In the general case the calculation of the lift coefficient C_y is very complicated because the wing chord b is a function of its thickness (connected with the parameter ε) and of the camber f (connected with h). But within the limits of small quantities these parameters can be assumed to be approximately the same as those for a symmetrical profile

$$b=4c,\ \frac{d}{b}=1{,}3\varepsilon,\ \text{i.e. } \varepsilon=\frac{d}{1{,}3b}=0{,}77\frac{d}{b}.\ \text{where}$$

$$C_y=2\pi\left(1+0{,}77\frac{d}{b}\right)\left(\alpha+\frac{2f}{b}\right). \qquad (3.5.20)$$

where f is the maximum camber of the center line of the profile.

The transformation of an ellipse. We notice that the N.Ye. Zhukovskiy transformation can also be applied to other smooth contours that pass through the point $\zeta = c$, the flow about which is known, e.g., to an ellipse. This yields a still greater variety of profile shapes (cf. Fig. 3.5.9,f).

Generalized Zhukovskiy profiles. To obtain profiles with a nonvanishing trailing edge angle ω, N.Ye. Zhukovskiy has applied to the circle the general transformation

$$\frac{z-ic}{z+ic}=\left(\frac{\zeta-c}{\zeta+c}\right)^n,\quad n=\frac{2\pi-\omega}{\pi}. \qquad (3.5.21)$$

The frame of these profiles consists of two circular arcs intersecting at the trailing edge at an angle ω (Fig. 3.5.10). The

profile shape is changed by changing the position of the center of the circle and of its size. The chord of these profiles is equal to $2\kappa c$. The lift coefficient is

$$C_y = \frac{4\pi}{\kappa} \sin(\alpha + \beta). \qquad (3.5.22)$$

Rounding of the profile at the leading edge. If the generating circle is so chosen that it enclosed both the points $\zeta = \pm c$, then, using Transformation (3.5.13), we obtain a profile without corner points. For such profiles the determination of the circulation becomes an indefinite problem.

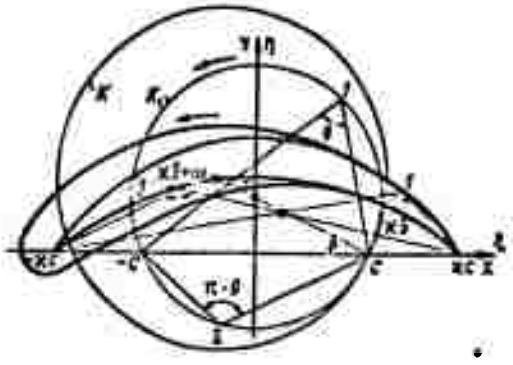


Fig. 3.5.10. Generalized Zhukovskiy profile (nonvanishing trailing edge angle). The circle K_1 is transformed to two intersecting arcs (the profile frame).

Comparison with experiment. Fig, 3.5.11 shows the polars of one and the same Zhuvskiy profile for various degrees of roughness of the surface. The points on the polars corresponding to one and the same angle of attack lie on straight lines whose sections with the C_y-axis give the C_y values holding for zero profile losses. It can be shown that those C_y values that correspond to zero drag are in very good agreement with the theoretical values*. It follows from these experiments that for a well polished surface, such as is commonly used in laboratory practice, the value $dC_y/d\alpha = 5.4$ is virtually

independent of the Re number.

Systematic investigations show that the values of $dC_y/d\alpha$ retains its significance for other Zhukovskiy profiles too, regardless of their thickness, and also for profiles with other contours but with zero trailing edge angle; (Fig. 3.5.12). However, $dC_y/d\alpha$ decreases with increasing trailing edge angle ω. This is seen from Fig. 3.5.12 where the values of $dC_y/d\alpha$ are given for a series of profiles whose trailing edge angles vary proportional to the profile thickness. This result disagrees with Relations (3.5.18) and (3.5.20), after which $dC_y/d\alpha$ increases with the profile thickness and the trailing edge angle.

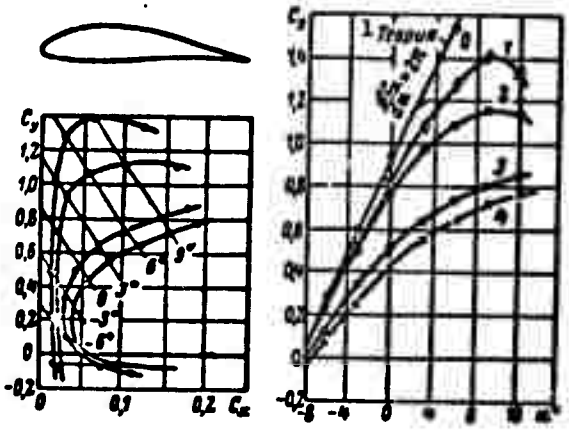


Fig. 3.5.11. Experimental polars of a Zhukovskiy profile with various degrees of roughness of the surface and the extrapolation of the lift to zero profile drag. 1) Theory.

These results show that the appearance of a circulation about the wing is determined by the conditions under which the starting vortex forms. Obviously, this process is connected with the effect of viscosity; not directly, as would be expressed in the dependence $dC_y/d\alpha$ on the Re number, but indirectly, due to a change of the form of the motion.

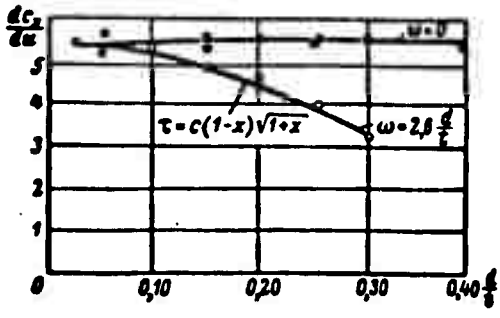


Fig. 3.5.12. Experimental results of a series of profiles with various trailing edge angles.

In practical applications the influence of the trailing edge angle can be taken into account by the relation

$$\frac{dC_y}{d\alpha} = 2\pi k e^{-\frac{\theta}{\pi}} = 2\pi k\left(1-\frac{\theta}{\pi}\right), \quad k = \frac{5.4}{2\pi} \approx 0.85. \tag{3.5.23}$$

Chaplygin profiles. Instead of applying one and the same transforming function to various circles, S.A. Chaplygin suggested transforming one and the same circle by a suitable function containing a sufficient number of parameters determining the profile shape. A very class of profiles is obtained by the transformation

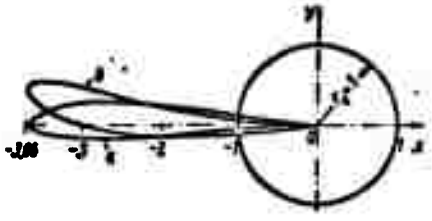


Fig. 3.5.13. Chaplygin profiles, $z = \frac{(\zeta-1)^k}{(\zeta-\varepsilon_0)^{k-1}}$: a) With $\varepsilon_0 = 0.1$; b) with $\varepsilon_0 = 0,1\ (1+i)$.

$$z = \frac{(\zeta-1)^{2-k}}{(\zeta-\varepsilon_0)^{1-k}}; \tag{3.5.24}$$

where k is a real parameter determining the trailing edge angle (equal to $k\pi$) and $\varepsilon_0 = \xi_0 + i\eta_0$ is the complex parameter that influences the profile shape.

The variety of profiles can be enlarged by generalizing the S.A. Chaplygin function by increasing the number of profile shape parameters [9.8]:

$$z = \frac{(\zeta-1)^{2-k}}{\left(\zeta - \Sigma\frac{a_n}{\zeta^n}\right)^{1-k}}. \tag{3.5.25}$$

However, this complication considerably encumbers the whole investigation of the influence of each parameter $\varepsilon_0, \tau_0, \eta_0$ on the profile shape and its aerodynamic characteristics.

The transforming Chaplygin Function (3.5.24) has its simplest form with k = 0 (zero trailing edge angle):

$$z = \frac{(\zeta - 1)^2}{\zeta - \zeta_0}. \qquad (3.5.26)$$

Figure 3.5.13 shows two Chaplygin profiles.

3.6. SOLUTION OF THE PROBLEM OF THE FLOW ABOUT A BODY BY THE METHOD OF CONTINUOUSLY DISTRIBUTED SINGULARITIES

Method of vortex sheets. As it has been shown above (cf. Section 2.6) in the case of a velocity potential the viscosity at a distant from the body does not affect the motion of the fluid and the pressure distribution in it. But from the boundary conditions it follows that the supposition on a motion potential cannot hold near the boundary of the body. Certainly there must exist here a region of vortex motion – a "vorticity layer" as it was called by N.Ye. Zhukovskiy.

In this very thin boundary layer, whose thickness is equal to

$$\delta = l\frac{5.5}{\sqrt{\mathrm{Re}}} \quad \left(\mathrm{Re} = \frac{w_0 l}{\nu}\right),$$

for a plate of length l, the speed changes from zero at the boundary to w_0 corresponding to potential flow. This sharp change of speed involves the formation of high intensity vortices.

If dy is an element normal to the body lying in the boundary layer, $dA_c = w_x dy$ will be the area of vortex formation per second. In the case of a plane flow the angular rate of rotation of particles is equal to $\frac{1}{2}\left(\frac{\partial w_y}{\partial x} - \frac{\partial w_x}{\partial y}\right) \approx \frac{1}{2}\frac{\partial w_x}{\partial y}$, since the velocity w_y varies only little in the x-direction and the total velocity of the boundary layer vortices formed per second is equal to

$$\int_0^{\infty} 2\omega\, dA_z = -\int_0^{\infty} \frac{\partial w_x}{\partial y} w_x\, dy = -\frac{w_0^2}{2}. \qquad (3.6.1)$$

It follows from this expression that the vortex flux per unit time does not depend on the thickness of the vortical boundary layer; it is mainly determined by the shape of the body. Therefore, in the limiting case of viscosity $\nu \to 0$, corresponding to $Re = wl : \nu \to \infty$, and, therefore, $\delta \to 0$, the boundary layer goes over to an infinitely thin vortex sheet with the same vortex intensity. This establishes the correspondence between the velocity jump (its discontinuity) in an inviscid fluid, formally introduced at the boundary of a solid body, and the limiting case of a vortical boundary layer that really exists.

Vorticity of a vortex sheet. If the tangential velocity on a vortex sheet is w_v and under it w_n (Fig. 3.6.1), then, calculating the circulation $\delta\Gamma$ of the vortex sheet element δl, the local vorticity per unit length can be determined:

$$\gamma(l) = \lim_{\delta l \to 0} \frac{\delta\Gamma}{\delta l} = w_v - w_n. \qquad (3.6.2)$$

In the case of a real flow the vortex sheet does not remain localized but is entrained by the stream and enters the trailing zone of potential flow in the form of a free vortex sheet, which immediately disintegrates, however, into single vortices of finite size and intensity.

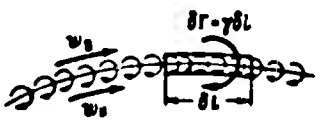


Fig. 3.6.1. The line of speed discontinuity is equivalent to a vortex sheet with the circulation $\gamma = \frac{d\Gamma}{dl}$ per unit length, equal to $w_v - w_n$.

During the flow around a body, at the place where the vortices are downwashed by the stream, new vortices of the same intensity are immediately formed since they are determined by the speed of

the potential flow. The vortex sheet can therefore be regarded as an adjacent vortex sheet the total vorticity of which determines the vorticity of the adjacent Zhukovskiy vortex.

The vortex system of a wing profile. Let us apply a vortex layer of the vorticity $\gamma(s)$ to a profile contour (s is the leading edge angle referred to the camber line). For convenience we shall take the clockwise circulation as positive (in order that the lift is directed upward along the y-axis).

To develop a theory of a none too thick and none too strongly bent profile the vorticity can be considered and determined separately for the camber line of the profile (i.e., for an infinitely thin profile) and for a symmetrical profile at zero angle of attack (Fig. 3.6.2).

In fact, since for reasons of symmetry the vorticity $\gamma_{mv}(s)$ on the upper contour of a symmetrical profile is equal but of opposite sign to $\gamma_{mn}(s)$ on the lower contour, i.e., $\gamma_{mn}(s) = -\gamma_{mv}(s)$, then, writing down the total vorticity of the vortex sheet on the upper and lower profile contours

$$\gamma_в(s) = \gamma_c(s) + \gamma_m; \quad \gamma_н(s) = \gamma_c(s) - \gamma_m,$$

we obtain

$$\gamma_c = \frac{\gamma_в + \gamma_н}{2}; \quad \gamma_m = \frac{\gamma_в - \gamma_н}{2}. \tag{3.6.3}$$

Camber line equation. We place the coordinate origin in the middle of the chord. Bearing in mind the application of trigonometric series, we assume (Fig. 3.6.3)

$$x = -\frac{b}{2}\cos\vartheta, \tag{3.6.4}$$

where the angle ϑ is measured clockwise from the negative x-semi-axis and

$$y = \frac{b}{2}\sum B_n \cos n\vartheta \qquad (0 < \vartheta < \pi). \tag{3.6.5}$$

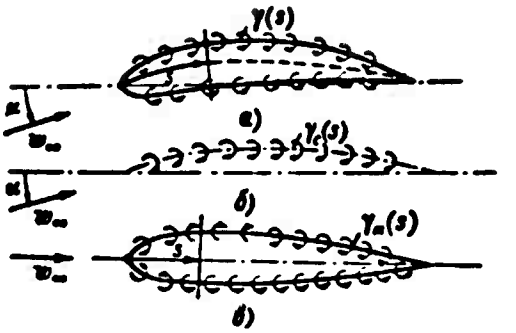


Fig. 3.6.2. Vortex system of a profile in a flow at an angle of attack α (a) can be built up from the camber line vortex system of the profile with the angle of attack α (b) and the vortex system for a symmetric profile with zero angle of attack (c).

If the profile equation is given in the form $y = f(x)$ the coefficients g_n are determined, as is well known, by formula

$$g_0 = \frac{1}{\pi}\int_0^{\pi} f(\vartheta)\,d\vartheta, \quad g_n = \frac{2}{\pi}\int_0^{\pi} f(\vartheta)\cos n\vartheta\,d\vartheta. \tag{3.6.6}$$

If the form of the camber line is given graphically we apply the trapezoidal rule and, taking into consideration that at the ends of the section the ordinates are equal to zero and replacing the integrals by sums, we shall have

$$g_0 = \frac{1}{\pi}\sum_i f(\vartheta_i)\,\delta\vartheta_i;$$

$$g_n = \frac{2}{\pi}\sum_i f(\vartheta_i)\cos n\vartheta_i\,\delta\vartheta_i.$$

Subdividing the whole interval $(0,\pi)$ into $\underline{k}$ equal parts, i.e., assuming $\delta\vartheta_i = \pi/k$ and $\vartheta_i = i\pi/k$, we obtain

$$g_0 = \frac{1}{\pi}\sum_{i=0}^{k-1} f(\vartheta_i)\frac{\pi}{k} = \frac{1}{k}\sum_{i=0}^{k} f(\vartheta_i); \quad g_n = \frac{2}{k}\sum_{i=0}^{k-1} f(\vartheta_i)\cos n\vartheta_i. \tag{3.6.7}$$

In explicit form we have

$$g_n = \frac{2}{k}\left[y_1\cos\frac{\pi n}{k} + y_2\cos 2\frac{\pi n}{k} + y_3\cos 3\frac{\pi n}{k} + \ldots + y_{k-1}\cos n\pi\right],$$

where the quantity $\underline{y}$ must be taken in terms of the semi-chord of the wing.

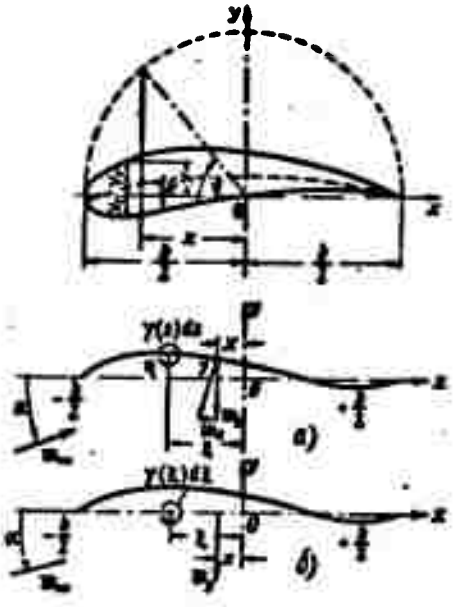


Fig. 3.6.3. Scheme for calculating the induced speeds of a vortex sheet positioned on the slightly curved camber line, exactly (a) and approximately (b).

Furthermore, a more accurate formula, such as Simpson's rule, can also be used.

Speed determination for the points of the camber line. The complex conjugate speed induced at the point $z = x + iy$ by the vortex sheet placed along the camber line, is, owing to (3.2.13), equal to

$$\overline{w}_a(x,y)=\frac{1}{2\pi}\int_{(a)}\frac{\gamma(s)\,ds}{z-z(s)}.$$

Assuming the profile to be slightly curved, we may replace the integration along the camber line by integration along the chord (cf. Fig. 3.6.3,b). Then

$$\overline{w}_a(x,y)=w_{x,a}-iw_{y,a}=\frac{1}{2\pi}\int_{-\frac{b}{2}}^{\frac{b}{2}}\frac{\gamma(\xi)\,d\xi}{(x+iy)-\xi}=\frac{1}{2\pi}\int_{-\frac{b}{2}}^{\frac{b}{2}}\frac{(x-\xi)-iy}{(x-\xi)^2+y^2}\gamma(\xi)\,d\xi.$$

The speed components on the chord are

$$\left.\begin{aligned}w_{x,a}(x,0)&=\frac{1}{2\pi}\lim_{y\to 0}\int_{-\frac{b}{2}}^{\frac{b}{2}}\frac{y}{(x-\xi)^2+y^2}\gamma(\xi)\,d\xi,\\ w_{y,a}(x,0)&=-\frac{1}{2\pi}\int_{-\frac{b}{2}}^{\frac{b}{2}}\frac{\gamma(\xi)\,d\xi}{x-\xi}.\end{aligned}\right\}\qquad(3.6.8)$$

Speed on the axis. The integral determining the x-component of the speed ($y \to 0$) is an improper one. To determine it the whole path of integration must be divided into sections $\left(-\frac{b}{2}, x-\varepsilon\right)$, $(x-\varepsilon, x+\varepsilon)$, $\left(x+\varepsilon, \frac{b}{2}\right)$ and the limit be found of the expression obtained for

$\varepsilon \to 0$ and $y \to 0$.

It is, however, simpler to find the speed of the vortex sheet by using Relation (3.6.2) and writing it in the form

$$w_{x_2}(x, +0) - w_x(x, -0) = \gamma(x). \qquad (*)$$

But, since we are considering speeds induced only by the vortex sheet lying on a straight line, their components along the x-axis are equal and opposite.

Thus,

$$w_{x_2}(x, +0) = -w_{x_2}(x, -0).$$

Taking Formula(*) into account we obtain

$$w_{x_2}(x, +0) = \frac{\gamma(x)}{2}; \quad w_{x_2}(x, -0) = -\frac{\gamma(x)}{2}, \qquad (3.6.9)$$

i.e., the speed discontinuity is equal to the vorticity of the vortex sheet at this point.

Thus, the total speed above and below the camber line and arbitrarily close to it will be

$$w_{2_0} = w_{\infty_x} + \frac{\gamma(x)}{2}, \quad w_{1_0} = w_{\infty_x} - \frac{\gamma}{2}. \qquad (3.6.10)$$

Integral equation of the theory of thin profiles. At the points of the camber line the speed is equal to $w_{\infty x}$. With a small angle of attack α we have

$$w_{\infty_x} = w_\infty \cos\alpha \approx w_\infty, \quad w_{\infty_y} = w_\infty \sin\alpha = w_\infty \alpha. \qquad (3.6.11)$$

Therefore, by virtue of (3.6.8),

$$w_y = w_\infty \alpha - \frac{1}{2\pi} \int_{-\frac{b}{2}}^{\frac{b}{2}} \frac{\gamma(\xi)\, d\xi}{x - \xi}; \quad w_x \approx w_\infty$$

and the boundary condition $dy : dx = w_y : w_x$ yields the basic equation of the theory of thin profiles

$$\alpha - \frac{dy}{dx} = \frac{1}{2\pi w_\infty} \int_{-\frac{b}{2}}^{\frac{b}{2}} \frac{\gamma(\xi)\, d\xi}{x - \xi}. \qquad (3.6.12)$$

The integral entering this equation is termed singular since

its integrand tends to infinity as $x \to \xi$. When calculating it we have to take the main value (denoted by $\int^{*}$) which is determined by the equality

$$\int_{-\frac{b}{2}}^{\frac{b}{2}} \frac{\gamma(\xi)\,d\xi}{\xi - x} = \lim_{\varepsilon \to 0} \left[\int_{-\frac{b}{2}}^{x-\varepsilon} \ldots + \int_{x+\varepsilon}^{\frac{b}{2}} \ldots \right]. \qquad (3.6.13)$$

The determination of the vorticity $\gamma(\xi)$ for a given profile is called the direct problem. The determination of the profile shape for an assumed $\gamma(\xi)$-distribution is called the inverse problem. In the first case of the direct problem the solution is reduced to solving the integral Eq. (3.6.12); with the help of its right-hand side which is known, the integral function $\gamma(\xi)$ is found. The inverse problem is solved by a quadrature.

Choice of a suitable vorticity distribution in the vortex sheet. To solve Eq. (3.6.12) it is convenient to make use of a geometrical progression by representing the function $\gamma(\xi)$ in the form of a suitable trigonometric series. In order to properly build up the series expressing $\gamma(\xi)$ we consider the flow about the profile edges. The leading edge behaves in the flow as the edge of an infinite plane. We have shown above (cf. Part 3.3) that at the plate edge, in our case as $\xi \to -\frac{b}{2}$, the velocity tends to infinity as $1 : \sqrt{\frac{b}{2} + \xi}$. The vorticity of the vortex layer also tends to infinity at this point.

According to the Zhukovskiy-Chaplygin condition the velocity at the trailing edge is the same above and below the profile; owing to (3.6.2) the vorticity of the layer is equal to zero. Hence in a trigonometric series we must have for the vorticity a term which is proportional to

$$\sqrt{\frac{\frac{\delta}{2}-t}{\frac{\delta}{2}+t}}=\sqrt{\frac{1+\cos\theta}{1-\cos\theta}}=\operatorname{ctg}\frac{\theta}{2}. \qquad (3.6.14)$$

which takes the flow conditions at the ends into account (remember that $\xi = -\frac{\delta}{2}\cos\theta$). Within the interval $(0<\theta<\pi)$ the remaining part of the vorticity can be assumed to be expressed by a sine series since at the ends of the interval $(0,[\pi])$ this series vanishes and does not violate the boundary conditions described by Function (3.6.14).

Thus, the series must read

$$\gamma(\theta)=2w_\infty\left[a_0\operatorname{ctg}\frac{\theta}{2}+\sum_{n=1}^{\infty}a_n\sin n\theta\right], \qquad (3.6.15)$$
$$(0<\theta<\pi),$$

where the factor w_∞ is introduced to make the coefficient a_n dimensionless.

Velocity at the axis (y = 0). Assuming $t=-\frac{\delta}{2}\cos\varphi$ and substituting the value of $\gamma(\varphi)$ in the second integral of (3.6.8) we find

$$\frac{w_{y=0}}{w_\infty}=-\frac{1}{2w_\infty}\int_{-\frac{\delta}{2}}^{\frac{\delta}{2}}\frac{\gamma(t)\,dt}{t-x}=\frac{1}{\pi}\int_0^{\pi}\frac{a_0\operatorname{ctg}\frac{\varphi}{2}+\sum_{n=1}^{\infty}a_n\sin n\varphi}{\cos\theta-\cos\varphi}\sin\varphi\,d\varphi=$$

$$=\frac{1}{\pi}\int_0^{\pi}\frac{a_0(1+\cos\varphi)+\frac{1}{2}\sum_{n=1}^{\infty}a_n[\cos(n-1)\varphi-\cos(n+1)\varphi]}{\cos\theta-\cos\varphi}d\varphi. \qquad (3.6.16)$$

For calculating the integrals of the form

$$K_p=\int_0^{\pi}\frac{\cos p\varphi}{\cos\theta-\cos\varphi}d\varphi \qquad (3.6.17)$$

entering (3.6.16) we assume $e^{i\varphi} = z$ and denote by C the circumference of the unit circle and so we find first

$$K_0=\int_0^{\pi}\frac{d\varphi}{\cos\theta-\cos\varphi}=\frac{1}{2}\int_0^{2\pi}\frac{d\varphi}{\cos\theta-\cos\varphi}= \qquad (3.6.18)$$

$$-\int_C \frac{dz}{iz\left[-\left(z+\frac{1}{z}\right)+2\cos\theta\right]} = i\int_C \frac{dz}{z^2-2z\cos\theta+1} =$$

$$= i\int_C \frac{dz}{(z-e^{i\theta})(z-e^{-i\theta})} = \frac{i}{e^{i\theta}-e^{-i\theta}}\int_C\left[\frac{1}{z-e^{i\theta}}-\frac{1}{z-e^{-i\theta}}\right]dz =$$

$$= \frac{1}{2\sin\theta}(\pi i-\pi i) = 0. \qquad (3.6.18)$$

Here

$$K_1 = \int_0^{2\pi}\frac{\cos\varphi}{\cos\theta-\cos\varphi}d\varphi = \int_0^{2\pi}\frac{\cos\varphi-\cos\theta+\cos\theta}{\cos\theta-\cos\varphi}d\varphi = -\pi.$$

Multiplying the identity

$$\cos(p+1)\varphi+\cos(p-1)\varphi = 2\cos p\varphi\cdot\cos\varphi$$

by $d\varphi/(\cos\vartheta - \cos\varphi)$ and integrating the expression obtained from 0 to π we arrive at the recurrence formula

$$K_{p+1}+K_{p-1} = 2\cos\theta\cdot K_p,$$

and, knowing K_0 and K_1, we can use it to successively calculate K_2, K_3,... etc. By direct substitution in the recurrence formula we can satisfy ourselves that

$$K_p = -\pi\frac{\sin p\theta}{\sin\theta}. \qquad (3.6.19)$$

Therefore Expression (3.6.16) now assumes the following form:

$$\frac{w_{y_0}}{w_\infty} = -\frac{1}{2\pi w_\infty}\int_{-\frac{b}{2}}^{\frac{b}{2}}\frac{\gamma(\xi)\,d\xi}{\xi-x} =$$

$$= -\frac{1}{\pi}\left\{-\pi a_0-\frac{\pi}{2}\sum_{n=1}^{\infty}a_n\frac{-\sin(n-1)\theta-\sin(n+1)\theta}{\sin\theta}\right\} =$$

$$= -\left(a_0-\sum_{n=1}^{\infty}a_n\cos n\theta\right) \qquad (3.6.20)$$

Connection with profile geometry. Determining

$$\frac{dy}{dx} = \frac{dy}{d\theta}\frac{d\theta}{dx} = -\sum_{n=1}^{\infty}nB_n\frac{\sin n\theta}{\sin\theta}$$

from (3.6.4) and (3.6.5), and taking (3.6.20) into account, we ob-

tain, by virtue of (3.6.12)

$$\varepsilon-\left(a_0-\sum_{k=1}^{n} a_k\cos k\theta\right)=-\sum_{s=1}^{n} ng_s\frac{\sin n\theta}{\sin\theta}. \qquad (3.6.21)$$

Hence, as also in (3.6.6), we have

$$\varepsilon-a_0=-\frac{1}{\pi}\sum_{s=1}^{n} ng_s\int_0^{\pi}\frac{\sin n\theta}{\sin\theta}\,d\theta,$$

$$a_k=-\frac{2}{\pi}\sum_{s=1}^{n} ng_s\int_0^{\pi}\frac{\sin n\theta}{\sin\theta}\cos k\theta\,d\theta=$$

$$=-\frac{1}{\pi}\sum_{s=1}^{n} ng_s\int_0^{\pi}\frac{\sin(n+k)\theta+\sin(n-k)\theta}{\sin\theta}\,d\theta.$$

However, since

$$\sin m\theta-\sin(m-2)\theta=2\sin\theta\cdot\cos(m-1)\theta,$$

we have

$$\int_0^{\pi}\frac{\sin m\theta}{\sin\theta}\,d\theta=2\int_0^{\pi}\cos(m-1)\theta\,d\theta+$$

$$+\int_0^{\pi}\frac{\sin(m-2)\theta}{\sin\theta}\,d\theta=\int_0^{\pi}\frac{\sin(m-2)\theta}{\sin\theta}\,d\theta.$$

Thus, applying the recurrence formula, we obtain

$$\int_0^{\pi}\frac{\sin m\theta}{\sin\theta}\,d\theta=\begin{cases}0, & \text{если } m=2s\\ \pi, & \text{если } m=2s-1\\ & (s=1,2,3,\ldots).\end{cases} \qquad (3.6.22)$$

Therefore,

$$\varepsilon-a_0=-\sum_{s=1}^{n} ng_s=-\sum_{s=1}^{n}(2s-1)g_{2s-1}$$

(n is an odd number).

Assuming that n + k (and n − k) are odd numbers, we obtain

$$a_k=-\sum_{s=1}^{n} ng_s-\frac{1}{\pi}\sum_{s=1}^{k} ng_s\int_0^{\pi}\frac{\sin(n-k)\theta}{\sin\theta}\,d\theta-$$

$$-\frac{1}{\pi}\sum_{s=n-k+1}^{n} ng_s\int_0^{\pi}\frac{\sin(n-k)\theta}{\sin\theta}\,d\theta=$$

$$=-\sum_{s=1}^{n} ng_s+\sum_{s=1}^{k} ng_s-\sum_{s=n-k+1}^{n} ng_s=2\sum_{s=n-k+1}^{n} ng_s.$$

Putting $n - k = 2s - 1$ we finally arrive at

$$\left.\begin{aligned} a_0 &= -2\sum_{s=1}^{\infty}(2s+k-1)A_{k+2s-1} \\ &\qquad (k=1,2,3\ldots), \\ a_0 &= \alpha + \sum_{s=1}^{\infty}(2s-1)B_{2s-1}. \end{aligned}\right| \tag{3.6.23}$$

Lift. To determine the lift arising at the wing profile the Zhukovskiy formula $R = \rho w_\infty \Gamma$ can be applied, where $\Gamma = \int_{-b/2}^{b/2}\gamma(\xi)\,d\xi$ stands for the circulation of the vortex sheet replacing the wing. This gives us

$$R_y = \rho w_\infty \int_{-b/2}^{b/2}\gamma(\xi)\,d\xi = 2\rho w_\infty^2 \int_0^{\pi}\left(a_0 \operatorname{ctg}\frac{\vartheta}{2} + \right.$$

$$\left. + \sum a_n \sin n\vartheta\right)\frac{b}{2}\sin\vartheta\,d\vartheta =$$

$$= b\rho w_\infty^2\left[\int_0^{\pi} a_0(1+\cos\vartheta)\,d\vartheta + \sum_{n=1}^{\infty} a_n \int_0^{\pi}\sin n\vartheta \sin\vartheta\,d\vartheta\right] =$$

$$= b\rho w_\infty^2 \pi\left(a_0 + \frac{a_1}{2}\right)$$

and

$$C_y = 2\pi\left(a_0 + \frac{a_1}{2}\right). \tag{3.6.24}$$

Moment. Calculating the moment necessitates determining the pressure distribution. Since outside the profile (the camber line) the motion is a potential one, we have, according to the Bernoulli equation

$$p_0 + \frac{\rho w_0^2}{2} = p_\infty + \frac{\rho w_\infty^2}{2} = \text{const}.$$

Therefore

$$p_0 - p_\infty = \rho\frac{w_\infty^2 - w_0^2}{2} = \rho\frac{(w_\infty + w_0)(w_\infty - w_0)}{2} = \rho w_c \gamma. \tag{3.6.25}$$

This relation is called the local Zhukovskiy theorem.

The velocity $w_c = \frac{1}{2}(w_0 + w_\infty)$ is composed of the velocity of the parallel undisturbed flow and the velocity induced by all singularities located at finite distances from the wing, without the velocity

from the singularity at the point considered. For a slightly curved profile the longitudinal component is very small and will be neglected in all our calculations; therefore

$$w_t \approx w_n. \tag{3.6.26}$$

This yields, by virtue of (3.6.25), the pressure coefficient

$$C_p = \frac{p_n - p_0}{\frac{1}{2}\rho w_\infty^2} = \frac{2\gamma}{w_\infty}. \tag{3.6.27}$$

Now the moment with respect to the leading edge is

$$M = \int_{-\frac{b}{2}}^{\frac{b}{2}} \left(\frac{b}{2} + x\right) p\, dx = \rho w_\infty \int_0^\pi 2w_\infty \left(a_0 \operatorname{ctg}\frac{\vartheta}{2} + \right.$$

$$\left. + \sum_{n=1}^{\infty} a_n \sin n\vartheta\right) \frac{b}{2}(1 - \cos\vartheta)\frac{b}{2}\sin\vartheta\, d\vartheta =$$

$$= \frac{\pi}{4}\rho w_\infty^2 b^2 \left(a_0 + a_1 - \frac{a_2}{2}\right). \tag{3.6.28}$$

Hence the coefficient of the trailing edge moment is obtained as

$$C_m = \frac{M}{\frac{\rho w_\infty^2}{2} b^2} = \frac{\pi}{2}\left(a_0 + a_1 - \frac{a_2}{2}\right). \tag{3.6.29}$$

The position of the pressure center e in terms of the wing chord is found from the relation M = eY, namely

$$\frac{e}{b} \approx \frac{C_m}{C_y} = \frac{1}{4} + \frac{\pi(a_1 - a_2)}{4c_y}; \tag{3.6.30}$$

whence for $a_1 = a_2$ the position of the pressure center does not vary with the angle of attack.

Approximate relations. A good approximation for the camber line of profiles actually used is obtained by adding the ordinates of two parabola curves (Fig. 3.6.4) – or curve P described by equation $y_p = p(1 - x^2)$ and curve S (cubic parabola) described by equation $y_s = sx(x^2 - 1)$, (the chord is $b = 2, -1 \leq x \leq 1$). These curves have maxima equal to $y_{p\ max} = p$ and $y_{s\ max} = \frac{2\sqrt{3}}{9}s$ at $\vartheta = 90^\circ$

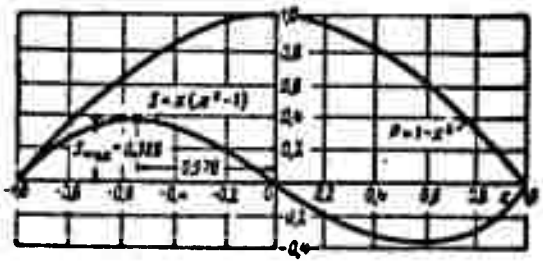


Fig. 3.6.4. The P and S curves.

and $\vartheta = 54^{\circ}50'$, respectively. Since $b = 2$, $x = -\cos\vartheta$ and the transition to the variable ϑ gives

$$y = \frac{p}{2} + \frac{s}{4}\cos\vartheta - \frac{p}{2}\cos 2\vartheta - \frac{s}{4}\cos 3\vartheta,$$

whence

$$g_0 = \frac{s}{2} = a - a_0, \quad g_1 = 2p = a_1, \quad g_2 = \frac{3s}{2} = a_2 \qquad (3.6.31)$$

and

$$C_y = 2\pi\left(a_0 + \frac{a_1}{2}\right) = 2\pi\left(a + p - \frac{s}{2}\right) = 2\pi(a + a_0); \quad a_0 = p - \frac{s}{2},$$

where α_0 is the angle of the first profile axis. As can be seen, the straight line connecting the ordinate of the camber line at the midpoint of its chord and the trailing edge gives the first profile axis (Fig. 3.6.5). If $a_1 = a_2$, i.e., $4p = 3s$, then, owing to (3.6.30), we obtain profiles with a constant pressure center; for these $e = 1/4$ and is independent of the angle of attack.

It has to be noticed that the theory of thin profiles yields better agreement between calculated data and experiment for profiles of small thickness than for what are literally thin profiles in the form of a very thin bent leaf. This is explained by the more regular flow about them in the trailing edge zone.

To draw a profile with a rounded leading edge, the ordinates of the thickness curve are plotted at the corresponding abscissas onto both sides from the camber line. The thickness curves, e.g., those suggested by Munk, have the equation (Fig. 3.6.6)

$$\tau_1=(1-x)\sqrt{1+x^2};\quad \tau_2=(1-x)\sqrt{1-x^2}. \tag{3.6.32}$$

The maximum ordinate τ_{max} of the first curve is equal to 1.09 for $x = -1/3$, and that of the second curve is equal to 1.30 for $x = 0.5$. The angle between the trailing edge tangents is equal to $2.60\ \tau_{max}/2$ for the first curve and zero for the second curve.

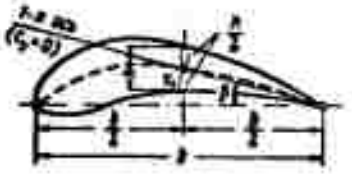


Fig. 3.6.5. Graphical method for an approximate determination of the first axis.

Circulation-free flow about a symmetrical profile. This can be found by the method of vortex sheets. If the angle of attack is equal to zero, then for reasons of symmetry this problem is more easily solved by the method of sources distributed on the profile axis.

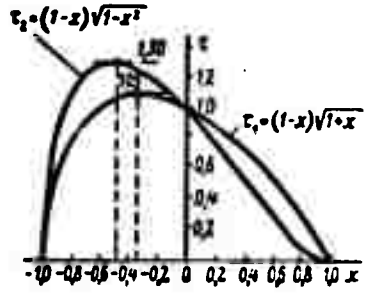


Fig. 3.6.6. Thickness curves.

Let us assume plane sources (and sinks) be continuously distributed on the ξ-axis, so that $\delta Q(\xi)$ is the flow rate of the sources at the section $\delta\xi$ near point ξ (Fig. 3.6.7). Let us denote by

$$q(\xi)=\lim_{\delta\xi\to 0}\frac{\delta Q(\xi)}{\delta\xi} \tag{3.6.33}$$

the flow rate from the sources at point ξ referred to the unit length of the axis (source density). The problem is to determine the source distribution characterized by the function $q(\xi)$ in such a way that if a parallel flow is superimposed on the flow generated by the sources we obtain a closed line with the form of the profile contour given, i.e., that the profile contour given is a streamline for which $dy/dx = w_y/w_x$.

The condition that the contour be closed requires

$$\int_{-b/2}^{b/2} q(t)\,dt = 0. \qquad (3.6.34)$$

The profile equation. Let us bring the equation of the upper part of the profile ($y_m \geq 0$) to the form

$$x = -\frac{b}{2}\cos\theta, \quad y_m = \frac{b}{2}\sum_{n=1}^{\infty} h_n \sin n\theta \quad (0 \leq \theta \leq \pi). \qquad (3.6.35)$$

If the profile equation is given in the form $y = f(x)$ we have

$$h_n = \frac{2}{\pi}\int_0^{\pi} f(\theta)\sin n\theta\,d\theta, \qquad (3.6.36)$$

and if the profile is given graphically, then, as in (3.6.7), we divide the interval $(0, -\pi)$ into k parts and, since $y_0 = y_k = 0$, we can write

$$h_n = \frac{2}{k}\left[y_1 \sin\frac{n\pi}{k} + y_2 \sin 2\frac{n\pi}{k} + \ldots + y_{k-1}\sin(k-1)\frac{n\pi}{k}\right].$$

Assuming, for example, $k = 4$ (cf. Fig. 3.6.7), we obtain hence

$$\frac{2y_m}{b} = h_1 \sin\theta + h_2 \sin 2\theta + h_3 \sin 3\theta,$$

where

$$h_1 = \frac{\sqrt{2}}{4}(y_1 + y_2\sqrt{3} + y_3); \quad h_2 = \frac{y_1 - y_3}{2};$$

$$h_3 = \frac{\sqrt{2}}{4}(y_1 - y_2\sqrt{2} + y_3).$$

Velocity at the points of the profile. The complex conjugate velocity at the point $z = x + iy$ from sources distributed along the chord will be (due to 3.2.5)

$$\overline{w}_0 = w_{0x} - iw_{0y} = \frac{1}{2\pi}\int_{-b/2}^{b/2} \frac{q(t)\,dt}{z - t} = \frac{1}{2\pi}\int_{-b/2}^{b/2} \frac{q(t)\,dt}{(x + iy) - t}.$$

This yields

$$w_{0x} = \frac{1}{2\pi}\int_{-b/2}^{b/2} \frac{(x-t)q(t)\,dt}{(x-t)^2 + y^2}, \quad w_{0y} = \frac{1}{2\pi}\int_{-b/2}^{b/2} \frac{yq(t)\,dt}{(x-t)^2 + y^2}. \qquad (3.6.37)$$

We shall consider a thin profile with $y_m : b \ll 1$. Then, when calculating the velocities at the points of the contour which are generated by the sources, we may assume

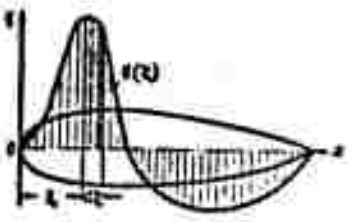


Fig. 3.6.7. Source-sink distribution on the axis of a symmetrical profile.

$$w_{0x}(x, y_m) = w_{0x}(x, 0);$$
$$w_{0y}(x, y_m) = w_{0y}(x, 0).$$

Comparing (3.6.37) and (3.6.8), and repeating the considerations made on deriving (3.6.8) and (3.6.9), we can write

$$w_{0x}(x, y_m) = \frac{1}{2\pi} \int_{-b/2}^{b/2} \frac{q(t)}{x - t} dt; \qquad (3.6.38)$$

$$w_{0y}'(x, y_m) = \pm \frac{q(x)}{2}. \qquad (3.6.39)$$

where the sign (+) applies to $y_m > 0$ and (-) to $y_m < 0$.

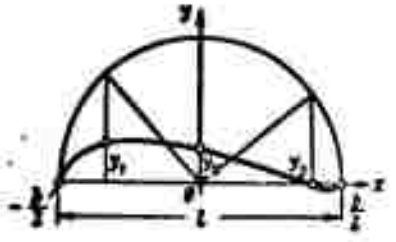


Fig. 3.6.8. The upper half of a symmetrical profile.

The integral equation. From the boundary condition that the profile contour has to be a streamline,

$$\frac{dy}{dx} = \frac{w_y}{w_x} = \frac{q(x):2}{w_\infty + \frac{1}{2\pi} \int_{-b/2}^{b/2} \frac{q(t)}{x - t} dt},$$

we obtain the integral function for determining function q(x):

$$\frac{dy}{dx}\left(w_\infty + \frac{1}{2\pi} \int_{-b/2}^{b/2} \frac{q(t)}{x - t} dt \right) = \frac{q(x)}{2}. \qquad (3.6.40)$$

In the case of a sufficiently thin profile we may neglect the additional induced velocity w_x as compared with the velocity of the undisturbed flow w_∞ and then

$$q(x) = 2w_\infty \frac{dy}{dx}. \qquad (3.6.41)$$

This equation can be used for approximately determining the function q(x).

If $y_m = \frac{b}{2} \sum_{n=1}^{\infty} h_n \sin n\theta$, we have

$$q(\theta) = 2w_\infty \frac{\sum_{n=1}^{\infty} n h_n \cos n\theta}{\sin \theta}. \qquad (3.6.42)$$

Here

$$w_x = w_\infty + \frac{1}{2\pi}\int_{-\frac{b}{2}}^{\frac{b}{2}} \frac{q(\xi)}{x-\xi}\,d\xi = w_\infty\left(1 + \frac{1}{\pi}\sum_{n=1}^{\infty} n h_n \int_0^{\pi} \frac{\cos n\varphi}{\cos\varphi - \cos\vartheta}\,d\varphi\right) =$$

$$= w_\infty\left[1 - \sum C_n \cos n\vartheta\right]. \qquad (3.6.43)$$

where, as on deriving (3.6.23),

$$\left.\begin{aligned} C_0 &= \sum_{s=1} (2s-1)\,h_{2s-1}, \\ &\cdots\cdots\cdots\cdots\cdots \\ C_n &= 2\sum_{s=1} (n+2s-1)\,h_{n+2s-1} \quad n \geqslant 1. \end{aligned}\right\} \qquad (3.6.44)$$

$$w_y = w_\infty \frac{\sum n h_n \cos n\vartheta}{\sin\vartheta}. \qquad (3.6.45)$$

Vorticity of a vortex shield. If the contour of a symmetrical profile is replaced by a vortex sheet, the vorticity of the sheet can be found from (3.6.41), calculating (by 3.6.2) $\gamma(\vartheta) = w_y - w_n$ at the speed discontinuity surface. This yields (with 3.6.43)

$$\gamma(\vartheta) = -2w_\infty \sum h_n \cos n\vartheta. \qquad (3.6.46)$$

Radii of curvature of the profile edges. If it is required that the radii of curvature of the leading and trailing edges of the profile should have given values, R and r, respectively, i.e., that at the points $\vartheta = 0$ and $\vartheta = \pi$ the y_m-curve touches the circles of radii R and r, then, as may be shown, the coefficients h_n will satisfy the condition

$$\left.\begin{aligned} \sum_{n=1}^{\infty} (-1)^n h_n n &= -\sqrt{\frac{2r}{b}}, \\ \sum h_n n &= -\sqrt{\frac{2R}{b}}. \end{aligned}\right\} \qquad (3.6.47)$$

Example. If the trailing edge angle is put equal to zero and if we break off after the second term, we obtain a profile which is similar to the Zhukovskiy profile for which

$$-h_1 + 2h_2 = 0; \quad -h_1 + 2h_2 = -\sqrt{\frac{2R}{b}}.$$

i.e., $h_1 = 2h_2$

$$y = \frac{b}{2}(-2A_2 \sin\theta + A_2 \sin 2\theta) = \frac{b}{4}\sqrt{\frac{2R}{b}}\sin\theta(1+\cos\theta). \qquad (3.6.48)$$

Comparing (3.6.48) with the equation of the symmetrical profile found in (3.5) we see that they agree, with $\varepsilon = \sqrt{\frac{2R}{b}}$ and $\bar{d} = \frac{d}{b} = \frac{1}{4}\sqrt{\frac{2R}{b}}$. The vorticity of the vortex layer is $\gamma(\theta) = -2w_\infty(2A_2\cos\theta + A_3\cos 2\theta) = w_\infty\sqrt{\frac{2R}{b}}(2\cos\theta + \cos 2\theta)$. Therefore, $C_p = \frac{2\gamma}{w_\infty} = \sqrt{\frac{2R}{b}}(2\cos\theta + \cos 2\theta)$. we note also that for two profiles, 1 and 2, with the relative thicknesses d_1 and d_2

$$\frac{C_{p1}}{C_{p2}} = \frac{\bar{d}_1}{\bar{d}_2}. \qquad (3.6.49)$$

3.7. JET FLOW ABOUT A BODY

The form of motion. The viscosity proves to exert a great effect on the form of motion. The boundary layer separated from the body disintegrates into single vortices which fill the entire zone behind the body (Fig. 3.7.1). The continuously forming vortical region has a relatively small speed of motion and is separated from the rest of the fluid by a rather sharply marked discontinuity line. This makes it possible to schematically represent the plane flow of an inviscid fluid in the following manner: the streamline impinging upon the profile at point O is split up into two lines running along the profile to points A_1 and A_2. Here they become separated from the contour, and together with the section A_1BA_2 bound the contour of region II where the vortex motion is observed. The motion in region I may be considered as a potential one.

The resting body represents an obstacle for the fluid and in first approximation we may regard the fluid in region II, extending to infinity, as being at rest. Thus the speed changes jumplike along the lines A_1C_1 and A_2C_2.

GRAPHIC NOT REPRODUCIBLE

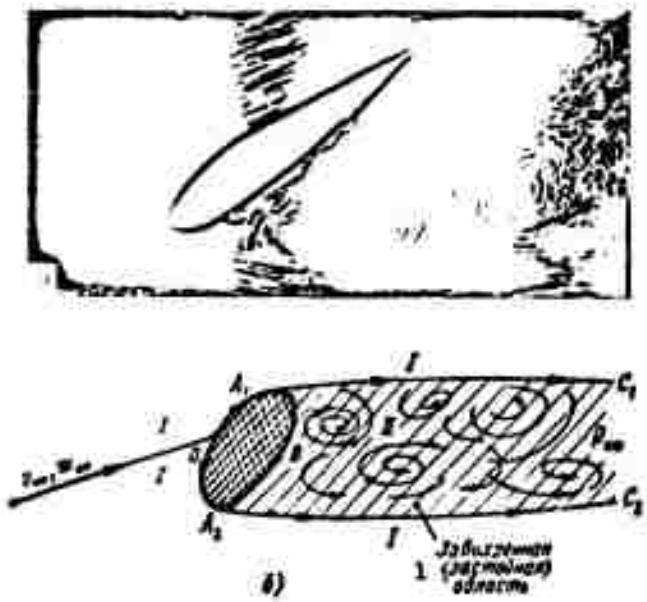


Fig. 3.7.1. Photograph (a) and scheme (b) of a jet flow about a body. 1) Vortex (stagnant) field.

Since the pressure in the stagnant region is constant and equal to the pressure at infinity, p_∞, it follows from the Bernoulli equation that the speed along the discontinuity lines is constant.

This form of motion has been studied by G. Kirchhoff and N. Ye. Zhukovskiy.

A plane plate. Let us place the coordinate origin at the stagnation point of a plane plate arranged at the angle of attack, α, with a stream of incompressible fluid of speed w_∞ flowing around it. The x-axis is directed along the plate. (Fig. 3.7.2).

Solving the problem by the hodograph method we assume $\chi=\Phi+i\Psi$ to be the complex potential in the P-region of the flow (outside the stagnant region), $\bar{w}=w_x-iw_y=\frac{d\chi}{dz}$ the complex conjugate velocity and

$$z=\int\frac{d\chi}{\bar{w}}. \qquad (3.7.1)$$

Therefore, if χ is determined as a function of $\bar{w}$, then, replacing $d\chi$ by its $\bar{w}$-expression and integrating in (3.7.1), we

find the solution $z = F(\overline{w})$ of this problem.

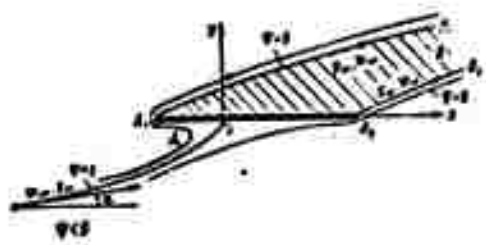


Fig. 3.7.2. Jet flow about a plane with an angle of attack.

Let us investigate those regions which contain the points $\overline{w}$ and χ in their planes when z varies in the P-region of the flow.

Let us begin with the variable $\overline{w}$ (Fig. 3.7.3,a). At the point O of the P-region the speed is equal to zero ($\overline{w} = 0$), along the line OA_2 the variable is positive and increases from O to w_∞; along the line OA_1 the variable $\overline{w}$ drops from O to $-w_\infty$ and over the free jets A_1B_1 and A_2B_2 (B_1B_2 and B lie at infinity) the velocity is equal in magnitude to w_∞ and is thus represented by a point on the circle of radius w_∞. Thus, the function $\overline{w} = \overline{w}(z)$ transforms the boundary of the P-region to a line consisting of half the circle of radius w_∞ and its horizontal diameter. Since the speed in the P-region is finite, the region of change of the quantity $\overline{w}$ we obtain in the $\overline{w}$-plane is the interior of the above semicircle. Furthermore, since the P-region is always to the left of the path $OA_1B_1B_2A_2O$ the lower semicircle will correspond to the region Q in the w-plane. The corresponding boundary points of the regions P and Q_w are designated by the same letters. At infinity $w_x = w_\infty \cos\alpha$, $w_y = w_\infty \sin\alpha$. $\overline{w} = w_x - iw_y = w_\infty e^{-i\alpha}$, therefore, one point B in the w-plane such that the angle A_2OB is equal to α corresponds to the three points B_1, B_2, and B in the z-plane.

Let us now consider the complex potential $\chi = \Phi + i\Psi$ (cf. Fig.

3.7.3,b). It is determined accurately to within a constant and it can be assumed that at $z = 0$ the χ-function also vanishes. But along a profile contour and free jets that are streamlines, the stream function $\Psi = 0$ on the whole boundary of the P-region. At the same time the potential Φ increases along the boundary of the P-region from 0 to ∞. It follows from this that all points of the plane

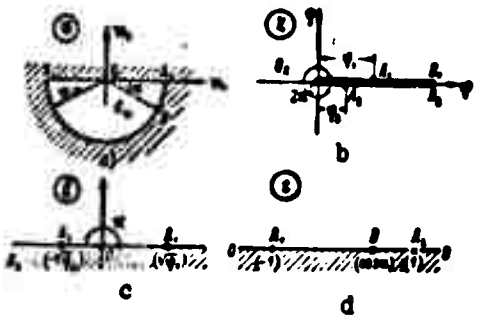


Fig. 3.7.3. The interior of the semicircle which represents the region of change of the quantity $\bar{w}$ corresponds to the whole region of flow, P (cf. Fig. 3.7.2) (a). The points of the χ-plane from which the positive half of the real axis is removed correspond to all points of the region of flow, P, (b). The transformation $\chi = g^2$ maps the region Q_χ to the upper semi-plane g, the positive semiaxis being cut up (c). The transformation $t = \frac{1}{2w_*}\left(\bar{w} + \frac{w_*^2}{\bar{w}}\right)$ maps Q_w to the region Q_t representing the upper semi-plane $\underline{t}$ (d).

of the plane $\chi = \Phi + i\Psi$ without the positive half of the real axis correspond to the inner points of the P-region; since the real semiaxis is the boundary of the Q_χ-region, it has to be considered as a double-shore section and this in such a way that the points A_1 and A_2 lie on opposite sides.

The positions of the points A_1 and A_2 are determined from the abscissas Φ_1 and Φ_2 which we do not know beforehand, but the features of the region Q_χ (and also of the region $Q_{\bar{w}}$) are given.

To find the relation between χ and $\bar{w}$, we map the regions Q_χ and $Q_{\bar{w}}$ to the upper semiplanes $\underline{g}$ and $\underline{t}$, respectively. We know (3.3) that $\chi = g^2$ transforms an angle of 2π to an angle of π, i.e., the

Q_χ-plane with a cut along the semiaxis $\underline{x}$ is mapped to the upper g-plane (cf. Fig. 3.7.3,c).

The transformation (cf. the mapping of a circle to a plate)

$$t=\frac{1}{2}\left(\frac{\bar{w}}{w_\infty}+\frac{w_\infty}{\bar{w}}\right)$$

transforms Q_w to the region Q_t, i.e., to the upper half of the t-plane (cf. Fig. 3.7.3,d). The inverse transition is effected by the function $w_\infty/\bar{w}=t+\sqrt{t^2-1}$. From the theory of functions of a variable it is known that, in the general case, a semi-plane is transformed to a semi-plane by a linear rational function

$$g=\frac{At+B}{Ct+D}.$$

Since the points g = 0 and ∞ correspond to the points $t = \infty$ and $t = \cos\alpha$, the condition determining the coefficients A, B, C, D will read $A=0;\ C\cos\alpha+D=0$.

Therefore

$$g=\frac{h}{t-\cos\alpha},$$

where $\underline{h}$ is a constant.

We replace $\underline{t}$ by the variable ω

$$t=\frac{1-\cos\alpha\cos\omega}{\cos\alpha-\cos\omega},\quad (-1<t<1;\ 0<\omega<\pi),$$

and find

$$\chi=g^2=\frac{h^2}{(t-\cos\alpha)^2}=\frac{4h^2}{\left(\frac{\bar{w}}{w_\infty}+\frac{w_\infty}{\bar{w}}-2\cos\alpha\right)}=\frac{h^2(\cos\alpha-\cos\omega)^2}{\sin^4\alpha};$$

$$\frac{d\chi}{d\omega}=\frac{2h^2(\cos\alpha-\cos\omega)\sin\omega}{\sin^4\alpha};$$

$$\frac{w_\infty}{\bar{w}}=t+\sqrt{t^2-1}=\frac{1-\cos\alpha\cos\omega+\sin\alpha\sin\omega}{\cos\alpha-\cos\omega}=\frac{1-\cos(\alpha+\omega)}{\cos\alpha-\cos\omega}.$$

Now the width of the plate is

$$b=\int_{-1}^{+1}\frac{d\chi}{dt}\cdot\frac{dt}{\bar{w}}=\int_{\pi}^{0}\frac{d\chi}{d\omega}\frac{d\omega}{\bar{w}}=$$

$$=\frac{1}{w_\infty}\int_0^\pi\frac{2h^2\sin\omega(1-\cos\alpha\cos\omega+\sin\omega\sin\alpha)}{\sin^4\alpha}d\omega=$$

$$=\frac{1}{w_\infty}\frac{h^2(4+\pi\sin\alpha)}{\sin^4\alpha}, \qquad (3.7.2)$$

whence we have

$$h^2=bw_\infty\frac{\sin^4\alpha}{4+\pi\sin\alpha}.$$

The pressure force R of a flow on a plate of width b is

$$R=\int_0^b(p-p_\infty)dx,$$

where p_∞ is the pressure in the stagnant zone. Using the Bernoulli equation, we can write $R=\frac{\rho}{2}\int_0^b\left(1-\frac{w_x^2}{w_\infty^2}\right)dx$. But on the plate we have $dy=0$, $dz=dx$; therefore $w^2=\bar{w}^2$ and $dx=d\chi/\bar{w}$. This gives us

$$R=\frac{\rho}{2}\int_{-1}^{1}\left(1-\frac{\bar{w}^2}{w_\infty^2}\right)\frac{d\chi}{dt}\frac{dt}{\bar{w}}.$$

Nothing that

$$\frac{w_\infty}{\bar{w}}\left(1-\frac{\bar{w}^2}{w_\infty^2}\right)=\frac{w_\infty}{\bar{w}}-\frac{\bar{w}}{w_\infty}=2\sqrt{t^2-1}$$

and going over to the variable ω we find

$$2\sqrt{t^2-1}=2\frac{\sin\alpha\sin\omega}{\cos\alpha-\cos\omega},$$

and therefore

$$R=\frac{\rho}{2}\int_0^\pi w_\infty 2\frac{\sin\alpha\sin\omega}{\cos\alpha\cos\omega}\cdot\frac{2h^2(\cos\alpha-\cos\omega)\sin\omega}{\sin^4\alpha}d\omega=$$

$$=\frac{2\rho h^2}{\sin^3\alpha}w_\infty\int_0^\pi\sin^2\omega d\omega=\frac{\pi\rho b\sin\alpha}{4+\pi\sin\alpha}w_\infty^2. \qquad (3.7.3)$$

The coefficient of this force is

$$C_R=\frac{R}{b\frac{\rho w_\infty^2}{2}}=\frac{2\pi}{4+\pi\sin\alpha}\sin\alpha. \qquad (3.7.4)$$

The lift and head drag coefficients for a plane plate are

$$C_x=\frac{2\pi\sin^2\alpha}{4+\pi\sin\alpha},\quad C_y=\frac{2\pi\cos\alpha\sin\alpha}{4+\pi\sin\alpha}. \tag{3.7.5}$$

If the plate is positioned normally to the flow, $\alpha = \pi/2$, and

$$R=\frac{\pi}{\pi+4}\rho b w_\infty^2,\quad C_x=\frac{2\pi}{\pi+4}. \tag{3.7.6}$$

Comparison with experiment. For small angles of attack, α, we obtain

$$C_y\approx\frac{\pi}{2}\alpha,$$

from (3.7.5), which is one quarter of the lift coefficient calculated after the theory of N.Ye. Zhukovskiy assuming nonseparating flow.

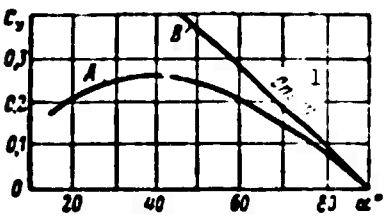


Fig. 3.7.4. Comparison of the results of the theory of jet flow (curve A) with the results of experiments (curve B) with a plate. 1) Experiment.

As can be seen from Fig. 3.7.4, the agreement with experiments is better for large angles of attack. This is because when the angles of attack are large the flow becomes separated from the body and a vortex field with lowered pressure arises instead of the stagnant zone; therefore the head drag is higher.

Vortex drag. The interfare between the flow separated from the body and the stagnant zone is a discontinuity surface of the tangential velocity and can be represented in the form of a vortex layer. It can be shown that this layer is unstable and disintegrates into a row of single vortices.

If the continuous vortex distribution is replaced by a row of discrete vortices, if a small disturbance is imposed on them, and if the vortex position is calculated over definite time intervals, then, as can be seen from Fig. 3.7.5, the vorticity will be concentrated at the points of intersection of the curve of initial disturbance with the x-axis; this leads to a disintegration of the vortex

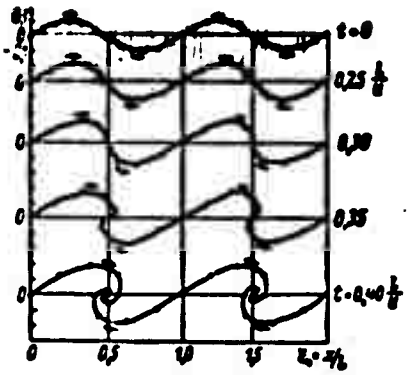


Fig. 3.7.5. The vortex sheet disintegrates into a row of equally distant discrete vortices. The vorticity is concentrated at the points of intersection of the initial disturbance curve with the x-axis.

sheet into a row of equally distant discrete vortices.

If there are two interfaces the two rows of vortices forming with circulations of equal magnitude and opposite signs can arrange themselves either symmetrically with respect to the middle line of the rows or in a chessboard pattern (Fig. 3.6.7). If l is the distance between two adjacent vortices of one row and h is the distance between the rows, then, as Karman (solving the problem of imposing small disturbances) has shown, the staggered array is more stable and stability will be greatest when [3.2]

$$\operatorname{ch}\frac{\pi h}{l}=\sqrt{2}.$$

The calculations show that in this case the vortex layers will move in the positive direction of the x-axis at a speed of

$$u=\frac{\Gamma}{2l}\operatorname{th}\frac{\pi h}{l}=\frac{\Gamma}{2l}\frac{1}{\sqrt{2}}, \qquad (3.7.7)$$

where Γ is the vorticity.

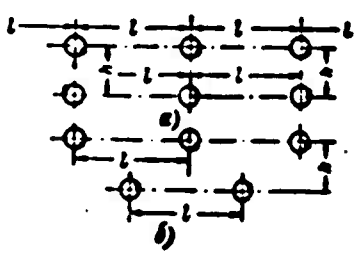


Fig. 3.7.6. Symmetrical (a) and chessboard arrangement (b) of vortices.

According to Karman the drag force X per unit length is determined by the formula

$$X=\rho l u w_{\infty}\left[0{,}7936\frac{u}{w_{\infty}}-0{,}3141\left(\frac{u}{w_{\infty}}\right)^{2}\right], \qquad (3.7.8)$$

where w_{∞} is the rate of motion of the body. The quantities l and u can be obtained by photographing the flow over

certain time intervals. The comparison of the calculations using Formula (3.7.8) with experiments with a plane and a circular cylinder have shown good agreement.

3.8. SPATIAL FLOWS

Source in space. A point in space from which a fluid streams out radially, continuously and uniformly to all sides is called a source; the amount Q of fluid streaming per unit time through a closed surface enclosing the source is called the flow rate of the source.

If Φ is the velocity potential, then, according to its definition and from the symmetry condition, we have

$$w_r = \frac{\partial \Phi}{\partial r} = \frac{Q}{4\pi r^2}; \quad \frac{\partial \Phi}{\partial \theta} = 0.$$

Therefore

$$\frac{Q}{4\pi r^2} = \frac{d\Phi}{dr} \quad \text{и} \quad \Phi = -\frac{Q}{4\pi r}. \tag{3.8.1}$$

When $Q < 0$ the motion of the fluid is directed to the center; this point is called the sink.

Flow about a half-body. When a body with a rounded front part moves in a quiescent fluid, the fluid particles are pushed aside by it as if a source moving at the same speed as the body existed inside the latter. When we now reverse the motion and assume that the fluid streams about a resting body of the same shape we obtain the streamline pattern of steady motion shown in Fig. 3.8.1.

If the coordinate origin is taken as being in the source, the potential of the whole flow can be written as

$$\Phi = w_\infty x - \frac{Q}{4\pi\sqrt{x^2 + y^2 + z^2}}. \tag{3.8.2}$$

On the symmetry axis y = 0, z = 0 a point will exist at which the velocity from the source, $w_{x_0} = \frac{Q}{4\pi x^2}$ will be equal and opposite

to the velocity w_∞ of the parallel flow. This is the stagnation point and its abscissa is given by

$$x_0 = -\sqrt{\frac{Q}{4\pi w_\infty}}. \qquad (3.8.3)$$

When constructing the streamlines we shall see that all the fluid coming from the source will be inside the surface obtained by rotating the streamline passing through the stagnation point about the x-axis. This surface of revolution can be taken as the solid boundary of what is called the "half-body."

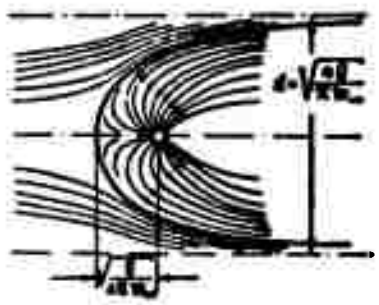


Fig. 3.8.1. A single source with the flow rate Q introduced into a parallel stream gives the flow pattern around a semi-infinite body of revolution (which is called the "half-body").

Thus, the source distorts the streamlines of a parallel flow in the same way as a half-body with a correspondingly rounded front part would. Since all the fluid from the source is inside the surface of revolution, then, denoting by d the diameter at infinity of the half-body, we deduce that the speed of the flow from a source at infinity equal to $4Q/\pi d^2$ must be equal to the speed w_∞ of the parallel flow, and hence we obtain for the diameter of the half-body

$$d = \sqrt{\frac{4Q}{\pi w_\infty}} = 4x_0. \qquad (3.8.4)$$

The dipole. This is the totality of a source and a sink of equal flow rates Q (Fig. 3.8.2,a) which increase unlimitedly if the distance $2l$ between them tends to zero, the product $M = 2Ql$ remaining constant. This product is called the dipole moment (cf. Fig. 3.8.2,b). The dipole potential at some point P is defined by

$$\Phi = -\lim_{r_1 \to \infty,\ l \to 0} \frac{Q}{4\pi}\left(\frac{1}{r_1} - \frac{1}{r_2}\right) = -\lim_{r_1 \to \infty,\ l \to 0} \frac{Q}{4\pi}\frac{r_2 - r_1}{r_1 r_2}. \qquad (3.8.5)$$

$r_1 \to r_2$ if $\theta_1 \to \theta_2$, where $r_1 - r_2 = 2l\cos\theta$, θ being the angle between $\vec{r}$ and the x-axis. Since $M = 2lQ = \text{const}$ the dipole potential is

$$\Phi = \frac{M}{4\pi r^2}\cos\theta. \qquad (3.8.6)$$

The dipole streamlines are shown in the upper part of Fig. 3.8.2,b.

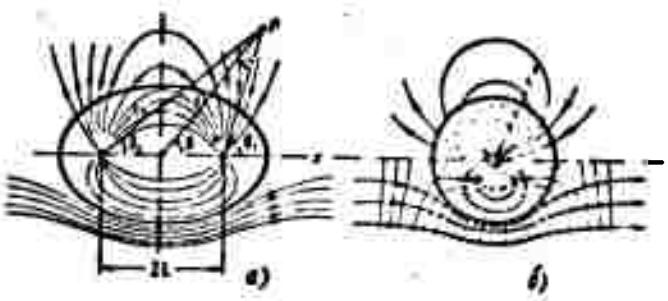


Fig. 3.8.2. The streamlines of a source and a sink of equal intensity in a parallel stream are the same as the streamlines of a uniform stream flowing around an oval body (a). The flow about a sphere is obtained by imposing a parallel flow on a dipole (source plus sink with $l \to 0$, $Q \to \infty$ so that $2lQ = \text{const}$). Above (b) – the streamlines of a dipole and below those of a dipole and a parallel flow.

Flow about a sphere. This can be studied by superimposing a parallel flow $\Phi = w_\infty x$ ($w_x = w_\infty$; $w_y = w_z = 0$) on a dipole flow (cf. Fig. 3.8.2,a). The streamlines of a flow about a sphere are shown in the lower part of the figure.

If the radius of the sphere is R, it can be shown that the potential of the flow about the sphere will read

$$\Phi = w_\infty x\left[1 + \frac{R^3}{2(x^2+y^2+z^2)^{3/2}}\right]. \qquad (3.8.7)$$

Source – sink distribution along the axis of rotation of a body. In the case of a flow about a body of revolution in the direction of the symmetry axis the flow will be axisymmetric; it can be obtained as the result of the source – sink distribution along the axis of rotation of the body.

If the flow rate per unit length at a given point ξ (source

density) is denoted by ϱ, we have

$$q(\xi)=\lim_{\delta V\to 0}\frac{\delta Q}{\delta V}. \qquad (3.8.8)$$

For closed surfaces all the fluid coming from the sources must be absorbed by the sinks, i.e., the function $q(\xi)$ has to fulfil the condition

$$\int_{\delta} q(\xi)\,d\xi=0. \qquad (3.8.9)$$

Determination of the velocity field of an incompressible fluid from the given source distribution. Let us consider the case of an unbounded incompressible fluid with zero speed at infinity and let curl $\vec{w}$ = 0 and div $\vec{w}$ = 0 in the whole region with the exception of the volume V where div $\vec{w} = \theta(x, y, z)$.

Since curl $\vec{w}$ = 0, there exists a unique speed potential Φ so that $\vec{w} = \vec{\nabla}\Phi$. Introducing the value of $\vec{w}$ in the equation div $\vec{w} = \theta(x, y, z)$ we obtain the Poisson equation for determining Φ:

$$\vec{\nabla}\cdot\vec{\nabla}\Phi=\Delta\Phi=\frac{\partial^2\Phi}{\partial x^2}+\frac{\partial^2\Phi}{\partial y^2}+\frac{\partial^2\Phi}{\partial z^2}=\theta(x, y, z). \qquad (3.8.10)$$

Thus the problem is reduced to determining this function $\Phi(x, y, z)$, that satisfies the Poisson equation in the region V.

We now subdivide the volume V into small volumes δV. Since $\theta(x, y, z)\neq 0$, we may assume that inside every volume there is a source with the intensity (flow rate per unit volume) $\theta_i=\theta(\xi_i, \eta_i, \zeta_i)$. Using now Solution (3.8.1), owing to the linearity of the equation the approximate solution can be written in the form

$$\tilde{\Phi}(x, y, z)=-\sum_i\frac{\theta_i(\xi_i, \eta_i, \zeta_i)}{4\pi r_i}\delta V_i, \qquad (3.8.11)$$

where

$$r_i=\sqrt{(x-\xi_i)^2+(y-\eta_i)^2+(z-\zeta_i)^2}$$

is the distance from the point (x, y, z) to the cource at the point (ξ_i, η_i, ζ_i). The limiting transition with $\delta V_i=0$ gives us the value

of Φ in the form of the integral:

$$\Phi(x, y, z) = -\frac{1}{4\pi}\int_V \frac{\theta(\xi, \eta, \zeta)}{\sqrt{(x-\xi)^2+(y-\eta)^2+(z-\zeta)^2}}\, dV. \qquad (3.8.12)$$

Determination of the velocity field from the given vorticity. Let now div $\vec{w}$ = 0 but curl $\vec{w}$ = 2ω ($\neq$ 0). We shall assume that

$$\vec{w} = \operatorname{rot}\vec{A}. \qquad (3.8.13)$$

Taking the curl of this expression we obtain (cf. Appendix 2)

$$\operatorname{rot}\operatorname{rot}\vec{A} = \vec{\nabla}(\vec{\nabla}\cdot\vec{A}) - \vec{\nabla}\cdot\vec{\nabla}\vec{A} = \operatorname{grad}\operatorname{div}\vec{A} - \Delta\vec{A} \qquad (3.8.14)$$

Vector $\vec{A}$ can be so chosen that it satisfies the condition

$$\vec{\nabla}\cdot\vec{A} = 0. \qquad (3.8.15)$$

and the solution of the problem is reduced to solving the vector equation

$$\Delta\vec{A} = -\operatorname{rot}\vec{w} = -2\vec{\omega}$$

or the system of scalar equations

$$\Delta A_x = -2\omega_x,\ \Delta A_y = -2\omega_y,\ \Delta A_z = -2\omega_z. \qquad (3.8.16)$$

In analogy to the potential Φ (scalar), the vector $\vec{A}$ is called the vector potential.

Solving (3.8.16) we obtain

$$A_x = \int_V \frac{2\omega_x}{4\pi r}\, dV, \quad A_y = \int_V \frac{2\omega_y}{4\pi r}\, dV, \quad A_z = \int_V \frac{2\omega_z}{4\pi r}\, dV,$$

whence

$$\vec{w} = \operatorname{rot}\int_V \frac{2\vec{\omega}}{4\pi r}\, dV. \qquad (3.8.17)$$

Velocity field of an arbitrarily shaped vortex tube. Since the vortex line can only be either stretched to infinity or closed, no vortex section may exist. Let the vortex field about the point ξ, η, ζ (Fig. 3.8.3) be a vortex tube of very small cross section δA along which the vorticity is

$$\Gamma = 2\omega\delta A.$$

Noticing that the angular velocity components are

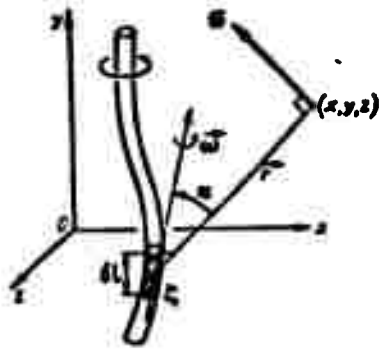


Fig. 3.8.3. Single spatial vortex line.

$w_x = w\cos(w, x) = w\frac{dx}{dl}$; $w_y = w\frac{dy}{dl}$; $w_z = w\frac{dz}{dl}$

and the volume element is $dV = \Delta A \cdot dl$, we find from (3.8.17) that

$$\vec{w} = \frac{\Gamma}{4\pi}\int \frac{d\vec{l}\times\vec{r}}{r^3}. \quad (3.8.18)$$

Equation (3.8.18) is analogous to the equation expressing the Biot-Savart law in electrodynamics; this law establishes that a vortex line element of vorticity Γ and length dl induces the velocity

$$dw = \frac{\Gamma}{4\pi}\frac{\sin\alpha}{r^2}dl, \quad (3.8.19)$$

at point P with the coordinates (x, y, z), which is directed normally to the plane containing $d\vec{l}$ and $\vec{r}$.

Here r is the distance from the element to point P, α the angle between the radius vector drawn from the element to point P and the direction of the vortex element.

The rectilinear vortex line. Let us determine the velocity induced at various points in space by the rectilinear section AB of a vortex line with the circulation Γ (Fig. 3.8.4).

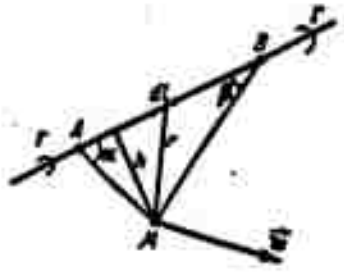


Fig. 3.8.4. The speed induced at various points in space by the rectilinear section AB of a vortex line with a circulation Γ .

Noting that at a given point M all the elements of a rectilinear vortex will possess elementary velocities $d\vec{w}$ directed similarly (along the normal to the plane passing through section AB and point M, in the same sense as the rotation generated by the vortex) we find according to (3.8.19) when using the obvious equalities (h is the shortest distance from the point M to section AB):

$$h = r\sin\alpha, \quad dl = -d(h\operatorname{ctg}\alpha) = h\frac{d\alpha}{\sin^2\alpha}.$$

Then

$$|dw| = \frac{\Gamma}{4\pi}\frac{\sin\alpha\sin^2\alpha}{h^2}\frac{h\,d\alpha}{\sin^2\alpha} = \frac{\Gamma}{4\pi h}\sin\alpha\,d\alpha.$$

Integrating with respect to α from $\alpha = \theta$ до $\alpha = \pi - \beta$ gives the sought value of the velocity $\underline{w}$ induced by the vortex section AB:

$$w = \frac{\Gamma}{4\pi h}\int_{\theta}^{\pi-\beta}\sin\alpha\,d\alpha = \frac{\Gamma}{4\pi h}(\cos\theta + \cos\beta). \qquad (3.8.20)$$

For $\alpha, \beta \to 0$ we obtain the formula known from plane motion theory for the speed induced by an infinitely long rectilinear vortex line

$$w = \frac{\Gamma}{2\pi h}. \qquad (3.8.21)$$

If α varies from 0 to $\pi/2$ (vortex half-line) we have

$$w = \Gamma : 4\pi h, \qquad (3.8.22)$$

i.e., the velocity is half what it should be according to the conditions of symmetry referring to the plane normal to the vortex axis.

Manuscript Page No.

[Footnotes]

135 A motion whose parameters depend on two coordinates is called two-dimensional.

162 Here and in what follows, the letter χ does not denote a definite form of functional dependence but stands for the complex potential.

196 Frame of the Zhukovskiy profile is the term applied to the mapping of the circle passing through the points $\zeta = \pm c$ with the center at the point of intersection of the first axis with the imaginary axis. The frame of a Zhukovskiy profile lies close to the camber line.

197 Wieselberger, Vorträge aus der Aero – und hydrodynamik (Lectures on Aerodynamics and Hydrodynamics) Innsbruck, Berlin, 1924.

BLANK PAGE

REFERENCES

3.1. Sedov, L.I., Ploskiye zadachi gidrodinamiki i aerodinamiki [Two-Dimensional Problems of Hydrodynamics and Aerodynamics], GTTI [State Technical and Theoretical Press], 1950.

3.2. Golubev, V.V., Lektsiya po teorii kryla [Lectures on the Theory of the Wing], Gostekhizdat [State Publishing House for Technical Literature], 1949.

3.3. Fabrikant, N.Ya., Aerodinamika [Aerodynamics], Part I, GTTI, 1949.

Manuscript Page No.	[Transliterated Symbols]
187	кр = kr = krylo = wing
202	в = v = vysshaya = upper
202	н = n = nizshaya = lower
202	с = s = sloy = layer
214	и = i = istochnik = source

Chapter 4

ONE-DIMENSIONAL FLOWS. FLOWS IN TUBES AND CHANNELS

A flow is said to be one-dimensional if all its physical parameters are functions of only one spatial (in the general case curvilinear) coordinate and of time. The most important of these flows is the rectilinear one-dimensional gas flow whose system of equations has the form (flow along x-axis)

$$\left.\begin{aligned} &\frac{\partial \rho}{\partial t}+\frac{\partial(\rho w)}{\partial x}=0,\\ &\frac{\partial w}{\partial t}+w\frac{\partial w}{\partial x}=f-\frac{1}{\rho}\frac{\partial p}{\partial x}+\frac{4}{3}\nu\frac{\partial^2 w}{\partial x^2},\\ &\rho c_v\frac{\partial T}{\partial t}+\rho c_v w\frac{\partial T}{\partial x}-\lambda\frac{\partial^2 T}{\partial x^2}+p\frac{\partial w}{\partial x}=\frac{4}{3}\mu\left(\frac{\partial w}{\partial x}\right)^2\\ &p=p(\rho, T), \text{ for a perfect gas } p=\rho RT. \end{aligned}\right\} \qquad (4.0.1)$$

In this system the last term of the right-hand side of the second equation characterizes the stress of normal viscosity forces acting on sections normal to the direction of motion, and the third term of the left-hand side of the third equation stands for the heat supplied via thermal conductivity.

If in the case of rectilinear motion speed and temperature vary inconsiderably, and the terms characterizing the effects of viscosity and thermal conductivity are very small and can be neglected. Moreover, since the parameters do not vary perpendicularly to the direction of motion the tangential stresses of friction, $\tau=\mu\frac{\partial w}{\partial n}$ vanish; owing to this there will also be no heat exchange perpendicular to the streamline, $q_n=-\lambda\frac{\partial T}{\partial n}=0$, and therefore these Eqs. (4.0.1) go over to the equations of motion of an inviscid thermally nonconductive gas.

4.1. THE FORMS OF ACTION

Let us consider a stream tube whose cross section A varies smoothly, $\delta A : (\sqrt{A}\delta x) \ll 1$, where δx is a length element of the stream tube, and its axis deviates only little from a straight line (i.e., $\sqrt{A} : R \ll 1$, where R is the radius of curvature of the tube axis). Then the speed components with respect to the normals to the tube axis can be neglected and the flow can be considered as one-dimensional and rectilinear.

The continuity equation for the steady flow in the stream tube (ρ and $\underline{w}$ being constant over the cross section) reads

$$\rho w A = \text{const}; \quad \rho_1 w_1 A_1 = \rho_2 w_2 A_2. \tag{4.1.1}$$

Hence we can obtain the changes of the gas parameters that <u>geometrically</u> affect the flow through a change of the cross-sectional area of the stream tube.

In real channels the flow parameters (for example, the velocity) can vary with the cross section. If, however, the parameter distribution varies slightly from section to section, then, subdividing the flow into stream tubes of sufficiently small cross section and averaging over the cross section, the flow in the channel can with sufficient accuracy be considered as being one-dimensional for the parameters averaged over the cross section.

If, during the motion of the gas a mass of gas is led either towards or away from it (for example, by injection and combustion of fuel, or by vapor condensation) the flow rate of the gas is changed, and along with this also other parameters. Such an influence on the flow is described as <u>flow-rate induced</u>.

The influence on the gas motion of drag forces due to friction is called <u>influence of drag forces</u> (friction).

<u>Thermal influences</u> on the flow are realized by supply or release of heat (from outside as well as through chemical reactions in the flow,

dissociation of molecules, etc.)

Mechanical influences are connected with a supply or withdrawal of energy by means of a compressor (turbine).

4.2. GASDYNAMIC FUNCTIONS

Parameters of decelerated flow. From the energy equation of a flow element of a one-dimensional adiabatic ($\lambda = 0$) flow of an inviscid gas ($\mu = 0$) which is perfectly insulated to energy ($L_j = 0$) and when there are no volume forces ($\bar{f} = 0$),

$$c_p T + \frac{w^2}{2} = \text{const} \tag{4.2.1}$$

it follows that if the velocity diminishes to zero the gas temperature assumes a certain value T_0. This temperature is called the adiabatic stagnation temperature of the flow; it is determined by the relation

$$c_p T_0 = c_p T + \frac{w^2}{2}. \tag{4.2.2}$$

This is the temperature a gas will assume when it is brought to a standstill by an adiabatic process; it is sometimes called the total temperature.

By virtue of Relation (2.3.6), $\frac{p_2}{p_1} = \left(\frac{\rho_2}{\rho_1}\right)^k e^{\frac{s_2 - s_1}{c_v}}$, the pressure p_0 and the density ρ_0, corresponding to the temperature T_0 depends on the process of passing from the state p, ρ, T to the state p_0, ρ_0, T_0 (Fig. 4.2.1). Stagnation pressure p_0 and stagnation density ρ_0 of the flow are called the pressure and the density which are obtained in an isentropic change of state. In this case from (2.3.5), $p_2 : p_1 = (\rho_2 : \rho_1)^k$, and therefore

$$\frac{p}{p_0} = \left(\frac{T}{T_0}\right)^{\frac{k}{k-1}}, \quad \frac{\rho}{\rho_0} = \left(\frac{T}{T_0}\right)^{\frac{1}{k-1}}. \tag{4.2.3}$$

The parameters of the decelerated flow are briefly called the stagnation or total parameters.

Notice that the stagnation pressure so defined will be the highest

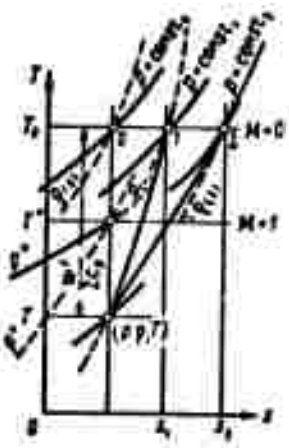


Fig. 4.2.1. The stagnation pressure and density of the flow are obtained by an isentropic transition from point p, ρ, T along the curve $T = T_0$; they are largest when the speed is reduced to zero.

pressure reached when the velocity is reduced to zero.

Characteristic velocities. From Eqs. (4.2.2), (4.2.3) and the equation of state

$$w = \sqrt{2c_p(T_0 - T)} = \sqrt{\frac{2k}{k-1}\frac{p_0}{\rho_0}\left[1 - \left(\frac{p}{p_0}\right)^{\frac{k-1}{k}}\right]} \quad (4.2.4)$$

follows, and, if the temperature T tends to zero, the velocity w tends to its maximum value

$$w_{max} = \sqrt{2c_pT_0} = \sqrt{\frac{2}{k-1}}a_0 \quad (4.2.5)$$

Using Eqs. (4.2.2) and (4.2.5) the local sonic speed (2.7) can be related with a_0, w_{max} and w:

$$a = a_0^2 - \frac{k-1}{2}w^2, \quad \frac{a^2}{a_0^2} + \frac{w^2}{w_{max}^2} = 1. \quad (4.2.6)$$

When the speed of the flow is increased from $w = 0$ to $w = w_{max}$ the local sonic speed a_0 in quiescent gas to zero.

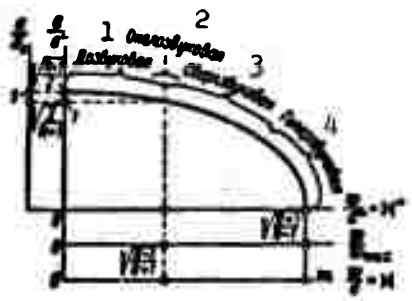


Fig. 4.2.2. With the flow velocity w increasing from zero to w_{max} the local sonic speed a diminishes after the elliptic rule to zero. 1) Subsonic; 2) transsonic; 3) supersonic; 4) hypersonic.

The velocity of the gas flow at which the propagation rate of sound becomes equal to the flow velocity itself (i.e., $w = a$), is called critical velocity and is denoted by a*; it is determined from (4.2.6):

$$a^* = \sqrt{\frac{2}{k+1}}a_0 \quad (4.2.7)$$

(for air $a^* = 0.9129\ a_0$).

With the help of the energy Eq. (4.2.2) we can find the relation linking the gas parameters in two cross sections of one stream tube. In

order to make the calculations it is convenient to introduce a stagnation cross section corresponding to a flow with w = 0. This gives for any adiabatic flow

$$\frac{T}{T_0}=1-\frac{w^2}{2c_pT_0}=1-\frac{w^2}{w^2_{max}}=1-\frac{k-1}{k+1}\frac{w^2}{a^{*2}}=1-\frac{k-1}{k+1}M^{*2},$$

where $M^* = w/a^*$ is the dimensionless velocity coefficient.

The connection between Mach's number $M = w/a$ and the velocity coefficient $M^* = w/a^*$ is immediately established by the relations

$$\left.\begin{aligned} M^2&=\frac{w^2}{a^2}=\frac{w^2}{c_0^2-\frac{k-1}{2}w^2}=\frac{2}{k+1}\frac{M^{*2}}{1-\frac{k-1}{k+1}M^{*2}},\\ M^{*2}&=\frac{w^2}{a^{*2}}=\frac{w^2}{\frac{2}{k+1}\left(c^2+\frac{k-1}{2}w^2\right)}=\frac{k+1}{2}\frac{M^2}{1+\frac{k-1}{2}M^2}. \end{aligned}\right\} \qquad (4.2.8)$$

Fundamental gasdynamic functions. These are the dependences of the ratios T/T_0, p/p_0 and ρ/ρ_0 from the Mach number $M(M^*)$ namely

the temperature function

$$\frac{T}{T_0}=1-\frac{k-1}{k+1}M^{*2}=\frac{1}{1+\frac{k-1}{2}M^2}; \qquad (4.2.9)$$

and we want to stress that this relation is true for any process which is insulated to energy;

the pressure function and the density function

$$\left.\begin{aligned} \frac{p}{p_0}&=\left(1-\frac{k-1}{k+1}M^{*2}\right)^{\frac{k}{k-1}}=\left(1+\frac{k-1}{2}M^2\right)^{-\frac{k}{k-1}},\\ \frac{\rho}{\rho_0}&=\left(1-\frac{k-1}{k+1}M^{*2}\right)^{\frac{1}{k-1}}=\left(1+\frac{k-1}{2}M^2\right)^{-\frac{1}{k-1}}. \end{aligned}\right\} \qquad (4.2.10)$$

The two latter relations are valid only for isentropic flows, i.e., when S = const. The fundamental gasdynamic functions are given in Fig. 4.2.3 (for k = 1.4).

Critical parameters. The parameters of a moving gas, T^*, p^*, ρ^*, whose velocity is equal to that of sound, i.e., $M = M^* = 1$, and a

cross section A* of the stream tube in which M = M* = 1, are called critical. With the help of (4.2.9) we obtain with M = M* = 1

$$\frac{T^*}{T_0}=\frac{2}{k+1},\quad \frac{p^*}{p_0}=\left(\frac{2}{k+1}\right)^{\frac{k}{k-1}},\quad \frac{\rho^*}{\rho_0}=\left(\frac{2}{k+1}\right)^{\frac{1}{k-1}}. \tag{4.2.11}$$

For air (k = 1.4)

$$T^*=0{,}8333T_0;\ p^*=0{,}5283p_0;\ \rho^*=0{,}6339\rho_0.$$

The mass flow function. As the charactetistic of the mass (flow rate) of outflowing gas it is useful to introduce the conception of the mass flow density j = ρw equal to the mass of gas passing per unit time through the unit cross-sectional area. The mass flow density is well characterized by the dimensionless ratio ρw/ρ*a*, which, as this follows from the equation ρwA = ρ*a*A* (4.11), determines the area ratio A*/A. For an isentropic flow

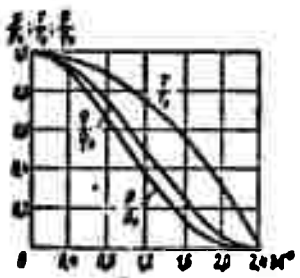


Fig. 4.2.3. Gasdynamic functions of temperature, T/T_0, pressure p/p_0, and density ρ/ρ_0 for a diatomic gas (k = = 1.4).

$$\left.\begin{aligned} j(M^*)&=\frac{\rho w}{\rho^* a^*}=\frac{A^*}{A}=\frac{\rho}{\rho_0}\frac{\rho_0}{\rho^*}\frac{w}{a^*}=\\ &=\left(\frac{k+1}{2}\right)^{\frac{1}{k-1}}M^*\left(1-\frac{k-1}{k+1}M^{*2}\right)^{\frac{1}{k-1}} \end{aligned}\right\} \tag{4.2.12}$$

and correspondingly

$$j(M)=\frac{\rho w}{\rho^* a^*}=M\left[\frac{2}{k+1}\left(1+\frac{k-1}{2}M^2\right)\right]^{-\frac{k+1}{2(k-1)}}.$$

It is easily seen that j(M*) reaches a maximum which is equal to unity for M* = M = 1 (Fig. 4.2.4).

In certain calculations the mass flow density j(M*) is more conveniently expressed in a form where p is contained explicitly, i.e.,

$$\left.\begin{aligned} j(M^*)&=\frac{\rho w}{\rho^* a^*}=M^*\left(\frac{k+1}{2}\right)^{\frac{1}{k-1}}\frac{\rho}{\rho_0}=\frac{\rho}{\rho_0}\left(\frac{k+1}{2}\right)^{\frac{1}{k-1}}\frac{M^*}{1-\frac{k-1}{k+1}M^{*2}}=\\ &=\frac{\rho}{\rho_0}y(M^*). \end{aligned}\right\} \tag{4.2.13}$$

with

$$y(M^*)=\left(\frac{k+1}{2}\right)^{\frac{1}{k-1}}\frac{M^*}{1-\frac{k-1}{k+1}M^{*2}}. \qquad (4.2.14)$$

The gasdynamic flow rate functions are shown in Fig. 4.2.4.

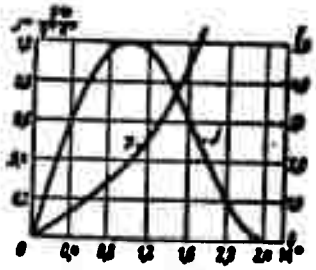


Fig. 4.2.4. Gasdynamic flow rate functions $\rho w/\rho^* a^*$ and $y(M^*)$ for diatomic gases ($k = 1.4$).

The impulse function. The impulse flux density is the momentum of the mass of gas, K, flowing per second through the unit cross-sectional area A of the stream tube, where the pressure is p, the density is ρ and the velocity is w:

$$\frac{K}{A}=\frac{\rho A+mw}{A}=p+\rho w^2 \qquad (4.2.15)$$

($m = \rho wA$). Relating this quantity to the doubled velocity pressure ρw^2 we obtain

$$\frac{K}{\rho w^2 A}=1+\frac{p}{\rho w^2}=1+\frac{1}{kM^2}=\frac{k+1}{2k}\frac{1+M^{*2}}{M^{*2}}=\frac{k+1}{2k}\frac{1}{M^*}\left(M^*+\frac{1}{M^*}\right).$$

whence follows

$$\left.\begin{aligned} K=pA+\rho w^2 A=\frac{k+1}{2k}ma^*\left(M^*+\frac{1}{M^*}\right)= \\ =\frac{k+1}{2k}ma^* z(M^*). \end{aligned}\right\} \qquad (4.2.16)$$

where

$$z(M^*)=M^*+\frac{1}{M^*}.$$

In certain calculations it is suitable to use the impulse expressed in terms of pressures, the total pressure p_0 and the static pressure p; in these cases

$$\frac{K}{\rho_0 A}=\frac{p}{p_0}(1+kM^2)=\left(1-\frac{k-1}{k+1}M^{*2}\right)^{\frac{1}{k-1}}(1+M^{*2})= \\ =\left(\frac{2}{k+1}\right)^{\frac{1}{k-1}}y(M^*)z(M^*)=f(M^*); \qquad (4.2.17)$$

$$\frac{K}{pA}=1+kM^2=\frac{1+M^{*2}}{1-\frac{k-1}{k+1}M^{*2}}= \qquad (4.2.18)$$

$$= \left(\frac{2}{k+1}\right)^{\frac{1}{k-1}} y(M^*) z(M^*) = \frac{1}{r(M^*)}. \qquad (4.2.18)$$

Let us denote by K* the value of K for M* = 1 and notice another relation important for practical calculations:

$$\frac{K}{K^*} = \frac{1}{2} z(M^*). \qquad (4.2.19)$$

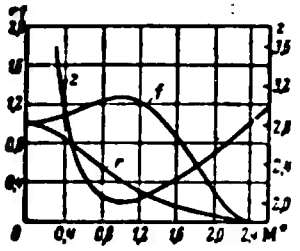


Fig. 4.2.5. The hydrodynamic function of impulse z(M*) and the auxiliary functions f(M*), r(M*) for k = 1.4.

The gasdynamic functions of impulse z(M*), f(M*), r(M*) are given in Fig. 4.2.5.

Gasdynamic functions of p/p_0. Since, according to (4.2.4),

$$w = \sqrt{\frac{2k}{k-1}\frac{p_0}{\rho_0}\left[1-\left(\frac{p}{p_0}\right)^{\frac{k-1}{k}}\right]},$$

we have

$$M^2 = \frac{w^2}{a^2} = \frac{2}{k-1}\left[\left(\frac{p_0}{p}\right)^{\frac{k-1}{k}} - 1\right], \quad M^{*2} = \frac{w^2}{a^{*2}} = \frac{k+1}{k-1}\left[1-\left(\frac{p}{p_0}\right)^{\frac{k-1}{k}}\right];$$

with

$$\frac{T}{T_0} = \left(\frac{p}{p_0}\right)^{\frac{k-1}{k}}, \quad \frac{\rho}{\rho_0} = \left(\frac{p}{p_0}\right)^{\frac{1}{k}}, \quad \frac{\rho a}{\rho^* a^*} = \frac{A^*}{A} =$$
$$= \sqrt{\frac{k+1}{k-1}}\left(\frac{k+1}{2}\right)^{\frac{1}{k-1}}\left(\frac{p}{p_0}\right)^{\frac{1}{k}}\sqrt{1-\left(\frac{p}{p_0}\right)^{\frac{k-1}{k}}}. \qquad (4.2.20)$$

Approximate relations. Sometimes it is convenient to calculate by using the approximate relations

$$\left(\frac{k+1}{2}\right)^{\frac{1}{k-1}} \approx 1{,}75 - 0{,}125k; \quad \left(\frac{k+1}{2}\right)^{\frac{k}{k-1}} \approx 1{,}05 + 0{,}5k. \qquad (4.2.21)$$

For M*-values in their limits $0 < M^* < 1.5$ the ratio ρ/ρ_0 is almost independent of k, namely

$$\frac{\rho}{\rho_0} = \left(1 - \frac{M^{*2}}{5}\right)^2. \qquad (4.2.22)$$

Furthermore,

$$\frac{p}{p_0} = \left(1 - \frac{M^{*2}}{5}\right)^3\left(1 + \frac{1{,}5-k}{3}M^{*4}\right) \qquad (0 \leqslant M^* \leqslant 2). \qquad (4.2.23)$$

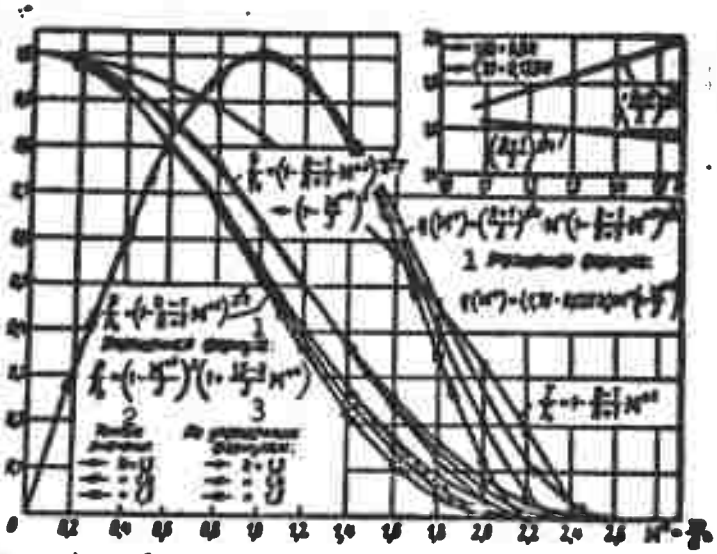


Fig. 4.2.6. Gasdynamic functions of temperature, pressure, density and flow rate plotted according to accurate and simplied formulas. 1) Simplified formula; 2) exact values; 3) according to simplied formulas.

where, if $M^* < 1$, the second factor in the parentheses can be taken equal unity. Finally

$$\frac{\rho w}{\rho^* a^*} = (1.75 - 0.125\lambda)\, M^* \left(1 - \frac{M^{*2}}{5}\right)^3. \qquad (4.2.24)$$

The accuracy of these relations is seen from the graph of Fig. 4.2.6.

4.3. GEOMETRICAL INFLUENCE AND FLOW RATE INFLUENCE

Geometrical nozzle. Dividing Expression (4.1.1) by ρwA and differentiating it we obtain

$$\frac{dp}{p} + \frac{dw}{w} + \frac{dA}{A} = 0.$$

But from the equation of motion we deduce that along a stream tube

$$w\,dw = -\frac{dp}{\rho} = -\frac{dp}{d\rho}\frac{d\rho}{\rho} = -a^2\frac{d\rho}{\rho}.$$

Thus

$$\left(1-\frac{w^2}{a^2}\right)\frac{dw}{w}+\frac{dA}{A}=0. \qquad (4.3.1)$$

It follows from this relation that in a subsonic flow ($w < a$), if $1-\frac{w^2}{a^2}>0$, the increase in speed ($dw > 0$) can be reached only by reducing the cross-sectional area ($dA < 0$). Therefore, in a subsonic flow the velocity decreases as the cross sectional area of the stream tube is increased. Completely different conditions are obtained for supersonic flow $w > a$, if $1-\frac{w^2}{a^2}<0$. Equality (4.3.1) shows that if the cross-sectional area is increased ($dA > 0$) in a supersonic flow the velocity increases as well ($dw > 0$) and, therefore, if the cross section is reduced, the velocity must drop too (Fig. 4.3.1).

1 Сечение трубки тока	2 Скорость: Дозвуковая $w<a$ 3	Сверхзвуковая $w>a$ 4
$\frac{dA}{dx}>0$	Замедление $\frac{dw}{dx}<0$ 5	Ускорение $\frac{dw}{dx}>0$ 6
$\frac{dA}{dx}<0$	Ускорение $\frac{dw}{dx}>0$ 6	Замедление $\frac{dw}{dx}<0$ 5

Fig. 4.3.1. Change of speed along stream tube as dependent on the type of flow and the change of cross-sectional area of the tube. 1) Cross section of stream tube; 2) speed; 3) subsonic; 4) supersonic; 5) deceleration; 6) acceleration.

This law of the contrary effect of the geometrical influence on the flow in subsonic and supersonic streams is a particular case of the general law of influence reversal [4.1], valid for all kinds of influences.

Owing to (4.3.1) the maximum speed of subsonic flow in a convergent channel can be reached only at its exit and the magnitude of it cannot exceed sonic speed. In accordance with the parameters of the gas at the intake and the exit of the convergent channel and with the channel dimensions, the mass of gas passing through per second can be only less than or equal to the mass of gas for which critical velocity has established at the channel exit; any further increase in mass of the gas passing through is impossible; in this case the channel is

could to display a choking effect.

In order to reach a supersonic flow by means of geometrical influence a subsonic flow needs be accelerated in the convergent part of the channel to the speed of sound that can be reached in the narrowest section – at the throat – then the channel becomes divergent (Fig. 4.3.2). In fact, at the exit $dA = 0$ and, therefore, $w = a = a^*$.

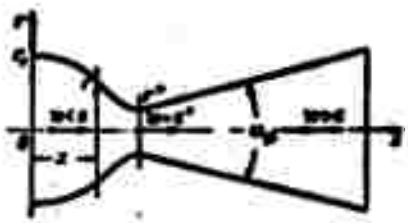


Fig. 4.3.2. In order to obtain supersonic speeds a subsonic flow is accelerated in a convergent nozzle to sonic speed and then, in the divergent part, a speed greater than that of sound is reached.

This geometrical form of a nozzle has first been suggested in 1889 by the Swedish engineer Laval. The operation of this geometrical nozzle is based on the fact that when the speed of flow exceeds the critical speed, the mass flow density ρw drops for all gases as the speed increases (ct. Fig. 4.2.3) and, therefore, in order to conserve the total mass of gas, ρwA, passing through, the nozzle cross section has to grow if it is required to obtain an accelerated flow with $w > a$.

Design of a geometrical nozzle. In the framework of one-dimensional theory the geometrical nozzle is designed on the basis of the continuity equation $\rho wA = \text{const}$ and the energy equation $c_p T + \frac{w^2}{2} = c_p T_0$. The fundamental relation linking the change of cross-sectional area with the parameters of the gas is the flow rate function

$$\frac{A^*}{A} = \frac{\rho w}{\rho^* a^*} = \left(\frac{k+1}{2}\right)^{\frac{1}{k-1}} M \left(1 - \frac{k-1}{k+1} M^2\right)^{\frac{1}{k-1}}. \qquad (4.3.2)$$

The calculation becomes considerably easier if we make use of the tables of gasdynamic functions.

In calculations based on the one-dimensional theory the supersonic part is usually assumed in the form of a cone (cf. Fig. 4.3.2). To

prevent separation of the flow (due to viscosity) the angle of divergence of the cone, α_r, is made not larger than 12-14°, though in special cases (in order to reduce the dimensions) it is made larger. The entry part follows a smooth curve, for example, that given by Vitoshinkiy's formula (8.4.12).

A more perfect geometrical nozzle can be designed by the method of characteristics (see Part 5.8).

In practical calculations it is convenient to use a relation obtained from (4.2.12):

$$\frac{m}{A^*} = \rho^* a^* = \frac{\rho^*}{\rho_0}\rho_0\sqrt{\frac{2}{k+1}}a_0 = \left(\frac{2}{k+1}\right)^{\frac{k+1}{2(k-1)}}\frac{\rho_0}{\sqrt{T_0}}\sqrt{\frac{k}{R}}$$

or

$$\frac{m\sqrt{T_0}}{A^*p_0} = \sqrt{\frac{k}{R}\left(\frac{2}{k+1}\right)^{\frac{k+1}{k-1}}} = \text{const.} \qquad (4.3.3)$$

where m is the mass flow per second.

For air (k = 1.4; R = 288 m^2/sec^2deg), introducing the weight flow per second, G = mg, we obtain

$$\frac{G\sqrt{T_0}}{A^*p_0} = 0.4. \qquad (4.3.4)$$

Outflow nozzle. It follows from the expression m = ρwA that

$$\frac{dm}{m} = \frac{d\rho}{\rho} + \frac{dw}{w} + \frac{dA}{A}.$$

In a tube of constant cross section dA = 0 and, since $d\rho/\rho = -w\,dw/a^2$, we have

$$\frac{dm}{m} = (1 - M^2)\frac{dw}{w}. \qquad (4.3.5)$$

Since m = jA we have for a geometrical nozzle (m = const) dj/j = -dA/A and from (4.3.1) we obtain $\frac{dj}{j} = (1 - M^2)\frac{dw}{w}$, i.e., when in a cylindrical tube the mass flow of the gas is changed the same change in speed can be reached as when using a geometrical nozzle. To realize a transition to sonic speed in a cylindrical tube gas has to be added

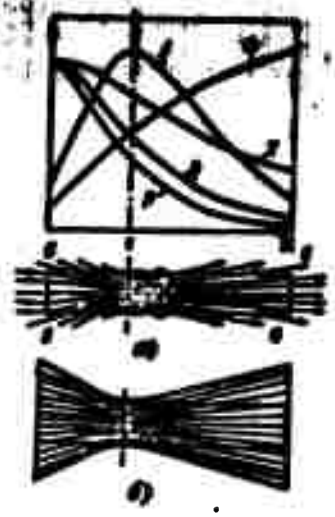


Fig. 4.3.3. Outflow nozzle and change of the parameters along it (a); an outflow nozzle can be designed when the law of variation of mass flow density ρw is maintained in the same way as in a geometrical nozzle (b).

in the subsonic part of it and to be removed in the supersonic part; such a nozzle is called outflow nozzle.

Figure 4.3.3 shows a diagram of an outflow nozzle and the change of parameters along it and also a diagram for designing an outflow nozzle from a geometrical one by introducing a porous cylindrical tube of a cross section equal to the critical. With equal mass flow of both nozzles the change of mass flow of gas in the critical cross section is inversely proportional to the change in cross-sectional area of the geometrical nozzle.

Example of calculating a geometrical nozzle. A compressor feeds per second 1.5 kg of air of pressure $p_0 = 8$ atm and temperature $T_0 = 400^\circ K$ to the receiver of a gasdynamic tube. The areas of the throat and of the operating part are to be determined in order to obtain $M = 3$ at the exit.

Solution :

$$A^* = \frac{G\sqrt{T_0}}{0.4 p_0} = \frac{1.5\sqrt{400}}{0.4 \cdot 80\,000} = 0.00094 \text{ m}^2; \quad d^* = 34.6 \text{ mm};$$

$$a^* = \sqrt{\frac{2}{k+1}}\sqrt{kRT_0} = \sqrt{\frac{2}{1.4+1}}\sqrt{1.4 \cdot 29.27 \cdot 9.81 \cdot 400} = 318 \text{ m/sec}$$

$$T^* = \frac{2}{k+1} T_0 = \frac{2}{1.4+1} 400 = 0.833 \cdot 400 = 333^\circ K;$$

$$p^* = \left(\frac{2}{k+1}\right)^{\frac{k}{k-1}} p_0 = 0.528 \cdot 80\,000 = 42\,250 \text{ kg/m}^2 = 4.225 \text{ atm};$$

$$\rho^* = \frac{p^*}{RT^*} = \frac{42\,250}{9.81 \cdot 29.27 \cdot 333} = 0.441 \text{ kg} \cdot \text{sec}^2/\text{m}^4$$

$$\frac{\rho w}{\rho^* a^*} = \frac{A^*}{A} = \left(\frac{k+1}{2}\right)^{\frac{k+1}{2(k-1)}} \frac{M}{\left(1 + \frac{k-1}{2} M^2\right)^{\frac{k+1}{2(k-1)}}} = 0.226.$$

Therefore, at the exit

$$A = \frac{A^*}{0.226} = \frac{0.00004}{0.226} = 0.0004\ m^2 \quad d = 71.6\ mm;$$

$$\rho = \rho_0\left(1 + \frac{k-1}{2}M^2\right)^{-\frac{1}{k-1}} = 0.0531\ kg\cdot sec^2/m^4$$

$$T = T_0\left(1 + \frac{k-1}{2}M^2\right)^{-1} = 143^\circ K;$$

$$a = \sqrt{kRT} = 20.1\sqrt{T} = 20.1\sqrt{143} = 240\ m/sec$$

$$w = a \cdot M = 240 \cdot 3 = 720\ m/sec.$$

In the receiver $\rho_0 = \rho^*: 0.6339 = 0.441 : 0.6339 = 0.696$ kg. sec^2/m^4.

When the angle of divergence of the nozzle is taken as about 12° we obtain for the length of the supersonic part

$$\frac{71.6 - 34.6}{2\,tg\,6^\circ} \approx 175\ mm.$$

Conditions of isentropic gas flow through the nozzle. Let us denote by m* the mass of gas flow when the speed in the narrowest cross section A_{min} has the critical value a*, and by m the gas mass flowing through any other cross section A of the nozzle when the speed in A_{min} is not equal to a*. In order to obtain m/m* explicitly we write

$$\frac{A}{A^*} = \frac{\rho^* a^*}{\rho w}\frac{m}{m^*} = \left(\frac{2}{k+1}\right)^{\frac{1}{k-1}}\frac{m}{m^*}\frac{1}{M^*\left(1 - \frac{k-1}{k+1}M^{*2}\right)^{\frac{1}{k-1}}} =$$

$$= \frac{m}{m^*}\left(\frac{2}{k+1}\right)^{\frac{1}{k-1}}\sqrt{\frac{k-1}{k+1}}\frac{1}{\left(\frac{\rho}{\rho_0}\right)^{\frac{1}{k}}\sqrt{1 - \left(\frac{\rho}{\rho_0}\right)^{\frac{k-1}{k}}}}.$$

Let us represent the change of A/A* in dependence on the ratio m/m* for various values by a graph (Fig. 4.3.4). For convenience we plot in the graph the curves M* = w/a* as a function of $p = p_0$.

Let us consider the case m = m* when $A_{min} = A^*$. Let A_v be the given exit cross section (in Fig. 4.3.4 we have taken $A_v = 1.6\ A^*$). Drawing the straight line A_v/A_{min} parallel to the axis p/p_0 at the points α_1 and α_2 of their intersection with the curve $A/A^* = f(p/p_0)$

With $m = m^*$ we find the ratios $(p_v/p_0)_{\alpha_1}$ and $(p_v/p_0)_{\alpha_2}$ corresponding to the pressures $p_{v\alpha_1}$ and $p_{v\alpha_2}$ in the exit cross section.

If, in the exit cross section, the pressure is equal to $p_{v_1} = \left(\frac{p_v}{p_0}\right)_1 p_0$ the pressure on the nozzle axis will continuously decrease with correspondingly steady increase of the speed until minimum exit pressure $p_{v\alpha_1}$ and the speed w_{α_1} are reached at the exit (or, correspondingly, $M^*_{\alpha_1}$). These conditions are called <u>rated characteristics</u>.

If, however, the pressure at the exit is equal to $p_{v_2} = \left(\frac{p_v}{p_0}\right)_2 p_0$ the curve A/A^* reaches a minimum equal to unity at $p : p_0 = p^* : p_0$ and $w = a^*$, whereupon the pressure again starts growing with correspondingly decreasing speed until the pressure at the exit becomes equal to $p_{v\alpha_2}$ and the speed assumes the value w_{α_2}. Consequently, the flow will be subsonic everywhere except at the cross section A_{min} where it assumes the speed of sound (curve $0\alpha_2$ of Fig. 4.3.4,b).

If, however, in this part of the nozzle the mass of gas flow is $m < m^*$ (dashed curve), the pressure at the exit is determined by the intersection of the curves A_v/A_{min} and A/A^*, in this case at the points β_1 and β_2, and will be equal to $(p_v/p_0)Q$ and $(p_v/p_0)\beta_2$. If, however, (p/p_0) deviated from unity, the minimum of A/A^* will not be reached since the lowest value of A/A^* is already reached at point ε where the pressure is $(p/p_0)_\varepsilon$. The flow in the narrowest cross section therefore reaches its highest (subsonic) speed $w_\varepsilon < a^*$ and then the pressure will grow up to the prescribed value $p_v\beta_2$ at the exit with decreasing the speed to the value w_β at the exit. The flow will be subsonic everywhere.

With $m > m^*$, as can be seen from Fig. 4.3.4 (dot-dash curve) there is no value of pressure at the exit for which the minimum value $A/A^* = 1$ can be reached. The nozzle cannot be passed through by a gas mass $m > m^*$. This phenomenon is called the <u>choking effect</u> of the flow.

RAPHIC NOT
EPRODUCIBLE

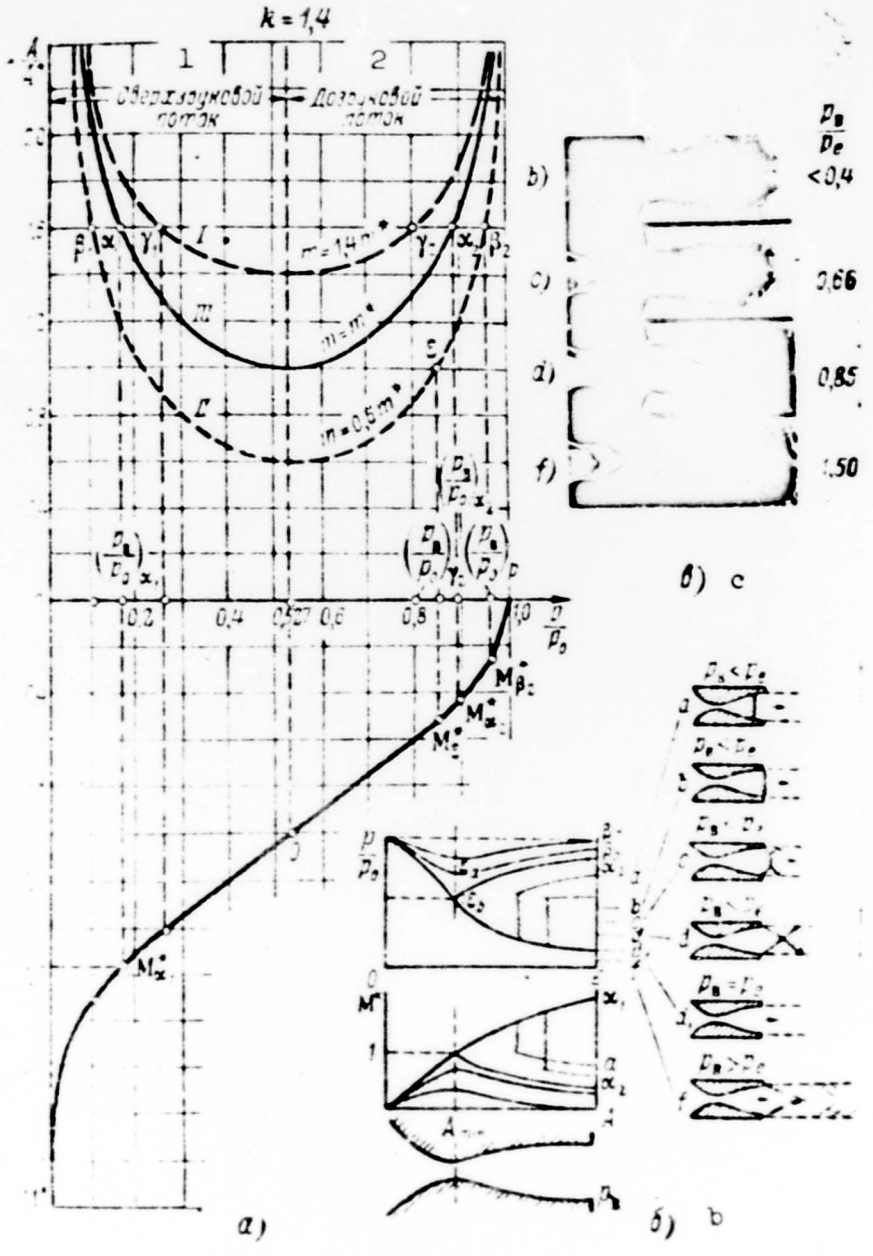


Fig. 4.3.4. Change of parameters in a geometrical nozzle (a). Change of pressure and speed along the nozzle axis for various values of the pressure at the exit (b); p_v-pressure at the nozzle exit, p_e-counterpressure. 1) Supersonic flow; 2) subsonic flow.

A second type of isentropic nonrated flow characteristic in the divergent part will be observed at a pressure smaller than p_{a_1}, the re-expansion of the gas and the corresponding pressure increase will occur outside the nozzle.

Formation of normal compression shocks. Let us consider the flow of a gas (cf. Fig. 4.3.4) of mass m^* with a pressure of p_v at the exit which is in the range $p_{a_1} < p_v < p_{a_2}$. The experiment shows that the flow in the nozzle passes through the throat and assumes a speed greater than that of sound. But since the pressure at the exit is greater than p_{va_1}, the gas in the supersonic part of the nozzle cannot expand completely to reach p_{va_1} corresponding to continuous velocity increase, and in a certain section x_1 downstream in the flow (before the nozzle exit is reached) the pressure grows by a jump to a value which is almost equal to the pressure at the exit, and the speed jumps down from supersonic to subsonic. At the same time, the greater the counterpressure the closer to the critical cross section does the shock occur. With dropping counterpressure the shock is shifted with respect to the flow and, passing through the nozzle exit, it then takes place outside the nozzle near its exit.

The kinematic relation for a normal shock. Let us consider a steady compression shock ($u = 0$). The conditions of dynamic compatibility (2.7.22) for it will be

$$\left.\begin{aligned} &\rho_1 w_1 = \rho_2 w_2, \quad p_1 - p_2 = \rho_2 w_1 (w_2 - w_1), \\ &C_p T_1 + \frac{w_1^2}{2} = C_p T_2 + \frac{w_2^2}{2}, \quad \frac{p_1}{\rho_1 T_1} = \frac{p_2}{\rho_2 T_2}. \end{aligned}\right\} \tag{4.3.6}$$

Calculating the product $w_1 w_2$ we find

$$w_1 w_2 = \rho_1 w_1 \frac{w_2}{\rho_1} = \frac{p_1 - p_2}{w_2 - w_1} \frac{w_2}{\rho_1} = \frac{p_1 - p_2}{\left(1 - \frac{w_1}{w_2}\right)\rho_1} = \frac{p_1 - p_2}{\rho_1 - \rho_2}$$

and, by virtue of (2.7.23) and (2.7.24),

$$w_1 w_2 = k \frac{p_2 + p_1}{\rho_2 + \rho_1} = k \frac{p_1}{\rho_1} \frac{1 + \frac{p_2}{p_1}}{1 + \frac{\rho_2}{\rho_1}} = a_1^2 \frac{1 + \frac{k+1}{k-1}\frac{p_2}{p_1} - 1}{1 + \frac{k+1}{k-1}\frac{\rho_2}{\rho_1}} = \frac{a_1^2}{\frac{k+1}{2} - \frac{k-1}{2}\frac{w_1}{w_2}}.$$

Nothing that $a_1^2 = a_0^2 - \frac{k-1}{2} w_1^2$, we obtain

$$\left.\begin{aligned} w_1 w_2 &= \frac{2}{k+1} a_0^2 = a^{*2}; \\ M_1^* M_2^* &= 1. \end{aligned}\right\} \qquad (4.3.7)$$

and thus

Collection of formulas for normal shock. We give here without their derivation, expressions for the parameters behind a normal compression shock in dependence of M_1^* and M_1 of the inflowing stream:

$$\left.\begin{aligned} M_2^* &= \frac{1}{M_1^*}, \quad M_2^2 = \frac{M_1^2 + \frac{2}{k-1}}{\frac{2k}{k-1} M_1^2 - 1}, \\ \frac{p_2}{p_1} &= \frac{M_1^*}{M_2^*} = M_1^{*2} = \frac{k+1}{2} \frac{M_1^2}{1 + \frac{k-1}{2} M_1^2}, \\ \frac{\rho_2}{\rho_1} &= \frac{\frac{k+1}{k-1} M_1^{*2} - 1}{\frac{k+1}{k-1} - M_1^{*2}} = \frac{2kM_1^2 - (k-1)}{k+1}, \\ \frac{T_2}{T_1} &= \frac{\frac{k+1}{k-1} M_1^{*2} - 1}{\frac{k+1}{k-1} - M_1^{*2}} \frac{1}{M_1^{*2}} = \frac{\left(\frac{2kM_1^2}{k-1} - 1\right)\left(1 + \frac{k-1}{2} M_1^2\right)}{\frac{(k+1)^2}{2(k-1)} M_1^2}. \end{aligned}\right\} \qquad (4.3.8)$$

The pressure recovery coefficient. To obtain the characteristics of energy dissipation between two cross sections of a stream tube on both sides of the shock we often make use of the pressure recovery coefficient which is defined as the ratio of the total pressures, $\nu = p_{02}/p_{01}$. On both sides of the normal shock we have

$$\frac{p_1}{p_{01}} = \left(1 - \frac{k-1}{k+1} M_1^{*2}\right)^{\frac{k}{k-1}};$$

$$\frac{p_2}{p_{02}} = \left(1 - \frac{k-1}{k+1} M_2^{*2}\right)^{\frac{k}{k-1}} = \left(1 - \frac{k-1}{k+1} \frac{1}{M_1^{*2}}\right)^{\frac{k}{k-1}},$$

and therefore

$$\nu = \frac{p_{02}}{p_{01}} = \frac{p_2}{p_1} \left(\frac{1 - \frac{k-1}{k+1} M_1^{*2}}{1 - \frac{k-1}{k+1} \frac{1}{M_1^{*2}}}\right)^{\frac{k}{k-1}} = M_1^{*2} \left(\frac{1 - \frac{k-1}{k+1} M_1^{*2}}{1 - \frac{k-1}{k+1} \frac{1}{M_1^{*2}}}\right)^{\frac{1}{k-1}} \qquad (4.3.9)$$

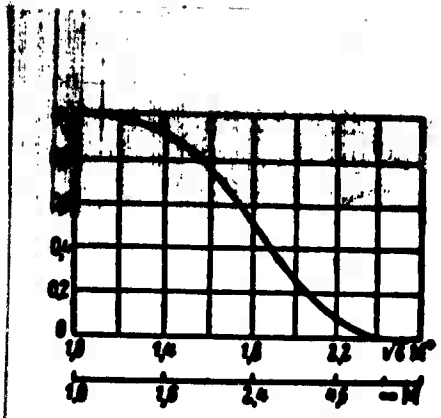


Fig. 4.3.5. The pressure recovery coefficient in a normal compression shock.

The pressure recovery coefficient can also be related with the change of entropy. In fact, since in a normal compression shock $T_{01} = T_{02}$ the equation

$$\frac{s_2 - s_1}{c_p} = \ln \frac{T_2}{T_1} - \frac{k-1}{k+1} \ln \frac{p_2}{p_1}$$

gives $\left.\frac{s_2 - s_1}{c_p}\right|_{T_{01}=\text{const}} = -\frac{k-1}{k} \ln \frac{p_{02}}{p_{01}}$,

and therefore

$$\nu = \frac{p_{02}}{p_{01}} = e^{-\frac{s_2 - s_1}{R}}. \qquad (4.3.10)$$

The values of the normal shock in dependence of M_1 are represented in Fig. 4.3.5.

4.4. INFLUENCE OF FRICTION

Semiempirical theory of turbulency. Laminar flows are described by the Navier-Stokes equations. The second type of flow, the turbulent kind, is very difficult to investigate theoretically, whether in the case of a compressible fluid or even in that of an incompressible one. If the problem of the inner structure of turbulent flow is, however, not closely examined, practical problems can be solved to a satisfactory degree of accuracy with the help of the semiempirical theories of turbulence, which, by means of empirical interrelations, link the time-averaged speeds with the forces of the so-called forces of apparent viscosity, derived from the supposition that the mixing is equivalent to an increased effect of viscosity.

Here arises the well-known analogy between viscosity in laminar flow connected with the molecular transfer of the molecule momenta and the apparent viscosity in turbulent flow, connected with molar transfer of the momenta of moles of sufficiently large volumes of fluid.

The turbulent tangential stresses are determined by the formula

$$\tau' = \rho\varepsilon\frac{d\tilde{w}_x}{dy}, \qquad (4.4.1)$$

analogous in its form to the relation valid for the tangential stresses in laminar flow

$$\tau = \rho\nu\frac{dw_x}{dy}.$$

Here ε, the apparent kinematic viscosity of turbulent flow, corresponds to the kinematic viscosity of laminar flow, $\nu = \mu/\rho$. Among the semiempirical theories of turbulence there are two which are the most known: the theory of the mixture length of L. Prandtl and the similarity hypothesis developed by T. Karman. In first approximation it is possible, however, to reduce Jarman's theory to L. Prandtl's theory of the mixture length [4.4].

The theory of the mixture length. In its conception this is connected with the molecular-kinetic representation of the mechanics of inertial friction (viscosity) of fluids. Let us consider such a flow along a wall lying in the xz-plane, so that $\tilde{w}_x = \tilde{w}_x(y)$; $\tilde{w}_y = 0$; $\tilde{w}_z = 0$. The fluid quantity passing during the short time interval dt through the areal element dA of the plane yz is equal to $dA\rho w_x dt$, and the mean value of the momentum component of this mass with respect to the y-axis after the time t_0 will be

$$\frac{dA}{t_0}\int_0^{t_0}\rho w_x w_y\,dt. \qquad (4.4.2)$$

Substituting $w_x = \tilde{w}_x + w_x'$; $w_y = \tilde{w}_y + w_y' = w_y'$ in (4.4.2) we obtain

$$dA\frac{1}{t_0}\int_0^{t_0}\rho\tilde{w}_x w_y'\,dt + dA\frac{1}{t}\int_0^{t_0}\rho w_x' w_y'\,dt = \frac{dA}{t}\int_0^{t_0}\rho w_x w_y'\,dt.$$

The term established by the velocity pulsations is a consequence of the turbulence and can be rewritten in the form $\rho dA\overline{w_x' w_y'}$. According to the momentum theorem this is the force, acting on the surface element dA and, therefore, dividing it by dA, we obtain the x-component

of the tangential stress:

$$|\tau_{xy}| = \rho |\overline{w_x' w_y'}|. \tag{4.4.3}$$

The quantity defined as

$$w_* = \sqrt{|\overline{w_x' w_y'}|} = \sqrt{\frac{|\tau|}{\rho}} \tag{4.4.4}$$

and having the dimension of a velocity, is called the velocity corresponding to the tangential stress of friction on the wall or simply the dynamic velocity.

According to the theory of the mixture length there are fluid volumes of finite dimensions in the flow which move over a certain distance in longitudinal and transverse directions as an nondestroyed whole.

Considering the change of mean velocity of longitudinal motion of these volumes when passing over from one to another fluid layer we can assume (hypothesis of L. Prandtl) that the magnitude of velocity pulsation (averaged modulus of pulsatory velocity) is proportional to the gradient of averaged velocity

$$|\overline{w_y'}| = l \left| \frac{d\tilde{w}_x}{dy} \right|. \tag{4.4.5}$$

The quantity l, called the mixture length, can be represented as being the transverse distance in the flow that has to be traveled by a fluid particle moving at the mean velocity of its original layer in order that its velocity may become, in the new site, equal to the mean velocity.

Furthermore it is supposed that the magnitude of transverse pulsatory velocity is proportional to the magnitude of pulsatory velocity of longitudinal motion $|\overline{w_x'}|$, i.e.,

$$|\overline{w_y'}| = \text{const} |\overline{w_x'}| = \text{const} \, l \left| \frac{d\tilde{w}_x}{dy} \right|. \tag{4.4.6}$$

Introducing the above constant into the quantity l of the mixture

length which is yet unknown we can, on the basis of (4.4.5) and (4.4.6) and by virtue of (2.6.13), write

$$|\overline{\tilde{w}_x'\tilde{w}_y'}| = \overline{|\tilde{w}_x'\tilde{w}_y'|} = \overline{|\tilde{w}_x'||\tilde{w}_y'|} = |\overline{\tilde{w}_x'}||\overline{\tilde{w}_y'}| = l^2\left(\frac{d\tilde{w}_x}{dy}\right)^2. \qquad (4.4.7)$$

Then Formula (4.4.3) will read

$$|\tau_{xy}| = \rho l^2\left(\frac{d\tilde{w}_x}{dy}\right)^2. \qquad (4.4.8)$$

Since the sign of τ changes with the change of sign of $d\tilde{w}_x/dy$ it is convenient to give Formula (4.4.8) the form

$$\tau_{xy} = \rho l^2\left|\frac{d\tilde{w}_x}{dy}\right|\frac{d\tilde{w}_x}{dy}. \qquad (4.4.9)$$

Comparing (4.4.1) with (4.4.9), the coefficient $\rho\varepsilon$ of turbulent transfer can be written in the form

$$\varepsilon = l^2\left|\frac{d\tilde{w}_x}{dy}\right|. \qquad (4.4.10)$$

Let us now make use of the assumption (Prandtl's hypothesis) that at the wall the mixture length is proportional to the distance, i.e., $l = \kappa y$, where κ = const.

Then (4.4.9) can be rewritten in the form

$$\frac{\tau}{\rho} = \kappa^2 y^2\left(\frac{d\tilde{w}_x}{dy}\right)^2, \quad d\tilde{w}_x = \frac{\sqrt{\tau/\rho}}{\kappa y}dy. \qquad (4.4.11)$$

Introducing the assumption that the tangential stresses are constant and equal to the stress at the wall, we have

$$\tilde{w}_x = \frac{1}{\kappa}\sqrt{\frac{\tau}{\rho}}\ln y + \text{const}. \qquad (4.4.12)$$

It is convenient to write this formula in terms of the dynamic velocity

$$\tilde{w}_x = \frac{w_*}{\kappa}\ln y + C. \qquad (4.4.13)$$

Determining the constant of integration from the tube axis condition $\tilde{w}_x = \tilde{w}_{max}$ for $y = r_0$, we obtain the velocity distribution in the turbulent flow according to the mixture length theory:

$$\frac{\tilde{w}_{max}-\tilde{w}_x}{w_*}=\frac{1}{\varkappa}\ln\frac{r_0}{y}. \qquad (4.4.14)$$

As was shown above (p. 100), the tangential stresses in a tube really decrease with increasing distance from the wall ($\tau/\tau_0 = r/r_0$ and along the axis $\tau = 0$). The velocity changes, however, particularly, in the immediate proximity of the wall, so that the assumption as to the constancy of the tangential stress leads to relations which are in good agreement with the experimental ones. In tubes, the mixture length l becomes smaller than $\varkappa y$ as the distance from the walls increases, but, as is shown by experiment, Relations (4.4.13)-(4.4.14) remain valid almost to the tube axis itself.

Notice that the mixture length l has the same meaning as the transverse turbulence scale (cf. p. 112) in the statistical theory, and their numerical values coincide [4.2], [4.3]. Thus, the intuitive notion of the semiempirical theory on the "mixture length" acquires a definite physical meaning in the statistical theory.

Experimental data on the friction in tubes. In order to determine the pressure drop Δp in the turbulent flow in a tube a great many formulas have been suggested in various periods of time. But only the most recent formulas have been based on the similarity theory. One of the first of these formulas was given by Blasius; it is applicable if

$$w_m d/\nu < 10^5,$$

where $w_m = V : \frac{\pi d^2}{4}$ is the axial velocity averaged over the cross section, V is the fluid volume passing through per second, and d is the tube diameter.

Determining the drag coefficient ζ from the equality

$$\Delta p = \zeta \frac{l}{d}\frac{\rho w_m^2}{2}, \qquad (4.4.15)$$

Blasius ascertained on the basis of experiments (Fig. 4.4.1) that

$$\zeta = \frac{0{,}316}{\sqrt[4]{Re}} \quad \left(Re = \frac{w_m d}{\nu}\right). \tag{4.4.16}$$

Comparing (4.4.16) with the expression for the stresses on the wall, $\tau_0 = \frac{\Delta p}{2l} r_0$, obtained from the equilibrium condition of the fluid element in the tube, $\tau_0 \cdot 2\pi r_0 l = \Delta p \cdot \pi r_0^2$, we find

$$\tau_0 = \frac{\zeta}{4} \frac{\rho w_m^2}{2} \tag{4.4.17}$$

If we introduce $r_0 = d/2$ in (4.4.15) and (4.4.16) instead of d, i.e., if we put

$$\Delta p = \zeta \frac{l}{r_0} \frac{\rho w_m^2}{2}.$$

then

$$\zeta = \frac{0{,}133}{\sqrt[4]{Re}} \frac{\rho w_m^2}{2} \text{ where } Re = \frac{w_m r_0}{\nu}; \tag{4.4.18}$$

with

$$\tau_0 = 0{,}03325 \rho w_m^{\frac{7}{4}} \nu^{\frac{1}{4}} r_0^{-\frac{1}{4}} = \rho w_*^2. \tag{4.4.19}$$

where $w_* = \sqrt{\tau_0 : \rho}$ is the dynamic velocity.

For a laminar flow $w = \frac{\Delta p}{4\mu l}(r_0^2 - r^2)$, and, since $w_{max} = \frac{\Delta p}{4\mu l} r_0^2$, when introducing $y = r_0 - r$, we then find

$$w = w_{max} \frac{y}{r_0}\left(2 - \frac{y}{r_0}\right) = w_{max} f\left(\frac{y}{r_0}\right).$$

Furthermore,

$$\tau_0 = \mu \left.\frac{\partial w}{\partial y}\right|_{y=0} = \frac{\Delta p}{2l} r_0 = \frac{2\mu r_0}{r_0^2 - r^2} w = \frac{2\mu}{y} \frac{1}{2 - \frac{y}{r_0}} w \approx 2 \frac{\rho w_*^2}{2} \left(\frac{\nu}{y w_*}\right).$$

can be found from (2.6.5). The quantity yw_*/ν can be called the dimensionless distance. Thus, in a laminar flow the velocity distributions are similar to $w = w_{max}(y/r_0)$ and the friction stress τ_0 at the wall does not depend on the tube radius – it is determined by the distance y from the wall and the velocity w at this distance y.

The law of the seventh-order root. Let us assume that also in turbulent motion $\tilde{w} = w_{max} f(y/r_0)$ and that the stress at the wall is independent of the tube radius, but we suppose that the velocity distributions are similar, i.e.,

$$\tilde{w} = w_{max}\left(\frac{y}{r_0}\right)^q = \text{const}\, w_m \left(\frac{y}{r_0}\right)^q. \qquad (4.4.20)$$

Substituting this in (4.4.19) we find

$$\tau_0 = \text{const}\, \rho \nu^{\frac{1}{4}} w^{\frac{7}{4}} \left(\frac{\eta}{y}\right)^{\frac{7}{4}} q\, r_0^{-\frac{1}{4}},$$

and since the tube radius r_0 must not enter the expression for τ_0, i.e., $r_0^{\frac{7}{4}q} \cdot r_0^{-\frac{1}{4}}$ must be equal to unity or, what is the same, $\frac{7}{4}q - \frac{1}{4} = 0$, so we have $q = \frac{1}{7}$. Therefore, within the limits of applicability of Blasius' formula (4.4.16), for a turbulent flow

$$\tilde{w} = w_{max}\left(\frac{y}{r_0}\right)^{\frac{1}{7}} = w_{max}\left(1 - \frac{r}{r_0}\right)^{\frac{1}{7}}. \qquad (4.4.21)$$

Furthermore form Equality (4.4.19)

$$\tau_0 = \rho w_*^2 = \rho w_*^{\frac{7}{4}} w_*^{\frac{1}{4}} = 0{,}03325 \rho w_m^{\frac{7}{4}} r_0^{-\frac{1}{4}} \nu^{\frac{1}{4}}$$

follows and we obtain

$$\frac{w_m}{w_*} = 6{,}99\left(\frac{w_* r_0}{\nu}\right)^{\frac{1}{7}}. \qquad (4.4.22)$$

If in (4.4.20) the constant is denoted by K_w, i.e., if we put $w_{max} = K_w w_m$, then instead of (4.4.22) we can write

$$\frac{\tilde{w}}{w_*} = 6{,}99 K_w \left(\frac{w_* y}{\nu}\right)^{\frac{1}{7}}. \qquad (4.4.23)$$

In order to determine K_w we write

$$w_m = \frac{1}{\pi r_0^2}\int_0^{r_0} \tilde{w} \cdot 2\pi r\, dr = 2 w_{max} \int_0^1 \left(1 - \frac{r}{r_0}\right)^{\frac{1}{7}} \frac{r}{r_0} d\frac{r}{r_0} = 0{,}816 w_{max},$$

i.e.,

$$K_w = \frac{w_{max}}{w_m} = \frac{1}{0{,}816} = 1{,}225.$$

Here

$$\frac{\tilde{w}}{w_*} = 8{,}57\left(\frac{w_* y}{\nu}\right)^{\frac{1}{7}}.$$

The relation

$$\frac{\tilde{w}}{w_*} = 8{,}74\left(\frac{w_* y}{\nu}\right)^{\frac{1}{7}} \qquad (4.4.24)$$

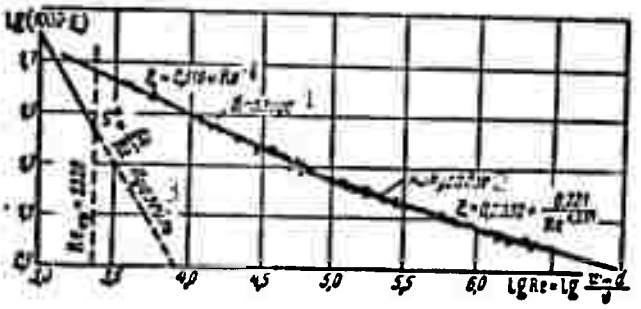


Fig. 4.4.1. Dependence of the drag coefficient of a smooth tube on the Reynolds number Re in turbulent (Blasius, Nikuradze) and laminar (Poiseuille) flows. 1) Blasius; 2) Nikuradze; 3) Poiseuille.

yields better agreement with the experiment (Fig. 4.4.2).

Generalization of the law of the seventh-order root. On the above suppositions that the velocity $\tilde{w}$ and the friction stress τ_0 were exclusively determined by the conditions at the wall and were independent of the tube radius we can take

$$\tilde{w} = f(\mu, \rho, \tau_0) y^q$$

With the help of a dimensional analysis we can show that

$$\tilde{w} = \text{const}\, \mu^{-q} \rho^{\frac{q-1}{2}} \tau_0^{\frac{q+1}{2}} y^q,$$

whence

$$\tau_0 = \zeta \frac{\tilde{\rho w}^2}{2} \left(\frac{\nu}{y\tilde{w}}\right)^{\frac{2q}{q+1}}, \quad \frac{\tilde{w}}{\tilde{w}^*} = f\left(\frac{y\tilde{w}}{\nu}\right)^q. \tag{4.4.25}$$

The exponent q has to be determined from experiment; it depends on the Reynolds number Re and its values are given in Fig. 2.6.6. As has been shown above (cf. Part 2.6), the velocity distribution tends to uniformity as the Re number increases. The influence of the viscosity diminishes in the whole stream and reduces to a smaller and smaller zone in the immediate proximity of the wall.

Logarithmic law of velocity distribution (4.4.11). As is shown by experiments, this law deduced for a plate, well describes the experi-

mental points for tubes within a very wide range of Re numbers if it is put in the form

$$\frac{\tilde{w}}{w_*} = 2{,}5 \ln \frac{w_* y}{\nu} + 5{,}5. \qquad (4.4.26)$$

With $y = r_0$ we find

$$\frac{w_{max}}{w_*} = 2{,}5 \ln \frac{w_* r_0}{\nu} + 5{,}5.$$

Calculating the foregoing equation from the latter one, we obtain

$$\frac{w_{max} - \tilde{w}}{w_*} = 2{,}5 \ln \frac{r_0}{y}. \qquad (4.4.27)$$

Hence it follows that the difference between the "dimensionless velocities," namely the local and the maximum ones, is a function of

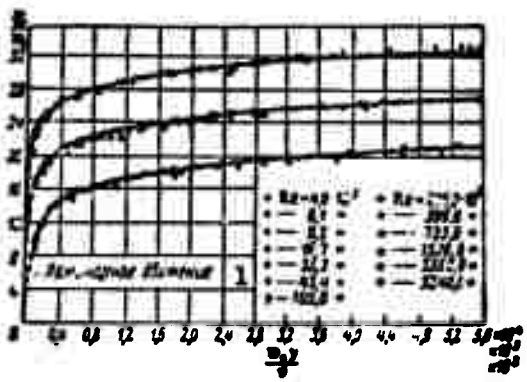


Fig. 4.4.2. Generalized velocity distribution over the tube cross section; $\tilde{w}/w_* = f(w_* y/\nu)$. 1) Laminar motion.

the ratio y/r_0 and independent of the viscosity of the fluid. In a logarithmic velocity distribution law the ratio of these "velocities" cannot be represented as a power function of y/r_0. Consequently, the supposition of conservation of kinematic similarity for flows in tubes with all Reynolds numbers is in general not true.

Let us calculate the velocity w_m averaged over the cross section, using $\tilde{w}$ determined from (4.4.27):

$$w_m = \frac{1}{r_0^2} \int_0^{r_0} \tilde{w} 2\pi r \, dr = w_{max} + \frac{5w_*}{r_0^2} \int_0^{r_0} \ln \frac{y}{r_0} r \, dr.$$

Since $r = r_0 - y$, $dr = -dy$, we have

$$w_m = w_{max} - 3{,}75 w_*.$$

The real velocity distribution near the wall does not correspond to this formula; the experiment shows that it is better described by the relation

$$w_m = w_{max} - 4{,}03 w_*.$$

Substituting w_{max} from (4.4.26) in the latter equation we obtain

$$w_m = 2{,}5 w_* \ln \frac{w_* r_0}{\nu} + 1{,}47 w_*$$

or

$$\frac{w_m}{w_*} = 2{,}5 \ln \frac{w_*}{w_m} \frac{w_m r_0}{\nu} + 1{,}47. \qquad (4.4.28)$$

Since

$$\tau_0 = \frac{\zeta}{8} \rho w_m^2 = \rho w_*^2,$$

we have

$$\frac{w_*}{w_m} = \frac{\sqrt{\zeta}}{2{,}828}.$$

Substituting the latter expression in (4.4.28) we obtain after transforming it

$$\frac{1}{\zeta} = 2{,}035 \lg (\mathrm{Re} \sqrt{\zeta}) - 1{,}01. \qquad (4.4.29)$$

Over a very wide interval of Re numbers the experimental results are better described by a relation which deviates somewhat from (4.4.29), namely (Fig. 4.4.3):

$$\frac{1}{\sqrt{\zeta}} = 2 \lg (\mathrm{Re} \sqrt{\zeta}) - 0{,}8. \qquad (4.4.30)$$

Viscous boundary layer. When we calculate the stress of friction on a wall in the case of exponential velocity distribution we obtain (since $q < 1$)

$$\tau_0 = \mu \left(\frac{\partial w}{\partial y}\right)_{y=0} = \mu w_A \left[\left(\frac{y}{r_0}\right)^{q-1}\right]_{y=0} = \infty.$$

The tangential stress at the wall tends to zero also with a

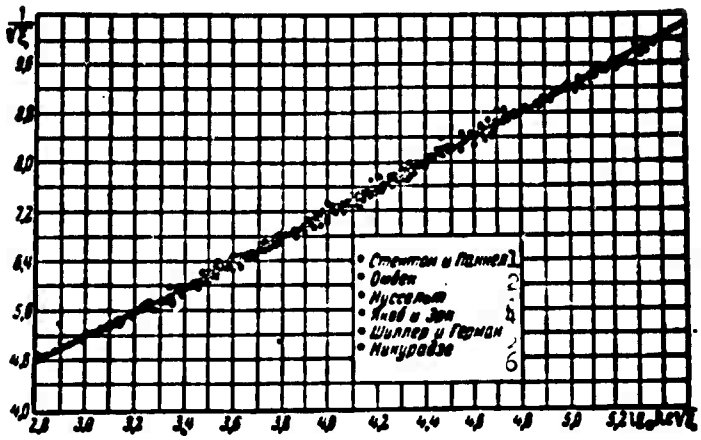


Fig. 4.4.3. $1:\sqrt{\zeta}$ as a function of $\log(\mathrm{Re}\sqrt{\zeta})$. The straight line corresponds to Formula (4.4.30). 1) Stenton and Pannel; 2) Ombek; 3) Nusselt; 4) Jakob and Erk; 5) Schiller and Herman; 6) Nikuradze.

logarithmic velocity distribution.

In order to eliminate this inconsistency with the experiment we assume for all types of flows a very thin layer to exist in the immediate proximity of the wall, which shall be called the viscous boundary layer*; the velocity in it is assumed to vary according to a linear law from zero at the wall to the value $w^* = \sqrt{\tau_0 : \rho}$. This assumption is verified by measurements.

Roughness. The results discussed above refer to smooth tubes. The study of the laws of resistance in rough tubes is rendered difficult by the great variety of geometrical forms of roughness and, therefore, by the great number of parameters determining the roughness. The resistance exerted by the wall to the motion of the fluid, depends not only on the shape and height but also on the number of the rough protuberances occurring per unit area of the wall, and, besides, on their arrangement on the surface. In the case of the so-called wavy roughness (Fig. 4.4.4,a) when the distance between the crests of the waves of roughness is greater than the wave amplitude ($h \gg 1$) the

resistance does not depend on the roughness and is the same as in smooth tubes. In tubes with the so-called grainy (sandy) roughness (cf. Fig. 4.4.4,b) when the height of the protuberances is of the same magnitude as the distance between them (h : l≈1), the main part is played by the ratio between the thickness δ_v of the viscous boundary layer and the height h of the protuberances of roughness. In the case of small Re numbers the protuberances of roughness are completely covered by the viscous layer and they do not cause the flow to separate and form vortices (cf. Fig. 4.4.5) and the roughness does not raise the resistance. Such a surface behaves as if it were hydraulically smooth (provided the heaps of roughness do not disturb the laminarity of the flow [4.4]).

With increasing Reynolds number the viscous layer may become so thin, that the peaks of the protuberances begin to reach into the turbulent "core" which leads to the formation of vortices (Fig. 4.4.5,c) and the drag becomes independent of the Reynolds number – this is what is called the region of self-similation.

Figure 4.4.5 represents the experimental results on the determination of the resistance of rough tubes of various diameters and having various dimensions of the roughness profile produced by glueing grains of sand onto the tube walls. In the range of low Reynolds numbers rough tubes behave as smooth ones. But, starting from a certain Reynolds number the value of which increases with increasing relative roughness ($2r_0/h$), the resistance curve for rough tubes deviates from the resistance curve for smooth tubes.

At the same time the resitance curve of turbulent flow can be subdivided into three characteristical regions:

1. Conditions without roughness effect, where ζ depends only on the Re number and is independent of the relative roughness r_0/h. The

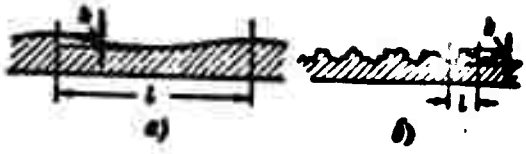


Fig. 4.4.4. Types of roughness. a) Wavy roughness $h/l \ll 1$; b) grainy roughness, $h/l \sim 1$.

roughness protuberances are completely covered by the viscous layer.

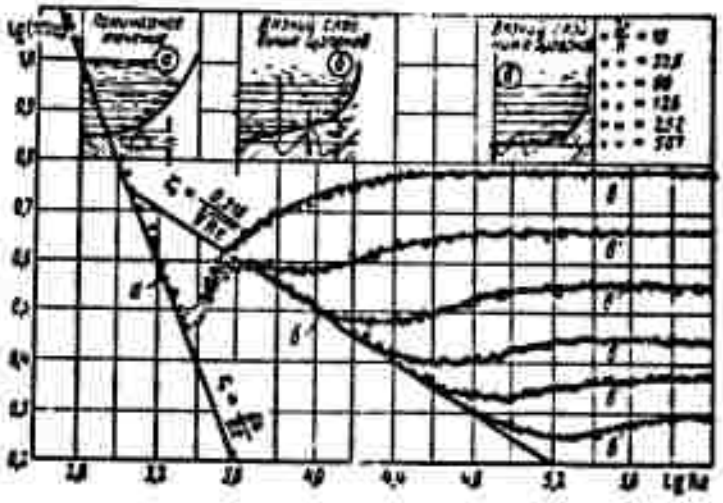


Fig. 4.4.5. Resistance law for rough tubes. Smooth flow: a) laminar, b) turbulent, – the elevations are covered by the viscous layer. Rough flow: the peaks of the elevations protrude into the viscous layer. In a turbulent flow for each value of relative roughness D/h three regimes are possible: smooth, transient and rough (self-similating).

2. Transient conditions, where ζ still depends on Re but starts depending on the factor r_0/h. Some of the roughness protuberances partly protrude the viscous layer.

3. Conditions with full roughness effect, where all roughness protuberances protrude the viscous layer.

Experiments show that the velocity distribution in rough tubes is the same as in smooth ones and that it is governed by the logarithmic law

$$\frac{\tilde{w}_x}{w_*} = 2{,}5 \ln \frac{y}{h} + f\left(\frac{w_* h}{\nu}\right). \qquad (4.4.31)$$

where the constant B is replaced by the function $f(w_* h/\nu)$ of the dimensionless parameter $w_* h/\nu$.

Under the conditions of point (3), i.e., with the full roughness effect B = 8.5 and Formula (4.4.28) assumes the form

$$\frac{\tilde{w}_x}{w_*} = 2.5 \ln \frac{y}{h} + 8.5.$$

From the velocity distributions obtained for rough tubes the resistance law can be derived. For example, in the case of full roughness effect (third mode) we have

$$\zeta = \frac{1}{\left(2 \lg \frac{r_0}{h} + 1.74\right)^2}. \qquad (4.4.32)$$

Equation of adiabatic motion of a viscous gas in a cylindrical tube. For a cylindrical tube the continuity equation reads

$$j = \rho w = \frac{m}{A} = \text{const}. \qquad (4.4.33)$$

When a gas moves in a tube it is subjected to friction forces from the walls which are not taken into account in the Eq. (4.1.1) of one-dimensional motion

$$\frac{dw}{dt} = -\frac{1}{\rho}\frac{\partial p}{\partial x} + \frac{4}{3}\nu \frac{\partial^2 w}{\partial x^2}.$$

The simplest way of approximately accounting for the forces of frictional resistance is the hydraulic method which consists in adding the pressure drop necessary to overcome the friction:

$$dp_{тр} = \zeta \frac{dx}{D} \frac{\rho w^2}{2}.$$

Here we obtain

$$\frac{dw}{dt} = -\frac{1}{\rho}\frac{dp}{dx} - \zeta \frac{w^2}{2D}. \qquad (4.4.34)$$

Determining the temperature T from the energy Eq. (4.2.9) and substituting it in the equation of state we find

$$p = \rho \frac{k+1}{2k} a^* \left(1 - \frac{k-1}{k+1} M^{*2}\right) = \frac{k+1}{2k} j a^* \frac{1 - \frac{k-1}{k+1} M^{*2}}{M^*}. \qquad (4.4.35)$$

Taking j = const into account, this yields

$$\frac{d\rho}{dM^*} = -\frac{k+1}{2k} j a^{*2} \frac{1+\frac{k-1}{k+1}M^{*2}}{M^{*3}} =$$

$$= -\frac{k+1}{2k} \rho a^{*2} \frac{1+\frac{k-1}{k+1}M^{*2}}{M^*}. \qquad (4.4.36)$$

We substitute the expression for $d\rho/\rho$ obtained from this in (4.4.34) and find

$$w\,dw - \frac{k+1}{2k} a^{*2} \frac{1+\frac{k-1}{k+1}M^{*2}}{M^*} dM^* = -\zeta \frac{w^2}{2D} dx,$$

whence

$$\frac{dM^*}{M^*} = \frac{k}{k+1} \frac{M^{*2}}{1-M^{*2}} \zeta \frac{dx}{D}. \qquad (4.4.37)$$

The presence of the factor $(1-M^{*2})$ in Eq. (4.4.37) determines the influence of the law of reversal of action. For $M^* < 1$, i.e., in the subsonic flow of a viscous gas the velocity increases downstream since $1 - M^{*2} > 0$ and with $dx > 0$ the right-hand side is positive and therefore also the left-hand side has to be positive, i.e., $dM^* > 0$. Conversely, in a supersonic flow $M^* > 1$, $1 - M^{*2} < 0$ and Eq. (4.4.37) requires that $dM^* < 0$, i.e., that the velocity of a supersonic flow of viscous gas decreases.

In order to determine the influence of the viscosity on the other parameters of an adiabatic flow we derive from the equation ρw = const

$$\frac{d\rho}{\rho} = -\frac{dw}{w} = -\frac{dM^*}{M^*} = -\frac{k}{k+1} \frac{M^{*2}}{1-M^{*2}} \zeta \frac{dx}{D}. \qquad (4.4.38)$$

Dividing (4.4.36) by (4.4.35) we obtain

$$\frac{d\rho}{\rho} = -\frac{1+\frac{k-1}{k+1}M^{*2}}{1-\frac{k-1}{k+1}M^{*2}} \frac{dM^*}{M^*} =$$

$$= -\frac{k}{k-1} \frac{M^{*2}}{1-M^{*2}} \frac{1+\frac{k-1}{k+1}M^{*2}}{1-\frac{k-1}{k+1}M^{*2}} \zeta \frac{dx}{D}. \qquad (4.4.39)$$

Using the equation of state we can write

$$\frac{dT}{T}=\frac{dp}{p}-\frac{d\rho}{\rho}=-\frac{2\frac{k-1}{k+1}M^{*2}}{1-\frac{k-1}{k+1}M^{*2}}\frac{dM^*}{M^*}=$$

$$=-\frac{2k(k-1)}{(k+1)^2}\frac{M^{*4}}{1-M^{*2}}\frac{1}{1-\frac{k-1}{k+1}M^{*2}}\zeta\frac{dx}{D}. \qquad (4.4.40)$$

By definition, $a^2 = kRT$. Therefore

$$\frac{da}{a}=\frac{1}{2}\frac{dT}{T}=-\frac{\frac{k-1}{k+1}M^{*2}}{1-\frac{k-1}{k+1}M^{*2}}\frac{dM^*}{M^*}=$$

$$=-\frac{k(k-1)}{(k+1)^2}\frac{M^{*4}}{1-M^{*2}}\frac{1}{1-\frac{k-1}{k+1}M^{*2}}\zeta\frac{dx}{D}; \qquad (4.4.41)$$

$$\frac{dM}{M}=\frac{dw}{w}-\frac{da}{a}=\frac{1}{1-\frac{k-1}{k+1}M^{*2}}\frac{dM^*}{M^*}=$$

$$=-\frac{k}{k+1}\frac{M^{*2}}{1-M^{*2}}\frac{1}{1-\frac{k-1}{k+1}M^{*2}}\zeta\frac{dx}{D}. \qquad (4.4.42)$$

In order to determine the change of total pressure we use the relation linking the pressure p at any point with the isentropic stagnation pressure p_0

$$p_0=p\left(1-\frac{k-1}{k+1}M^{*2}\right)^{\frac{k}{k-1}}. \qquad (4.4.43)$$

This gives

$$\frac{dp_0}{p_0}=\frac{dp}{p}+\frac{2k}{k+1}\frac{M^{*2}}{1-\frac{k-1}{k+1}M^{*2}}\frac{dM^*}{M^*}=\frac{M^{*2}-1}{1-\frac{k-1}{k+1}M^{*2}}\frac{dM^*}{M^*}=$$

$$=-\frac{k}{k+1}\frac{M^{*2}}{1-\frac{k-1}{k+1}M^{*2}}\zeta\frac{dx}{D}. \qquad (4.4.44)$$

The change of impulse $K=\frac{k+1}{2k}ma^*\left(M^*+\frac{1}{M^*}\right)$ can be determined by the formula

$$\frac{dK}{K}=\frac{\left(1-\frac{1}{M^{*2}}\right)dM^*}{M^*+\frac{1}{M^*}}=\frac{M^{*2}-1}{M^{*2}+1}\cdot\frac{dM^*}{M^*}=$$

$$=-\frac{k}{k+1}\frac{M^{*2}}{1+M^{*2}}\zeta\frac{dx}{D}. \qquad (4.4.45)$$

The change of entropy is (by definition)

$$dS=\frac{dQ}{T}=\frac{c_v dT+p d\frac{1}{\rho}}{T}=c_v\frac{dT}{T}-R\frac{d\rho}{\rho}=c_p\frac{dT}{T}-R\frac{d\rho}{\rho}$$

or

$$\frac{dS}{R}=\frac{k}{k-1}\frac{dT}{T}-\frac{d\rho}{\rho}.$$

Since in the case considered the flow is adiabatic, i.e., there is no external heat supply and the total temperature T_0 is constant, we have

$$\frac{dS}{R}=-\frac{dp_0}{p_0}=-\frac{M^{*2}-1}{1-\frac{k-1}{k+1}M^{*2}}\frac{dM^*}{M^*}=$$
$$=\frac{k}{k+1}\frac{M^{*2}}{1-\frac{k-1}{k+1}M^{*2}}\zeta\frac{dx}{D}. \qquad (4.4.46)$$

Noticing that the quantity $1-\frac{k-1}{k+1}M^{*2}$ is always positive because $M^{*2}_{max}=\frac{k+1}{k-1}$), the viscosity effects on each of the gas parameters considered for a cylindrical tube in dependence on the type of flow can be collected in the following table:

1 Параметр	2 Поток	
	3 дозвуковой	4 сверхзвуковой
5 Скорость w	Увеличивается 14	Уменьшается 15
6 Плотность ρ	Уменьшается 15	Увеличивается 14
7 Давление p	•	•
8 Температура T	•	•
9 Скорость звука a	•	•
Число M 10	Увеличивается 14	Уменьшается 15
11 Полное давление p_0	15 Уменьшается	
12 Импульс K	•	
13 Энтропия S	14 Увеличивается	

1) Parameter; 2) flow; 3) subsonic; 4) supersonic; 5) velocity w, 6) density ρ; 7) pressure p; 8) temperature T; 9) sonic speed a; 10) Mach number M; 11) total pressure p_0; 12) Impulse K; 13) entropy S; 14) increases; 15) decreases.

Change of number M*. Rewriting Eq. (4.4.37) in the form

$$\left(\frac{1}{M^{*2}}-1\right)\frac{dM^*}{M^*}=\frac{k}{k+1}\zeta\frac{dx}{D}, \qquad (4.4.47)$$

we find the integral of this equation

$$\chi(M^*)=\ln M^{*2}+\frac{1}{M^{*2}}=-\frac{2k}{k+1}\int\zeta\frac{dx}{D}+C. \qquad (4.4.48)$$

Thus, if we denote by M_1^* and M_2^* the value of M* in the cross sections x_1 and x_2 of the tube, we have

$$\chi(M_2^*)-\chi(M_1^*)=-\frac{2k}{k+1}\int_{x_1}^{x_2}\zeta\frac{dx}{D}. \qquad (4.4.49)$$

In most cases met in practice Re = ρwD/μ varies slowly since in gases μ varies relatively slowly with the temperature and Re is so large that ζ can be taken as constant. Assuming $x_1 = 0$ and $x_2 = l$ we obtain

$$\chi(M_1^*)-\chi(M_2^*)=\frac{2k}{k+1}\zeta\frac{l}{D}. \qquad (4.4.50)$$

Owing to the law of the viscosity-induced change of velocity the number M* at the exit of a cylindrical tube cannot exceed unity. This determines the extreme tube length l_{max} for each value of M_1^* at the inlet by the condition that at the exit M = M* = 1; whence the relation

$$\chi(M_1^*)-\chi(1)=\ln M_1^{*2}+\frac{1}{M_1^{*2}}-1=\frac{2k}{k+1}\zeta\frac{l_{max}}{D}. \qquad (4.4.51)$$

In order to obtain a clear idea of the extreme tube length values, the values of l_{max}/D are given in the following for air (k = 1.4) with ζ = 0.015 for various values of M_1^* (M_1) at the exit:

M_1^*	0	0,25	0,50	1,00	1,30	1,70	2,0	$\sqrt{6}$
M_1	0	0,229	0,466	1,00	1,40	2,156	3,16	∞
$l_{max}:D$	∞	700	92	0	7	23	49	55

Determination of the gas parameters for various tube cross sections. From Eq. (4.4.33) we obtain $\rho w = \rho^* a^*$.

$$\rho M^* = \text{const} = \rho^*, \quad \rho : \rho^* = 1 : M^*. \qquad (4.4.52)$$

Rewriting (4.4.39) in the form

$$\frac{d\rho}{\rho}+\frac{1+\frac{k-1}{k+1}M^{*2}}{1-\frac{k-1}{k+1}M^{*2}}\frac{dM^*}{M^*}=\frac{d\rho}{\rho}+\frac{dM^*}{M^*}+2\frac{\frac{k-1}{k+1}M^*dM^*}{1-\frac{k-1}{k+1}M^{*2}}=0$$

and integrating, we find

$$\left.\begin{aligned}\frac{\rho M^*}{1-\frac{k-1}{k+1}M^{*2}}&=\text{const}=\frac{\rho^*}{1-\frac{k-1}{k+1}},\\ \frac{\rho}{\rho^*}&=\frac{k+1}{2}\frac{1-\frac{k-1}{k+1}M^{*2}}{M^*}.\end{aligned}\right\}\qquad(4.4.53)$$

Further we have from (4.4.52) and (4.4.53)

$$\left.\begin{aligned}\frac{T}{T^*}&=\frac{k+1}{2}\left(1-\frac{k-1}{k+1}M^{*2}\right);\\ \frac{a}{a^*}&=\sqrt{\frac{k+1}{2}\left(1-\frac{k-1}{k+1}M^{*2}\right)}.\end{aligned}\right\}\qquad(4.4.54)$$

Since $M=w:a=(w:a^*)\cdot(a^*:a)$, we have

$$\frac{M}{M^*}=\frac{a^*}{a}=\sqrt{\frac{2}{k+1}\frac{1}{1-\frac{k-1}{k+1}M^{*2}}}.\qquad(4.4.55)$$

In order to determine p_0/p_0^* we have from (4.4.44)

$$\frac{dp_0}{p_0}+\frac{1-M^{*2}}{1-\frac{k-1}{k+1}M^{*2}}\frac{dM^*}{M^*}=\frac{dp_0}{p_0}+\frac{dM^*}{M^*}+$$

$$+\frac{\frac{k-1}{k+1}M^*dM^*}{1-\frac{k-1}{k+1}M^{*2}}-\frac{M^*dM^*}{1-\frac{k-1}{k+1}M^*}=0;$$

which we integrate, obtaining

$$p_0M^*\left(1-\frac{k-1}{k+1}M^{*2}\right)^{\frac{1}{k-1}}=\text{const}=p_0^*\left(1-\frac{k-1}{k+1}\right)^{\frac{1}{k-1}}$$

or

$$\frac{p_0}{p_0^*}=\left(\frac{2}{k+1}\right)^{\frac{1}{k-1}}\frac{1}{M^*\left(1-\frac{k-1}{k+1}M^{*2}\right)^{\frac{1}{k-1}}}=\frac{\rho^*a^*}{\rho w};\qquad(4.4.56)$$

$$\frac{K}{K^*}=\frac{1}{2}\left(M^*+\frac{1}{M^*}\right).\qquad(4.4.57)$$

Since according to (4.4.46) $dS:R+dp_0:p_0=0$,

we have

$$S:R+\ln p_0=\text{const}=S^*:R+\ln p_0^*$$

or

$$\frac{S-S^*}{R}=-\frac{1}{k-1}\ln\left[M^*\left(1-\frac{k-1}{k+1}M^{*2}\right)\right]+$$
$$+\frac{1}{k-1}\ln\left(\frac{2}{k+1}\right). \qquad (4.4.58)$$

In order to determine the change of an arbitrary parameter, e.g., p between the cross section x_1 where $M^* = M_1^*$ and x_2 where $M^* = M_2^*$, we make use of the identity

$$\frac{p_2}{p_1}=\frac{(p:p^*)_{M_1^*}}{(p:p^*)_{M_2^*}}. \qquad (4.4.59)$$

The calculated graphs are given in Fig. 4.4.6.

The position of the compression shock. Equation (4.4.51) shows that for each reduced length $\frac{2k}{k+1}\zeta\frac{l_{max}}{D}$ of subsonic flow there exists a maximum value of the number M_1^* at the inlet. If the tube length is taken larger the number M_1^* at the inlet must be so reduced that the number M^* of the flow at the exit becomes equal to unity.

On the other hand, if the flow is supersonic, the minimum number M_1^* at the inlet can be found permitting the solution to Eq. (4.4.51). If M_1^* is smaller, a compression shock of such intensity and in such a section arises in the tube that at the outlet $M_1^* = 1$.

Let us denote the distance of the shock from the inlet by l_{sk}. Then, if M_{sk}^* and $\hat{M}_{ca}^*$ are the coefficients of speed M^* before and behind the shock, respectively, (Fig. 4.4.7), by virtue of (4.3.7) and (4.4.51), we may write the system of equations as

$$\left.\begin{aligned} &M_{ca}^*\hat{M}_{ca}^*=1,\\ &\left(\frac{1}{M_1^{*2}}+\ln M_1^{*2}\right)-\left(\frac{1}{M_{ca}^{*2}}+\ln M_{ca}^{*2}\right)=\frac{2k}{k+1}\zeta\frac{l_{ca}}{D},\\ &\ln\hat{M}_{ca}^{*2}+\frac{1}{\hat{M}_{ca}^{*2}}-1=\frac{2k}{k+1}\zeta\frac{l-l_{ca}}{D}. \end{aligned}\right\} \qquad (4.4.60)$$

Finding a consistent solution to this system, we find l_{sk}, M_{sk}^* and

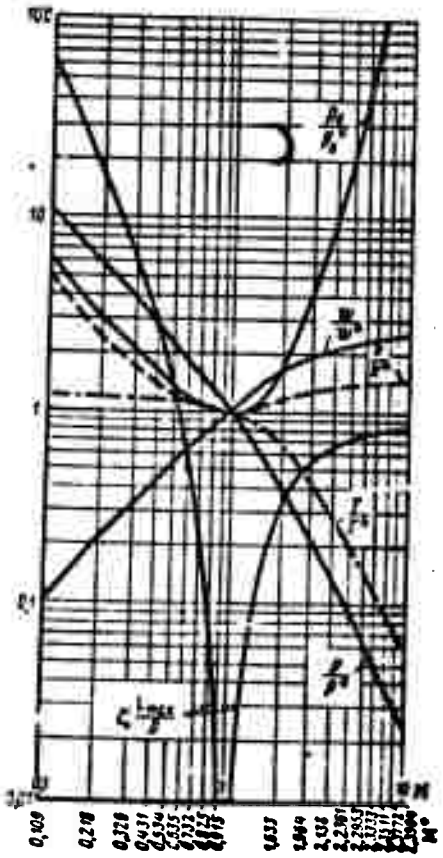


Fig. 4.4.6. Graph for calculating the flow of a viscous gas.

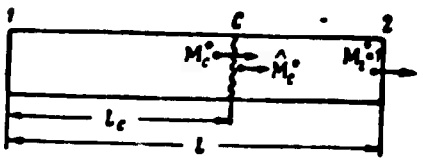


Fig. 4.4.7. Position of the shock in the flow of a viscous fluid in a cylindrical tube.

4.5. THERMAL INFLUENCE

The system of equations. In many cases of gas motion in tubes, heat is exchanged with the external medium. For example, the gas can give up or receive heat through the wall; during the motion of the gas, fuel may be burnt in it, etc. In order to investigate this kind of flow we shall consider a steady motion of a gas in a cylindrical tube without friction and without volume forces, which is described by the continuity equation

$$j=\frac{m}{A}=\rho w=\text{const} \qquad (4.5.1)$$

and the equation of motion $w\frac{dw}{dx}+\frac{1}{\rho}\frac{dp}{dx}=0$. which, after integration, (since ρw = const) we can write in the form

$$p+\rho w^2=\text{const.} \qquad (4.5.2)$$

If we denote by ${}_1Q_2$ the heat supplied to a section between the cross sections 1 and 2, then

$${}_1Q_2=c_p(T_{02}-T_{01})$$

and, by virtue of the law of energy conservation,

$$\left(c_pT_2+\frac{w_2^2}{2}\right)-\left(c_pT_1+\frac{w_1^2}{2}\right)=c_p(T_{02}-T_{01}). \qquad (4.5.3)$$

The gas is assumed to be perfect

$$p=\rho RT. \qquad (4.5.4)$$

It follows from Eq. (4.5.2) that when a gas flows without friction through a cylindrical tube the resulting pressure forces in the direction of motion are given by

$$R=A(p_1-p_2)=Ap_1w_1(w_2-w_1)=0, \tag{4.5.5}$$

i.e., a heat supply to the cylindrical tube does not change the momentum of the gas and, therefore, does not induce a reaction force.

Thermal nozzle. If we substitute in Expression (4.5.4)

$$\frac{dp}{p}=\frac{d\rho}{\rho}+\frac{dT}{T}.$$

$\frac{p}{}$ by $\frac{p^2}{k}$, we obtain with $\frac{dp}{p}=-w\,dw$ and $\frac{d\rho}{\rho}+\frac{dw}{w}=0$:

$$-\frac{kw\,dw}{a^2}=\frac{d\rho}{\rho}+\frac{dT}{T}=-\frac{dw}{w}+\frac{dT}{T},$$

whence

$$(1-kM^2)\frac{dw}{w}=\frac{dT}{T}. \tag{4.5.6}$$

But, by definition

$$M=w:a,\ \text{i.e.,}\ \frac{dM}{M}=\frac{dw}{w}-\frac{da}{a},$$

and, since $a^2 = kRT$, we have $2\frac{da}{a}=\frac{dT}{T}$, which gives

$$\frac{dM}{M}=\frac{dw}{w}-\frac{1}{2}\frac{dT}{T}.$$

Thus

$$(1-kM^2)\left(\frac{dM}{M}+\frac{1}{2}\frac{dT}{T}\right)=\frac{dT}{T},\quad \frac{dT}{T}=\frac{1-kM^2}{1+kM^2}\frac{dM^2}{M^2}. \tag{4.5.7}$$

Noticing that $T_0=T\left(1+\frac{k-1}{2}M^2\right)$, we obtain

$$\frac{dT_0}{T_0}=\frac{dT}{T}+\frac{\frac{k-1}{2}M^2}{1+\frac{k-1}{2}M^2}\frac{dM^2}{M^2}=\left(\frac{1-kM^2}{1+kM^2}+\frac{\frac{k-1}{2}M^2}{1+\frac{k-1}{2}M^2}\right)\frac{dM^2}{M^2}$$

or

$$\frac{dT_0}{T_0}=\frac{1-M^2}{(1+kM^2)\left(1+\frac{k-1}{2}M^2\right)}\frac{dM^2}{M^2}. \tag{4.5.8}$$

Here, by virtue of (4.5.6)-(4.5.8)

$$\frac{dw}{w}=\frac{1}{1-kM^2}\frac{dT}{T}=\frac{1}{1+\frac{k-1}{2}M^2}\frac{dM^2}{M^2}=$$

$$=\frac{1+\frac{k-1}{2}M^2}{1-M^2}\frac{dT_0}{T_0}=\frac{1+\frac{k-1}{2}M^2}{1-M^2}\frac{k-1}{a_0^2}dQ=\frac{(k-1)dQ}{(1-M^2)a^2}. \qquad (4.5.9)$$

The presence of the factor $(1-M^2)$ shows that by a unilateral influence – by supply of heat ($dQ > 0$) – sonic velocity ($M = 1$) cannot be passed through. If, however, during the motion in a cylindrical tube in the range $M < 1$ heat is supplied to the cylinder and is, with $M > 1$, led off, the transition through sonic velocity can be realized. This is the basis of the so-called thermal nozzle (Fig. 4.5.1). Thus, the law of reversal of action is valid also for the motion of an inviscid gas with heat exchange.

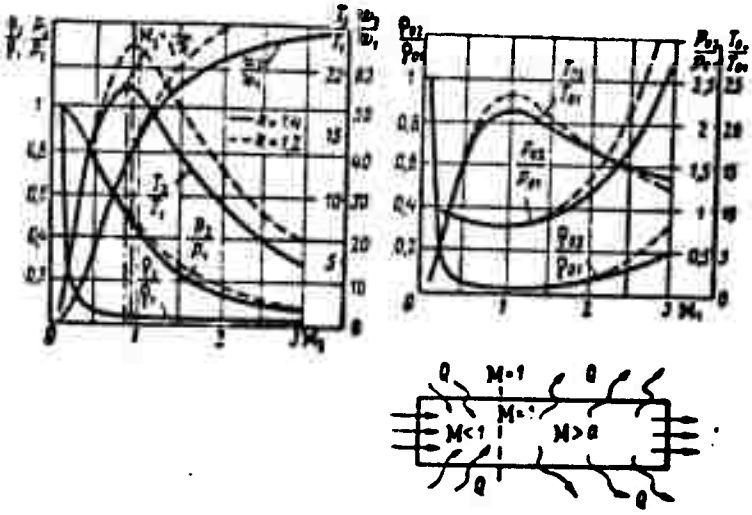


Fig. 4.5.1. Change of the parameters of a gas moving in a thermal nozzle independent of the Mach number M ($k = 1.4$; $M_1 = 0.1$).

Change of the gas parameters in a cylindrical tube. With the help of the logarithmic derivatives of Eqs. (4.5.1)-(4.5.4) and Relations (4.5.8)-(4.5.9) we find:

$$\frac{dp}{p}=-\frac{dw}{w}=-\frac{1+\frac{k-1}{2}M^2}{1-M^2}\frac{dT_0}{T_0}=-\frac{k-1}{1-M^2}\frac{dQ}{a^2}; \qquad (4.5.10)$$

$$\frac{dp}{p}=-\frac{dw}{w}+\frac{dT}{T}=-\frac{kM^2}{1+kM^2}\frac{dM^2}{M^2}=$$

$$=-\frac{kM^2}{1-M^2}\left(1+\frac{k-1}{2}M^2\right)\frac{dT_0}{T_0}=-\frac{kM^2}{1-M^2}\frac{(k-1)\,dQ}{a^2}; \qquad (4.5.11)$$

$$\frac{dp_0}{p_0}=\frac{dp}{p}+\frac{kM^2/2}{1+\frac{k-1}{2}M^2}\frac{dM^2}{M^2}=-\frac{kM^2}{2}\frac{dT_0}{T_0}=-\frac{kM^2}{2}\frac{k-1}{a_0^2}dQ, \qquad (4.5.12)$$

i.e., heat supply causes the pressure to drop and removal of heat raises it, independently of whether the flow is subsonic or supersonic.

Since, according to (4.5.2) $K=A(p+\rho w^2)=\text{const}$, (4.5.13), we have dK/K = 0, in accordance with the above mentioned fact that heat supply cannot change the momentum. Furthermore,

$$\frac{dS}{c_v}=\frac{dp}{p}-k\frac{d\rho}{\rho}=-k\left(1+\frac{k-1}{2}M^2\right)\frac{dT_0}{T_0}=$$
$$=-k(k-1)\left(1+\frac{k-1}{2}M^2\right)\frac{dQ}{a_0^2}. \qquad (4.5.14)$$

i.e., in the case of heat supply both the entropy and the total pressure always drop.

The gas parameters. We consider two cross section of a cylindrical tube in which a gas is flowing and heat is exchanged; by virtue of (4.5.1)-(4.5.4) the following relations will hold:

$$p_1\left(1+\frac{k w_1^2}{k\,p_1/\rho_1}\right)=p_2\left(1+\frac{k w_2^2}{k p_2/\rho_2}\right).$$

$$\frac{p_2}{p_1}=\frac{1+kM_1^2}{1+kM_2^2}=\frac{1+M_1^{*2}}{1+M_2^{*2}}\frac{1-\frac{k-1}{k+1}M_2^{*2}}{1-\frac{k-1}{k+1}M_1^{*2}}; \qquad (4.5.15)$$

$$\frac{w_2}{w_1}=\frac{w_2^2}{w_1^2}\frac{w_1}{w_2}=\frac{M_2^2}{M_1^2}\frac{p_2}{p_1}\frac{\rho_1}{\rho_2}\frac{w_1}{w_2}=\frac{M_2^2}{M_1^2}\frac{1+kM_1^2}{1+kM_2^2}=\frac{M_2^{*2}(1+M_1^{*2})}{M_1^{*2}(1+M_2^{*2})}; \qquad (4.5.16)$$

$$\frac{\rho_2}{\rho_1}=\frac{w_1}{w_2}=\frac{M_1^2}{M_2^2}\frac{1+kM_2^2}{1+kM_1^2}=\frac{M_1^{*2}(1+M_2^{*2})}{M_2^{*2}(1+M_1^{*2})}; \qquad (4.5.17)$$

$$\frac{T_2}{T_1}=\frac{p_2}{p_1}\frac{\rho_1}{\rho_2}=\frac{M_2^2}{M_1^2}\left(\frac{1+kM_1^2}{1+kM_2^2}\right)^2=$$
$$=\frac{M_2^{*2}}{M_1^{*2}}\left(\frac{1+M_1^{*2}}{1+M_2^{*2}}\right)^2\frac{1-\frac{k-1}{k+1}M_2^{*2}}{1-\frac{k-1}{k+1}M_1^{*2}}; \qquad (4.5.18)$$

$$\frac{K_2}{K_1}=1; \tag{4.5.19}$$

$$\frac{p_{02}}{p_{01}}=\frac{p_2}{p_1}\left(\frac{1+\frac{k-1}{2}M_2^2}{1+\frac{k-1}{2}M_1^2}\right)^{\frac{k}{k-1}}=$$

$$=\frac{1+M_1^2}{1+M_2^2}\left(\frac{1-\frac{k-1}{k+1}M_1^2}{1-\frac{k-1}{k+1}M_2^2}\right)^{\frac{1}{k-1}}; \tag{4.5.20}$$

$$\frac{T_{02}}{T_{01}}=\frac{T_2}{T_1}\frac{1+\frac{k-1}{2}M_2^2}{1+\frac{k-1}{2}M_1^2}=\frac{M_2^2}{M_1^2}\left(\frac{1+M_1^2}{1+M_2^2}\right)^2. \tag{4.5.21}$$

For two cross sections with equal gas temperature, $T_2 = T_1$, we obtain from (4.5.18) either $M_2 = M_1$ or $M_2 = 1/kM_1$.

From these relations it follows further that with increasing Mach number M: - the velocity increases and pressure and density monotonically drop; - the temperature (the thermodynamic temperature T and the adiabatic stagnation temperature T_0) have a maximum, and the total pressure p_0 has a minimum: T in the cross section where $M_2 = \sqrt{1:k}$, and T_0 and p_0 in the critical cross section.

In fact, when we differentiate (4.5.18) with respect to M_2^2, taking M_1 = const and T_1 = const, from the extremum condition

$$\frac{1}{T_1}\frac{dT_2}{dM_2^2}=\frac{(1+kM_1^2)^2}{M_1^2}\frac{d}{dM_2^2}\frac{M_2^2}{(1+kM_2^2)^2}=0,$$

we find

$$\left.\begin{aligned}(1+kM_2^2)^2-2kM_2(1+kM_2^2)=0,\quad M_2=\sqrt{1:k},\\ M_2^*=\sqrt{\frac{k+1}{3k-1}}.\end{aligned}\right\} \tag{4.5.22}$$

Since $\left.\frac{d^2T_2}{dM_2^4}\right|_{M_2^2=\frac{1}{k}}<0$, this will be the maximum; the value of the maximum temperature in dependence on the number M_1 at the tube inlet will be

$$\frac{T_{max}}{T_1} = \frac{(1+kM_1^2)^2}{4kM_1^2} = \frac{k+1}{8kM_1^{*2}} \frac{(1+M_1^{*2})^2}{1-\frac{k-1}{k+1}M_1^{*2}}. \qquad (4.5.23)$$

Figure 4.5.1 gives the graphs of the change of the parameters of gas motion in dependence on M.

Thus, in a subsonic flow, in the section between $M_1 = 1/k$ to $M = 1$ the gas temperature decreases regardless of the heat supply, and the velocity increases, i.e., the increment of kinetic energy is greater than the increment of heat content. Notice that the absolute value of temperature drop is small:

$$T_{max} : T_1 = (1+k)^2 : 4k.$$

Sometimes it is convenient to use gas parameters that are referred to their critical values: they are obtained by putting $M_1 = 1$ and $M_2 = M$ in the above obtained formulas (Fig. 4.5.2):

$$\frac{w}{a^*} = \frac{\rho^*}{\rho} = \frac{(1+k)M}{1+kM^2}, \quad \frac{T}{T^*} = \frac{(1+k)^2M^2}{(1+kM^2)^2}, \quad \frac{p}{p^*} = \frac{1+k}{1+kM^2}; \qquad (4.5.24)$$

$$\left.\begin{aligned} \frac{T_0}{T_0^*} &= \frac{2(k+1)M^2\left(1+\frac{k-1}{2}M^2\right)}{(1+kM^2)^2}, \\ \frac{p_0}{p_0^*} &= \frac{k+1}{1+kM^2}\left[\frac{2\left(1+\frac{k-1}{2}M^2\right)}{k+1}\right]^{\frac{k}{k-1}}; \end{aligned}\right\} \qquad (4.5.25)$$

$$\left.\begin{aligned} \frac{S-S^*}{c_p} &= -\ln M^2\left(\frac{1+k}{1+kM^2}\right)^{1+k}, \\ q &= \frac{T_{02}-T_{01}}{T_{01}} = \frac{T_0}{T_{01}} - 1 = \frac{(T_0T_0^*)_2}{(T_0T_0^*)_1} - 1. \end{aligned}\right\} \qquad (4.5.26)$$

Thermal resistance. The drop of total pressure (4.5.20) arising when heat is supplied to the moving gas may be considered as a certain thermal resistance. In a subsonic flow with small Mach numbers M, the approximate amount of drop of total pressure will be

$$\frac{\Delta p_0}{p_0} = \frac{p_{01}-p_{02}}{p_{01}} \approx 1 - \frac{1+kM_1^2}{1+kM_2^2} = \frac{k(M_2^2-M_1^2)}{1+kM_2^2}. \qquad (4.5.27)$$

The amount of heat, $Q = c_p(T_{02}-T_{01})$, needing to be supplied to the gas

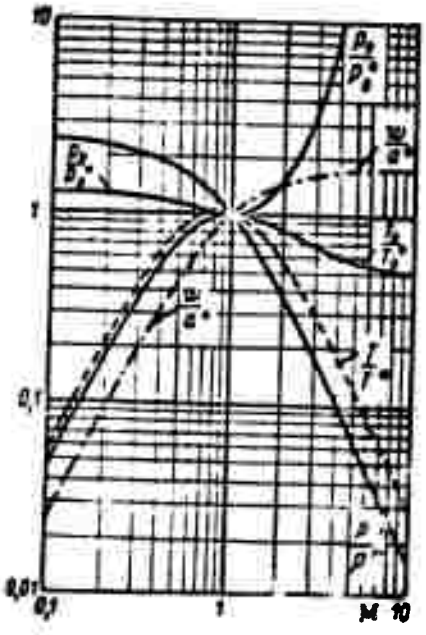


Fig. 4.5.2. Dimensionless parameters when the motion is accompanied by heat exchange.

in order to change the velocity in any cross section from the value M_1 to the value M_2, is determined in dimensionless form from the relation

$$q_0 = \frac{Q}{c_p T_{01}} = \frac{T_{02}}{T_{01}} - 1 = \frac{1+\frac{k-1}{2}M_2^2}{1+\frac{k-1}{2}M_1^2}\frac{M_2^2}{M_1^2}\left(\frac{1+kM_1^2}{1+kM_2^2}\right)^2 =$$

$$= \frac{(M_2^{*2}-M_1^{*2})(1-M_1^{*2}M_2^{*2})}{M_1^{*2}(1+M_2^{*2})^2}. \qquad (4.5.28)$$

The left-hand side of this equation must be assumed as given; it can thus be the heat supplied to the gas when heating it or condensing vapor in it, or, conversely, heat, eliminated from the gas during evaporation, etc.; the right-hand side depends on M_1 and $M_2(M_1^*, M_2^*)$.

Figure 4.5.3 shows three curves of q_0 as functions of M_2^* for the three values $M_1^* = 0.1$, 0.2, and 0.3 for ($k = 1.4$). The maximum amount of heat corresponding to critical heating $M_2^* = M_2 = 1$, will be

$$q_{max} = \frac{1}{2(1+k)}\frac{1}{M_1^2}\frac{1+kM_1^2}{1+\frac{k-1}{2}M_1^2} = \left(\frac{1-M_1^{*2}}{2M_1^*}\right)^2. \qquad (4.5.29)$$

As can be seen from Fig. 4.5.4, in the subsonic range q_0 increases sharply with decreasing M_1 and with $M_1 \to 0$ $q_0 \to \infty$.

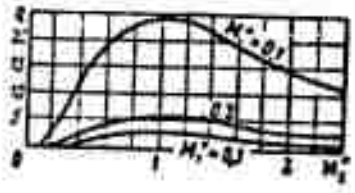


Fig. 4.5.3. Amount of heat that needs be supplied in order to change M_1^* to M_2^*.

The heat release is governed by an independent kinetic law; therefore its release in an amount greater than $q_{0max}(M_1)$, without disturbing this process, (for example, total combustion) gives rise to this increase in resistance and to the corresponding rearrangement of the flow,

where M_1 drops to a value for which this set free heat q_0 will be critical.

It follows from the graphs $q_0 = f(M_2^*)$ (cf. Fig. 4.5.3) schematically given in Fig. 4.5.5 that in the flow of a gas with constant densities of mass flow (ρw), of impulse ($p + \rho w^2$) and of initial number $M(M^*)$ there are two values of M_2^* corresponding to each value of q_0 - a subsonic, $M_2^* < 1$, and a supersonic, $M_2^* > 1$. A transition from subsonic to supersonic velocity is possible only by way of changing the influence, when first heating the gas (up to $M^* = 1$) and then cooling it (path 12'32" in the diagram of 4.5.5). On the other hand, in the case of unilateral direction of influence (heating) a transition from supersonic velocity, $M^* > 1$, to subsonic, $M^* < 1$, can be achieved only by a jump – either along the path 12'2", or the path 12"'2", or the path 1ab2";a steady transition through the maximum 3 is connected with a change in the sign of the influence.

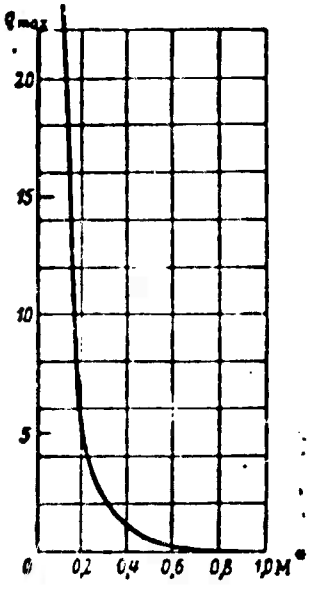


Fig. 4.5.4. Maximum amount of heat supplied to the gas in dependence on the initial number M_1.

Fanneau lines. In order to trace the adiabatic flow of a viscous gas in a cylindrical tube a TS graph is convenient. In this case the continuity equation and the energy equation read

$$J = \frac{m}{A} = \rho w = \text{const}; \quad c_p T + \frac{w^2}{2} = c_p T_0 = \text{const}$$

whence after introducing the entropy into them we obtain

$$\frac{S - S_1}{c_v} = \ln \frac{T}{T_1} - (k-1) \ln \frac{\rho}{\rho_1} = \ln \frac{T}{T_1} - (k-1) \ln \frac{w_1}{w} = \ln \frac{T}{T_1} - \frac{k-1}{2} \ln \frac{T_0 - T_1}{T_0 - T}. \qquad (4.5.30)$$

The relation so obtained immediately established the connection between the entropy increment and the temperature, in-

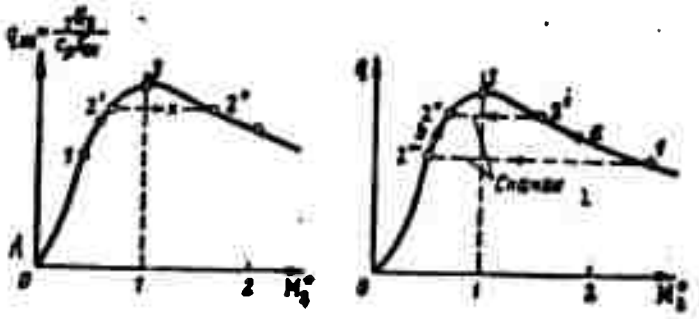


Fig. 4.5.5. In the case of unilateral influence a transition from subsonic to supersonic flow is impossible: left-hand – the path 12'2" is forbidden, point 2" can be reached only via point 3; right-hand – along the path 12'32" a transition from supersonic to subsonic flow is possible, but only via a jump. 1) Jump.

dependently of the mechanism and the magnitude of the resistance forces. The graphical representation of this relation is named Fanneau lines.

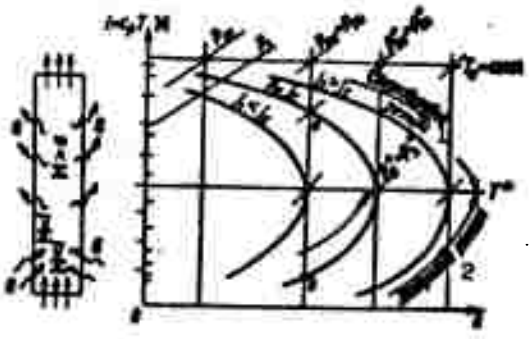


Fig. 4.5.6. Fanneau lines characterizing the energy-insulated (c_pT_0 = const) flow of a viscous gas in a cylindrical tube ($j = \rho w$ = = const) in the presence of resistance. 1) Supersonic flow; 2) subsonic flow.

If we take the critical values $T_1 = T^*$ and $S_1 = S^*$ as the fixed parameters we obtain

$$\frac{S-S^*}{c_p} = \ln\frac{T}{T^*} - \frac{k-1}{2}\ln\frac{\frac{k-1}{2}T^*}{\frac{k-1}{2}T^*-T^*} =$$

$$= \ln\left(\frac{2}{k-1}\right)^{\frac{k-1}{2}}\frac{T}{T^*}\left(\frac{k+1}{2}-\frac{T}{T^*}\right)^{\frac{k-1}{2}}. \qquad (4.5.31)$$

Figure 4.5.6 shows the Fanno lines for three different values of mass flow density, $j_1 < j_0 < j_2$.

When solving the equation $dS/dT = 0$ we can show that the maximum value of S is reached at the critical temperature. Thus the lower branch of the curve describes the subsonic flow and the upper branch the supersonic. The direction of the process must finally be such that the entropy increases.

The above deduced relation makes it possible to find for each T/T^* the values $M^*, M, p:p^*, a:a^*$ etc.

If we take into account that the speed of flow, $w = \sqrt{2c_p(T_0 - T)}$, the sonic speed, $a = \sqrt{kRT}$, the temperature axis may be regarded as the axis (with variable scale) of w, a, M, M* and thus the plot can be used for determining the flow parameters at all cross sections.

The graphical means is particularly convenient to investigate flows of "imperfect" gases, i.e., of gases whose equation of state cannot be given in the form $p = \rho RT$ but is given in the form of graphs (phase diagrams). In this case for a given value of $j = \rho w = \text{const}$ we assume several values of ρ (or $v = 1/\rho$) and determine the w for these and after this we use the energy equation $c_pT + \frac{w^2}{2} = c_pT_0 = \text{const}$ to find $i = c_pT$.

Raleigh lines. In the case of zero friction, the mass flow density $j = \rho w$ and the momentum $K = A(p + \rho w^2)$ as well are constant, independently of the heat exchange during gas motion in a cylindrical tube. Consequently, in the diagram of iS(TS) a curve can be drawn along which

$$j = \rho w = \text{const}; \quad K = p + \rho w^2 = \text{const}.$$

This curve is called Raleigh line.

For its construction we first write

$$\frac{S - S_1}{c_v} = \ln \frac{T}{T_1} - (k-1) \ln \frac{\rho}{\rho_1} = \ln \frac{T}{T_1} - (k-1) \ln \frac{w_1}{w}.$$

Expressing now the velocity in terms of temperature from the

relation

$$K = p + \rho w^2 = \frac{\rho RT}{w} + \rho w, \text{ we find } \frac{S - S_1}{c_v} = f(T, T_1)$$

for various K and λ.

Compression shock in the iS graph. Since for a normal shock the condition of dynamic compatibility gives

$$\rho w = \text{const}, \quad p - \rho w^2 = \text{const}, \quad c_p T + \frac{w^2}{2} = c_p T_0 \qquad (4.5.32)$$

then, obviously, the state of the gas before and after the shock must be determined by the points of intersection of the Fanneau and Raleigh curves; the direction of the process corresponds to the condition of entropy increase (Fig. 4.5.7).

Mechanism of comoustion. Combustion is the term applied to a rapidly occurring exothermal chemical reaction. Combustion is usually accompanied by the appearance of flames, these being the gas volume in which the combustion takes place. It can be more or less sharply divided into four regions (Fig. 4.5.8): 1) the region of fresh gas; 2) the zone of heating and of the associated decomposition of the gas under the influence of high temperature; 3) the zone of complete combustion of the gas (its thickness is of the order of 10^{-4} - 10^{-2} cm); 4) the region of the combustion products.

Let us consider the combustion reaction in the tube. If the amount (mass) of substance burnt per unit time is denoted by $m_g = \rho V$ and the area of the flame front by A, then the mass rate of the reaction, as it is called, will be $w_m = m/A$ (kg/m^{2}sec) and the normal propagation rate of the reaction will be $w_N = V/A$ (m/sec).

The experiment shows that two essentially different modes of reaction propagation are possible: 1) slow burning propagated with 1-2 m/sec, and 2) detonation with a velocity of 2-3 km/sec. In the case of slow burning, all pressure changes (propagated at sonic speed)

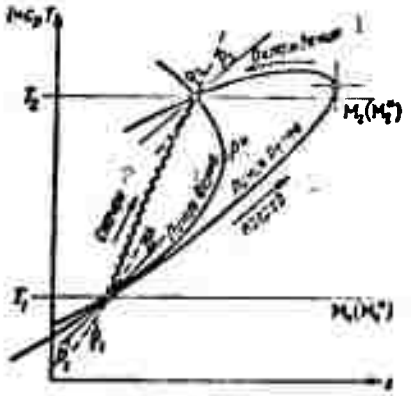


Fig. 4.5.7. The Raleigh lines characterize the motion of an inviscid gas ($\mu = 0$) in a cylindrical tube, $\rho w = \text{const}$, when the total impulse is conserved, $p + \rho w^2 = \text{const}$, independently of the heat exchange. 1) Cooling; 2) jump; 3) Fanneau l ; 4) Raleigh line; 5) heating

thrust well ahead of the flame front and are offset with the ambient pressure, $p_1 \approx p_2$. In the case of detonation when the reaction-front speed is greater than sonic speed, there arise great local pressure increases; in the gas located before the reaction front the disturbances do not arise before the gas is reached by the wave front. The front of the detonation wave is manifested as a shock wave of high intensity and this causes the gas temperature to rise so much that the chemical reaction takes place in a certain zone behind the front in the form of an explosion with release of heat. The energy expended by the shock wave in irreversibly heating the compressible gas is taken from the energy of the chemical reaction. The width of the front of the detonation wave is of the order of a mean free path — the П (heating) zone is considerably narrower than the Г (combustion) zone.

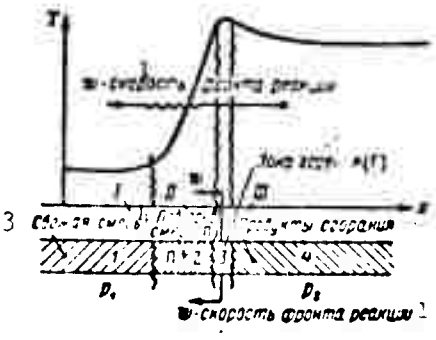


Fig. 4.5.8. Diagram of heating of a quiescent gas; the mixture is heated by virtue of the thermal conductivity of the gas. 1) w-velocity of the reaction front; 2) combustion zone, 3) fresh mixture; 4) heating of the mixture; 5) combustion products.

If the motion is reversed, i.e., a velocity w_1 is imparted to the gas which is equal to the oppositely directed velocity of the reaction front, the shock wave can be considered as stationary, with the gas passing through it. At the same time M_1 will be the ratio between the speed of the fresh mixture to

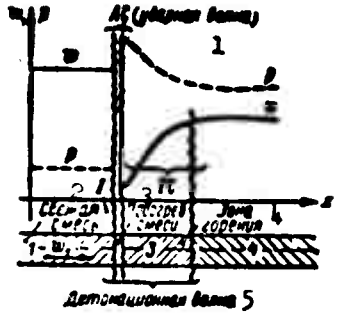


Fig. 4.5.9. Schematic representation of detonation; the mixture is heated by a shock wave. The detonation wave consists of two layers: the first layer is the adiabatic shock wave (AS) and the second one the thermal shock (TS). 1) (Shock wave); 2) fresh mixture; 3) heating of mixture; 4) combustion zone.

the speed of sound in it. The change of the gas parameters for the reversed motion during the detonation is given in Fig. 4.5.9; the supersonic speed ($M_1 > 1$) of the fresh mixture in the zone of the wave front decreases to subsonic ($M_2 < 1$) whereas pressure and temperature sharply increase, the mixture is heated and decomposed; in the combustion zone, combustion takes place at subsonic speed, heat is supplied to the gas and its speed increases according to the scheme given in Fig. 4.5.5; the pressure decreases somewhat and the combustion products dissipate with subsonic speed.

Thermal shocks. The very small extension of the combustion zone in which the heat is set free allows the assumption, in schematizing the effect that it originates from a shock. In the case of slow burning the thermal shock arises in a subsonic flow. This is explained by the fact that in this case the main part is played by the kinetic processes (thermal conductivity, turbulence of the flow, etc.).

The detonation – a very rapidly occurring process – excludes kinetic processes. The detonation wave may be considered as the layer of two shocks, a normal adiabatic compression shock of a thickness of the order of a mean free path (and therefore excluding kinetic processes), in which compression and ignition of the mixture takes place, and a thermal rarefaction shock in the subsonic flow in which the combustion process occurs (pat 12'"2" in Fig. 4.5.5).

According to this approximate scheme there also occurs a condensa-

tion shock in the course of which the latent heat of evaporation is set free.

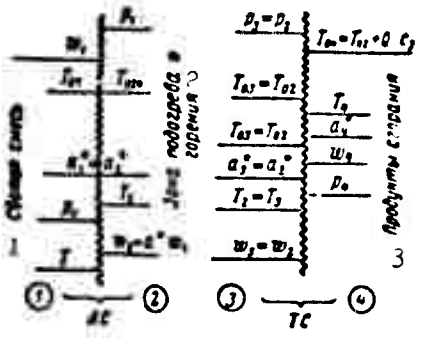


Fig. 4.5.10. Gas parameters in a detonation wave. 1) Fresh mixture; 2) heating and combustion zone; 3) combustion products.

Gas parameters in the detonation. It is convenient to calculate these parameters in the reversed motion, assuming that the gas is flowing with a velocity equal to that of shock wave propagation while the shock wave is stationary (Fig. 4.5.10).

The shock wave parameters are calculated with the formulas of the normal compression shock (4.3.8):

$$\left.\begin{aligned} &T_{01}=T_{02},\quad M_2^{\circ}=\frac{1}{M_1^{\circ}},\quad \frac{T_2}{T_1}=\frac{1-\frac{k-1}{k+1}\frac{1}{M_1^{*2}}}{1-\frac{k-1}{k+1}M_1^{*2}},\\ &\frac{p_2}{p_1}=\frac{M_1^{*2}-\frac{k-1}{k+1}}{1-\frac{k-1}{k+1}M_1^{*2}}. \end{aligned}\right\} \quad (4.5.33)$$

In order to calculate the thermal shock with the designations of Fig. 4.5.10 we have, first of all, by virtue of $T_{03}=T_{02}=T_{01}$, $M_3^{\circ}=M_3^{\circ}$ and of Eqs. (4.5.19), (4.5.28):

$$\frac{T_{04}}{T_{02}}=\frac{M_4^{*2}(1+M_3^{*2})^2}{M_3^{*2}(1+M_4^{*2})^2}=\frac{M_4^{*2}}{M_1^{*2}}\frac{(1+M_1^{*2})^2}{(1+M_4^{*2})^2}.$$

Evolving the square roots of this equation we obtain

$$\left.\begin{aligned} &M_3^{*2}-\sqrt{\frac{T_{04}}{T_{01}}}\frac{1+M_4^{*2}}{M_4^{\circ}}M_3^{\circ}+1=0,\\ &M_4^{*2}-\sqrt{\frac{T_{01}}{T_{04}}}\frac{1+M_3^{*2}}{M_3^{\circ}}M_4^{\circ}+1=0. \end{aligned}\right\} \quad (4.5.34)$$

Solving the first of them we find

$$M_3^{\circ}=\frac{1}{M_1^{\circ}}=\frac{1+M_4^{*2}}{2M_4^{\circ}}\left[1\pm\sqrt{1-\frac{4M_4^{*2}}{(1+M_4^{*2})^2}\frac{T_{01}}{T_{04}}}\right]\sqrt{\frac{T_{04}}{T_{01}}}. \quad (4.5.35)$$

The minus sign refers here to the case of heat release (e.g.,

combustion and condensation) in a subsonic flow ($M_2^* < 1$), and the plus sign to supersonic flow ($M_2^* > 1$). For the conditions of the thermal crisis ($M_4^* = 1$) we have

$$M_2^{**} = \sqrt{\frac{T_{01}}{T_{02}}}\left(1 \pm \sqrt{\frac{\Delta T_0}{T_{02}}}\right), \quad M_1^{**} = \frac{1}{M_2^{**}} = \frac{\sqrt{\frac{T_{02}}{T_{01}}}}{1 \pm \sqrt{\frac{\Delta T_0}{T_{02}}}}. \tag{4.5.36}$$

The latter expression determined the maximum possible velocity at the inlet of the combustion chamber when, in the subsequent course, the flow reaches the value $M_4^* = 1$ at the chamber exit.

Steady regime of detonation. This is determined by the conditions $M_1^* > 1$ and $M_2^* = \frac{1}{M_1^*} < 1$; solving (4.5.34), we obtain

$$M_4^* = \frac{1 + M_2^{*2}}{2M_2^*}\left[1 - \sqrt{1 - \frac{4M_2^{*2}}{(1 + M_2^{*2})^2}\frac{T_{02}}{T_{01}}}\right]\sqrt{\frac{T_{01}}{T_{02}}}. \tag{4.5.37}$$

Usually M_2^* is considerably smaller than unity, and, with little heating, $Q = c_p(T_{02} - T_{01})$

$$M_4^* \approx \frac{M_2^*}{1 + M_2^{*2}}\sqrt{\frac{T_{02}}{T_{01}}} \approx M_2^*\sqrt{\frac{T_{02}}{T_{01}}} = M_2^*\sqrt{1 + \frac{Q}{c_p T_{01}}}. \tag{4.5.38}$$

The stronger the compression shock, i.e., the greater the propagation rate of the shock wave, the higher is the stagnation temperature of the hot mixture $T_{01} = T_1\left(1 - \frac{k-1}{k+1}M_1^{*2}\right)^{-1}$ and, in the limiting case with $M_1 \to \infty$

$$M_1 \to \sqrt{\frac{k+1}{k-1}}; \quad T_{01} = T_{02} \to \infty; \quad M_2 \to 0.$$

At the same time the relative heating and the speed of the combustion products drop sharply ($M_4^* \approx M_2^*$), i.e., the detonation wave degenerates to a compression shock. This is easily seen when the variable stagnation temperature is replaced by the temperature of the cold gas:

$$M_4^{*2} = \frac{1}{M_1^*}\sqrt{1 + \frac{Q}{c_p T_1}\left(1 - \frac{k-1}{k+1}M_1^{*2}\right)} \tag{4.5.39}$$

Usually the detonation (shock) wave arises as the result of a local explosion in a hot mixture. The detonation wave propagates to

the cold gas and, causing there a considerable local heating, brings the gas to ignition. In this region $M_2^* \approx M_1^* < 1$. With increasing from the explosion center the shock wave weakens, its propagation rate drops and the speed of the combustion products and the relative heating increase; with $M_4^* = 1$ the propagation of the detonation assumes a steady character.

Then

$$M_2^* = \frac{1}{M_1^*} = \sqrt{\frac{T_{04}}{T_{01}}} - \sqrt{\frac{T_{04}}{T_{01}} - 1}, \quad \frac{T_{04}}{T_{01}} = \left(\frac{1+M_2^{*2}}{2M_2^*}\right)^2; \tag{4.5.40}$$

$$q_0 = \frac{T_{04} - T_{01}}{T_{01}} = \left(\frac{M_1^{*2}-1}{2M_1^*}\right)^2 = \left(\frac{1-M_2^{*2}}{2M_2^*}\right)^2.$$

$$q_1 = \frac{T_{04} - T_{01}}{T_1} = \frac{(M_1^{*2}-1)^2}{4M_1^{*2}\left(1 - \frac{k-1}{k+1} M_1^{*2}\right)}. \tag{4.5.41}$$

The latter equation determines the propagation rate of the wave

$$M_1^{*2} = \frac{1+2q_1}{1+4q_1\frac{k-1}{k+1}}\left[1 \pm \sqrt{1 - \frac{1+4q\frac{k-1}{k+1}}{(1+2q_1)^2}}\right]. \tag{4.5.42}$$

The sign (+) refers to heating by detonation and the sign (−) to slow heating.

The following approximate relations hold for $q_1 > 1$:

for the speed of the detonation wave

$$M_{1\Delta}^{*2} = \frac{2(1+2q)}{1+4q_1\frac{k-1}{k+1}} - \frac{2}{1+2q}$$

and for the speed of the wave of slow burning

$$M_{1M}^{*2} = \frac{1}{2(1+2q_1)}. \tag{4.5.43}$$

Figure 4.5.11 gives the graph of the dependence of M_1^* on q_1 for $k = 1.4$. The upper branch of the curve (in the supersonic region of the motion) corresponds to minimum steady speed of detonation propagation; the points above it correspond to unsteady detonation and the points below it to the physically impossible transition to sonic speed with supply of heat (thermal crisis). The lower branch (in the sub-

sonic region) gives the maximum combustion velocity; the points below this branch of the curve correspond to the infinite multiplicity of regimes of normal slow burning at low speeds.

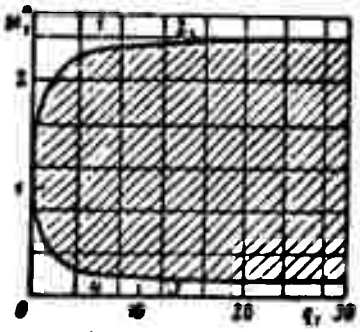


Fig. 4.5.11. Dependence of the propagation rate of the combustion wave on the thermal characteristic of a hot mixture. 1) Region of unsteady detonation; 2) steady regime of detonation; 3) maximum detonation rate; 4) region of slow burning.

Thus, the regimes in the shaded region are not feasible owing to the effect of thermal crisis. This explains the jump-like character of the transition from normal heating to detonation. It should also be noted that a very small thermal influence suffices for the burning rate to become much lower and the detonation rate higher than sonic speed.

The remaining parameters are calculated by means of (4.5.14)-(4.5.19).

Absolute velocities. In a coordinate system fixed to the quiescent gas the absolute particle velocity is right behind the shock wave front equal to $w_p = w_1 - w_2$, and the velocity of the combustion products is $w_g = w_1 - w_4$.

In detonations $w_1 > w_4 > w_2$; therefore the flame front and the front of the combustion products move in the same direction as the shock wave front, but $w_p > w_g$. In the case of normal burning $w_1 = w_2 < w_4$ and the directions of motion of the front of flames and combustion products are opposite.

4.6. THE LAW OF REVERSAL OF INFLUENCE

The above considered forms of isolated influences on the flow show that each of them changes the local parameters of the gas in the sub- and supersonic flows in opposite directions. This property is called the law of reversal of influence [4.1],[4.7]; it was carefully studied by L.A. Vulis. In order to be definite, let us agree to denote

as normal influence, such action as accelerates a subsonic flow.

Combined influence. Let us isolate in a channel of variable cross section of length dx; let, owing to lateral inflow, the mass in this section be raised by an amount of dm. Let the amount of heat supplied from outside be dQ = mdq and the work done by the gas and transferred to the outside be dL = mdl (Fig. 4.6.1).

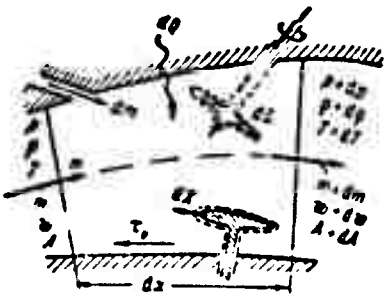


Fig. 4.6.1. Combined influence on a flow.

The continuity equation m = ρAw yields

$$\frac{dm}{m} = \frac{d\rho}{\rho} + \frac{dA}{A} + \frac{dw}{w}. \qquad (4.6.1)$$

The momentum equation is

$$pA + \rho\, dA - (p + dp)(A + dA) - \tau_0\, dA_\delta - dX - (m + dm)(w + dw) - w_d\, dm = mw;$$

where τ_0 is the tangential friction stress at the wall, dA_δ the wall area dX the resistance force acting on bodies inside the channel, and w_d the projection of the velocity with which the additional mass dm of gas flows in, along the velocity direction of the main flow.

Assuming

$$\gamma = \frac{w_d}{w};\quad \frac{dA_\delta}{A} = 4\frac{dx}{D}\ (D = \text{hydraulic diameter}^*),$$

$$\tau_0 = C_f \frac{\rho w^2}{2} = C_f \frac{kpM^2}{2},$$

we obtain

$$\frac{dp}{p} + \frac{kM^2}{2}\frac{dw^2}{w^2} + \frac{kM^2}{2}\left(4C_f\frac{dx}{D} + \frac{2dX}{kpAM^2}\right) - kM^2(1-\gamma)\frac{dm}{m} = 0. \qquad (4.6.2)$$

Let us write the energy equation (first law of thermodynamics) in the form

$$[m(i + di) + i_d\, dm] - [mi + i_d\, dm] + (m + dm)\left(\frac{w^2}{2} + d\frac{w^2}{2}\right) - \left(m\frac{w^2}{2} + \frac{w_d^2}{2}dm\right) = m\,dq - m\,dl.$$

The change of gas temperature, dT, may occur owing to the change in enthalpy $di = d\left(c_p T + \frac{p}{\rho}\right)$ and to that of a chemical reaction, di_2, so that

$c_p dT = dl + dh$; here i_{dT} is the enthalpy of the mass dm at the temperature T of the main gas flow, and i_d the enthalpy at the temperature of its entry into the channel.

After a transformation we obtain

$$dq - dl = dl + d\frac{w^2}{2} + \left(i_{dT} - i_d + \frac{w^2 - w_d^2}{2}\right)\frac{dm}{m}. \qquad (*)$$

Defining

$$i_{dT} - \left(i_d + \frac{w_d^2}{2}\right) = i_{dT} - i_{0d} = \tilde{c}_{p\,d}(T - T_{0d}), \quad \tilde{c}_{p\,d} = \frac{1}{T - T_{0d}}\int_{T_{0d}}^{T} c_{p\,d}\,dT, \qquad (4.6.3)$$

where i_{0d} and T_{0d} are the enthalpy and stagnation temperature of the mass dm, we find

$$dq - dl + dh = c_p dT + d\frac{w^2}{2} = c_p dT_0. \qquad (4.6.4)$$

Here

$$dh = dh_2 - \left[\tilde{c}_{p\,d}(T - T_{0d}) + \frac{w^2}{2}\right]\frac{dm}{m} \qquad (4.6.5)$$

and T_0 is the stagnation temperature, determining the whole energy of supplied heat, mechanical work, chemical reaction, introduced additional gas, etc.:

$$T_0 = T + \frac{w^2}{2c_p} = T\left(1 + \frac{k-1}{2}M^2\right), \quad \frac{dT_0}{T_0} = \frac{dT}{T} + \frac{\frac{k-1}{2}M^2}{1 + \frac{k-1}{2}M^2}\frac{dM^2}{M^2}. \qquad (4.6.6)$$

Dividing (4.6.4) by c_pT we can write it in the form

$$\frac{dq - dl + dh}{c_pT} = \frac{dT}{T} + \frac{k-1}{2}M^2\frac{dw^2}{w^2} = \left(1 + \frac{k-1}{2}M^2\right)\frac{dT_0}{T_0}. \qquad (4.6.7)$$

The equation of state $p = \rho RT$ yields

$$\frac{dp}{p} = \frac{d\rho}{\rho} + \frac{dT}{T}. \qquad (4.6.8)$$

The stagnation pressure in the stream is

$$p_0 = p\left(1 + \frac{k-1}{2}M^2\right)^{\frac{k}{k-1}}, \quad \frac{dp_0}{p_0} = \frac{dp}{p} + \frac{kM^2/2}{1 + \frac{k-1}{2}M^2}\frac{dM^2}{M^2}. \qquad (4.6.9)$$

By definition, $M^2 = w^2 : a^2$; $a^2 = kRT$. Therefore

$$\frac{dM^2}{M^2} = \frac{dw^2}{w^2} - \frac{dq^2}{a^2} - \frac{da^2}{a^2} = \frac{dT}{T} \qquad (4.6.10\text{-}11)$$

The system of Eqs. (4.6, 1, 2, 4, 8, 10, 11) together with the entropy equation

$$\frac{dS}{c_p} = \frac{dT_0}{T_0} - \frac{k-1}{k}\frac{dp_0}{p_0} \qquad (4.6.12)$$

links 12 parameters from which four can be singled out as independent ones and eight will be functions of them. The selection of the independent parameters is subject to the condition that they must be directly measurable. Usually the following are taken as the independent variables:

$$\frac{dA}{A}, \frac{dT_0}{T_0}, 4\zeta\frac{dx}{D} + \frac{2dX}{kpAM^2} - 2\gamma\frac{dm}{m}, \frac{dm}{m}. \qquad (4.6.13)$$

Then their functions will be

$$\frac{dM^2}{M^2}, \frac{dw}{w}, \frac{dT}{T}, \frac{dp}{p}, \frac{dp_0}{p_0}, \frac{d\rho}{\rho}, \frac{dS}{c_p}, \frac{dq}{a}. \qquad (4.6.14)$$

Applying the common methods of eliminating the unknowns we found the expressions for all the dependent parameters given in the (following) table.

In order to determine the arbitrary function standing in the first vertical column, the function standing in the horizontal line needs be multiplied by the independent variable placed in the top line.

All influence factors multiplied by $1-M^2$ change their sign according as $M > 1$ or $M < 1$, besides changing the direction of action.

Let us note that the work dl enters Eq. (4.6.4) with a sign oppositely to the sign of heat supplied (or liberated in chemical reactions). Therefore in a cylindrical tube the transition from subsonic to supersonic flow can be achieved if, in its subsonic part, a turbine is arranged with blades to which the gas will impart mechanical energy, and if in its supersonic part a compressor is installed whose blades will perform work under the influence of the gas. Such an arrangement

M	$\frac{dA}{A}$	$\frac{dT_0}{T_0}$	$\zeta\frac{dx}{D}+\frac{2dX}{kpAM^2}-2\gamma\frac{dm}{m}$	$\frac{dm}{m}$
$\frac{dM^2}{M^2}$	$-\frac{2\left(1+\frac{k-1}{2}M^2\right)}{1-M^2}$	$\frac{1+kM^2}{1-M^2}\left(1+\frac{k-1}{2}M^2\right)$	$\frac{kM^2}{1-M^2}\left(1+\frac{k-1}{2}M^2\right)$	$2\frac{1+kM^2}{1-M^2}\left(1+\frac{k-1}{2}M^2\right)$
$\frac{dw}{w}$	$-\frac{1}{1-M^2}$	$\frac{1}{1-M^2}\left(1+\frac{k-1}{2}M^2\right)$	$\frac{kM^2}{2(1-M^2)}$	$\frac{1+kM^2}{1-M^2}$
$\frac{da}{a}$	$\frac{(k-1)M^2}{2(1-M^2)}$	$\frac{1-kM^2}{2(1-M^2)}\left(1+\frac{k-1}{2}M^2\right)$	$-\frac{k(k-1)M^4}{4(1-M^2)}$	$-\frac{k-1}{2}M^2\frac{1+kM^2}{1-M^2}$
$\frac{dT}{T}$	$\frac{(k-1)M^2}{1-M^2}$	$\frac{1-kM^2}{1-M^2}\left(1+\frac{k-1}{2}M^2\right)$	$-\frac{k(k-1)M^4}{2(1-M^2)}$	$-(k-1)M^2\frac{1+kM^2}{1-M^2}$
$\frac{dp}{p}$	$\frac{kM^2}{1-M^2}$	$-\frac{1}{1-M^2}\left(1+\frac{k-1}{2}M^2\right)$	$-\frac{kM^2}{2(1-M^2)}$	$-\frac{(k+1)M^2}{1-M^2}$
$\frac{dp}{p}$	$\frac{kM^2}{1-M^2}$	$\frac{kM^2}{1-M^2}\left(1+\frac{k-1}{2}M^2\right)$	$-\frac{kM^2[1+(k-1)M^2]}{2(1-M^2)}$	$-\frac{2kM^2}{1-M^2}\left(1+\frac{k-1}{2}M^2\right)$
$\frac{dp_0}{p_0}$	0	$-\frac{kM^2}{2}$	$-\frac{kM^2}{2}$	$-kM^2$
$\frac{ds}{c_p}$	0	$1+\frac{k-1}{2}M^2$	$\frac{k-1}{2}M^2$	$(k-1)M^2$

Example:

$$\frac{dM^2}{M^2}=-\frac{2}{1-M^2}\left(1+\frac{k-1}{2}M^2\right)\frac{dA}{A}+\frac{1+kM^2}{1-M^2}\left(1+\frac{k-1}{2}M^2\right)\frac{dT_0}{T_0}+$$

$$+\frac{kM^2}{1-M^2}\left(1+\frac{k-1}{2}M^2\right)\left(\zeta\frac{dx}{D}+2\frac{dX}{kpAM^2}-2\gamma\frac{dm}{m}\right)+2\frac{1+kM^2}{1-M^2}\left(1+\frac{k-1}{2}M^2\right)\frac{dm}{m}$$

is called a mechanical mixture.

Evaporation and condensation. These are processes widespread in engineering. The coolant fluid spray is used in order to cool the flow. During condensation the latent heat of evaporation is set free.

The calculation of the influence of these processes presents no great difficulties and can be done on the basis of the fact that the additional mass dm_L adds to the evaporated fluid, and in Eq. (4.6.1) we shall have $dm = dm_d + dm_L$ (for condensation dm_L is negative). The corresponding additional terms enter the momentum equation (they are small since the additional mass is usually small) and the energy equation, which are connected with the liberation of heat.

In a subsonic flow the fluid spray diminishes the speed of the flow and raises the pressure and density; in a supersonic flow the speed is raised and pressure and density drop.

Change of the physical properties. A change in molecular weight and of the specific heat ratio $k = c_p/c_v$ also influence the processes of gas motion. In order to take them into account the universal gas constant R_y can be introduced, defined by $R = R_y/\mu$ where μ is the molecular weight. Then the equation of state

$$p = \rho \frac{R_y}{\mu} T \quad \text{gives} \quad \frac{dp}{p} = \frac{d\rho}{\rho} - \frac{d\mu}{\mu} + \frac{dT}{T}$$

instead of (4.6.8). Correspondingly Eq. (4.6.11) is changed and $\frac{da^2}{a^2} = \frac{dT}{T} - \frac{d\mu}{\mu} + \frac{dk}{k}$. At the same time the number of independent parameters is increased. Without giving the calculations we remark that a reduction in molecular weight accelerates the subsonic flow and decelerates the supersonic flow. A change in the exponent k increases the Mach number M decreases and the sonic speed increases both in the subsonic and in the supersonic region of flow; all the other motion parameters remain unaffected by a change of k.

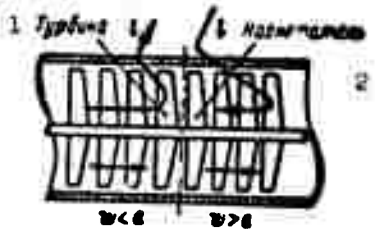


Fig. 4.6.2. Mechanical nozzle. 1) Turbine; 2) compressor.

Manuscript Page No.

[Footnotes]

260 It is sometimes called laminar sublayer; the flow structure in it will be considered in greater detail in what follows.

287 The hydraulic radius is the ratio between the area of the flow cross section and the wetted perimeter.

REFERENCES

4.1. Vulis, L.A., Termodinamika gazovykh potokov [Thermodynamics of Gas Flows], Gosenergoizdat [State Power Press], 1950.

4.2. Obukhov, A.M., Turbulentnost' [Turbulence], Collection entitled "Mekhanika v SSSR na tridtsat' let" [Mechanics in the USSR over 30 Years], GTTI [State Technical and Theoretical Press], 1950.

4.3. Minskiy, Ye.M., Turbulentnost' ruslovogo potoka [Turbulence of Channel Flows], Gidroizdat [State Publishing House for Hydraulic Engineering Literature], 1952.

4.4. Sovremennoye sostoyaniye gidroaerodinamiki vyazkoy zhidkosti [Present State of Hydroaerodynamics of the Viscous Fluid], IL [Foreign Literature Press], 1948.

4.5. Khitrin, L.N., Fizika goreniya i vzryva [Physics of Combustion and Explosion], MGU [Moscow State University], 1957.

4.6. Zel'dovich, Ya.B. and Kompaneyets, A.S., Teoriya detonatsii [De-

tonation Theory], GTTI, 1955.

4.7. Abramovich, G.N., Prikladnaya gazovaya dinamika [Applied Gas-dynamics], GTTI, 1953.

4.8. Shapiro, The Dynamics and Thermodynamics of Compressible Fluid Flow, Ronald Press Co., N.Y., 1953.

BLANK PAGE

Chapter 5

PLANE POTENTIAL MOTIONS OF A GAS

5.1. FUNDAMENTAL EQUATIONS

The present chapter deals with the investigation of plane gas flows. The fundamental system of equations of a steady plane flow of compressible inviscid medium

$$\frac{\partial}{\partial x}(\rho w_x)+\frac{\partial}{\partial y}(\rho w_y)=0; \tag{5.1.1}$$

$$\left.\begin{aligned} w_x\frac{\partial w_x}{\partial x}+w_y\frac{\partial w_x}{\partial y}&=-\frac{1}{\rho}\frac{\partial p}{\partial x},\\ w_x\frac{\partial w_y}{\partial x}+w_y\frac{\partial w_y}{\partial y}&=-\frac{1}{\rho}\frac{\partial p}{\partial y}; \end{aligned}\right\} \tag{5.1.2}$$

$$w_x\frac{\partial S}{\partial x}+w_y\frac{\partial S}{\partial y}=0; \tag{5.1.3}$$

$$p=p(\rho, S) \tag{5.1.4}$$

serves to determine the functions ρ, p, w_x, w_y, S, with the boundary conditions formulated in (2.'). Notice that besides the convective acceleration induced nonlinearity, a linearity arises also because of the fact that now $\rho = \rho(x, y)$.

The velocity potential. If we assume that $\operatorname{curl}_z \vec{w}=\frac{\partial w_y}{\partial x}-\frac{\partial w_x}{\partial y}=0$ at each point of the flow, then, as has been shown above (cf. Part 2.7), the entropy is the same for all points of the flow (S = const).

Then Eq. (5.1.3) is identically satisfied and Eq. (5.1.4) assumes the form $p=\frac{\rho_0}{\rho_0^k}\rho^k=C\rho^k$, where C is a constant quantity as this follows from (2.3.5).

Then the velocity field is characterized by the potential Φ defined by the relation $\vec{w}=\nabla\Phi$.

However, in contradistinction to the velocity potential of an incompressible fluid, the equation that is satisfied by the potential Φ in a compressible gas will now be nonlinear.

In fact, if we take into account that $\frac{dp}{d\rho} = a^2(x, y)$, we can write Eq. (5.12) in the form

$$w_x \frac{\partial w_x}{\partial x} + w_y \frac{\partial w_x}{\partial y} = -\frac{a^2}{\rho} \frac{\partial \rho}{\partial x};$$
$$w_x \frac{\partial w_y}{\partial x} + w_y \frac{\partial w_y}{\partial y} = -\frac{a^2}{\rho} \frac{\partial \rho}{\partial y}.$$

Multiplying the first of these equations by w_x, the second by w_y and adding them up we obtain with (5.1.1)

$$(w_x^2 - a^2) \frac{\partial w_x}{\partial x} + (w_y^2 - a^2) \frac{\partial w_y}{\partial y} + w_x w_y \left(\frac{\partial w_x}{\partial y} + \frac{\partial w_y}{\partial x} \right) = 0. \qquad (5.1.5)$$

Replacing here w_x and w_y by Φ we arrive at

$$\left[\left(\frac{\partial \Phi}{\partial x} \right)^2 - a^2 \right] \frac{\partial^2 \Phi}{\partial x^2} + 2 \frac{\partial \Phi}{\partial x} \frac{\partial \Phi}{\partial y} \frac{\partial^2 \Phi}{\partial x \partial y} + \left[\left(\frac{\partial \Phi}{\partial y} \right)^2 - a^2 \right] \frac{\partial^2 \Phi}{\partial y^2} = 0, \qquad (5.1.6)$$

whereupon (4.2.6)

$$a^2 = a_0^2 - \frac{k-1}{2} \left[\left(\frac{\partial \Phi}{\partial x} \right)^2 + \left(\frac{\partial \Phi}{\partial y} \right)^2 \right]$$

follows.

Equation (5.1.6) is nonlinear. Only in the case of an infinitely large propagation rate of the small disturbances (incompressible fluid, $\rho = \rho_0$) does it go over to the linear Laplace equation

$$\frac{\partial^2 \Phi}{\partial x^2} + \frac{\partial^2 \Phi}{\partial y^2} = 0.$$

The stream function. Eq. (5.1.1) is identically satisfied if we introduce the function $\Psi(x, y)$ by means of the relation

$$\rho w_x = \rho_0 \frac{\partial \Psi}{\partial y}, \quad \rho w_y = -\rho_0 \frac{\partial \Psi}{\partial x}. \qquad (5.1.7)$$

where ρ_0 is the density at an arbitrary point in the flow.

Since by definition for the streamlines $dx : w_x = dy : w_y$, $d\Psi = \frac{\partial \Psi}{\partial x} dx +$

$+\frac{\partial\Psi}{\partial y}dy=\frac{1}{\rho_0}(\rho w_x dy-\rho w_y dx)=0$ will be valid along the streamline, which means that the streamlines are characterized by the equation $\Psi(x,y)=$ const. The function $\Psi(x,y)$, as in the case of the incompressible flow, is called the stream function.

If w_x and w_y in Eq. (5.1.5) are replaced by their Ψ-functions obtained from (5.1.7) we obtain the nonlinear equation for Ψ:

$$\left[1-\frac{\rho_0^2}{\rho^2a^2}\left(\frac{\partial\Psi}{\partial y}\right)^2\right]\frac{\partial^2\Psi}{\partial x^2}+2\frac{\rho_0^2}{\rho^2a^2}\frac{\partial\Psi}{\partial x}\frac{\partial\Psi}{\partial y}\frac{\partial^2\Psi}{\partial x\partial y}+$$
$$+\left[1-\frac{\rho_0^2}{\rho^2a^2}\left(\frac{\partial\Psi}{\partial x}\right)^2\right]\frac{\partial^2\Psi}{\partial y^2}=0, \qquad (5.1.8)$$

with

$$a^2=a_0^2-\frac{k-1}{2}\left(\frac{\rho_0^2}{\rho^2}\right)\left[\left(\frac{\partial\Psi}{\partial x}\right)^2+\left(\frac{\partial\Psi}{\partial y}\right)^2\right].$$

With $\rho=\rho_0$ this equation likewise goes over into the Laplace equation

$$\frac{\partial^2\Psi}{\partial x^2}+\frac{\partial^2\Psi}{\partial y^2}=0,$$

which we have already used for investigating plane flows of an incompressible fluid.

Owing to the nonlinearity of the equations for Φ and Ψ the apparatus of the theory of functions of complex variables cannot be applied directly in gasdynamics. The sum of the particular solutions of the homogeneous linear equation is again a solution to this equation. Nonlinear equations do not possess this important property, which accounts for the difficulties in solving them.

Nonlinear equations are often solved by the method of successive approximations and sometimes they are reduced to linear equations. In the latter case the substitutes for the independent variables are chosen in such a way that the nonlinear equations are transformed to linear ones. It should be noticed, however, that great difficulties

arise in satisfying the given boundary conditions for these new equations. The other course open is to linearize the equation of motion of the gas approximately and so to obtain approximate solutions.

5.2. APPROXIMATE LINEARIZATION OF THE EQUATION FOR THIN BODIES

Statement of the problem. A great many practical problems are related to gas flows which deviate only slightly from undisturbed parallel flow and which are almost always met when long bodies with smooth contours are placed in a flow at small angles of attack*. In these cases the exact nonlinear equations can be replaced by approximate linear equations.

Linearized equation for the velocity potential. Let the velocity of an undisturbed parallel flow (Fig. 5.2.1) be w_∞, the pressure p_∞, the density ρ_∞, and w', p', ρ' the corresponding quantities characterizing the disturbances of these parameters caused by a thin body brought into the flow so that $w=w_\infty+w'$, $p=p_\infty+p'$, $\rho=\rho_\infty+\rho'$, with $|w'|:w_\infty \ll 1$, $|p'|:p_\infty \ll 1$, $|\rho'|:\rho_\infty \ll 1$. Let us assume the flow to be vortex-free and let us take the x-axis in the direction of the velocity w_∞; we can then

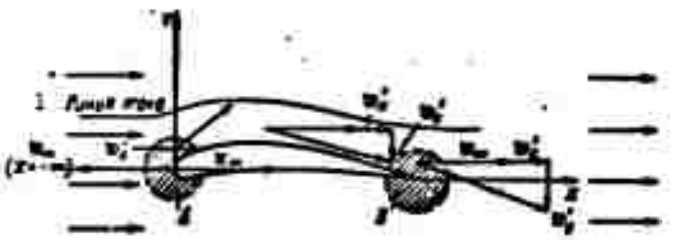


Fig. 5.2.1. For long bodies only in the small (shaded) regions A and B is the velocity of the disturbance of the same order of magnitude as the velocity of the undisturbed flow. 1) Streamline.

write the velocity potential of the total motion in the form

$$\Phi(x,y)=w_\infty x+\varphi(x,y) \qquad (5.2.1)$$

where $\varphi(x,y)$ is the disturbance potential, i.e.,

$$w'_x=\frac{\partial\varphi}{\partial x},\quad w'_y=\frac{\partial\varphi}{\partial y}. \qquad (5.2.2)$$

Since

$$a_0^2 = a_\infty^2 + \frac{k-1}{2} w_\infty^2 = a^2 + \frac{k-1}{2} [(w_\infty + w_x')^2 + w_y'^2],$$

we have

$$a^2 = a_\infty^2 + \frac{k-1}{2} w_\infty^2 - \frac{k-1}{2} w_\infty^2 \left[\left(1 + \frac{w_x'}{w_\infty}\right)^2 + \frac{w_y'^2}{w_\infty^2} \right] =$$

$$= a_\infty^2 - \frac{k-1}{2} w_\infty^2 \left(2 \frac{w_x'}{w_\infty} + \frac{w'^2}{w_\infty^2} \right)$$

or

$$\frac{a^2}{a_\infty^2} = 1 - \frac{k-1}{2} M_\infty^2 \left(2 \frac{w_x'}{w_\infty} + \frac{w_x'^2 + w_y'^2}{w_\infty^2} \right) =$$

$$= 1 - (k-1) M_\infty^2 \frac{w_x'}{w_\infty} + 0\left(M_\infty^2 \frac{w'^2}{w_\infty^2} \right)$$

and

$$\frac{1}{a^2} = \frac{1}{a_\infty^2} \cdot \frac{1}{1 - (k-1) M_\infty^2 \frac{w_x'}{w_\infty} + 0\left(M_\infty^2 \frac{w'^2}{w_\infty^2} \right)} =$$

$$= \frac{1}{a_\infty^2} \left[1 + (k-1) M_\infty^2 \frac{w'^2}{w_\infty^2} \right] + 0\left(M_\infty^2 \frac{w'^2}{w_\infty^2} \right).$$

where the symbol $0(z^n)$ denotes a quantity of the order of z^n.

Let us calculate the factors of the second derivatives of the velocity potential Eq. (5.1.6), writing the main terms as

$$1 - \frac{w_x^2}{a^2} = 1 - \frac{a_\infty^2}{a^2} \frac{(w_\infty + w_x')^2}{a_\infty^2} =$$

$$= 1 - \left[1 + (k-1) M_\infty^2 \frac{w_x'}{w_\infty} + 0\left(M_\infty^2 \frac{w'^2}{w_\infty^2} \right) \right] M_\infty^2 \left(1 + \frac{w_x'}{w_\infty} \right)^2 =$$

$$= 1 - M_\infty^2 - 2 M_\infty^2 \frac{w_x'}{w_\infty} - (k-1) M_\infty^4 \frac{w_x'}{w_\infty} + 0\left(M_\infty^2 \frac{w'^2}{w_\infty^2} \right) =$$

$$= 1 - M_\infty^2 + 0\left(M_\infty^2 \frac{w_x'}{w_\infty} \right);$$

$$1 - \frac{w_y^2}{a^2} = 1 - \frac{w_y'^2}{w_\infty^2} \frac{w_\infty^2}{a_\infty^2} \frac{a_\infty^2}{a^2} = 1 + 0\left(M_\infty^2 \frac{w_y'^2}{w_\infty^2} \right);$$

$$\frac{w_x w_y}{a^2} = \frac{(w_\infty + w_x') w_y'}{w_\infty^2} \frac{w_\infty^2}{a_\infty^2} \frac{a_\infty^2}{a^2} =$$

$$= M_\infty^2 \frac{w_y'}{w_\infty} + 0\left(M_\infty^2 \frac{w_x' w_y'}{2 w_\infty^2} \right) \approx M_\infty^2 \frac{w_y'}{w_\infty}.$$

Since

$$\frac{\partial^2\Phi}{\partial x^2}=\frac{\partial^2\varphi}{\partial x^2};\quad \frac{\partial^2\Phi}{\partial x\,\partial y}=\frac{\partial^2\varphi}{\partial x\,\partial y};\quad \frac{\partial^2\Phi}{\partial y^2}=\frac{\partial^2\varphi}{\partial y^2},$$

the approximate equation will be the disturbance potential equation, namely

$$(1-M_\infty^2)\left(1+\frac{M_\infty^2\frac{v_x'}{v_\infty}}{1-M_\infty^2}\right)\frac{\partial^2\varphi}{\partial x^2}+M_\infty^2\frac{v_y'}{v_\infty}\frac{\partial^2\varphi}{\partial x\,\partial y}+$$
$$+\left[1+0\left(M_\infty^2\frac{v_y'^2}{v_\infty^2}\right)\right]\frac{\partial^2\varphi}{\partial y^2}=0.$$

Assuming that

$$\frac{M_\infty^2}{|1-M_\infty^2|}\frac{v_x'}{v_\infty}\ll 1,\quad M_\infty^2\frac{v_y'}{v_\infty}<1 \tag{5.2.3}$$

and retaining the first-order small terms, we obtain the approximate linearized equation for the disturbance potential,

$$(1-M_\infty^2)\frac{\partial^2\varphi}{\partial x^2}+\frac{\partial^2\varphi}{\partial y^2}=0. \tag{5.2.4}$$

The stream function equation is linearized in the same way; we obtain

$$(1-M_\infty^2)\frac{\partial^2\psi}{\partial x^2}+\frac{\partial^2\psi}{\partial y^2}=0.$$

<u>The pressure coefficient</u>. In the flow about smooth-contour bodies the area of a stream tube cross section varies only very little; owing to this the product ρw varies but little too.

The equation of motion along the streamlines is therefore obtained in the form

$$\int_{p_\infty}^{p} dp=p-p_\infty=-\int_{v_\infty}^{v=v_\infty+v_x'}\rho w\,dw\approx-\rho_\infty v_\infty v_x'. \tag{5.2.5}$$

The order of magnitude of the discarded terms can be obtained from the energy equation

$$\frac{v^2}{2}+\frac{k}{k-1}\frac{p}{\rho}=\frac{v_\infty^2}{2}+\frac{k}{k-1}\frac{p_\infty}{\rho_\infty}$$

and the isentropy relation $p = c\rho^k$. The pressure coefficient then reads

$$C_p = \frac{p - p_\infty}{\frac{\rho_\infty v_\infty^2}{2}} = -2\frac{v_x'}{v_\infty} = -\frac{2}{v_\infty}\frac{\partial \eta}{\partial x}. \qquad (5.2.6)$$

Subsonic and supersonic plane flows. If we assume that $\frac{\partial v_x'}{\partial x} > 0$ indicates that the flow velocity increases along the stream tube, and $-\frac{\partial v_y'}{\partial y} > 0$ — that the stream tube widens, then it follows from the equation $(1 - M_\infty^2)\frac{\partial v_x'}{\partial x} + \frac{\partial v_y'}{\partial y} = 0$ that in a subsonic flow $(1 - M_\infty^2 > 0)$ the acceleration of the flow is connected with a decrease of the stream tube cross section, and that in a supersonic flow $(1 - M_\infty^2 < 0)$ an acceleration of the flow requires that the stream tube widens; consequently, the slope of the stream lines changes sign at the transition from subsonic to supersonic flow.

The theory of differential equations with second order partial derivations shows that the type of the equation with second-order partial derivatives, $A\frac{\partial^2 \varphi}{\partial x^2} + 2B\frac{\partial \varphi}{\partial x}\frac{\partial \varphi}{\partial y}\frac{\partial^2 \varphi}{\partial x \partial y} + C\frac{\partial^2 \varphi}{\partial y^2} = 0$ is determined by the sign of its discriminant $B^2 - AC$.

In our case $B = 0$ and $B^2 - AC = -(1 - M_\infty^2)$. If $1 - M_\infty^2 > 0$, i.e., if the flow is subsonic, it is qualitatively similar to the flow of an incompressible fluid; the disturbances introduced into the flow are propagated over the whole region occupied by the flow. If $B^2 - AC < 0$, the equation is said to belong to the elliptic type*.

If $M_\infty > 1$ the flow is supersonic; $B^2 - AC = M_\infty^2 - 1 > 0$ is an equation of the hyperbolic type; the disturbances introduced into the flow are propagated only in a certain part of the whole region occupied by the flow. Interfaces (lines in the plane motion) exist which separate the region of disturbed motion from the undisturbed ones. These lines are called characteristics. In a subsonic flow the disturbances are propagated over all the flow. Hence follows the character, the type of the disturbances: in the presence of characteristics (supersonic flow) the disturbances are concentrated. When they occupy the whole region of the flow they are, if not attenuated, propagated to

infinity. In subsonic flows the perturbations are propagated over the whole region and become attenuated at infinity.

5.3. FLOW ABOUT A WAVY SURFACE

As an example that illustrates well the application of the perturbation method and the differences between subsonic and supersonic flows let us consider the plane flow along a wavy wall that is sinusoidal in shape

$$y = h \sin \frac{2\pi x}{l}, \tag{5.3.1}$$

where the amplitude h is assumed to be much smaller than the period l (Fig. 5.3.1).

Boundary conditions. Since the wall must coincide with streamlines, we have

$$\left(\frac{dy}{dx}\right)_w = 2\pi \frac{h}{l} \cos \frac{2\pi x}{l} = \left(\frac{v_y}{v_x}\right)_w. \tag{5.3.2}$$

When the formulation of the problem is linearized,

$$\frac{v_y}{v_x} = \frac{v'_y}{v_\infty + v'_x} \approx \frac{v'_y}{v_\infty} = \frac{1}{v_\infty} \frac{\partial \varphi}{\partial y}.$$

Hence follows the first boundary condition: for $y = h \sin \frac{2\pi x}{l}$ the disturbance potential φ has to satisfy the equation

$$\frac{\partial \varphi}{\partial y} = v_\infty \cdot 2\pi \frac{h}{l} \cos \frac{2\pi x}{l}, \tag{5.3.3}$$

and the stream function $\Psi = 0$, or, since $\Psi = v_\infty y + \psi$,

$$\psi = -v_\infty h \sin \frac{2\pi x}{l}. \tag{5.3.4}$$

The second boundary condition is obtained from the fact that the velocity must be finite at infinity, i.e., as $y \to \infty$ the derivatives of the functions φ and ψ must not tend to infinity.

Subsonic flow. If we put $n^2 = 1 - M_\infty^2$ then $n^2 > 0$ for a subsonic flow. Rewriting the linearized equation in the form

$$n^2 \frac{\partial^2 f}{\partial x^2} + \frac{\partial^2 f}{\partial y^2} = 0$$

(where f stands for φ or ψ) we can seek the solution to the equation in the form of a product of the function $\zeta(x)$, depending only on x, and the function $\eta(y)$, depending only on y:

$$f(x,y)=\zeta(x)\eta(y).$$

Differentiating $f(x,y)$ twice and dividing by $f(x,y)$, we obtain

$$\frac{\zeta''(x)}{\zeta(x)}+\frac{1}{n^2}\frac{\eta''(y)}{\eta(y)}=0.$$

Since one term depends only on x and the other only on y, both of them must be equal to one and the same constant, but with opposite sign, i.e.,

$$\frac{\zeta''(x)}{\zeta(x)}=k,\quad \frac{1}{n^2}\frac{\eta''(y)}{\eta(y)}=-k.$$

Thus, depending on the sign of k the solution to Eq. (5.3.4) will be either an exponential function ($k > 0$) or a trigonometrical function ($k < 0$)*.

We shall now seek the stream function. If

$$\psi=\zeta(x)\eta(y),$$

it follows from the boundary condition for $y = h \sin(2\pi x/l)$, i.e., near $y=0$, $\psi=-w_0 h\sin\frac{2\pi x}{l}$, that $\zeta(x)$ must be a trigonometrical function of the form $a \sin px$ and at the same time $\eta(y)$ will be an exponential function; by virtue of the second boundary condition (finiteness of $\eta(y)$ it will have the form be^{-py}. Thus

$$\psi=A\sin px e^{-py}.$$

In order to determine A and h we write the boundary conditions as

$$-w_0 h\sin\frac{2\pi x}{l}=A\sin px e^{-hp\sin\frac{2\pi x}{l}}\approx$$
$$\approx A\sin px\left(1-nph\sin\frac{2\pi x}{l}\right).$$

This equation can be satisfied if we put $p = 2\pi/l$ and if the

term of the order of $\varkappa ph = \sqrt{1-M_\infty^2}\,2\pi\frac{h}{l}$ on the right-hand side is neglected compared with unity, which is permissible since we have initially assumed that $h/l \ll 1$.

This means that the boundary conditions (5.3.3) and (5.3.4) at the wall, i.e., at $y = h\sin\frac{2\pi x}{l}$ are replaced by approximate relations formulated for y = 0.

In this approximation we therefore obtain $A = -w_\infty h$;

$$\psi = -w_\infty h e^{-\frac{2\pi y}{l}\sqrt{1-M_\infty^2}} \sin\frac{2\pi x}{l}. \quad (5.3.5)$$

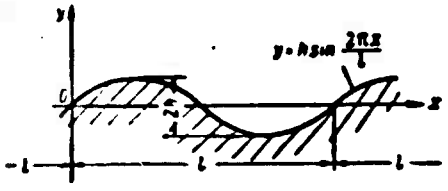


Fig. 5.3.1. Wavy sine-shaped wall. 1) is the wavelenght and h) the amplitude.

Similarly

$$\varphi = -\frac{w_\infty h}{\sqrt{1-M_\infty^2}} e^{-\frac{2\pi y}{l}\sqrt{1-M_\infty^2}} \cos\frac{2\pi x}{l}. \quad (5.3.6)$$

We have now

$$w'_x = \frac{\partial\varphi}{\partial x} = w_\infty \frac{2\pi h}{l\sqrt{1-M_\infty^2}} e^{-\frac{2\pi y}{l}\sqrt{1-M_\infty^2}} \sin\frac{2\pi x}{l}; \quad (5.3.7)$$

$$w'_y = \frac{\partial\varphi}{\partial y} = w_\infty \frac{2\pi h}{l} e^{-\frac{2\pi y}{l}\sqrt{1-M_\infty^2}} \cos\frac{2\pi x}{l}; \quad (5.3.8)$$

$$C_p = -2\frac{w'_x}{w_\infty} = -\frac{4\pi h}{l\sqrt{1-M_\infty^2}} e^{-\frac{2\pi y}{l}\sqrt{1-M_\infty^2}} \sin\frac{2\pi x}{l}. \quad (5.3.9)$$

It follows from these expressions that the greater $M_\infty (M_\infty < 1)$, the more slowly the disturbances are attenuated.

The pressure coefficients for a compressible gas, C_{ps}, and of an incompressible fluid, C_{pn}, are simply linked by

$$C_{ps} = \frac{C_{pn}}{\sqrt{1-M_\infty^2}}. \quad (5.3.10)$$

Since the linearized equation has been obtained on the supposition that $|w'| : w_\infty \ll 1$, the limits of applicability of the solution found are determined by the condition

$$\left|\frac{w'}{w_\infty}\right|_{max} = \frac{2\pi h}{l\sqrt{1-M_\infty^2}} \ll 1,$$

i.e., the relative thickness admitted becomes smaller as M_∞ increases.

Supersonic flow, $M_\infty > 1$. A flow for which $1 - M_\infty^2 < 0$ is described

by the wave equation

$$\frac{\partial^2 f}{\partial x^2} - \frac{1}{m^2}\frac{\partial^2 f}{\partial y^2} = 0, \qquad (5.3.11)$$

where $m = \sqrt{M_\infty^2 - 1} > 0$ and $f = \varphi$ or ψ.

The total integral of this equation, as was found in (2.7.8), has the form

$$f(x, y) = f_1(x - my) + f_2(x + my). \qquad (5.3.12)$$

where f_1 and f_2 are arbitrary functions of (x - my) and (x + my), respectively.

Assuming x - my = const and, correspondingly, x + my = const, we obtain two sets of straight lines on which each of the functions f_1 and f_2 and all disturbance parameters, w', p', ρ',... are constant. These straight lines, along which the disturbance parameters remain constant are the characteristics (Fig. 5.3.2).

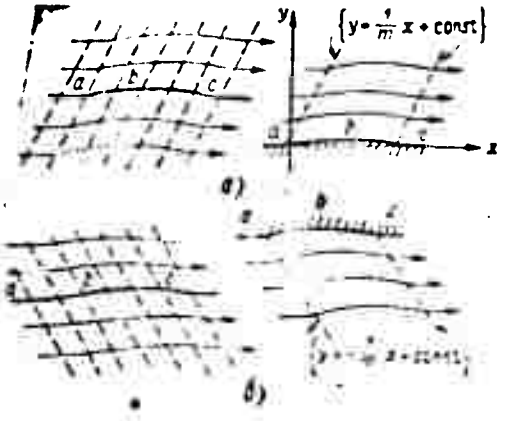


Fig. 5.3.2. + Mach lines (a) and - mach lines (b).

In the flow considered the - Mach lines $y = \frac{1}{m}C_2 - \frac{x}{m}$ in the upper semiplane, for y > 0, are inclined against the flow, i.e., the disturbances must be propagated upstream; this is impossible for a supersonic flow and so we have to take $f_2 = 0$. Thus, in the upper semiplane only the + Mach lines remain:

$$y=\frac{1}{m}x+C_1=\frac{1}{\sqrt{M_\infty^2-1}}x+C_1.$$

It can be shown by the same considerations that in the lower semi-plane the + Mach lines cannot exist since the disturbances would otherwise propagate against the flow; consequently, for $y < 0$ only the - Mach lines remain:

$$y=-\frac{1}{m}x+C_2=-\frac{1}{\sqrt{M_\infty^2-1}}+C_2.$$

As in the case of $M_\infty < 1$, the boundary conditions at the wall can be taken for $y = 0$; then

$$\frac{\partial\varphi}{\partial y}=w_\infty\frac{2\pi h}{l}\cos\frac{2\pi x}{l},\quad \psi=-w_\infty h\sin\frac{2\pi x}{l}. \tag{5.3.4}$$

For the stream function at $y = 0$ we shall therefore have

$$-w_\infty h\sin\frac{2\pi x}{l}=f_1(x),$$

hence we obtain the stream function equation in the form

$$\psi=f_1(x-my)=-w_\infty h\sin\frac{2\pi(x-my)}{l}. \tag{5.3.13}$$

For the velocity potential $\varphi = f_1(x - my)$ we have at $y = 0$

$$\left.\frac{\partial\varphi}{\partial y}\right|_{y=0}=-mf_1(x)=w_\infty\frac{2\pi h}{l}\cos\frac{2\pi x}{l}.$$

Hence

$$\varphi=-w_\infty\frac{h}{\sqrt{M_\infty^2-1}}\sin\frac{2\pi(x-my)}{l}. \tag{5.3.14}$$

Notice that the second boundary condition (finite values for φ and ψ with $x \to \infty$ and $y \to \infty$) is automatically satisfied.

For the velocity of the disturbance and for the pressure coefficient, we have

$$w_x'=-w_\infty\frac{2\pi h}{l\sqrt{M_\infty^2-1}}\cos\left[\frac{2\pi}{l}(x-y\sqrt{M_\infty^2-1})\right]; \tag{5.3.15}$$

$$w_y'=w_\infty\frac{2\pi h}{l}\cos\left[\frac{2\pi}{l}(x-y\sqrt{M_\infty^2-1})\right]; \tag{5.3.16}$$

$$C_p=-2\frac{w_x'}{w_\infty}=\frac{4\pi h}{l\sqrt{M_\infty^2-1}}\cos\left[\frac{2\pi}{l}(x-y\sqrt{M_\infty^2-1})\right].$$

At the wall surface ($y \approx 0$)

$$C_{p\,cp}=\frac{4\pi h}{l\sqrt{M_\infty^2-1}}\cos\frac{2\pi x}{l}=\frac{2\alpha_m}{\sqrt{M_\infty^2-1}}, \qquad (5.3.17)$$

where $\alpha_m=\frac{dy}{dx}=\frac{2\pi h}{l}\cos\frac{2\pi x}{l}$ denotes the slope of the stream line, which is often called the local angle of attack.

Comparison of the results. In both cases the applicability limits of the solution are determined by the condition $|\bar{w}_x'|:w_\infty \ll 1$, which gives $2\pi h:l\sqrt{1-M_\infty^2}\ll 1$, for the subsonic and $2\pi h:l\sqrt{M_\infty^2-1}\ll 1$, for the supersonic flow.

The supersonic flow differs qualitatively from the subsonic flow: without their magnitude being changed, the disturbances are propagated to infinity along the straight lines (Fig. 5.3.3, b)

$$x-y\sqrt{M_\infty^2-1}=C_1.$$

Comparing the pressure distribution curves in subsonic and supersonic flows, we ascertain (Fig. 5.3.4) that a force arises which acts in the direction of motion on the body placed in the flow, which is not so in a subsonic flow. This force is called the wave drag.

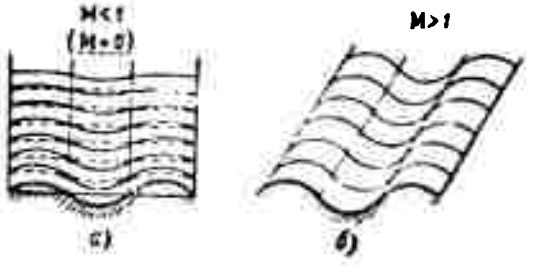


Fig. 5.3.3. The greater the Mach number M of a subsonic flow the more slowly the disturbances are attenuated (a); in a supersonic flow the disturbances flow off to infinity without being changed (b).

Transition through sonic speed. With $M_\infty \to 1$, if $\left(\frac{h}{l}\right)^2 < \frac{M_\infty^2-1}{4\pi^2}$, Eq. (5.2.4) formally goes over to a parabolic equation

$$\frac{\partial^2\varphi}{\partial y^2}=0.$$

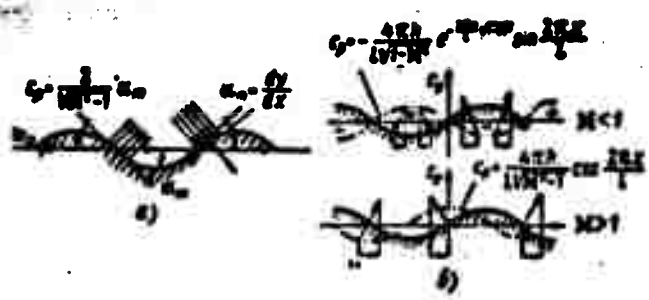


Fig. 5.3.4. In a supersonic flow a force proportional to the local angle of attack arises on each element (a). In a subsonic flow the projection of the pressure forces onto the velocity direction is equal to zero (b). In a supersonic flow it differs from zero.

In the region $M_\infty = 1$, however, Eqs. (5.2.4) and (5.2.5) become invalid by virtue of Condition (5.2.3), and in order to solve the problem in this so-called nearsonic (transsonic) region another equation has to be formulated. Owing to (5.3.17) the pressure coefficient C_p tends to infinity for $M_\infty = 1$ (Fig. 5.3.5). Thus, when passing over to $M_\infty = 1$ from the side $M_\infty < 1$ the drag is equal to zero, and when coming from the side $M_\infty > 1$ it tends to infinity.

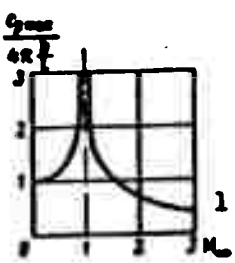


Fig. 5.3.5. According to the linearized theory $C_p \to \infty$ as $M_\infty \to 1$.

Notice that the linearized equations also lose validity when the M_∞'s are very large, i.e., in the so-called hypersonic range.

5.4. LINEARIZED SUBSONIC PLANE FLOW

A plane subsonic flow of compressible gas streaming about a sufficiently thin cylindrical body at a small angle of attack can be described by the linearized equation for the disturbance potential:

$$\beta^2 \frac{\partial^2 \varphi}{\partial x^2} + \frac{\partial^2 \varphi}{\partial y^2} = 0, \quad \beta^2 = 1 - M_\infty^2; \tag{5.4.1}$$

with the boundary conditions:

a) the disturbances are attenuated at infinity, i.e., with $x \to \pm\infty$, $y \to \pm\infty$;

$$\left.\begin{aligned} w'_x &= \frac{\partial \varphi}{\partial x} = 0, \\ w'_y &= \frac{\partial \varphi}{\partial y} = 0; \end{aligned}\right\} \qquad (5.4.2)$$

b) the body contour l must coincide with streamlines, i.e.,

$$\left(\frac{dy}{dx}\right)_l = \frac{v_y}{v_x} = \frac{w'_y}{v_\infty + w'_x} \approx \frac{1}{v_\infty}\left(\frac{\partial \psi}{\partial y}\right)_l. \qquad (5.4.3)$$

The bases of the method of solution. Since Eq. (5.4.1) differs from the Laplace equation (for an incompressible fluid) only by a factor n^2 in the $\partial^2\varphi/\partial x^2$ term, this equation can of course be transformed to the Laplace equation by substituting the variables. From the physical point of view this means that we can try to find an incompressible fluid flow corresponding to each compressible fluid flow. The correspondence must be mutually unique. After having found the solution in the plane of motion of an incompressible flow, we must indicate a way of making the reverse transition and of transferring the results of the solution to the plane of a compressible gas.

Substitution of the variables. Let us denote the quantities referring to the flow of an incompressible fluid by the sign "~" and put

$$\tilde{x} = \lambda_x x, \quad \tilde{y} = \lambda_y y, \quad \tilde{\varphi}(\tilde{x}, \tilde{y}) = \lambda_\varphi \varphi(x, y), \qquad (5.4.4)$$

where λ_x, λ_y, λ_φ are constants.

Then

$$\left.\begin{aligned} \frac{\partial \varphi}{\partial x} &= w'_x = \frac{\lambda_x}{\lambda_\varphi}\frac{\partial \tilde{\varphi}}{\partial \tilde{x}} = \frac{\lambda_x}{\lambda_\varphi}\tilde{w}'_x, \\ \frac{\partial^2 \varphi}{\partial x^2} &= \frac{\partial w'_x}{\partial x} = \frac{\partial}{\partial x}\frac{\partial \varphi}{\partial x} = \frac{\lambda_x^2}{\lambda_\varphi}\frac{\partial^2 \tilde{\varphi}}{\partial \tilde{x}^2}, \\ \frac{\partial \varphi}{\partial y} &= w'_y = \frac{\lambda_y}{\lambda_\varphi}\frac{\partial \tilde{\varphi}}{\partial \tilde{y}} = \frac{\lambda_y}{\lambda_\varphi}\tilde{w}'_y, \quad \frac{\partial^2 \varphi}{\partial y^2} = \frac{\lambda_y^2}{\lambda_\varphi}\frac{\partial^2 \tilde{\varphi}}{\partial \tilde{y}^2} \end{aligned}\right\} \qquad (5.4.5)$$

and instead of (5.4.1) we obtain

$$n^2\lambda_x^2\frac{\partial^2 \tilde{\varphi}}{\partial \tilde{x}^2} + \lambda_y^2\frac{\partial^2 \tilde{\varphi}}{\partial \tilde{y}^2} = 0.$$

If we put

$$M_x^2 = \lambda_y^2, \text{ i. e. } \lambda_y : \lambda_x = M_\infty.$$

then we obtain the Laplace equation

$$\frac{\partial^2 \tilde{\varphi}}{\partial \tilde{x}^2} + \frac{\partial^2 \tilde{\varphi}}{\partial \tilde{y}^2} = 0. \tag{5.4.6}$$

which describes the motion of an incompressible fluid in the $\tilde{x}$, $\tilde{y}$-plane with the potential $\tilde{\varphi}(\tilde{x}, \tilde{y})$ (Fig. 5.4.1).

Correspondence of the boundary conditions. In order to establish complete correspondence between the flows it is necessary to consider the boundary conditions again. As can be seen from (5.4.2) the boundary conditions at infinity are satisfied: as $\tilde{x} \to \infty$ and $\tilde{y} \to \infty$, both $\tilde{w} \to 0$ and $w_y' \to 0$. Going over to the boundary conditions at the body, we have to notice that

$$\left(\frac{\partial \varphi}{\partial x}\right)_L = \frac{\lambda_x}{\lambda_y}\left(\frac{\partial \tilde{\varphi}}{\partial \tilde{x}}\right)_{\tilde{L}}. \tag{5.4.7}$$

Here

$$\left(\frac{\partial \varphi}{\partial y}\right)_L = \frac{\lambda_y}{\lambda_\varphi}\left(\frac{\partial \tilde{\varphi}}{\partial \tilde{y}}\right)_{\tilde{L}}$$

and, therefore, the equation $\left(\frac{\partial \varphi}{\partial x}\right)_L = \frac{1}{w_\infty}\left(\frac{\partial \varphi}{\partial y}\right)_L$ goes over to

$$\left(\frac{\partial \tilde{\varphi}}{\partial \tilde{x}}\right)_{\tilde{L}} = \frac{1}{w_\infty}\frac{\lambda_y^2}{\lambda_x \lambda_\varphi}\left(\frac{\partial \tilde{\varphi}}{\partial \tilde{y}}\right)_{\tilde{L}}.$$

Thus, if we put

$$\lambda_y^2 = \lambda_x \lambda_\varphi, \quad w_\infty = \tilde{w}_\infty \tag{5.4.8}$$

then

$$\left(\frac{\partial \tilde{\varphi}}{\partial \tilde{x}}\right)_{\tilde{L}} = \frac{1}{\tilde{w}_\infty}\left(\frac{\partial \tilde{\varphi}}{\partial \tilde{y}}\right)_{\tilde{L}}. \tag{5.4.9}$$

The equations $M_x^2 = \lambda_y^2$ and $\lambda_y^2 = \lambda_x \lambda_\varphi$ do not determine the quantities λ_x, λ_y and λ_φ except by the ratios. One of them can be arbitrarily chosen. If we put $\lambda_y = 1$, then $\lambda_x = 1/n$ and $\lambda_\varphi = 1/\lambda_x = n$.

Moreover, regardless of the choice of λ_x and λ_y, the connection between the shape of the body placed in a compressible gas flow and

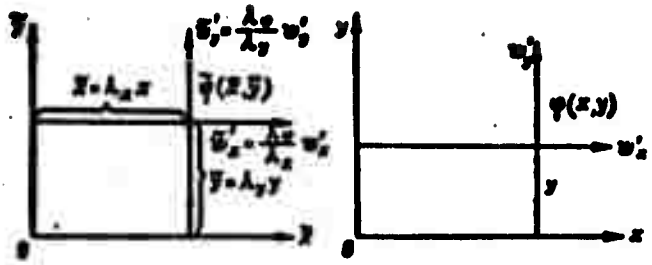


Fig. 5.4.1. In an affine transformation of the coordinates and of the velocity potential $\tilde{x}=\lambda_x x, \tilde{y}=\lambda_y y, \tilde{\varphi}=\lambda_\varphi \varphi$. the equation for the disturbance potential $a^2\varphi_{xx}+\varphi_{yy}=0$ goes over to the Laplace equation $\tilde{\varphi}_{\tilde{x}\tilde{x}}+\tilde{\varphi}_{\tilde{y}\tilde{y}}=0$.

the shape of the corresponding body placed in an incompressible fluid flow can be formulated by the relation

$$\left(\frac{dy}{dx}\right)_l : \left(\frac{d\tilde{y}}{d\tilde{x}}\right)_{\tilde{l}} = \frac{\lambda_x}{\lambda_y} = \frac{1}{\sqrt{1-M_\infty^2}}. \qquad (5.4.10)$$

This indicates that the slope of each element of the body in the compressible gas is greater than the slope of the corresponding element of the body in the incompressible fluid flow by $1 : \sqrt{1-M_\infty^2}$. Owing to this, the angle of attack, the thickness of the body and its camber are greater by the same factor (Fig. 5.4.2). For the angle of attack this is obvious since it is proportional to the slope of the streamline. For the body thickness we have

$$\frac{d}{l} = \frac{\tilde{d}:\lambda_y}{\tilde{l}:\lambda_x} = \frac{\lambda_x}{\lambda_y}\frac{\tilde{d}}{\tilde{l}}.$$

For maximum camber

$$\frac{f}{l} = \frac{\tilde{f}:\lambda_y}{\tilde{l}:\lambda_x} = \frac{\lambda_x}{\lambda_y}\frac{\tilde{f}}{\tilde{l}}.$$

The coefficients of pressure, lift and moment. The connection between the pressure distributions will be

$$C_p = -\frac{2}{w_\infty}\left(\frac{\partial\varphi}{\partial x}\right)_l = -\frac{2}{w_\infty}\frac{\lambda_x}{\lambda_\varphi}\frac{\partial\tilde{\varphi}}{\partial\tilde{x}} =$$

$$= \frac{1}{a^2}\left[-\frac{2}{w_\infty}\left(\frac{\partial\tilde{\varphi}}{\partial x}\right)_l\right] = \frac{\tilde{C}_p}{M_\infty^2-1}. \qquad (5.4.11)$$

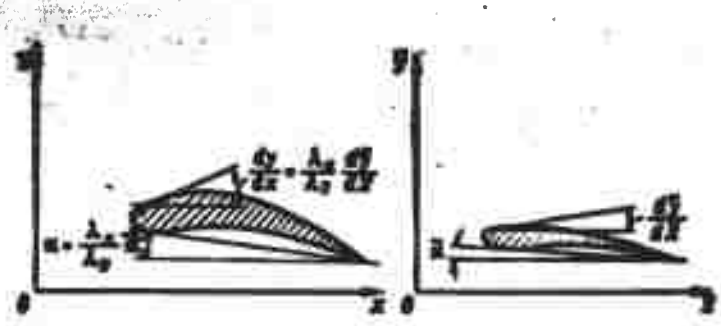


Fig. 5.4.2. Correspondence of the boundary conditions with the affine transformation $\tilde{x}=\lambda_x x,\ \tilde{y}=\lambda_y y,\ \tilde{\varphi}=\lambda_y \varphi$ consists in that the slope of each streamline element in the compressible gas is obtained by multiplying the slope of the corresponding element in the incompressible fluid by λ_x/λ_y.

The coefficients of lift and moment (b is the profile chord) are

$$C_y=\frac{R_y}{\frac{\rho v_\infty^2}{2}A}=\frac{\oint p\,dx}{\frac{\rho v_\infty^2}{2}b}=\frac{\oint (p-p_\infty)dx}{\frac{\rho v_\infty^2}{2}b}=\oint C_p\,d\left(\frac{x}{b}\right)=$$

$$=\oint \tilde{C}_p\frac{1}{n^2}d\left(\frac{\tilde{x}}{\tilde{b}}\right)=\frac{\tilde{C}_y}{M_\infty^2-1}; \qquad (5.4.12)$$

$$C_m=\frac{M}{\frac{\rho v_\infty^2}{2}Ab}=\oint C_p\frac{x}{b}d\left(\frac{x}{b}\right)=\frac{\tilde{C}_m}{M_\infty^2-1}. \qquad (5.4.13)$$

Thus, the pressure coefficient C_p at any point (x,y) of the compressible gas flow streaming about a sufficiently smooth and thin body will be greater by a factor of $n^2=1:(1-M_\infty^2)$ than the coefficient $\tilde{C}_p$ at the corresponding point $(\tilde{x},\tilde{y})$ of the incompressible fluid flow streaming about a body whose thickness, angle of attack and maximum camber are smaller than those of the given body by a factor of $\sqrt{1-M_\infty^2}$. The correspondence is established by the choice of λ_x and λ_y satisfying the condition $n\lambda_x = \lambda_y$ and the relations $\tilde{x} = \lambda_x X$ and $\tilde{y} = \lambda_y Y$.

For practical applications it is important to solve the following problems:

1) to determine the pressure distribution over a thin profile in a compressible flow when the pressure distribution is given for the same profile positioned at the same angle of attack in the incompressible flow;

2) to know to change the formula of the given profile so that the pressure distribution in the compressible gas flow is the same as that over the reference profile in the incompressible flow.

Pressure distribution over a given body. Since $C_p = \tilde{C}_p/n^2$ for a subsonic gas flow round a body whose thickness is greater than the thickness of the similar body in the incompressible fluid by a factor of 1/n, reducing the thickness of the body in the gas flow by the same factor gives us the flow about like bodies; the pressure distribution over them are linked by the relation

$$C_p = \frac{\tilde{C}_p}{\sqrt{1-M_\infty^2}} \qquad (5.4.14)$$

owing to the fact that the ratio of the pressures at the corresponding points of similar sufficiently long bodies in one and the same medium is equal to the ratio of their thicknesses (3.6.49).

Determination of the shape of the body for a given pressure distribution. The solution of this problem is used in boundary layer theory for a compressible gas. It is solved by the same method. Let the primed quantities belong to the bodies of altered shape; the requirement

$$\frac{C_p}{\tilde{C}'_p} = \frac{C_p}{\tilde{C}_p}\cdot\frac{\tilde{C}_p}{\tilde{C}'_p} = 1 - \frac{1}{n^2}\frac{\tilde{C}_p}{\tilde{C}'_p}$$

leads us, taking (3.6.49) into account, to

$$\tilde{C}_p : \tilde{C}'_p = n^2 - \tilde{d} : \tilde{d}'.$$

But $d/\tilde{d} = 1/n$ and therefore

$$\frac{d}{\tilde{d}'} = \frac{d}{\tilde{d}}\cdot\frac{\tilde{d}}{\tilde{d}'} = \frac{1}{n}n^2 = n = \sqrt{1-M_\infty^2}; \quad \tilde{d}' = \frac{d}{\sqrt{1-M_\infty^2}}.$$

i.e., the pressure distribution in the gas flow will be the same as in the incompressible fluid flow if the ordinates of the body placed in the incompressible fluid are multiplied by $\sqrt{1-M_\infty^2}$.

Improvement of the solution to the linearized equation. Linearized equations are obtained on the supposition that the disturbances are very small. Regarding the number M_∞, the supposition states that its influence is uniform over the whole space occupied by the gas. Laitone* has suggested applying the solution found in each small region of the flow, i.e., replacing the M_∞ in the solution found by the local Mach number M and taking

$$C_p = \frac{\tilde{C}_p}{\sqrt{1-M_\infty^2}}. \tag{5.4.15}$$

Since

$$C_p = \frac{p-p_\infty}{\frac{\rho_\infty w_\infty^2}{2}} = \frac{p_\infty\left(\frac{p}{p_\infty}-1\right)}{\frac{\rho_\infty w_\infty^2}{2}} = 2\frac{\left(\frac{p}{p_\infty}-1\right)}{kM_\infty^2}$$

and

$$\frac{p}{p_\infty} = \left(\frac{1+\frac{k-1}{2}M_\infty^2}{1+\frac{k-1}{2}M^2}\right)^{\frac{k}{k-1}},$$

we have

$$C_p = \frac{2}{kM_\infty^2}\left[\left(\frac{1+\frac{k-1}{2}M_\infty^2}{1+\frac{k-1}{2}M^2}\right)^{\frac{k}{k-1}}-1\right] \tag{5.4.16}$$

or

$$\left(\frac{kM_\infty^2}{2}C_p+1\right)^{\frac{k-1}{k}}\left(1+\frac{k-1}{2}M^2\right) = \left(1+\frac{k-1}{2}M_\infty^2\right). \tag{5.4.17}$$

When the disturbances are small, C_p will also be small and we can assume

$$\left(1+\frac{\varkappa M_\infty^2}{2}c_p\right)^{\frac{\varkappa-1}{\varkappa}}\approx 1+\frac{\varkappa-1}{2}c_p M_\infty^2.$$

Then, solving (5.4.17) for M^2, we obtain

$$M^2\approx M_\infty^2-\left(1+\frac{\varkappa-1}{2}M_\infty^2\right)M_\infty^2 c_p \qquad (5.4.18)$$

and from (5.4.15)

$$c_p=\frac{\tilde{c}_p}{\sqrt{1-M_\infty^2}+\frac{M_\infty^2\left(1+\frac{\varkappa-1}{2}M_\infty^2\right)\tilde{c}_p}{2\sqrt{1-M_\infty^2}}}. \qquad (5.4.19)$$

Laitone's solution is compared with the linearized one in the graph of Fig. 5.4.3. In what follows also the exacter solutions to (5.11.26) are given.

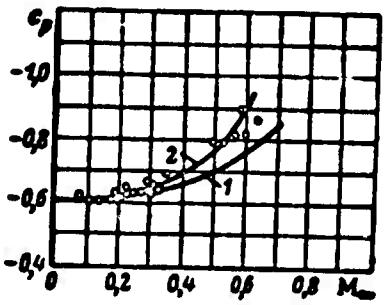


Fig. 5.4.3. Comparison of Eq. (5.4.14) – curve 1 – and the exacter Eq. (5.4.19) – curve 2 – with experiment.

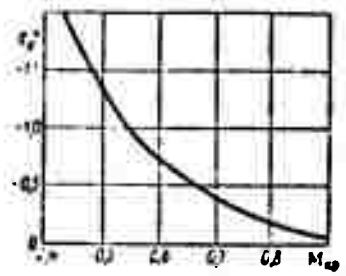


Fig. 5.4.4. Dependence of the critical pressure coefficient (corresponding to M = M* = 1) C_p^* on M_{kr}.

The critical Mach number M. The relations found allow us to determine the Mach number M of the undisturbed flow corresponding to the beginning of shock stall, i.e., to the appearance of regions near the body where the flow velocity is equal to the local velocity of sound. This Mach number M is termed critical and is denoted by M_{kr}.

From (5.4.16) we obtain the C_p^* values corresponding to M = 1

$$C_p^*=\frac{2}{\varkappa M_{cp}^2}\left[\left(\frac{1+\frac{\varkappa-1}{2}M_{cp}^2}{1+\frac{\varkappa-1}{2}}\right)^{\frac{\varkappa}{\varkappa-1}}-1\right]. \qquad (5.4.20)$$

C_p^* is shown as a function of M_{kr} in Fig. 5.4.4.

From (5.4.18) we obtain approximately

$$C_p^*=\frac{M_{cp}^2-1}{M_{cp}^2\left[1+\frac{\varkappa-1}{2}M_{cp}^2\right]}. \qquad (5.4.21)$$

5.5. THE LINEARIZED PLANE SUPERSONIC FLOW

General form of the solution to a linearized equation. For $M_\infty > 1$ the coefficients of the equation

$$(1-M_\infty^2)\frac{\partial^2\varphi}{\partial x^2}+\frac{\partial^2\varphi}{\partial y^2}=0 \qquad (5.5.1)$$

have different signs and the equation belongs to the hyperbolic group.

If we assume $m^2 = M_\infty^2 - 1$ the total integral of this equation will read

$$\varphi = w_\infty f_1(x-my) + w_\infty f_2(x+my), \qquad (5.5.2)$$

where $f_1(x - my)$ and $f_2(x + my)$ are arbitrary functions of $x - my$ and $x + my$, respectively, the forms of which are determined from the boundary conditions [cf. (2.7.10)].

Range of applicability of the solution. The linearization of the equations was based on the supposition (5.2.3) that

$$\frac{M_\infty^2\left|\frac{w'}{w_\infty}\right|}{M_\infty^2-1}\ll 1;\quad M_\infty^2\frac{|w'_y|}{w_\infty}\ll 1.$$

As was pointed out these equations lose their validity in the near-sonic range ($M_\infty \approx 1$), as they do when M_∞ is very large, namely in the hypersonic range.

If we take into account that w'_x/w_∞ and w'_y/w_∞ are of the same order of magnitude as the body's thickness ratio d/l we can say that the linearized equations are valid if

$$M_\infty^2\frac{d}{l}\ll 1\ ;\quad \frac{M_\infty^2}{M_\infty^2-1}\frac{d}{l}\ll 1.$$

Streamlines. We find from (5.5.2) that

$$w'_x=\frac{\partial\varphi}{\partial x}=w_\infty(f'_1+f'_2),\quad w'_y=\frac{\partial\varphi}{\partial y}=-w_\infty m(f'_1-f'_2). \qquad (5.5.3)$$

where f'_1 and f'_2 are the derivatives of f_1 and f_2 with respect to $(x - my)$ and $(x + my)$, respectively.

We then have for the streamlines

$$\frac{dy}{dx}=\frac{w_y}{w_x}=\frac{w'_y}{w_\infty+w'_x}=\frac{w'_y}{w_\infty}\left(1-\frac{w'_x}{w_\infty}\right)\approx$$
$$\approx\frac{w'_y}{w_\infty}=m(f'_2-f'_1). \qquad (5.5.4)$$

Since for the linearization we have assumed that $|w'_x|:w_\infty\ll 1$, we have for the case considered $M_\infty>1$, $|w'_y|:w_\infty\ll 1$ and $m\left|\frac{dy}{dx}\right|\ll 1$.

We can therefore write

$$dy=m(f'_2-f'_1)\,dx\approx m[f'_2(dx+m\,dy)-f'_1(dx-m\,dy)],$$

whence we obtain the streamline equation

$$y=m(f_2-f_1)+\text{const}. \qquad (5.5.5)$$

The pressure distribution. If we take (5.5.5) and (5.2.6) into account we can write

$$C_p=-2\frac{w'_x}{w_\infty}=-2(f'_1+f'_2)\approx\frac{2}{\sqrt{M_\infty^2-1}}\cdot\frac{f'_1+f'_2}{f'_1-f'_2}\cdot\frac{dy}{dx}. \qquad (5.5.6)$$

Characteristics. The general solution $\varphi=w_\infty(f_1+f_2)$ can be considered as the sum of the two particular solutions $\varphi_1=w_\infty f_1$ and $\varphi_2=w_\infty f_2$. Let us discuss each of them.

Let $f_2 = 0$. Then, assuming $x - my = \text{const}$ we find that along the set of straight lines $y=\frac{1}{m}x+\text{const}$ the disturbance potential $\varphi=w_\infty f_1(x-my)$ will have one and the same value; as has been said, these straight lines are called the characteristics or the Mach lines. Along these lines the pressure coefficient, the velocity of the disturbance, the slope of the streamlines, etc. will be constant. Thus, for example, the streamlines can be obtained by simply shifting one of them along the straight line

$$y=\frac{1}{m}x+\text{const}. \qquad (5.5.7)$$

The slope of these lines with respect to the x-axis is the direction of the undisturbed flow and is determined by the equation

$$\operatorname{tg}\mu=\frac{1}{m}=\frac{1}{\sqrt{M_\infty^2-1}},\quad \sin\mu=\frac{1}{M_\infty}=\frac{a_\infty}{w_\infty}. \qquad (5.5.8)$$

The second particular solution determines the second set of straight lines (Mach lines, waves) $y=-\frac{1}{m}x+\text{const}$, with the same properties.

Thus the whole space occupied by the moving gas is covered by the two families of characteristics: $y=\pm\frac{1}{m}x+\text{const}$. The characteristics $y=\frac{1}{m}x+C_1$, with the slope angle $+\mu$ above the axis will be called the + Mach lines and the lines $y=-\frac{1}{m}x+C_2$ are the − Mach lines and join the x-axis from below at the angle $(-\mu)$.

Choice of the sign of the characteristics. This choice is determined by the physical significance of the problem. Let us elucidate this by means of the example of a thin profile (Fig. 5.5.1). Let us assume that the region below the x-axis and the line abc is solid.

Since in a supersonic flow the disturbances can be propagated only downstream in the upper semiplane, only + Mach lines can arise, i.e., here $f_2 = 0$.

If we assume the upper semiplane to be solid, we find that in the lower semiplane only − Mach lines exist, for which $f_1 = 0$. This results in the form of motion shown in Fig. 5.5.1.

Flow about the outside of an obtuse angle. Let us consider a supersonic gas flow streaming at a velocity of $w_\infty = w_1$ about an angle greater than π, equal to $\pi + \vartheta$ with $\vartheta \ll \pi$ (Fig. 5.5.2). Let the coordinate origin be placed at the vertex of the angle (source of disturbances). Since in the shaded region there is no flow, $f_2 = 0$. The net of Mach lines resolves itself to only the + Mach lines.

For $-\infty \leq x \leq 0$, the streamline equation is $y = \text{const}$ and since $f_2 = 0$ from (5.5.5) follows that $f_1 = 0$. When $0 \leq x \leq \infty$ the streamline equation is $\frac{dy}{dx} = -\vartheta = -mf_1$, and integrating it we arrive at $f_1 = \frac{\vartheta}{m}(x - my) = \vartheta\left(\frac{x}{m} - y\right)$.

By virtue of (5.5.2) the disturbance potential is now obtained

in the form

$$\varphi = -w_1 \delta \left(y - \frac{x}{m} \right). \qquad (5.5.9)$$

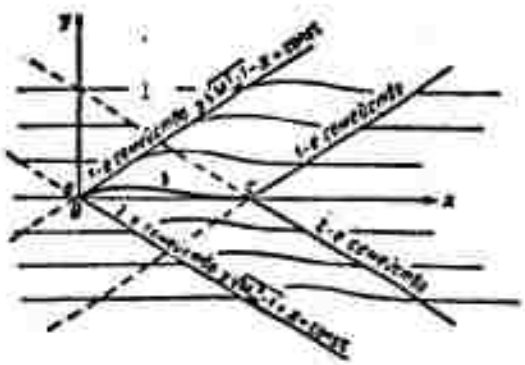


Fig. 5.5.1. In the upper semiplane (y > 0) the – Mach lines contradict the physical significance: in a supersonic flow the disturbances can be propagated only downstream and not upstream: the same holds for the + Mach lines in the lower semiplane (y < 0). 1) 1st family.

The components of the disturbance velocity are

$$w'_x = \frac{\partial \varphi}{\partial x} = \frac{\delta}{m} w_1, \quad w'_y = -w_1 \delta. \qquad (5.5.10)$$

When coming from the origin of coordinates at an angle of $\nu_1 = \operatorname{arctg} \frac{1}{\sqrt{M_\infty^2 - 1}}$, we meet no disturbances and the velocity potential is $\Phi_1 = w_1 x$ before the straight line $y = \frac{1}{m} x_{1_1}$. At this straight line the velocity w_1 receives at each point the increment w'_x and w'_y and the subsequent flow occurs at the velocity w_2 parallel to the wall OB.

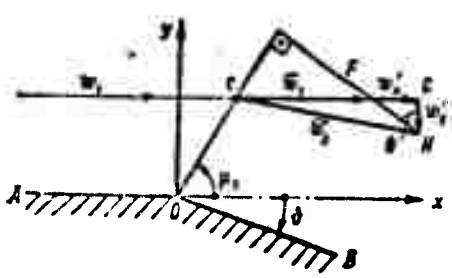


Fig. 5.5.2. Flow outside an obtuse angle.

It can be seen from the triangle FGH that the disturbance velocity vector w' is perpendicular to the disturbance lines.

Hence follows the method of constructing the velocity vector $\vec{w}_2$: we draw the straight line CH through the origin of the vector $\vec{w}_1$ parallel to the wall OB and another straight line through its tip, perpendicular

to the Mach line; point H where these straight lines intersect is the tip of the vector $\vec{w}_2$ and its origin will be at the point C.

The pressure coefficient

$$C_p = \frac{p_2 - p_1}{\frac{\rho_1 w_1^2}{2}} = -2\frac{w_x'}{w_1} = \frac{-2\vartheta}{m} = \frac{-2\vartheta}{\sqrt{M_1^2 - 1}} \qquad (5.5.11)$$

is negative, i.e., $p_2 < p_1$; the Mach lines in such a flow are called rarefaction lines.

Flow inside an obtuse angle. Let now the flow be inside the angle $\pi - \vartheta$ ($\vartheta \ll \pi$) (Fig. 5.5.3). Reversing all the considerations discussed above we obtain $f_2 = 0$ and, changing the sign of the angle $-\vartheta$ to $+\vartheta$,

$$\varphi = w_1 \vartheta \left(y - \frac{x}{m}\right); \qquad (5.5.12)$$

$$w_x' = -\frac{\vartheta}{m} w_1, \quad w_y' = w_1 \vartheta. \qquad (5.5.13)$$

Here the velocity is $w_2 < w_1$, the flow is slowed down and instead of rarefaction, the pressure increases, $p_2 > p_1$:

$$C_p = \frac{2(p_2 - p_1)}{\rho_1 w_1^2} = -2\frac{w_x'}{w_1} = \frac{2\vartheta}{\sqrt{M_1^2 - 1}}. \qquad (5.5.14)$$

When the pressure increases on passing through the Mach lines we shall denote the Mach lines as compression (pressure) lines (waves).

In what follows the rarefaction lines will be drawn in the figures as solid lines and the compression (pressure) lines as wavy lines.

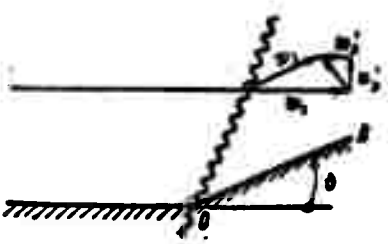


Fig. 5.5.3. Flow inside an obtuse angle.

Flow about a curvilinear wall. The flows inside and outside the obtuse angle considered are fundamental in the linearized theory of supersonic flows, and the flow about curvilinear contours can be reduced to them. For example, a slightly convex wall (shown in Fig. 5.5.4 by the dashed line) can be replaced by a polygon. In the roughest approximation (cf. Fig. 5.5.4,a) it can be replaced by an angle

$$w_x' = \frac{\theta}{\sqrt{M_\infty^2 - 1}}; \quad w_y' = w_1\theta; \quad C_p = -\frac{2\theta}{\sqrt{M_\infty^2 - 1}}.$$

All these quantities remain unchanged when the calculation is made more accurately (cf. Fig. 5.5.4,b) since $\theta = \theta_1 + \theta_2$. Replacing the wall curve by a polygon with a large number of sides makes it possible to construct the shape of the streamline in a more accurate manner.

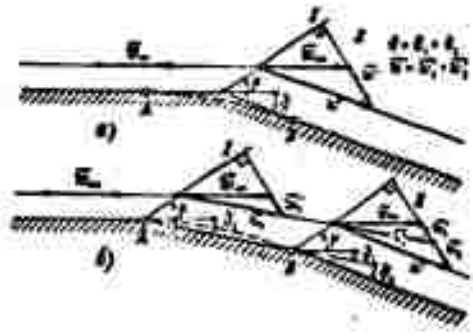


Fig. 5.5.4. Within the framework of the linearized theory the flow velocity in region II will be one and the same if it is calculated more roughly according to scheme a or more exactly according to scheme b. But with increasing number of subdivisions, the shape of the streamline becomes exacter.

5.6. A PLANE WING IN A SUPERSONIC FLOW

The plane plate. Figure 5.6.1 shows the Mach lines for a plate arranged at the angle of attack α in a supersonic flow. When passing through the line A1 the velocity increases and will be equal to

$$w_1 = \sqrt{(w_x' + w_1)^2 + w_y'^2} \approx w_1 + w_x'.$$

It decreases by the same amount on passing through the line B1, i.e., it becomes equal to w_1. The same happens if we trace any other streamline below AB. On the other side rarefaction will occur, $C_p = -2\frac{w_x'}{w_1} = -\frac{2\alpha}{\sqrt{M^2 - 1}}$, and the pressure at the lower side (cf. Fig. 5.6.1,a) will be of the same value.

The force N is normal to the plate and its coefficient is

$$N = \frac{4\alpha}{\sqrt{M_\infty^2 - 1}} b \frac{p_\infty - p_1}{2}, \quad C_N = \frac{4\alpha}{\sqrt{M_\infty^2 - 1}}. \qquad (5.6.1)$$

Hence the coefficients of lift, C_y, and drag, C_x, are obtained as

$$C_y = \frac{4\alpha}{\sqrt{M_\infty^2 - 1}}, \quad C_x = C_{N\alpha} = \frac{4\alpha^2}{\sqrt{M_\infty^2 - 1}}. \tag{5.6.2}$$

The pressure center will lie at the midpoint of the plate. The moment is therefore $M = R_y b/2$ and the coefficient of the moment

$$C_m = \frac{M}{\frac{\rho_1 w_1^2}{2} b^2} = \frac{2\alpha}{\sqrt{M_\infty^2 - 1}}. \tag{5.6.3}$$

The lift distribution, As has been shown, the fact that a lift appears at the plate in a subsonic flow is due to the appearance of a circulation whose magnitude is determined by the Zhukovskiy-Chaplygin

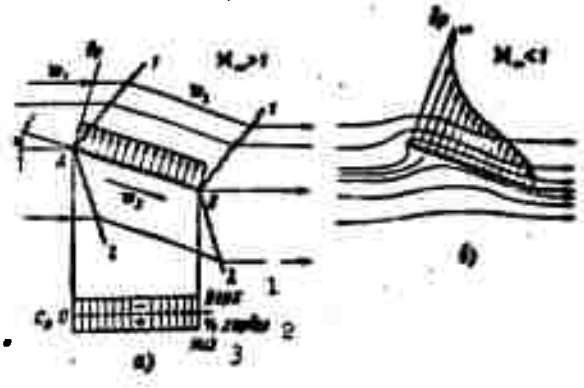


Fig. 5.6.1. Pressure distribution and Mach lines for a plane plate arranged at the angle α in a supersonic flow (a) and in a subsonic flow (b). 1) Above; 2) chord; 3) below.

condition. Since the pressures from below and above are equal in the trailing edge region, the pressure difference will vanish here and therefore the lift will be zero at the profile section in the trailing edge region. In a supersonic motion the lift at the rear edge will be finite.

The lift distribution about the leading edge will also be different in the two cases. For $M_\infty < 1$, theory predicts infinite lift density at the trailing edge where the flow induces negative pressure.

Wheb $M_\infty > 1$ a similar flow cannot occur at the leading edge and the difference between the pressure on the upper and lower surface remains finite (cf. Fig. 5.6.1).

Circulation and lift. We can satisfy ourselves that Zhukovskiy's lift formula applies to the linearized solution of the problem of a plate located in a supersonic flow. In fact, calculating the circulation around a plate (cf. Fig. 5.6.1) yields

$$\Gamma = b(w_2 - w_3) = b\left[\left(w_1 + \frac{\alpha}{m} w_1\right) - \left(w_1 - \frac{\alpha}{m} w_1\right)\right] = b \cdot 2 \frac{\alpha}{m} w_1$$

and the lift will therefore be

$$R_y = \rho_1 w_1 \Gamma = \frac{4\alpha}{\sqrt{M^2 - 1}} \frac{\rho_1 w_1^2}{2} b,$$

(assuming ρ = const), i.e., it is the same as that given by (5.6.1).

Drag. We have to notice the presence of a drag when considering a wing of infinite span in a supersonic flow. In a subsonic flow the lift-induced drag appears only in the case of a finite wing.

In a supersonic flow, regardless of the plate's span, the downwards directed velocity component will be $w_y = -w_1\alpha$. Applying Zhukovskiy's theorem (3.2) we obtain from this

$$R_x = \rho_1 w_1 \Gamma = \rho_1 w_1 \alpha b 2 \frac{\alpha}{m} w_1 = \frac{4\alpha^2}{\sqrt{M^2 - 1}} b \frac{\rho_1 w_1^2}{2},$$

which has also been found before. As will be shown in what follows, the drag does depend on the shape of the body. From the point of view of energy considerations it is connected with the formation of disturbances (waves) traveling to infinity, and it is therefore called the wave drag.

Arbitrary thin profile. Let us now consider a sufficiently thin arbitrary profile (Fig. 5.6.2). Let δl_v be an element of the upper surface inclined to the undisturbed flow at an angle of $\vartheta - \alpha$, and δl_n an element of the lower surface inclined at an angle of $\vartheta_n + \alpha$. Since the profile is thin, then, if we take the ξ -axis coincident

with the chord and the η -axis normal to the leading edge, we may write

$$u_0 = U_\infty = \text{const} \quad \theta_0 = \frac{\partial \eta_0}{\partial \xi};$$

$$\theta_0 = \frac{\partial \eta_0}{\partial x}.$$

Noticing that

$$C_{p,0} = -\frac{2}{\sqrt{M_\infty^2 - 1}}(\theta_0 - \alpha) \quad C_{p,0} = -\frac{2}{\sqrt{M_\infty^2 - 1}}(\theta_0 - \alpha),$$

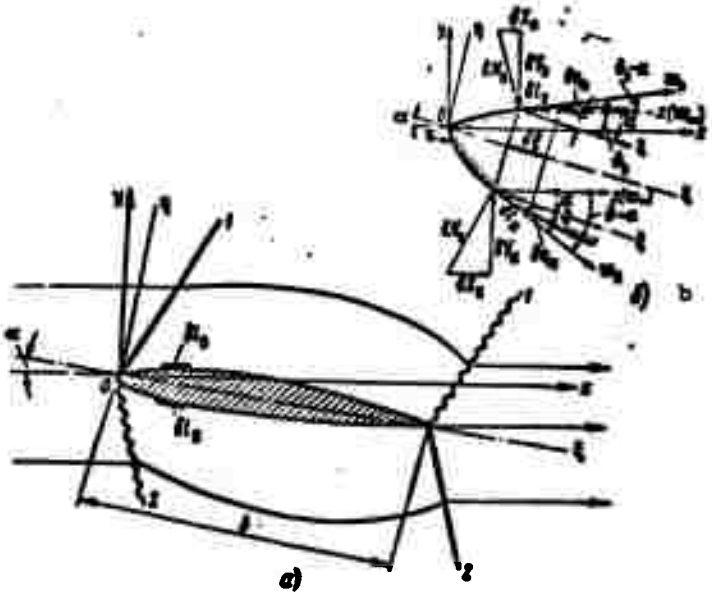


Fig. 5.6.2. Flow about an arbitrary thin profile (a). Profile element on large scale (b).

we obtain

$$R_y = \int_0^b (C_{p,0} - C_{p,0}) \frac{\rho_\infty w_\infty^2}{2} d\xi = \frac{2}{\sqrt{M_\infty^2 - 1}} \frac{\rho_\infty w_\infty^2}{2} \int_0^b \left[\left(\frac{d\eta_0}{d\xi} + \alpha\right) - \left(\frac{d\eta_0}{d\xi} - \alpha\right)\right] d\xi = \frac{2}{\sqrt{M_\infty^2 - 1}} \frac{\rho_\infty w_\infty^2}{2} 2b\alpha = \frac{4\alpha}{\sqrt{M_\infty^2 - 1}} b \frac{\rho_\infty w_\infty^2}{2}.$$

for the wing's lift, taking into account that

$$\int_0^b \left(\frac{d\eta_0}{d\xi}\right) d\xi = \int_0^b \left(\frac{d\eta_0}{d\xi}\right) d\xi = 0.$$

Consequently the lift coefficient

$$C_y = \frac{4\alpha}{\sqrt{M_\infty^2 - 1}} \qquad (5.6.4)$$

is independent of the shape of the profile. The profile's wave drag, however, depends on the lift and on the shape of the profile. In fact,

$$R_x = \int_0^b [C_{p_+}(\vartheta_+ + \alpha) + C_{p_-}(\vartheta_- - \alpha)] \frac{\rho_\infty v_\infty^2}{2} d\xi =$$

$$= \frac{2}{\sqrt{M_\infty^2 - 1}} \frac{\rho_\infty v_\infty^2}{2} \int_0^b \left[\left(\frac{d\eta_0}{d\xi} + \alpha \right)^2 + \left(\frac{d\eta_0}{d\xi} - \alpha \right) \right] d\xi =$$

$$= \frac{2}{\sqrt{M_\infty^2 - 1}} \frac{\rho_\infty v_\infty^2}{2} b \left\{ 2\alpha^2 + \frac{1}{b} \int_0^b \left[\left(\frac{d\eta_0}{d\xi} \right)^2 + \left(\frac{d\eta_0}{d\xi} \right)^2 \right] d\xi \right\}. \qquad (5.6.5)$$

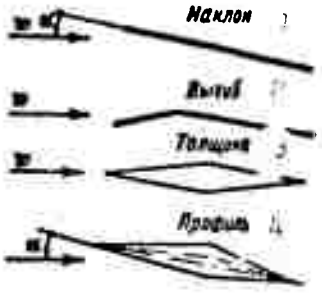


Fig. 5.6.3. The influences on the flow about a thin profile can in general be assumed to consist of the effect of a plate at the angle of attack of the profile, the bend of its camber line and the thickness. 1) Slope; 2) camber; 3) thickness; 4) profile.

The superposition principle. A slightly disturbed flow can be described by linear equations. This makes it possible to study the effects of the profile's camber, angle of attack, thickness, and bend separately. According to the superposition principle the result of several simultaneous effects exerted on the system considered is equal to the algebraic sum of the results which would be obtained if each of these effects were exerted separately. For example, the pressure distribution over the profile as shown in Fig. 5.6.3, can be found by adding the pressures caused by the effect of the angle of attack, the camber and the thickness, i.e., by summing the pressures exerted on three profiles: 1) a plane plate at the angle of attack of the profile, 2) the camber line of the profile considered at zero angle of attack, and 3) a symmetrical profile constructed from the thickness curve (3.6).

5.7. REFLECTION AND INTERSECTION OF WAVES

Reflection from a plane wall. Let us now consider a finite flow, for example, a supersonic flow in a channel (Fig. 5.7.1) with one wall

that has a break (flow about the outside of an obtuse angle near a plane wall).

A rarefaction wave (+ Mach line), coming from point O hits the plane wall at point 1. The flow behind the line O1 is deflected by the angle ϑ and therefore it must separate at point 1. The boundary condition requires that the flow does not become separated, i.e., at point 1 the flow must be deflected by the same angle ϑ. This will take place if a rarefaction wave (−Mach line) departs from point 1 (flow in the lower semiplane). Now, in order that the flow parallel to the wall CD does not separate at point 3, this point must be the origin of a rarefaction wave (+ Mach line), which again deflects the flow by the angle ϑ and so on. Since within the framework of the

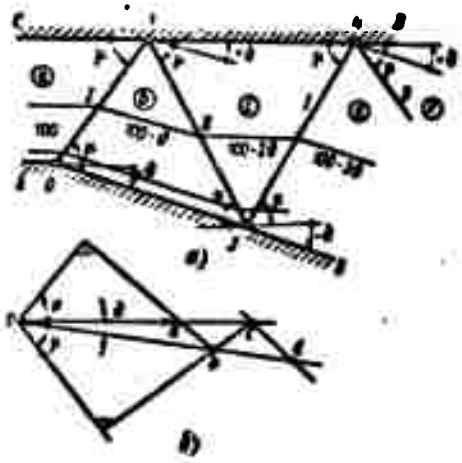


Fig. 5.7.1. The type of a wave remains unchanged when it is reflected from a plane wall; a rarefaction (compression) wave remains a rarefaction (compression) wave and in the linearized flow the angle of incidence is equal to the angle of reflection (a). Construction of velocity hodograph for the case of a wave reflected from a plane wall (b).

linearized theory the deflection angle is one and the same (ϑ) the wave 13 can be considered as the reflected wave O1, the angle of incidence being equal to the angle of reflection. The wave 34 can be considered as the wave 13 reflected from the wall OB, etc. Thus, when a wave is reflected from a plane wall the type of the wave remains

unchanged.

Change of pressure. It is found from the relation

$$C_p = \frac{p - p_\infty}{\frac{\rho_\infty v_\infty^2}{2}} = \frac{2\vartheta}{\sqrt{M_\infty^2 - 1}}. \qquad (5.7.1)$$

In practical calculations it is convenient to determine

$$\frac{p}{p_\infty} - 1 = \frac{2}{\sqrt{M_\infty^2 - 1}} \frac{\pi}{180^\circ} \vartheta^\circ \frac{\rho_\infty v_\infty^2}{2p_\infty} = \frac{1}{A} \vartheta^\circ,$$

where

$$\frac{1}{A} = \frac{2}{\sqrt{M_\infty^2 - 1}} \frac{\pi}{180^\circ} \frac{\rho_\infty v_\infty^2}{2p_\infty}, \quad A = \frac{\sqrt{M_\infty^2 - 1}}{k M_\infty^2} \frac{180^\circ}{\pi} \qquad (5.7.2)$$

or $\frac{\sqrt{M_\infty^2 - 1}}{k M_\infty^2} \frac{180^\circ}{\pi} \frac{p}{p_\infty} = A + \vartheta^\circ$. We determine the quantity P by the equation

$$P = A \frac{p}{p_\infty} = \frac{\sqrt{M_\infty^2 - 1}}{k M_\infty^2} \cdot \frac{180^\circ}{\pi} \cdot \frac{p}{p_\infty}; \qquad (5.7.3)$$

then, after having passed through a + Mach line, the increment δP of the quantity P will be

$$\left.\begin{array}{l} \delta P = \vartheta^\circ, \\ \text{and, after having passed through a} - \text{Mach line, it will be} \\ \delta P = -\vartheta^\circ. \end{array}\right\} \qquad (5.7.4)$$

The constant A is chosen here as a number convenient for the numerical calculations, e.g., 100.

In Fig. 5.7.1, when passing through the + Mach line 01 the angular increment amounts to $-\vartheta^\circ$, and the pressure in the range b is characterized by the quantity $100 - \vartheta^\circ$; when passing through the - Mach line 13, the angular increment $+\vartheta^\circ$ and, therefore, $P = \vartheta^\circ$, so that the pressure in the region c will be $100 - \vartheta - \vartheta = 100 - 2\vartheta$, etc.

The velocity hodograph. In the following we shall frequently make use of the velocity hodograph. In order to construct it, for example, in the case of a gas flow in a channel with a sharp bend in one of its walls (cf. Fig. 5.7.1), we construct the velocity vector of the undisturbed flow, Oa, originating at an arbitrary point O. In the region b the velocity vector will be Ob; its construction has been described

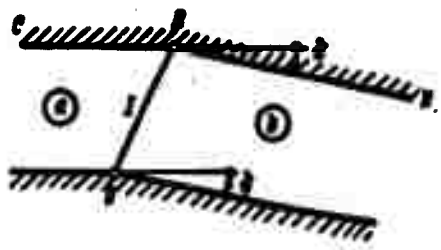


Fig. 5.7.2. Extinction of a wave by the sharp bend at point B in the wall CD.

when the flow outside the obtuse angle was considered and can moreover be seen from the figure. We continue to use the same method in order to construct the velocity vector in the region Oc, then the velocity vector Od in the region d, and so on; the velocity increases all the time, as it must do.

Extinction of a wave. Returning to the example discussed above, it can be shown that no reflection can occur if at point B the wall has a sharp bend whose angle is equal to ϑ (Fig. 5.7.2). The incident wave OB will be extinguished by the sharp bend in the wall.

Reflection of a wave from a free boundary. Let us now consider the flow from a free boundary where the pressure must remain unchanged ($p = \text{const}$). Let, for example, a uniform flow coming out of a nozzle whose upper wall is cut off and whose lower wall has a sharp bend with an angle of ϑ (Fig. 5.7.3).

The rarefaction wave O1 intersects the free boundary at point 1. Since the pressure must remain unchanged behind the rarefaction line in the region of point 1, it is necessary that a "compression wave" 12 departs from point 1; at the same time it is only the pressure change that keeps its value when the flow is deflected inwards by the angle ϑ. For the pressure to resume the initial value the flow must be deflected inwards once more by the angle ϑ, the total deflection thus amounting to an angle of 2ϑ. The compression wave 12 is reflected from the surface of the wall OB as a compression wave which, in turn, is reflected from the free surface as the rarefaction wave 34, and so on.

Thus, when waves are reflected from a free surface their type is

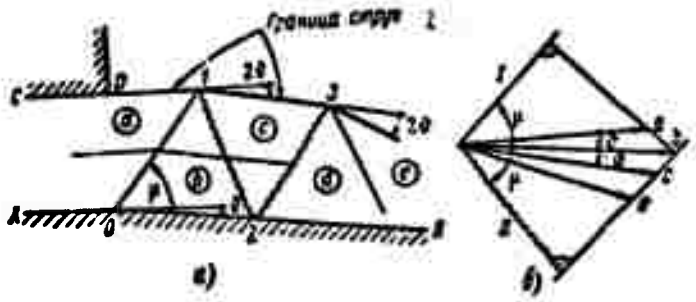


Fig. 5.7.3. When a wave is reflected from a free surface it changes in type (a). Velocity hodograph of the flow from a free surface (b). 1) Boundary of the jet.

changed to the opposite.

Intersection of waves. Let us consider a straight initially parallel channel with a sharp bend in the walls with the angles of ϑ_a and ϑ_b (Fig. 5.7.4,a).

From the vortices of the bend angles O' and O" a compression wave O'1' and a rarefaction wave O"1", respectively, depart. The state in region d can be determined if we go there from region a either through region b or thorugh c.

When passing through b

$$p_d-p_a=(p_d-p_b)+(p_b-p_a)=-(\vartheta_d-\vartheta_b)+(\vartheta_b-\vartheta_a)=\\=-\vartheta_d+2\vartheta_b-\vartheta_a.$$

When passing through region c

$$p_d-p_a=(p_d-p_c)+(p_c-p_a)=(\vartheta_d-\vartheta_c)-\\-(\vartheta_c-\vartheta_a)=\vartheta_d-2\vartheta_c+\vartheta_a.$$

Adding these equations yields

$$p_d-p_a=\vartheta_b-\vartheta_c;$$

substracting them yields

$$\vartheta_d+\vartheta_a=\vartheta_c+\vartheta_b.$$

Thus, when linearized waves intersect they do not interfere because of the linearity of the equation; each of the waves behaves as

if the others did not exist.

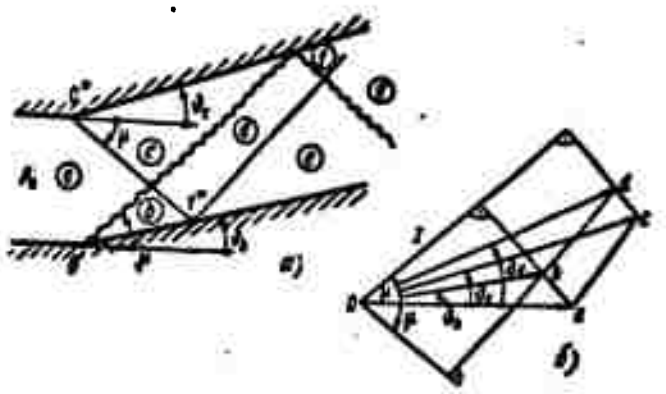


Fig. 5.7.4. When the waves intersect they do not interfere (a). Velocity hodograph for intersecting waves (b).

A nozzle under off-design conditions. The discussed cases of reflections and intersections of compression and rarefaction waves render it possible to construct the flow pattern at the outlet of a geometrical nozzle under off-design conditions (provided the deviations from the design system are small).

Figure 5.7.5,a describes a flow pattern construction for the case of overexpansion, when the pressure of the atmosphere into which the flow streams is higher than that in the jet. In this case two compression waves arise at the end of the nozzle, with intensities such that the pressure at the boundary of the jet is equal to atmospheric pressure (cf. Fig. 4.3.4).

Figure 5.7.5,b shows the pattern of a jet in the case of underexpansion. Instead of compression waves rarefaction waves arise at the end of the nozzle.

Regions of dependence and influence. As has been shown with $M_\infty > 1$ the general solution to the linearized equation of disturbance potential

$$m^2 \frac{\partial^2 \varphi}{\partial x^2} = \frac{\partial^2 \varphi}{\partial y^2}; \quad m^2 = M_\infty^2 - 1 = \operatorname{ctg}^2 \mu$$

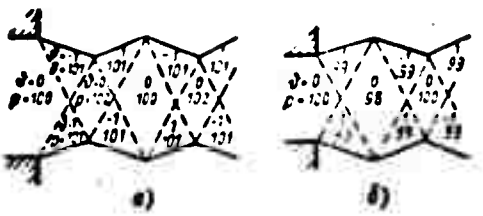


Fig. 5.7.5. Nozzle under off-design conditions. Flow pattern in the case of overexpansion (a). Flow pattern in the case of underexpansion (b).

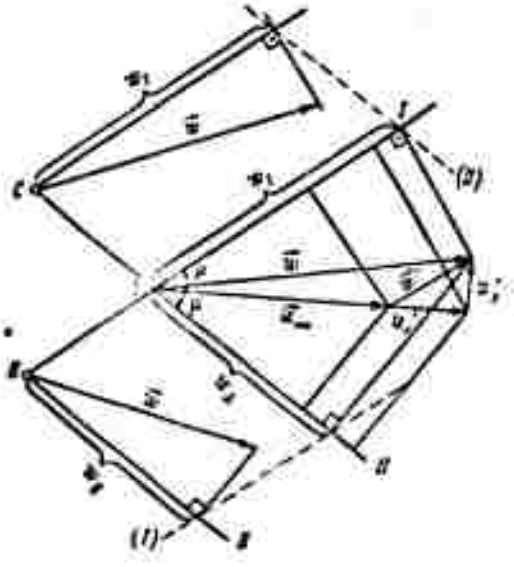


Fig. 5.7.6. Projection of the velocity vector on the Mach line.

has the form

$$\varphi = w_\infty f_1(x - my) + w_\infty f_2(x + my).$$

Taking into account that, owing to (5.5.4),

$$w'_x = \frac{\partial \varphi}{\partial x} = w_\infty (f'_1 + f'_2); \quad w'_y = m w_\infty (f'_2 - f'_1)$$

projecting the velocity vector $\vec{w}$ onto a + Mach line, and bearing in mind, we obtain $m \sin\mu = \frac{\sqrt{M_\infty^2 - 1}}{M_\infty} = \sqrt{1 - \frac{1}{M_\infty^2}} = \sqrt{1 - \sin^2\mu} = \cos\mu$

(Fig. 5.7.6):

$$w_I = w_\infty \cos\mu + w'_x \cos\mu + w'_y \sin\mu = w_\infty [\cos\mu + (f'_1 + f'_2)\cos\mu + (f'_2 - f'_1)\cos\mu] = w_\infty \cos\mu (1 + 2f'_2);$$

$$w_{II} = w_\infty \cos\mu + w'_x \cos\mu - w'_y \sin\mu = w_\infty \cos\mu (1 + 2f'_1).$$

Since $f_1^+ = \text{const}$ along a straight + Mach line, the projection w_{II} of the velocity vector $\vec{w}$ onto a straight – Mach line remains constant along the former. Similarly, when moving along a straight – Mach line the velocity vector projection onto the straight + Mach Line remains constant.

It follows from this that if the velocity vector is given for a certain line AB not coinciding with a characteristic (Mach line), then the velocity vector $\vec{w}$ in the rhomb ACBD is defined by this vector, the rhomb being formed by the characteristics passing through the points A and B (Fig. 5.7.7).

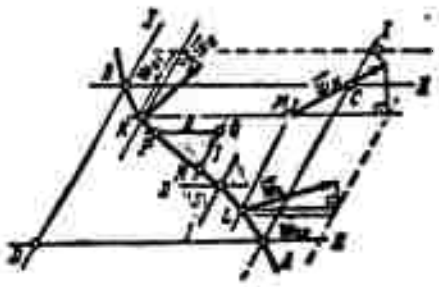


Fig. 5.7.7. If we know the velocity at points on the line AB we can determine the velocity at any point M inside the rhomb ABCD formed by the characteristics passing through the points A and B. The region PRQ is the region of dependence for point Q. The shaded region at point S is the region of its influence.

In fact, the velocity projection at point M onto the straight line II must be equal to the given projection of the velocity $\vec{w}_2$ at point L onto the same straight line, w_{LII}. Exactly the same projection of the velocity vector $\vec{w}_M$ onto a + Mach line, w_{MI}, must be equal to the given projection w_{KI} of the velocity vector $\vec{w}_K$ onto a + Mach line, whence we obtain the velocity vector $\vec{w}_M$.

The state at the point Q is determined by the conditions on the arc PR on which the changes of state at the sections AR and BP have no influence; therefore the region PRQ is called the region of dependence for point Q.

The change in flow conditions at point S can become apparent only in the shaded region bounded by characteristics passing through this point, and lying downstream of it. This region is therefore termed

the region of influence (effect) for point S.

5.8. CHARACTERISTICS

Mach lines as characteristics. In plane slightly disturbed supersonic flows, described by the linearized equation (for the disturbance potential φ)

$$(1-M^2)\frac{\partial^2\varphi}{\partial x^2}+\frac{\partial^2\varphi}{\partial y^2}=0 \qquad (M=\text{const}),$$

two families of straight lines have been found to exist:

$$x-my=C_1,\quad x+my=C_2, \tag{5.8.1}$$

along which all parameters of motion remain constant; these are the families of the characteristics. The tangent of the angle of slope of these straight lines to the x-axis, more exactly, to the velocity vector, is

$$\tan\mu=\frac{dy}{dx}=\pm\frac{1}{m}=\frac{1}{\sqrt{M^2-1}};\quad \sin\mu=\frac{a}{w}. \tag{5.8.2}$$

Thus, the characteristics or Mach lines bound the region of disturbed motion. In subsonic flows no such lines exist. All the parameters of its motion vary continuously and in a steady flow these variations cover the whole region occupied by the flow.

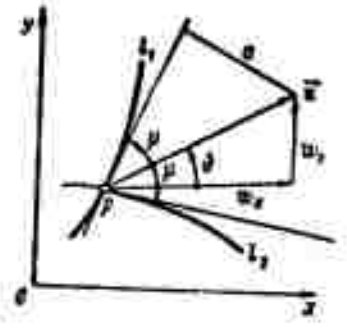


Fig. 5.8.1. The direction of the characteristics will be changed together with the Mach number M.

If the disturbances in the supersonic flow are not small then we shall obtain the following equation for the velocity potential:

$$(w_x^2-a^2)\frac{\partial^2\Phi}{\partial x^2}+2w_xw_y\frac{\partial^2\Phi}{\partial x\,\partial y}+(w_y^2-a^2)\frac{\partial^2\Phi}{\partial y^2}=0; \tag{5.8.3}$$

the characteristics for each flow determined by Eq. (5.8.3) will now be its own. Considering an arbitrary flow we find its Mach angle defined by the relation $\sin\mu = a/w$ and define

as a characteristic any line whose tangent to any point of it subtends the angle μ to the direction of the velocity at this point. Two characteristics l_1 and l_2 will pass through each point of the flow (Fig. 5.8.1), their angular coefficients being determined by the relations

$$y'_{I,II}=\left(\frac{dy}{dx}\right)_{I,II}=\operatorname{tg}(\theta\pm\mu). \tag{5.8.4}$$

Noticing that

$$\operatorname{tg}(\alpha\pm\beta)=\frac{\operatorname{tg}\alpha\pm\operatorname{tg}\beta}{1\mp\operatorname{tg}\alpha\operatorname{tg}\beta};\quad \operatorname{tg}\theta=\frac{w_y}{w_x};\quad \operatorname{tg}\mu=\frac{a}{\sqrt{w^2-a^2}},$$

we can write

$$\left.\begin{aligned} y'_I&=\left(\frac{dy}{dx}\right)_I=\frac{\operatorname{tg}\theta+\operatorname{tg}\mu}{1-\operatorname{tg}\theta\operatorname{tg}\mu}=\frac{\dfrac{w_y}{w_x}+\dfrac{a}{\sqrt{w^2-a^2}}}{1-\dfrac{w_y}{w_x}\dfrac{a}{\sqrt{w^2-a^2}}};\\ y'_{II}&=\left(\frac{dy}{dx}\right)_{II}=\frac{\operatorname{tg}\theta-\operatorname{tg}\mu}{1+\operatorname{tg}\theta\cdot\operatorname{tg}\mu}=\frac{\dfrac{w_y}{w_x}-\dfrac{a}{\sqrt{w^2-a^2}}}{1+\dfrac{w_y}{w_x}\dfrac{a}{\sqrt{w^2-a^2}}}. \end{aligned}\right\} \tag{5.8.5}$$

But when z_1 and z_2 are the roots of the quadratic equation $z^2 + pz + q = 0$, then $z_1 + z_2 = -p$ and $z_1 z_2 = q$, and therefore, assuming $z_1 = y'_I$, $z_2 = y'_{II}$, we obtain the differential equation of the characteristics

$$(w_x^2-a^2)\left(\frac{dy}{dx}\right)^2-2w_xw_y\frac{dy}{dx}+(w_y^2-a^2)=0. \tag{5.8.6}$$

Equations (5.8.4) and (5.8.5) can be written in the form

$$\left(\frac{dy}{dx}\right)_{I,II}=\frac{w_xw_y\pm a\sqrt{w^2-a^2}}{w_x^2-a^2}. \tag{5.8.7}$$

In the general case of a quasilinear second-order partial differential equation

$$A\frac{\partial^2\Phi}{\partial x^2}+2B\frac{\partial^2\Phi}{\partial x\,\partial y}+C\frac{\partial^2\Phi}{\partial y^2}+D\frac{\partial\Phi}{\partial x}+E\frac{\partial\Phi}{\partial y}+F=0, \tag{5.8.8}$$

where A, B, C, ... can be functions of x, y, Φ, $\partial\Phi/\partial x$, and $\partial\Phi/\partial y$, the characteristics equations are introduced for each solution and are determined by the relation

$$A\left(\frac{dy}{dx}\right)^2 - 2B\frac{dy}{dx} + C = 0. \qquad (5.8.9)$$

In accordance with this,

$$\frac{dy}{dx} = \frac{B \pm \sqrt{B^2 - AC}}{A}. \qquad (5.8.10)$$

Velocity variation along the characteristics. It is possible to determine the characteristics in the x,y-plane and the integrals of the differential Eq. (5.8.3) when we know the velocity field $w_x(x,y)$, $w_y(x,y)$, i.e., when we have found a solution to the basic system (5.8.3), (5.8.6).

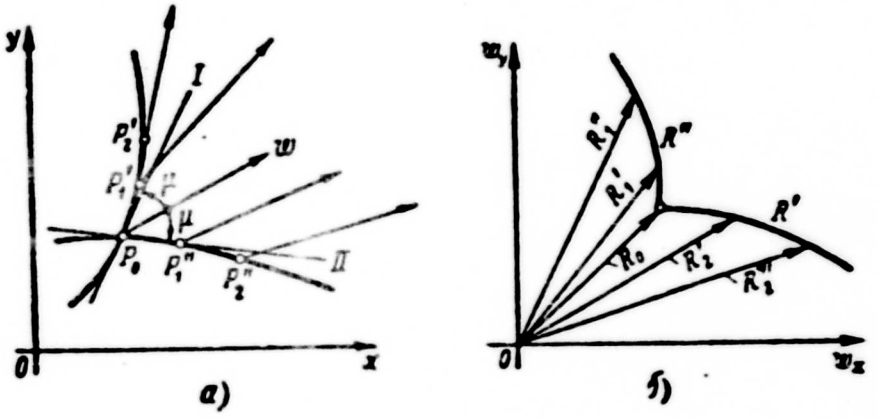


Fig. 5.8.2. The relation linking w_x and w_y on the characteristics of the (x,y)-plane can be considered as a mapping of these characteristics on the hodograph plane w_x, w_y. a) Physical plane; b) plane of velocity hodograph.

It is possible, however, to determine the relation between w_x (x,y) and w_y (x,y) along these characteristics independently of a solution to System (5.8.3), (5.8.6). The relation between w_x (x,y) and w_y (x,y) on the characteristics of the (x,y)-plane can be considered as a mapping of these characteristics on the hodograph plane ($w_x w_y$), and the curves R' and R" (Fig. 5.8.2) determining this relation are called the characteristics in the hodograph plane.

Let us now determine the relation between the changes of w_y and w_x, i.e., between dw_y and dw_x, when x and y vary along the characteristics; dy and dx are linked by Eq. (5.8.7) or, in general form,

by (5.8.10)

$$dy = m_{1,II}\,dx = \frac{B \pm \sqrt{B^2 - AC}}{A}\,dx,$$

where $m_I = \frac{dy}{dx} = \frac{B + \sqrt{B^2 - AC}}{A}$ for the first family and $m_{II} = \frac{dy}{dx_{II}} = \frac{B - \sqrt{B^2 - AC}}{A}$ for the second family.

We have

$$dw_y = \frac{\partial w_y}{\partial x}dx + \frac{\partial w_y}{\partial y}dy = \left(\frac{\partial w_y}{\partial x} + m_{1,II}\frac{\partial w_y}{\partial y}\right)dx;$$

$$dw_x = \frac{\partial w_x}{\partial x}dx + \frac{\partial w_x}{\partial y}dy = \left(\frac{\partial w_x}{\partial x} + m_{1,II}\frac{\partial w_x}{\partial y}\right)dx.$$

Since the flow is a potential flow, $\frac{\partial w_x}{\partial y} = \frac{\partial w_y}{\partial x}$, and

$$dw_x = \left(\frac{\partial w_x}{\partial x} + m_{1,II}\frac{\partial w_y}{\partial x}\right)dx; \quad dw_y = \left(\frac{\partial w_x}{\partial y} + m_{1,II}\frac{\partial w_y}{\partial y}\right)dx.$$

Determining from (5.8.3)

$$\frac{\partial w_x}{\partial x} = -\frac{2w_x w_y}{w_x^2 - a^2}\frac{\partial w_x}{\partial y} - \frac{w_y^2 - a^2}{w_x^2 - a^2}\frac{\partial w_y}{\partial y}$$

and using the notations $A = w_x^2 - a^2$, $B = w_x w_y$, $C = w_y^2 - a^2$, we obtain

$$dw_x = \left(\frac{\partial w_x}{\partial x} + m_{1,II}\frac{\partial w_y}{\partial x}\right)dx = \left(-\frac{2B}{A}\frac{\partial w_x}{\partial y} - \frac{C}{A}\frac{\partial w_y}{\partial y} + \right.$$

$$\left. + m_{1,II}\frac{\partial w_y}{\partial x}\right)dx = -\frac{2B - m_{1,II}A}{A}\left[\frac{\partial w_x}{\partial y} + \frac{C}{m_{1,II}A}\frac{\partial w_y}{\partial y}\right]dx.$$

But

$$m_{1,II}^2 A - 2Bm_{1,II} + C = 0,$$

whence

$$\frac{C}{2B - m_{1,II}A} = m_{1,II}; \quad \frac{C}{A} = m_I \cdot m_{II}.$$

Therefore

$$dw_x = -\frac{C}{Am_{1,II}}\left(\frac{\partial w_x}{\partial y} + m_{1,II}\frac{\partial w_y}{\partial y}\right)dx = -\frac{C}{Am_{1,II}}dw_y =$$

$$= -\frac{m_I \cdot m_{II}}{m_{1,II}}dw_y$$

or

$$\frac{dw_y}{dw_x} = -\frac{m_{1,II}}{m_I m_{II}} = n_{1,II}. \qquad (5.8.11)$$

Thus, if x and y vary along the + Mach lines in the x,y-plane ($m_{I,II} = m_I$), then w_x and w_y vary in accordance with the equation

$$\left(\frac{dw_y}{dw_x}\right)_I = n_I = -\frac{1}{m_{II}} = -\frac{A}{B-\sqrt{B^2-AC}} = -\frac{w_x^2-a^2}{w_xw_y-a\sqrt{w^2-a^2}},$$

and if along the second family ($m_{I,II} = m_{II}$), then

$$\left(\frac{dw_y}{dw_x}\right)_{II} = n_{II} = -\frac{1}{m_I} = -\frac{A}{B+\sqrt{B^2-AC}} = -\frac{w_x^2-a^2}{w_xw_y+a\sqrt{w^2-a^2}}.$$

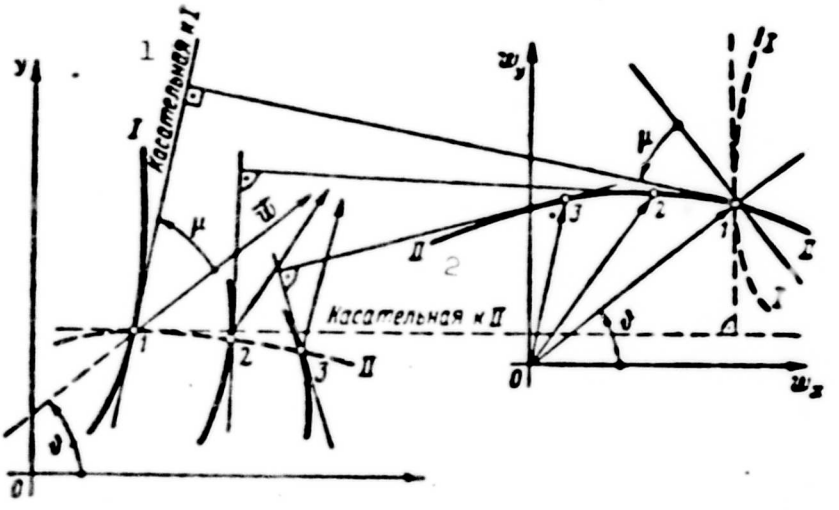


Fig. 5.8.3. The normal to the + Mach line in the physical x,y-plane is the tangent at the corresponding point to the – Mach line in the velocity hodograph plane w_x, w_y. 1) Tangent to I; 2) tangent to II.

Here we have

$$\left(\frac{dy}{dx}\right)_{I,II} \cdot \left(\frac{dw_y}{dw_x}\right)_{II,I} = -1, \qquad (5.8.12)$$

i.e., the normal to the tangent of the + Mach line in the physical plane of the flow is a tangent at the corresponding point to the – Mach line in the hodograph plane (Fig. 5.8.3).

Equation of the characteristics in the velocity hodograph plane. Equation (5.8.11) is a differential equation in the variables w_x and w_y. Since it does not contain the variables x and y, the characteristics in the velocity hodograph plane have one and the same shape for all flows in the physical plane, but the characteristics in the physical plane will be different.

In order to integrate Eq. (5.8.11) we introduce the polar coordinates w and ϑ:

$$w_x = w\cos\theta = a^* M^* \cos\theta; \quad w_y = w\sin\theta = a^* M^* \sin\theta,$$

Noticing that when $\underline{w}$ varies along the characteristics (Fig. 5.8.4), $\pm \operatorname{tg}\mu = \frac{dw}{w\,d\theta} = \frac{1}{\sqrt{M^2-1}}$, holds in the hodograph plane, we have

$$d\theta = \pm \frac{dw}{w} \operatorname{ctg}\mu = \pm \frac{dw}{w}\sqrt{M^2-1}$$

or, by virtue of (4.2.8),

$$d\theta = \pm \frac{dM^*}{M^*}\sqrt{\frac{2}{k+1}\frac{M^{*2}}{1-\frac{k-1}{k+1}M^{*2}} - 1} = \pm\sqrt{\frac{M^{*2}-1}{1-\frac{k-1}{k+1}M^{*2}}}\frac{dM^*}{M^*}. \tag{5.8.13}$$

In order to integrate this equation we put

$$\operatorname{ctg}\mu = \sqrt{\frac{M^{*2}-1}{\frac{k-1}{k+1}\left(\frac{k+1}{k-1} - M^{*2}\right)}} = K\sqrt{\frac{M^{*2}-1}{K^2 - M^{*2}}} = z \quad \left(K^2 = \frac{k+1}{k-1}\right).$$

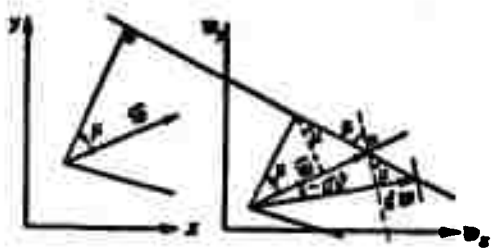


Fig. 5.8.4. For deriving the equation of the characteristics in the velocity hodograph plane.

Then

$$z^2 = K^2\frac{M^{*2}-1}{K^2-M^{*2}}; \quad M^{*2} = K^2\frac{z^2+1}{z^2+K^2}.$$

Differentiating this gives

$$\frac{dM^*}{M^*} = K^2\left(\frac{z}{z^2+1} - \frac{z}{z^2+K^2}\right)dz.$$

Therefore

$$\pm d\theta = \frac{dM^*}{M^*}\operatorname{ctg}\mu = K^2\left(\frac{z^2}{z^2+1} - \frac{z^2}{z^2+K^2}\right)dz = K^2\left(\frac{K^2}{z^2+K^2} - \frac{1}{z^2+1}\right)dz.$$

When we integrate we obtain

$$\pm\theta = \sqrt{\frac{k+1}{k-1}}\operatorname{arctg}\sqrt{\frac{M^{*2}-1}{\frac{k+1}{k-1}-M^{*2}}} - \operatorname{arctg}\sqrt{\frac{M^{*2}-1}{1-\frac{k-1}{k+1}M^{*2}}} + \theta_0 = \nu(M^*) + \theta_0. \tag{5.8.14}$$

$$\sqrt{\frac{k+1}{k-1}}\operatorname{arctg}\sqrt{\frac{k-1}{k+1}(M^2-1)}-\operatorname{arctg}\sqrt{M^2-1}+\vartheta_0=\nu(M)+\vartheta_0. \qquad (5.8.14)$$

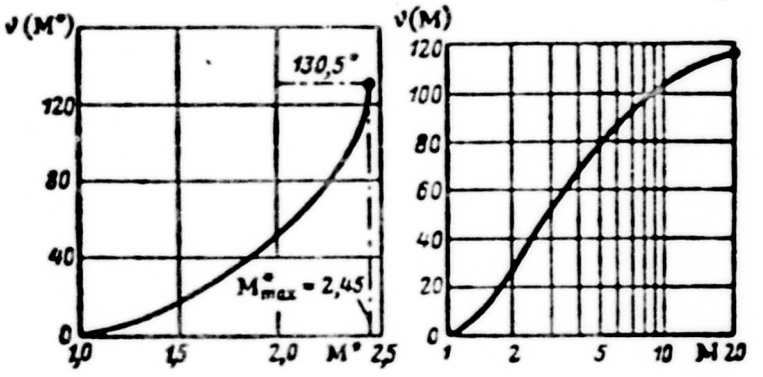


Fig. 5.8.5. The angle ν as a function of M* and as a function of M for K = 1.4.

Figure 5.8.5 gives the values of ν (in degrees) as functions of M* and M for k = 1.4.

The two curves $\vartheta=\nu(M)+\vartheta_0$ and $-\vartheta=\nu(M)+\vartheta_0$ are epicycloids (Fig. 5.8.6,b).

Since M* = 1 corresponds to w = a* and $M^*_{max}=\sqrt{\frac{k+1}{k-1}}$ these epicycloids are obtained by rolling the circle of radius $\frac{1}{2}\left(\sqrt{\frac{k+1}{k-1}}-1\right)a^*$ about the circle of radius a (M* = 1) with no slipping.

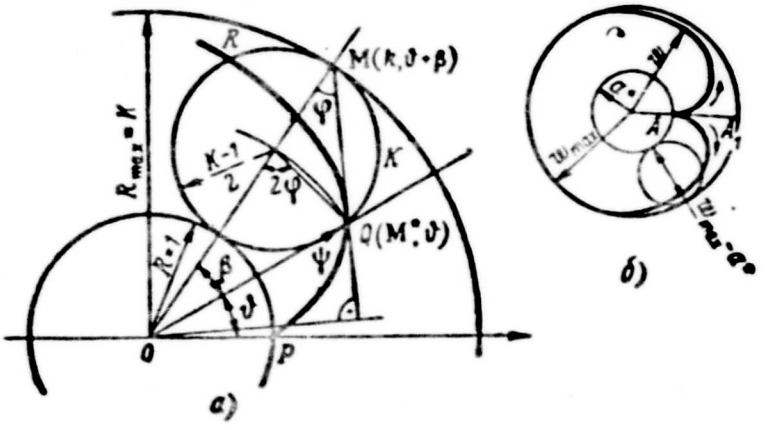


Fig. 5.8.6. The epicycloid PQR is obtained by rolling the circle K of radius (K-1)/2 round the unit circle (a). The constructed epicycloid (b).

In fact (cf. Fig. 5.8.6,a), the epicycloid equation for a circle of radius (K-1)/2 rolling around a unit circle is

$$(\vartheta+\beta)=\frac{1}{2}(K-1)2\varphi.$$

Since $\beta + \varphi = \psi$, we have

$$\vartheta=(K-1)\varphi-\beta=K\varphi-\psi. \qquad (5.8.15)$$

From the triangle OQM we have

$$M^{*2}=K^2+[(K-1)\cos\varphi]^2-2K(K-1)\cos^2\varphi,$$

whence

$$\cos^2\varphi=\frac{K^2-M^{*2}}{K^2-1};\quad \operatorname{tg}^2\varphi=\frac{M^{*2}-1}{K^2-M^{*2}}.$$

Moreover,

$$\operatorname{tg}\psi=\frac{K\sin\varphi}{K\cos\varphi-(K-1)\cos\varphi}=K\operatorname{tg}\varphi=K\sqrt{\frac{M^{*2}-1}{K^2-M^{*2}}}.$$

Substituting the results in (5.8.15) we obtain

$$\vartheta=K\operatorname{arc\,tg}\sqrt{\frac{M^{*2}-1}{K^2-M^{*2}}}-\operatorname{arc\,tg}K\sqrt{\frac{M^{*2}-1}{K^2-M^{*2}}}. \qquad (5.8.16)$$

which agrees with (5.8.14).

An arbitrary characteristic is obtained from a base corresponding to C = 0 either by rotating it through an arbitrary angle ϑ_0 or by mirror reflection in the real axis x (the angle ϑ changes sign).

Choice of the constant in the characteristics equation. The characteristics in the velocity hodograph plane differ from each other by a constant, C, entering Eq. (5.8.14). It is therefore convenient to enumerate the characteristics in such a way as to make the calculatory operations in practical applications as simple as possible.

Let us assume

$$\vartheta=\nu(M^*)-C_1;$$
$$-\vartheta=\nu(M^*)-C_2.$$

Then

$$\nu(M^*)=\frac{C_1+C_2}{2};\quad \vartheta=\frac{C_2-C_1}{2}.$$

Therefore, if we re-enumerate the epicycloid so that the velocity direction (angle ϑ) corresponds to the difference of the numbers of

the epicycloids passing through one and the same point on the hodograph plane, then the variation of the angle $\nu(M^*)$ and hence of M^* (i.e., of the magnitude of the velocity $\underline{w}$) will depend on the sum of these two numbers. Besides, each pair of epicycloids for which the difference of the numbers is constant must intersect at one and the same radius ϑ, and the epicycloids having one and the same value of the sum of the numbers will intersect at the points of one circle M^*.

$$C_1 = 1200 - 2q, \quad C_2 = 800 - 2s, \tag{5.8.17}$$

is frequently taken, where $\underline{q}$ and $\underline{s}$ are the epicycloid numbers.

Then

$$\vartheta = \frac{C_2 - C_1}{2} = -200 - s + q = (q - s) - 200;$$

$$\nu(M^*) = \frac{C_1 + C_2}{2} = 1000 - q - s = 1000 - (q + s).$$

Figure 5.8.7 shows epicycloids and their enumeration. A diagram of the characteristics for k = 1.4 is given in Appendix 6., and the values of $\nu(M^*)$ are tabulated in Appendix 8.

The adiabatic ellipse. If the x-axis is directed along the tangent to a Mach line and the y-axis is perpendicular to it then (Fig. 5.8.8)

$$\sin\mu = \frac{a}{w} = \frac{w_y}{w}.$$

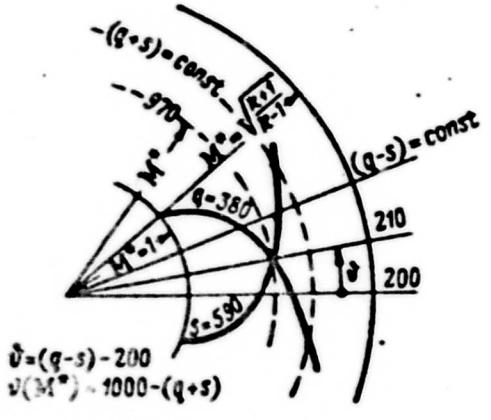


Fig. 5.8.7. Enumeration of characteristics.

By comparison we find that the velocity projection on the y-axis is equal to sonic velocity:

$$a^2 = \frac{k+1}{2}a^{*2} - \frac{k-1}{2}(w_x^2 + w_y^2) = w_y^2,$$

whence

$$\frac{w_x^2}{\frac{k+1}{k-1}a^{*2}} + \frac{w_y^2}{a^{*2}} = 1. \tag{5.8.18}$$

The ratio of the axes of the ellipse (5.8.18), which is called the adiabatic ellipse, depends only on the number $k = c_p/c_v$. The major semiaxis is

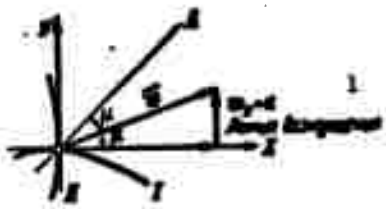


Fig. 5.8.8. The projection of the velocity vector onto the normal to a characteristic at any point is equal to the velocity of sound at this point. 1) Mach line.

equal to $\sqrt{\frac{k+1}{k-1}}a^*$, and the minor semi-axis to a^*. One certain ellipse can therefore be used to analyze arbitrary motions of one certain gas (that gas whose $\underline{k}$ is equal to the $\underline{k}$ of the ellipse). In order to determine the direction of the characteristics the center of the ellipse is placed at the origin of the velocity vector at the point considered and the ellipse is rotated until the tip of the velocity vector comes to lie on it (Fig. 5.8.9). This will occur in two positions of the adiabatic ellipse and in each of these the major axis will be directed along the tangent to the characteristic.

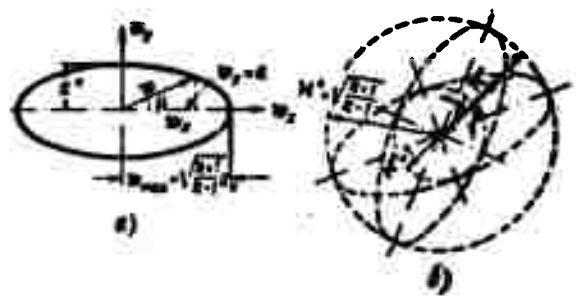


Fig. 5.8.9. Adiabatic ellipse for supersonic flow analysis (a). If we draw the velocity vector at any point on the ellipse, the major axis will be the tangent to a characteristic (b).

Four basic problems on potential gas flow solved by the method of characteristics (Fig. 5.8.10). I. The velocity distribution is given for the line AB which is not a characteristic in the physical x,y-plane. Find the velocity distribution in the region bounded by the line AB and a pair of Mach lines, one plus and one minus, passing through the points A and B. These two characteristics are assumed to

be given.

II. The velocity distribution is given along a plus and a minus Mach line, AB and AC. Determine the velocity distribution in the field bounded by these Mach lines and two other Mach lines passing through points B and C, respectively, and intersecting at point D, which are also assumed to be given.

III. The velocity distribution is given along the characteristic AB which intersects a solid wall at point A. Find the velocity distribution in a region bounded by this wall, a given characteristic AB and the characteristic BC intersecting the wall at point C, which is also to be determined.

IV. The velocity distribution is given along a certain characteristic AB intersecting the free surface AC. Find the velocity distribution in the region bounded by AB, AC and a minus Mach line. This problem differs from problem III in that the velocity direction along AC is not given and in that the pressure is constant over the free surface, p = const, so that

$$M^* = \sqrt{\frac{k+1}{k-1}}\sqrt{1-\left(\frac{p}{p_0}\right)^{\frac{k-1}{k}}} = \text{const.}$$

The boundary conditions to these four basic problems allow us to construct the net of characteristics inside the given region and so to obtain the solutions. The net of characteristics is constructed in an approximate manner, by replacing the curved lines on which the boundary conditions are given by the sides of a polygon. The more sides we take, the more accurate is the solution. Let us demonstrate here the solution of problem I; for details we refer, for example, to the course by N. Ye. Kochin, I.A. Kibel' and N.V. Roze in "Theoreticheskaya gidromekhanika" (Theoretical Hydromechanics) [5.5].

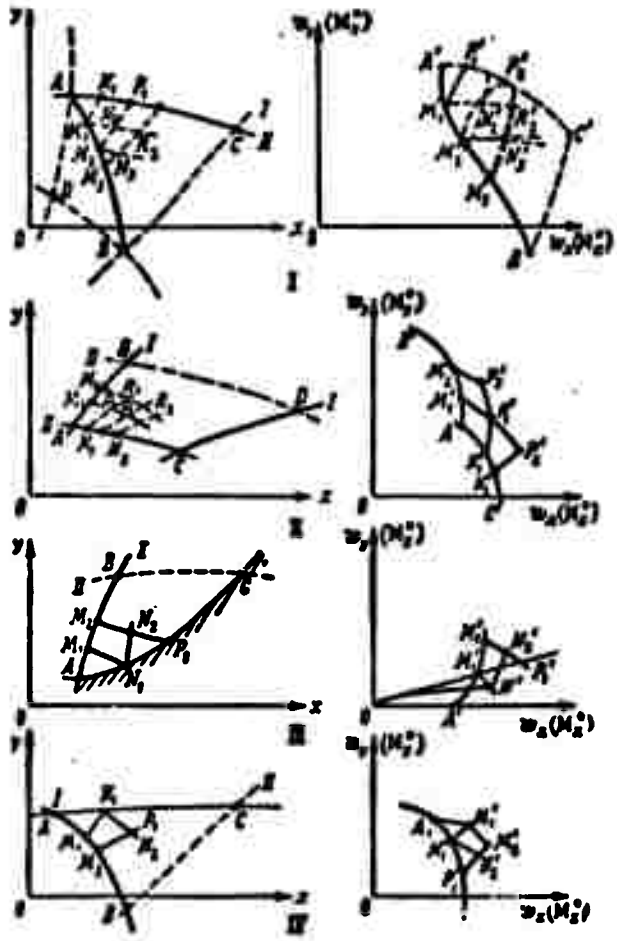


Fig. 5.8.10. If the velocity distribution is given on the line AB, which is not a characteristic, the velocity distribution can be found in the region bounded by AB and a plus and a minus Mach line (I). Knowing the velocity distribution on a plus and a minus Mach line, AB and AC, we can find the velocity distribution in the region bounded by these Mach lines and their conjugates, BD and CD (II).
We can find the velocity field in a region bounded by a solid wall, the Mach line AB with a given velocity distribution, and the characteristic BC (III).
From the given velocity distribution along a characteristic AB the velocity distribution can be determined in the region bounded by AB, a free surface AC and a – Mach line (IV).

Replacing the curve AB by the polygon $AM_1M_2M_3\ldots$ we construct its image on the hodograph plane, $A'M_1'M_2'M_3'\ldots$ Then, with the help of the adiabatic ellipse we mark at each point A, M_1, M_2,... the Mach line elements, i.e., the characteristics AP_1, M_1P_1, M_1N_1, M_2N_2,... etc.

In order to determine the velocities at the points of intersection P_1, N_2, N_3,... we can use the net of characteristics. To the motion with respect to the elements, for example, of the –Mach line M_1N_2, on the hodograph plane will correspond the motion with respect to the epicycloid of the + Mach line M_1' N_2', and to the motion with respect to the element of the + Mach line M_2N_2 will correspond the motion with respect to the epicycloid of the – Mach line M_2' N_2'. Their intersection determines the point N_2' – point N_2 of the image. Thus we find the velocity at the points N_3, N_4,... – and can hence construct the velocity distribution on the line P_1, N_2, N_3,... and its image P_1' N_2' N_3' .. Repeating the process for this line, we can construct the line $P_2R_2R_3$... and so on, until the region ABC is completely covered and thus also region ABC.

The streamlines can easily be drawn since we know that the velocity at each point is directed along the bisector of the angle enclosed by the characteristics. The pressure is determined by the Bernoulli equation.

5.9. FINITE DISTURBANCES IN A SUPERSONIC FLOW

Classification of discontinuities. Surfaces which impose a jump on the parameters characterizing the state of a gas that pass through them are called discontinuity surfaces. They are tangential if the velocity of the flow at each point is tangential to them and normal if the discontinuity surface is perpendicular to the direction of the flow. As a rule tangential discontinuities are unstable.

Furthermore, as we already know, the discontinuities are termed strong if the flow parameters themselves, the velocity, pressure, temperature, etc. are discontinuous, and weak if it is only the derivatives of the flow parameters that display a jump.

An example of a strong discontinuity is afforded by the velocity

jump at the surface of a body placed in the flow of an inviscid fluid.

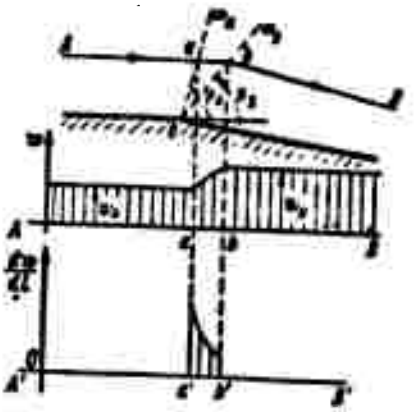


Fig. 5.9.1. Weak velocity discontinuity – the derivative of the velocity jumps as is passes through the Mach lines Oa and Ob.

Rarefaction waves are an example of a weak discontinuity. In fact, (Fig. 5.9.1), when moving along a streamline AabB of a flow streaming round the outside of an obtuse angle, the velocity at the section Aa will not vary and will be equal to w_A, whereas the velocity at the section bB will be constant but equal to w_B. Since $w_B > w_A$, $\mu_B > \mu_A$ $\left(\mu = \operatorname{arc\,tg} \frac{1}{\sqrt{M^2-1}}\right)$ and from point O we can draw the two lines Om_A and Om_B bounding parallel flows: the line Om_A bounds the undisturbed flow from the right, which is parallel to the wall AO, and the line Om_B bounds the flow from the left, which is parallel to the wall OB and inside which no changes occur either. The change of the velocity from w_A to w_B begins at the line Om_A and stops at the line Om_B (cf. Fig. 5.9.1), and for the streamline considered – from point a to point b.

The velocity derivative with respect to the streamline on the path Aa and bB is equal to zero. At point a it changes jumpkile from zero to a certain value and at point b it jumps back to zero.

The parameters change in an essentially different way when a supersonic gas flows inside an abtuse angle. Since the flow is slowed down, $\mu_B > \mu_A$ (Fig. 5.9.2). The region between a and b must be both the region of the undisturbed flow with the parameters A and the same region with the parameters B; in this very region, moreover, the flow parameters must change from the values corresponding to region A to the values corresponding to region B. This inconsistency is removed when we introduce a discontinuity line between Om_B and Om_A. This scheme

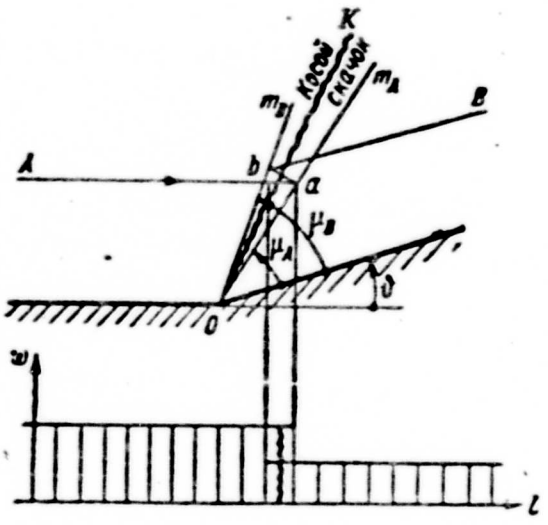


Fig. 5.9.2. Strong velocity discontinuity – velocity, pressure, etc. jump as they pass through the line OK. 1) Diagonal shock.

is verified by experiment – in this region there arises what is called a diagonal compression shock.

In the foregoing, when considering the linearized flow we have assumed that the disturbances are very small; we therefore assumed $\mu_A \approx \mu_B$, the region $m_A O m_B$ was replaced by a line and the low-intensity compression shock was considered as a pressure wave.

Prandtl-Meyer flow. The flow about an angle greater than 180° was investigated by Prandtl and Meyer in 1908. In order to find the streamline equation for this kind of flow we notice that up to the line Om_1 determined by the angle $\mu_1 = \operatorname{arc\,tg} \frac{1}{\sqrt{M_1^2-1}}$, the flow is uniform and parallel to the x-axis. It will

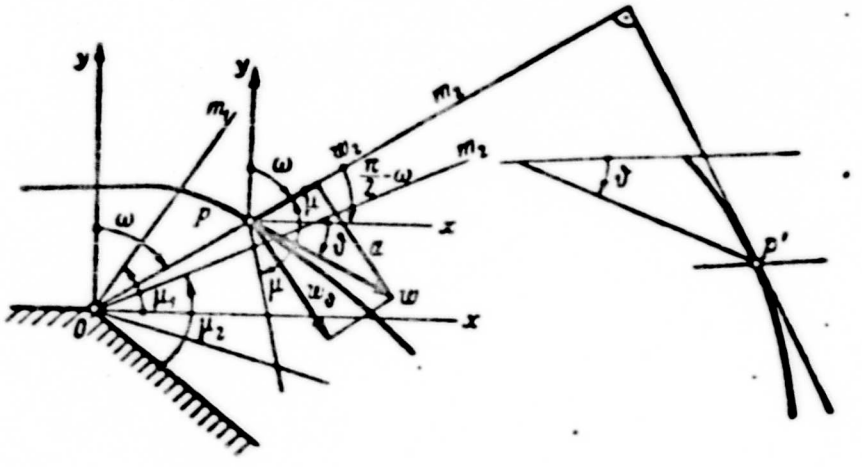


Fig. 5.9.3. For deriving the streamline equation for a Prandtl-Meyer flow.

also be parallel beyond the line Om_2 determined by the angle $\mu_2 = \operatorname{arc\,tg} \frac{1}{\sqrt{M_2^2-1}}$ counted from the direction of the velocity w_2. In the sector $m_1 O m_2$ which is called the sector of rarefaction, the stream-

lines will be curvilinear.

A continuous turn of the flow through the finite angle θ can be considered as the limit of an infinitely large number of turns through infinitely small angles. All rays originating at the vertex of the angle in the region of the Mach sector are therefore Mach lines. They will be + Mach lines on the physical plane of the flow; - Mach lines will correspond to them on the hodograph plane.

Let $\underline{r}$ be the radius vector drawn from the vertex O of the angle to point P on the streamline (Fig. 5.9.3) and the angle ω be included between $\underline{r}$ and the y-axis.

Decomposing the velocity $\underline{w}$ into its radial and normal components w_r and w_ϑ, respectively, we can write

$$\frac{1}{r}\frac{dr}{d\omega}=\frac{w_r}{w_\vartheta}=\operatorname{ctg}\mu=\sqrt{M^2-1}=$$
$$=K\sqrt{\frac{M^2-1}{K^2-M^2}}\quad\left(K=\sqrt{\frac{k+1}{k-1}}\right).$$

whence

$$\mu=\operatorname{arctg}K\sqrt{\frac{M^2-1}{K^2-M^2}}=\frac{\pi}{2}-\operatorname{arctg}K\sqrt{\frac{M^2-1}{K^2-M^2}};$$

we rewrite (5.8.14) in the form ($\vartheta_0 = 0$):

$$\theta=K\operatorname{arctg}\sqrt{\frac{M^2-1}{K^2-M^2}}-\operatorname{arctg}K\sqrt{\frac{M^2-1}{K^2-M^2}}=$$
$$=K\operatorname{arctg}\left(\frac{1}{K}\operatorname{ctg}\mu\right)-\frac{\pi}{2}+\mu.$$

However, it follows from Fig. 5.9.3 that

$$\omega+\mu-\theta=\frac{\pi}{2},$$

i.e., that

$$\mu-\frac{\pi}{2}=\theta-\omega.$$

Thus

$$\theta=K\operatorname{arctg}\left(\frac{\operatorname{ctg}\mu}{K}\right)+\theta-\omega$$

or

$$\omega = K \operatorname{arc\,tg} \frac{\operatorname{ctg} \mu}{K}.$$

Therefore

$$\operatorname{tg} \frac{\omega}{K} = \frac{\operatorname{ctg} \mu}{K}; \quad \operatorname{ctg} \mu = \frac{1}{r} \frac{dr}{d\omega} = K \operatorname{tg} \frac{\omega}{K}.$$

Integrating this equation we obtain

$$r = r_0 \left(\cos \frac{\omega}{K} \right)^{-K}. \tag{5.9.1}$$

where r_0 is the value of $\underline{r}$ at $\omega = 0$.

The limiting (maximum) value of the angle of turn, θ_{max}, is obtained from the condition that for any streamline with finite value of r_0 the radius vector $\underline{r}$ can be arbitrarily large. It follows from (5.9.1) that this is the case when $\cos(\omega/K) = 0$ which gives us $\theta_{max} = K\pi/2$. In this case

$$\operatorname{ctg} \mu_2 \Big|_{\omega \to K\frac{\pi}{2}} = K \operatorname{tg} \frac{\omega}{K} \Big|_{\omega \to K\frac{\pi}{2}} \to \infty,$$

i.e., the outermost characteristic coincides with a streamline. But $\cot \mu \to \infty$ if $M^* \to K = \sqrt{\frac{k+1}{k-1}}$ (corresponding to $M \to \infty$), i.e., the maximum angle of turn corresponds to outflow into vacuum and the flow velocity is equal to w_{max}.

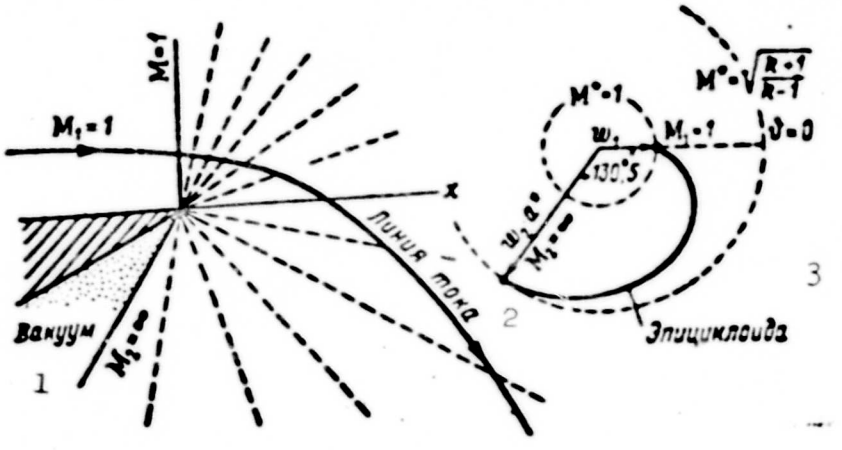


Fig. 5.9.4. The flow cannot be deflected by an angle greater than $\left(\sqrt{\frac{k+1}{k-1}} - 1\right)\frac{\pi}{2}$. (For air $k = 1.4$ and $\theta_{max} = 130.5^\circ$). 1) Vacuum; 2) streamline; 3) epicycloid.

The maximum angle of deflection is

$$\theta_{max} = \nu_{max} - \frac{\pi}{2} = \frac{\pi}{2}\left(\sqrt{\frac{k+1}{k-1}} - 1\right).$$

For air ($k = 1.4$) $\theta_{max} \approx 130.5^\circ$. Thus, when the angle of deflection exceeds 130.5° there remains a region in space which is theoretically not occupied by the air stream (Fig. 5.9.4). The numerical values of the flow parameters for $k = 1.4$ are given in Appendix 8.

Diagonal compression shocks. Let us now consider a supersonic flow inside an angle of less than 180° and discard the supposition that the deviations of the angle from 180° are small. We assume that the angle is curved, and that the curve can be replaced by a polygon. In a flow this polygon will give rise to a system of pressure waves (Mach lines) emanating from each angle of the polygon. The fundamental difference between these compression waves and the rarefaction lines has been explained above.

Since the slope angle of these rarefaction lines increases downstream they will form a system like that shown in Fig. 5.9.5,a, and the disturbances which sum up where the lines are curved assume a finite value – a compression shock arises in the flow, whose parameters are subject to a finite discontinuity (cf. photograph of Fig. 5.9.5,b). A discontinuity whose plane includes with the direction of velocity an angle that differs from 90° is called a diagonal shock.

Conditions of dynamic consistency. Let us subdivide the reference surface (Fig. 5.9.6) by two streamlines and sections parallel to the discontinuity plane in front of and behind it and let us formulate the conservation laws for the gas streaming through it. Decomposing the velocity before and after the discontinuity into the component normal to the discontinuity, w_n, and component along it, w_t, the continuity equation can be written down as

$$\rho_1 w_{1n} = \rho_2 w_{2n}. \tag{5.9.2}$$

Since the resultant pressure force $(p_1-p_2)A$ will act perpendicular to the discontinuity plane, then, projecting the momentum onto the tangent to the discontinuity plane, we obtain

$$0 = \rho_1 w_{1n}(w_{2t} - w_{1t})$$

or, since $\rho_1 w_{1n} \neq 0$.

$$w_{2t} = w_{1t} = w_t. \tag{5.9.3}$$

i.e., the tangential velocity component remains unchanged when passing through the plane of a diagonal shock.

For a direction perpendicular to the discontinuity plane

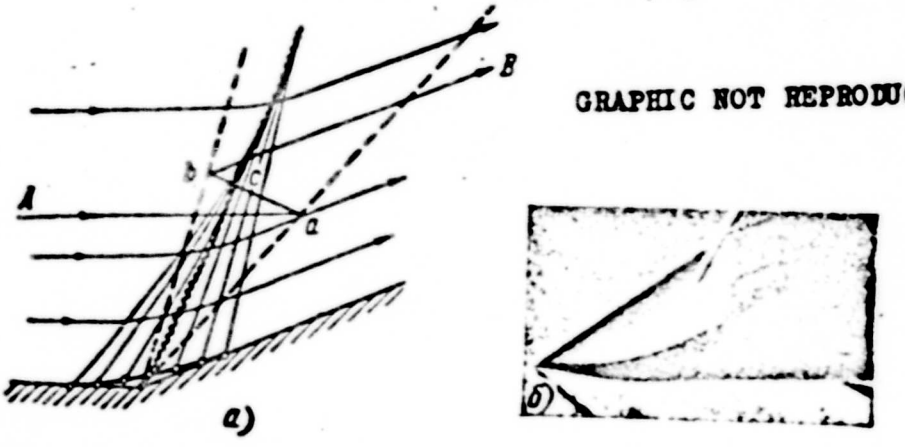
$$p_1 - p_2 = \rho_1 w_{1n}(w_{2n} - w_{1n}). \tag{5.9.4}$$

The energy equation yields

$$c_p T_1 + \frac{w_{1n}^2 + w_t^2}{2} = c_p T_2 + \frac{w_{2n}^2 + w_t^2}{2} = c_p T_0$$

or

$$c_p T_1 + \frac{w_{1n}^2}{2} = c_p T_2 + \frac{w_{2n}^2}{2} = c_p T_0 - \frac{w_t^2}{2}. \tag{5.9.5}$$



GRAPHIC NOT REPRODUCIBLE

Fig. 5.9.5. Formation of diagonal compression shock when a supersonic flow streams about a curved wall as curved compression lines of the linearized solution (a); photograph of diagonal shock (b).

For a perfect gas

$$\frac{p_1}{\rho_1 T_1} = \frac{p_2}{\rho_2 T_2}. \tag{5.9.6}$$

The Hugoniot curve. Comparing Relations (5.9.2) - (5.9.6)

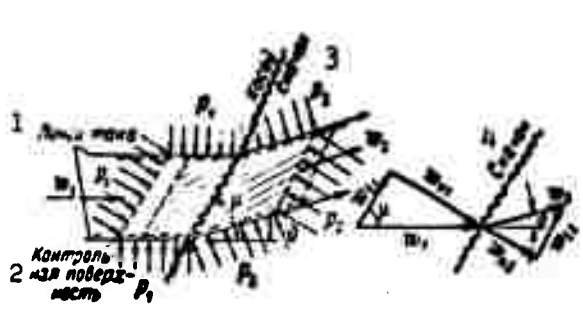


Fig. 5.9.6. For deriving the conditions of dynamic consistency for a diagonal shock. 1) Streamline; 2) reference surface; 3) diagonal shock; 4) discontinuity.

with the analogous Relations (2.7.22) for the normal shock, we can show that they agree completely if we replace w in the normal shock by w_n of the diagonal shock and define a reference stagnation temperature in the diagonal shock by the equation

$$T_{0\Phi} = T_0 - \frac{w_t^2}{2c_p}. \tag{5.9.7}$$

The conclusions given above for the normal shock therefore remain valid for the diagonal shock too when velocities and temperatures are replaced as indicated, i.e., when the equation of the Hugoniot curve can be written in one of the following forms:

$$\frac{p_2 - p_1}{\rho_2 - \rho_1} = k\frac{p_2 + p_1}{\rho_2 + \rho_1}, \quad \frac{p_2}{p_1} = \frac{\frac{k+1}{k-1}\frac{\rho_2}{\rho_1} - 1}{\frac{k+1}{k-1} - \frac{\rho_2}{\rho_1}}, \quad \frac{\rho_2}{\rho_1} = \frac{\frac{k+1}{k-1}\frac{p_2}{p_1} + 1}{\frac{k+1}{k-1} + \frac{p_2}{p_1}}. \tag{5.9.8}$$

Furthermore,

$$w_{1n}w_{2n} = a_\Phi^{*2} = \frac{2}{k+1}kRT_{0\Phi} = \frac{2}{k+1}kR\left(T_0 - \frac{w_t^2}{2c_p}\right) = a^{*2} - \frac{k-1}{k+1}w_t^2 \tag{5.9.9}$$

or, what is the same,

$$\frac{p_2 - p_1}{\rho_2 - \rho_1} = a^{*2} - \frac{k-1}{k+1}w_t^2.$$

It follows from this relation that the velocity drop behind the shock is greatest when the shock is normal, i.e., when $w_t = 0$. It

should be stressed that by virtue of the tangential component the velocity behind the shock can also remain supersonic.

Practical formulas for calculating a diagonal compression shock. We have from Fig. 5.9.6.

$$w_{1\tau} = w_1 \cos\mu; \quad w_{2\tau} = w_2 \cos(\mu - \theta).$$

Since

$$w_{1\tau} = w_{2\tau}, \text{ то } \frac{w_1}{w_2} = \frac{\cos(\mu-\theta)}{\cos\mu}.$$

Moreover,

$$w_{1n} = w_1 \sin\mu; \quad w_{2n} = w_2 \sin(\mu - \theta),$$

which, together with the continuity equation, gives

$$\frac{\rho_2}{\rho_1} = \frac{w_1 \sin\mu}{w_2 \sin(\mu-\theta)} = \frac{\cos(\mu-\theta)\sin\mu}{\cos\mu \sin(\mu-\theta)} = \frac{\operatorname{tg}\mu}{\operatorname{tg}(\mu-\theta)}. \tag{5.9.10}$$

Equation (5.9.4) can now be rewritten in the form

$$p_2 - p_1 = \rho_1 w_1^2 \left(1 - \frac{\rho_2}{\rho_1}\frac{w_{2n}^2}{w_{1n}^2}\right) = \rho_1 w_1^2 \sin^2\mu \left(1 - \frac{\rho_1}{\rho_2}\right).$$

Since $p_1 w_1^2 = k p_1 M_1^2$, we have

$$\frac{p_2}{p_1} = 1 + kM_1^2 \sin^2\mu \left(1 - \frac{\rho_1}{\rho_2}\right). \tag{5.9.11}$$

When we substitute the expression for ρ_1/ρ_2 from the equation of the Hugoniot curve (5.9.8) into the first equation (5.9.11), we obtain

$$\frac{p_2}{p_1} = 1 + kM_1^2 \sin^2\mu \left(1 - \frac{\frac{k-1}{k+1} + \frac{p_2}{p_1}}{\frac{k+1}{k-1}\frac{p_2}{p_1} + 1}\right).$$

Solving it with respect to p_2/p_1 we find

$$\frac{p_2}{p_1} = \frac{2k}{k+1} M_1^2 \sin^2\mu - \frac{k-1}{k+1}. \tag{5.9.12}$$

When $\mu = 90^\circ$ this equation goes over into Eq. (4.3.8) for the normal compression shock. If $\sin\mu = \frac{1}{M_1}$, the diagonal shock degenerates to a weak wave with $p_2 = p_1$.

Equations (5.9.9) - (5.9.12) express the connection between the variables μ, θ, M_1, M_2, $p_2 : p_1$, $\rho_2 : \rho_1$; any two from them can be taken as in-

dependent variables.

If we use the velocity coefficient M* and introduce $w_{1n} = w_1 \sin\mu$, $w_t = w_1 \cos\mu$, into (5.9.4) we obtain

$$p_1 - p_2 = \rho_1 (w_{1n} w_{2n} - w_{1n}^2) = \rho_1 a_1^{*2} \left(1 - \frac{k-1}{k+1} M_1^{*2} \cos^2\mu - M_1^{*2} \sin^2\mu\right).$$

With

$$\frac{p_1}{\rho_1} = \frac{p_0}{\rho_0} \frac{T_1}{T_0} = \frac{a_0^2}{k} \frac{T_1}{T_0} = \frac{k+1}{2k} a^{*2} \left(1 - \frac{k-1}{k+1} M_1^{*2}\right),$$

we find

$$\frac{p_2}{p_1} = 1 - \frac{\rho_1}{p_1} a_1^{*2} \left(1 - \frac{k-1}{k+1} M_1^{*2} \cos^2\mu - M_1^{*2} \sin^2\mu\right) =$$

$$= \frac{M_1^{*2} \left[1 - \frac{4k}{(k+1)^2} \cos^2\mu\right] - \frac{k-1}{k+1}}{1 - \frac{k-1}{k+1} M_1^{*2}}. \qquad (5.9.13)$$

If $\mu = 90^\circ$, this relation goes over to (4.3.8). In this way we obtain $M_2^2 = \dfrac{M_1^2 + \frac{2}{k-1}}{\frac{2k}{k-1} M_1^2 \sin^2\mu - 1} + \dfrac{M_1^2 \cos^2\mu}{\frac{k-1}{2} M_1^2 \sin^2\mu + 1}$;

$$M_2^{*2} = \frac{w_2^2}{a^{*2}} = \frac{w_{2n}^2 + w_t^2}{a^{*2}} = \left(\frac{a^{*2} - \frac{k-1}{k+1} w_t^2}{a^* w_1 \sin\mu}\right)^2 + \frac{w_1^2 \cos^2\mu}{a^{*2}} = M_1^{*2} \cos^2\mu +$$

$$+ \frac{\left(1 - \frac{k-1}{k+1} M_1^{*2} \cos^2\mu\right)^2}{M_1^{*2} \sin^2\mu}. \qquad (5.9.14)$$

Taking into account that $a_0^2 = a_1^2 + \frac{k-1}{2} w_1^2 = \frac{k+1}{2} a^{*2}$ or $a^{*2} = \frac{2}{k+1} a_1^2 + \frac{k-1}{k+1} w_1^2$

Relation (5.9.9)

$$w_{1n} w_{2n} = a^{*2} - \frac{k-1}{k+1} w_t^2 = \frac{2}{k+1} a_1^2 + \frac{k-1}{k+1} (w_{1n}^2 + w_t^2) -$$

$$- \frac{k-1}{k+1} w_t^2 = \frac{2}{k+1} a_1^2 + \frac{k-1}{k+1} w_{1n}^2,$$

leads us to

$$\frac{w_{2n}}{w_{1n}} = \frac{2}{k+1} \frac{a_1^2}{w_{1n}^2} + \frac{k-1}{k+1} =$$

$$= \frac{k-1}{k+1} \left(1 + \frac{2}{k-1} \frac{1}{M_1^2 \sin^2\mu}\right) \frac{1 - \frac{k-1}{k+1} M_1^{*2} \cos^2\mu}{M_1^{*2} \sin^2\mu} = \frac{\rho_1}{\rho_2}. \qquad (5.9.15)$$

But on the other hand (5.9.2) and (5.9.10) yield

$$\frac{w_{2n}}{w_{1n}}=\frac{\rho_1}{\rho_2}=\frac{\operatorname{tg}(\mu-\theta)}{\operatorname{tg}\mu}=\frac{1}{\operatorname{tg}\mu}\cdot\frac{\operatorname{tg}\mu-\operatorname{tg}\theta}{1+\operatorname{tg}\mu\operatorname{tg}\theta},$$

whence

$$\operatorname{ctg}\theta=\frac{1+\frac{w_{2n}}{w_{1n}}\operatorname{tg}^2\mu}{\operatorname{tg}\mu\left(1-\frac{w_{2n}}{w_{1n}}\right)}=\operatorname{tg}\mu\,\frac{\frac{1}{\operatorname{tg}^2\mu}+\frac{k-1}{k+1}+\frac{2}{k+1}\frac{1}{M_1^2\sin^2\mu}+1-1}{1-\frac{k-1}{k+1}-\frac{2}{k+1}\frac{1}{M_1^2\sin^2\mu}}=$$

$$=\operatorname{tg}\mu\left[\frac{\frac{k+1}{2}M_1^2}{M_1^2\sin^2\mu-1}-1\right]. \qquad (5.9.16)$$

The Hugoniot curve is a curve that represents the interrelation between the velocity vector behind the shock, w_2, and the velocity vector in front of the shock, w_1. In order to find the equation of this curve we decompose the velocity w_2 into the components w_{2x} and w_{2y} and choose the axes such that $w_{1x} = w_1$ and $w_{1y} = 0$ (Fig. 5.9.7).

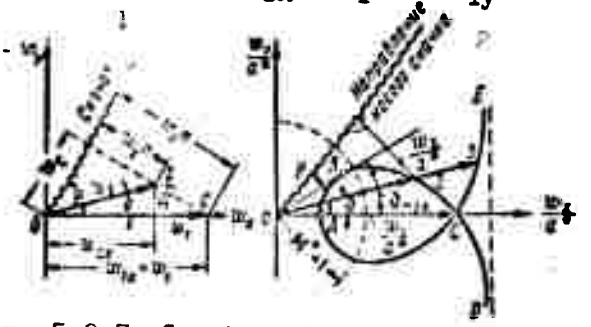


Fig. 5.9.7. Construction of the Hugoniot curve. 1) Shock; 2) direction of diagonal shock.

Then $w_{1n}=w_1\sin\mu$; $w_t=w_1\cos\mu$;

$$w_{2n}=w_{1n}-\sqrt{w_{2y}^2+(w_1-w_{2x})^2}=w_1\sin\mu-\sqrt{w_{2y}^2+(w_1-w_{2x})^2}$$

and Eq. (5.9.9) reads

$$w_1\sin^2\mu-w_1\sin\mu\sqrt{w_{2y}^2+(w_1-w_{2x})^2}=a^{*2}-\frac{k-1}{k+1}w_1^2\cos^2\mu.$$

From Fig. 5.9.7 it can be seen that

$$\operatorname{tg}\mu=\frac{w_1-w_{2x}}{w_{2y}}.$$

Hence we obtain for the equation of the Hugoniot curve

$$\left(\frac{w_{2y}}{a^*}\right)^2=\frac{\left(\frac{w_1}{a^*}-\frac{w_{2x}}{a^*}\right)^2\left(\frac{w_1w_{2x}}{a^{*2}}-1\right)}{\frac{2}{k+1}\left(\frac{w_1}{a^*}\right)^2-\frac{w_1w_{2x}}{a^{*2}}+1}. \qquad (5.9.17)$$

The Hugoniot curve is a third order curve (strophoid) with w_x as the symmetry axis. The point A corresponds to a normal compression shock.

The infinite branches CD and CE of the polar do not correspond to any real state; for their points (points 3) $w_{2n}/w_{1n} > 1$, i.e., $\rho_1/\rho_2 > 1$, which contradicts the second law of thermodynamics. Thus, two shock waves (points 1 and 2) correspond to each angle ϑ of deflection of the flow. At the point B points 1 and 2 coincide, and here the maximum deflection of the flow is at the angle $\vartheta = \vartheta_{max}$. The branch AB of the Hugoniot curve specifies the "strong" shocks, and BC the "weak" ones; the flow past the "strong" shocks is subsonic (Fig. 5.9.8).

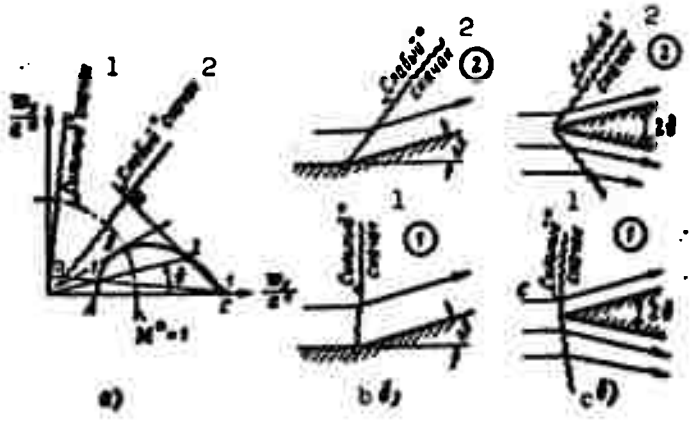


Fig. 5.9.8. Two possible types of diagonal shocks: "strong" and "weak" shocks. a) on the Hugoniot curve, b) inside an obtuse angle; c) for a wedge. 1) "Strong" shock; 2) "weak" shock.

The experiment shows that inside an obtuse angle "weak" shocks occur, having a smaller slope angle and a greater velocity past the shock (branch BC).

Flow about a wedge. Two cases may arise when a supersonic flow streams about a wedge at zero angle of attack: $\vartheta < \vartheta_{max}$ and $\vartheta > \vartheta_{max}$, where ϑ is half the vertex andgle of the flow and ϑ_{max} is the maximum angle of flow deflection (Fig. 5.9.9, a and b).

Experiment shows that with $\vartheta < \vartheta_{max}$ only a shock wave is produced

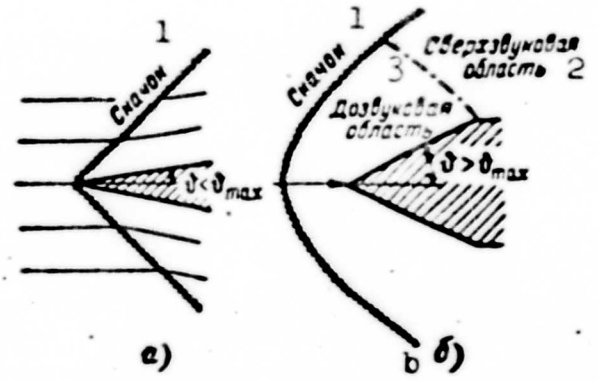


Fig. 5.9.9. Flow about a wedge. a) Attached shock $\vartheta < \vartheta_{max}$; b) detached shock $\vartheta > \vartheta_{max}$. 1) Shock; 2) supersonic region, 3) subsonic region.

that corresponds to point 2 of the Hugoniot curve (cf. Fig. 5.9.9,a). In this case we obtain an attached diagonal compression shock.

When $\vartheta > \vartheta_{max}$ the compression shock leaves from the wedge placed in front of it and forms a so-called detached shock (cf. Fig. 5.5.9,b). The shock wave forms a curve corresponding to all points of the Hugoniot curve from A to C (cf. Fig. 5.9.7). In the central part of the wave surface the shock is a normal one.

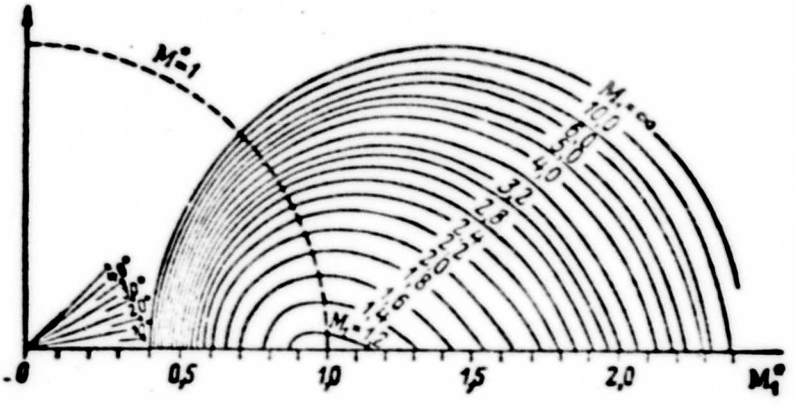


Fig. 5.9.10. Set of Hugoniot curves for various M_1 and k = 1.4.

Figure 5.9.10 gives the family of Hugoniot curves for k = 1.4 and for various Mach numbers M. The region inside the arc of radius M* = 1 is the region of subsonic velocities w_2 and that outside the

arc is the supersonic region. This graph can be used to determine the velocity w_2 behind the shock for various velocities w_1 and for various values of the angle through which the flow is deflected at the shock.

5.10. THE METHOD OF SUCCESSIVE APPROXIMATIONS FOR SUBSONIC FLOWS

In the linearization of the equations of motion of a compressible gas the disturbances have been assumed to be so small that their products are negligible. The solution obtained is a first approximation. This naturally raises the problem of the second, third and further approximations, considering the terms small of second, third, and higher orders. It can be solved by expanding the velocity potential in powers of the number M_∞ or of a parameter characterizing the thickness of the body.

Expansion of the velocity potential in a power series of M_∞. Such a series will contain only even powers of M_∞, i.e., M_∞^0, M_∞^2, M_∞^4, ... This is immediately evident from the fact that if we choose the x_1-axis at any point of the flow to coincide with the direction of the velocity at this point, the potential equation in the new coordinates will have the form

$$\frac{\partial^2\Phi}{\partial x_1^2}+\frac{\partial^2\Phi}{\partial y_1^2}=\frac{w^2}{a^2}\frac{\partial^2\Phi}{\partial x_1^2}.$$

The approximation corresponding to $M_\infty = 0$ holds for the motion of an incompressible fluid, which can be obtained by solving the velocity potential equation

$$\frac{\partial^2\Phi}{\partial x^2}+\frac{\partial^2\Phi}{\partial y^2}= =\frac{1}{a^2}\left[\left(\frac{\partial\Phi}{\partial x}\right)^2\frac{\partial^2\Phi}{\partial x^2}+2\frac{\partial\Phi}{\partial x}\frac{\partial\Phi}{\partial y}\frac{\partial^2\Phi}{\partial x\,\partial y}+\left(\frac{\partial\Phi}{\partial y}\right)^2\frac{\partial^2\Phi}{\partial y^2}\right]. \tag{5.10.1}$$

and assuming $a = \infty$, i.e., by solving the Laplace equation $\Delta\Phi = 0$. Substituting the solution found, $\Phi = \Phi_0(x,y)$, the zeroth approximation, into the right-hand side of Eq. (5.10.1) and solving the Poisson equation obtained,

$$\frac{\partial^2\Phi}{\partial x^2}+\frac{\partial^2\Phi}{\partial y^2}=F[\Phi_0(x,y)]. \qquad (5.10.2)$$

we find the first approximation, $\Phi_1 = \Phi_1(x,y)$. When we substitute the latter in the right-hand side of (5.10.1) and solve the new Poisson equation, we obtain the second approximation. Continuing this procedure we shall find more and more new approximations in the form of a series

$$\Phi=\Phi_0+M_\infty^2\Phi_1+M_\infty^4\Phi_2+\dots. \qquad (5.10.3)$$

When the difference between two subsequent approximations of the velocity potential tends to zero, the process is convergent. Depending on the shape of the body this process can be convergent only for a number M_∞ not exceeding the critical value M_{kr} which corresponds to the appearance of regions in the flow where the stream velocity becomes equal to the sonic velocity; from the mathematical point of view this is connected with a change in the type of the equation.

Figure 5.10.1 shows the velocity distribution around a circular cylinder for $M_\infty = 0.4$ in first, second and third approximation*. When $\vartheta < 45^\circ$ the local velocity shows a slight increase for an incompressible fluid; a converse picture is obtained for $90^\circ < \vartheta^\circ < 45^\circ$. The maximum local velocity is expressed in this case by

$$\frac{v_{max}}{v_\infty}=2+\frac{7}{6}M_\infty^2+\left[\frac{281}{120}+\frac{71}{120}(k-1)\right]M_\infty^4+\dots \qquad (5.10.4)$$

or (for k = 1.4) by

$$\frac{v_{max}}{v_\infty}=2+1.167M_\infty^2+2.58M_\infty^4+7.53M_\infty^6+\dots$$

The results of calculations in different approximations become more divergent as the number M_∞ increases. The method is therefore only a rough one when M_∞ ia a large subsonic number.

Calculations in third approximation show that sonic speed arises when $M_\infty = 0.404$; which is, therefore, the critical number for a cylinder.

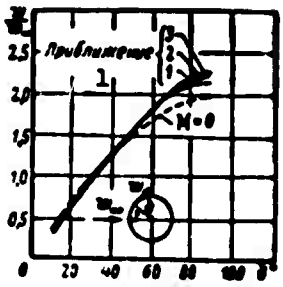


Fig. 5.10.1. Velocity distribution about a circular cylinder for $M_\infty = 0$ and $M_\infty = 0.4$. 1) Approximation.

Expansion of the thickness parameter into a power series. For a uniform flow streaming parallel to the x-axis about a body, the velocity potential can in general be written in the form

$$\Phi = w_\infty x + \varphi(x, y) \qquad (5.10.5)$$

where $\varphi(x,y)$ denotes the part of the potential due to the presence of the body. If no body is present, $\varphi(x,y) = 0$. For example, for a plate at zero angle of attack, $\Phi = \Phi_0 = w_\infty x$. The additional potential can be assumed to depend on the body thickness, and we can assume that $\varphi(x,y) = 0$, where δ is a parameter characterizing the body thickness, and write

$$\Phi = w_\infty x + \sum_{n=1} \delta^n \varphi_n(x, y) \qquad (5.10.6)$$

Neglecting all powers of δ in (5.10.6) higher than the first, and substituting in (5.10.1), we obtain the linearized equation

$$(1 - M_\infty^2) \frac{\partial^2 \varphi_1}{\partial x^2} + \frac{\partial^2 \varphi_1}{\partial y^2} = 0.$$

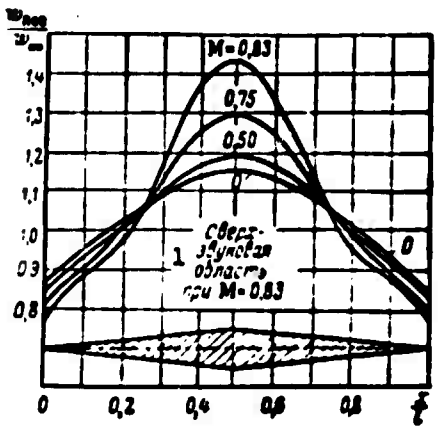


Fig. 5.10.2. Velocity distribution about a profile of 10% thickness for various Mach numbers M. 1) Supersonic region for M = 0.83.

The equation for φ_2 has the form

$$(1 - M_\infty^2) \frac{\partial^2 \varphi_2}{\partial x^2} + \frac{\partial^2 \varphi_2}{\partial y^2} = -\frac{M_\infty^2}{w_\infty} \left[(k+1) \frac{\partial \varphi_1}{\partial x} \frac{\partial^2 \varphi_1}{\partial x^2} + (k-1) \frac{\partial \varphi_1}{\partial x} \frac{\partial \varphi_1}{\partial y} + 2 \frac{\partial \varphi_1}{\partial y} \frac{\partial^2 \varphi_1}{\partial x \partial y} \right].$$

It should be noted that solving the problem by this method is a rather cumbersome task. Fig. 5.10.2 shows the velocity distribution over a profile of 10% thickness for various M_∞ numbers.

5.11. THE HODOGRAPH METHOD

The method of exact linearization. Two methods exist which can be used to transform the nonlinear equations of a plane potential motion of a compressible gas exactly to linear equations. One of them, based on the Legendre transformation consists in choosing the velocities w_x and w_y as the independent x and y and going over from the velocity potential Φ to the conjugate potential $\Phi_c = xw_x + yw_y - \Phi$. It can be shown that the equation for the conjugate potential has the form

$$\left(1-\frac{w_y^2}{a^2}\right)\frac{\partial^2\Phi_c}{\partial w_x^2}+2\frac{w_x w_y}{a^2}\frac{\partial^2\Phi_c}{\partial w_x \partial w_y}+\left(1-\frac{w_x^2}{a^2}\right)\frac{\partial^2\Phi_c}{\partial y^2}=0.$$

By analogy with the stream function, the components $q_x = \rho w_x$ and $q_y = \rho w_y$ of the mass flow density vector $\vec{\rho w}$ are taken as the independent variables; the stream function is replaced by a conjugate stream function $\Psi_c = -(xq_y + yq_x + \Psi)$, yielding the linear equation

$$\left(1-\frac{q_x^2}{\rho^2 a^2}\right)\frac{\partial^2\Psi_c}{\partial q_x^2}-2\frac{q_x q_y}{\rho^2 a^2}\frac{\partial^2\Psi_c}{\partial q_x \partial q_y}+\left(1-\frac{q_y^2}{\rho^2 a^2}\right)\frac{\partial^2\Psi_c}{\partial q_y^2}=0.$$

The Legendre transformation maps the physical plane of the motion onto the plane of mass flow density. This is the disadvantage of the method, since the values of the mass flow density are not uniquely determined; to each value of ρw correspond one value $w < a$ and another value $w > a$ (Fig. 4.2.4).

Chaplygin transformation. This second transformation leads to investigating the motion on the hodograph plane. In this case the velocity potential and the stream function remain unchanged. Difficulties arise, however, on establishing the boundary conditions.

This method is widely used in practice because the linearity of the equations makes it possible to obtain complex solutions by adding simple exact solutions. Moreover, with certain simple boundary conditions the exact solutions can be successfully applied to a study of mixed sub- and super-sonic flows when the approximate methods no longer apply.

Finally there also exist approximate methods of solving the problem on the hodograph plane which enable us to overcome the difficulties connected with satisfying the boundary conditions.

We introduce the stream function Ψ:

$$w_x = \frac{\partial \Phi}{\partial x} = \frac{\rho_0}{\rho} \frac{\partial \Psi}{\partial y}, \quad w_y = \frac{\partial \Phi}{\partial y} = -\frac{\rho_0}{\rho} \frac{\partial \Psi}{\partial x} \tag{5.11.1}$$

and obtain $z = x + iy$; $\overline{w} = w_x - iw_y = we^{-i\theta}$.

Then

$$\overline{w}\,dz = we^{-i\theta}dz = (w_x dx + w_y dy) + i(w_x dy - w_y dx) =$$
$$= d\Phi + i\frac{\rho_0}{\rho} d\Psi; \quad dz = \left(d\Phi + i\frac{\rho_0}{\rho} d\Psi\right)\frac{e^{i\theta}}{w}. \tag{5.11.2}$$

When $\rho = \rho_0$ this relation reduces to that found before:

$$\overline{w} = \frac{d\chi}{dz}; \quad (\chi = \Phi + i\Psi).$$

Let us now consider z (or x,y) as a function of w and $\theta = \arctg \frac{w_y}{w_x}$; then $\Phi = \Phi(w, \theta)$; $\Psi = \Psi(w, \theta)$.

To find the equation satisfied by thse functions we calculate

$$\frac{\partial z}{\partial w} = \left(\frac{\partial \Phi}{\partial w} + i\frac{\rho_0}{\rho}\frac{\partial \Psi}{\partial w}\right)\frac{e^{i\theta}}{w}; \quad \frac{\partial z}{\partial \theta} = \left(\frac{\partial \Phi}{\partial \theta} + i\frac{\rho_0}{\rho}\frac{\partial \Psi}{\partial \theta}\right)\frac{e^{i\theta}}{w}.$$

The equation $\frac{\partial^2 z}{\partial w\,\partial \theta} = \frac{\partial^2 z}{\partial \theta\,\partial w}$ under the condition $\rho = \rho(w)$ reads

$$\left(\frac{\partial^2 \Phi}{\partial \theta\,\partial w} + i\frac{\rho_0}{\rho}\frac{\partial^2 \Psi}{\partial \theta\,\partial w}\right)\frac{e^{i\theta}}{w} + \left(\frac{\partial \Phi}{\partial w} + i\frac{\rho_0}{\rho}\frac{\partial \Psi}{\partial w}\right) i\frac{e^{i\theta}}{w} =$$
$$= \left[\frac{\partial^2 \Phi}{\partial w\,\partial \theta} + i\frac{\rho_0}{\rho}\frac{\partial^2 \Psi}{\partial w\,\partial \theta} + i\frac{d}{dw}\left(\frac{\rho_0}{\rho}\right)\frac{\partial \Psi}{\partial \theta}\right]\frac{e^{i\theta}}{w} -$$
$$- \left(\frac{\partial \Phi}{\partial \theta} + i\frac{\rho_0}{\rho}\frac{\partial \Psi}{\partial \theta}\right)\frac{e^{i\theta}}{w}.$$

Taking into account that $\frac{\partial^2 \Phi}{\partial \theta\,\partial w} = \frac{\partial^2 \Phi}{\partial w\,\partial \theta}$, and comparing the real and imaginary parts we find

$$\left.\begin{aligned} \frac{\partial \Phi}{\partial \theta} &= w\frac{\rho_0}{\rho}\frac{\partial \Psi}{\partial w}, \\ \frac{\partial \Phi}{\partial w} &= \left[\frac{d}{dw}\left(\frac{\rho_0}{\rho}\right) - \frac{dw}{w}\left(\frac{\rho_0}{\rho}\right)\right]\frac{\partial \Psi}{\partial \theta} = w\frac{d}{dw}\left(\frac{1}{w}\frac{\rho_0}{\rho}\right)\frac{\partial \Psi}{\partial \theta}. \end{aligned}\right| \tag{5.11.3}$$

However, $w\,dw = -\frac{d\rho}{\rho} = -a^2\frac{d\rho}{\rho}$; $\frac{d}{dw}\left(\frac{\rho_0}{\rho}\right) = -\frac{\rho_0}{\rho^2}\left(-\frac{\rho w}{a^2}\right) = \frac{\rho_0}{\rho}\frac{w}{a^2}$.

Therefore

$$\frac{\partial \vartheta}{\partial w} = -\frac{\rho}{\rho_0 w}$$

$$\frac{\partial \Phi}{\partial w} = -\frac{\rho_0}{\rho w}\left(1-\frac{w^2}{a^2}\right)\frac{\partial \Psi}{\partial \vartheta} = -\frac{\rho_0}{\rho}\frac{1-M^2}{w}\frac{\partial \Psi}{\partial \vartheta}. \qquad (5.11.4)$$

These equations are linear; the coefficients of the derivatives depend only on the independent variables $\underline{w}$ and ϑ.

To eliminate Φ we use the condition $\frac{\partial^2 \Phi}{\partial w \partial \vartheta} = \frac{\partial^2 \Phi}{\partial \vartheta \partial w}$, which gives

$$\frac{\rho_0}{\rho}\frac{\partial \Psi}{\partial w} + w\frac{d}{dw}\left(\frac{\rho_0}{\rho}\right)\frac{\partial \Psi}{\partial w} + w\frac{\rho_0}{\rho}\frac{\partial^2 \Psi}{\partial w^2} = -\frac{\rho_0}{\rho}\frac{1-M^2}{w}\frac{\partial^2 \Psi}{\partial \vartheta^2}$$

(ρ and M depending only on $\underline{w}$) and therefore

$$w^2\frac{\partial^2 \Psi}{\partial w^2} + \left(1+\frac{w^2}{a^2}\right)w\frac{\partial \Psi}{\partial w} + \left(1-\frac{w^2}{a^2}\right)\frac{\partial^2 \Psi}{\partial \vartheta^2} = 0. \qquad (5.11.5)$$

System (5.11.4) is analogously solved with respect to $\partial\Psi/\partial w$ and $\partial\Psi/\partial\vartheta$, giving

$$\left(1-\frac{w^2}{a^2}\right)w^2\frac{\partial^2 \Phi}{\partial w^2} + w\left(1+\frac{w^4}{a^4}\right)\frac{\partial \Phi}{\partial \vartheta} + \left(1-\frac{w^2}{a^2}\right)\frac{\partial^2 \Phi}{\partial \vartheta^2} = 0. \qquad (5.11.6)$$

These equations were obtained by S.A. Chaplygin in 1902 and are named after him.

Let us trace the transition to the physical plane of flow after having found the solutions to (5.11.5) and (5.11.6), i.e., the functions $\Phi(w, \vartheta)$ and $\Psi(w, \vartheta)$ on the hodograph plane.

Then, determining the real and imaginary parts we have from (5.11.2)

$$dx = \frac{1}{w}\cos\vartheta\, d\Phi - \frac{\rho_0}{\rho w}\sin\vartheta\, d\Psi, \quad dy = \frac{1}{w}\sin\vartheta\, d\Phi + \frac{\rho_0}{\rho w}\cos\vartheta\, d\Psi; \qquad (5.11.7)$$

which, after integrating, gives $x = x(\vartheta, w)$, $y = y(\vartheta, w)$, and also $w = w(x, y)$, $\vartheta = \vartheta(x, y)$, $\Phi = \Phi(x, y)$ и $\Psi = \Psi(x, y)$.

Subsidiary flow. If the fluid is incompressible, $\rho = \rho_0$ and, rewritten in the coordinates $(\tilde{w}, \vartheta)$, the equations in the hodograph plane, (5.11.3), take the form

$$\frac{\partial \Phi}{\partial \vartheta} = \tilde{w}\frac{\partial \Psi}{\partial \tilde{w}}, \quad \frac{\partial \Phi}{\partial \tilde{w}} = -\frac{1}{\tilde{w}}\frac{\partial \Psi}{\partial \vartheta}. \qquad (5.11.8)$$

Let us state that in Eq. (5.11.3) the velocity $\underline{w}$ is a certain function of the velocity $\tilde{w}$ of an incompressible fluid. This unknown

function of $\underline{w}$ is so determined that Eq. (5.11.3) becomes symmetrical, as similar to (5.11.8) as possible, and assumes the form

$$\frac{\partial\Phi}{\partial\vartheta}=\tilde{w}\sqrt{K}\frac{\partial\Psi}{\partial\tilde{w}},\quad \frac{\partial\Phi}{\partial\tilde{w}}=-\frac{1}{\tilde{w}}\sqrt{K}\frac{\partial\Psi}{\partial\vartheta}. \tag{5.11.9}$$

where $\sqrt{K}$ is a certain function of $\tilde{w}$, introduced by S.A. Chaplygin.

Owing both to the condition $w = w(\tilde{w})$ and to $\rho = \rho(\tilde{w})$, Eq. (5.11.3) can be written in terms of the variables $\tilde{w},\vartheta$ in the form

$$\frac{\partial\Phi}{\partial\vartheta}=w\frac{\rho_0}{\rho}\frac{d\tilde{w}}{dw}\frac{\partial\Psi}{\partial\tilde{w}};\quad \frac{d\Phi}{d\tilde{w}}=w\frac{d}{d\tilde{w}}\left(\frac{1}{w}\frac{\rho_0}{\rho}\right)\frac{\partial\Psi}{\partial\vartheta},$$

whence by comparison with (5.11.9) we arrive at

$$\frac{w}{\tilde{w}}\frac{\rho_0}{\rho}\frac{d\tilde{w}}{dw}=\sqrt{K},\quad -w\tilde{w}\frac{d}{d\tilde{w}}\left(\frac{1}{w}\frac{\rho_0}{\rho}\right)=\sqrt{K}. \tag{5.11.10}$$

Going over to the velocity coefficients $M^*=w:a^*$, $\tilde{M}^*=\tilde{w}:a^*$, where $a^*=\sqrt{\frac{2k}{k+1}RT_0}$, multiplying and differentiating these equations, and applying the gasdynamic function yields

$$\left.\begin{aligned}&\frac{\rho}{\rho_0}=\left(1-\frac{k-1}{k+1}M^{*2}\right)^{\frac{1}{k-1}},\\ &\sqrt{K}=\frac{\rho_0}{\rho}\sqrt{1+M^*\frac{d\rho}{\rho dM^*}}=\sqrt{\frac{1-M^{*2}}{1+\frac{k-1}{k+1}M^{*2}}},\end{aligned}\right\} \tag{5.11.11}$$

or

$$\sqrt{K}=\sqrt{1-M^2}\left(1+\frac{k-1}{2}M^2\right)^{\frac{1}{k-1}}=\frac{\rho_0}{\rho}\sqrt{1-M^2}.$$

The first equation of (5.11.10) now gives

$$\frac{d\tilde{M}^*}{\tilde{M}^*}=\sqrt{\frac{1-M^{*2}}{1-\frac{k-1}{k+1}M^{*2}}}\frac{dM^*}{M^*}. \tag{5.11.12}$$

The analytical expression of the connection between M^* and $\tilde{M}^*$ has a rather complicated form. Figure 5.11.1 gives a graphical representation of this relation of the dependence between $K^{1/2}$ and M^* from Eq. (5.11.11). To solve System (5.11.3) S.A. Khristianovich assumes that the functions Φ and Ψ can be expressed as series of the form

$$\Phi=\Phi_1+\Phi_2+\ldots,\quad \Psi=\Psi_1+\Psi_2+\ldots \qquad (5.11.13)$$

and that $\sqrt{K}\approx\sqrt{K_\infty}$ can be adopted to obtain the first approximation in System (5.11.9). Furthermore, if the Mach numbers M are small, the values of $K^{1/2}$ differ slightly from unity, as can be seen from Fig. 5.11.1 and from expanding $K^{1/2}$ into a power series of M:

$$\sqrt{K}=\sqrt{1-M^2}\left(1-\frac{k-1}{2}M^2\right)^{\frac{1}{k-1}}=1-\frac{k-1}{2}M^4+\ldots,$$

where the lowest power of M is the fourth.

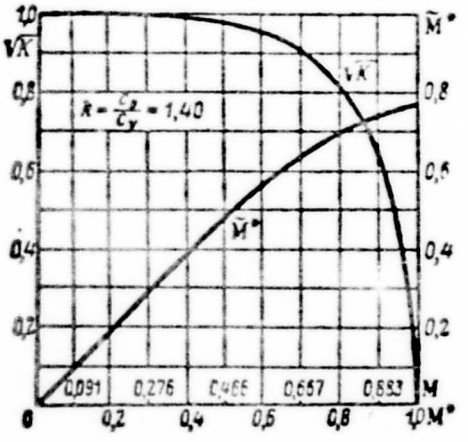


Fig. 5.11.1. Chaplygin function $\sqrt{K}=\frac{\rho_0}{\rho}\sqrt{1-M^2}$ and connection between the velocity coefficients of compressible and incompressible flows, $\tilde{M}^*=f(M^*)$.

Thus, if we restrict ourselves to the first approximation and suppose that $\Phi\approx\Phi_1$, $\Psi\approx\Psi_1$, then, solving the equation of gasdynamics leads to finding the solutions to the corresponding equations of motion of an incompressible fluid in the hodograph plane $(\tilde{w},\vartheta)$. Going over to the establishment of the correspondence between the points of the flow, we have to take into account that the x and y coordinates determined by integrating (5.11.7) will depend on the path of integration, since the values of Φ and Ψ were given approximately. These considerations make it expedient to integrate along streamlines for which Ψ = const, i.e., for which $d\Psi = 0$. When calculations are being made on the boundaries of the flow, for example, on the contour of the body placed in the flow, they become deformed and the larger the number $M(\tilde{M}^*)$, the greater is the deformation. It may happen that a closed contour (wing profile) goes over into an open one. The calculations show, however, that for small Mach numbers M and sufficiently long contours the boundaries change but slightly.

Since we cannot linger to consider these very profound and complicated bases of the method of S.A. Kristianovich [5.2], [5.3], which go beyond the scope of the course, we have to point out that the relation found between M* and $\tilde{M}$* allows us to determine the pressure coefficients C_p in the gas flow if the pressure coefficient $\tilde{C}_p$ in an incompressible fluid flow is given. More precisely, for $M^*_\infty(M_\infty)$ given we find $\tilde{M}^*_\infty$ from the graph (5.11.1), and from the equation

$$\tilde{C}_p = \frac{p - p_\infty}{\frac{\rho_\infty v_\infty^2}{2}} = 1 - \frac{\tilde{M}^{*2}}{\tilde{M}^{*2}_\infty}$$

we find the value of $\tilde{M}$* at the point considered to which the M* will correspond, and hence we have

$$C_p = \frac{p - p_\infty}{\frac{\rho_\infty v_\infty^2}{2}} = 2\frac{p_\infty}{\rho_\infty v_\infty^2}\left(\frac{p}{p_\infty} - 1\right) =$$

$$= \frac{k+1}{k}\frac{1 + \frac{k-1}{k+1}M_\infty^{*2}}{M_\infty^{*2}}\left[\left(\frac{1 - \frac{k-1}{k+1}M^{*2}}{1 - \frac{k-1}{k+1}M_\infty^{*2}}\right)^{\frac{k}{k-1}} - 1\right].$$

Unfortunately there is no convenient analytical expression for the relation between C_p and $\tilde{C}_p$; there are, however, tables and graphs which give $C_p = f(\tilde{C}_p, M_\infty, k)$.

Approximate solutions. In a sufficiently large range of subsonic Mach numbers M the function $\sqrt{K} = \frac{\rho_0}{\rho}\sqrt{1 - M^2} = \left(1 + \frac{k-1}{2}M^2\right)^{\frac{1}{k-1}}(1 - M^2)^{\frac{1}{2}}$, introduced by S.A. Chaplygin has been shown to deviate little from unity. If we put $K^{1/2} = 1$ this corresponds formally to $k = -1$ for any $M < 1$.

In nature no gases exist for which $k = c_p/c_v$ is negative; for calculations on subsonic flows it is, however, very useful to introduce such an imaginary gas with an isentropic curve $p/\rho^k = \text{const}$ described by the equation of the straight line $p\rho = \text{const}$, or, in a more general form, by

$$p = \frac{A}{\rho} + B. \qquad (5.11.14)$$

When the constants A and B are properly chosen, this straight line can be made a tangent to the true isentropic curve (Fig. 5.11.2), or a secant passing through two given points which can be chosen at will.

For an incompressible gas the "isentropic curve" has the form ρ = const. S.A. Chaplygin took the tangent at the point p_0, ρ_0, which gives a good approximation at small velocities, S.A. Khristianovich (in first approximation) and also Karman and Tsiang took the tangent at the point p_∞, ρ_∞ corresponding to an undisturbed flow (cf. Fig. 5.11.2).

If k = −1, from the energy equation $a_*^2 + \frac{k-1}{2} w_*^2 = a^2 + \frac{k-1}{2} w^2$ follows

$$a_*^2 - w_*^2 = a^2 - w^2 = a_0^2 = \text{const},$$

$$a = \sqrt{a_0^2 + w^2} \tag{5.11.15}$$

At the same time the critical velocity $a^* = \sqrt{\frac{2}{k+1}} a_0$ becomes infinite, i.e, in an imaginery gas for which k = −1, the velocity of sound cannot be reached and there is no sense in using the velocity coefficient M* = w/a*, since for k = −1 the number M* is zero everywhere. The dimensionless velocity, however, can be determined as the ratio of the flow velocity and a certain constant characterizing the velocity of the given flow.

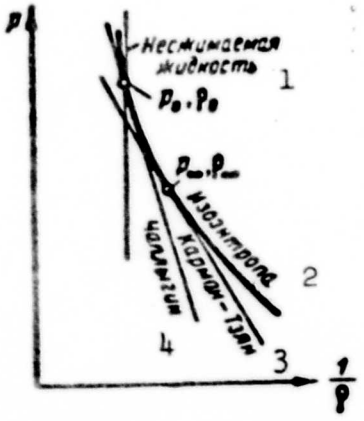


Fig. 5.11.2. Various approximations of the adiabatic curve by straight lines. 1) Incompressible fluid; 2) isentropic line; 3) Karman – Tsiang; 4) Chaplygin.

Since $\tilde{w} \frac{\partial}{\partial \tilde{w}} = \frac{\partial}{\partial \ln \tilde{w}}$, it is convenient to introduce the variable $d\tilde{s} = \frac{d\tilde{w}}{\tilde{w}}$ or $\tilde{s} = \ln \tilde{w}$; at the same time Eqs. (5.11.8) become Cauchy-Riemann equations:

$$\frac{\partial \Phi}{\partial \theta} = \frac{\partial \Psi}{\partial \tilde{s}}, \quad \frac{\partial \Phi}{\partial \tilde{s}} = -\frac{\partial \Psi}{\partial \theta},$$

$$d\tilde{s} = \frac{d\tilde{w}}{\tilde{w}}. \tag{5.11.16}$$

In System (5.11.4) which we rewrite in the form

$$\frac{\partial\Phi}{\partial\theta}=\sqrt{K}\frac{w}{\sqrt{1-M^2}}\frac{\partial\Psi}{\partial w},\quad \frac{w}{\sqrt{1-M^2}}\frac{\partial\Phi}{\partial w}=-\sqrt{K}\frac{\partial\Psi}{\partial\theta}. \tag{5.11.17}$$

it is likewise convenient to substitute $ds=\sqrt{1-M^2}\frac{dw}{w}$ and write

$$\frac{\partial\Phi}{\partial\theta}=\sqrt{K}\frac{\partial\Psi}{\partial s},\quad \frac{\partial\Phi}{\partial s}=-\sqrt{K}\frac{\partial\Psi}{\partial\theta},\quad ds=\sqrt{1-M^2}\frac{dw}{w}. \tag{5.11.18}$$

If we now put ds = $\tilde{ds}$ and $K^{1/2} = -1$, this system of approximate equations will describe the compressible gas flow in the hodograph plane, which coincides with the flow of an isentropic fluid (5.11.16). At the corresponding points of these flows the velocity potentials and stream functions will be equal and the velocity directions will coincide. The boundary conditions of these flows, determined by (5.11.7) will, however, as has already been shown, differ more as M approaches unity more closely. As long as M is small the changes in the boundaries can be ignored.

Since w = w(s), Eq. (5.11.3) can be written in the form

$$\frac{\partial\Phi}{\partial\theta}=\frac{w(s)}{w'(s)}\frac{\rho_0}{\rho}\frac{\partial\Psi}{\partial s};\quad \frac{\partial\Phi}{\partial s}=-\left[-\frac{d}{ds}\left(\frac{\rho_0}{\rho}\right)-\frac{\rho_0}{\rho}\frac{w'(s)}{w(s)}\right]\frac{\partial\Psi}{\partial\theta}=$$
$$=w\frac{d}{ds}\left(\frac{\rho_0}{\rho w}\right)\frac{\partial\Psi}{\partial\theta}.$$

If we introduce the dimensionless velocity coefficients μ and $\tilde{\mu}$ for $\underline{w}$ and $\tilde{w}$, respectively, referring $\underline{w}$ and $\tilde{w}$ to a certain constant which is characteristic of the given flow velocity, we then have

$$\frac{\mu(s)}{\mu'(s)}\frac{\rho_0}{\rho}=\sqrt{K},\quad -\mu\frac{d}{ds}\left(\frac{\rho_0}{\mu\rho}\right)=\sqrt{K}. \tag{5.11.19}$$

If $K^{1/2} = 1$ this will be a set of ordinary differential equations. In order to solve them we put $z = \rho_0/\rho$ in (5.11.19); then

$$\mu z\frac{ds}{d\mu}=1;\quad \mu\frac{d}{ds}\left(\frac{s}{\mu}\right)=1 \tag{*}$$

or

$$\frac{d}{ds}\left(\frac{1}{\mu^2}\frac{d\mu}{ds}\right)=-\frac{1}{\mu};\quad \frac{d}{ds}\left[\frac{d(1:\mu)}{ds}\right]=\frac{1}{\mu};\quad \frac{d^2u}{ds^2}=u\quad\left(u=\frac{1}{\mu}\right)$$

and

$$\mu=\frac{C_1\tilde{\mu}}{1-C_2\tilde{\mu}} \quad \left(\tilde{\mu}=e^{s}\right).$$

Eliminating μ from the set (*) we find $z^2 - dz/ds = 1$, and integration yields

$$s=\ln\tilde{\mu}=\frac{1}{2}\ln\frac{z-1}{z+1}+\text{const}; \quad \frac{\rho_0}{\rho}=\frac{1+C_2\tilde{\mu}^2}{1-C_2\tilde{\mu}^2}.$$

Taking into account that $\lim_{\mu\to 0}(\mu/\tilde{\mu}) = 1$, we find $C_1 = 1$; here

$$\mu=\frac{\tilde{\mu}}{1-C\tilde{\mu}^2}, \quad \tilde{\mu}=\frac{2\mu}{1+\sqrt{1+4C\mu^2}}, \quad \frac{\rho_0}{\rho}=\frac{1+C\tilde{\mu}^2}{1-C\tilde{\mu}^2}=\sqrt{1+4C\mu^2} \qquad (5.11.20)$$

If the velocities $\underline{w}$ and $\tilde{w}$ refer to $2a_0$, i.e., $\mu=w:2a_0$, $\tilde{\mu}=\tilde{w}:2a_0$, then, when calculating $\sqrt{K}=\frac{\rho_0}{\rho}\sqrt{1-\frac{w^2}{a^2}}=1$ we find C = 1 and

$$\mu=\frac{\tilde{\mu}}{1-\tilde{\mu}^2}, \quad \tilde{\mu}=\frac{2\mu}{1+\sqrt{1+4\mu^2}}, \quad \frac{\rho_0}{\rho}=\frac{1+\tilde{\mu}^2}{1-\tilde{\mu}^2}=\sqrt{1+4\mu^2}. \qquad (5.11.21)$$

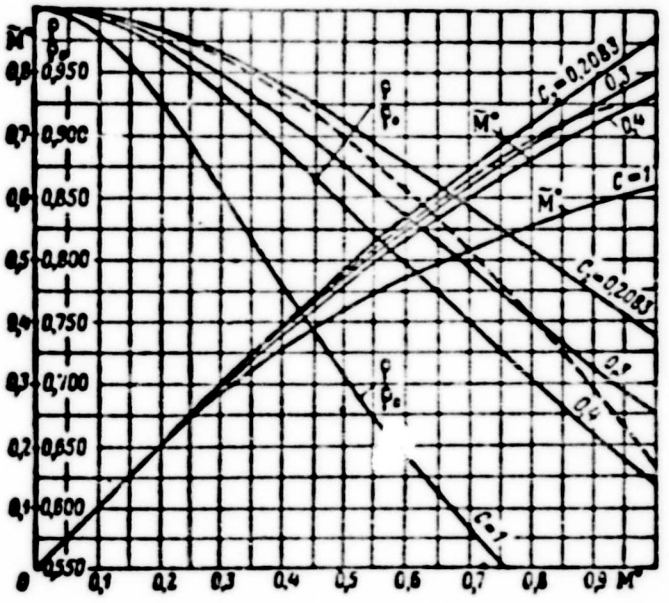


Fig. 5.11.3. Dependence of ρ/ρ_0 and $\tilde{M}^*$ on M^* for various values of the constant.

If the velocity coefficients μ and $\tilde{\mu}$ are determined by the ratios $w:a^*=M^*$ and $\tilde{w}:a^*=\tilde{M}^*$ respectively, where $a^*=\sqrt{\frac{2k}{k+1}RT_0}$, then we obtain from (5.11.20)

$$M^*=\frac{\tilde{M}^*}{1-CM^{*2}}, \quad \tilde{M}^*=\frac{2M^*}{1+\sqrt{1+4CM^{*2}}}, \quad \frac{\rho_0}{\rho}=\frac{1+C\tilde{M}^{*2}}{1-C\tilde{M}^{*2}}=\sqrt{1+CM^{*2}}. \qquad (5.11.22)$$

The dependence of $\tilde{M}^*$ and ρ_0/ρ on M^* is shown in Fig. 5.11.3. The

dashed curves give the exact values of ρ_0/ρ and $M^* = f(\tilde{M}^*)$ got from the formula of S.A. Khristianovich as a result of integrating (5.11.14). The constanct C is chosen according to the range in which the M* values vary.

The pressure coefficient. Differentiating (5.11.14) we obtain $dp = -(A:\rho^2)d\rho$ and since $a^2 = \frac{dp}{d\rho}$, we have $A = -\rho^2 a^2 = -\rho_0 a_0^2 = -\rho_\infty a_\infty^2$. Determining $p_\infty = -\rho_\infty a_\infty^2 + B$, we find for the imaginary gas with k = −1

$$p = p_\infty + \rho_\infty a_\infty^2\left(1 - \frac{\rho_\infty}{\rho}\right), \quad C_p = \frac{2(p-p_\infty)}{\rho_\infty v_\infty^2} = \frac{2}{M_\infty^2}\left(1 - \frac{\rho_\infty}{\rho}\right). \tag{5.11.23}$$

For an incompressible fluid

$$\tilde{C}_p = \frac{2(\tilde{p}-\tilde{p}_\infty)}{\tilde{\rho}\tilde{v}_\infty^2} = 1 - \frac{\tilde{v}^2}{\tilde{v}_\infty^2} = 1 - \frac{\tilde{\mu}^2}{\tilde{\mu}_\infty^2}. \tag{5.11.24}$$

Therefore

$$C_p = \frac{2}{M_\infty^2}\left(1 - \frac{\rho_\infty}{\rho_0}\frac{\rho_0}{\rho}\right) = \frac{2}{M_\infty^2}\left(1 - \frac{1-\tilde{\mu}_\infty^2}{1+\tilde{\mu}_\infty^2}\frac{1+\tilde{\mu}^2}{1-\tilde{\mu}^2}\right) =$$
$$= \frac{4}{M_\infty^2}\frac{\tilde{\mu}_\infty^2 - \tilde{\mu}^2}{(1+\tilde{\mu}_\infty^2)(1-\tilde{\mu}_\infty^2+\tilde{\mu}_\infty^2-\tilde{\mu}^2)} =$$
$$= \frac{4}{M_\infty^2}\frac{\tilde{\mu}^2\tilde{C}_p}{(1+\tilde{\mu}_\infty^2)(1-\tilde{\mu}_\infty^2+\tilde{\mu}_\infty^2\tilde{C}_p)}.$$

Noticing that $\frac{\rho_0}{\rho}\sqrt{1-M_\infty^2} = 1 - \sqrt{1+4\mu_\infty^2}\sqrt{1-M_\infty^2}$ and taking (5.11.24) into account, we find

$$M_\infty^2 = \frac{1}{4}\frac{M_\infty^2}{1-M_\infty^2}, \quad \tilde{\mu}_\infty = \frac{2\mu_\infty}{1+\sqrt{1+4\mu_\infty^2}} = \frac{M_\infty}{1+\sqrt{1-M_\infty^2}}. \tag{5.11.25}$$

Substituting this into the expression for C_p and making some simple transformations, we obtain

$$C_p = \frac{\tilde{C}_p}{\sqrt{1-M_\infty^2} + \frac{M_\infty^2}{2(1+\sqrt{1-M_\infty^2})}\tilde{C}_p}. \tag{5.11.26}$$

This is the formula given by Karman and Tsiang in 1939. As can be seen, it is obtained from an exacter solution, given by S.A. Khristianovich as a first approximation.

A profile in a subsonic gas flow. This is one of the most complex

problems of aeromechanics. The very fact that the above-mentioned Chaplygin method is a method of passing over to the hodograph plane and of replacing the exact adiabatic curve by a linear relation between pressure and specific volume is of great significance in the solution of this problem. After S.A. Chaplygin (1902) had developed the method, N.A. Slezkin (1937) and Tsiang (1939) applied it to solving the problem of an unstalled circulation-free flow about a profile.

In 1940 S.A. Khristianovich developed the method for solving the problem of a profile in a subsonic gas flow with circulation, establishing the correspondence between the physical plane of flow and the flow of an incompressible fluid about an imaginary distorted profile. In order to establish the correspondence the method of successive approximations is used, Φ and Ψ being substituted in the form of the series (5.11.13). The method of S.A. Khristianovich was further improved in 1946 in a paper [5.3] published together with I.M. Yur'yev; another imaginary flow was introduced in order to obtain a unique solution.

L.I. Sedov and his pupils succeeded in their most recently published papers inasmuch as they directly continued the Chaplygin method, which thus led to a simpler method of calculating subsonic gas flows [5.1]. A discussion of these papers would overstep the bounds of the course and here we can only outline the paper by L.I. Sedov on which the studies of his pupils are based.

It follows from Eq. (5.11.16)

$$\frac{\partial \Phi}{\partial \vartheta} = \frac{\partial \Psi}{\partial s}; \quad \frac{\partial \Phi}{\partial s} = -\frac{\partial \Psi}{\partial \vartheta}$$

that $\Phi + i\Psi$ is an analytical function of the complex variable $s - i\vartheta$, i.e., also of the variable $e^{s-i\vartheta}$. We put $e^s = \tilde{w}/2a_0$ and we shall consider the variable

$$2a_0 e^{s-i\vartheta} = \tilde{w} e^{-i\vartheta} \qquad (5.11.27)$$

as the complex velocity in the auxiliary plane ζ of incompressible fluid flow; we shall moreover assume that its complex potential is expressed by the relation

$$\Phi + i\Psi = w^* f(\zeta), \tag{5.11.28}$$

where w^* is a certain constant with the dimension of a velocity which is introduced because of dimensional considerations.

In order to establish the relation between the variables z and ζ which should map the Chaplygin gas flow on the z-plane onto the fluid plane ζ, we rewrite Eq. (5.11.2) for dz, taking into account that according to (5.11.21)

$$w = \frac{4a_0^2 \tilde{w}}{4a_0^2 - \tilde{w}^2}; \quad \frac{\rho}{\rho_0} = \frac{4a_0^2 + \tilde{w}^2}{4a_0^2 - \tilde{w}^2};$$

$$dz = \frac{e^{i\theta}\left(4a_0^2 - \tilde{w}^2\right)}{4a_0^2 \tilde{w}} d\Phi + i \frac{4a_0^2 + \tilde{w}^2}{4a_0^2 - \tilde{w}^2} d\Psi \frac{e^{i\theta}\left(4a_0^2 - \tilde{w}^2\right)}{4a_0^2 \tilde{w}} =$$

$$= \frac{e^{i\theta}}{\tilde{w}} (d\Phi + i d\Psi) - \frac{\tilde{w}}{4a_0^2} e^{i\theta} (d\Phi - i d\Psi) =$$

$$= d\zeta - \frac{\tilde{w} e^{2i\theta}}{4a_0^2} d\bar{\zeta}. \tag{5.11.29}$$

or, in the form suggested by Tsiang,

$$dz = d\zeta - \tilde{w}^2 \overline{\left(\frac{df}{d\zeta}\right)^2 d\zeta}. \tag{5.11.30}$$

In the ζ-plane we have a certain (unknown) excluded contour which is the image of the profile given in the z-plane. Together with the contour on the ζ-plane the excluded region can be mapped to the interior of the parameteral t-plane with the help of the function

$$\zeta = \frac{a_{-1}}{t} + a_0 t + a_1 t^2 + \ldots. \tag{5.11.31}$$

Since as $\zeta \to \infty$, $t \to 0$, and assuming that $\left.\frac{df}{d\zeta}\right|_{t=0} = 1$, we obtain

$$\frac{d\zeta}{dt} = -\frac{a_{-1}}{t^2} + a_0 + 2a_1 t + \ldots = A \frac{\Phi(t)}{t^2}, \quad (A = -a_{-1}). \tag{5.11.32}$$

Though the coefficients A, a_0, a_1, a_2,... are unknown, we know the complex potential on the t-plane, namely

$$f(t) = -A\left(t + \frac{1}{t}\right) - \frac{\Gamma}{2\pi i\tilde{w}} \ln t. \qquad (5.11.33)$$

The fundamental Eq. (5.11.30) can here be rewritten in the form

$$dz = A\frac{\Phi(t)}{t^2}dt - \frac{\tilde{r}^2}{\Phi(t)}(t - e^{i\alpha_0})^2(t + e^{-i\alpha_0})^2\frac{dt}{t^2}, \qquad (5.11.34)$$

where $\Gamma = 4\pi a\tilde{w}_\infty \sin\alpha_0$.

Decomposing dz into real and imaginary parts and integrating, we obtain $\underline{x}$ and $\underline{y}$ as functions of the parameter $\underline{t}$. The unknown coefficients a_k appear in these formulations. If we assume in the series of $\underline{x}$ and $\underline{y}$ that $t = e^{i\tau}$ and if we let τ run through the interval $(0,2\pi)$, we obtain the parametral equation of the contour in the z-plane as the image of the circle $|t| = 1$ in the t-plane. The condition needed to determine the coefficients a_k is the requirement that the contour should coincide with the given profile in the z-plane.

Examples for solving this problem approximately are dealt with in the papers by L.I. Sedov's pupils.

5.12. NEARSONIC FLOWS

Nearsonic flows are flows whose velocities differ only a little from the local sonic velocity. Such flows can be subsonic everywhere and supersonic and mixed everywhere, i.e., these flows can be partly subsonic and partly supersonic. The theoretical investigation of mixed flows is difficult since the differential equations which describe these motions, the so-called Euler-Triccomi equations, are very complicated. Experimental investigation is rendered difficult by the great influence of the stream boundaries on the flow around the model.

Approximate differential equation of nearsonic flows. Let us consider a thin profile placed in a nearsonic flow whose velocity w_∞ is only slightly disturbed and is near to the velocity of sound, i.e.,

$$(a^* - w_\infty) : a^* \ll 1; \quad (a^* - w_x) : a^* \ll 1; \quad w_y : a^* \ll 1.$$

Let us calculate the coefficients of Eq. (5.1.6):

$$a^2-w_x^2=a_0^2-\frac{k-1}{2}w^2-w_x^2=\frac{k+1}{2}a^{*2}-\frac{k-1}{2}(w_x^2+w_y^2)-w_x^2=$$

$$=\frac{k+1}{2}(a^{*2}-w_x^2)-\frac{k-1}{2}w_y^2=\frac{k+1}{2}(a^*-w_x)(-a^*+w_x+2a^*)-$$

$$-\frac{k-1}{2}w_y^2=-\frac{k+1}{2}(a^*-w_x)^2+(k+1)(a^*-w_x)a^*-\frac{k-1}{2}w_y^2\approx$$

$$\approx(k+1)a^*(a^*-w_x),$$

$$w_xw_y=-w_y(a^*-w_x)+w_ya^*\approx w_ya^*, \qquad (*)$$

$$a^2-w_y^2=\frac{k+1}{2}a^{*2}-\frac{k-1}{2}(w_x^2+w_y^2)-w_y^2=\frac{k-1}{2}(a^{*2}-w_y^2)-$$

$$-\frac{k+1}{2}w_y^2+a^{*2}\approx a^{*2}+(k-1)(a^*-w_x)a^*.$$

Neglecting the term $(k-1)a^*(a^*-w_x)\frac{\partial w_y}{\partial y}$, we then obtain instead of (5.1.6)

$$-(k+1)(w_x-a^*)\frac{\partial w_x}{\partial x}-2w_y\frac{\partial w_x}{\partial y}+a^*\frac{\partial w_y}{\partial y}=0. \qquad (5.12.1)$$

Let us therefore assume for the velocity potential

$$\Phi=a^*x+(1-M_\infty^*)\varphi,\quad M_\infty^*=\frac{w_\infty}{a^*}. \qquad (5.12.2)$$

Then

$$\left.\begin{aligned}w_x&=\frac{\partial\Phi}{\partial x}=a^*-(1-M_\infty^*)\frac{\partial\varphi}{\partial x}=a^*+w_x'.\\ w_y&=\frac{\partial\Phi}{\partial y}=(1-M_\infty^*)\frac{\partial\varphi}{\partial y}=w_y'.\end{aligned}\right\} \qquad (5.12.3)$$

Substituting in Eq. (5.12.1) we obtain

$$-(k-1)(1-M_\infty^*)\frac{\partial\varphi}{\partial x}\frac{\partial^2\varphi}{\partial x^2}-2(1-M_\infty^*)\frac{\partial\varphi}{\partial y}\frac{\partial^2\varphi}{\partial x\partial y}+$$

$$+a^*\frac{\partial^2\varphi}{\partial y^2}=0. \qquad (5.12.4)$$

Since the boundary conditions at infinity require that $x\to\infty$, $y\to\infty$, $w_x\to w_\infty$ и $w_y\to 0$, we obtain from Eq. (5.12.3) with $x,y\to\pm\infty$

$$\frac{\partial\varphi}{\partial x}=-a^*,\quad \frac{\partial\varphi}{\partial y}=0. \qquad (5.12.5)$$

If $(dy/dx)_L$ is the slope of the profile surface to the chord and $\delta = d/b$ is the relative profile thickness, then, since we have supposed that the disturbances are small, the boundary conditions on the profile surface will be

$$\frac{v_y}{v_x} = \frac{w_y}{a^*} - \left(\frac{dy}{dx}\right)_L = \delta h,$$

where $h = \left(\frac{dy}{dx}\right)_L : \delta$ is a dimensionless function of the order of one. Owing to the small profile thickness we obtain from (5.12.3) for $y = -0$, $0 \leqslant x : b < 1$

$$(1 - M_\infty^*)\frac{\partial \varphi}{\partial y} = a^* \delta h. \qquad (5.12.6)$$

Similarity rule for nearsonic flows [5.6]. Let us try now to determine a dimensionless coordinate function f that would be one and the same for similar flows which have one and the same value of a certain parameter, K, which depends on the number M_∞^* and the thickness $\delta = d/b$. This can be done if we put

$$\xi = \frac{x}{b}, \quad \eta = \frac{y}{b(k+1)^m \delta^n} \quad \left(\delta = \frac{d}{b}\right). \qquad (5.12.7)$$

where the powers m and n are unknown as yet and the disturbance potential is taken in the form

$$\varphi = ba^* f(\xi, \eta). \qquad (5.12.8)$$

Then, going over to the new coordinates ξ, η, we find subsequently

$$\left.\begin{aligned}
&\frac{\partial \varphi}{\partial x} = \frac{\partial \varphi}{\partial \xi}\frac{d\xi}{dx} = a^* \frac{\partial f}{\partial \xi}, \\
&\frac{\partial}{\partial x}\frac{\partial \varphi}{\partial x} = \frac{\partial}{\partial \xi}\frac{\partial \varphi}{\partial x}\frac{d\xi}{dx} = \frac{a^*}{b}\frac{\partial^2 f}{\partial \xi^2}, \\
&\frac{\partial}{\partial y}\frac{\partial \varphi}{\partial x} = \frac{\partial}{\partial \eta}\frac{\partial \varphi}{\partial x}\frac{d\eta}{dy} = \frac{a^*}{b(k+1)^m \delta^n}\frac{\partial^2 f}{\partial \xi \partial \eta}, \\
&\frac{\partial \varphi}{\partial y} = \frac{\partial \varphi}{\partial \eta}\frac{d\eta}{dy} = \frac{a^*}{(k+1)^m \delta^n}\frac{\partial f}{\partial \eta}, \\
&\frac{\partial}{\partial y}\frac{\partial \varphi}{\partial y} = \frac{\partial}{\partial \eta}\frac{\partial \varphi}{\partial y}\frac{d\eta}{dy} = \frac{a^*}{b(k+1)^{2m}\delta^{2n}}\frac{\partial^2 f}{\partial \eta^2}.
\end{aligned}\right\} \qquad (5.12.9)$$

Substituting these values in Eq. (5.12.4) we obtain

$$-(k+1)^{2m+1}(1 - M_\infty^*)\delta^{2n}\frac{\partial f}{\partial \xi}\frac{\partial^2 f}{\partial \xi^2} + \frac{\partial^2 f}{\partial \eta^2} = -2(1 - M_\infty^*)\frac{\partial f}{\partial \eta}\frac{\partial^2 f}{\partial \xi \partial \eta}. \qquad (5.12.10)$$

The corresponding boundary conditions will be

$$\xi, \ \eta \to \pm\infty, \ \frac{\partial f}{\partial \xi} = -1, \ \frac{\partial f}{\partial \eta} = 0; \qquad (5.12.11)$$

$$\eta = 0, \ 0 \leqslant \xi \leqslant 1, \ \frac{\partial f}{\partial \eta} = \frac{(k+1)^m \delta^{n+1}}{1 - M_\infty^*} h(\xi). \qquad (5.12.12)$$

It can be seen from Eqs. (5.12.10) and (5.12.12) that if we put

$$2m+1=-m \text{ and } 2n=-(n+1), \text{ i.e., } m=-\frac{1}{3},\ n=-\frac{1}{3}$$

and introduce the parameter K by the relation

$$K=\frac{1}{2}\left(\frac{k+1}{2}\right)^{\frac{1}{3}}(1-M_{-}^{*})^{-\frac{2}{3}}, \tag{5.12.13}$$

we then obtain instead of (5.12.10), (5.12.11) and (5.12.12) the equation for a nearsonic flow

$$-2K\frac{\partial f}{\partial \xi}\frac{\partial^2 f}{\partial \xi^2}+\frac{1}{\sqrt[3]{2}}\frac{\partial^3 f}{\partial \eta^3}=4K\sqrt[3]{\frac{v^3}{k+1}}\frac{\partial f}{\partial \eta}\frac{\partial^2 f}{\partial \xi \partial \eta} \tag{5.12.14}$$

and the boundary conditions corresponding to (5.12.11) and (5.12.12) will be

$$\xi,\ \eta\to\pm\infty,\ \frac{\partial f}{\partial \xi}=-1,\ \frac{\partial f}{\partial \eta}=0; \tag{5.12.15}$$

$$\eta=0,\ 0<\xi<1,\ \frac{\partial f}{\partial \eta}=\frac{1}{2\sqrt[3]{2}K}h(\xi). \tag{5.12.16}$$

At the same time the dimensionless coordinates (5.12.7) will be

$$\xi=\frac{x}{b},\ \eta=\frac{y}{b}\sqrt[3]{(k+1)\delta}. \tag{5.12.17}$$

If $1-M_{\infty}^{*}$ and δ are quantities of the same order of magnitude, then the right-hand side of (5.12.14) can be neglected and we can write

$$-2\sqrt[3]{2}K\frac{\partial f}{\partial \xi}\frac{\partial^2 f}{\partial \xi^2}+\frac{\partial^3 f}{\partial \eta^3}=0. \tag{5.12.18}$$

When the boundary conditions (5.12.15) and (5.12.16) are taken into account, it follows that if K has one and the same value for different flows, the dimensionless function $f(\xi,\eta)$ will also have the same value for them. The parameter K may thus be regarded as a similarity criterion for nearsonic flows.

For further calculations it is convenient to introduce M_{-} in the place of M_{∞}^{*}. For this we write

$$1-M_{-}^{*}=1-\frac{v_{-}}{a_{-}}\frac{a_{-}}{a^{*}}=1-M_{-}\frac{a_{-}}{a^{*}}=(1-M_{-})\frac{a_{-}}{a^{*}}+\left(1-\frac{a_{-}}{a^{*}}\right).$$

Since $a_\infty^2 = \frac{k+1}{2}a^{*2} - \frac{k-1}{2}w_\infty^2$, we have

$$\frac{a_\infty}{a^*} = \sqrt{\frac{\frac{k+1}{2}}{1+\frac{k-1}{2}M_\infty^2}} = \sqrt{\frac{1}{1+2\frac{k-1}{k+1}(M_\infty-1)+\frac{k-1}{2}(M_\infty-1)^2}}.$$

Expanding this into a series of $M_\infty - 1$, we obtain

$$\frac{a_\infty}{a^*} \approx 1 + \frac{k-1}{k+1}(1-M_\infty).$$

We now have

$$1 - M_\infty^* \approx \frac{2}{k+1}(1-M_\infty) \qquad (5.12.19)$$

and

$$K = \frac{1-M_\infty^*}{\sqrt[3]{\frac{2}{k+1}k^2}} \approx \frac{1-M_\infty}{\sqrt[3]{\left(\frac{k+1}{2}k\right)^2}}; \qquad (5.12.20)$$

$K > 0$ corresponds to the subsonic flow condition $M_\infty < 1$ and $K < 0$ to the supersonic.

The pressure coefficient. If the disturbances are assumed to be small the pressure coefficient can be written in the form

$$C_p = \frac{2(p-p_\infty)}{\rho_\infty w_\infty^2} = -2\frac{w_x - w_\infty}{w_\infty} = -2\left(\frac{w_x}{a^*}\frac{a^*}{w_\infty} - 1\right) \approx$$
$$\approx -2\left(\frac{w_x}{a^*} - 1\right). \qquad (5.12.21)$$

According to (5.12.3), however,

$$\frac{w_x}{a^*} = \frac{1}{a^*}\frac{\partial\Phi}{\partial x} = \frac{1}{a^*}\left|a^* + (1-M_\infty^*)\frac{\partial\varphi}{\partial x}\right|.$$

Therefore, when (5.12.19) is taken into account,

$$C_p = -\frac{2}{a^*}(1-M_\infty^*)\frac{\partial\varphi}{\partial x} = -2(1-M_\infty^*)\frac{\partial f}{\partial\xi} =$$
$$= -\frac{4}{k+1}(1-M_\infty)\frac{\partial f}{\partial\xi}. \qquad (5.12.22)$$

Since the function $f(\xi,\eta)$ depends only on the shape of the profile and on K, we can use (5.12.13) and (5.12.19) to write

$$C_p = \frac{2(1-M_\infty)}{k+1} G(K, \xi, \eta) = K \sqrt[3]{\frac{2\delta}{k+1}} G(K, \xi, \eta), \qquad (5.12.23)$$

where $G(K,\xi,\eta)$ is a function of K, ξ, and η, the form of which is determined by the family of profiles.

Thus, if we know the distribution of pressure C_p at M_∞ for a profile with the thickness ratio δ_1, then, by virtue of (5.12.23), the pressure coefficient for a profile of the same family with the thickness ratio δ_2 will read

$$C_{p2} = C_{p1} \sqrt[3]{\left(\frac{\delta_2}{\delta_1}\right)^2} \qquad (5.12.24)$$

with

$$M_{\infty 2} = 1 - (1 - M_{\infty 1}) \sqrt[3]{\left(\frac{\delta_2}{\delta_1}\right)^2}. \qquad (5.12.25)$$

The lift coefficient is

$$C_y = \frac{1}{b} \oint C_p \, dx = \oint C_p \, d\bar{x} = \sqrt[3]{\frac{2\delta}{k+1}} H(K) = \frac{2}{k+1} \frac{(1-M_\infty) H(K)}{K}. \qquad (5.12.26)$$

Finally, the shape drag (pressure) coefficient is

$$C_{xp} = \frac{1}{b} \oint C_p \, dy = \frac{1}{b} \oint C_p \left(\frac{dy}{dx}\right)_l dx = \oint C_p \bar{h} \, d\bar{x} = \frac{\sqrt[3]{2}\sqrt[3]{\delta^2}}{\sqrt{k+1}} B(K) = \sqrt[3]{\frac{2}{k+1}} \cdot \sqrt{\left(\frac{1-M_\infty}{K}\right)^3} B(K). \qquad (5.12.27)$$

All functions B(K) and H(K), and also the function G(K), are functi ns of only K and the thickness distribution $h(\xi)$. The case $M_\infty = 1$ corresponds to K = 0, regardless of the thickness. From here the functions B, G and H depend on the profile shape, i.e., on the thickness distribution and not on the thickness ratio $\delta = d/b$. For similar profiles C_y is proportional to $\delta^{2/3}$ and $C_{xp} \sim \delta^{5/3}$, and the lift/drag ratio of the profile, $1/\mu = C_y/C_x$, is inversely proportional to δ.

Description of the transition from subsonic to mixed flow. Let us consider the transition from subsonic to mixed flow in a plane

Laval nozzle (Fig. 5.12.1). If the counter-pressure is large the flow is subsonic everywhere and $M < 1$; but above a certain M-value small regions in which $M > 1$ appear in the throat (cf. Fig. 5.12.1,a and b). As the counterpressure drops the velocity in the nozzle increases until sonic speed is reached in the narrowest cross section (throat) (cf. Fig. 5.12.1, c). Any further pressure drop at the exit leads to a normal compression shock arising at the walls. In this case, before the throat the flow will have a Mach number $M < 1$, in the region between throat and normal shock $M < 1$, and behind the normal shock again $M < 1$ (cf. Fig. 5.12.1,d). As the velocity increases further the normal shock becomes closed behind the throat; the region of supersonic flow grows until it occupies the whole region behind the throat (cf. Fig. 5.12.1,e).

Figure 5.12.2 is a schematic diagram of the flow of a nearsonic stream about a subsonic profile. At $M_\infty = 0.7$ the local Mach number M reaches unity and a small region of supersonic flow appears. As long as M_∞ is slightly larger than M_{kr} no shocks arise besides a λ shock. Then, as M_∞ increases the supersonic region grows in its size and shifts smoothly backwards without giving rise to shocks. The interaction of the λ shock with the boundary layer leads to premature stalling (at $M_\infty = 0.9$ – cf. Fig. 5.12.2).

When M_∞ is further increased ($M_\infty = 0.95$) the λ shock is displaced backwards and becomes intensified. Even at $M_\infty = 1.05$ a clearly marked normal detached shock appears at the profile nose. As M_∞ increases it becomes curved and approaches the profile ($M_\infty = 1.3$). By way of example, the coefficients C_x and C_y are shown as functions of M_∞ for a subsonic NACA 23012 profile arranged at an angle of attack of $\alpha = 1.6$ (Fig. 5.12.3).

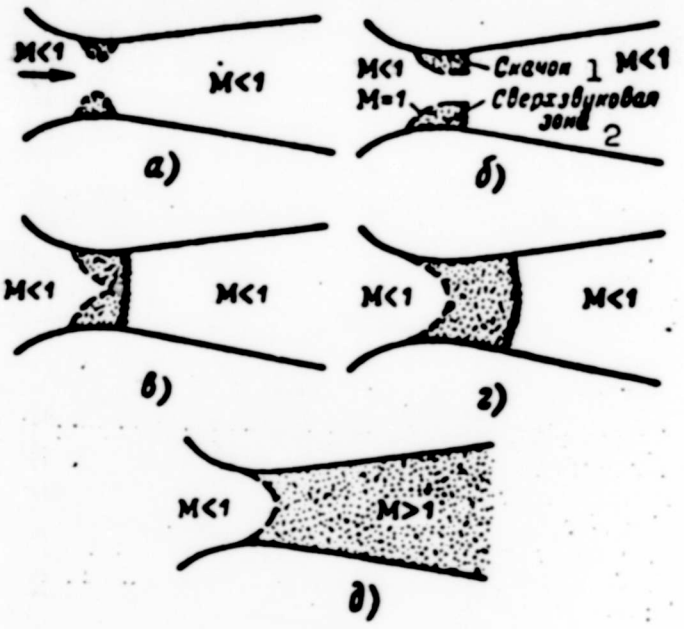


Fig. 5.12.1. Transition through sonic speed in a Laval nozzle. 1) Shock; 2) supersonic zone.

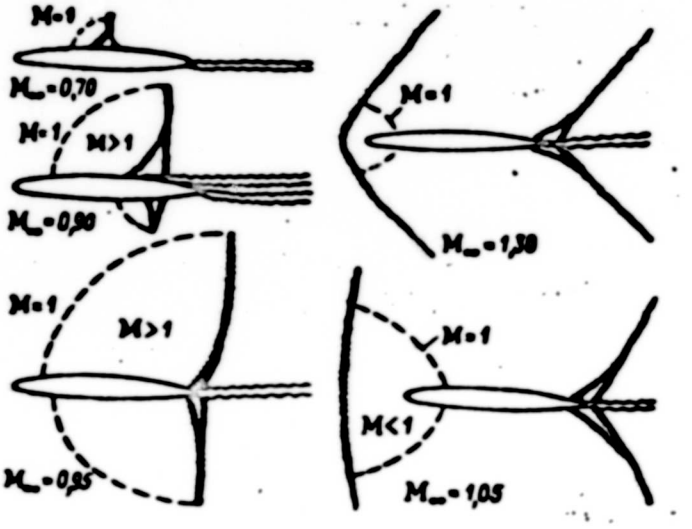


Fig. 5.12.2. Character of flow about an airfoil profile at the transition through sonic speed.

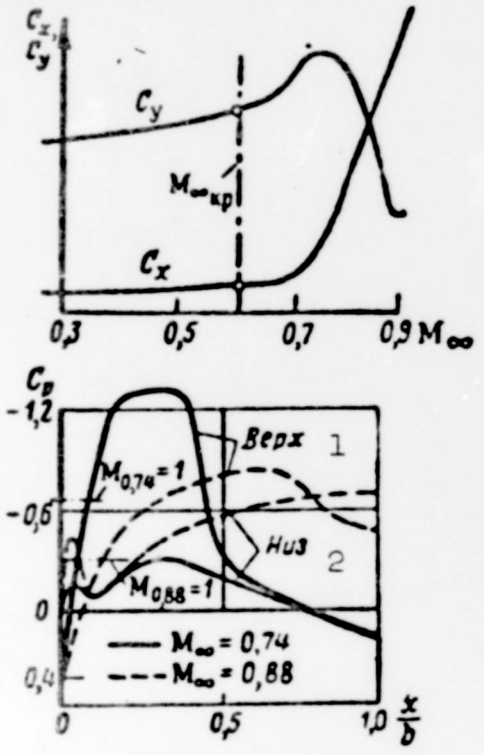


Fig. 5.12.3. Pressure distribution over a profile and lift and drag coefficients as functions of M (M close to unity). 1) Above; 2) below.

5.13. HYPERSONIC FLOWS

Flows with very large numbers M_∞ – usually M_∞ is taken to be greater than 7/8 – are called <u>hypersonic</u>*. The theory of hypersonic flows [5.7] is of freat practical significance, especially nowadays, for example, in connection with rocket flights at very high speeds. Flight at these velocities is possible at very great altitudes where air density and drag are small.

With increasing M_∞ the specific heat ratio $k = c_p/c_v$ varies from $k = 1.4$ to $k = 1$ because of the dissociation of the gas molecules constituting the air (isothermal change of state of the air), during which the air at the surface of the bodies placed in the flow is strongly heated. At large M_∞ the diagonal compression shock is adjacent to the body surface and its influence is restricted to a relatively thin layer of air at the profile surface.

<u>Approximate differential equation of hypersonic flows.</u> Let us consider a vortex-free plane flow about a thin profile. Let the velocity disturbance potential be denoted by φ, and assuming $\Phi(x, y) = w_\infty x + \varphi(x, y)$, we can write for it

$$\left(1-\frac{w_x^2}{a^2}\right)\frac{\partial^2\varphi}{\partial x^2}-2\frac{w_x w_y}{a^2}\frac{\partial^2\varphi}{\partial x\,\partial y}+\left(1-\frac{w_y}{a^2}\right)\frac{\partial^2\varphi}{\partial y^2}=0. \qquad (5.13.1)$$

where

$$w_x = w_\infty+\frac{\partial\varphi}{\partial x},\quad w_y=\frac{\partial\varphi}{\partial y},\quad a^2=a_\infty^2+\frac{k-1}{2}(w_\infty^2-w^2)= \\ =a_\infty^2-\frac{k-1}{2}\left[2w_\infty\frac{\partial\varphi}{\partial x}+\left(\frac{\partial\varphi}{\partial x}\right)^2+\left(\frac{\partial\varphi}{\partial y}\right)^2\right]. \qquad (5.13.2)$$

Owing to the suppositions adopted

$$a_\infty \ll w_\infty, \quad \frac{\partial \varphi}{\partial x} \ll w_\infty, \quad \frac{\partial \varphi}{\partial y} \ll w_\infty \tag{5.13.3}$$

we can approximately derive from (5.13.1)

$$\left[1-(k+1)\frac{M_\infty}{a_\infty}\frac{\partial \varphi}{\partial x}-\frac{k-1}{2}\frac{1}{a_\infty^2}\left(\frac{\partial \varphi}{\partial y}\right)^2-M_\infty^2\right]\frac{\partial^2 \varphi}{\partial x^2}-$$
$$-2\frac{M_\infty}{a_\infty}\frac{\partial \varphi}{\partial y}\frac{\partial^2 \varphi}{\partial x \partial y}+\left[1-(k-1)\frac{M_\infty}{a_\infty}\frac{\partial \varphi}{\partial x}-\right. \tag{5.13.4}$$
$$\left.-\frac{k+1}{2}\frac{1}{a_\infty^2}\left(\frac{\partial \varphi}{\partial y}\right)^2\right]\frac{\partial^2 \varphi}{\partial y^2}=0.$$

In the same way as when analyzing nearsonic flows we introduce the dimensionless coordinates

$$\xi=\frac{x}{b}, \quad \eta=\frac{y}{d}=\frac{y:b}{d:b}=\frac{y:b}{\delta} \quad \left(\delta=\frac{d}{b}\right) \tag{5.13.5}$$

to obtain the similarity criteria and we assume the disturbance potential in the form

$$\varphi=\frac{a_\infty b}{M_\infty} f(\xi, \eta). \tag{5.13.6}$$

Then, assuming $\delta^2 \ll 1$ and neglecting the higher-order small terms we obtain from (5.13.4)

$$\left[1-(k-1)\frac{\partial f}{\partial \xi}-\frac{k+1}{2(M_\infty \delta)^2}\left(\frac{\partial f}{\partial \eta}\right)^2\right]\frac{\partial^2 f}{\partial \eta^2}=$$
$$=(M_\infty \delta)^2\frac{\partial^2 f}{\partial \xi^2}+2\frac{\partial f}{\partial \eta}\frac{\partial^2 f}{\partial \eta \partial \xi}. \tag{5.13.7}$$

The boundary conditions for $x \to \infty$ are $\frac{\partial \varphi}{\partial x} \to 0$, $\frac{\partial \varphi}{\partial y} \to 0$, and at the profile surface they read $(\partial \varphi/\partial y): w_\infty = (dy/dx)_L$; in the new variables, neglecting the higher-order small terms, we have

$$\left.\begin{array}{ll} \text{for} & \xi \to -\infty \quad \partial f/\partial \xi \to 0, \ \partial f/\partial \eta \to 0, \\ & (\partial f/\partial y)_L = M_\infty^{1/3} h(\xi). \end{array}\right\} \tag{5.13.8}$$

and at the profile surface

Here $\eta(\xi) = (dy/dx)_L : \delta$ is a dimensionless function of the thickness distribution, independent of the thickness ratio δ.

Considering (5.13.7) and (5.13.8) we can see that the similarity criterion for hypersonic flows is the parameter

$$K_1 = M_\infty \delta \tag{5.13.9}$$

The force coefficient. Using the exact connection between p and p_∞ for an isentropic flow (4.2.9), the expression for φ (5.13.6) and the determination of the pressure coefficient $C_p = \frac{2(p-p_-)}{\rho_- v_-^2} = \frac{2}{kM_-^2}\left(\frac{p}{p_-}-1\right)$, we can show that

$$C_p = \delta^2 P(K_h, k, \xi, \eta) = \frac{1}{M_-^2} K_h P(K_h, k, \xi, \eta), \tag{5.13.10}$$

where

$$P(K_h, k, \xi, \eta) = \frac{2}{K_h^2 k}\left\{\left[1-(k-1)\frac{\partial f}{\partial \xi}+\frac{k-1}{2K_h^2}\left(\frac{df}{\partial \eta}\right)^2\right]^{\frac{k}{k-1}}-1\right\}. \tag{5.13.11}$$

For the family of profiles having the same thickness distribution (i.e. with camber and angle of attack proportional to δ) and the same $k = c_p/c_v$, the function P depends only on K_h.

Therefore

$$\left.\begin{aligned} C_y &= \frac{1}{b}\oint C_p\, dx = \delta^2 Q(K_h, k) = \frac{1}{M_-^2} K_h^2 Q(K_h, k), \\ C_x &= \frac{1}{b}\oint C_p\, dy = \delta^3 R(K_h, k) = \frac{1}{M_-^3} K_h^3 R(K_h, k). \end{aligned}\right\} \tag{5.13.12}$$

Example. Let us assume that we know C_x and C_y from testing an 8% symmetrical profile with $M_\infty = 5$ and an angle of attack of $\alpha = 6^\circ$. From the expression of the similarity criterion (5.13.9) it follows that $K_h = 5 \cdot 0.08 = 0.4$ and therefore a similar 4% profile, for example, with $M_\infty = 0.4/0.04 = 10$ and an angle of attack $\alpha = 0.04/0.08) \cdot 6^\circ = 3^\circ$ will have the coefficients

$$C_{x4\%} = \left(\frac{0.04}{0.08}\right)^3 C_{x8\%} = \frac{1}{8} C_{x8\%};\quad C_{y4\%} = \left(\frac{0.04}{0.08}\right)^2 C_{y8\%} = \frac{1}{4} C_{y8\%}.$$

Infinitely large number M_∞. When M_∞ is unlimitedly increased, K_h and the P-function (5.13.11) increase unlimitedly and together with them the functions Q and R will not depend on the thickness ratio δ. In this case, as can be seen from (5.13.12), C_y will be proportional to δ^2, and C_x proportional to δ^3 which is in agreement with Newton's

corpuscular theory.

Manuscript Page No.

[Footnotes]

296 Only near the stagnation points where the total velocity becomes zero is the disturbance velocity comparable with the velocity of the undisturbed flow.

299 The notation has been set up by analogy with the algebraic second-order curves governed by the general equation $ax^2+2bxy+cy^2+dx+ey+f=0$. If $B^2-AC=0$ the equation is parabolic.

301 Remember that the equation of the form $F''(t) = kF(t)$ is well known as the equation describing the oscillations of a point under the action of a force proportional to the displacement of the point from its equilibrium position. To solve it we put $F(t) = e^{pt}$. Then $F''(t) = p^2e^{pt}$, and therefore $p^2 = k$ и $k = p^2$. The number k can be both positive and negative. If $k > 0$, then, assuming $k = p^2$, we obtain $p = \pm p$ и $F(t) = a_1e^{pt} + a_2e^{-pt}$. If $k < 0$, then, assuming $k = -p^2 = -\alpha^2$ we find $p = \pm ip$ и $F(t) = b_1e^{ipt} + b_2e^{-ipt} = (b_1+b_2)\cos pt + i(b_1-b_2)\sin pt = d_1\cos pt + d_2\sin pt$.

312 E.V. Laitone, New Compressibility Correction for Two-Dimensional Subsonic Flow, Jour. Aero. Sci., Vol. 18, No. 5 (1951), p. 350.

357 I. Imai, On the Flow of a Compressible Fluid Past a Circular Cylinder, Proc. Phys. Math. Soc. Japan, Vol. 23, 1941.

379 This is connected with the fact that the properties of air streaming with Mach numbers M greater than 7-8 begin to deviate considerably from those of an ideal gas.

REFERENCES

5.1. Sedov, L.I., Ploskiye zadachi gidrokinamiki i aeromekhaniki [Two-Dimensional Problems of Hydrodynamics and Aerodynamics], GTTI [State Technical and Theoretical Press], 1952.

5.2. Khristianovich, S.A., Obtekaniye tel gazom pri bol'shikh dozvukovykh skorostyakh [Flow of Gas Around Bodies at High Subsonic Velocities], Trudy TsAGI [Trans. Central Aerohydrodynamics Institute], No. 483, 1940.

5.3. Khristianovich, S.A. and Yur'yev, I.M., Obtekaniye krylovogo pro-

filya pri dokriticheskoy skorosti potoka [Flow Past a Wing Profile at Subcritical Stream Velocities], "Prikladnaya matematika i mekhanika" [Applied Mathematics and Mechanics], XI, 1, 1947.

5.4. Ferri, A., Aerodinamika sverkhzvukovykh techeniy [Aerodynamics of Supersonic Flows], GITTI, 1952.

5.5. Kochin, N.Ye., Kibel', I.A. and Roze, N.V., Teoreticheskaya gidromekhanika [Theoretical Fluid Mechanics], GITTI, 1955.

5.6. Karman, T., Zakony podobiya dlya transzvukovogo potoka [Similarity Laws for Transonic Flow], Collection entitled "Gazovaya dinamika" [Gasdynamics], IL [Foreign Literature Press], 1950.

5.7. Chernyy, G.G., Techeniya gaza s bol'shoy sverkhzvukovoy skorostyyu [Flow of Gas at High Supersonic Velocity], Fizmatgiz [State Publishing House for Physicomathematical Literature], 1959.

BLANK PAGE

Chapter 6

THE BOUNDARY LAYER

6.1. EQUATIONS OF MOTION IN THE BOUNDARY LAYER

Prandtl's equations. Let us consider a two-dimensional steady flow ($w_z=0$, $\partial/\partial z=0$; $\partial/\partial t=0$) of a viscous incompressible fluid along the plane boundary of a solid (it is, however, possible to show that the derivations apply to the case of a curvilinear wall as well). The continuity equation and equations of motion (no volume forces) will then read:

$$\left.\begin{aligned} &\frac{\partial w_x}{\partial x}+\frac{\partial w_y}{\partial y}=0,\\ &w_x\frac{\partial w_x}{\partial x}+w_y\frac{\partial w_x}{\partial y}=-\frac{1}{\rho}\frac{\partial p}{\partial x}+\nu\left(\frac{\partial^2 w_x}{\partial x^2}+\frac{\partial^2 w_x}{\partial y^2}\right),\\ &w_x\frac{\partial w_y}{\partial x}+w_y\frac{\partial w_y}{\partial y}=-\frac{1}{\rho}\frac{\partial p}{\partial y}+\nu\left(\frac{\partial^2 w_y}{\partial x^2}+\frac{\partial^2 w_y}{\partial y^2}\right). \end{aligned}\right\} \qquad (6.1.1)$$

Let the x-axis be directed along the boundary and the y-axis along its normal. Let us now estimate the magnitudes of the individual terms entering this equation, with greater accuracy than we did before on p. 105. For this purpose we introduce a characteristic scale of length, l, on the x-axis, and as the scale of the y-axis we choose the boundary layer thickness δ; we put

$$x=\xi l;\quad y=\eta\delta,$$

where ξ and η are dimensionless quantities.

Multiplying the continuity equation by dy and integrating it between the limits 0 and δ, we obtain the vertical velocity component at the boundary layer surface, $[w_y(x,0)=0]$:

$$w_y(x,\delta)=-\int_0^{\delta}\frac{\partial w_x}{\partial x}dy=-\frac{\delta}{l}\int_0^{\delta}\frac{\partial w_x}{\partial\xi}d\eta.$$

If the velocity w_x changes from zero at the boundary to a certain value w_{0x} at the outer boundary of the layer, which is comparable with a certain velocity $\underline{w}$ characteristic of the given flow, (for example with the velocity of the undisturbed flow), then the derivative $\partial w_x/\partial\xi$ will depend a little on the layer thickness and will be a quantity of the order of $\underline{w}$. The value of the transverse velocity w_y inside the layer will therefore be of the order of $\delta w/\underline{l}w$.

The situation in the left-hand side of the equation is then: the order of magnitude of the first term $w_x\frac{\partial w_x}{\partial x}$ is equal to $w^2/\underline{l}$; the order of magnitude of the second term $w_y\frac{\partial w_x}{\partial y}$ is equal to $w^2/\underline{l}$.

Taking the pressure head $\rho w^2/2$ as the pressure scale the situation in the right-hand side of this equation is that the order of magnitude of the first term $\frac{1}{\rho}\frac{\partial p}{\partial x}$, is equal to $w^2/\underline{l}$; the order of magnitude of the second term $\frac{\partial^2 w_x}{\partial x^2}=\frac{\nu}{l^2}\frac{\partial}{\partial\xi}\frac{\partial w_x}{\partial\xi}$ is equal to $\nu w/\underline{l}^2$; the order of magnitude of the third term $\nu\frac{\partial^2 w_x}{\partial y^2}=\frac{\nu}{\delta^2}\frac{\partial}{\partial\eta}\frac{\partial w_x}{\partial\eta}$, is equal to $\nu w/\delta^2$.

Considering the order of magnitude of all terms of the equation in comparison with the order of magnitude of $w^2/\underline{l}$ we find that the term $\nu\frac{\partial^2 w_x}{\partial x^2}$ will be of the order of $\frac{\nu w}{l^2}:\frac{w^2}{l}=\frac{\nu}{wl}=\frac{1}{Re}$, and the order of magnitude of the term $\nu\frac{\partial^2 w_x}{\partial y^2}$ will be $\frac{\nu w}{\delta^2}:\frac{w^2}{l}=\frac{\nu l}{\delta^2 w}=\frac{l^2}{\delta^2}\frac{1}{Re}$.

By mutually comparing the terms characterizing the influence of the viscosity we can show that $\nu\frac{\partial^2 w_x}{\partial y^2}$ will be $\underline{l}^2/\delta^2$ times as large as $\nu\frac{\partial^2 w_x}{\partial x^2}$. Experiment shows that at large Re the ratio $\delta/\underline{l}$ is small. At large Re numbers the term $\nu\frac{\partial^2 w_x}{\partial x^2}$ can therefore be neglected.

When we assume further that all terms of the equation must be of one and the same order we come to the conclusion we arrived at before (cf. p.105), viz., that the layer thickness must have the order of magnitude of

$$\delta \sim l : \sqrt{\frac{wl}{\nu}} = l : \sqrt{\mathrm{Re}}. \qquad (6.1.2)$$

Estimating similarly the order of magnitude of the terms of the second equation, we obtain

$$w_x \frac{\partial w_y}{\partial x} \sim \frac{w^2}{l}; \quad w_y \frac{\partial w_y}{\partial y} \sim \frac{w^2}{l}; \quad \frac{1}{\rho}\frac{\partial p}{\partial y} \sim \frac{w^2}{\delta};$$

$$\nu \frac{\partial^2 w_y}{\partial x^2} \sim \frac{\nu w}{l^2}; \quad \nu \frac{\partial^2 w_y}{\partial y^2} \sim \frac{\nu w}{\delta^2}.$$

Since all the terms of the second equation are very small compared with the term $\partial p/\partial y$, we can assume that for large Re numbers

$$\frac{\partial p}{\partial y} = 0, \qquad (6.1.3)$$

i.e., that the pressure inside the boundary layer is constant along the normal to the body contour and equal to the pressure on the outer boundary of the layer at the normal considered.

Thus the approximate equations of continuity and motion in the boundary layer can be written in the form

$$\left.\begin{aligned} &\frac{\partial w_x}{\partial x} + \frac{\partial w_y}{\partial y} = 0, \\ &w_x \frac{\partial w_x}{\partial x} + w_y \frac{\partial w_x}{\partial y} = -\frac{1}{\rho}\frac{\partial p}{\partial x} + \nu \frac{\partial^2 w_x}{\partial y^2}, \\ &\frac{\partial p}{\partial y} = 0. \end{aligned}\right\} \qquad (6.1.4)$$

Let us stress that the boundary layer thickness δ inside which the viscous forces play a considerable part is a quantity of the order of $1/\mathrm{Re}^{1/2}$. These equations are called Prandtl's boundary layer equations; they make it possible to determine the velocity distribution in the boundary layer from a given pressure distribution dp/dx.

A more rigorous derivation shows [6.1] that the boundary layer equations are the general equations of a viscous fluid for large Reynolds numbers.

The plane plate. We can simplify the boundary layer equations in the case of a plane plate in a steady flow, (6.1.4), if we take

into account that the velocity of the outer potential flow is uniform and equal to the velocity w_0 of the undisturbed flow at inifinity. In this case it follows from the Bernoulli equation $p+\frac{\rho w^2}{2}=\text{const}$ that the pressure p will be constant too since $\partial p'/\partial x+\rho w_0 w_0'=0$. where $w_0'=0$, i.e., $\partial p/\partial x=0$; then

$$\left.\begin{aligned} &w_x\frac{\partial w_x}{\partial x}+w_y\frac{\partial w_x}{\partial y}=\nu\frac{\partial^2 w_x}{\partial y^2},\quad \frac{\partial w_x}{\partial x}+\frac{\partial w_y}{\partial y}=0.\\ &\text{The boundary conditions}\\ &\text{for}\qquad y=0,\quad 0<x<l \qquad w_x=0,\quad w_y=0;\\ &\text{for}\qquad y\to\infty \qquad\qquad w_x\to w_0. \end{aligned}\right\} \qquad (6.1.5)$$

The principal difficulty in solving the system is that the boundary condition for $y = 0$ must be satisfied at the finite section $0 \leq x \leq l$. It has proved simpler to seek a solution for an infinitely long plate which coincides with the positive x-axis and then apply this solution to the finite section given. In this case the length will not enter the boundary conditions and, since it does not enter Eqs.(6.1.5), the solution will not contain this length l either. It has to be noticed that Eqs. (6.1.5) were obtained for large Re number and that the solution will therefore be valid only for parts with $x > > 0$, sufficiently far from the leading edge.

Let us assume that the velocity distributions in the boundary layer are similar for all sections $x = \text{const}$, i.e.,

$$\frac{w_x}{w_0}=f\left(\frac{y}{\delta}\right).$$

Owing to the estimate (6.1.2) we can suppose that

$$\left.\begin{aligned} &\text{where}\qquad \frac{w_x}{w_0}=f\left(\frac{y}{x}\sqrt{\mathrm{Re}_x}\right)=f\left(\frac{y}{x}\sqrt{\frac{w_0 x}{\nu}}\right)=f(\eta),\\ &\eta=\frac{y}{x}\sqrt{\frac{w_0 x}{\nu}}. \end{aligned}\right\} \qquad (6.1.6)$$

The definition of the stream function $\Psi(\eta)$ leads to

$$w_x = \frac{\partial \Psi}{\partial y} = \frac{\partial \Psi}{\partial \eta}\frac{\partial \eta}{\partial y} = \frac{1}{\sqrt{\frac{x\nu}{w_0}}}\frac{\partial \Psi}{\partial \eta} = \frac{w_0}{\sqrt{x w_0 \nu}}\frac{\partial \Psi}{\partial \eta} = w_0 \Phi'(\eta).$$

Therefore

$$\Psi = \sqrt{w_0 x \nu}\int \Phi'(\eta)\, d\eta = \sqrt{w_0 x \nu} f(\eta),$$

i.e., $f'(\eta) = \Phi(\eta)$. Now

$$w_y = -\frac{\partial \Psi}{\partial x} = \frac{1}{2}\sqrt{\frac{w_0 \nu}{x}}\,[\eta f'(\eta) - f(\eta)].$$

Boundary conditions:

For $\eta = 0$ $w_x = w_y = 0$.

For $\eta = \infty$ $w_x = w_0$, $w_y = 0$.

All terms of Eq. (6.1.5) can thus be expressed by a single function, $f(\eta)$; calculating the derivatives $\partial w_x/\partial x$, $\partial^2 w_x/\partial x^2$ and $\partial w_x/\partial y$ and substituting them into (6.1.5) we obtain an ordinary differential equation for f:

$$ff'' + 2f''' = 0$$

with the boundary conditions: $f'(\eta) = 0$ at $\eta = 0$ and $f(\eta) = 0$ and $f'(\eta) = 1$ at $\eta = \infty$.

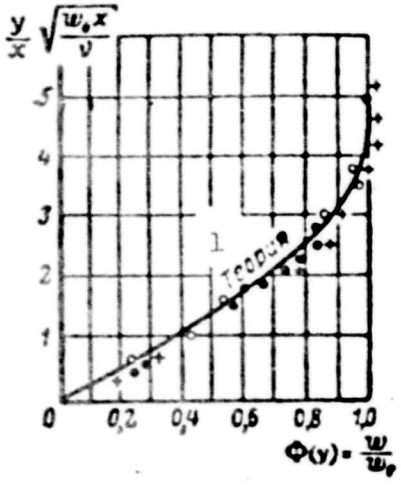


Fig. 6.1.1. Velocity distribution in the boundary layer of forces on a plate in a laminar flow. 1) Theory.

The results of a numerical solution of this equation are given in Fig. 6.1.1 for comparison, together with the experimental data, in the form of a function $\Phi(\eta) = w_x/w_0 = f'(\eta)$.

It can be seen from the figure that, although the solution found is asymptotic, the velocity is virtually equal to the velocity w_0 of the undisturbed flow as early as at $y = 5{,}5\frac{x}{\sqrt{Re_x}}$. For a plate placed in laminar flow this value can be taken as

the thickness of the boundary layer at a distance x, in which all viscosity effects are concentrated.

The stress of the friction forces on the plate is

$$\tau_0 = \mu \left.\frac{\partial w_x}{\partial y}\right|_{y=0} = 0{,}332 \sqrt{\frac{\mu \rho w_0^3}{x}} = 0{,}664 \frac{\rho w_0^2}{2} \sqrt{\frac{\mu}{\rho x w_0}}. \qquad (6.1.7)$$

The coefficient C_{fm} of local friction is determined from the relation $\tau_0 b\,dx = C_{fm} b\,dx \frac{\rho w_0^2}{2}$. Its value is obtained from

$$C_{fm} = \frac{\tau_0}{\frac{\rho w_0^2}{2}}. \qquad (6.1.8)$$

The frictional force R_f for one side of a plate of width b and length l is

$$R_f = b \int_0^l \tau_0 dx = 0{,}664 \frac{\rho w_0^2}{2} \sqrt{\frac{\nu}{l w_0}} \cdot 2bl$$

and the mean coefficient of friction for the whole plate, referred to a wetted surface, is

$$C_f = \frac{R_f}{A \frac{\rho w_0^2}{2}} = \frac{1{,}328}{\sqrt{Re}}. \qquad (6.1.9)$$

The method of successive approximations. This method, suggested by M. Ye. Shvets [6.2], is very effective for solving problems on laminar boundary layers.

Eliminating the vertical component with the help of the second equation of (6.1.5) and introducing the dimensionless quantities $x' = x : l$; $y' = y : \frac{l}{\sqrt{Re}}$; $w'_x = w_x : w_0$; $w'_y = w_y : \frac{w_0}{\sqrt{Re}}$; $Re = \frac{w_0 l}{\nu}$, we obtain the first equation of (6.1.5) in the form

$$\frac{\partial^2 w'_x}{\partial y'^2} = w'_x \frac{\partial w'_x}{\partial x'} - \frac{\partial w'_x}{\partial y'} \int_0^{y'} \frac{\partial w'_x}{\partial x'} dy'. \qquad (6.1.10)$$

the solution of this equation must satisfy the following boundary conditions: at $y' = 0$, $w'_x = 0$, and at $y' = b' = b : \frac{l}{\sqrt{Re}}$ $w'_x = 1$.

The first approximation is obtained when the right-hand side of

gives $w_x = \frac{y}{\delta} w_0$. The second approximation is obtained by substituting the value found for w_x in the right-hand side; when integrated twice, this gives

$$w'_x = \frac{y'}{\delta'} + \frac{y'}{24}\left(1 - \frac{y'^2}{\delta'^2}\right)\frac{d\delta'}{dx'}.$$

When we determine the quantity $\left(\frac{\partial w'_x}{\partial y'}\right)_{\delta'} = 0$ from $\delta' = 4\sqrt{x'}$, we find further

$$\tau' = \left(\frac{\partial w'_x}{\partial y'}\right)_{y'=0} = \frac{1}{\delta'} + \frac{1}{24}\frac{d\delta'}{dx} = \frac{0{,}333}{\sqrt{x'}};$$
$$w'_x = \frac{1}{3}\frac{y'}{x'} - \frac{1}{768}\frac{y'}{x'^3}.$$

In dimensioned quantities, we have

$$\tau = 0{,}666\,\frac{\rho w_0^2}{2}\sqrt{\frac{\nu}{w_0 x}},$$
$$w_x = w_0\left[\frac{y}{x}\sqrt{\frac{w_0 x}{\nu}} - \frac{1}{768}\frac{y^4}{x^4}\left(\frac{w_0 x}{\nu}\right)^2\right]. \qquad (6.1.11)$$

Notice that this method can also be used for a boundary layer with longitudinal pressure drop.

The turbulent boundary layer. According to the two modes of flow of a viscous fluid, we distinguish between laminar and turbulent boundary layers. In a laminar boundary layer the motion of the fluid occurs in layers without velocity pulsation; in a turbulent boundary layer chaotic velocity pulsation governed only by statistical laws and accompanied by the molar mixing of the fluid takes place.

Let us consider the longitudinal flow about a plane plate arranged along the x-axis in a turbulent stream which, for simplicity, is assumed to be two-dimensional: $\tilde{w}_z = 0$, and $\tilde{w}_x = w$, $\tilde{w}_y = 0$. The frictional stress τ_0 at the wall is obtained from (2.6.15) as

$$\tau_0 = \mu\frac{dw}{dy} - \rho\overline{w'_x w'_y}. \qquad (6.1.12)$$

In the immediate proximity of the wall the first component plays

the major role and distant from the wall the second one predominates. We determine the distance y_0 at which the effect of molecular viscosity μ is essential by taking into account that in this zone the order of magnitude of the velocity is equal to $w_* = \sqrt{\tau_0 : \rho}$ and that the corresponding Re number $\mathrm{Re} = \frac{y_0 w_*}{\nu}$ must be of the order of one; hence $y_0 = \nu : w_*$. Since $\tau_0 = \mu \frac{dw}{dy}$, we have

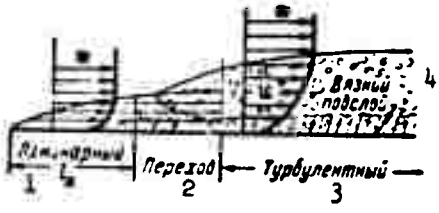


Fig. 6.1.2. Boundary layer structure on a plate. 1) Laminar; 2) transient; 3) turbulent; 4) viscous sublayer.

$$\tilde{w} = \frac{\tau_0}{\mu} y = \frac{w_*^2}{\nu} y. \qquad (6.1.13)$$

Thus (Fig. 6.1.2), there exists in the immediate proximity of the wall an adjacent thin layer of fluid in which the average velocity is small and varies linearly from zero to the value $w_* = \sqrt{\tau_0 : \rho}$. As was said before (cf. Part 4.4), this layer is called the viscous sublayer. In a tubulent flow the longitudinal components of the pulsators velocities are much larger than the transverse ones, and the flow in the viscous sublayer will also be turbulent, the averaged velocities, however, being governed by a linear law. Outside the zone of the viscous sublayer (there is no sharp interface between the viscous sublayer and the remaining fluid flow) the turbulent stresses $\overline{\rho w_x' w_y'}$ play the main part.

In order to determine the motion in a fluid of the density ρ producing the stress τ_0, we notice that we can combine the quantities ρ, τ_0 and y determining this motion to form a single expression whose dimension is that of $\sqrt{\tau_0 : \rho} : y$, so we arrive at the equality

$$\frac{d\tilde{w}}{dy} = \frac{1}{\kappa y} \sqrt{\frac{\tau_0}{\rho}}, \qquad (6.1.14)$$

where κ is a so-called universal constant which is determined only by experiment from the results of measurements in tubes.

Integrating (6.1.14) we obtain a logarithmic velocity distribu-

$$\frac{\tilde{w}}{w_*} = \frac{w_*}{\varkappa}(\ln y + C) = \frac{w_*}{\varkappa}\ln\frac{yw_*}{\nu} + C; \qquad (6.1.15)$$

where $\frac{yw_*}{\nu}$ is the so-called dimensionless distance from the wall.

Experiments yield for tubes (4.4.26)

$$\frac{\tilde{w}}{w_*} = 2{,}5\lg\frac{yw_*}{\nu} + 5{,}5.$$

In the immediate proximity of the wall where the conditions correspond more to the flow along a plate, experiment [6.1] gives instead of (4.4.26)

$$\frac{\tilde{w}}{w_*} = 2{,}4\lg\frac{yw_*}{\nu} + 5{,}84. \qquad (6.1.16)$$

The quantity τ_0 or, what is the same, w_* depends on the number $\mathrm{Re}_x = \frac{w_0 x}{\nu}$ and there exists a critical number Re_x at which the laminar form of flow changes over to become turbulent. Thus, as the velocity increases (the other conditions remaining unchanged) the transient zone approaches the leading edge of the plate or of another streamlined body. The structure of a boundary layer of finite thickness is shown in Fig. 6.1.2.

Integral relations. Besides the difficulties arising on solving the approximate boundary layer equations which are due to the nonlinearity of the latter, there are those due to the necessity of satisfying the boundary conditions at the wall, where the fluid velocity must be equal to zero, and at infinity, where the viscosity effect vanishes. This solution supposes, strictly speaking, an unlimited thickness of the boundary layer in which the velocity asymptotically approaches the velocity of the undisturbed flow. Theoretical estimates, as made above (cf. p. 387) and as verified by experiment, however, show that in a laminar flow, for example even at a distance of the order of $1/\mathrm{Re}^{1/2}$, there is virtually no difference between the velocity

of a potential flow and the velocity in the boundary layer. The idea of the boundary layer has proved to be very fruitful. It leads to the replacement of the differential equations for each point of the flow in the boundary layer by integral relations, which are obtained by applying the conservation laws to the length elements of the layer. The method of the integral relations is based on operating with a certain kind of averaged parameters, proves to be relatively insensitive to the accuracy of the law governing the longitudinal velocity distribution with respect to the normal, adopted in the calculation; calculations show that in many cases it is sufficient for the distribution applied to be more or less plausible.

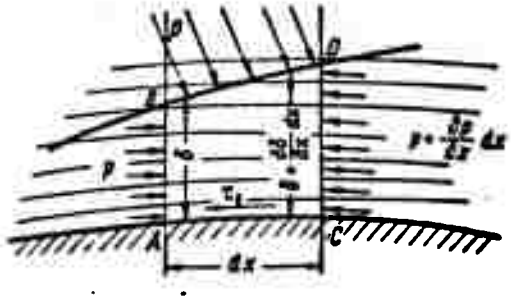


Fig. 6.1.3. The integral relations are obtained when the conservation laws are applied to boundary layer element ABCD of length dx.

The impulse equation. The mass passing per second through the section AB (Fig. 6.1.3) $m = \int_0^\delta \rho w_x dy$. is augmented in the section CD by $\frac{dm}{dx} dx = \frac{d}{dx}\left(\int_0^\delta \rho w_x dy\right) dx$ since this mass of fluid streams in through the face BD. This is accompanied by an increase in momentum within the volume ABCD, which is equal to

$$w_0 \frac{dm}{dx} dx = w_0 \frac{d}{dx}\left(\int_0^\delta \rho w_x dy\right) dx,$$

where $w_0 = w_0(x)$ is the velocity at the boundary layer surface.

The projection onto the x-axis of the momentum flux through the

All momentum changes in the volume ABCD will therefore be given by

$$\left(I+w_0\frac{dm}{dx}dx\right)-\left(I+\frac{dI}{dx}dx\right)=$$

$$=w_0\frac{d}{dx}\int_0^\delta \rho w_x\,dy\,dx-\frac{d}{dx}\int_0^\delta \rho w_x^2\,dy\,dx.$$

They must be equal to the impulse of the forces per second, these forces consisting of the frictional force $\tau_0 dx$ at the fact AC and the resulting pressure force equal to $p\frac{d\delta}{dx}dx$, as can be seen from Fig. 6.1.3. Thus, reducing by dx gives

$$w_0\frac{d}{dx}\int_0^\delta \rho w_x\,dy-\frac{d}{dx}\int_0^\delta \rho w_x^2\,dy=-\tau_0-p\frac{d\delta}{dx}. \qquad (6.1.17)$$

In an incompressible fluid $p+\frac{\rho w_0^2}{2}=\text{const}$, at the boundary layer, and therefore $\frac{dp}{dx}=-\rho w_0\frac{dw_0}{dx}$.

If we write $d\delta/dx$ in the form $\frac{d}{dx}\int_0^\delta dy$ and take into account that

$$\frac{d}{dx}w_0\int_0^\delta \rho w_x\,dy=\frac{dw_0}{dx}\int_0^\delta \rho w_x\,dy+w_0\frac{d}{dx}\int_0^\delta \rho w_x\,dy,$$

then regrouping the terms in (6.1.17) gives

$$\frac{d}{dx}\int_0^\delta \rho w_x(w_0-w_x)\,dy+\frac{dw_0}{dx}\int_0^\delta \rho(w_0-w_x)\,dy=\tau_0. \qquad (6.1.18)$$

In the further calculations made for an incompressible fluid it will be convenient to write the first integral in the form $w_0^2\delta^{**}$, and the second as $w_0\delta^*$, where

$$\left.\begin{aligned}\delta^*&=\int_0^{\delta\ldots}\left(1-\frac{w_x}{w_0}\right)dy,\\ \delta^{**}&=\int_0^{\delta\ldots}\frac{w_x}{w_0}\left(1-\frac{w_x}{w_0}\right)dy,\end{aligned}\right\} \qquad (6.1.19)$$

and the sign $\int_0^{\delta\ldots}$ means that we integrate beginning from a certain virtually arbitraty value δ up to any distance from the wall.

The quantities δ^*, δ^{**} have the dimension of a length and are

called the displacement thickness and the thickness of impulse loss, respectively.

Here we obtain instead of (6.1.18)

$$\frac{d}{dx}(w_0^2\delta^{**})+w_0\frac{dw_0}{dx}\delta^{*}=\frac{\tau_0}{\rho_0}$$

or

$$\frac{d\delta^{**}}{dx}+\frac{w_0'}{w_0}(2\delta^{**}+\delta^{*})=\frac{\tau_0}{\rho_0 w_0^2}. \qquad (6.1.20)$$

This fundamental integral relation of the boundary layer theory, obtained by T. Karman, is called the impulse equation.

The energy equation. This equation was derived by L. S. Leybenzon in a similar way*. When the energy conservation law is applied to the laminar boundary layer elements, it can be written in the form

$$\frac{1}{2}\frac{\delta^{**}}{w_0^3}\frac{d}{dx}(w_0^3\delta^{***})=\int_0^{\delta,\infty}\left[\frac{\partial}{\partial(y:\delta^{**})}\left(\frac{w_x}{w_0}\right)\right]^2 d\frac{y}{\delta^{**}}. \qquad (6.1.21)$$

We introduce here the thickness of energy loss

$$\delta^{***}=\int_0^{\delta,\infty}\frac{w_x}{w_0}\left(1-\frac{w_x^2}{w_0^2}\right)dy. \qquad (6.1.22)$$

The right-hand side of Eq. (6.1.21) is called the dimensionless energy dissipation D*. It characterizes the work of frictional forces in the boundary layer which is converted to heat.

Conventional thicknesses of the boundary layer. The thicknesses of displacement, δ*, impulse loss, δ**, and energy loss δ***, characterize the zone of viscosity effect much more accurately than the very indistinct conception of the boundary layer thickness as the distance from the wall at which the viscous forces are comparable with the forces of inertia. This distance is often taken as that distance from the wall where the velocity in the boundary layer differs from the velocity at its outer boundary by some small predetermined amount: 1%, 0.1% etc.

plained if the determination is generalized to the case of a compressible gas and $\rho_0 w_0 \delta^* = \int_0^\infty (\rho_0 w_0 - \rho w_x) dy$ is rewritten in the form $\int_0^\infty \rho w_x dy = \rho_0 w_0 (\delta - \delta^*)$. We can now show (Fig. 6.1.4) that the displacement thickness is that distance by which the gas flow needs be removed from the wall of the body in order to keep its mass flow unchanged when the body is in the potential flow of an incompressible fluid.

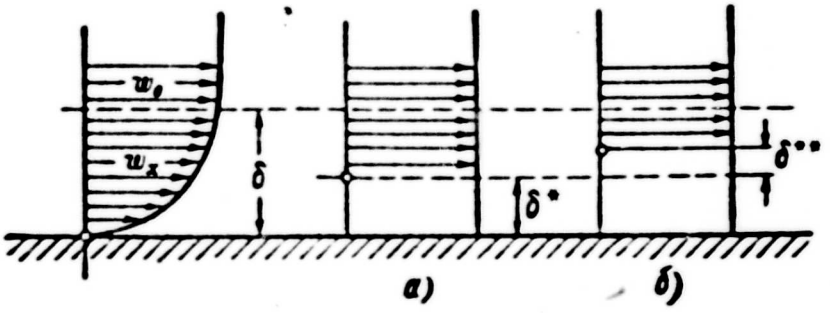


Fig. 6.1.4. The displacement thickness is the distance by which the gas flow needs be removed from the wall in order to take the effect of the viscosity on the flow into account (a); impulse loss thickness, (b).

In exactly the same way it follows from the definition $\rho_0 w_0^2 \delta^{**} = \int_0^\infty \rho w_x (w_0 - w_x) dy$ that

$$\int_0^\infty \rho w_x^2 dy = \int_0^\infty \rho w_0 w_x dy - \rho_0 w_0^2 \delta^{**} =$$

$$= w_0 \int_0^\infty \rho w_x dy - \rho_0 w_0^2 \delta^{**} = \rho_0 w_0^2 [\delta - (\delta^* + \delta^{**})]$$

i.e., the impulse loss thickness is a distance in addition to the displacement thickness by which the flow must be removed from the body wall in order to keep the momentum unchanged when the body is in the potential flow of an incompressible fluid.

It should be noticed that the pressure distribution over the body is in good agreement with experimental results when the calculation is made according to the theory of the potential flow of an inviscid

gas about a body whose contours are increased by the displacement thickness.

In the roughest approximation, i.e., linear velocity distribution in the boundary layer of an incompressible fluid, $w_x = w_0 \frac{y}{\delta}$ we shall have

$$\delta^* = \frac{1}{2}\delta; \quad \delta^{**} = \frac{1}{6}\delta; \quad \delta^{***} = \frac{1}{4}\delta.$$

Separation of the boundary layer. Experiment shows that in the motion of a fluid with a positive pressure gradient, the motion of the fluid is reversed (Fig. 6.1.5) at a certain point, or, more exactly, region, at the body surface. In physical terms, this can be explained as follows: as the fluid moves in the direction of increasing pressure, the particles of the fluid closest to the body surface have the lowest velocity due to friction; these particles are first slowed down, and then, under the action of the pressure directed against the main flow, start moving in the opposite direction, thus causing the boundary layer to separate.

It follows from the figure showing the velocity distribution in the boundary layer (Fig. 6.1.6) that at the place of separation the derivative of the velocity with respect to the normal to the wall vanishes at the wall itself:

$$\left(\frac{\partial w_x}{\partial y}\right)_{y=0} = 0. \qquad (6.1.23)$$

It follows from the boundary layer equations that as $y \to 0$ $\left.\frac{\partial^2 w_x}{\partial y^2}\right|_{y=0} = \frac{1}{\rho}\frac{\partial p}{\partial x}$ at the separation point $\left.\frac{\partial w_x}{\partial y}\right|_{y=0} \to 0.$, but, since as the distance from the wall increases, $w_x > 0$, we have $\left.\frac{\partial^2 w_x}{\partial y^2}\right|_{y=0} > 0.$ and, moreover, dp/dx will be positive, i.e., in the separation zone the fluid moves from the region of lower pressure to that of higher. Owing to the Bernoulli equation the velocity w_0 of the main flow will drop.

Behind the place of separation, the reverse motion gives rise to

the region of the outer flow and change the form of motion.

Since in a laminar layer $\delta/l \sim 1/\sqrt{\mathrm{Re}}$; $\omega_y/\omega_x \sim 1/\sqrt{\mathrm{Re}}$ and when Re is changed only the transverse scales (length and velocity) change, the motion remains similar, then (cf. Fig. 6.1.6) 1) the position of the separation site is independent of the Reynolds number, and, by virtue of the same considerations. 2) the angle between the direction of the separated layer and the tangent to the body surface at the separation point is inversely proportional to the square root of Re:

$$\varepsilon_{\text{отр}} \sim 1:\sqrt{\mathrm{Re}}. \qquad (6.1.24)$$

NOT REPRODUCIBLE

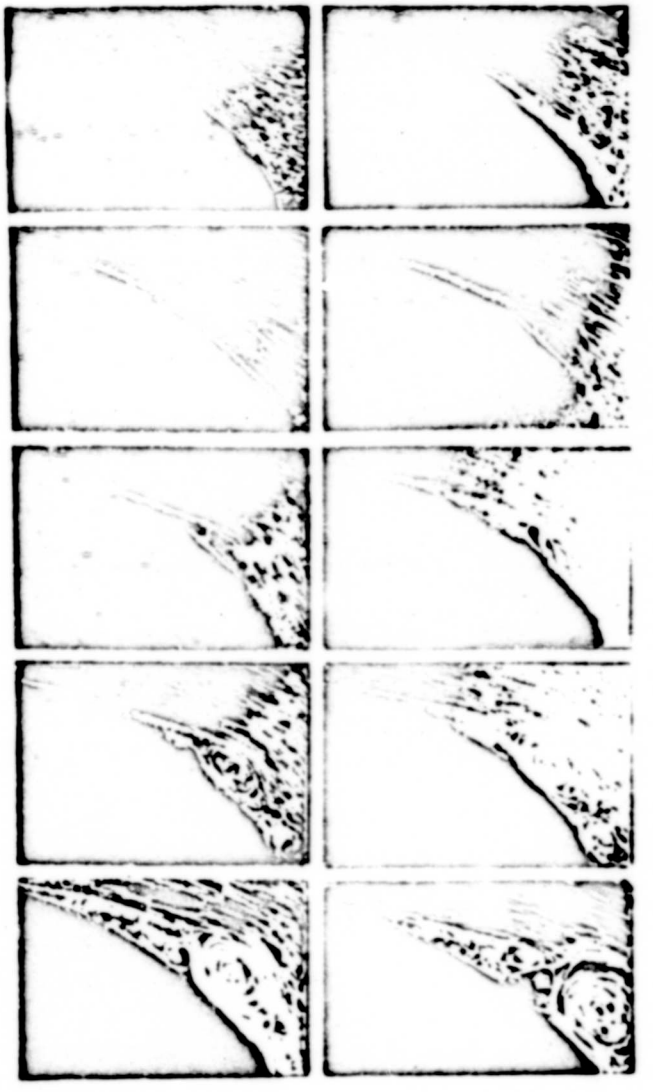


Fig. 6.1.5. Photograph of flow in the rear region of the body where dp/dx > 0 (after Prandtl).

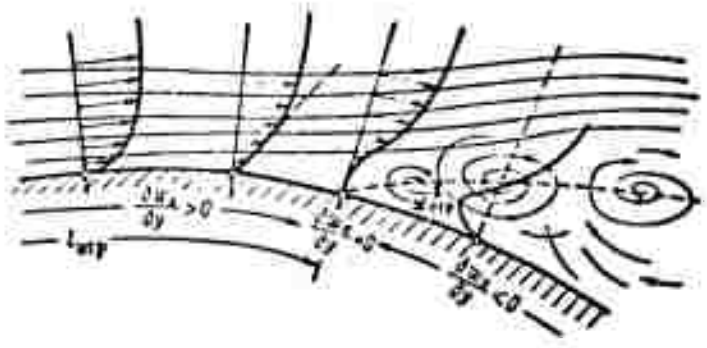


Fig. 6.1.6. Schematic representation of reverse flow and separation of the boundary layer.

6.2. CORRESPONDENCE BETWEEN THE INTERNAL AND EXTERNAL PROBLEMS

Velocity distribution. For the laminar flow of a fluid in a round tube it has been found that

$$w = w_0 \frac{r_0^2 - r^2}{r_0^2} = w_0 \frac{2r_0 y - y^2}{r_0^2} = w_0 \left(2\frac{y}{r_0} - \frac{y^2}{r_0^2}\right). \qquad (6.2.1)$$

where $y = r_0 - r$ is the distance from the tube walls. The frictional stress at the wall is

$$\tau_0 = \mu \frac{\partial w}{\partial y}\Big|_{y=0} = \mu w_0 \frac{2}{r_0} = \frac{2\mu}{r_0} \frac{r_0^2 w}{2r_0 y - y^2}\Big|_{y=0} =$$

$$= \rho w^2 \left(\frac{\nu}{wy}\right) \frac{1}{1 - \frac{y}{2r_0}}\Big|_{y=0} = \rho w^2 \left(\frac{\nu}{wy}\right)$$

or, introducing the dynamic velocity, $w_* = \sqrt{\tau_0 : \rho}$

$$w = w_* \sqrt{\frac{yw}{\nu}}. \qquad (6.2.2)$$

i.e., the velocity distribution near the wall is determined only by the conditions in this region - the frictional stress τ_0 at the wall and the dimensionless distance yw/ν. This conclusion is true also for a turbulent flow in a round tube; for example, for Re numbers to which the empirical inverse seventh-power law applies, $w = w_0 (y : r_0)^{\frac{1}{7}}$, the frictional stress at the wall is expressed by the equality

$$\tau_0 = 0.0456 \frac{\rho w^2}{2} \left(\frac{\nu}{yw}\right)^{\frac{1}{4}}$$

$$w = 6{,}65 w_* \left(\frac{y w_*}{\nu}\right)^{\frac{1}{7}}. \qquad (6.2.3)$$

These facts, already established in the 20s, furnish the basis for the supposition that the velocity distribution in a boundary layer for an external flow streaming around a body will be the same as that for the flow in a tube at the same Re number if the boundary layer thickness δ and the velocity w_0 at its surface are assumed to play the same part as the tube radius r_0 and the flow velocity w_0 at the tube axis (Fig. 6.2.1).

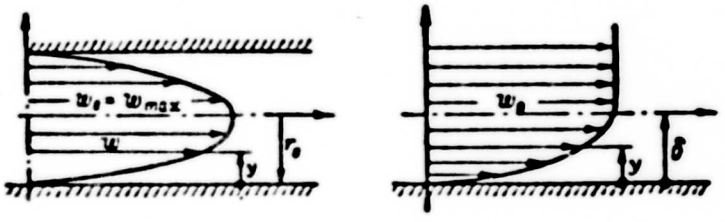


Fig. 6.2.1. Correspondence between internal and external flow problems.

$$\frac{w}{w_0} = f\left(\frac{y}{r_0}\right) = f\left(\frac{y}{\delta}\right).$$

The region of transition from laminar to turbulent flow. It has been shown by very carefully made experiments on the determination of the transition region between laminar and turbulent conditions in the boundary layer of a plate that the correspondence applies to this transient state of the flow as well. It can be seen from Fig. 6.2.2 that if the Re number is determined from the thickness δ of the boundary layer, $\mathrm{Re}_\delta = \frac{w_0 \delta}{\nu} = \frac{w_0 5{,}5x}{\nu\sqrt{\mathrm{Re}_x}} = 5{,}5\sqrt{\mathrm{Re}_x}$, then a sharp increase of the boundary layer thickness on a plate, due to the transition from a laminar to a turbulent form of motion, occurs at Re $\approx$ 3000/4000, a value which is of the same order of magnitude as Re_{kr} = 2200 for a round tube*. In this connection we have to take the very imprecise determination of the boundary layer thickness δ into consideration. If we introduced, for example, the displacement thickness δ^*, we would then obtain Re_{kr}

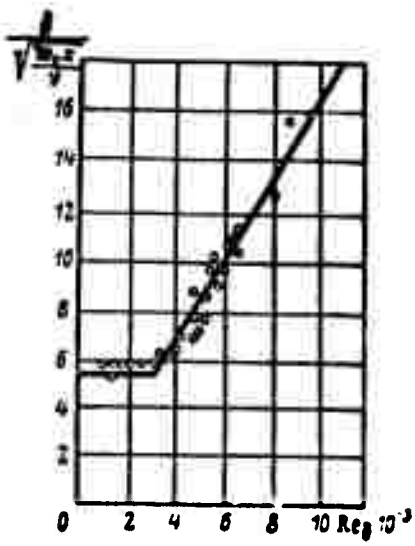


Fig. 6.2.2. At $Re = \frac{w_\infty \delta}{\nu} \sim 3100$ the boundary layer thickness and the frictional stresses on the plate increase sharply; this critical value corresponds to the transition from laminar to turbulent flow.

for a plate of the order of 1000/1500. The characteristic length apparently lies between these figures and consequently Re_{kr} will be closer to 2200.

Figure 6.2.3 shows us an oscillogram of the velocity pulsation in the boundary layer of a plate, from which it can be seen that the inflowing turbulent stream becomes steady by internal friction. The pulsation frequency first drops sharply and then, as the boundary layer thickness and Re_x number increase, the state of the laminar layer becomes unsteady, the disturbances grow and new disturbances that occupy the region of the turbulent boundary layer arise.

The transition from the laminar boundary layer to a turbulent one and its connection with the magnitude of pulsation is seen from Fig. 6.2.4, which represents the pulsation distribution, characterized by the quantity

$$K_0 = \frac{1}{w_0} \sqrt{\frac{1}{t_p} \int_0^{t_p} (w_{ist} - \tilde{w})^2 \, dt},$$

where w_{ist} is the true velocity, $\tilde{w}$ the averaged velocity, and t_p the averaging interval. As can be seen, the site of maximum pulsation coincides with the region of sharp change of the boundary layer surface. In this region the laminar form of flow loses steadiness. The magnitude of these local pulsations depends slightly on the degree of turbulence of the incoming flow, characterized by the number K_0.

of the transient region. Since for a laminar flow $Re_\delta = 5{,}5\sqrt{Re_x}$, i.e., $Re_x = Re_\delta^2 : 30$ and $Re_{кр} = \frac{w_0 l_{кр}}{\nu} = Re_{\delta кр}^2 : 30$, the position of the transient region depends on the initial turbulence. Figure 6.2.5 gives the results of experiments which verify this.

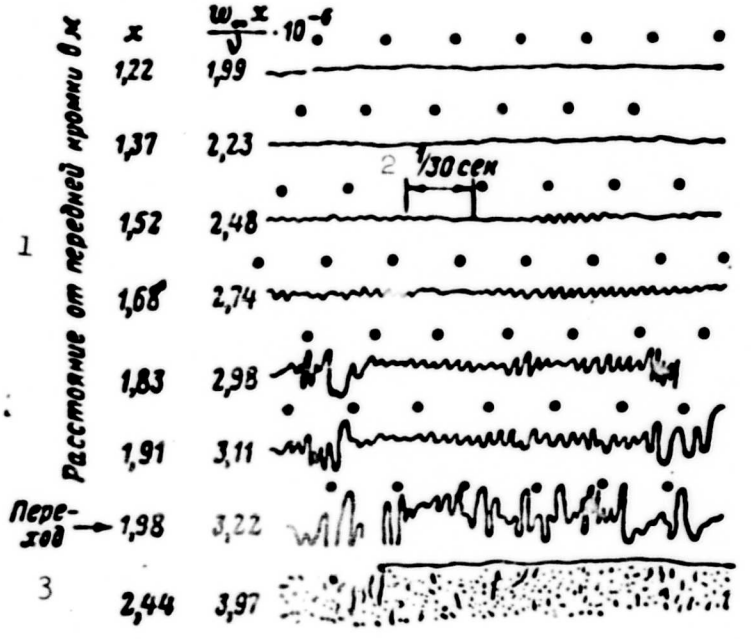


Fig. 6.2.3. Oscillogram of pulsations and random ("natural") disturbances in a laminar boundary layer on a plane plate which is placed in a longitudinal air stream. The measurements were made at a distance of 0.57 mm from the wall; the velocity of the incoming flow was w_∞ = = 24 m/sec; the marks (dots) indicate the time intervals, which were 1/30 sec. 1) Distance from leading edge in m; 2) sec; 3) transition.

Example 1. In order to calculate the laminar boundary layer on a plate from the correspondence with the flow in a tube we choose the velocity distribution in the form $\frac{w_x}{w_0} = 2\frac{y}{\delta} - \frac{y^2}{\delta^2}$. Here $\frac{dp}{dx} = 0$; $w_0' = 0$ and

$$w_0^2 \frac{d}{dx}\int_0^\delta \rho \frac{w_x}{w_0}\left(1 - \frac{w_x}{w_0}\right) dy = \rho w_0^2 \frac{d\delta}{dx}\int_0^1 (2z - z^2)(1 - 2z + z^2)\, dz = \frac{2}{15}\rho w_0^2 \frac{d\delta}{dx} = \tau_0,$$

where $\tau_0 = \mu \left.\frac{\partial w_x}{\partial y}\right|_{y=0} = \mu \frac{2w_0}{\delta}$. Assuming $\delta = 0$ at $x = 0$ we obtain

$$\delta = \frac{5{,}48x}{\sqrt{Re_x}}. \qquad (6.2.4)$$

The frictional force and coefficient for a plate of width b and length l will be

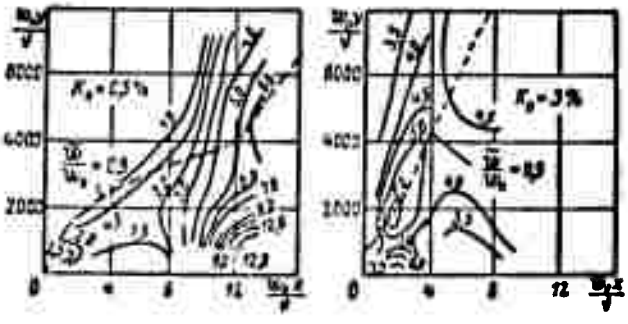
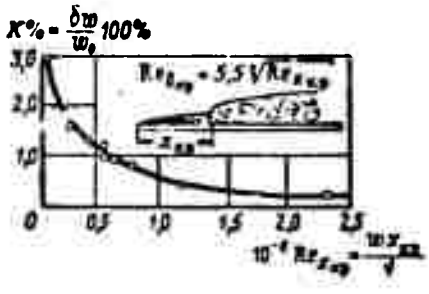


Fig. 6.2.4. Velocity pulsation distribution $\frac{\Delta w}{w_0}\,100\%$ on a plane plate for two values of initial turbulence (w_0 is the velocity of the incoming flow). The lines are lines of equal pulsation velocities.



6.2.5. Influence of initial turbulence on the position of the transition point.

The frictional force and coefficient for a plate of width b and length l will be

$$\left.\begin{aligned} R_f &= 2b\int_0^l \tau_0\,dx - 2b\int_0^l 2w_{0^3}\frac{\sqrt{\rho w_0 x}}{5{,}48} = \\ &= \frac{1{,}46}{\sqrt{\mathrm{Re}}}\,2bl\frac{\rho w_0^2}{2}, \quad C_f = \frac{1{,}46}{\sqrt{\mathrm{Re}}}. \end{aligned}\right\} \quad (6.2.5)$$

As was shown by (6.1.9), Blasius' exact solution gives

$$C_f = \frac{1{,}328}{\sqrt{\mathrm{Re}}}.$$

Example 2. The turbulent boundary layer on a plate can be calculated by applying a power law, for example, the inverse seventh power law: $w_x = w_0(y:\delta)^{1/7}$.

Since dp/dx = 0 p = const here, and from the momentum conservation law we obtain

$$\frac{d}{dx}\int_0^\delta \rho w_0\left(\frac{y}{\delta}\right)^{\frac{1}{7}} w_0\left[1-\left(\frac{y}{\delta}\right)^{\frac{1}{7}}\right]dy = \frac{7}{72}\rho w_0^2\frac{d\delta}{dx} = \tau_0$$

From Eq. (4.4.24) $\frac{w_0}{w_*} = 8{,}74\left(\frac{y w_*}{\nu}\right)^{\frac{1}{7}}$ we obtain

$$w_* = \sqrt{\tau_0:\rho} = 0{,}15 w_0^{\frac{7}{8}}\left(\frac{\nu}{y}\right)^{\frac{1}{8}},$$

whence

$$\tau_0 = \rho w_0^2 = 0.0225 \rho w_0^{\frac{7}{4}} \left(\frac{\nu}{y}\right)^{\frac{1}{4}} = \frac{7}{72} \rho w_0^2 \frac{d\delta}{dx}.$$

When we assume that the turbulent boundary layer begins at the leading edge of the plate (i.e., $\delta = 0$ at $x = 0$) we find by integration

$$\frac{4}{5} \delta^{\frac{5}{4}} = 0.235 \left(\frac{\nu}{w_0}\right)^{\frac{1}{4}} x, \quad \delta = 0.37 \sqrt[5]{\frac{\nu}{w_0}} x^{\frac{4}{5}}. \tag{6.2.6}$$

Substituting δ in the expression for τ_0 we obtain for the friction drag of the plate

$$R_f = 2b \int_0^l \tau_0 \, dx = 0.0376 \frac{\rho w_0^2}{2} \left(\frac{\nu}{w_0}\right)^{\frac{1}{5}} 2b \int_0^l \frac{dx}{\sqrt[5]{Re}} =$$

$$= 2bl \frac{\rho w_0^2}{2} \frac{0.072}{\sqrt[5]{Re}}. \tag{6.2.7}$$

whence the friction drag coefficient calculated for one side of the plate is obtained as

$$C_f = \frac{0.072}{\sqrt[5]{Re}}. \tag{6.2.8}$$

Agreement with experiment is better if we take

$$C_f = \frac{0.074}{\sqrt[5]{Re}}.$$

Figure 6.2.6 shows the dependence of the coefficient of friction for a smooth plane plate at various Re numbers.

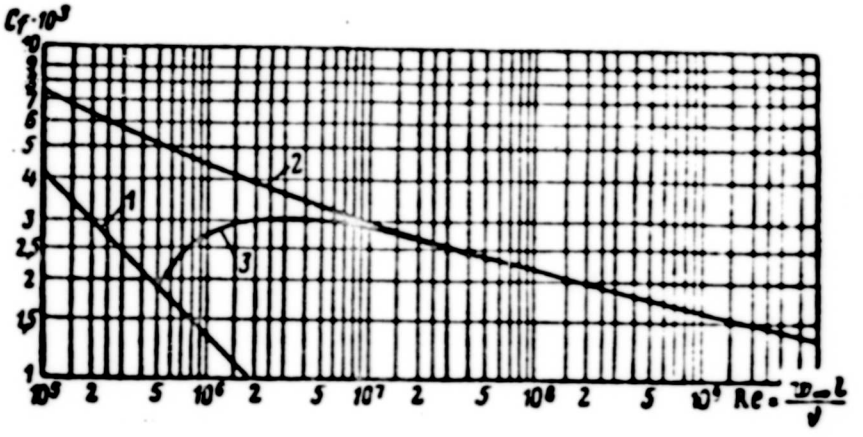


Fig. 6.2.6. Friction drag coefficient for smooth plate when the boundary layer is laminar (1), turbulent (2) and mixed (3).

Example 3. In order to determine the friction drag coefficient for a plate with mixed boundary layer we assume that at the site where the laminar layer goes over to a turbulent layer (Prandtl's hypothesis) the thickness of the turbulent layer is just the same as it would be if it began at the leading edge of the plate (Fig. 6.2.7). In this case we can say the friction drag will be smaller than the friction drag of the whole plate with a completely turbulent boundary layer by the quantity

$$\frac{\underline{l}_{\underline{l}}}{\underline{l}} (C_{f\ turb} - C_{f\ lam})$$

where $C_{f\ turb}$ and $C_{f\ lam}$ must be chosen for the Re numbers determined from the length of the laminar section of the boundary layer, since only in this section does the drag increase. Therefore, noting that $Re_{kr} = w_0 \underline{l}_{kr}/\nu$ and $Re = w_0 \underline{l}/\nu$, i.e., $\underline{l}_d/\underline{l} = Re_{kr}/Re$ we may say that this reduction is equal to $\frac{Re_{kr}}{Re} \times (C_{f\ турб} - C_{f\ лам})_{Re_{kr}}$. For the natural turbulence of the atmosphere $Re_{kr} = 485{,}000$; this Re corresponds to $C_{f\ turb} = 0.00539$ and $C_{f\ lam} = 0.00290$. Thus,

$$\Delta C_f = \frac{485\,000\,(0{,}00539 - 0{,}00190)}{Re} = \frac{1700}{Re}$$

and

$$C_{fc} = \frac{0{,}074}{\sqrt[5]{Re}} - \frac{1700}{Re}. \qquad (6.2.9)$$

For another initial turbulence (another Re_{kr}) the coefficient 1700 must be correspondingly calculated.

Although Prandtl's hypothesis, which is the simplest from the standpoint of calculation, has no physical basis at all, the results of calculations made on this hypothesis (6.2.9) coincide satisfactorily with experiment.

Drag of a rough plate. This is calculated on the basis of the correspondence between the flow in a tube and on a plate. The results

of the calculations (made under the supposition that the boundary layer is turbulent from the leading edge on) are shown in Fig. 6.2.8 by the values of the coefficient C_f of local friction given as functions of the local Re_x numbers for various values of the parameter x/h. On the basis of the correspondence between the external and the internal problems the relative roughness is determined as the ratio of the height h of the protuberances and the boundary layer thickness δ. The coefficient of over-all friction for the whole plate is given in Fig. 6.2.9.
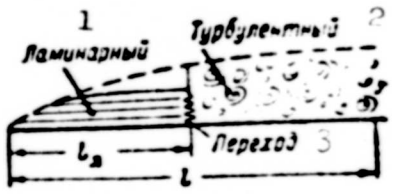


Fig. 6.2.7. For the calculation of a mixed boundary layer. 1) Laminar; 2) turbulent; 3) transient.

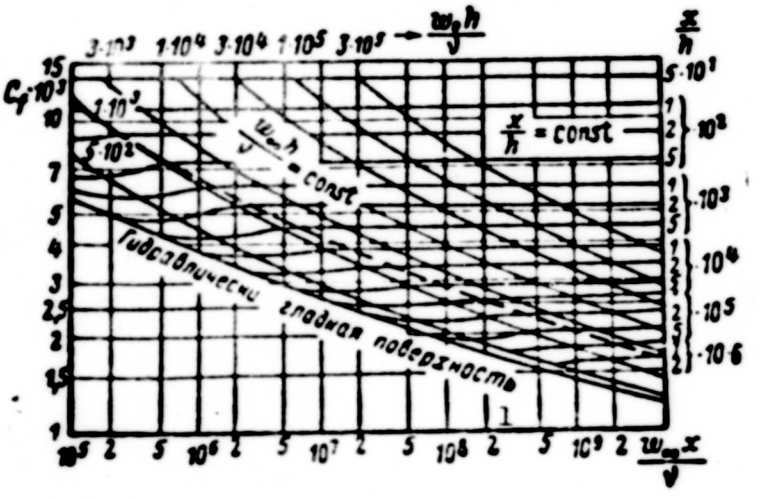


Fig. 6.2.8. Local friction coefficient for a plane plate with sandy roughness. 1) Hydraulically smooth surface.

Notice that the ratio h/r_0 = const is constant along the tube and that for the plate h/δ decreases (i.e., the boundary thickness increases). We may therefore observe along the plate a flow with full roughness effect and transient and smooth flow as well.

Admissible roughness. This is determined by the thickness of the viscous boundary layer, on the supposition that no vorticity may arise beyond the irregularities completely immersed in this layer. The admissible height h_d of the protuberances on the plate (for sandy rough-

ness) is defined by the relation

$$\frac{h_0}{\delta} = \frac{4}{\mathrm{Re}\sqrt{c_f}}. \qquad (6.2.10)$$

Figure 6.2.10 [6.3] gives the curves determining the height of the protuberances of admissible roughness for a profile in laminar and turbulent boundary layers. As the height of the protuberances increases the transition point in a laminar flow approaches the leading edge; in a turbulent flow the protuberances which exceed the admissible

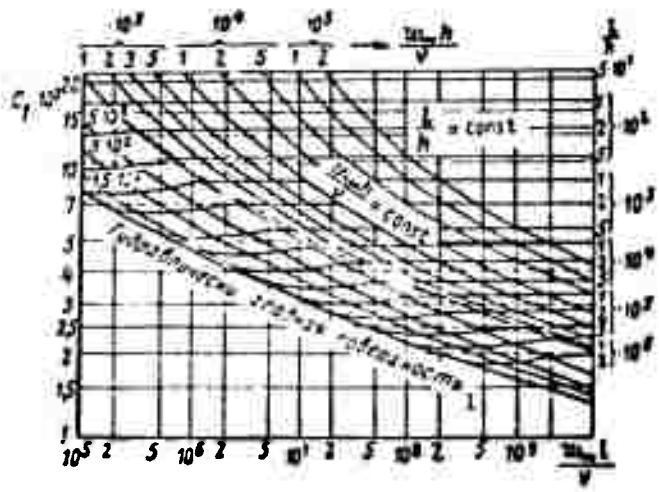


Fig. 6.2.9. Coefficient of over-all friction for a plane plate with sandy roughness. 1) Hydraulically smooth surface.

height give rise to rough turbulent flow.

Influence of the pressure gradient. The influence of the pressure gradient on the plate's boundary layer can be estimated if we consider the flow near the wall of a straight convergent or divergent channel.

Figure 6.2.11 gives the velocity distribution curves for various divergence angles of the channel; from these we see that in convergent channels the boundary layer thickness is considerably smaller than in a longitudinal flow along a plate (i.e., $\alpha = 0$) and that in a divergent channel it is considerably larger. In the case of a steady flow (when the boundary layers join at the channel axis) the radial velocity

distribution is symmetrical and the boundary layer does not become separated as long as the vortex angle of the divergent channel does not exceed 4°. At larger angles the velocity distribution changes considerably. At $\alpha = 5^\circ$ separation may occur on one of the walls. Experiments showed that separation occurs between the limits of $\alpha = 4.8$ to 5.1°. At $\alpha = 6^\circ$ separation can be observed clearly on one of the walls and the reverse motion is beginning.

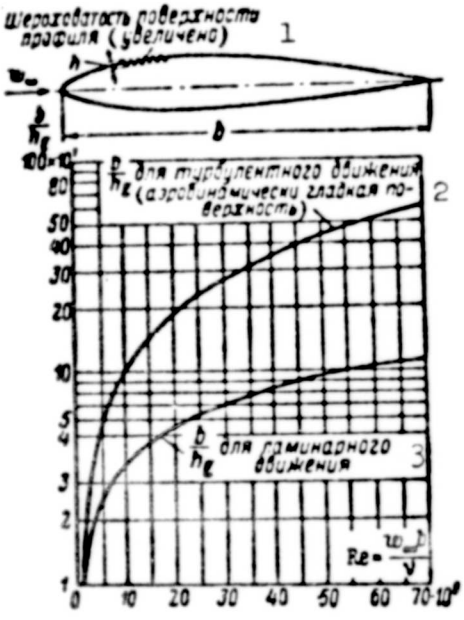


Fig. 6.2.10. Admissible height of (sandy type) roughness protuberances in laminar and turbulent flows. 1) Roughness of profile surface (enlarged); 2) for turbulent motion (aerodynamically smooth surface); 3) for laminar motion.

Boundary layer on a wing. This is calculated on the basis of the correspondence to the flow in a tube, the velocity distribution being assumed to satisfy the power law $w_x = w_0 (y/\delta)^q$ [6.4]. If we assume that the stress τ_0 at the wall is bound to depend only on the conditions close to the wall, μ, ρ, y, w need not depend on the tube radius r_0, or, in other words, if $w = f(\mu, \rho, y, \tau_0)$, then, assuming $w = \text{const}\ \mu^\alpha \rho^\beta \tau_0^\gamma y^\varepsilon$, it follows from dimensionally considerations that $w = \text{const} \left(\frac{\mu}{\rho}\right)^{\frac{q-1}{2}} \tau_0^{\frac{q+1}{2}} y^q$; solving this for τ_0 we find

$$\left.\begin{aligned} \tau_0 &= c\left(\frac{\rho w^2}{2}\right)\left(\frac{\nu}{yw}\right)^m, \\ m &= \frac{2q}{q+1}. \end{aligned}\right\} \qquad (6.2.11)$$

Substituting (6.2.11) in the impulse equation, we obtain the equation

$$z' + A\frac{f'}{f} z - B\left(\frac{w_0}{\nu}\right)^m f^{m/n} = 0.$$

where

$$z=\delta^{1-n};\quad f=\frac{w_0^2}{w_m^2};$$
$$A=\frac{(2q+3)(3q+1)}{2(q+1)};$$
$$B=\frac{(3q+1)(2q+1)}{2(q+1)}. \qquad (6.2.12)$$

and the drag coefficients ζ, a function of Re, is determined only by the parameter q. The values of ζ can be taken from the table:

$q=\frac{1}{6}$	$\frac{1}{7}$	$\frac{1}{8}$	$\frac{1}{9}$	$\frac{1}{10}$
$\zeta=0{,}050$	0,045	0,039	0,032	0,0245

Integrating Eq. (6.2.12) gives

$$\left(\frac{\delta}{l}\right)^{1-n}=B\,\mathrm{Re}^{n}f^{-A}\int_0^{x/l}f^{-\frac{n}{2}+A}\,d\frac{x}{l}. \qquad (6.2.13)$$

Another way of using the results of the semi-empirical theory to calculate the turbulent boundary layer is based on representing the tangential stress τ (or $\tau^{1/2}$) (and not the velocity) by a polynomial whose coefficients are obtained from the boundary conditions at the wall and at the outer boundary of the layer [6.4] with the help of the equations of motion in the boundary layer. The representation of $\tau^{1/2}$ (and not of τ) allows us to avoid the complex transcendental equations and lead to fairly simple algebraic relations for the velocity distribution, which are convenient

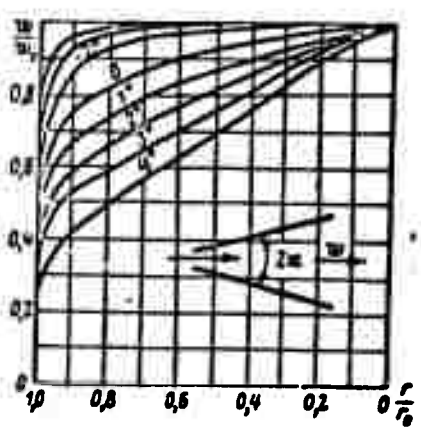


Fig. 6.2.11. Velocity distributions in divergent and convergent channels.

for the calculations. At the same time the impulse equation is exactly integrated and represented in a form convenient for carrying out successive approximations [6.5].

Logarithmic velocity distribution. If we consider the longitudinal flow about a square plate, $w_0' = 0$, and use a logarithmic velocity distribution

$$\frac{w_x}{w_*} = 2{,}5 \ln \frac{y w_*}{\nu} + 5{,}5,$$

we have

$$\frac{w_0 - w_x}{w_*} = -2{,}5 \ln \frac{y}{\delta}. \tag{6.2.14}$$

whence

$$\frac{\delta^{**}}{\delta} = \int_0^1 \frac{w_x}{w_0}\left(1 - \frac{w_x}{w_0}\right) d\frac{y}{\delta} = \frac{w_*^2}{w_0^2} \int_0^1 \frac{w_x}{w_*} \frac{w_0 - w_x}{w_*} d\frac{y}{\delta}.$$

Or, introducing $\mathrm{Re}^{**} = \frac{w_0 \delta^{**}}{\nu}$ and $\mathrm{Re}_\delta = \frac{w_0 \delta}{\nu}$, we obtain

$$\frac{\mathrm{Re}^{**}}{\mathrm{Re}_\delta} = A_1 \frac{w_*}{w_0} + A_2 \frac{w_*^2}{w_0^2}, \tag{6.2.15}$$

where

$$A_1 = -2{,}5 \int_0^1 \ln \frac{y}{\delta} d\frac{y}{\delta} = 2{,}5;$$

$$A_2 = -6{,}25 \int_0^1 \left(\ln \frac{y}{\delta}\right)^2 d\frac{y}{\delta} = -12{,}5.$$

Since $w_* : w_0 = \sqrt{\tau_0 : \rho w_0^2}$, eliminating Re_δ from (6.2.15) give us

$$1 : \sqrt{\tau_0 : \rho w_0^2} = 5{,}75\left[\lg \mathrm{Re}^{**} - 5{,}75 \lg\left(1 - 5\sqrt{\tau_0 : \rho w_0^2}\right) + 3{,}22\right]. \tag{6.2.16}$$

An approximate solution to this equation may be written in the form

$$1 : \sqrt{\tau_0 : \rho w_0^2} = 5{,}75 \lg \mathrm{Re}^{**} + 3{,}8,$$

and hence

$$\frac{\tau_0}{\rho w_0^2} = \frac{1}{(5{,}75 \lg \mathrm{Re}^{**} + 3{,}8)^2} = \frac{1}{33(\lg \mathrm{Re}^{*} + 0{,}66)^2}. \tag{6.2.17}$$

The results of experiments on plates at large Re numbers yielded the approximate relation

$$\frac{\tau_0}{\rho w_0^2} = \frac{1}{153.2\sqrt[4]{Re^{**}}}. \qquad (6.2.18)$$

which will be used a little later.

6.3. UNIVERSAL METHOD OF CALCULATING THE BOUNDARY LAYER ON CURVILINEAR SURFACES

The shape factor. The velocity distribution in a boundary layer is determined by the quantites dp/dx and τ_0; in dimensionless form we can write

$$\frac{w_x}{w} = \varphi\left(\frac{y}{l}, \frac{\rho w l}{\mu}, \frac{l}{\rho w^2}\frac{dp}{dx}\right),$$

where l and w are the characteristic linear dimension and the velocity for which we take in the further calculations δ** and w_0, respectively. Then, taking into account that $\frac{dp}{dx} = -\rho w_0 w_0'$ we can write

$$\frac{w_x}{w_0} = \varphi\left(\frac{y}{\delta^{**}}, \frac{w_0\delta^{**}}{\nu}, \frac{w_0'\delta^{**}}{w_0}\right) = \varphi\left(\frac{y}{\delta^{**}}, Re^{**}, Eu^{**}\right). \qquad (6.3.1)$$

On solving the problem it proved possible to combine the two effective parameters Re**, characterizing the tangential stresses, and Eu**, characterizing the dimensionless pressure drop (i.e., the shape of the body), into one universal parameter $f(Re^{**}, Eu^{**})$, which is independent of the Re number; its introduction simplifies the solution of the impulse equation

$$\frac{d\delta^{**}}{dx} + \frac{w_0'\delta^{**}}{w_0}\left(2 + \frac{\delta^*}{\delta^{**}}\right) = \frac{\tau_0}{\rho w_0^2} \qquad (6.3.2)$$

whereby its right-hand side becomes a function of this parameter, $\tau_0 : \rho w_0^2 = \Phi(f)$. This combined parameter $f(Re^{**}, Eu^{**})$, allowing for the shape of the body (Eu**) and the tangential stress distribution (Re**) is called the shape factor.

We thus put

$$w_x = w_0 f[y : \delta^{**}, f(x)]. \qquad (6.3.3)$$

to obtain $f(Re^{**}, Eu^{**})$ and $\tau_0 : \rho w_0^2 = \Phi(f)$ in the form

$$f = \mathrm{Eu}^{**}\, G(\mathrm{Re}^{**}); \tag{6.3.4}$$

$$\frac{\tau_0}{\rho w_0^2} = \frac{\zeta(f)}{G(\mathrm{Re}^{**})}. \tag{6.3.5}$$

Following L.G. Loytsyanskiy, we first consider a laminar boundary layer for which $\tau = \mu \frac{\partial w_x}{\partial y}$.

Calculating

$$\tau_0 = \mu \left(\frac{\partial w_x}{\partial y}\right)_{y=0} = \mu \frac{w_0}{\delta^{**}} \left.\frac{\partial (w_x : w_0)}{\partial (y : \delta^{**})}\right|_{y=0} = \rho w_0^2 \frac{\nu}{w_0 \delta^{**}} \zeta(f); \tag{6.3.7}$$

$$\delta^{*} = \int_0^{\delta} \left(1 - \frac{w_x}{w_0}\right) dy = \delta^{**} \int_0^{\delta} \left[1 - \varphi\left(\frac{y}{\delta^{**}}, f\right)\right] d\frac{y}{\delta^{**}} = \tag{6.3.8}$$

$$= H(f)\,\delta^{**},$$

we rewrite the impulse equation in the form

$$\frac{d\delta^{**}}{dx} + \frac{\dot{w}_0}{w_0} \delta^{**} [2 + H(f)] = \frac{\nu}{w_0 \delta^{**}} \zeta(f).$$

Multiplying it by $2\frac{w_0 \delta^{**}}{\nu}$ yields the equation

$$w_0 \frac{d}{dx}\left(\frac{\dot{w}_0 \delta^{**2}}{\nu} \frac{1}{w_0}\right) = 2\zeta(f) - \frac{\dot{w}_0 \delta^{**2}}{\nu} [2 + H(f)]. \tag{6.3.9}$$

The dimensionless combination $\frac{\dot{w}_0 \delta^{**2}}{\nu} = \frac{w_0 \delta^{**}}{\nu} \frac{\dot{w}_0 \delta^{**}}{w_0}$ entering this equation is a product of Re** and Eu**, i.e., $G(\mathrm{Re}^{**}) = \mathrm{Re}^{**}$; if this product is taken as the shape factor $f(x) = \frac{\dot{w}_0 \delta^{**2}}{\nu}$, then for this function f equation (6.3.9) remains an ordinary differential equation

$$\left.\begin{aligned} \frac{d}{dx}\left(\frac{f}{w_0}\right) &= \frac{1}{w_0} F(f), \\ F(f) &= 2\{\zeta(f) - f[2 + H(f)]\}. \end{aligned}\right\} \tag{6.3.10}$$

Carrying out the differentiation we obtain the equation

$$\frac{df}{dx} = \frac{\dot{w}_0}{w_0} F(f) + \frac{\dot{w}_0}{w_0} f. \tag{6.3.11}$$

which can be integrated if the form of the function $w_0(x)$ is given; the calculation of the laminar boundary layer is reduced here to finding the functions F(f), ζ(f) and H(f).

For a turbulent boundary layer we make use of the expression of τ_0 found previously for a plane plate (6.2.17) in the case of a logarithmic velocity profile:

$$\frac{c_0}{\rho w_0^2} = \frac{1}{33(\lg Re^{**} + 0{,}66)^3}. \qquad (6.3.12)$$

Since $w_0' = 0$ on the plate, we have for it $f = 0$ and $\zeta(f)_{f=0} = \zeta(0)$ = const; let us assume that const = 1, i.e., include the constant in the function $G(Re^{**})$; we then obtain for a plate

$$G(Re^{**}) = 33(\lg Re^{**} + 0{,}66)^3. \qquad (6.3.13)$$

As was said before (6.2.18), the results of evaluating experimental data on the drag of the plane plates at large Re' numbers can be well represented by the relation

$$G(Re^{**}) = 153{,}2\sqrt[6]{Re^{**}}, \qquad (6.3.14)$$

which, over a wide range of large Re numbers virtually coincides with Eq. (6.3.13).

In order to formulate the shape factor for a turbulent boundary layer we multiply both sides of the impulse equation by $G(Re^{**})$; we obtain

$$G(Re^{**})\frac{d\delta^{**}}{dx} + (2+H)f = \zeta. \qquad (6.3.15)$$

We rewrite the first component in the form

$$G(Re^{**})\frac{d\delta^{**}}{dx} = \frac{d}{dx}\left[G(Re^{**})\frac{w_0'\delta^{**}}{w_0} - \frac{w_0}{w_0'}\right] - \zeta^{**}G'(Re^{**})\frac{d\,Re^{**}}{dx} =$$

$$= \frac{d}{dx}\left(f\frac{w}{w_0'}\right) - \zeta^{**}G'(Re^{**})\left(\frac{w_0}{\nu}\frac{d\delta^{**}}{dx} + \frac{w_0'\delta^{**}}{\nu}\right) =$$

$$= \frac{d}{dx}\left(f\frac{w_0}{w_0'}\right) - Re^{**}G(Re^{**})\frac{d\delta^{**}}{dx} - Re^{**}\frac{G'(Re^{**})}{G(Re^{**})}f =$$

$$= \frac{d}{dx}\left(f\frac{w_0}{w_0'}\right) - \frac{Re^{**}G'(Re^{**})}{G(Re^{**})}\frac{d\delta^{**}}{dx} - \frac{Re^{**}G'(Re^{**})}{G(Re^{**})}f$$

or

$$[1 + m(Re^{**})]G(Re^{**})\frac{d\delta^{**}}{dx} = \frac{d}{dx}\left(f\frac{w_0}{w_0'}\right) - m(Re^{**})f,$$

where we put

$$m(Re^{**}) = \frac{Re^{**}[G'(Re^{**})]}{G(Re^{**})} = \frac{d\ln G(Re^{**})}{d\ln Re^{**}}. \qquad (6.3.16)$$

At the same time the impulse Eq. (6.1.19) assumes the form

$$\frac{d}{dx}\left(f\frac{w_0}{w_0}\right)=(1+m)\zeta-[2+m+(1+m)H]f$$

or

$$\left.\begin{aligned}\frac{df}{dx}&=\frac{\dot{w}_0}{w_0}F(f)+\frac{\dot{w}_0}{w_0}f,\\ F(f)&=(1+m)\zeta-[3+m+(1+m)H]f.\end{aligned}\right\}\qquad(6.3.17)$$

The form of this equation is the same as that of the equation for f in a laminar layer, into which it goes over at m = 1, and by virtue of (6.3.9). G(Re**) = Re**.

<u>One-parametric family of velocity distributions</u>. In order to find the functions F(f), ζ(f) and H(f) we assume a family of velocity distributions in the boundary layer cross sections to be given by the polynomial.

$$w_x=w_0(a_0+a_1\eta+a_2\eta^2+\ldots+a_N\eta^N).\qquad(6.3.18)$$

where $\eta = 1 - y/\delta$, and the coefficients a_0, a_1, a_2,... of the polynomial are functions of x. In order to determine the coefficients we write the boundary conditions as

$$w_x=w_y=0\qquad\text{for } y=0,\ \eta=1;$$
$$w_x=w_0;\ w_y=0;\ \frac{\partial w_x}{\partial y}=0\qquad\text{for } y=\delta,\ \eta=0.$$

The additional coefficients needed to determine the coefficients can be obtained from the differential equations of the boundary layer.

Since $w_x = w_y = 0$ at y = 0, we have

$$\frac{\partial^2 w_x}{\partial y^2}=\frac{1}{\rho\nu}\frac{dp}{dx}=-\frac{w_0}{\nu}\frac{dw_0}{dx}=-\frac{w_0\dot{w}_0}{\nu}.\qquad(6.3.19)$$

Differentiating the second equation of System (6.1.4) with respect to y

$$\frac{\partial w_x}{\partial y}\frac{\partial w_x}{\partial x}+w_x\frac{\partial^2 w_x}{\partial x\,\partial y}+\frac{\partial w_y}{\partial y}\frac{\partial w_x}{\partial y}+w_y\frac{\partial^2 w_x}{\partial y^2}=\nu\frac{\partial^3 w_x}{\partial y^3}$$

or

$$\frac{\partial w_x}{\partial x}\left(\frac{\partial w_x}{\partial y}+\frac{\partial w_y}{\partial y}\right)+w_x\frac{\partial^2 w_x}{\partial x\,\partial y}+w_y\frac{\partial^2 w_x}{\partial y^2}=\nu\frac{\partial^3 w_x}{\partial y^3}$$

and taking into account that for an incompressible fluid $\frac{\partial w_x}{\partial x}+\frac{\partial w_y}{\partial y}=0$, we obtain

$$w_x\frac{\partial^2 w_x}{\partial x\,\partial y}+w_y\frac{\partial^2 w_x}{\partial y^2}=\nu\frac{\partial^3 w_x}{\partial y^3},$$

and hence for $y = 0$

$$\frac{\partial^3 w_x}{\partial y^3}=0. \qquad (6.3.20)$$

Since $w_x = w_0$, $w_y = 0$, $\frac{\partial w_x}{\partial y}=0$, at the boundary $y = \delta$,

$$\frac{\partial^2 w_x}{\partial y^2}=0. \qquad (6.3.21)$$

If the derivatives of w_x with respect to y are continuous up to the $(n - 1)$th order, including that at $y = \delta$, we have

$$\frac{\partial^n w_x}{\partial y^n}=0 \quad (n=1, 2, 3\ldots). \qquad (6.3.22)$$

This means that the graph of the functions $w_x = f(y)$ is a curve that touches the straight line $w_x = w_0$ at the upper surface of the boundary layer, and that the number n determines the order of osculation.

Here it follows from the condition $w_x = w_0$, $w_y = 0$, that if $y = \delta$, $a_0 = 1$ and from Condition (6.3.22) we find that $a_1 = 0$, $a_2 = 0,\ldots,$ $a_{n-1} = 0$.

Therefore,

$$w_x = w_0(1 + a_n\eta^n + a_{n+1}\eta^{n+1} + a_{n+2}\eta^{n+2}). \qquad (6.3.23)$$

Determination of the polygonal coefficients. In Expression (6.3.23) the boundary conditions at the upper boundary of the layer are allowed for by taking the coefficients from a_1 to a_{n-1} to be equal to zero, and the coefficients a_n are determined by the boundary conditions only at the body surface at $y = 0$ ($\eta = 1$). In our case, at $\eta = 1$, $w_x = 0$

$$\frac{\partial^2 w_x}{\partial y^2}=-\frac{w_0 w_0'}{\nu};\quad \frac{\partial^3 w_x}{\partial y^3}=0.$$

Substituting this into Series (6.3.23) we obtain a system of

three equations in the three unknowns a_n, a_{n+1}, a_{n+2} depending on n and $\lambda = \frac{w_0' \delta^2}{\nu}$:

$$1 + a_n + a_{n+1} + a_{n+2} = 0;$$

$$n(n-1)a_n + n(n+1)a_{n+1} + (n+2)(n+1)a_{n+2} = \frac{dw}{dx}\frac{\delta^2}{\nu} = \frac{w_0' \delta^2}{\nu} = \lambda;$$

$$n(n-1)(n-2)a_n + (n+1)n(n-1)a_{n+1} + (n+2)(n+1)na_{n+2} = 0.$$

The solution of this system yields

$$\left.\begin{aligned} a_n &= \frac{1}{2}\lambda - \frac{(n+2)(n+1)}{6}, \\ a_{n+1} &= -\frac{n}{n+1}\lambda + \frac{(n-1)(n-2)}{3} \\ a_{n+2} &= \frac{n-1}{2(n+1)}\lambda - \frac{(n-1)n}{6}. \end{aligned}\right\} \qquad (6.3.24)$$

Now,

$$H^*(\lambda) \quad \frac{\delta^*}{\delta} = \frac{1}{\delta}\int_0^\infty \left(1 - \frac{w_x}{w_0}\right)dy =$$

$$= -\frac{a_n}{n+1} - \frac{a_{n+1}}{n+2} - \frac{a_{n+2}}{n+3}; \qquad (6.3.25)$$

$$H^{**}(\lambda) = \frac{\delta^{**}}{\delta} = \frac{1}{\delta}\int_0^\infty \frac{w_x}{w_0}\left(1 - \frac{w_x}{w_0}\right)dy = H^* - \frac{a_n^2}{2n+1} -$$

$$- \frac{a_{n+1}^2}{2n+3} - \frac{a_{n+2}^2}{2n+5} - \frac{2a_n a_{n+1}}{n+1} - \frac{2a_n a_{n+2}}{2n+3} - \frac{2a_{n+1}a_{n+2}}{n+2}. \qquad (6.3.26)$$

Calculation of the laminar boundary layer. In this case the quantity ζ is also expressed in terms of λ; according to (6.3.7)

$$\left.\begin{aligned} \zeta &= \frac{\delta^{**}}{\mu w_0}\tau_0 = \frac{\delta^{**}}{w_0}\frac{\partial w_x}{\partial y}\Big|_{y=0} = \frac{\partial(w_x : w_0)}{\partial(y : \delta^{**})}\Big|_{y=0} = na_n\eta^{n-1} + \\ &+ (n+1)a_{n+1}\eta^n + (n+2)a_{n+2}\eta^{n+1} = H^{**}(\lambda)\,b(\lambda), \\ b(\lambda) &= \frac{\lambda}{n+1} + \frac{n+2}{3}. \end{aligned}\right\} \qquad (6.3.27)$$

The frictional stress

$$\tau_0 = \mu\frac{\partial w_x}{\partial y}\Big|_{y=0} = \sqrt{\rho\nu w_0' w_0}\,\frac{b(\lambda)}{\lambda} \qquad (6.3.28)$$

and the shape factor

$$f = \frac{w_0' \delta^{**2}}{\nu} = \frac{w_0' \delta^2}{\nu}\left(\frac{\delta^{**}}{\delta}\right)^2 = \lambda H^{**2} \qquad (6.3.29)$$

will also be functions of the two parameters λ and n.

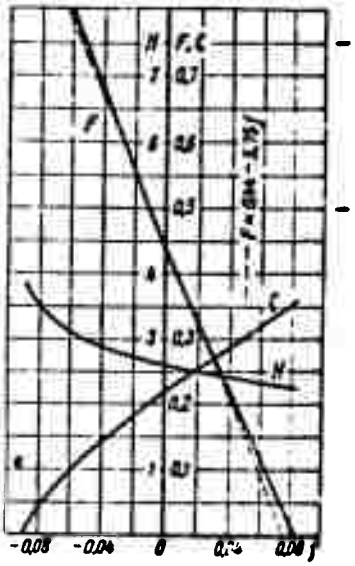


Fig. 6.3.1. The functions $F(f)$, $\zeta(f)$ and $H(f)$.

Applying the exact solutions of the boundary layer equation for $w_x = \text{const}\, x^m$, L.G. Loytsyanskiy obtained a relation linking n and λ in the form

$$n = 0.15\lambda + 4 \qquad (6.3.30)$$

and, fixing various values on n beforehand, he calculated the coefficients a_n, a_{n+1}, a_{n+2} and also the quantities H, H*, H**, ζ, b and f. The dependence of $F\zeta$ and H on f is given in a table presented below, and in Fig. 6.3.1.

It can be seen from the graph of Fig. 6.3.1 that the function F_{st} f is almost linear and we may put $F = p - qf$ where $p = 0.44$ and $q = 5.75$.

Table of the values of $f(f)$, $\zeta(f)$ and $H(f)$

f	$F(f)$	$\zeta(f)$	$H(f)$	f	$F(f)$	$\zeta(f)$	$H(f)$
−0,089	1,04	0,000	3,85	0,00	0,44	0,219	2,61
−0,085	1,00	0,019	3,66	0,01	0,38	0,236	2,55
−0,08	0,96	0,039	3,50	0,02	0,33	0,253	2,50
−0,07	0,88	0,071	3,28	0,03	0,275	0,270	2,46
−0,06	0,81	0,097	3,12	0,04	0,22	0,286	2,41
−0,05	0,74	0,120	3,00	0,05	0,17	0,302	2,36
−0,04	0,68	0,142	2,90	0,06	0,12	0,318	2,32
−0,03	0,615	0,162	2,82	0,07	0,07	0,335	2,28
−0,02	0,55	0,181	2,74	0,08	0,02	0,350	2,24
−0,01	0,50	0,200	2,67	0,084	0,003	0,357	2,22

In this case Eq. (6.3.11) assumes the form of the linear equation

$$\frac{df}{dx} = \left(\frac{\dot{w}_0}{w_0} - q\frac{\dot{w}_0}{w_0}\right) f + p\frac{\dot{w}_0}{w_0}. \qquad (6.3.31)$$

its integral will be

$$f = p\frac{\dot{w}_0}{w_0^q}\int_0^x w_0^{q-1}\,d\zeta = 0.44\,\frac{\dot{w}_0}{w_0^{5.75}}\int_0^x w_0^{4.75}\,d\zeta =$$

$$\approx 0{,}46\frac{w_0'}{w_0^6}\int_0^x w_0^5\,d\xi. \qquad (6.3.32)$$

where the value $x = 0$ corresponds to the forward stagnation point.

Having obtained the velocity distribution, for example from a calculation of the flow potential for the given body, we calculate f with Eq. (6.3.32) and then we can find all re- δ^*, δ^{**}, τ_0 etc. from the table.

The separation point of a laminar boundary layer. For a curvilinear surface this point is found from the condition that on the surface $\tau_0 = 0$, a condition to which the value $f = -0.089$ corresponds. The relation applying to the separation point is thus

$$\frac{w_0'\delta^{**2}}{\nu} = -0{,}089. \qquad (6.3.33)$$

Method for calculating the laminar boundary layer. From the distribution $w_0(x)$ given in a series of cross sections we find $w_0'(x)$ and from Eq. (6.3.32) we find $f(x)$ and, therefore, δ^{**}; we then find $\zeta(x)$ from the graph 6.3.1 or the table, and hence $\tau_0 = \mu\frac{w_0}{\delta^{**}}\zeta$, $\delta^* = \delta^{**}H(f)$ and the abscissa of the separation point.

Let us point out that from (6.3.32) and the definition $f = \frac{w_0'\delta^{**2}}{\nu}$ we obtain an expression for δ^{**} which does not contain w_0':

$$\frac{\delta^{**2}}{\nu} = \frac{0{,}46}{w_0^6}\int_0^x w_0^5\,d\xi, \qquad (6.3.34)$$

from which δ^{**} can be found without graphically differentiating the curve $w_0(x)$.

Calculations of the turbulent boundary layer. The idea of the shape factor has proved very fruitful for calculating the turbulent layer too. Following L.G. Loytsyanskiy, we introduce normalized quantities, the shape factor being normalized in such a way that at the separation point it equals unity, i.e., $\bar{F} = f : f_s$ where f_s is the value of the unnormalized shape factor f at the separation point ($x = x_s$)

The functions $\zeta(f)$ and $H(f)$ are so normalized that at $f = 0$ (at the point of minimum pressure) the values of $\zeta(f)$ and $H(f)$ become equal to unity; thus

$$\bar{f}=f:f_s,\ \bar{\zeta}=\zeta:\zeta(0),\ \bar{H}=H:H(0), \tag{6.3.35}$$

where $\zeta(0)$ and $H(0)$ are the values of the unnormalized parameters at the point of minimum pressure (at $f = 0$), which are different for laminar and turbulent boundary layers. The values of the normalized quantities $\bar{f}$, $\bar{\zeta}$ and $\bar{H}$ are given in the table.

Values of the Parameters

$\bar{f}$	$\bar{\zeta}$	$\bar{H}$	$\bar{F}$	$\bar{f}$	$\bar{\zeta}$	$\bar{H}$	$\bar{F}$
−0,95	1,63	0,85	0,00	0,0	1,00	1,00	−4,90
−0,90	1,60	0,86	−0,24	0,1	0,93	1,02	−5,48
−0,80	1,53	0,87	−0,74	0,2	0,85	1,04	−6,04
−0,70	1,47	0,88	−1,24	0,3	0,77	1,07	−6,64
−0,60	1,41	0,90	−1,76	0,4	0,69	1,10	−7,28
−0,50	1,34	0,915	−2,28	0,5	0,60	1,125	−7,88
−0,40	1,28	0,93	−2,78	0,6	0,515	1,16	−8,56
−0,30	1,21	0,95	−3,30	0,7	0,42	1,20	−9,28
−0,20	1,14	0,97	−3,82	0,8	0,31	1,26	−10,04
−0,10	1,08	0,985	−4,36	0,9	0,175	1,35	−10,80
0,00	1,00	1,00	−4,90	1,0	0,0	1,48	−11,68

Written in terms of the normalized quantities the differential Eq. (6.3.17) has the form

where

$$\left.\begin{aligned}&\frac{d\bar{f}}{d\bar{x}}=\frac{w_0'}{w_0}\bar{F}(\bar{f})+\frac{w_0'}{w_0}\bar{f},\\&\bar{F}(\bar{f})=\frac{1+m}{f_s}\zeta_0\bar{\zeta}(\bar{f})-[3+m+(1+m)H_0\bar{H}(\bar{f})]\bar{f}.\end{aligned}\right\} \tag{6.3.36}$$

Applying the experimentally well verified supposition due to L.G. Loytsyanskiy that the functions $\bar{\zeta}(\bar{f})$ and $\bar{H}(\bar{f})$ are the same for laminar and turbulent boundary layers and determining the values of m, f_s and H_0 from experimental results, makes it possible to substitute the expression $\bar{\zeta}(\bar{f})$ and $\bar{H}(\bar{f})$ taken from the table into Formula (6.3.36) and so to determine $\bar{F}(\bar{f})$ for the turbulent layer. With an accuracy sufficient for practical purposes the function $\bar{F}(\bar{f})$ can be assumed

to be the same for turbulent and laminar layers and to be a linear function of $\bar{f}$:

$$F(\bar{f}) = p - q\bar{f}. \tag{6.3.37}$$

Experiment yields $\bar{p} = 0.6$; $q = 4.8$.

Substituting (6.3.37) in (6.3.36) and integrating it yields

$$\bar{f}(x) = \frac{w_0'(x)}{[w_0(x)]^q}\left[C - p\int_0^x [w_0(\xi)]^{q-1}\,d\xi\right]. \tag{6.3.38}$$

Since $\bar{f}$ is finite at $x = 0$ then, if the layer is completely turbulent, $C = 0$, we have

$$\bar{f}(x) = -\frac{pw_0'}{w_0^q}\int_0^x w_0^{q-1}\,d\xi \tag{6.3.39}$$

or, substituting the values $p = 0.6$ and $q = 0.48$ for the turbulent layer, we shall have

$$\bar{f}(x) = -0{,}6\,\frac{w_0'}{w_0^{0.48}}\int_0^x w_0^{0.8}\,d\xi. \tag{6.3.40}$$

Transition of a laminar to a turbulent boundary layer on a curvilinear surface. When the drag of a wing is being calculated it is necessary to know the position of the point (more exactly, of the region) of transition on the wing profile where the laminar boundary layer goes over to a turbulent one.

The separation conditions of the laminar layer (6.3.33) can be rewritten in the following manner:

$$\frac{\nu w_0'}{w_0^3}\left(\frac{w_0\delta^{**}}{\nu}\right)^2 = \frac{\nu w_0'}{w_0^2}\,\mathrm{Re}^{**} = -0{,}089, \tag{6.3.41}$$

whence it can be seen that the thicker the boundary layer, the smaller are the gradients of the velocity w_0' of the outer flow at which the laminar boundary layer becomes separated.

At a certain distance from the separation site the laminar layer loses steadiness, becomes turbulent and disintegrates into individual

vortices which are carried along downstream.

Owing to the presence of disturbances streaming towards the wing of to the production of disturbances on the wing surface, e.g., owing to its roughness, the laminar layer already becomes unsteady before the separation point x_s. The presence of disturbances in the boundary layer leads to pulsations of the velocity and its derivatives, inducing reverse motion and vortex formation.

Thus, depending on the intensity of the disturbances, the beginning of the region of unsteady vortex formation may lie much farther upstream than the separation point x_s of the steady laminar layer, and even farther upstream than the point of minimum pressure. We take this region as the transition region and in order to take the influence of these disturbances into account we introduce the parameter $j = j(\mathrm{Re}_x, \mathrm{Eu}_x) = j\left(\frac{w_0 x}{\nu}, \frac{w_0'}{w_0}\right)$. Noticing that $\frac{\nu w_0'}{w_0^2} = \frac{\nu}{w_0 x}\frac{x w_0'}{w_0} = \mathrm{Eu}_x \mathrm{Re}_x'$ and keeping the form of the parameter $\frac{\nu w_0'}{w_0^2}\mathrm{Re}^{**2} = -0{,}089$, that characterizes the separation of the laminar boundary layer unchanged, we find that at the separation point

$$\left(\frac{\nu w_0'}{w_0^2} + j\right)\mathrm{Re}^{**2} = -0{,}089. \qquad (6.3.42)$$

To a first approximation, the quantity j can be taken as a constant and, as is shown by a re-calculation of the experimental results, j varies from -0.5 to -2.5; it depends only on the character of the flow and is almost independent of the magnitude of the velocity, of the profile shape, etc.

Passing over to the dimensionless quantities $\bar{w}_0 = w_0 : w_\infty$, $\bar{x} = x : b$, we find from (6.3.34) that

$$\mathrm{Re}^{**2} = \frac{w_\infty b}{\nu}\frac{0{,}46}{\bar{w}_0^6}\int_0^{\bar{x}} \bar{w}_0^5 d\bar{x} = \mathrm{Re}\,\varphi(\bar{x}). \qquad (6.3.43)$$

where

$$\varphi=\frac{0.46}{\bar{w}_0^4}\int_0^{\bar{x}}\bar{w}_0^5\,d\bar{x},\quad \mathrm{Re}=\frac{w_0 b}{\nu}. \tag{6.3.44}$$

In dimensionless quantites $\frac{\nu w_0'}{w_0^2}=\frac{1}{\mathrm{Re}}\frac{\bar{w}_0'}{\bar{w}_0^2}$.

Substituting this in (6.3.42) we obtain

$$\left(\frac{1}{\mathrm{Re}}\frac{\bar{w}_0'}{\bar{w}_0^2}+j\right)\mathrm{Re}\,\varphi(\bar{x})=Q(\bar{x},\ j,\ \mathrm{Re})=-0.089. \tag{6.3.45}$$

When we determine the values and construct the graph of the function $Q(\bar{x}, j, \mathrm{Re})$ with the values C_y, j, Re for a given profile, we can find the value $\bar{x}=\bar{x}_p$ at which Eq. (6.3.45) will be satisfied.

Boundary layer equations for a compressible gas. These equations must take thermodynamic processes into account too, i.e., the system of Eqs. (6.1.4) must be completed by adding the energy equation and taking the temperature dependences of viscosity and thermal conductivity into account. The energy equation can be derived in the same way, by estimating the magnitudes of the individual terms of the diffrential energy Eq. (2.3.10).

Omitting the rather cumbersome calculations, we give two forms of the energy equation [6.1] for a steady laminar plane boundary layer in a viscous gas:

first form, containing the enthalpy: $i_0=i+\frac{w_x^2}{2}=c_pT+\frac{w_x^2}{2}$.

second form, containing the absolute temperature

$$\left.\begin{aligned}\rho w_x\frac{\partial i_0}{\partial x}+\rho w_y\frac{\partial i_0}{\partial y}&=\frac{1}{\mathrm{Pr}}\frac{\partial}{\partial y}\left(\mu\frac{\partial i_0}{\partial y}\right)+\left(\frac{1}{\mathrm{Pr}}-1\right)\frac{\partial}{\partial y}\left(\mu\frac{\partial i}{\partial y}\right)\\ \rho c_p\left(w_x\frac{\partial T}{\partial x}+w_y\frac{\partial T}{\partial y}\right)&=w_x\frac{\partial p}{\partial x}+\mu\left(\frac{\partial w_x}{\partial y}\right)^2+\frac{\lambda}{\mu}\frac{\partial}{\partial y}\left(\mu\frac{\partial T}{\partial y}\right).\end{aligned}\right\} \tag{6.3.46}$$

The equations of continuity and momentum conservation will read

$$\left.\begin{aligned}\frac{\partial(\rho w_x)}{\partial x}+\frac{\partial(\rho w_y)}{\partial y}&=0,\\ \rho w_x\frac{\partial w_x}{\partial x}+\rho w_y\frac{\partial w_x}{\partial y}&=-\frac{\partial p}{\partial x}+\frac{\partial}{\partial y}\left(\mu\frac{\partial w_x}{\partial y}\right).\end{aligned}\right\} \tag{6.3.47}$$

A.A. Dorodnitsyn's transformation. A universal method of boundary layer calculation based on representing the profile in the boundary layer in the form of a function of a single parameter was generalized by A.A. Dorodnitsyn for the case of a compressible gas [6.6].

Choosing the first form of the energy Eq. (6.3.46) and keeping in mind that $\frac{\partial p}{\partial y}=0$, we can write the system of boundary layer equations as

$$\left.\begin{gathered}\frac{\partial(\rho w_x)}{\partial x}+\frac{\partial(\rho w_y)}{\partial y}=0,\\ \rho w_x\frac{\partial w_x}{\partial x}+\rho w_y\frac{\partial w_x}{\partial y}=-\frac{dp}{dx}+\frac{\partial}{\partial y}\left(\mu\frac{\partial w_x}{\partial y}\right),\\ \rho w_x\frac{\partial i_0}{\partial x}+\rho w_y\frac{\partial i_0}{\partial y}=\frac{1}{\mathrm{Pr}}\frac{\partial}{\partial y}\left(\mu\frac{\partial i_0}{\partial y}\right)-\\ -\left(\frac{1}{\mathrm{Pr}}-1\right)\frac{\partial}{\partial y}\left(\mu w_x\frac{\partial w_x}{\partial y}\right)\\ \left(i_0=I+\frac{w_x^2}{2}=c_pT+\frac{w_x^2}{2};\ \mathrm{Pr}=\frac{\mu c_p}{\lambda}\right),\\ p=\rho RT,\quad \mu=\mu(T),\quad \lambda=\lambda(T).\end{gathered}\right\}\qquad(6.3.48)$$

Assuming for simplicity that Pr = 1 and that no heat exchange with the walls occurs ($\partial T/\partial y = 0$ for $y = 0$), we obtain $i_0 = \text{const}$ as a particular integral of the energy equation, i.e., the total heat content is equal for all points of the boundary layer, and we therefore have for them

$$\frac{T}{T_0}=\left(1-\frac{w_x^2}{2c_pT_0}\right);\qquad \frac{p}{p_0}=\left(1-\frac{w_0^2}{2i_0}\right)^{\frac{k}{k-1}}\qquad(6.3.49)$$

We put

$$\lambda=\frac{w_x}{\sqrt{2i_0}},\quad \lambda_0=\frac{w_0}{\sqrt{2i_0}}\qquad(6.3.50)$$

and introduce the new independent variables (the so-called Dorodnitsyn variables)

$$\xi=\int_0^x\frac{\rho}{\rho_0}dx=\int_0^x(1-\lambda_0^2)^{\frac{k}{k-1}}dx,\quad \eta=\int_0^y\frac{\rho}{\rho_0}dy=\int_0^y\frac{(1-\lambda_0^2)^{\frac{k}{k-1}}}{1-\lambda^2}dy.\qquad(6.3.51)$$

where it is taken into account that $\rho/\rho_0=pT_0/p_0T$

Then, assuming that the viscoisty μ satisfies the law $\mu=\mu_0(T/T_0)^n$ and taking into account that

$$\frac{\partial}{\partial x}=\frac{\rho}{\rho_0}\frac{\partial}{\partial\xi}+\frac{\partial\eta}{\partial x}\frac{\partial}{\partial\eta};\quad \frac{\partial}{\partial y}=\frac{\rho}{\rho_0}\frac{\partial}{\partial\eta};$$

we obtain from the second equation of System (6.3.48)

$$\left.\begin{aligned} &\nu_0 = \frac{\mu_0}{\rho_0}, \quad w_0' = \frac{\partial w_0}{\partial \xi}, \\ &w_x \frac{\partial w_x}{\partial \xi} + \left[\frac{w_y}{1-a^2} + \frac{w_x}{(1-a_0^2)^{\frac{k}{k-1}}} \frac{d\tau}{dx} \right] \frac{\partial w_x}{\partial \eta} - \\ &= \frac{1-a^2}{1-a_0^2} w_0 w_0' + \nu_0 \frac{\partial}{\partial \eta} \left[(1-a^2)^{n-1} \frac{\partial w_x}{\partial \eta} \right]. \end{aligned}\right\} \qquad (6.3.52)$$

Putting

$$\bar{w}_y = \frac{w_y}{1-a^2} + \frac{w_x}{(1-a_0^2)^{\frac{k}{k-1}}} \frac{\partial \eta}{\partial x}. \qquad (6.3.53)$$

we can rewritte (6.3.52) in the form

$$w_x \frac{\partial w_x}{\partial \xi} + \bar{w}_y \frac{\partial w_x}{\partial \eta} = \frac{1-a^2}{1-a_0^2} w_0 w_0' + \nu_0 \frac{\partial}{\partial \eta} \left[(1-a^2)^{n-1} \frac{\partial w_x}{\partial \eta} \right]. \qquad (6.3.54)$$

Introducing the stream function Ψ

$$\rho w_x = \frac{\partial \Psi}{\partial y}; \quad \rho w_y = -\frac{\partial \Psi}{\partial x}$$

and going over to the variables ξ, η we obtain

$$w_x = \frac{1}{\rho_0} \frac{\partial \Psi}{\partial \eta}; \quad \frac{w_y}{1-a^2} = -\frac{1}{\rho_0} \frac{\partial \Psi}{\partial \xi} - \frac{w_x}{(1-a_0^2)^{\frac{k}{k-1}}} \frac{\partial \eta}{\partial x},$$

i.e.,

$$\bar{w}_y = -\frac{1}{\rho_0} \frac{\partial \Psi}{\partial \xi}.$$

At the same time, the continuity Eq. (6.3.48) will read

$$\frac{\partial w_x}{\partial \xi} + \frac{\partial \bar{w}_y}{\partial \eta} = 0. \qquad (6.3.55)$$

Solving System (6.3.54)-(6.3.55) analogously to the system of Eqs. (6.1.4) for an incompressible fluid, we can find the distributions of velocities w_x and w_y from the given pressure distribution.

On the basis of these considerations and also of Eq. (6.1.18), we can write down the integral relation

$$\frac{d}{d\xi} \int_0^{\delta_\eta} w_x (w_0 - w_x) d\eta + w_0' \int_0^{\delta_\eta} \left(\frac{1-a^2}{1-a_0^2} w_0 - w_x \right) d\eta = \nu_0 \left(\frac{\partial w_x}{\partial \eta} \right)_{\eta=0}. \qquad (6.3.56)$$

where δ_η denotes the value of η for which $w_x = w_0$.

Introducing the conventional thickness of displacement and the thickness of impulse loss by analogy with (6.1.19)

$$\delta_1^* = \int_0^\delta \left(1 - \frac{w_x}{w_0}\right) d\eta; \quad \delta_2^{**} = \int_0^\delta \frac{w_x}{w_0}\left(1 - \frac{w_x}{w_0}\right) d\eta$$

and omitting the subscript η at δ we can rewrite Eq. (6.3.56) in the form

$$\frac{d\delta^{**}}{dt} + \left(2\frac{w_0'}{w_0} - \frac{\alpha_0\alpha_0'}{1-\alpha_0^2}\right)\delta^{**} + \frac{w_0'}{w_0(1-\alpha_0^2)}\delta^* = \frac{\nu_0}{w_0^2}\left(\frac{\partial w_x}{\partial \eta}\right)_{\eta=0}. \qquad (6.3.57)$$

where

$$\alpha_0' = \frac{d\alpha_0}{dt} = \frac{1}{\sqrt{2L_0}} w_0'$$

If we assume that the velocity distributions in the boundary layer cross sections can be given by the single-parameter family

$$w_x = w_0 \varphi\left(\frac{\eta}{\delta^{**}}, f\right); \qquad (6.3.58)$$

then

$$\left.\begin{aligned} \frac{\delta^*}{\delta^{**}} = H(f) &= \int_0^\delta \left[1 - \varphi\left(\frac{\eta}{\delta^{**}}, f\right)\right] d\left(\frac{\eta}{\delta^{**}}\right), \\ \left(\frac{\partial w_x}{\partial \eta}\right)_{\eta=0} &= \frac{w_0}{\delta^{**}}\varphi'(0, f) = \frac{w_0}{\delta^{**}}\zeta(f). \end{aligned}\right| \qquad (6.3.59)$$

Substituting (6.3.59) in (6.3.57) we find

$$\left.\begin{aligned} &\frac{1}{2}\frac{d}{dt}\frac{\delta^{**2}}{\nu_0} + \left[2\frac{w_0'}{w_0} - \frac{\alpha_0\alpha_0'}{1-\alpha_0^2}\right]\frac{\delta^{**2}}{\nu_0} + \\ &+ \frac{w_0'}{w_0(1-\alpha_0^2)}\frac{\delta^{**2}}{\nu_0}H(f) = \frac{\zeta(f)}{w_0} \end{aligned}\right| \qquad (6.3.60)$$

or, multiplying by $(1-\alpha_0^2)$ and noticing that

$$\left.\begin{aligned} &\frac{d}{dt}\frac{(1-\alpha_0^2)\delta^{**}}{\nu_0} = (1-\alpha_0^2)\frac{d}{dt}\frac{\delta^{**2}}{\nu_0} - 2\frac{\delta^{**2}}{\nu_0}\alpha_0\frac{\alpha_0'}{dt}, \\ &\frac{1}{2}\frac{d}{dt}\frac{(1-\alpha_0^2)\delta^{**2}}{\nu_0} = \frac{1-\alpha_0^2}{w_0}\left\{\zeta(f) - \frac{\delta^{**2}w_0'}{\nu_0(1-\alpha_0^2)}[2+H(f)]\right\}. \end{aligned}\right| \qquad (6.3.61)$$

Let us choose as the shape factor

$$f = \frac{w_0'\delta^{**2}}{\nu_0(1-\alpha_0^2)}. \qquad (6.3.62)$$

The differential equation defining it will then be (6.3.61)

$$\left.\begin{aligned} &\frac{d}{dt}\left[\frac{(1-\alpha_0^2)^2}{w_0'} f\right] = \frac{1-\alpha_0^2}{w_0} F(f), \\ &F(f) = 2[\zeta(f) - f[2+H(f)]] \end{aligned}\right| \qquad (6.3.63)$$

or, if the differentiation in (6.3.63) is carried out

$$\frac{df}{d\xi} = F(f)\frac{d}{d\xi}\ln\frac{w_0}{\sqrt{1-a_0^2}} + f\frac{d}{d\xi}\ln\frac{w_0'}{(1-a_0^2)^2}. \qquad (6.3.64)$$

If we return in Eq. (6.3.64) to the variable x we have

$$\frac{df}{dx} = F(f)\frac{d}{dx}\ln\frac{w_0}{\sqrt{1-a_0^2}} + f\frac{d}{dx}\ln\frac{w_0'}{(1-a_0^2)^{2+\frac{k}{k-1}}} \quad \left(w_0' = \frac{dw_0}{dx}\right) \qquad (6.3.65)$$

At $\alpha = \alpha_0 = 0$ Eq. (6.3.65) goes over to the equation for an incompressible medium.

Equation (6.3.65) can be integrated if we know F(f). Since Expression (6.3.58) for w_x/w_0 does not depend explicitly on the number M_∞, it must be the same for both compressible and incompressible fluids. The forms of the functions F(f), H(f) and $\zeta(f)$ must therefore be equal too. Assuming therefore that F(f) = p - qf, we find by integrating (6.3.65) that

$$f = \frac{p w_0'}{w_0(x)^q (1-a_0^2)^m}\int_0^x w_0(\xi)^{q-1}(1-a_0^2)^{m-1}\,d\xi \qquad (6.3.66)$$

where

$$m = -2 + \frac{k}{k-1} - \frac{q}{2}.$$

Notice that the number M_∞ influences the velocity distribution (6.3.58) implicitly through the quantities w_0, δ^{**}, η, and f.

For the coefficient of friction we have

$$C_f = \frac{2\tau_0}{\rho_0 w_0^2} = \frac{2\mu_0}{\rho_0 w_0^2}\left(\frac{\partial w_x}{\partial \eta}\right)\left(\frac{\partial \eta}{\partial y}\right)_{y=\eta=0}. \qquad (6.3.67)$$

Substituting the value of the quantity $(\partial w_x/\partial \eta)_{\eta=0}$ form (6.3.59) into (6.3.66) and knowing the relation linking η and y, we obtain

$$C_f = \frac{2\nu_0}{w_0 \delta^{**}}(1-a_0^2)\zeta(f) = \frac{2\sqrt{\nu_0}}{w_0}(1-a_0^2)^{\frac{1}{2(k-1)}}\sqrt{\frac{w_0'}{f}}\,\zeta(f). \qquad (6.3.68)$$

The calculation of profiles by the above method shows that the separation point lies considerably closer to the leading edge of the profile in a compressible gas than it does in incompressible fluid,

which leads to an increased profile drag.

6.4. BOUNDARY LAYER AND SHOCK WAVES

The sound barrier. The investigation of boundary layers at near-sonic velocities proves very complex, particularly at the transition from $M < 1$ to $M > 1$. This transition through the so-called "sound barrier" ($M = 1$), is accompanied by vibrations of the aircraft and a deterioration in its controllability; these phenomena are caused by the unsteady interaction between the boundary layer and the shock waves leading to the separation of the boundary layer. Similar effects arise on the blades of turbines, guide mechanisms and propellers when the air speed relative to the blade profile approaches the sonic speed.

Let us consider the flow about an airfoil profile placed in a nearsonic stream. At the leading part of the profile $\partial p/\partial x < 0$ and behind the point of maximum profile thickness the flow is slowed down and $\partial p/\partial x > 0$.

At M_∞ numbers close to unity, the acceleration of the flow at the leading part of the profile may lead to a local Mach number M in the region of maximum thickness being equal to 1. Further, owing to the expansion of the flow (as in the Laval nozzle) the M number exceeds unity. Past the profile, however, the flow remains subsonic, as before. This means that in the rear part of the profile the supersonic flow must pass over to subsonic flow. Since a transition from supersonic to subsonic flow is virtually impossible without shocks, a shock wave must arise in this region. Experiments showed that the character of this wave depends on the Re number at the site where the shock wave "contacts" the profile and on whether the boundary layer at this "contact" site is laminar or turbulent. The word "contact" may only be used conditionally because the shock cannot touch the

wall. Since the flow before the shock is supersonic we can in fact subdivide the boundary layer on the profile before the shock into two zones: a supersonic zone ($M > 1$) and a subsonic zone ($M < 1$) adhering directly to the profile, separated by the interface $M = 1$ (Fig. 6.4.1). The compression shock may arise only in the supersonic zone of the flow, and therefore, cannot pass through the subsonic part of the boundary layer or touch the profile surface.

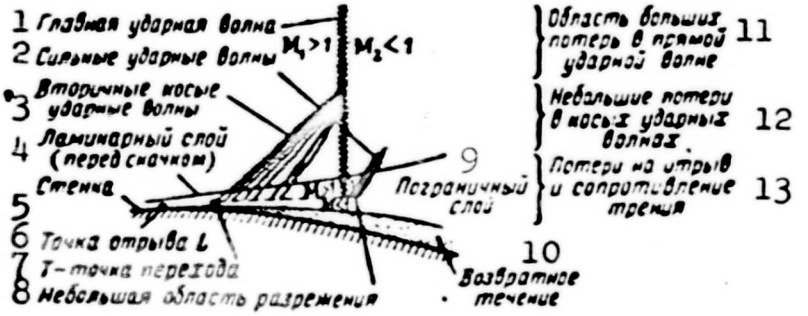


Fig. 6.4.1. Boundary layer structure and λ-shaped shock. 1) Main shock wave; 2) strong shock waves; 3) secondary diagonal shock waves; 4) laminar layer (before the shock); 5) wall; 6) separation point L; 7) transition point T; 8) small region of rarefaction; 9) boundary layer; 10) back flow; 11) region of large losses in the normal shock wave; 12) small losses in the diagonal shock waves; 13) losses due to separation and frictional drag.

Laminar boundary layer. In this case a λ-shaped shock arises at the profile in the region of the shock wave (cf. Fig. 6.4.1). Near the profile surface in the subsonic part of the boundary layer the pressure changes continuously from pressure p_1 before and pressure p_2 after the shock. In the supersonic zone a pressure shock occurs, from p_1 to p_2. This leads to the pressure at the wall in the shock zone not being equal to the pressure at a point at a small normal distance y from the wall, i.e., $\frac{\partial p}{\partial y} \neq 0$.

On the other hand, since the shock propagates only in the supersonic part of the boundary layer and the pressure gradient in the

shock becomes theoretically infinite, $\partial p/\partial x$ will differ from zero in the shock zone of the boundary layer.

Thus, in the shock zone of a boundary layer

$$\frac{\partial p}{\partial x} \neq 0, \quad \frac{\partial p}{\partial y} \neq 0.$$

The presence of a noticeable longitudinal gradient $\partial p/\partial x$ in the laminar boundary layer causes it to become thicker and even to separate. The thickening of the boundary layer before the direct shock wave gives rise to a secondary diagonal shock wave or several weaker diagonal shock waves which, above the boundary layer, join the strong normal shock wave. The whole of this wave system is called a λ-shaped shock wave.

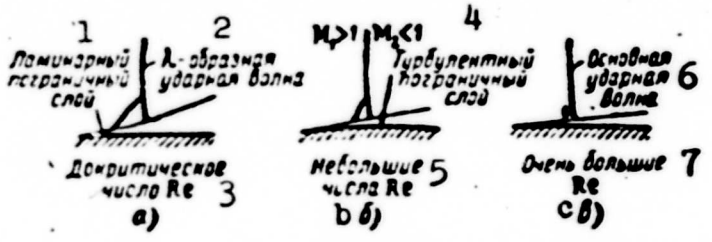


Fig. 6.4.2. Development of a λ-shaped shock with M = const and increasing Re number. 1) Laminar boundary layer; 2) λ-shaped shock wave; 3) subcritical Re number; 4) turbulent boundary layer; 5) small Re numbers; 6) main shock wave; 7) Re very large.

The turbulent boundary layer. This layer has a greater store of kinetic energy than the laminar one. It is less sensitive to pressure changes an therefore in a strongly turbulent boundary layer the system of diagonal λ shocks is replaced by a single shock wave (Fig. 6.4.2,c).

From the point of view of total pressure loss in shocks, the λ-shaped system is preferrable to the normal shock. The λ-shaped shock is, however, usually accompanied by separation, which, finally, is very undiserable. A particularly promising method of rendering separation after the λ-shock impossible is that of sucking off the boundary

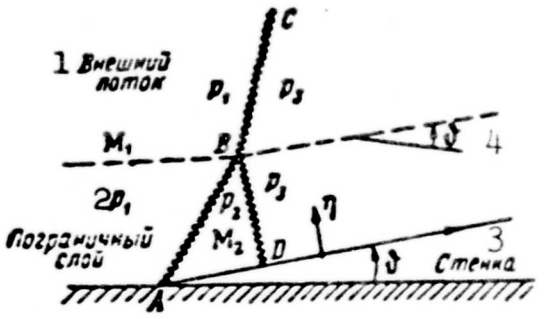


Fig. 6.4.3. Diagram of λ-shaped shock in the region of separation of a turbulent boundary layer. 1) External stream; 2) boundary layer; 3) wall.

layer.

Conditions of separation. A schematization of the flow as given in Fig. 6.4.3 makes it possible to analyze [6.10] the conditions of separation of a turbulent boundary layer in a supersonic flow. At the separation pressure let a shock wave AB be formed in the boundary layer and let the flow leave the wall at the angle ϑ. The centrifugal forces then appearing must be counterbalanced by the pressure, whose gradient transverse to the flow is equal to $\partial p/\partial n$. We shall assume that the outer flow changes its direction together with the boundary layer surface by the same angle ϑ; to this deflection correspond the shock wave BC and a pressure shock $p_3 - p_1$. In the boundary layer a shock wave BD corresponds to the pressure shock $p_3 - p_2$.

The experiment shows that in the separation zone the Mach numbers M are linked by the relation

$$M_2^2 = AM_1^2, \tag{6.4.1}$$

where A is a constant.

Let us put

$$M_1^2 \sin^2 \mu = 1 + \varepsilon;$$

it then follows from (5.9.12) that

$$\frac{p_2}{p_1} = \frac{2k}{k+1} M_1^2 \sin^2 \mu - \frac{k-1}{k+1} = \frac{2k}{k+1} \varepsilon + 1. \tag{6.4.2}$$

Since large pressure gradients cannot arise in the boundary layer, the quantity ε must be small. Determining the ratio a_1^2/a_1^2 from the energy equation $a_1^2 + \frac{k-1}{2} w_1^2 = a_2 + \frac{k-1}{2} w_2^2$ using (5.9.12) and (5.9.15), and neglecting small terms of higher than first order, we find

$$\frac{a_2^2}{a_1^2}=\frac{1+\frac{k-1}{2}M_1^2}{1+\frac{k-1}{2}M_2^2}=\frac{T_2}{T_1}=\frac{p_2}{p_1}\frac{\rho_1}{\rho_2}=$$

$$=\frac{2k}{k+1}\left(M_1^2\sin^2\mu-\frac{k-1}{2k}\right)\frac{2}{k+1}\left(\frac{k-1}{2}+\frac{1}{M_1^2\sin^2\mu}\right)=$$

$$=\frac{4k}{(k+1)^2}\left(\varepsilon+\frac{k+1}{2k}\right)\left(\frac{k+1}{2}-\varepsilon\right)\approx 2\frac{k-1}{k+1}\varepsilon+1.$$

This gives us

$$\varepsilon=\frac{k+1}{2(k-1)}\left(\frac{a_2^2}{a_1^2}-1\right)=\frac{k+1}{2(k-1)}\left(\frac{1+\frac{k-1}{2}M_1^2}{1+\frac{k-1}{2}M_2^2}-1\right)=$$

$$=\frac{k+1}{4}\frac{M_1^2-M_2^2}{1+\frac{k-1}{2}M_2^2} \qquad (6.4.3)$$

and instead of (6.4.2) we obtain

$$\frac{p_2}{p_1}=1+\frac{kM_1^2}{2}\frac{1-A}{1+\frac{k-1}{2}AM_1^2}. \qquad (6.4.4)$$

Figure 6.4.4 shows the experimental values of the ratio p_2/p_1 as a function of M_1; better agreement is obtained with Formula (6.4.4) if we take A = 0.65*.

If we assume that the deflection of the boundary layer in the separation zone takes place continuously and lay the ξ-axis along the flow and the η-axis along the normal, we obtain from the equilibrium condition

$$-\frac{\partial p}{\partial \eta}=\rho w^2\frac{d\theta}{d\xi} \qquad (6.4.5)$$

and, consequently,

$$p-p_2=\frac{d\theta}{d\xi}\int_0^\delta \rho w^2\,d\eta. \qquad (6.4.6)$$

Using A.A. Dorodnitsyn's transformation (cf. p. 421) and some considerations on the velocity distribution in the boundary layer we can obtain [6.10].

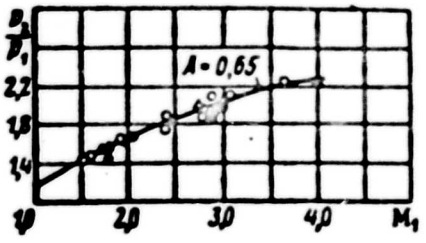


Fig. 6.4.4. The pressure p_2 behind the diagonal shock of a λ-shaped shock in the separation zone of a turbulent boundary layer (k = 1.4).

$$\frac{p_3}{p_1}=\frac{p_2}{p_1}\left(1+0{,}328\frac{kAM_1^2\theta}{1+\frac{k-1}{2}AM_1^2}\right); \quad (6.4.7)$$

$$\theta=\frac{\sqrt{M_1^2-1}}{kM_1^2}\left(\quad -1\right). \quad (6.4.8)$$

If we write

$$G=-0{,}328\frac{A\sqrt{M_1^2-1}}{1+\frac{k-1}{2}AM_1^2},$$

$$\text{then } \frac{p_3}{p_1}=\frac{p_2}{p_1}\frac{1+G}{1+\frac{p_2}{p_1}G}\approx\frac{p_2}{p_1}\left[1+G\left(1-\frac{p_2}{p_1}\right)\right]. \quad (6.4.9)$$

The values of the experimental points and the curve representing Eq. (6.4.9) are shown in Fig, 6.4.5.

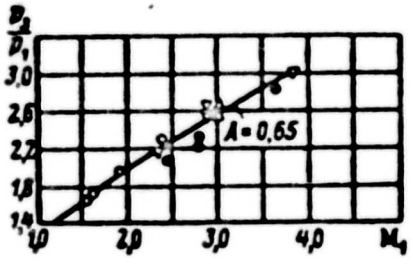


Fig. 6.4.5. The pressure p_3 behind the normal shock of a λ-shaped shock (total pressure shock) in the separation zone of a turbulent boundary layer (k = 1.4).

These relations can be applied to determining the separation and the appearance of shock waves in a nozzle.

6.5. AERODYNAMIC HEATING

Aerodynamic (kinetic) heating. A body in a gas flow streaming with high supersonic velocity is heated. Owing to the friction in the boundary layer and the compression in the stagnation zones at the leading edge kinetic energy is converted to heat. Since air at this temperature is adjacent to the body surface (Fig. 6.5.1), the heat goes over from the boundary layer to the body, the rate of this transition increasing with the velocity.

The temperature difference between the body surface and the free stream depends on the flow conditions.

If we suppose that at the forward stagnation point pure adiabatic compression occurs, then for this point we have

$$T_0=T_\infty+\frac{w_\infty^2}{2c_p}=T_\infty\left(1+\frac{k-1}{2}M_\infty^2\right) \quad (6.5.1)$$

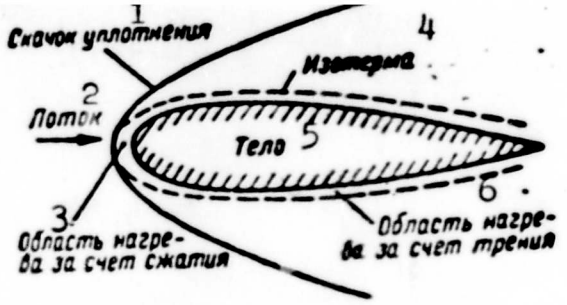


Fig. 6.5.1. Region of heating at supersonic flying speed. 1) Compression shock; 2) flow; 3) zone of heating due to compression; 4) isotherm; 5) body; 6) zone of heating due to friction.

(Figure 6.5.2). Experiment shows that near a body in the flow is not only a velocity induced (viscous) boundary layer but also a temperature-induced boundary layer, in which the temperature varies rapidly from its value at the boundary of the body to the value in the outer stream. From the theoretical point of view the temperature boundary layer (like the velocity-induced, dynamical boundary layer) has an infinitely large thickness. In practice, however, the temperature does not vary any more even at a short distance from the wall; this distance may be conventionally adopted as the thickness δ_T of the temperature layer.

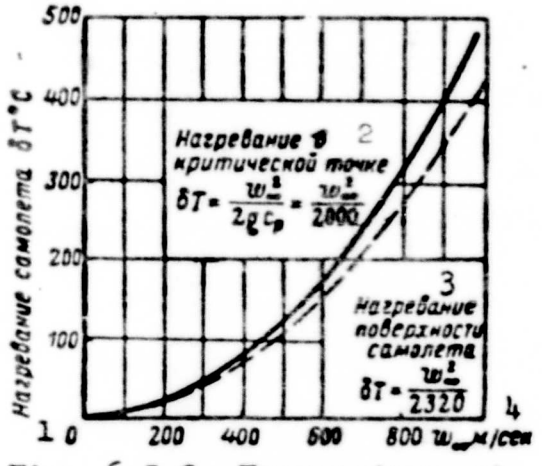


Fig. 6.5.2. Temperature at the stagnation point of the wing of an aircraft as a function of the speed. 1) Heating of the aircraft; 2) heating at the stagnation point; 3) heating of aircraft surface; 4) m/sec.

Equation (6.5.1) can be looked upon as a first approximation. The heat liberated in the viscous boundary layer must be added to the drag-induced heat and the heat removed due to thermal conductivity through the thin thermal boundary layer must be subtracted. The Prandtl number (cf. p.), $Pr = \mu c_p/\lambda$ is a measure of the relative magnitude of these two oppositely directed effects.

In strongly rarefied gases or at very high cosmic velocities, however, radiant heat plays the main part. If these influences are ignored, then at M = 3 the temperature in the boundary layer will be about 600°K.

Similarity criteria. The presence of heat exchange makes it necessary to consider in greater detail the similarity criteria established above (2.5.2).

The presence of temperature fields in the gas at high strengths of the volume forces $\underline{f}$, for example in the rotating cavities of turbines, may lead to an increase in magnitude of the buoyancy forces arising due to changes in volume.

If we denote the coefficient of thermal expansion by β and the particle temperature increment due to heating by ΔT, then the buoyancy force per unit mass, due to the change in volume, will be $f\beta\Delta T$. This quantity represents the strength of the buoyancy force. The similarity criterion, when allowance is made for buoyancy [second equation of the system (2.5.1)] therefore assumes the form $lf\beta\Delta T/w^2$. This similarity criterion is usually given as the product

$$\frac{f\beta\Delta T l^3}{\nu^2}\frac{\nu^2}{l^2w^2}=Gr\frac{1}{Re^2}. \qquad (6.5.2)$$

The dimensionless number

$$Gr=\frac{f\beta\Delta Tl^3}{\nu^2} \qquad (6.5.3)$$

is called the Grashof number.

Unfortunately there are no papers dealing with the analysis of the influence of buoyancy on the flow in the turbine section through which steam passes, though it is possible that at $Gr \sim Re^2$ this force should be taken into account*. In connection with the flow about airplanes under usual conditions the buoyancy effect is meaningless.

Heat transfer, i.e., the process of the propagation of heat through a space may, as is well known, be achieved in three ways: thermal conduction, convection and thermal radiation. The thermal conductivity is connected with the molecular transfer of heat and is similar to other transfer processes such as diffusion (transfer of mat-

ter), viscosity (transfer of momentum) and electrical conduction (transfer of electrons). According to Fourier's law

$$\vec{q} = -\lambda \vec{\nabla} T. \qquad (6.5.4)$$

i.e., the heat flux (amount of heat passing per unit time through a unit area of an isothermal surface) is proportional to the temperature gradient. The coefficient of thermal conductivity, λ, characterizing the ability of the material to conduct heat, is a physical constant of the material.

In nonsolid bodies such as liquids and gases, the heat is transferred via individual finite volumes (moles) of the medium. The radiant heat transfer connected with the conversion of heat into energy of electromagnetic oscillations occurs independently of the presence of an intermediary substantial medium. It is accepted that the heat exchanges due to thermal conduction and convection are united by the single conception by contact heat.

Usually, especially at the interface with the surrounding medium, all the three modes of heat exchange coexist. In order to estimate the total heat exchange at the body surface quantitatively we make use of Newton's relation

$$q = \alpha(T_s - T_\infty) = \alpha \Delta T. \qquad (6.5.5)$$

where $\Delta T = T_s - T_\infty$ is the temperature difference between the wall (T_s) and the fluid (T_∞); α in kgm/sec-m^2 is the coefficient of heat transfer (heat exchange) determined either for each individual point or for the whole surface as a certain mean value.

The heat transfer coefficient α affects all the conditions of interaction of the body with the surrounding medium – the temperature of body and medium, the velocity and nature of the medium's motion, the size and shape of the body, the state of the surface, etc. For example, liquid drops are virtually opaque for infrared (thermal) ra-

diation, which, therefore, does not influence heat exchange involving liquid drops. On the other hand, in strongly rarefied media (upper atmospheric layers, interplanetary space) heat is virtually exchanged by radiation alone.

The fundamental difficulties are connected with the proper choice of the temperature T_∞ of the medium. If the body is located in a virtually unbounded space, T_∞ has to be taken the temperature at a sufficiently large distance from the body. In other more complex cases T_∞ represents some means temperature of the surrounding medium.

Let us consider the heat exchange conditions at the interface of a body to a liquid (or gas); heat is transferred here owing to the thermal conductivity alone. According to Eq. (6.5.4), when heat is transferred from the fluid to the wall, the heat flux is equal to

$$\vec{q}\cdot(-\vec{n}) = q = \vec{n}\cdot\lambda\vec{\nabla}T = \lambda\frac{\partial T}{\partial n}\Big|_{n\to 0};$$

on the other hand (according to (6.5.5)), $q = \alpha\,(T_\infty - T_s)$. Combining (6.5.4) and (6.5.5) makes it possible to introduce a dimensionless heat transfer coefficient, the Nusselt number

$$\mathrm{Nu} = \frac{\alpha l}{\lambda}. \qquad (6.5.6)$$

which is sometimes incorrectly designated as a similarity criterion. The heat flux (6.5.5) may here be expressed by the relation $q = \mathrm{Nu}\frac{\lambda}{l}\delta T$. In the American and British literature the Stanton number is widely used; it is defined as

$$\mathrm{St} = \frac{\mathrm{Nu}}{\mathrm{Re\,Pr}} = \frac{\alpha l}{\lambda}\frac{\mu}{\rho w l}\frac{\lambda}{c_p\mu} = \frac{\alpha}{\rho w c_p}. \qquad (6.5.7)$$

Remembering the discussions in (2.5), we can say that the velocity (w/w_∞) and temperature (T/T_∞) fields and also the Nusselt number (Nu) are functions of the position (x/l, y/l, z/l) and of the similarity criteria $\mathrm{Re} = \frac{wl}{\nu}$, $\mathrm{Pr} = \frac{c_p\mu}{\lambda}$, $\mathrm{M} = \frac{w}{a}$ and $\mathrm{Gr} = \frac{\beta g \delta T l^3}{\nu^2}$. . Among these the numbers Re, Pr and M are of fundamental significance. The influence of the

temperature difference δT between body and gas is taken into account by comparing it with the adiabatic temperature increment $\delta T_{ad} = T_0 - T_\infty = \frac{v_\infty^2}{2c_p}$ in the form of the dimensionless ratio

$$\frac{\delta T_{ad}}{\delta T} = \frac{v_\infty^2}{2c_p \delta T}. \qquad (6.5.8)$$

from which it follows that the production of heat by friction and compression influences the temperature field essentially only at large speeds, when the temperature of aidabatic compression is comparable with the temperature difference δT between the body and gas. e.g., on the flight of rockets to great altitudes. If this is of the order of absolute temperature of the body, then the dimensionless temperature can be simply expressed in terms of the Mach number M, namely

$$\frac{v_\infty^2}{2c_p \delta T} \approx \frac{v_\infty^2}{2c_p T_\infty} = \frac{k-1}{2} M_\infty^2. \qquad (6.5.9)$$

Thickness of the thermal boundary layer. Let us consider the term of the dimensionless energy Eq. (2.5.1) that takes the heat transfer into account, $\frac{k}{\mathrm{Pr\,Re}} \vec{\nabla} \cdot \vec{q}$. . For plane motion, considering $\vec{\nabla} \cdot \vec{q}$, we obtain

$$\frac{k}{\mathrm{Pr\,Re}} \left(\frac{\partial^2 T_1}{\partial x_1^2} + \frac{\partial^2 T_1}{\partial y_1^2} \right).$$

where the subscript "1" denotes the dimensionless quantities, and where $x = x_1 l$, $y = y_1 l$.

In the expression the order of magnitude of the first term in the parentheses will be T/l^2 and that of the second term T/δ_t^2, where δ_t denotes the thickness of the thermal boundary layer, i.e., the distance from the wall at which a sharp temperature change occurs (Fig. 6.5.3). Neglecting therefore the term $\partial^2 T_1 / \partial x_1^2$ as compared with the term $\partial^2 T_1 / \partial y_1^2$, we find that if the heat transfer due to conduction is of the same order of magnitude as the convective heat transfer, we have $\frac{1}{\mathrm{Pr\,Re}} \frac{l^2}{\delta_t^2} \approx 1$ or $\delta_t^2 / l^2 \approx 1/\mathrm{Pr\,Re}$. Noticing that δ_d is the thickness of the dynamic (velocity-induced) boundary layer, $\delta_d \approx \frac{l}{\sqrt{\mathrm{Re}}}$ we have

$$\frac{\delta_t}{\delta_d} \approx \frac{1}{\sqrt{Pr}}. \qquad (6.5.10)$$

For gases Pr ≈ 1 and $\delta_t \approx \delta_d$, i.e., the thicknesses of the thermal and the dynamic boundary layers are quantities with equal orders of magnitude.

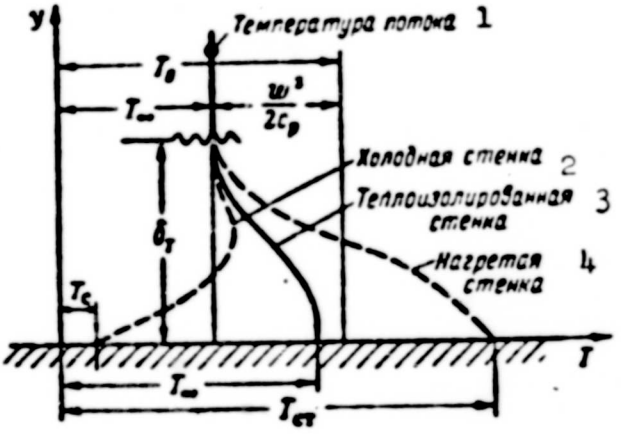


Fig. 6.5.3. Curve of temperature distribution near a wall. 1) Temperature of the flow; 2) cold wall; 3) heat insulated wall; 4) hot wall.

Analogy between friction and heat exchange. The similar structure of the formulas applying to local friction and to heat transfer during approach to the wall indicates the similarity of the mechanisms of the processes connected with these effects:

$$q = -\lambda \frac{\partial T}{\partial y}\Big|_{y=0}, \quad \tau_0 = \mu \frac{\partial w}{\partial y}\Big|_{y=0}. \qquad (6.5.11)$$

Integrating these two expressions gives us the amount of heat passing through the surface enclosed by the flow, and the frictional drag:

$$Q = b\int_0^l q(x)\,dx = A\frac{T_c - T_\infty}{\delta_T}; \quad R_f = b\int_0^l \tau_0(x)\,dx = B\frac{w_\infty}{\delta_d}.$$

where A and B are numerical factors.

For gases the Prandtl number Pr is near to unity and the thickness of the thermal δ_t and dynamic δ_d boundary layers are equal by virtue of (6.5.10), $\delta_t \approx \delta_d$. Therefore

$$q=-\lambda\frac{dT}{dy}\Big|_{y=0}\approx-\lambda\frac{T_\infty-T_c}{\delta_T}\approx\lambda\frac{T_c-T_\infty}{\delta_\Delta}\approx\frac{\lambda}{\mu}\frac{T_c-T_\infty}{w_\infty}\tau_0.$$

and, since

$$\alpha=\frac{q}{T_c-T_\infty}.$$

$$\mathrm{Nu}_x=\frac{\alpha x}{\lambda}=\frac{\tau_0 x}{\mu w_\infty}=\mathrm{Re}_x\frac{\tau_0}{\rho w_\infty^2}.$$

Introducing the local drag coefficient C_{fm} for a plate (6.1.8) in a laminar flow, we obtain

$$\mathrm{Nu}_x=\mathrm{Re}_x\frac{C_{fm}}{2}.\quad \mathrm{St}_x=\frac{\mathrm{Nu}_x}{\mathrm{Pr}\,\mathrm{Re}_x}=\frac{1}{\mathrm{Pr}}\frac{C_{fm}}{2}. \tag{6.5.12}$$

Like the solution (6.1.7), this solution applies to flow sections ($x > 0$) sufficiently distant from the leading edge (cf. p. 386).

The turbulent boundary layer. A similar relation exists for a turbulent flow, where the viscous sublayer immediately adherent to the wall plays the leading part. In this case (6.5.12) is replaced by

$$\mathrm{St}=\frac{1}{s}\frac{C_f}{2}. \tag{6.5.13}$$

where the number s is determined by the equation [6.13].

$$s=\mathrm{Pr}_T\left[1+5\sqrt{\frac{C_f}{2}}\left\{\frac{1}{5\kappa}(1-\mathrm{Pr}_T)\left[\frac{\pi^2}{6}+\frac{3}{2}(1-\mathrm{Pr}_T)+\right.\right.\right.$$
$$\left.\left.\left.+\left(\frac{\mathrm{Pr}_\Delta}{\mathrm{Pr}_T}-1\right)+\ln\left[1+\frac{5}{6}\left(\frac{\mathrm{Pr}_\Delta}{\mathrm{Pr}_T}-1\right)\right]\right\}\right]$$

and κ is a universal constant in the theory of mixing length (cf. p. 254); $\mathrm{Pr}_\Delta=\frac{\mu c_p}{\lambda}$; $\mathrm{Pr}_T=\frac{\mu_{турб}c_p}{\lambda_{турб}}$ are the Prandtl numbers for laminar and turbulent flows, respectively. If $\mathrm{Pr}_l=\mathrm{Pr}_t=1$ then $s=1$ and (6.5.13) goes over to (6.5.12).

Without pausing to dwell on detail which can be found in special literature [6.13], it must be pointed out that the coefficient of local friction decreases considerably as the Mach number M increases. Fig. 6.5.4 gives the dependence of the ratio of the coefficient of local friction in a compressible flow to the coefficient of local friction in an incompressible flow on the Mach number M, as calculated using the theories of Prandtl and Karman, for two values of the Re number. The experimental points are plotted too; it can be seen that

they lie between the points obtained from the calculations based on these theories.

Plane plate. If Pr = 1, the lines T = const and the lines w_x = = const coincide regardless of the form of the dependences $\mu(T)$ and $\lambda(T)$.

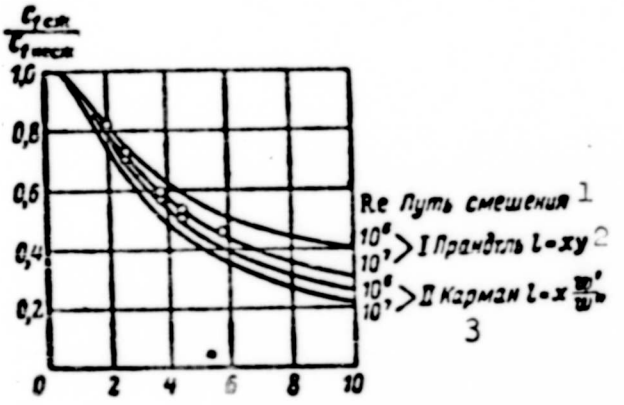


Fig. 6.5.4. Comparison of the local surface friction coefficients obtained theoretically and experimentally for a turbulent boundary layer on plates with Re = $10^6/10^7$. Calculation was carried out using Prandtl's theory of the mixture length, $\underline{l} = xy$, and Karman's theory, $\underline{l} = xw'/w$. 1) Mixture length; 2) Prandtl; 3) Karman.

Let us in fact take the energy equation in the second form (6.3.46) and write the system of equations for dp/dx = 0:

$$\left.\begin{aligned} \frac{\partial(\rho w_x)}{\partial x}+\frac{\partial(\rho w_y)}{\partial y}=0, \quad (*)\\ \rho\left(w_x\frac{\partial w_x}{\partial x}+w_y\frac{\partial w_x}{\partial y}\right)=\frac{\partial}{\partial y}\left(\mu\frac{\partial w_x}{\partial y}\right), \quad (**)\\ \rho\left(w_x\frac{\partial T}{\partial x}+w_y\frac{\partial T}{\partial y}\right)=\frac{\mu}{c_p}\left(\frac{\partial w_x}{\partial y}\right)^2+\frac{1}{\mathrm{Pr}}\frac{\partial}{\partial y}\left(\mu\frac{\partial T}{\partial y}\right). \quad (***)\end{aligned}\right\} \qquad (6.5.14)$$

Let us assume $T = T(w_x)$. Then the third equation of the system will be

$$\rho\left(w_x\frac{\partial w_x}{\partial x}+w_y\frac{\partial w_x}{\partial y}\right)\frac{dT}{dw_x}=\frac{\mu}{c_p}\left(\frac{\partial w_x}{\partial y}\right)^2+\frac{1}{\mathrm{Pr}}\frac{\partial}{\partial y}\left(\mu\frac{\partial w_x}{\partial y}\frac{dT}{dw_x}\right);$$

when we carry out the integration in the last term, allowing for Eq. (**) of the system, we obtain

$$\left(1-\frac{1}{\mathrm{Pr}}\right)\frac{dT}{dw_x}\frac{\partial}{\partial y}\left(\mu\frac{\partial w_x}{\partial y}\right)=\frac{1}{c_p}\left(\frac{\partial w_x}{\partial y}\right)^2+\left(\mu+\lambda\frac{d^2T}{dw_x^2}\right).$$

We see from this that the supposition that $T = T(w_x)$, i.e.,

that the lines T = const and w_x = const coincide, can be a solution to System (6.5.14) if at the same time

$$\Pr = 1, \quad \frac{dT}{dw_x} = -\frac{\mu}{\lambda} = -\frac{1}{c_p}. \tag{6.5.15}$$

Integrating the second Eq. (6.5.15) we obtain

$$T(w_x) = -\frac{w_x^2}{2c_p} + C_1 w_x + C_2. \tag{6.5.16}$$

The constants C_1 and C_2 must be determined from the boundary conditions.

Let us consider the conditions of heat transfer when the boundary conditions have the form: T = T_s at w_x = 0; T = T_∞ at $w_x = w_\infty$. (6.5.17)

This gives

$$\frac{T - T_c}{T_\infty} = \left(1 - \frac{T_c}{T_\infty}\right)\frac{w_x}{w_\infty} + \frac{w_\infty^2}{2c_p T_\infty}\frac{w_x}{w_\infty}\left(1 - \frac{w_x}{w_\infty}\right) =$$

$$= \left(1 - \frac{T_c}{T_\infty}\right)\frac{w_x}{w_\infty} + \frac{k-1}{2} M^2 \frac{w_x}{w_\infty}\left(1 - \frac{w_x}{w_\infty}\right). \tag{6.5.18}$$

The problem of the direction of the heat flux is solved by the sign of $\left.\frac{dT}{dw_x}\right|_{w_x \to 0}$ (since $\left.\frac{\partial w_x}{\partial y}\right|_{y \to 0} > 0$).

Differentiating (6.5.18) we obtain for y → 0 (which corresponds to $w_x \to 0$)

$$\frac{w_\infty}{T_\infty}\left.\frac{dT}{dw_x}\right|_{y \to 0} = 1 - \frac{T_c}{T_\infty} + \frac{w_\infty^2}{2c_p T_\infty}. \tag{6.5.19}$$

If $\left.\frac{dT}{dw_x}\right|_{y \to 0} > 0$, then the heat is transferred from the gas to the wall.

It can therefore happen that in a gas flow whose temperature T_∞ is lower than the wall temperature T_s ($T_\infty - T_s < 0$) the heat flux will be directed from the gas to the wall – this will occur if $T_c - T_\infty < \frac{k-1}{2} M^2$.

In the general case of $P_r \neq 1$ the direction of the heat transfer from the wall to the gas or from the gas to the wall is determined by the inequality $T_c - T_\infty \gtrless \sqrt{\Pr}\frac{w_\infty^2}{2c_p}$.

The > sign refers to heat transfer from the wall to the gas and the < sign to transfer from the gas to the wall.

The case of no heat exchange, $\left.\frac{dT}{dy}\right|_{y=0}=0$ and therefore $dT/dw_x = 0$ at $w_x = 0$ and $T = T_\infty$ at $w_x = w_\infty$ leads to the solution

$$T=T_\infty+\frac{w_\infty^2}{2c_p}\left(1-\frac{w_x^2}{w_\infty^2}\right).$$

The wall temperature T_w, corresponding to $w_x = 0$, is called the proper wall temperature. In the general case of $Pr \neq 1$:

$$T_w-T_\infty=\sqrt{Pr}\frac{w_\infty^2}{2c_p}.$$

The recovery coefficient. The calculations show that it is convenient to define the proper wall temperature by the expression

$$T_w=T_\infty+\sigma\frac{w_\infty^2}{2c_p},\quad \frac{T_w}{T_\infty}=1+\sigma\frac{k-1}{2}M^2. \qquad (6.5.22)$$

Here σ denotes the so-called recovery coefficient; it expresses the ratio of the difference between the proper wall temperature and the stagnation temperature of the gas to the difference between the same temperatures under the same conditions when there is no external heat exchange and purely adiabatic stagnation:

$$\sigma=\frac{T_w-T_\infty}{T_0-T_\infty}. \qquad (6.5.23)$$

Other definitions of the temperature recovery coefficient also exist [6.12], [6.13].

For a laminar boundary layer, as can be seen by comparing (6.5.20) and (6.5.22), we have $\sigma = (Pr)^{1/2}$.

Many formulas exist for a turbulent boundary layer. Good agreement with experiment is obtained with the formula [6.14].

$$\sigma=1-4{,}55(1-Pr)Re^{-\frac{1}{7}}. \qquad (6.5.24)$$

For a supersonic turbulent layer, on the average $\sigma = 0.90/0.98$.

Calculation of heat transfer. Let us write the expression for the heat flux in terms of the Stanton number, assuming that the temperature and Mach number at the boundary layer surface are T_δ and M_δ, respectively:

$$q = \mathrm{St}\left[T_i\left(1 + r\frac{k-1}{2}M_\delta^2\right) - T_w\right] = \rho w c_p. \qquad (6.5.25)$$

Figure 6.5.5 shows the composite graph of the dependence of the Stanton number St on the numbers Re and M for a plane plate. This graph can be used for calculating the heat transfer for other bodies. For example, for cones the local heat transfer coefficient is taken as being equal to the heat transfer coefficient calculated for a plate at a Re number equal to half that of the cone at the same Mach number M and with the same ratio of wall temperature to free stream temperature, but with the Re number for the cone [6.13].

However, these and all the relations presently available for other shapes (cylinder, sphere) are based on more or less plausible suppositions; they have complex forms and to state them would be to go beyond the limits of our course.

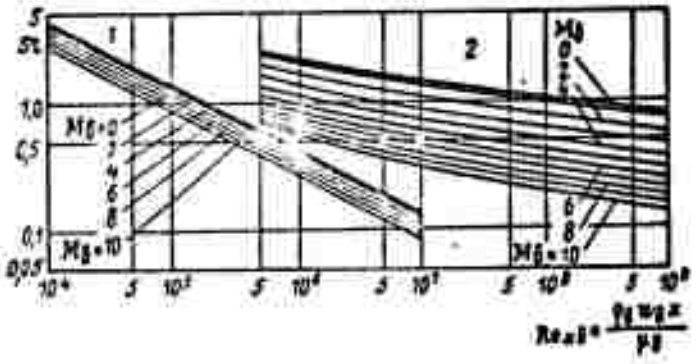


Fig. 6.5.5. Dependence of the dimensionless St number on the numbers M and Re for an isolated plane plate in free flight. 1) Laminar; 2) turbulent.

Boundary layer control. A laminar boundary layer is in the position

to "survive" only very slight pressure increases without separation occurring. In a turbulent flow the danger of separation of the boundary layer from the body in the flow is reduced since the boundary layer has a greater store of kinetic energy owing to the transfer of a certain momentum from the external flow during turbulent mixing. The separation, increasing the head drag, reduces the lift. Drag and heat transfer are much higher in turbulent flow than in laminar flow.

Boundary layer control essentially tends to avoid separation and to extend the laminar part of the boundary layer on the body. The latter is of especial importance for nearsonic and supersonic velocities; for nearsonic velocities the extension of the laminar part is accompanied by avoiding separation with simultaneous replacement of the normal shock wave by a system of diagonal λ shocks with lower total pressure losses, and for supersonic velocities by a decrease in kinetic (aerodynamic) heating of the body because the laminar boundary layer transfers less heat to the wall than the turbulent one (cf. Fig. 6.5.5).

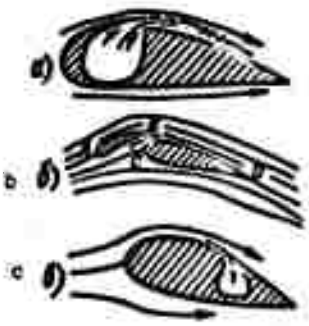


Fig. 6.5.6. Various systems for boundary layer control. a) Air jettisoning; b) flap; c) boundary layer suck-off.

Figure 6.5.6 represents three methods of boundary layer control with the help of additional devices: forcing air into the boundary layer, the high-lift wing (leading edge flap or flap), sucking off the air from the boundary layer.

In the first variant air is forced through slits into the boundary layer from high-pressure containers within the wing. The injected air raises the kinetic energy of the boundary layer and so hinders separation. In the second variant the fluid stream extracted from the gap between the leading-edge flap AB and the main wing CD withdraws the boundary layer formed on the leading edge flaps into the

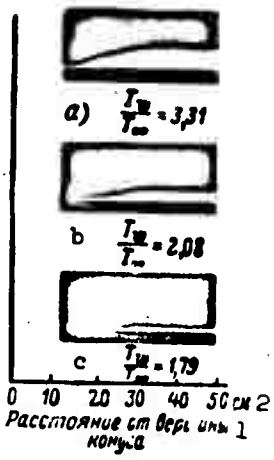


Fig. 6.5.7. Boundary layer structure in the case of cooling: a) without cooling, T_w/T_∞ = 3.31; b) cooling, T_w/T_∞ = 2.08; c) cooling, T_w/T_∞ = 1.79. 1) Distance from cone vertex; 2) cm.

the outer flow before separation can occur. Beginning at point C a new boundary layer forms which may reach the trailing edge without being separated.

Sucking off the boundary layer reduces its thickness, and a thin boundary layer has less tendency to go over to the turbulent state than a thicker one. Besides, sucking off a laminar boundary layer raises the convexity of the velocity distribution and increases its stability, or, what is the same, leads to a higher critical Re number.

Boundary layer control is particularly significant for gliding and ballistic rockets. Delaying the transition from laminar to turbulent boundary layer may lead to a reduction of the pressure gradient, for example, when a very long body which also reduces the wave drag is used.

A very effective method of boundary layer control is to cool the laminar layer at the surface, e.g., by fuel circulation. Cooling stabilizes the flow and raises the convexity of the velocity distribution. Fig. 6.5.7 shows schematic diagrams of a boundary layer drawn after photographs, which make the stabilizing effect of cooling apparent [6.13].

Manuscript Page No.

[Footnotes]

394 Starting from the boundary layer equations, V.V. Golubev obtained a general formula of integral relations yielding Karman's impulse equation and Laybenso's energy equation as particular cases.

399 L.G. Loytsyanskiy, Aerodynamics of the boundary layer, Part III, §2, GTTI, 1941.

430 In paper[6.10]in the denominator of Eq. (6.3.4) the factor A is omitted and from the conditions of coincidence with experiment the author obtains tne value A = 0.55.

433 For example, in the case of a turbine, 1 m in diameter, turning at 15,000 rpm, $f = r\omega^2 \approx 0.5 \cdot 1500^2$. For a temperature drop $\Delta T = 100°C$ (possible if the secondary air is badly mixed in the combustion chamber), a flow velocity of 300 m/sec and a profile chord of 0.1 m, we obtain

$$\frac{Gr}{Re^2} = \frac{0.5 \cdot 1500^2 \cdot 0.1^3 \cdot 100}{273 \cdot 300^2 \cdot 0.1^2} = 0.45.$$

REFERENCES

6.1. Loytsyanskiy, L.G., Mekhanika zhidkosti i gaza [Mechanics of Liquids and Gases], GTTI [State Technical and Theoretical Press], 1952.

6.2. Shvets, M.Ye., O priblizhennom reshenii nekotorykh zadach gidrodinamiki pogranichnogo sloya [Approximate Solution of Certain Problems in the Hydrodynamics of the Boundary Layer], "Prikladnaya matematika i mekhanika" [Applied Mathematics and Mechanics], No. 3, 1949.

6.3. Goshek, I., Aerodinamika bol'shikh skorostey [Aerodynamics of High Speeds], IL [Foreign Literature Press], 1954.

6.4. Fedyayevskiy, K.K., Raschet treniya poverkhnostey s mestnoy i obshchey sherokhovatostiyu [Friction Calculations for Surfaces with Local and General Roughness], Trudy TsAGI [Trans. Central

Aerohydrodynamics Institute], No. 250, 1936.

6.5. Fedyaevskiy, K.K. and Ginevskiy, A.S., Metod rascheta turbulentnogo pogranichnogo sloya pri nalichii prodol'nogo gradienta davleniya [Method for Calculation of Turbulent Boundary Layer in Presence of Longitudinal Pressure Gradient], ZhTF [Journal of Technical Physics], XXXII, 2, 1957.

6.6. Dorodnitsyn, A.A., Laminarnyy pogranichnyy sloy v szhimayemom gaze [Laminar Boundary Layer in a Compressible Gas], Sbornik teoreticheskikh rabot po aerodinamike [Collection of Theoretical Papers in Aerodynamics], Oborongiz [State Scientific and Technical Publishing House of the Defense Industry], 1957.

6.8. Shlikhting, Teoriya pogranichnogo sloya [Theory of the Boundary Layer], IL [Foreign Literature Press], 1956.

6.9. Struminskiy, V.V., Teoriya prostranstvennogo pogranichnogo sloya na skol'zyashchem kryle [Theory of the Three-Dimensional Boundary Layer on the Slipping Wing], Sbornik teoreticheskikh rabot po aerodinamike [Collection of Theoretical Papers in Aerodynamics], Oborongiz, 1957.

6.10. A. Mager, On the Model of the Free Shock Separated Turbulent Boundary Layer, "Journ. Aeron. Sci," No. 2, 1956.

6.11. Bam-Zelikovich, G.M., Raschet otryva pogranichnogo sloya [Calculating Detachment of the Boundary Layer], Izv. OTN AN SSSR [Bull. Div. Tech. Sci., Acad. Sci. USSR], No. 12, 1954.

6.12. Khilton, Kh., Aerodinamika bol'shikh skorostey [Aerodynamics of High Speeds], IL [Foreign Literature Press], 1955.

6.13. Van Drayst, Ye., Problemy aerodinamicheskogo nagreva [Problems of Aerodynamic Heating]. "Voprosy raketnoy tekhniki" [Problems of Rocket Engineering], No. 5 (41), 1957.

6.14. Shirokov, M.F., Fizicheskiye osnovy gazodinamiki [Physical Found-

ations of Gasdynamics], Fizmatgiz [State Publishing House of Physicomathematical Literature], 1958.

Chapter 7

WING OF FINITE SPAN

7.1. WING OF FINITE SPAN IN INCOMPRESSIBLE FLUID

Vortex sheet behind the wing. At the end of the formation process of the starting vortex and of the circulatory motion about a wing (this process being closely connected with the fluid's viscosity), the motion assumes a steady character.

The circulation about a wing of infinite span is determined from the Zhukovskiy-Chaplygin condition by Relation (3.5.10)

$$\Gamma = 4\pi r_0 w_\infty \sin \alpha_a \approx \pi w_\infty b \sin \alpha_a \approx \pi b w_\infty \alpha_a,$$

where α_a is the aerodynamic angle of attack, r_0 the radius of the generating circle, and $b \approx 4r_0$ the chord of the wing.

Owing to frictional losses, the coefficient π in this expression is replaced by a somewhat smaller quantity, k_∞, which is determined by experiment; thus

$$\Gamma = k_\infty w_\infty b \alpha_a. \qquad (7.1.1)$$

The lift of the element dl of an infinite wing will be

$$dR_y = \rho w_\infty \Gamma dl = k_\infty \rho w_\infty^2 b \alpha_a dl,$$

and the lift coefficient

$$C_y = \frac{R_y}{\frac{\rho w_\infty^2}{2} A_{cp}} = 2k_\infty \alpha_a = \left(\frac{dc_y}{d\alpha}\right)_\infty \alpha_a.$$

For a wing of finite span, the fluid at its ends will flow from a region of higher pressure (under the wing, if $C_y > 0$, i.e., if the aerodynamic angle of attack is positive) into a rarefaction zone (Fig. 7.1.1). Owing to this, the velocity above the wing will have a

component directed from the ends of the wing to its center, and under the wing the additional velocity components will be directed from the center of the wing to its ends; behind the wing a vortex zone of finite thickness forms, with vortices whose axes flow off in the direction of the stream.

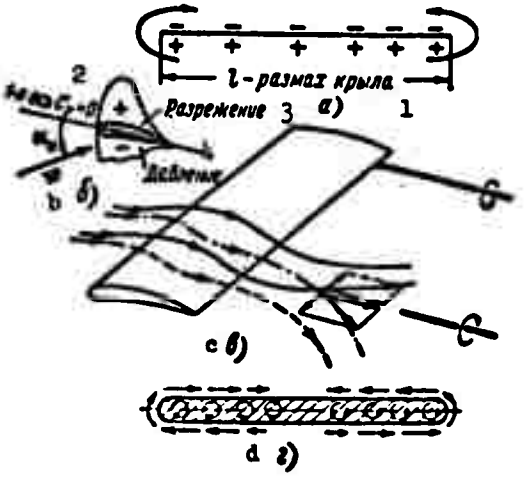


Fig. 7.1.1. Overflow of a fluid at the ends of a wing with $C_y > 0$ (a). Pressure distribution on the profile (b). Formation of vortex zone behind the wing (c). Section through the vortex zone behind the wing (d). 1) Span of wing; 2) first axis; 3) rarefaction; 4) pressure.

The vorticity of the vortex sheet is independent of its thickness; the sheet thickness may be taken as being equal to zero, and behind the wing the vortex sheet can be regarded as being equivalent to the velocity discontinuity surface.

We shall assume that the whole lift of a finite cylindrical wing is concentrated on a certain straight line (lifting line) running through the span of the wing where the vortex sheet also originates.

Connection between the circulation on the wing and the vorticity in the sheet. Let us place the coordinate origin at the midpoint of the lifting line (of the span), the x-axis being directed along the stream, and the z-axis along the lifting line (Fig. 7.1.2). Let us

consider a finite section of the layer between z = l/2 and z. If C_1 is a certain contour enveloping the separated section, then the vorticity of the vortex sheet on this section will be equal to the circulation Γ with respect to the contour C_1. If the contour is displaced along the vortex band, the wing section z can be reached without a single vortex line being intersected, and therefore the circulation in this section will be Γ (z).

Thus, the vorticity of the vortex sheet adjacent to the section between the end of the wing and a certain wing cross section is equal to the circulation in this wing section. If we consider now two neighboring sections, z and z + dz (Contours C_1 and C_2), then the vorticity of the vortex band dz will be equal to $(d\Gamma/dz)dz$, i.e., to the difference of the circulations in the sections z and z + dz. The continuous formation of a vortex sheet during the motion of a finite wing is connected with the consumption of energy in the form of work done by the drag force of the wing.

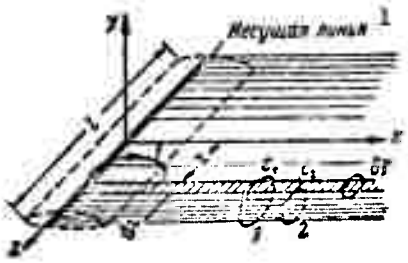


Fig. 7.1.2. The vorticity of the (free) wake vortices at an arbitrary wing section is equal to the change in circulation in this section. 1) Lifting line.

Fundamental equation for a finite wing. In order to determine the forces acting on a finite wing it is necessary to find the distribution of the additional (induced) velocities due to the presence of the vortex sheet. An exact solution of this problem requires allowance for the motion of the sheet itself and for its possible distortion, and is therefore very complex. In order to solve the problem approximately we suppose: 1) that the mean velocity circulation is small compared with the speed of the main flow; 2) that the intrinsic motion of the vortex sheet itself can be neglected, and 3) that the vortex lines

forming the band are straight and directed along the streamlines.

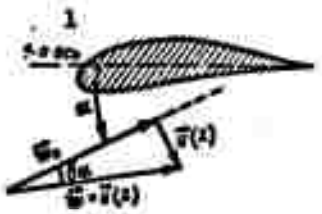


Fig. 7.1.3. Velocity on a wing profile. 1) First axis.

The theory of the finite wing is based on the hypothesis of plane cross sections: it is supposed that the wing profile in each of its cross sections is subject to the conditions associated with the plane flow at its (local) velocity at infinity.

Let us consider a wing element in the cross section z (Fig. 7.1.3). The velocity $u(z)$ induced by the vortex sheet is directed downwards (if $C_y > 0$); it reduces the angle of attack by $\delta_z = \operatorname{arctg} u(z)/w_\infty$ and raises the velocity to the value of $w_\infty/\cos\delta_z$.

When the above assumptions are made about the magnitudes of the induced velocities

$$\delta_z \approx \operatorname{tg}\delta_z = u/w_\infty; \quad \cos\delta_z \approx 1$$

and owing to (7.1.1) the angle of attack will not be α_a but $\alpha_a - \delta_z = \alpha_a - \frac{u}{w_\infty}$. We can therefore write the equation of the finite wing theory as:

$$\Gamma(z) = k_\infty(z)\, w_\infty b(z)\left[\alpha_a(z) - \frac{u(z)}{w_\infty}\right]. \qquad (7.1.2)$$

From the symmetry conditions for a vortex with the vorticity Γ, which extends along the x-axis from $-\infty$ to $+\infty$ it can be shown that the velocity induced by a semi-vortex beginning at $x = 0$ and reaching to infinity ($x = \infty$) will lie in the plane zOy and will amount to half its value, i.e., it will be equal to $\Gamma/4\pi r$. The velocity $u(z)$, induced by the vortex sheet between $x = 0$ and $x = \infty$ at the point z (Fig. 7.1.4) will therefore be

$$u(z) = \frac{1}{4\pi}\int_{-\frac{l}{2}}^{\frac{l}{2}} \frac{d\Gamma}{d\zeta}\,\frac{d\zeta}{z-\zeta}.$$

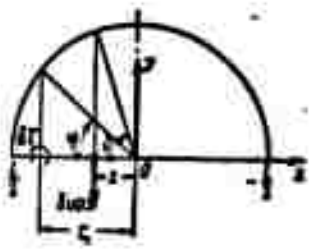


Fig. 7.1.4. Velocity induced at point z by the vortex at point ζ.

Substituting this in (7.1.2), we obtain the basic integro-differential equation of Prandtl's theory of a finite wing in the form

$$\Gamma(z)=k_{\infty}(z)\,w_{\infty}b(z)\left[\alpha_1(z)-\frac{1}{4\pi w_{\infty}}\int_{-\frac{l}{2}}^{\frac{l}{2}}\frac{d\Gamma}{d\zeta}\frac{d\zeta}{\zeta-z}\right]. \quad (7.1.3)$$

Zhukovskiy's theorem (Fig. 7.1.5) gives the forces acting on the wing as

$$\left.\begin{aligned} R_y&=\rho w_{\infty}\int_{-\frac{l}{2}}^{\frac{l}{2}}\Gamma(z)\,dz,\\ R_{x_1}&=\rho\int_{-\frac{l}{2}}^{\frac{l}{2}}\Gamma(z)\,u(z)\,dz. \end{aligned}\right\} \quad (7.1.4)$$

Solution of the basic equation of the finite wing. In order to solve the basic integro-differential equation we put

$$z=\frac{l}{2}\cos\vartheta \qquad (0<\vartheta<\pi). \quad (7.1.5)$$

Since at the ends of the wing at $\vartheta = 0$ and $\vartheta = \pi$ the pressure leveling causes the lift and also the circulation to vanish, it is convenient to represent the circulation in the form of a series of multiple sines, namely

$$\Gamma(\vartheta)=2w_{\infty}l\sum_{n=1}^{\infty}B_n\sin n\vartheta. \quad (7.1.6)$$

The vortex sheet originating at $x = 0$ and extending to infinity induces at the wing itself a velocity which can now be written in the form

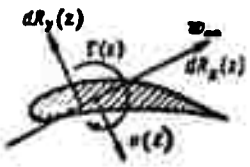


Fig. 7.1.5. The forces $dR_y(z)$ and $dR_{x1}(z)$ on the element dz of a finite wing.

$$u(\vartheta)=\frac{1}{4\pi}\int_0^{\pi}\frac{2w_{\infty}l\sum_{n=1}^{\infty}nB_n\cos n\varphi}{\frac{l}{2}\cos\varphi-\frac{l}{2}\cos\vartheta}\,d\varphi;$$

where the variable angle φ determined the position

of the vortex. However, as has been found on considering the fine wing (cf. 3.6.19),

$$K_p = \int_0^{\pi} \frac{\cos p\varphi}{\cos\varphi - \cos\vartheta}\, d\varphi = \pi \frac{\sin p\vartheta}{\sin\vartheta}.$$

We therefore have the following expression for the point determined by the angle ϑ:

$$\frac{a(\vartheta)}{w_\infty} = \frac{\sum_{n=1}^{\infty} nB_n \sin n\vartheta}{\sin\vartheta}. \qquad (7.1.7)$$

The basic integro-differential equation then assumes the following form:

$$2w_\infty l \sum_{n=1}^{\infty} B_n \sin n\vartheta = k_\infty w_\infty b \left(\alpha_0 - \frac{\sum_{n=1}^{\infty} nB_n \sin n\vartheta}{\sin\vartheta}\right).$$

If we introduce the notation $\mu = \frac{k_\infty b}{2l}$, we have

$$\sum_{n=1}^{\infty} B_n \sin n\vartheta = \mu\left(\alpha_0 - \frac{\sum_{n=1}^{\infty} nB_n \sin n\vartheta}{\sin\vartheta}\right). \qquad (7.1.8)$$

or

$$\sum_{n=1}^{\infty} B_n \sin n\vartheta\,(n\mu + \sin\vartheta) = \mu\alpha_0 \sin\vartheta. \qquad (7.1.9)$$

Many methods exist for determining the series of coefficients B_n for the circulation with the help of this equation [7.1]. For example, in the case of a symmetrical wing we may restrict ourselves to only four coefficients, and, requiring that the series of (7.1.9) broken off after the first four terms satisfies Eq. (7.1.9) exactly at the points $\vartheta = \frac{\pi}{8}, \frac{\pi}{4}, \frac{3}{8}\pi, \frac{\pi}{2}$, we obtain a set of four equations for determining the first four coefficients B_n.

The forces on the wing. In order to determine the lift R_y and the drag R_{xi} we have

$$R_y = \rho w_\infty \int_0^{\pi} 2w_\infty l \sum_{n=1}^{\infty} B_n \sin n\vartheta \frac{l}{2} \sin\vartheta\, d\vartheta = \pi B_1 l^2 \frac{\rho w_\infty^2}{2}; \qquad (7.1.10)$$

$$R_{x_1}=\rho\int_0^{\pi}2w_{\infty}l\left(\sum_{n=1}^{\infty}B_n\sin n\theta\right)\left(w_{\infty}\sum_{n=1}^{\infty}nB_n\sin n\theta\frac{1}{\sin\theta}\right)\frac{l}{2}\sin\theta\,d\theta=$$

$$=\rho w_{\infty}^2 2l\frac{l}{2}\frac{\pi}{2}\sum_{n=1}^{\infty}nB_n^2=\pi l^2\frac{\rho w_{\infty}^2}{2}\sum_{n=1}^{\infty}nB_n^2. \qquad (7.1.11)$$

The respective coefficients are

$$\left.\begin{aligned}C_y&=\pi B_1\frac{l^2}{\lambda_{kr}}=\pi B_1 A,\\ C_{x_1}&=\pi\frac{l^2}{\lambda_{kr}}\sum_{n=1}^{\infty}nB_n^2=\pi A\sum_{n=1}^{\infty}nB_n^2.\end{aligned}\right\} \qquad (7.1.12)$$

where $A=\frac{l^2}{\lambda_{kr}}$ — is the aspect ratio, l the span and A_{kr} the area of the wing.

Since all coefficients B_n enter (7.1.12) as squares and the lift is determined by the first coefficient B_1 alone, and when $C_y \neq 0$, the induced drag will be minimum if all $B_n = 0$ vanish with the exception of B_1.

In this case $\Gamma=2w_{\infty}lB_1\sin\theta$.

Or, taking into account that

$$\sin\theta=\sqrt{1-\left(\frac{2z}{l}\right)^2},$$

we have

$$\Gamma=2w_{\infty}lB_1\sqrt{1-\left(\frac{2z}{l}\right)^2};$$

at $z = 0$

$$\Gamma_0=2w_{\infty}lB_1$$

and we can also write

$$\Gamma=\Gamma_0\sqrt{1-\left(\frac{2z}{l}\right)^2}$$

or

$$\frac{\Gamma^2(z)}{\Gamma_0^2}+\frac{z^2}{(l/2)^2}=1. \qquad (7.1.13)$$

Thus, a wing will have minimum drag if its circulation with respect to the span satisfies an elliptical distribution law.

In this case the induced velocity

$$w(z)=w_0 B_1=\frac{\Gamma_0}{2l} \qquad (7.1.14)$$

is constant over the whole span of the wing: all points of the vortex sheet have the same velocity, i.e., it moves like a solid surface. In this case the induced drag coefficient (7.1.12) and the down-wash (7.1.7) will be

$$C_{x_i}=\frac{1}{\pi\lambda}C_y^2,\quad \delta_2=\frac{w}{v_\infty}=\frac{C_y}{\pi\lambda}. \qquad (7.1.15)$$

With elliptical circulation distribution there exists a simple interrelation between the slope angles of C_y with respect to α for $\Lambda = \infty$ when Λ is given.

We put

$$C_y=2k_\infty\alpha_\infty=2k\alpha_\lambda.$$

Since

$$\alpha_\lambda=\alpha_\infty+\delta_2=\alpha_\infty+\frac{C_y}{\pi\lambda},$$

then

$$2k_\infty\alpha_\infty=2k\alpha_\infty+\frac{2kC_y}{\pi\lambda},$$

whence

$$2k=\frac{2k_\infty}{1+\frac{2k_\infty}{\pi\lambda}}. \qquad (7.1.16)$$

When the circulation deviates from the elliptical distribution the induced drag increases, but only slightly. The correction to the angle of attack is more considerable. The down-wash (induced velocity) is constant along the span only in the case of an elliptical wing ($w(z)=\frac{\Gamma}{2l}$ = const). For all other circulation distributions it will be variable. The true aerodynamic angle of attack, $\alpha-\frac{w(z)}{v}$ will therefore differ for different sections.

In determining the mean rake angle $\delta\tilde{\alpha}$ we take into account that any reduction of the angle of attack by the angle $\delta\alpha$ causes a reduc-

tion in lift at the section which amounts to

$$\Delta R_y = -\frac{\rho w_\infty^2}{2} 2k \int_{-l/2}^{l/2} b(z) \alpha_e(z)\, dz.$$

For a part of the wing with the same profile and with the area A_{kr} this reduction can be estimated in the case of a plane flow by introducing a mean rake angle with the help of the relation

$$\Delta R_y = 2k \frac{\rho w_\infty^2}{2} A_{kr} \tilde{\alpha}_e,$$

whence

$$\tilde{\alpha}_e = \frac{1}{A_{kr}} \int_{-l/2}^{l/2} b \alpha_e\, dz. \qquad (7.1.17)$$

However,

$$\alpha_e = \frac{u(z)}{w_\infty} = \frac{\sum_{n=1}^{\infty} n B_n \sin n\vartheta}{\sin \vartheta}.$$

Therefore, in the case considered,

$$\tilde{\alpha}_e = \frac{b}{A_{kr}} \int_{-l/2}^{l/2} \frac{u(z)}{w_\infty} dz = \frac{1}{l} \int_0^{\pi} \frac{\sum_{n=1}^{\infty} n B_n \sin n\vartheta}{\sin \vartheta} \frac{l}{2} \sin \vartheta\, d\vartheta =$$

$$= \frac{1}{2} \int_0^{\pi} \sum_{n=1}^{\infty} n B_n \sin n\vartheta\, d\vartheta.$$

If we take now into account that

$$\int_0^{\pi} \sin n\vartheta\, d\vartheta = \frac{1}{n} \int_0^{\pi} \sin n\vartheta\, dn\vartheta = \frac{1}{n} (1 - \cos \pi n) \begin{cases} 0, & n = 2s, \\ \frac{2}{n}, & n = 2s-1, \end{cases}$$

we obtain

$$\tilde{\alpha}_e = (B_1 + B_3 + B_5 + \dots) = \sum_{s=1}^{\infty} B_{2s-1}. \qquad (7.1.18)$$

For an elliptical wing

$$\tilde{\alpha}_e = \alpha_e = B_1.$$

Thus

$$\frac{\tilde{\alpha}_e}{\alpha_0} = \frac{\sum_{n=1}^{\infty} B_{2n-1}}{B_1} = 1 + \tau,$$

whence

$$\tau = \frac{B_3 + B_5 + B_7 + \dots}{B_1}; \qquad (7.1.19)$$

τ is a coefficient that accounts for the difference between the angle of attack of the wing having any given circulation distribution and that of a wing with elliptical circulation distribution (Fig. 7.1.6).

Форма крыла в плане 1	Удлинение 2	$\frac{1+\delta}{\pi}$	$\frac{1+\tau}{\pi}$
Эллиптическое крыло 3	5-8	0,318	0,318
Трапециевидное крыло 4 $\frac{b_0}{b_r} = \frac{1}{3} : \frac{2}{3}$	5-8	0,318	0,318
Прямоугольное крыло 5	6	0,335	0,315
Крыло со скошенными назад концами 6	5-8	0,318	0,338
Крыло с закругленными концами 7	5-8	0,318	0,365
Ромбовидальное крыло 8	-	0,375	0,362

Fig. 7.1.6. Table of the coefficients of influence, $(1 + \delta)$ and $(1 + \tau)$, for various wing plans. 1) Wing plan; 2) aspect ratio; 3) elliptical wing; 4) tapered wing; 5) unswept wing; 6) wing with rearwards raked tips; 7) wing with rounded tips; 8) diamond-shaped wing.

The moments of a finite wing. The lift of the wing will in general give rise to a moment about the x-axis:

$$M_x = -\int_{-\frac{b}{2}}^{\frac{b}{2}} z\,dR_y = -\rho w_\infty \int_{-\frac{b}{2}}^{\frac{b}{2}} z\Gamma(z)\,dz =$$

$$= \rho w_\infty \int_0^\pi 2w_\infty \frac{l}{2} \sum_{n=1}^{\infty} B_n \sin n\vartheta \frac{l}{2} \cos\vartheta \frac{l}{2} \sin\vartheta\,d\vartheta =$$

$$= \frac{\rho w_\infty^2 l^3}{4} \int_0^\pi \sum_{n=1}^{\infty} B_n \sin n\vartheta \sin 2\vartheta\,d\vartheta = \frac{\pi}{8} \rho w_\infty^2 l^3 B_2. \qquad (7.1.20)$$

For a wing with a symmetrical load distribution, B_{2n} and $M_x = 0$. The induced drag of an asymmetric wing yields a moment about the y-axis; in the case of symmetrical load distribution both M_y and M_x vanish. The moment M_z can be given for each wing section in the form (theory of the fine wing)

$$c_m = c_{m_0} + \frac{1}{4} c_y.$$

It can be calculated relatively easily if it is assumed, as usual, that the lift is concentrated at a distance of 1/4 from the leading edge.

Calculation of the wing characteristics. In the foregoing we have obtained Expression (7.1.12) for the coefficient of induced drag of a wing:

$$C_{x_i} = \frac{R_{x_i}}{\frac{\rho v_\infty^2}{2} A_{wp}} = \pi \Lambda \sum_{n=1}^{\infty} n B_n^2.$$

We multiply and divide the right-hand side by B_1^2 and make use of the relation $B_1 = C_y \pi \Lambda$, and thus obtain

$$C_{x_i} = \pi \Lambda \left(\frac{C_y}{\pi \Lambda}\right)^2 \frac{\sum_{n=1}^{\infty} n B_n^2}{B_1^2}$$

or

$$C_{x_i} = \frac{C_y^2}{\pi \Lambda}(1+\sigma),$$

where

$$1+\sigma = \frac{\sum_{n=1}^{\infty} n B_n^2}{B_1^2}. \qquad (7.1.21)$$

Let the subscript "1" refer to the given wing and "2" to the wing whose characteristic is to be determined.

Supposing that the profile drag coefficient remains constant and that C_y is the same for both wings, we can write for the first wing

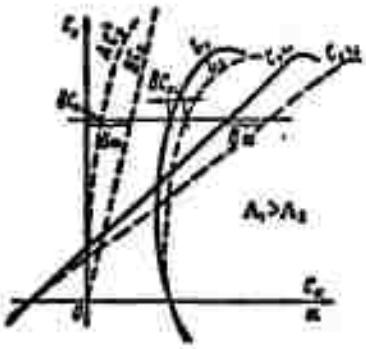


Fig. 7.1.7. Recalculation of wing characteristics for a different aspect ratio.

$$C_{x1} = C_{xp} + C_{xi1} = C_{xp} + \frac{1+\varepsilon_1}{\pi\lambda_1} C_y^2;$$

$$\alpha_1 = \alpha_\infty + \delta\alpha_1 = \alpha_\infty + \frac{1+\tau_1}{\pi\lambda_1} C_y$$

and for the second one

$$C_{x2} = C_{xp} + C_{xi2} = C_{xp} + \frac{1+\varepsilon_2}{\pi\lambda_2} C_y^2;$$

$$\alpha_2 = \alpha_\infty + \delta\alpha_2 = \alpha_\infty + \frac{1+\tau_2}{\pi\lambda_2} C_y.$$

Hence we obtain for the increment of the drag coefficient

$$\left.\begin{aligned} \delta C_{xi} &= C_{x2} - C_{x1} = \left(\frac{1+\varepsilon_2}{\pi\lambda_2} - \frac{1+\varepsilon_1}{\pi\lambda_1}\right) C_y^2 \\ \text{and for that of the angle of attack} \quad \delta\alpha &= \alpha_2 - \alpha_1 = \left(\frac{1+\tau_2}{\pi\lambda_2} - \frac{1+\tau_1}{\pi\lambda_1}\right) C_y. \end{aligned}\right\} \quad (7.1.22)$$

It should be kept in mind that the angles are given in radians.

Thus, if a polar curve of first kind (Fig. 7.1.7) is given and if for convenience C_y is plotted as a function of the angle of attack, α, on the same graph, then, drawing the parabola

$$\delta C_{xi} = \left(\frac{1+\varepsilon_2}{\pi\lambda_2} - \frac{1-\varepsilon_1}{\pi\lambda_1}\right) C_y^2 = AC_y^2$$

and the straight line $\left(\frac{1+\tau_2}{\pi\lambda_2} - \frac{1+\tau_1}{\pi\lambda_1}\right) C_y = BC_y$, we obtain the curves L and $C_y = f(\alpha)$ for the given wing by transposing the values of δC_{x1} and $\delta\alpha$ for a series of C_y values.

Finite wing in subsonic linearized gas flow. Since in a subsonic linearized gas flow

$$2k_{\infty c} = 2k_{\infty} : \sqrt{1-M_\infty^2} = 2k_\infty m$$

and

$$dR_y = \frac{\rho w_\infty^2}{2} b(z) C_y dz = \rho w_\infty \Gamma dz,$$

we obtain from the relation $C_y = 2k_\infty (\alpha + \alpha_0)$

$$\Gamma(z) = \frac{w_\infty}{2} b(z) C_y = w_\infty b(z) k(z) \left[\alpha(z) + \alpha_0(z) + \frac{1}{2\pi w_\infty} \int_{-l/2}^{l/2} \frac{d\Gamma}{dz} \frac{dz}{\zeta - z}\right].$$

The dimensionless form derived by dividing by $b_{max}w_\infty$ will be ($z^* = z/l$)

$$\Gamma^*(z) = \frac{\Gamma(z)}{b_{max}w_\infty} = k_0(z)\frac{b(z)}{b_{max}}\left[\frac{\alpha(z)}{m} + \frac{\alpha_0(z)}{m} + \frac{1}{4\pi}\frac{b_{max}}{lm}\int_{-1/2}^{1/2}\frac{d\Gamma^*}{dz^*}\frac{dz^*}{\zeta^* - z^*}\right].$$

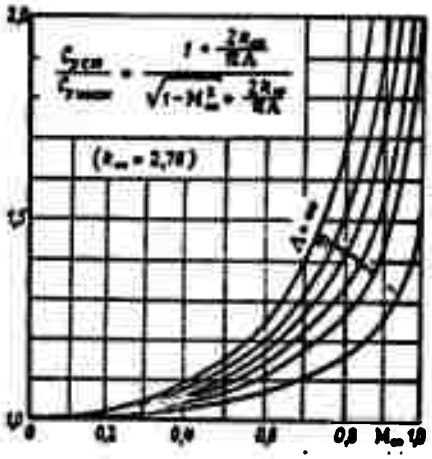


Fig. 7.1.8. Influence of aspect ratio Λ on the coefficient C_y for various numbers M_∞ in subsonic flow.

The distribution of the circulation with respect to a finite wing in a subsonic flow will thus be the same as that with respect to a certain wing in an incompressible fluid flow which differs from the given one by its angle of attack, α, and its zero-lift angle, α_0, being increased by a factor of $1:\sqrt{1-M_\infty^2}$ and by the aspect ratio being reduced by a factor of $\sqrt{1-M_\infty^2}$

Since the lift curve slope $dc_y/d\alpha$ for a wing with an aspect ratio of $\Lambda = l^2:A_{wp}$ in an incompressible fluid is determined by Relation (7.1.16)

$$\frac{dC_y}{d\alpha} = 2k = \frac{2k_0}{1+\frac{2k_0}{\pi\Lambda}},$$

thus, in a subsonic gas flow,

$$\frac{C_{y\,\alpha}}{C_{y\,\alpha\,\infty}} = \frac{1+\frac{2k_0}{\pi\Lambda}}{\sqrt{1-M_\infty^2}+\frac{2k_0}{\pi\Lambda}}. \qquad (7.1.23)$$

As $\Lambda \to \infty$ $C_{y\,\alpha}:C_{y\,\alpha\,\infty} = 1:\sqrt{1-M_\infty^2}$: as $\Lambda \to 0$, C_y becomes independent of the number M_∞.

Figure 7.1.8 shows how Λ influences C_y when α = const, for one profile and various M_∞.

7.2. METHODS OF RAISING M_{kr}

Swept wing. This is a wing whose span axis includes a certain angle χ with the lateral axis (Fig. 7.2.1). The wing axis is usually placed at one fourth of the local chords. The angle χ is called the angle of sweep.

Let the wing axis include the angle χ with the wind velocity. The components of the velocity w_∞ will then be

$$w_{\infty n} = w_\infty \cos\chi \quad \text{и} \quad w_{\infty l} = w_\infty \sin\chi.$$

Since the lift arising on a wing placed in an oblique flow is determined solely by the normal velocity component $w_{\infty n} = w_\infty \cos\chi < w_\infty$, the effective number M_∞ will be

$$M_n = M_\infty \cos\chi. \qquad (7.2.1)$$

The shock stall on a wing in an oblique can therefore arise only when $w_{\infty n}$ and not the total velocity w_∞ exceeds the critical value, i.e., when $M_{nkr} > M_{kr}$. Figure 7.2.2 shows the function $C_x = f(M_\infty)$ for wings with various sweeps and aspect ratios.

Streamlines of swept wing in subsonic flow. Figure 7.2.3 shows how the streamlines of a swept wing are curved at the rarefaction face. The undisturbed velocity component $w_\infty \sin\chi$ will be constant and the component $w_\infty \cos\chi$ will vary during the flow about the wing. Sufficiently far from the wing, at the points A and G, the flow is undisturbed. As it approaches the wing the normal component ($w_\infty \cos\chi$) of the particle velocity begins to decrease and, as can be seen from the velocity triangle, the particles are deflected to the right. At point B the trajectory is a tangent to the trailing edge contour (since there is no normal velocity component). Behind point B the pressure drops and the velocity increases as far as point D (the point of minimum pressure). At point C the pressure is zero. Behind point D the velocity decreases as far as point F. Point E is

analogous to point C.

Advantages and disadvantages of a swept wing. The main advantage of swept wings is the reduction of drag at high velocities, which is due to the instant at which shock waves arise shifting towards higher M_∞ numbers. The increment of M_{kr} of a swept wing (sweep χ) compared with an unswept wing ($\chi = 0$) is theoretically equal to

$$\delta M = \frac{M_{\text{кр}\chi=0}}{\cos\chi} - M_{\text{кр}\chi=0} = M_{\text{кр}\chi=0}\left(\frac{1}{\cos\chi} - 1\right). \qquad (7.2.2)$$

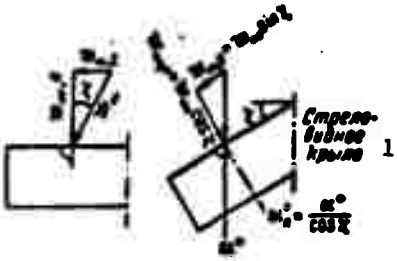


Fig. 7.2.1. A swept wing is equivalent to a wing in an oblique air stream. 1) Swept wing.

However, owing to the influence of the boundary layer and especially of the center effect (no sweep in the central part of the wing) the increment of M_{kr} will be less.

As shown by experiment [7.3] the true increment of M_{kr} can be determined from the relation

$$\delta M = M_{\text{кр}\chi=0}\left(\frac{1}{\sqrt{\cos\chi}} - 1\right). \qquad (7.2.3)$$

A disadvantage of wings with positive sweep is the premature

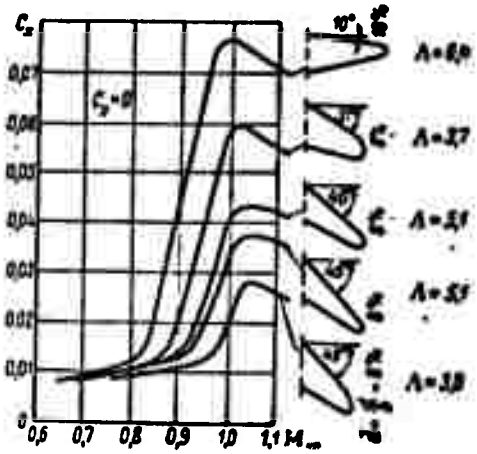


Fig. 7.2.2. Influence of sweep and aspect ratio of a wing on its drag coefficient.

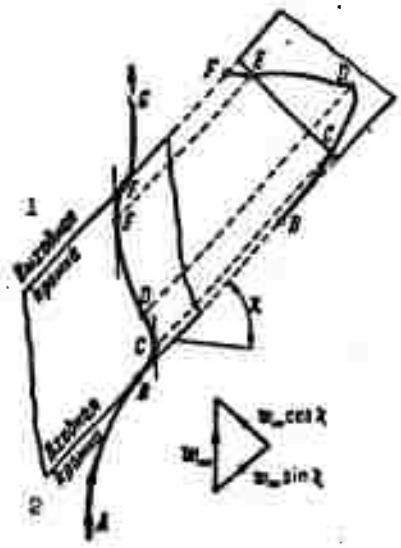


Fig. 7.2.3. Curvature of streamlines of a swep wing in a subsonic flow. 1) Trailing edge; 2) leading edge.

separation of the flow from the wing tips (this gives rise to the deterioration of controllability at low velocities in aircraft with wings of $\chi > 0$, i.e., at take off and landing). A wing with negative sweep ($\chi < 0$) does not suffer from these shortcomings.

Furthermore, as the sweep increases C_y diminishes and the effectiveness of the landing flaps and slots decreases.

Wing of small aspect ratio. A second way of raising M_{kr} is to reduce the aspect ratio of the wing, Experiment shows that near $M_\infty = 1$ the drag decreases in the shock stall region as the aspect ratio becomes smaller (Fig. 7.2.4). Airplanes for nearsonic or supersonic flight speeds therefore have a small aspect ratio which, from the standpoint of strength, is also economical.

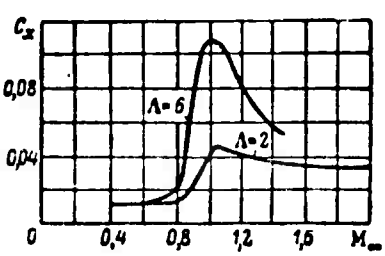


Fig. 7.2.4. Influence of aspect ratio of a wing on its drag in high-speed flows.

Also included among the small aspect ratio wings are delta wings which are plane triangular wings (Λ=1÷2).

7.3. WING OF FINITE SPAN IN SUPERSONIC FLOW [7.5]

In theory, finite wings in a subsonic flow constitute a vortex sheet consisting of elementary horseshoe vortices: an adjacent vortex and two free vortices, which together form the vortex sheet. In the solution of the linearized problem on a finite wing in a supersonic

flow, the flow pattern can be built up with the help of particular solutions of the wave equation. For an elementary flow bounded by the surface of the Mach cone each of these solutions yields the concentrated lift applied to the vertex of the cone. At a sufficiently large distance behind the wing, the flow near the axis coincides with the flow near subsonic horseshoe vortices (Fig, 7.1.3). Thus, an induced drag also exists in the case of a supersonic flow. Within the framework of the linear theory the relationship between induced drag and lift is considered to be one and the same in both cases.

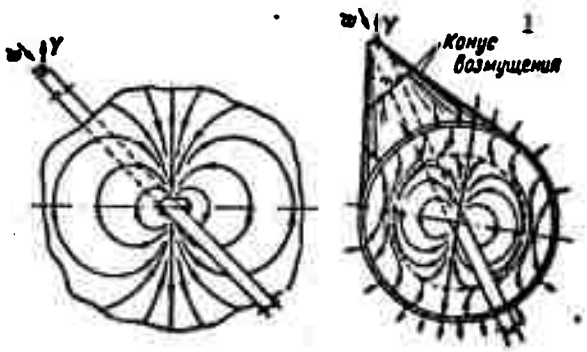


Fig. 7.3.1. Horseshoe vortex in subsonic and supersonic flows. 1) Mach cone.

Region of plane flows. Since not all disturbances leave the bounds of their Mach cone, a certain part of the finite wing, lying between the Mach cones, will be in a zone of plane flow.

Figure 7.3.2 shows these zones with several design shapes of finite wings shaded in. As can be seen, it is possible that the flow about an unswept profile is entirely plane. Calculations are made on such wings by the methods of plane flow with subsequently introduced corrections.

Supersonic and subsonic edges. We decompose the velocity of an undisturbed oblique flow about an unswept wing (Fig. 7.3.3) into the

two components along the leading edge $w_{\infty,l} = w_\infty \sin\chi$, and perpendicular to it, $w_{\infty,n} = w_\infty \cos\chi$.

Since the sonic velocity is $a_\infty = w_\infty \sin\mu$, we can divide the normal velocity component of the flow by it to obtain

$$M_{\infty,n} = \frac{w_{\infty,n}}{a_\infty} = \frac{\cos\chi}{\sin\mu}. \qquad (7.3.1)$$

This will be the number M_∞ of the corresponding plane flow.

If the angle $\mu+\chi<90°$, the corresponding flow is supersonic (cf. Fig. 7.3.3,a), and if $\mu+\chi>90°$, it is subsonic (cf. Fig. 7.3.3,b). In the first case the leading edge is called supersonic, in the second subsonic. The character of the flow about the trailing edges is determined similarly.

Plane flow for wing with positive sweep. Let us consider a wing of infinite span with χ as its angle of sweep and α as its angle of attack. Let the leading edge be placed in front of a Mach line. The normal velocity component will then be supersonic (Fig. 7.3.4).

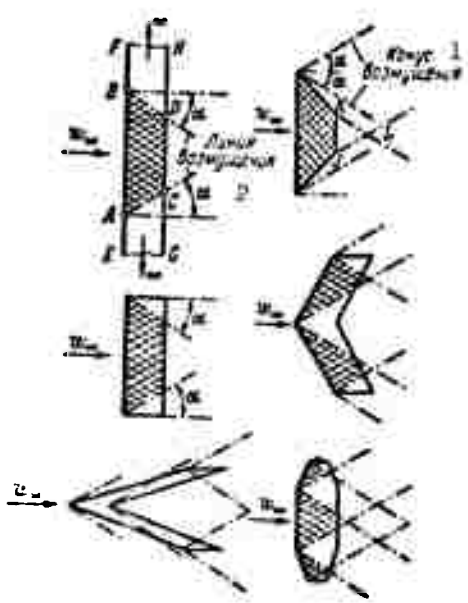


Fig. 7.3.2. Zone of plane flow for various wing plans in a supersonic flow, shaded. 1) Mach cone; 2) Mach line.

Let us decompose the velocity or the corresponding number M_∞ into three components: $M_\infty \cos\chi \cos\alpha$ in the plane of the wing normal to the leading edge, $M_\infty \sin\alpha$ normal to the plane of the wing, and $M_\infty \sin\chi \cos\alpha$ in the plane of the wing along the leading edge. Let us denote a flow in which the component along the leading edge is taken to be zero as an equivalent flow. For such a flow (subscript "e") we obtain from Fig. 7.3.5

$$M_{\infty,n} = \sqrt{(M_\infty \sin\alpha)^2 + (M_\infty \cos\alpha \cos\chi)^2} = \tag{7.3.2}$$
$$= M_\infty \sqrt{1 - \sin^2\chi \cos^2\alpha};$$
$$\alpha_n = \operatorname{arc\,tg} \frac{M_\infty \sin\alpha}{M_\infty \cos\alpha \cos\chi} = \operatorname{arc\,tg} \frac{\operatorname{tg}\alpha}{\cos\chi}; \tag{7.3.3}$$
$$\bar{d}_n = \frac{d}{b\cos\chi} = \frac{\bar{d}}{\cos\chi}. \tag{7.3.4}$$

where $\bar{d}$ is the thickness ratio.

From the relations

$$C_y \equiv \frac{R_y}{\frac{\rho_\infty a_\infty^2}{2} M_\infty^2 lb}; \quad C_{y,n} \equiv \frac{R_y}{\frac{\rho_\infty a_\infty^2}{2} M_{\infty,n}^2 (b\cos\chi)\left(\frac{l}{\cos\chi}\right)}.$$

We obtain

$$C_y = C_{y,n}\left(\frac{M_{\infty,n}}{M_\infty}\right)^2 = C_{y,n}(1 - \sin^2\chi\cos^2\alpha). \tag{7.3.5}$$

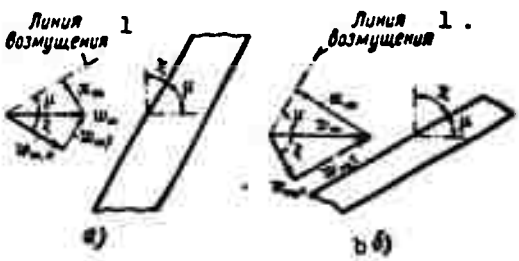


Fig. 7.3.3. Supersonic leading edge $w_{\infty,n} > a_\infty$ (a). Subsonic leading edge, $w_{\infty,n} < a_\infty$ (b). 1) Mach line.

If we assume that the tangential velocity component does not influence the drag, then the total pressure drag component in the w_∞-direction will be equal to $R_\chi \cos\chi$.

Therefore

$$C_x = C_{x,n}\cos\chi\left(\frac{M_{\infty,n}}{M_\infty}\right)^2 = C_{x,n}\cos\chi(1 - \sin^2\chi\cos^2\alpha) \tag{7.3.6}$$

or

$$C_x = C_{x,n}\cos\chi\left(\frac{M_{\infty,n}}{M_\infty}\right)^2 = C_{x,n}\cos\chi(1 - \sin^2\chi\cos^2\alpha). \tag{7.3.7}$$

For a given profile with given M_∞, χ, α and $\bar{d}$, the correspond-

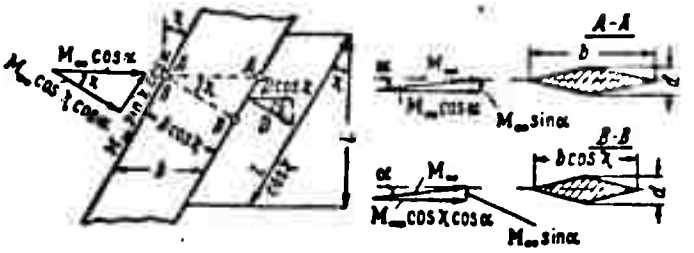


Fig. 7.3.4. For the analysis of a swept wing of infinite span.

ing values of $M_{\infty e}$, α_e and $\bar{d}_e$ can be obtained with the help of (7.3.2)-(7.3.4).

The corresponding values of the force coefficients C_{ye} C_{xe} are determined on the theory of plane flow. The values of C_y and C_x for a swept wing are determined from Formulas (7.3.5) and (7.3.7).

The total drag coefficient can be found by summing the frictional drag coefficient C_f and the pressure drag coefficient C_x,

$$C_{x\,\text{сумм}} = C_x + C_f. \tag{7.3.8}$$

Approximate formulas. For small angles of attack

$$\cos\alpha \approx 1; \quad \operatorname{tg}\alpha \approx \alpha.$$

In this case Eqs. (7.3.2), (7.3.3) can be rewritten in the form

$$\left.\begin{aligned} M_{\infty e} \approx M_\infty \cos\chi; \quad \alpha_e \approx \frac{\alpha}{\cos\chi}; \quad C_y \approx C_{y_e}\cos^2\chi; \\ C_{x\,\text{сумм}} \approx C_{x_e}\cos^2\chi + C_f \end{aligned}\right\} \tag{7.3.9}$$

Thin profile at small angle of attack. The linear theory yields for a fine profile at small angle of attack [cf. (5.6.4)-(5.6.5)]

$$C_{y_e} = \frac{4\alpha_e}{\sqrt{M_{\infty e}^2 - 1}}; \quad C_{x_e} = \frac{4}{\sqrt{M_{\infty e}^2 - 1}}(\alpha_e^2 + \beta\bar{d}_e^2).$$

where the coefficient β depends only on the profile shape. Substituting this in (7.3.9) we shall have

$$C_y = \frac{4\cos\chi}{\sqrt{M_\infty^2\cos^2\chi - 1}}\alpha; \tag{7.3.10}$$

$$C_{x\,сумм} = \frac{4\cos\chi}{\sqrt{M_\infty^2\cos^2\chi - 1}}\alpha^2 + \frac{4\cos^2\chi}{\sqrt{M_\infty^2\cos^2\chi - 1}}\beta\bar{d}_e^2 + C_f \qquad (7.3.11)$$

The first term of the right-hand side of Eq. (7.3.11) represents the drag induced by the lift. This drag component is proportional to the lift squared.

The second term represents the wave drag. When $\bar{d}_e$ is constant, the magnitude of the drag decreases as the sweep line increases, but when the leading edge contour is close to the Mach line (i.e., $M_\infty \cos\chi \to 1$), the wave drag increases.

Conical flows. These are flows in which all three velocity components are constant along the straight lines originating at one point. The simplest example represents a flow streaming about a circular cone. Generalizations of this type of flow represent more complex cases of a conical flow (Fig. 7.3.5).

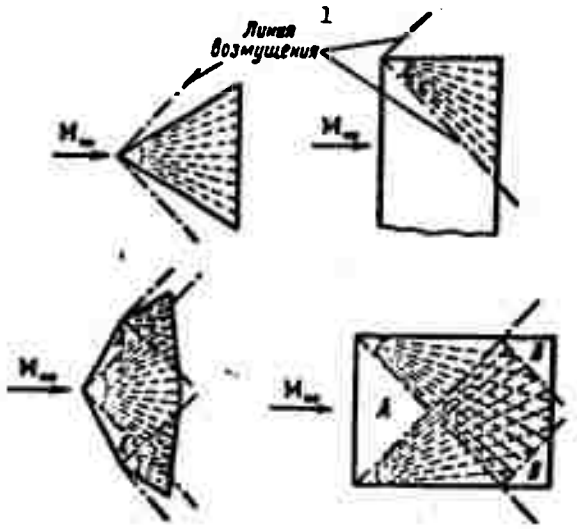


Fig. 7.3.5. The shaded areas show the conical flow for various wing plans. 1) Mach line.

Since the velocity components of a conical flow are independent of the radius, then, using the spherical coordinate system r, ϑ, φ, it can be shown that w_r, w_ϑ, w_φ will satisfy a Laplace equation.

It can be solved using the technique pertaining to the theory of functions of complex variables. This constitutes the effectiveness of applying the conical flow method in solving certain problems of flows about thin bodies.

Comparison of wings of various design shapes. The graph of Fig. 7.3.6 gives a comparison of lift characteristics for three different design shapes of wings. With $A\sqrt{M_\infty^2-1}<2.8$ the unswept wing gives the largest value of $\frac{dC_y}{d\alpha}\sqrt{M_\infty^2-1}$. If $2.8<A\sqrt{M_\infty^2-1}<5$, a delta wing with the trailing edge perpendicular to the wind is best in order to obtain the largest value of $\frac{dC_y}{d\alpha}\sqrt{M_\infty^2-1}$. And, finally, with $A\sqrt{M_\infty^2-1}>5$ a delta wing with positive sweep of the trailing edges is best. Figure 7.3.7 gives a comparison of the induced drags for the same design shapes as dealt with in the foregoing case. The unswept wing has the largest drag.

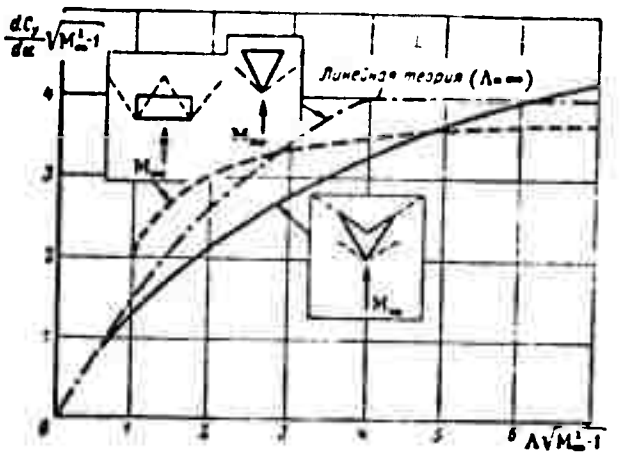


Fig. 7.3.6. Comparison of the slope of the lift characteristics for three different wing plans. 1) Linear theory.

Comparison of calculation with experimental data. A comparison [7.1] of the calculated and experimental characteristics of lift versus aspect ratio shows good agreement. Disagreement between theory and experiment is obtained in the case where the Mach line is close

to or coincides with the leading edge of the wing. Let us note that the linear theory deviates greatly from the calculation for the position of the pressure center.

The body drag of a delta wing with a wedge-like cross section and a subsonic leading edge can be considerably reduced, by bringing the line of maximum profile thickness near to the leading edge. This, however, changes the pressure considerably and the boundary layer becomes turbulent; this, in turn, raises the surface friction drag and the total drag is thus increased.

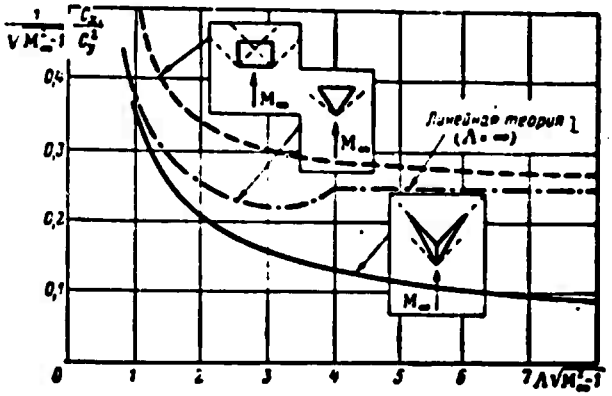


Fig. 7.3.7. Comparison of induced drag of various wing plans. 1) Linear theory.

REFERENCES

7.1. Arzhanikov, N.S. and Mal'tsev, V.I., Aeromekhanika [Aerodynamics], Oborongiz [State Scientific and Technical Publishing House of the Defense Industry], 1952.

7.2. Khilton, U.F., Aerodinamika bol'shikh skorostey [Aerodynamics of High Speeds], IL [Foreign Literature Press], 1953.

7.3. Goshek, I., Aerodinamika bol'shikh skorostey [Aerodynamics of High Speeds], IL, 1954.

7.4. Karman, T., Sverkhzvukovaya aerodinamika [Supersonic Aerodynamics], IL, 1948.

7.5. Krasil'shchikova, Ye.A., Krylo konechnogo razmakha v skhimayemom potoke [Wing of Finite Span in Compressible Flow], GTTI [State Technical and Theoretical Press], 1952.

7.6. A. Puskett and H. Stewart, Aerodynamic Performance of Delta Wings at Supersonic Speeds, "Journ. Aeron. Sci.," 14, No. 10, 1947.

BLANK PAGE

Chapter 8

AIR INTAKES, NOZZLES, JETS

8.1. THRUST OF JET ENGINES

Rocket motors and air-breathing jet engines. The thrust of a jet engine (RD) is the reaction against the gas flow leaving the RD. These gases are produced by combustion of the fule. The process of fuel combustion is accompanied by a liberation of chemical energy, which is imparted to the gaseous combustion products in the form of thermal energy (internal, $c_v T$) and pressure energy (p/ρ). Their sum gives the total energy, i.e., the enthalpy $i = c_v T + pv$ (heat content) of the gas. During the subsequent expansion of the combustion products in a special tube (nozzle) these forms of energy are partly converted into the jet's kinetic energy.

The oxidation (combustion) of the fuel may be induced by an oxidizer carried in the RD itself or by the oxygen taken from the surrounding air in which the RD is operating.

Jet engines carrying all the propellant they need, i.e., fuel plus oxidizer, are called rocket motors (RRD) or simply rockets. An RD taking its oxygen from the surrounding air is called an air-breathing jet engine (VRD).

The operation of (VRD) is limited by the presence of a sufficient oxygen content in the atmosphere. Therefore the altitude of flight of a vehicle powered by a VRD is bounded by certain limits.

Supplying heat to an open air stream does not produce a jet with raised velocity, and the only result of such a process will be

to increase the ambient air temperature. In order to produce a jet with raised velocity, heat must be supplied at increased pressure. Only in this case does the operating cycle executed by the air as it changes its state perform work which differs from zero and which may be used to move the vehicle. For this purpose the fuel combustion zone must be enclosed by a cowling which will receive the thrust, i.e., the result of the change in the static pressure on its surface. This set-up is the simplest type of jet engine and is called the ram-jet engine.

Let us consider the sequence of changes in state of the mass carrier in this engine.

Along the line 1-2 the air is compressed (in the given case by dynamic head, in other types of VRD by a compressor). The air then enters the combustion chamber into which the fuel is also delivered. The fuel mixture forming is ignited. In a VRD as shown in Fig. 8.1.1, a, burning occurs at constant pressure, whereas in the combustion chamber of the engine represented in Fig. 8.1.1,b, the valves K_1 and K_2 are closed during the combustion of the fuel mixture and combustion takes place at constant volume (line 2-3). The combustion products produced stream into the inlet part of the nozzle where they expand (line 3-4) and convert part of their thermal and volume energies into kinetic energy before being expelled through the nozzle. The remainder of the energy diffuses with the combustion products into space. The parameters of state of the expelled combustion product particles reach equilibrium with the parameters of state of the surrounding air particles.

The reaction – the recoil – of the emitted jet will constitute the thrust of the RD.

Thus, during the operation of the RD the mass carrier (gas)

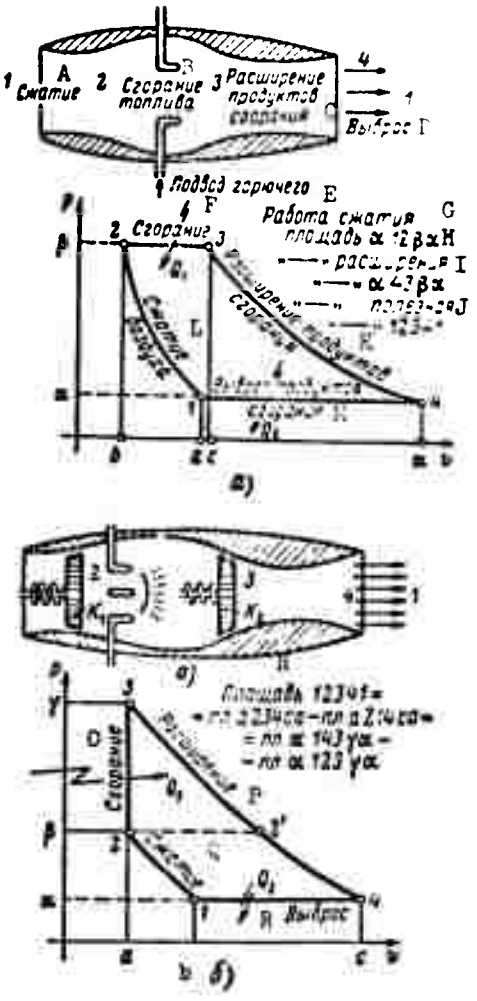


Fig. 8.1.1. Cyclic processes for ram-jet engines with heat supply at constant pressure (a), and constant volume (b). A) Compression; B) fuel combustion; C) expansion of combustion products; D) expulsion; E) fuel supply; F) combustion; G) compression work; H) area; I) expansion; J) effective; K) expansion of combustion products; L) compression of air; M) expulsion of combustion products; N) area; O) heating; P) expansion; Q) compression; R) expulsion.

does not perform a closed cycle: the mass carrier leaves the engine after having done work. If, however, we take into account that at large distances from the engine, where they have mixed with the surrounding medium, the combustion products emitted have virtually the same parameters of state as the induced air, and if we further notice that the ultimate fate of each individual portion of mass

carrier is of no interest, we can establish the convention of regarding the process as being closed, assuming that the parameters of state of the mass carrier are led back via line 4-1 to their initial values. Under this assumption each volume of air taken from in front of the engine is identified with the same volume of air far behind the engine. Figure 8.1.1 shows such conventionally cyclic ram-jet engine processes.

Since the volume of the whole rocket fuel is negligibly small as compared with the volume of the combustion products, the difference between the cycle of an RRD and the cycle of a VRD will consist in that the line 1-2 will be virtually straight, almost coinciding with the ordinate axis (Fig. 8.1.2).

Solid fuel rocket motor (RRDTT). The RRDTT is most applied and has its widest use in rocket missiles (RS). Powder is used here as the propellant which in general contains both the fuel and the oxidizer in solid form (Fig. 8.1.3).

Such a state of aggregation of the fuel determines the extraordinary simplicity of the construction of the engine which consists of a combustion chamber containing the powder charge, and the exhaust nozzle.

Liquid fuel rocket motors (ZhRD) carry the fuel (plus oxidizer) in liquid form with them.

A great advantage exhibited by the ZhRD as compared with the RRDTT is the possibility of controlling them, and, in particular, its cut off and repeated launching. The fundamental disadvantage of the ZhRD is the low efficiency: the fuel required to obtain a thrust of 1 kg is 20-50 times greater than in a reciprocating engine. The ZhRD is therefore only economical as a short duration motor, since only in this case does the gain in weight of the ZhRD as compared

with the weight of a piston engine (a factor of 20-30) compensate the large weight of the fuel.

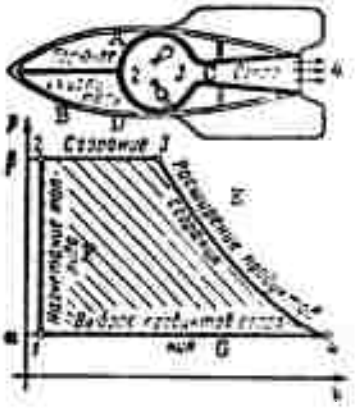


Fig. 8.1.2. Cyclic process of liquid fuel rocket motor (ZhRD). A) Fuel; B) oxidizer; C) nozzle; D) combustion; E) expansion of combustion products; F) compression of fuel; G) expulsion of combustion products.

Jet engines (VRD). Since the weight of the oxidant is 3 to 5 times as large of the weight of the propellant, the application of jet engines carrying only the propellant is of great interest to aviation. The complete combustion of a large amount of fuel within a short time interval requires, however, sufficiently large amounts of air and a sufficiently high pressure in the combustion chamber. Jet engines can be subdivided into two large groups: those with and those without compressors.

In the VRD with no compressor the pressure is raised solely by virtue of the dynamic head, whereas in the VRD with a compressor the pressure is mainly produced by a specially mounted compressor.

VRD with no compressor. The VRD with no compressor, or ram-jet engine, as was indicated above, is an open tube of variable cross section oriented in the direction of motion. The dynamic head is used to achieve precompression of the air in the engine, which is produced by the forward motion of the engine. It therefore follows first of all that this engine must be started by being brought into motion by some other means, for example, by a take-off ZhRD or by towing. The thermal efficiency of a jet engine increases with pressure and, since the dynamic head increases with the square of the velocity, the efficiency of an engine with no compressor is very



Fig. 8.1.3. Schematic diagram of rocket missile with powder propellant motor. 1) Igniter; 2) powder; 3) stabilizer; 4) nozzle; 5) warhead; 6) end plate; 7) control instruments.

low at low velocities.

If heat supply (fuel combustion) occurs at constant pressure (p = const) the engine operates continuously and is called a ram-jet engine (VRD).

If the heat supply occurs at constant volume (v = const) the combustion chamber volume must be periodically constant at the times of completion of the cycle. The operation of the engine has a periodic character and the engine is therefore called a pulsed ram-jet engine (PuVRD).

Figure 8.1.4 shows a schematic diagram of a continuously operating ram-jet engine. In subsonic flight the velocity in the diffuser drops along the section 1-2 and the pressure increases from the value p_1 to the value p_2. The section 2-3 represents the combustion chamber, and the section 3-4 the exhaust nozzle in which the pressure drops to its initial value p, which is equal to the pressure of the surrounding air. If the speed of flight exceeds the speed of sound, then, as is well known, a continuous transition from supersonic to subsonic speed is impossible, This transition is always accompanied by the occurrance to subsonic speeds with smaller losses special measures, which will be discussed later, can be applied; they make it possible to have a single shock or a system of diagonal compression shocks at the inlet of the engine. After this, the changes in velocity and pressure throughout the whole length of the VRD will have the same character for both subsonic and supersonic flight. The velocity and pressure characteristics are given in Fig. 8.1.4, which shows also the TS graphs of the engine's operation for

these two flight regimes.

The specific weight of the ram-jet engine is by about 10 times as small as the weight of the usual propellant plant. It can, however, be used only at very high speeds, when the efficiency is sufficiently high; this can be seen from the following table:

1 Скорость полета w м/сек	200	400	600	800	1000
2 Полный к. п. д. η %	3	10	30	50	80

1) Speed of flight, w, m/sec; 2) total efficiency, η, %.

Jet engine with a compressor. Jet engines in which air is compressed with the help of a specially mounted compressor constitute

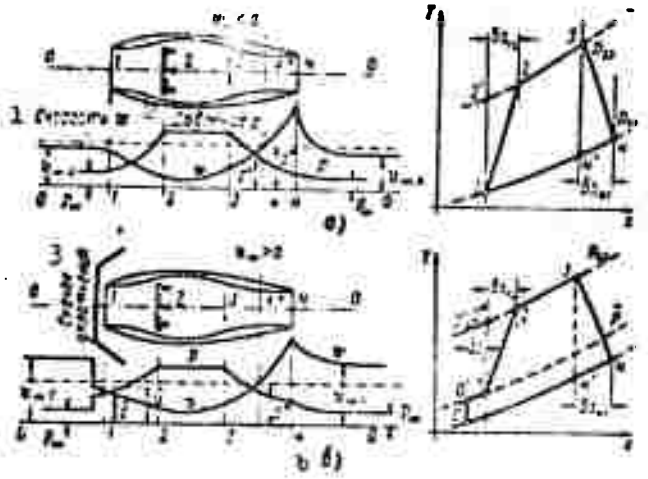


Fig. 8.1.4. Continuously operating ram-jet engine in flight at subsonic speed (a) and supersonic speed (b). 1) Speed; 2) pressure; 3) compression shock.

the large group of the VRD with compressors which are at present the most widely used power plants in aviation.

If the compressor is driven by a piston engine, the jet engine is called motor compressor jet engine (MKVRD). The widest range of application, however, was reached by engines whose compressors are

driven by a special gas turbine. These jet engines are called turbo-compressor jet engines (TKVRD).

The turbo-compressor VRD (TKVRD). The prospects for jet engines had been brightening in connection with the successful construction of a sufficiently reliably operating gas turbine, and with the industrial solution of the problem of producing it. The fact that both compressors an turbines belong to a common class of machine types, the absence of reciprocal motion, and of a complex valve-controlled distributing mechanism, the full balance with excellent weight relations renders the combination "gas turbine – compressor" especially successful.

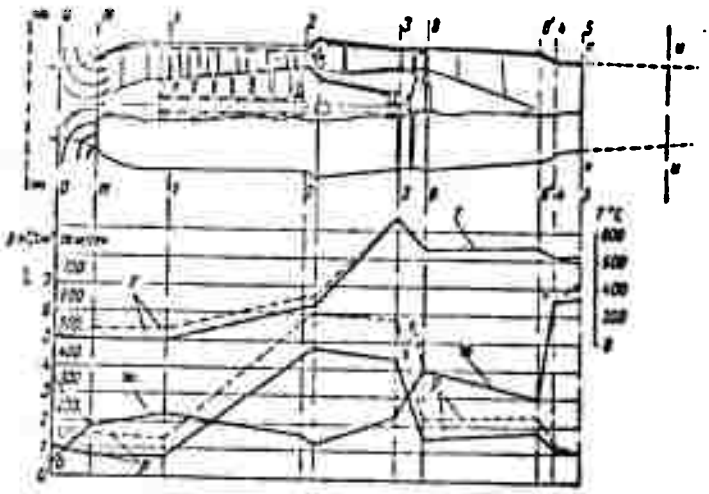


Fig. 8.1.5. Section through TKVRD with an axial-flow compressor and curve of parameter variation along the engine. 1) p, kg/cm^2, w, m/sec.

Figure 8.1.5 gives a section through a turbo-compressor jet engine (TKVRD) with an axial-flow compressor, and Fig. 8.1.6 shows a centrifugal flow.

From the point of view of economy, turbo-compressor jet engines are ineffective at low speeds of flight and become comparable with the propeller plants driven by piston engines at flying speeds of

700-900 km/kr. It must be pointed out, however, that the TKVRD have a much smaller weight per unit of thrust than piston engines do.

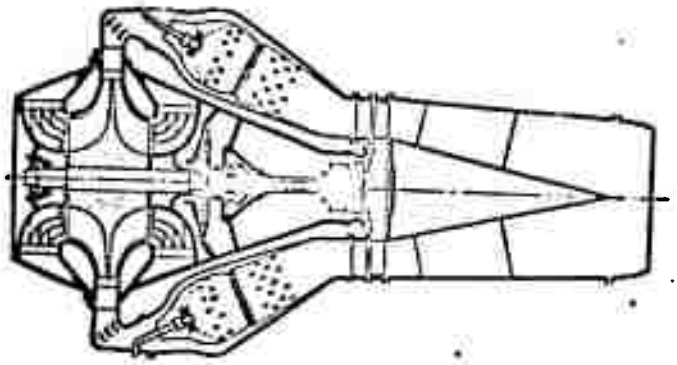


Fig. 8.1.6. Section through a centrifugal-flow TKVRD.

Serious difficulties in the development of the TKVRD are occasioned by the hard operational conditions of the gas turbine blades, which limit the lifetime of the TKVRD. The large centrifugal forces which arise as they rotate and the high temperatures of the combustion products give rise to considerable plastic deformation, or creep, in the blades.

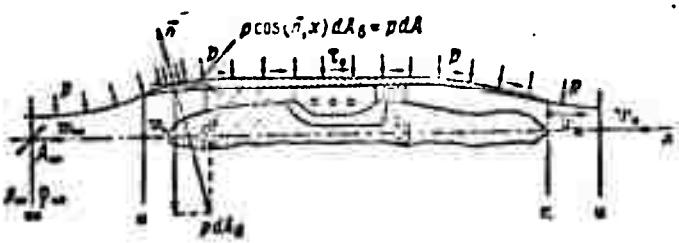


Fig. 8.1.7. Schematic diagram of pressure distribution over the outer surface of the cowling of a jet engine.

Since reducing the engine's revolutions raises the bulk and lowering the temperature reduces the efficiency, the work on turbo-compressors is mainly aimed at developing methods of cooling the machine units and producing particularly strong and heat-resistant steels.

Effective thrust. The flight of a vehicle – aircraft, rocket, etc., – is determined by the effective thrust of its power plant, i.e., by the difference between the [illegible] and drag of the engine. When the engine is placed in a cowling (Fig. 8.1.7) the effective thrust is the resultant of the [illegible] forces on the outer surface A_{nrzh} of the cowling (external force) and its inner surface A_{vn} (internal force*), including the inner surface and those parts of the engine which are [illegible] ring inside the cowling. In view of the [illegible] on determining the control surface, the external force (drag of cowling) is usually calculated directly, e.g., from the [illegible] distribution on the outer surface of the cowling. Let us denote by dA the projection of an element of

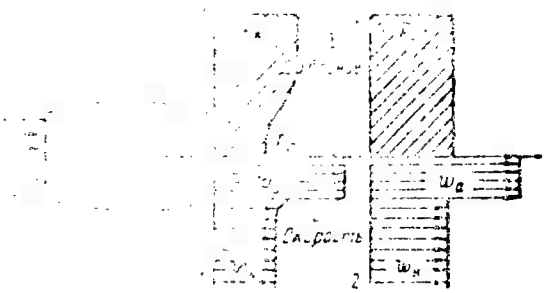


Fig. [illegible]. Diagram of velocity distribution [illegible] engine. 1) Pressure; 2) velocity.

the lateral cowling [illegible] plane normal to the engine axis (flying velocity) and substitute the angle "[illegible]" to the projection of the normal on the axis in flight direction (cf. Fig. 8.1.7). Then, assuming the flow [illegible] constant over the cross section of the jet in the [illegible] denoting by R_{tr} the force of friction on the outer surface of the cowling, A_{obt}, we can write

$$[\text{illegible}] = \int_{A_{nr}} p\cos(\vec{n}, x)\,dA = \int_{A_{vn}} p\cos(\vec{n}, x)\,dA =$$

$$= -[(p + \rho v^2)A_a + [\text{illegible}]A_a] - \left[\int_{A_{obt}} p\,dA + R_{tr}\right]. \qquad (8.1.1)$$

The resultant of all forces (effective thrust) remains one and the same, no matter where the control sections are chosen. The first control section is conveniently taken in the free flow where it is very simple to determine the flow parameters.

In order to choose the second control section, we make use of the empirical fact that the nonuniformity of the pressure distribution is smoothed considerably sooner than the nonuniformity in the velocity distribution.

As experiments show, the pressure distribution is already uniform at a distance equal to the diameter of the outlet nozzle, and it is equal there to the pressure of the surrounding medium, whereas the velocity at this distance differs considerably from the flying speed. The second section is therefore sometimes taken far downstream from the exit. As was said before, the thrust remains unchanged and independent of the choice of the control sections, but the magnitudes of the internal and external forces change by the magnitude of the axial pressure component with respect to the stream tube of the jet outside the engine, if, for example, the control sections are taken in the free flow and at the nozzle edge of the engine. Noticing that the change of the total impulse of the part of the jet entering the engine between the cross sections A_∞ and A_n is equal to zero, i.e.,

$$[(p+\rho w^2)A]_\infty + \int_{A_{s,n}} p\,dA - [(p+\rho w^2)A]_n = 0$$

(s and n denote the surfaces of the jet section), we may write

$$F = \{[(p+\rho w^2)A]_n - [(p+\rho w^2)A]_\infty\} - \left\{\int_{A_{s,n}} p\,dA + \int_{A_{\text{edge}}} p\,dA + R_p\right\}. \qquad (8.1.2)$$

Conventional thrust and additional drag. In practical work use is generally made of the excess pressure with respect to the pressure

of the undisturbed flow, p_∞. Owing to the fact that the integral over the surface of a closed volume must be zero we can write

$$p_\infty A_\infty + \int_{A_{c.s}} p_\infty \, dA + \int_{A_{обт}} p_\infty \, dA - p_\infty A_\infty = 0.$$

Equation (8.1.2) can therefore be rewritten in the form

$$F = \underbrace{(p_\infty - p_\infty) A_\infty + m_\infty w_\infty - m_\infty w_\infty}_{\text{условная (обычная) тяга}} - \underbrace{\int_{A_{c.s}} (p - p_\infty) \, dA}_{\text{дополнительное сопротивление}} - \underbrace{\int_{A_{обт}} (p - p_\infty) \, dA}_{\text{(обычное) сопротивление}} + R_p. \qquad (8.1.3)$$

The expression in the first brace, the conventional thrust, coincides with the usual definition of the thrust, and therefore the conventional thrust is often simply called the thrust. The drag, however, determined in the usual way, must then be increased by the amount of the additional drag, i.e., the resultant of the pressure forces acting on the free part of the jet entering the engine. As will be shown, in a subsonic flow the additional drag is compensated by the thrust (suction) of the forward part of the cowling.

Since $(p - p_\infty)$ represents an excess pressure, the expression $[(p - p_\infty) + \rho w^2] A$ may be called the excess impulse.

Referring all forces to the product of the dynamic head of the undisturbed flow and the mid-sectional area A_d of the engine, we obtain the following coefficients:

$$C_F = \frac{2F}{\rho w_\infty^2 A_d}, \quad C_x = \frac{2X}{\rho w_\infty^2 A_d}, \quad C_{x\,тр} = \frac{2X_{тр}}{\rho w_\infty^2 A_d}.$$

The mass flow coefficient φ. This is one of the fundamental parameters characterizing the operation of the air intake (of the engine); it is the ratio of the true air-mass flow G passing through the cowling per unit time to the mass flow G_∞ at which the flow parameters in the inlet cross section are equal to the parameters of the

undisturbed (free) flow:

$$\varphi = \frac{G}{G_\infty} = \frac{\rho_n w_n A_n}{\rho_\infty w_\infty A_n} = \frac{\rho_\infty w_\infty A_\infty}{\rho_\infty w_\infty A_n} = \frac{A_\infty}{A_n} \qquad (8.1.4)$$

If the fluid is incompressible, then $\varphi = w_n/w_\infty$. The mass flow coefficient is thus equal to the ratio of the cross sectional area A_∞ of the air jet passing through the cowling where the flow is undisturbed, to the area of the inlet cross section, A_n, of the iar intake.

Thrust and drag distributions over the cowling elements. The theoretical shape of the jet for various operational conditions of the air intake (in a subsonic flow) is shown in Fig. 8.1.9. The flow about the elementary sector of the air intake in the inlet zone is analogous to the circulatory flow about a profile, and, depending on the operational conditions (mass flow coefficient φ), the vector $\vec{R}$ of aerodynamic force per unit length of the contour of the inlet section may change. Finally, of great significance to the motion of the aircraft is the axial component (thrust), since the radial component will be taken up by the construction of the air intake.

Figure 8.1.10 shows the distribution curves of the pressure coefficient C_p for the upper contour of the air intake, with various values of the mass flow coefficient $\varphi = w_n/w_\infty$, from which it can be seen that for all flow conditions the resulting pressure distributed over the outer surface of the air intake is directed forward in the inlet zone.

Let us agree for the following to take the minimum cross section A_n of the inner channel as the interface separating the outer and inner surfaces and to denote it as the entry cross section.

Experiments (Fig. 8.1.11) show (at M = 0) that for sufficiently long cowlings the pressure distribution on the outer surface in the

inlet zone is determined only by the operational conditions of the cowling (air intake) and by the mass flow coefficient φ, and is independent of both the flow conditions in the rear zone and the flow conditions in the inner channel. It thus remains indifferent whether there is a central body (or a lattice) in the inner channel or not (Fig. 8.1.12). It is therefore possible to consider the external

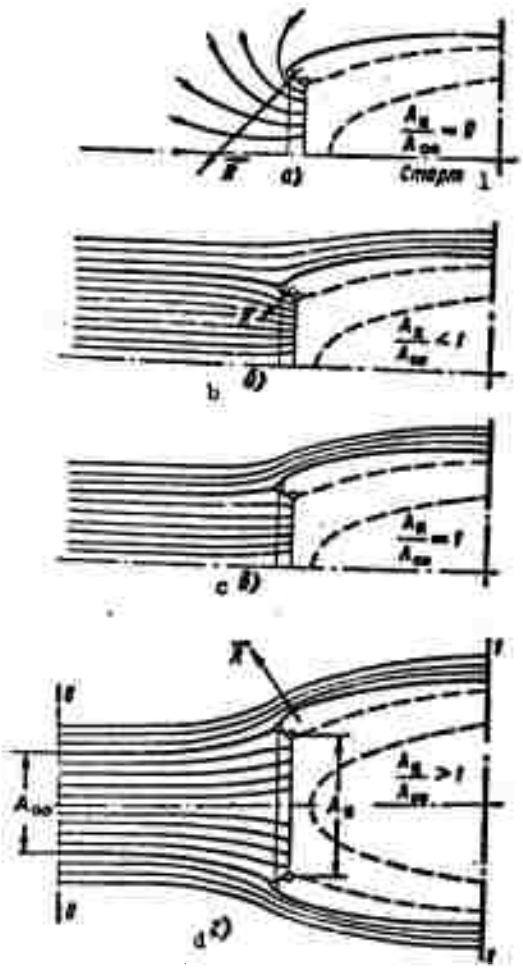


Fig. 8.1.9. Schematic diagram of flow about an air intake for various flying conditions; the velocity grows in these diagrams from zero at the start (a) to the calculated value (b). 1) Starting.

flow about the inlet part (air intake), rear part, and inner channel separately and independently of each other. These conditions make it convenient to decompose the change in excess impulse into three parts

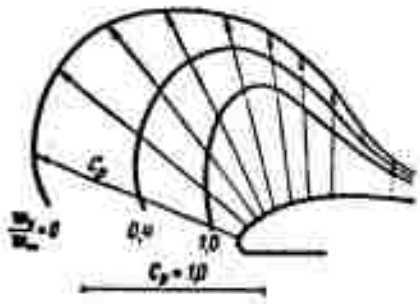


Fig. 8.1.10. Pressure distribution on the upper contour of the air intake for various flying conditions.

by adding and subtracting at the right-hand side of Eq. (8.1.2) the expression

$$[(p_k-p_\infty)+\rho_k w_k^2]\,A_k+[(p_a-p_\infty)+\rho_a w_a^2]\,A_a.$$

Regrouping the terms gives

$$F=\{[(p_a-p_\infty)+\rho_a w_a^2]\,A_a-[(p_\infty-p_\infty)+\rho_\infty w_\infty^2]\,A_\infty-$$
$$-\int_{A_{c.s}}(p-p_\infty)\,dA\Big\}+\Big\{[(p_k-p_\infty)+\rho_k w_k^2]\,A_k-[(p_a-p_\infty)+$$
$$+\rho_a w_a^2]\,A_a-\int_{A_{c.t}}(p-p_\infty)\,dA\Big\}+\Big\{[(p_a-p_\infty)+\rho_a w_a^2]\,A_a-$$
$$-[(p_k-p_\infty)+\rho_k w_k^2]\,A_k-\int_{A_{c.n}}(p-p_\infty)\,dA\Big\}. \quad (8.1.5)$$

Each pair of braces contains the change of excess impulses

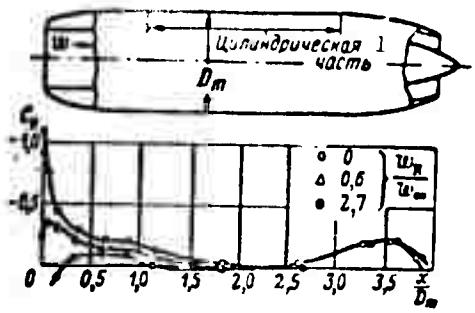


Fig. 8.1.11. Pressure distribution over the outer surface of the jet engine housing in dependence on the ratio w_n/w_∞ (at low flying speeds $M \approx 0$). 1) cylindrical part.

$[(p-p_\infty)+\rho w^2]A$, characterizing the conventional thrust for the sections ∞-n, n-k and k-i of the jet passing through the engine; the integrals represent the drag due to the pressure distributed over the lateral stream tube surface of the jet sections mentioned above.

Thrust of the air intake. The integral in the first braces of (8.1.5), $\int_{A_{c.s}}(p-p_\infty)\,dA$ represents the projection on the engine axis of the resultant of the pressure forces distributed over the lateral

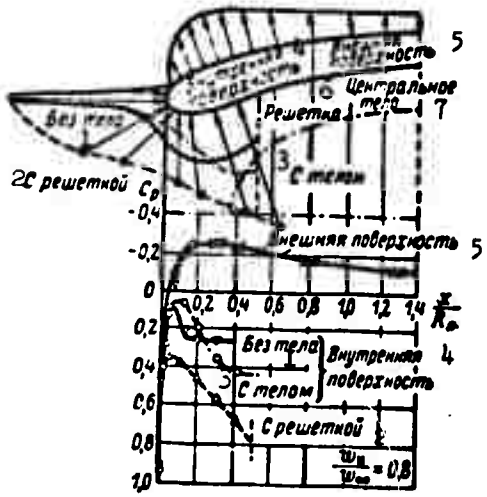


Fig. 8.1.12. Dependence of pressure distribution over the outer surface of the air intake on the flow conditions inside. 1) With no body; 2) with lattice; 3) with body; 4) inner surface; 5) outer surface; 6) lattice; 7) central body.

surface of the jet entering the engine, from the free flow section to the cowling inlet. As we have mentioned above, this force is called the additional drag and is equal to the change of excess impulse for this part of the jet, i.e., the expression in the first braces vanishes. In fact,

$$[(p_a - p_\infty) + \rho_a w_a^2] A_a - [(p_\infty - p_\infty) + \rho_\infty w_\infty^2] A_\infty -$$
$$- \int_{A_{c.a}} (p - p_\infty)\, dA = [(p + \rho w^2) A]_a - [(p + \rho w^2) A]_\infty -$$
$$- p_\infty A_a + p_\infty A_\infty + \int_{A_{c.a}} p_\infty\, dA - \int_{A_{c.a}} p\, dA = J_a - J_\infty - \int_{A_{c.a}} p\, dA.$$

since

$$p_\infty A_\infty + \int_{A_{c.a}} p_\infty\, dA - p_\infty A_a = \oint_A p_\infty\, dA = 0$$

and therefore

$$(pA)_a - (pA)_\infty + \int_{A_{c.a}} p\, dA + (\rho_a w_a^2 A_a - \rho_\infty w^2 A_\infty) = 0,$$

i.e.,

$$(pA)_a - (pA)_\infty + \int_{A_{c.a}} p\, dA = \rho w_\infty A_\infty (w_\infty - w_a). \qquad (8.1.6)$$

This force is the result of the influence of the forward part of the cowling – the air intake – on the flow. Let us in fact consider the cowling as an air intake which goes over smoothly to a cylindrical surface that extends to infinity (Fig. 8.1.13). In order to avoid integrating along an unknown streamline, we choose the control sections: AK far in front of the inlet where the flow is uniform and undisturbed, and BCEFH far behind the inlet in the region of the cylindrical part where the flow parameters may be assumed to be steady (cf. Fig. 8.1.11); i.e., inside the channel they are assumed to be equal to those at the inlet and outside the cowling they are assumed to be equal to the parameters of the undisturbed flow.

If we denote by F_N the force acting on an isolated volume in the direction of the flow, we can write

$$F_N + p_\infty A_\infty - p_\infty (A_\infty - A_d) - p_n A_n = \rho_\infty w_\infty^2 (A_\infty - A_d) + \rho_n w_n^2 A_n + (\rho_\infty w_\infty A_d - \rho_n w_n A_n) w_\infty - \rho_\infty w_\infty^2 A_\infty$$

or, noticing that $A_d = A_n + A_0$,

where A_0 is the projection of the area of the air intake on the plane normal to the flow (cf. Fig. 8.1.13),

$$F_N = (p_n - p_0) A_n - p_\infty A_0 + \rho_n w_n A_n (w_n - w_0).$$

Taking the flying direction as positive for the force, we obtain for the conventional thrust of the air intake $F_N = -\int_A (p - p_\infty) dA_0$

$$F_N = -\int_{A_0} (p - p_\infty) dA_0 \quad \rho_n w_n A_n (w_n - w_\infty) + (p_n - p_\infty) A_n. \qquad (8.1.7)$$

At low flying speeds, when the compressibility of the flow can be neglected, $\rho_\infty = \rho_n = \rho$, and when we take into account that according to Bernoulli's equation $p_n + \frac{\rho w_n^2}{2} = p_\infty + \frac{\rho w_\infty^2}{2}$, we obtain

$$F_N = \frac{\rho w_\infty^2}{2} A_n \left(1 - \frac{w_n}{w_\infty}\right)^2 = \frac{\rho w_\infty^2}{2} A_n (1 - \varphi)^2. \qquad (8.1.8)$$

Thus, regardless of the outer contour of the air intake it is acted on by an axial force which depends only on its operational

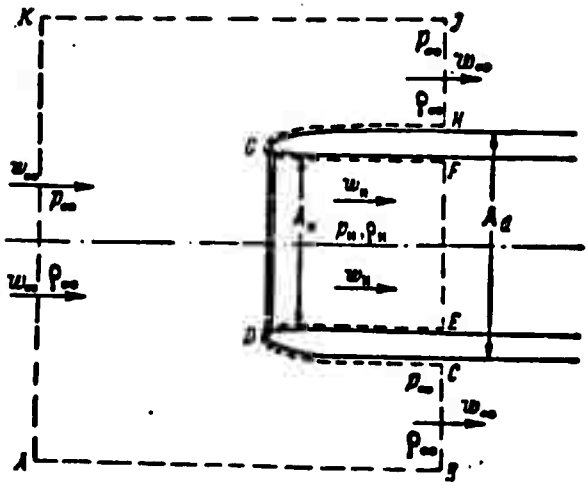


Fig. 8.1.13. Air intake in the form of a semi-infinite cowling and control contour for the determination of the forces acting on the air intake.

conditions, and which is determined by the mass flow coefficient φ. This statement is verified by experiment (Fig. 8.1.14). If $\varphi = 1$, i.e., if the flow rate is unchanged, then $F_N = 0$. The other limiting case $\varphi = 0$, occurs when the inner channel is closed, and then $F_N = \frac{\rho w_\infty^2}{2} A_H$. This force is exactly equal to the pressure the flow exerts on the plate closing the channel.

The thrust of the air intake. The thrust of the air intake is determined only by the momentum change in the free flow, i.e., between the cross section in the undisturbed flow and the inlet of the air intake, and, consequently, only by the mass flow coefficient φ. The type of the air intake can, therefore, have no influence on this momentum change and in this respect the air intakes shown in Fig. 8.1.15 are equivalent. The pressure distributions over these air intakes will, however, be different and for the same total amount of thrust the thrust components will be different. This leads to the widely held but erroneous opinion that embedded air intakes, i.e., such which lie in one plane with the surrounding surface are advan-

tageous [8.1].

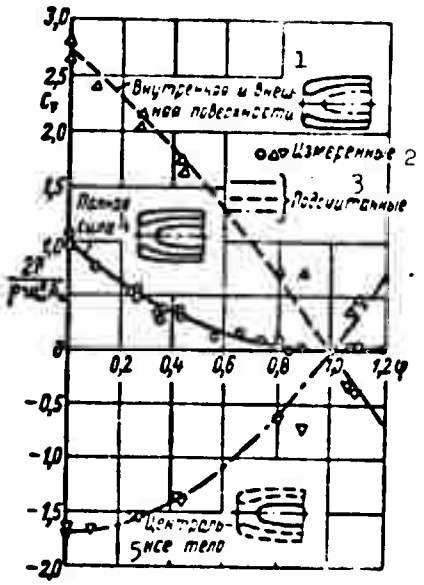


Fig. 8.1.14. The thrust of the air intake is determined by the velocity ratio alone. 1) Inner and outer surfaces; 2) measured; 3) calculated; 4) total force; 5) central body.

Drag of the rear part. The integral in the third braces of (8.1.5) is equal to the resultant force of the pressure distributed over the lateral surface of the jet leaving the engine. As in the consideration of the entry part of the air intake it can be shown that the expression in the third braces is equal to zero and that this force is the result of the influence of the rear part of the air intake of the flow. Its direction coincides with the direction of the outflowing reactive jet, i.e., it is directed against the flying direction and therefore appears as a drag. This can be shown when we consider the rear zone with its cylindrical part extending to infinity on the upstrem side (as if the air intake were placed in a reverse flow).

Usually $p_1 = p_\infty$ and the drag of the rear part is

$$F_{xp} = \rho_a w_a^2 A_a - [(p_a - p_\infty) + \rho_a w_a^2] A_a. \qquad (8.1.9)$$

The thrust of the engine. The second braces of (8.1.5) represents the thrust of the engine exactly. As we know already, the integral in it is called the conventional drag. In the subsonic flow of an inviscid gas the drag of an arbitrary infinite body, which can be taken as the resultant of the pressure distributed over its entire surface, is zero. In a subsonic flow the sum of the three integrals entering the braces of (8.1.5) is therefore equal to zero and

the force acting on the envelope will be composed of the thrust of the entry part and the drag of the rear part of the air intake.

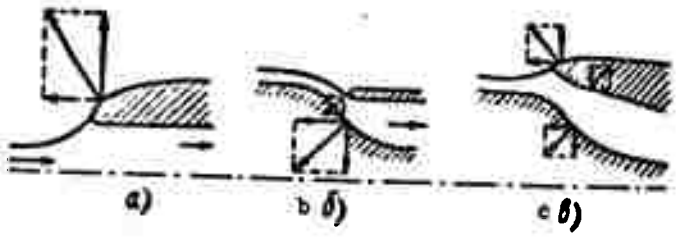


Fig. 8.1.15. The magnitude of the thrust is determined only by the change in momentum of the entering flow regardless of where it takes place, but its point of application depends on where the momentum change takes place: in the free flow (a), in the channel (b), or partially in the free flow and partially in the channel (c).

The conditions met in a supersonic flow, where the flow is accompanied by the formation of the compression shocks and irreversible energy dissipation, will be different. The cowling drag will be finite

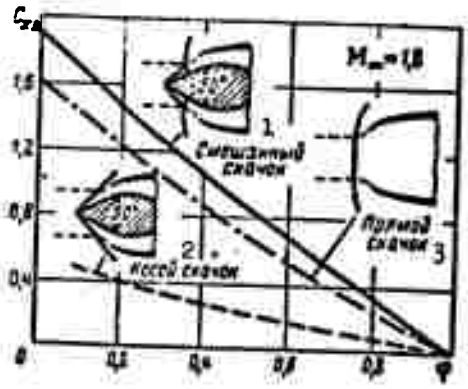


Fig. 8.1.16. The coefficient of additional drag for three types of compression shocks at the inlet. 1) Mixed shock; 2) diagonal shock; 3) normal shock.

and the additional drag will exceed the thrust of the air intake. Figure 8.1.16 gives the curves of variation of the additional drag coefficient calculated for three types of compression shock systems at the inlet, as a function of the mass flow φ; the necessity of designing the supersonic flow inlet properly is obvious.

As we have already mentioned, the device used to produce the

drag in a jet engine consists of an annular cowling, whose forward part, the air intake, serves to separate a certain amount of air. Besides this, the cowling serves to improve the external aerodynamics of the power plant, i.e., to reduce its drag.

The engine is sometimes arranged fairly far from the air intake and in this case the air from the air intake reaches the engine through a channel. The position of the air intake on the aircraft depends on the position of the engine; we distinguish between head intakes, arranged directly at the nose of the fuselage with the inlet parts consisting of sufficiently long cowlings (engine housing), off-axis intakes (on the side of the fuselage), wing intakes (in the wings of the aircraft), wing root intakes, positioned at the joint of the wing with the fuselage, etc. The air intakes (especially those for supersonic flight) are sometimes called diffusers. The air stream entering the engine must be highly uniform since even the slightest nonuniformities in the flow may disturb the regular operation of the engine. The uniformity of the flow is determined to a considerably degree by the construction of the air intake.

It is also very important for a jet engine that the nozzle through which the thrust-producing jet of combustion products is emitted should be accurately designed.

8.2. AIR INTAKES

Air intake parameters. The energy losses in the inlet system lead to a drop in total pressure. The ratio between the total pressure at the end of the inlet system, p_{0k}, and the total pressure of the undisturbed flow, $p_{0\infty}$, characterizes the quality of the inlet system and is called the pressure recovery coefficient

$$\sigma_0 = \frac{p_{0k}}{p_{0\infty}} = \frac{p_{0k}}{p_\infty \left(1 + \frac{k-1}{2} M_\infty^2\right)^{\frac{k}{k-1}}}. \qquad (8.2.1)$$

The quality of the air intake is also characterized by the ratio between the total pressure losses and the dynamic head in the exit cross section of the air intake channel. This ratio is called the loss coefficient

$$\zeta_к = \frac{2(p_{0\infty} - p_{0к})}{\rho_к w_к^2} = \frac{2\Delta p_0}{\rho_к w_к^2}. \qquad (8.2.2)$$

Sometimes the total pressure losses are referred to the dynamic head of the undisturbed flow; in this case the loss coefficient is

$$\zeta_\infty = \frac{2(p_{0\infty} - p_{0к})}{\rho_\infty w_\infty^2} = \frac{2\Delta p_0}{\rho_\infty w_\infty^2} = \zeta_к \frac{\rho_к w_к^2}{\rho_\infty w_\infty^2}. \qquad (8.2.3)$$

It is easy to show that

$$\sigma_0 = 1 - \frac{k}{k-1}\zeta_\infty M_\infty^2 \left(1 - \frac{k-1}{k+1} M_\infty^2\right)^{\frac{1}{k-1}}. \qquad (8.2.4)$$

The geometrical characteristic of the inner channel is the relative inlet, i.e., the ratio of inlet cross section A_n to exit cross section A_k:

$$f = \frac{A_n}{A_к}. \qquad (8.2.5)$$

As we have already mentioned, the operational conditions are characterized by the mass flow coefficient φ (8.1.3).

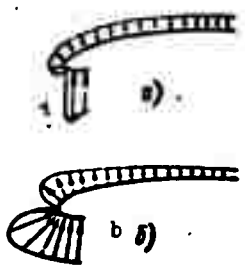


Fig. 8.2.1. Pressure distribution over the outer surface of the air intake, for optimum shape (a) and in the general case (b).

Optimum subsonic air intake. The pressure coefficient $C_p = \frac{2(p - p_\infty)}{\rho w_\infty^2} = 1 - \frac{w^2}{w_\infty^2}$ (at M = 0) depends at each point only of the ratio of the local velocity w to the velocity of the undisturbed flow, w_∞. To produce a thrust in the air intake the coefficient C_p must be negative, i.e., the local velocity must exceed the velocity of the undisturbed flow.

Since the nonuniformity in the pressure distribution is connected with a premature separation of the flow, and at large velocities

with the onset of shock stall, then, as we have shown in Part 3.3, the optimum contour will be the one for which the velocity is the same at all of its points and the highest velocity reached at rated flight conditions, i.e., $w/w_\infty = w_{max}/w_\infty$. In this case the static pressure will be constant along the outer contour (Fig. 8.2.1).

In the case of optimum shape of the outer part the integral in (8.1.7) will therefore be equal to $C_p p \frac{w_\infty^2}{2}(A_d - A_n)$ and the thrust will be

$$C_P = \frac{2P}{\rho w_\infty^2 A_n} = C_p\left(\frac{A_d}{A_n} - 1\right) = -\left(1 - \frac{w_{max}^2}{w_\infty^2}\right)\left(\frac{A_d}{A_n} - 1\right). \qquad (8.2.6)$$

whence we obtain for the general case

$$\frac{A_d}{A_n} \geqslant 1 + \frac{\left(1 - \frac{w_n}{w_\infty}\right)^2}{\frac{w_{max}^2}{w_\infty^2} - 1}. \qquad (8.2.7)$$

The equality sign in (8.2.6) determines the optimum midsection of the air intake of every inlet for a given maximum velocity w_{max} of the external flow for rated conditions, w_n. The sign > refers to a cowling with variable pressure distribution on the outer surface.

Influence of compressibility in a subsonic flow. For a compressible gas we obtain from

$$\left.\begin{aligned} &\frac{p_n}{p_\infty} = \left(\frac{\rho_n}{\rho_\infty}\right)^k; \quad \frac{k}{k-1}\frac{p_\infty}{\rho_\infty} + \frac{w_\infty^2}{2} = \frac{k}{k-1}\frac{p_n}{\rho_n} + \frac{w_n^2}{2} \\ &\frac{p_n}{p_\infty} = \left[1 + \frac{k-1}{2k}\frac{\rho_\infty}{p_\infty}\frac{w_\infty^2 - w_n^2}{2}\right]^{\frac{k}{k-1}} = \\ &= \left[1 + \frac{k-1}{2} M_\infty^2\left(1 - \frac{w_n^2}{w_\infty^2}\right)\right]^{\frac{k}{k-1}}, \\ &\frac{\rho_n}{\rho_\infty} = \left(\frac{p_n}{p_\infty}\right)^{\frac{1}{k}}; \end{aligned}\right| \qquad (8.2.8)$$

and, owing to (8.1.7) the thrust of the outer part of the air intake will be

$$C_{F_N}=\frac{2F_N}{\rho_\infty w_\infty^2 A_n}=2\frac{\rho_n}{\rho_\infty}\frac{w_n}{w_\infty}\left(\frac{w_n}{w_\infty}-1\right)+\frac{2p_\infty}{\rho_\infty w_\infty^2}\left(\frac{p_n}{p_\infty}-1\right)=$$

$$=2\frac{w_n}{w_\infty}\left(\frac{w_n}{w_\infty}-1\right)\left[1+\frac{k-1}{2}M_\infty^2\left(1-\frac{w_n^2}{w_\infty^2}\right)\right]^{\frac{1}{k-1}}+$$

$$+\frac{2}{kM_\infty^2}\left\{\left[1+\frac{k-1}{2}M_\infty^2\left(1-\frac{w_n^2}{w_\infty^2}\right)\right]^{\frac{k}{k-1}}-1\right\}. \qquad (8.2.9)$$

At the surface $\frac{p}{p_\infty}=\left[1+\frac{k-1}{2}M_\infty^2\left(1-\frac{w_{max}^2}{w_\infty^2}\right)\right]^{\frac{k}{k-1}}$, and the formula for the optimum midsection of the air intake (8.2.7) is transformed to

$$\frac{A_d}{A_n}=1-\frac{2F_N}{\rho_\infty w_\infty^2 A_n}\frac{1}{C_p}=1+\frac{C_{F_N}}{2}\frac{kM_\infty^2}{1-\left[1+\frac{k-1}{2}M_\infty^2\left(1-\frac{w_{max}^2}{w_\infty^2}\right)\right]^{\frac{k}{k-1}}}\approx$$

$$\approx 1-\frac{C_{F_N}}{1-\frac{w_{max}^2}{w_\infty^2}}. \qquad (8.2.10)$$

The thrust coefficient C_{F_N} in Eq. (8.2.10) is determined with allowance for the compressibility according to Formula (8.2.9).

The calculations made with Eqs. (8.2.9)-(8.2.10) show (Fig. 8.2.2) that the compressibility in a subsonic flow exerts no essential influence either on the thrust F_N or on the areal ratio A_d/A_n, and that the optimum midsection of the air intake can therefore be preliminary calculated with the help of Expression (8.2.7).

In the case of a flight with a different M_∞ the optimum shape of the outer part of the air intake will also be different. If the optimum shape of the outer part of the air intake is determined (experimentally or theoretically) for an incompressible flow and if $C_{p_{M=0}}$ is given, then the optimum shape for a compressible flow can be obtained from its previously determined longitudinal dimensions by multiplying them by $1:\sqrt{1-M_\infty^2}$ [8.1].

In this case and for round air intakes the ratio

$$\frac{C_{p_M}}{C_{p_{M=0}}}=\frac{1}{\sqrt{1-M_\infty^2}}, \qquad (8.2.11)$$

obtained in the linearized theory is in good agreement with experiment.

The outer contour of the air intake. On calculating the air intake contour by the method of connected singularities (cf. p. 200) we consider the flow of an incompressible parallel stream from annular sources, sinks and vortices, arranged on a cylindrical surface.

If for a given singularity distribution the stream function Ψ can be calculated on the site x, r (x, r, ϑ being the cylindrical coordinates), then the shape of the air intake can be determined since it is always possible to find the stream-lines Ψ = const. Such a method of calculation is however laborious. It is complicated enough to solve the inverse problem, i.e., to determine the distribution of the annular sources, sinks and vortices for a given air intake and a given velocity distribution on its contour. It can be reduced to solving a certain integral equation [8.1].

The calculation of the optimum shape of a plane air intake under the condition of constant pressure along its outer surface by the method of conformal mapping has been discussed before (cf. Part 3.3).

It has been proven by an experimental selection of the best shapes of air intakes that air intake shapes with almost constant pressure distribution are similar. This empirical conclusion makes it possible to obtain simple geometrical relations for different shapes of air intakes. Particularly good results were obtained with air intakes whose contours are ellipses joined at the leading edge (Fig. 8.2.3).

In this case the outer profile is determined by the formula

$$\frac{r}{R_d} = \frac{R_0}{R_d} + \left(1 - \frac{R_0}{R_d}\right)\sqrt{1 - \left(1 - \frac{R_d}{l}\frac{x}{R_d}\right)^2} \qquad (8.2.12)$$

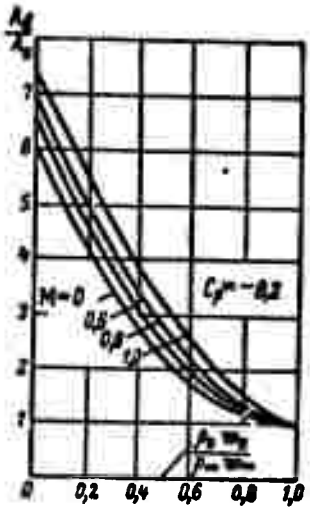


Fig. 8.2.2. Change of midsectional area in dependence on the dimensionless mass flow φ for various M_∞ in subsonic flight.

and the inner profile by

$$\frac{r}{R_d} = \frac{R_0}{R_d} - \left(\frac{R_0}{R_n} - 1\right)\frac{R_n}{R_d}\sqrt{1-\left(1-\frac{R_n}{l_n}\frac{x}{R_n}\right)^2}. \quad (8.2.13)$$

In order to calculate with the help of these formulas it is convenient to introduce the ratio A_n/A_d and the coefficients K_1, K_2, K_3, K_4:

$$\left.\begin{aligned} K_1 &= \frac{R_0}{R_n}, \quad \frac{R_0}{R_d} = K_1\sqrt{\frac{A_n}{A_d}}, \\ K_2 + K_3\left(\frac{A_n}{A_d}\right)^2 &= \frac{R_d}{l}, \quad \frac{1}{K_4(K_1-1)} = \frac{R_n}{l_n}. \end{aligned}\right\} \quad (8.2.14)$$

Different radii of curvature of the air intake nose (thickness of leading edge). Correspond to different values of these coefficients. The values of the coefficients for the three groups of air intakes, A, B, and C, for which aerodynamic characteristics are available [8.1], are given in the following table.

Группа 1	Радиус закругления носка 2	K_1	K_2	K_3	K_4
A	3 Большой	1,15	0,2	12,5	1,5
B	4 Средний	1,10	0,2	12,5	1,3
C	5 Малый	1,03	0,2	7,5	1,0

1) Group; 2) nose curvature radius, 3) large; 4) medium; 5) small.

Group C corresponds to smallest leading edge thickness.

An air intake is completely determined by its group and its aerial ratio A_n/A_d. The air intakes are designated by figures giving the areal ratio A_n/A_d in per cent together with the group, e.g., C-27.

The aerodynamic characteristics of air intakes (Fig. 8.2.4)

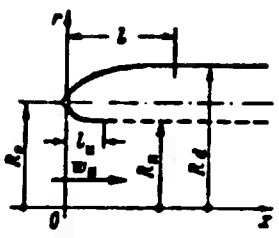


Fig. 8.2.3. Geometrical parameters of round air intake.

show that the pressure distribution on the largest part of the profile of group C is more uniform and that this group is therefore nearer than group A to the optimum shape, but more sensitive to changes in w_n/w_∞ near the leading edge. The rarefaction peaks and the resulting higher speeds at the leading edge are explained by the strong curvature of the ellipse near the nose. Other geometrical curves may provide lead dges

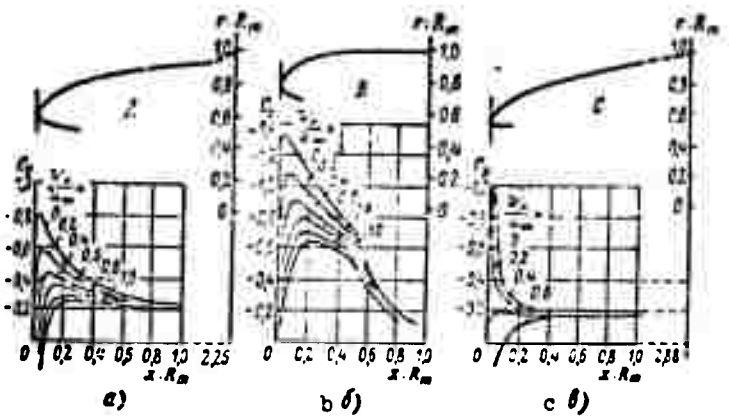


Fig. 8.2.4. Pressure distributions for air intakes of groups A, B and C.

with less curvature; this avoids the appearance of large rarefaction peaks (e.g., the air intakes of the NACA-1 series).

The thicker edges of the air intakes of group A (less curved nose) reduce the rarefaction at the edge. When A_n/A_d is given, however, the maximum velocity on the outer surface obtained is larger than in the flow about an optimum shape (Fig. 8.2.5).

For "elliptical" air intakes an increase in thickness of the edges therefore raises the danger of shock stall appearance at the outer surface (cf. Fig. 8.2.5, b). Under take-off conditions the thick edges afford a smoother inflow of air (Fig. 8.2.6). Under these

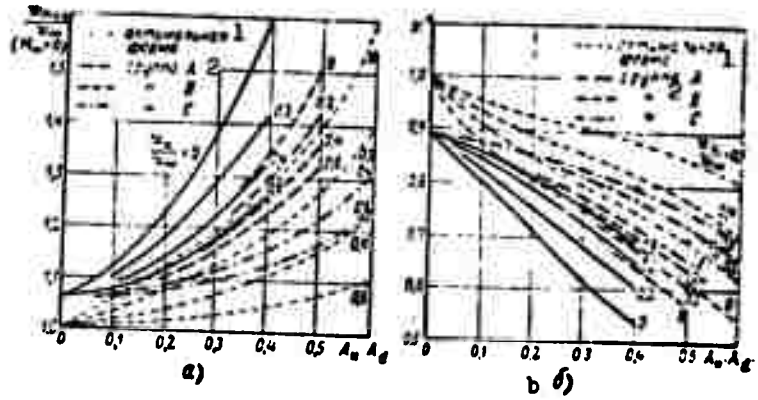


Fig. 8.2.5. Maximum velocities at the outer surface (a) and calculated critical numbers M_∞^* (b) for air intakes of the groups A, B and C. 1) Optimum shape; 2) group.

operational conditions sharp edges may lead to separation of the flow from the walls, to vortex formation and to energy losses. At the same time the pressure drops and with it the thrust of the jet engine, just at the moment when it should be maximum (take-off). In order to avoid the losses due to flow separation, the air intakes are furnished with slots (Fig. 8.2.7) which are opened during the start to provide an additional air inlet.

When air intakes are designed, the thickness of the leading edges is taken as large as possible without leading to shock stall. Note that the more closely the shape of an air intake approaches optimum shape, the larger in size the supersonic zones forming on the outer surface of the air intake may be when the flow velocity exceeds the maximum, and the faster the drag will grow when M_{kr} is reached.

The inner channel. The mean velocity w_n in the narrowest section of the air intake determines both the flow about the outer surface and the flow in the inner channel. In the same way it connects the two conditionally independent flows, and it is a given quantity in the design of the inner channel. Depending on the given velocity w_1

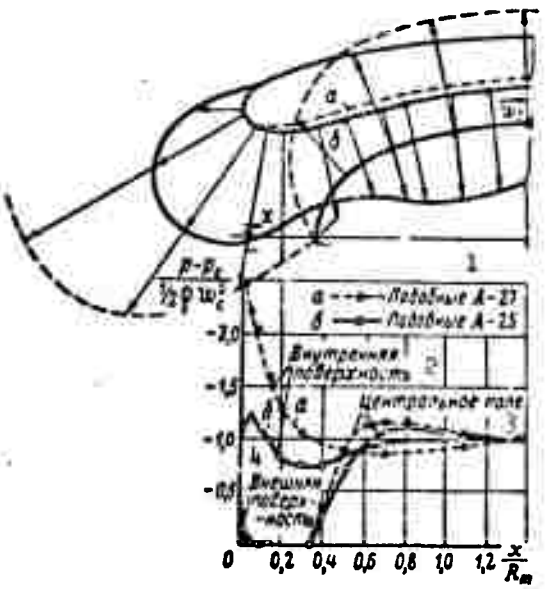


Fig. 8.2.6. Influence of the curvature of the inner contour on the pressure distribution on the leading edge during take-off. 1) Similar to; 2) inner surface; 3) central field; 4) outer surface.

the exit from the inner channel may be divergent ($w_1 < w_n$), convergent ($w_1 > w_n$) or parallel-sided ($w_1 = w_n$). The inner channel may have a round or oval cross section. At the exit it goes sometimes over to an annular cross section because of the necessity of placing a central body in the air intake (in order to mount the forward bearing of the compressor or of the engine assembly). In any case the nature of the flow for a given length of the inner channel is determined by the relative inlet $f_1 = A_n/A_1$.

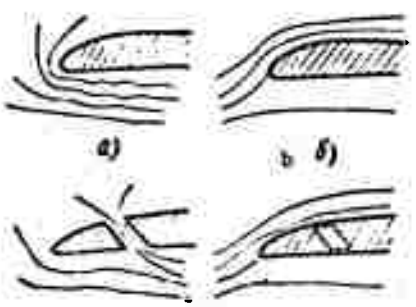


Fig. 8.2.7. Air intakes with slot during take-off (a) and during flight (b).

Applying the momentum equation to an air intake and allowing for the changes in shape of its inner channel (of the relative inlet f_1), we

can find the total thrust F of the air intake in a manner similar to that in which we determined the thrust of the inner surface (M = 0):

$$\frac{F}{\frac{1}{2}\rho w_\infty^2 A_1} = \left(1 - \frac{w_1}{w_\infty}\right)^2. \qquad (8.2.15)$$

The thrust F_N of the outer surface of the air intake as determined before, is equal to

$$\frac{F_N}{\frac{1}{2}\rho w_\infty^2 A_n} = \left(1 - \frac{w_n}{w_\infty}\right)^2$$

or

$$\frac{F_N}{\frac{1}{2}\rho w_\infty^2 A_n} = \frac{A_n}{A_1}\left(1 - \frac{A_1}{A_n}\frac{w_1}{w_\infty}\right)^2 = f_1\left(1 - \frac{1}{f_1}\frac{w_1}{w_\infty}\right)^2. \qquad (8.2.16)$$

The difference between the total thrust F of the air intake and F_N of its outer surface constitutes the thrust of the inner surface. The latter is equal to zero for an inner channel of constant area, $f_1 = 1$, negative for a convergent channel, $f_1 > 1$, and positive for a divergent channel, $f_1 < 1$.

The divergence of the inner channel is convenient from the point of view of design, since keeping the mass flow G, the total thrust F and the velocity ratio w_{max}/w_∞ at the outer surface unchanged makes it possible to raise the ratio w_n/w_∞ and therefore to reduce the midsectional area A_d of the air intake in accordance to Expression (8.2.6). The flow in divergent channels is, however, connected with the possibility of boundary layer separation and vortex formation, which may lead to additional energy losses. Details about this will be given in what follows.

Convergent channels have smaller energy losses than divergent ones, as can be seen from Fig. 8.2.8, which shows the loss coefficient curves. Convergent channels yield a more uniform flow at their ends but require a larger air intake midsection when the outer surface

possesses the optimum shape.

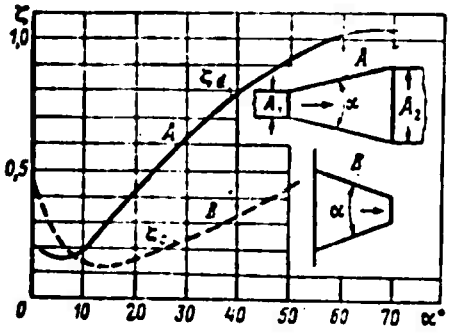


Fig. 8.2.8. Dependence of loss coefficient ζ for divergent and convergent channels on the vertex angle α.

For an inner channel of constant cross-sectional area $f_1 = 1$, containing a central body (positioned behind the middle cross section), we can take the surface of a stream tube as the inner surface to a first approximation, the central body being in an undisturbed parallel flow with the velocity w_n. The mass flow required must then take place. In the case of equal velocities at the channel entry and exit, $w_n = w_1$, the pressure will be nonuniformly distributed along a streamline. It will be higher in front of the central body where the flow is slowed down and lower at the surface of the central body where the flow is accelerated. Uniform pressure distribution can be achieved by correcting the streamlines.

In a subsonic flow in a diffusor the flow velocity decreases and the static pressure increases, i.e., the flow is decelerated in the presence of a positive pressure gradient.

This counterpressure may lead to separation of the boundary layer from the diffuser walls and to the production of vortices, which entails considerable energy losses, i.e., losses in total pressure (Fig. 8.2.9). The separation of the laminar or turbulent boundary layers occurs at the site where the kinetic energy of the flow is entirely consumed in overcoming the frictional forces. The position of the separation point depends on the initial velocity of the flow, on the pressure gradient and on the roughness of the surface. When the inlet velocity w_n is constant the separation point in a conical diffusor moves closer to the inlet as the positive pressure gradient

increases, i.e., as the divergence angle α of the diffusor increases. The upstream displacement of the separation point of the boundary layer, as the divergence angle α of the diffusor increases, leads to an extension of the vortex zone over a great part of the flow and hence to an increase in losses (cf. Fig. 8.2.9).

HIC NOT REPRODUCIBLE

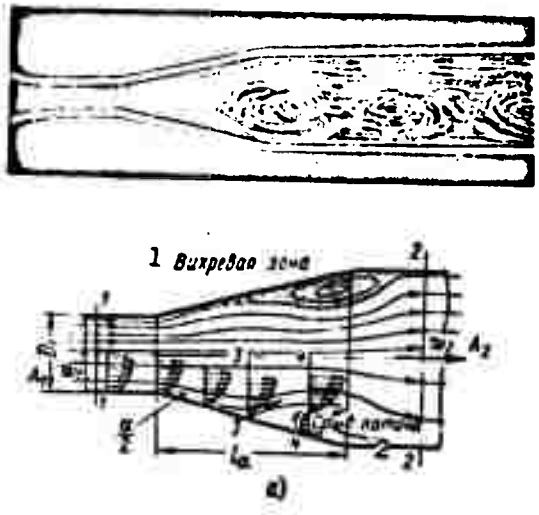


Fig. 8.2.9. Separation of the flow from the walls and vortex formation in a diffusor. 1) Vortex zone; 2) separation of flow.

When the relative inlet f_1 of a conical diffusor is kept constant, the losses due to vortex formation decrease but the frictional losses increase as the angle of divergence decreases, since the wetted surface then increases in area. The optimum angle of divergence for a conical diffusor is α_{opt} = 10-15°. We should notice that as the angle of divergence decreases the diffusor length increases and the gross weight of the air intake increases as well.

Ignoring the changes in density and the losses in a conical diffusor, we obtain from the Bernoulli equation

$$p - p_н = \frac{\rho}{2}(w_н^2 - w^2) = \frac{\rho w_н^2}{2}\left(1 - \frac{A_н^2}{A^2}\right) = \frac{\rho w_н^2}{2}\left(1 - \frac{d_н^4}{d^4}\right) =$$

$$= \frac{k p_n}{2} M_n^2 \left[1 - \frac{1}{\left(1 + 2 \frac{l}{d_n} (\operatorname{tg} \frac{\varphi}{2}) \right)^4} \right]. \qquad (8.2.17)$$

w, p, d denote here the velocity, pressure and diameter at the distance x from the inlet. In a conical diffusor (Fig. 8.2.10,a) the steep pressure increase in the first longitudinal sections of the diffusor may cause the boundary layer to separate early. In order to avoid this the channel walls can be profiled in such a way that the longitudinal gradient is a constant (cf. Fig. 8.1.10,b). In this case dp/dx = const and from the Bernoulli equation $\rho w\, dw + dp = 0$. neglecting the density variation, we obtain $w\, dw$ = const along a streamline, and hence

$$x = \frac{w_n^2 - w^2}{2c} = \frac{w_n^2}{2c}\left(1 - \frac{d_n^4}{d^4}\right), \quad \left(c = \frac{1}{\rho} \frac{dp}{dx}\right). \qquad (8.2.18)$$

The length corresponding to complete stagnation of the flow ($d \to \infty$) is equal to $w_n^2/2c$.

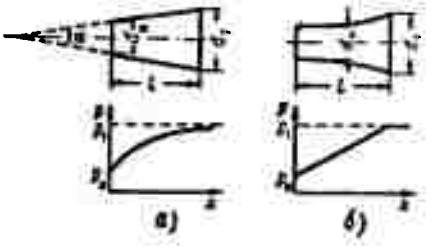


Fig. 8.2.10. Conical (a) and isogradient (b) diffusors.

The separation of the boundary layer sets in later in isogradient diffusors than in conical ones, and the energy losses in the former are therefore smaller (Fig. 8.2.11). The advantages of using isogradient diffusors instead of conical ones are particularly appearent for short channels with $l < 4d$.

The principal losses in the diffusor are the vortex losses. The frictional losses are relatively small and can often be neglected. The energy losses due to the vortices in the diffusor can be estimated from the losses arising on sudden expansion

$$\Delta p = \psi \Delta p_{удар} = \psi \rho \frac{(w_n - w_1)^2}{2}, \qquad (8.2.19)$$

where ψ is the shock moderation coefficient which, as was shown by

experiments with a conical diffusor, depends on the angle of divergence, α.

In the case of an angle of divergence $\alpha > 40°$ (Fig. 8.1.12) the vortex losses are greater ($\psi > 1$) than they are when expansion occurs suddenly. This is explained by the instability of the vortex zone, which is periodically washed downstream and consumes additional energy in being renewed. If the density variations in the diffusor are neglected, the loss coefficient ζ can be expressed in terms of the shock moderation coefficient ψ:

$$\zeta = \frac{2\Delta p}{\rho w_1^2} = \psi\left(\frac{A_1}{A_0} - 1\right)^2. \qquad (8.2.20)$$

The losses in the diffusor are sometimes conveniently estimated from the ratio between the isentropic work done by the gas when it is compressed from a pressure corresponding to the total inlet pressure, and the dynamic head in the inlet cross section. This <u>loss coefficient</u>

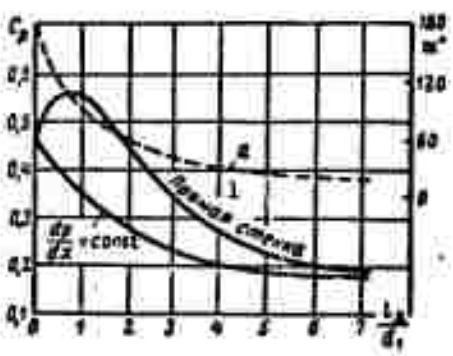


Fig. 8.2.11. Dependence of loss coefficient ζ on the length for straight and isogradient diffusors. 1) Straight wall.

$$\zeta_{sz} = \frac{L_{sz}}{\frac{w_0^2}{2}} = \frac{\frac{2k}{k-1} RT_{01}\left[\left(\frac{p_{0z}}{p_{01}}\right)^{\frac{k-1}{k}} - 1\right]}{\frac{w_0^2}{2}} \qquad (8.2.21)$$

makes it possible to estimate the influence of compressibility. On the basis of experimental data [8.3] (Fig. 8.2.13) the compressibility becomes apparent (ζ_{szh} increases) only when the velocities are nearsonic ($M > 0.7$). The changes of the loss coefficient ζ_{szh} for $M < 0.3$ are explained by the great influence of the Reynolds number.

In calculations on diffusors for nearsonic inlet velocities

($M_n > 0.7$), the compressibility of the flow therefore has to be taken into account. Figure 8.2.14 shows the results of testing conical diffusors over a wide range of subsonic velocities [8.3]. The diffusors tested were provided with a cylindrical inlet part before the diffusor, the length of which was equal to the diameter of the diffusor inlet opening. The dependence of the total pressure recovery coefficient ν_0 is determined as a function of the Mach number M_n at the beginning of the cylindrical part. The Mach number M_n' at the end of the cylindrical part is somewhat higher for nearsonic velocities (Fig. 8.2.15). The flow velocity reaches the velocity of sound right at the diffusor inlet, provided the Mach number M_n at the beginning of the cylindrical part is near 0.9. When the Mach number M_n at the beginning of the cylindrical part is further increased, the flow becomes supersonic in the first part of the diffusor and then goes over to subsonic speed via a normal shock. At the same time the pressure recovery coefficient suddenly drops.

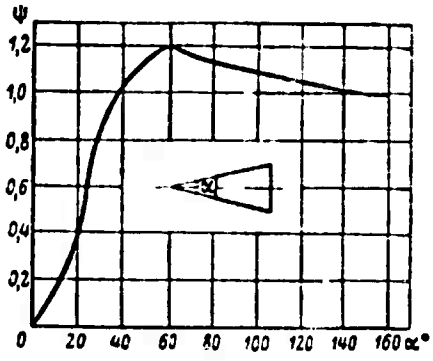


Fig. 8.2.12. Dependence of shock moderation coefficient ψ on the vertex angle α of a conical diffusor.

Supersonic air intakes. A peculiarity of the supersonic air intake is that the flow is slowed down by a shock. The transition from supersonic to subsonic flow velocities occurs in a normal compression shock, and at $M > 1.2$-1.5 it is accompanied by considerable losses in total pressure. As was shown by G.I. Petrov and Ye. P. Ukhov it is convenient when dealing with flight at high Mach numbers M to pre-decelerate the supersonic flow in diagonal compression shocks (Fig. 8.2.16), since the energy losses are then smaller. The total pressure recovery coef-

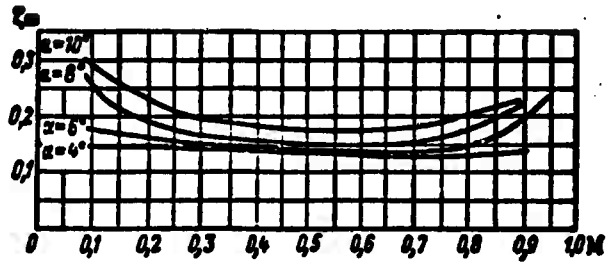


Fig. 8.2.13. Dependence of loss coefficient ζ on the Mach number M at the inlet of a conical diffusor for various vertex angles.

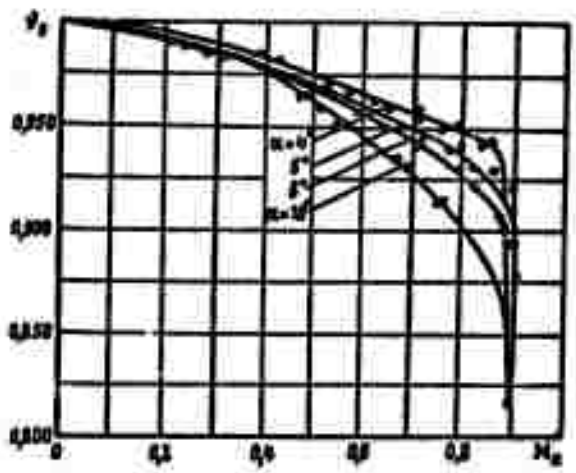


Fig. 8.2.14. Dependence of the total pressure recovery coefficient ν_0 on the Mach number M_n at the beginning of the cylindrical part at the inlet of the conical diffusor for various vertex angles.

ficient ν_0 for the system of shocks (one or several diagonal shocks plus one final normal shock) is in this case larger than it is when there is a single normal shock instead of the system (Fig. 8.2.17). The supersonic flow is decelerated on the outer surfaces of the air intake (wedge, cone) arranged in front of its inlet, and also inside the air intake by specially shaped inner surfaces. Notice that when a supersonic flow is decelerated the number of diagonal shocks is de-

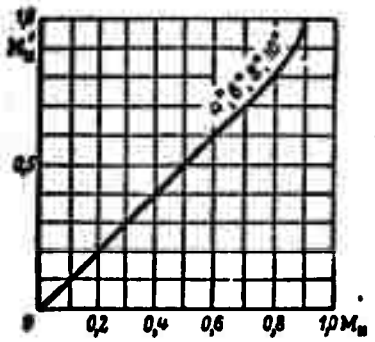


Fig. 8.2.15. Dependence of the Mach number M_n' right at the inlet of a conical diffusor on the Mach number M_n at the beginning of the cylindrical part.

termined by the number of breaks of the surface on which deceleration occurs. In the case of infinitely many breaks and, therefore, an infinite number of infinitely weak diagonal compression shocks it is theoretically possible to obtain isentropic deceleration of the flow with smooth surface contours.

In supersonic flight the velocity behind a normal shock remains high as compared with the required velocity at the exit of the air intake. The inner channel must effect further subsonic recovery and is therefore made divergent ($f_1 > 1$). A supersonic air intake achieves deceleration of both supersonic and subsonic flows and is often called a diffusor. Depending on the number of shocks in which a supersonic flow is slowed down stepwise, we distinguish between the single-shock diffusor, simply called a diffusor, and the two- or multi-shock diffusors.

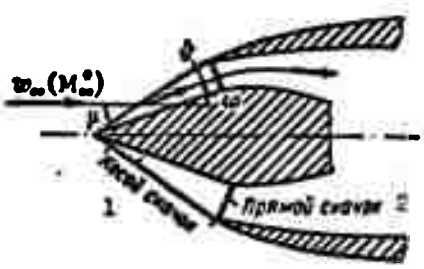


Fig. 8.2.16. Air intake with two shocks, the first being diagonal and the second normal. 1) Diagonal shock; 2) normal shock.

The leading edges of the supersonic air intake, unlike those of the subsonic air intake, are made sharp in order to reduce the drag. Flow about thick edges at supersonic speeds entails the appearance of detached additional shocks in front of the edges, which raises the external drag. During starting, however, the sharp edges of supersonic air intakes lead to great losses in total pressure of the air flow due to separation of the

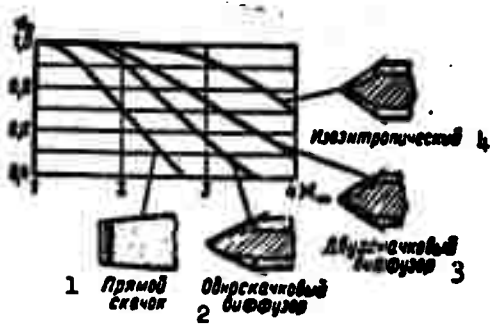


Fig. 8.2.17. Total pressure recovery coefficient in dependence on the number of shocks and the Mach number of the incoming flow. 1) Normal shock; 2) single-shock diffusor; 3) two-shock diffusor; 4) isentropic diffusor.

subsonic flow as it streams about the sharp edges.

Additional drag. When the streamtube in front of the air intake is cylindrical, i.e., when the mass flow coefficient $\varphi = 1$, there is no additional drag; it increases as the coefficient φ decreases.

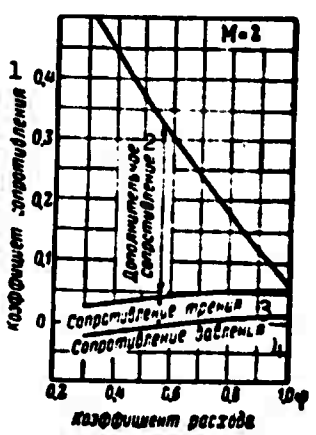


Fig. 8.2.18. Dependence of the coefficients of pressure drag, friction and additional drag on the mass flow coefficient for an engine model with $M_\infty = 2$. 1) Drag coefficient; 2) additional drag; 3) frictional drag; 4) pressure drag.

For a subsonic air intake in this case the additional drag arising when φ decreases is small and, as we have shown, it is compensated by an additional thrust on the outer surface owing to increased rarefaction on it.

For a supersonic air intake the additional drag increases rapidly as φ decreases and is not compensated by a rarefaction on the outer surface. This is explained by the flow about the outer surface of the air intake being preliminarily decelerated in the normal compression shock in front of the air intake, and, having become subsonic, being unable to cause appreciable rarefaction. This is also why

the frictional forces vary but slightly when φ varies. The change in additional drag is however great, since the pressure excess $p-p_\infty$ acting on the outer surface of the internal flow in front of the air intake and behind the normal compression shock is appreciable (Fig. 8.2.18).

If the mass flow $\underline{m}$ of the engine is given, the area A_∞ of the undisturbed stream tube can be calculated from the relation

$$m=\rho_\infty w_\infty A_\infty=\frac{kp_\infty}{a_\infty}M_\infty A_\infty\sqrt{1+\frac{k-1}{2}M_\infty^2}=$$
$$=\frac{kp_{0\infty}}{\sqrt{kRT_{0\infty}}}\frac{M_\infty A_\infty}{\left(1+\frac{k-1}{2}M_\infty^2\right)^{\frac{k+1}{2(k-1)}}}. \qquad (8.2.22)$$

The total pressure $\hat{p}_0$, the static pressure $\hat{p}$ and the Mach number $\hat{M}$ right behind the normal shock wave are calculated from the well known Eq. (4.3.8).

If the flow between the normal shock wave and the inlet is assumed to be isentropic, we obtain the Mach number M_n at the inlet of the air intake from the relation

$$\frac{\hat{M}}{\left(1+\frac{k-1}{2}\hat{M}^2\right)^{\frac{k+1}{2(k-1)}}}=\varphi\frac{M_\infty}{\left(1+\frac{k-1}{2}M_\infty^2\right)^{\frac{k+1}{2(k-1)}}}. \qquad (8.2.23)$$

The static pressure at the inlet is

$$p_n=\frac{\hat{p}_0}{\left(1+\frac{k-1}{2}M_n^2\right)^{\frac{k}{k-1}}}. \qquad (8.2.24)$$

The additional drag can be determined from the given parameters of the internal flow in the inlet section of the air intake as the difference of the momenta of the internal flow in this section and in a section of undisturbed flow:

$$X_A=(p_n-p_\infty)A_n+kp_nA_nM_n^2-kp_\infty A_nM_n^2. \qquad (8.2.25)$$

Figure 8.2.18 shows experimental graphs of the drag components

for one air intake at M = 2 in dependence of φ [8.16].

Single-shock air intake. If a subsonic air intake with a divergent inner channel is made with sharp edges and a conical outer surface it may be used at relatively low supersonic flying speeds ($M_\infty < 2$) with satisfactory results. The transition from supersonic flow velocities occurs in this case through one (normal) compression shock, and this is why such an air intake is called single-shock air intake. The position of the shock depends on the operational conditions of the air intake, i.e., on the mass flow coefficient φ. If the mass flow coefficient φ > 1, the normal compression shock arises in front of the air intake (Fig. 8.2.20,a). In this case the shock front lies normal to the internal flow, since its velocity has the same direction on both sides of the shock and it has a curved surface for the flow about the outer surface where the velocity changes its direction immediately behind the compression shock. The subsonic internal flow is slowed down partly in front of the air intake and partly within it. The external subsonic recovery occurs virtually without losses and leads to a reduction in frictional losses in the air intake, which is due to a reduction in inlet velocity; the total pressure recovery coefficient will therefore be high for the subsonic flow, which exerts a positive effect on the specific thrust of the engine.

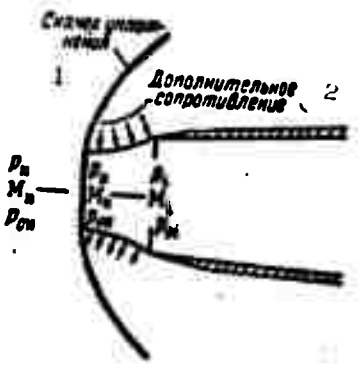


Fig. 8.2.19. For calculating the additional drag. 1) Compression shock; 2) additional shock.

These operational conditions (φ < 1) of the air intake are however connected with the appearance of a large additional drag, which in turn reduces the effective thrust of the engine. It should be borne in mind that when the specific thrust is high, the total thrust drops

as the air mass flow decreases.

The case when the outer drag is zero ($\varphi = 1$, $X_d = 0$) can be taken as the rated (critical) conditions of operation of a single-shock air intake. To the rated regime corresponds maximum air mass flow

$$m_{max} = \frac{G_{max}}{g} = \rho_\infty w_\infty A_\infty.$$

The normal shock is placed immediately at the inlet of the air intake and the external supersonic flow is decelerated by a diagonal compression shock. The latter occurs when the supersonic flow is deflected by the conical outer surface of the air intake. The external drag of the oblique lip of the air intake is minimum under rated conditions.

It proves impossible to raise the true mass flow further since there are no types of disturbances inside the engine which could bring the supersonic flow in front of the air intake. The increase of the reduced mass flow $G(T_1/p_1)^{1/2}$ that is caused by the drop of the pressure p_1 at the exit may, however, lead to an acceleration of the supersonic flow entering the air intake. The transition from supersonic to subsonic flow inside the air intake (cf. Fig. 8.2.20,c) is accompanied by a normal compression shock which is stronger than that under rated conditions, and it is common knowledge that this leads to a decrease in total pressure and to a decrease in the effective thrust of the engine, the latter being due to the drop in total thrust, which occurs when the minimum external drag and the maximum flow rate remain constant.

The total pressure recovery coefficient ν_0 for a single-shock air intake is determined by the product of the total pressure recovery coefficient ν_{0p} of the normal shock and the total pressure recovery

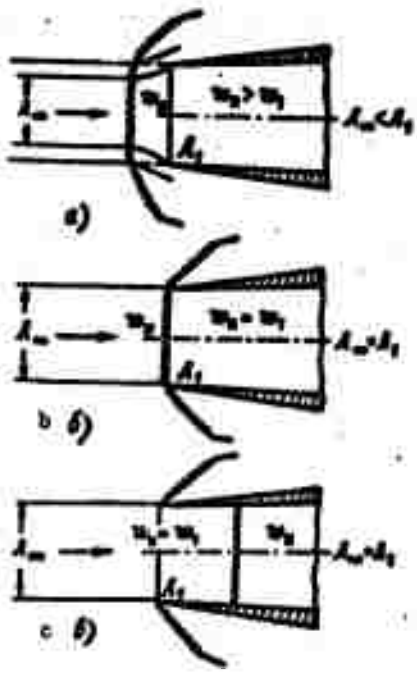


Fig. 8.2.20. Various operational conditions of single-shock air intake.

coefficient ν_{0d} of the inner channel (diffusor);

$$\nu_0 = \nu_{0d} \cdot \nu_{0s} = M_\infty^2 \left[\frac{1 - \frac{k-1}{k+1} M_\infty^2}{1 - \frac{k-1}{k+1} \frac{1}{M_\infty^2}} \right]^{\frac{1}{k-1}} \nu_{0s}. \quad (8.2.26)$$

The parameters of the flow immediately behind the normal compression shock (velocity, static and total pressure, temperature) are determined from the well known relations for normal shock (4.3.8).

The flow inside a single-shock air intake is taken to be adiabatic and calculations are made on it in the same way as in the case of a subsonic air intake.

The additional drag of an air intake at off-design operational conditions ($\varphi < 1$) is determined from Eq. (8.2.25).

The external drag of the oblique lips of the air intake can be determined from the given pressure distribution behind a diagonal compression shock on the outer surface of the cone.

Multi-shock air intakes. Let us consider a plane two-shock air intake (Fig. 8.2.21,IIa) in which the supersonic flow is preliminarily decelerated in a diagonal compression shock – at the wedge – and then goes over to subsonic flow in a normal compression shock right at the inlet. The front of the diagonal shock includes the angle μ with the direction of the undisturbed flow (μ is called the angle of the diagonal shock). This is then a two-shock air intake. Figure

8.2.21 shows various diagrams of three- and four-shock air intakes; the behavior of such shock systems is determined by the number and the relative position of the breaks on the central body and on the inner surface of the air intake.

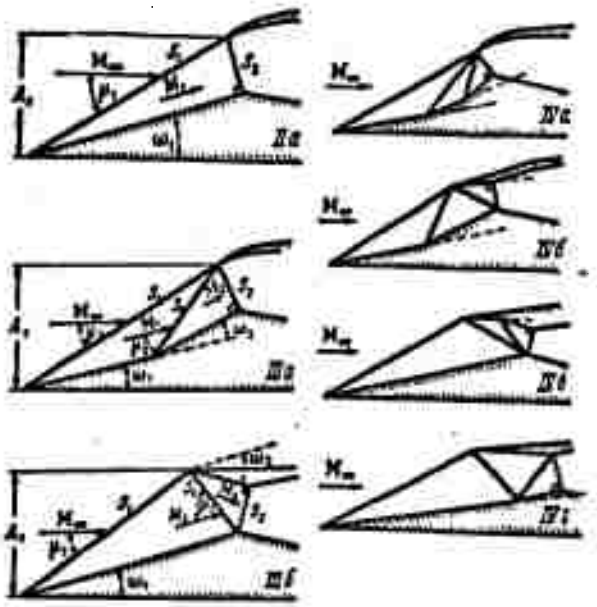


Fig. 8.2.21. Diagrams of multi-shock air intakes.

In order to prevent the wedge from affecting the external flow, the shock front must touch the leading edge of the air intake. Making use of the relations determined before which link the parameters of the flow behind the diagonal compression shock, we find for a two-shock air intake:

$$M_1^{*2} = M_\infty^{*2}\cos^2\mu + \frac{\left(1-\frac{k-1}{k+1}M_\infty^{*2}\cos^2\mu\right)^2}{M_\infty^{*2}\sin^2\mu}; \qquad (8.2.27)$$

$$\frac{p_1}{p_\infty} = \frac{M_\infty^{*2}\left[1-\frac{4k}{(k+1)^2}\cos^2\mu\right]-\frac{k-1}{k+1}}{1-\frac{k-1}{k+1}M_\infty^{*2}}; \qquad (8.2.28)$$

$$\sigma_{\text{вх}} = \frac{p_{01}}{p_{0\infty}} = \frac{p_{01}}{p_1}\cdot\frac{p_1}{p_\infty}\cdot\frac{p_\infty}{p_{0\infty}} = \frac{p_1}{p_\infty}\left(\frac{1-\frac{k-1}{k+1}M_\infty^{*2}}{1-\frac{k-1}{k+1}M_1^{*2}}\right)^{\frac{k}{k-1}}. \qquad (8.2.29)$$

The pressure change in a normal shock may be determined from the given value of the Mach number M_2^* in front of the normal shock, using the well known relation

$$\frac{p_2}{p_1} = \frac{M_1^{*2} - \frac{k-1}{k+1}}{1 - \frac{k-1}{k+1} M_1^{*2}}; \quad \nu_{0s} = \frac{p_{02}}{p_{01}} = M_1^{*2} \left(\frac{1 - \frac{k-1}{k+1} M_1^{*2}}{1 - \frac{k-1}{k+1} \frac{1}{M_1^{*2}}} \right)^{\frac{1}{k-1}}$$

The total pressure recovery coefficient ν_{0s} of the system of (two) shocks is determined by the relation

$$\nu_{0s} = \nu_{01} \nu_{02}.$$

The pressure recovery coefficient ν_0 for the whole air intake is equal to

$$\nu_0 = \nu_{0s} \nu_{0d} = \nu_{01} \nu_{02} \nu_{0d}. \qquad (8.2.30)$$

where ν_{0d} is the pressure recovery coefficient for the inner channel, where the flow is subsonic.

The maximum recovery coefficient ν_{0s} of the shock system corresponds to the optimum angle μ_{opt} of the diagonal shock and hence to the optimum angle ω of the wedge for given M_∞ of the flight, (Fig. 8.2.22).

At small angles (in the region to the left of the dashed line A) the diagonal shock is replaced by a weak wave and the deceleration of the flow occurs principally in the normal compression shock; at large angles μ (in the region to the right of the dashed line B) the diagonal shock transforms the supersonic velocity to a subsonic one directly. The deceleration in such a strong diagonal shock is insignificant, since the energy losse in it differ only slightly from the losses in a normal shock and the higher velocity behind the diagonal shock leads to an increase in frictional losses in the inner channel.

It follows from the graphs that replacing a single-shock air intake ($\mu = 90°$) by a two-shock air intake raises the total pressure

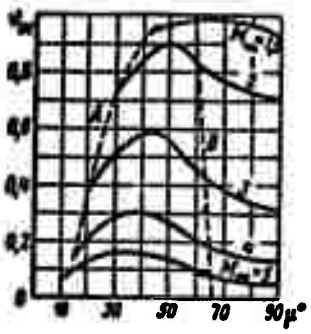


Fig. 8.2.22. Dependence of total pressure recovery coefficient for a system of two shocks (diagonal + normal) on the angle of the diagonal shock.

recovery coefficient by 27% at $M_\infty = 2$ and by 70% at $M_\infty = 3$. The gain in pressure recovery of a two-shock air intake compared with a single-shock air intake is therefore particularly appreciable at supersonic velocities when $M \geq 2$.

Let us notice that the optimum angle of diagonal shock determined in order to obtain a maximum static pressure recovery coefficient,

$$\nu = \frac{p_2}{p_{0\infty}} = \frac{p_2}{p_1}\frac{p_1}{p_0}\frac{p_0}{p_{0\infty}}$$

is somewhat smaller than the optimum angle of diagonal shock determined from the condition that the total pressure recovery coefficient (Fig. 8.2.23) should be a maximum.

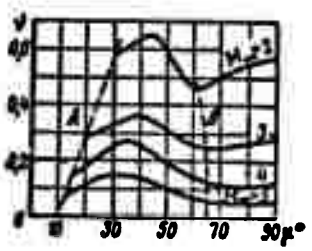


Fig. 8.2.23. Dependence of the static pressure recovery coefficient for a system of two shocks (diagonal + normal) on the angle of the diagonal shock.

In the case of an axisymmetric round air intake the wedge used to produce the diagonal shock is replaced by a cone. Under symmetrical flow conditions a compression shock with conical front is set up in front of the cone. The vertex of the cone and the front of the compression shock virtually coincide. The main distinctive feature of the symmetric flow about the cone is that the streamlines behind the diagonal shock do not remain parallel to the cone surface but behave as if they were pressed towards it. This follows from the flow conditions for a conical surface. The angle of deflection of the flow grows continuously from its minimum value immediately behind the diagonal shock, and approaches

the semiangle ω_{kon} of the cone asymptotically (Fig. 8,2.24). In order to ensure that the diagonal shock angle μ remains the same in the semi-angle ω_{kon} of the cone must exceed the angle ω_{kl} of the wedge. In other words, when $\omega_{kon} = \omega_{kl}$ the cone decelerated the flow less ($\mu_{kon} = \mu_{kl}$).

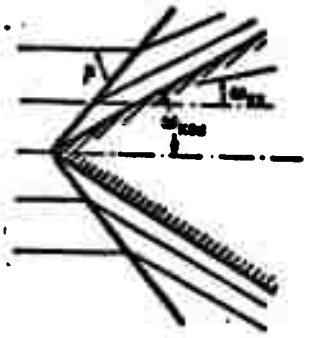


Fig. 8.2.24. Diagram of supersonic flow about a cone.

By way of approximation it can be assumed that for the diagonal shock angles to be equal, $\mu_{kon} = \mu_{kl}$, the Mach numbers behind the diagonal shock must be equal for wedge and cone. It is then possible to reduce the calculation of an axisymmetric air intake to that of a plane air intake. The vertex angle of the cone, $2\omega_{kon}$, can be determined from the wedge angle $2\omega_{kl}$ with the help of the graph shown in Fig. 8.2.25.

Optimum compression shock system. Let us follow G.I. Petrov and Ye. P. Ukhov in considering a supersonic flow near a wall (Fig. 8.2.26) whose contour is represented by a broken line. At the i-th corner a diagonal shock arises with the Mach number M_i^* in front of it. Let the Mach number of the flow streaming against the wall be M_1^* and the total pressure p_{01}, let the flow pass through (m-1) diagonal shocks and let the last, m-th shock be a normal one. If the angles of deflection of the velocity, $\omega_1, \omega_2, \ldots, \omega_m$ are given, then, making use of the diagonal shock diagram (cf. Appendix 8) representing Relations (5.9.13), (5.9.14) and (5.9.16) graphically, we may find the shock angle μ_i and the Mach number M_{i+1}^* behind the shock [8.4].

In order to determine the total head drop for a diagonal shock, we take into account that $T_{01} = T_{02}$ and write down

$$\frac{p_{02}}{p_{01}} = \frac{p_{02}T_{02}}{p_0T_{01}} = \frac{p_{02}}{p_2}\frac{p_2}{p_1}\frac{p_1}{p_{01}} =$$

$$= \left(\frac{T_{02}}{T_2}\right)^{\frac{1}{k-1}}\frac{p_2}{p_1}\left(\frac{T_1}{T_{01}}\right)^{\frac{1}{k-1}} = \left(\frac{T_1}{T_2}\right)^{\frac{1}{k-1}}\frac{p_2}{p_1} = \left(\frac{p_1}{p_2}\right)^{\frac{1}{k-1}}\left(\frac{p_2}{p_1}\right)^{\frac{k}{k-1}}.$$

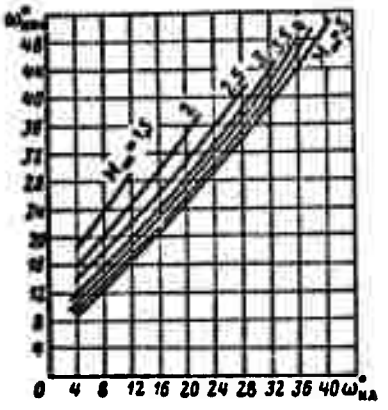


Fig. 8.2.25. Dependence of the semiangle of the cone vertex on the angle of deflection of the flow in the shock (from the wedge angle) for various flow speeds.

Thus

$$\frac{p_{01+1}}{p_{01}} = \left\{\frac{1-\frac{k-1}{k+1}M_i^{*2}}{M_i^{*2}\left[1-\frac{4k}{(k-1)^2}\cos^2\mu_i\right]-\frac{k-1}{k+1}}\right\}^{\frac{1}{k-1}} \times$$

$$\times\left[\frac{M_i^{*2}\sin^2\mu_i}{1-\frac{k-1}{k+1}M_i^{*2}\cos^2\mu_i}\right]^{\frac{k}{k-1}}. \qquad (8.2.31)$$

This relation is represented graphically in Fig. 8.2.27, in dependence on the angle of deflection ω_1 of the flow and on the velocity of the incoming stream, M_1^*.

The total pressure recovery coefficient after the passage of all m shocks will be

$$\sigma_0 = \frac{p_{0m+1}}{p_{01}} = \frac{p_{0m+1}}{p_{0m}}\cdot\frac{p_{0m}}{p_{0m-1}}\cdots\frac{p_{02}}{p_{01}}. \qquad (8.2.32)$$

A system of m shocks, the last of which is a normal shock, for which the total pressure recovery coefficient is a maximum for a given value of M_1^* will be called the optimum system.

It can be shown that for a given system of (m-1) diagonal shocks and one normal shock this will be the case when the entropy jumps arising are equal in all the diagonal shocks, or, what comes to the same thing, if the pressure recovery coefficients for each diagonal shock passing through have the same value, namely

$$\frac{p_{0i+1}}{p_{0i}} = \frac{p_{02}}{p_{01}}.$$

Without going into details as to the solution and investigation of optimum shock systems, we give in Fig. 8.2.28 the results of cal-

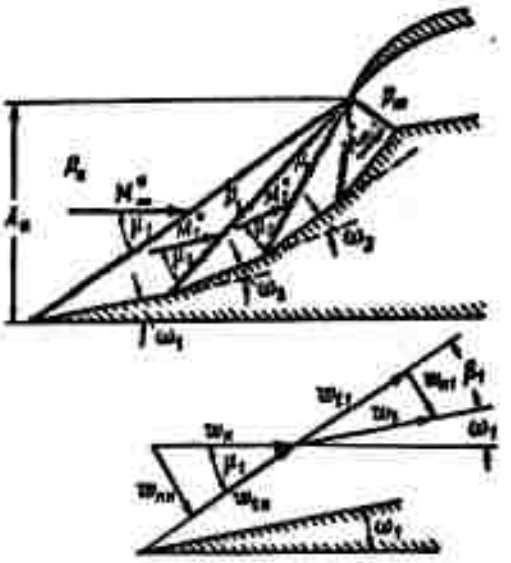


Fig. 8.2.26. For calculating the optimum system of plane compression shocks.

culating the maximum pressure recovery coefficient in dependence on the number of the (m-1) diagonal shocks and the final normal shock. It can be seen from the graphs that the pressure recovery coefficient increases rapidly at large M_1^* as the number of shocks increases.

We can use the same method to solve the problem of the transition of m diagonal shocks when the parameters of the last shock are given. In particular, if we adopt the condition that the flow velocity behind the last, m-th diagonal shock must be equal to the velocity of sound we find that the maximum recovery coefficient will have the highest value; the solution for such a system is represented in Fig. 8.2.29.

It can be shown that systems which are optimum as to the total pressure, are optimum with respect to the static pressure as well.

The profiling of the wedge is based on the condition that the plane of all compression shocks must intersect at a single point on the leading edge of the diffusor.

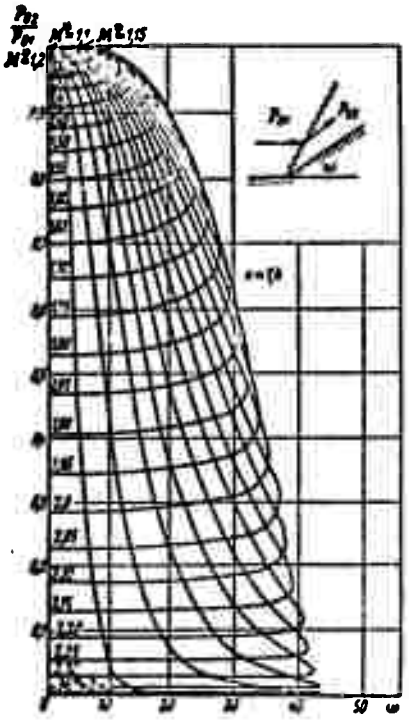


Fig. 8.2.27. Maximum total pressure recovery coefficient ν_0 as a function of the number m of plane shocks and the number M_∞^* of the incoming flow.

The dimensions of the diffusor throat are chosen according to the design parameters of this section and the given flow rate G.

Air intake characteristics. Let us consider the throttle characteristics of air intakes, i.e., the dependence of the basic parameters on the standard air mass flow $G_v(T_1)^{1/2}/p_1$ when the Mach number M of the flight is constant. The standard mass flow will in this case be proportional to the minimum cross-sectional area of the throttle in the air intake. For a ram-jet engine the nozzle serves as the throttle and for a turbo-jet engine the engine itself. The design conditions demand that the minimum cross sectional area of the throttle be so chosen that the final normal shock is positioned at the narrowest cross section of the air intake, i.e., at its leading edges (critical state, Fig. 8.2.30,b). In this case the thrust will be at its highest, since the total pressure recovery obtained is at its best and the external drag is minimum because the stream entering the air intake is cylindrical as a whole and there is no additional drag. Operation under critical conditions therefore corresponds to maximum effective thrust of the engine.

As the minimum cross-sectional area of the throttle increases, the standard mass flow surpasses the critical value. Under these transcritical conditions the final normal shock is shifted behind the

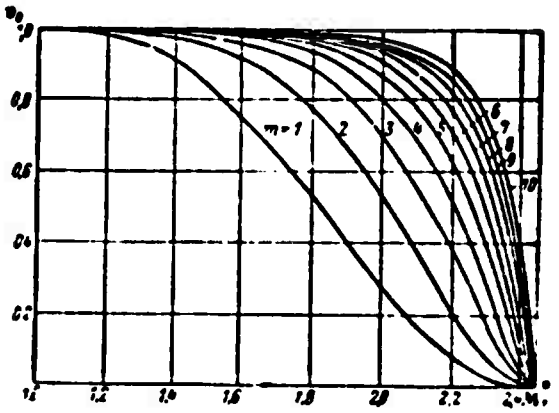


Fig. 8.2.28. Maximum static pressure recovery coefficient ν as a function of M_∞^* of the incoming flow in dependence on the number of shocks, m.

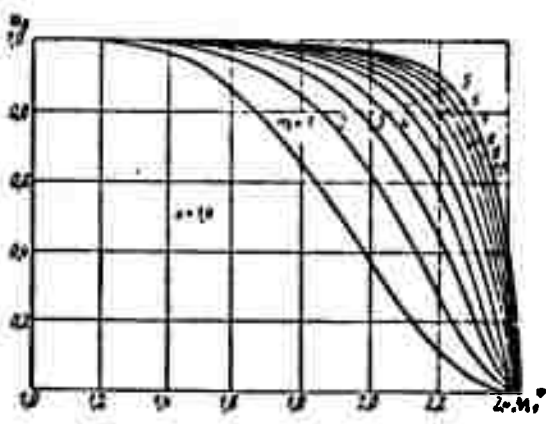


Fig. 8.2.29. Dependence of optimum total pressure recovery coefficient on M_∞ of the incoming flow for various shock systems.

minimum cross section into the air intake and becomes more powerful; the total pressure recovery coefficient then drops. In fact the air mass flow remains unchanged, but owing to the drop of pressure p_1 the standard mass flow increases. The external drag remains minimum but the effective thrust is lowered because of the lower pressure recovery coefficient.

When the minimum cross sectional area of the throttle is re-

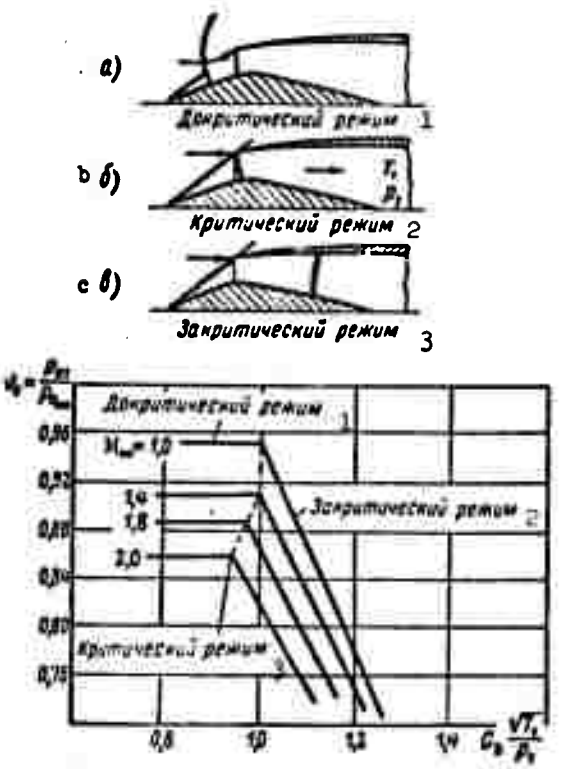


Fig. 8.2.30. Throttle characteristics of a typical two-shock air intake. 1) Subcritical state; 2) critical state; 3) transcritical state.

duced the mass flow through the air intake drops below the critical value (subcritical state). In this case a detached compression shock arises from a site in front of the leading edges of the air intake. Since the true air mass flow decreases, the part of the flow that enters the air intake carries it along downstream after it has passed through the normal detached shock.

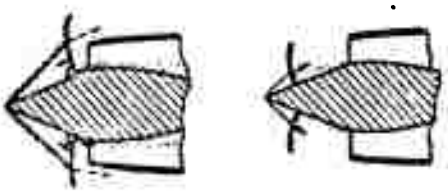


Fig. 8.2.31. For explaining the surge of the air intake.

We already know that such a flow is connected with the appearance of a considerable additional drag. Besides this, the detached shock leads to an extension of the system of diagonal compression shocks which

exerts an adverse influence on the total pressure recovery.

The subcritical state is sometimes accompanied by a significant pulsation of the flow (which is termed the surge of the air intake). An example of the causes of the appearance of surges is afforded by boundary layer separation on the cone surface (Fig. 8.2.31) or on the lips. A separated boundary layer diminishes the effective area of the minimum cross section of the air intake and this exercises an adverse effect on the total pressure recovery in the subsonic part of the air intake. At the same time the outlet pressure p_1 decreases. The position of the throttle remains unchanged, and in order to keep the standard mass flow constant the true air mass flow must be decreased as well. This causes the compression shock to be shifted upstream, which in turn yields favorable conditions for the boundary layer to be pressed against the surface. This raises the effective area of the minimum cross section, the flow passes through the subsonic part of the air intake with smaller losses, the pressure p_1 at the outlet grows, the true air mass flow rises, and this leads to the compression shock moving downstream. The downstream displacement of the attached shock gives rise to a new separation of the boundary layer and the process is repeated.

The surge of the air intake may be caused by slight oscillations of the pressure and of the air mass flow at the exit. Such oscillations occur in the operation of a turbo-jet engine.

Similar behavior is observed in the case of the slight pressure and mass flow oscillations which may accompany the operation of a turbo-jet engine, since arbitrary disturbances at the outlet of the air intake travel upstream in the subsonic flow and affect the position of the normal shock.

It follows from the two-shock air intake throttle characteristics

considered (cf. 8.2.30) that as M_∞ of the flight decreases they are shifted to higher values of the total pressure recovery coefficient.

The dashed line connecting the critical points represents the dependence of the critical mass flow on the number M_∞ of the flight (velocity characteristics of the critical flow) and characterizes the coordination of air intake and engine. For the two-shock air intake considered the critical mass flow increases as the Mach number M of the flight decreases.

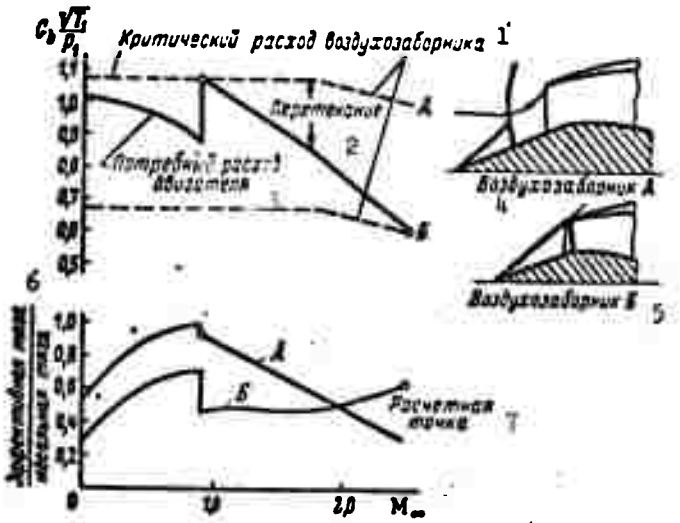


Fig. 8.2.32. Air intake characteristics for various design conditions. 1) Critical Mass flow of air intake; 2) excessive flow; 3) mass flow consumed by engine; 4) air intake A; 5) air intake B; 6) effective thrust/ideal thrust; 7) reference point.

The air mass flow consumed by a typical turbo-jet engine (velocity characteristic of the engine) does not coincide with the critical mass flow of the air intake (velocity characteristic of the critical mass flow of the air intake) in all flying speed ranges. It is therefore impossible to select an air intake which would separate under critical conditions in all flying speed ranges.

By way of example, the solid lines in Fig. 8.2.32 show the change in air mass flow consumed by a typical turbo-jet engine in

dependence on the Mach number M of the flight, while the dashed lines show the change in the critical mass flows of two air intakes, A and B. It is assumed that under cruising flight conditions at M = 0.9 the flying altitude varies from sea level up to 10,500 m. The break in the curve of consumed air mass flow at M = 0.9 corresponds to climb.

The design conditions for the air intake A are the conditions of cruiser flight at M = 0.9, and for the smaller air intake B they are the conditions of maximum velocity with M = 2.5.

The lower graph shows the change in the effective thrust of the engine divided by the ideal thrust, i.e., the thrust obtained with total pressure recovery, as a function of the flying speed M for the air intakes A and B.

The effective thrust of the air intake A assumes a high value design condition but drops rapidly as the flying speed decreases, because an additional drag arises under subcritical conditions. At subsonic flying speeds the mass flow for which a choking effect arises in the air intake is considered to be critical. For the air intake A the critical mass flow exceeds the consumed air mass flow in the engine. The decrease in effective thrust at velocities below the design velocity is due to the large losses in total pressure in the flow about the sharp edges. The lower the flying speed, i.e., the larger the ratio of the velocity in the throat of the air intake to the velocity of the undisturbed flow, the greater are the losses in total pressure at the inlet. This fact explains the low value of the thrust at the intake.

The air intake B possesses a high thrust at the reference point M = 2.5. At lower velocities it will operate in the transcritical state and its thrust will drop as M decreases, due to the low pressure

recovery. During flight this air intake is totally incapable of producing the thrust required.

Air intake control. In order to obtain correspondence between the velocity characteristics of air intake and engine, and also to prevent the air intake from surging, the air intakes are subjected to control. The control has to ensure that the diagonal and normal compression shocks assume the positions necessary to produce optimum values of the effective thrust of the engine and stable operation under all flight conditions.

Control may be achieved with the help of an air bypass behind the leading edges of the air intake, high-lift leading edges, or a change in geometry or in position of the stagnation surfaces, etc.

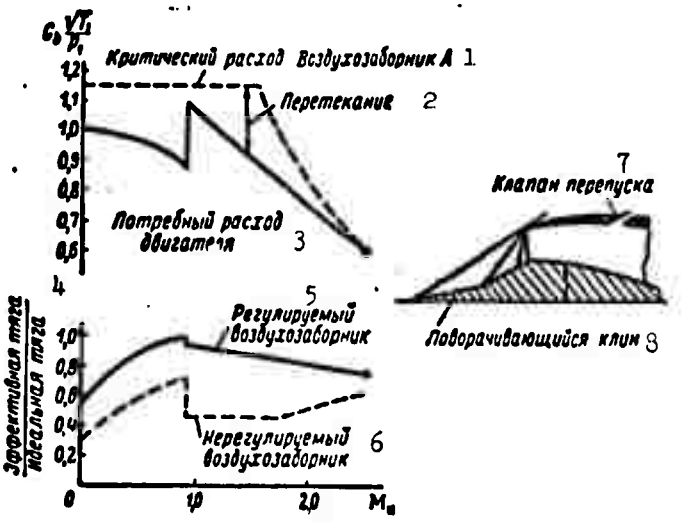


Fig. 8.2.33. Control effects on the air intake characteristics. 1) Critical flow of air intake A; 2) excessive flow; 3) air flow consumed by engine; 4) effective thrust/ideal thrust; 5) controlled air intake; 6) noncontrolled air intake; 7) by-pass valve; 8)

Figure 8.2.33 depicts the change in effective thrust of the engine as a function of the Mach number M of flight for controlled and noncontrolled air intakes. In the given example, when the flying speed drops below the design speed, control is achieved first by

turning the wedge until the forward face lies parallel to the flow, and then by letting the air pass through special by-pass valves. At subsonic flying speeds the by-pass is closed so as to reduce the input losses by lowering the relative velocities at the input. The thrust during flight is then low, however. It can be considerably raised if the by-pass valve is opened upwards, i.e., if it is made operate as an additional air intake.

The flying characteristics of air intakes can be significantly improved with the help of high-lift leading edges. During flight the air intake must have round leading edges to prevent the flow from separating. As the velocity increases, the round edges must be replaced by sharp edges in order to reduce the total drag.

To prevent the air intake from surging, a cylindrical ring whose diameter exceeds the diameter of the inlet lip can be mounted in front of the air intake (Fig. 8.2.34). Such a ring raises the frictional drag under normal flight conditions only slightly and has no influence on the operation of the inlet channel.

In cases of possible surging under subcritical conditions the operation of a many-shock air intake system goes over to steady operational conditions with a single shock in front of the ring. In this case the pressure recovery coefficient drops. The surplus air which cannot pass through the engine is led off through an axial gap between lip and ring. The higher the Mach number M of flight, the wider this gap must be opened to obtain optimum results.

With an annular air intake the position of the diagonal shocks may be controlled by displacing the cone axially or by changing its geometry, and the position of the normal shock by an air by-pass. In order to obtain optimum results both control systems must be coordinated.

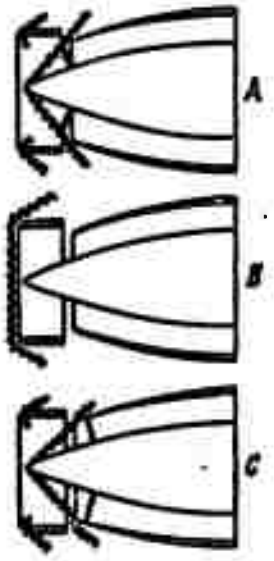


Fig. 8.2.34. Schematic diagrams of anti-surge arrangements in the form of a cylindrical ring in front of the air intake.

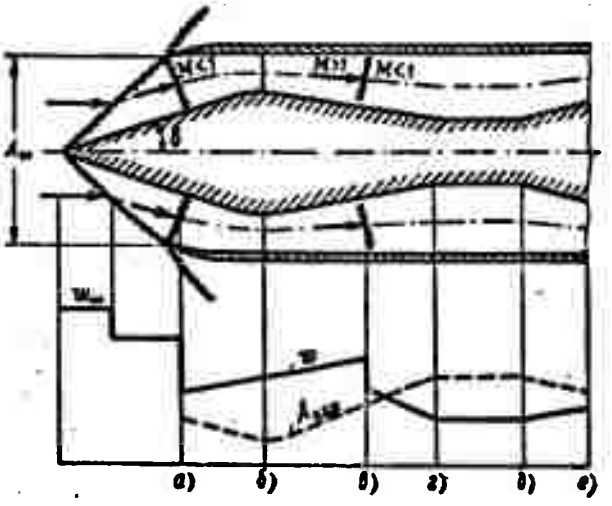


Fig. 8.2.35. Air intake with supersonic flow in the inner channel.

The compression shock system in front of the air intake can be made insensitive to pressure and mass flow oscillations in the engine by accelerating the subsonic flow behind the leading edges in a Laval nozzle to make it supersonic and by allowing the secondary deceleration of the flow to occur in a normal compression shock (Fig. 8.2.35). In this case the disturbances cannot penetrate the supersonic zone. They will influence only the position of the second normal compression shock.

8.3. COWLINGS

The thin cowling. The air intakes considered in the foregoing part may be considered as semi-infinite cowlings. Let us now consider a cowling of finite length and small thickness and curvature, when the acceleration arising on its outer surface is small. Let us assume that at a certain distance from the inlet the velocity on the cowling surface can be taken as approximately equal to the velocity w_∞ of the undisturbed flow. The flow about the forward part of the cowling, of

the air intake, (amounting to 2-3 maximum diameters) is assumed to be known.

Let us first consider the flow about the rear part of the cowling alone. As we have said already, the flow about the rear part of a sufficiently long and thin cowling does not depend on the flow about the forward part (cf. Fig. 8.1.11). We can therefore calculate the flow about the rear part of the cowling under the supposition that the cowling is infinitely long in the upstream direction.

It is theoretically possible to solve this problem by the singularity method. The walls of the rear part of a round cowling are in this case represented by a continuous row of annular sources and sinks. The difference from the air intake design consists in the flow behind the air intake being uniform, since the velocity of the jet differs from the velocity of the surrounding flow. This nonuniform flow can be replaced by an equivalent uniform flow with a vortex sheet (discontinuity surface) at the interface to the jet; the magnitude of the discontinuity is determined from the difference between the velocities inside and outside the jet. This method of calculation is however complex and laborious.

The sum F_k off the forces acting on the rear part of the cowling differs slightly from zero and vanishes completely for the values of $p-p_\infty$ met with in practice; it can therefore be assumed that the shape of the surface does not influence the magnitude of this force. The surface shape of the rear part of the cowling does, however, influence the pressure distribution and consequently the local velocities. The maximum local rarefaction will arise at the position where the cylindrical part of the cowling goes over to the curved rear part (Fig. 8.3.1). In order to avoid shock stall it is necessary that at this site the critical Mach number M should be as high as

possible and the velocity increment negligible. Satisfying these requirements in practice means that the transition from the cylindrical part of the cowling to the rear part must be made smoothly and that the radius of curvature of the surface must be sufficiently large.

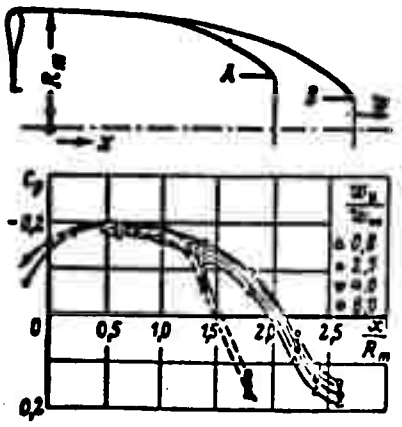


Fig. 8.3.1. Pressure distribution on the outer surface of rear part of the cowling.

The jet carries along and accelerates particles of the external flow and gives rise to an additional rarefaction at the surface of the rear part. The external drag increment due to this rarefaction is small (1-2% of the total thrust) at subsonic velocities, and it is therefore unimportant in determining the optimum shape of the rear part of the cowling.

Thick optimum cowling. Let us consider an annular cowling with a finite length L and a thickness such that the velocity on its outer surface will differ considerably from the velocity of the undisturbed flow (Fig. 8.3.2). Let us assume that the outer surface has a symmetry plane passing through the thickest part of the cowling. Applying the momentum theorem to the reference volume ABCDEFGHJK (cf. Fig. 8.3.2) and supposing that the pressure distribution on the outer surface is uniform we obtain

$$\frac{1}{2}\rho(w_a - w_\infty)^2 A_a - \frac{1}{2}\rho(w_{max}^2 - w_\infty^2)(A_d - A_a) + \\ + \frac{1}{2}\rho\int_A (w - w_\infty)^2 dA = 0. \qquad (8.3.1)$$

A denotes here the surface of integration, BCHJ, a plane that lies at the maximum diameter of the cowling but at a distance from it such that the cowling has no more influence. If the thickness of

the cowling is finite, the nature of the pressure distribution at this plane must be taken into account. Kuheman and Weber [8.1] suggest using the following power to describe the decrease of w with increasing distance from the cowling:

$$w - w_\infty = \frac{w_{max} - w_\infty}{(r:R_d)^n}. \qquad (8.3.2)$$

where R_d is the radius corresponding to A_d, r is the distance from the axis to the point where the velocity is determined, and n = 3 for short cowlings and n = 2 for long cowlings. In this case the relation corresponding to (8.2.6) will be

$$\frac{A_d}{A_n} > \left\{1 + \frac{[(w_n:w_\infty)-1]^2}{(w_{max}-w_\infty)^2-1}\right\}:\left[1 - \frac{1}{n-1}\,\frac{(w_{max}:w_\infty)-1}{(w_{max}-w_\infty)+1}\right]. \qquad (8.3.3)$$

Comparing the reduced inlet area (A_n/A_d) of an air intake having a semi-infinite outer surface of optimum shape (8.2.7) with the reduced inlet area $(A_n/A_d)_0$ of an optimum cowling of finite length (8.3.3) we arrive at the relation

$$\frac{(A_n:A_d)_0}{(A_n:A_d)_\infty} = 1 - \frac{1}{n-1}\,\frac{(w_{max}:w_n)-1}{(w_{max}:w_n)+1}. \qquad (8.3.4)$$

Consequently, for the same ratio w_{max}/w_∞ a finite cowling has a reduced area that is smaller than that of the forepart of a semi-infinite cowling (air intake). The difference is insignificant for velocity ratios w_{max}/w_n encountered in practice.

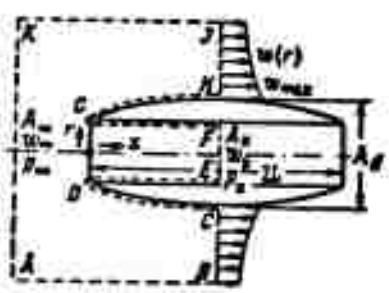


Fig. 8.3.2. Optimum contour of finite length with constant pressure distribution on the outer surface.

The length L_{vx} of the inlet part of an annular cowling for small values of w_{max}/w_∞ may be determined with sufficient accuracy from the empirical relation [8.1]:

$$\frac{R_d}{L_{vx}} = 3{,}9\left[1 + 0{,}4\left(\frac{w_n}{w_\infty}\right)^2\right]\left(\frac{w_{max}}{w_\infty} - 1\right). \qquad (8.3.5)$$

where R_d is the maximum outer radius and the length L_{vx} of the optimum cowling.

The thin annular profile. In the case of an annular profile (Fig. 8.3.3), i.e., an annular cowling whose length does not exceed twice the diameter of the inlet cross section, the flows about inner and outer surfaces must be considered together. The cowlings of radial piston engines or the outer rings of marine screws and propellers may serve as examples for annular profiles.



Fig. 8.3.3. Annular wing.

Let an annular profile be generated by having a certain profile rotated about its longitudinal axis. The aerodynamic characteristics of an annular profile, i.e., the pressure distribution along the contour, the resulting forces and the mass flow passing through can be theoretically determined. The exact calculation allowing for the thickness of the profile presents considerable difficulties. Let us set out the steps of a simplified calculation.

The annular profile is replaced by an extended sheet of vortices with the vorticity $\gamma(x)$, along its axial arc ($\underline{x}$ is measured in fractions of the chord $\underline{b}$ and varies from zero to one). The profile is in this case assumed to be infinitely thin.

The axial and radial velocity components w_x and w_r, determined by the vortex distribution, depend on the profile shape $r(x)$ and must satisfy the boundary condition

$$\frac{dr}{dx} = \frac{w_r(x, r)}{w_\infty + w_x(x, r)}. \qquad (8.3.6)$$

If the vortex distribution is given, the shape of the profile and its aerodynamic characteristics can be determined. And, conversely,

a given profile shape enables us to find the corresponding vortex distribution and to determine the aerodynamic characteristics.

Since the vortex distribution and the profile itself are usually unknown, it is very difficult to obtain a solution. It can be assumed as a first approximation that the annular vortices are distributed over a cylindrical surface with a radius equal to the mean distance from the axis to the chord. The linearized equation thus obtained is solved by numerical integration (usually with the help of series expansions).

Let us point out that a lift due to the presence of adjacent vortices arise on an annular wing placed in a flow at an angle of attack. At the same time, the form drag on the wing is accompanied by an induced drag.

8.4. JET NOZZLES

The jet nozzle of the engine serves to convert the potential energy of the gas into kinetic energy, with the aim of producing a thrust. The latter is approximately equal to

$$F = m_k(w_k - w_\infty) + (p_k - p_\infty)A_k. \qquad (8.4.1)$$

The subscript "k" refers here to the parameters at the nozzle edge.

For a supersonic nozzle at constant flying speed (w_∞ = const), and constant air mass flow (G = mg), an increase in the exhaust velocity w_k causes the first component to increase and the second term in the thrust Formula (8.4.1) to decrease, since it can be shown that $p_k - p_\infty$ drops faster than A_k rises.

In order to determine the exhaust velocity corresponding to maximum thrust, we rewrite (8.4.1) in the form

$$F = m\left(w_k - w_\infty + \frac{p_k - p_\infty}{\rho_k w_k}\right). \qquad (8.4.2)$$

For extreme thrust we obtain from (8.4.2)

$$\frac{dF}{dp_k}=m\left[\frac{dw_k}{dp_k}+\frac{1}{\rho_k w_k}-\frac{p_k-p_\infty}{(\rho_k w_k)^2}\frac{d(\rho_k w_k)}{dp_k}\right]=0.$$

From the Bernoulli equation $dp = -\rho w\, dw$ we obtain $\frac{dw_k}{dp_k}=-\frac{1}{\rho_k w_k}$ and, consequently,

$$\frac{p_k-p_\infty}{(\rho_k w_k)^2}\frac{d(\rho_k w_k)}{dp_k}=0 \qquad (8.4.3)$$

with $p_k - p_\infty = 0$ or $\frac{d(\rho_k w_k)}{dp_k}=0$.

We take $\frac{d^2(\rho_k w_k)}{dp_k^2}$, so that the case $p_k = p_\infty$ corresponds to maximum thrust and $\frac{d(\rho_k w_k)}{dp_k}=0$ to minimum thrust.

The operational conditions of the nozzle with $p_k = p_\infty$ are, as previously mentioned, called design conditions.

The above considerations also apply to a subsonic nozzle, for which an increase in exhaust velocity leads to a more intense decrease of the second component in (8.4.1) due to the drop of $p_k - p_\infty$.

Subsonic nozzles. A convergent nozzle is used as the subsonic nozzle, whose exhaust velocity cannot exceed the critical velocity of sound in the narrowest (exit) cross section.

The critical pressure is determined by Relation (4.2.10)

$$\frac{p_2^*}{p_0}=\left(\frac{2}{k+1}\right)^{\frac{k}{k-1}}. \qquad (8.4.4)$$

and the isentropic exhaust velocity, if w_1 is the initial gas velocity by

$$w_{2is}=\sqrt{\frac{2k}{k-1}RT_0\left[1-\left(\frac{p_2}{p_0}\right)^{\frac{k-1}{k}}\right]+w_1^2}. \qquad (8.4.5)$$

The quantity w_1 is usually neglected, and it is then assumed that $p_1 \approx p_0$, $T_1 \approx T_0$. The mass flow $\underline{m}$ of the gas will be

$$m=\rho_2 w_{2is} A_2. \qquad (8.4.6)$$

Noticing that $\frac{p_2}{p_1}=\left(\frac{p_2}{p_1}\right)^k$, we obtain

$$m = A_2 \sqrt{\frac{2k}{k-1} p_1 \rho_1 \left(\frac{p_2}{p_1}\right)^{\frac{2}{k}} \left[1 - \left(\frac{p_2}{p_1}\right)^{\frac{k-1}{k}}\right]}. \qquad (8.4.7)$$

This function has been investigated in Chapter 4; its graph is shown in Fig. 8.4.1. Maximum mass flow is reached at the critical pressure ratio. The left-hand part of the curve (dashed) virtually fails to correspond to reality since a drop in counterpressure below the critical value does not influence the change in mass flow and the outlet velocity therefore remains constant and equal to the critical velocity.

At subcritical exhaustion the pressure in the exit cross section is equal to the external counterpressure p_2 and at transcritical exhaustion it exceeds p_2 and is equal to the critical value, determined by Eq. (8.4.6).

In a real exhaustion process (Fig. 8.4.2) the entropy of the flow increases due to the losses. This leads to a drop in the true exhaust velocity w_2 compared with the isentropic velocity w_{2iz}. The ratio of these coefficients is termed <u>nozzle efficiency</u>

$$\varphi = w_2 : w_{2iz}. \qquad (8.4.8)$$

As experiments show, the principal losses are due to friction. φ therefore depends on the Re number. At large Re numbers the value of φ does not drop below 0.92, not even for nozzles with roughly treated inner surfaces.

The performance of the nozzle may also be estimated from the ratio of the true flow rate G to the theoretical flow rate G_t (in the case of isentropic expansion) which is designated as the mass flow coefficient

$$\mu = G : G_t. \qquad (8.4.9)$$

A nozzle is sometimes evaluated with the help of the ratio of the kinetic energy of the true process to the energy available in

isentropic expansion (Fig. 8.4.2):

$$\eta = \frac{w_2^2}{w_{2ad}^2} = \frac{T_0 - T_2}{T_0 - T_{2ad}} = \frac{w_2^2}{2c_p(T_0 - T_{2ad})} = \frac{k-1}{2} \frac{w_{2ad}^2 : a^2}{1 - (p_2 : p_0)^{\frac{k-1}{k}}}. \quad (8.4.10)$$

As can be seen,

$$\varphi = \sqrt{\eta} \quad (8.4.11)$$

Subsonic nozzles are produced with straight or curvilinear walls. The latter can yield higher values of the coefficients φ, μ and η and uniformity of the flow at the exit. In aerodynamic tubes, for example, a nozzle form is used which, theoretically, ensures uniform axisymmetric flow in the inlet and exit planes, determined by Vitoshinskiy's formula [8.5]:

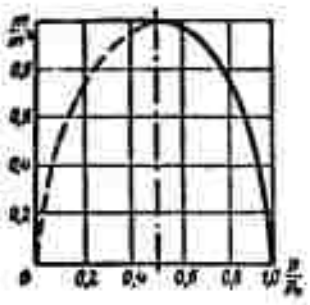


Fig. 8.4.1. Gas mass flow from a convergent nozzle.

$$\frac{r}{r_2} = \frac{1}{\sqrt{1 - \left(1 - \frac{r_2^2}{r_1^2}\right) \frac{[1 - (x^2 : l^2)]^2}{[1 - (3x^2 : l^2)]^3}}}; \quad (8.4.12)$$

where r, x are cylindrical coordinates, l is the nozzle length, r_1, r_2 are the radii of the inlet and exit cross sections, repectively (cf. Fig. 8.4.3).

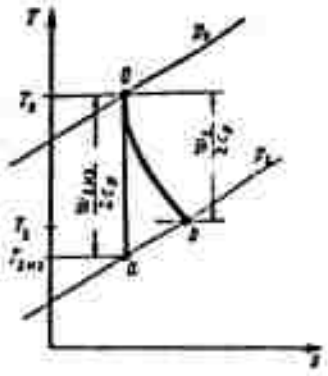


Fig. 8.4.2. For determining the nozzle performance.

Modern gas turbines usually employ convergent conical nozzles which are simple in shape, stable, rigid, and cheap in production. The experiment shows that the application of convergent nozzles in the range of transcritical pressure drop ($p_2/p_1 < 3$-4) do not exert much influence on the thrust losses with drops amounting up to 4, and only with pressure drops $p_2/p_1 > 4$ is it necessary to go over to divergent nozzles [8.6].

A great disadvantage of divergent nozzles is that they operate normally only under design conditions. Any deviation from the design

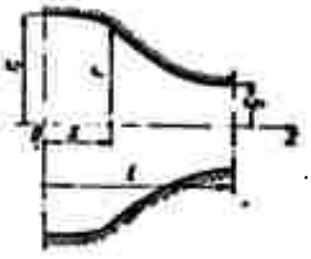


Fig. 8.4.3. Subsonic Vitoshinskiy nozzle.

conditions entails great losses and a decrease in thrust.

Figure 8.4.4 represents graphically the change in nozzle efficiency φ in dependence on the pressure drop for various vertex angles of the cone and various diameter ratios of the nozzles [8.6].

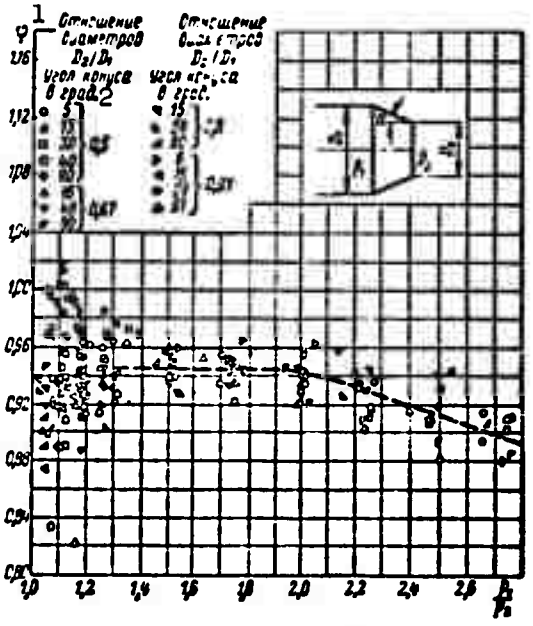


Fig. 8.4.4. Nozzle efficiency φ in dependence on the pressure drop in conical nozzles. 1) Ratio of diameters; 2) vertex angle of cone in degrees.

Supersonic nozzle (cf. Part 4.3). The calculation formulas, according to the stagnation parameters (4.3.3), give

$$\frac{G\sqrt{T_0}}{A^* p_0} = \sqrt{\frac{k}{R}\left(\frac{2}{k+1}\right)^{\frac{k+1}{k-1}}} \quad (k = 0.4 \text{ for air}) \qquad (8.4.13)$$

According to the pressure drop (4.2.20)

$$A = \frac{m}{\sqrt{\frac{2k}{k-1}\rho_0 p_0 \left(\frac{p}{p_0}\right)^{\frac{2}{k}}\left[1-\left(\frac{p}{p_0}\right)^{\frac{k-1}{k}}\right]}},$$

$$\frac{A}{A^*} = \sqrt{\frac{k-1}{2}} \frac{\left(\frac{2}{k+1}\right)^{\frac{k+1}{2(k-1)}}}{\left(\frac{p}{p_0}\right)^{\frac{1}{k}}\left[1-\left(\frac{p}{p_0}\right)^{\frac{k-1}{k}}\right]^{\frac{1}{2}}}. \qquad (8.4.14)$$

The thrust of a conical nozzle. If the gas mass m passes through the nozzle every second, then $j_s = m/A_s$ mass units will pass through a unit area of the sphere's surface (Fig. 8.4.5), A_s being the surface area of the sphere of radius R, and, assuming w = const and ρ = const for the points of the sphere, we obtain j = const for all points of the sphere. The mass of gas passing through a spherical surface element is then $dj = j_s dA_s$.

The thrust calculated from this supposition (with $w = m/\rho A_s$) is therefore equal to

$$F_c = \iint_{A_c} w \cos\alpha \, dj = w j_c \iint_{A_c} \cos\alpha \, dA_c = \frac{m^2}{\rho A_c^2} \iint_{A_c} \cos\alpha \, dA_c.$$

where the integral is extended over the entire surface A_s and the angle α determines the position of the element dA_s on the sphere.



Fig. 8.4.5. Influence of vertex angle of a conical nozzle on the magnitude of the thrust of the engine.

If we assume that the velocity at the nozzle exit is parallel to the nozzle axis and has one and the same value, the thrust can be calculated from the relation

$$F_a = mw = \frac{m^2}{\rho A_p},$$

where A_p is the generating area of the nozzle cone. Then

$$\zeta = \frac{F_c}{F_a} = \frac{A_a}{A_c^2} \iint_{A_c} \cos\alpha \, dA_c.$$

Taking into account that $dA_c = 2\pi R^2 \sin\alpha \, d\alpha$, we obtain

$$A_c = 2\pi R^2 \int_0^{\alpha_p} \sin\alpha \, d\alpha = 2\pi R^2 (1 - \cos\alpha_p);$$

$$\iint_{A_c} \cos\alpha \, dA_c = 2\pi R^2 \int_0^{\alpha_p} \sin\alpha \cos\alpha \, d\alpha = \pi R^2 \sin^2\alpha_p.$$

Since $A_a = \pi R^2 \sin^2\alpha_p$, we have

$$\zeta = \frac{F_c}{F_a} = \frac{\sin^4\alpha_p}{4(1-\cos\alpha_p)^2} = \left(\frac{1+\cos\alpha_p}{2}\right)^2 = \cos^4\frac{\alpha_p}{2}. \qquad (8.4.15)$$

If the nozzle thrust is determined from the condition for the axial velocity at the nozzle exit, then the true thrust must be determined by multiplying this velocity by the coefficient ζ which takes the influence of the vertex angle of the nozzle on its thrust into account.

The subsonic part of the nozzle. This can be calculated with Vitoshinskiy's formula (8.4.12). Sometimes it is designed "by rule of thumb," influenced by general considerations on the smoothness of the curve.

The transient section (nozzle throat). The region where M* lies between 0.85 and 1.15 and where the flow goes over from subsonic to supersonic speed has a great influence on the development of the supersonic flow. If this section has an unsuitable shape, compression shocks form and hence a nonuniform pressure distribution occurs in the whole supersonic range of flow. A more complete but rather complex solution to this problem is given in the work of V. Astrov, L. Levin, Ye. Pavlov and S. Khristianovich [8.7].

The much simpler method due to I.M. Yur'yev [8.8] is based on

several particular solutions of approximate equations of plane and axisymmetric gas flows.

It can easily be shown that the velocity potential equation for a plane and axisymmetric flows may be written in the form

$$\left(1-\frac{w_x^2}{a^2}\right)\frac{\partial^2\Phi}{\partial x^2}+\left(1-\frac{w_y^2}{a^2}\right)\frac{\partial^2\Phi}{\partial y^2}-2\frac{w_x w_y}{a^2}\frac{\partial^2\Phi}{\partial x\,\partial y}+ +\frac{B}{y}\frac{\partial\Phi}{\partial y}=0, \tag{8.4.16}$$

where B = 0 for a plane flow and B = 1 for an axisymmetric flow.

Let us put

$$\left.\begin{aligned} &w_x=a^*+w_x', \quad a^2=a^{*2}-\frac{k-1}{2}(w^2-a^{*2}),\\ &(w^2=(a^*+w_x')^2+w_y^2), \quad \Phi=a^*x+\varphi=a^*(x+\varphi^*). \end{aligned}\right\} \tag{8.4.17}$$

Substituting these values into (8.4.16) and neglecting the small quantities which are second and higher orders of w_x' and w_y, we find

$$-(k+1)\frac{\partial\varphi^*}{\partial x}\frac{\partial^2\varphi^*}{\partial x^2}+\frac{\partial^2\varphi^*}{\partial y^2}-2\frac{\partial\varphi^*}{\partial y}\frac{\partial^2\varphi}{\partial x\,\partial y}+\frac{B}{y}\frac{\partial\varphi^*}{\partial y}=0. \tag{8.4.18}$$

We shall seek the particular solution of (8.4.18) in the form

$$\varphi^*=\frac{1}{2}ax^2+xf_1(y)+f_2(y). \tag{8.4.19}$$

Substituting (8.4.19) in (8.4.18) yields a system of ordinary equations:

$$\left.\begin{aligned} &f_1'(y)-2f_1^2(y)-(k+1)a^2+\frac{B}{y}f_1(y)=0,\\ &f_2'(y)-\left[2f_1(y)-\frac{B}{y}\right]f_2'(y)-(k+1)af_1(y)=0. \end{aligned}\right\} \tag{8.4.20}$$

In the case of a plane flow the solutions will read

$$\left.\begin{aligned} &f_1(y)=-\frac{1}{2}\ln\cos\left[\sqrt{2(k+1)}\,ay\right],\\ &f_2(y)=\frac{1}{8a}\left[\ln^2\cos\left(\sqrt{2(k+1)}\,ay\right)-\right.\\ &\qquad -2\ln\left(\sqrt{2(k+1)}\,ay\right)-\\ &\qquad \left.-\ln^2\operatorname{tg}\left(\frac{\pi}{4}-\sqrt{\frac{k+1}{2}}\,ay\right)\right. \end{aligned}\right\} \tag{8.4.21}$$

The two functions $f_1(y)$ and $f_2(y)$ are both even functions.

The additional velocity components will be

$$\left.\begin{aligned}
\frac{w'_x}{a^*} &= \frac{\partial \varphi^*}{\partial x} = ax - \frac{1}{2}\ln\left(\cos\sqrt{2(k+1)}\,ay\right),\\
\frac{w'_y}{a^*} &= \frac{\partial \varphi^*}{\partial y} = \sqrt{\frac{k+1}{2}}\left\{\left[ax + \frac{1}{2}\ln\sec\left(\sqrt{2(k+1)}\,ay\right) + \right.\right.\\
&\quad \left.\left. + \frac{1}{2}\right]\operatorname{tg}\left(\sqrt{2(k+1)}\,ay\right) + \right.\\
&\quad \left. + \frac{1}{2}\sec\left(\sqrt{2(k+1)}\,ay\right)\ln\operatorname{tg}\left(\frac{\pi}{4} - \sqrt{\frac{k+1}{2}}\,ay\right)\right\}.
\end{aligned}\right\} \qquad (8.4.22)$$

The streamlines are determined by numerical integration of the equations

$$\frac{dy}{dx} = \frac{w_y}{a^* - w'_x}. \qquad (8.4.23)$$

The equipotential lines and the lines of equal velocities will be

$$x + \varphi^*(x, y) = \text{const}, \quad \left(1 + \frac{\partial \varphi^*}{\partial x}\right)^2 + \frac{\partial \varphi^{*2}}{\partial y} = M^{*2} = \text{const}. \qquad (8.4.24)$$

For an axisymmetric nozzle (y is replaced by r)

$$\left.\begin{aligned}
f_1(r) &= -\frac{1}{2}\ln S(r), \text{ где } S(r) = \sum_{n=0}^{\infty}\frac{(-1)^n\left(\sqrt{2(k+1)}\,ar\right)^n}{2^{2n}(n!)^2},\\
f_2(r) &= -\frac{(k+1)a}{2}\int_0^r \frac{dr}{rS(r)}\int_0^r rS(r)\ln S(r)\,dr.
\end{aligned}\right\} \qquad (8.4.25)$$

The series $S(r)$ converges rapidly.

The additional velocity components are equal to

$$\left.\begin{aligned}
\frac{w'_x}{a^*} &= \frac{\partial \varphi^*}{\partial x} = ax - \frac{1}{2}\ln S(r),\\
\frac{w'_r}{a^*} &= \frac{\partial \varphi^*}{\partial r} = -\frac{xS'(r)}{2S(r)} - \frac{(k+1)a}{2rS(r)}\int_0^r rS(r)\ln S(r)\,dr.
\end{aligned}\right\} \qquad (8.4.26)$$

The streamline is obtained by numerical integration of the equation

$$\frac{dr}{dx} = \frac{w_r}{a^* + w'_x}. \qquad (8.4.27)$$

The supersonic section. Calculations are made on the super-

sonic section of a plane nozzle (behind the throat) by the method of characteristics we have described before (cf. Chapter 5).

The calculation of an axisymmetric nozzle with the help of the method of characteristics was carried out by F. I. Frankl [8.9].

The above method was applied in a much simpler way by I. M. Yur'yev [8.10], who used particular solutions of the approximate velocity potential equation, which in the general case of a three-dimensional flow has the form

$$\left(1-\frac{w_x^2}{a^2}\right)\frac{\partial^2\Phi}{\partial x^2}+\left(1-\frac{w_y^2}{a^2}\right)\frac{\partial^2\Phi}{\partial y^2}+\left(1-\frac{w_z^2}{a^2}\right)\frac{\partial^2\Phi}{\partial z^2}-$$
$$-2\frac{w_x w_y}{a^2}\frac{\partial^2\Phi}{\partial x\,\partial y}-2\frac{w_y w_z}{a^2}\frac{\partial^2\Phi}{\partial y\,\partial z}-2\frac{w_z w_x}{a^2}\frac{\partial^2\Phi}{\partial z\,\partial x}=0. \qquad (8.4.28)$$

Under similar suppositions about the smallness of w_x', w_y and w_z this equation can be reduced to the form

$$F(w_x)\frac{\partial^2\Phi}{\partial x^2}+\frac{\partial^2\Phi}{\partial y^2}+\frac{\partial^2\Phi}{\partial z^2}=0. \qquad (8.4.29)$$

where

$$\Phi=a^*(x+\varphi^*);\ w_x=a^*(1+w_x');\ F(w_x)=\frac{a^{*2}-w_x^2}{a^{*2}-\frac{w_x^2}{K^2}};$$

$$K^2=\frac{k+1}{k-1}.$$

A solution can however be found for a somewhat different equation:

$$-[(k+1)w_x'+kw_x'^2]\frac{\partial^2\varphi^*}{\partial x^2}+\frac{\partial^2\varphi^*}{\partial y^2}+\frac{\partial^2\varphi^*}{\partial z^2}=0. \qquad (8.4.30)$$

The difference between the function $F(w_x)$ determined from (8.4.29) and the function $-[(k+1)w_x'+kw_x'^2]$ is very small, as is shown in Fig. 8.4.6. Notice that the function $-(k+1)w_x$ satisfies the Triccomi equation. The particular solution has the form

$$\varphi^*=f_1(y,z)x^2+f_2(y,z)x+f_3(y,z). \qquad (8.4.31)$$

Substituting (8.4.31) into (8.4.30) gives the system

$$\left.\begin{aligned}
\frac{\partial^2 f_1}{\partial y^2}+\frac{\partial^2 f_1}{\partial z^2}-8kf_1^2=0,\\
\frac{\partial^2 f_2}{\partial y^2}+\frac{\partial^2 f_2}{\partial z^2}-8kf_1^2 f_3-4(k+1)f_1^2=0,\\
\frac{\partial^2 f_3}{\partial y^2}+\frac{\partial^2 f_3}{\partial z^2}-2f_1[(k+1)f_3+kf_2^2]=0.
\end{aligned}\right\} \qquad (8.4.32)$$

For an axisymmetric flow ($r = [\,y^2 + z^2\,]^{1/2}$).

of ordinary differential equations

$$\left.\begin{aligned}
\frac{d^2 f_1(r)}{dr^2}+\frac{1}{r}\frac{df_1(r)}{dr}-8kf_1^2(r)=0. \quad (*)\\
\frac{d^2 f_2(r)}{dr^2}+\frac{1}{r}\frac{df_2(r)}{dr}-\\
-8kf_1^2(r)f_3(r)-4(k+1)f_1^2(r)=0. \quad (**)\\
\frac{d^2 f_3(r)}{dr^2}+\frac{1}{r}\frac{df_3(r)}{dr}-\\
-2f_1(r)[(k+1)f_3(r)+kf_2^2(r)]=0. \quad (***)
\end{aligned}\right\} \qquad (8.4.33)$$

The first equation of (8.4.33) is satisfied by the function $1/2\ (2kr)^{1/2}$.

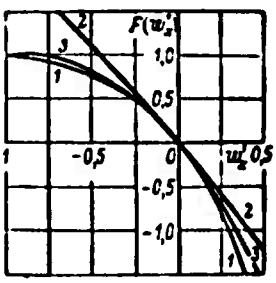


Fig. 8.4.6. Curve 1 represents the equation $\frac{a^{*2}-w_x^{*2}}{a^{*2}-\frac{w_x^{*2}}{K^2}}$

Curve 3 the function $-[(k+1)w_x^{*}+kw_x^{*2}$

and the straight line 2 the equation $-(k+1)w_x^{*}$

We shall however seek a solution which is continuous on the r-axis, and for which we put

$$f_1(r)=Cg(Cr), \qquad (8.4.34)$$

where C is an arbitrary constant and g(r) is a particular solution which we determine from the condition g(0) = 1 and, therefore, g'(0) = 0.

$$f_3(r)=\left\{D+4(k+1)\int_0^r r^{-1}f_1^{-2}(r)\left(\int_0^r rf_1^2(r)\,dr\right)dr\right\}f_1(r). \qquad (8.4.35)$$

where D is an arbitrary constant.

We find now from (8.4.33***)

$$f_2(r)=2\int_0^r\frac{dr}{r}\left\{\int_0^r[(k+1)f_3(r)+kf_2^2(r)]f_1(r)\,dr\right\}. \qquad (8.4.36)$$

The values of g(r) and g'(r) are best determined by a numerical integration of the equation for the function

$$k(r)=\frac{1}{f_1^2(r)}. \qquad (8.4.37)$$

The function g(r) can be determined fairly exactly by the function sec (2.2335r).

The nozzle contour is obtained by integrating the equation

$$\frac{dr}{dx}=\frac{\frac{d\varphi^*}{dr}}{1+\frac{d\varphi^*}{dr}}. \qquad (8.4.38)$$

If D = 0 the line M* = 1 passes through the origin.

Optimum nozzles. Maximum thrust is obtained for nozzle contours which produce a parallel jet with the pressure in the jet equal to the ambient pressure. The rear sections of such nozzles almost fail to participate in the thrust production since the surface in this section is almost parallel to the nozzle axis and therefore it does not receive any forces directed along the nozzle axis. If the rear section of such a nozzle is cut off, then, with insignificant thrust losses, essential savings in weight are made with the surface reached by the flow.

Guderley and Hantsch [8.11] set themselves the task of finding the contour of nozzles which produce maximum thrust for given mass flow, length and exit cross section. When the mass flow is fixed a two-papametric family of nozzles is obtained. One can also demand that the design of nozzle contours be such that not only the mass flow but also the length are given. These contours however depend on the external pressure too, since in this case a two-parametric many-shaped solution is obtained. In this case the solution for a nozzle satisfying the conditions of the problem for given length and pressure is likewise a solution to the problem of a nozzle with given length and exit cross-section area. Fig. 8.4.7 shows contours for the pressure ratios 0, 0.02 and 0.05; in this graph we also

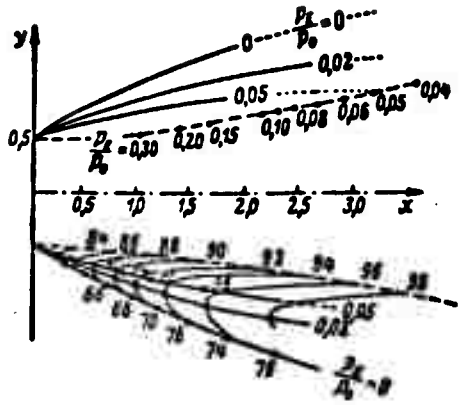


Fig. 8.4.7. Nozzle contours for pressure ratios p_E/p_0 = 0, 0.02, 0.05. Above we see the locus of the endpoints of nozzle contours designed for parallel exhaustion. Below the curves of equal thrust as percentages of the maximum attainable thrust (in the case of parallel exhaust) for the accelerating nozzle chosen, with p_E/p_0 = = 0.2; the maximum values correspond to the vertical tangent – on the contours p_E/p_0 = 0 and p_E/p_0 = 0.05 the points of these maximum values are plotted.

plotted the locus of the endpoints of nozzle contours designed for parallel exhaustion.

The calculations on nozzles of various lengths with given ratios between external and stagnation pressures show that the contours obtained are determined by curves which are virtually general.



Fig. 8.4.8. Notations for nozzle calculation.

Nozzles calculated by the method of Guderley and Hantsch have a break in the throat. In order to avoid this, G. Rao [8.12] determined the contour of a jet nozzle giving maximum thrust without this break. As the calculations show [8.13] the transient section of the nozzle can be constructed using two arcs (Fig. 8.4.8). Choosing the relative length of the nozzle for a given ratio of exit and throat radii we find from the graph (Fig. 8.4.9) the slope angles of

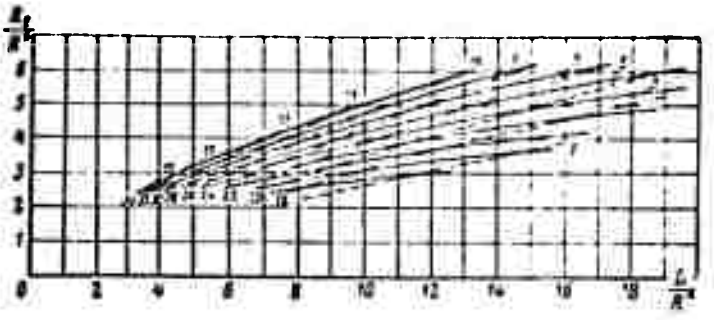


Fig. 8.4.9. The angles θ_E/θ_M as functions of R_E/R^* and L/R^*.

the nozzle walls to the axis at the inlet and exit and we can construct the angle MQE. Dividing each of the straight line segments into the same number of parts, we can use the common method to determine the parabola. The nozzle contours obtained differ little from the exact ones calculated by the characteristics method; for an areal ratio of $A_E/A^* = 25/1$ and a length of $L/R = 12/1$ the error does not exceed 3%.

Figure 8.4.10 shows the graph representing the influence of the specific heat ratio $k = c_p/c_v$ on the nozzle contour.

It should be noted that nozzle contours constructed with G. Rao's method depend on the nozzle length. Besides this, calculations showed that a considerable improvement of the characteristics of nozzles with optimum thrust, compared with conical nozzles of the same length, is reached only when the gases are highly rarefied.

Allowance for the boundary layer. A boundary layer forms on the nozzle surface whose influence was not yet taken into account. The displacement thickness δ^* of the boundary layer increases downstream (Fig. 8.4.11). If the core flow is assumed to be isentropic, the exit velocity can be determined from Formula (8.4.5). In this case we can assume that the cross-sectional area of the flow core, A_f, is determined for a plane-parallel nozzle of width b by the condition

and

$$\frac{A_\phi}{A} = 1 - \frac{2\delta^*}{b} \tag{8.4.39}$$

$$\frac{A_\phi}{A} = \left(1 - \frac{\delta^*}{R}\right)^2 \approx 1 - \frac{2\delta^*}{R} \tag{8.4.40}$$

for an axisymmetric nozzle with a local radius R.

In the formulas determining the exhaust velocity for a given nozzle we should use not the true but the fictitious nozzle areas A_f.

Taking the boundary layer into account leads to the value obtained for the velocity in the core flow of a subsonic nozzle being higher than in the ideal case (when the boundary layer is not taken into account), and that for a supersonic nozzle being lower.

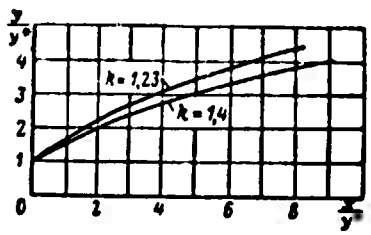


Fig. 8.4.10. Influence of $k = c_p/c_v$ on the nozzle contour.

Differentiating (4.3.2) and raplacing dA and dM* by δA and δM* we can write

$$\frac{\delta A}{A} = \frac{M^{*2} - 1}{1 - \frac{k-1}{k+1} M^{*2}} \frac{\delta M^*}{M^*}. \tag{8.4.41}$$

If we now assume M* = 1 + δM* for the throat region, we obtain

$$\frac{\delta A}{A} \approx \frac{k+1}{2} \frac{\delta M^{*2}}{M^{*2}}.$$

It follows from this by the way that a slight change in the cross-sectional area of the nozzle near its throat gives rise to a great change in velocity.

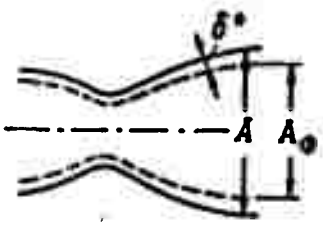


Fig. 8.4.11. Displacement thickness of the boundary layer in a nozzle.

If we replace δA/A by 2δ*/b we can estimate the influence of the boundary layer on the velocity in a geometrical nozzle.

$$\frac{\delta M^*}{M^*} = 2\frac{\delta^*}{b} \frac{1 - \frac{k-1}{k+1} M^{*2}}{M^{*2} - 1}. \tag{8.4.42}$$

8.5. THE FLOW IN CURVILINEAR CHANNELS

The internal problem. Besides the consideration of the so-called external problems, the construction of the flow about a solid body (or a system of bodies), the solution of what is called the internal problem – the construction of the flow in a channel of given shape – is of basic significance in engineering practice.

If the region of real inlet (the air intake) or that of the outlet (nozzle) can be efficiently designed by methods as described in Parts 8.2-8.4, the problem of constructing the flow in the main section of the channel remains unsolved except in the case of the simplest diffusor with a straight-line axis (cf. Part 8.2). Meanwhile the shape of the channel is determined with allowance for widely differing considerations and may be rather complex.

In solving the internal problem we shall assume that not only the shape of the channel but also the flow rate of the fluid is given, since the mass m flowing through the channel per unit time is equal to

$$m = \int_A \rho w \, dA. \qquad (8.5.1)$$

where w is the velocity component normal to an element of area dA. It is however also possible to formulate the reverse problem – to determine the shape of the channel from the velocity distribution given on the walls. In this and other cases the fluid is assumed to be inviscid and the motion potential. The viscosity can be taken into account by calculating the boundary layer and introducing the displacement thickness δ^* at the channel walls into the calculation.

Velocity distribution transverse to a plane channel. G. Yu. Stepanov who developed A. Stodola's considerations on the flow in a plane curvilinear channel (Fig. 8.5.1), assumed that the equipotential lines of the flow in the channel intersect the channel walls at the

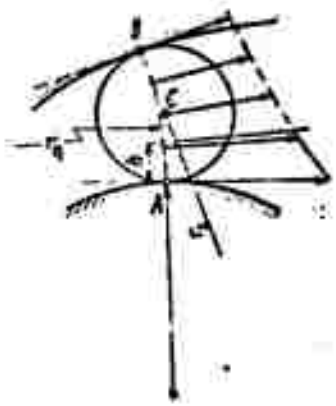


Fig. 8.5.1. The velocity distribution in the channel is hyperbolic. The tangency points A and B of the circle inscribed in the channel determine the ends of the equipotential lines AB which can be taken in the form of a circular arc AB (dashed).

point where they are touched by the circles inscribed in the channel (points A and B in Fig. 8.5.1), and that the transverse velocity distribution in the channel is described by the hyperbolic law

$$w = \frac{\text{const}}{r_1 + h} = \frac{r_1 w_1}{r_1 + h}, \qquad \frac{w}{w_1} = \frac{r_1}{r_1 + h}. \qquad (8.5.2)$$

This distribution is exact in the case of a potential flow in a channel of constant width and curvature (the field due to the vortex at the center of the circles determining the channel boundaries).

A.N. Sherstyuk [8.17] remarked that in the two limiting cases of a channel with $r_2 = \infty$ and $r_2 = r_1 + b$ (Fig. 8.5.2) the velocity distribution on the channel boundaries

$$\frac{w_1}{w_2} = 1 + \frac{b}{2r_1}; \quad \frac{w_1}{w_2} = 1 + \frac{b}{r_1}$$

can be described by the single relation

$$\frac{w_2}{w_1} = \frac{1 - b/2r_2}{1 + b/2r_1}, \qquad (8.5.3)$$

which, as is shown by calculation, is sufficiently accurate also for intermediary cases defined by the condition that $r_2 \geq r_1 + b$.

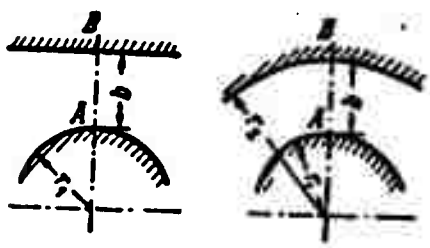


Fig. 8.5.2. Two limiting cases of a channel: $r_2 = \infty$; $r_2 = r_1 + b$.

In order to determine the velocities on intermediary streamlines we make use of the fact that the ratio $\frac{w(r_1 + h)}{w_1 r_1}$ varies slightly transversely to the chan-

nel, and we can write

$$\frac{w_1(r_1+h)}{w_1 r_1}=1+qB. \qquad (8.5.4)$$

where B is a small constant quantity and q is a monotonic function, $q = q(h/b)$, $q = 0$ for $h = 0$ and $q = 1$ for $h = b$. Thus, taking (8.5.3) into account, we use the relation (8.5.4) for $q = 1$

$$\frac{w_2(r_1+b)}{w_1 r_1}=\frac{\left(1-\frac{b}{2r_2}\right)(r_1+b)}{\left(1+\frac{b}{2r_1}\right)r_1}=1+B,$$

to find

$$B=\frac{b}{2r_1+b}\left(1-\frac{r_1+b}{r_2}\right). \qquad (8.5.5)$$

Since the quantity qB is small, the form of the function q does not exert much influence on the velocity distribution. The calculations show that the formulas are obtained more simply and that the results are more exact if we do not apply the simplest linear relation $q = h/b$ but a somewhat more complex one:

$$q=\frac{h}{b}\frac{r_1+h}{r_1+b}. \qquad (8.5.6)$$

In tnis case

$$\frac{w}{w_1}=\frac{r_1}{r_1+h}+B\frac{h}{b}\frac{r_1}{r_1+b}. \qquad (8.5.7)$$

we see that the second component of the right-hand side is a correction to the parabolic velocity distribution.

Calculation of the flow of an incompressible fluid in a plane channel. Substituting Relation (8.5.7) with $\rho = \text{const}$ in (8.5.1) and integrating, we obtain the volume flow rate (for a channel height equal to unity):

$$V=\int_0^b w\,dh=$$

$$=w_1\left[r_1\ln\left(1+\frac{b}{r_1}\right)+\frac{b}{2r_1+b}-\frac{b}{2(r_1+b)}-\frac{b^2}{2(2r_1+b)r_2}\right]. \qquad (8.5.8)$$

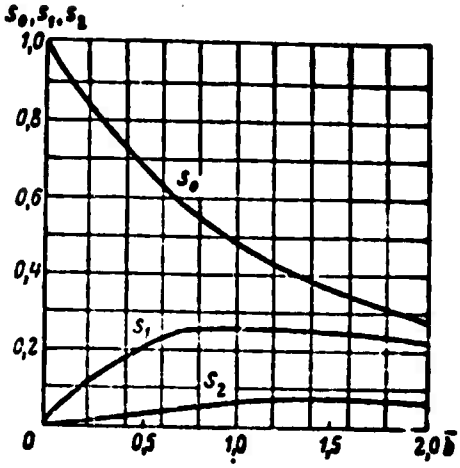


Fig. 8.5.3. Auxiliary functions S_0, S_1, and S_2 for calculation of flow in curvilinear channel as functions of $b/r_1 = \bar{b}$.

formula

$$M_2^* = M_1^* \frac{1 - \frac{b}{2r_1}}{1 + \frac{b}{2r_1}}. \quad (8.5.15)$$

The transverse velocity distribution in the channel may be determined according to Eq. (8.5.7) since the compressibility has no influence on it [8.18], [8.19].

8.6. JETS

Fundamental suppositions. A jet is a fluid (gas) stream bounded by tangential velocity discontinuity surfaces. We have to distinguish between the slipstream motion, when the flows are parallel on the two sides of the discontinuity surface, and counterflow, when the flows are in opposite directions.

The jet is described as free when the fluid streams out into a quiescent unbounded medium. If jet and medium have the same physical properties, the jet is said to be submerged.

We distinguish between a jet in a slipstream, when the velocity in the jet exceeds the velocity of the surrounding flow, and the wake behind the body in the flow, when the velocity in the jet behind the body is smaller than the velocity of the surrounding flow. These cases are both examples of slipstream motion. The interface of two flows moving with equal velocities can be considered as a particular case of a jet second boundary lies at infinity.

In any case the jet boundary has a tangential velocity discontinuity only at its very beginning, for example, in the exit plane of the nozzle from which the flow issues, or at the place where mixing of the two flows with different velocities sets in (the boundary layer formation on solid walls is disregarded here). According to the motion of the jet the velocity discontinuity as a result of viscous friction and turbulent mixing (transverse momentum transfer)

can be replaced by a region of finite thickness with continuous velocity distribution, which is termed a jet boundary layer.

A laminar jet boundary layer can be observed at very low Re numbers*. The equations of motion which were derived for the laminar boundary layer near a solid wall (6.1.4) can be used to investigate it. In the given case the solution differs in that a boundary condition which is characteristic of a solid wall – zero velocity of the fluid at the surface in the flow – does not exist.

The laminar jet boundary layer is of no practical interest and is not dealt with here.

The mechanism of motion in a turbulent boundary layer leads to turbulence and does not depend on the Re number since the influence of the ordinary "molecular" viscosity is negligibly small here. The viscosity terms can therefore be neglected in the equations describing the motion in a turbulent jet boundary layer, which are the same for jet turbulent layers near a solid wall.

Since a solid wall has no influence on the nature of the flow in a jet boundary layer the flow is usually said to be free and the turbulence is called free turbulence.

The structure of a free jet. A free jet becomes turbulent right after emission through an opening (except in the case of a very low exhaust velocity which is not considered here). Owing to turbulent mixing of the jet particles and the quiescent surrounding fluid and to momentum transfer, the jet expands as the distance increases, its mass grows and the velocity drops (Fig. 8.6.1).

The divergent surface originating at the edges of the opening separates the boundary layer of the jet from the inner core of constant velocities (equal to exhaust velocity) and from the remaining medium (of zero velocity).

The transient cross section passing through the vertex of the jet core cone separates the initial zone from the main zone. The latter is completely filled with the boundary layer and the velocity on its axis drops gradually.

Both experiment and theory show that at any cross section of the jet the transverse velocity components are small compared with the longitudinal velocity and can be neglected.

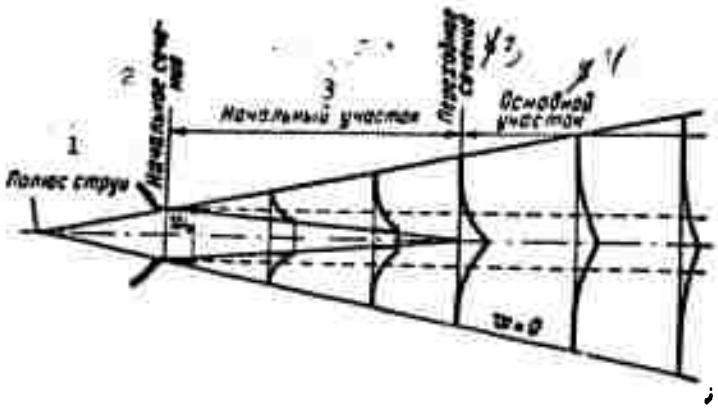


Fig. 8.6.1. Structure of free jet. 1) Apex of jet; 2) initial cross section; 3) transient cross section; 4) main zone.

The longitudinal velocity distribution curves of a jet are shown in Fig. 8.6.2. It is characteristic that the distributions of the dimensionless velocities (the local maximum velocity w_m at the jet axis is taken as the unit) are similar for all boundary layer cross sections. This indicates that the lines of equal dimensionless velocities are rays, originating at the edges of the opening for the initial zone, and at the apex* for its main zone (Fig. 8.6.3). The equation for the lines of equal dimensionless velocities may therefore be represented in the form [8.10].

$$\frac{w}{w_m} = f\left(\frac{y}{x}\right); \qquad (8.6.1)$$

where x is the distance from the jet apex to the cross section given,

and y is the distance from the jet axis to the point at which the velocity is determined.

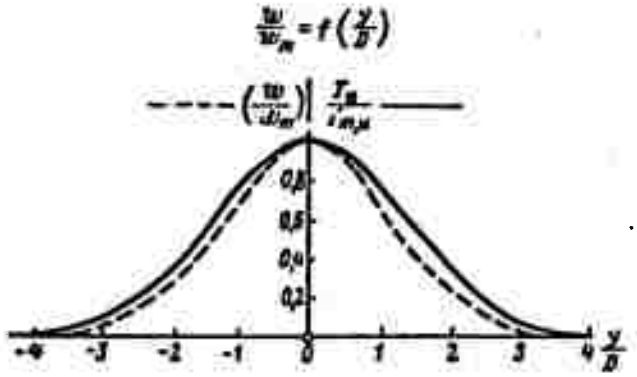


Fig. 8.6.2. Velocity and temperature of the main zone of the jet.

The velocity variation along the jet axis is determined from the condition that the momentum per unit mass flow must be constant in any jet cross section, i.e.,

$$\int_A \rho w^2 dA = \text{const.} \qquad (8.6.2)$$

where A is the cross sectional area of the jet.

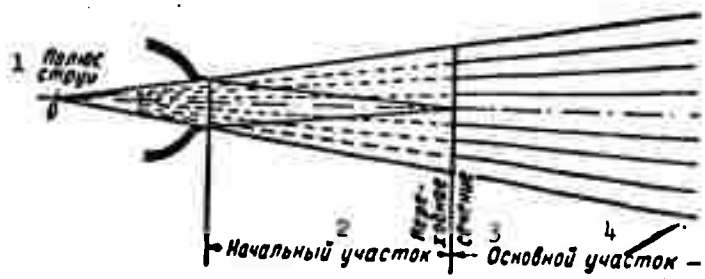


Fig. 8.6.3. Lines of equal dimensionless velocities of a free jet. 1) Apex of jet; 2) initial zone; 3) transient cross section; 4) main zone.

For an axisymmetric jet

$$w_m^2 x^2 \int_0^{\frac{R_{cp}}{x}} \left(\frac{w}{w_m}\right)^2 \frac{y}{x} \frac{dy}{x} = \text{const.} \qquad (8.6.3)$$

where R_{gr} is the radius of the outer boundary of the jet cross section considered.

By virtue of (8.6.1)

$$\int_0^{\frac{R_{gr}}{x}} \left(\frac{w}{w_m}\right)^2 \frac{y}{x}\,\frac{dy}{x} = \text{const}, \tag{8.6.4}$$

and therefore (8.6.3) yields

$$w_m = \frac{\text{const}}{x}, \tag{8.6.5}$$

i.e., the velocity at the center of a circular cross section of an axisymmetric jet drops in inverse proportion to the distance from the apex.

The proportionality constant in Eq. (8.6.4) may be determined theoretically or by experiment from the velocity distributions of each cross section of the main zone of the jet.

In practice it is more convenient to measure the distance not from the apex but from the initial cross section. In this case the relation [8.14]

$$\frac{w_m}{w_n} = \frac{0.93}{\frac{bs}{R_n} + 0.29}; \tag{8.6.6}$$

will apply [8.14]; s is here the distance to the initial cross section of the jet, R_n the radius of this cross section, b an elementary constant that depends on the flow structure in the initial cross section (b = 0.7-0.8).

The flow rate of the gas through the cross section of the jet for the main zone is equal to

$$V = \int_0^{R_{gr}} w 2\pi R\,dR. \tag{8.6.7}$$

Calculating the ratio between V and the gas flow rate V_n in the

initial cross section leads to the relation

$$\frac{V}{V_n} = 2{,}18\frac{b_s}{R_n} + 0{,}29, \qquad (8.6.8)$$

where $b_s/R_n > 0.67$.

The dimensionless flow rate for the initial zone of the jet ($b_s/R_n \leq 0.67$) can be determined with the help of the formula

$$\frac{V}{V_n} = 1 + 0{,}76\frac{b_s}{R_n} + 1{,}32\left(\frac{b_s}{R_n}\right)^2, \quad \frac{b_s}{R_n} \leqslant 0{,}67. \qquad (8.6.9)$$

The weakly heated jet. Let us assume that a weakly heated free jet whose density can be assumed to be constant is propagated in a medium with the temperature T_{vn}.

Let the temperature T at each point of the jet (apart from its axis) exceed T_{vn} by $T_i = T - T_{vn}$ and let us assume

$$T_{m.n} = T_m - T_{vn}; \quad T_{n.n} = T_n - T_{vn}.$$

respectively, for the axis of the main zone and in the initial cross section.

Experiments show that the distribution of the excess temperatures T_i is similar to the velocity distribution (cf. Fig. 8.6.2), the difference being that a temperature difference is more rapidly leveled out than a velocity difference.

In this case both the isothermal lines and the lines of equal dimensionless velocities in the main zone of the jet are straight rays, originating from the apex, which are described by the expression

$$\frac{T_n}{T_{m.n}} = f\left(\frac{y}{x}\right). \qquad (8.6.10)$$

The temperature decrease along the jet axis is determined by the constancy of the enthalpy of the free jet in an arbitrary cross section, expressed in terms of the surplus temperature T_i, i.e.,

$$\int_A \rho T_n w\, dA = \text{const}. \qquad (8.6.11)$$

For the circular cross section of an axisymmetric jet

$$x^2 w_m T_{m,n} \int_0^{\frac{R_{cp}}{x}} \frac{T_n}{T_{m,n}} \frac{w}{w_m} \frac{y\,dy}{x^2} = \text{const.} \qquad (8.6.12)$$

It follows from (8.6.10) that the integral in Eq. (8.6.12) is a constant quantity and therefore

$$T_{m,n} = \frac{\text{const}}{x}. \qquad (8.6.13)$$

Experiments show that the temperature distributions are not similar to the velocity distributions and therefore the constants of Eqs. (8.6.5) and (8.6.13) are different.

The expression for $T_{m,1}$, corresponding to Expression (8.6.5) can, by analogy with (8.6.6), be written in the form

$$\frac{T_{m,n}}{T_{n,n}} = \frac{0.70}{\frac{bx}{R_n} + 0.29}. \qquad (8.6.14)$$

Let us notice that the decrease in mean temperature along the free jet is governed by the same law as the decrease in mean velocities (in contradistinction to the maximum temperatures and velocities), i.e.,

$$\frac{T_{cp}}{T_n} = \frac{w_{cp}}{w_n}. \qquad (8.6.15)$$

As a matter of fact it follows from the constancy of momentum in any cross section that

$$\rho V w_{cp} = \rho V_n w_n,$$

i.e.,

$$\frac{V}{V_n} \frac{w_{cp}}{w_n} = 1, \qquad (8.6.16)$$

and from the enthalpy constancy that

$$\rho V T_{cp,n} = \rho V_n T_{n,n},$$

$$\frac{V}{V_n} \frac{T_{cp,n}}{T_{n,n}} = 1. \qquad (8.6.17)$$

Comparing (8.6.16) with (8.6.17) yields (8.6.15). The velocities and temperatures are averaged in this case with respect to mass flow:

$$w_{cp} = \frac{\int_A \rho w^2 dA}{\int_A \rho w dA}; \quad T_{cp.m} = \frac{\int_A T_m \rho w dA}{\int_A \rho w dA}.$$

The propelling jet. If the jet is arbitrarily heated it is necessary to take the compressibility of the gas into account. In this case the momentum conservation law reads

$$\int_0^{\bar{r}} \rho w^2 dA = \rho_m w_m^2 A_m$$

or, in a dimensionless form

$$\int_0^{\bar{r}} \frac{\rho}{\rho_m} \left(\frac{w}{w_m}\right)^2 \frac{dA}{A_m} = 1. \qquad (8.6.18)$$

Applying the equation of state to the case p = const, $\rho/\rho_n = T_n/T$ yields the initial expression for calculations on a propelling jet.

$$\int_0^{\bar{r}} \frac{T_m}{T} \left(\frac{w}{w_m}\right)^2 \frac{dA}{A_m} = 1. \qquad (8.6.19)$$

The temperature drop along the axes of a propelling jet is determined as before from the condition of enthalpy conservation in jet of compressible gas,

$$\int_0^{\bar{r}} \rho T_m w dA = \rho_m T_{m.m} w_m A_m$$

or, in a dimensionless form

$$\int_0^{\bar{r}} \frac{\rho}{\rho} \frac{T_n}{T_{n.n}} \frac{w}{w_m} \frac{dA}{A_m} = \int_0^{\bar{r}} \frac{T_m}{T} \frac{T_n}{T_{n.n}} \frac{w}{w_m} \frac{dA}{A_m} = 1. \qquad (8.6.20)$$

Figure 8.6.4 shows typical velocity and temperature distributions for a subsonic propelling jet. The transient cross section for the velocity is located at the distance of about six diameters from the exit cross section, and for the temperature at about five.

For the main section the rays corresponding to a velocity equal to half the velocity w_m on the axis leave the apex at an angle of

about 5°. For analogous rays at half the temperature ($T_1 = 0.5\ T_{m,i}$)

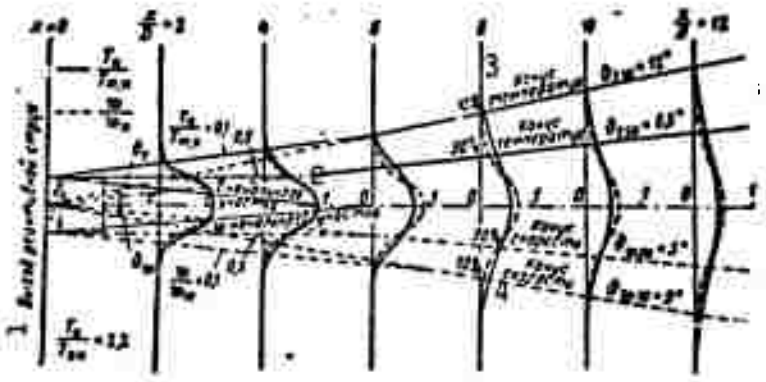


Fig. 8.6.4. Propelling jet. 1) Reaction stream outlet; 2) of the initial zone; 3) temperature cone; 4) velocity cone.

the angle is 6.5°. If the jet boundary is defined as a surface where the jet parameters amount to 1/10 of the corresponding parameters on the axis, then the semi-angle of the jet boundary cone amounts to about 9° for the velocity and to about 12° for the temperature (cf. Fig. 8.6.4).

When a plane-parallel gas jet is propagated in slipstream motion the increase in the ratio of the slipstream velocity to the constant exhaust velocity leads to an elongation of the initial zone, to a construcion of the jet boundaries and to a less intense drop of the dimensionless axial velocity as the distance from the nozzle increases. A detailed consideration of the influence of the slipstream on a free jet can be found in the special literature [8.1], [8.14], [8.15].

8.7. THE EJECTOR

Ejection. The ejector is a jet apparatus used to press (suck off) the medium to be ejected with the help of a jet of the ejecting (working) medium whose pressure is relatively high. Ejectors, which can be used instead of ventilators, compressors and pumps, have no mechanical drive and no moving parts.

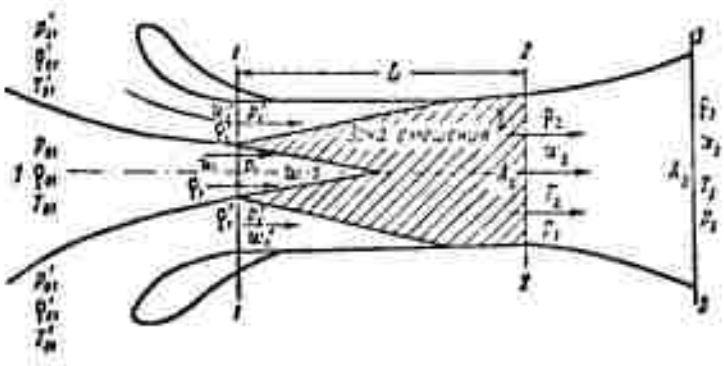


Fig. 8.7.1. Schematic diagram of an ejector.
1) Mixing zone.

Figure 8.7.1 is a schematic representation of an ejector. From the nozzle 1 the gas whose stagnation parameters are p_{01}, ρ_{01}, T_{01}, flows into the mixing chamber, acquiring at the nozzle exit the parameters p_1, ρ_1, T_1 and the velocity w_1. In the mixing chamber the jet of this gas entrains the gas to be ejected, which has the stagnation parameters p'_{01}, ρ'_{01}, T'_{01}, such that in the nozzle exit plane – the beginning of the mixing chamber – its parameters are p'_1, ρ'_1, T'_1, w'_1 and the cross-sectional area is A'_1. In the mixing chamber the gas mixture becomes homogeneous because of the intense turbulent exchange, and at the mixing chamber exit the parameters of the mixture will be p_2, ρ_2, T_2, and w_2.

In order to simplify the solution of the problem we shall assume in what follows that 1) there is no heat exchange with the environment, 2) the gas to be ejected and the ejecting have the same specific heat ratio, 3) the mixing chamber is cylindrical, i.e.,

$$A_1+A'_1=A_2, \qquad (8.7.1)$$

4) there is no friction, and 5) the velocity and pressure fields are uniform in the cross sections chosen.

Losses in the ejector. The losses in an ejector are essentially kinetic energy losses on mixing. If the pressure along the mixing

chamber is constant, the mass and momentum conservation laws yield the equalities

$$m_1 + m_1' = m_2, \quad m_1 w_1 + m_1' w_1' = m_2 w_2. \tag{8.7.2}$$

Forming the difference between the kinetic energies of the gases before and after mixing leads to the kinetic energy losses

$$\left(\frac{m_1 w_1^2}{2} + \frac{m_1' w_1'^2}{2}\right) - \frac{(m_1 + m_1') w_2^2}{2} = \frac{1}{2} \frac{m_1 m_1'}{m_1 + m_1'} (w_1 - w_1')^2, \tag{8.7.3}$$

i.e., thy are proportional to the square of the relative velocity of the gas to be ejected and the ejecting gas. Other losses will arise in the ejector owing to the leveling of the gas parameters before mixing, and to friction and losses in the diffusor, which usually is mounted at the end of the mixing chamber.

The ejection equation. There is no need to know the processes in the mixing chamber in detail to be able to calculate the conditions of steady ejector operation. The fundamental relations can be obtained by applying the conservation laws in their integral forms. Taking the reference cross sections at the inlet and the exit of the mixing chamber, we can write the mass conservation law (8.7.2) in the form

$$\rho_1 w_1 A_1 + \rho_1' w_1' A_1' = \rho_2 w_2 A_2. \tag{8.7.4}$$

The momentum conservation law gives

$$p_1 A_1 + p_1' A_1' - p_2 A_2 = \rho_2 w_2^2 A_2 - \rho_1' w_1'^2 A_1' - \rho_1 w_1^2 A_1 \tag{8.7.5}$$

or, taking into account that owing to (4.2.15) $(p + \rho w^2) A = K$,

$$K_1 + K_1' = K_2. \tag{8.7.6}$$

If there is no heat exchange we can write the energy conservation law expressing the equality of the changes in the internal and kinetic energy of the work done by the pressure forces (the potential energy of position and the work done by frictional forces are neglected) in the form

$$\left(\frac{w_2^2}{2}+c_{p_2}T_2\right)\rho_2 w_2 A_2-\left(\frac{w_1'^2}{2}+c'_{p_1}T_1'\right)\rho_1' w_1' A_1'-$$
$$-\left(\frac{w_1^2}{2}+c_{p_1}T_1\right)\rho_1 w_1 A_1=p_1 A_1 w_1+p_1' A_1' w_1'-p_2 A_2 w_2 \qquad (8.7.7)$$

or

$$m_1\left(c_{p_1}T_1+\frac{w_1^2}{2}\right)+m_1'\left(c'_{p_1}T_1'+\frac{w_1'^2}{2}\right)=m_2\left(c_{p_2}T_2+\frac{w_2^2}{2}\right). \qquad (8.7.8)$$

In terms of stagnation parameters for one and the same c_p we have

$$m_1T_{01}+m_1'T_{01}=m_2T_{02}. \qquad (8.7.9)$$

These equations must be supplemented by the equation expressing the cylindricality of the mixing chamber (8.7.1).

The ejection equation in gasdynamic functions. Rewriting the momentum equation in the form

$$K=mw+pA=m\left(w+\frac{pA}{m}\right)=m\left(w+\frac{a^2}{kw}\right)=$$
$$=m\left[w+\frac{a_0^2}{kw}\left(1-\frac{k-1}{k+1}M^{*2}\right)\right]=\frac{k+1}{2k}ma^*\left(M^*+\frac{1}{M^*}\right)=$$
$$=\frac{k+1}{2k}ma^*z(M^*), \qquad (8.7.10)$$

and reducing (8.7.6) by (k + 1)/2k will lead to

or
$$\left.\begin{aligned} m_1a_1^*z_1+m_1'a_1'^*z_1'&=m_2a_2^*z_2\\ m_1z_1\sqrt{T_{01}}+m_1'z_1'\sqrt{T_{01}}&=m_2z_2\sqrt{T_{02}}\end{aligned}\right\} \qquad (8.7.11)$$

Taking into account that

$$m=\rho wA=\frac{w}{\rho^*a^*}A\rho^*a^*=$$
$$=\lambda(M^*)A\frac{\rho^*}{a^*}\frac{2}{k+1}a_0^2=\lambda A\frac{\rho^*}{a^*}\frac{2}{k+1}k\frac{p_0}{\rho_0},$$

we obtain

$$p_0=\frac{k+1}{2k}\left(\frac{2}{k+1}\right)^{\frac{1}{k-1}}\frac{ma^*}{\lambda(M^*)A}. \qquad (8.7.12)$$

Substituting the value of A obtained from (8.7.12) into Eq. (8.7.1) we get

or

$$\left.\begin{aligned}\frac{m_1 a_1^*}{j_1 p_{01}}+\frac{m_1' a_1'^*}{j_1' p_{01}'}&=\frac{m_2 a_2^*}{j_2 p_{02}},\\ \frac{m_1\sqrt{T_{01}}}{j_1 p_{01}}+\frac{m_1'\sqrt{T_{01}'}}{j_1' p_{01}'}&=\frac{m_2\sqrt{T_{02}}}{j_2 p_{02}};\end{aligned}\right\} \qquad (8.7.13)$$

where $j(M^*)$ is a function of the mass flow (4.2.12)

$$j(M^*)=\left(\frac{k+1}{2}\right)^{\frac{1}{k-1}} M^*\left(1-\frac{k-1}{k+1}M^{*2}\right)^{\frac{1}{k-1}}.$$

Let us define the mass ratio of ejected gas to ejecting gas as the ejection coefficient

$$\varkappa=\frac{m_1'}{m_1}. \qquad (8.7.14)$$

Then, dividing (8.7.11) by $m_1 (T_{01})^{1/2}$ and taking into account that by virtue of (8.7.9)

$$\frac{m_2 a_2^*}{m_1 a_1^*}=\frac{m_1+m_1'}{m_1 a_1^*}\sqrt{\frac{m_1 T_{01}+m_1' T_{01}'}{m_1+m_1'}}=\sqrt{1+\varkappa}\sqrt{1+\varkappa\frac{T_{01}'}{T_{01}}},$$

we obtain

$$z(M_1^*)+\varkappa\sqrt{\frac{T_{01}'}{T_{01}}}z(M_1'^*)=\sqrt{1+\varkappa}\sqrt{1+\varkappa\frac{T_{01}'}{T_{01}}}z(M_1^*). \qquad (8.7.15)$$

Dividing (8.7.13) by $m_1 a_1^*$ gives us an equation linking the total pressures

$$\frac{1}{p_{01} j(M_1^*)}+\frac{1}{p_{02}' j(M_1'^*)}\varkappa\sqrt{\frac{T_{01}'}{T_{01}}}=\frac{\sqrt{1+\varkappa}}{p_{02} j(M_2^*)}\sqrt{1+\varkappa\frac{T_{01}'}{T_{01}}} \qquad (8.7.16)$$

or

$$p_{02}=p_{01}'\frac{\sqrt{1+\varkappa}\sqrt{1+\varkappa\frac{T_{01}'}{T_{01}}}}{1+\frac{p_{01}'}{p_{01}}\varkappa\sqrt{\frac{T_{01}'}{T_{01}}}\frac{j(M_1^*)}{j(M_1'^*)}}\frac{j(M_1^*)}{j(M_2^*)}. \qquad (8.7.17)$$

The ratio of the cross-sectional areas A_1 and A_2 is found with the help of (8.6.12) in the form

$$\frac{A_1'}{A_1}=\frac{m_1'}{m_1}\frac{a_1'}{a_1}\frac{p_{01}}{p_{01}'}\frac{j_1'}{j_1}=\varkappa\sqrt{\frac{T_{01}'}{T_{01}}}\frac{p_{01}}{p_{01}'}\frac{j(M_1^*)}{j(M_1'^*)}. \qquad (8.7.18)$$

The system of Eqs. (8.7.15), (8.7.17) and (8.7.18) is used for

the calculations.

The conditions at the exit. The mixing chamber may be followed a diffusor, a confusor, a cylinder, or a nozzle. The pressure at the exit of the device following the mixing chamber is usually given. The losses in this device were considered above and we may write

$$p_{03} = \frac{p_{02}}{\zeta}. \tag{8.7.19}$$

If the degree of divergence is

$$\frac{A_3}{A_2} = \beta, \tag{8.7.20}$$

than it follows from the equalities of masses, $m_2 = m_3$, and total temperatures, $T_{02} = T_{03}$, that owing to (8.7.12) we can write

$$\tau(M_3^*) = \tau(M_2^*)\frac{\zeta}{\beta}, \tag{8.7.21}$$

whence we find M_2^*.

The length of the mixing chamber. Since a free jet exists in certain zones of the ejector, we can make use of the laws governing it to determine the additional ejection coefficient κ' and the mixing chamber length L.

The law of mass increase along the axis of a free air jet (8.6.8) enables us to derive the following approximate relation for the additional ejection coefficient κ' due to turbulent mixing of the particles of the jet with the ejected gas:

$$\left.\begin{aligned} \kappa' &= 0{,}2235\left(\frac{R_2}{R_1}-1\right)+0{,}114\left(\frac{R_2}{R_1}-1\right)^2 \\ &\text{and} \\ \kappa' &= -0{,}3675+0{,}6425\left(\frac{R_2}{R_1}-1\right) \end{aligned}\right| \quad \text{with} \quad \left|\begin{aligned} \frac{R_2}{R_1} &\leqslant 3.28 \\ \frac{R_2}{R_1} &\geqslant 3.28 \end{aligned}\right|, \tag{8.7.22}$$

where R_1 and R_2 are the radii of the ejector nozzle and the mixing chamber, respectively.

Applying the continuity equation for the additional ejected gas

$$\kappa' + 1 = \left(1 + \frac{A_1}{A_1'}\right)\frac{\rho_2 w_2}{\rho_1 w_1}$$

and the law of axial velocity variation for a free jet (8.6.6) and also taking into account that the velocity distribution w_x/w_0 differs only slightly from the mass velocity distribution $\rho_x w_x/\rho_1 w_1$, we can write

$$\frac{w_x}{w} \approx \frac{\rho_x w_x}{\rho_1 w_1} \approx \frac{0,96}{bx:R_1}.$$

In particular we have for the end of the mixing chamber (cross section 2-2)

$$\frac{\rho_2 w_2}{\rho_1 w_1} = \frac{0,96}{bL:R_1}$$

or

$$\frac{L}{rR} = \frac{0,48}{e} \frac{1}{1+x'} \frac{R_2}{R_1}.$$

The calculation shows that the length of the mixing chamber which is necessary to level out the velocity field must be approximately equal to ten times its diameter. This conclusion is sufficiently well verified by experiment.

Manuscript Page No.

[Footnotes]

478 Conventional notation: With respect to the cowling this force is, in the final analysis, an external force (cf. Introduction).

551 The Re number is defined as $w_m R/\nu$, where R is the radius of the jet cross section and w_m is the maximum velocity in it.

552 The term apex is understood to mean the point of intersection between axis and the outer boundary of the jet.

REFERENCES

8.1. Kyukheman, D. and Veber, I., Aerodinamika aviatsionnykh dvigateley [Aerodynamics of Aircraft Engines], IL [Foreign Literature Press], 1956.

8.2. Abramovich, G.I., Prikladnaya gazovaya dinamika [Applied Gasdynamics], GTTI [State Technical and Theoretical Press], 1953.

8.3. Stsillard, K.S., Issledovaniye diffzorov pri bol'shikh skorostyakh [High-Speed Study of Diffusors], Tekhn. zametki TsAGI [Engineering Notes of the Central Aerohydrodynamics Institute], 1958.

8.4. Sedov, L.I., Ploskiye zadachi gidrodinamiki i aerodinamiki [Two-Dimensional Problems of Hydrodynamics and Aerodynamics], GTTI, 1950.

8.5. Witoszynski, E., Uber Strahlerweiterung and Strahlablenkung, Vortäge aus dem Gebiete der Aer- und Hydrodynamik [Jet Expansion and Jet Deflection: Contributions from the Field of Aero- and Hydrodynamics], Innsbruck, 1922, Berlin, 1924.

8.6. Shayrer, G. and Grey, R., Kachestvo sopel reaktivnykh dvigateley [Quality of Jet Engine Nozzles], "Voprosy raketnoy tekhniki" [Problems of Rocket Engineering], No. 3 (9), IL, 1952.

8.7. Astrov, V., Levin, L., Pavlov, Ye. and Khristianovich, S., O raschete sopel Lavalya [On Calculations for Laval Nozzles], "Prikl. mat. i mekh." [Applied Mathematics and Mechanics], VII, 1943.

8.8. Yur'yev, I.M., K raschetu sopel [Nozzle Design], "Prikl. mat. i mekh.," IXX, 1955.

8.9. Frankl', F.I., Sverkhzvukovyye techeniya osevoy simmetrii [Axisymmetric Supersonic Flows], 1934.

8.10. Yur'yev, I.M., O raschete sopla [Nozzle Design], Izv. OTN AN SSSR [Bull. Div. Tech. Sci. Acad. Sci. USSR], Mekh. i Mashinostr [13], No. 4, 1959.

8.11. Guderley, G. and Khantsh, Ye., Nailuchshiye formy sverkhzvukoykh osesimmetrichnykh reaktivnykh sopel [Optimum Forms for Supersonic Axisymmetric Jet Nozzles], In collection entitled "Mekhanika,"

[Mechanics], 4 (38), IL [Foreign Literature Press], 1956.

8.12. Rao, G.V.R., Exhaust Nozzle Contour for Optimum Thrust, Jet Propulsion, June, 1958.

8.13. Rae, G.V.R., Approximation of Optimum Thrust Nozzle Contour, ARS-Journal, June, 1960.

8.14. Abramovich, G.N., Turbulentnyye svobodnyye strui zhidkostey i gazov [Turbulent Free Liquid and Gas Jets], Gosenergoizdat [State Power Press], 1948.

8.15. Borodachev, V.Ya., Rasprostraneniye v poputnom potoke ploskoparallel'noy strui szhimayemoy zhidkosti [Propagation of a Plane-Parallel Jet of Compressible Fluid in an Accompanying Flow], Oborongiz [State Scientific and Technical Publishing House of the Defense Industry], 1954.

8.16. Evvard, Dzh.D., Diffuzory i sopla, Aerodinamika chastey samoleta pri bol'shikh skorostyakh [Diffusors and Nozzles; Aerodynamics of Airplane Parts at High Speeds], Vol. VII of Series "Aerodinamika bol'shikh skorostey i reaktivnaya tekhnika" [High-Speed Aerodynamics and Jet Propulsion Engineering], IL, 1959.

8.17. Sherstyuk, A.N., Priblizhennyy metod rascheta krivolineynykh kanalov [Approximate Method for the Design of Curvilinear Channels], "Teploenergetika" [Thermal Engineering], No. 8, 1955.

8.18. Samoylovich, G.S. and Sherstyuk, A.N., Raschet krivolineynykh osesimmetrichnykh kanalov [Calculations for Curvilinear Axisymmetric Channels], Izv. OTN AN SSSR [Bull. Div. Tech. Sci. Acad. Sci. USSR], No. 4, 1958.

Chapter 9

HYDRODYNAMIC LATTICES

9.1. FUNDAMENTAL INFORMATION ON PROFILE LATTICES

In turbine theory the so-called two-dimensional hydrodynamic lattices are very important. Such a lattice is a system of like profiles arranged at equal distances (lattice spacing l) either along a straight line up to infinity on both sides, thus forming a straight lattice, or

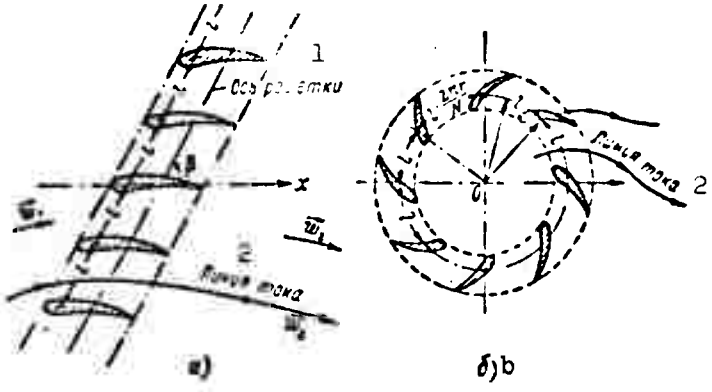


Fig. 9.1.1. The straight lattice is obtained by displacing the profile by equal distances (lattice spacing) l on both sides to infinity (a), and the circular lattice when the profile is repeated on a circle (b). 1) Lattice axis; 2) streamline.

along a circle (where the spacing must be an integer contained in the length of the circumference), i.e., a circular lattice (Fig. 9.1.1).

The solutions to the problems of the airfoil profile in a channel, of the impact of a fluid on a profile, of taking the wind tunnel boundary effects on the results of testing in this tunnel into account, etc., all reduce to the solutions of lattice problems.

Types of turbines. Turbines are machines which interact energeti-

cally with a fluid by changing its momentum with respect to the axis of rotation of its main part, the working wheel. The working wheel is a system of bodies – blades – mounted on the whole rotating hub and interacting with the fluid flow. The wheel in a tubrine rotates due to the action of the flow: it transfers the energy obtained from the flow to other mechanisms. If the working wheel is rotated by an energy source other than the flow and transfers the energy to the fluid (gas), thus displacing it, then it will be a pump – a ventilator, compressor, or propelling screw (Fig. 9.1.2).

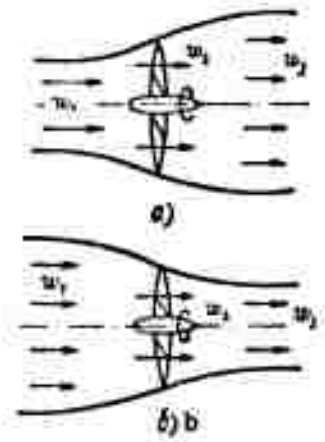


Fig. 9.1.2. Schematic diagram of the simplest turbines. a) Air vane (turbine) – the air passing through the working wheel, gives up part of its energy to it and flows off with lower velocity, causing the stream to widen; b) propelling screw (propeller) – the air is accelerated by the action of the working wheel and flows off at an increased velocity; the cross section of the stream is diminished.

Classification of turbomachines according to their mechanisms. According to the shape of the flow in the working wheel, we distinguish between the following turbines (Fig. 9.1.3).

axial-flow turbines, in which the flow passing through the working wheel is mainly axial in direction (cf. Fig. 9.1.3, a, b);

radial-axial turbines, if the flow in the working wheel changes its direction from axial to radial, e.g., the centrifugal pump, compressor, or radial-flow turbine (cf. Fig. 9.1.3, c, d);

diagonal (mixed) turbines, in which the flow in the working wheel has both an axial and a radial velocity component (cf. Fig. 9.1.3, e).

Generally speaking, all turbines are reversible, i.e., any one of them can operate as both turbine and pump (compressor).

If turbines are to operate regularly the fluid must be supplied and removed in definite directions. Regular operation is achieved with the help of inlets and outlets. Their mutual position is determined by the form of flow required.

Absolute and relative motion. The motion of the fluid in the turbine channels will be designated according to what the coordinate system refers to. In a quiescent coordinate system, for example, fixed to a body at rest, the motion is said to be absolute. If the motion is considered however in a coordinate system connected with the rotating working wheel, it will be a relative motion. The motion of the working wheel itself is a transport motion; when the motion is steady it is a uniform rotation about a fixed axis, with the angular velocity ω. If we

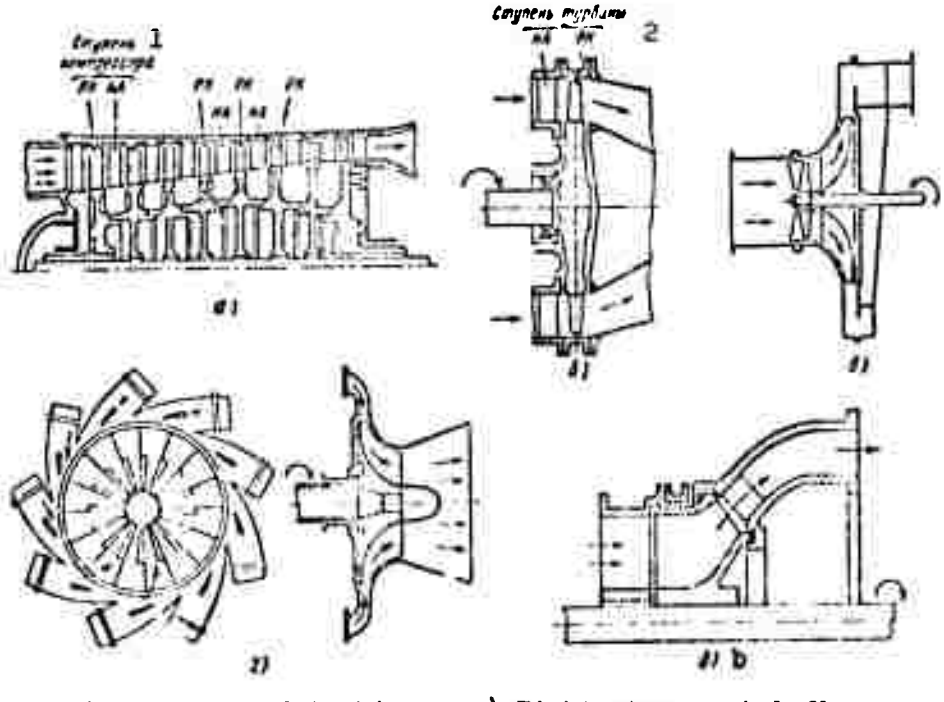


Fig. 5.1.3. Types of turbines. a) Eight-stage axial-flow compressor; b) single-stage axial-flow turbine; c) centrifugal compressor; d) radial centripetal turbine. 1) Stage of compressor; 2) stage of turbine.

denote the relative particle velocity by $\vec{w}$, the transport velocity by $\vec{u}$, and the absolute velocity by $\vec{c}$, then, as is well known from mechanics,

$$\vec{c} = \vec{w} + \vec{u}. \qquad (9.1.1)$$

The geometrical representation of this equation is called the triangle of velocities. It is usually constructed at the inlet and outlet of the working wheel.

Axial-flow turbines. In an axial-flow turbine the gas is brought into the desired direction by the impeller intake guide mechanism and is then led to the working wheel, where energy is exchanged between the gas flow and the wheel.

The working wheel is followed by another (aligning) guide mechanism, which leads the flow either to the next working wheel or to the turbine exit. These two parts – the guide mechanism and the working wheel – constitute a stage. In a turbine stage the guide mechanism (GM) has to be arranged in front of the working wheel (WW) and in a compressor stage behind it. According to the number of stages we distinguish single-, two- three-stage etc., turbines, or, correspondingly, compressors.

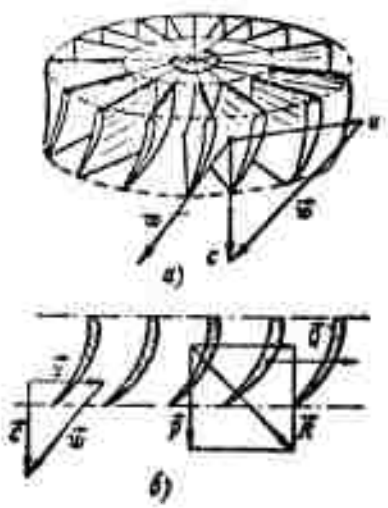


Fig. 9.1.4. Cross section of axial-flow turbine unrolled to a linear profile lattice. a) Triangle of velocities $\vec{c} = \vec{u} + \vec{w}$; b) triangle of forces $\vec{R} = \vec{P} + \vec{Q}$.

In a turbine the gas performs mechanical work; in a compressor mechanical work is expended to compress the gas.

In his paper "Modification of Kirchhoff's method of Determining the Motion of an Unknown Streamline" (1889), N.Ye. Zhukovskiy indicated the possibility of replacing the flow in an axial turbine by the flow through a linear profile lattice. For this purpose the flow between two cylindrical surfaces placed close together (Fig. 9.1.4) is unrolled onto a plane. The cross section of each blade appears

as a profile. Since the flow about each profile is identical, and since each of the profiles must have like profiles to its left and to its right, the row of profiles must extend to infinity on both sides. If the radial velocity component in the axial-flow turbine is taken as zero, the motion in the involute will be two-dimensional (plane); this arrangement is called a plane linear lattice.

Radial-flow turbines. Radial-flow turbines are termed centrifugal if the gas moves from the center to the periphery (cf. Fig. 9.1.3, c) and centripetal if the flow moves towards the machine axis (cf. Fig. 9.1.3, d).

In gas turbine engines (aircraft and stationary engines) compressors of the centrifugal and axial types are used at present; the latter are always multi-staged, while the turbines are mostly single- or multi-stage axial-flow turbines.

Active and reactive turbines. When considering one-dimensional flow through a stage, we denote the work done by a unit mass of gas by l. We then obtain from the energy equation for the absolute motion of a gas flow element in an axial-flow turbine (Fig. 9.1.5)

$$i_1+\frac{c_1^2}{2}=i_2+\frac{c_2^2}{2}=i_3+\frac{c_3^2}{2}+l. \qquad (9.1.2)$$

The hot compressed gas with the parameters p_1, ρ_1, T_1 first enters the convergent channel of the guide mechanism (nozzle) (cf. Fig. 9.1.5) and thus increases in velocity; at the same time, the pressure and temperature drop, i.e., the potential energy of the gas is converted into kinetic energy in the nozzle. From the nozzle the gas is led to the working wheel. As it flows about the turbine blades the pressure will be less on the convex side of the profiles than on the concave side. The circumferential component of the force resulting from this pressure difference rotates the working wheel; the kinetic energy of the gas is

converted into mechanical work.

If the gas pressure p_2 at the nozzle exit (in front of the working wheel) is equal to the pressure p_3 behind the wheel, then, provided there are no losses, we find that the whole energy of the gas becomes kinetic energy in the nozzle; this type of turbine is said to be active. Its working wheel channel cross sections have to be chosen such that (cf. Fig. 9.1.5, a) the relative velocities are equal on both sides of the working wheel. The circumferential force arises due to a change in only the direction of the momentum vector.

The other limiting case represents the purely reactive turbine, where the gas parameters in the nozzle remain completely unchanged. The process of gas expansion and energy conversion occurs as a whole in the working wheel, in whose channels the pressure and temperature drop and the relative velocity increases. The circumferential force arises owing to the momentum vector of the outcoming stream (cf. Fig. 9.1.5, b) changing in both magnitude and direction.

Hence we can see that the expressions "active" and "reactive" turbine are conventional. The process of gas expansion in a turbine usually occurs both in the nozzle and in the working wheel (Fig. 9.1.6); such turbines are said to be reactive. The flow cross section between the profiles in the turbine decreases and the lattice is called a turbine lattice. More exactly, such a turbine is denoted as a confusor.

In a compressor the gas is compressed both in the working wheel and in the guide mechanism behind it. The velocity in the compressor channels drops, pressure and temperature rise. The channel cross sections increase downstream and owing to the geometry these lattices are termed diffusor lattices; less accurately, they are said to be compressor lattices.

A subsonic flow in the channels of a diffusor lattice has the same

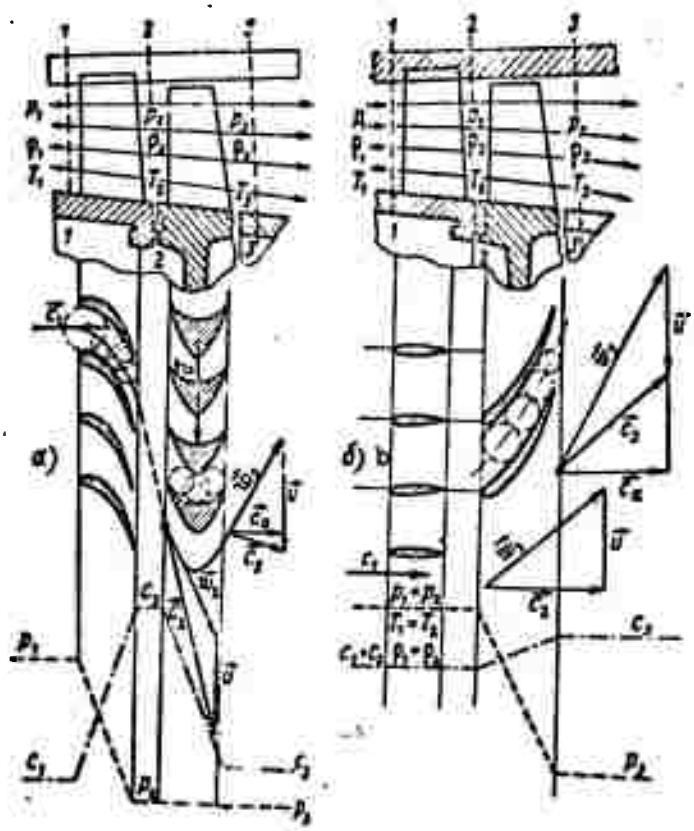


Fig. 9.1.5. Idealized diagrams of turbine stages: if the potential energy is entirely converted into kinetic energy in the guide mechanism we have an active turbine (a); if this is done in the working wheel, we have a reactive turbine (b).

character as the flow in a diffusor – the velocity drops, and the pressure rises. The boundary layer on the profiles therefore grows rapidly. If the pressure gradients are large it becomes separated and reverse flow arises. Owing to this the potential motion of an inviscid fluid differs considerably from that of a real viscous fluid.

In the channels of a confusor lattice the motion is accelerated. The boundary layer in them is very thin and separates with difficulty. The motion of a real viscous fluid is very similar to the potential motion of an inviscid fluid. The theoretically calculated properties of confusor lattices correspond well with experimental data, which cannot be said of diffusor lattices.

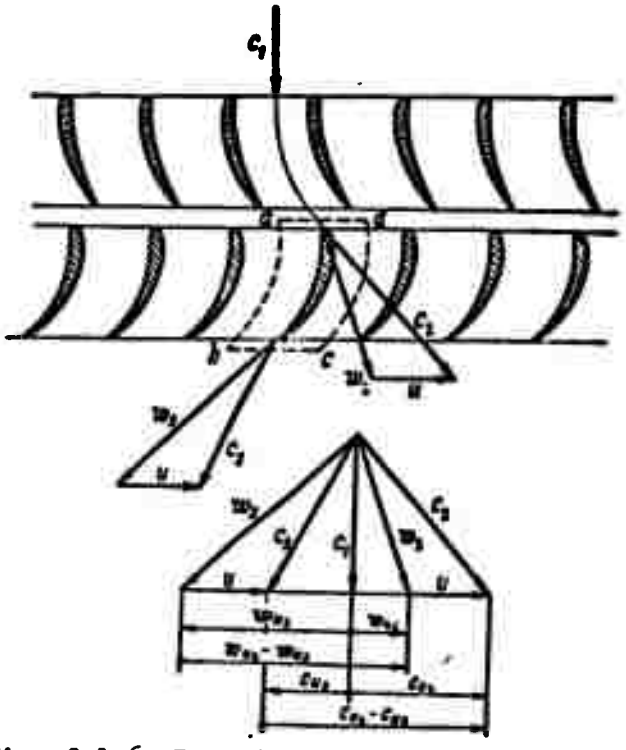


Fig. 9.1.6. Reactive turbine; the gas expansion occurs in the channels of both the working wheel and the guide mechanism.

Moreover, the confusor (turbine) lattice can operate as a compressor, and conversely, the diffusor lattice can work as a turbine. They are then said to operate under off-design conditions.

Second form of the Euler turbine equation. When we multiply Eq. (2.2.7) by the angular velocity or rotation (ω) of the working wheel and assume that $\underline{m} = 1$, we obtain for the work done by 1 kg mass of gas in a turbine stage

$$l_т = M\omega = u_1 w_{u1} - u_2 w_{u2}. \qquad (9.1.3)$$

Instead of w_y, w_u from turbine theory is used here to denote the tangential component of relative velocity, and the subscripts 1 and 3 refer respectively to input and output of the stage. When we consider a compressor stage we have to alter the sign of l_{1-3}. Taking into account

that

$$\left.\begin{aligned} w_{u2}-w_{u1}&=c_{u2}-c_{u1},\\ w_i^2&=c_i^2+u_i^2-2u_ic_{ui}\quad (i=2,\ 3).\end{aligned}\right\} \tag{9.1.4}$$

follows from Eq. (9.1.1), $\vec{c} = \vec{w} + \vec{u}$, we obtain

$$l_u=u_3c_{u3}-u_2c_{u2}=\frac{c_3^2-c_2^2}{2}-\frac{w_3^2-w_2^2}{2}+\frac{u_3^2-u_2^2}{2}. \tag{9.1.5}$$

For an axial-flow turbine $u_2 = u_3$, and instead of (9.1.5)

$$l_u=\frac{c_3^2-c_2^2}{2}-\frac{w_3^2-w_2^2}{2}. \tag{9.1.6}$$

The reactivity ratio. The first term in the Euler equation $(c_3^2 - c_2^2)/2$ characterizes the energy expended in changing the absolute velocity of the flow, i.e., in changing the kinetic energy of 1 kg mass of gas.

The second term is connected with the change in relative velocity. It is the energy expended in changing the velocity in the working wheel channel.

The third term, connected with the change in circumferential velocity, characterizes the fraction of work done by the wheel, which is related to the pressure rise due to centrifugal forces. The sum of the last two terms $\frac{1}{2}[(u_2^2 - w_2^2) + (u_3^2 - w_3^2)]$ characterizes the change in potential energy of 1 kg of gas. The fraction of total energy converted in the working wheel of the turbine corresponds to the reactivity ratio of the stage, i.e., to the ratio between the work l_p done by the gas (or on it) owing to the change in potantial energy in the working wheel and the total work $l_p + l_k$ done by or on the gas:

$$r_\text{т}=\frac{l_p}{l_p+l_k}=\frac{w_3^2-w_2^2+u_3^2-u_2^2}{c_3^2-c_2^2+w_2^2-w_3^2+u_3^2-u_2^2}. \tag{9.1.7}$$

The reactivity ratio may vary within wide limits; it can be equal to or less than zero and larger than unity. With it the triangle of velocities changes too. For an active axial-flow stage we have

$w_2 = w_3$ и $r_2 = 0$; если $c_0 = c_{2s}$ то $l_a = 0, r_a = 1$.

Geometrical and kinematic parameters of a plane linear lattice. In addition to the common geometrical parameters (cf. Fig. 3.5.1), the chord b, the maximum thickness d, the maximum camber f, the position of the maximum camber b_f and the position of maximum thickness b_d, conceptions referring to the camber of the profile and to the directions of the leading and trailing edges are introduced into turbine engineering in order to characterize the profile geometrically (Fig. 9.1.7). The direction of the leading edge is determined by the acute angle θ_1 between the chord and the tangent unit vector to the camber line at the leading edge, directed downstream; the trailing edge direction θ_2 is determined correspondingly. The camber of the profile is characterized by the angle of camber (cf. Fig. 3.5.1)

$$\theta = \theta_1 + \theta_2.$$

The straight line joining the corresponding points of the lattice profiles in the direction of their camber line curvature is called the axis (front of the lattice; its unit vector is denoted by $\vec{i}_0$. The lattice spacing (period) l is the distance on the lattice axis between the corresponding points of neighboring profiles. For a turbine lattice under design conditions its direction of motion coincides with the axis, whereas for a compressor it is oppositely directed.

A linear profile lattice is obtained as a result of unrolling the wheel cross section of an axial-flow turbine with a cylindrical surface on a plane. The axis of rotation of the working wheel coincides with the axis of the cylinder and is perpendicular to the axis (front) of the lattice; for the lattice too, it is convenient to keep the unit vector $\vec{i}_\omega$ (of the angular velocity $\vec{\omega}$) as a normal to the lattice front directed from inlet to outlet. If turning the unit vector $\vec{i}_\omega$ anticlockwise (clockwise) through a right angle aligns with the lattice axis, we

shall denote the lattice as right-handed (left-handed). Positive angles are measured anticlockwise in the right-handed lattice and clockwise in the left-handed lattice.

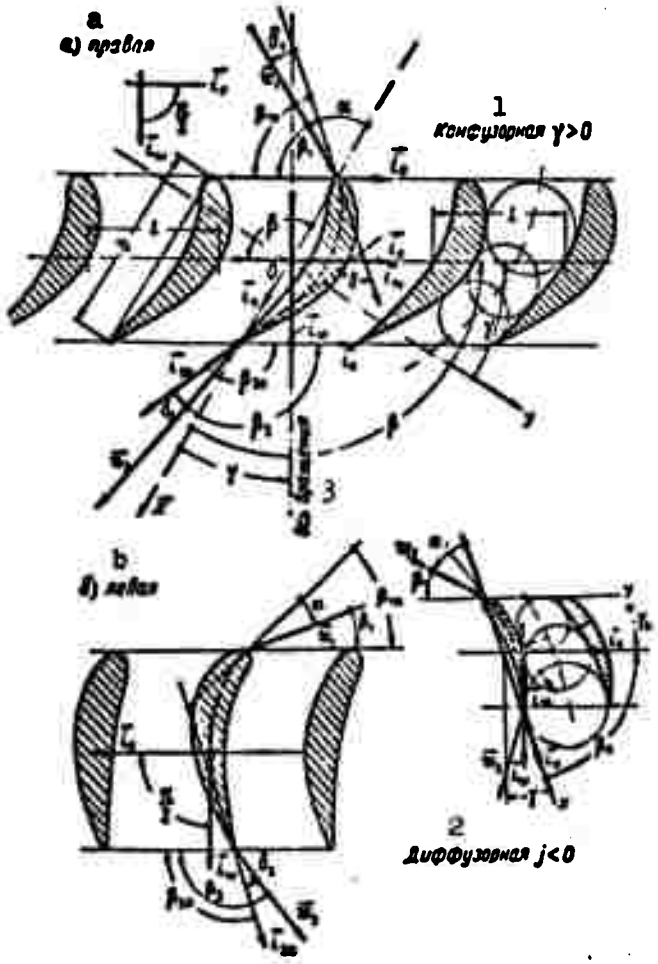


Fig. 9.1.7. Geometrical and kinematic lattice parameters. The type of the lattice is determined by the direction in which the axis of rotation $\vec{i}_\omega$ is turned to make it coincide with the lattice axis $\vec{i}_O$. a) right-handed (all angles counted anticlockwise are positive); b) left-handed (all angles counted clockwise are positive). 1) Confusor; 2) diffusor; 3) axis of rotation.

The position of the profile in the lattice is determined by the rigging angle of incidence, β, which is the smallest angle through which the chord unit vector $\vec{i}_p$ (directed from the leading edge to the trailing edge of the profile along its chord) must be rotated to coin-

cide with the lattice axis, which we shall therefore the angle of the lattice axis, β. It is sometimes convenient to determine the position of the profile by the stagger angle γ which is the angle through which the unit vector $\vec{i}_p$ has to be rotated to coincide with the unit vector $\vec{i}_\omega$ of lattice rotation (Fig. 9.1.8). If $\gamma > 0$ we have a confusor (turbine) lattice, and if $\gamma < 0$ the lattice is of the diffusor (compressor) type.

Besides the rigging angle of incidence, β, of the profile, the geometrical forward rigging angle β_{1p} (and backward rigging angle β_{2p}) are introduced; these are the smallest angles through which the unit vector of inlet (outlet) direction must be rotated to coincide with the lattice axis. Here we have $\theta = \beta_{2p} - \beta_{1p}$.

In theoretical considerations of lattices the coordinate origin is often placed at the chord's midpoint, the x-axis being oriented along the chord unit vector and the y-axis being obtained by turning the x-axis anticlockwise through 90° (right-handed coordinate system).

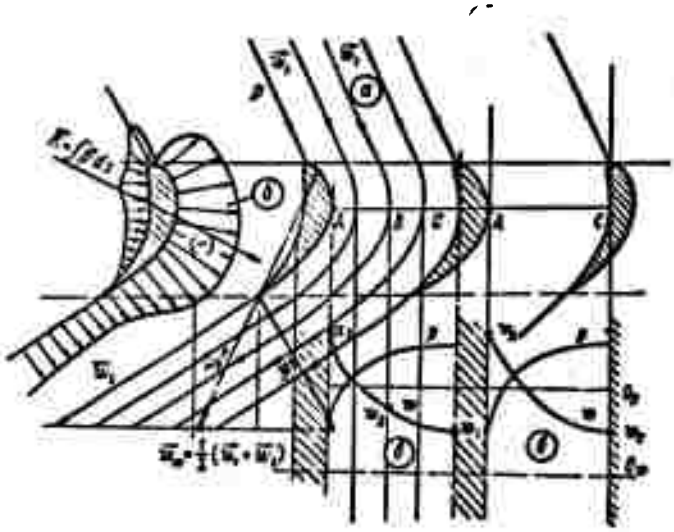


Fig. 9.1.8. Form of flow through a fixed lattice of profiles. a) Velocity field; b) pressure distribution on the profile; c) pressure and velocity in the channel between the profiles.

The kinematic lattice parameters determine the velocity direction.

The angle β_1 (β_p) between the velocity direction at the inlet (outlet) and the lattice axis is called the forward (backward) rigging angle.

The angle of attack α (α_m) is the angle between the direction of the velocity $\vec{w}_1$ ($\vec{w}_m$) and the profile chord

$$\alpha = \beta - \beta_1.$$

The angle of influx, δ_1, is the angle between the direction of the velocity $\vec{w}_1$ and the unit vector of the inflow direction:

$$\delta_1 = \beta_{1л} - \beta_1.$$

The angle of lag, δ_2, is the angle between the direction of the velocity $\vec{w}_2$ and the unit vector of the outflow direction:

$$\delta_2 = \beta_{2л} - \beta_2.$$

Finally, there is another essential lattice parameter, namely the density of the lattice, i.e., the ratio $b/l = \bar{b}$.

The form of motion of the flow through a fixed linear lattice. Let us consider the two-dimensional potential motion of an incompressible inviscid fluid through a fixed linear lattice of profiles. The flow through a linear lattice is assumed to be periodic, i.e., on any straight line parallel to the axis of the lattice (see Fig. 9.1.8) the flow parameters at any given point of the straight line will be the same as those lying at distances of $\pm$ nl (n = 1, 2, 3, ...). Theoretically, the flow parameters level off and become equal only at infinity upstream and downstream from the lattice. In practice, for streamlined profiles it is already at small distances (1 to 2 periods) both upstream and downstream from the lattice that the nonuniformity of the lattice parameters becomes negligibly small and that their values are the same as at infinity.*

Let us decompose the flow as a whole into the streamlines. If the flow does not separate and the walls of the lattice profile are impenetrable, the contours of each of them will be streamlines. Each profile will have its own streamline, coming from infinity, splitting at the

forward stagnation point, recombining at the backward stagnation point and flowing off to infinity. The Zhukovskiy-Chaplygin condition will be valid and necessary even for lattices of profiles with sharp trailing edges; infinitely large velocities cannot arise, and the flow must leave each of the lattice profiles smoothly, i.e., the backward stagnation point must lie on the trailing edge.

In a flow about a profile in a lattice, as in a flow round an isolated profile, the velocity will be greater on the convex side of the profile than on the concave side, and the pressure will be lower. Owing to the pressure difference a force will be acting on the profile which is directed from the concave to the convex side. This can also be derived from the momentum conservation law, according to which a change in direction of the velocity $\vec{w}_1$ to $\vec{w}_2$ must give rise to a force $\vec{R}$ directed from the concave to the convex side of the profile surface.

Structure of the flow in a lattice of profiles. Provided the period is not too large, the flow between two neighboring profiles may be considered as a flow in a channel. In this case all considerations discussed in Part 8.5 remain valid. We have to take into account that this method does not apply to the inflow region of the profile. This can be seen in Fig. 9.1.9, which gives a graph of the velocity distribution on a profile in a confusor lattice for an incompressible fluid flow.

Deflection of the flow through a lattice of profiles. The force of finite magnitude arising on an isolated profile cannot alter the momentum of an infinite mass of fluid passing per unit time. Therefore, a single profile (or a finite number of them) does not change the form of the flow at a sufficiently large distance from it.

When a flow passes through a lattice of profiles the infinite mass of fluid is affected by an infinite number of profiles which are able to change the momentum of the whole mass of the fluid.

The angle $\beta_1(\beta_p)$ between the velocity direction at the inlet (outlet) and the lattice axis is called the forward (backward) rigging angle.

The angle of attack α (α_m) is the angle between the direction of the velocity $\vec{w}_1(\vec{w}_m)$ and the profile chord

$$\alpha = \beta - \beta_1.$$

The angle of influx, δ_1, is the angle between the direction of the velocity $\vec{w}_1$ and the unit vector of the inflow direction:

$$\delta_1 = \beta_{1a} - \beta_1.$$

The angle of lag, δ_2, is the angle between the direction of the velocity $\vec{w}_2$ and the unit vector of the outflow direction:

$$\delta_2 = \beta_{2a} - \beta_2.$$

Finally, there is another essential lattice parameter, namely the density of the lattice, i.e., the ratio $b/l = \bar{b}$.

The form of motion of the flow through a fixed linear lattice. Let us consider the two-dimensional potential motion of an incompressible inviscid fluid through a fixed linear lattice of profiles. The flow through a linear lattice is assumed to be periodic, i.e., on any straight line parallel to the axis of the lattice (see Fig. 9.1.8) the flow parameters at any given point of the straight line will be the same as those lying at distances of $\pm$ nl (n = 1, 2, 3, ...). Theoretically, the flow parameters level off and become equal only at infinity upstream and downstream from the lattice. In practice, for streamlined profiles it is already at small distances (1 to 2 periods) both upstream and downstream from the lattice that the nonuniformity of the lattice parameters becomes negligibly small and that their values are the same as at infinity.*

Let us decompose the flow as a whole into the streamlines. If the flow does not separate and the walls of the lattice profile are impenetrable, the contours of each of them will be streamlines. Each profile will have its own streamline, coming from infinity, splitting at the

forward stagnation point, recombining at the backward stagnation point and flowing off to infinity. The Zhukovskiy-Chaplygin condition will be valid and necessary even for lattices of profiles with sharp trailing edges; infinitely large velocities cannot arise, and the flow must leave each of the lattice profiles smoothly, i.e., the backward stagnation point must lie on the trailing edge.

In a flow about a profile in a lattice, as in a flow round an isolated profile, the velocity will be greater on the convex side of the profile than on the concave side, and the pressure will be lower. Owing to the pressure difference a force will be acting on the profile which is directed from the concave to the convex side. This can also be derived from the momentum conservation law, according to which a change in direction of the velocity $\vec{w}_1$ to $\vec{w}_2$ must give rise to a force $\vec{R}$ directed from the concave to the convex side of the profile surface.

Structure of the flow in a lattice of profiles. Provided the period is not too large, the flow between two neighboring profiles may be considered as a flow in a channel. In this case all considerations discussed in Part 8.5 remain valid. We have to take into account that this method does not apply to the inflow region of the profile. This can be seen in Fig. 9.1.9, which gives a graph of the velocity distribution on a profile in a confusor lattice for an incompressible fluid flow.

Deflection of the flow through a lattice of profiles. The force of finite magnitude arising on an isolated profile cannot alter the momentum of an infinite mass of fluid passing per unit time. Therefore, a single profile (or a finite number of them) does not change the form of the flow at a sufficiently large distance from it.

When a flow passes through a lattice of profiles the infinite mass of fluid is affected by an infinite number of profiles which are able to change the momentum of the whole mass of the fluid.

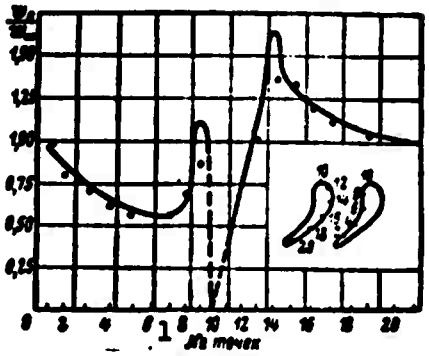


Fig. 9.1.9. Velocity distribution on a profile in an incompressible fluid flow, calculated by the channel method. 1) Number of points.

Let us consider a contour formed by two streamlines (though this is not necessary) separated by the length of a spacing and by straight line sections parallel to the lattice axis lying so far in front of and behind the lattice that the velocity distributions on them can be taken as uniform (Fig. 9.1.10). The mass of fluid passing per unit time between the streamlines AB and DC through the sections AD and BC is finite. The change in momentum per unit time of this mass will therefore be finite too, and equal to the difference in momentum of the volumes AA'D'D and BB'C'C.

Two fundamental lattice relations may be indicated (for simplicity we consider an incompressible fluid, $\rho = \text{const}$). The first results from the mass conservation law:

$$w_1 \sin\beta_1 = w_2 \sin\beta_2 = w_a; \qquad (9.1.8)$$

the second reads

$$w_1 \cos\beta_1 = w_2 \cos\beta_2 + \frac{\Gamma}{t}. \qquad (9.1.9)$$

where Γ is the circulation about one profile. It can be obtained by calculating the circulation with respect to the contour ABCDA in Fig. 9.1.10:

$$-\Gamma = \int_{ABCDA} \vec{w}\cdot d\vec{r} = \int_{AB} \vec{w}\cdot d\vec{r} + \int_{BC} \ldots + \int_{CD} \ldots + \int_{DA}.$$

Since the flow is periodic, $\int_{AB} \vec{w}\cdot d\vec{r} = -\int_{CD} \vec{w}\cdot d\vec{r}$, and in the case of uniform velocity distributions on BC and AB we have

$$\Gamma = t(w_1 \cos\beta_1 - w_2 \cos\beta_2). \qquad (9.1.10)$$

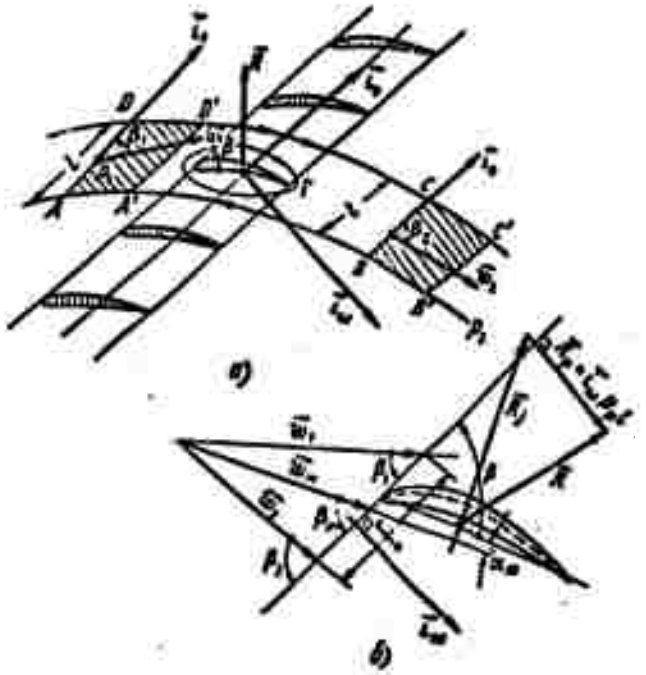


Fig. 9.1.10. Deflection of the flow by the profile lattice. The amount of fluid passing through the lattice is determined by the normal velocity component, therefore (with ρ = const) $w_1 \sin \beta_1 = w_2 \sin \beta_2$; the circulation with respect to the contour formed by the two streamlines one spacing apart and by closing straight lines parallel to the lattice axis is $\Gamma = t(w_1 \cos \beta_1 - w_2 \cos \beta_2)$.

This expression does not depend on how distant the sections AD and BC are taken as being. In Fig. 9.1.10 these relations are given in the form of triangles of velocities.

Dividing Expression (9.1.9) by $w_z = w_1 \sin \beta_1 = w_2 \sin \beta_2$, we obtain

$$\operatorname{ctg} \beta_1 = \operatorname{ctg} \beta_2 + \frac{\Gamma}{t w_z} \qquad (9.1.11)$$

Energy exchange between moving lattice and flow. For an energy exchange between working wheel and flow, and correspondingly between lattice and flow, it is necessary that a transport motion exists at the working wheel (lattice). With zero transport motion at the working wheel, then, although there is a momentum change and forces arise on the blades of the wheel, the work done by these forces will be equal to

zero.

Thus, when energy is exchanged, the absolute motion of the flow will be unsteady. It follows from (2.3.25) that the total change in specific energy is connected with the local change in motion:

$$\frac{dl}{dt} = \frac{1}{\rho}\frac{\partial p}{\partial t}. \qquad (9.1.12)$$

Equation (9.1.12) expresses the fact that the change in total energy of any particle, determined by the left-hand side of (9.1.12), will differ from zero during the particle's motion only when this motion occurs in the field of variable pressure ($\partial p/\partial t \neq 0$). In turbines this variable pressure field is produced by the blades of the working wheel as it rotates.

When rotation is uniform, the relative motion will be steady and the pressure distribution will be the same as it would be if it were connected with the profile.

In the absolute system of coordinates fixed to the turbine body, however, the spatial periodicity of the relative motion will be a periodic function of time (Fig. 9.1.11, c).

If the velocity of the transport motion is u, then the distance traveled in the time δt will be $\delta l = u\,dt$. It follows that $\delta t = \delta l/u$. The scale of length can thus be transformed to a time scale by dividing it by u and the division gives us the pressure as a function of time. The trajectory of a particle's absolute motion is obtained by plotting its positions at short intervals of time, δt.

The forces acting on a linear lattice. Let us divide two streamlines, AB and CD, by the length of the spacing (cf. Fig. 9.1.10) and let us denote the force acting on the profile in the lattice by $\vec{R}$.

We then apply the momentum theorem (2.2.17) to the fluid volume enclosed between these lines and the sections AD and BC, parallel to the lattice axis and placed far upstream and downstream of the lattice, where the velocity distribution is uniform; first we shall suppose

that the fluid is incompressible (ρ = const).

If we take into account that the continuity equation reads $\rho\vec{w}_1\cdot\vec{i}_n=\rho\vec{w}_2\cdot\vec{i}_n$, then

$$\vec{R}=l(p_1-p_2)\vec{i}_n+l(\rho\vec{w}\cdot\vec{i}_n)(\vec{w}_1-\vec{w}_2)=l(p_1-p_2)\vec{i}_n-$$
$$-l(\rho\vec{w}\cdot\vec{i}_n)\vec{w}_d; \qquad (9.1.13)$$

where $\vec{w}_d$ denotes the velocity of deflection of the flow, $\vec{w}_2-\vec{w}_1$.

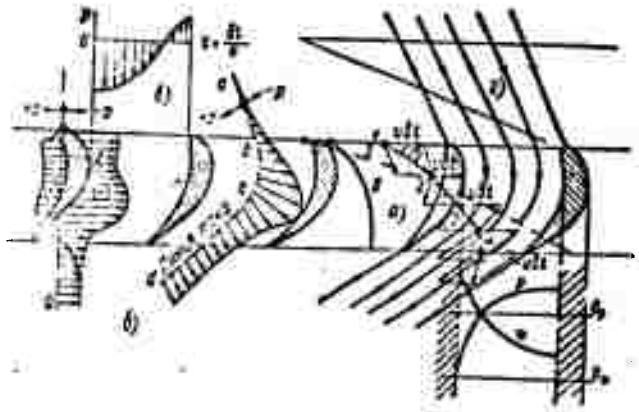


Fig. 9.1.11. Lattice in uniform motion. a) The particle trajectories and streamlines in absolute motion, I and II paths of particles along concave and convex side of blade, III – path of particle in the middle of the channel; b) pressure distribution on the profile and along a streamline; c) the spatial periodicity at any point of the absolute system of coordinates becomes a periodic time function in the relative motion; d) streamlines in relative motion.

To obtain the viscosity effect in explicit form we consider it by the rather widely used "hydraulic" method, i.e., by determining the pressure losses p_μ due to friction, between the sections AB and BC [cf. (4.4.34)]. Since there are no other dissipative factors, the Bernoulli equation assumes the form

$$p_1+\frac{\rho w_1^2}{2}=p_2+\frac{\rho w_2^2}{2}+p_\mu. \qquad (9.1.14)$$

In this case (9.1.13) can be written as

$$p_1-p_2=\rho\frac{w_1^2-w_2^2}{2}+p_\mu=\rho\frac{\vec{w}_2+\vec{w}_1}{2}\cdot(\vec{w}_2-\vec{w}_1)+p_\mu=$$
$$=\rho\vec{w}_m\cdot\vec{w}_d+p_\mu. \qquad (9.1.15)$$

where $\vec{w}_m = 1/2(\vec{w}_1 + \vec{w}_2)$ denotes half the geometrical sum of the velocities at infinity in front of and behind the profile (cf. Fig. 9.1.10, b).

Therefore

$$\vec{R} = l(\rho\vec{w}_m \cdot \vec{w}_d)\vec{i}_\omega - l(\rho\vec{w}_m \cdot \vec{i}_\omega)\vec{w}_d + i_\omega p_\mu = \\ = l[\rho\vec{w}_m \times (\vec{i}_\omega \times \vec{w}_d)] + \vec{i}_\omega p_\mu l.$$

Since $\vec{\Gamma}_\omega \perp \vec{w}_d$ we have

$$|l(\vec{i}_\omega \times \vec{w}_d)| = |l(\vec{w}_2 - \vec{w}_1) \cdot \vec{i}_0| = \Gamma,$$

i.e., we may regard the vector $\underline{l}(\vec{\Gamma}_\omega \times \vec{w}_d)$ as the vector $\vec{\Gamma}$ of circulation about the profile;* denoting $p_\mu l$ by R_μ we have

$$\vec{R} = \rho\vec{w}_m \times \vec{\Gamma} + \vec{i}_\omega R_\mu. \qquad (9.1.16)$$

In the case of zero viscosity the lift of the profile in the lattice placed in an incompressible fluid flow is equal to the product of the fluid's density, the magnitude of half the vector sum of the velocities at infinity in front of and behind the profile, and the circulation around the profile; its direction is obtained by turning the velocity vector $\vec{w}_m$ through a right angle against the direction of circulation. This theorem was stated by N.Ye. Zhukovskiy; the force $R = \rho w_\infty \Gamma$ is the Zhukovskiy force.

As will be shown in what follows (cf. Part 9.7), this relation is somewhat modified if we consider a compressible fluid (gas).

In a viscous incompressible fluid $2\vec{w}_m = \vec{w}_1 + \vec{w}_2$; $\vec{w}_2 - \vec{w}_1 = \vec{w}_d$ and the circulation Γ has to be determined from the real velocities. This means that the drag force R_μ which is equal in magnitude to the product of dynamic head losses in the lattice and the lattice spacing, and which is directed along the axis of rotation of the lattice, has to be added to the Zhukovskiy force. The viscosity effect becomes thus apparent both directly through the drag force R_μ and indirectly (implicitly)

through a change in the velocities $\vec{w}_1$ and $\vec{w}_2$ at infinity and in the circulation Γ.

The lift and drag coefficients of a profile in a lattice. They are usually determined from the mean velocity w_m:

$$R_y = C_y \frac{\rho w_m^2}{2} A, \quad R_x = C_x \frac{\rho w_m^2}{2} A. \qquad (9.1.17)$$

We see from Fig. 9.1.12 that the viscosity effect on a profile in a turbine lattice will cause $C_{y\ rt}$ to exceed $C_{y\ iz}$, and that when it operates as a pump, $C_{y\ n}$ will be smaller than $C_{y\ iz}$. Fig. 9.1.13 shows the graphs of the changes in C_y, C_x, and $\mu = C_x/C_y$ after V.I. Lechev's experiments* for a blade profile of a reversible pump – turbine, arranged in a lattice under turbine and pump conditions, and also isolated.

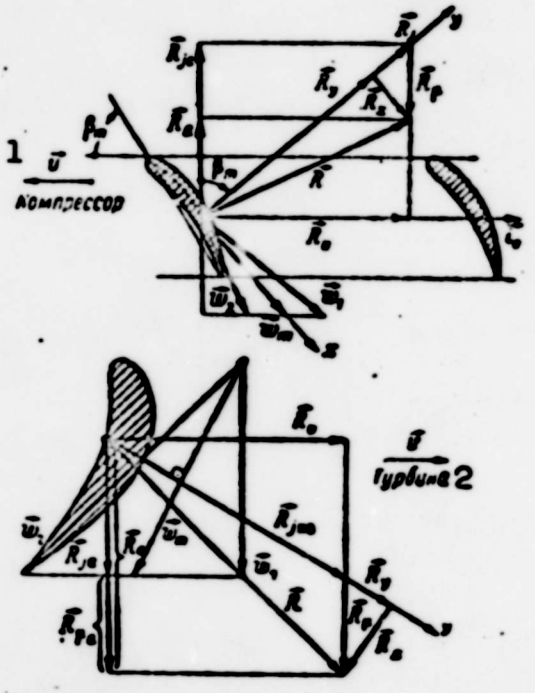


Fig. 9.1.12. The lift R_y of a profile in a turbine (compressor) lattice is greater (smaller) than the lift R_j of an isolated profile. 1) Compressor; 2) turbine.

Conditions of flow about a lattice. As we have indicated, turbines are reversible machines and the flow about one and the same lattice of

profiles may correspond to the machine's operation either as a turbine or as a compressor. For lattices operating under turbine conditions, the inlet pressure exceeds the outlet pressure p_2, the inlet velocity w_1 is smaller than the outlet velocity w_2 and the circumferential force R_u coincides with the direction of the transport velocity $\vec{u}$ ($\vec{R}_u = \vec{1}_0 R_u$, with $\vec{u} = u\vec{1}_0$).

When the lattice operates under compressor conditions all these relations are reversed: $p_1 < p_2$, $w_1 > w_2$, and R_u is directed oppositely to $\vec{u}$ ($\vec{R}_u = -\vec{1}_0 R_u$).

The conception of the turbine (compressor) lattice coincides with the conception of a confusor (diffusor) lattice only if the flow satisfies the design conditions (Fig. 9.1.14).

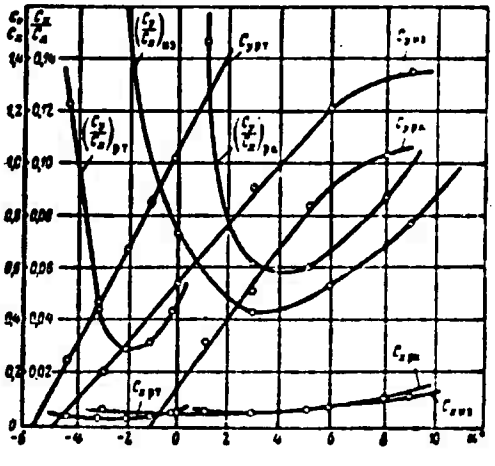


Fig. 9.1.13. Experimental graph of the dependence of $C_{y\,r}$ and $C_{y\,iz}$.

Lattice efficiency. In analogy to the linear diffusor, an efficiency is sometimes defined for a compressor lattice as the ratio of the pressure increment really obtained in a viscous fluid and the pressure increment that would be obtained in an inviscid fluid for the same values of the velocities w_1 and w_2 (i.e., with the same triangle of velocities):

$$\eta_{p.s} = \frac{(p_2 - p_1)_\mu}{p_2 - p_1} = \frac{R_a}{R_{ja}}.$$

Taking into account that (cf. Fig. 9.1.12)

$$R_a = R_y \cos\beta_m - R_x \sin\beta_m; \quad R_u = R_y \sin\beta_m + R_x \cos\beta_m = R_{ja} \operatorname{ctg}\beta_m$$

we obtain

$$\eta_{p.s} = \frac{R_y \cos\beta_m - R_x \sin\beta_m}{(R_y \sin\beta_m + R_x \cos\beta_m)\operatorname{ctg}\beta_m} = \frac{1 - \mu \operatorname{tg}\beta_m}{1 + \mu \operatorname{ctg}\beta_m} = \frac{\operatorname{tg}\beta_1}{\operatorname{tg}(\beta_1 + \gamma)}. \qquad (9.1.18)$$

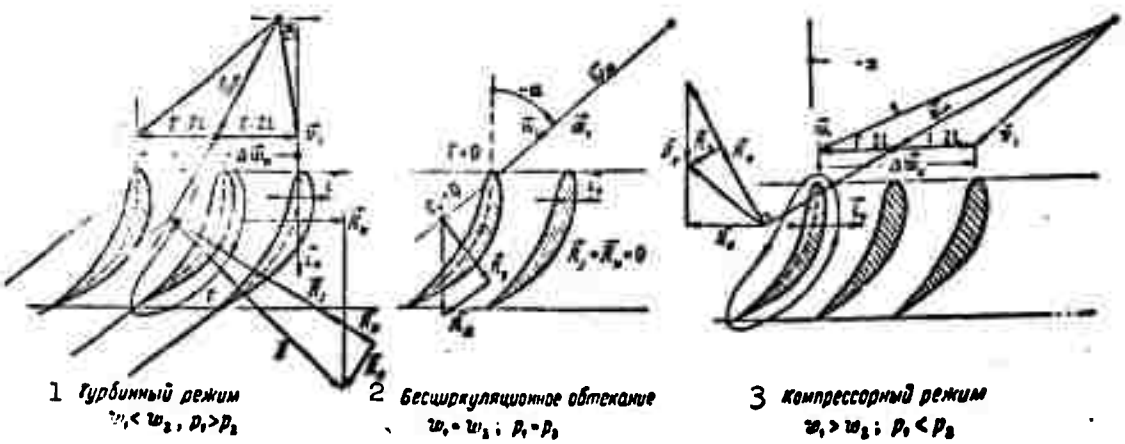


Fig. 9.1.14. Various conditions of a flow through a confusor lattice. 1) Turbine conditions; 2) circulation-free flow; 3) compressor conditions.

In order to obtain a given deflection of the flow in a turbine lattice (the same circumferential force), the pressure difference must be greater for a viscous fluid than for an inviscid one. Correspondingly,

$$\eta_{p.T} = \frac{p_2 - p_1}{(p_2 - p_1)_\mu} = \frac{R_{ja}}{R_a} = \frac{R_y \sin\beta_m - R_x \cos\beta_m}{(R_y \cos\beta_m + R_x \sin\beta_m)\operatorname{tg}\beta_m} = \frac{1 - \mu \operatorname{ctg}\beta_m}{1 - \operatorname{tg}\beta_m} = \frac{\operatorname{tg}(\beta_1 - \gamma)}{\operatorname{tg}\beta_1} \qquad (9.1.19)$$

This definition of the efficiency coincides with the energetic definition as the ratio of work put in and work taken out. In fact, for a compressor lattice, for example, we have

$$\eta = \frac{L_{полезн}}{L_{полезн} + L_{потер}} = \frac{L_{полезн}}{L_{затрач}} = \frac{R_a w_a}{R_a u} = \frac{R_a}{R_a \operatorname{ctg} \beta}.$$

which agrees with the above formulation.

9.2. POTENTIAL FLOW OF INCOMPRESSIBLE FLUID THROUGH A LATTICE OF THIN PROFILES

The theory of the lattice wing due to Chaplygin and Zhukovskiy. In his paper "Theory of the Lattice Wing" (1911), S.A. Chaplygin gave a solution to the problem of the flow through an infinite lattice of profiles. He considered a lattice of plane plates arranged parallel to the imaginary axis y (Fig. 9.2.1). S.A. Chaplygin used a rather complicated procedure of mapping this lattice to the upper semi-plane of the variable u in such a way that both sides of the plates constituting the lattice on the z-plane are transferred to form real axis of the u-plane, and he established the interrelation between direction and magnitude of the flow velocity far in front of and behind the plate lattice and then he used the formula named after him to find the forces arising on the plates constituting the lattice. In this paper S.A. Chaplygin indicated a method of constructing a lattice of profiles with rounded leading edges and sharp trailing edges.

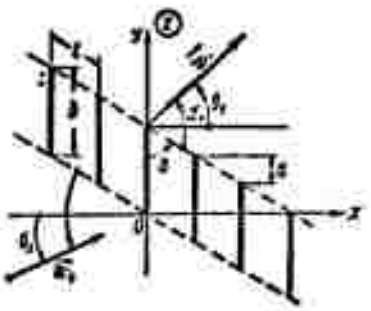


Fig. 9.2.1. Lattice of plane plates as considered by S.A. Chaplygin in 1911.

Soon after S.A. Chaplygin's paper appeared, N.Ye. Zhukovskiy published his third article "Vortex Theory of the Propelling Screw," in which the problem of the plane plate lattice was solved directly by constructing the characteristic function. In what follows, the relations between the parameters of the plate lattice will be derived by the method of conformal mapping of the exterior of this lattice to the exterior of a circle.

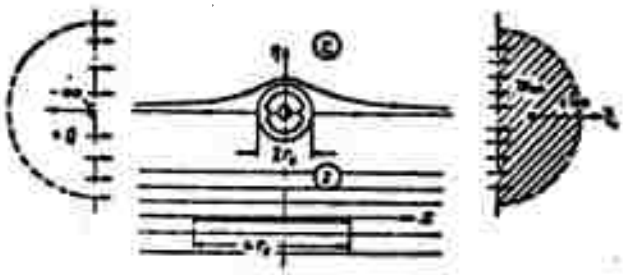


Fig. 9.2.2. The flow about a circle of a plane-parallel stream can be considered as the flow from two dipoles; one lies at the center of a circle, the other at infinity.

Lattice of unstaggered plane plates. Considering the uniform flow as flow from a dipole (Fig. 9.2.2) located at infinity (p. 149), let us now separate the source and the sink constituting the dipole at the point $z = 0$ of the circle, placing the sink at point $+mr_0$ and the source,

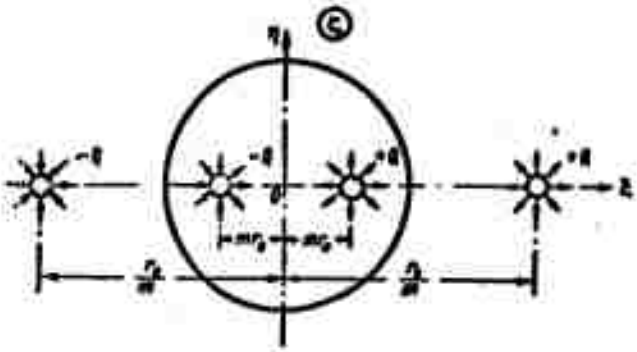


Fig. 9.2.3. To make the circle of radius r_0 become a streamline enclosing the singularities placed at the points mr_0 and $-mr_0$ identical singularities must be placed at the points $-r_0/(-m)$ and r_0/m.

having the same intensity Q, at the point $-mr_0$ $(m < 1)$. In order to make the circle of radius r_0 into a streamline, a sink must then be placed at point r_0/m and a source at point $-r_0/-m$ (Fig. 9.2.3), both with the intensity Q. Let us put $Q = w_\infty h$, h being a certain length whose meaning will be explained in what follows. The complex potential of such a flow has the form

$$\chi(\zeta)=\frac{w_\infty h}{2\pi}\left[\ln\frac{\zeta+\frac{r_0}{m}}{\zeta-\frac{r_0}{m}}+\ln\frac{\zeta+mr_0}{\zeta-mr_0}\right].$$

For the subsequent calculations it is convenient to add the constant quantity [$\ln(-1)=\ln e^{\pi i}$] to the potential and write

$$\chi_1(\zeta)=\frac{w_\infty h}{2\pi}\left[\ln\frac{r_0+m\zeta}{r_0-m\zeta}+\ln\frac{\zeta+mr_0}{\zeta-mr_0}\right]. \qquad (9.2.1)$$

If we now take

$$z=\frac{h}{2\pi}\left[\ln\frac{r_0+m\zeta}{r_0-m\zeta}+\ln\frac{\zeta+mr_0}{\zeta-mr_0}\right]. \qquad (9.2.2)$$

as the function mapping it to the exterior of the circle, we shall then have a uniform plane-parallel flow in the z-plane

$$\chi(z)=w_\infty z. \qquad (9.2.3)$$

The points $\zeta = r_0/m$ and $\zeta = -r_0/m$ go over to the z-plane at infinity. Since the singularities are conserved in this transformation the source and the sink are displaced to infinity, the former along the negative semi-axis and the latter along the positive semi-axis.

Owing to the conformity of the mapping,* the numerical values of velocity potential and stream function are conserved and so are the numerical characteristics of the singularities (source-sink intensity, dipole moments, vorticities). On passing around** any external singularity, e.g., the source at point r_0/m, we obtain the intensity $Q = w_\infty h$. Corresponding to this in the z-plane, where the velocity w_∞ is parallel to the x-axis, there will be a flow through sections of length h on the y-axis, i.e., corresponding to the whole flow from the source on the ζ-plane of the circle there will be a flow in a band of width h in the z-plane.

Passing around the source a second time raises the intensity by Q; it is convenient to imagine this circumvention occurring on a second plane – a screw surface of infinitely small pitch (Fig. 9.2.4); corresponding to it, there will be a second band lying alongside of the first.

A third band will correspond to a third circumvention, and so on. The planes formed by stratifying the ζ-plane constitute the so-called many-leaved Riemann surface. Infinitely many circumventions of the source (or another singularity) lead to an infinite multitude of bands lying side by side (their widths are equal to $\underline{h}$ in the given case) and covering the whole z-plane.

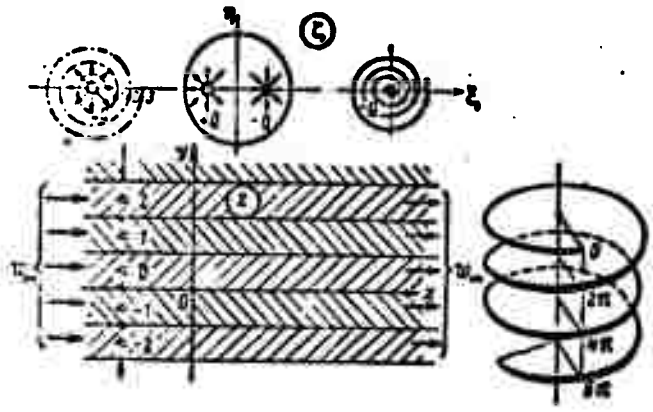


Fig. 9.2.4. Totality of infinitely many circumventions of the source (sink) yielding infinitely many bands lying side by side (of width $\underline{h}$ in the figure) covering the whole z-plane. Right, a perspective diagram of the Riemann surface and the circumventions about a source.

Let us investigate where the point $\zeta = r_0 e^{i\vartheta}$ of the circle is transposed to. Making use of the many-valuedness of the logarithm,* we can write

$$z=\frac{h}{2\pi}\left[\ln\frac{r_0+mr_0e^{i\vartheta}}{r_0-mr_0e^{i\vartheta}}+\ln\frac{r_0e^{i\vartheta}+mr_0}{r_0e^{i\vartheta}-mr_0}+2\pi ik\right]=$$
$$=\frac{h}{2\pi}\left[\ln\frac{(e^{i\vartheta}+m)(1+me^{i\vartheta})}{(e^{i\vartheta}-m)(1-me^{i\vartheta})}+2\pi ik\right]= \quad 5$$
$$=\frac{h}{2\pi}\left[\ln\frac{m^2+m(e^{i\vartheta}+e^{-i\vartheta})+1}{m^2-m(e^{i\vartheta}+e^{-i\vartheta})+1}+2\pi ik\right]=$$
$$=\frac{h}{2\pi}\ln\frac{1+2m\cos\vartheta+m^2}{1-2m\cos\vartheta+m^2}+ikh=x+iy.$$

whence

$$x=\frac{h}{2\pi}\ln\frac{1+2m\cos\vartheta+m^2}{1-2m\cos\vartheta+m^2},\quad y=kh \qquad (k=0,\pm1,\pm2\ldots \quad (9.2.4)$$

We see that corresponding to the point of the circle in the ζ-

plane there will be an infinite totality of twice traveled line sections in the z-plane, parallel to the x-axis, of the length $b=\frac{h}{\pi}\ln\frac{1+m}{1-m}$ and the spacing h, arranged symmetrically with respect to the y-axis, i.e., an unstaggered lattice (Fig. 9.2.5).

Lattice of plane plates arranged one after the other. If vortices of the strength $\Gamma = w_\infty d$ (Fig. 9.2.6) are located at the points mr_0 and

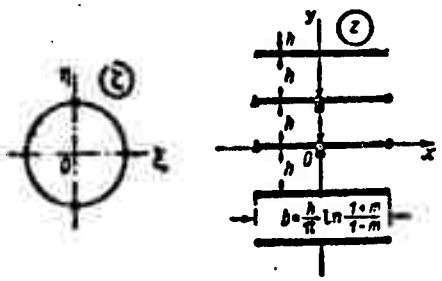


Fig. 9.2.5. Function $z=\frac{h}{2\pi}\ln\frac{(r_0+m\zeta)(\zeta+mr_0)}{(r_0-m\zeta)(\zeta-mr_0)}$ maps the circle on the ζ-plane to an unstaggered lattice of plane plates.

$-r_0/m$, and vortices of the strength $-w_\infty d$ ($m < 1$, real) at the points $-mr_0$ and $+r_0/m$, then the stream function will read

$$\chi_3(\zeta)=-i\frac{w_\infty d}{2\pi}\left(\ln\frac{r_0+m\zeta}{r_0-m\zeta}-\ln\frac{\zeta+mr_0}{\zeta-mr_0}\right). \qquad (9.2.5)$$

To obtain the flow $w_\infty z$ on the z-plane we have to apply the mapping function

$$z=-i\frac{d}{2\pi}\left(\ln\frac{r_0+m\zeta}{r_0-m\zeta}-\ln\frac{\zeta+mr_0}{\zeta-mr_0}\right). \qquad (9.2.6)$$

The vortices at the points $\pm r_0/m$ are displaced to infinity. Corresponding in the x-plane to one circumvention of the vortex there will be a displacement along the straight line section of length $d = \Gamma/w_\infty$, and to the whole interior of the circle – the band of width d. On the second circumvention of the vortex, the whole region outside the circle will be mapped as the second band of width d, and so on. The whole z-plane will look as if it were made up of bands of width d glued togeth-

er along the x-axis (cf. Fig. 9.2.6) and the ζ-plane will be a Riemann surface with infinitely many leaves. The circle (more exactly, the infinite multitude of circles on the infinitely leaved Riemann surface) is mapped to a system of straight line sections constituting part of the straight streamlines.

In order to determine the length of the sections we put $\zeta = r_0 e^{i\vartheta}$. Then

$$z = x + iy = -i\frac{d}{2\pi}\left[\ln\frac{(1+me^{i\vartheta})(e^{i\vartheta}-m)}{(1-me^{i\vartheta})(e^{i\vartheta}+m)} + 2\pi ik\right] =$$
$$= -i\frac{d}{2\pi}\ln\frac{1-m^2-2im\sin\vartheta}{1-m^2+2im\sin\vartheta} + kd.$$

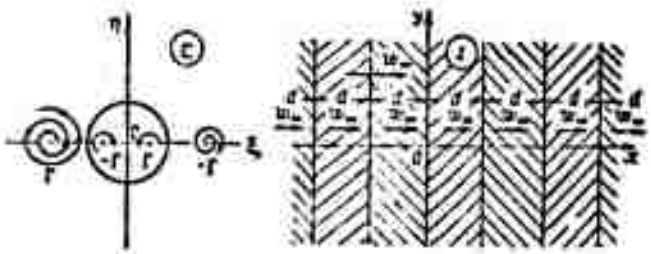


Fig. 9.2.6. To one leaf of the Riemann surface on the ζ-plane corresponds a band of width α on the z-plane.

Taking into account that

$$\ln\frac{a-bi}{a+bi} = \ln\frac{e^{-i\varphi}}{e^{i\varphi}} = -2i\varphi + 2\pi is; \quad \varphi = \operatorname{arctg}\frac{b}{a},$$

we obtain

$$z = x + iy = -i\frac{d}{2\pi}\left[-2i\operatorname{arctg}\frac{2m\sin\vartheta}{1-m^2} + 2\pi i(k+s)\right] =$$
$$= -\frac{d}{\pi}\operatorname{arctg}\frac{2m\sin\vartheta}{1-m^2} + nd,$$

i.e.,

$$x = -\frac{d}{\pi}\operatorname{arctg}\frac{2m\sin\vartheta}{1-m^2} + nd; \quad y = 0. \qquad (9.2.7)$$

The circle is therefore mapped to a row of sections of length (chord)

$$b=\frac{2d}{\pi}\operatorname{arctg}\frac{2m}{1-m^2},$$

arranged on the real x-axis with spacings equal to d (unstaggered lattice, Fig. 9.2.7).

Staggered (diagonal) lattice. Superimposing the two flows considered above we obtain

$$\chi_0(\zeta)=\chi_1+\chi_2=\frac{w_\infty}{2\pi}\left[(h-id)\ln\frac{r_0+m\zeta}{r_0-m\zeta}+(h+id)\ln\frac{\zeta+mr_0}{\zeta-mr_0}\right].$$

With

$$d=l\sin\beta;\quad h=l\cos\beta;$$

we have

$$\chi_0=\frac{w_\infty l}{2\pi}\left[e^{-i\beta}\ln\frac{r_0+m\zeta}{r_0-m\zeta}+e^{i\beta}\ln\frac{\zeta+mr_0}{\zeta-mr_0}\right]. \qquad (9.2.8)$$

Function

$$z=\frac{l}{2\pi}\left[e^{-i\beta}\ln\frac{r_0+m\zeta}{r_0-m\zeta}+e^{i\beta}\ln\frac{\zeta+mr_0}{\zeta-mr_0}\right] \qquad (9.2.9)$$

maps the flow from the vortex sources at the points $\pm r_0/m$ streaming around the circle, to the flows $\chi_0(z) = w_\infty z$ on the z-plane. Using Eqs. (9.2.4) and (9.2.7) obtained before we can write the real and imaginary parts of the mapping function in the form

$$\frac{x}{l}=\frac{\cos\beta}{2\pi}\ln\frac{1+2m\cos\vartheta+m^2}{1-2m\cos\vartheta+m^2}-\frac{\sin\beta}{\pi}\operatorname{arctg}\frac{2m\sin\vartheta}{1-m^2}+k\sin\beta;$$

$$\frac{y}{l}=k\cos\beta \qquad (k=0,\pm1,\pm2,\ldots). \qquad (9.2.10)$$

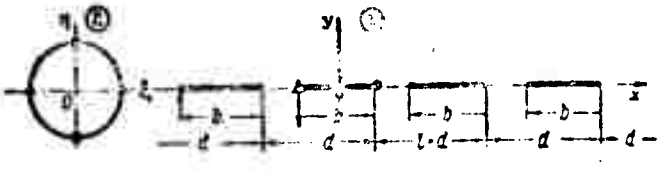


Fig. 9.2.7. Mapping of the circle to a lattice of plates arranged on the real x-axis.

In this case the circle on the infinitely leaved Riemann surface goes over to an infinite row of straight line sections, parallel to the

real x-axis, their axis enclosing the angle β with the imaginary y-axis (Fig. 9.2.8).

In fact, corresponding to each circumvention of the circle, when the number $\underline{k}$ is constant, there will be a double circumvention of the straight line section parallel to the real axis ($y = k \cos \beta = \text{const}$). When $\underline{k}$ is changed by unity ($\underline{k}$ being an integer) $\underline{y}$ changes by the quantity $\underline{l} \cos \beta$, and all abscissas of the subsequent section acquire the same constant increment $\underline{l} \sin \beta$.

The length of the sections (chords) must be determined by calculating the distance between the beginning and the end-point of the section, the distance between leading and trailing edges, where $dz/d\zeta = 0$.

This yields

$$e^{-i\beta}\left(\frac{m}{r_0 + m\zeta_p} - \frac{-m}{r_0 - m\zeta_p}\right) + e^{i\beta}\left(\frac{1}{\zeta_p + mr_0} - \frac{1}{\zeta_p - mr_0}\right) = 0;$$

where ζ_p is a point on the circle at which $dz/d\zeta = 0$.

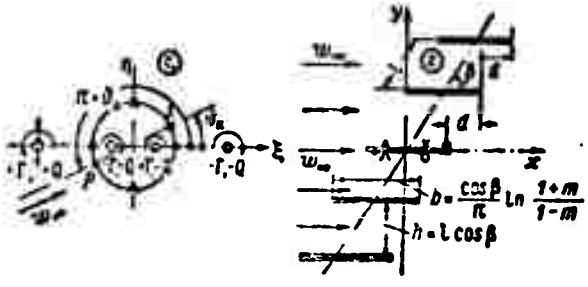


Fig. 9.2.8. Mapping of a circle to a diagonal lattice of plane plates.

Assuming $\zeta_p = r_0 e^{i\vartheta}$ and solving this equation we obtain

$$e^{-i\beta}(e^{2i\vartheta} - m^2) = e^{i\beta}(1 - m^2 e^{2i\vartheta}),$$

whence

$$e^{2i\vartheta} = \frac{(1+m^2)\cos\beta + i(1-m^2)\sin\beta}{(1+m^2)\cos\beta - i(1-m^2)\sin\beta}$$

or

$$\operatorname{tg}\beta = i\frac{(1+m^2)(1-e^{2i\theta})}{(1-m^2)(1+e^{2i\theta})} = \frac{1+m^2}{1-m^2}\operatorname{tg}\theta. \qquad (9.2.11)$$

Equation (9.2.11) determines two angles corresponding to the points S and P on the circle which go over to the beginning and the end of the section:

$$\theta_н = \operatorname{arc\,tg}\left(\frac{1-m^2}{1+m^2}\operatorname{tg}\beta\right);\quad \theta_к = \theta_н + \pi = \operatorname{arc\,tg}\left(\frac{1-m^2}{1+m^2}\operatorname{tg}\beta\right) + \pi,$$

for which

$$\sin\theta_к = -\sin\theta_н;\quad \cos\theta_к = -\cos\theta_н.$$

We have therefore from (9.2.10)

$$2\pi\frac{x_к - x_н}{l} = 2\cos\beta\ln\frac{1+2m\cos\theta_н + m^2}{1-2m\cos\theta_н + m^2} - 4\sin\beta\operatorname{arc\,tg}\frac{2m\sin\theta_н}{1-m^2}. \qquad (9.2.12)$$

Calculating

$$\sin\theta_н = \frac{\operatorname{tg}\theta_н}{\sqrt{1+\operatorname{tg}^2\theta_н}} = \frac{(1-m^2)\sin\beta}{\sqrt{(1-m^2)^2 + 4m^2\cos^2\beta}};$$

$$\cos\theta_н = \frac{1}{\sqrt{1+\operatorname{tg}^2\theta_н}} = \frac{(1+m^2)\cos\beta}{\sqrt{(1-m^2)^2 + 4m^2\cos^2\beta}}$$

and substituting in (9.2.12) we obtain

$$\frac{\pi b}{2l} = \cos\beta\ln\frac{\sqrt{(1-m^2)^2 + 4m^2\cos^2\beta} + 2m\cos\beta}{1-m^2} + \sin\operatorname{arc\,tg}\frac{2m\sin\beta}{\sqrt{(1-m^2)^2 + 4m^2\cos^2\beta}}. \qquad (9.2.13)$$

This relation, linking the parameter m, the lattice density $\frac{l}{b}$ and the angle β of the lattice is given in the table.

$\frac{l}{b}$	0°	±15°	±30°	±45°	±60	±75°	±90°
0	1	1	1	1	1	1	—
0,25	0,996	0,997	0,998	0,999	1,000	1,000	—
0,50	0,916	0,919	0,938	0,965	0,987	0,999	—
0,75	0,781	0,782	0,810	0,848	0,911	0,975	—
1,00	0,656	0,658	0,685	0,722	0,775	0,857	1
1,25	0,557	0,561	0,579	0,609	0,647	0,697	0,725
1,50	0,481	0,484	0,499	0,518	0,542	0,566	0,585

TABLE (cont'd)

1,75	0,419	0,423	0,435	0,450	0,464	0,477	0,482
2,00	0,371	0,375	0,383	0,395	0,404	0,411	0,421
2,25	0,335	0,339	0,343	0,350	0,355	0,359	0,363
2,50	0,314	0,315	0,317	0,320	0,323	0,325	0,326
∞	0	0	0	0	0	0	0

Thus, Function (9.2.9) maps the flow in the plane outside the circle of radius r_0 with real w_∞ to a uniform flow $w_\infty z$ which is parallel to the real axis, and therefore, parallel to the plates (zero angle of attack for each of the plates).

Lattice of plates with nonzero angle of attack. To obtain a flow in the z-plane with an angle of attack $\alpha \neq 0$ we consider first a circulation-free flow about a cylinder in the ζ-plane [cf. (9.2.9)], the flow having the angle of attack α,

$$\chi_{6\alpha}(\zeta) = \frac{w_\infty l}{2\pi}\left(e^{-i(\alpha+\beta)}\ln\frac{r_0+m\zeta}{r_0-m\zeta} + e^{i(\alpha+\beta)}\ln\frac{\zeta+mr_0}{\zeta-mr_0}\right) \qquad (9.2.14)$$

and apply Transformation (9.2.9) to it. This does not change the geometry of the lattice of plates obtained by mapping the cylinder. The velocity distribution, however, will be different. Since

$$(w_x - iw_y)_{6\alpha} = \frac{d\chi_{6\alpha}}{dz} = \frac{d\chi_{6\alpha}}{d\zeta}\frac{d\zeta}{dz}$$

and

$$\frac{d\chi_{6\alpha}}{d\zeta} = \frac{w_\infty l}{2\pi}\left[e^{-i(\alpha+\beta)}\left(\frac{m}{r_0+m\zeta} - \frac{-m}{r_0-m\zeta}\right) + e^{i(\alpha+\beta)}\left(\frac{1}{\zeta+mr_0} - \frac{1}{\zeta-mr_0}\right)\right] = \frac{mr_0 l w_\infty}{\pi}\left(\frac{e^{-i(\alpha+\beta)}}{r_0^2-m^2\zeta^2} - \frac{e^{i(\alpha+\beta)}}{\zeta^2-m^2r_0^2}\right);$$

$$\frac{dz}{d\zeta} = \frac{lmr_0}{\pi}\left(\frac{e^{-i\beta}}{r_0^2-m^2\zeta^2} - \frac{e^{i\beta}}{\zeta^2-m^2r_0^2}\right),$$

we have

$$(w_x - iw_y)_{6\alpha} = -\frac{d\chi_{6\alpha}}{dz} = \frac{d\chi_{6\alpha}}{d\zeta}\frac{d\zeta}{dz} =$$

$$= w_\infty \frac{(\zeta^2-m^2r_0^2)e^{-i(\alpha+\beta)} - (r_0^2-m^2\zeta^2)e^{i(\alpha+\beta)}}{(\zeta^2-m^2r_0^2)e^{-i\beta} - (r_0^2-m^2\zeta^2)e^{i\beta}}. \qquad (9.2.15)$$

The point $z = \pm\infty$ corresponds to $\zeta = \pm r_0/m$. Substituting these values, we obtain from (9.2.15)

$$(w_x - iw_y)_{z\to\pm\infty} = w_\infty e^{-i\alpha}, \qquad (9.2.16)$$

i.e., the flow far in front of and behind the lattice is directed at the angle α to the real axis, or, what is the same, at the angle α to each of the plates (Fig. 9.2.9). The separation points on the circle are found if we put $d\chi_{bts}/d\zeta = 0$. Applying (9.2.11), we obtain the coordinates of the separation points of the flow:

$$\left.\begin{aligned}\theta_{01} &= \operatorname{arctg}\left[\frac{1-m^2}{1+m^2}\operatorname{tg}(\alpha+\beta)\right],\\ \theta_{02} &= \pi + \operatorname{arctg}\left[\frac{1-m^2}{1+m^2}\operatorname{tg}(\alpha+\beta)\right].\end{aligned}\right\} \qquad (9.2.17)$$

As can be seen from Relation (9.2.16), the flow $\chi_{bts}(z)$ about the lattice of plates considered does not influence the velocity at infinity. According to Zhukovskiy's theorem the force acting on any of the plates will be zero, because the circulation around the profile is equal to zero. When the flow hits the plate at the angle of attack α, the velocities at the leading and trailing edges become infinite, since the angles of the partition points on the circle are determined by Relation (9.2.17) and they do not coincide for $\alpha \neq 0$ with the points corresponding to the leading and trailing edges, defined by Eq. (9.2.11). To satisfy the Zhukovskiy-Chaplygin condition for smooth flow about the trailing edge, a circulatory flow must be superimposed on the flow round the cylinder such that the point corresponding to the trailing edge coincides with the backward stagnation point.

Purely circulatory flow through a lattice of plane plates. A purely circulatory flow about a cylinder can be achieved by placing vortices with the circulations $\Gamma/2$ inside the circle at the points $\pm mr_0$, where, in order to conserve the streamline circumferences, vortices with the circulations $-\Gamma/2$ must be placed at the points $\pm r_0/m$ (Fig. 9.2.10).

The characteristic function of the flow [cf. (3.2.12)] reads

$$\chi_k(\zeta) = -\frac{\Gamma}{4\pi i}\ln\frac{\zeta^2 - m^2 r_0^2}{\zeta^2 - \frac{r_0^2}{m^2}}. \qquad (9.2.18)$$

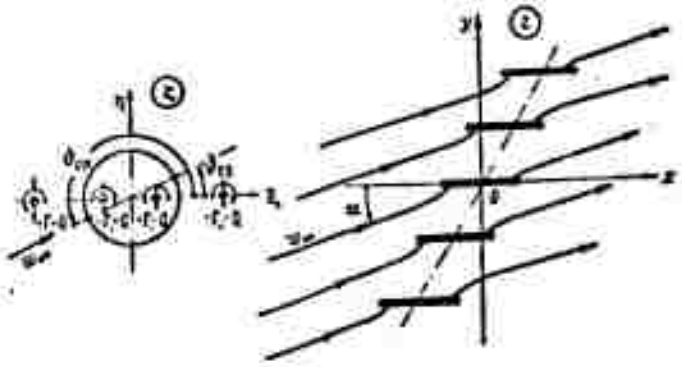


Fig. 9.2.9. Circulation-free flow about a lattice of plane plates at an angle of attack α.

Maintaining as before the mapping function in the form (9.2.9) and taking into account that conformal mapping does not change the numerical characteristics of the singularities (intensity, circulation), we shall have a circulatory flow, Γ, around each of the profiles (cf. Fig. 9.2.10). The external vortices, -Γ/2, at the points $\pm r_0/m$ are shifted to infinity.*

The velocity at any point of the ζ-plane outside the circle will be

$$(w_\zeta - iw_\eta)_k = \frac{d\chi_k}{d\zeta} = i\frac{\Gamma}{4\pi}\left(\frac{2\zeta}{\zeta^2 - m^2 r_0^2} - \frac{2\zeta}{\zeta^2 - \frac{r_0^2}{m^2}}\right) =$$

$$= i\frac{\Gamma r_0^2 \zeta}{2\pi}\frac{m^4 - 1}{(\zeta^2 - m^2 r_0^2)(m^2\zeta^2 - r_0^2)}.$$

At the points of the circ $\zeta = r_0 e^{i\vartheta}$

$$(w_\zeta - iw_\eta)_k = i\frac{\Gamma}{2\pi r_0}\frac{(1-m^4)e^{i\vartheta}}{[m^2 e^{-2i\vartheta} + (1+m^4) - m^2 e^{2i\vartheta}]e^{2i\vartheta}} =$$

$$= i\frac{\Gamma}{2\pi r_0}\frac{(1-m^4)(\cos\vartheta + i\sin\vartheta)}{(1-m^2)^2 + 4m^2\sin^2\vartheta}. \qquad (9.2.19)$$

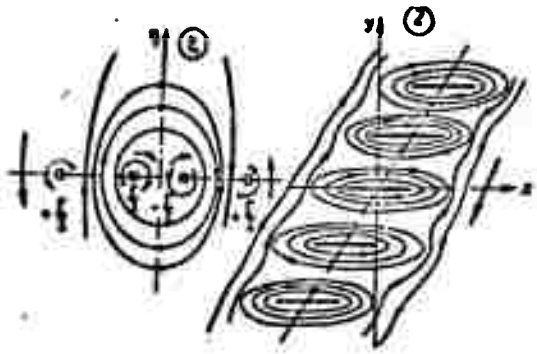


Fig. 9.2.10. Flow about a lattice of plane plates by a purely circulatory stream.

The general case. In order to obtain the flow about a lattice of plates with a given angle of attack, α, and nonvanishing circulation we have to superimpose Flows (9.2.14) and (9.2.18) on the ζ-plane of the circle:

$$\chi_\zeta(\zeta)=\chi_{\zeta\alpha}(\zeta)+\chi_{\zeta\Gamma}(\zeta)=\frac{w_\infty l}{2\pi}\left[e^{-i(\alpha+\beta)}\ln\frac{r_0+m\zeta}{r_0-m\zeta}+\right.$$

$$\left.+e^{i(\alpha+\beta)}\ln\frac{\zeta+mr_0}{\zeta-mr_0}\right]+i\frac{\Gamma}{4\pi}\ln\frac{\zeta^2-m^2r_0^2}{\zeta^2-\frac{r_0^2}{m^2}} \qquad (9.2.20)$$

and map the flow obtained on the z-plane with the help of Function (9.2.9):

$$z=\frac{l}{2\pi}\left(e^{-i\beta}\ln\frac{r_0+m\zeta}{r_0-m\zeta}+e^{i\beta}\ln\frac{\zeta+mr_0}{\zeta-mr_0}\right).$$

The magnitude of the circulation Γ is determined from the Zhukovskiy-Chaplygin condition on the smooth flow about the trailing edge of the profile. For this purpose the backward separation point on the circle must go over to the trailing edge.

At the separation point $\zeta_z = r_0 e^{i\vartheta_k}$ where $\vartheta_k = \pi + \arctg\left(\frac{1-m^2}{1+m^2}\operatorname{tg}\frac{\gamma}{2}\right)$, the total flow velocity on the circle,

$$w_\zeta - iw_\eta = -\frac{mr_0 l w_\infty}{\pi}\left(\frac{e^{-i(\alpha+\beta)}}{r_0^2-m^2\zeta^2}-\frac{e^{i(\alpha+\beta)}}{\zeta^2-m^2r_0^2}\right)+$$

$$+i\frac{\Gamma r_0^2\zeta}{2\pi}\cdot\frac{m^4-1}{m^2r_0^2)(m^2\zeta^2-r_0^2)}$$

must be equal to zero. Omitting the subscript "k" of ϑ we find from this condition that

$$\Gamma = -\frac{2mlw_\infty}{i}\frac{(e^{2i\vartheta}-m^2)e^{-i(\alpha+\beta)}-(1-m^2e^{2i\vartheta})e^{i(\alpha-\beta)}}{(1-m^4)e^{i\vartheta}} =$$
$$= 2i\frac{(e^{i\vartheta}-m^2e^{-i\vartheta})e^{-i(\alpha+\beta)}-(e^{-i\vartheta}-m^2e^{i\vartheta})e^{i(\alpha+\beta)}}{1-m^4}mlw_\infty.$$

But, as we already know,

$$\sin\vartheta = \frac{(1-m^2)\sin\beta}{R};\quad \cos\vartheta = \frac{(1+m^2)\cos\beta}{R},$$

where, for brevity, we put $R = \sqrt{(1-m^2)^2+4m^2\cos^2\beta}$.

Therefore,

$$e^{i\vartheta} = \cos\vartheta + i\sin\vartheta = \frac{(1+m^2)\cos\beta + i(1-m^2)\sin\beta}{R} = \frac{e^{i\beta}+m^2e^{-i\beta}}{R};$$

$$e^{i\vartheta}-m^2e^{-i\vartheta} = \frac{1}{R}[e^{i\beta}+m^2e^{-i\beta}-m^2(e^{-i\beta}-m^2e^{i\beta})] = \frac{(1-m^4)e^{i\beta}}{R};$$

$$e^{-i\vartheta}-m^2e^{i\vartheta} = \frac{(1-m^4)e^{-i\beta}}{R}.$$

Consequently,

$$\Gamma = 2i\frac{(1-m^4)e^{i\beta}e^{-i(\alpha+\beta)}-(1-m^4)e^{-i\beta}e^{i(\alpha+\beta)}}{R(1-m^4)}mlw_\infty =$$
$$= 2i\frac{e^{-i\alpha}-e^{i\alpha}}{R}mlw_\infty = \frac{4mlw_\infty}{\sqrt{(1-m^2)^2+4m^2\cos^2\beta}}\sin\alpha. \qquad (9.2.21)$$

For an isolated plate

$$\Gamma_\infty = \pi bw_\infty\sin\alpha.$$

Thus, denoting the ratio of lattice profile lift to isolated profile lift as the coefficient of lattice influence on the lift, we obtain

$$k = \frac{\Gamma}{\Gamma_\infty} = \frac{4ml}{b\pi\sqrt{(1-m^2)^2+4m^2\cos^2\beta}}. \qquad (9.2.22)$$

The values of k are given in Fig. 9.2.11.

For $\beta = 0$

$$k_{\beta=0} = \frac{4ml}{\pi b(1+m^2)}.$$

In this case

$$\frac{\pi b}{2l} = \ln\frac{(1+m)^2}{1-m^2} = \ln\frac{1+m}{1-m}$$

or

$$\frac{1+m}{1-m}=e^{\frac{\pi b}{2l}}.$$

Solving this equation, we find

$$m=\frac{e^{\frac{\pi b}{2l}}-1}{e^{\frac{\pi b}{2l}}+1};\quad \frac{m}{1+m^2}=\frac{1}{2}\operatorname{th}\frac{\pi b}{2l}.$$

Therefore, for $\beta = 0$

$$k_{\beta=90^\circ}=\frac{4ml}{\pi b(1-m^2)};\quad \frac{2m}{1-m^2}=\operatorname{tg}\frac{\pi b}{2l} \qquad (9.2.23)$$

If $\beta = \pi/2$ we find by analogy that

$$k_{\beta=0}=\frac{2l}{\pi b}\operatorname{th}\frac{\pi b}{2l}.$$

and finally

$$k_{\beta=\frac{\pi}{2}}=\frac{2l}{\pi b}\operatorname{tg}\frac{\pi b}{2l}. \qquad (9.2.24)$$

Change of angle of attack. As was shown (cf. Fig. 9.1.10), the velocity along straight lines parallel to the lattice front will have a constant component Γ/l regardless of the position of these straight lines. The profile's angle of attack therefore varies with the flow velocity at infinity in front of the lattice; the amount of this variation is determined by the relation

$$\operatorname{tg}\alpha_{\text{в ср}}=\frac{w_\infty\sin\alpha+\frac{\Gamma}{l}\cos\beta}{w_\infty\cos\alpha-\frac{\Gamma}{l}\sin\beta}=$$

$$=\frac{\sqrt{(1-m^2)^2+4m^2\cos^2\beta}+4m\cos\beta}{\sqrt{(1-m^2)^2+4m^2\cos^2\beta}+4m\sin\beta\operatorname{tg}\alpha}\operatorname{tg}\alpha. \qquad (9.2.25)$$

Deflection of the flow. The relations between the angles of inflow and outflow of the stream for a lattice of plane plates can be found from Equalities (Fig. 9.2.12)

$$w_a=w_1\sin\beta_1=w_m\sin\beta_m=w_2\sin\beta_2,$$

$$w_2\cos\beta_2+\frac{\Gamma}{2l}=w_m\cos\beta_m=w_1\cos\beta_1-\frac{\Gamma}{2l},$$

from which

$$\operatorname{ctg}\beta_m=\operatorname{ctg}\beta_2+\frac{\Gamma}{2lw_m\sin\beta_m}=\frac{1}{2}(\operatorname{ctg}\beta_1+\operatorname{ctg}\beta_2). \qquad (9.2.26)$$

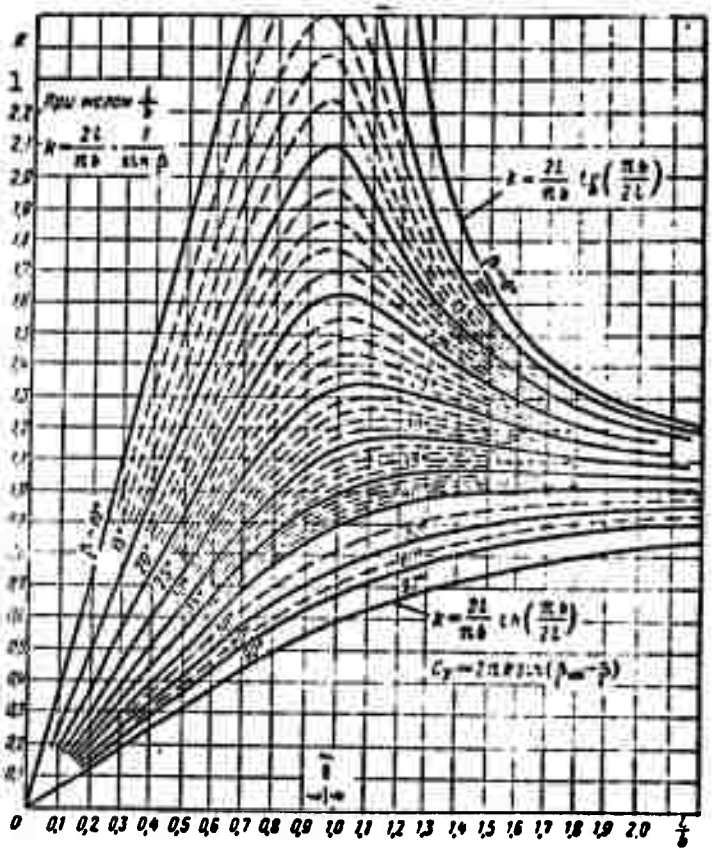


Fig. 9.2.11. Coefficient of influence of the lattice of plane plates on the lift, $k=\frac{\Gamma_{реш}}{\Gamma_{нр}}=\left(\frac{dC_y}{d\alpha}\right)_{реш}:\left(\frac{dC_y}{d\alpha}\right)_{нр}=\frac{4ml}{\pi b\sqrt{(1-m^2)^2+4m^2\cos^2\beta}}$. 1) For small l/b.

results.

Noticing that the angle of attack $\alpha = \beta - \beta_m$ is also determined by the circulation through the relation $\Gamma = k\Gamma_0 = k\pi b w_\infty \sin\alpha$, we find

$$\operatorname{ctg}\beta_m = \operatorname{ctg}\beta_2 + \frac{k\pi b w_\infty \sin\alpha}{2l w_m \sin\beta_m} = \operatorname{ctg}\beta_2 + k\frac{\pi b}{2l}(\sin\beta\operatorname{ctg}\beta_m - \cos\beta),$$

whence

$$\operatorname{ctg}\beta_m = \frac{\operatorname{ctg}\beta_2 - k\frac{\pi b}{2l}\cos\beta}{1 - k\frac{\pi b}{2l}\sin\beta} = \frac{1}{2}(\operatorname{ctg}\beta_1 + \operatorname{ctg}\beta_2).$$

We find from this equation

$$\operatorname{ctg}\beta_2 = A\operatorname{ctg}\beta_1 + B, \qquad (9.2.27)$$

where

$$A=\frac{1-k\frac{\pi b}{2l}\sin\beta}{1+k\frac{\pi b}{2l}\sin\beta}, \quad B=\frac{2k\frac{\pi b}{2l}\cos\beta}{1+k\frac{\pi b}{2l}\sin\beta}, \quad k=\left(\frac{dC_y}{d\alpha}\right)_0. \tag{9.2.27}$$

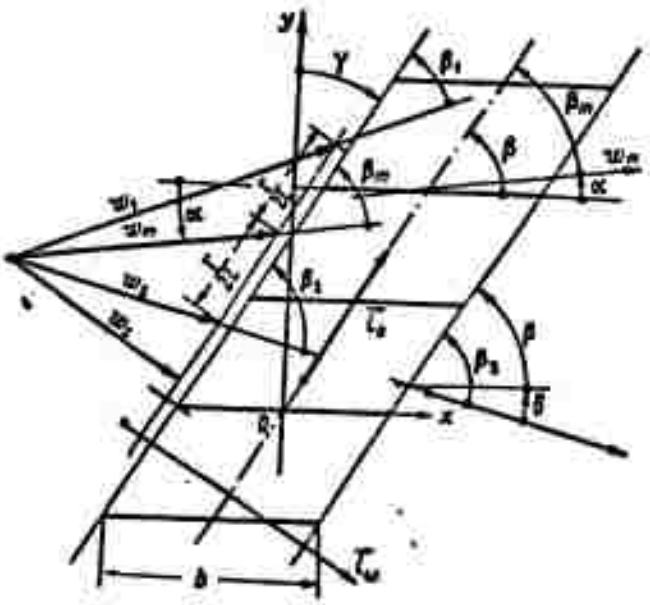


Fig. 9.2.12. For deriving the relation $\operatorname{ctg}\beta_1 = A\operatorname{ctg}\beta_2 + B$ between the angles of inflow and outflow, β_1 and β_2, respectively.

The values of A, B, and the angle of lag $\delta = \beta - \beta_2$ (cf. Fig. 9.2.12) for a lattice of plates are given in Figs. 9.2.13-15. As we can see,

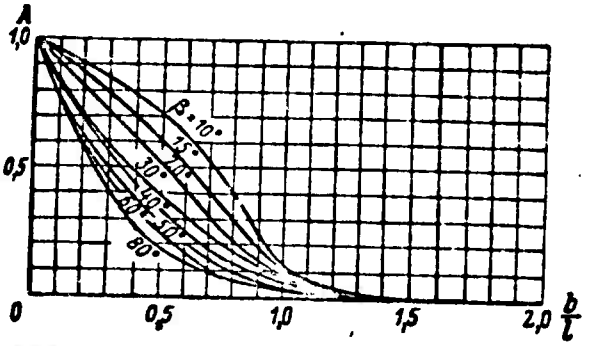


Fig. 9.2.13. The coefficient A(b/l,β) for a lattice of plates.

for a lattice density $0 \leq l/b \leq 1$ the coefficient A and the angle of

lag, δ, are close to zero, and $\cot \beta_2 \approx B$. This result is well verified by experiment.

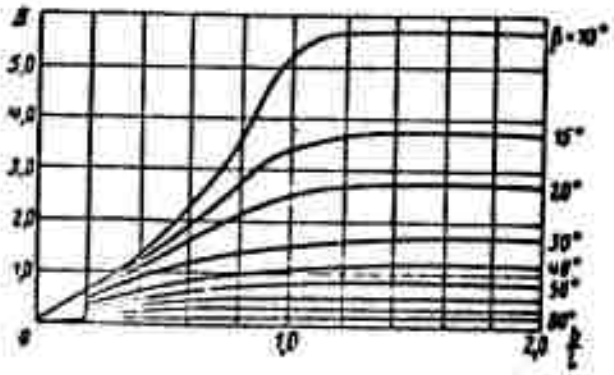


Fig. 9.2.14. The coefficient $B(b/l, \beta)$ for a lattice of plates.

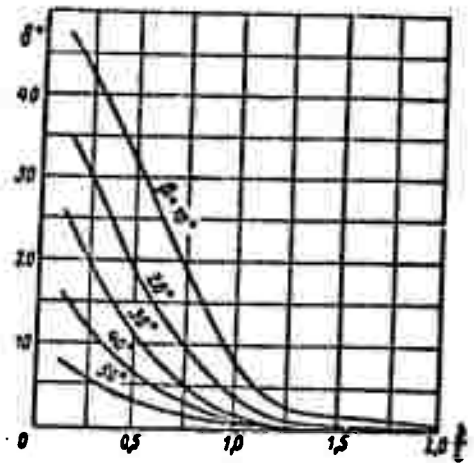


Fig. 9.2.15. The angle of lag, δ, for a lattice of plates.

Lattice of solid Zhukovskiy profiles. As for the isolated profiles obtained, we assume that in the ζ-plane the mapping circle of radius R, which is somewhat larger than the radius r_0 of the initial circle, is mapped to the lattice of plates. If the mapping circle passes through the backward separation point of the initial circle and if the forward separation point lies inside it, then, making use of Transformation (9.2.9) we obtain in the z-plane a lattice of solid profiles with

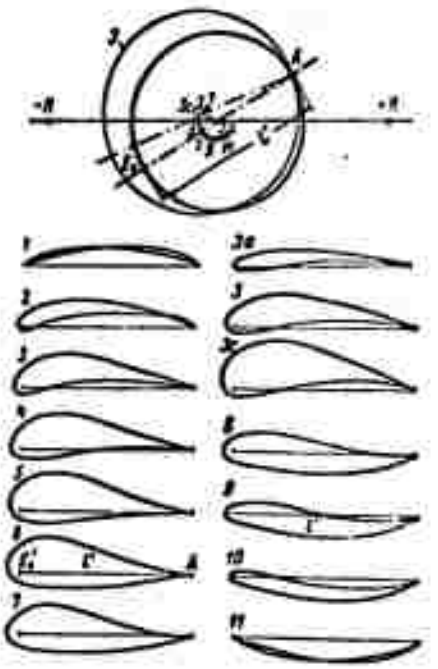


Fig. 9.2.16. Conformal mapping of the circle 2 with the help of a function mapping the circle 1 to a lattice of plates yields a lattice of solid curved profiles. Each number inside the circle indicates the center of the circle yielding the profile with the same number. The profiles 1, 2 and 11 are self-intersecting.

rounded leading edges and sharp trailing edges. The shape of the profile will be determined by the position of the center of the mapping circle; however, only slightly curved profiles which do not intersect themselves (Profiles 1, 2 and 11 in Fig. 9.2.16) are self-intersecting) are obtained.

9.3. SOLUTION OF THE PROBLEM OF A PROFILE LATTICE BY THE METHOD OF VORTEX SHEETS

The most heavily loaded parts of the blades in turbines are the profiles far from the axis of rotation. Strength considerations make it possible to satisfy the requirements of aeromechanics and to make these profiles like the guide vane profiles, i.e., thin. The investigation of lattices of such profiles of small camber allows us to employ the method of vortex sheets positioned on the camber line of the profile.

Despite the difficulties of obtaining a general analytical solution by this method, there exist well elaborated graphical-analytical procedures for finding a solution to any special case of arbitrary profile lattices. This is ensured by the widespread practical application of the vortex sheet method in the design offices of our plants.

In order to investigate the influence of the geometrical parameters of a lattice of solid profiles on its aerodynamic properties it is, however, convenient to use the method of conformal mapping of profile

lattices to circle lattices; the flow about a circular lattice can be graphically investigated by the method of vortex sheets.

Lattice of thin profiles. Let us renumber all the profiles of the lattice in the upper semiplane with positive numbers and those in the lower semiplane with negative numbers, according to the sequence (0, $\pm$ 1, $\pm$ 2, $\pm$ 3,...) attributing the number "zero" to the fundamental profile whose chord coincides with the x-axis and whose midpoint is traversed by the y-axis, (Fig. 9.3.1). The coordinates of the midpoint of the chord of the k_{-n} profile will be $kl\cos\beta$ and $kl\sin\beta$. We place a vortex sheet on the camber line of each profile, which has the vorticity $\gamma(s)$, equal to the discontinuity $w_v - w_n$ of the tangential velocity component at the point s. Since the flow conditions in the leading and trailing edge regions of each profile of the lattice are the same as the condition of the flow around a like isolated profile, then, if the profile's camber is assumed to be small ($y/b \ll 1$, $x \approx s$) and the variables $s \approx x = (b/2)\cos\vartheta$ are substituted, it is convenient to seek the vorticity of the vortex sheet in the form of a series

$$\gamma(\vartheta)=2w_m\left(a_0\operatorname{ctg}\frac{\vartheta}{2}+\sum_{n=1}^{\infty}a_n\sin n\vartheta\right). \qquad (9.3.1)$$

where w_m is the magnitude of half the vector sum of the velocities far in front of and behind the lattice, which will be denoted in what follows as the velocity of the undisturbed flow.

The circulation about a profile in a lattice (cf. p. 210) is equal to

$$\Gamma=\int_{-\frac{b}{2}}^{\frac{b}{2}}\gamma(s)\,ds=\int_0^{\pi}2w_m\left(a_0\operatorname{ctg}\frac{\vartheta}{2}+\sum_{n=1}^{\infty}a_n\sin n\vartheta\right)\frac{b}{2}\sin\vartheta\,d\vartheta=$$
$$=\pi\left(a_0+\frac{a_1}{2}\right)bw_m. \qquad (9.3.2)$$

Hence the lift per unit length of the airfoil is given by

$$R_y = \rho w_m \Gamma = 2\pi\left(a_0 + \frac{a_1}{2}\right) b \frac{\rho w_m^2}{2} = C_y b \frac{\rho w_m^2}{2}, \qquad (9.3.3)$$

i.e., it is determined by only the first two coefficients of Series (9.3.1); the other terms redistribute the circulation without changing its total amount.

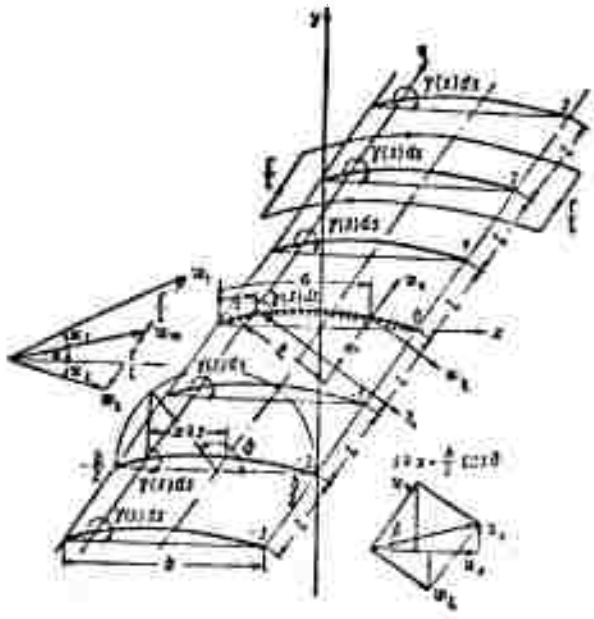


Fig. 9.3.1. Lattice of thin slightly curved profiles.

If α, the angle of attack of a profile with the mean velocity w_m, is as indicated in Fig. 9.3.1, then, by virtue of Relations (9.1.9) and (9.1.10), the angles α_1 and α_2 between the velocities w_1 and w_2 and the profile chord (x-axis) are determined by the relation

$$\operatorname{tg}\alpha_{1,2} = \frac{w_m \sin\alpha \pm \frac{\Gamma}{l}\sin\beta}{w_m \cos\alpha \pm \frac{\Gamma}{l}\cos\beta} = \frac{\sin\alpha \pm \pi\left(a_0 + \frac{a_1}{2}\right)\frac{b}{l}\sin\beta}{\cos\alpha \pm \pi\left(a_0 + \frac{a_1}{2}\right)\frac{b}{l}\cos\beta}. \qquad (9.3.4)$$

The velocity induced by the vortex sheets. This velocity is the same at corresponding points on each of the profiles; we shall therefore determine it for the fundamental profile. It will be composed, on the one hand, of the velocity induced by the vortex sheet belonging to

this profile; like that for an isolated profile, this velocity is equal to

$$w_{00y} = -w_\infty\left(a_0 - \sum_{n=1}^{\infty} a_n \cos n\theta\right) \qquad (9.3.5)$$

and, on the other hand, of the velocity induced by the vortex sheets of all other profiles. In order to determine this second velocity component, we consider an infinite row of identical vortices, $\gamma(s)ds$, positioned on the camber line points of each of the profiles, corresponding to points of the fundamental profile, which we take as the origin of the coordinates (ξ, η), the η-axis lying in the direction of the lattice axis. The complex potential at the point ζ of the fundamental profile in the (ξ, η) coordinate system of the vortex $\gamma(s)ds$ on the kth airfoil will be

$$\frac{\gamma(s)\,ds}{2\pi i}\ln(\zeta + kl) = \frac{\gamma(s)\,ds}{2\pi i}\left[\ln\left(1 + \frac{\zeta}{kl}\right) + \ln kl\right].$$

Omitting the constant $\ln kl$, which is unessential for the potential, and summing over the action of all profiles, we obtain the complex potential at the point $\zeta = \xi + i\eta$:

$$\chi_p(\zeta) = \int_{s=-b/2}^{s=b/2} \frac{\gamma(s)\,ds}{2\pi i}\left[\ln\left(1 + \frac{\zeta}{l}\right) + \ln\left(1 - \frac{\zeta}{l}\right) + \ln\left(1 + \frac{\zeta}{2l}\right) + \right.$$
$$\left. + \ln\left(1 - \frac{\zeta}{2l}\right) + \ldots\right] = \frac{1}{2\pi i}\int_{s=-b/2}^{s=b/2} \gamma(s) \sum_{k=1}^{\infty} \ln\left(1 - \frac{\zeta^2}{k^2 l^2}\right) ds =$$
$$= \frac{1}{2\pi i}\int_{s=-b/2}^{s=b/2} \gamma(s) \ln \prod_{1}^{\infty}\left(1 - \frac{\zeta^2}{k^2 l^2}\right) ds.$$

It is proved in mathematical lectures that

$$\sin x = x \prod_{k=1}^{\infty}\left(1 - \frac{x^2}{k^2\pi^2}\right).$$

Then

$$\chi_p(\zeta) = \frac{1}{2\pi i}\int_{s=-\frac{b}{2}}^{s=\frac{b}{2}} \gamma(s)\left(\ln \sin\frac{\pi\zeta}{l} - \ln\zeta\right) ds.$$

The complex velocity at point ζ of the fundamental profile due to all "foreign" vortices is

$$(w_i - i\omega_\eta)_0 = -\frac{d\Gamma_0}{d\zeta} = \frac{1}{2\pi i}\int_{s=-\frac{b}{2}}^{s=\frac{b}{2}} \gamma(s)\left[\frac{\pi}{l}\operatorname{ctg}\frac{\pi\zeta}{l} - \frac{1}{\zeta}\right]ds.$$

Since

$$\operatorname{ctg}\frac{\pi\zeta}{l} = \frac{\cos\frac{\pi(\xi+i\eta)}{l}}{\sin\frac{\pi(\xi+i\eta)}{l}} = \frac{\cos\frac{\pi\xi}{l}\operatorname{ch}\frac{\pi\eta}{l} + i\sin\frac{\pi\xi}{l}\operatorname{sh}\frac{\pi\eta}{l}}{\sin\frac{\pi\xi}{l}\operatorname{ch}\frac{\pi\eta}{l} - i\cos\frac{\pi\xi}{l}\operatorname{sh}\frac{\pi\eta}{l}},$$

we have

$$\left.\begin{aligned}
w_{0\xi} &= \frac{1}{l}\int_{s=-\frac{b}{2}}^{s=\frac{b}{2}} \gamma(s)\left[-\frac{\frac{1}{2}\operatorname{sh}\frac{2\pi\eta}{l}}{\operatorname{ch}\frac{2\pi\eta}{l} - \cos\frac{2\pi\xi}{l}} + \right.\\
&\left. + \frac{1}{2\pi}\frac{\frac{\eta}{l}}{\left(\frac{\xi}{l}\right)^2 + \left(\frac{\eta}{l}\right)^2}\right]ds = \frac{1}{l}\int_{s=-\frac{b}{2}}^{s=\frac{b}{2}} \gamma(s)\, a(\xi, \eta)\, ds.\\
w_{0\eta} &= \frac{1}{l}\int_{s=-\frac{b}{2}}^{s=\frac{b}{2}} \gamma(s)\left[\frac{\frac{1}{2}\sin\frac{2\pi\xi}{l}}{\operatorname{ch}\frac{2\pi\eta}{l} - \cos\frac{2\pi\xi}{l}} - \right.\\
&\left. - \frac{1}{2\pi}\frac{\frac{\xi}{l}}{\left(\frac{\xi}{l}\right)^2 + \left(\frac{\eta}{l}\right)^2}\right]ds = \frac{1}{l}\int_{s=-\frac{b}{2}}^{s=\frac{b}{2}} \gamma(s)\, b(\xi, \eta)\, ds.
\end{aligned}\right\} \qquad (9.3.6)$$

In the (x, y)-coordinate system

$$w_{0x} = w_{0\xi}\sin\beta + w_{0\eta}\cos\beta, \quad w_{0y} = w_{0\eta}\sin\beta - w_{0\xi}\cos\beta. \qquad (9.3.7)$$

In the Leningrad Metal Works imeni I.V. Stalin the functions $a(\xi, \eta) = \text{const}$ and $b(\xi, \eta) = \text{const}$, introduced by A.F. Lesochin and L. A. Simonov [9.4] were calculated and their values plotted on a nomogram (Fig. 9.3.2).

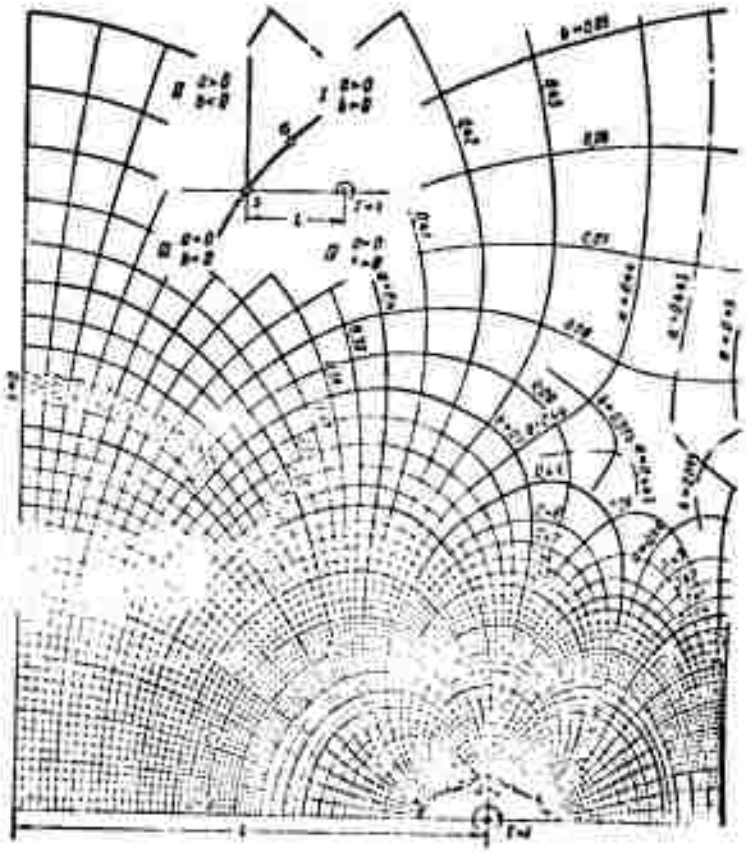


Fig. 9.3.2. Functions $a(\xi, \eta)$ and $b(\xi, \eta)$ are the projections on the ξ- and η-axes of the velocity induced at point $(\xi + i\eta)$ by an infinite row of vortices with the circulation $\Gamma = 1$, arranged on the axis passing through the coordinate origin, assuming that there is no vortex at the origin; the signs of the functions a and b are governed by the following rule: the sign of a coincides with the sign of η, and the sign of b with that of ξ.

If a given lattice is drawn on a tracing paper to such a scale that its period is equal to the period on the nomogram then, when the profile is so positioned that the point s lies at the coordinate origin of the nomogram and the lattice axis coincides with its η-axis, the values written against the lines $a(\xi, \eta) = \text{const}$ and $b(\xi, \eta) = \text{const}$ intersecting at a point $\sigma(\xi, \eta)$ chosen on the camber line will be the values of the functions a and b at this point. From the physical point of view this will be the projection of the velocity onto the axes ξ and

η at the point σ considered (with the coordinates ξ and η) of an infinite row of vortices, each with the circulation $\Gamma = 1$, placed at points that correspond to the coordinate origin, whereas the vortex located at the coordinate origin (coinciding with the point $\underline{s}$ of the fundamental profile) is eliminated (cf. Fig. 9.3.2).

In order to calculate the integrals entering w_ξ and w_η (9.3.6), it is convenient to return to the variable $\underline{s} = b/2 \cos \vartheta$. Then

$$\frac{1}{2w_\infty}\gamma(s) = a_0\sqrt{\frac{1+2s/b}{1-2s/b}} + a_1\sqrt{1-(2s/b)^2} -$$

$$+ a_2 2\frac{s}{b}\sqrt{1-(2s/b)^2} + \ldots$$

Going over to the dimensionless variable $s_1 = 2s/b$ and omitting the subscript for the variable under the integral sign, i.e., assuming $b = 2$ for the chord, we arrive at

$$\frac{1}{w_\infty}w_{0\xi} = -\frac{b}{l}\int_{-1}^{1} a(s,\sigma)\left[a_0\sqrt{\frac{1+s}{1-s}} + a_1\sqrt{1-s^2} + \right.$$

$$\left. + 2a_2 s\sqrt{1-s^2} - \ldots\right]ds = \frac{b}{l}\int_{-1}^{1}\frac{a(s,\sigma)}{\sqrt{1-s^2}}\left[a_0(1+s) + a_1(1-s^2) + \right.$$

$$\left. + 2a_2 s(1-s^2) + \ldots\right]ds = \frac{b}{l}\int_{-1}^{1}\frac{f(s)\,ds}{\sqrt{1-s^2}}. \qquad (9.3.8)$$

where f(s) denotes the numerator function. The formula for $w_{0\eta}$ reads analogously.

The integral $I_0 = \int_{-1}^{1}\frac{f(s)\,ds}{\sqrt{1-s^2}}$ is calculated by approximation. If we put $\underline{s} = \cos\theta$ then, as can be seen, $I_0 = \int_0^\pi f(\cos\theta)\,d\theta$. Applying the trapezoidal rule and dividing the interval into four parts, we obtain

$$I_0 = \frac{\pi}{6}\left[f(-1) + 2f\left(-\frac{1}{2}\right) + 2f\left(\frac{1}{2}\right) + f(1)\right].$$

The integral can be calculated more accurately if the interval is

divided into more parts and if we apply, for example, Hermite's formula:*

$$\int_{-1}^{+1}\frac{f(s)\,ds}{\sqrt{1-s^2}}=\frac{\pi}{n}\sum f(x_i)+R(f);$$

$$x_i=\cos\frac{(2i-1)\pi}{2n}\qquad(i=1,\ 2,\ 3\ldots,\ n);$$

$$R(f)=\frac{\pi}{(2n)!\,2^{2n-1}}f^{(2n)}(\xi)\qquad(0<\xi<\pi).$$

When the angle of attack and the camber are small, the velocities induced by the vortex sheets are small compared with the velocity of the undisturbed flow; their components along the chord can be neglected and the velocity calculation can be carried out on the profile chord. Calculating the velocities $K(\sigma) = w_{00y}/w_m$, induced by the "own" vortex layer according to (9.3.2) and the velocities $L(\sigma) = w_{0y}/w_m$ from the "foreign" vortices

$$\frac{1}{lw_m}\int_{-1}^{+1}\gamma(\sigma,\ s)\,[b(s,\ \sigma)\sin\beta-a(s,\ \sigma)\cos\beta]\,ds=$$

$$=\frac{1}{lw_m}\int_{-1}^{+1}\gamma(s,\ \sigma)\,c(s,\ \sigma)\,ds$$

for a series of points of the profile (chord), and then adding them to the velocity $w_{my} \approx w_m\alpha$ of the undisturbed flow, we can write with the boundary condition $dy/dx = w_y/w_x$ the following set of equations

$$\alpha+K(\sigma)+L(\sigma)=\frac{dy}{dx}(\sigma).\qquad(9.3.9)$$

Here dy/dx (σ) denotes the angles of slope of the tangent to the camber line of the profile at those points σ for which the velocities $K(\sigma)$ and $L(\sigma)$ were determined.

These equations contain the unknown coefficients a_0, a_1, a_2, ... of the series expansion of (9.3.1) for the circulation; solving Set (9.3.10) enables us to determine as many of the coefficients a_0, a_1, a_2, ... as we have equations in the set; details as to the solution of the problem are given in special textbooks, e.g., [9, 13].

Lattice of thin profiles with small camber. In this case the complex velocity at the point x_0 of the fundamental profile induced by the vortex sheet of the kth profile will be

$$\overline{w}_{0k}=(w_x-iw_y)_{0k}=\frac{1}{2\pi i}\int\limits_{-\frac{b}{2}}^{\frac{b}{2}}\frac{\gamma(x)\,dx}{x_k-x_0}$$

or, if the vorticity is replaced by the expression for it,

$$w_{0k}=\frac{1}{2\pi i}\sum_{k=-\infty}^{\infty}{}'\int_0^{\pi}\frac{2w_m\left(a_0\operatorname{ctg}\frac{\varphi}{2}+\sum\limits_{n=1}^{\infty}a_n\sin n\varphi\right)}{kle^{i\beta}-\frac{b}{2}\cos\varphi+\frac{b}{2}\cos\beta}\cdot\frac{b}{2}\sin\varphi\,d\varphi=$$

$$=\frac{w_m}{\pi i}\sum_{k=-\infty}^{\infty}{}'\int_0^{\pi}\frac{a_0(1+\cos\varphi)+\frac{1}{2}\sum a_n[\cos(n-1)\varphi-\cos(n+1)\varphi]}{2k\frac{l}{b}e^{i\beta}+\cos\beta-\cos\varphi}\,d\varphi.$$

Assuming $s=2k\frac{l}{b}e^{i\beta}+\cos\beta$ (s does not lie on the section − 1, + 1), we find

$$I_p=\int_0^{\pi}\frac{\cos p\varphi}{s-\cos\varphi}\,d\varphi=\frac{(s-\sqrt{s^2-1})^p}{\sqrt{s^2-1}}$$

and after this we calculate w_{0kx} and w_{0ky} in the form of trigonometrical series with coefficients depending on the lattice parameters. It is, however, rather complicated to obtain the general expression, but when we restrict ourselves to a small number of terms of the power series expansion of the ratio b/l, we obtain simple expressions. For example, if we neglect the terms of higher than fourth order in b/l and add the velocity induced by the own vortex sheet and the velocity w_m parallel to the flow then the calculations yield

$$\frac{w_x}{w_m}=-\left(\cos\alpha-a_0q_2-\frac{a_1}{2}q_2\right)+(2a_0q_2+a_1q_2)\cos\beta;$$

$$\frac{w_y}{w_m}=\left[\sin\alpha-a_0(1-p_2)+\frac{a_1}{2}p_2\right]-$$

$$-[2a_0p_2-a_1(1-p_2)]\cos\beta+a_2\cos2\beta,$$

where

$$p_{2n}=\left(\frac{b}{2l}\right)^{2n}S_{2n}\cos 2n\beta;\quad q_{2n}=\left(\frac{b}{2l}\right)^{2n}S_{2n}\sin 2n\beta;$$

$$S_{2n}=\sum_{k=1}^{\infty}\frac{1}{k^{2n}};\quad S_2=\frac{\pi^2}{6}=1{,}645,\quad S_4=\frac{\pi^4}{90}=1{,}082;$$

$$S_6=\frac{\pi^6}{945}=1{,}017 \text{ and so on.}$$

For the camber line of the profile formed by the P-curve $y_p=\frac{b}{2}p(1-x^2)$ and the S-curve $y_s=\frac{b}{2}sx(x^2-1)$ (cf. Fig. 3.6.4); substituting $x=-(b/2)\cos\vartheta$ gives us

$$\frac{2y}{b}=\frac{p}{2}+\frac{s}{4}\cos\vartheta-\frac{p}{2}\cos 2\vartheta-\frac{s}{4}\cos 3\vartheta$$

and

$$\frac{dy}{dx}=\frac{s}{2}+2p\cos\vartheta+\frac{3}{2}s\cos 2\vartheta.$$

The boundary condition for the camber line $w_y/w_x = d_y/d_x$ gives us

$$a_0-a_0(1-p_2)+\frac{a_2}{2}p_2=\frac{s}{2};\quad -2a_0p_2+a_1(1-p_2)=2p;\quad a_2=\frac{3}{2}s.$$

Usually s is very small and then

$$a_0\approx\frac{a}{1-p_2}-\frac{s}{2};\quad a_1\frac{1-p_2}{2}=a\frac{p_2}{1-p_2}+p-s\frac{p_2}{2};\quad a_2=\frac{3}{2}s.$$

Therefore

$$C_y=2\pi\left(a_0+\frac{a_1}{2}\right)=\frac{2\pi}{(1-p_2)^2}\left[a+\left(p-\frac{s}{2}\right)(1-p_2)\right].$$

When w_x and w_y are more accurately calculated it is possible to determine the pressure distribution over the lattice profile, using Relation (3.6.25)

$$p_x-ip_y=ip_T(w_x-iw_y).$$

Sparse lattice of plane plates. Let us consider a lattice of plane plates with y = 0, dy/dx = 0 and small b/l.

Restricting ourselves to the two terms a_0 and a_1 of the series expansion we obtain

$$a_0=\frac{a}{1-p_2};\quad a_1=\frac{2l\cdot a_0}{1-p_2};\quad p_2=\left(\frac{1}{2}\cdot\frac{b}{l}\right)^2 s\cos 2\beta=0{,}411\frac{b^2}{l^2}\cos 2\beta.$$

For an isolated plane plate

$$C_{y\infty} = 2\pi\alpha,$$

whereas for the lattice with the degree of accuracy adopted,

$$C_{yp} = 2\pi\left(a_0 + \frac{a_1}{2}\right) = 2\pi a_0\left(1 + \frac{a_1}{a_0}\right) = 2\pi\alpha\,\frac{1+\rho_2}{(1-\rho_2)^2}.$$

Thus

$$k = \frac{C_{yp}}{C_{y\infty}} = \frac{1+\rho_2}{(1-\rho_2)^2} \approx \frac{1 + 0{,}411\,\frac{b^2}{l^2}\cos 2\beta}{1 - 0{,}822\,\frac{b^2}{l^2}\cos 2\beta}. \quad (9.3.10)$$

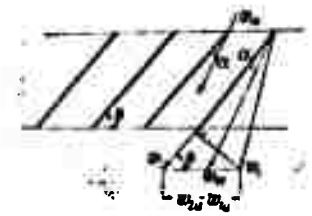


Fig. 9.3.3. Dense lattice of plane plates – the velocity at the outlet coincides with the direction of the plates.

Comparison with the exact solution that agreement is good for $l/b > 1.5$.

Dense lattice of plates. When the density is high ($b/l \gg 1$) the velocity at the exit of the lattice coincides with the direction of the plates. In this case it follows from the triangle of velocities (Fig. 9.3.3) that

$$w_m \sin\alpha = \frac{\Delta w_a}{2}\sin\beta$$

and therefore the coefficient of influence of the lattice is given by

$$k = \frac{\Gamma_p}{\Gamma_\infty} = \frac{l\Delta w_a}{\pi b w_m \sin\alpha} = \frac{1}{\pi}\,\frac{l}{b}\,\frac{\Delta w_a}{w_m \sin\alpha} = \frac{2l}{\pi b \sin\beta}. \quad (9.3.11)$$

It can be seen from Fig. 9.2.11 that up to $l/b = 0.8$–0.9, k is an almost linear function of l/b and that the agreement with the exact solution is good.

Flow about a lattice of discs. Let us consider a lattice of discs of radius r and with the spacing l in parallel uniform flow of inviscid incompressible fluid with the velocity w_m parallel to the x-axis (Fig. 9.3.4). Let us enumerate all discs according to the sequence of numbers $\pm 1, \pm 2, \ldots$, the positive numbers for the upper and the negative numbers for the lower semiplane, the number "0" being attributed to the fundamental disc placed at the coordinate origin.

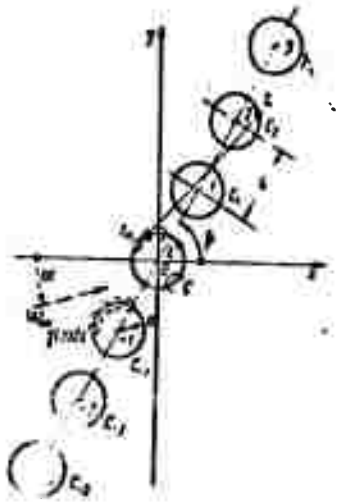


Fig. 9.3.4. Lattice of discs.

We replace each of the discs by quiescent fluid and place at the boundary of each disc a vortex sheet with the vorticity $\gamma(s)$ per unit length [cf. 3.6.2)]:

$$\gamma(s)=w_+(s)-w_-(s)=w(s). \quad (9.3.12)$$

Owing to (3.2.13) the complex velocity at the point z_0 of the fundamental disc, induced by the vortex sheet on the kth disc will be equal to

$$(w_x-iw_y)_k=\frac{1}{2\pi i}\int_{l_k}\frac{w(s)\,ds}{z_0-\zeta}. \quad (9.3.13)$$

From the identity

$$\overline{w}(\zeta)\,d\zeta=(w_\xi-iw_\eta)(d\xi+i\,d\eta)=(w_\xi\,d\xi+w_\eta\,d\eta)+ i(w_\xi\,d\eta-w_\eta\,d\xi)$$

and the boundary condition $\operatorname{Im}\{\overline{w}(\zeta)\,d\zeta\}=w_\xi\,d\eta-w_\eta\,d\xi=0$, expressing the fact that the normal component of the circumferential velocity vanishes, it follows that

$$R\{\overline{w}(\zeta)\,d\zeta\}=w(s)\,ds=w(s)\,|d\zeta|.$$

Since the complex coordinate of any point of the kth circle ($k=\pm1, \pm2, \pm3, \ldots$) can be written in the form

$$\zeta=z+kle^{i\beta}, \quad (9.3.14)$$

where z is a point on the fundamental circle that corresponds to the point ζ on the kth circle (cf. Fig. 9.3.4), the expression for the complex velocity (9.3.13) can be rewritten in the form

$$(w_x-iw_y)_k=\frac{1}{2\pi i}\int_{\zeta}\frac{w(s)\,|ds|}{z_0-kle^{i\beta}-z}, \quad (9.3.15)$$

where the path of integration, l_k, is replaced by the contour C, i.e., the circle at the origin of coordinates. The physical meaning of this is that instead of finding the velocity at the point z_0 on the contour

of the fundamental disc due to the vortex sheet of the kth circle we determine the identical velocity at the corresponding point on the kth circle due to the vortex on the fundamental circle.

Summing over k from $-\infty$ to $+\infty$ (excluding k = 0 which is indicated by a dash at the summation sign, Σ') we find that the complex velocity at the fundamental circle due to the external singularities is equal to

$$\frac{1}{2\pi i}\sum_{k=-\infty}^{\infty}{}'\int_C \frac{w(s)\,|dz|}{z_0 - kle^{i\vartheta} - z}.$$

This expression is summed by calculating the influence that each pair of circles symmetrically disposed with respect to the fundamental circle exerts on the latter, beginning with the nearest pair, k = ± 1:

$$\sum_{k=\pm 1,\ \pm 2,\ldots} \frac{1}{2\pi i}\int_C \frac{w(s)\,|dz|}{z_0 - z - kle^{i\vartheta}} = \frac{1}{2\pi i}\int_C w(s)\sum_{k=1}^{\infty}\left(\frac{1}{z_0 - z - kle^{i\vartheta}} + \right.$$

$$\left. + \frac{1}{z_0 - z + kle^{i\vartheta}}\right)|dz| = \frac{1}{2\pi i}\int_C w(s)\sum_{k=1}^{\infty}\frac{2(z_0 - z)}{(z_0 - z)^2 - (kle^{i\vartheta})^2}\,|dz|. \qquad (9.3.16)$$

In addition to the velocity induced by the external vortex sheets, at each point of the fundamental circle a velocity will arise owing to its own vortex sheet (for k = 0) which is equal to

$$\frac{1}{2\pi i}\int_C^{\bullet} \frac{w(z)}{z_0 - z}\,|dz|. \qquad (9.3.17)$$

where the sign $\int^{\bullet}$ means that we have to take the principal value of the integral (cf. p. 205).

Calculating

$$\overline{w}\,dz = (w_x - iw_y)(dx + i\,dy) = (w_x\,dx + w_y\,dy) + i(w_y\,dx - w_x\,dy),$$

we obtain (cf. Fig. 9.3.6)

$$w(s) = w_x\frac{dx}{ds} + w_y\frac{dy}{ds} = R\left\{(w_x - iw_y)\frac{dz_0}{ds}\right\},$$

where R $\{\ldots\}$ denotes the real part.

The fundamental equation. Let us add the velocity induced by all vortex sheets of the lattice to the velocity of the undisturbed paral-

lel flow, w_m. If we multiply the complex velocity obtained at the point z of the fundamental cylinder by dz_0/ds, then the real part of this product gives the total velocity at the point z_0 considered; owing to the boundary condition it will be directed along the tangent to the body contour at this point. It was shown, however, in (3.6.9) that the tangential velocity arbitrarily close above the vortex sheet is equal to half the velocity discontinuity at this point.

By virtue of (3.3.12) this yields the fundamental equation

$$R\left\{\left[\frac{1}{2\pi i}\int_{\zeta}\gamma(s)\sum_{k=1}^{\infty}\frac{2(z_0-z)}{(z_0-z)^2-(kle^{i\beta})^2}|dz|+\right.\right.$$

$$\left.\left.+\frac{1}{2\pi i}\int_{\zeta}^{\infty}\frac{\gamma(s)}{z_0-z}|dz|+w_m\right]\frac{dz_0}{ds}\right\}=\frac{\gamma(s)}{2}.$$

Supposing $u = (z_0 - z)/le^{i\beta}$, we can write

$$\sum_{k=1}^{\infty}\frac{z_0-z}{(z_0-z)^2-(kle^{i\beta})^2}=-\frac{1}{z_0-z}\sum_{k=1}^{\infty}\frac{u^2}{k^2-u^2},$$

if

$$\sum_{k=1}^{\infty}\frac{u^2}{k^2-u^2}=\sum_{k=1}^{\infty}\frac{\frac{u^2}{k^2}}{1-\frac{u^2}{k^2}}=u^2\sum_{k=1}^{\infty}\frac{1}{k^2}\frac{1}{1-\frac{u^2}{k^2}}=$$

$$=u^2\left[\sum_{p=0}^{\infty}u^{2p}+\frac{1}{2^2}\sum_{p=0}^{\infty}\left(\frac{u}{2}\right)^{2p}+\frac{1}{3^2}\sum_{p=0}^{\infty}\left(\frac{u}{3}\right)^{2p}+\dots\right]=$$

$$=\sum_{r=1}^{\infty}u^{2r}\sum_{m=1}^{\infty}\frac{1}{m^{2r}}=\sum_{r=1}^{\infty}S_{2r}u^{2r},$$

with

$$\sum_{m=1}^{\infty}\left(\frac{1}{m}\right)^{2r}=S_{2r}.$$

The calculations show that the numerical values of S_{2r} rapidly

tend to unity:

$$S_3=\frac{\pi^2}{6}=1{,}64493;\quad S_4=\frac{\pi^4}{90}=1{,}08232;\quad S_6=\frac{\pi^6}{945}=1{,}01734.$$

In this case the fundamental equation assumes the form

$$\frac{w(s)}{2}+R\left\{\frac{1}{2\pi i}\int_{\zeta}\frac{w(s)}{(z-z_0)}\cdot\frac{dz_0}{ds}|dz|\right\}=$$

$$=R\left\{w_m\frac{dz_0}{ds}+\frac{1}{\pi i}\int_{\zeta}\frac{w(s)}{z-z_0}\sum_{k=1}^{\infty}S_k\left(\frac{z_0-z}{l}e^{-i\beta}\right)^{2k}\frac{dz_0}{ds}|dz|\right\}. \qquad (9.3.18)$$

The solution of this equation is rendered more simply if, following N.Ye. Kochin, we consider the general case of the flow about a lattice of discs as the result of superimposing three simpler flows (Fig. 9.3.5): 1) a circulation-free transverse flow (w_1); 2) a circulation-free longitudinal flow (w_2) and; 3) a purely circulatory flow (w_3) [9.5].

The transverse flow. In this case $\beta = \pi/2$. From the symmetry condition (cf. Fig. 9.3.5, a) we have $w_1(\vartheta) = -w_1(-\vartheta)$, i.e., the function $w_1(\vartheta)$ is odd and can be represented by a series of the form $\sum_{n=1}^{\infty}\beta_n\sin n\vartheta$. Moreover, $w_1(\vartheta) = w_1(\pi-\vartheta)$, i.e., $\sum_{n=1}^{\infty}\beta_n\sin n\vartheta=\sum_{n=1}^{\infty}\beta_n\sin n(\pi-\vartheta)$, where all even coefficients must vanish. The series for the velocity $w_1(\vartheta)$ therefore has the form

$$w_1(\vartheta)=\sum_{n=0}^{\infty}\beta_{2n+1}\sin(2n+1)\vartheta, \qquad (9.3.19)$$

where the velocity of the undisturbed flow, w_m, is taken to be equal to unity.

Let us assume that $z = re^{i\varphi}$ and $z_0 = re^{i\vartheta}$ on the circle. Then, substituting (9.3.19) into the left-hand side of the fundamental equation (9.3.18) and taking into account that $2i\sin x = e^{ix} - e^{-ix}$, we find that

$$\frac{1}{2}\sum_{n=0}^{\infty}\beta_{2n+1}\sin(2n+1)\vartheta+$$

$$+R\left\{\frac{1}{2\pi i}\int_0^{2\pi}\frac{\sum_{n=0}^{\infty}\beta_{2n+1}\sin(2n+1)\vartheta}{re^{i\varphi}-re^{i\vartheta}}\frac{ire^{i\vartheta}d\vartheta}{rd\vartheta}rd\varphi\right\}=$$

$$=-\frac{1}{2}\sum_{n=0}^{\infty}\beta_{2n+1}\sin(2n+1)\vartheta+R\left\{\sum_{n=0}^{\infty}\frac{1}{2i}e^{i\vartheta}\beta_{2n+1}\left[\int_0^{2\pi}\frac{e^{i(2n+1)\varphi}}{e^{i\varphi}-e^{i\vartheta}}d\varphi-\right.\right.$$

$$\left.\left.-\int_0^{2\pi}\frac{e^{-i(2n+1)\varphi}}{e^{i\varphi}-e^{i\vartheta}}d\varphi\right]\right\}. \qquad (9.3.20)$$

The calculations show [9.6], that the real part of the expression in the braces of (9.3.20) is equal to zero and, thus, the left-hand

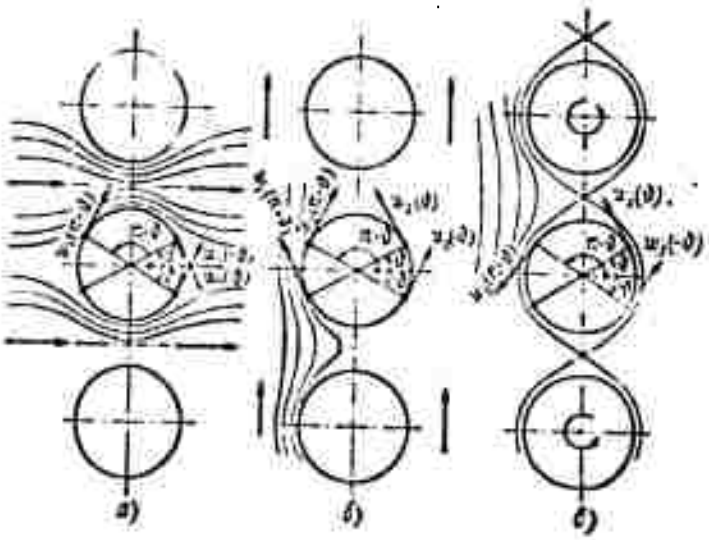


Fig. 9.3.5. Special cases of flows past a lattice of discs. a) Transverse circulation-free flow, $w_1(\vartheta) = w_1(-\vartheta) = w_1(\pi-\vartheta)$; b) longitudinal circulation-free flow, $w_2(\vartheta) = w_2(-\vartheta) = w_2(\pi-\vartheta)$; c) purely circulatory flow.

side of Eq. (9.3.18) is equal to

$$\frac{1}{2}\sum_{n=0}^{\infty}\beta_{2n+1}\sin(2n+1)\vartheta.$$

Let us consider the right-hand side of the fundamental equation (9.3.18). We find first of all that

$$R\left\{\frac{dz_0}{ds}\right\}=R\left\{\frac{re^{i\vartheta}i\,d\vartheta}{rd\vartheta}\right\}=-\sin\vartheta. \qquad (9.3.21)$$

Substituting Expression (9.3.19) for $w_1(\vartheta)$ in the integral of the right-hand side we find after some not too complicated but rather cumbersome transformations that the right-hand side as a whole is equal to

$$-\sin\vartheta+\sum_{n=0}\beta_{2n+1}\sum_{k=1}(-1)^k C_{2k}\binom{2k-1}{2(k+1)}\sin(2k-2n-1)\vartheta.$$

Here $C_{2k}=S_{2k}\left(\frac{2r}{l}\right)^{2k}=S_{2k}q^{2k}$ and $\binom{m}{n}=\frac{m!}{(m-n)!\,n!}$ is a binomial coefficient.

Comparing the coefficients of the sines of arcs of equal multiplicity of the expressions found, we obtain an infinite set of equations

$$\left.\begin{aligned}-\frac{1}{2}\beta_1&=1+\sum_{s=1}^{\infty}(-1)^s\beta_{2s-1}C_{2s},\\ -\frac{1}{2}\beta_{2n+1}&=\sum_{s=1}^{\infty}(-1)^s\beta_{2s-1}C_{2(s+n)}\binom{2s+2n-1}{2n}\\ &\qquad(n=1,2,3\ldots).\end{aligned}\right\}\qquad(9.3.22)$$

It can be solved by means of the method of successive approximations [9.5].

Without pausing to dwell on the technique of calculation [9.6], we give the final expression for β_{2n+1} in the form

$$\beta_{2n+1}=\frac{4S_2q^2}{4-S_2^2q^4}B_{2n+1}(q,n),$$

where the functions $B_{2n+1}(q, n)$ are represented as power series in q with coefficients depending on n.

Omitting the general expression for $B_{2n+1}(q, n)$ we list here the values accurate up to the term in q^{12}:

$$\begin{aligned}-B_1&=1{,}216q^2+1+0{,}0666q^6+0{,}110q^8+0{,}100q^{10}+0{,}0664q^{12}+\ldots\\ B_3&=0{,}494q^2+0{,}406q^4+0{,}157q^8+0{,}156q^{10}+0{,}077q^{12}+\ldots\\ -B_5&=0{,}193q^4+0{,}159q^6+0{,}132q^{10}+0{,}122q^{12}+\ldots\\ B_7&=0{,}051q^6+0{,}055q^8+0{,}081q^{12}+\ldots\\ -B_9&=0{,}0214q^8+0{,}176q^{10}+\ldots\\ B_{11}&=0{,}0055q^{10}+0{,}0054q^{12}+\ldots\\ -B_{13}&=0{,}0019q^{12}+\ldots\end{aligned}$$

The longitudinal flow. In this case $\beta = 0$ and from the symmetry conditions (cf. Fig. 9.3.5, b) we have $w_2(\vartheta) = w_2(-\vartheta) = -w_2(\pi - \vartheta)$; therefore

$$w_2(\vartheta) = \sum_{n=0} a_{2n+1} \cos(2n+1)\vartheta. \qquad (9.3.23)$$

The solution to the fundamental equation (9.3.18) obtained by the same method yields

$$a_{2n+1} = \frac{4S_2 q^2}{1 - S_2^2 q^4} A_{2n+1}(q, n).$$

The values of A_{2n+1} accurate up to the term in q^{12} are the following:

$$A_1 = 1,2116q^2 - 1 + 0,0666q^6 - 0,110q^8 + 0,100q^{10} - 0,0664q^{12} + \ldots$$
$$A_3 = -0,486q^2 + 0,406q^4 + 0,157q^8 - 0,136q^{10} + 0,077q^{12} + \ldots$$
$$A_5 = -0,193q^4 + 0,159q^6 + 0,132q^{10} - 0,122q^{12} + \ldots$$
$$A_7 = -0,051q^6 + 0,055q^8 + 0,081q^{12} + \ldots$$
$$A_9 = -0,0214q^8 + 0,0176q^{10} + \ldots$$
$$A_{11} = -0,0065q^{10} + 0,0054q^{12} + \ldots$$
$$A_{13} = -0,0019q^{12} + \ldots$$

The circulatory flow. For a lattice of discs with its axis laid along the y-axis (cf. Fig. 9.3.5, b) a repetition of the above considerations leads to the relations

$$w_3(\vartheta) = \sum_{n=0} a_{2n} \cos 2n\vartheta; \quad a_{2n} = (-1)^n \frac{\Gamma}{2\pi r} A_{2n}$$
$$A_0 = 1$$
$$A_2 = -1,645q^2 + 0,667q^6 - 0,228q^{10} + \ldots$$
$$A_4 = -0,270q^4 + 0,521q^8 - 0,0114q^{12} + \ldots$$
$$A_6 = -0,0632q^6 + 0,270q^{10} - \ldots$$
$$A_8 = -0,0162q^8 + 0,116q^{12} - \ldots$$
$$A_{10} = -0,0032q^{10} + \ldots$$
$$A_{12} = -0,00098q^{12} + \ldots$$

If the angle β of the lattice axis deviates from $\pi/2$, then

$$w_3(\vartheta) = \sum (\alpha_{2n} \cos 2n\vartheta + \beta_{2n} \sin 2n\vartheta);$$

$$\begin{matrix} u_{2n} \\ v_{2n} \end{matrix} = -\frac{\Gamma}{2\pi r} A_{2n} \begin{matrix} \cos 2n\vartheta \\ \sin 2n\vartheta \end{matrix}.$$

The magnitude of the circulation Γ has to be determined from other considerations. Fig. 9.3.6 gives the numerical values and the graphs

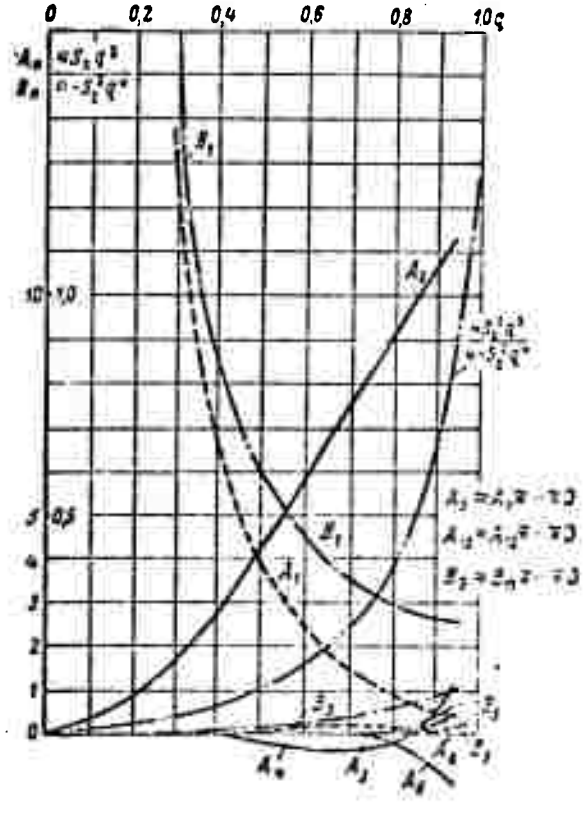


Fig. 9.3.6. Graph of variation of A_n and B_n as dependent on q.

of the variations of A_n and B_n in dependence on q, from which we see that even for very dense lattices with q near unity these values become negligibly small even when $k \approx 8$-10 and in the calculations we can restrict ourselves to q^8-q^{10} as the highest powers.

The velocity potential on the circle. It is determined from the relation $w_r = \frac{\partial \varphi}{\partial r}\Big|_{r=r_0} = 0$, $w_\vartheta = \frac{1}{r}\frac{\partial \varphi}{\partial \vartheta}\Big|_{r=r_0} = w(\vartheta)$. For $r_0 = 1$ the velocity potential $\varphi(1, \vartheta) \equiv \varphi^*(\vartheta)$ on the circle is equal to $\int w(\vartheta)d\vartheta$. When the

velocity of the undisturbed flow is $w_m = 1$, the transverse flow through the lattice of discs, owing to (9.3.19), is given by

$$\left.\begin{aligned}\varphi_1^{(*)}(\vartheta) &= \int \sum_{n=0}^{\infty} \beta_{2n+1} \sin(2n+1)\vartheta \, d\vartheta = \\ &= -\sum_{n=0}^{\infty} \frac{\beta_{2n+1}}{2n+1} \cos(2n+1)\vartheta\end{aligned}\right| \qquad (9.3.24)$$

and the longitudinal flow, according to (9.3.21), by

$$\left.\begin{aligned}\varphi_2^{*}(\vartheta) &= \int \sum_{n=0}^{\infty} \alpha_{2n+1} \cos(2n+1)\vartheta \, d\vartheta = \\ &= \sum_{n=0}^{\infty} \frac{\alpha_{2n+1}}{2n+1} \sin(2n+1)\vartheta.\end{aligned}\right|$$

Lattice of staggered discs. In the general case the velocity distribution is obtained by adding the velocities of the three fundamental flows, that of the transverse flow, $w_1(\vartheta)$, of the longitudinal flow, $w_2(\vartheta)$, and of the circulatory flow, $w_3(\vartheta)$. Supposing (Fig. 9.3.7) that $\theta = \vartheta + \gamma = \vartheta + \frac{\pi}{2} - \beta$ and $w_m = 1$, we obtain

$$w(\vartheta) = w_1(\vartheta)\cos\gamma + w_2(\vartheta)\sin\gamma + \frac{\Gamma}{2\pi} w_3(\vartheta). \qquad (9.3.25)$$

The values of w_1, w_2, w_3, φ_1^*, φ_2^* and dependent on $\theta = \vartheta + \gamma$ are given in Appendix 9.

The complex potential of a flow through a lattice of discs. Starting from the fact that the tangential velocity $w(\vartheta)$ on the circle is equal to the vorticity of the vortex sheet, $\gamma(\vartheta)$, at this point . . (9.3.12), we can use the solution found to the problem of the flow through a lattice of discs to derive the complex potential of the whole flow. In fact, the complex potential at any point z of an elementary vortex $\gamma(\zeta)|d\zeta|$, placed at the kth circle at the point $\zeta + kle^{i\beta}$ will be $\frac{1}{2\pi i}\gamma(\zeta)\ln[z-(\zeta+kle^{i\beta})]|d\zeta|$. and that of the whole vortex sheet of the kth circle will be

$$\frac{1}{2\pi i}\int_c \gamma(\zeta)\ln[z-(\zeta+kle^{i\beta})]\,|d\zeta|.$$

where c denotes a circle with the center at the origin of coordinates. Summing over all k from $-\infty$ to $+\infty$ and adding the complex potential of the parallel flow, we find

$$\chi(z) = w_m z + \frac{1}{2\pi i}\int_c \gamma(\zeta)\ln(z-\zeta)\,|d\zeta| +$$

$$+ \sum_{k=-\infty}^{+\infty}{}' \frac{1}{2\pi i}\int_c \gamma(\zeta)\ln\left(1-\frac{z-\zeta}{kle^{i\beta}}\right)|d\zeta|,$$

where the dash at the summation sign indicates that the value k = 0 has to be omitted in summing over k, since the potential of the sheet of the fundamental circle is taken into account by the second term of the right-hand side.

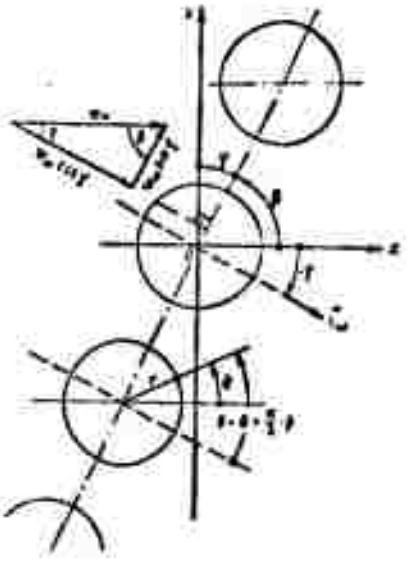


Fig. 9.3.7. The general case of zero circulation flow about a lattice of circles may be regarded as the sum of two particular cases – transverse with velocity $w_m \cos\gamma$ and longitudinal with velocity $w_m \sin\gamma$.

Integration leads to the following form of the complex potential of the lattice of discs:*

$$\frac{1}{w_-}\chi(z) = z + i\sum_{n=0}^{\infty}{}' \frac{(-1)^{n-1} r_0^{n-1}}{n!} a_{-n}\frac{d^n}{dz^n}\ln\sin\frac{\pi z}{le^{i\beta}}, \quad (9.3.25)$$

where $a_0 = \alpha_0$, $a_{-n} = \frac{\alpha_n + i\beta_n}{2}$,

and α_n and β_n are expressions obtained previously.

Denoting the expression $\pi/le^{i\beta}$ by λ and performing the differentiation, we obtain the complex potential of the lattice of discs of unit radius when $w_m = 1$ is the velocity of the undisturbed flow:

$$\chi(z) = z - ia_0\ln\sh\lambda z + ia_{-1}\lambda\operatorname{ctg}\lambda z +$$
$$+\frac{1}{2}ia_{-2}\lambda^2\sh^{-2}\lambda z + \frac{1}{3}ia_{-3}\lambda^3\frac{\ch\lambda z}{\sh^3\lambda z} + \quad (9.3.26)$$
$$+\frac{1}{12}ia_{-4}\lambda^4\frac{1+2\ch^2\lambda z}{\sh^4\lambda z} + \ldots$$

As we can see, the sum of all terms of the right-hand side of (9.3.26) with the exception of the first term is a periodic function of the period $\underline{l}e^{i\beta}$.

Lattice of approximately circular contours. The potential of dipoles uniformly arranged on sections of the imaginary axis (Fig. 9.3.8) with the period $\underline{l}$, and placed in a plane-parallel flow having the velocity $w_m = 1$ along the real axis, has the form

$$\gamma(\zeta) = \zeta + \frac{m}{2l}\int_{-\lambda}^{+\lambda} \operatorname{cth}\frac{\pi(\zeta - ip)}{l}\,dp = \zeta + \frac{lm}{2\pi}\ln\frac{\operatorname{sh}\frac{\pi(\zeta - i\lambda)}{l}}{\operatorname{sh}\frac{\pi(\zeta + i\lambda)}{l}}.$$

m is the dipole moment per unit length (Fig. 9.3.8, a). As E.L. [illegible] [9.9] has shown, if the stream function is zero we obtain a lattice of profiles whose contours deviate only slightly from circles with their centers on the imaginary axis.

E.L. Blokh and A.S. Ginevskiy [9.9] showed in their paper that the complex potential of the transverse flow through a lattice of "near-circles" can be obtained by arranging dipoles of equal moment m_1 on the imaginary axis in a parallel uniform flow occurring along the real axis, at a distance $\underline{l}$ from each other, and vortex pairs of equal intensity m_2 but opposite sense of rotation on both sides of the dipoles at a distance of λ (cf. Fig. 9.3.8, b) where ($w_m = 1$)

$$\gamma_p(\zeta) = \zeta - \frac{lpm_1}{\sin 2p\lambda}\ln\frac{\operatorname{sh}[p(\zeta + i\lambda)]}{\operatorname{sh}[p(\zeta - i\lambda)]} + pm_2\operatorname{cth} p\zeta$$

Here $p = \pi/\underline{l}$, m_1, m_2 and λ are parameters subject to the following conditions: 1) the points $\zeta = \pm 1$ must be stagnation points ($w = 0$); 2) $\eta = \pm 1$ when $\zeta = 0$; 3) at the points $\zeta = 0$ and $\eta = \pm 1$ the radius of curvature is $R = 1$. The authors solved the transcendental equations obtained by choosing numerical values for the parameters for a series of values of $q = 2r_0/\underline{l}$ between 0.5 and 1. The presence of three parameters makes it possible to obtain contours which are very similar to circles.

The results of an analysis of the shape of the "near-circles" show that the greatest deviation of the radius vector of a "near-circle" from the radius of a circle amounts to less than 0.6%.

The longitudinal and circulatory flow about "near-circles" can be calculated fairly simply from the transverse flow.

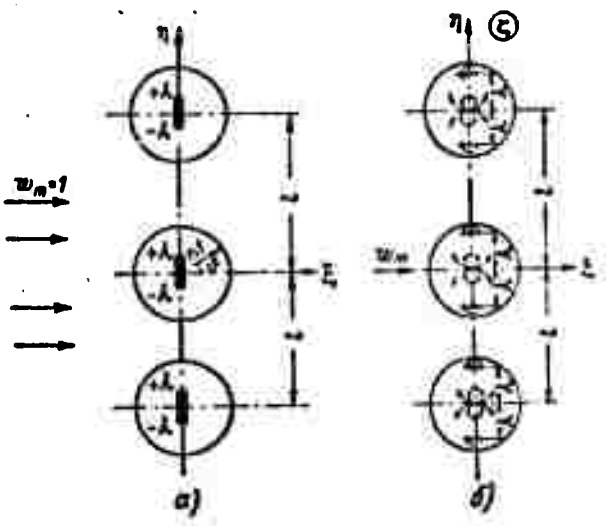


Fig. 9.3.8. Dipoles placed in a plane-parallel flow and uniformly arranged on sections of length 2λ of the imaginary axis (a) with the period l, together with the dipoles on the imaginary axis with the period l and vortices (b) on both sides of the dipoles give a lattice of "near-circles."

9.4. MAPPING OF A LATTICE OF CIRCLES TO A LATTICE OF THEORETICAL PROFILES

To construct a lattice of theoretical solid profiles, which are very important for the analysis of the general properties of lattices, it is natural to attempt to apply N.Ye. Zhukovskiy's method of rounding to a lattice of circles [9.8].

In fact, let us compare the complex potential of a circulation-free flow for a unit circle (the velocity at infinity being assumed equal to unity)

$$\chi_0 = \zeta + \frac{1}{\zeta} \qquad (9.4.1)$$

with the potential of a circulation-free flow about a lattice of circles (9.3.26) of unit radius for the velocity $w_m = 1$ of the undisturbed flow,

$$\chi_p = \zeta + g(\zeta); \qquad (9.4.2)$$

where $g(\zeta)$ is a periodic function with a period equal to $le^{i\beta}$. Since unlimited increase of the spacing l causes the lattice of circles to

degenerate to a single circle, we have $g(\zeta) \to 1/\zeta$ as $\underline{1} \to \infty$.

Moreover, the function $g(\zeta)$ is finite at infinity, and, since the velocity remains unchanged, we must have $\left.\frac{dg}{d\zeta}\right|_{\zeta=\infty} \to 0$. Further, if we calculate the potential of a circulation-free flow on the contour of a circle,

$$\omega(\zeta) = \varphi^* + i\psi^* = \cos\vartheta + i\sin\vartheta + R\{g(\zeta)\} + iIm\{g(\zeta)\} = \\ = \cos\vartheta + i\sin\vartheta + \varphi + i\psi,$$

then, noticing that the circular contour is a streamline for which $\psi^* = 0$, we obtain the imaginary part of $g(\zeta)$ on the circular contour in the form $Im\{g(\zeta)\} = \psi = -\sin\vartheta$, whereas in accordance with (9.3.25) the real part of $g(\zeta)$ on the circular contour will be

$$R(g(\zeta)) = \varphi(\vartheta) = -\cos\vartheta + \varphi_1^*(\vartheta+\gamma)\cos\gamma + \\ + \varphi_2^*(\vartheta+\gamma)\sin\gamma,$$

where φ_1^* and φ_2^* are determined by Formulas (9.3.24).

Thus, on the contour of the circle

$$g(\zeta) = \varphi(\vartheta) - i\sin\vartheta = \varphi_1^*(\vartheta+\gamma)\cos\gamma + \varphi_2^*(\vartheta+\gamma)\sin\gamma - \cos\vartheta. \qquad (9.4.3)$$

But on the contour of each circle of the lattice in the ζ-plane the imaginary part $\chi(\zeta)$ vanishes, and therefore, mapping the diagonal lattice onto the plane with the help of Function (9.4.2), i.e., assuming

$$z = \chi_p(\zeta) = \zeta + g(\zeta),$$

we obtain in the z-plane a diagonal lattice of plates with the parallels to the real axis of the z-plane staggered to the same extent. In exactly the same way the unit circle is mapped to a section of the real axis if (9.4.1) is taken as the mapping function.

It can therefore be shown that the function $g(\zeta)$ plays the same role in a flow about a lattice of circles as the function $1/\zeta$ in the flow about an isolated circle. Hence, if the function $1/\zeta$ is explicitly separated when the function $z = f(\zeta)$ conformally maps an isolated cir-

cle to a profile, i.e., if we take $z = \zeta + f(1/\zeta)$ and replace $1/\zeta$ by the function $g(\zeta)$ putting $z = \zeta + f[g(\zeta)]$, then we can expect to obtain a lattice of profiles in the z-plane which have shapes similar to the initial isolated profile with the same period $le^{i\beta}$ as the function $g(\zeta)$, (Fig. 9.4.1).

The mapping function. There are many methods of solving the problem of conformal mapping of a lattice of circles to a lattice of given profiles. The simplest one is obviously to extend S.A. Chaplygin's method of obtaining an isolated profile on a lattice of circles. As we have indicated in the foregoing (cf. Part 3.5), S.A. Chaplygin has shown that a great variety of profile shapes can be obtained by applying one and the same mapping function (3.5.24), containing a sufficient number of parameters determining the profile shape, to one and the same

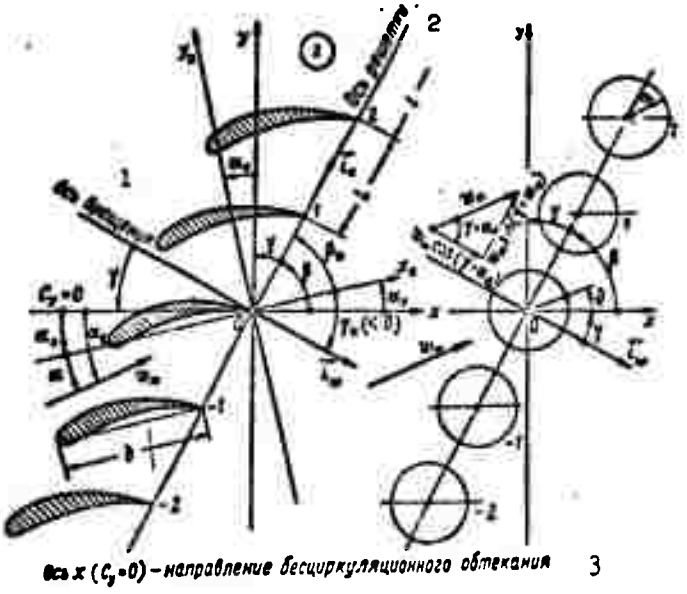


Fig. 9.1.4. Mapping of a lattice of profiles to a lattice of circles. 1) Axis of rotation; 2) lattice axis; 3) the x-axis ($C_y = 0$) is the direction of the circulation-free flow.

circle. An investigation of this function by A.S. Ginevskiy and Ye.I. [9.10], [9.11], with $k = 0$ (which corresponds to an angle of zero

at the profile's trailing edge).

$$z=\frac{(\zeta-1)^2}{\zeta-\varepsilon_0} \qquad (9.4.4)$$

showed that it yields sufficient variety of profile lattice shapes in dependence on the complex parameter $\varepsilon_0 = \xi_0 + i\eta_0$. Following a paper by A.S. Ginevskiy we shall deal with this method in what follows.

In order to separate $1/\zeta$, we rewrite (9.4.4) in the form

$$z=\frac{(\zeta-1)^2+(\zeta-\varepsilon_0)(\zeta-1)-(\zeta-\varepsilon_0)(\zeta-1)}{\zeta-\varepsilon_0}=$$

$$=\zeta-1+\frac{(\zeta-1)(\varepsilon_0-1-\varepsilon_0+\varepsilon_0)}{\zeta-\varepsilon_0}=\zeta-1-\frac{(\zeta-1)(\varepsilon_0-1)}{\zeta-\varepsilon_0}=$$

$$=\zeta-1-(1-\varepsilon_0)\frac{1-\frac{1}{\zeta}}{1-\varepsilon_0\frac{1}{\zeta}}.$$

This function maps the unit circle to a profile whose trailing edge $z = 0$ corresponds to the point $\zeta_0 = 1$ on the circle. In a more general case, corresponding to the transition $\zeta_0 \neq 1$ at the trailing edge $z = 0$ we have to write the mapping function in the form

$$z=\zeta-\zeta_0-\left(1-\varepsilon_0\frac{1}{\zeta_0}\right)\frac{\frac{1}{\zeta_0}-\frac{1}{\zeta}}{1-\varepsilon_0\frac{1}{\zeta}}. \qquad (9.4.5)$$

As has already been shown, the transforming function for a lattice is constructed by replacing $1/\zeta$ by the periodic function $g(\zeta)$.

Thus, if we take ϑ_0 to denote the polar angle of the point corresponding to the trailing edge and g_0 the value of the function $g(\zeta)$ at the point $\zeta_0 = e^{i\vartheta_0}$, then the function mapping the lattice of unit circles to a lattice of Chaplygin profiles has the form

$$z=\zeta-e^{i\vartheta_0}-(1-\varepsilon_0 g_0)\frac{g_0-g(\zeta)}{1-\varepsilon_0 g(\zeta)}. \qquad (9.4.6)$$

The equation of the profil contour. As has been shown (9.4.3)

$$g(\zeta)=\varphi(\vartheta)-i\sin\vartheta,\quad g_0=g(e^{i\vartheta_0})=\varphi(\vartheta_0)-i\sin\vartheta_0, \qquad (9.4.7)$$

holds for the contour of a circle where $\varphi(\vartheta)$ is the velocity potential of a circulation-free flow about a lattice of circles from which the

potential of the uniform parallel flow is calculated.

Substituting $\zeta = e^{i\vartheta}$ and $\zeta_0 = e^{i\vartheta_0}$ in (9.4.5) now, we obtain the values $z = x + iy$ for the points of the profile contour

$$z = x + iy = e^{i\vartheta} - e^{i\vartheta_0} - [1 - (\xi_0 + i\tau_0)(\varphi_0 - i\sin\vartheta_0)]\frac{(\varphi_0 - i\sin\vartheta_0) - (\varphi - i\sin\vartheta)}{1 - (\xi_0 + i\tau_0)(\varphi - i\sin\vartheta)},$$

whence the coordinates of the profile

$$\left.\begin{aligned} x &= \cos\vartheta - \cos\vartheta_0 - \frac{(A_0C - B_0D)A + (B_0C + A_0D)B}{A^2 + B^2}, \\ y &= \sin\vartheta - \sin\vartheta_0 - \frac{(B_0C + A_0D)A - (A_0C + B_0D)B}{A^2 + B^2}, \end{aligned}\right\} \qquad (9.4.8)$$

where

$$\begin{aligned} A_0 &= 1 - \xi_0\varphi_0 - \tau_0\sin\vartheta_0, & B_0 &= \xi_0\sin\vartheta_0 - \tau_0\varphi_0, \\ A &= 1 - \xi_0\varphi - \tau_0\sin\vartheta, & B &= \xi_0\sin\vartheta - \tau_0\varphi, \\ C &= \varphi_0(\vartheta_0) - \varphi(\vartheta), & D &= \sin\vartheta - \sin\vartheta_0. \end{aligned}$$

The quantities φ_1^* and φ_2^* necessary to calculate the profile coordinates can be taken from the table in Appendix 9. The values of the angles ϑ_0 and the velocity potentials on the circle at the point defined by this angle are given in Tables 1 and 2 in Appendix 10.

For sparse lattices $q < 0.5$ and, restricting ourselves to terms containing q^2, we obtain

$$\vartheta_0 = -\left(\operatorname{arctg}\frac{0{,}823q^2\sin 2\gamma}{1 + 0{,}823q^2\cos 2\gamma} + \gamma\right).$$

where

$$\begin{aligned} \varphi_1^* &= b_1\cos\vartheta - b_3\cos 3\vartheta + b_5\cos 5\vartheta, \\ \varphi_2^* &= a_1\sin\vartheta - a_3\sin 3\vartheta - a_5\sin 5\vartheta, \end{aligned}$$

$$\begin{aligned} b_1 &= 2 + 1{,}645q^2 + 1{,}354q^4 + 1{,}112q^6 + \ldots, \\ b_3 &= 0{,}270q^4 + 0{,}222q^6 + \ldots; \\ b_5 &= 0{,}0634q^6 + \ldots; \\ a_1 &= 2 - 1{,}645q^2 + 1{,}354q^4 - 1{,}112q^6 + \ldots; \\ a_3 &= 0{,}270q^4 - 0{,}222q^6 + \ldots; \\ a_5 &= 0{,}0634q^6 + \ldots. \end{aligned}$$

The profile lattice is thus determined by the parameters $\gamma = \pi/2 - \beta$ and $q = 2r/t$, varying within the limits $-\frac{\pi}{2} \leqslant \gamma \leqslant \frac{\pi}{2}$, $0 < q < 1$ characterizing the slope angles of the lattice and its density, and

by the parameters ξ_0 and η_0 on which the shape of the camber line and the profile thickness depend.

In order to calculate lattices of profiles for given values of the geometrical density parameters $\bar{b} = b/l$, of the (geometrical) rigging angle of incidence, $\beta_p = \beta - \alpha_0$ (correspondingly, of the geometrical stagger $\gamma_p = \pi/2 - \beta_p$), of the camber $\bar{f} = f/b$ and of the thickness $\bar{d} = d/b$, it is necessary to know the relationship between these and the following parameters of the lattice of circles: the density $q = 2r_0/l$ of the lattice of circles, the aerodynamic stagger γ, and the transformation parameters ξ_0 and η_0. It is impossible to determine this relationship in analytical form. It has been established on the basis of calculations on a great number of profile lattices.

Shape of camber line and thickness curve. The limits within which the parameters ξ_0 and η_0 vary are determined by the condition that no self-intersection should occur (cf. Fig. 9.2.16), i.e., that the function $z(\zeta)$ and $dz/d\zeta$ should have no zeros in the whole region outside the circles with the exception of the point corresponding to the trailing edge of the profile. A limiting case will therefore be a second cusp on the profile and the point on the circle corresponding to it. General considerations lead to the conclusion that the limiting values of the parameters ξ_0 and η_0 depend on the density $q = 2/l$ of the lattice of circles and on its stagger angle γ. The sparser the lattice, i.e., the smaller q, the greater is the range of admissible values of ξ_0 and η_0.

Calculations on a series of profiles showed [9.10] that profiles obtained by the Chaplygin transformation (9.4.4) have a camber line which is very similar to a circular arc, and that the shape of the symmetrical part of the lattice profile, namely the thickness curve over a very wide range of densities b/l, the rigging angle $\beta_g = \beta - \alpha_0$, the

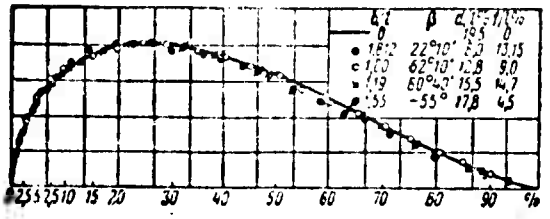


Fig. 9.4.2. The thickness curve virtually does not change over wide intervals of lattice parameter variation.

camber $\bar{f} = f/t$, and the thickness $\bar{d} = d/b$, are virtually unchanged (cf. Fig. 9.4.2). At the same time, within the limits of absence of self-interaction, we have for an isolated profile ($q = 0$)

$$v_0 = -\frac{2(1-0.77\bar{d})\bar{f}}{4\bar{f}^2-1}; \quad \xi_0 = 1 + \frac{\eta_0}{2\bar{f}}.$$

In Appendix 10 tables and graphs give the values of ξ_0, η_0, and α_0 in dependence on $\bar{f}$, $\bar{d}$, γ, and $b/\underline{l}$ and also the connection between $b/\underline{l}$ and $\underline{q}$ obtained from calculations.

Velocity distribution on the profile contour. This is determined by the relation $\bar{w}(z) = \bar{w}(\zeta)\frac{d\zeta}{dz}$, where $\left.\frac{d\zeta}{dz}\right|_{\substack{y\to 0\\ x\to\infty}} = 1$ and, owing to (9.3.25), if α_a is the angle of attack which is equal to the angle between the vector of mean velocity w_m and the direction of the circulation-free flow,

$$\frac{1}{w_m}\bar{w}(\zeta) = w_1(\zeta)\cos(\gamma+\alpha_a) + w_2(\zeta)\sin(\gamma+\alpha_a) + \frac{\Gamma}{2\pi r_0 w_m} w_3(\zeta).$$

When $w_m = 1$ at the boundary of a unit circle $\zeta = e^{i\vartheta}$

$$w(\vartheta) = w_1(\vartheta+\gamma)\cos(\gamma+\alpha_a) + w_2(\vartheta+\gamma)\sin(\gamma+\alpha_a) + \frac{\Gamma}{2\pi} w_3(\vartheta+\gamma). \qquad (9.4.9)$$

The sum of the first two terms of the right-hand side (9.4.9) gives the velocity on the contour of the circle in a circulation-free flow for $\alpha_a = 0$, referred to w_m (9.3.25),

$$w_0 = w_1\cos\gamma + w_2\sin\gamma.$$

Hence the polar angle of the stagnation point ϑ_0 on the circle, where, by definition, $w_0 = 0$, can be calculated from the expression

$$w_1(\vartheta_0+\gamma)\cos\gamma+w_2(\vartheta_0+\gamma)\sin\gamma=0 \qquad (9.4.10)$$

for various values of q and γ (cf. Appendix 10). The point on the circle determined by this angle must go over to the trailing edge of the profile.

The magnitude of the circulation Γ is chosen according to the Zhukovskiy-Chaplygin postulate on smooth flow about the profile's trailing edge, i.e., from the condition that Expression (9.4.9) becomes zero at point $\vartheta = \vartheta_0$ for all angles of attack; this gives

$$\Gamma=-2\pi w_\infty\frac{w_1(\vartheta_0+\gamma)\cos(\gamma+\alpha_0)+w_2(\vartheta_0+\gamma)\sin(\gamma+\alpha_0)}{w_2(\vartheta_0+\gamma)}$$

or, owing to (9.4.10),

$$\Gamma=-2\pi w_\infty\sin\alpha_0\frac{w_1(\vartheta_0+\gamma)\sin\gamma-w_2(\vartheta_0+\gamma)\cos\gamma}{w_2(\vartheta_0+\gamma)}. \qquad (9.4.11)$$

Substituting this in (9.4.9) we obtain the velocity at the points of the circle when the circulation is chosen according to the Zhukovskiy-Chaplygin condition at the trailing edge of the profile

$$w_0=w_0(\cos\alpha_0-G\sin\alpha_0).$$

where

and

$$\left.\begin{aligned}G&=\frac{1}{w_0}\left[\left(w_1-\frac{w_{10}}{w_{20}}w_2\right)\sin\gamma-\left(w_2-\frac{w_{20}}{w_{20}}w_2\right)\cos\gamma\right]\\ w_{10}&=w_1(\vartheta_0+\gamma),\quad w_{20}=w_2(\vartheta_0+\gamma),\quad w_{30}=w_2(\vartheta_0+\gamma)\end{aligned}\right\}(9.4.12)$$

are the velocity components at the point that corresponds to the trailing edge. These velocities can be calculated once and for all (cf. Appendix 10) and it is then easier to calculate $w(\vartheta)$. It is considerably more difficult to calculate the expression for $dz/d\zeta$. If we restrict ourselves however to calculating the magnitude of the velocity at the profile contour

$$w_z = |\overline{w}(z)| = |\overline{w}(\zeta)| \left|\frac{d\zeta}{dz}\right| = \frac{w_3(\vartheta)}{\sqrt{\left(\frac{dx}{d\vartheta}\right)^2 + \left(\frac{dy}{d\vartheta}\right)^2}} \qquad (9.4.13)$$

(where $w_3(\vartheta)$ is the magnitude of the velocity at the contour of a circle in the lattice, x and y are the profile coordinates), then in this case too the expression for w_z has a rather complex form. Omitting the intermediary transformations we can give the final formulas for the determination of dx/dϑ and dy/dϑ [9.10]:

$$\left.\begin{aligned}
&-\frac{dx}{d\vartheta} = \sin\vartheta + a\frac{d\varphi}{d\vartheta} + \\
&+\frac{(K'A + L'B + KA' + LB')(A^2+B^2) - 2(KA+LB)(AA'+BB')}{(A^2+B^2)^2}, \\
&\frac{dy}{d\vartheta} = (1+a)\cos\vartheta - \\
&-\frac{(L'A + A'L - K'B - KB')(A^2+B^2) - 2(LA+KB)(AA'+BB')}{(A^2+B^2)^2}, \\
&K = A_0C - B_0D, \quad -K' = A_0\frac{d\varphi}{d\vartheta} + B_0\cos\vartheta, \\
&A' = -\left(\xi_0\frac{d\varphi}{d\vartheta} + \tau_{w0}\cos\vartheta\right), \\
&L = B_0C + A_0D, \quad L' = A_0\cos\vartheta - B_0\frac{d\varphi}{d\vartheta}, \\
&B' = \xi_0\cos\vartheta - \tau_{w0}\frac{d\varphi}{d\vartheta}, \quad \frac{d\varphi}{d\vartheta} = \sin\vartheta + \varpi_0.
\end{aligned}\right\} \qquad (9.4.14)$$

Let us point out that most of the quantities entering the expressions for dx/dϑ, dy/dϑ and for the velocity of the profile are determined when the profile coordinates are calculated.

The pressure coefficient. If we know the velocity distribution, we find the pressure coefficient at each point in terms of the pressure head due to the mean velocity:

$$C_{pm} = \frac{p - p_m}{\frac{\rho w_m^2}{2}} = 1 - \left(\frac{w_\zeta}{w_m}\right)^2 \qquad (9.4.15)$$

or due to the velocity w_1 of the undisturbed incoming flow

$$C_{p1} = \frac{p - p_1}{\frac{\rho w_1^2}{2}} = 1 - \left(\frac{w_\zeta}{w_1}\right)^2. \qquad (9.4.16)$$

The lift coefficient in a lattice. Substituting the expression for Γ from (9.4.11) into the relation $2\Gamma = C_y b w_m$ and putting

$$\Gamma^* = -\frac{w_{10} - \sin\gamma - w_{20}\cos\gamma}{2w_{20}}, \qquad (9.4.17)$$

we find, when taking $b = 2\bar{b}/q$ and $\alpha_p = \alpha + \alpha_0$ into account, that

$$C_y = \frac{8\pi}{b}\Gamma^*(q,\gamma)\sin\alpha_p - \frac{4\pi q}{b}\Gamma^*(q,\gamma)\sin(\alpha+\alpha_0). \qquad (9.4.18)$$

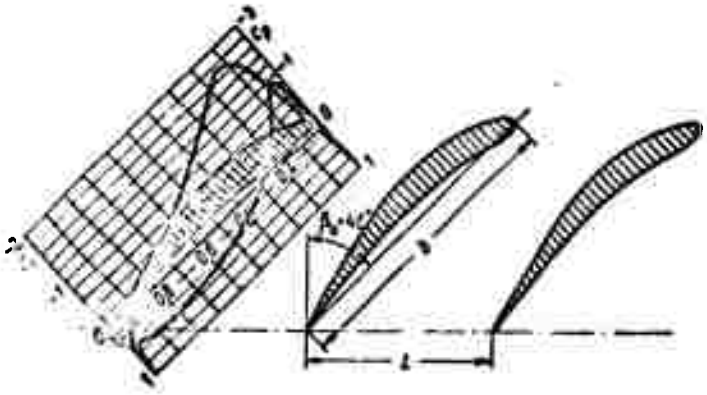


Fig. 9.4.3. Lattice of profiles calculated by way of example and the pressure distribution over a profile ($b:l=1.5$; $\gamma_s=46°$; $d:b=10.2\%$; $\bar{f}=8.2\%$).

The values of Γ^* are given in Appendix 10 (Table 7) as functions of q and γ. On the basis of a series of lattices calculated by means of a two-parametric family of Chaplygin profiles, obtained by Transformation (9.4.6) with the two parameters ξ_0 and η_0 ($\varepsilon_0 = \xi_0 + i\eta_0$), curves were drawn representing the dependence of $dC_y/d\alpha$ and α_0 on the following geometrical lattice parameters: the geometrical stagger ($\gamma = \pi/2 - \beta$), the density b/l, the thickness ratio $\bar{d} = d/l$ and the camber $\bar{f} = f/b$ of the profile, which render the calculations much easier (Fig. 9.4.3, cf. also Part 9.13); they are given in Appendix 10 where an example of the calculation is given too.

Deflection of flow from a lattice. The connection of the geometrical and aerodynamic lattice characteristics with the triangle of velocities is determined in the same way as for a lattice of plane plates (cf. Part 9.2), by relations analogous to (9.2.26)-(9.2.27):

$$\left.\begin{aligned} &\operatorname{ctg}\beta_m=\frac{1}{2}(\operatorname{ctg}\beta_1+\operatorname{ctg}\beta_2) \qquad (\beta=\beta_r-\alpha_0).\\ &\operatorname{ctg}\beta_2=A\operatorname{ctg}\beta_1+B;\\ &A=\frac{1-\frac{b}{4l}\frac{dC_y}{d\alpha}\sin\beta}{1+\frac{b}{4l}\frac{dC_y}{d\alpha}\sin\beta}; \quad B=\frac{\frac{b}{4l}\frac{dC_y}{d\alpha}\cos\beta}{1+\frac{b}{4l}\frac{dC_y}{d\alpha}\sin\beta}. \end{aligned}\right\} \qquad (9.4.19)$$

This makes it possible to solve the so-called converse problem, i. e., to choose the lattice for a given deflection of the flow. This problem is solved by means of the graphs $dC_y/d\alpha$ and α_0; if the two lattice parameters β_1 and β_2 and two profile parameters, e.g., d/b and b/l are given, we find f/b and β.

9.5. CONSTRUCTION OF PROFILE LATTICES

The problems considered in Parts 9.2-9.4 refer mainly to the flow structure and the so-called lattices of theoretical profiles, the class of which is not very large. Despite the auxiliary tables available, the construction of lattices is a rather complex task.

The great value of solving this series of problems consists in the determination of the lattice characteristics to be analytically or graphically represented. Meanwhile, the constructor must have a sufficiently simple and reliable method of constructing lattices displaying given properties, for example, a given velocity distribution over the lattice profile or a more or less definite profile geometry determined by the constructional requirements. In this part we shall consider several solutions to these problems; unless it is otherwise stated, the fluid is assumed to be incompressible and inviscid.

The principal streamline. This is the name given to the streamline which, coming from infinity to the profile, branches at the leading edge, runs along the profile, rejoins at the trailing edge (or leaves the profile contour forming the stagnant zone) and runs off behind the profile to infinity. In Fig. 9.5.1 this is the line $AB^{CDEFG}_{PQRST}KL$.

The channel method. As we have shown, when the flow between two neighboring profiles in a sufficiently dense lattice is regarded as a curved channel, the velocity distributions both over the profile contour and over the channel cross sections can be determined by a method described in Part 8.5. Unfortunately this method does not render it possible to construct the flow reliably in the leading and trailing edge zones and thus to take the angle of inflow into account.

The velocity hodograph. This is used to investigate the flow through lattices of plane plates by N.Ye. Zhukovskiy's method. In recent years this method was developed in connection with the development of turbocompressor aircraft engines by both native and foreign scientists. In what follows we shall deal with the method due to G.Yu. Stepanov [9.17].

When we draw the velocity vector from any point O along the principal streamline ABCDEFGKL-ABPQRSTKL and join the tips of the vectors by a smooth curve, we obtain the velocity hodograph of this streamline (cf. Fig. 9.5.1). The other streamlines in the channel formed by the principal streamlines begin at infinity A and end at infinity B. Their velocity hodographs will begin at point A and end at point L, the ends of the velocity vectors $\vec{w}_1$ and $\vec{w}_2$ of the flow at infinity in front of and behind the lattice. The velocity hodograph of the flow through the channel formed by the principal streamlines will therefore have the form of a flow from the source A to the sink L.

We shall first consider the flow of an incompressible fluid. From the condition of conservation of the mass flow through the lattice [cf. (9.1.9)] the straight line AB will be parallel to the lattice axis (front). The mass flow from the source and the corresponding sink is then obtained by multiplying the velocity component normal to the lattice axis by the lattice period, i.e., by the equation

$$Q = w_1 \sin\beta_1 l = w_2 \sin\beta_2 l. \qquad (9.5.1)$$

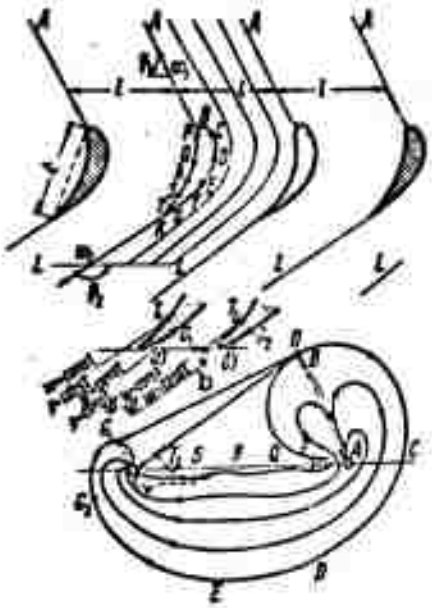


Fig. 9.5.1. Velocity hodograph of profile lattice. In the region of thick trailing edges a stagnant zone forms, with the boundary conditions on the departing streamlines. a) Constant velocity and pressure; b) constant direction of the velocity.

As in the case considered of the lattice of unstaggered plane plates (cf. Part 9.2), a multiple circumvention of the source may be considered as being performed on a Riemannian surface. Corresponding to one circumvention of the source on the hodograph plane, there will be a transition over one lattice spacing on the physical plane of the flow.

The equation given is insufficient to determine w_1 and β_1 (or correspondingly w_2 and β_2). A second equation can be obtained from Eq. (9.1.10) which determines the circulation about the profile $\Gamma = w_1 l \cos\beta_1 - w_2 l \cos\beta_2$.

Corresponding to the constant velocity along the front of a lattice with the period l, at infinity in front of the lattice, $w_1 \cos\beta_1$, and behind it, $w_2 \cos\beta_2$, in the physical plane of flow there is a vortex at the point A with the circulation $\Gamma_1 = w_1 l \cos\beta_1$, and a vortex

at the point L of the circulation $\Gamma_2 = w_2 l \cos \beta_2$ in the hodograph plane (cf. the lattice of plane plates, arranged one after the other (Part 6.2). We can thus assume that the flow in the hodograph plane is produced by a vortex-source at the point $A(Q = l w_1 \sin \beta_1, \ \Gamma_1 = l w_1 \cos \beta_1)$ and a vortex-sink at the point $L(Q = l w_2 \sin \beta_2, \ \Gamma_2 = l w_2 \cos \beta_2)$.

The trailing edge. In the flow about a trailing edge of finite thickness a stagnant zone forms, beginning at the points G and T and extending to infinity. As the boundary condition determining the streamlines that bound the stagnant zone we can take, for example, the conservation of the constancy of velocity and pressure on the streamlines or the constancy of the direction on the streamlines (cf. Fig. 9.5.1, a and b). In this case there will be only a sink along at point L and the continuity equation yields

$$l w_1 \sin \beta_1 = l w_2 (1 - \sigma) \sin \beta_2; \qquad (9.5.2)$$

where $\sigma = c/b$ is the relative thickness of the jet zone.

Construction of streamlines. Let us integrate along a streamline (Ψ = const) on the velocity hodograph the expression

$$dz = dx + i dy = \frac{d\Phi}{\overline{w}} = \frac{d\Phi}{\overline{w}},$$

where Φ is the velocity potential, $\overline{w}$ the conjugate complex velocity and dz a streamline element. The direction of the streamline element $dz = e^{i\vartheta} ds$ coincides with the direction of the velocity $w_x + i w_y = w e^{i\vartheta}$, and so in order to be able to construct a streamline we only need to know the length of its element

$$ds = \frac{d\Phi}{w}. \qquad (9.5.3)$$

The method of constructing a profile coinciding with the principal streamline is based on these considerations.

The velocity potential. The velocity potential at corresponding points in the hodograph plane and in the flow plane is the same. In order to determine it in the hodograph plane it is convenient to make use of the conformal mapping of the interior of the hodograph to the interior of the unit circle in such a way that the tip of the vector $\vec{w}_1$

(vortex-source at A) goes over to the center of the circle and the tip of the vector $\vec{w}_2$ lying on the contour of the hodograph (vortex-sink or sink in separated flow – at point L) goes over to a point lying on the circle, for example, the point with the central angle $\vartheta = 0$, (Fig. 9.5.2).

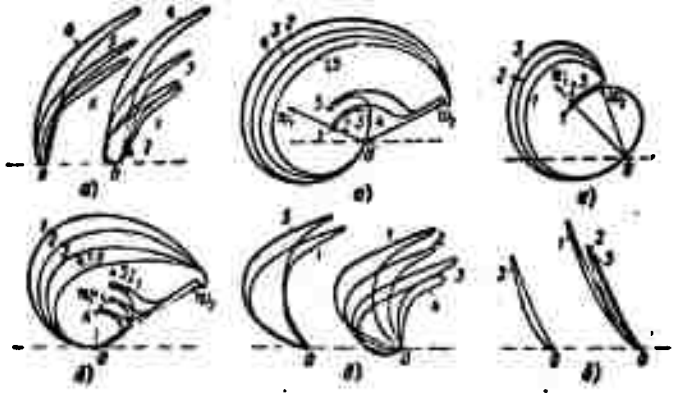


Fig. 9.5.2. Hodographs and lattices. a) Of reactive type ($\beta_1 = 90^\circ$, $\beta_2 = 120^\circ$); b) of active type ($\beta_1 = 25^\circ$, $\beta_2 = 115^\circ$); c) of compressor type ($\beta_1 = 47^\circ$, $\beta_2 = 198^\circ$).

Calculating the complex potential of the circle from the vortex-source (Γ,Q) lying at its center and the sink (-Q) on its contour, we find

$$\Phi = \frac{\Gamma}{2\pi}\vartheta - \frac{Q}{\pi}\ln\sin\frac{\vartheta}{2}. \qquad (9.5.4)$$

At the leading edge branching point (B) of the flow about a profile (at the origin O of the hodograph plane) the velocity becomes zero. Corresponding to it there is a point on the circle, which is determined by the condition that $d\Phi/d\vartheta = 0$ at this point, and hence

$$\vartheta_0 = 2\arctg\frac{Q}{\Gamma}. \qquad (9.5.5)$$

The inflection zone on the inner side of the profile (saddle) corresponds to the zone of the slit about point P. The length of this slit is so chosen that the original of the branching point B of the flow is

a point on the circle, determined by Eq. (9.5.5).

Choice of the velocity hodograph. In order to construct a lattice according to a given triangle of velocities (inlet velocity w_1, outlet velocity w_2, and the corresponding rigging angles β_1 and β_2, related by the expression $w_1 \sin \beta_1 = w_2 \sin \beta_2$, we must know in addition the lattice period $\underline{1}$, the maximum velocity w_{max}, the velocity at the profile back, w_{sp}, parallel to the inlet velocity w_1, and the velocity w_{vn} at the inflection point of the profile's saddle contour, and also the thickness σ and the angle ω at the trailing edge of the profile.

For diffusor (compressor) lattices $w_{max} = (1{,}05 \div 1{,}5) w_1$, $w_{cn} \approx w_{max}$, $w_{sp} \approx w_2$. For confusor (turbine) lattices $w_{max} = (1{,}05 \div 1{,}35) w_2$, $w_{cn} = (1{,}1 \div 2{,}5) w_1$, $w_{sp} = (0{,}5 \div 1{,}7) w_1$.

It should be borne in mind that as the velocity w_{sp} increases, the camber of the profile increases and the profile becomes shorter. For active lattices it is recommended to take the velocity at the profile back to be constant. The trailing edge angle $\omega = 5$ to 10°.

After having chosen the characteristic properties by the circular arcs the hodograph contour is drawn. Fig. 9.5.2 shows several types of lattices and their velocity hodographs [9.18].

Mapping of the hodograph region on a circle. As we shall see, this transformation is most simply achieved by ellectrical stimulation with an apparatus [9.18] consisting (Fig. 9.5.3) of an electrolytic tank 1, two electrodes 2, 3, two shunts 4 of copper wire 1.5-2.0 mm and 0.75 mm in diameter, respectively, and the headphones 5. The electrolytic tank is made of a piece of plasticine (10 x 25) pasted on glass along the hodograph; it is positioned horizontally and filled with water. The system is fed by alternating current from the 120-220 v mains; the current is fed through a lamp to the electrodes. The image of the hodograph, the circle, is subdivided into 16 equal parts which are marked by the figures 0, 1, 2, ... 15 (16).

The following sequence of sumulation can be recommended. 1) The electrode 2 is fixed at the point where the vector $\vec{w}_1$ has its tip, i.e., at the point corresponding to the center of the circle; 2) we shall assume that the position of the electrode at the tip of the vector $\vec{w}_2$ corresponds to point 0 (the original of point L) of the circle at $\vartheta = 0.3$). If one of the contacts is now fixed at an arbitrary point M, then, if the other contact is shifted along the contour until the signal in the headphones becomes null the point can be found whose image on the circle is the point N which is symmetrical to the image M ($\vartheta_M = -\vartheta_N$); 4) If the position of the contacts is fixed at the points M and N and the electrode 3 shifted along the contour of the hodograph, point 8 on the circle ($\vartheta_8 = 180^\circ$) can be found from the cessation of the signal in the headphones. In order to determine the points 4 and 12 we place the contacts at the points B and L and, shifting the electrode 3 over the hodograph contour, we find successively point 4 ($\vartheta_4 = 90^\circ$) and then point 12 ($\vartheta_{12} = 270^\circ$). 6) The length of the slit is so chosen that the point on the circle with ϑ_k as calculated by Formula (9.5.5) becomes the image of the origin 0 (B) of the hodograph vectors.

The construction of a lattice. Lattices are constructed by graphoanalytical methods. We determine the mean velocity $\vec{w}_{sr}$ and the mean increment of the potential, $\Delta\Phi$, on the selected section and from (9.5.3) we calculate the length of the profile element

$$\Delta s = \frac{\Delta\Phi}{w_{sr}},$$

which we lay off in the direction of the mean velocity $\vec{w}_{sr}$. It is convenient to begin the construction at the branching point of 0 (B).

If the lattice obtained and its profile do not satisfy certain requirements (mainly constructive in nature), then the velocity hodograph is to be corrected and all the calculations are repeated. When the

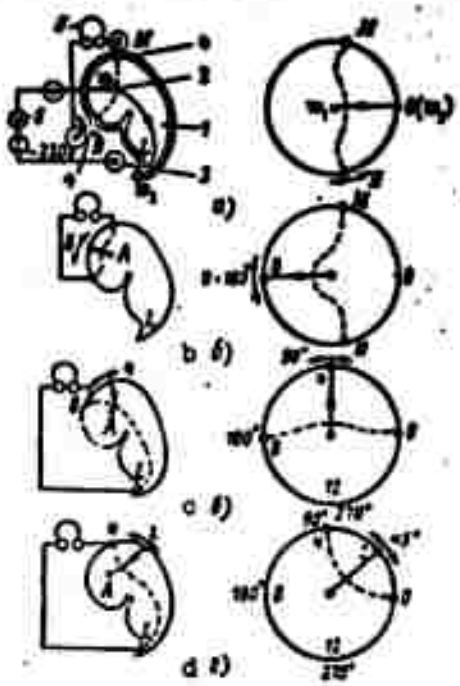


Fig. 9.5.3. Conformal mapping of the velocity hodograph to a circle by the method of electrodynamic simulation. a) Determination of the two symmetrical points M and N; b) determination of the point $\vartheta_1 = 180^\circ$; c) separation of the points $\vartheta = 98^\circ$ and $\vartheta = 270^\circ$; d) separation of the points $\vartheta_2 = 45^\circ$ (the circle is subdivided into 16 equal sections).

shape of the profile is altered we have to keep in mind that the shape of the back exerts a great influence on the flow, and when the conditions on the back are satisfactory, attempts should be made to restrict the changes in shape to the saddle if possible.

9.6. CIRCULAR LATTICE OF PROFILES

The centrifugal compressor (CC). The blades of a CC, forming a circular lattice, rotate and bring the air contained in its channels into rotation. Under the action of the centrifugal forces arising, the air is accelerated and its density, pressure and temperature are raised. In the diffusor the speed of the air drops and owing to the reduction of kinetic energy the pressure and temperature increase. It is very important to guide the flow in the diffusor properly, since this is

where the compressor losses are greatest. This explains the great variety of diffusor types used; they are investigated and estimated in the blade machine lectures.

A multi-stage CC consists of several stages mounted on a single shaft so that the air streams from the first to the second, from the second to the third stage, and so on.

Let us consider a vortex-source at the coordinate origin of the plane

$$\chi(\zeta)=\frac{Q-i\Gamma}{2\pi}\ln\zeta=\frac{Q-i\Gamma}{2\pi}(\ln r+i\vartheta). \qquad (9.6.1)$$

The logarithmic spirals $r_1=C_1\exp\frac{\Gamma}{Q}\vartheta$, $r_2=C_2\exp\frac{\Gamma}{Q}\vartheta$ will be the streamlines and equipotential lines, respectively, of this flow. Let us assume the streamline sections between $r = R_1$ and $r = R_2$ with the spacing $2\pi/N$ (N being an integer) are solid. The corresponding circular lattice is that of a nonmoving CC with infinitely thin blades describing logarithmic spirals.

Let us determine the flow parallel to the x-axis on the z-plane, $\chi(z) = w_\infty z$, i.e., the image of the flow (9.6.1), for which we put

$$z=A\ln\zeta+B. \qquad (9.6.2)$$

This is a periodic function with the period $i2\pi k$; corresponding each logarithmic spiral there will be an infinite multitude of straight lines parallel to the x-axis. Corresponding to the spiral sections, i.e., to the circular lattice there will be an infinite array of straight line sections, i.e., a lattice of plane plates. Thus Function (9.6.2) maps the circular lattice of logarithmic spirals to a lattice of plane plates (Fig. 9.6.1).

In order to establish the correspondence between the lattice parameters we put $A = A_1 + iA_2$, $B = B_1 + iB_2$. Then $x=B_1-A_2\vartheta+A_1\ln r$, $y=B_2+A_1\vartheta+A_2\ln r$.

Let the first blade of the circular lattice with the endpoints $\vartheta = A$, $r = R_1$ and $\vartheta = 0$, $r = R_2$, go over to the section $x = + b/2$ of

the real axis.

For a plate with $y = 0$ we have $B_2 + A_1\vartheta + A_2 \ln r = 0$, for the second plate with $y = h$ we have

$$B_2 + A_1\left(\vartheta + \frac{2\pi}{N}\right) + A_2 \ln r = h \quad A_1 = \frac{Nh}{2\pi} \tag{9.6.3}$$

This gives us

$$\left.\begin{aligned} -\frac{b}{2} &= B_1 - A_2\lambda + A_1 \ln R_1, \quad 0 = B_2 + A_1\lambda + A_2 \ln R_1, \\ \frac{b}{2} &= B_1 + A_1 \ln R_2, \qquad\qquad 0 = B_2 + A_2 \ln R_2 \end{aligned}\right\} \tag{9.6.4}$$

Solving the set of equations (9.6.4) we find

$$A_2 = A_1 \frac{\lambda}{\ln \frac{R_2}{R_1}} = \frac{Nh\lambda}{2\pi \ln \frac{R_2}{R_1}}, \quad A = -\frac{Nh}{2\pi \ln \frac{R_2}{R_1}}\left(\ln \frac{R_2}{R_1} + \Omega\right); \tag{9.6.5}$$

$$B_1 = -\frac{Nh}{4\pi \ln \frac{R_2}{R_1}}\left(\lambda^2 - \ln R_1 R_2 \ln \frac{R_2}{R_1}\right); \quad B_2 = -\frac{Nh\lambda}{2\pi \ln \frac{R_2}{R_1}} \ln R_2;$$

$$B = -\frac{Nh}{4\pi \ln \frac{R_2}{R_1}}\left(\lambda^2 - \ln R_1 R_2 \cdot \ln \frac{R_2}{R_1} - i2\lambda \ln R_2\right) =$$

$$= -\frac{Nh}{4\pi \ln \frac{R_2}{R_1}}(i\lambda + \ln R_1 R_2)\left(i\lambda + \ln \frac{R_2}{R_1}\right). \tag{9.6.6}$$

Now

and, consequently,

$$\left.\begin{aligned} \ln \zeta &= \varkappa z - \frac{B}{A}, \quad \varkappa = \frac{2\pi}{Nh} \frac{\ln \frac{R_2}{R_1} - \Omega}{\ln \frac{R_2}{R_1} + \frac{\lambda^2}{\ln (R_2 : R_1)}}; \\ -\frac{B}{A} &= \ln \sqrt{R_1 R_2} + \frac{\Omega}{2} \\ \zeta &= \sqrt{R_1 R_2}\, e^{\varkappa z + \frac{\Omega}{2}}. \end{aligned}\right\} \tag{9.6.7}$$

At the same time it follows from (9.6.4) and (9.6.5) that

$$b = A_1 \ln \frac{R_2}{R_1} + A_2; \quad \lambda = \frac{Nh}{2\pi}\left(\ln \frac{R_2}{R_1} + \frac{\lambda^2}{\ln (R_2 : R_1)}\right); \quad d = -A_2$$

From the relation $w_z = w_\zeta \frac{d\zeta}{dz} = \frac{Q - i\Gamma}{2\pi} \frac{\zeta}{A} = w_*$ it follows that

$$\frac{Q}{H}=w_{\infty}h,\quad \frac{\Gamma}{N}=-\frac{2\pi w_{\infty}}{\ln(R_2:R_1)},\quad \operatorname{arctg}\frac{Q}{\Gamma}=-\frac{1}{\lambda}\ln\frac{R_2}{R_1}. \qquad (9.6.8)$$

For $\Gamma = 0$ we have $\lambda = 0$, i.e., the lattice of radial blades goes over to a lattice of plane plates. For the latter

$$\zeta=\sqrt{R_1R_2}e^{\frac{2\pi z}{Nh}}. \qquad (9.6.9)$$

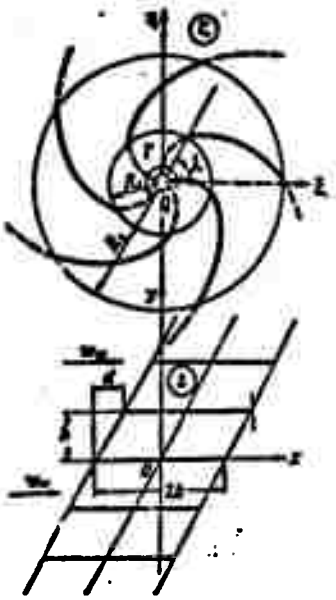


Fig. 9.6.1. Mapping of a circular lattice of logarithmic spirals to a lattice of plane plates.

Function (9.6.9) obtained can be taken as the transforming function in order to map a linear lattice of solid profiles to a circular lattice of solid profiles, and the relation $w_z = w_\zeta(d\xi/dz)$ can be used to determine the velocity at any point of it.

In the considered case of a flow the circulation about each of the profiles is equal to zero, as can be seen from Fig. 9.6.2. Therefore, no interaction of forces will occur between lattice and flow. In fact, in accordance with (9.1.9), the moment generated by one blade of the circular lattice when 1 kg of fluid mass passes through the lattice is

$$\frac{1}{N}M=r_2c_{2u}-r_1c_{1u}=\frac{1}{N}\left(r_2\frac{\Gamma_n}{2\pi r_2}-r_1\frac{\Gamma_v}{2\pi r_1}\right)=\frac{1}{2\pi N}(\Gamma_n-\Gamma_v),$$

where Γ_n and Γ_v are the circulations about the outer and inner circles (cf. Fig. 9.6.2), respectively.

In our case $\Gamma_n = \Gamma_v$ and $M = 0$.

In order to obtain a nonvanishing moment the profile must be arranged at a certain angle of attack and the Zhukovskiy-Chaplygin condition on a smooth flow about the trailing edge must be satisfied. This causes a circulation to arise about the profile and in connection with it the circulation with respect to a contour enclosing the whole cir-

cular lattice will differ from the circulation of the vortex on the axis of rotation of the circular lattice. Fig. 9.6.3 shows a flow of this type when there is no vortex at the lattice axis and the flow is radial.

Rotation of circular lattice. If the wheel rotates uniformly, the period of pressure change is $\delta t = \frac{2\pi r}{N} \frac{1}{r\omega} = \frac{2\pi}{N\omega}$.. Since the moment acting on the particle is $\delta M = \delta p \delta r \delta b r$, the work performed on the particles (or by the particles in the case of a turbine) per unit time (i.e., the power) will be equal to $\delta M\omega = \delta p \delta r \delta b r\omega$. The mass of a particle is $\delta m = \rho \delta r \delta b \frac{2\pi r}{N}$, and therefore the change in specific energy of a particle is $\frac{\delta l}{\delta t} = \frac{\delta M\omega}{\delta m} = \frac{\delta p N}{\rho 2\pi}$, i.e., it is equal to $\frac{1}{\rho}\frac{\partial p}{\partial t} = \frac{\delta p N\omega}{\rho 2\pi}$. This is in agreement with Relation (9.1.12) obtained previously and with the conclusion that in order to obtain a change in energy it is necessary to change the pressure with time.

Let us note that as the number N of blades increases at constant power, the slope of p(t) also remains constant – and the "saw-tooth" character of the pressure change with time is retained (Fig. 9.6.4). This is also true when the number of blades is raised to infinity; in this limiting case the flow becomes axisymmetric and unsteady.

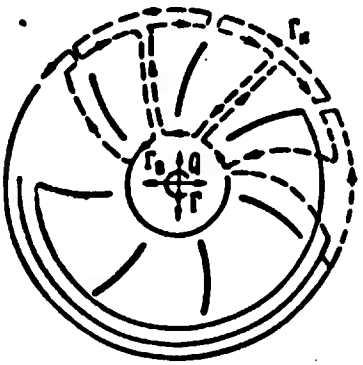


Fig. 9.6.2. The circulation about each blade Γ_b is equal to $(\Gamma_n - \Gamma_v)/k$.

If the wheel rotates, the absolute motion remains a potential motion but will be unsteady.

If the wheel rotates uniformly, then in a coordinate system fixed to it the wheel will be at rest, and the flow through it will be steady relative to it. Finally, this is highly convenient and in many cases this simplifies the investigation.

The Bernoulli equation in the Relative motion. As we know, the laws of mechanics remain valid in uniformly ro-

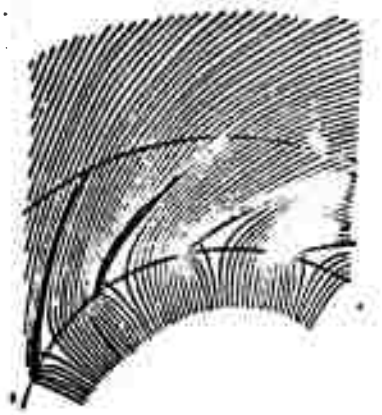


Fig. 9.6.3. A circulatory flow is superimposed on the radial flow from a plane source at the origin of coordinates such that the flow about the trailing edge is smooth.

tating systems if the radially directed centrifugal force $mr\omega^2$ and the Coriolis force are added to the forces acting in the absolute coordinate system; the magnitude per unit mass (tension) of the Coriolis force is determined by the vector product $2\vec{\omega} \times \vec{w}$ and its direction is perpendicular to the angular velocity of rotation and the relative velocity.

The centrifugal force is directed radially and its magnitude per unit mass is $f_c = \omega^2 r$; its potential is U_c, which is found by integration:

$$U_c = -\int \omega^2 r\, dr = \text{const} - \frac{\omega^2 r^2}{2}.$$

The gravity potential is $U_t = -gz$. The Coriolis force is perpendicular to the relative velocity. Applying the Bernoulli equation we find that along a streamline

$$P + \frac{w^2}{2} + gz - \frac{\omega^2 r^2}{2} = \text{const}, \qquad (9.6.10)$$

where the pressure function $P = \int dp/\rho$ (in an isotropic process for a gas $P = \frac{k}{k-1}\frac{p}{\rho}$; for an incompressible fluid $P = p/\rho$.

The constant in this equation is, generally speaking, different for different streamlines, but for flows which are free from rotation in the absolute coordinate system (even in unsteady but potential flows) it is the same for all streamlines.

In fact, for an absolute unsteady potential motion the Legendre integral (2.2.14) can be written in the following form

$$\frac{\partial \varphi}{\partial t} + P + \frac{c^2}{2} + U = f(t), \qquad (9.6.11)$$

where $\underline{c}$ is the absolute velocity of motion.

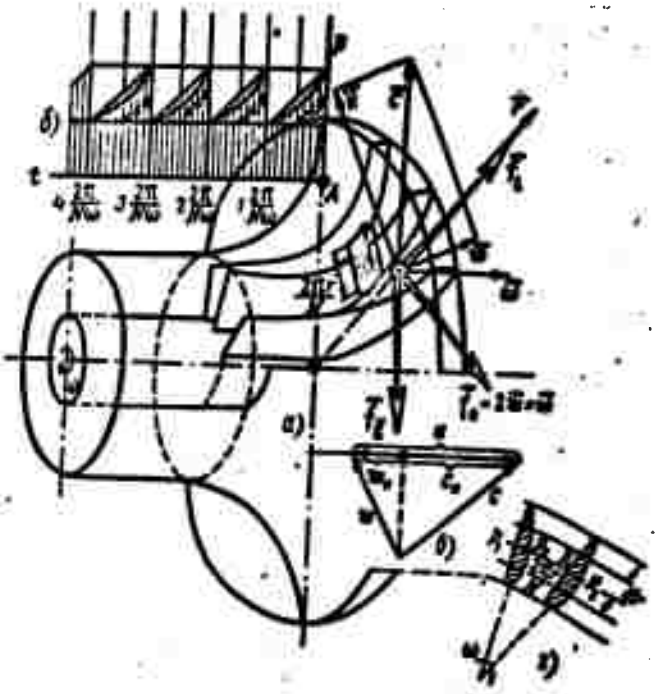


Fig. 9.6.4. Diagram of radial-flow turbine (a). For an observer at rest the pressure change with time at point A in space is periodic with the period $2\pi/\omega N$ (N is the number of blades and ω the angular velocity)(b); when the number of blades is doubled the pressure distribution (with unchanged power) will be as shown by the dashed line, the ratio $\partial p/\partial t$ remains unchanged. The triangle of velocities (c) and the axial view of a channel between the blades (d).

The value of f(t) will at each instant of time be equal for all streamlines.

Since the relative motion is steady, the potential must remain constant at each point of the rotating flow; its total variation must therefore vanish:

$$\frac{\partial \varphi}{\partial t} + \omega r \frac{\partial \varphi}{\partial l} = 0$$

Here ωr is the linear velocity of rotation (transport velocity); dl is a linear element in the direction of motion and therefore $\partial\varphi/dl$ is the velocity component of the absolute flow in the direction of rotation, equal to c_u.

Thus,

$$\frac{\partial \varphi}{\partial t} = -c_u \omega r.$$

From the triangle of velocities (cf. Fig. 9.6.4), $c^2-2\omega r c_u=w^2-(\omega r)^2$. Therefore

$$p+\frac{w^2-(\omega r)^2}{2}+U_g=\text{const}. \qquad (9.6.12)$$

where the constant is the same for all streamlines.

Let us consider an example - the uniform rotation about the z-axis with the angular velocity ω of a rectangular channel of constant cross section, in which the fluid flow in the absolute system of coordinates is a potential flow (Fig. 9.6.5).

Let us assume that in relative motion

$$w_x=w=w_1+2\omega y,\quad w_y=w_z=0.$$

In absolute motion

$$c_x=w_1+\omega y,\quad c_y=\omega x,\quad c_z=0.$$

In relative motion this flow is vortical at each point of the stream, since $\text{rot}_x\vec{w}=\text{rot}_y\vec{w}=0$, $\text{rot}_z\vec{w}=\frac{1}{2}\left(\frac{\partial w_y}{\partial x}-\frac{\partial w_x}{\partial y}\right)=-\omega$. . In absolute motion curl $\vec{c}$ = 0.

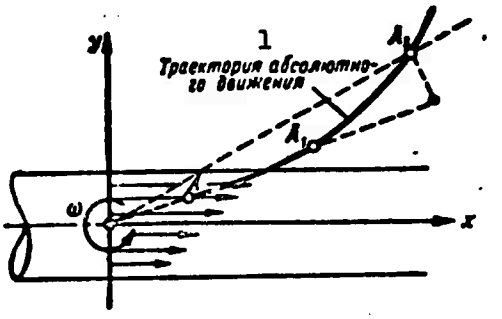


Fig. 9.6.5. In uniform motion of a rectangular channel the motion inside, which is potential in the absolute coordinate system, will be vortical in relative motion . 1) Trajectory of absolute motion.

The volume force components will be: the centrifugal force $f_{cx}=\omega^2 x$, $f_{cy}=\omega^2 y$, $f_{cz}=0$; the Coriolis force $f_{kx}=0$, $f_{ky}=-2\omega w_x$, $f_{kz}=0$; the gravitational force $f_{gx}=f_{gy}=0$, $f_{gz}=-g$.

Assuming that in relative motion each particle moves uniformly in a straight line (cylindrical channel), i.e., that its acceleration is

zero, we can write the projection of the equation of relative motion as

$$0=\omega^2x-\frac{1}{\rho}\frac{\partial p}{\partial x};\quad 0=\omega^2y-2\omega w_1-4\omega^2y-\frac{1}{\rho};\quad 0=-g-\frac{1}{\rho}\frac{\partial p}{\partial z}.$$

Multiplying the first equation by dx, the second by dy, and the third by dz, and integrating, we obtain

$$\frac{\omega^2}{2}(x^2-3y^2)-2\omega w_1y-U_g-P=\text{const}\left(P=\int\frac{dp}{\rho},\ U_g=gz\right).$$

But

$$w^2=w_x^2=w_1^2+4\omega yw_1+4\omega^2y^2,$$

and, therefore,

$$P+U_g-\frac{\omega^2(x^2+y^2)}{2}+\frac{w^2-w_1^2}{2}=\text{const}.$$

Since w_1 = const, we have

$$P+\frac{w^2-\omega^2r^2}{2}+U_g=\text{const}. \qquad (9.6.13)$$

Before the integration, the equation of motion was multiplied by the arbitrarily positioned element $d\vec{r}=\vec{i}dx+\vec{j}dy+\vec{k}dz$, therefore, the constant of integration is independent of the position since it was the same for all streamlines in Eq. (9.6.12) as well.

Velocity distribution in the channels of a CC. From the equation of motion of a fluid in a coordinate system fixed to the working wheel (relative motion), $\frac{d\vec{w}}{dt}=\vec{f}-\frac{1}{\rho}\vec{\nabla}p$, we find the velocity distribution in the channels of the CC.

Neglecting the force f_g of the Earth's gravity and taking into account that the centrifugal force f_c is radially directed ($\vec{f}_c = \omega^2\vec{r}$), and the Coriolis force $\vec{f}_k = 2\vec{w} \times \vec{\omega}$ lies in the plane of rotation of the wheel and is directed along the normal $\vec{n}$ to the relative velocity, i.e., to the streamline, and also that $\vec{f}=\vec{f}_c+\vec{f}_k=\omega^2\vec{r}+2w\omega\vec{n}$, we find that all forces and velocities lie in the plane of rotation (Fig. 9.6.6).

Projecting the equation of motion onto the direction of the tangent to the streamline, we obtain (9.6.6)

$$\frac{dw}{dt} = \omega^2 r \sin\beta - \frac{1}{\rho}\frac{dp}{dl}, \qquad (9.6.14)$$

where β is the angle between the normal $\vec{n}$ to the streamline and the radius $\vec{r}$.

If R is the radius of curvature of the streamline, the projection onto the normal $\vec{n}$ of the streamline gives us

$$-\frac{w^2}{R} = \omega^2 r \cos\beta - 2w\omega - \frac{1}{\rho}\frac{dp}{dn}. \qquad (9.6.15)$$

If the motion depends only on the radius r, then

$$\frac{dp}{dl} = \frac{dp}{dr}\frac{dr}{dl} = \frac{dp}{dr}\sin\beta; \quad \frac{dr}{dl} = \sin\beta.$$

Noticing that $w = dl/dt$ and supposing that $P = \int dp/\rho$, we can rewrite Eq. (9.6.14) in the form $w\,dw = \omega^2 r\,dr - dp$, whose solution reads

$$\frac{w^2}{2} - \frac{\omega^2 r^2}{2} + P = f(n). \qquad (9.6.16)$$

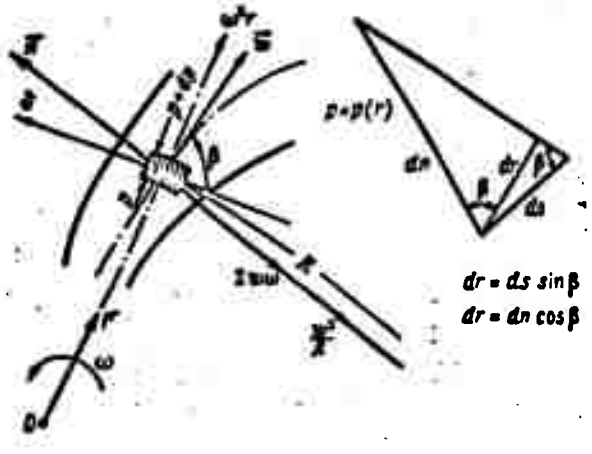


Fig. 9.6.6. Forces and velocities in the plane of rotation. The strength of the volume forces $\vec{f}$ is composed of the strength of the gravitational force, of the strength of the centrifugal force $\vec{f}_c = \omega^2\vec{r}$, and the strength of the Coriolos force $\vec{f}_k = 2\vec{w} \times \vec{\omega}$, lying in the plane of rotation of the wheel, and directed along the normal to the relative velocity, i.e., to the streamline.

If we suppose that the rotation of the flow at the inlet (if there is any) is produced by a vortex at the origin of coordinates, the absolute motion will be potential everywhere. In front of the inlet of the

lattice, as well as behind the outlet from the lattice, the absolute motion will be steady. Since the motion in the channel is assumed to be frictionless, the potentiality of the absolute motion is not violated for this region either. Therefore, f(n) must be the same for all streamlines; it was shown above that this is a constant quantity.

Thus,

$$\frac{w^2-u^2r^2}{2}+P=\text{const.} \qquad (9.6.17)$$

Differentiating this equation with respect to the normal $\underline{n}$

$$w\frac{dw}{dn}-\omega^2 r\frac{dr}{dn}+\frac{dP}{dn}=0,$$

we introduce dP/dn into Eq. (9.6.15) and, noticing that $\frac{1}{\rho}\frac{dp}{dn}=\frac{dP}{dn}$ and $dr=dn\cos\beta$, we obtain $w\frac{dw}{dn}-\omega^2 r\cos\beta+\frac{w^2}{R}+\omega^2 r\cos\beta-$ whence for blades bent forward (cf. Fig. 9.6.6),

$$\left.\begin{aligned}\frac{dw}{dn}&=2\omega+\frac{w}{R},\\ \frac{dw}{dn}&=2\omega-\frac{w}{R}.\end{aligned}\right\} \qquad (9.6.18)$$

and for blades bent backward

For radial blades ($R\to\infty$)

$$\frac{dw}{dn}=2\omega,\quad w=2\omega n+\text{const.} \qquad (9.6.19)$$

i.e., the relative (in the case considered, radial) velocity increases in the direction of the normal to the radius in the direction or rotation.

If there is a large number of blades, the radius of curvature of the blades is large compared with the transverse channel dimensions and can be taken as constant for all streamlines at a section normal to the streamlines passing through in the middle of the channel.

Therefore, from (9.6.18),

$$\frac{d\frac{w}{R}}{2\omega\mp\frac{w}{R}}=\frac{dn}{R},$$

whence we obtain after integration

$$\mp \ln\left(2\omega \mp \frac{w}{R}\right) = \frac{n}{R} + C.$$

where the upper sign applies to blades bent backward.

Denoting the velocity in the middle of the channel (n = 0) by w_m, we have

$$\left(2\omega \mp 2\frac{w}{R}\right) : \left(2\omega \mp 2\frac{w_m}{R}\right) = e^{\mp \frac{n}{R}}.$$

For $n/R \ll 1$ we can assume $e^{\mp \frac{n}{R}} = 1 \mp \frac{n}{R}$, where

$$w = \left(1 \mp \frac{n}{R}\right) w_m + 2\omega n.$$

Let us denote by w_1 the velocity on what is called the <u>driving side of the blade</u> (the blade surface that turns in the same direction as the rotation), for which $n = -d/2$, and by w_2 the velocity on the driven side, $n = +d/2$, so we obtain from (9.6.20) [sic].

$$w_1 = \left(1 \pm \frac{d}{2R}\right) w_m - \omega d; \quad w_2 = \left(1 \mp \frac{d}{2R}\right) w_m + \omega d. \qquad (9.6.20)$$

The velocity distribution is therefore linear in character, with $w_m = (w_1 + w_2)/2$.

The pressure difference between the two sides of the blade is determined from the Bernoulli equation for relative motion

$$p_1 + \frac{w_1^2 - \omega^2 r_1^2}{2} = p_2 + \frac{w_2^2 - \omega^2 r_2^2}{2}.$$

Supposing the process is isentropic, $p = \text{const}\ \rho^k$, we have $p = \int \frac{dp}{\rho} = \frac{k}{k-1}\frac{p}{\rho}$ and therefore

$$\left.\begin{aligned} &\frac{k}{k-1}\left(\frac{p_2}{\rho_2} - \frac{p_1}{\rho_1}\right) = \frac{w_1^2 - w_2^2}{2} = \frac{d}{R} w_m^2 - 2\omega w_m d, \\ &\frac{p_2}{p_1}\frac{\rho_1}{\rho_2} - 1 = d\frac{k-1}{k} w_m^2 \left(\frac{1}{R} - 2\frac{\omega}{w_m}\right)\frac{\rho_1}{p_1}, \\ &\frac{p_2}{p_1} = \left[1 + \frac{k-1}{k}\frac{\rho_1}{p_1} d w_m^2 \left(\frac{1}{R} - 2\frac{\omega}{w_m}\right)\right]^{\frac{k}{k-1}}. \end{aligned}\right\} \qquad (9.6.21)$$

Notice that $p_2 = p_1$ when $\omega/w_m = 1/2R$, i.e., the pressure difference vanishes; to these conditions corresponds $w_1 = w_2 = w_m$.

If the velocity is incompressible, $P = p/\eta$, then

$$p_2 - p_1 = \rho \frac{w_1^2 - w_2^2}{2} = \rho w_{1u}^2 \left(\frac{1}{R} - 2\frac{s}{w_{1u}}\right) d. \qquad (9.6.22)$$

As $d = 2\pi r/N \to 0$, i.e., as the number N of blades tends to infinity, though the pressure difference tends to zero, the product $(p_2 - p_1)N$ remains constant and the power consumed by the compressor maintains its value; at the same time it is supposed that the thickness of the blades is equal to zero, their capacity being conserved.

For radial blades ($R \to \infty$) we obtain from (9.6.20), (9.6.21) and (9.6.22):

$$\left.\begin{aligned} &\text{for } \rho = \text{const} && \frac{p_2}{p_1} = 1 - 2\frac{\rho w_1^2}{p_1}\left(1 + \frac{w_{1d}}{w_1}\right)\frac{w_{1d}}{w_1}; \\ &\text{for } \rho = \text{const } p^{1/k} && \frac{p_2}{p_1} = \left[1 - 2(k-1)M_1^2\left(1 + \frac{w_{1d}}{w_1}\right)\frac{w_{1d}}{w_1}\right]^{\frac{k}{k-1}}. \end{aligned}\right\} \qquad (9.6.23)$$

The critical velocity in relative motion. It follows from the energy equation in relative motion

$$c_p T + \frac{w^2}{2} = \text{const} + \frac{(\omega r)^2}{2} = c_p T_{0\,otn}$$

(where $T_{0\,otn}$ is the stagnation temperature in relative motion) that the total energy of a particle varies as the particle is displaced radially. Since the sonic speed in a gas depends only on its temperature,

$$a^2 = k\frac{dp}{d\rho} = k\frac{p}{\rho} = kRT,$$

the critical velocity (determined as the gas velocity that is equal to the velocity of sound) will no longer be constant along a flow element but will vary with the radius. If we denote it by a^*_{otn}, we can write

$$\begin{aligned} c_p T + \frac{w^2}{2} &= \frac{w^2}{2} + \frac{a^2}{k-1} = c_p T_{0\,otn} = \\ &= \frac{k+1}{2(k-1)} a^{*2}_{otn} = \text{const} + \frac{(\omega r)^2}{2}. \end{aligned} \qquad (9.6.24)$$

In order to determine the constant in this equation, we take usually the given conditions at the inlet of the working wheel. For this,

taking into account that $c_r = w_r$, $c_z = w_z$, $c_u - u = w_u$, we write $c^2 - 2uc_u + u^2 = w^2$, and from Eq. (9.6.24) we find that if $c_pT_{0z} = c_pT + \frac{c^2}{2}$ denotes the enthalpy of the flow at the inlet,

$$\text{const} = c_pT + \frac{w^2}{2} - \frac{(\omega r)^2}{2} = c_pT + \frac{c^2}{2} - uc_u = c_pT_{0z} - (uc_u)_{0z},$$

whence

$$a^*_{otn} = 2\frac{k-1}{k+1}\left(c_pT + \frac{w^2}{2}\right) = 2\frac{k-1}{k+1}\left[c_pT_{0z} - (\omega rc_u)_{0z} + \frac{(\omega r)^2}{2}\right] =$$
$$= a^*_{0z} - 2\frac{k-1}{k+1}\left[(\omega rc_u)_{0z} - \frac{(\omega r)^2}{2}\right]. \qquad (9.6.25)$$

For a streamline of an axial-flow compressor the critical velocity in relative motion is the same along one radius. As the radius is changed, not only the stagnation temperature $T_{0\ otn} = \text{const} + u^2/2p$ in relative motion but also the stagnation pressure and density in this motion will change.

Equation for the compression shock in relative motion. Repeating the discussion pertaining to (2.6.2) we obtain

$$\left.\begin{aligned} &\rho_1 w_1 = \rho_2 w_2, \\ &p_1 - p_2 = \rho_1 w_1 (w_2 - w_1), \\ &c_pT_1 + \frac{w_1^2}{2} = c_pT_2 + \frac{w_2^2}{2}, \\ &p = \rho RT. \end{aligned}\right\} \qquad (9.6.26)$$

The similarity in the form of the compression shock equations in absolute and relative motion results from the fact that the shock equations do not contain forces proportional to the gas mass, which are added as a result of the transition from the absolute to the relative system.

Solving System (9.6.26) and introducing the quantity a^*_{otn} from Eq. (9.6.25), we obtain the basic relation

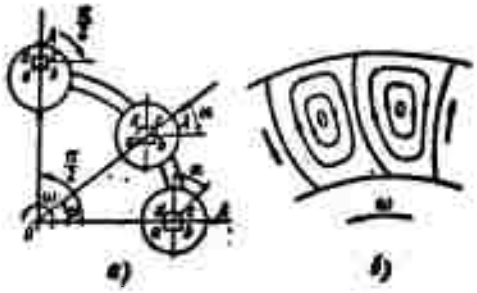
$$w_1 w_2 = a^{*2}_{otn} \qquad (9.6.27)$$

and therefore all conclusions drawn before with respect to absolute motion can be taken over with appropriate corrections for relative motion.

The axial vortex. As already indicated, the relative motion between the blades of the working wheel will be a vortical motion. From the physical point of view we can visualize the appearance of this motion if we consider the rotation of a cylindrical cavity, e.g., a circle filled with an inviscid fluid, about an axis, as shown in Fig. 9.6.7. Each particle of the inviscid fluid filling the closed cavity will rotate relative to the container walls like a solid particle, with the same angular velocity but in the opposite direction. This kind of motion will also be found in a cavity (closed channel) of any other shape.

This motion is described as the motion caused by an axial vortex.

We shall assume that the motion due to the axial vortex will not be changed if the channel is opened, i.e., if we take away the surfaces which prevent the fluid from streaming radially through the channel. On this assumption the motion in the rotating lattice can be determined by superimposing the transport motion from the whole wheel and the motion from the axial vortex on the flow in a quiescent lattice.



Fir. 9.6.7. When a cylinder filled with an inviscid fluid rotates about the axis, each fluid particle contained in a closed cavity rotates relative to the container walls with the same angular velocity, but in the opposite direction (a); the same is true for a channel in a centrifugal compressor (b).

Under the influence of the axial vortex the circumferential velocity component at the outlet (the most important for the power and capacity of the CC) is diminished by c_u'' and becomes equal (Fig. 9.6.8) to

$$c_{u2} = c_{u2\infty} - c_u^* = R_2\omega - c_u^*.$$

The quantity

$$\sigma = \frac{R_2\omega - c_u^*}{R_2\omega} = 1 - \frac{c_u^*}{R_2\omega} \qquad (9.6.28)$$

is called the slip.

To estimate the influence of the axial vortex, Stodola made use of (Fig. 9.6.8)

$$c_u^* = \frac{\omega d}{2} = \frac{\pi\omega R}{N}\sin\beta_2 \qquad (9.6.29)$$

(N is the number of blades).

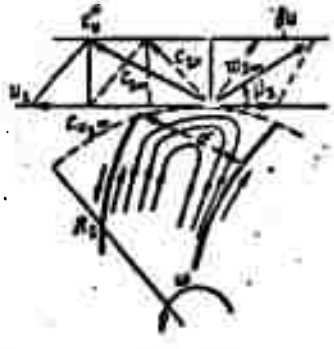


Fig. 9.6.8. Under the influence of an axial vortex the circumferential velocity component at the outlet is reduced by the amount c_u^*.

This estimate, however, is satisfactory only if the number of blades is large enough.

Let us consider in greater detail the motion of the fluid in uniformly rotating cavities.

The absolute motion of an incompressible and inviscid fluid in a cavity is a potential motion to which the relations

$$\frac{\partial c_y}{\partial x} - \frac{\partial c_x}{\partial y} = 0, \quad \frac{\partial^2\Phi}{\partial x^2} + \frac{\partial^2\Phi}{\partial y^2} = 0, \quad \frac{\partial^2\Psi}{\partial x^2} + \frac{\partial^2\Psi}{\partial y^2} = 0. \qquad (9.6.30)$$

apply.

The relative motion in uniform rotation of the cavity is vortical; for it the velocity potential is zero and the equation of the stream-function Ψ_0 is

$$\frac{\partial w_y}{\partial x} - \frac{\partial w_x}{\partial y} = \frac{\partial^2\Psi_0}{\partial x^2} + \frac{\partial^2\Psi_0}{\partial y^2} = -2\omega.$$

If we take into account that in uniform rotation

$$w_x = c_x - \omega y; \quad w_y = c_y + \omega x,$$

then from the stream function equation

$$d\Psi_0 = w_x dy - w_y dx = d\Psi - \omega(x\,dx + y\,dy)$$

we obtain

$$\Psi_0 = \Psi - \frac{\omega}{2}(x^2 + y^2). \qquad (9.6.31)$$

i.e., in order to find the stream function of the relative motion in the cavity we have to calculate $\omega r^2/2$ from the stream function of absolute motion. At the walls Ψ_0 = const, and hence the boundary condition for the determination of the function Ψ satisfying Eq. (9.6.31) are

$$\Psi_{контур} = \frac{\omega}{2}(x^2 + y^2) + \text{const}. \qquad (9.6.32)$$

The axial vortex in elliptical and triangular cavities. The flow from the axial vortex can be found in the converse way – by choosing the function Ψ satisfying the differential equation (9.6.30), the shape of the cavity and the flow in it. Let us give two examples, considered by N.Ye. Zhukovskiy.*

As the first example, let us take $\Psi = n\omega(x^2 - y^2)$. We can satisfy ourselves by direct verification that $\Delta\Psi = 0$. The stream function for relative motion is

$$\Psi_0 = \Psi - \frac{1}{2}\omega(x^2 + y^2) = \left[\left(n - \frac{1}{2}\right)x^2 + \left(n + \frac{1}{2}\right)y^2\right]\omega.$$

The streamline equation, which is also the contour equation reads

$$\left(n - \frac{1}{2}\right)x^2 - \left(n + \frac{1}{2}\right)y^2 = \frac{\text{const}}{\omega}$$

or

$$\frac{x^2}{(1/2) + n} + \frac{y^2}{(1/2) - n} = \frac{\text{const}}{(1/4) - n^2}.$$

Assuming const = $1/4 - n^2$, we obtain the equation of an ellipse with the semiaxis

$$a = \sqrt{\frac{1}{2} + n}; \quad b = \sqrt{\frac{1}{2} - n}.$$

This ellipse will also be the contour of the cavity.

The streamlines in absolute motion

$$\Psi = n\omega(x^2 - y^2) = \frac{a^2 - b^2}{a^2 + b^2}\omega(x^2 - y^2) + \text{const}$$

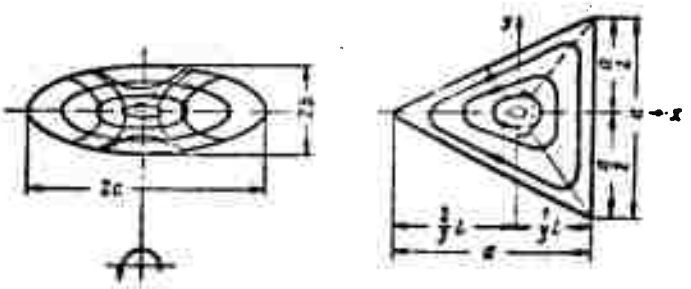


Fig. 9.6.9. Streamlines of axial vortex for ellipse and triangle.

are equilateral hyperbolas (Fig. 9.6.9); at the same time

$$c_x = \frac{\partial \Psi}{\partial y} = 2n\omega y = \frac{\partial \Phi}{\partial x};$$

$$c_y = -\frac{\partial \Psi}{\partial x} = 2n\omega x = \frac{\partial \Phi}{\partial y}.$$

Integrating the first equation we obtain the velocity potential in the form $\Phi = 2n\omega xy + f(y)$. Differentiating it with respect to y and putting it equal to $c_y = \partial\Phi/\partial y$, we find $\Phi = 2n\omega xy$.

The second example: we put $\Psi = \frac{n\omega}{2}(x^3 - 3xy^2)$.

Then

$$\Psi_0 = \frac{\omega}{2}[n(x^3 - 3xy^2) + x^3 + y^3] =$$

$$= \frac{\omega}{2}[nx^3 + x^3 - y^2(3nx - 1)].$$

Solving the equation $\Psi_0 = \text{const} = C$ for y^2, we find

$$y^2 = \frac{1}{3}\left(x + \frac{2}{3n}\right)^2 + \frac{\frac{4}{27n^2} - \frac{2}{\omega}C}{3nx - 1}$$

or, with $n = 1/a$,

$$y^2 = \frac{1}{3}\left(x + \frac{2a}{3}\right)^2 + a\frac{\frac{4}{27}a^2 - \frac{2}{\omega}C}{3x - a}.$$

If we take as the contour the streamline for which $C = 2\omega a^2/27$, then the equation for the contour boundaries reduces to three straight lines:

$$3x - a = 0; \quad y - \frac{1}{\sqrt{3}}\left(x + \frac{2a}{3}\right) = 0; \quad y + \frac{1}{\sqrt{3}}\left(x + \frac{2a}{3}\right) = 0.$$

Thus, the cavity is constituted by the three sides of an equilateral triangle; for the case of uniform rotation the streamlines in it are given in Fig. 9.6.9.

Radial channels. In order to solve the problem on the fluid motion in a CC with an arbitrary number of radial channels* it is necessary to know the motion due to the axial vortex in the cavity constituted by the radial walls with the angle α and the circular arcs of R_1 and R_2 which correspond to the inlet and outlet ($R_2 > R_1$) of the channel.

Since the absolute motion is a potential motion, we have

$$\left.\begin{aligned} c_r &= \frac{\partial \Phi}{\partial r} = \frac{1}{r}\frac{\partial \Psi}{\partial \vartheta} = \frac{\partial \Psi_0}{\partial r} = w_r \\ c_\vartheta &= \frac{1}{r}\frac{\partial \Phi}{\partial \vartheta} = -\frac{\partial \Psi}{\partial r} = -\frac{\partial \Psi_0}{\partial r} - \omega r = w_\vartheta - \omega r. \end{aligned}\right\} \qquad (9.6.33)$$

The streamline equation (continuity equation) is

$$w_r r\, d\vartheta - w_\vartheta\, dr = 0. \qquad (9.6.34)$$

If we substitute the expressions for w_r and w_ϑ from (9.6.33), into the continuity equation (9.6.34), we find that

$$\frac{1}{r}\frac{\partial \Phi}{\partial \vartheta}\, dr - r\frac{\partial \Phi}{\partial r}\, d\vartheta + \omega r\, dr = 0. \qquad (9.6.35)$$

We shall seek the general solution to Eq. (9.6.35) in the form of a sum of particular solutions of the Laplace equation $\frac{\partial^2 \Phi}{\partial r^2} + \frac{1}{r}\frac{\partial \Phi}{\partial r} + \frac{1}{r^2}\frac{\partial^2 \Phi}{\partial \vartheta^2} = 0$.

$$\Phi = \sum_{m=1}^{\infty}\left[\left(A_m r^m + \frac{B_m}{r^m}\right)\sin m\vartheta + \left(C_m r^m + \frac{D_m}{r^m}\right)\cos m\vartheta\right]. \qquad (9.6.36)$$

Since the walls are radial, symmetry conditions mean that a reversal of the direction of rotation (or, what is the same, of the angle ϑ) will cause the potential to change its sign and the series will not contain cosine terms, i.e., $C_m = D_m = 0$ and

$$\Phi = \sum_{m=1}^{\infty}\left(A_m r^m + \frac{B_m}{r^m}\right)\sin m\vartheta. \qquad (9.6.37)$$

In order to determine the coefficients A_m, B_m, we make use of the boundary conditions: if $\alpha = 2\pi/N$, then 1) on the radial walls, with $\vartheta = \pm\frac{\alpha}{2}$, $w_\vartheta = 0$ and $c_\vartheta = \frac{1}{r}\frac{\partial\Phi}{\partial\vartheta} = -\omega r$, we have $\partial\Psi/\partial\vartheta = -\omega r^2$; 2) on the radii $r = R_1$ and $r = R_2$ the radial component of $\vec{c}$ vanishes: $c_r = \partial\Psi/\partial r = 0$.

Omitting the intermediary calculations, we give the final form of the solution:

$$\Phi = -\frac{\omega r^2}{2}\frac{\sin 2\vartheta}{\cos\alpha} - \frac{8\omega}{\pi\cos\alpha}\sum_{k=1}^{\infty}\frac{(-1)^k}{(m^2-4)(2k-1)} \times$$

$$\times \frac{(R_2^{m+2} - R_1^{m+2})r^{2m} - (R_1R_2)^{m+2}(R_2^{m-2} - R_1^{m-2})}{(R_2^{2m} - R_1^{2m})r^m}\sin m\vartheta. \qquad (9.6.38)$$

$$\left(\alpha = \frac{2\pi}{N};\quad m = \frac{2k-1}{\alpha}\pi;\quad m > 2,\ N > 4\right).$$

If we retain only one term of the sum then we obtain

$$\Phi = -\frac{\omega r^2}{2}\frac{\sin 2\vartheta}{\cos\alpha} +$$

$$+\frac{8\omega}{\pi\cos\alpha}\frac{\left(R_2^{\frac{N}{4}+2} - R_1^{\frac{N}{4}+2}\right)r^{\frac{N}{4}} - (R_1R_2)^{\frac{N}{4}+2}\left(R^{\frac{N}{4}+2} - R_1^{\frac{N}{4}+2}\right)}{\left(\frac{\pi^2}{4\alpha^2} - 4\right)(R_2^N - R_1^N)r^{-\frac{N}{2}}}\sin\frac{N\vartheta}{4}. \qquad (9.6.39)$$

If $R_1 \ll R_2$, then

$$\Phi = -\frac{\omega r^2}{2}\frac{\sin 2\vartheta}{\cos\alpha} + \frac{8\omega}{\pi\cos\alpha}\sum_{m=1}^{\infty}\frac{(-1)^k}{2k-1}\frac{R_2^2}{m^2-4}\left(\frac{r}{R_2}\right)^m\sin m\vartheta. \qquad (9.6.40)$$

Omitting the calculations we give the expression for the stream function (for $R_1 \ll R_2$)

$$\Psi = \frac{\omega r^2}{2}\frac{\cos 2\vartheta}{\cos\alpha} - \frac{8\omega}{\pi\cos\alpha}\sum_{m=1}^{\infty}\frac{(-1)^k}{2k-1}\frac{R_2^2}{m^2-4}\left(\frac{r}{R_2}\right)^m\cos m\vartheta. \qquad (9.6.41)$$

Restricting ourselves to the first term we obtain, with $R_1 \ll R_2$

$$\Psi = \frac{\omega r^2}{2}\frac{\cos 2\vartheta}{\cos\alpha} - \frac{8\omega}{\pi\cos\alpha}\frac{4\alpha^2R_2^2}{\pi^2 - 16\alpha^2}\left(\frac{r}{R}\right)^{\frac{N}{4}}\cos\frac{N}{2}\vartheta. \qquad (9.6.42)$$

The calculations show that the center of the axial vortex coincides with the center of the circle inscribed in an impeller sector (fig. 9.6.10), i.e., with $r_0 = r_3\frac{\sin\frac{\alpha}{2}}{1+\sin\frac{\alpha}{2}}$. Since the angular velocity of

the vortex coincides with the angular velocity of the impeller rotation, the ratio of the linear velocity due to the vortex on the impeller rim to the linear velocity of the impeller itself will be

$$w_{0u} : wr_2 = r_0 : r_2 = \frac{\sin\frac{\varepsilon}{2}}{1+\sin\frac{\varepsilon}{2}}. \qquad (9.6.43)$$

The accuracy of this ratio is seen from Fig. 9.6.10.

Despite the inaccuracy of the boundary conditions used (cf. page 657) the solution obtained is, as Fig. 9.6.10 shows, in good agreement with experiment even when the number of blades is low.

Determination of the form of motion of the axial vortex by the method of analogy. Considering the torsion of a prismatic rod, Saint Venant has made the supposition that in any cross section all stress components with the exception of the tangential stresses (τ_{zx} and τ_{zy}) vanish (Fig. 9.6.11).

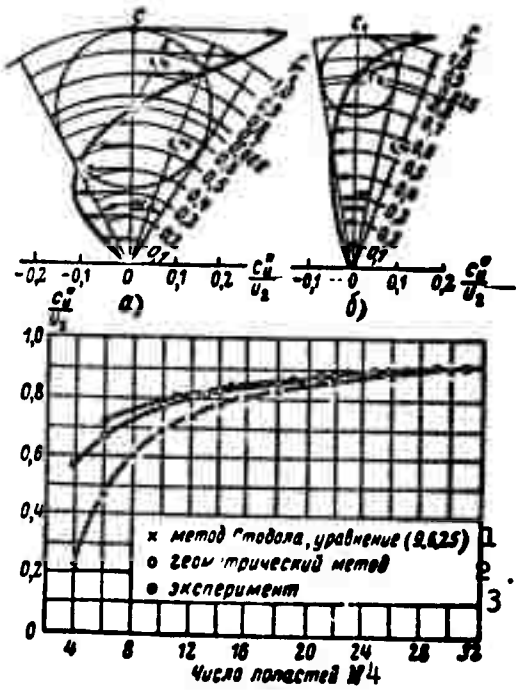


Fig. 9.6.10. Geometrical method of determining the influence of an axial vortex in radial channels. 1) Stodola's method, Eq. (9.6.25); 2) geometrical method; 3) experiment; 4) number of blades, N.

If there are no volume forces, the equilibrium conditions lead to the system of equations

$$\frac{\partial \tau_{zx}}{\partial z} = 0, \quad \frac{\partial \tau_{zy}}{\partial z} = 0, \quad \frac{\partial \tau_{zx}}{\partial x} + \frac{\partial \tau_{zy}}{\partial y} = 0. \tag{9.6.44}$$

The first two equations show that the stresses on all cross sections are equal. The third equation makes it possible to introduce a function Φ such that

$$\tau_{zx} = \frac{\partial \Phi}{\partial y}, \quad \tau_{zy} = -\frac{\partial \Phi}{\partial y}. \tag{9.6.45}$$

The appearance of stresses is however connected with certain deformations, which cannot be arbitrary.

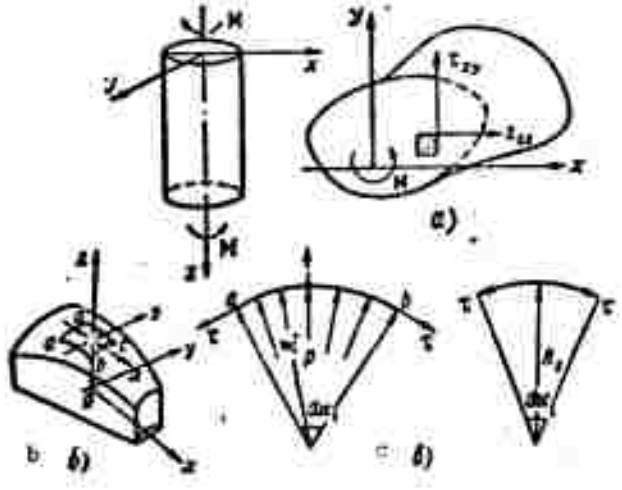


Fig. 9.6.11. Analogy between the problem concerning the tangential stress distribution on torsion of a prismatic bar and the problem of the motion of an axial vortex in a channel of the same cross section (a); a membrane fastened on a plane contour (b) and equilibrium of a membrane element (c).

In lectures on elasticity theory it is proved that the so-called compatibility conditions for the case of elastic deformations lead to the relations

$$\frac{\partial^2 \tau_{zx}}{\partial x^2} + \frac{\partial^2 \tau_{zy}}{\partial y^2} = 0; \quad \frac{\partial^2 \tau_{zx}}{\partial x^2} + \frac{\partial^2 \tau_{zx}}{\partial y^2} = 0.$$

Substituting τ_{zx} and τ_{zy} into these equations we find

$$\frac{\partial}{\partial x}\left(\frac{\partial^2 \Phi}{\partial x^2} + \frac{\partial^2 \Phi}{\partial y^2}\right) = 0, \quad \frac{\partial}{\partial y}\left(\frac{\partial^2 \Phi}{\partial x^2} + \frac{\partial^2 \Phi}{\partial y^2}\right) = 0,$$

i.e.,

$$\frac{\partial^2\Phi}{\partial x^2}+\frac{\partial^2\Phi}{\partial y^2}=\text{const}. \qquad (9.6.46)$$

This is the Poisson equation which is satisfied by the motion connected with the axial vortex (see page 660, the equation for Ψ_0). The solution of the problem on the tangential stress distribution on the torsion of a prismatic bar can therefore be directly transferred to the motion of an axial vortex in a channel of the same cross section as the bar. This analogy was first mentioned by N.Ye. Zhukovskiy in his work "On the Motion of a Solid Body with Cavities Filled with a Homogeneous Dropable Fluid," published in 1885.

From the purely practical point of view, in order to solve the problem of the axial vortex in a channel of given cross section it is more convenient to use the membrane analogy.

Let a membrane, i.e., a very thin film, be fastened to an arbitrary plane contour (cf. Fig. 9.6.11) and let the pressure on the membrane be greater by the amount p on one side than on the other side. The membrane therefore bulges, and the distances of its points from a certain plane parallel to the plane of the contour will be different; let us denote them by z. Let us consider the equilibrium of an element abcd:

$$pR_1\,d\alpha_1R_2\,d\alpha_2=2\tau R_1\,d\alpha_1\sin\frac{d\alpha_2}{2}+2\tau R_2\,d\alpha_2\sin\frac{d\alpha_1}{2},$$

whence

$$\frac{1}{R_1}+\frac{1}{R_2}=\frac{p}{\tau}. \qquad (9.6.47)$$

but

$$\frac{1}{R_1}=\frac{\partial^2 z}{\partial x^2};\quad \frac{1}{R_2}=\frac{\partial^2 z}{\partial y^2}$$

and therefore,

$$\frac{\partial^2 z}{\partial x^2}+\frac{\partial^2 z}{\partial y^2}=\frac{p}{\tau}=\text{const}. \qquad (9.6.48)$$

Thus, the distances of the points to the membrane fastened on a certain plane contour and subjected to a constant pressure are governed by the same equation as the tangential stresses on a rod of the same cross section undergoing torsion, or as the stream function of an axial vortex in a channel of the same cross section, or as the velocity

distribution in a viscous fluid executing laminar motion through a tube of the same cross section.

9.7. LATTICES OF PROFILES IN SUBSONIC GAS FLOW

The influence of the compressibility. The high gas velocity in the channels of turbines makes it necessary to take the compressibility of the gas into account.

The influence of the compressibility affects not only the aerodynamic properties of profiles but also the configuration of the triangles of velocities. The influence of the compressibility of the gas on a flow about the profile in a lattice is much greater than in the case of the flow about an isolated profile.

Experience shows that in subsonic flows the angle of deflection of the flow about the profile lattice varies little as the flow velocity changes, i.e., that the shape of the middle streamlines is determined by the lattice profile.

Shock stall and choking effect for a lattice. The compressibility however, proves to exert a very great influence on the velocity and pressure distribution on the profile.

In this case, apart from the possibility of the appearance of shock stall which is connected, as for a free profile with the appearance of zones at the profile contour in which the local velocity is such that $M = 1$, a choking effect may arise at the lattice, if the local velocity in the narrowest cross section between the profiles reaches sonic speed. If we assume that the direction of the velocity in the narrowest channel cross section of width h is independent of the direction of the incoming flow and that the velocity is uniform over the cross section, then, neglecting the losses, we can write (Fig. 9.7.1) the continuity equation in the form

$$j(M^*_{max})\, l \sin \beta_1 = j(M^*)\Big|_{M^*=1} h.$$

$$j(M^*)=\left(\frac{k+1}{2}\right)^{\frac{1}{k-1}} M^*\left(1-\frac{k-1}{k+1}M^{*2}\right)^{\frac{1}{k-1}}.$$

whence

$$j(M^*_{1\max})=\frac{h}{l\sin\beta_1}; \qquad (9.7.1)$$

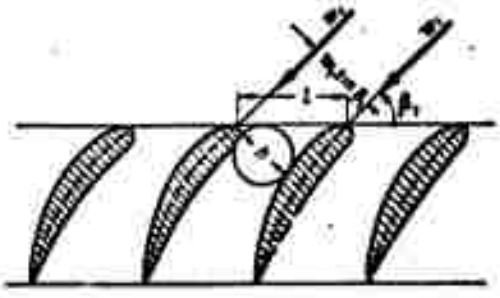


Fig. 9.7.1. If M_1^* of the flow exceeds the value $M_{1\ max}^*$ for which $j(M_{1\ max}^*) = h/l \sin \beta_1$, then a choking effect arises at the lattice.

from which it follows that the quantity $M_{1\ max}^*$ depends on the geometrical parameters of the lattice: the shape of the profile, its thickness and camber, the rigging angle of incidence, and the density of the lattice.

Experience shows that the onset of shock stall at $M_{1\ kr}^*$ and the formation of small supersonic zones does not lead to a sudden change in the flow conditions whereas when $M_{1\ max}^*$ is reached the flow pattern changes qualitatively. A change in the aerodynamic characteristics usually occurs at $M_{1кр}^* < M_1^* < M_{1max}^*$.

The lift of a profile in a lattice placed in a subsonic flow. The lift of a lattice profile in an incompressible fluid is determined by N.Ye. Zhukovskiy's formula $R_y = \rho w_m \Gamma$, where the characteristic velocity

$\vec{w}_m$ is equal to half the vector sum of the velocities in front of and behind the lattice. Considering a profile lattice in a compressible gas we can write the momentum equation as

$$\vec{R}=(p_1-p_2)\vec{i}_\infty l+\rho_1 l(\vec{i}_\infty\cdot\vec{w}_1)\vec{w}_1-\rho_2 l(\vec{i}_\infty\cdot\vec{w}_2)\vec{w}_2, \qquad (9.7.2)$$

which, by virtue of the continuity equation

$$\rho_1 l(\vec{i}_\infty\cdot\vec{w}_1)=\rho_2 l(\vec{i}_\infty\cdot\vec{w}_2) \qquad (9.7.3)$$

can be rewritten in the form

$$\vec{R}=l(p_1-p_2)\vec{i}_\infty-\rho_1 l(\vec{i}_\infty\cdot\vec{w}_1)\vec{w}_2.$$

In the case of a compressible gas we also put

$$\vec{w}_m=\frac{\vec{w}_1+\vec{w}_2}{2} \qquad (9.7.4)$$

and let ρ_m be a certain density satisfying the continuity equation for the velocity $\vec{w}_m$. Rewriting (9.7.4) in the form

$$2\frac{\rho_m\vec{w}_m}{\rho_m}=\frac{\rho_1\vec{w}_1}{\rho_1}+\frac{\rho_2\vec{w}_2}{\rho_2}$$

and multiplying it scalarly by $\vec{i}_\omega$, owing to (9.7.3) we obtain

$$2\frac{\vec{i}_\infty\cdot\rho_m\vec{w}_m}{\rho_m}=\frac{\vec{i}_\infty\cdot\rho_1\vec{w}_1}{\rho_1}+\frac{\vec{i}_\infty\cdot\rho_2\vec{w}_2}{\rho_2}=(\vec{i}_\infty\cdot\rho_m\vec{w}_m)\left(\frac{1}{\rho_1}+\frac{1}{\rho_2}\right),$$

where $\vec{i}_\infty\cdot\rho_1\vec{w}_1=\vec{i}_\infty\cdot\rho_2\vec{w}_2=\vec{i}_\infty\cdot\rho_m\vec{w}_m$ because of the definition of ρ_m adopted.

Hence

$$\frac{1}{\rho_m}=\frac{1}{2}\left(\frac{1}{\rho_1}+\frac{1}{\rho_2}\right),\ \rho_m=\frac{2\rho_1\rho_2}{\rho_1+\rho_2},\ v_m=\frac{v_1+v_2}{2}, \qquad (9.7.5)$$

i.e., the characteristic specific volume ($v = 1/\rho$) equals half the sum of the specific volumes in front of and behind the lattice.

In order to determine $p_1 - p_2$, we have from (4.2.9):

$$\frac{1}{p_0}(p_1-p_2)=\left(1-\frac{k-1}{k+1}M_1^{*2}\right)^{\frac{k}{k-1}}-\left(1-\frac{k-1}{k+1}M_2^{*2}\right)^{\frac{k}{k-1}}=$$
$$=\left[1-\frac{k}{k+1}M_1^{*2}+\frac{k}{2(k+1)^2}M_1^{*4}\pm\ldots\right]-$$
$$-\left[1-\frac{k}{k+1}M_2^{*2}+\frac{k}{2(k+1)^2}M_2^{*4}\pm\ldots\right]=$$

$$= \frac{k}{k+1}(M_2^{*2} - M_1^{*2})\left[1 - \frac{1}{2(k+1)}(M_1^{*2} + M_2^{*2}) + O(M^{*4})\right].$$

Composing the expression

$$\frac{\rho_m}{\rho_0} = \frac{2}{\rho_0}\frac{\rho_1\rho_2}{\rho_1+\rho_2} =$$

$$= 2\frac{\left[1 - \frac{1}{k+1}M_1^{*2} + \frac{2-k}{2(k+1)^2}M_1^{*4} + \ldots\right]\left[1 - \frac{1}{k+1}M_2^{*2} + \frac{2-k}{2(k+1)^2}M_2^{*4} + \ldots\right]}{1 - \frac{1}{k+1}M_1^{*2} + \frac{2-k}{2(k+1)^2}M_1^{*4} + \ldots + 1 - \frac{1}{k+1}M_2^{*2} + \frac{2-k}{2(k+1)^2}M_2^{*4} + \ldots} \approx$$

$$\approx 1 - \frac{1}{2(k+1)}(M_1^{*2} + M_2^{*2}) + O(M^{*4}),$$

we obtain to within an accuracy of M^{*2}

$$p_1 - p_2 = p_0\frac{k}{k+1}(M_2^{*2} - M_1^{*2})\frac{\rho_m}{\rho_0} =$$

$$= \rho_m(\vec{w}_2 - \vec{w}_1)\frac{\vec{w}_2 + \vec{w}_1}{2} = \rho_m\vec{w}_m \cdot \vec{w}_d. \qquad (9.7.6)$$

Therefore, to the same approximation

$$\vec{R} = l\rho_m(\vec{w}_m \cdot \vec{w}_d)\vec{i}_\infty - l\rho_m(\vec{w}_m \cdot \vec{i}_\infty)\vec{w}_d = \rho_m\vec{w}_m \times \vec{w}_d. \qquad (9.7.7)$$

The lift of a profile in a lattice at subsonic velocities can thus be approximately determined with N.Ye. Zhukovskiy's formula if the velocity and the specific volume are determined by half the sum of the velocity vectors and half the sum of the specific volumes, respectively, in front of and behind the lattice. The direction of the force is obtained when the velocity vector is turned through 90° against the direction of circulation. The relative error of Formula (9.7.7)* for $4/3 < k < 3/2$ does not exceed $0.2\,(M_1^{*2} - M_2^{*2})^2$.

Numerical calculation of the gas flow in a lattice. This circulation, when allowing for the compressibility of the gas, can be made using methods described in Part 8.5 which afford reliable results everywhere except in the inlet region. In order to calculate the flow in the inlet region we have to adopt the hypothesis of a flow which does not separate at the edges; in this case the channel contour must be produced along straight lines which are tangents to the camber line of the

profile.

The camber line method of numerically calculating the gas flow in a lattice of profiles, suggested by Ch'ung Hu-Wu and Brown [9.14] is based on the assumption that a change of the flow density component ρw_x on the central line of the flow in a channel of a profile lattice follows upon a change in width with respect to the lattice spacing, and that the central line of the flow (halving the flow in the channel) deviates but slightly from the central line of the channel; calculations show that it is somewhat less curved and lies somewhat closer to the suction surface (Fig. 9.7.2).

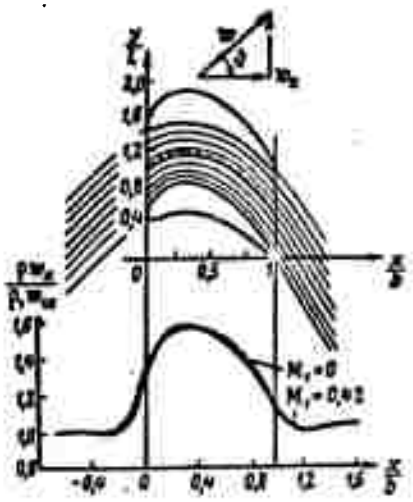


Fig. 9.7.2. The central line of the flow depends only little on the Mach number M.

Let the streamline equation in the middle part of the channel be $\Psi(x, y) = 0$. Considering an arbitrary quantity q along this line as a function of x alone, i.e., $q = [x, y(x)]$, we have

$$\frac{dq}{dx} = \frac{\partial q}{\partial x} + \frac{\partial q}{\partial y}\frac{dy}{dx}. \qquad (9.7.8)$$

Noticing that along a streamline

$$\frac{dy}{dx} = \frac{\frac{\partial \Psi}{\partial x}}{\frac{\partial \Psi}{\partial y}} = \frac{w_y}{w_x} = \operatorname{tg}\vartheta, \qquad (9.7.9)$$

we can write the equations of continuity and absence of vortices in the form

$$\frac{d(\rho w_x)}{dx} + \frac{\partial(\rho w_y)}{\partial y} + \frac{\partial(\rho w_x)}{\partial y}\operatorname{tg}\vartheta = 0; \qquad (9.7.10)$$

$$\frac{dw_y}{dx} - \frac{\partial w_x}{\partial y} - \frac{\partial w_y}{\partial y}\operatorname{tg}\vartheta = 0. \qquad (9.7.11)$$

Denoting by the subscript "v" all quantities referring to the corresponding quantities at the inlet, we can formulate the density equation as

$$p_0 = \frac{p}{p_1} = \frac{p}{p_0}\frac{p_0}{p_1} = \left(\frac{1-\frac{w^2}{2i_0}}{1-\frac{w_1^2}{2i_0}}\right)^{\frac{1}{k-1}} =$$

$$= \left(\frac{1-\frac{w_x^2}{2i_0\cos^2\beta}}{1-\frac{w_1^2}{2i_0}}\right)^{\frac{1}{k-1}} = \left(\frac{1-\frac{w_{x0}^2\rho_0^2 w_{x1}^2}{2i_0\cos^2\beta\rho_0^2}}{1-\frac{w_1^2}{2i_0}}\right)^{\frac{1}{k-1}}$$

or

$$\rho_0 w_{x0}^2 = \frac{2i_0}{w^2}\rho_0^2\left[1-\rho_0^{k-1}\left(1-\frac{w^2}{2i_0}\right)\right]\cos^2\beta_0. \qquad (9.7.12)$$

Solving it for example with the method of successive approximations, we find the density, and after this, from (9.7.10) and (9.7.11), the velocity components along the central line.

The flow parameters with respect to the channel width are determined by means of a Taylor series:

$$q(y) = q_m + (y-y_m)\left(\frac{\partial q}{\partial y}\right)_m + \frac{(y-y_m)^2}{2!}\left(\frac{\partial^2 q}{\partial y^2}\right)_m +$$
$$+ \frac{(y-y_m)^3}{3!}\left(\frac{\partial^3 q}{\partial y^3}\right)_m + \ldots \qquad (9.7.13)$$

Examples of calculations on common turbine lattices show that the first two or three terms of this series are completely sufficient for obtaining the accuracy required in engineering.

Linearized solution for subsonic flow. We have shown before (cf. Part 5.4) that the flow of a compressible gas in the x, y plane can be put equal to the flow of an incompressible fluid in the x_n, y_n plane if

$$x_n = \lambda_x x,\ y_n = \lambda_y y,\ \varphi_n(x_n, y_n) = \lambda_\varphi \varphi(x, y), \qquad (9.7.14)$$

where the constants λ_x, λ_y, and λ_φ are interrelated by the system of the two equations

$$\lambda_y = n\lambda_x,\ \lambda_y^2 = \lambda_x\lambda_\varphi \quad \left(n^2 = \sqrt{1-M_\infty^2}\right) \qquad (9.7.15)$$

so that one of the constants can be arbitrarily chosen. The boundary conditions on the contours of the corresponding bodies $y = f(x)$ and a

gas and $y_n = f_n(x_n)$ in a fluid [illegible], independently of λ_x and λ_y,

$$\frac{df}{dx} = \frac{\lambda_x}{\lambda_y}\frac{df_n}{dx_n} = \frac{1}{\sqrt{1-M_\infty^2}}\frac{df_n}{dx_n}. \qquad (9.7.16)$$

As in the case of an isolated profile (cf. p. 310), the factors λ can be chosen either so that we obtain equal pressure distributions on a profile in an incompressible fluid and in a gas, or so that we find the pressure distribution on a profile in a gas if we know the pressure distribution on the same profile in a fluid.

In the first case all geometrical lattice parameters, including the profile, are subject to deformation, and in the second case the profile remains unchanged, which is in many cases more convenient.

Considering the second case we put $\lambda_x = 1$, $\lambda_y = n$, then

$$\lambda_\varphi = n^2 \quad (n^2 = 1 - M^2). \qquad (9.7.17)$$

i.e., $x_n = x$, $y_n = y\sqrt{1-M_\infty^2}$, $\varphi_n = (1-M_\infty^2)\varphi$, , and consider a not too dense lattice of sufficiently fine slightly curved profiles at small angles of attack. Let the distance between the profiles of the lattice, along the normals to the velocity, be $\underline{h}$.

Since the corresponding profile in a fluid will be $\underline{m}$ times as thick, then, in order to have its shape unchanged we shall assume that it corresponds to a profile in a gas with ordinates $1/n$ times larger. In accordance with (9.7.14), the distance along the normal to the velocity – in particular the projection $\underline{h}$ of the spacing on it – will be $\underline{n}$ times smaller, i.e., $h_n = h\,(1 - M_\infty^2)^{1/2}$ thus when the profile shape is maintained in liquid and gas, the lattice in liquid (Fig. 9.7.3) corresponding to a profile lattice in gas will be denser. At the same time

$$l_n = \sqrt{x^2 + h_n^2} = \sqrt{x^2 + n^2h^2} = l\sqrt{1 - M_\infty^2\sin^2\beta} =$$
$$= l\sqrt{\cos^2\beta + n^2\sin^2\beta}. \qquad (9.7.18)$$

The angle of the lattice axis also varies; as Fig. 9.7.3 shows, it will be

$$\operatorname{tg}\beta_\infty = n \operatorname{tg}\beta. \tag{9.7.19}$$

Further, since the disturbances arising in the stream are proportional to the thickness, we have for the construction of the triangles of velocities

$$\left.\begin{aligned} w'_x &= \frac{\lambda_x}{\lambda_\varphi} w'_{\infty x} \frac{d}{d_1} = \frac{1}{n^2} w'_{\infty x} n = \frac{1}{\sqrt{1-M_\infty^2}} w'_{\infty x}, \\ w'_y &= \frac{\lambda_y}{\lambda_\varphi} w'_{\infty y} \frac{d}{d_1} = \frac{n}{n^2} w'_{\infty y} n = w'_{\infty y}; \end{aligned}\right\} \tag{9.7.20}$$

hence results that the angle of attack remains unchanged.

By virtue of (5.4.14) the pressure and lift coefficients will be

$$C_p = \frac{C_{p\infty}}{\sqrt{1-M_\infty^2}}. \tag{9.7.21}$$

$$C_y = \frac{C_{y\infty}}{\sqrt{1-M_\infty^2}}. \tag{9.7.22}$$

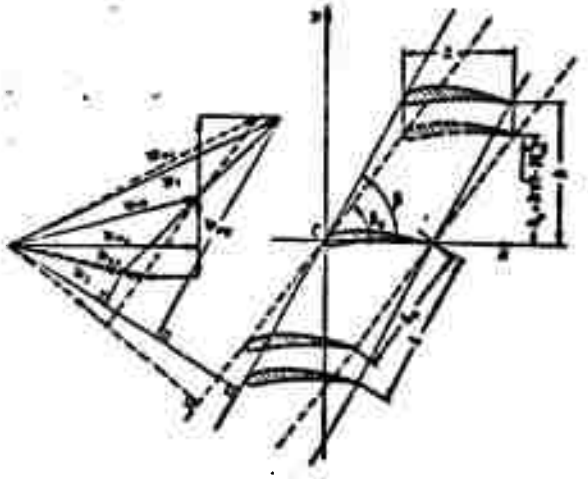


Fig. 9.7.3. Corresponding to a flow about a lattice in a subsonic gas stream there is a flow about a lattice of the same profiles in an incompressible liquid, whose spacing and slope angle are smaller by $(1 - M_\infty^2)^{1/2}$.

The improved formula for C_p remains valid; it is obtained by introducing the local Mach number M, and yields [cf. (5.4.19)]

$$c_p = \frac{c_{p,s}}{\sqrt{1-M_\infty^2} + \frac{M_\infty^2\left(1+\frac{k-1}{2}M_\infty^2\right)}{2\sqrt{1-M_\infty^2}}c_{p,s}} \qquad (9.7.23)$$

The distribution of the pressure $c_{p\,n}$ in a fluid must finally be found for a lattice with the spacing $\underline{1}_n$ and the angle β_n of the axis, determined according to the equations (9.7.18)-(9.7.19).

9.8. ALLOWANCE FOR THE VISCOSITY EFFECT

The flow of a viscous fluid about a profile in a lattice is connected with a change in the form of the motion. This influences the

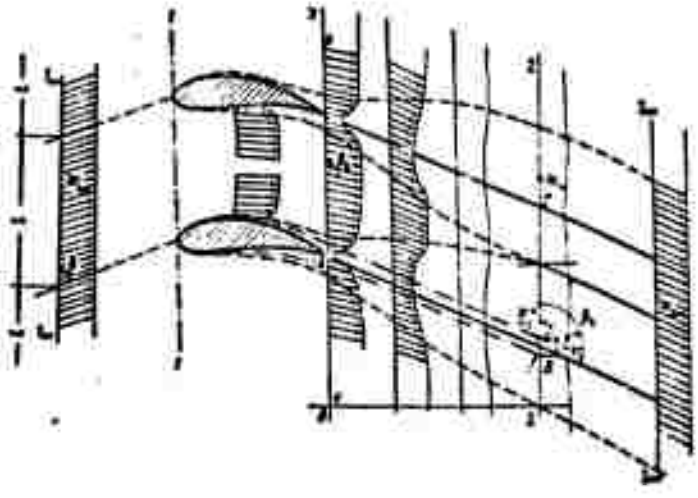


Fig. 9.8.1. Velocity distribution in wake cross sections behind a lattice.

pressure distribution (especially when the flow becomes separated) and gives rise to an irreversible dissipation of energy both in the boundary layer and in the wake. Behind the lattice this wake consists of the boundary layers from each of the lattice profiles and a potential core between them. The velocities in the wake level out, the thickness of the wake grows and at a certain distance behind the lattice the wakes fuse together. This cross section will be designated by the subscript "2." The inhomogeneities of the velocity distribution, $\vec{w}_1 - \vec{w}_2$ (Fig. 9.8.1), are then so small that the squares of their magnitudes

can be neglected in the calculations. This applies to confusor lattices because of the thin boundary layer, while the diffusor lattices usually have a relatively large period. It should also be borne in mind that the gas flow passing through a system of quiescent and rotating turbine wheels arranged one after another becomes strongly turbulent; this favors the leveling of velocities.

The profile drag coefficient. Following an investigation of L.G. Loytsyanskiy [9.3], we lay the y-axis along the front of the lattice and consider a viscous incompressible fluid flowing about it. We denote by y_0 the ordinate of the point at which two neighboring layers join and assume that at the corresponding cross section 2-2 we have $w/w_2 = w_x/w_{2x}$. Then, denoting by dn an element of the normal to the principal streamline in the wake, we can write

$$\delta_2^* = \int_{y_0}^{y_0+t} \left(1 - \frac{w}{w_2}\right) dn = \int_{y_0}^{y_0+t} \left(1 - \frac{w_x}{w_{2x}}\right) \cos\beta_2 \, dy = \delta_{2y}^* \cos\beta_2. \qquad (9.8.1)$$

where δ_{2y}^* denotes the displacement thickness along the y-axis at the cross section 2-2; it will prove convenient to introduce this into the calculations below.

From the condition of mass flow conservation between streamlines at the distance of a lattice period we can write $\int_{y_0}^{y_0+t} w_x \, dy = w_{2x} t$, whence

$$w_{2x} - w_{2x} = \frac{1}{t} \int_{y_0}^{y_0+t} (w_{2x} - w_x) \, dy = w_{2x} \frac{\delta_{2y}^*}{t} = w_{2x} \varepsilon. \qquad (9.8.2)$$

The quantity

$$\varepsilon = \frac{\delta_{2y}^*}{t} = \frac{1}{t} \int_{y_0}^{y_0+t} \left(1 - \frac{w_x}{w_{2x}}\right) dy$$

characterizes the degree of nonuniformity of the flow in the wake; therefore, neglecting powers of ε higher than the first we can write

$$w_{2x} = w_{2x}(1+\varepsilon), \quad w_{2y} = w_{2y}(1+\varepsilon), \quad w_2 = w_2(1+\varepsilon). \qquad (9.8.3)$$

Applying the impulse theorem to the mass of the fluid flowing between the streamlines at a distance equal to the lattice period and between the cross sections 2 and 2∞, we find $p_2 \approx p_{2\infty}$ to within the degree of accuracy adopted. In fact,

$$(p_2-p_{2\infty})l=\rho w_{2\infty x}^2 l-\int_{y_0}^{y_0+t}\rho w_x^2\,dy=\rho w_{2\infty x}^2 l-\int_{y_0}^{y_0+t}\rho[w_{2x}-$$
$$-(w_{2x}-w_x)]^2\,dy=\rho(w_{2\infty x}^2-w_{2x}^2)l+2\rho w_{2x}^2\delta_{2y}=\rho w_{2\infty x}^2\varepsilon^2=0(\varepsilon^2).$$

For a potential core of the stream we find that substituting (9.8.3) in the Bernoulli equation under the same assumptions gives

$$p_{1\infty}-p_2=\frac{1}{2}\rho[(w_{2x}^2+w_{2y}^2)-(w_{1\infty x}^2+w_{1\infty y}^2)]=$$
$$=\frac{\rho}{2}[w_{2\infty x}^2+2\varepsilon w_{2\infty x}+w_{2\infty y}^2+2\varepsilon w_{2\infty y}-w_{1\infty x}^2-w_{1\infty y}^2]=$$
$$=\frac{\rho}{2}[(w_{2\infty x}^2-w_{1\infty x}^2)+2\varepsilon(w_{2\infty x}+w_{2\infty y})+(w_{2\infty y}^2-w_{1\infty y}^2)]=$$
$$=\frac{1}{2}\rho(w_{2\infty}^2-w_{1\infty}^2)+\rho w_{2\infty}^2\varepsilon. \qquad (9.8.4)$$

The losses in head drag p_μ due to viscosity (9.8.4) and the drag R_μ per unit length of the wing in the lattice will be

$$\left.\begin{aligned} p_\mu&=p_{1\infty}-p_{2\infty}+\rho\frac{w_{2\infty}^2-w_{1\infty}^2}{2}=\rho w_{2\infty}^2\varepsilon=\rho w_{2\infty}^2\frac{\delta_{2y}^*}{l\cos\beta_2}.\\ R_\mu&=p_\mu l=\rho w_{2\infty}^2\frac{\delta_{2y}^*}{\cos\beta_2}.\end{aligned}\right\} \qquad (9.8.5)$$

If we take into account that

$$\delta_2^{**}=\int_{y_0}^{y_0+t}\frac{w}{w_2}\left(1-\frac{w}{w_2}\right)dn=\int_{y_0}^{y_0+t}\frac{w_2-(w_2-w)}{w_2}\,\frac{w_2-w}{w_2}\,dn\approx$$
$$\approx\int_{y_0}^{y_0+t}\frac{w_2-w}{w_2}\,dn=\delta_{2y}^*,$$

we can also write

$$p_\mu=\rho w_{2\infty}^2\frac{\delta^{**}}{l\cos\beta_2},\quad R_\mu=\rho w_{2\infty}^2\frac{\delta^{**}}{\cos\beta_2}. \qquad (9.8.6).$$

In practical calculations the boundary layer parameters at the cross section 2-2, the position of which is uncertain, are replaced by the corresponding parameters at the trailing edge of the profile. For this we write the impulse equation for the wake in the form

$$\frac{d\delta^{**}}{ds}=\frac{1}{w_0}\frac{dw_0}{ds}(2\delta^{**}+\delta^{*})=\frac{c_f}{2w_0}.$$

where s is a curvilinear coordinate, referred to the principal streamline. Since $\tau_0 = 0$ in the wake, we have

$$\frac{d\delta^{**}}{ds}+\frac{w_0'}{w_0}(2\delta^{**}+\delta^{*})=0 \qquad (9.8.7)$$

or, denoting δ^*/δ^{**} by H,

$$\frac{1}{\delta^{**}}\frac{d\delta^{**}}{ds}=-(H+2)\frac{1}{w_0}\frac{dw_0}{ds}.$$

We characterize the values of the parameters at the trailing edge by the subscript "k" and integrate by parts from the trailing edge to the cross section 2, and taking $\delta_2^* = \delta_2^{**}$ and $w_2/w_{2\infty} = 1 + \varepsilon$ into account, we obtain

$$\ln\frac{\delta_k^{**}}{\delta_2^{**}}+(H_k+2)\ln\frac{w_k}{w_{2\infty}}=-\int_{H_k}^{1}\ln\frac{w_0}{w_{2\infty}}dH. \qquad (9.8.8)$$

Solving this with respect to δ_2^{**}, we find

$$\delta_2^{**}=\delta_k^{**}\left(\frac{w_k}{w_{2\infty}}\right)^{H_k+2}\exp\int_{1}^{H_k}\ln\frac{w_{2\infty}}{w_0}dH. \qquad (9.8.9)$$

Experiments show that for an isolated profile $\ln(w_{2\infty}/w_0) = \text{const}\,(H-1)$. Therefore $\ln\frac{w_{2\infty}}{w_0}:\ln\frac{w_{2\infty}}{w_k}=(H-1):(H_k-1)$.

At the same time

$$\int_{1}^{H_k}\ln\frac{w_{2\infty}}{w_0}dH=\int_{1}^{H_k}\frac{H-1}{H_k-1}\ln\frac{w_{2\infty}}{w_k}dH=\frac{H_k-1}{2}\ln\frac{w_{2\infty}}{w_k},$$

i.e.,

$$\exp\int_{1}^{H_k}\ln\frac{w_{2\infty}}{w_0}dH=\left(\frac{w_{2\infty}}{w_k}\right)^{\frac{H_k-1}{2}}$$

and

$$\delta_2^{**}:\delta_k^{**}=(w_k:w_{2\infty})^{\frac{H_k+3}{2}}. \qquad (9.8.10)$$

The quantity H_k does not depend on the value of the shape parame-

ter (6.3) at the trailing edge. If the velocity distribution is far from being equal to that under separation conditions, then the quantity H_k changes from 1.5 for small Re number to 1.3 for large ones, and on an average we can take $H_k = 1.4$ [9.3]. Then

$$(\delta_1^{**} : \delta_2^{**}) = (w_1 : w_{2\infty})^{3.2}. \tag{9.8.11}$$

Now

$$p_\mu = \rho w_{2\infty}^2 \left(\frac{w_2}{w_{2\infty}}\right)^{3.2} \frac{\delta_2^{**}}{l\cos\beta_2}, \quad R_\mu = \rho w_{2\infty}^2 \left(\frac{w_2}{w_{2\infty}}\right)^{3.2} \frac{\delta_2^{**}}{\cos\beta_2}. \tag{9.8.12}$$

If we introduce the mean value of half the sum of the vector $\vec{w}_m = \frac{1}{2}(\vec{w}_1 + \vec{w}_2)$ into the consideration and take into account that $w_m \cos\beta_m = w_{2\infty}\cos\beta_{2\infty}$ and that $R_x = R_\mu \cos\beta_m$:

$$p_\mu = \rho w_{2\infty}^2 \frac{w_2}{w_m}\left(\frac{w_2}{w_{2\infty}}\right)^{3.2} \frac{\delta_2^{**}}{l\cos\beta_m} =$$

$$= \frac{\rho w_m^2}{2} 2\left(\frac{w_2}{w_m}\right)^{3.2}\left(\frac{w_m}{w_{2\infty}}\right)^{0.2} \frac{\delta_2^{**}}{l\cos\beta_m}; \tag{9.8.13}$$

$$R_\mu = \frac{\rho w_m^2}{2} 2\left(\frac{w_2}{w_m}\right)^{3.2}\left(\frac{w_m}{w_{2\infty}}\right)^{0.2} \frac{\delta_2^{**}}{\cos\beta_m}. \tag{9.8.14}$$

$$R_x = \frac{\rho w_m^2}{2} 2\delta_2^{**}\left(\frac{w_2}{w_m}\right)^{3.2}\left(\frac{w_m}{w_{2\infty}}\right)^{0.2}; \tag{9.8.15}$$

$$C_{xp} = \frac{2R_x}{\rho w_m^2 b} = 2\left(\frac{w_2}{w_m}\right)^{3.2}\left(\frac{w_m}{w_{2\infty}}\right)^{0.2} \frac{\delta_2^{**}}{b}. \tag{9.8.16}$$

The factor $^5(w_m/w_{2\infty})^{1/2}$ differs but little from unity, and the last relation mentioned virtually coincides with the profile drag coefficient for an isolated profile

$$C_{xp} = 2\left(\frac{w_2}{w_m}\right)^{3.2} \frac{\delta_2^{**}}{b}. \tag{9.8.17}$$

If we retain ε in the second power, then, according to the results of I.L. Povkh [9.21]

$$p_\mu = \rho w_{2\infty}^2 [1 + (2{,}5 + \sin^2\beta_2)\varepsilon]. \tag{9.8.18}$$

This relation is satisfactorily confirmed by experiment.

Circulation about a profile in a lattice. The disturbances caused

by the appearance of lift and drag on an isolated profile (or a finite number of profiles) are considerably attenuated at small distances from it. This is explained by the fact that finite disturbances cannot alter the state of an infinite fluid mass. During the flow through a lattice of profiles the disturbances induced by an infinite number of profiles change the flow parameters at infinity.

The most correct way of taking these changes into account obviously consists in determining the pressure distribution in an inviscid fluid streaming about a semi-body formed by constructing streamlines passing through the stagnation points, at the displacement thickness δ^* calculated from the true pressure distribution (Fig. 9.8.2) on both sides of the profile considered (or on a lattice of profiles). In practice the shape of the semi-body can be determined by the method of successive approximations.

This calculation is however tedious, and yields no analytical expression making it possible to estimate the influence of the parameters on the aerodynamic properties of the lattice. This influence can be estimated to a certain degree by means of very general theoretical considerations and experimental data.

In the consideration of the vortex system of an airfoil profile it was shown that the vorticity of the boundary layer formed per unit time and passing through the boundary layer cross section is equal to $\int_0^\delta 2\omega_z w_x dy = \int_0^\delta \frac{\partial w}{\partial y} w dy = \frac{w_\delta^2}{2}$. Calculations show that the profile lift determined with Zhukovskiy's formula, $\rho w_\infty \Gamma$, in which the circulation has been calculated from the experimentally determined velocity distribution agrees well with the lift calculated from the pressure distribution. In this case the contour for which the circulation was calculated must intersect the wake perpendicularly, in which case the tangential

velocity component to the contour of the wake becomes zero. It is important to note that for these contours the circulation is independent of the length of the contour (Fig. 9.8.3).

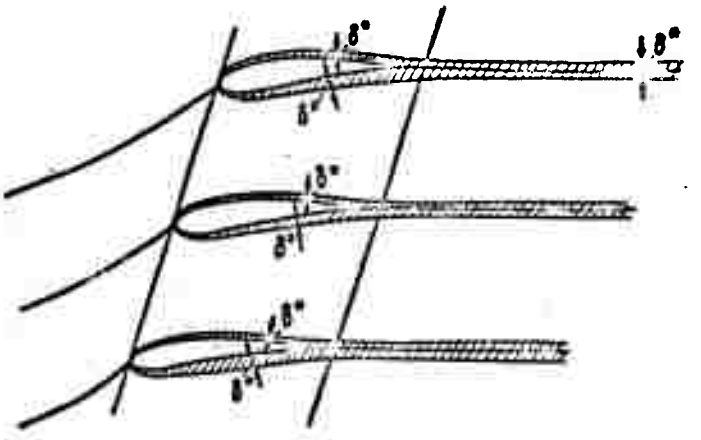


Fig. 9.8.2. Diagram of flow through a lattice of profiles the thickness of which is augmented by the displacement thickness $\delta^* = \delta_p \sin \beta_k$.

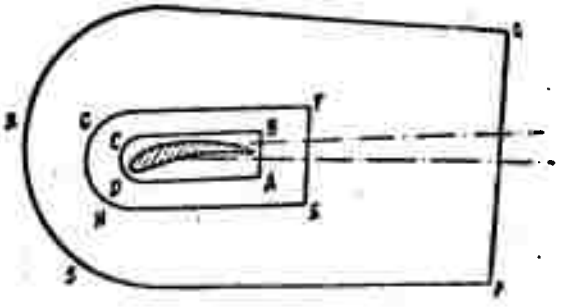


Fig. 9.8.3. When the circulation around to contours APCD, EFQH, and PQRS is calculated, the values obtained are almost the same.

When the process of build-up of circulations about a wing (cf. p. 184) is finished, the motion becomes steady, the starting vortex stops growing and the vorticities of the upwash and of the downwash must be the same, i.e.,

$$\varpi_{0u}^2 = \varpi_{0d}^2. \qquad (9.8.18)$$

If $Re \to \infty$, i.e., if $\delta \to 0$ this condition goes over to the Zhukov-

skiy-Chaplygin condition.

For an isolated plate of length 2b, arranged in the flow at an angle α, the complex velocity is

$$\frac{1}{w_\infty}\overline{w}(z)=\cos\alpha-i\frac{z\sin\alpha+\frac{\Gamma}{2\pi w_\infty}}{\sqrt{z^2-b^2}},$$

where $\underline{z}$ is a complex coordinate in the plane of flow. If δ_v and δ_n are the boundary layer thicknesses at the trailing edge for the upper and lower surface of the plate, respectively, then the condition that the velocities at this point be equal gives rise to an expression for the circulation:

$$\Gamma=-2\pi b\sin\alpha\left(1-\frac{2\sqrt{\delta_v\delta_n}}{b}\right)w_\infty.$$

With

$$\delta_v=\delta_n=0\quad\Gamma=-2\pi bw_\infty\sin\alpha.$$

Therefore,

$$\frac{\Gamma}{\Gamma_{sov}}=1-\frac{2\sqrt{\delta_v\delta_n}}{b}. \qquad (9.8.19)$$

For a lattice of unstaggered plates ($\beta = \pi/2$) and a lattice arranged along a straight line ($\beta = 0$),

$$\frac{\Gamma}{\Gamma_{sov}}=1-2k\frac{\sqrt{\delta_v\delta_n}}{b},\quad k_{\frac{\pi}{2}}=\frac{\pi b}{b\,\mathrm{sh}\frac{\pi b}{l}},\quad k_0=\frac{\pi b}{l\sin\frac{\pi b}{l}}. \qquad (9.8.20)$$

In the general case of an arbitrarily staggered lattice we can assume that

$$\frac{\Gamma}{\Gamma_{sov}}=1-2k\left(\frac{b}{l},\beta\right)\frac{\sqrt{\delta_v\delta_n}}{b}.$$

Figure 9.8.4 shows a graph of the values of $\underline{k}$ for plane plates plotted on the basis of numerical calculations [9.22]. When it is assumed that the boundary layer thicknesses at the trailing edge of the plate δ_v and δ_n should depend slightly on the geometrical parameters it can be shown that for a dense lattice ($b/\underline{l} > 1$), $\Gamma/\Gamma_{sov} \to 1$; whereas, if $\beta > 45^\circ$, $\Gamma_{sov} - \Gamma$ decreases monotonically so that Γ/Γ_{sov} tends to

unity as b/l increases, and when $\beta < 45^{\circ}$, $(\Gamma_{sov} - \Gamma)$ first grows, reaches a maximum at $b/l = 1$, and then drops

The influence of viscosity on the deflection of the flow. The disturbances caused by the lattice of profiles alters the parameters of the flow at infinity. Since the principal cause of the change in the direction of the velocity in the viscous fluid flow at infinity as compared with the flow of an inviscid fluid is the asymmetry of the boundary layer development in the channel between the blades, it can be assumed that the deviation in velocity is proportional to the difference in the displacement thicknesses.

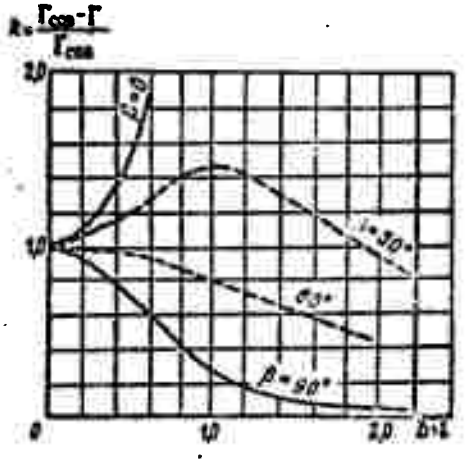


Fig. 9.8.4. The influence of the viscosity on the circulation for a lattice of plane plates with different densitities and staggers.

The velocity direction at the trailing edge will therefore be reflected from the velocity direction behind the lattice in the flow of an inviscid fluid towards the side of the surface on which the displacement thicknesses are smaller.

In order to estimate the influence of the viscosity and compressibility on the deflection of the flow we apply the equations of continuity and momentum [illegible] reference surface ABCD (cf. Fig. 9.8.1);

since the following calculations are only slightly complicated by allowing for compressibility, the gas will be considered as viscous and compressible.

We shall suppose that, 1) the total pressure in the potential core of the flow is equal to the total pressure in front of the lattice, 2) the flow in the cross section 2-2 is uniform and all the gas parameters repeat themselves in the same way in each interval, 3) the direction of the velocity at each cross section is constant along an interval and in the core of the flow the magnitude is constant too; hence the static pressure in the cross section k-k is constant along an interval both in the core and in the boundary layer.

Let us denote by the subscript "c" those parameters which correspond to an inviscid gas flowing through a lattice. The condition of constancy of mass flow through the cross sections 2-2 and k-k then gives

$$\rho_k w_k \left(t - \frac{\delta^*}{\sin\beta_k}\right) \sin\beta_k = \rho_2 w_2 t \sin\beta_2 = \rho_c w_c t \sin\beta_c. \qquad (9.8.21)$$

Assuming

$$\frac{\delta^*}{t\sin\beta_k} = \frac{\delta_0^* + \delta_n^*}{t\sin\beta_k} = \Delta^*, \qquad (9.8.22)$$

we find that

$$\sin\beta_2 = \frac{\rho_k w_k (1-\Delta^*)}{\rho_2 w_2} \sin\beta_k. \qquad (9.8.23)$$

Projecting the momentum equation onto the lattice axis we obtain

$$\rho_2 w_2^2 \sin\beta_2 \cos\beta_2 = \sin\beta_k \cos\beta_k \int_0^t \rho w^2 d\left(\frac{y}{t}\right) =$$

$$= \sin\beta_k \cos\beta_k \rho_k w_k^2 \left[1 - \int_0^1 \left(1 - \frac{\rho w}{\rho_k w_k}\right) d\frac{y}{t} - \int_0^1 \frac{\rho w}{\rho_k w_k}\left(1 - \frac{w}{w_k}\right) d\frac{y}{t}\right].$$

but

$$\int_0^1 \left(1 - \frac{\rho w}{\rho_k w_k}\right) d\frac{y}{t} = \frac{1}{\sin\beta_k} \int_0^1 \left(1 - \frac{\rho w}{\rho_k w_k}\right) d\frac{n}{t} = \Big| \qquad (9.8.24)$$

$$= \frac{\beta_2^* + \dots}{l \sin \beta_2} = \Delta^*,$$

$$\int_0^1 \frac{\rho w}{\rho_2 w_2} \left(1 - \frac{w}{w_2}\right) d\frac{y}{l} = \frac{\beta_1^{**} + \beta_2^{**}}{l \sin \beta_2} = \Delta^{**}. \qquad (9.8.24)$$

Therefore $\rho_2 w_2^2 \sin \beta_2 \cos \beta_2 = \rho_2 w_2^2 \sin \beta_2 \cos \beta_2 (1 - \Delta^* - \Delta^{**})$ and, by virtue of (9.8.21) $w_2 \cos \beta_2 (1 - \Delta^*) = w_2 \cos \beta_2 (1 - \Delta^* - \Delta^{**})$, which gives

$$\cos \beta_2 = \frac{w_2}{w_2} \frac{1 - \Delta^* - \Delta^{**}}{1 - \Delta^*} \cos \beta_2. \qquad (9.8.25)$$

Dividing this by (9.8.23), we obtain Stepanov's formula

$$\operatorname{ctg} \beta_2 = \frac{\rho_2}{\rho_2} \frac{1 - \Delta^* - \Delta^{**}}{(1 - \Delta^*)^2} \operatorname{ctg} \beta_2. \qquad (9.8.26)$$

Supposing $\beta_k = \beta_c + \varepsilon$, where ε is a small quantity, we can write

$$\operatorname{ctg} \beta_2 = \operatorname{ctg} (\beta_c + \varepsilon) = \frac{\operatorname{ctg} \beta_c - \varepsilon}{1 + \varepsilon \operatorname{ctg} \beta_c} \qquad (9.8.27)$$

and therefore,

$$\operatorname{ctg} \beta_2 = \frac{\rho_2}{\rho_2} \frac{1 - \Delta^* - \Delta^{**}}{(1 - \Delta^*)^2} \frac{\operatorname{ctg} \beta_c - \varepsilon}{1 + \varepsilon \operatorname{ctg} \beta_c}. \qquad (9.8.28)$$

Experiment shows [9.21] that if we put

$$\frac{\sin \beta_c}{\sin \beta_2} = 1 + \eta, \qquad (9.8.29)$$

then the quantity η for sufficiently dense lattices ($b/\underline{l} > 1.2$) does not depend on the shape of the profile but varies from $\eta = 0.01$ (for small stagger angles j_p) to $\eta = 0.03$ (for large j_p) ε and η are linked by the relationships

$$\frac{\sin \beta_2}{\sin \beta_c} = \frac{\sin (\beta_c + \varepsilon)}{\sin \beta_c} = \frac{1}{1 + \eta} \approx \frac{\sin \beta_c + \varepsilon \cos \beta_c}{\sin \beta_c} = 1 + \varepsilon \operatorname{ctg} \beta_c$$

and

$$\varepsilon \operatorname{ctg} \beta_c = \frac{1}{1 + \eta} - 1 = -\frac{\eta}{1 + \eta}; \quad \varepsilon = -\frac{\eta}{1 + \eta} \operatorname{tg} \beta_c;$$

therefore

$$\operatorname{ctg} \beta_2 = \frac{\rho_2}{\rho_2} \frac{1 - \Delta^* - \Delta^{**}}{(1 - \Delta^*)^2} \frac{\operatorname{ctg} \beta_c + \frac{\eta}{1 + \eta} \operatorname{tg} \beta_c}{1 - \frac{\eta}{1 + \eta}} =$$

$$= \frac{\rho_2}{\rho_2} \frac{1 - \Delta^* - \Delta^{**}}{(1 - \Delta^*)^2} \left(\operatorname{ctg} \beta_c + \frac{2\eta}{\sin 2\beta_c}\right). \qquad (9.8.30)$$

In most of the calculations we can assume $\rho_2 = \rho_k$.

The formula obtained enables us to take the influence of the viscosity of the gas on the direction of flow behind the lattice into account; to do this it is necessary to know the boundary layer parameters at the trailing edge of the profile.

The loss coefficient. In many calculations it is convenient to replace the drag coefficient (9.8.16) by the loss coefficient ζ which is defined as the ratio of the energy lost per unit mass of gas at the lattice inlet. It is convenient to subdivide the energy losses into two parts, namely the losses connected with the passage of the gas through the channel between the profiles, and the losses connected with turbulent mixing in the flow behind the lattice.

The energy dissipated in the section 11-kk (cf. Fig. 9.8.1) can be determined by the expression

$$E_a = \int_0^l \left(\frac{w_1^2}{2} + \int_{p_2}^{p_1} \frac{dp}{\rho} - \frac{w^2}{2} \right) \rho w \sin \beta_2 \, dy. \qquad (9.8.31)$$

and since no losses occur in the potential core of the flow,

$$\frac{w_1^2}{2} + \int_{p_2}^{p_k} \frac{dp}{\rho} = \frac{w_k^2}{2}. \qquad (9.8.32)$$

where the potential energy is referred to its value at the cross section kk.

Substituting (9.8.32) in (9.8.31) we obtain

$$E_a = \frac{\sin \beta_2}{2} \left(w_k^2 \int_0^l \rho w \, dy - \int_0^l \rho w^2 \, dy \right). \qquad (9.8.33)$$

But

$$\int_0^l \rho w \, dy = l \int_0^1 [\rho_2 w_2 - (\rho_2 w_2 - \rho w)] \, d\frac{y}{l} = l \rho_2 w_2 (1 - \Delta^*);$$

$$\int_0^l \rho w^2 \, dy = \rho_2 w_2^2 l \left[1 - \int_0^1 \left(1 - \frac{\rho w}{\rho_2 w_2} \right) d\frac{y}{l} - \int_0^1 \frac{\rho w}{\rho_2 w_2} \left(1 - \frac{w^2}{w_2^2} \right) d\frac{y}{l} \right.$$

Here $\Delta^{***}=\frac{\delta_{k\,n}^{***}+\delta_{k\,s}^{***}}{l\sin\beta_k}$ is the relative energy loss thickness at the trailing edge of the profile. Substituting this into (9.8.33) we find that

$$E_a=\frac{1}{2}l\rho_k w_k^3\sin\beta_k\Delta^{***} \qquad (9.8.34)$$

and that the loss coefficient in the channel is

$$\zeta_a=\frac{E_a}{\rho_1 w_1 l\sin\beta_1\frac{w_1^2}{2}}=\frac{\rho_k w_k^3}{\rho_1 w_1^3}\frac{\sin\beta_k}{\sin\beta_1}\Delta^{***}$$

or, taking into account that, according to the continuity equation $\rho_1 w_1 \sin\beta_1 = \rho_k w_k \sin\beta_k\ (1-\Delta^*)$, we have

$$\zeta_a=\frac{\Delta^{***}}{(1-\Delta^*)^3}\left(\frac{\rho_1\sin\vartheta_1}{\rho_k\sin\vartheta_k}\right)^2. \qquad (9.8.35)$$

The losses in the wake behind the lattice are

$$E_{ca}=\int_0^l\left(\frac{w^2}{2}+\int_{p_k}^{p}\frac{dp}{\rho}-\frac{w_2^2}{2}\right)\rho w\sin\vartheta_k\,dy. \qquad (9.8.36)$$

Projecting the momentum equation for the mass in the reference volume ABCD onto the axis of rotation (the normal to the front) of the lattice we find that, in view of the expressions for Δ^* and Δ^{**} . . (9.8.24):

$$p_k-p_2=\rho_2 w_2^2\sin\vartheta_2-\rho_k w_k^2\sin\vartheta_k(1-\Delta^*-\Delta^{**})$$

and, putting $\rho_2=\rho_k$,

$$\zeta_{ca}=\frac{E_c}{\frac{\rho_1 w_1^2}{2}l\sin\beta_1}=\left\{\frac{2\Delta^{**}+\Delta^{*2}}{(1-\Delta^*)^2}-\frac{\Delta^{***}}{(1-\Delta^*)^3}-\right.$$
$$\left.-\left[\frac{1-\Delta^*-\Delta^{**}}{(1-\Delta^*)^2}-1\right]^2\sin\beta_k\right\}\left(\frac{\rho_1\sin\beta_1}{\rho_k\sin\beta_k}\right)^2. \qquad (9.8.37)$$

Adding ζ_l and ζ_{sl}, we find the total loss coefficient:

$$\zeta=\left[\frac{2\Delta^{**}+\Delta^{*2}}{(1-\Delta^*)^2}-\frac{\Delta^*-\Delta^{*2}-\Delta^{**}}{(1-\Delta^*)^2}\sin\beta_k\right]\left(\frac{\rho_1\sin\beta_1}{\rho_k\sin\beta_k}\right)^2. \qquad (9.8.38)$$

Assuming that $w_2 = w_c$ in (9.2.1) and neglecting the second component in the bracket , we obtain

$$\zeta = \frac{2\delta^{**} + \Delta^{**2}}{(1-\Delta^{**})^2}\left(\frac{\rho_1 \sin\beta_1}{\rho_2 \sin\beta_2}\right)^2. \qquad (9.8.39)$$

The influence of roughness. Experiments show [9.23] that when the sandy roughness does not exceed a certain admissible value h_d, the drag of a lattice of profiles is virtually the same as that of a lattice consisting of smooth profiles. The admissible roughness for a completely turbulent flow is determined by the relation

$$\frac{w_p h_d}{\nu} = 27{,}3\frac{(w_p l:\nu)^{0.107}}{(w_0:w_p)^{1.268}} \approx 30\frac{\sqrt[10]{w_p l:\nu}}{\sqrt[8]{(w_0:w_p)\sqrt{w_0:w_p}}}. \qquad (9.8.40)$$

where w_0 is the velocity of a potential flow past a profile in the lattice and w_p is the reduced velocity, equal to w_1 for a diffusor and to w_2 for a turbine lattice.

If the roughness exceeds the permissible value, the increment of the drag coefficient can be determined from the relation

$$\frac{\zeta_{sup}}{\zeta_s} = \frac{C_{f\,sup}}{C_{f\,s}},$$

where C_f is the drag of a plane plate.

9.9. A LATTICE OF PROFILES IN A SUPERSONIC FLOW

For given power and mass flow of gas, the size and weight of a turbine can be reduced by raising the speed of flow in its elements to values exceeding sonic speed. This is of special importance for the axial-flow compressor. A supersonic flow streaming through a lattice of profiles with thick rounded leading edges, like a flow about an isolated body, is accompanied by the formation of shock waves and a sharp associated increase in drag. Depending on the profile of the channel between the blades and on the intensity of the shock, the subsonic flow behind the shock wave can once again pass through sonic speed. In a very dense lattice the head shock waves formed in front of each profile can fuse together to form a shock which is periodic in shape and intensity. Since the drag increases greatly when a shock wave forms, it is

assumed that it is unsuitable to make use of supersonic velocities in a compressor. The pressure losses in a normal shock at moderate Mach numbers M, however, are not very large (cf. Fig. 4.3.5), and the transition to a system of diagonal shocks makes it possible to reduce the losses even at high M numbers.

A supersonic flow can be produced in either the guide wheel or the working wheel. By way of example, Fig. 9.9.1 shows the triangles of velocities for axial flow compressors of various designs, in which the axial component is subsonic throughout.

The relative velocity w_1 can be raised to sonic speed by imparting a rotation to the flow in the inlet guide mechanism. The supersonic velocity of the absolute motion, c_2, at the inlet of the GM (guide mechanism) is reached at the expense of the rotation of the working wheel. By profiling the channel between the blades appropriately, the relative velocity w_2 at the outlet of the working wheel can be made supersonic.

Conditions of supersonic flow through a lattice of profiles. One of the most important pecularities of supersonic flows is the fact that disturbances bounded by characteristics (or shocks) are propagated only downstream. At the same time, as we have already shown, the velocity component normal to a characteristic is equal to the local velocity of sound (Fig. 9.9.2). Depending on the magnitude of the velocity and the structure of the lattice, the waves and the lattice profiles will interact in different ways. This enables us to distinguish between the main types of flows [9.24].

Let us first consider the simplest case of flow through a lattice, when the axial velocity component exceeds the speed of sound. Let the lattice be sufficiently sparse so that all characteristics are directed into the lattice and do not touch the neighboring profiles (cf. Fig. 9.9.3, I). The lattice profiles do not then influence each other; the

flow in front of the lattice is undisturbed, while the flow about each profile in the lattice is the same as it would be about an isolated profile. Behind the lattice, however, the velocity field will be nonuniform owing to the interaction of rarefaction and compression waves.

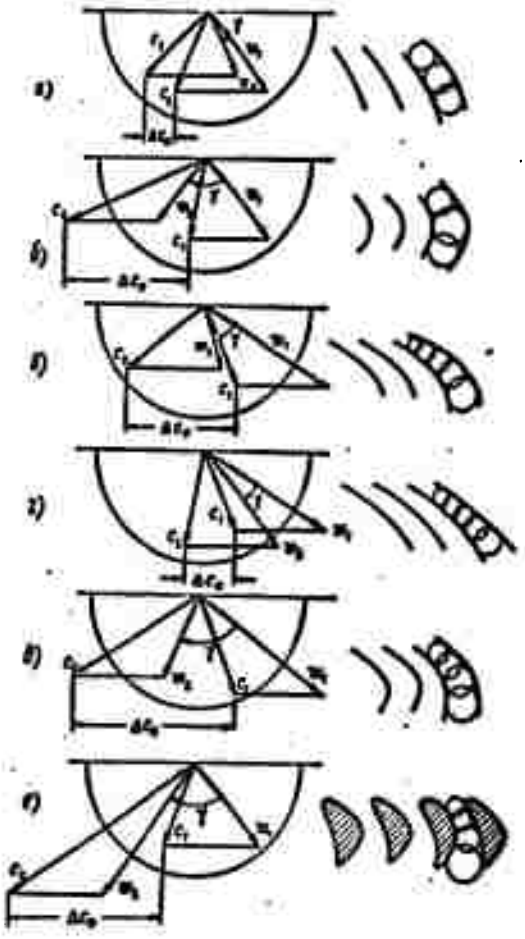


Fig. 9.9.1. Triangles of velocities for axial-flow compressors of various designs and blade shapes. The rotation of the flow is characterized by the angle. a) Subsonic stage; b) supersonic velocity in the GM; c) supersonic velocity at the inlet of the WW, due to the intense twisting of the flow directed against the rotation; d) supersonic velocity at inlet and outlet of WW; e) supersonic velocities at the inlet of WW and GM; f) supersonic velocities in WW due to the geometry of the channel.

Such a flow will occur if the axial velocity component $w_z = w_1 \sin(\beta-\alpha)$ exceeds $w_\infty \sin \mu_n$; the condition that the rarefaction wave om_1' passes by point A_1 will be (Fig. 9.9.3)

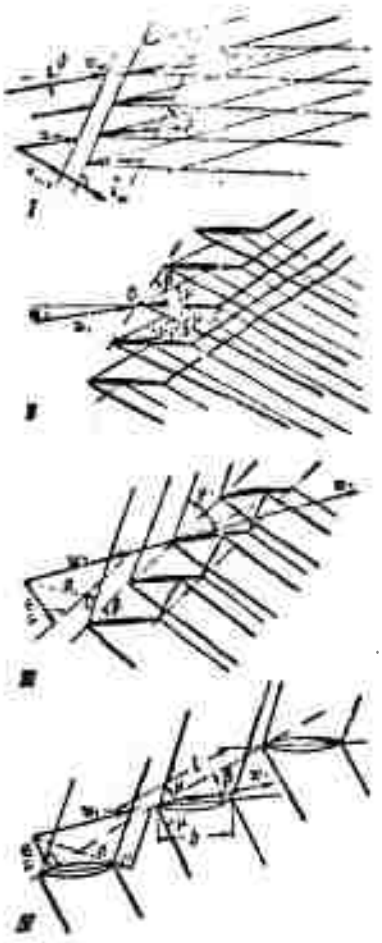


Fig. 9.9.2. Diagram of supersonic flow through a lattice. I) the axial velocity component exceeds the sonic speed and the profiles do not interfere; II) the parameters of the left-hand diagram of supersonic flow about a lattice are $w_a > a_* / \sin\beta > \sin(\alpha + \mu_p) : \sin(\beta - \alpha - \mu_p)$. The flow in front of the lattice is undisturbed, the profiles interfere, but the flow about the individual profile sections (oc and ob), occurs without interference; III) The axial component of the incoming flow is subsonic and the flow in front of the lattice is disturbed; IV) the flow about each profile of the lattice is the same as it would be about an isolated profile.

$$\frac{t}{b} \geqslant \frac{\sin(\alpha + \mu_p)}{\sin(\beta - \alpha - \mu_p)};$$

where μ_p is the limiting angle of the rarefaction wave.

If we now reduce the density of the lattice or the velocity of the flow, then the angle μ may become greater than the angle μ_p. The Mach [illegible] of one profile strike the neighboring profiles and so the pro-

files come into interaction. This second mode of flow (cf. Fig. 9.9.2, II) will be observed as long as $\beta > \alpha + \mu_p$, and a certain part of each profile will therefore be outside the disturbance zone; the field behind the lattice is nonuniform. The axial velocity component $w_z =$

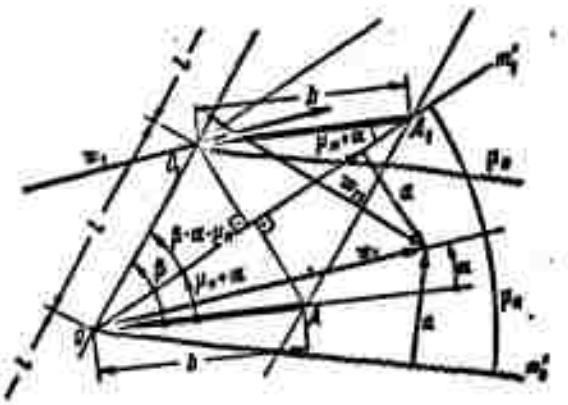


Fig. 9.9.3 The condition of absence of interference between the profiles for Diagram I (cf. Fig. 9.9.2).

$= w_1 \sin(\beta-\alpha)$ will exceed the local sonic speed $\underline{a}$ if $\beta > \alpha + \mu$; in the limiting case $\beta = \alpha + \mu_p$ it is equal to the sonic speed, $w_{1z} = \underline{a}$.

Any further reduction in lattice density or in the velocity of the incoming flow leads to the condition $\beta < \alpha + \mu_p$. The axial velocity component of the undisturbed flow becomes smaller than the sonic speed (cf. Fig. 9.9.2, III) and in the third mode of flow, the flow in front of the lattice will be distu bed. If the lattice is only slightly staggered, the Mach waves from one profile will fall upon the neighboring profiles.

Raising the stagger angle of the lattice can lead to the Mach waves from each profile bypassing the neighboring profiles and to the flow about each of the profiles being equal to the flow about an isolated profile (cf. Fig. 9.9.2, IV).

In all modes of flow considered the profiles were assumed to be thin and the channel cross section was taken as being virtually con-

stant. If we account for the possibility of geometrical influence of cross-sectional changes of the channel between the blades on the flow, then the modes considered become more complex because the velocity in the channel varies.

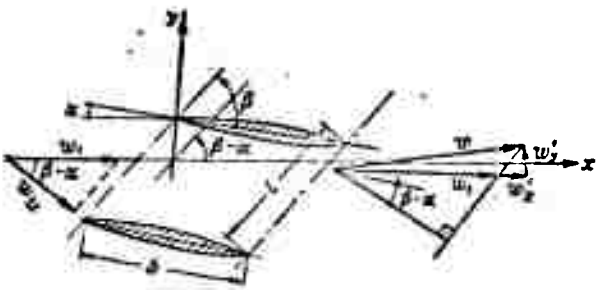


Fig. 9.9.4. I and II) Modes of supersonic flow about lattices of thin profiles (cf. Fig. 9.9.2).

Still more complex is the form of flow with two lattices – the working wheel and the guidance mechanism.

Velocity field behind a lattice of profiles with a supersonic axial component. Let us first consider the modes I and II (cf. Fig. 9.9.2) of a supersonic flow about thin profile lattices (Fig. 9.9.4). Since the flow is uniform in front of the lattice, the continuity equation leads to

$$\rho_1 l w_1 \sin(\beta-\alpha)=\int_0^l \rho\left[(w_1+w_x')\sin(\beta-\alpha)-w_y'\cos(\beta-\alpha)\right]d\xi. \quad (9.9.1)$$

Within the scope of linearized theory

$$\frac{\rho}{\rho_\infty}=1-m^2\frac{w_x'}{w_\infty}\qquad (m^2=M_\infty^2-1),$$

and, retaining only the first order small terms, we obtain from Eq. (9.9.1)

$$l w_1=\int_0^l\left[\left(1-M_1^2\frac{w_x'}{w_1}\right)w_1+w_x'-w_y'\operatorname{ctg}\beta\right]d\xi$$

$$\int_0^l [(M_1^2-1)w'_x + w'_y \operatorname{ctg}\beta]\,dt = 0.$$

Introducing the averaged quantities $w'_{x\,cp} = \frac{1}{l}\int_0^l w'_x\,dt$; $w'_{y\,cp} = \frac{1}{l}\int_0^l w'_y\,dt$, we find

$$(M_\infty^2-1)w'_{x\,cp} = -w'_{y\,cp}\operatorname{ctg}\beta \qquad (9.9.2)$$

or, since $1/(M_\infty^2 - 1) = \tan^2\mu_1$

$$w'_{y\,cp} = -w'_{x\,cp}\operatorname{ctg}^2\mu_1 \operatorname{tg}\beta. \qquad (9.9.3)$$

Hence the mean angle through which the lattice deflects the flow is

$$\delta_{cp} \approx \frac{w'_{y\,cp}}{w_1} = -\frac{w'_{x\,cp}}{w_1}\operatorname{ctg}^2\mu_1 \operatorname{tg}\beta.$$

The velocity field is determined with the method of characteristics described before (cf. Part 5.8). The boundary conditions are provided by the fact that the lattice profiles must be streamlines. If the x-axis is directed along the velocity of the undisturbed flow and if $y'(x)$ denotes the angle between the tangent to the profile contour and the chord (Fig. 9.9.5), then, within the limits of accuracy of the theory of small disturbances, the boundary condition can be formulated as

$$y'_1(x) - \alpha = \frac{w'_y}{w_1 + w'_x} \approx \frac{w'_y}{w_1}. \qquad (9.9.4)$$

In the case of slightly curved thin profiles we may assume that the boundary conditions refer to the chord of the profile. This assumption simplifies the solution of the problem considerably, since in many cases the Mach waves are reflected several times from the profile contours.

Since there are no free surfaces in the case of a supersonic flow through a lattice of profiles, we can, when constructing the flow pattern, make use of the rules governing reflection from a solid wall, namely: 1) the nature of the wave remains unchanged when it is reflec-

ted from a solid wall, and 2) the angle of incidence of the wave is equal to the angle of reflection (Fig. 9.9.6).

Lattices which accelerate a supersonic flow with no wave drag. It is possible to design a lattice which, theoretically, will deflect a supersonic flow without disturbing its isentropy. For this purpose let us find the number M_2 after deflection from the number M_1 of the incoming flow and the angle of deflection. We draw at the distances of the lattice period chosen two broken straight lines, AOB and $A_1O_1B_1$, which are formed when the incoming flow and the deflected flow intersect at given angles (Fig. 9.9.7). From the point O we draw the characteristics corresponding to the numbers M_1 and M_2 to the points of intersection, C and D. The profile chord b is thus determined. In the section CD we construct the curve according to Eq. (5.9.1)

$$r=r_0\left[\cos\left(\sqrt{\frac{k-1}{k+1}}\varphi\right)\right]^{\frac{k+1}{k-1}}.$$

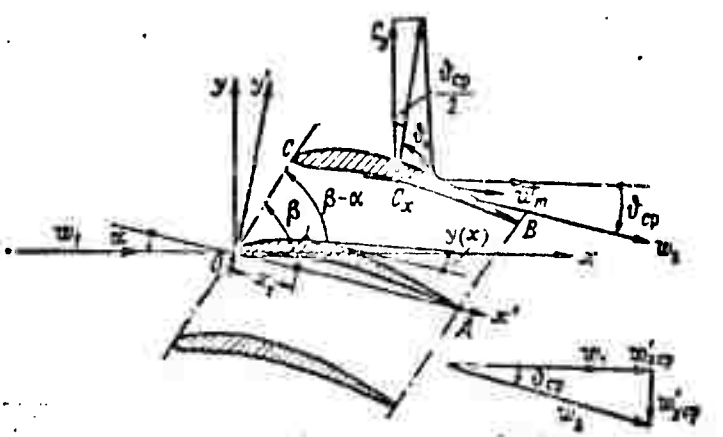


Fig. 9.9.5. The boundary conditions on the profile can be obtained within the limits of accuracy of perturbation theory.

The parameters p_i, ρ_i, T_i ($i = 1, 2$) are determined for M_1 and M_2, respectively.

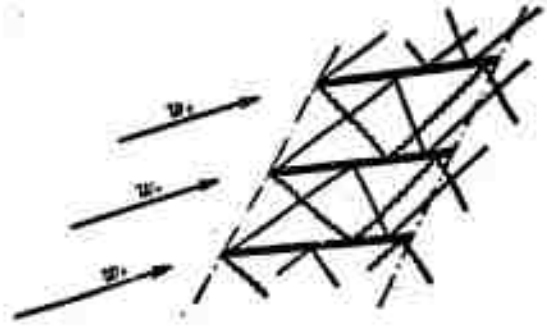


Fig. 9.9.6. Mach waves in a lattice of profiles.

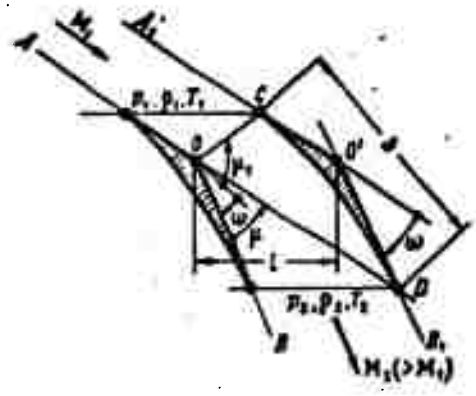


Fig. 9.9.7. Construction of lattice of profiles accelerating a flow with no wave drag.

Applying the method of characteristics it is theoretically possible to construct the lattice of a supersonic active turbine (Fig. 9.9.8). It is however fairly improbable that the flow can be compressed without shock waves forming (on the section DAB).

Lattices which decelerate a supersonic flow. It is theoretically possible to obtain a diffusor lattice of profiles by reversing a lattice that accelerates a supersonic flow, as considered above (cf. Fig. 9.9.7). Instead of the rarefaction waves in the zone OCD compression waves will arise. In this zone, as in the case of a reversed geometrical nozzle, compression shocks may arise. In order to avoid one strong

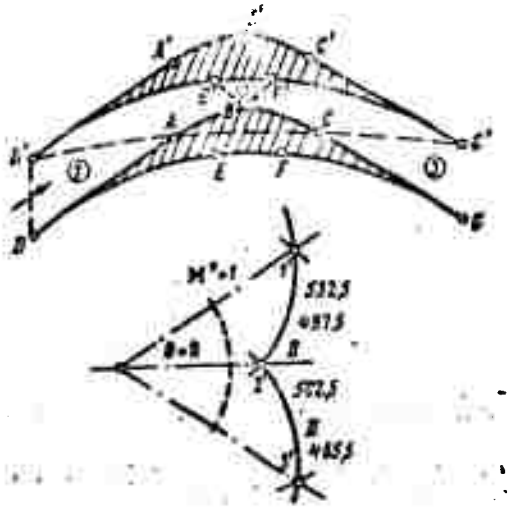


Fig. 9.9.8. Construction of supersonic lattice of profiles with no wave drag by the method of characteristics.

normal compression shock, conscious efforts are made to produce systems of diagonal compression shocks with a final normal shock in the compressor lattice. The losses can then be made very small.

The forces on a profile in the lattice. In order to determine the forces acting on a profile we apply the law of conservation of momentum to the gas mass enclosed in the volume CABCC (cf. Fig. 9.9.5)

$$w'_x = w'_y = 0; \quad C_p = \frac{2(p-p_1)}{\rho w_1^2} = 0; \quad p = p_1.$$

Behind the lattice these quantities will vary from point to point, and therefore the x-component of the force $\vec{R}$ arising on the profile will be

$$-R_x + \int_0^t (p_1 - p_2) \sin(\beta - a)\, d\xi =$$

$$= \int_0^t \rho \left[(w_1 + w'_x) \sin(\beta - a) - w'_y \cos(\beta - a) \right] w'_x\, d\xi$$

or

$$C_x = \frac{2R_x}{b_1 w_1^2} = \frac{1}{b}\int_0^l \left\{C_p \sin\beta - \frac{2p}{\rho_1}\left[\left(1+\frac{w_x'}{w_1}\right)\sin\beta + \frac{w_y'}{w_1}\cos\beta\right]\frac{w_x}{w_1}\right\} dl$$

and analogously

$$C_y = \frac{2R_y}{b_1 w_1^2} = \frac{1}{b}\int_0^l \left\{C_p \cos\beta - \frac{2p}{\rho_1}\left[\left(1+\frac{w_y'}{w_1}\right)\sin\beta + \frac{w_y'}{w_1}\cos\beta\right]\frac{w_y}{w_1}\right\} dl. \qquad (9.9.5)$$

Using the relation for $p:\rho_1 = 1 - m_1^2\frac{w_x}{w_1}$, we obtain

$$C_x = \frac{1}{b}\int_0^l \left\{\left[\left(\frac{w_x'}{w_y'}\right)^2 (M_1^2-1) + \left(\frac{w_y'}{w_1}\right)^2\right]\sin\beta + 2\frac{w_x' w_y'}{w_1^2}\cos\beta\right\} dl.$$

$$C_y = -\frac{2}{b}\int_0^l \left(\frac{w_x'}{w_1}\cos\beta + \frac{w_y'}{w_1}\sin\beta\right) dl. \qquad (9.9.6)$$

Introducing the averaged values $w'_{x\ sr}$ and $w'_{y\ sr}$ and taking into account that according to (9.9.2)

$$\frac{w_{y\,cp}'}{w_{x\,cp}'} = -\operatorname{tg}\beta\cdot\operatorname{ctg}^2\rho_1;$$

$$C_y\frac{b}{l} = 2\frac{w_{x\,cp}'}{w_1}\sin\beta\operatorname{tg}\beta(\operatorname{ctg}^2\rho_1 - \operatorname{ctg}^2\beta),$$

we find

$$C_x = \frac{l}{b}\left\{\left[\left(\frac{w_{x\,cp}'}{w_{y\,cp}'}\right)^2 (M_1^2-1) + \left(\frac{w_{y\,cp}'}{w_1}\right)^2\right]\sin\beta + 2\frac{w_{x\,cp}' w_{y\,cp}'}{w_1^2}\cos\beta\right\}$$

and

$$C_y = \frac{l}{b}2\frac{w_{x\,cp}'}{w_1}\sin\beta\cdot\operatorname{tg}\beta(\operatorname{ctg}^2\rho_1 - \operatorname{ctg}^2\beta). \qquad (9.9.7)$$

Substituting this into the expression for the angle ϑ_{sr} of deflection of the flow and for C_x, we find

$$\vartheta_{cp} = \frac{w_{y\,cp}'}{w_1} = -\frac{C_y b}{2l}\frac{\operatorname{ctg}^2\rho_1}{\sin\beta(\operatorname{ctg}^2\rho_1 - \operatorname{ctg}^2\beta)}; \qquad (9.9.8)$$

$$C_x = C_y^2 \frac{b}{l} \frac{\operatorname{ctg}^2 \mu_1}{4 \sin \beta (\operatorname{ctg}^2 \mu_1 - \operatorname{ctg}^2 \beta)}. \qquad (9.9.9)$$

If we use the expression found previously for $C_p = -2w'_x/w_1$, then the mean value of the pressure coefficient behind the lattice will be

$$C_{p\,cp} = -C_y \frac{b}{l} \frac{\cos \beta}{\sin^2 \beta (\operatorname{ctg}^2 \mu_1 - \operatorname{ctg}^2 \beta)}. \qquad (9.9.10)$$

Denoting by ϑ_0 the angle between the direction of the total aerodynamic force and the velocity of the undisturbed flow (cf. Fig. 9.9.5) we can write

$$\vartheta_0 = \frac{\pi}{2} - \operatorname{arc\,tg} \frac{C_x}{C_y} \approx \frac{\pi}{2} - C_y \frac{b}{l} \frac{\operatorname{ctg}^2 \mu_1}{4 \sin \beta (\operatorname{ctg}^2 \mu_1 - \operatorname{ctg}^2 \beta)} =$$

$$= \frac{\pi}{2} + \frac{\vartheta_{cp}}{2}. \qquad (9.9.11)$$

Hence we see that the total force $\vec{R}$ is normal to half the vector sum of the velocities, $\vec{w}_m = \frac{1}{2}(\vec{w}_1 + \vec{w}_2)$ (cf. Fig. 9.9.6).

It is possible to connect the lift with the circulation round a profile in a lattice. We have, by definition,

$$\Gamma = l w_{a\,cp} - l w_{n\,cp} = l [(w_1 + w'_{cp}) \cos \beta + w'_{y\,cp} \sin \beta - w_1 \cos \beta] =$$

$$= l w'_{x\,cp} \cos \beta \left(1 + \frac{w'_{y\,cp}}{w_{x\,cp}} \operatorname{tg} \beta\right) = l w'_{x\,cp} \cos \beta (1 - \operatorname{tg}^2 \beta \operatorname{ctg}^2 \alpha) =$$

$$= l w_1 \frac{C_y b}{2l} \frac{\cos \beta (1 - \operatorname{tg}^2 \beta \operatorname{ctg}^2 \alpha)}{\sin \beta \operatorname{tg} \beta (\operatorname{ctg}^2 \alpha - \operatorname{ctg}^2 \beta)}. \qquad (9.9.12)$$

Thus, within the scope of the linear theory, Zhukovskiy's formula remains valid for a supersonic flow.

Lift and lattice geometry. These quantities are interrelated by the boundary conditions which express that the profile in the lattice must coincide with streamlines. If the x-axis lies in the direction of the undisturbed flow, then

$$f'(x) = \frac{w'_y}{w_1 + w_x} \approx \frac{w'_y}{w_1}, \qquad (9.9.13)$$

where $f(x)$ is the equation of a lattice profile contour. Let us stress that the profile is supposed to be thin, slightly curved and arranged at a small angle of attack.

If $y'(x)$ is the angle between the tangent to the profile contour and the chord, and α is the angle of attack, we may put

$$f'(x)=y'(x)+\alpha. \tag{9.9.14}$$

As was shown in Part 5.5, the relations

$$\xi=x-my \text{ and } \eta=x+my$$

determine the characteristics of the Mach lines of Eq. (5.5.1)

$$(M_\infty^2-1)\frac{\partial w_x'}{\partial x}-\frac{\partial w_y'}{\partial y}=0.$$

Rewriting this equation and the condition for the absence of vortices $\frac{\partial w_x'}{\partial y}-\frac{\partial w_y'}{\partial x}=0$ in the variables (ξ, η) we obtain

$$\frac{\partial}{\partial\xi}\left(w_x'\sqrt{M_\infty^2-1}-w_y'\right)-\frac{\partial}{\partial\eta}\left(w_x'\sqrt{M_\infty^2-1}+w_y'\right)=0,$$
$$\frac{\partial}{\partial\xi}\left(w_x'\sqrt{M_\infty^2-1}-w_y'\right)+\frac{\partial}{\partial\eta}\left(w_x'\sqrt{M_\infty^2-1}+w_y'\right)=0,$$

and hence

$$\frac{\partial}{\partial\xi}\left(w_x'\sqrt{M_\infty^2-1}-w_y'\right)=0;\quad \frac{\partial}{\partial\eta}\left(w_x'\sqrt{M_\infty^2-1}+w_y'\right)=0,$$

i.e.,

$$w_x'+\frac{w_y'}{\sqrt{M_\infty^2-1}}=\text{const}=c_\xi \quad \text{along the line } \xi=\text{const}$$
$$w_x'-\frac{w_y'}{\sqrt{M_\infty^2-1}}=\text{const}=c_\eta \quad \text{along the line } \eta=\text{const} \tag{9.9.15}$$

i.e., the projection of the disturbance velocity vector at points lying on a Mach line of one sign onto a Mach line of the other sign is a constant quantity.

Thus, at the points of intersection of two characteristics

$$w_x'=\frac{c_\xi+c_\eta}{2},\quad w_y'=\frac{c_\xi-c_\eta}{2}\sqrt{M_\infty^2-1}. \tag{9.9.16}$$

i.e., in order to determine the velocity field in a certain region we need know the constants c_ξ and c_η on the characteristics.

Taking now into account that according to (5.2.6) and (5.5.10)

$$C_p = -\frac{2}{w_1} w_x, \quad \frac{w_x}{w_y} = \operatorname{ctg} \frac{w_x}{w_y} = \frac{1}{m} = \operatorname{tg} \mu_1$$

we can write for the profile contour

$$\left.\begin{aligned} C_p(x) - 2f'(x)\operatorname{ctg}\mu_1 &= -2\frac{c_\xi}{w_1} \quad \text{on the line} \\ C_p(x) + 2f'(x)\operatorname{ctg}\mu_1 &= -2\frac{c_\eta}{w_1} \quad \text{on the line} \end{aligned}\right\} \qquad (9.9.17)$$

On Mach lines coming from the zones of the undisturbed flow, $c_\xi = c_\eta = 0$; therefore the pressure at points of the profile lying outside the disturbances of neighboring profiles will be the same as that on isolated profiles:

on the upper surface

$$C_{p_+} = 2\operatorname{tg}\mu_1 f'_+(x).$$

on the lower surface

$$C_{p_-} = -2\operatorname{tg}\mu_1 f'_-(x). \qquad (9.9.18)$$

When the formula

$$C_p - 2f'(x)\operatorname{tg}\mu_1 = -2\frac{c_\xi}{w_1}, \quad C_p + 2f'(x)\operatorname{tg}\mu_1 = -2\frac{c_\eta}{w_1} \qquad (9.9.19)$$

is used to determine c_ξ, c_η for wave reflected from these sections we can find the pressure at the points of the neighboring profile from which the lines were reflected. If this process is continued the pressure on the whole lattice profile contour can be determined. The arrows in Fig. 9.9.9 indicate the Mach lines as they are reflected between two neighboring profiles in the lattice. The sections c and d of the profile adjacent to the leading edge are outside the disturbance zones of the neighboring profiles and are touched by the lines from the undisturbed flow.

In order to simplify the problem, V.V. Keldysh [9.24] assumes that the reflection inside the lattice does not occur from the profile contour but from its chord, and that the boundary conditions are given for the chord. He obtained practical formulas for the determination of the flow on a profile in the lattice under various conditions of flow.

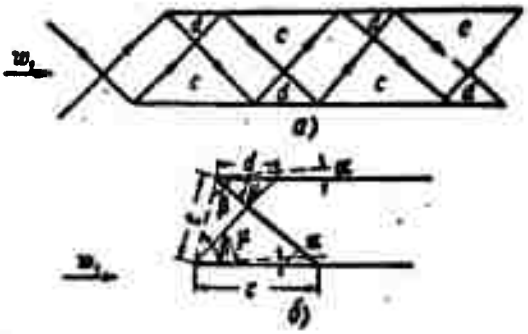


Fig. 9.9.9. Reflection of the Mach lines in a profile lattice (a); c and d are profile sections lying outside the disturbance zones of the neighboring profiles (b).

The guiding properties of a supersonic lattice of profiles. Let us consider a supersonic flow through a sufficiently dense lattice of profiles, where the axial component is smaller than the sonic velocity, $w_{1z} < a$, and the wave from one profile falls upon the other (Fig. 9.9.10). As can be seen from the diagram, $OA \sin(\mu + \alpha) = l \sin(\mu + \alpha - \beta)$; and therefore $OA = l \frac{\sin(\mu + \alpha - \beta)}{\sin(\mu + \alpha)}$ will then be smaller than b when $\frac{l}{b} < \frac{\sin(\mu + \alpha)}{\sin(\mu + \alpha - \beta)}$.

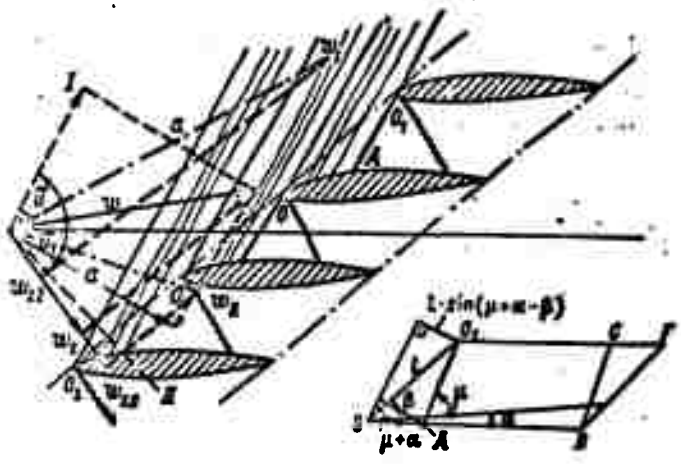


Fig. 9.9.10. If the axial velocity component is smaller than sonic speed the disturbances propagate into the region in front of the lattice. If the section OA is a straight line, then the nonuniformity vanishes and the velocity w_1 will be directed in the direction of OA.

If this condition is not satisfied, the Mach waves coming from one profile will not fall upon the other profile and the flow about each

profile of this lattice will be the same as the flow about an isolated profile.

Let $w_{1s} < a; \frac{t}{b} < \frac{\sin(\mu+\varepsilon)}{\sin(\mu+\varepsilon-\beta)}$. . In this case the flow in front of the lattice will be disturbed and nonuniform. The nonuniformity will be periodic in the strip OA. Therefore, if the section OA is straight line section, then the nonuniformity vanishes and the flow at the inlet of the lattice will have the same direction as the straight line section OA. Thus, in the case considered, strictly speaking, the expression "velocity of undisturbed flow" becomes meaningless because the whole flow in front of the lattice will be disturbed. It will, however, be uniform, and, by convention, we may take it as being undisturbed. Its velocity will be parallel to the straight line at the inlet section of the upper profile surface. This section OA is called the guiding section of the profile.

If the axial velocity in a compressor (w_{zI} in Fig. 9.9.10) is smaller than the velocity in the direction of flow along OA, then rarefaction waves will go out from the leading edges, and, when passing through these the axial velocity will grow until the relative velocity becomes parallel to the section OA. If, however, the axial velocity is large (w_{zII} in Fig. 9.9.10), compression shocks will reduce the axial velocity until the relative velocity becomes parallel to the section OA. The axial velocity, and therefore the volume flow of gas through a compressor with given circumferential velocity, will thus be determined by the slope of the line OA. On these circumstances we can say that the lattice has guidance properties.

Manuscript Page No.

[Footnotes]

577 The nonuniformity in velocity decreases according to an exponential law.

583 In the case of a viscous fluid the contour C is assumed to be taken on the boundary layer surface.

584 V.I. Dechev, Investigation of Conditions of Flow Through a Profile Lattice of the Reversible Pump-turbine of Axial-flow Type. Thesis. Kharkov Polytechnic Institute imeni V.I. Lenin, 1958.

589 * Strictly speaking, the mapping (9.2.2) is not conformal since it is not one to one: there is a branching point. It will be conformal in the limits of the strip (see below).

589 ** Corresponding to each circumvention of the flow there is an increment in the mass flow through a contour enclosing the source which is equal to $\oint w_r r \, d\vartheta = Q$.

590 The equation $e^w = z$ has infinitely many roots, each of which will be called a logarithm of the number z and be denoted by Log z. Let $z = r(\cos\varphi + i\sin\varphi)$, then $w = \operatorname{Log} z = \log r + \varphi i + 2k\pi i$, where log r is taken to denote the real logarithm of the positive number r. Consequently, Log z is an infinitely many-valued function.

598 Two pairs of vortices are taken because of the symmetry condition. The problem could also be solved with a single pair of vortices - one (Γ) at the point mr_0 (or $-mr_0$) and its conjugate ($-\Gamma$) at the point $-r_0/m$ (or r_0/m).

612 I.N. Berezin and N.P. Zhidkov, Methods of calculation, Vol. 1, Fizmatgiz, 1959, page 266.

624 A.I. Borisenko, Characteristic Function of the Flow Through a Lattice of Circular Cylinders, Trudy Laboratorii AN USSR, Kiev, 1955.

660 N.Ye. Zhukovskiy, On the Motion of a Solid Body With Cavities filled With a Homogeneous Dropable Fluid, Izbr. sochineniya, Vol. 1, GTTI, 1948.

662 V.M. Mayzel',
DVU, Kharkov, 1930.
Exactly the same solution was given in the paper of K. Raddy "Vortices and their Influence upon the Characteristics of a Centrifugal Compressor with Unswept Blades." Journ. Roy. Aeron. Sci. 58, No. 542, 1954. Collection "Problems in Rocket Engineering," No. 3 (27), IL, 1955.

670 L.G. Loytsyanskiy, Mechanics of Fluid and Gas, GTTI, 1957, page 359.

REFERENCES

9.1. Proskura, G.F., Gidrodinamika turbomashin [Hydrodynamics of Turbine Machines], Mashgiz [State Scientific-Technical Press for Machine Construction Literature], 1954.

9.2. Kochin, N.Ye., Gidrodinamicheskaya teoriya reshetok [Hydrodynamic Theory of Grids], GTTI [State Technical and Theoretical Press], 1949.

9.3. Loytsyanskiy, L.G., Soprotivleniye reshetki profiley obtekayemoy vyazkoy neszhimayemoy zhidkost'yu [Resistance of Profile Grid to Viscous Incompressible Fluid Flow Past It], "Prikl. mat. i mekh." [Applied Mathematics and Mechanics], XI, No. 4, 1947.

9.4. Simonov, L.A., Potentsial'nyye techeniya v reshetkakh profiley [Potential Flows in Profile Grids], Tr. TsAGI [Trans. Central Aerohydrodynamics Institute], 1948.

9.5. Kochin, N.Ye., Vliyaniye shaga reshetki na yeye gidrodinamicheskiye kharakteristiki [Influence of Grid Spacing on Its Hydrodynamic Characteristics], "Prikl. mat. i mekh.," V, No. 2, 1941, also "Sobraniye sochineniy," [Collected Works], Vol. II, AN SSSR, 1949.

9.6. Borisenko, A.I., Teoriya gidrodinamicheskoy reshetki krugovykh tsilindrov [Theory of Circular-Cylinder Hydrodynamic Grid], Tr. Laboratorii AN USSR [Trans. Lab. Acad. Sci. UkrSSR], Kiev, I: 3.

9.7. Samoylovich, G.S., Raschet gidrodinamicheskikh reshetok [Calculations for Hydrodynamic Grids], "Prikl. mat. i mekh.," XII, No. 2, 1950.

8. Blokh, E.L., Issledovaniye ploskoy reshetki, sostavlennoy iz teoreticheskikh profiley konechnoy tolshchiny [Investigation of a Two-Dimentional Grid Made Up of Theoretical Profiles of Finite Thickness], Tr. TsAGI, No. 611, 1947.

9.9. Blokh, E.L. and Ginevskiy, A.S., O potentsial'nom obtekanii reshetki krugov [Potential Flow Around Circle Grids], Collection entitled "Promyshl. aerodinamika" [Industrial Aerodynamics], No. 4, TsAGI [Central Aerohydrodynamics Institute], 1953.

9.10. Ginevskiy, A.S., Issledovaniye aerodinamicheskikh kharakteristik reshetok profiley napravlyayushchego apparata i rabochego kolesa osevogo kompressora [Investigation of Aerodynamic Characteristics of Profile Grids on Guide Assembly and Rotor of Axial-Flow Compressor], TsAGI [Central Aerohydrodynamics Institute], 1956.

9.11. Umnov, Ye.I., Potentsial'noye obtekaniye neszhimayemoy zhidkost'yu reshetok iz teoreticheskikh profiley [Potential Flow of an Incompressible Fluid Past Grids of Theoretical Profiles], 1951.

9.12. Dovzhik, S.A., Profilirovaniye lopatok osevogo dozvukovogo kompressora [Profiling Blades of an Axial-Flow Subsonic Compressor], Collection entitled "Promyshl. aerodinamika," No. 11, Oborongiz [State Scientific and Technical Publishing House of the Defense Industry], 1958.

9.13. Kolton, A.Yu and Etinberg, I.E., Osnovy teorii i gidrodinamicheskogo rascheta vodyanykh turbin [Foundations of Theory and Hydrodynamic Design of Water Turbines], Mashgiz, 1958.

9.14. Chun Khu-Vu and Braun, K., Teoriya pryamoy i obratnoy zadachi rascheta potoka szhimayemoy zhidkosti v reshetkakh profiley [Theory of Direct and Inverse Problems of Calculating Flow of Compressible Fluid in Profile Grids], Collection entitled "Voprosy raketnoy tekhniki" [Problems of Rocket Engineering], No. 1 (13), IL [Foreign Literature Press], 1953.

9.15. Teoreticheskaya gidromekhanika [Theoretical Fluid Dynamics], Collection of articles No. 16 edited by L.I. Sedov, Oborongiz, 1955.

9.16. Fedorov, R.M., Raschet dozvukovogo potentsial'nogo techeniya gaza vokrug ploskoy reshetki profiley [Calculation of Subsonic Potential Flow of a Gas Around a Plane Profile Grid], 1953.

9.17. Stepanov, G.Yu., Gazodinamicheskiye metody rascheta ustanovivshegosya obtekaniya reshetok turbomashin [Gasdynamic Methods for Calculating Steady-State Flow Through Turbine Grids], 1956.

9.18. Stepanov, G.Yu and Naumova, L.G., Metodika profilirovaniya ploskikh reshetok po zadannomu godografu skorosti [Technique of Profiling Plane Grids from a Specified Velocity Hodograph], Tekhn. otchet instituta im. Baranova [Technical Report of the Baranov Institute], 1959.

9.19. Markov, N.M., Raschet aerodinamicheskikh kharakteristik lopatochnogo apparata turbomashin [Calculating Aerodynamic Characteristics of Turbine-Machine Bucket Assemblies], Mashgiz, 1955.

9.20. Zysina-Molozhen, L.M., Raschet poter' v reshetkakh profiley turbomashin [Calculation of Losses in Turbomachine Profile Grids], "Aerogidrodinamika" [Aerohydrodynamics], Tr. TsKTI [Trans. Central Scientific Research Institute for Boilers and Turbines], 1954.

9.21. Povkh, I.L., Vliyaniye vyazkosti na velichinu i napravleniye skorosti za reshetkoy [Influence of Viscosity on Magnitude and Direction of Velocity Behind a Grid], Tr. LPI [Trans. Leningrad Polytechnic Institute], No. 5, 1953.

9.22. Ginevskiy, A.S., Vliyaniye vyazkosti zhidkosti na velichinu tsirkulyatsii vokrug profilya gidrodinamicheskoy reshetki [Influence of Fluid Viscosity on Magnitude of Circulation Around a Hydrodynamic Grid Profile], Collection entitled "Promyshl. aerodin." [Industrial Aerodynamics], No. 9, Oborongiz, 1957.

.. Speidel, L., Einfluss der Oberflächenrauhigkeit auf die Strö-

ungverluste in eben Schaufelgittern [Influence of Surface Roughness on Flow Losses in Plane Bucket Grids], "Forsch. Geb. Ingenierwesens" [Research from the Field of Engineering], No. 5, 1954.

9.24. Keldysh, V.V., Reshetki profiley v sverkhzvukovom potoke [Profile Grids in Supersonic Flow], Sb. teoretich. rabot TsAGI [Collected Papers of the TsAGI], Oborongiz, 1957.

Chapter 10

SOME SPECIAL PROBLEMS

10.1. CAVITATION

Cavitation effects. In the hydrodynamics of incompressible fluids the medium is considered as a continuous, homogeneous, dropable fluid. When the fluid moves at great local velocities the pressure in individual regions of the flow may be lower than the saturated vapor pressure ($p_{n.p}$), the pressure at which the fluid starts boiling. In these regions the fluid starts to evaporate vigorously and cavities (voids) form as bubbles filled with vapor or with a gas which was dissolved in the fluid. Such a flow with two phases is termed a cavitational flow, and the effect of formation of gas-phase volumes in a homogeneous fluid itself is termed cavitation. A cavitational fluid flow is also characterized by considerable changes in its physico-chemical properties.

If the pressure in the fluid rises as the motion of the fluid continues, the cavities (voids) formed close. At the same time the fluid surrounding a bubble moves at a great velocity to its center. When the fluid elements come into collision at the end of the process of filling the cavity, the pressure shock arising amounts to several hundred atmospheres. This process of bubble collapse occurs at a very high speed; it is reminiscent of the explosion of a "microscopic mine" and is accompanied by a characteristic sharp noise.

Cavitation in a tube of variable cross section. The simplest arrangement for investigating cavitation effects is a channel that is

first convergent and then divergent. At sufficiently high speeds of flow the pressure may drop to the saturation pressure in the throat and then rise again in the divergent part. In this case the main moving core of water behind the throat is laterally surrounded by a foam-like mixture of bubbles filled with vapor and air. Figure 1.10.1 shows the curves of pressure variation along the axis of a rectangular channel of constant height and variable width. The flow rate of the water passing through the channel is kept constant but the counterpressure is altered with the help of a throttle. If the counterpressure is large enough (Curves 1, 2, 3) and when the absolute pressure in the

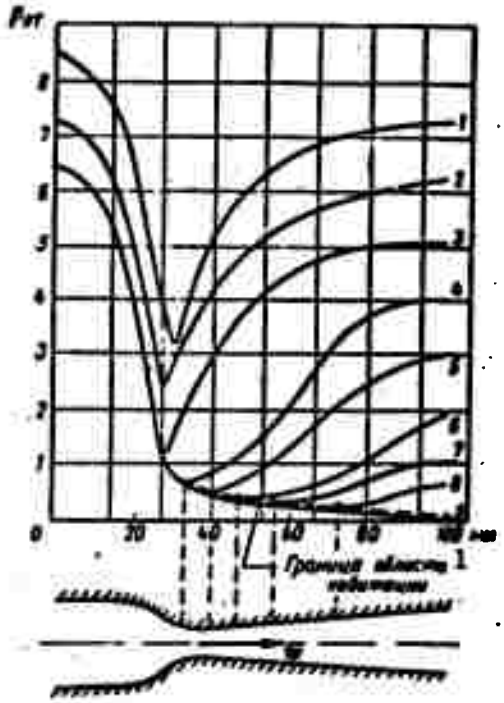


Fig. 10.1.1. Cavitation in a tube with a constriction. 1) Boundary of cavitation zone.

throat is sufficiently high, there is no cavitation and the pressure recovers almost completely (with the exception of frictional and shape variation losses). But when the pressure in the throat becomes low

enough,cavitation occurs (curves 6-9) and the pressure in the divergent section does not recover in accordance with the velocity drop since much energy has been lost. The zone of cavitation ends where the curves start rising. In Fig. 10.1.1 these zones are indicated by the dashed lines. The local change in fluid volume that accompanies the growing cavitation, the appearance of zones where the flow is separated from the body it streams around, e.g., the wing profile, leads to an increase in drag and a reduction in lift. This causes the efficiency of the turbine wheels to drop sharply. Figure 10.1.2 shows typical pump characteristics, the dashed lines indicate the normal course of the characteristics; cavitation begins at $Q = Q_k$.

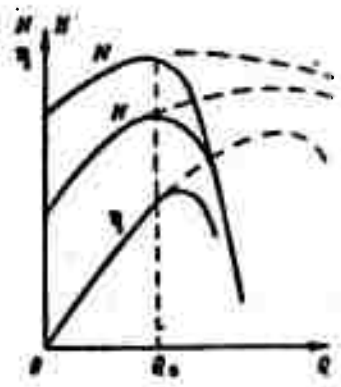


Fig. 10.1.2. Effect of cavitation on turbine characteristics..

Cavitation-induced destruction of metals. The deterioration of the operation of water-driven machines under cavitation conditions is accompanied by an unusual destruction of their working parts. Since the velocity is increased near the surfaces of the working parts, the process of bubble colapse, accompanied by local hydraulic shocks (explosions) leads to destruction of the surface of the protecting film (erosion). This process of shock destruction is accompanied by chemical destruction (corrosion) since the air separated from the water during cavitation contains more oxygen than ordinary air. Under the action of the hydraulic shock this air enriched in oxygen is pressed into the pores of the metal, which it oxidizes; and then, after the pressure has dropped, it is re-extracted. This physico-mechanical effect is accompanied by electrization (by friction), which produces ions exhibiting particularly marked chemical activity.

The combined action of all these factors destroys the surface layer of the metal. On the surface of a metal there are fine pits and grooves which are rapidly deepened and widened, thus causing individual pieces of metal to fall off. The metal assumes a spongy structure down to large depths.

The cavitation number. From the energy equation for a flow element in the steady motion of an incompressible fluid

$$p+\frac{\rho w^2}{2}=p_0+\gamma(y_0-y)+\frac{\rho w_0^2}{2}=p_{cr}+\frac{\rho w_0^2}{2}$$

we obtain

$$\frac{p_{cr}-p}{\frac{\rho w_0^2}{2}}=\frac{w^2}{w_0^2}-1. \qquad (10.1.1)$$

If the pressure p at any point of the region reaches the saturation pressure $p_{n.p}$ then cavitation will arise. As the quantity characterizing the appearance of cavitation we therefore take the number

$$K=\frac{p_{cr}-p_{n.p}}{\frac{\rho w_0^2}{2}}. \qquad (10.1.2)$$

The right hand side of Eq. (10.1.1) is determined by the motion of the flow, i.e., by the channel in the internal problem or by the shape of the body in the flow in the external problem, for example.

In the external problem the minimum pressure $p = p_{min}$ is reached at the body surface in the zone of maximum velocity w_{max}. Figure 10.1.3,a shows a vector diagram of the pressure distribution $C_p = -\frac{p-p_{cr}}{\frac{\rho w_0^2}{2}}=1-\frac{w^2}{w_0^2}$ over the wing profile for a certain definite angle of attack. In the zone where the pressure is smaller than the saturated vapor pressure cavitation may arise. For practical calculations and graphical construction it is more convenient to make use of the curve of pressure distribution at the wing profile, in which the pressures are referred to the chord's normal (Fig. 10.1.3,b).

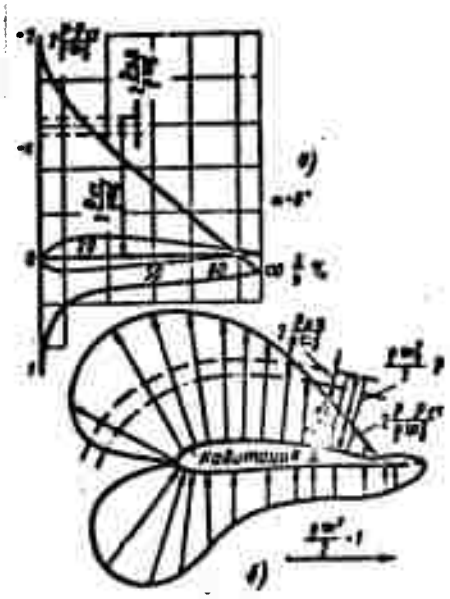


Fig. 10.1.3. Pressure distribution at the profile in the zone of cavitation. 1) Cavitation.

If we take the saturated vapor pressure to be $p_{n.p} = 0$, we find, for example, that the motion of a thin wing profile in water can be realized at a speed of 20 m/sec without cavitation if the static pressure satisfies the relation

$$p_{cr} : \frac{\rho v_0^2}{2} = \frac{2p_{cr}}{100 \cdot 10^2} = 1{,}9 \text{ or}$$

$$p_{cr} = 1{,}9 \frac{100 \cdot 10^2}{2} = 9500 \text{ kg/m}^2$$

whereas at a speed of 20 m/sec it must be equal to 38,000 kg/m^2. In the first case the velocity of 20 m/sec can be reached, for example, in a motion immediately above the free surface of water at sea level, whereas in the case of motion at 30 m/sec speed, the wing must be immersed to a depth of at least 28 m.

Influence of the air and dust content on the appearance of cavitation. One of the decisive factors determining the appearance of cavitation is the amount of air dissolved in the water. A completely degasified pure fluid with no dust impurities withstands considerable stresses and can by strongly overheated without bubbles forming.

It has been established that the process of formation of cavities in a fluid that contains dissolved gas and suspended solid impurities (dust) begins around the finest vapor or gas bubbles. The dimensions of these formation centers are very small and their presence can be observed only by raising the temperature or diminishing the pressure. Experiments indeed show that if water, for example, is subjected to a high pressure of the order of 500-1000 atm for several minutes, it no

longer cavitates under conditions under which it would have shown cavitation.

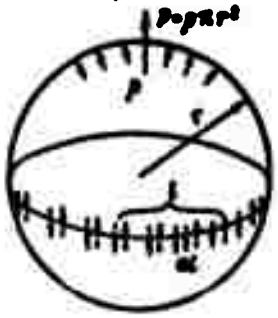


Fig. 10.1.4. Equilibrium of a spherical bubble.

The presence of suspended particles of fine dust or microorganisms facilitates the appearance of cavitation. This can be explained by the fact that the force of cohesion between fluid and dust material is smaller than the force of cohesion between the molecules of the fluid. Less energy is therefore necessary to separate the fluid from the dust particle, thus forming a microscopic cavity, than to form a like cavity in the body of the fluid.

Let us consider a spherical bubble filled with gas (Fig. 10.1.4). We think it is being cut through by a diametral plane and assume the force of surface tension acting on both semi-spheres to be equal to $2\pi r\sigma$ where σ is the coefficient of surface tension. If the gas pressure inside the bubble is denoted by p_n the force on each half of the bubble will be equal to $p_n\pi r^2$. Since the bubble is in equilibrium, $p_n\pi r^2 = 2\pi r\sigma$ and the pressure inside the bubble is $p_n = 2\sigma/r$.

On the basis of this, the critical pressure at which cavitation may arise, is determined by the relation

$$p_{cr} < p_{n.s} - \frac{2\sigma}{r}. \qquad (10.1.3)$$

Dust contained in the liquid plays the same role as air bubbles; the critical pressure is therefore determined by the same relation, if r is the radius of the non-wettable particle.

Cavitation arises especially easily at the surface of solid bodies. This can obviously be explained by the above indicated decrease in surface energy at the interface between the solid body and the fluid. Moreover, the air trapped at the surface and in the pores of solid

GRAPHIC NOT REPRODUCIBLE

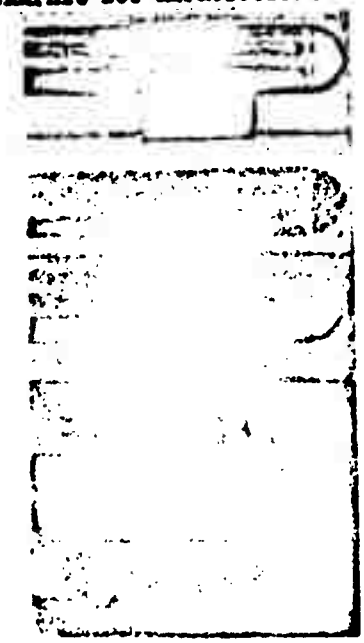


Fig. 10.1.5. Cavitation is caused by a small pressure difference, e. g., in the experiment at a pressure difference corresponding to a water column whose height was equal to the body diameter (50 mm).

bodies can easily form bubbles on the surface. This is confirmed by the fact that the presence of cohesion and friction accelerates the formation of cavities.

This surface tension effect mentioned above may, together with the pressure of the surrounding fluid, the pressure of saturation and the radius of the bubbles formed, constitute the basis of stating a dimensionless similarity criterion, σ/rp, as a characteristic of the effect. Besides this, when the cavitation is sufficiently developed, the effect is subject to a certain periodicity. If, for example, f denotes the frequency, then the dimensionless parameter fr/w has to serve as one of the criteria of dynamic similarity. Therefore, if the other factors, such as the gas content of the fluid, are left aside, the usual parameter $K=(p_{cr}-p_{n.s})\colon \frac{\rho w^2}{2}$ cannot give a full idea of such a complex process as cavitation.

Three forms of fluid motion. The first subcavitational flow regime at large values of K is single-phase flow, such as a flow of an incompressible fluid (or the flow of a gas at small Mach numbers M). As K decreases (Fig. 10.1.5), relatively few bubbles arise in the flow to begin with, but their number increases as K further decreases. This second type of flow is called the two-phase type and can be termed cavitational flow in contradistinction to the third type, the separating [illegible]ctional flow, which is obtained when K is still further decreased

and the number of bubbles has become so large that they merge to form voids which cover a part of the streamlined body. In this third type of flow a decrease in size of the voids, and the problem of the separating flow can be treated with the jet theory.

The second cavitational flow is characterized rather arbitrarily as the flow of a liquid with a relatively small number of cavitation bubbles. In the total mass of flow here the pressure distribution, with the exception of the small cavitational domains, which are sufficiently isolated from each other, is the same as in a subcavitational flow (Fig. 10.1.6).

The process of formation and disappearance of a single cavitation bubble. High-speed moving pictures make it possible to investigate the process of formation and the behavior of a single bubble of the fundamental element of the cavitation process. Direct measurements of the displacement of a bubble during its motion along a model render it possible (Fig. 10.1.7) to subdivide the whole period of time the bubble exists into the following stages: 1) production and growth to maximum diameter, 2) first disappearance and first recovery (from the first disappearance and growth to the second maximum diameter), 3) the second disappearance and the second recovery, 4) the third and sometimes fourth, fifth, and further disappearances and reappearances, and then the final disappearance.

To solve the question what the cavitation bubbles are filled with we notice that the pressure in a bubble must be very low. This follows from the fact that the zone where cavitation arises is characterized by a very small pressure difference. In fact, regarding the photographs (cf. Fig. 10.1.5) of the flow about a semi-sphere for various cavitation numbers, from top to bottom, $K = 0.62, 0.55, 0.45, 0.40, 0.31$, we can see that the cavitation zone is nonsymmetrical; it begins

above and the zone of developing cavitation is broader above. The only difference in the flow conditions consists in the hydrostatic pressure being 50 mm water column (body diameter) lower above than below. At p_{st} = 2800 kg/cm^2 (0.28 m water column) this amounts to only 1.8%. The sensitivity to such an insignificant pressure change proves that the pressure inside the bubble must be insignificant as well, namely of the order of the saturated vapor pressure at this temperature. Furthermore, a comparison of two neighboring frames shows that a slight change in pressure in the flow leads to a considerable change in the degree of cavitation.

Observations show that the bubbles can be assumed to be spherical and therefore the forces and velocities to be directed radially. Let us consider a certain fluid particle near the leading edge of the body. Since the pressure at the leading edge is higher than the static pressure of the undisturbed flow, the particle, which is moving along a streamline, receives centrifugal acceleration. As the pressure drops at the body surface (cf. Fig. 10.1.6) the acceleration decreases and at the point where the pressure is equal to the pressure of the undisturbed flow (point A) the acceleration becomes zero. The further motion of the particle must occur along a straight line that is a tangent to the body at this point. But a further pressure drop at the surface presses the particle towards the body surface. The maximum pressure difference is reached at the point where the pressure at the body surface becomes equal to the saturated vapor pressure. A bubble that separates from the body surface forms here.

The bubble formed first expands, regardless of the fact that the forces of surface tension tend to reduce its volume. Then, under the influence of the pressure increase, beginning at point C, the dimensions of the bubble diminish until it disappears completely. The bub-

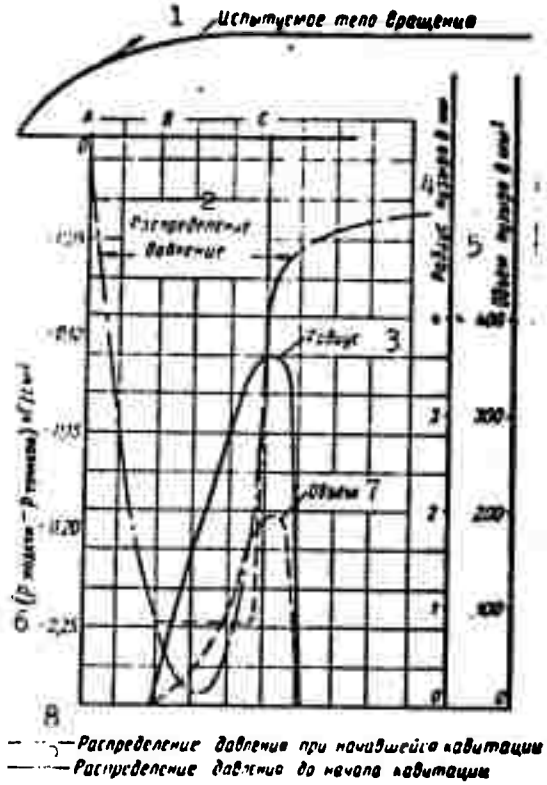


Fig. 10.1.6. Pressure distribution on a body of revolution before and after the appearance of cavitation. 1) Body of revolution under investigation; 2) pressure distribution; 3) radius; 4) bubble radius in mm; 5) bubble volume in mm^3; 6) $P_{model}-P_{tunnel}$) kg/cm^2; 7) volume; 8) pressure distribution at the beginning of cavitation; 9) pressure distribution before the beginning of cavitation.

ble then reappears and vanishes again; this process is repeated two to three times.

In answering the question what there is inside in the bubble we make some estimates. Let us assume that a bubble of radius R contains air which is given off by a layer of thickness δR around the bubble (Fig. 10.1.8). Let us suppose that the amount of air dissolved at atmospheric pressure and room temperature is equal to 2%.

Then, denoting by P_A the pressure inside the bubble, we can write the equation

$$P_A \frac{4}{3}\pi R^3 = 1 \cdot 0{,}02 \cdot 4\pi R^2 \delta R, \qquad (10.1.4)$$

whence

$$p_A = 0{,}06\frac{\delta R}{R}.$$

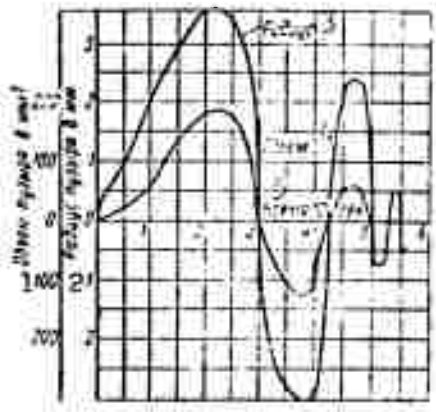


Fig. 10.1.7. Bubble dimensions as a function of time. 1) Bubble volume in mm3; 2) bubble radius in mm; 3) radius; 4) volume; 5) time, 10^{-3} sec.

Assuming that the diffusion rate of air in water amounts to 10 to 20 mm/sec, we find that after a time of 0.002 sec the thickness obtained is $\delta R \approx 0.03$ mm. For a bubble diameter of 3 mm we obtain an inside pressure of

$$p_A = 0{,}06\frac{0{,}03}{3} = 0{,}0006\ \text{atm}.$$

This pressure is much smaller than the pressure of the surrounding fluid because the assumption that the bubble should contain only air is highly improbable.

The second limiting assumption in considering the bubble as being filled with vapor at a pressure equal to the saturation pressure; this is something that can be directly verified by measuring the pressure in sufficiently large bubbles. The expansion of the bubbles obviously occurs at the expense of evaporating of fluid surrounding the bubble. In the absence of heat sources we must assume that the heat necessary for evaporation is obtained from the surrounding fluid.

Let us assume that the thickness of the fluid layer that evaporates into the bubble is equal to δR_p and let the heat needed in this process be obtained at the expense of a cooling of the layer δR_0 from the temperature T_{zh} of the fluid stream to the temperature T_p of the vapor formed and of the liquid shell adjacent to the bubble (cf. Fig. [illegible] 8,b). If we denote by γ_p the specific weight of the vapor and by γ the specific weight of the fluid, then the mass conservation law

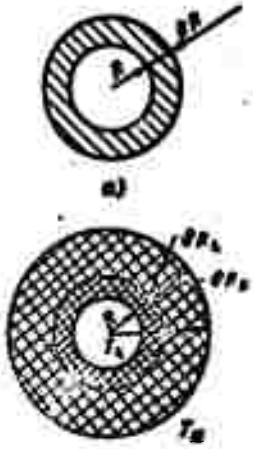


Fig. 10.1.8. Structure of cavitation bubble (schematic).

$$4\pi R^2 \delta R_0 \gamma_{ж} = \frac{4}{3}\pi R^3 \gamma_{ж}$$

leads to the relation

$$\frac{\delta R_0}{R} = \frac{\gamma_0}{3\gamma_{ж}} = \frac{v_{ж}}{3v_0},$$

where $v_{ж} = \frac{1}{\gamma_{ж}}$; $v_0 = \frac{1}{\gamma_0}$ – denote the specific volumes of fluid and vapor, respectively. In order to determine the thickness of the cooled layer, we make use of the energy equation

$$4\pi R^2 \delta R_0 c_{ж} \frac{T_{ж} - T_0}{2} = A\pi R^2 \delta R_0 Q_0,$$

where c_{zh} is the specific heat of the fluid and Q_p the specific heat of evaporation. From the latter equation we obtain

$$\delta R_0 = \delta R_0 \frac{2Q_0}{(T_{ж} - T_0)c_{ж}}. \qquad (10.1.5)$$

At room temperature (20°C) we have

$$v_{ж} = \frac{1}{1000}\ \text{m}^3/\text{kg}\quad v_0 = 57.8\ \text{m}^3/\text{kg}$$

If we assume the bubble radius to be R = 3.8 mm, this gives us the thickness of the evaporating layer as $\delta R_0 = \frac{v_{ж}}{v_0}\cdot\frac{R}{3} = \frac{1}{1000\cdot 57,8}\cdot\frac{3,8}{3} = 2,2\cdot 10^{-5}$ mm.

Under the same conditions we obtain for water

$$c_{ж} = 1\ \text{kcal/kg-°C}\quad Q_0 = 590\ \text{kcal/kg}$$

Assuming the temperature drop to be $T_{zh} - T_p = 10°$ we obtain

$$\delta R_0 = \delta R_0 \frac{2Q_0}{(T_{ж} - T_0)c_{ж}} = 2,2\cdot 10^{-5}\,\frac{2\cdot 590}{10} = 2,6\cdot 10^{-3}.$$

Thus we obtain the following dimensions: diameter of the layer giving off the air: $3\cdot 10^{-2}$ mm, thickness of the liquid layer evaporating: $2.2\cdot 10^{-5}$ mm, thickness of the layer delivering heat: $2.6\cdot 10^{-3}$ mm; if we imagine a layer two meters in diameter, then the thickness of the layer giving off air would be 16 mm, the thickness of the liquid layer evaporating would amount to $1.2\cdot 10^{-2}$ mm and the layer cooled down would be 1.2 mm thick. Comparing these values it becomes clear

that the evaporation of the liquid layer is a very natural process. This does not, however, exclude the diffusion of air, and in all probability a cavitation bubble is filled with an air-vapor mixture at saturated vapor pressure.

The collapse of a bubble. After a bubble, continually increasing in size, has reached the volume C (cf. Fig. 10.1.6) where the pressure at the body surface begins to rise, it starts growing smaller. At the first instant of the collapse the temperature of the air-vapor mixture in its interior is lower than the temperature of the surrounding liquid.

Owing to the compression suffered by the bubble on being reduced in size, the temperature of the air-vapor mixture contained in it rises because of both the compression work of the mixture and the heat of condensation of the vapor. The temperature gradient therefore changes its sign.

The graph in Fig. 10.1.7 shows the bubble size as a function of time; we can see that the collapse time is much shorter than the expansion time, and that the rate of collapse increases as the bubble size decreases. In accordance with this the condensation rate grows too. The reappearance of the bubble indicates that the kinetic energy of the fluid moving towards the center is converted to potential energy of compression of the same fluid and, very probably, partly into compression energy of the gas and noncondensed vapor.

The process of periodical appearance and disappearance of the bubble is damped because of frictional losses and heat transfer. Usually a bubble reappears 4 to 5 times, then vanishes for good. It should be remarked that a considerable part of the fluid's kinetic energy is transferred to the body at the surface of which the cavitation bubble and becomes apparent there as noise, vibration and erosion.

Cavitation damage. We must begin by pointing out that damage is always observed at the beginning of the region of pressure rise, i.e., in regions of bubble collapse (Fig. 10.1.9).

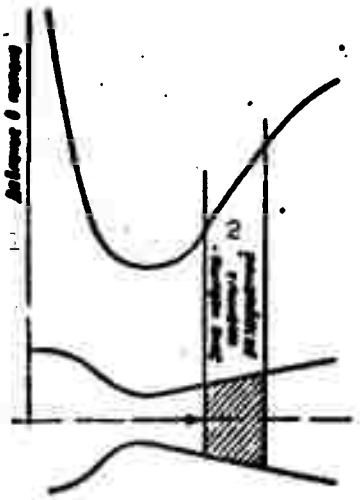


Fig. 10.1.9. Zone of cavitational disturbance with recompression. 1) Pressure in the flow; 2) zone of cavitational disturbance.

In order to estimate the amount of pressure arising as a cavitation bubble fills, we may consider the simplest mechanism of filling an empty void of radius R_0 up to a given radius r_0 (Fig. 10.1.10).

To simplify the calculations we assume that the disturbances are propagated linearly. Let δR be the width of the disturbance range and τ the time during which the density rises from the gas density (virtually zero) to a certain value ρ_1 (which corresponds to a pressure rise up to p_1). If $\underline{a}$ is the propagation rate of the disturbance, then $\tau = \delta R/a$. The fluid mass increment in the disturbance zone during the time δt ($\ll \tau$) will be

$$4\pi R^2 \Delta R \frac{\rho_1 - \rho_r}{\tau} \delta t - 4\pi R^2 a \rho_1 \delta t;$$

this mass increase occurs at the expense of fluid streaming into the disturbance zone, and therefore

$$4\pi R^2 a (\rho_1 - \rho_r) \delta t = \rho 4\pi R^2 w \delta t,$$

where ρ_1 is the density of the undisturbed fluid.

Hence $\rho_1 a = \rho w$.

The increase in velocity from the value "zero" to the value $\underline{w}$ is connected with the momentum change $\rho_m 4\pi R^2 \Delta R w$, where $\rho < \rho_m < \rho_1$, which must be equal to the impulse $p_1 4\pi R^2 \tau$ of the forces. Putting them equal, we obtain $p_1 = \rho_m a w$. Since $\rho_1 \approx \rho_m \approx \rho$, the final pressure during the

collapse will be $p_1 = \rho a w$ where w is the collapse velocity. Since $a = (E/\rho)^{1/2}$, where E is Young's modulus (for water $E = 20.9 \cdot 10^6$ kg/m^2), $p_1 = w (\rho E)^{1/2}$.

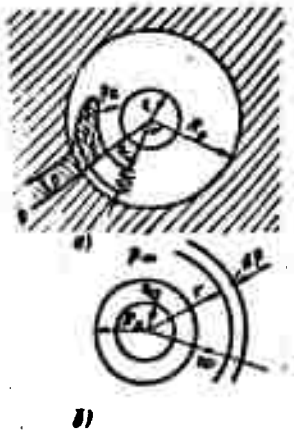


Fig. 10.1.10. For calculating the pressure during the collapse of a bubble.

It should be noted that the velocity w is found to be of the order of magnitude of sonic speed (for water $a \approx 1500$ m/sec) and hence $p_1 = 100 \cdot 1500^2 = 2.25 \cdot 10^8$ kg/m^2. The velocity at which the fluid moves during the collapse does in fact differ from sonic velocity. Apart from this it should be mentioned that in order for a surface to be damaged it is not at all necessary that a bubble should collapse on it. Calculations confirm considerable pressures arise in a certain region near a collapsing bubble.

To show this, Rayleigh considered an infinite mass of homogeneous fluid inside which a spherical volume of radius R_0 disappears suddenly. The fluid being assumed to be inviscid and incompressible, it is necessary to determine the pressure and velocity at an arbitrary point, assuming the pressure p_∞ at infinity to be constant.

If r and R are the radii of two spherical surfaces inside and outside the bubble where the fluid velocities are w and W, respectively (cf. Fig. 10.1 10), then the continuity equation yields $wr^2 = WR^2$. The kinetic energy of the fluid at a certain instant of time that corresponds to the instant when the bubble radius is just equal to R, $\frac{\rho}{2}\int_R^\infty w^2 4\pi r^2\,dr = 2\pi\rho W^2 R^3$, must be equal to the work done by the pressure forces $p_\infty \frac{4}{3}\pi(R_0^3 - R^3)$ in reducing the bubble radius from the value R_0 to R.

Thus

$$p_\infty \frac{4}{3}\pi(R_0^3 - R^3) = 2\pi\rho W^2 R^3, \quad W^2 = \frac{2p_\infty}{3\rho}\left(\frac{R_0^3}{R^3} - 1\right). \qquad (10.1.6)$$

But $W = dR/dt$ and therefore

$$t = \int_0^{R_0} \frac{dR}{W} = \sqrt{\frac{3\rho}{2p_\infty}} \int_0^{R_0} \frac{R^{3/2}}{(R_0^3 - R^3)^{1/2}}\, dR = R_0 \sqrt{\frac{3\rho}{2p_\infty}} \int_0^1 \frac{\beta^{3/2}}{\sqrt{1-\beta^3}}\, d\beta. \qquad (10.1.7)$$

where

$$\beta = \frac{R}{R_0}.$$

The total time of collapse is obtained by integrating from 0 to 1, namely

$$t_{\text{коллапс}} = R_0 \sqrt{\frac{\rho}{6p_\infty}} \frac{\Gamma\left(\frac{5}{6}\right) - \Gamma\left(\frac{1}{2}\right)}{\Gamma\left(\frac{4}{3}\right)} = 0{,}91468 R_0 \sqrt{\frac{\rho}{p_\infty}}. \qquad (10.1.8)$$

where $\Gamma(x)$ is the well-known gamma function*.

The solution obtained leads to an infinitely large velocity as $R \to 0$. This can be avoided if the solution is improved by taking the compressibility of the air-vapor mixture in the bubble into account. If the compression is assumed to be an isothermal process, the work of the pressure forces must be diminished by the gas compression work which is equal to $p_A 4\pi R_0^3 \ln \frac{R_0}{R}$. where p_A is the initial gas pressure in the bubble. From the equation

$$p_\infty \frac{4}{3}\pi R^3 \left(\frac{R_0^3}{R^3} - 1\right) - 4\pi R^3 \frac{R_0^3}{R^3} p_A \ln \frac{R_0}{R} = 2\pi\rho W^2 R^3$$

we find here

$$W^2 = \frac{2p_\infty}{\rho}\left(\frac{R_0^3}{R^3} - 1\right) - \frac{2p_A R_0^3}{\rho R^3} \ln \frac{R_0^3}{R^3}. \qquad (10.1.9)$$

The smallest bubble radius R_{min} is determined from the condition $W = 0$. If we write $R_0^3/R_{min}^3 = \alpha$, this results in

$$\frac{p_\infty}{p_A} = \frac{\alpha}{\alpha - 1} \ln \alpha$$

or

$$\alpha^{\frac{\alpha}{\alpha-1}} = e^{\frac{p_\infty}{p_A}}. \qquad (10.1.10)$$

Since p_∞/p_A is a rather large quantity, α will be very large and

we can therefore replace (10.1.10) by

$$a = e^{\rho - \varphi_A}. \qquad (10.1.11)$$

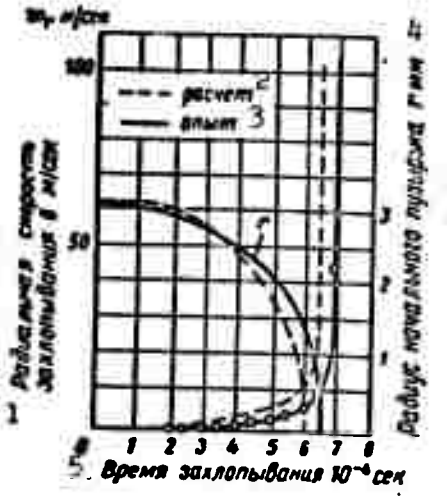


Fig. 10.1.11. Comparison of the calculated bubble radius and the calculated bubble radius and the calculated velocity with the measured values. 1) Radial collapse velocity in m/sec; 2) calculation; 3) experiment; 4) initial bubble radius in mm; 5) duration of collapse, 10^{-4} sec.

The agreement of calculated and measured values of the bubble radius as a function of time is sufficiently good (Fig. 10.1.11).

The pressure is determined from the equation of motion assuming that the empty bubbles are spherical in shape and that the velocity and acceleration are therefore both directed radially:

$$\frac{dw}{dt} = \frac{\partial w}{\partial t} + w\frac{\partial w}{\partial r} = -\frac{1}{\rho}\frac{\partial p}{\partial r}. \qquad (10.1.12)$$

From the continuity equation we have $wr^2 = WR^2$.

Without giving the calculations we can write down the result:

$$\frac{p_{max}}{p_\infty} = 1 + \frac{a-4}{3}\sqrt[3]{\frac{a-4}{4(a-1)}} - \frac{a-1}{3}\left(\frac{a-1}{4a-4}\right)^3 = 1 + \frac{(a-4)^{4/3}}{4^{4/3}(a-1)^{1/3}}. \qquad (10.1.13)$$

For $R \to 0$ (α) is large and

$$\frac{p_{max}}{p_\infty} = \frac{e}{4^{1/3}} = 0.158\frac{R_0^3}{R^3}. \qquad (10.1.14)$$

If we substitute the values of W found with Eq. (10.1.6) into the expression for $p_1 = W(\rho E)^{1/2}$ we obtain for the momentary pressure on a rigid sphere of radius:

$$\frac{p_1}{p_\infty} = \sqrt{\frac{2}{3}\frac{E}{p_\infty}}\sqrt{\frac{R_0^3}{R^3} - 1}. \qquad (10.1.15)$$

The following table gives the values of velocity and pressure calculated with (10.1.6), (10.1.13) and (10.1.14).

$R_0 : R$	W [1] no (10.1.6)	$\frac{p_{max}}{p_\infty}$ (no 10.1.13)	$\frac{p_{max}}{p_\infty}$ no (10.1.14)
3	57	8	800
5	130	40	1700
10	580	300	5500
20	1000	2500	14500
50	4000	40000	57000

1) According to.

The values of the calculated and experimental collapse velocities are shown in Fig. 10.1.11. The divergences observed can be explained by the fact that the calculations did not take the compressibility into account, which results in a shortening of the time and in an increase in velocity.

Influence of surface tension and viscosity. The forces of surface tension exert a considerable influence on the process of bubble collapse.

Taking the tension forces on the basis of [10.1.3] into account leads to the following relations. For bubbles filled with vapor at a pressure p_p, the hydrostatic pressure of the surrounding fluid being p_0

$$\frac{\rho}{p_0} = \sqrt{\frac{2}{3}\frac{R_0^3}{R^3}}\sqrt{\left[\left(1 - \frac{p_p}{p_0}\right) + \frac{3\sigma}{p_0 R_0}\right]\frac{E}{p_0}}.$$

We see from this formula that the collapse may occur without considerable changes in the external fluid pressure, only under the influence of the surface tension forces, where $p_0 = p_p$ and

$$p = \sqrt{\frac{2R_0^3}{R^3} \cdot \varepsilon p_0}.$$

If the bubbles are assumed to be filled with air at a pressure p_A then

$$\frac{p}{p_A} = \left\{\frac{1}{p_A}\left[p_A + 1.2\left(\frac{p_0}{3} + \frac{\sigma}{R_0}\right)\right]\right\}^{3.5}.$$

The pressures calculated theoretically are too high, which raises the question why the cavitational destruction does not process much faster in reality. This may perhaps be explained by the fact that the latent heat of condensation which is set free on the process of bubble collapse reduces the shock pressure. Moreover, the viscosity of the fluid should be taken into account.

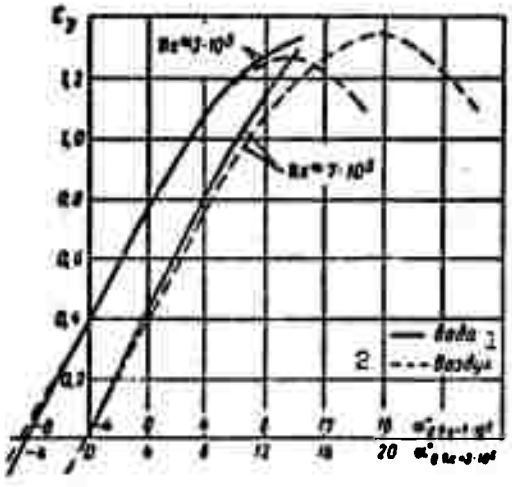


Fig. 10.1.12. Profile characteristic according to data obtained by testing it in water and air. 1) Water; 2) air.

Cavitation on hydrodynamic profiles. Going over to the problem of the behavior of a wing profile under calvitation conditions we should first of all point out that there are very few experimental studies in

this field. This is mainly due to the difficulties arising in performing experiments on effects which last thousandths or tenthousandths of a second. Under the conditions of developing cavitation the flow becomes unsteady and the forces acting on the model are subject to very intense fluctuations. The experimental conditions are still more complicated when a profile in a lattice is under investigation.



Fig. 10.1.13. Calculation of cavitation according to a profile characteristic obtained in a wind tunnel test. 1) Cavitation on the lower surface; 2) calculated from the pressure distribution obtained in a wind tunnel test; 3) cavitation on the upper surface.

From the point of view of hydrodynamics, the flow and the conditions of a fluid flow about the body before cavitation sets in are equivalent to the flow about the same body of a gas at small Mach numbers M (M = w/a, where w is the flow velocity and a the velocity of sound). The availability of much experimental material from wind tunnel tests on various profiles and the great simplicity of such tests renders extremely important the problem of determining the beginning of the cavitation on a profile in a liquid from data obtained on testing this profile in air.

The profile characteristics C_y and C_x as functions of the angle of attack obtained in tests in water under conditions that exclude the possibility of cavitation, at Re = $2.87 \cdot 10^5$ and $7.3 \cdot 10^5$, and in air at Re = $3.31 \cdot 10^5$ and $6.38 \cdot 10^5$ are shown in Fig. 10.1.12. The main data

obtained in the tests are given in a table (see below).

The values of the parameter $K=\frac{p_{ст}-p_{min}}{\frac{\rho w_0^2}{2}}$, at which cavitation sets in are shown as functions of the angle of attack in Fig. 10.1.13. The values of the cavitation number K_p, determined from the pressure distribution curve obtained in a wind tunnel test are plotted on the same graph:

$$K_p=\frac{p_{ст}-p_{min}}{\frac{\rho w_0^2}{2}}.$$

Среда 1	$Re=\frac{wl}{\nu}$	Угол атаки нуля подъемной силы α_0 5	Наклон кривой подъемной силы по α $\frac{dC_y}{d\alpha_0}$ 6	$C_{y\,max}$	$C_{x\,min}$	C_{m0}
Воздух 2	$3{,}31\cdot10^5$	24,35	0,094	1,27	0,011	—0,096
	$6{,}38\cdot10^5$	—4,25	0,094	1,36	0,012	—0,094
Вода 3	$2{,}87\cdot10^5$	—3,95	0,098	1,36	0,014	—0,102
	$5{,}63\cdot10^5$	—4,05	0,102	1,39	0,013	—0,101
	$7{,}30\cdot10^5$	—4,15	0,104	—	0,0105	—0,102
	$9{,}03\cdot10^5$	—4,25	0,106	—	0,011	—0,101
Теория 4	—	—4,58	0,120	—	—	—0,137

1) Medium; 2) air; 3) water; 4) theory; 5) zero lift angle of attack, α_0; 6) slope of lifting line with respect to α.

As can be seen, the agreement is quite good for angles of attack between -2 and $+8°$.

It should be noticed that cavitational erosion occurs in the initial stage of cavitation, i.e., when the individual bubbles collapse near or at the body surface. In the further stages, the bubbles collapse sufficiently far from the body not to destroy its surface.

REFERENCES

10.1.1. Prandtl', L., Gidroaeromekhanika [Hydroaerodynamics], IL [Foreign Literature Press], 1951.

10.1.2. Kvyatkovskiy, V.S., Rabochiy protsess osevoy gidroturbiny [Work Cycle of the Axial Hydroturbine], Trudy VIGM [Trans. All-Union Institute of Hydromachinery], XIV, 1951.

10.1.3. Knapp, R.T., Cavitation Mechanics and Its Relation to the Design of Hydraulic Equipment. Inst. of Mech. Eng. Proc. A, Vol. 166, No. 2, 1952.

10.2. ATOMIZATION OF A FLUID

Atomization denotes the disintegration of a fluid jet into very fine particles. The degree of atomization plays an important part in bringing about the combustion process.

Disintegration of a jet. This is caused by the action of aerodynamic forces which are external with respect to the jet, and internal forces which are connected with the turbulence of the flow.

Let us consider a fluid jet at low discharge velocity (Fig. 10.2.1,a). Under the action of the surface tension forces arising at the nozzle exit, oscillations arise in the jet which thus loses stability and disintegrates into drops (cf. Fig. 10.2.1,b). As the discharge velocity increases, the jet becomes curved and the pulsations causing its disintegration into large drops increase. Then, under the influence of the aerodynamic forces, these drops are split up into finer ones – this being the secondary disintegration (Fig. 10.2.2).

When the discharge velocity is raised further, then, under the action of the aerodynamic drag forces of the medium into which the fluid to be sprayed is injected, it assumes the form of a torch right behind the nozzle exit (Fig. 10.2.3); we notice a central zone (the core) I, containing the large drops, and a zone II which consists of fine drops and thin filaments which easily disintegrate into droplets.

NOT REPRODUCIBLE

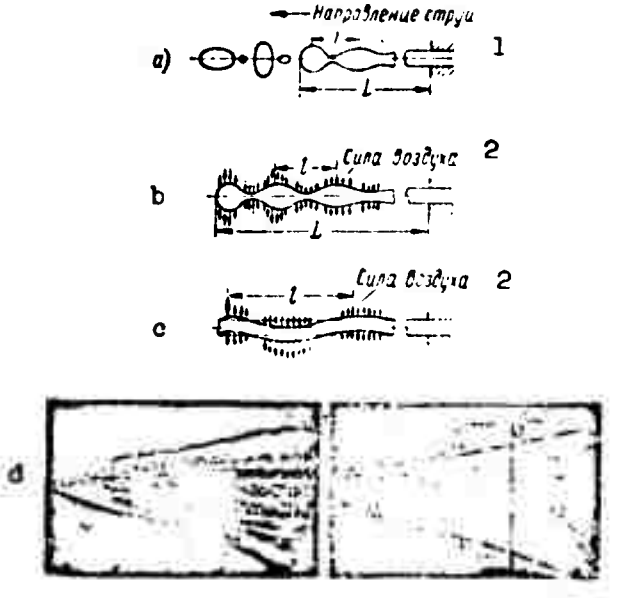


Fig. 10.2.1. Schematic representation of the disintegration of a jet: a) Drop formation without jet; b) the jet disintegrates into drops as a consequence of oscillations caused by initial disturbances in the nozzle; the aerodynamic forces enhance the amplitudes of the oscillations; c) the jet disintegrates under the influence of wavelike oscillations; d) at large discharge velocities the fluid disintegrates at once into fine droplets – the spray torch is formed. 1) Direction of jet; 2) aerodynamic force.

The spraying angle α increases with increasing discharge velocity.

We may observe four characteristic forms of jet disintegration.

At relatively small discharge velocities of the liquid into the surrounding medium the jet disintegrates mainly under the influence of a static instability caused by the surface tension forces. In practice the aerodynamic drag forces of the medium have no influence on the

APHIC NOT REPRODUCIBLE

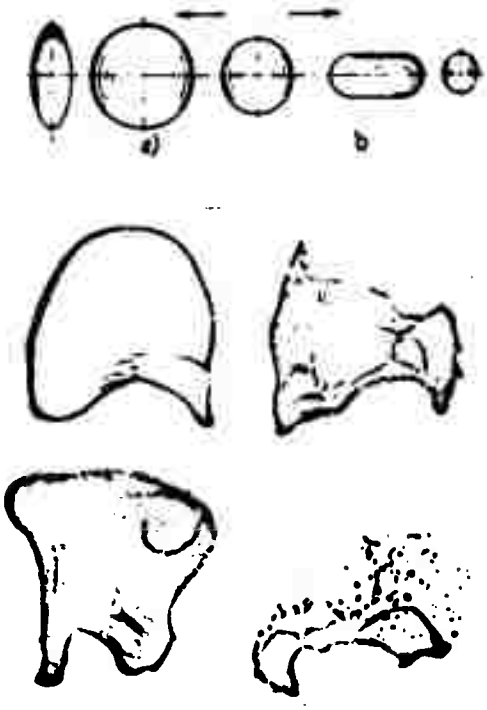


Fig. 10.2.2. Destruction of drops by the air stream. Scheme of drop: the drop is flattened to a disc with round edges (a) and then elongated to a cylinder with spherical ends (b).

disintegration of the jet. The jet remains continuous if the ratio of wavelength $\frac{l}{}$ to jet diameter D does not exceed a certain value. According to Rayleigh, the jet disintegrates into drops if

$$\frac{l}{D}=\sqrt{2}\pi\sqrt{1+3\sqrt{\frac{\mu^2}{\rho\sigma D}}}. \qquad (10.2.1)$$

Here μ is the absolute viscosity (g-sec/cm^2); ρ is the mass density (g-sec^2/cm^4); σ is the surface tension (g/cm).

For this mode of disintegration it is characteristic that the drop dimensions do not change after the disintegration of the jet and there is no secondary break up. The drops formed keep the direction of motion of the jet and perform oscillations; at times they thicken, at times they flatten (cf. Fig. 10.2.1,a). By virtue of the large inter-

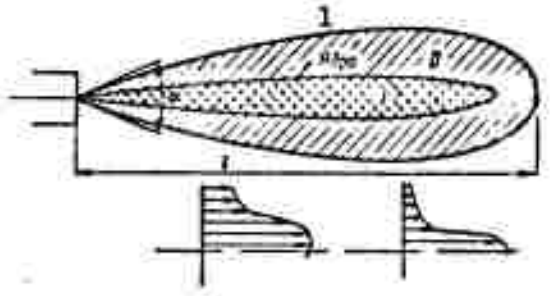


Fig. 10.2.3. Structure of a fluid spray torch consisting of the core I containing the large drops, and of the zone II containing small droplets and fine filaments. 1) Core.

nal friction the oscillations of the drops of a viscuous fluid are strongly damped. It should be kept in mind that the quality of treatment of the working nozzle surface has a great influence on the length of the continuous part of the jet and on the instant at which disintegration sets in.

As the discharge velocity increases the aerodynamic forces begin to act, giving rise to the second mode of disintegration. The action of the aerodynamic forces is shown schematically in Fig. 10.2.1,b.

The third mode of disintegration is observed at still higher velocities – the fluid jet begins to perform wavelike oscillations which lead to disintegration (cf. Fig. 10.2.1,c).

The fourth mode of disintegration – atomization – occurs when the discharge velocity is raised further (above 100 m/sec for kerosene). The disintegration of the fluid jet begins at the nozzle exit itself (cf. Fig. 10.2.1,d).

The pressure of the medium into which the discharge occurs has a great influence on the process of atomization; the higher it is, the more intense is the disintegration.

Figure 10.2.4 illustrates the limits of discharge velocities as dependent on the counterpressure for one grade of fuel.



Fig. 10.2.4. The limits of the various modes of disintegration. The calculated curves are obtained with the equation $w = w_1 \rho_1/\rho$, the counterpressure being p_1; ρ and ρ_1 are the corresponding air densities; x = 2 for Curve 1, x = 3 for Curve 2 and x = 2.7 for Curve 3. 1) Experimental data for w, calculated data; 2) zone of atomization; 3) zone of formation of wavy surface; 4) zone of disintegration; 5) m/sec; 6) atm.

The second, third and fourth modes of disintegration of the jet are connected with the secondary break up, i.e., under the action of the aerodynamic forces the drops formed are broken up into finer droplets.

The final drop dimensions when a fluid is atomized under the action of the aerodynamic forces are virtually independent of the conditions of primary disintegration and are determined by the conditions of the secondary break up, namely the relative velocity, the density of the surrounding medium and the physical properties of the fluid.

The similarity criteria. Owing to the complexity of the effect of fluid atomization we must resort to investigating it experimentally, making use of the theory of similarity. When the characteristic dimension is denoted by $\underline{l}$, the forces participating in the effect will be the aerodynamic forces of the fluid, $\sim\rho_{zh}w_{zh}^2\underline{l}^2$, and of the gas, $\sim\rho_g w_g^2\underline{l}^2$, the viscous forces, $\sim\mu w\underline{l}$, and the surface tension forces, $\sim\sigma\underline{l}$. Therefore, apart from the Reynolds criteria $\frac{\rho w_{zh}\underline{l}}{\mu_{zh}}$, $\frac{\rho_g w_g \underline{l}}{\mu_g}$, one of the similarity criteria will be the number determining the order of magnitude of the surface tension forces relative, for example, to the aerodynamic forces, $We = \sigma/\rho_{zh}w^2\underline{l}$. The influence of the aerodynamic forces (air) can be taken into account by the ratio ρ_g/ρ_{zh}; the dimensionless com-

bination $\mu^2/\sigma\rho l$ entering Rayleigh. Formula (10.2.1) may be regarded as a similarity criterion, equal to $1/(Re^2/We) = \mu^2/\sigma\rho l$.

Thus, for example, if we denote by d the mean jet diameter, then

$$\frac{d}{l} = \left(\frac{\sigma}{\rho_{\infty} w^2 l}, \frac{\mu_{\infty}^2}{\sigma\rho l}, \frac{\rho_r}{\rho_{\infty}}\right). \qquad (10.2.2)$$

At large Re numbers the influence of the viscous forces is small, in the same way that at large ratios ρ_{zh}/ρ_g the influence of this ratio is small and the disintegration process is described by the simplified relation

$$\frac{d}{l} = f\left(\frac{\sigma}{\rho w^2 l}\right). \qquad (10.2.3)$$

The maximum drop diameter. It is determined from the supposition [10.2.4] that the product of the function of the determining criteria (where the characteristic diameter is $l = D_{max}$) is a constant quantity

$$Z_1\left(\frac{\sigma}{\rho_{\infty} w^2 D_{\infty}}\right) Z_2\left(\frac{\mu_{\infty}^2}{\sigma\rho_{\infty} D_{\infty}}\right) Z_3\left(\frac{\rho_r}{\rho_{\infty}}\right) = \text{const}. \qquad (10.2.4)$$

Experiment shows that $D_{max} \sim 1/w^2$. Hence, supposing that the function Z_1 is the first power of the argument, we can put $Z_1 = \sigma/\rho_{zh} \cdot w^2 D_{zh}$.

According to Rayleigh, the ratio of the drop diameters on the disintegration of jets of inviscid and viscous fluids of equal density is

$$\frac{D_0}{D_c} = \sqrt[6]{1 + 3\sqrt{\frac{\mu_{\infty}^2}{\sigma\rho_{\infty} D_1}}}. \qquad (10.2.5)$$

If we further take into account that $D_{max} \to 0$ if $\sigma \to 0$ and $D_{max} > 0$ if $\mu_{zh} \to 0$, then we can take for Z_2 a relation of the form

$$Z_2 = \left(1 + a_1 \frac{\mu_{\infty}}{\sigma\rho_{\infty} D}\right)^{\frac{1}{12}}.$$

As has already been shown, the influence of the ratio ρ_g/ρ_{zh} is small and if we take into account that $D_{zh} > 0$ if $\rho_g \to 0$, then, with

$z_3 = 1 - \alpha_2 \rho_g/\rho_{zh}$, we obtain the equation for determining D_{max}

$$\frac{\sigma}{\rho w^2 D_m} = \left(1 + a_1 \frac{\mu_m^2}{\sigma \rho_m D_m}\right)^{\frac{1}{12}} \left(1 - a_2 \frac{\rho_r}{\rho_m}\right) = K. \qquad (10.2.6)$$

Evaluation of experimental results yields the values of the constants

$$K = 4{,}8 \cdot 10^{-1}, \quad a_1 = 10^4, \quad a_2 = 0{,}5. \qquad (10.2.7)$$

The drop size can also be estimated under the assumption that the break-up of large drops sets in when the drag becomes equal to the surface tension

$$\sigma \pi D_m = \frac{\pi D^2}{4} \frac{\rho_r w^2}{2} c_x;$$

whence

$$\frac{\sigma}{\rho_m w^2 D_m} = \frac{c_x}{A} = \frac{f(\mathrm{Re})}{A} \quad (A = \mathrm{const}). \qquad (10.2.8)$$

Figure 10.2.5 shows the function $C_x = f(Re)$ for a sphere. Experiments [10.2.1] show that A = 5.6 for the upper limit of stability (break-up of 100% of the drops) and A = 4.0 for the lower limit (break-up of 10% of the drops).

Figure 10.2.2 depicts various forms of deformation of a spherical drop. The drop is either flattened to a disc or extended to a cylinder. The second variant is more probable since the cylindrical form is less sensitive to disturbances in symmetry. The fluid's viscosity obviously does not influence the mode of deformation of a drop.

When the surface tension is low and the drop dimensions large, the deformation at individual points of the drop surface will be proportional to the aerodynamic pressure which (Fig. 10.2.6) causes its deformation and, together with this, changes the pressure distribution. A drop which is deformed assumes the shape of a thin-walled cupola which is rapidly destroyed (cg. Fig. 10.2.2).

Size distribution of the drops. The size distribution of the

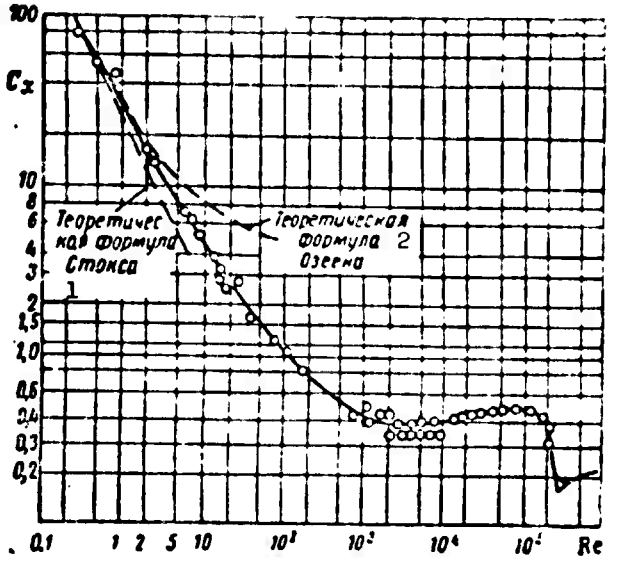


Fig. 10.2.5. Drag coefficient $C_x = f(Re)$ for a ball. 1) Theoretical formula of Stokes; 2) theoretical formula of Ozeyen.

drops can be investigated by means of statistical methods [10.2.4]. For this purpose we suppose that all the fluid disintegrates into N molecules, each of the volume V, which, joined to a drop, are distributed over k-cells in such a way that in the cell $\underline{i}$ of volume Q_i there are N_i molecules which form a drop whose diameter lies between D_i and $D_i + dD$. The distribution of molecules will be the same if they all exchange their positions; the number of permutations is N! Taking into account that this number includes the combinations in which the molecular positions in one and the same cell are exchanged (and this gives no new possibilities), we obtain the number of possible ways of achieving a given distribution in the form

$$\frac{N!}{N_1!N_2!\ldots N_k!}. \qquad (10.2.9)$$

According to the theorem of multiplying the probabilities of independent events the probability of this distribution will be

$$P = \frac{N!}{N_1!N_2!\ldots N_k!}. \qquad (10.2.10)$$

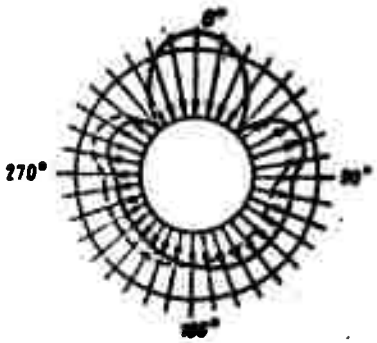


Fig. 10.2.6. Pressure diagram for flow about a sphere.

Applying Stirling's formula in N! = N ln N and going over to the logarithm of the probability, we obtain

$$\ln P = N \ln N - \sum_{i=1}^{n} N_i \ln N_i. \qquad (10.2.11)$$

Let us determine the most probable distribution, which corresponds to the maximum of this function, taking into account that the total volume of the fluid and the total surface of the drop during the exchange process, where $V = \Sigma V_1 = \text{const}$ are independent of the distribution and must be constant

$$V = \sum_{i=1}^{n} V_i = \text{const}, \quad A = \sum_{i=1}^{n} A_i V_i = \text{const}, \qquad (10.2.12)$$

where A_1 is the surface of a cell of unit volume ($V_1 = 1$). Let us introduce the function g_0 of the fluid volume density in the cell volume

$$g_i = V_i : Q_i.$$

Then, denoting by v the volume of one molecule, we obtain

$$\left.\begin{aligned} \ln P &= \frac{V}{v}\ln\frac{V}{v} - \sum_{i=1}^{n}\frac{g_i Q_i}{v}\ln\frac{g_i Q_i}{v} \\ \sum V_i &= \sum g_i Q_i = \text{const}\ (*); \quad \sum A_i g_i Q_i = \text{const}\ (**). \end{aligned}\right\} \qquad (10.2.13)$$

on condition that

Putting the first variation of this equation equal to Condition (10.2.13) and equating it to zero, we obtain

$$-\delta \ln P = \sum \delta g_i \frac{Q_i}{v}\ln\frac{g_i Q_i}{v} + \sum\frac{Q_i}{v}\delta g_i + \frac{\alpha}{v}\sum \delta g_i Q_i + \frac{\beta}{v}\sum A_i Q_i \delta g_i = 0, \text{ where } \alpha \text{ and } \beta \text{ are constants.}$$

The variation of g_1 in the k-th cell is equivalent to all variations of g_1 except that where i = k, which is zero, and yields the equation

$$\delta g_k Q_k\left[\frac{\ln\left(g_k\frac{Q_k}{V_k}\right)}{v} + \frac{1}{v} + \frac{\alpha}{v} + \frac{\beta}{v}a_k\right] = 0,$$

for $v = 1$, returning to the subscript i,

$$\ln \frac{g_i Q_i}{V_i} + 1 + \alpha + \beta A_i = 0$$

and finally

$$g_i = \frac{v}{Q_i} e^{-(1+\alpha+\beta A_i)} = C_1 e^{-\beta A_i} \quad C_1 = \frac{v}{Q_i} e^{-(1+\alpha)}. \tag{10.2.14}$$

The function g_i obtained shows how the molecules are distributed in the cell Q_i.

The N_i molecules found in the i-th cell must form H_i spheres of the diameter D_i, which gives the equation

$$V_i = n_i \frac{\pi}{6} D_i^3, \quad g_i = \frac{\pi}{6} \frac{n_i}{Q_i} D_i^3 = h_i \frac{\pi}{6} D_i^3, \tag{10.2.15}$$

where $h_i = n_i/Q_i$ is the frequency function for the number of drops, which is analogous to the function g_i. Comparing (10.2.14) and (10.2.15) and solving with respect to h_i, we obtain

$$n_i = C_1 e^{-\beta Q_i} D^{-3}. \tag{10.2.16}$$

The total number of drops within the limits $0 \leq D \leq D_{max}$ will be

$$n_0 = C_1 \int_0^{D_{max}} e^{-\beta Q_i} D^{-3} dQ_i. \tag{10.2.17}$$

Normalizing Eq. (10.2.16) ... tain

$$\frac{dn}{n} = \frac{e^{-\beta Q_i} D^{-3} dQ_i}{\int_0^{D_{max}} e^{-\beta Q_i} D^{-3} dQ_i}. \tag{10.2.18}$$

In order to determine the surface area of a cell of unit volume we write

$$V_i = n_i \frac{\pi}{6} D_i^3, \quad A_i = \frac{V_i}{Q_i} = \frac{6}{D_i}. \tag{10.2.19}$$

On transition from cell to cell there are three possibilities - the volume, surface area or diameter of the drop may increase by a constant amount; experience shows that it is the diameter increase which takes place, i.e., $Q_i \sim \delta D$. Therefore, replacing dQ_i by dD and taking into account that $a_i = 6/D_i$, we obtain the frequency curve for

the number of drops

$$\frac{dn}{n_0} = \frac{e^{-\frac{\beta}{D_1}D^{-3}dD}}{\int_0^{D_{max}} e^{-\frac{\beta}{D}D^{-3}dD}} \qquad (10.2.20)$$

or, assuming $x = D : D_{max}$, $\tilde{\beta} = 6\beta : D_{max}$,

$$\frac{1}{n_0}\frac{dn}{dx} = \frac{e^{-\frac{\tilde{\beta}}{x}}}{x^3 \int_0^{D_{max}} e^{-(\tilde{\beta}:x)D^{-3}}dD}. \qquad (10.2.21)$$

This equation contains only one constant which has to be determined by experiment. Figure 10.2.7 is a graphical representation of this function for $\beta = 0.35$.

The drop trajectory. It is most simply calculated in a coordinate system moving along with the air stream [10.2.2].

Let us write the equation of motion, neglecting gravity and taking the x-axis as coincident with the velocity w_p of the surrounding flow (Fig. 10.2.8):

$$\frac{dw_x}{dt} = -\frac{R}{m}\cos\alpha, \quad \frac{dw_y}{dt} = -\frac{R}{m}\sin\alpha, \qquad (10.2.22)$$

where m is the drop mass and $R = C \frac{\rho w^2}{2}\frac{\pi D^2}{4}$ is the drag of the drop, which is directed oppositely to the velocity.

For a spherical drop at large Re numbers the coefficient C depends slightly on Re (cf. Fig. 10.2.5) and can be regarded as constant; here

$$\frac{dw_x}{dt} = -\frac{3}{4}\frac{C}{D}\frac{\rho_r}{\rho_m}\frac{w_x^2}{\cos\alpha}, \quad \frac{dw_y}{dt} = -\frac{3}{4}\frac{C}{D}\frac{\rho_r}{\rho_m}\frac{w_y^2}{\sin\alpha}.$$

Writing $l = \frac{4}{3}\frac{\rho_m}{\rho_r}\frac{D}{C}$, we obtain a simple form of the equation of motion

$$\frac{dw_x}{dt} = -\frac{w_x^2}{l\cos\alpha}, \quad \frac{dw_y}{dt} = -\frac{w_y^2}{l\sin\alpha}. \qquad (10.2.23)$$

The solution of this set will be

$$\frac{w_x}{w_x} = 1 + \frac{w_x t}{l\cos\alpha}, \quad \frac{}{w_y} = 1 + \frac{w_y t}{l\sin\alpha}, \qquad (10.2.24)$$

where u_x, u_y are the velocity components of the drop at the sprayer outlet. A second integration and transition to a fixed coordinate system yields the path of motion in parametric form

$$\left.\begin{aligned} x &= l\cos\alpha \ln\left(1+\frac{u_x+w_a}{l\cos\alpha}t\right)-w_a t = \\ &= l\cos\alpha\ln\left(1+\frac{a}{l}t\right)-w_a t. \\ y &= l\sin\alpha\ln\left(1+\frac{u_y}{l\cos\alpha}t\right)=l\sin\alpha\ln\left(1+\frac{a}{l}t\right). \end{aligned}\right\} \quad (10.2.25)$$

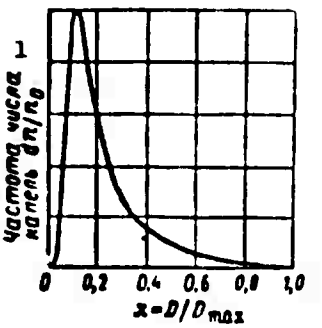


Fig. 10.2.7. Frequency curve (dimensionless) of the number of drops for $\beta = 0.35$. 1) Frequency of number of drops dn/n_0.

where

$$a=\sqrt{(u_x^2+w_a^2)^2+u_y^2}\,;\quad u_x+w_a=a\cos\varepsilon\,;\quad u_y=a\sin\varepsilon.$$

Let us call the region where the x-component of the velocity of the drop is equal to zero in the moving coordinate system the annular zone. In a coordinate system moving along with the flow, $w_x = w_p$ for the annular zone. The time of flight along it is according to (10.2.24)

$$t_a=\left(\frac{u_x+w_a}{w_a}-1\right)\frac{l\cos\alpha}{u_x+w_a}=\frac{u_x}{a}\frac{l}{w_a}. \quad (10.2.26)$$

The dimensions of the annular zone are obtained after substituting (10.2.26) into (10.2.25);

$$L=l\left[\cos\alpha\ln\left(1+\frac{u_x}{w_a}\right)-\frac{u_x}{a}\right],\quad R=l\sin\alpha\ln\left(1+\frac{u_x}{w_a}\right). \quad (10.2.27)$$

The effective spraying angle is

$$\operatorname{ctg}\frac{\varepsilon}{2}=\frac{L}{R}. \quad (10.2.28)$$

Centrifugal atomizers (Fig. 10.2.9). Centrifugal atomizers are widely used at present; they are characterized by tangential supply of the fluid to the lateral surface of a cylindrical chamber and subsequent motion of the fluid along a convergent spiral. The cylindrical part of the chamber tapers smoothly on one side to the dimensions of the outlet nozzle arranged at the center. The fluid passing through the

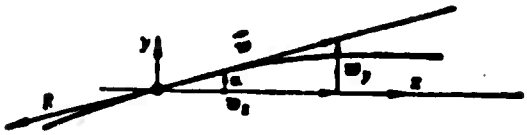


Fig. 10.2.8. For determining the trajectory of a drop.

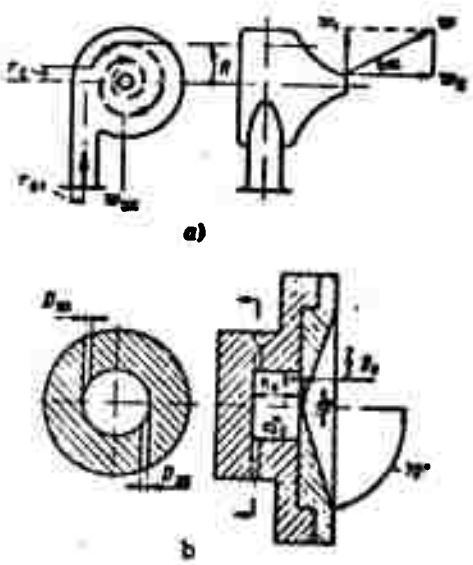
atomizer therefore executes rotational motion. When the fluid leaves the nozzle it flies off along straight radii. The angle of the spray lines is determined by the ratio

$$\operatorname{tg}\alpha=\frac{w_t}{w_0}. \qquad (10.2.29)$$

Neglecting gravitational forces, we can write the momentum conservation law as

$$w_{vkh}R=w_t r, \qquad (10.2.30)$$

where w_{vkh} is the velocity at the sprayer inlet, at the radius R, and w_t is the tangential component at the radius r of the sprayer exit.



a)

b

Fig. 10.2.9. Centrifugal atomizer: Schematic diagram (a) and plan of an experimental centrifugal atomizer (b).

The outlet pressure is given according to the Bernoulli equation by

$$p=H-\rho\frac{w_0^2+w_t^2}{2}\quad\left(H=p_{vx}+\frac{\rho w_{vx}^2}{2}=\text{const}\right) \qquad (10.2.31)$$

which, since $w_t \to \infty$ and $p \to -\infty$ as $r \to 0$, is impossible. In fact, as

the distance to the axis decreases, the velocity increases and the pressure drops only until it becomes equal to atmospheric pressure. Since this central region communicates with the atmosphere there will be an air vortex and the discharge occurs through an annular cross section which is bounded by circles of the nozzle radius r_c and the vortex radius r_v. The cross section of the fluid jet will be

$$A_ж = \pi(r_c^2 - r_в^2) = \varphi\pi r_c^2, \quad \varphi = 1 - \frac{r_в^2}{r_c^2}. \tag{10.2.32}$$

Considering the motion of a fluid element at the outlet cross section of the nozzle, and assuming the layer thickness to be unity, we can write:

$$r\,d\vartheta\,dp = \frac{\rho w_t^2}{r}\,dm; \quad dm = \rho r\,d\vartheta\,dr; \quad w_t r = w_{t_0} r_0. \tag{*}$$

whence

$$dp = \frac{\rho w_t^2}{r}\,dr = -\rho w_t\,dw_t; \quad p = -\frac{\rho w_t^2}{r} + \text{const}.$$

Since at the vortex boundary $w_t = w_{t\,v}$ the excess pressure is

$$p = \frac{\rho w_{t_0}^2}{2} - \frac{\rho w_t^2}{2}. \tag{10.2.33}$$

Substituting this into Eq. (10.2.31) we find that the axial velocity at the nozzle exit cross section is constant and satisfies the equation

$$\frac{\rho w_c^2}{2} = H - \frac{\rho w_{t_0}^2}{2}. \tag{10.2.34}$$

The fluid flow rate per second is

$$V = w_e A_ж = w_a \varphi \pi r_c^2 = w_0 \pi r_c^2 = w_{0x} \pi r_{0x}^2.$$

where $w_e = \varphi w_a$ is the equivalent velocity.

This gives

$$w_0 = w_e \frac{r_c^2}{r_{0x}^2}. \tag{10.2.35}$$

If we assume that for every particle at the inlet R is the same and equal to R_v the momentum Eq. (*) gives us

$$w_t = w_0 \frac{R_{ss}}{r} \frac{r_c^2}{r_0^2}, \quad w_{tc} = w_0 \frac{r_c^2}{r_{ss}^2}, \quad w_{t0} = w_0 \frac{R_{ss} r_c}{r_{ss}^2} \frac{1}{\sqrt{1-\varphi}}. \qquad (10.2.36)$$

Substituting the expression for the tangential velocity $w_{t\,v}$ at the vortex Boundary (10.2.36) and $w_e = \varphi w_a$ into (10.2.34), we find

$$\left.\begin{aligned} H &= \frac{w_0^2}{2}\left[\frac{1}{\varphi^2} + \frac{R_{ss} r_c^2}{r_{ss}^2 (1-\varphi)}\right], \\ w_0 &= \frac{\sqrt{2gH}}{\sqrt{\frac{1}{\varphi^2} + \frac{A}{1-\varphi}}} = k\sqrt{2gH}, \\ k &= \frac{1}{\sqrt{\frac{1}{\varphi^2} + \frac{A}{1-\varphi}}}, \quad A = \frac{R_{ss} r_c}{r_{ss}^2}. \end{aligned}\right\} \qquad (10.2.37)$$

Thus, the flow rate coefficient of the atomizer is determined by the geometrical characteristic A of the atomizer and the cross sectional coefficient φ.

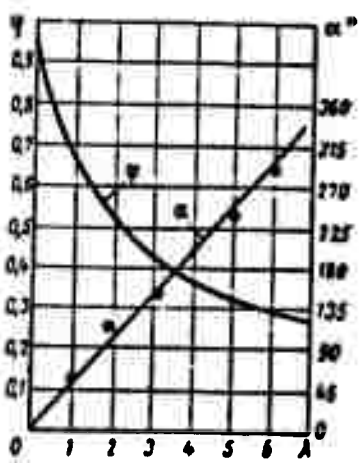


Fig. 10.2.10. Dependence of the cross section coefficient and the spraying angle on the geometrical characteristic A of the atomizer.

Following G.N. Abramovich [10.2.5] in assuming that the flow conditions set up in an atomizer will be those which correspond to maximum flow rate for a given pressure, we obtain an equation for $A = A(\varphi)$ from the condition $\frac{dk}{d\varphi} = 0$, which gives

$$A = \frac{1-\varphi}{\sqrt{\varphi^3 : 2}}, \quad k = \varphi\sqrt{\frac{\varphi}{2-\varphi}}. \qquad (10.2.38)$$

Here the spraying angle is

$$\operatorname{tg}\alpha = \frac{(1-\varphi)\sqrt{1}}{\sqrt{\varphi}\,(1+\sqrt{1-\varphi})}. \qquad (10.2.39)$$

Figure 10.2.10 represents graphically φ and α as functions of A.

As is shown by experiment (Fig. 10.2.11), for a centrifugal atomizer we have

$$k = k\left(A, \frac{D_s}{D_0}, \mathrm{Re}\right). \qquad (10.2.40)$$

where D_k is the diameter of the vortex chamber, and D_0 is the diameter of the atomizer nozzle.

In the range $Re < 1.6 \cdot 10^4$

$$\xi = 13 \frac{\sqrt{D_k : D_0}}{\sqrt[8]{Re}} \varphi \sqrt{\frac{\varphi}{2-\varphi}}. \qquad (10.2.41)$$

For $Re > 1.6 \cdot 10^4$ ξ does not depend on the viscosity or on D_k/D_0.

For the mean diameter of a drop during atomization by a centrifugal atomizer of a low-viscosity fluid we have the empirical formula

$$\frac{\bar{d}}{D_0} = 47{,}8A^{-0.6}\left(\frac{\rho v D_0}{\mu^2}\right)^{0.1}\left(\frac{\nu}{w_0 D_0}\right)^{0.7}. \qquad (10.2.42)$$

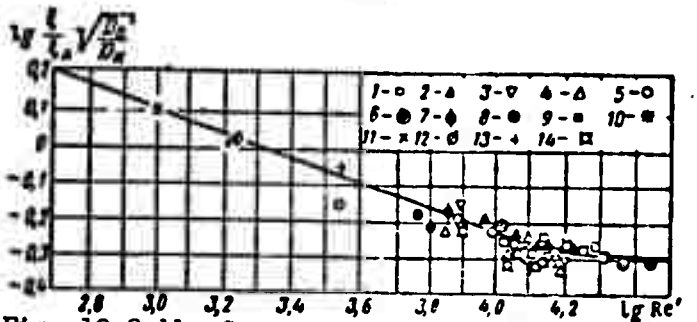


Fig. 10.2.11. Generalized dependence of $\frac{\tilde{D}}{D_0} = \left(\frac{\rho_2 w^2 D_0}{\sigma}\right)^{0.45}$ on $\frac{\mu_1}{\rho_1 v D_0}$.

For $Re > 3.5 \cdot 10^3$ and $\mu^2 : \sigma\rho D_0 > 3 \cdot 10^{-3}$ the spraying angle is determined by the formula

$$\operatorname{tg}\alpha = (\operatorname{tg}\alpha_A) 3{,}05 \cdot 10^{-2}\left(\frac{D_0}{D_k}\right)^{0.4}\left(\frac{\sigma\rho D_0}{\mu^2}\right)^{0.35}. \qquad (10.2.43)$$

where $\tan\alpha_A$ is obtained from Fig. 10.2.9. For $Re < 3.5 \cdot 10^3$ and $\mu^2 : \sigma\rho D_0 > 3 \times 10^{-4}$ $\tan\alpha$ depends on Re. For this region (according to experiments with an atomizer having A = 4.4)

$$\operatorname{tg}\alpha = \operatorname{tg}\alpha_A 1{,}88 \cdot 10^{-3}\left(\frac{\mu^2}{\rho\sigma D_0}\right)^{0.25}\left(\frac{w_0 D_0}{\nu}\right)^{0.9}. \qquad (10.2.44)$$

The spray density of a torch. The term spray density of a torch is understood to mean the mass flow of a fluid per unit area of the

torch cross section. It characterizes the torch structure and it can be expressed in fractions of the mean mass flow of the fluid, G/G_{sr}. In centrifugal atomizers the spray density for not too viscous fluids has a maximum on the axis (the influence of the air vortex); the vis-

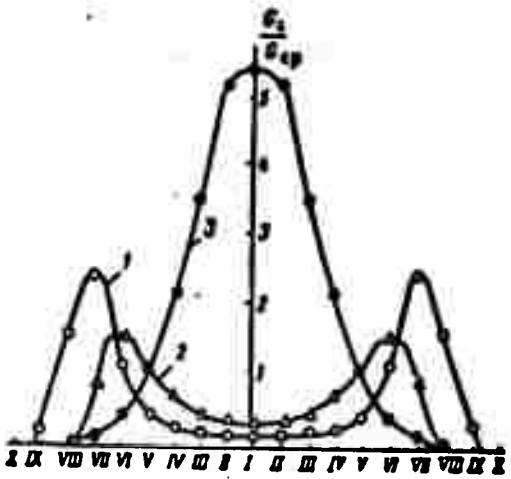


Fig. 10.2.12. Influence of viscosity on the relative density of spraying with a mechanical atomizer. 1) Water $\mu = 1.0 \cdot 10^{-4}$ kg sec./m^2; 2) kerosene, $\mu = 3.08 \cdot 10^{-4}$ kg·sec/m^2; 3) gas oil, $\mu = 7.84 \cdot 10^{-4}$ kg·sec/m^2.

cosity, however, considerably changes the spray density distribution and when the viscosity is high it becomes the same as it is for pneumatic nozzle atomizers (Fig. 10.2.12).

REFERENCES

10.2.1. Volynskiy, M.S., O droblenii kapel' zhidkosti v potoke vozdukha [Shattering of Liquid Droplets in a Stream of Air], 1948.

10.2.2. Frank-Kamenetskiy, D.A., O dvizhenii kapel' goryuchego po vylete iz forsunki [Motion of Fuel Droplets Through Nozzle Exit], 1947.

10.2.3. Kutateladze, S.S. and Styrinovich, M.A., Gidravlika gazozhidkostnykh sistem [Hydraulics of Gas-and-Liquid Systems], Gos-

energoizdat [State [illegible]], 1[illegible].

10.2.4. Tresh, Kh., Raspylivaniye [illegible]ti [Atomization of Li[illegible]], Collection entitled Voprosy raketnoy tekhniki [Problems of Rocket Engineering], No. 4, 1955.

10.2.5. Abramovich, G.N., Prikladnaya gazovaya dinamika [Applied Gas Dynamics], GTTI [State Technical and Theoretical Press], 1[illegible]3.

BLANK PAGE

10.3. MECHANICS OF RAREFIED GASES

The scope of gas mechanics. It is well known that a gas is an ensemble made up of a great number of molecules moving relative to each other in all possible directions and colliding with each other.

The forces of intermolecular interaction diminish so fast with increasing distance that the interaction can be considered as occurring when molecules come into contact. The process of molecular interaction can therefore be imagined as the collision of elastic spheres; this hypothesis is in sufficiently good agreement with experiment. At the same time if we neglect the action of external fields of forces (gravitational field, etc), we may assume that the molecules move uniformly in straight lines between collisions. The distance traveled by a molecule between two successive collisions is defined as its mean free path. It follows from this definition that the mean free path is a qualitative quantity which can be determined only as to its order of magnitude, as a certain "mean" distance.

Making use of the above simplifying suppositions we can, however, obtain an approximate quantitative expression for l. Obviously a molecule collides in the course of its motion with another molecule whose center lies inside a cylinder of radious σ which is the sum of the radii of the colliding molecules. The cross-sectional area of this cylinder is called the effective cross section

$$\pi\sigma^2 = \pi(R_1 + R_2)^2. \qquad (10.3.1)$$

Let us introduce a unit volume of gas in the form of a cylinder whose cross section is equal to the effective cross section. If N is the number of molecules in the unit volume and if all the molecules except one are at rest, then in a part of the cylinder with a volume of $1/N$ the molecule is in free motion. This means that the length of

this part of the cylinder will be equal to the length of a mean free path: $l = 1/\sigma^2 N$. A more precise consideration results in the fact that the mean free path is shorter by $2^{1/2}$:

$$l = \frac{1}{\sqrt{2}\sigma^2 N}. \qquad (10.3.2)$$

If the mean free path of the molecules is very short compared with the characteristic dimensions of the region of flow or the dimensions of the body placed in the flow, we can disregard the molecular structure of the gas and consider it as a continuous medium. In this case, as has already been pointed out in the introduction, the rather small physical gas volumes which are taken as elementary volumes in the mechanics of continuous media nevertheless contain a sufficiently large number of molecules for it to be possible to attribute a definite mass, velocity, etc. to each of them.

If the order of magnitude of the mean free path of the molecules becomes comparable to the body dimensions or exceeds them it becomes impossible to ignore the discontinuous structure of the gas and the continuous medium approximation becomes inapplicable. In this case the motion of the gas has to be investigated with the methods of the kinetic theory of gases. The state of the medium is in this case termed a rarefield state and the medium a rarefield gas. Gases in the rarefield state are investigated by means of the mechanics of rarefield gases, which is applied in many branches of engineering, e.g., in vacuum technology. The ratio of the mean free path l of the molecules to the characteristic dimension L (characteristic dimension of the body or characteristic dimension of the region of flow)

$$\mathrm{Kn} = \frac{l}{L} \qquad (10.3.3)$$

is called the Knudsen number; the condition of applicability of the continuity hypothesis can be represented by the inequality

$Kn \ll 1$.

The quantity l cannot be determined as the result of a direct experiment; it has to be expressed through other quantitatively measurable quantities into which it enters, for example, through the viscosity coefficient μ. As was shown (cf. Part 0.2),

$$\mu \approx \rho c l.$$

Taking into account that the mean velocity c of the molecules is of the order of sonic velocity ($c \sim a$), we can write

$$Kn = \frac{l}{L} \approx \frac{\mu}{\rho c L} \approx \frac{c}{\frac{\rho w L}{\mu}} \sim \frac{M}{Re}. \qquad (10.3.4)$$

For the condition of applicability of the continuity hypothesis we thus have the inequality

$$Kn = \frac{l}{L} = \frac{M}{Re} \ll 1. \qquad (10.3.5)$$

In the mechanics of rarefied gases we can distinguish between a whole series of flow regions. In fact, near a solid wall along which a gas is flowing there is always a layer of the thickness of the order of a mean free path l, in which the effects are microscopic in character. If the thickness δ of the boundary layer is large compared with the mean free path l, this layer near the wall can be ignored and the velocity of the viscous gas at the wall can be taken as being zero. If however $\delta \sim l$ the microscopic effects can no longer be neglected. In this case, by virtue of the absence of a direct contact with the surface, there is a certain finite microscopic velocity at the interface between the solid and the gas; the gas "slips" along the wall. This also gives rise to the concept of slip flow.

When the mean free path of molecules is much greater than the dimensions of the body, then the changes in motion of the molecules due to collisions between each other in the neighborhood of the body will

be much smaller than those due to collisions with the body. The flow in the vicinity of the body can in this case be considered to be a flow of mutually noninteracting (free) molecule. Hence the term free molecular flow.

Taking the boundary layer thickness as the characteristic length, we can write

$$\frac{l}{\delta} = \frac{l}{L}\frac{L}{\delta} = \mathrm{Kn}\frac{L}{\delta} \sim \frac{M}{\mathrm{Re}}\frac{L}{\delta}.$$

If $\mathrm{Re} \ll 1$ then $L/\delta \sim 1$; when $\mathrm{Re} \to 1$, as is well known, $L/\delta \sim \mathrm{Re}^{1/2}$ for a laminar flow. Therefore

$$\left.\begin{aligned} \frac{l}{\delta} &\sim \frac{M}{\mathrm{Re}} \quad \text{for } \mathrm{Re} \ll 1 \\ \frac{l}{\delta} &\sim \frac{M}{\sqrt{\mathrm{Re}}} \quad \text{for } \mathrm{Re} \gg 1. \end{aligned}\right\} \qquad (10.3.6)$$

Tzyan [10.3.6] suggests taking the range of slip flow in the interval $0{,}01 < \frac{l}{\delta} < 1{,}0$, and $\frac{l}{\delta} = 10$ for the boundary of the region of free molecular flow. These ranges are graphically represented in Fig. 10.3.1.

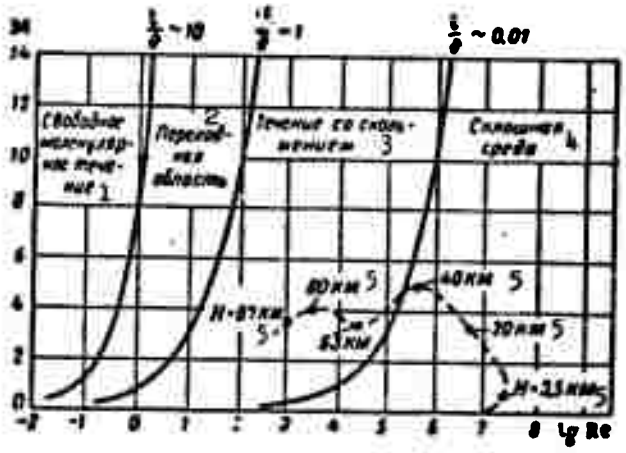


Fig. 10.3.1. Regions of gas mechanics. The dashed line gives the flying regime of a rocket; to each dot corresponds a certain height and flying speed. 1) Free molecular flow; 2) transient region; 3) slip flow; 4) continuous medium; 5) km.

To illustrate the extent of investigations carried out within the field of the mechanics of rarefield gases, Fig. 10.3.2 represents in an M-Re plot the regions in which the aerodynamics of the simplest body, a sphere, is being studied [10.3.10].

The distribution function of the molecules. Let us consider a perfect gas constituted by a system of molecules whose interactions can always be neglected except in the cases of collisions.

For the sake of simplicity we shall consider nonatomic molecules in the form of hard smooth spheres. The state of each molecule, which may be considered as being independent of the other molecules, will then be completely determined if we know its velocity $\vec{u}(u_x u_y u_z)$ and its coordinates $\vec{r}(x, y, z)$ at every instant of time t.

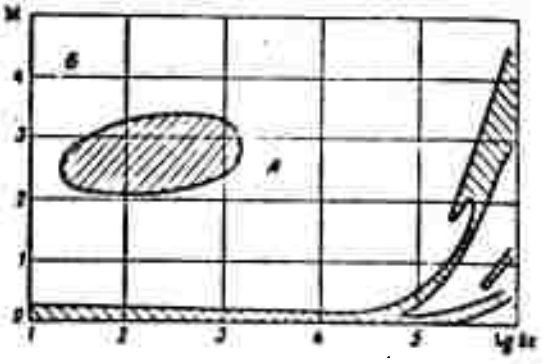


Fig. 10.3.2. The regions of gasdynamics of a sphere investigated are shaded. The region of slip flow (A) and the region of free molecular flow (B) are subject to investigation.

Let us denote a certain spatial volume by dV and the velocity in it by du, so that $dV = dx\,dy\,dz$, $du = du_x\,du_y\,du_z$. Let the function f of the point $\vec{r}$, the velocity $\vec{u}$ and the time t determine the probable number of molecules per unit volume whose velocities lie within a unit interval of velocities.

Then, denoting by dv the probable number of molecules contained in the elementary volume dr around point $\vec{r}$ and having velocities in

the interval between $\vec{u}$ and $\vec{v} + d\vec{u}$, we can write

$$dN = f(\vec{r}, \vec{u}, t)\,dx\,dy\,dz\,du_x\,du_y\,du_z = f(\vec{r}, \vec{u}, t)\,dV\,du.$$

The function $f(\vec{r}, \vec{u}, t)$ is called the <u>distribution function of the molecules</u>. Integrating it over all possible velocities of the molecules we find that the total number of molecules contained in a unit volume ($dV = 1$) is equal to

$$N = \int f(\vec{r}, \vec{u}, t)\,du. \qquad (10.3.7)$$

For a fixed instant of time the statistical mean $\tilde{\varphi}$ of any velocity $\varphi(\vec{u})$ is determined in the following way:

$$\overline{\varphi(\vec{u})} = \frac{1}{N}\int \varphi(\vec{u}) f(\vec{r}, \vec{u})\,du. \qquad (10.3.8)$$

This is a local mean value, i.e., it varies from point to point. Such mean values yield the local macroscopic characteristics of the gas. For example, if $\vec{u}$ is the velocity of a gas molecule, then its mean value, representing the macroscopic velocity $\vec{w}$ of the gas is

$$\vec{w} = \tilde{\vec{u}} = \vec{u} - \vec{c}, \qquad (10.3.9)$$

where $\vec{c}$ is the velocity relative to a coordinate system in which the gas is at rest, i.e., it is the <u>thermal velocity of the molecules</u>; $\vec{w}$ is determined by the formula

$$\vec{w}(\vec{r}) = \tilde{\vec{u}} = \frac{1}{N}\int \vec{u} f(\vec{r}, \vec{u}, t)\,du.$$

Its x-component is given by the expression

$$w_x(x, y, z) = \frac{1}{N}\iiint_{-\infty}^{+\infty} u_x f(x, y, z, u_x, u_y, u_z)\,du_x\,du_y\,du_z.$$

Analogous expressions are obtained for u_y and u_z. Let us stress once more that integration is carried out over all possible values of the velocities u_x, u_y, u_z.

If we know the distribution function of the molecules it is always possible to calculate the number of collisions between the mole-

cules and the surface of the solid body located in the gas, and also the momentum and energy transferred by the gas molecules to the body.

In other words, the dynamic and thermal interaction of body and gas is completely determined when the distribution function is known.

Boltzmann's kinetic equation. Let us consider the change in the number of molecules (which we call the "molecules $\vec{u}$") in the volume dV (dx, dy, dz), having velocities in the interval du (du_x du_y du_z) during the time interval δt, which is short compared with the mean free time but long compared with the duration of a collision. During this time the molecule does not suffer more than one collision. If no collision occurs during the time δt the variation of the distribution function f caused by the particle motion can be written in the form

$$\frac{df}{dt}\,dV\,du\,\delta t=\left(\frac{\partial f}{\partial t}+\frac{\partial f}{\partial x}\frac{dx}{dt}+\frac{\partial f}{\partial y}\frac{dy}{dt}+\frac{\partial f}{\partial z}\frac{dz}{dt}+\frac{\partial f}{\partial u_x}\frac{du_x}{dt}+\frac{\partial f}{\partial u_y}\frac{du_y}{dt}+\right.$$

$$\left.+\frac{\partial f}{\partial u_z}\frac{du_z}{dt}\right)dV\,du\,\delta t=\left(\frac{\partial f}{\partial t}+\vec{u}\cdot\vec{\nabla}f+\frac{\vec{F}}{m}\frac{\partial f}{\partial \vec{u}}\right)dV\,du\,\delta t.$$

Here

Здесь $\frac{\partial f}{\partial x}\frac{dx}{dt}+\frac{\partial f}{\partial y}\frac{dy}{dt}+\frac{\partial f}{\partial z}\frac{dz}{dt}=\frac{d\vec{r}}{dt}\cdot\frac{\partial f}{\partial \vec{r}}=\vec{u}\cdot\vec{\nabla}f,$

$$\frac{\partial f}{\partial u_x}\frac{du_x}{dt}+\frac{\partial f}{\partial u_y}\frac{du_y}{dt}+\frac{\partial f}{\partial u_z}\frac{du_z}{dt}=\frac{d\vec{u}}{dt}\cdot\frac{\partial f}{\partial \vec{u}},$$

with $\frac{d\vec{u}}{dt}=\frac{\vec{F}}{m}$, where $\vec{F}$ is an external force acting on the molecules.

This change in the number of "molecules $\vec{u}$" owing to their motion is equal to the difference between the increment $I_1 dV\,du\,\delta t$ and the diminuition $I_2 dV\,du\,\delta t$ of the number of "molecules $\vec{u}$" in the volume dV during the time δt, due to collisions

$$\frac{\partial f}{\partial t}+\vec{u}\cdot\vec{\nabla}f+\frac{\vec{F}}{m}\frac{\partial f}{\partial \vec{u}}=I_1-I_2.$$

Let us adopt a certain scheme of molecular collision: let us imagine the molecules as smooth hard spheres. The collision of two spheres of diameter σ may be represented as the collision between the center of a sphere and a sphere of radius σ (Fig. 10.3.3).

It is obvious that as the result of any collision "molecule $\vec{u}$" remains one and the same, and the number of collisions of the "molecules $\vec{u}$" with other molecules ("molecules $\vec{u}_1$") yields the diminuition I_2. Let us isolate part of the surface of the sphere of the "molecule $\vec{u}$" as an areal element $dA = \sigma^2 d\omega$, where $d\omega$ is the solid angle element. The number of "molecules $\vec{u}_1$" impinging on dA during the time δt is equal to the product of the volume of the oblique cylinder $\sigma^2 d\omega\,|(\vec{u}_1-\vec{u})\cdot\vec{l}|\,\delta t$, and the density of the "molecules $\vec{u}_1$", $f(\vec{r}, \vec{u}_1, t)$. The number of the "molecules $\vec{u}$" in the volume dV is equal to $f(\vec{r}, \vec{u}, t)dVdu$. Consequently, the number of collisions suffered by the "molecules $\vec{u}$" along the center line $\underline{\vec{l}}$ is equal to

$$\sigma^2 d\omega\,|(\vec{u}_1-\vec{u})\vec{l}\,|\,\delta t\, f(\vec{r}, \vec{u}_1, t)\,du_1 f(\vec{r}, \vec{u}, t)\,dV\,du.$$

Integration over all values of $\vec{u}_1$ and all directions $\underline{\vec{l}}$ yields

$$I_2 dV\,du\,\delta t = \frac{\sigma^2}{2}\int |(\vec{u}_1-\vec{u})\cdot\vec{l}|\, f(\vec{r}, \vec{u}_1, t)\, f(\vec{r}, \vec{u}, t)\,d\omega\,du_1 dV\,du\,\delta t.$$

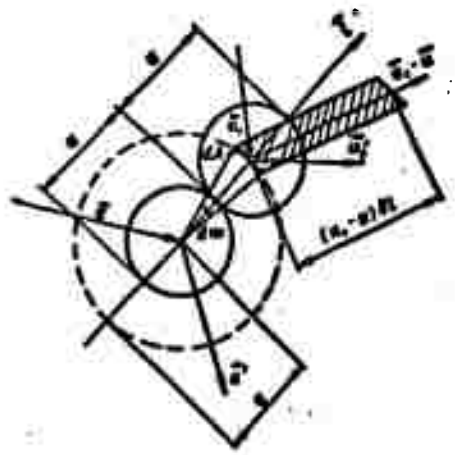


Fig. 10.3.3. The interactions of perfect gas molecules can be represented as the collisions of hard smooth balls.

The factor "1/2" has been introduced since integration needs be done only over the half of all molecules.

After the collision the "molecules $\vec{u}$" and "$\vec{u}_1$" acquire the velocities $\vec{u}'$ and $\vec{u}_1'$ such that the total momentum and the total energy remain unchanged, i.e.,

$$\left.\begin{aligned}\vec{u}+\vec{u}_1&=\vec{u}'+\vec{u}_1',\\ \vec{u}^2+\vec{u}_1^2&=\vec{u}'^2+\vec{u}_1'^2.\end{aligned}\right\} \qquad (*)$$

Therefore, as the result of a collision between the "molecule "$\vec{u}'$" and "$\vec{u}_1'$" is increased. After analogous considerations on the derivation of I_2 we obtain the number of "molecules $\vec{u}$" appearing as the result of collisions:

$$I_1\,dV\,du\,dt=\frac{\sigma^2}{2}\int\left|(\vec{u}_1'-\vec{u}')\cdot\vec{l}\right|f(\vec{r},\vec{u}_1',t)\times$$
$$\times f(\vec{r},\vec{u}',t)\,d\omega\,du_1'\,dV\,du'\,dt.$$

From Expression (*) follows*

$$\left|(\vec{u}_1-\vec{u})\cdot\vec{l}\right|=\left|(\vec{u}_1'-\vec{u}')\cdot\vec{l}\right|,$$

which enables us to simplify the expression for the difference $I_1 - I_2$.

Hence we obtain Boltzmann's kinetic equation for a monatomic perfect gas in the form of an integro-differential equation

$$\left.\begin{aligned}&\frac{\partial f}{\partial t}+\vec{u}\cdot\vec{\nabla}f+\frac{\vec{F}}{m}\frac{\partial f}{\partial\vec{u}}=\frac{\sigma^2}{2}\int\left|(\vec{u}_1-\vec{u})\cdot\vec{l}\right|(f_1'f'-f_1f)\,d\omega\,du_1,\\ &\text{where}\\ &f=f(\vec{r},\vec{u},t);\quad f_1=f(\vec{r},\vec{u}_1,t);\\ &f'=f(\vec{r},\vec{u}',t);\quad f_1'=f(\vec{r},\vec{u}_1',t).\end{aligned}\right\} \qquad (10.3.10)$$

For a perfect gas in static equilibrium, i.e., when its parameters remain unchanged for an arbitrary long period, the distribution function does not depend on $\vec{r}$ and t and $F = 0$. In this case it is called Maxwellian distribution function and Boltzmann's kinetic equation assumes the form

$$\int\left|(\vec{u}_1-\vec{u})\cdot\vec{l}\right|(f_1'f'-f_1f)\,d\omega\,du_1=0. \qquad (10.3.11)$$

From the physical point of view this expresses that the collisions between the molecules do not affect the distribution function. The motion of the molecules is such that when as the result of one pair of collisions the number of the "molecules $\vec{u}$" for example, diminishes by one, then immediately, as the result of another pair of collisions, the "molecule $\vec{u}_1$" is formed.

It follows directly from (10.3.11) that the Maxwellian distribution function satisfies the condition

$$ff' = f_1 f$$

or

$$\ln f_1 + \ln f' = \ln f_1 + \ln f.$$

This means that $\ln f$ remains unchanged when molecules collide, and $\ln f$ is said to be a generalized invariant for molecular collisions. But since in a collision the mass of the molecules, the momentum, and the energy are conserved, $\ln f$ must be a linear combination of m, $m\vec{u}$ and $mu^2/2$, i.e.,

$$\ln f = a_0 m + \vec{a}_1 \cdot m\vec{u} + a_2 \frac{mu^2}{2}.$$

Instead of the constants a_0, $\vec{a}_1$ and a_2 we introduce new constants, viz., the scalars α and β and the vector $\vec{A}$, represented in the form

$$\ln f = \alpha - \beta(\vec{u} - \vec{A})^2.$$

Then

$$f(\vec{u}) = ae^{-\beta(\vec{u}-\vec{A})^2}. \qquad (a = e^{\alpha})$$

In order to determine the constants a and $\vec{A}$ we notice that the number of molecules per unit volume whose velocities lie in the interval between u and $u + du$ is equal to $a \exp[-\beta(\vec{u}-\vec{A})^2] du_x du_y du_z$.

Integrating this expression from $-\infty$ to $+\infty$ we obtain the total number of molecules per unit volume:

$$N = a \int_{-\infty}^{+\infty} \iint e^{-j(\vec{u}-\vec{A})^2} du_x du_y du_z.$$

Moreover, by definition, the x-component of the macroscopic velocity of the gas is expressed by

$$w_x = \frac{1}{N} \int u_x f \, du =$$

$$= \frac{a}{N} \iiint_{-\infty}^{+\infty} u_x e^{-j[(u_x-A_x)^2+(u_y-A_y)^2+(u_z-A_z)^2]} du_x du_y du_z =$$

$$= \frac{a}{N} A_x \iiint_{-\infty}^{+\infty} e^{-j(\vec{u}-\vec{A})^2} du_x du_y du_z = A_x$$

(the integral giving zero contribution is canceled here).

Analogously we obtain $w_y = A_y$; $w_z = A_z$.

Thus, $\vec{A} = \vec{w}$ and $\vec{u} - \vec{A} = \vec{u} - \vec{w} = \vec{c}$, where $\vec{c}$ denotes the thermal velocity of the molecules. The calculations yield $a = (j/\pi)^{3/2}$ and, thus,

$$f = \left(\frac{j}{\pi}\right)^{\frac{3}{2}} e^{-jc^2}; \quad f = \sqrt{\left(\frac{j}{\pi}\right)^3} e^{-jc^2}.$$

The quantity j can be expressed in terms of the absolute gas temperature and Boltzmann's constant k. Taking into account that the mean kinetic energy per degree of freedom of the molecule is equal to $kT/2$, we obtain

$$\frac{3}{2} kT = \frac{\overline{mc^2}}{2} = \frac{1}{N} \frac{mN}{2} \left(\frac{j}{\pi}\right)^{\frac{3}{2}} \int_{-\infty}^{+\infty} \iiint c^2 e^{-jc^2} dc_x dc_y dc_z. \qquad (10.3.12)$$

Calculations yield $j = m/2kT$.

Thus, for a monatomic perfect gas in equilibrium the Maxwellian distribution function has the form

$$f = \left(\frac{m}{2\pi kT}\right)^{\frac{3}{2}} e^{-\frac{mc^2}{2kT}}. \qquad (10.3.13)$$

As follows from the definition, $\tilde{c}^2 = 3RT$.

The quantity $\sqrt{\tilde{c}^2} = \sqrt{\frac{3kT}{m}}$ is called the r.m.s. velocity. The mean velocity of thermal motion is

$$\tilde{c} = \frac{1}{N}\int_{-\infty}^{\infty}\int\int fc\,dc_x\,dc_y\,dc_z = \frac{N}{N}\left(\frac{m}{2\pi kT}\right)^{\frac{3}{2}}\int_{-\infty}^{\infty}\int\int ce^{-\frac{mc^2}{2kT}} \times$$

$$\times dc_x\,dc_y\,dc_z = \sqrt{\frac{8kT}{\pi m}}.$$

If the rectangular coordinates c_x, c_y, c_z are replaced by spherical ones, c, φ, ϑ, then the number of molecules per unit volume which have velocities in the interval between c and c + dc, is determined regardless of the direction by the expression

$$dw = 4\pi Nc^2 f\,dc.$$

The Maxwellian distribution is described by a curve (Fig. 10.3.4) whose equation reads

$$\varphi(c) = \frac{1}{N}\frac{dn}{dc} = 4\pi c^2 f. \qquad (10.3.14)$$

The velocity that corresponds to the highest value of $\varphi(c)$ is called the most probable velocity,

$$c_m = \sqrt{\frac{2\tilde{c}^2}{3}} = \sqrt{\frac{2kT}{m}}. \qquad (10.3.15)$$

The Maxwellian distribution function for a monatomic perfect gas in equilirbium may be expressed in the form

$$f = \left(\frac{1}{\pi c_m^2}\right)^{\frac{3}{2}} e^{-\frac{c^2}{c_m^2}} = \left(\frac{m}{2\pi kT}\right)^{\frac{3}{2}} e^{-\frac{mc^2}{2kT}}. \qquad (10.3.16)$$

Maxwell's distribution function is a particular solution to Boltzmann's equation. It may serve only as a first approximation in the search for the general form of the function $f(\vec{r}, \vec{u}, t)$.

It is shown in the kinetic theory of gases that when a polyatomic gas in a field of forces with a single-valued potential is in a state of statistical equilibrium, then its distribution function has the form

$$f = B\left(\frac{m}{2\pi kT}\right)^{3/2} e^{-\frac{E}{kT}},$$

where $E = E' + \Phi(x, y, z)$ is the total energy of the molecule, E' being independent of the coordinates and representing the part of the energy of translational, rotational and vibrational motions of the molecule.

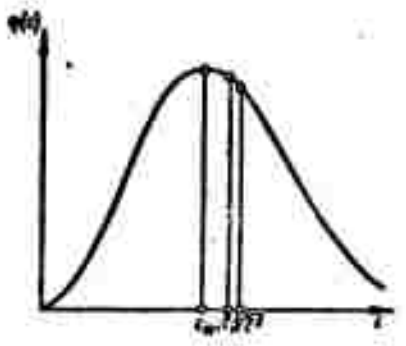


Fig. 10.3.4. Curve of the Maxwellian distribution funtion.

To the energy of translational motion, E_{post} (the only one in the case of a monatomic gas) we must therefore add the rotational energy E_{vr}, and the energy E_{kol} of a possible vibrational motion of the atoms in the molecule, and also the potential energy Φ of the field of forces.

The factor B is chosen from the condition

$$N = \int f dV dr d\omega,$$

where

$$f = B\left(\frac{m}{2\pi kT}\right)^{3/2} e^{-\frac{E_{post}+E_{vr}+E_{kol}+\Phi(x,y,z)}{kT}}; \qquad (10.3.17)$$

$d\omega$ is a volume element in the space determined by the parameters of the rotational and vibrational energies of the molecules. For example, in the case of a diatomic molecule (with $E_{kol} = 0$)

$$E_{vr} = \frac{J}{2}(\omega_1^2 + \omega_2^2),$$

where $J = \frac{m_1 m_2}{m_1 + m_2} b^2$ is the moment of inertia of the molecule (m_1, m_2 are the masses of the atoms and b is the distance between them); ω_1, ω_2 are the angular velocities of rotation of the atoms.

Interaction of the gas molecules with the surfaces of solids. Let us calculate the number of collisions per unit time of monatomic gas molecules possessing the distribution function $f(\vec{r}, u, \vec{t})$, with the surface A of a body which is at rest in the coordinate system chosen.

In unit time the surface element dA suffers collision with those molecules that are contained in a cylinder with the base dA and the generatrix $|\vec{u}|$ and move towards the surface element (Fig. 10.3.5), i.e., for which $(\vec{u}\cdot\vec{n}) < 0$, where $\vec{n}$ is the unit vector of the outer normal to dA. This number is equal to

$$dv = -dA \int\limits_{(\vec{u}\cdot\vec{n})<0} (\vec{u}\cdot\vec{n}) f\, dV.$$

The integration here is extended only over those values of u_x, u_y, u_z for which $\vec{u}\cdot\vec{n} < 0$.

The total number of collisions per unit time with the whole surface is obtained by integrating over the whole surface of the body:

$$v = -\int_A dA \int\limits_{(\vec{u}\cdot\vec{n})<0} (\vec{u}\cdot\vec{n}) f\, du, \qquad (10.3.18)$$

and that with a unit area of the surface is

$$v^0 = -N \int\limits_{(\vec{u}\cdot\vec{n})<0} (\vec{u}\cdot\vec{n}) f\, du. \qquad (10.3.19)$$

where N is the number of molecules per unit volume.

When gas molecules collide with the surface of solids, momentum and energy are exchanged between the gas molecules and the body surface. This interaction between the gas molecules and the molecules of the body surface, rather complex in its physical nature, can be estimated with the help of two experimental coefficients: the adhesion coefficient β and the accomodation coefficient γ.

The adhesion coefficient. The transfer of momentum from the gas molecules to the surface of the solid body is characterized by the adhesion coefficient β determining the interaction forces between solid and gas.

It is convenient to treat the interaction process as a collision, consisting of two stages; in the first stage the molecule, approaching

the wall, transmits what is called the active momentum to it, and in the second stage, when it moves away from the wall, i.e., it is "reflected," it transmits the reactive momentum. The total force, acting on a solid body in a gas flow is then equal to the sum of active and reactive momenta transferred to the body surface by the gas molecules colliding with it:

$$\vec{P}=\vec{P}_a+\vec{P}_r. \qquad (10.3.20)$$



Fig. 10.3.5. In unit time the areal element dA suffers collision with the molecules that are contained in the cylinder with the base dA and the generatrix $\vec{u}$ and move towards the surface ($\vec{u}\cdot\vec{n} < 0$).

If the mass of molecules is m, the momentum transferred per unit area of the body surface by the impinging molecules (active momentum) is

$$\vec{P}_a = -\int\limits_{(\vec{u}\cdot\vec{n})<0} m\vec{u}(\vec{u}\cdot\vec{n})f\,du.$$

Now we have to calculate the momentum transferred to the body by the molecules in the second stage of collision, i.e., when they are reflected from the body surface.

We can distinguish between two modes of reflection of molecules from the surface of a solid body: mirror reflection and diffuse reflection.

On the molecular scale the body surface must be considered as consisting of the molecules of the body substance arranged in an elastic lattice. Some of the molecules impinging on this surface suffer elastic mirror reflection, i.e., a reflection in which magnitude and direction of the tangential velocity component remain unchanged while the sign of the normal component is reversed. In mirror reflection all laws governing the absolutely elastic collision between a ball and a plane apply, i.e., the velocity distribution function of the molecules

is conserved.

The remainder of the molecules penetrate into the material of the body for a certain time, as if they were absorbed by the surface. A detailed study of the process of collision between molecules and body has proved the existence of such temporary molecular absorption. For a certain time the gas molecules leave the body with velocities having magnitudes and directions that do not depend on the velocities of the molecules at the instant when they impinge on the surface, It is an essential feature that the direction on emission does not depend on the direction of motion of the molecule before its impact on the surface.

The entire process of absorption and reemission is called diffuse reflection.

The adhesion coefficient β determines the fraction of diffusely reflected molecules. Thus, of all the molecules colliding with the body surface only a fraction β is diffusely reflected while the remainder $(1-\beta)$ undergo mirror reflection. The value of the coefficient β depends on the nature and the temperature of the gas and on the conditions at the body surface - on the treatment, material and temperature (of the body).

Experience has shown that it is diffuse reflection that predominates [10.3.4]:

Gas - surface	β % at 23°C
Air - mercury	100
Air - brass (mechanically treated)	100
Air - glass	89.0
Helium - oil	87.4
Air - oil	89.5
Carbon dioxide - oil	92

So as to simplify the calculations, we shall assume in what follows that the reflection of molecules from the surface of a solid body is entirely diffuse, i.e., we shall take $\beta = 1$. In this case the reactive momentum $\vec{P}_r$ represents the momentum transferred to a unit surface of the body by diffusely reflected molecules. If the diffusely reflected molecules possess the distribution function $f_d = f_d(\vec{r}, \vec{u}_d, t)$ which, generally speaking, differs from f, and the velocity $\vec{u}_d$ (the macroscopic velocity of the diffusely reflected gas being zero, $\tilde{\vec{u}} = 0$, because all directions of reflection are equally probable), then

$$\vec{P}_r = -\int_{\vec{u}_d \cdot \vec{n} > 0} m\vec{u}_d (\vec{u}_d \cdot \vec{n}) f_d \, du_d.$$

Integration extends here over all values of $\vec{u}_d$ for which $\vec{u}_d \cdot \vec{n} > 0$.

The total force acting on a unit area of the body surface is equal to

$$P = -\int_{(\vec{u}-\vec{u}_0)\cdot\vec{n}<0} m\vec{u}(\vec{u}\cdot\vec{n}) f \, du - \int_{(\vec{u}_d-\vec{u}_0)\cdot\vec{n}>0} m\vec{u}_d(\vec{u}_d\cdot\vec{n}) f_d \, du_d. \qquad (10.3.21)$$

and its projection onto a certain direction determined by the unit vector σ is equal to

$$P_\sigma = -m\int_{(\vec{u}-\vec{u}_0)\cdot\vec{n}<0} (\vec{u}\cdot\vec{\sigma})(\vec{u}\cdot\vec{n}) f \, du - m\int_{(\vec{u}_d-\vec{u}_0)\cdot\vec{n}>0} (\vec{u}_d\cdot\vec{\sigma})(\vec{u}_d\cdot\vec{n}) f_d \, du_d. \qquad (10.3.22)$$

The accommodation coefficient. The transfer of energy of the molecules on the body surface is characterized by the accommodation coefficient γ.

Let ε^0 be the total energy of a gas molecule. In the case of a monatomic gas (taking into account that $\vec{u} = \vec{c} + \vec{w}$)

$$\varepsilon^0 = \frac{mu^2}{2} = \varepsilon + m(\vec{c}\cdot\vec{w}) + \frac{mw^2}{2}. \qquad (10.3.23)$$

where $\varepsilon = mc^2/2$ determines the integral energy of the gas.

The mean value of the total energy is equal to

$$\tilde{\varepsilon}^0 = \tilde{\varepsilon} + \frac{m\tilde{c}^2}{2}, \qquad (10.3.24)$$

since by definition the mean value is $\tilde{c} = 0$.

The quantity $\tilde{\varepsilon}$ determines the internal energy of the gas, which is equal to mc_vT, where c_v is the specific heat at constant volume.

Now

$$\tilde{\varepsilon}_0 = mc_vT + \frac{m\tilde{c}^2}{2}. \qquad (10.3.25)$$

If the gas is macroscopically at rest, $\tilde{\varepsilon}_0 = mc_vT_0$, where T_0 is the adiabatic stagnation temperature of the gas.

Let us consider the transfer of energy by gas molecules at rest to the body surface, which has the temperature T_s.

Let $\tilde{\varepsilon}_0$ be the mean energy of the molecules impinging on the body, $\tilde{\varepsilon}_r^0$ the same of the reflected gas molecules, $\tilde{\varepsilon}_s$ the mean energy of the gas molecules whose temperature is equal to the temperature T_s of the body surface.

The accomodation coefficient γ is defined by the equation

$$\tilde{\varepsilon}_r = \gamma\tilde{\varepsilon}_s + (1-\gamma)\tilde{\varepsilon}^0, \quad \gamma = \frac{\tilde{\varepsilon}_r - \tilde{\varepsilon}^0}{\tilde{\varepsilon}_s - \tilde{\varepsilon}^0}. \qquad (10.3.26)$$

Thus, γ is the ratio of the mean energy transferred from the gas to the body to the energy which may in general be transferred at a given surface temperature T_s. In other, γ determines the fraction of those gas molecules which, after their collision with the body surface, possess a mean energy that corresponds to the temperature T_s. In the case of complete accomodation ($\gamma = 1$), $\tilde{\varepsilon}_r^0 = \tilde{\varepsilon}_s^0$. Without any accomodation ($\gamma = 0$) $\tilde{\varepsilon}_r^0 = \tilde{\varepsilon}^0$ is the energy of the reflected molecules, equal to the mean energy of the impinging molecules.

The value of the accomodation coefficient lies within the limits

$0 < \gamma < 1$. The values for some materials with surface temperatures between 40 and 70°C are given in what follows.

Поверхность 1		Коэффициент аккомодации γ 2	
		минимальный 3	максимальный 4
Матовый черный лак на бронзе 5		0,88	0,89
Бронза 6	полированная 7	0,91	0,94
	машинной обточки 8	0,89	0,93
	травленая 9	0,93	0,95
Литая сталь 10	полированная 7	0,87	0,93
	машинной обточки 8	0,87	0,88
	травленая 9	0,89	0,96
Алюминий 11	полированный 7	0,87	0,95
	машинной обточки 8	0,95	0,97

1) Surface; 2) accomodation coefficient γ; 3) minimum; 4) maximum; 5) dull black varnish on bronze; 6) bronze; 7) polished; 8) machined; 9) etched; 10) cast steel; 11) aluminum.

It is seen from the table that γ is close to unity and depends only slightly on the mechanical treatment of the surface.

The accomodation coefficient γ is related to the adhesion coefficient β by a relation which is obtained from (10.3.26) if $\tilde{\varepsilon}_r^0$ is replaced by its expression in terms of the energy $\tilde{\varepsilon}_d^0$ of the diffusely reflected molecules, $\tilde{\varepsilon}_r^0 = \beta\tilde{\varepsilon}_s^0 + (1-\beta)\tilde{\varepsilon}^0$. Then

$$\gamma = \beta\frac{\tilde{\varepsilon}^0 - \tilde{\varepsilon}_s^0}{\tilde{\varepsilon}^0 - \tilde{\varepsilon}_c^0}.$$

Or, if we introduce the stagnation temperature T_0, T_d and T_s of the incident, diffusely reflected and completely accomodated gas (having the wall temperature) respectively, then

$$\gamma = \beta\frac{T_0 - T_s}{T_0 - T_c}, \text{ for } \beta = 1 \quad \gamma = \frac{T_0 - T_s}{T_0 - T_c}. \qquad (10.3.27)$$

The total E* received by a unit area of the body surface per unit

time as the result of collisions with molecules is equal to the energy difference of the impinging and reflected molecules (under the assumption of diffuse reflection):

$$E^* = N \iiint_{(\vec{u}\cdot\vec{n})<0} \varepsilon^* (\vec{u}\cdot\vec{n}) f\, du - N_s \iiint_{\vec{u}_s\cdot\vec{n}>0} \varepsilon_s^* (\vec{u}_s\cdot\vec{n}) f_s\, du_s. \qquad (10.3.28)$$

The energy balance equation. This may be represented in the following form

$$E^* = E_1^* - E_2^* + Q^*, \qquad (10.3.29)$$

where E_1^* and E_2^* are the radiant energies emitted and received, respectively, by a unit area of the body surface; Q* is the amount of heat delivered to a unit area of the body surface from within (e.g., separation of heat from a surface cooling system).

Let us consider the components of this equation.

The body as a whole continuously absorbs and emits radiant energy. The amount of heat emitted by the body is determined by the Stefan - Boltzmann law under the assumption that the body behaves as a "black body," i.e., its radiation coefficient is independent of the wavelength

$$E_1^* = \varepsilon\sigma (T_s^4 - T^4). \qquad (10.3.30)$$

where ε is the degree of blackness (relative emissivity); $\sigma = 4.9 \cdot 10^{-8}$ kcal/m^2-kr-°K^4 is the constant for an absolutely black body; T_s is the temperature of the body surface; T is the effective temperature of the surrounding bodies onto which the radiation falls.

During flight in the atmosphere radiant energy may be transferred to a body in several ways (radiation from the Earth, the sun, etc.), but the main part of this energy is solar radiation. Allowance for solar radiation demands the introduction of the azimuthal altitude of the Sun and the direction of flight relative to the Sun. The mean val-

ue of the solar radiation at the boundary of the atmosphere (solar constant) for a surface lying perpendicular to the direction of the rays is $I_0 = 138.5$ kgm/m^2-sec. The amount of radiant energy received by a body from the Sun is determined by the relation

$$E_1^+ = I_0.$$

A body flying in the atmosphere also receives radiant energy from the Earth and the surrounding air but compared with the solar radiation the radiation of atmosphere and Earth can be neglected.

The problems of molecular aerodynamics. All the conclusions in the foregoing paragraph concern the interaction of bodies with a perfect gas, i.e., with a mechanical system of molecular particles whose mutual interaction is negligibly small.

The state of such a molecular system is characterized by the distribution function f satisfying Boltzmann's kinetic Eq. (10.3.10). If for a given state of the gas the distribution function is known to be a certain solution (or its approximation) to Boltzmann's kinetic equation, the formulas of the foregoing part enable us to establish the dynamic and energetic interactions between gas and body.

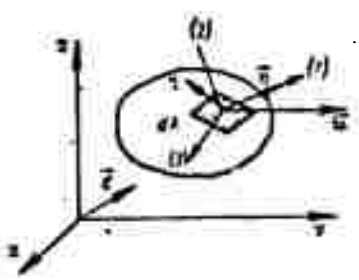


Fig. 10.3.6. A body moving in the system of coordinates x, y, z is connected with the system of rectangular coordinates 1, 2, 3 such that the axis 1 coincides with the direction of the outer normal $\vec{n}$.

In what follows we shall consider the problem of free molecular flow when the mean free path of the molecules considerably exceeds the characteristic linear dimensions of the problem. In this case, as we pointed out above, the collisions of the molecules with each other in the neighborhood of the body virtually does not influence the process of collisions between molecules and body surface. The molecules interact with the body surface indepen-

dently of each other. Such a gas is in statistical equilibrium and the distribution function of the molecules has the form of a Maxwellian distribution (when a monatomic gas is considered):

$$f=\left(\frac{m}{2\pi kT}\right)^{\frac{3}{2}} e^{-\frac{mc^2}{2kT}}=\left(\frac{1}{\pi c_m^2}\right)^{\frac{3}{2}} e^{-\frac{c^2}{c_m^2}}.$$

The reflected molecules do not affect the form of the distribution function because it is fairly improbable that they will collide with each other or with the remaining molecules. Thus, the presence of bodies in a highly rarefied gas does not change the equilibrium distribution function.

In this case the boundary conditions of the mechanics of continuous media are replaced by those of the physics of interaction of gas molecules and the surface of the solid body, which are expressed by the coefficients of accomodation, γ, and adhesion, β.

Let a body of arbitrary shape move in an inertial system of coordinates x, y, z in which the gas is at rest.

With the element dA of the body, having in the x, y, z system the velocity $\vec{w}$, a system of rectangular coordinates 1,2,3 is connected in such a way that the axis 1 is directed along the outer normal $\vec{n}$ (Fig. 10.3.6).

The distribution function of the molecules in the system fixed to the element dA reads

$$f=\frac{1}{(\pi c_m^2)^{\frac{3}{2}}} e^{-\left(\frac{\vec{u}+\vec{w}}{c_m}\right)^2}; \quad f_s=\frac{1}{(\pi c_{ms}^2)^{\frac{3}{2}}} e^{-\frac{c_s^2}{c_{ms}^2}};$$

where $c_m=\sqrt{\frac{2kT}{m}}$, $c_{ms}=\sqrt{\frac{2kT_s}{m}}$ are the most probable velocities of the impinging and reflected gas molecules, respectively.

Let us denote $a_1=\cos(1, \vec{w})$; $a_2=\cos(2, \vec{w})$; $a_3=\cos(3, \vec{w})$; $\xi=u_1:c_m$; $\eta=u_2:c_m$; $\zeta=u_3:c_m$; $w^0=w:c_m$. and, if $(\vec{u}\cdot\vec{n})<0$, then $-\infty<\xi<0$; $-\infty<\eta<\infty$; $-\infty<\zeta<\infty$.

Let $\vec{\sigma}$ be the unit vector of a certain constant direction, where

$$\frac{1}{c_m}\vec{\sigma}\cdot\vec{u}=\alpha_1'\xi+\alpha_2'\eta+\alpha_3'\zeta.$$

Here, taking into account that the first axis 1 coincides with the normal $\vec{n}$, the expressions entering (10.3.19) will be

$$\vec{n}\cdot\vec{u}=u_1=\xi c_m;\quad f=\frac{1}{(\pi c_m^2)^{\frac{3}{2}}}e^{-\left(\frac{\vec{c}+\vec{u}}{c_m}\right)^2}=$$

$$=\frac{1}{\pi\sqrt{\pi}c_m^3}e^{-\frac{1}{c_m^2}\left[\left(w_1^*+u_1\right)^2+\left(w_2^*+u_2\right)+\left(w_3^*+u_3\right)^2\right]c_m^2}$$

and, finally, $du=c_m^3 d\xi\, d\eta\, d\zeta$. Substituting all this into (10.3.19) we obtain

$$v^*=-\frac{Nc_m}{\pi\sqrt{\pi}}\int_{-\infty}^{\infty}\int_{-\infty}^{\infty}\int_{-\infty}^{\infty}\xi e^{-\left[\left(\xi+w_1^*\right)^2+\left(\eta+w_2^*\right)^2+\left(\zeta+w_3^*\right)^2\right]}d\xi\, d\eta\, d\zeta. \qquad (10.3.31)$$

In the same way the total force projection P_σ^* onto the $\vec{\sigma}$-axis is calculated according to Eq. (10.3.22) for a unit area of the body surface

$$P_\sigma^*=-\frac{mNc_m^2}{\pi\sqrt{\pi}}\int_{-\infty}^{\infty}\int_{-\infty}^{\infty}\int_{-\infty}^{\infty}\left(\alpha_1'\xi+\alpha_2'\eta+\alpha_3'\zeta\right)\xi e^{-\left[\left(\xi+w_1^*\right)^2+\left(\eta+w_2^*\right)^2+\left(\zeta+w_3^*\right)^2\right]}\times$$

$$\times d\xi\, d\eta\, d\zeta-\frac{mN_s c_{ms}^2}{\pi\sqrt{\pi}}\int_{-\infty}^{\infty}\int_{-\infty}^{\infty}\int_{-\infty}^{\infty}\alpha_1'\zeta_s^2 e^{-\left(\xi_s^2+\eta_s^2+\zeta_s^2\right)}d\xi_s\, d\eta_s\, d\zeta_s; \qquad (10.3.32)$$

$$E^*=-\frac{Nc_m^2}{\pi\sqrt{\pi}}\int_{-\infty}^{\infty}\int_{-\infty}^{\infty}\int_{-\infty}^{\infty}\frac{\varepsilon^*}{c_m^2}\xi e^{-\left[\left(\xi+w_1^*\right)^2+\left(\eta+w_2^*\right)^2+\left(\zeta+w_3^*\right)^2\right]}d\xi\, d\eta\, d\zeta-$$

$$-\frac{N_s c_{ms}^2}{\pi\sqrt{\pi}}\int_{-\infty}^{\infty}\int_{-\infty}^{\infty}\int_{-\infty}^{\infty}\frac{\varepsilon_s^*}{c_{ms}^2}\zeta_s e^{-\left(\xi_s^2+\eta_s^2+\zeta_s^2\right)}d\xi_s\, d\eta_s\, d\zeta_s; \qquad (10.3.33)$$

with $w_1^*=\alpha_1 w^*$, $w_2^*=\alpha_2 w^*$, $w_3^*=\alpha_3 w^*$.

Let us introduce the expression $\frac{2}{\sqrt{\pi}}\int_0^a e^{-x^2}dx=\Phi(a)$ for the probability integral and

$$\psi(a)=\frac{1}{\sqrt{\pi}}e^{-a^2}+a\left[1+\Phi(a)\right]. \qquad (10.3.34)$$

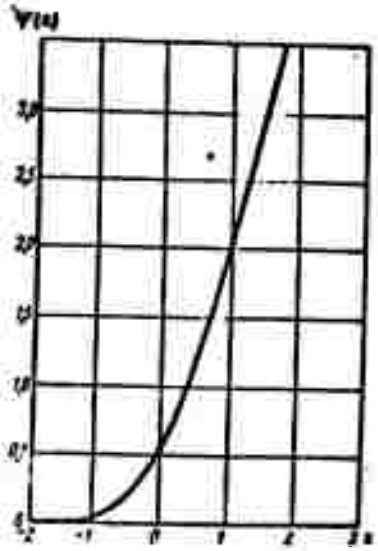


Fig. 10.3.7. Graph of the function ψ.

Let us note some relations for these functions, which we shall need in what follows:

$$\left.\begin{aligned} &\Phi(a) = -\Phi(-a);\quad \Phi(\infty) = 1;\\ &\psi(a) = \psi(-a) + 2a;\quad \psi(\infty) = \infty;\ \psi(-\infty) = 0. \end{aligned}\right\} \quad (10.3.35)$$

The function ψ (a) is graphically represented in Fig. 10.3.7.

Calculating the integrals in the expressions of ν^*, P^*_σ, E^*, we obtain

$$\nu^* = \frac{Nc_m}{2}\psi(s_1 w^0); \quad (10.3.36)$$

$$P^*_\sigma = -\frac{mNc_m}{2}\left\{(s_1 s_1' + s_2 s_2' + s_3 s_3')\, w^0 \psi(s_1 w^0) + \right.$$
$$\left. + \frac{s_1'}{2}\left[1 + \Phi(s_1 w^0)\right] + \frac{s_1'}{2}\frac{N_2 c_{m_2}^2}{N c_m^2}\right\}; \quad (10.3.37)$$

$$E^* = \frac{mNc_m^2}{2}\left\{\left(\frac{5}{4} + \frac{w^{02}}{2}\right)\psi(s_1 w^0) - \frac{e^{-s_1^2 w^{02}}}{4\sqrt{\pi}} - \frac{N_2 c_{m_2}^2}{N c_m^2\sqrt{\pi}}\cdot\right. \quad (10.3.38)$$

In order to determine the number N_d of diffusely reflected molecules we write

$$\nu_2^* = \frac{N_2 c_{m_2}}{\pi\sqrt{\pi}}\int_{-\infty}^{\infty}\int_{-\infty}^{\infty}\int_{-\infty}^{\infty}\zeta_2 e^{-(\xi_2^2+\eta_2^2+\zeta_2^2)}\, d\xi_2\, d\eta_2\, d\zeta_2 = \frac{N_2 c_{m_2}}{2\sqrt{\pi}}$$

and, since the mass of the molecules impinging on each unit are of the surface cf equal to the mass of the diffusely reflected molecules, $\nu^* m = \nu^*_{dm}$, we have

$$N_2 = \sqrt{\pi} N \frac{c_m}{c_{m_2}}\psi(s_1 w^0) = \sqrt{\pi} N \sqrt{\frac{T}{T_2}}\psi(s_1 w^0). \quad (10.3.39)$$

We express the ratio $\frac{c_{m_2}}{c_m} = \sqrt{\frac{T_2}{T}}$ in terms of γ, β and w^0, using Relation (10.3.27) and the expression for the stagnation temperature T_0:

$$T_0 = T\left(1 + \frac{w^2}{2c_p}\right) = T\left(1 + \frac{k-1}{k}w^2\right),$$

so that

$$\sqrt{\frac{T_2}{T}} = \sqrt{(1+\gamma)\left(1 + \frac{k-1}{k}w^{02}\right) + \gamma\frac{T_2}{T}} \quad (\text{for } \beta = 1) \quad (10.3.40)$$

Thus, the final expressions for force and energy referred to a unit area of the surface have the form

$$P_c^* = -\frac{\rho w^2}{2}\left\{(a_1 a_1' + a_2 a_2' + a_3 a_3')\frac{\psi(a_1 w^0)}{w^0} + \frac{a_1'}{2w^{02}}[1 + \Phi(a_1 w^0)] + \right.$$
$$\left. + \frac{a_1'}{2w^{02}}\sqrt{(1-\gamma)\left(1 + \frac{k-1}{k}w^{02}\right) + \gamma\frac{T_c}{T}}\sqrt{\pi}\psi(a_1 w^0)\right\}; \qquad (10.3.41)$$

$$E^* = \frac{\rho w^3}{2}\left[\left(\frac{w^{02}}{2} + \frac{5}{4} - \frac{T_s}{T}\right)\frac{\psi(a_1 w^0)}{w^{03}} - \frac{1}{4\sqrt{\pi}\, w^{03}}e^{-a_1^2 w^2}\right]. \qquad (10.3.42)$$

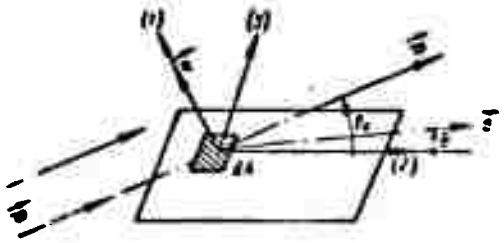


Fig. 10.3.8. Plate in a free molecular flow.

In order to determine the total force acting on the body in the flow of a highly rarefied gas, it is necessary to integrate the expression for P_c^* over the whole surface of the body. The dependence T_d/T on the surface points is then determined from the energy balance Eq. (10.3.29). From this function $T_c = T_c(\vec{w}^0, T, \gamma, \beta, E_1^*, E_2^*)$ and, consequently, the function $\sqrt{T_d : T} = G(\vec{w}, \vec{T}, \gamma, \beta, E_1^*, E_2^*)$ are determined.

In a translatory motion of the solid perfectly heat-conducting (T_s = const) body, G = const and this constant is determined from the energy balance Eq. (10.3.29).

Let us give some examples of calculating the forces acting on a perfectly heat-conducting body executing translatory motion.

The plate. Let θ_0 be the angle of attack of a plate (Fig. 10.3.8). On the upper surface of the plate

$$a_1 = -\sin\theta_0, \quad a_2 = \cos\theta_0, \quad a_3 = 0;$$
$$a_1' = -\sin\theta, \quad a_2' = \cos\theta, \quad a_3' = 0;$$

on the lower surface

$$a_1' = -\sin\theta, \quad a_2' = \cos\theta, \quad a_3' = 0;$$
$$a_1 = \sin\theta_0, \quad a_2 = \cos\theta_0, \quad a_3 = 0.$$

We find from Expression (10.3.41) that

$$P_n = -\frac{\rho v^2}{2} A \left\{2\left(\frac{\psi(v^0 \sin\theta_0)}{v^0 \sin\theta_0} - 1\right)(\sin\theta \sin\theta_0 + \cos\theta \cos\theta_0)\sin\theta_0 + \right.$$
$$\left. + \frac{1}{v_0^2} \sin\theta \Phi(v^0 \sin\theta_0) + \frac{\sqrt{\pi}}{v_0} \sqrt{\frac{T_1}{T}} \sin\theta \sin\theta_0 \right\}. \qquad (10.3.43)$$

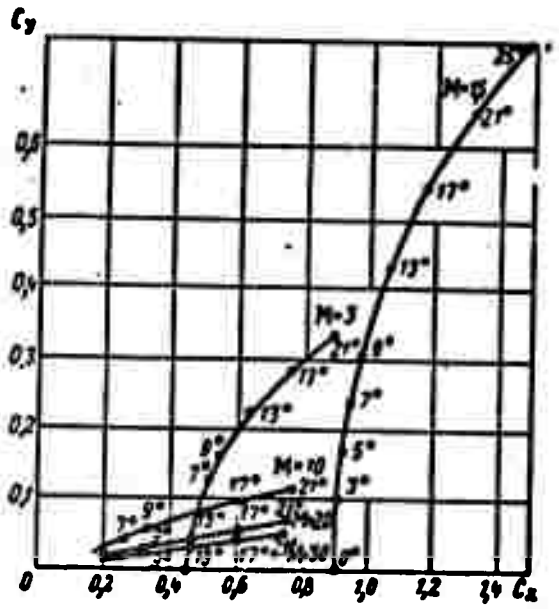


Fig. 10.3.9. Polar curves of a plane plate in a free molecular flow.

We find from this the coefficient of lift and head drag of the plate, assuming $\theta = -\pi/2 + \theta_0$ and $\theta = \pi + \theta_0$:

$$\left.\begin{aligned} C_x &= 2\left\{\left[\frac{\psi(v^0 \sin\theta_0)}{v^0 \sin\theta_0} - 1\right] + \frac{\Phi(v^0 \sin\theta_0)}{v^{02}} + \right. \\ &\left. + \frac{\sqrt{\pi}}{v_0} \sqrt{\frac{T_1}{T}} \sin\theta_0 \right\} \sin\theta_0, \\ C_y &= \left[\frac{\Phi(v^0 \sin\theta_0)}{v_0^2} + \frac{\sqrt{\pi}}{v^0} \sqrt{\frac{T_1}{T}} \sin\theta_0\right] \cos\theta_0. \end{aligned}\right\} \qquad (10.3.44)$$

The graph of Fig. 10.3.9 shows the polar curves for a plane plate at various angles of attack in air of $\rho = 10^{-7}$ kg-sec^2/m^4. It also contains a plot of the polar for a plate in air at sea level with M = = 0.

Body of revolution. Sphere. Let the equation of a body of revolu-

tion be $r=\sqrt{y^2+z^2}=r(x)$, and the vectors $\vec{v}$ and $\vec{w}$ lie in the plane $\underline{x}$, $\underline{y}$ (Fig. 10.3.10).

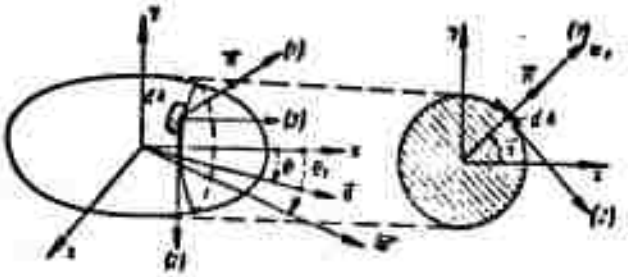


Fig. 10.3.10. Body of revolution in a free molecular flow.

Then $dA=r\sqrt{1+r'^2}\,dx\,d\varphi$;

$$a_1=-\frac{r'\cos\theta_0+\sin\theta_0\sin\varphi}{\sqrt{1+r'^2}};\quad a_1'=-\frac{r'\cos\theta+\sin\theta\sin\varphi}{\sqrt{1+r'^2}};$$
$$a_2=\cos\varphi\sin\theta_0;\quad a_2'=\cos\varphi\sin\theta_0;$$
$$a_3=\frac{\cos\theta_0-r'\sin\theta_0\sin\varphi}{\sqrt{1+r'^2}};\quad a_3'=\frac{\cos\theta-r'\sin\theta\sin\varphi}{\sqrt{1+r'^2}}.$$

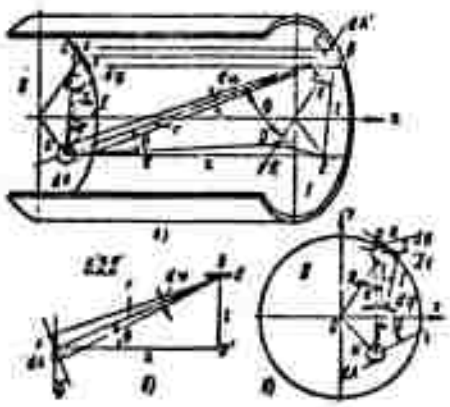


Fig. 10.3.11. Free molecular flow in a tube.

In order to determine the drag we have to put $\theta_0=0$, $\theta=\pi$. in these expressions.

Then

$$\left.\begin{aligned}a_1&=-a_1'=-\frac{r'}{\sqrt{1+r'^2}};\quad a_2=a_2'=0;\\ a_3&=-a_3'=\frac{1}{\sqrt{1+r'^2}}.\end{aligned}\right\}\quad(10.3.45)$$

For a sphere $a_1=-a_1'=\frac{x}{R}$; $a_2=a_2'=0$; $a_3=-a_3'=\frac{\sqrt{R^2-x^2}}{R}$.

Calculations give us the drag coefficient for a sphere

$$C_x=\left(2+\frac{2}{w^0}-\frac{1}{2w^{0.3}}\right)\Phi(w^0)+\frac{e^{-w^{0.2}}}{\sqrt{\pi}}\left(\frac{2}{w^0}+\frac{1}{w^{0.3}}\right)+\quad(10.3.46)$$
$$+2\sqrt{\frac{T_s}{T}}\frac{\sqrt{\pi}}{2w^0}.$$

Notice that since $c_m=\sqrt{\frac{2kT}{m}}=\sqrt{\frac{2}{k}}a$, where $\underline{a}$ is the sonic speed in the gas, we have $w^0=\frac{w}{c_m}=\sqrt{\frac{k}{2}}M$.

Free molecular flow in a tube. Let us suppose that the reflection from the tube walls is purely diffuse ($\beta = 1$). This means that the

surface element dA' of the tube behaves as if it were a source of molecules (Fig. 10.3.11). The number of molecules reemitted from the element dA' per unit time and impinging on the element dA of the plane of the cross section II is determined, if we assume Maxwellian velocity distribution after reflection, by the formula

$$\int_{-\infty}^{\infty} \frac{N'}{\pi^{\frac{3}{2}} c_m^3} e^{-\frac{u^2}{c_m^2}} u^3 du\, d\omega\, dA' \cos\theta' = \frac{N'}{4\pi} c \cos\theta'\, d\omega\, dA', \qquad (10.3.47)$$

where c_m is the most probable velocity, connected with the mean velocity by the relation $c = 2c_m/\pi^{1/2}$; $d\omega$ is the solid angle subtended by the element dA in the plane of the cross section II when viewed from dA'; θ' is the angle between the normal to dA' and the axis of the solid angle $d\omega$; N' is the number of molecules in a unit volume in the cross section I.

When point B', which corresponds to point K' of the element dA, is found in the plane of the cross section I (we denote the distance between B and B' by $\underline{l}$), and we consider the plane of the triangle K'BB' (cf. Fig. 10.3.11,b), we obtain

$$d\omega = \frac{dA \cos\theta}{r^2}, \quad x = r\cos\theta, \qquad (10.3.48)$$

where θ is the angle between the axis of the solid angle $d\omega$ and the line K'B'; $\underline{r}$ is the distance between dA and dA'.

We see from the diagram that

$$r\cos\theta' = l\cos\varepsilon; \quad r^2 = x^2 + l^2;$$
$$d\omega\cos\varepsilon = l\,d\sigma; \quad dA' = d\sigma\, dx, \qquad (10.3.49)$$

where θ' is the angle between the normal to the element dA' and the axis of the solid angle $d\omega$; ε is the angle between the normal and the direction of $\underline{l}$; $d\sigma$ is the projection of the element dA' on the plane of the cross section II (cf. Fig. 10.3.11,c); φ is the angle between the line connecting $d\sigma$ with dA and the fixed reference line (e.g., K'E); $d\varphi$ is the angle $d\sigma$ subtends at dA.

Let us assume that the density function of $\underline{x}$ can be represented by a series

$$N'(x)=N(x)+x\frac{dN}{dx}+\frac{x^2}{2!}\frac{d^2N}{dx^2}+\ldots \qquad (10.3.50)$$

where N' is the number of molecules per unit volume in the Section II. Let us restrict ourselves to the first two terms in Eq. (10.3.50). The number of molecules passing through the element dA of Section II per unit time is then equal to

$$dv=\frac{c\,dA}{4\pi}\int_{-\infty}^{\infty}\frac{\left(N+x\frac{dN}{dx}\right)x\,dx}{(x^2+l^2)^2}\int l^2\,d\tau=\frac{c\,dA}{8}\frac{dN}{dx}\int l\,d\tau.$$

The mass of gas flowing in the positive direction of the axis through Section II is

$$G=-\frac{mc}{8}\frac{dN}{dx}\int dA\int_0^{2\pi} l\,d\tau,$$

but $\frac{dmN}{dx}=\frac{d\rho}{dx}=\frac{1}{RT}\frac{dp}{dx}$ (assuming T = const)

and then

$$G=-\frac{1}{2\sqrt{2RT\pi}}\left(\int dA\int_0^{2\pi} l\,d\tau\right)\frac{dp}{dx}.$$

In the case of a round tube it is easy to calculate the expression in the parentheses when the y-axis is taken parallel to the direction of $\underline{l}$ (cf. Fig. 10.3.11,c):

$$\int dA\int_0^{2\pi} l\,d\tau=\int_0^{2\pi} d\tau\int l\,dA=\int_0^{2\pi} d\tau\int_{-R_0}^{R}dz\int_{-\sqrt{R_0^2-z^2}}^{\sqrt{R_0^2-z^2}}(\sqrt{R_0^2-x^2}-y)\,dy=\frac{16\pi R_0^3}{3}.$$

For a part of the tube of length L ($L \gg R_0$) we have approximately

$$G=\frac{4}{3}R_0^3\sqrt{\frac{2\pi}{RT}}\frac{p_1-p_2}{L}. \qquad (10.3.51)$$

Convective heat exchange with a free molecular flow. If we neglect radiant heat transfer, then the amount of heat transferred by

convection in the gas through a unit area per unit time is equal to

$$Q^* = -E^*, \tag{10.3.52}$$

where E* is the total energy transferred by the molecules. Under the assumption of diffuse reflection alone, E* is determined for a monatomic gas by Formula (10.3.42). We can write

$$-\frac{Q^*}{\frac{\rho w^3}{2}} = \left(\frac{5}{4} + \frac{w^{02}}{2} - \frac{T_s}{T}\right)\frac{\psi(w_1^0)}{w^{02}} - \frac{e^{-w_1^{02}}}{4\sqrt{\pi}\, w^{03}}. \tag{10.3.53}$$

We introduce for convenience the values averaged over the body surface of Q^*, $\frac{e^{-w_1^{02}}}{2\sqrt{\pi}\, w^{03}}$; $\frac{w_1^0[1+\Phi(w_1^0)]}{2w^0}$:

$$\left.\begin{aligned} \tilde{Q} &= \frac{1}{A}\int_\chi Q^*\, dA;\quad \tilde{G} = \frac{1}{A}\int_\chi \frac{e^{-w_1^{02}}}{2\sqrt{\pi}\, w^{03}}\, dA; \\ \tilde{F} &= \frac{1}{A}\int_\chi \frac{w_1^0[1+\Phi(w_1^0)]}{2w^0}\, dA, \end{aligned}\right\} \tag{10.3.54}$$

where A is the surface area of the body.

Integrating Eq. (10.3.55) and making use of the formulas for $\tilde{Q}$, $\tilde{G}$ $\tilde{F}$, and T_d/T, we obtain

$$\begin{aligned} -\frac{2\tilde{Q}}{\rho w^3} = \frac{2}{w^{02}}\Big[\frac{5}{4} + \frac{w^{02}}{2} - (1-\gamma)\Big(1 + \frac{k-1}{k} w^{02}\Big) - \\ - \gamma\frac{T_s}{T}\Big](\tilde{G}+\tilde{F}) - \frac{\tilde{G}}{2w^{02}}. \end{aligned} \tag{10.3.55}$$

This quantity characterizes the mean value of the heat transferred convectively through a unit area of the body surface per unit time.

Let us express (10.3.55) in terms of the Stanton number (6.5.7)

$$\mathrm{St} = \frac{\mathrm{Nu}}{\mathrm{Re}\,\mathrm{Pr}}.$$

If we take into account that $\mathrm{Pr} = \frac{c_p \mu}{\lambda}$, $\mathrm{Re} = \frac{\rho w L}{\mu}$; $\mathrm{Nu} = \frac{\alpha L}{\lambda}$,

we have

$$\mathrm{St} = \frac{\alpha}{\rho w c_p};\quad \alpha = \frac{\tilde{Q}}{T_e - T_r},$$

where α is the heat transfer coefficient and T_r the equilibrium temperature of the body surface. In order to determine the equilibrium temperature it is sufficient to put $\tilde{Q} = 0$:

$$\frac{2}{w^{02}}\left[\frac{5}{4}+\frac{w^{02}}{2}-(1-\gamma)\left(1+\frac{k-1}{k}w^{02}\right)-\gamma\frac{T_p}{T}\right](\tilde{G}+\tilde{F})-\frac{\tilde{Q}}{2w^{02}}=0.$$

Solving this with respect to T_0/T gives us

$$\gamma\frac{T_0}{T}=\frac{5}{4}+\frac{w^{02}}{2}-(1-\gamma)\left(1+\frac{k-1}{k}w^{02}\right)-\frac{\tilde{Q}}{4(\tilde{G}+\tilde{F})}. \qquad (10.3.56)$$

The equilibrium wall temperature determined thus applies only to bodies with infinitely large thermal conductivity, for which T_s is constant over the whole surface.

Introducing Relation (10.3.56) into (10.3.55), we find

$$St=\frac{\tilde{Q}}{\rho_\infty w(T_r-T_p)}=2\gamma\frac{k-1}{k}(\tilde{G}+\tilde{F}). \qquad (10.3.57)$$

so that

$$\frac{w^2}{w^{02}c_p}=\frac{c_m^2}{c_p}=\frac{2RT}{c_p}=2T\frac{k-1}{k}.$$

Formula (10.3.59) applies only to a monatomic gas with k = 5/3. If we take the energy of rotational and vibrational motions of the monatomic gas molecules into account, we find $St=\frac{k+1}{2k}\gamma(G+F)$ [10.3.2]. Rewriting (10.3.57) in the form

$$\frac{k}{4\gamma(k-1)}St=\frac{\tilde{G}+\tilde{F}}{2}, \qquad (10.3.58)$$

we find that the first term is a function of the Mach number M alone; M does not enter it explicitly but for a given shape of the body the quantities $\tilde{G}$ and $\tilde{F}$ are functions of the relative molecular velocity w^0 alone, and since

$$w^0=\frac{w}{c_m}=\sqrt{\frac{k}{2}}M,$$

$\tilde{G}$ and $\tilde{F}$ are functions of the Mach number M.

Thus, the calculation on the process of convective heat exchange in a free molecular flow for a given body can be reduced to calculating the quantities $\tilde{G}$ and $\tilde{F}$ and determining the number St from (10.3.57). Figures 10.3.12 and 10.3.13 show $\tilde{G}$ and $\tilde{F}$ graphically as functions of the relative molecular velocity w^0 and the number M for a plane plate,

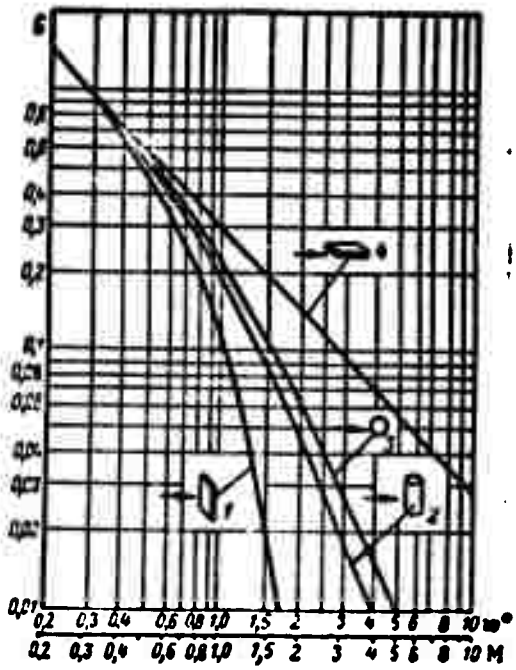


Fig. 10.3.12. Dependence of the function $\tilde{G}$ on w^0 and M.

a sphere and a circular cylinder for the flow directions indicated by the arrows. Figure 10.3.14 shows how St/γ of convective heat exchange

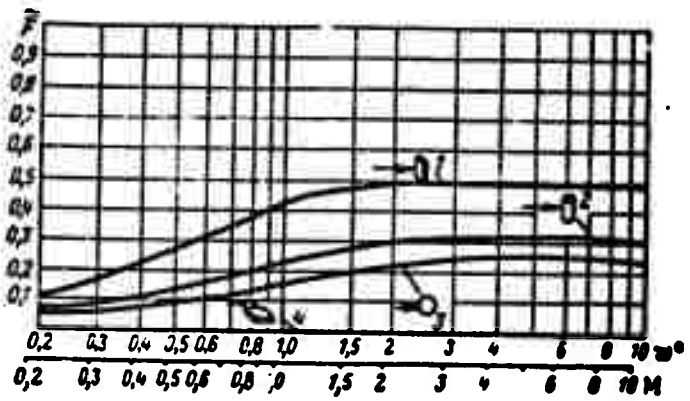


Fig. 10.3.13. Dependence of the function $\tilde{F}$ on w^0 and M.

of a plate, a sphere and a circular cylinder in a monatomic gas flow depend on w^0 and M.

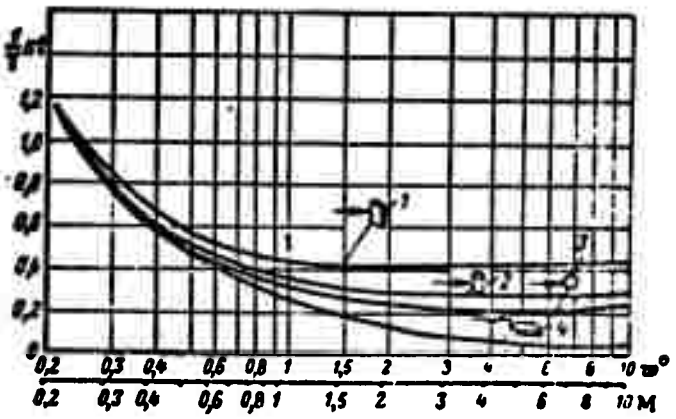


Fig. 10.3.14. Dependence of St on w^0 and M for bodies of various shapes.

It can be seen from Fig. 10.3.14 that the influence of the shape on St decreases as the relative molecular velocity w^0 (or M) decreases. On the other hand, though for large values of w^0 the influence of the shape is obvious for sufficiently large values of this parameter (e.g., $M > 2$), the variation of the number St for a body of arbitrary shape cannot exceed the value of $0.4\,\gamma$ (these considerations refer only to the case in which the whole surface participates in the heat exchange).

Flow with slipping. In those cases of gas motion in which the mean free path of the molecules is comparable to the characteristic dimension of the problem, i.e., when the continuous medium approximation is no longer applicable but when the distribution function of the molecules cannot yet be considered as being Maxwellian, the investigation becomes difficult since the distribution function is unknown. It must be obtained from the kinetic equation for a given approximation.

It is commonly known that in aeromechanics the heat flux is taken as being proportional to the temperature gradient and the stress – to the velocity gradient. Even if these assumptions are considered as being valid for rarefied gases, it is nevertheless necessary to take the changes in the body conditions into account.

In the continuous medium approximation when dimensions of the order of the mean free path of the molecules are disregarded, we can assume that the temperature of the gas layer at the wall is equal to the wall temperature and that the velocity of this layer is equal to the velocity of the wall. In rarefied gases this assumption cannot be admitted, since when the mean free path at the interface between solid and gas is finite, there exists a certain finite difference in temperatures and velocities.

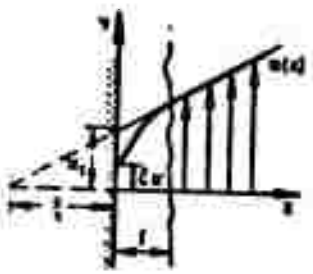


Fig. 10.3.15. In a flow with slipping on a solid wall there arises a discontinuity in the velocity w_σ.

In fact, let us consider the velocity distribution of a gas at a wall (Fig. 10.3.15). Near the wall (at short distances from it) the distribution law w(x) can always be assumed to be linear and $\partial w/\partial x = \text{const}$. At the wall itself, however, in a layer whose thickness is of the order of the mean free path $\underline{l}$, tne shape of the velocity distribution will be rather complex.

When determining the macroscopic gas velocity w(x) in this layer, at distances of the order of $\underline{l}$, we adopt certain conditions. At every site we shall determine this velocity as the mean velocity of the molecules and assume that it is the same everywhere as it is in the case of large gas volumes containing a sufficient number of molecules.

At the wall itself we shall have a certain value of the velocity δw connected with the fact that the gas at the wall is not in general in thermal equilibrium and the energy of the molecules may differ from the energy they would have were the gas at the same temperature as the wall. The value of δw can be obtained only by determining the whole course of the w(x) curve in the layer of the order of $\underline{l}$. This course and the value of δw are however not essential in order to determine

w(x) everywhere in the gas, because it is the linear part of w(x) that is of interest, i.e., the shape of the w(x) curve at distance greater than l. The equation of this linear section of the curve is determined by the gradient $\partial w/\partial x$ and by the section w_s which it cuts off from the ordinate. This section also determined what is called the slip velocity w_s at the wall; it is not a true but an extrapolated jump. If $\partial w/\partial x$ is equal to zero, this jump vanishes. If the gradients $\partial w/\partial x$ are not too large, we may therefore assume that

$$w_s = \zeta \frac{\partial w}{\partial x}. \qquad (10.3.59)$$

where ζ is called the slip coefficient.

The numerical value of ζ depends both on the nature and state of the gas and on the wall material. It follows from the definition of ζ that this quantity is of the order of the mean free path of the gas molecules; graphically ζ is the section that the linear part of the w(x) curve cuts off from the abscissa.

An analogous jump is performed by the temperature too:

$$\delta T = \zeta_T \frac{\partial T}{\partial x}, \qquad (10.3.60)$$

where δT is the difference between wall temperature and gas temperature.

If we take ζ and ζ_T as given, e.g., from experiment, then we can solve a series of slipstream problems. As an example we give the solution of a problem on a slipstream in a tube and the results of an experiment.

Slip flow in a tube. Let us consider a steady motion of an elementary cylinder of radius r cut out of a medium with a cylindrical surface, concentric with the tube.

It follows from the equilibrium between the pressure forces and the frictional forces

$$\pi r^2 \frac{dp}{dz} = 2\pi r\mu \frac{dw}{dr}$$

that

$$w = \frac{r^2}{4\mu}\frac{dp}{dz} + C. \qquad (10.3.61)$$

In the case of slipstream motion $w = w_s \mid r = R_0$ and since $w_s = -\zeta \frac{dw}{dr}\Big|_{r=R_0}$, we have $w_s = -\frac{R_0\zeta}{2\mu}\frac{dp}{dz}$ and therefore $C = -\frac{R_0^2}{4\mu}\times\left(1+\frac{2\zeta}{R_0}\right)\frac{dp}{dz}$, i. e.,

$$w = \frac{R_0^2}{4\mu}\left[\left(\frac{r}{R_0}\right)^2 - \left(1+\frac{2\zeta}{R_0}\right)\right]\frac{dp}{dz}. \qquad (10.3.62)$$

The expression for the flow of a continuous medium with the boundary conditions $w_{r=R_0} = 0$, as was found from (2.6.5), reads

$$w = \frac{R_0^2}{4\mu}\left[\left(\frac{r}{R_0}\right)^2 - 1\right]\frac{dp}{dz}.$$

Thus, in the case of a slipstream the velocity distribution equation acquires an additional term $2\zeta/R_0$, which is proportional to the slip coefficient.

Determining the mass flow through the tube cross section, $G = \rho g \int_0^{R_0} w 2\pi r\, dr$, we obtain (putting $\rho = p/RT$)

$$G = -\frac{\pi R_0^4 pg}{8\mu RT}\left(1+\frac{4\zeta}{R_0}\right)\frac{dp}{dz}. \qquad (10.3.63)$$

For a tube of length L, putting

$$p_{z=0} = p_1, \quad p_{z=L} = p_L,$$

$$G = \frac{\pi R_0^4 g}{16\mu L}\frac{p_1^2 - p_2^2}{RT}\left(1+\frac{4\zeta}{R}\right). \qquad (10.3.64)$$

REFERENCES

10.3.1. Shaaf, Aerodinamika na ochen' bol'shikh vysotakh [Aerodynamics at Very High Altitudes], Collection entitled "Mekhanika" [Mechanics], No. 2, IL [Foreign Literature Press], 1957.

10.3.2. Oppengeym, A., K obshchey teorii konvektivnogo teploobmena v svobodno molekulyarnom potoke [Toward a General Theory of

Convective Heat Transfer in Free Molecular Flow], Collection entitled "Mekhanika," No. 5, IL, 1953.

10.3.3. Braun et al., Techeniye v trubakh gazov pri nizkikh davleniyakh [Flow of Gases in Tubes at Low Pressures], Collection entitled "Mekhanika," No. 2, IL, 1950.

10.3.4. Milliken, R.A., Koeffitsienty skol'zheniya v gazakh i zakon otrazheniya molekul ot poverkhnostey tverdykh tel i zhidkostey [Slip Coefficients in Gases and Law of Reflection of Molecules from Surfaces of Solids and Liquids], Collection entitled "Gazovaya dinamika" [Gas Dynamics], IL, 1950.

10.3.5. Popov, S.G., Nekotoryye zadachi i metody eksperimental'noy aeromekhaniki [Certain Problems and Techniques of Experimental Aerodynamics], GTTI [State Technical and Theoretical Press], 1952.

10.3.6. Tzyan, Kh.Sh., Aerodinamika razrezhennykh gazov [Aerodynamics of Rarefied Gases], In collection entitled "Gazovaya dinamika," IL, 1950.

10.3.7. Timiryazev, A.K., Kineticheskaya teoriya materii [Kinetic Theory of Matter], GTTI, 1933.

10.3.8. Zommerfel'd, A., Termodinamika i statisticheskaya fizika [Thermodynamics and Statistical Physics], IL, 1955.

10.3.9. Kavanau, L.L., Issledovaniye dannogo davleniya pri techenii razrezhennogo gaza so sverkhzvukovymi skorostyami [Investigation of a Given Pressure in the Flow of a Rarefied Gas at Supersonic Speeds], TsAGI [Central Aerohydrodynamics Institute], Technical Translation No. 9265, 1957.

10.3.10. Mey, Vitt, Opredeleniye koeffitsientov soprotivleniya sharov v svobodnom polete [Determining Drag Coefficients of Spheres in Free Flight], In collection entitled "Voprosy raketnoy

tekhniki" [Problems of Rocket Engineering], No. 4, IL, 1954.

10.3.11. Landau, L.D. and Lifshits, B.M., Mekhanika sploshnykh sred [Mechanics of Continuous Media], 1st Edition, GTTI, 1944.

10.4. MAGNETOGASDYNAMICS

In this thirties effects connected with the compressibility of the medium were considered in aeromechanics. Nowadays it has become necessary to introduce into mechanics conceptions connected with the appearance of effects that are electromagnetic in character.

When the flow velocities are small, the gas temperatures are not high and no chemical or nuclear reactions occur in the flow, the amount of charged particles in the gas is negligibly small and the gas has virtually no electrical conductivity. But supersonic and hypersonic flows with intense shock waves greatly change the character of motion of the gas molecules; this leads to a marked ionization of the gas, which thus becomes an electrical conductor. Ionization appears in the reaction of combustion of the gas; it takes place in the high-temperature boundary layer of missiles and satellites as they move rapidly through the atmosphere, and so on.

When a conductive gas (or liquid) moves in a magnetic field, the induced (or external) electric fields give rise to currents in it and, as a result of an interaction of the latter with the magnetic field, forces arise which may be comparable to the aerodynamic forces. At the same time these currents alter the magnetic field itself. An interrelation exists between the electromagnetic and the gasdynamic (hydrodynamic) effects. Magnetogasdynamics (magnetohydrodynamics) is engaged in the investigation of the motion of an electrically conducting gas (fluid) in magnetic and electric fields.

Let us point out that the early work was carried out on magnetohydrodynamics and led to the development of pumps without moving parts for pumping liquid metals. The diagram of the simplest electromagnetic pump is shown in Fig. 10.4.1. Pumps of this type as used in atomic power plants for pumping liquid-metal coolants are described in detail

for example in the Collection of Papers of the Institute of Physics of the AS Latv. SSR [10.4.1].

In recent years the study of problems of electroconductive medium flow control with the help of a magnetic field has been developed with the aim of constructing power plants which make use for example of the magnetic acceleration of a plasma jet in order to decelerate satellites on their entry into the atmosphere, to reduce the heating of flying vessels etc. Great importance is attached to the solution of the problem of isulating a high-temperature plasma (ionized gas) from contact with the walls during thermonuclear reactions ("magnetic bottle").

The following discussions refer to an ionized gas.

The electric field. By analogy with the action of gravitational forces in the field of gravity, the action of an electric charge at a distance is explained with the help of an electric field.

The theory of the electric field is based on Coulomb's empirical law: two like point charges e_1, e_2 repel each other, unlike charges attract each other; if $\vec{r}$ is the distance between the charges the force of interaction is

$$\vec{F} = k\frac{e_1 e_2}{r^3}\vec{r}. \qquad (10.4.1)$$

Ignoring the effect of the charges on the medium, i.e., considering the effects in an absolute vacuum, we choose the unit of charge in the CGS system so that $k = 1$.

The force acting on the charge $e = 1$ is called the intensity (or strength) of the electric field

$$\vec{E} = \frac{e}{r^3}\vec{r}. \qquad (10.4.2)$$

The mechanic (or pondermotive) force acting on a charged body is determined by the product of field strength $\vec{E}$ and body charge e:

$$\vec{F} = e\vec{E}. \qquad (10.4.3)$$

The work done by the forces of the electric field along any path depend only on the positions of the beginning and the end of the path. It is therefore convenient to introduce the conception of the electromagnetic field potential into our considerations, taking it as the negative work done by the field forces when a positive unit charge is displaced:

$$d\varphi = -\vec{E}\cdot d\vec{l} \qquad \varphi = -\int_{\lambda}^{\delta} \vec{E}\cdot d\vec{l}. \tag{10.4.4}$$

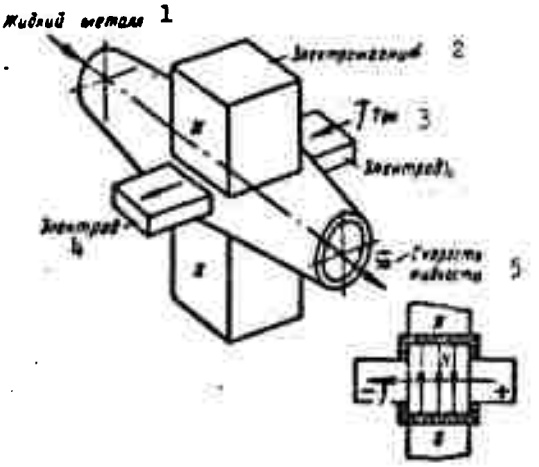


Fig. 10.4.1. The electromagnetic pump operates similarly to an electromotor: the motive force is produced by a conductor carrying current in a magnetic field. The action of an external electric field drives a current through the liquid metal, which plays the part of the conductor, in a direction perpendicular to the magnetic lines of force; the fluid moves perpendicularly to the current and to the field lines (left hand rule). 1) Liquid metal; 2) electromagnet; 3) current; 4) electrode; 5) velocity of liquid.

Conductors and dielectrics. Electrical conductors are bodies characterized by containing free charges such that when there exists a nonzero electric field strength $\vec{E}$ in a conductor, the free charges in it move, i.e., an electric current flows.

Unlike metals and electrolytes, nonconductors (dielectrics) have no free charges which can move over large distances. Under the influence of an external electric field the charges contained in the elec-

trolyte remain at their sites and are only somewhat displaced from their equilibrium positions into certain new equilibrium positions.

The ionized gas. Conduction in a gas comes about through the motion of charged particles and must therefore grow as the number of charged particles grows; their number is determined by the degree of ionization, α, and decreases as the probability of collisions with other particles, such as neutral atoms or molecules or charged particles, increases.

At room temperature the degree, α, is very close to zero and the air has a very low conductivity. If $\alpha = 1$, this means that the gas is completely ionized. A gas in this state is called a plasma, which is sometimes considered as the fourth state of aggregation of matter.

The degree of ionization α may exceed unity, which indicates that not only the first, but also the second and third electrons have been set free, i.e., the particle energy exceeds not only the first but also the second or third ionization potential. Such a high degree of ionization is encountered either at very high temperatures or at very low densities. If α is much smaller than unity, when the charged particles collide mainly with neutral molecules, then the conductivity σ is proportional to α and T, i.e.,

$$\sigma \sim \alpha \sqrt{T}. \qquad (10.4.5)$$

Since α depends itself on the temperature T, the dependence of σ on T is considerably greater.

If α is close to unity then the collisions between charged particles predominate, the conductivity therefore does not depend on α and

$$\sigma \sim T\sqrt{T}. \qquad (10.4.6)$$

Very important in practice is the case when it is possible to diminish the temperature dependence of σ, which may be achieved by adding to the gas an easily ionizable substance such as an alkali metal,

potassium, sodium etc. The substance added is completely ionized at a

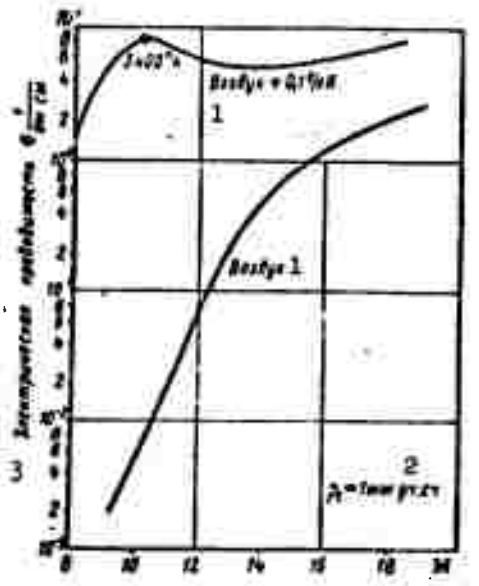


Fig. 10.4.2. Influence of additions of an easily ionizable substance (potassium) on the electrical conductivity of air. 1) Air; 2) mm Hg; 3) electrical conductivity, σ, $ohm^{-1}\ cm^{-1}$.

much lower temperature than the gas; when the temperature of the mixture is raised further, the conductivity does not increase any longer, the added substance is already completely ionized and the increase in ionization of the main gas (e.g., air) with increasing temperature is unimportant. This can be seen from Fig. 10.4.2, which shows the curves of the electrical conductivity of air measured in a shock tube [10.4.2] and of the electrical conductivity of air with an addition of 0.1% potassium (wt%) in dependence on the temperature (the Mach number M) [10.4.3].

It follows from Fig. 10.4.2 that small additions of easily ionizable substances can be used to make the air highly conductive at relatively low temperatures. Thus, for example, adding 0.1% of potassium (wt%) to air raises the conductivity of the air at 3000°K by a factor

of 10^4.

For the purpose of comparison we give data on the conductivity of a few substances: copper $6 \cdot 10^5$ $ohm^{-1}cm^{-1}$; liquid Na (100°C) $1 \cdot 10^5$ $ohm^{-1}cm^{-1}$; mercury $1.08 \cdot 10^4$ $ohm^{-1}cm^{-1}$; saturated aqueous solution of salt (25°C) 0.25 $ohm^{-1}cm^{-1}$; pure water $2 \cdot 10^{-7}$ $ohm^{-1}cm^{-1}$; air at 3000°K 10^{-3} $ohm^{-1}cm^{-1}$; air with an addition of 0.1% K 4.0 $ohm^{-1}cm^{-1}$.

Ohm's law. The fundamental empirical law of direct current – Ohm's law – expresses the fact that the amount of electricity, the current strength I, flowing per unit time through the cross section A of a conductor of length l and the potential difference $\varphi_2 - \varphi_1$ at the ends of the conductor are linked by the relation

$$I = \sigma \frac{\varphi_2 - \varphi_1}{l} A. \qquad (10.4.7)$$

The specific conductivity σ depends on the material of the conductor, and the direction of the current is by convention taken as coinciding with the direction in which positive charges would move under the influence of a field; it is conventionally assumed that the current flows from the higher to the lower one. If ρ is the resistivity ($\rho = 1/\sigma$) the resistance of a conductor is $l/\sigma A$.

This law applies to a large class of transfer effects in which the flow along a given section of its path is directly proportional to the potential difference applied to its ends. For an electric current this rule is known as Ohm's law, for a heat flow as the Fourier law and for momentum transfer as Newton's law of viscous friction.

The potential difference $\varphi_2 - \varphi_1$ may be expressed as a linear integral of the field strenth $\vec{E}$ taken from the initial to the final cross section of the conductor section considered, namely

$$\varphi_2 - \varphi_1 = \int_1^2 \vec{E} \cdot d\vec{l}, \qquad (10.4.8)$$

where $d\vec{l}$ is the length element of the conductor.

The linear integral of the electric field strength between the points 1 and 2 is called the voltage between these points

$$U_{1,2}=\int_1^2 \vec{E}\cdot d\vec{l}=\frac{I}{\sigma A}. \qquad (10.4.9)$$

Noticing that the current strength dI flowing through a filament of cross section dA is equal to dI = jdA, where $\underline{j}$ is the current density, we obtain $dI\underline{dl} = jdV$, dV being the volume of an element of the filament. Since the filament axis coincides with the streamline, i.e., $\underline{dl} \parallel \vec{j}$, the length element of each current filament, the totality of which constitutes the current I through a finite cross section, is equivalent to the volume element $\vec{j}dV$ of this current.

The current direction at each point of the conductor coincides with the direction of the electric field caused by the motion of the charges, i.e., the current density vector $\vec{j}$ must coincide in direction with the vector $\vec{E}$, and therefore

$$\vec{j}=\sigma\vec{E}, \qquad (10.4.10)$$

$$\vec{E}=\frac{1}{\sigma}\vec{j}. \qquad (10.4.11)$$

Joulean heat. The liberation of heat (heating of the conductor) is an inevitable result of the passage of current in the circuit.

The amount of heat Q liberated by the current per unit time is given according to Joule's law by

$$Q=I\int_1^2 \vec{E}\cdot d\vec{l}=\frac{I^2 l}{\sigma A}.$$

For an homogeneous cylindrical conductor the resistance is R = $= \underline{l}/A\sigma$. In this case the amount of heat liberated per unit volume is

$$q=\frac{Q}{V}=\frac{I^2}{\sigma A l A}=\frac{j^2}{\sigma A^2}=\frac{j^2}{\sigma}. \qquad (10.4.12)$$

The electrical induction vector (displacement vector). This vector $\vec{D}$ characterizes the excitation of the medium by the charges it contains. If Σe is the total charge contained in a region bounded by

the surface area A, then the electric induction vector $\vec{D}$ satisfies the equation

$$\oint_A (\vec{D}\cdot\vec{n})\,dA = \sum e.$$

As is shown by experiment, any variation with time of the vector $\vec{D}$ is accompanied by the appearance of current called displacement currents in the medium. Their density is determined by the equation

$$\vec{j}_{см} = \frac{\partial \vec{D}}{\partial t}. \qquad (10.4.13)$$

Unlike the conduction current, which characterizes the motion of electric charges, the displacement current characterizes the displacement of charges within the limits of the intermolecular space; at the same time the field of the free charges is changed as well.

The vector of electrical induction coincides in direction with the field strength vector

$$\vec{D} = \varepsilon\vec{E}. \qquad (10.4.14)$$

The proportionality factor ε (a physical constant of the material) characterizes the dielectric permeability of the medium.

The magnetic field. Between conductors through which electric currents flow there arise mechanical (ponderomotive) forces of interaction which depend on the strengths of these currents and the relative position of the conductors. We may thus imagine that at all points in space around an arbitrary current there exists a field of forces induced by this current. Experience shows that this field is the same as the field of forces of permanent magnets; it is therefore called the magnetic field of the current. Previously, in order to explain the magnetic effects the idea of magnetic charges interacting according to Coulomb's law was put forward and it was assumed that magnetization consists in a polarization of the molecules.

Later on a second source of magnetic fields was found to exist,

namely the electric currents, i.e., the moving electric charges, where the currents, like magnets, are themselves subject to ponderomotive forces in an external magnetic field. The suggestion has been made (Ampere) that the apparent existence of magnetic charges is in fact caused by the presence of current circuits in the molecules. The modern idea of the atom substantiates this hypothesis and explains the magnetic properties of the bodies in terms of firstly the revolution of the electrons about the atomic nucleus and secondly the self-rotation (spin) of the electrons. It can be shown that the magnetic properties of bodies are specified by correspondingly distributed molecular electric currents. However, this descriptive idea of the so-called "self-rotation" of the electron does not correspond to reality and it was left to quantum mechanics to explain the magnetic properties of the electron satisfactorily.

The magnetic field at each point in space may be characterized by a certain vector $\vec{H}$ which is called the magnetic field strength, where, as is shown by experiment, the force $d\vec{F}$ acting in a field of the strength $\vec{H}$ on a current element of the length $d\vec{l}$ through which a current of intensity I flows, is equal to

$$d\vec{F}=I\left(d\vec{l}\times_{P_0}\vec{H}\right). \qquad (10.4.15)$$

This formula can be considered as the definition of the notion of the "magnetic field strength."

The magnetic field of a current element is determined according to the Biot-Savart law (3.8.18) by

$$d\vec{H}=\frac{I}{r^3}\left(d\vec{l}\times\vec{r}\right). \qquad (10.4.16)$$

Here $\vec{r}$ is the distance from the current element $Id\vec{l}$ exciting the magnetic field $\vec{H}$ to the "point of observation" where the strength $\vec{H}$ of this field is determined. This law is analogous to that for the

field of a vortex line.

In order to characterize the magnetization by a quantity analogous to the vector of electrical induction, a vector of magnetic induction, $\vec{B}$, is introduced; it is connected with the magnetic field strength $\vec{H}$ by the relation

$$\vec{B}=\mu_e\vec{H}. \qquad (10.4.17)$$

where μ_e is the magnetic permeability of the medium (μ_{eC} = 1 for a vacuum, $\mu_e > 1$ for magnetics and $\mu_e < 1$ for diamagnetics).

The Lorentz force. Let us consider the motion of charged particles. In a perfect vacuum, in the presence of solely an electric field $\vec{E}$ the force

$$\vec{F}_e=Ze\vec{E},$$

acts on the particle, where Ze is the particle charge. In this case the particle moves in the direction in which the electric field strength vector is directed.

If a charged particle moves at a velocity $\vec{w}$ in vacuum where only a magnetic field $\vec{H}$ is present, then the force

$$\vec{F}_m=Ze\left(\vec{w}\times\mu_e\vec{H}\right).$$

will act upon it.

When an electric and a magnetic field act jointly on the particle the force will be

$$\vec{F}=Ze\left(\vec{E}+\vec{w}\times\mu_e\vec{H}\right). \qquad (10.4.18)$$

which is called the Lorentz force.

When $\vec{H}$ is constant and $\vec{w}\perp\vec{H}$, this force is equal to ZewH and must be balanced by the centrifugal force mw^2/R, i.e.,

$$Zew\dot{H}=\frac{mw^2}{R}.$$

where m is the mass of the charged particle; for an electron ($Z = 1$, $m = m_e$)

$$R=\frac{m_e w}{eH},$$

R is the radius of the electron's trajectory.

If w and H are constant then R is constant too, i.e., the trajectory is a circle. Therefore, in a homogeneous magnetic field of strength $\vec{H}$ (0, 0, H) an electron with the thermal velocity c will move in the xy-plane along a circle of radius

$$R=\frac{m_e c}{eH}. \qquad (10.4.19)$$

This radius is called the Larmor radius.

If a uniform electric field is simultaneously applied parallel to the magnetic field, then the particle trajectory will be a helical spiral.

Since an electron and an ion carry charges which are equal in magnitude and the mass of the electron is almost 1840 times smaller than the mass of the ion, the radius of curvature for the electron is correspondingly much smaller than the radius of curvature for the ion.

This radius of curvature is the most important linear dimension in magnetogasdynamic problems. The equations of magnetogasdynamics based on the assumption that the gas is a continuous medium, are applicable only when the radius of curvature of the particle trajectory is much larger than the mean free path of the particle. Since the radius of the trajectory of an electron is many times smaller than that of an ion, checks must be made on the radius of the trajectory of an electron.

The conductivity of the medium will be isotropic if the radius of curvature of the trajectories of the electrons which constitute the current in the magnetic field is large compared with the mean free

path l, i.e., if

$$H \ll \frac{mc}{ed}. \qquad (10.4.20)$$

For a liquid this condition is always satisfied, but for rarefied gases in strong magnetic fields it is not.

Induction. If a closed metallic conductor L to which no other elctromotive forces are applied moves in an external magnetic field H at a certain velocity $\vec{w}$, then, denoting by $\vec{u}$ the velocity of any of the "free" electrons relative to the conductor (so that the total velocity of any of the electron is $\vec{w}' = \vec{w} + \vec{u}$), we obtain the Lorentz force acting on it as

$$\vec{F} = e\left(\vec{w}' \times \mu_0 \vec{H}\right) = e\left(\vec{w} \times \mu_0 \vec{H}\right) + e\left(\vec{u} \times \mu_0 \vec{H}\right) = \vec{F} + e\left(\vec{u} \times \mu_0 \vec{H}\right).$$

The second right-hand term is perpendicular to the velocity $\vec{u}$ of the electron relative to the conductor and therefore the force corresponding to this term will not change the magnitude of this force $\vec{u}$ but will only bend the path of the electron in the conductor.

As regards the first force component, however,

$$\vec{F} = e\left(\vec{w} \times \mu_0 \vec{H}\right), \qquad (10.4.21)$$

it is nonzero only in moving conductors, and the force $\vec{F}$ is generally speaking not perpendicular to $\vec{u}$ and may therefore accelerate (or decelerate) the motion of the electrons relating to the conductor, i.e., it may excite electric currents. Thus, for example, in a section of the conductor L (Fig. 10.4.4) the Lorentz force acting on the electrons will drive them to the left with respect to the conductor. An electric current therefore arises in the conductor. Since the direction of the current is conventionally assumed to be opposite to the direction in which the negative charges move, the current is found to flow from the left to the right. This is the basis of the current induction effect which arises when a conductor is moved in a magnetic

field.

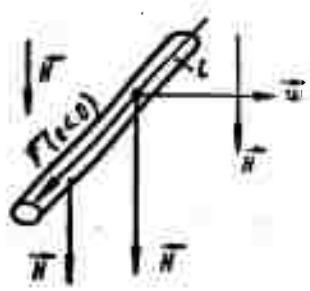


Fig. 10.4.3. The Lorentz force $\vec{F} = e(\vec{w} \times \mu_e \vec{H})$ accelerates a negatively charged particle according to the left hand rule.

Thus, the formula $\vec{j} = \sigma \vec{E}$ applies to conductors which are at rest relative to the field. If the conductor is moved with the velocity $\underline{w}$ (much smaller than the velocity of light), then

$$\vec{j} = \sigma\left(\vec{E} + \vec{w} \times \mu_e \vec{H}\right). \qquad (10.4.22)$$

This equation determines the conduction current induced by the simultaneous action of an external electric field $\vec{E}$ and the electric field induced in the conductor as it moves in the magnetic field. Comparing (10.4.18) and (10.4.22) with (10.4.2) and (10.4.4) the sum $\vec{E} + \vec{w} \times \mu_e \vec{H}$ may be considered as playing the part of an "effective" electric field strength.

If the medium moves, then the current contains not only the conduction current determined by (10.4.22), but also a convective component which is connected with the displacement of charges together with the substance of the medium:

$$\vec{j} = \rho_{sv}\vec{w} + \sigma\left(\vec{E} + \mu_e \vec{w} \times \vec{H}\right), \qquad (10.4.23)$$

where ρ_{sv} is the free charge density

If the conductivity of the medium is large enough the convective current in (10.4.23) can be neglected.

The displacement current. If the frequency ω of a periodically alternating field $E = E_0 \sin \omega t$ is given, the displacement current (10.4.13) is determined by the expression

$$j_{cm} = \frac{\partial D}{\partial t} = \varepsilon \omega E_0 \cos \omega t.$$

The displacement current may therefore be neglected when the density

$$\frac{j}{j_{ind}} \sim \frac{\omega}{\omega_0} \gg 1. \qquad (10.4.24)$$

is valid.

If the conduction current is sustained only by an electric field induced by the motion in a homogeneous magnetic field, $\vec{j} = \sigma\mu_0 \vec{w} \times \vec{H}$, the role of the frequency ω is played in this case by w/L (since w = L/t) where w and L are the characteristic velocity and the characteristic linear dimension of the flow. Condition (10.4.24) assumes the form

$$\frac{\sigma L}{\omega} \gg 1. \qquad (10.4.25)$$

Lenz's rule. The force (10.4.21) an electron experiences in the magnetic field $\vec{H}$ when it moves together with the conductor at the velocity $\vec{w}$ is equal to the force acting on an electron in an electric field of strength $\vec{E}'$, if

$$\vec{E}' = \vec{w} \times \mu_0 \vec{H}. \qquad (10.4.26)$$

Under the influence of the field $\vec{E}'$, and also, accordingly, under the influence of a field $\vec{H}$ equivalent to $\vec{E}'$, a current must arise in a closed contour L, the intensity I of which is obtained from Eq. (10.4.6):

$$\frac{I}{\sigma A} = \int_l \vec{E}' \cdot d\vec{l} = E_{ind}, \qquad (10.4.27)$$

where $1/\sigma A$ is the resistance of the contour L and E_{ind} is the induction of the vector $\vec{E}'$ along the contour L. The latter quantity is termed the induced electromotive force; according to (10.4.26) it is equal to

$$E_{ind} = \int (\vec{w} \times \mu_0 \vec{H}) \cdot d\vec{l} = -\int \vec{w} \cdot (d\vec{l} \times \mu_0 \vec{H}). \qquad (10.4.28)$$

This equation expresses the well known law of current induction in moving conductors. If we introduce the magnetic flux Φ into our

discussion, then $E_{ind} = -d\Phi/dt$, i.e., the induced electromotive force arising in the conductor is equal to the rate of change of the flux of the magnetic vector through a surface bounded by the contour of this conductor. The minus sign in this equation indicated that if the magnetic flux increases in magnitude, the direction of the induced electromotive force in this contour coincides with the direction of flow in a left-handed system and vice versa.

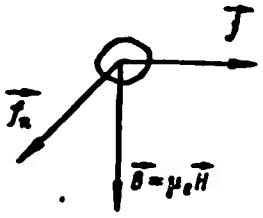


Fig. 10.4.4. The electric volume force $\vec{f}$ is determined by the vector product of current density $\vec{J}$ and magnetic induction $\vec{B} = \mu_e\vec{H}$.

Electric volume force. The term electric volume forces is understood to mean the volume forces arising in a conducting medium under the action of an electromagnetic field.

Taking into account that $Id\vec{l} = \vec{J}dV$ we can rewrite Expression (10.4.15) for a medium with magnetic permeability as

$$d\vec{F} = (\vec{J} \times \mu_e\vec{H})\,dV. \qquad (10.4.29)$$

The strength $\vec{f}_p$ of the electric (pondermotive) volume force (per unit volume) is then equal to

$$\vec{f}_n = \vec{j} \times \mu_e\vec{H}. \qquad (10.4.30)$$

These three vectors form a right-handed system (Fig. 10.4.4).

When the conductor is moved the electric volume forces perform negative work, i.e., they oppose the motion in accordance with Lenz's rule: induction currents arising in a conductor as it moves in a constant magnetic field are so directed that the electric volume forces exerted by these currents act so as to oppose the motion of the conductor.

In the general case the electric volume force includes the force due to the magnetic field acting on the charges associated with a unit

volume of the medium:

$$\vec{f}_{\text{в}}=\rho_{\text{св}}\vec{E}+\mu_{\text{в}}\vec{j}\times\vec{H}.$$

It is, however, possible to show that $\rho_{sv}\vec{E}$ is of the order of magnitude of w^2/c^2_{sveta} as compared with $\mu_{\text{в}}\vec{j}\times\vec{H}$, but in magnetogasdynamics the macroscopic velocities of the media are always much smaller than the velocity of light c_{sveta}, and therefore the terms of the order of w^2/c^2_{sveta} can be omitted. This means that in magnetogasdynamic problems the whole energy of the field is magnetic energy.

The Maxwell equations. The Maxwell equations link the four parameters that characterize the state of the electromagnetic field: the electric field strength vector $\vec{E}$, the displacement vector $\vec{D}$, the magnetic field strength vector $\vec{H}$ and the magnetic induction vector $\vec{B}$:

$$\left.\begin{gathered}\operatorname{rot}\vec{H}=\vec{j}+\frac{\partial\vec{D}}{\partial t};\quad \operatorname{rot}\vec{E}=-\frac{\partial\vec{B}}{\partial t};\quad \operatorname{div}\vec{B}=0;\quad \operatorname{div}\vec{D}=\rho_{\text{св}};\\ \frac{\partial\rho_{\text{св}}}{\partial t}=-\operatorname{div}\vec{j}_{\text{в}}\end{gathered}\right\}\qquad(10.4.30)$$

where ρ_{sv} is the density of the free electrons. By virtue of the equations $\vec{B}=\mu_{\text{в}}\vec{H}$; $\vec{D}=\varepsilon\vec{E}$, and when the displacement current is ignored, this system can be reduced to the two Maxwell equations*

$$\operatorname{rot}\vec{H}=\vec{j};\qquad(10.4.31)$$

$$\operatorname{rot}\vec{E}=-\mu_{\text{в}}\frac{\partial\vec{H}}{\partial t}\qquad(10.4.32)$$

and Ohm's law

$$\vec{j}=\sigma\left(\vec{E}+\mu_{\text{в}}\vec{w}\times\vec{H}\right).\qquad(10.4.33)$$

These equations are written in the absolute practical rationalized MKSA system (m, kg, sec, a) in which, for vacuum, $\mu_{\text{в}0}=4\pi\cdot10^{-7}$ ohm.sec/m and since

$$\frac{1}{\sqrt{\varepsilon_0\mu_0}}=c_{\text{света}}=3\cdot10^8\ \text{m/sec}$$

for a vacuum

$$\varepsilon_0 = \frac{1}{4\pi} \cdot \frac{1}{9 \cdot 10^9} \qquad \text{sec/ohm-m}$$

The electromagnetic field energy is determined by an equation which is obtained from the Maxwell equations and which has the form

$$\frac{\partial}{\partial t}\int_V \frac{\varepsilon E^2 + \mu_e H^2}{8\pi} dV = \int_A \vec{S}_n \vec{n}\, dA - \int_V \vec{j}\cdot\vec{E}\, dV. \qquad (10.4.34)$$

In this equation it is taken into account that the change in total electromagnetic energy in the volume V is equal to the flux of the Poynting vector $\vec{S} = \vec{F} \times \vec{H}$ through a surface A bounding the volume V, and to the Joulean heat arising inside the volume.

Poynting's flux vector is proportional to the fourth power of the a-c frequency ω, and for the frequencies encountered in gasdynamics it is very small compared with the Joulean heat. The change in electromagnetic field energy in magnetogasdynamic problems can therefore be due only to the electrical resistance of the medium, and the Joulean heat obtained must enter the energy equation of the gas flow. The Joulean heat per unit volume may be written in the form

$$q_{Jo} = \frac{j^2}{\sigma} \qquad (10.4.35)$$

If the properties of the medium differ from the properties of empty space, the integrand of the left-hand side of the electromagnetic energy equation assumes the form $\frac{\varepsilon E^2 + \mu_e H^2}{8\pi}$.

The equations of motion. The appearance of two new effects in a fluid in which a current flows, namely the appearance of the electric volume force $\vec{f}_p = \mu_e \vec{j} \times \vec{H}$ and the liberation of the Joulean heat j^2/σ, influences the form of the momentum equation (the force $\vec{f}_p/\rho$ must be added to the body force) and of the energy equation (the Joulean heat must be added to the heat supplied). The motion is described by the equations

$$\frac{\partial \rho}{\partial t} + \operatorname{div} \rho \vec{w} = 0; \tag{10.4.36}$$

$$\frac{d\vec{w}}{dt} = \vec{f} - \frac{1}{\rho}\nabla p - \frac{\mu_e}{\rho}(\vec{j} \times \vec{H}) + \nu\left(\nabla^2 \vec{w} + \frac{1}{3}\nabla\nabla \cdot \vec{w}\right); \tag{10.4.37}$$

$$\rho c_v \frac{dT}{dt} + p\nabla \cdot \vec{w} = \frac{f^2}{\sigma} + Q; \tag{10.4.38}$$

$$\operatorname{rot} \vec{H} = \vec{j}; \tag{10.4.39}$$

$$\operatorname{rot} \vec{E} = -\mu_e \frac{\partial \vec{H}}{\partial t}; \tag{10.4.40}$$

$$\vec{j} = \sigma(\vec{E} + \mu_e \vec{w} \times \vec{H}). \tag{10.4.41}$$

Moreover we shall assume that the equation of state of a perfect gas remains valid:

$$p = \rho RT. \tag{10.4.42}$$

Here $Q = \mu D + \lambda \Delta T$ denotes the total heat apart from the Joulean heat received by a fluid element, i.e., it includes the thermal conductivity and viscous dissipation. For simplicity the viscosity here is taken as being constant, through it should be remembered that it depends on T.

It follows from Eq. (10.4.38), which expresses the first law of thermodynamics, that the heat supplied to or removed from a moving medium becomes apparent in a change of internal energy and in the mechanic work performed, and that there are no other forms of energy conversion besides the Joulean heat mentioned above. In more complex cases, e.g., if the magnetic permeability is a function of the temperature or of the field strength then, according to the first law of thermodynamics, the energy Eq. (10.4.35) must be written in another, more expanded form.

We separate explicitly the work of the forces by scalar multiplication of the momentum equation by the velocity $\vec{w}$ and addition of it

to the energy Eq. (10.4.38), and we write the energy equation so that the terms which characterize the unsteadiness are separated:

$$c_v\frac{\partial T}{\partial t}+\frac{1}{2}\frac{\partial w^2}{\partial t}+p\frac{\partial}{\partial t}\left(\frac{1}{\rho}\right)+\vec{w}\cdot\nabla h_0=$$

$$=\frac{\mu_e}{\rho}\vec{w}\cdot(\vec{j}\times\vec{H})+\frac{j^2}{\rho\sigma}+\nu\left(\nabla^2\vec{w}+\frac{1}{3}\nabla\nabla\cdot\vec{w}\right)\cdot\vec{w}+Q. \qquad (10.4.43)$$

Here $h_0=c_vT+\frac{p}{\rho}+\frac{w^2}{2}=c_pT+\frac{w^2}{2}$ is the stagnation enthalpy. This form is convenient for steady-state problems since the first three terms of the left-hand side vanish and all that remains on the left is the rate of change of the stagnation enthalpy of the fluid particle. This rate of change consists of two magnetoaerodynamic terms – the mechanical work done by the electric volume force, and the Joulean heat. Their interrelation determines the character of variation of the motion parameters.

Similarity criteria in magnetogasdynamics. Let us eliminate $\vec{j}$ and $\vec{E}$ from Eqs. (10.5.36) – (10.4.41). For this purpose we substitute the expression for $\vec{j}$ from (10.4.39) into Eq. (10.4.37):

$$\frac{\partial\vec{w}}{\partial t}+\vec{w}\cdot\nabla\vec{w}+\frac{1}{\rho}\nabla p=\nu\left(\Delta\vec{w}+\frac{1}{3}\nabla\nabla\cdot\vec{w}\right)-$$

$$-\frac{\mu_e}{\rho}(\vec{H}\times\operatorname{rot}\vec{H}). \qquad (10.4.44)$$

and the expressions for $\vec{E}$ from (10.4.41) and for $\vec{j}$ from (10.4.39) in Eq. (10.4.40):

$$\frac{\partial\vec{H}}{\partial t}=\operatorname{rot}(\vec{w}\times\vec{H})-\frac{1}{\sigma\mu_e}\operatorname{rot}\operatorname{rot}\vec{H}=\operatorname{rot}(\vec{w}\times\vec{H})-\frac{1}{\sigma\mu_e}(\nabla\operatorname{div}\vec{H}-\Delta\vec{H}).$$

Making use of the condition $\operatorname{div}\vec{H}=0$, we obtain the so-called induction equation:

$$\frac{\partial\vec{H}}{\partial t}=\operatorname{rot}(\vec{w}\times\vec{H})+\nu_m\Delta\vec{H}, \qquad (10.4.45)$$

where $\nu_m=1/\mu_e\sigma$ is what is called the "magnetic viscosity"; it is introduced analogously to the viscosity coefficient ν, so that the term $\nu_m\Delta\vec{H}$ characterizes the dissipation of electromagnetic energy to

Joulean heat.

Let us put the first term of the right-hand side of Eq. (10.4.45), which characterizes the energy consumed in maintaining the currents in the moving medium, equal to the second, which characterizes the energy dissipation:

$$\frac{wH:L}{\nu_m H:L^2}=\frac{wL}{\nu_m}. \qquad (10.4.46)$$

The physical meaning of this quantity is analogous to the physical meanings of the common Reynolds number and the structure of the formula coincides with the structure Re = wL/ν. The dimensionless combination (10.4.46) was therefore the magnetic Reynolds number

$$Re_m=\frac{wL}{\nu}=\mu_0\sigma wL. \qquad (10.4.47)$$

For $Re_m \gg 1$ the electrical resistance of the medium and the Joulean losses connected with it can be neglected in the same way as the viscosity is "neglected" in normal hydromechanics at large Re numbers. In cosmic gasdynamics $Re_m \approx 10^6$ and higher, because of the food conductivity of the ionized gas and the huge dimensions of the objects considered [10.4.2]. In many problems where the common Re numbers are large, it is sufficient to restrict oneself to considering an inviscid fluid with infinite conductivity.

Under terrestrial conditions such Re_m values are not reached; e. g., in experiments with mercury and liquid sodium $Re_m \approx 10^{-2}$-10^0.

The magnetic number Re_m may be interpreted [10.4.2] as the ratio between the induced and applies magnetic field. The induced field can be determined from the Maxwell equation

$$\operatorname{curl} \vec{H} = \vec{j}$$

Repeating considerations analogous to those made on calculating the field of velocities $\vec{w}$ under the action of a given vortex distribution $2\vec{\omega} = \operatorname{curl} \vec{w}$, we find that the induced field will be proportional

to $\mu_e \sigma w H L$;

$$Re_m = \mu_e \sigma w l = \frac{\mu_e \sigma w H L}{H}.$$

Let us estimate the possible values of the Re_m number in magnetogasdynamics. If we take ρ = 1.0 ohm^{-1}cm^{-1} and L = 1 cm, then

$$Re_m = \mu_e \sigma w L = 10^{-5} w$$

(the coefficient 10^{-5} is introduced for conformity of the measuring units). Even if we put w $\approx 10^4$ m/sec, Re_m assumes an order of 10^{-1}. To estimate the order of magnitude of the last term of Eq. (10.4.44), which characterizes the electric volume force, we write it as a ratio to the dynamic head $\mu_e H^2/\rho w^2$. The quantity $H (\mu_e/\rho)^{1/2}$ has the dimension of a velocity and is called the velocity of Alven waves.

$$c_A = H \sqrt{\frac{\mu_e}{\rho}}. \qquad (10.4.48)$$

In order to explain the physical meaning of this velocity we consider [10.4.7] a medium of infinite conductivity, $\sigma \to \infty$, i.e., $\nu_m = 0$.

Equation (10.4.45) can be written in the form

$$\frac{\partial \vec{H}}{\partial t} - \mathrm{rot}(\vec{w} \times \vec{H}) = 0. \qquad (10.4.49)$$

and the continuity Eq. (10.4.36) in the form

$$\frac{\partial \rho}{\partial t} + \mathrm{div}\, \rho \vec{w} = \frac{\partial \rho}{\partial t} + \vec{w} \cdot \vec{\nabla} \rho + \rho \vec{\nabla} \cdot \vec{w} = \frac{d\rho}{dt} + \rho \vec{\nabla} \cdot \vec{w} = 0.$$

Combining them we obtain

$$\frac{d}{dt}\left(\frac{\vec{H}}{\rho}\right) = \frac{1}{\rho}\frac{d\vec{H}}{dt} - \frac{\vec{H}}{\rho^2}\frac{d\rho}{dt} = \frac{1}{\rho}(\vec{H} \cdot \vec{\nabla})\vec{w}, \qquad (10.4.50)$$

where $(\vec{H} \cdot \nabla)\,\vec{w}$ is the gradient of the velocity vector $\vec{w}$ with respect to the vector $\vec{H}$.

If $(\vec{H} \cdot \nabla)\,\vec{w} = 0$, i.e., if the velocity does not vary along the magnetic lines of force $\vec{H}$, and since it does not do so for one dimensional and cylindrical-symmetrical flows, then in these flows the quantity

$$\frac{\vec{H}}{\rho}=\vec{b} \text{ or } \vec{H}=\rho\vec{b}. \qquad (10.4.51)$$

is conserved.

This may be looked upon as a condition of "freezeability" of the magnetic field in the fluid.

In fact the change with time of the vector $\vec{H}$ flux through the surface A bounded by the contour L moving along with the gas will be

$$\frac{d}{dt}\int_A \vec{H}\cdot d\vec{A}=\lim_{u\to 0}\int_A \frac{\vec{H}(l+u)-\vec{H}(l)}{u}d\vec{A}+$$
$$+\lim_{u\to 0}\frac{1}{u}\left[\int_{A_t+u}\vec{n}\cdot\vec{H}\,dA-\int_{A_t}\vec{n}\cdot\vec{H}\,dA\right].$$

The first limit of the right-hand side will be $\int_A \frac{\partial\vec{H}}{\partial t}dA$. In order to calculate the second limit we consider the volume δV circumscribed by the contour L as it moves in the fluid during the time δt; its end faces will be A_t and $A_{t+\delta t}$ and the lateral surface A_{bok} has the generatrix $\vec{w}\delta t$:

according to Ostrogradskiy's formula

$$\int_{\delta V}\vec{\nabla}\cdot\vec{H}\,dV=\int_{A_t}\vec{H}\cdot d\vec{A}+\int_{A_{bok}}\vec{H}\cdot d\vec{A}+\int_{A_{t+u}}\vec{H}\cdot d\vec{A}$$

and when the direction of the normal $\vec{n}$ is taken into account

$$\int_{A_{t+u}}\vec{n}\cdot\vec{H}\,dA-\int_{A_t}\vec{n}\cdot\vec{H}\,dA=\int_{\delta V}\vec{\nabla}\cdot\vec{H}\,dV-\int_{A_{bok}}\vec{n}\cdot\vec{H}\,dA.$$

In the first integral the right-hand side is $dV=\vec{w}u\cdot\vec{n}\,dA$ and for it $\int_{\delta V}\nabla\cdot\vec{H}dV=u\int_A(\vec{\nabla}\cdot\vec{H})\vec{w}\cdot d\vec{A}$; the second integral can be transformed in the following way if it is taken into account that on the lateral surface $\vec{n}\cdot dA=d\vec{A}=\vec{w}u\times\vec{u}l$:

$$\int_{A_{bok}}\vec{n}\cdot\vec{H}\,dA=\int_L\vec{H}\cdot(\vec{w}u\times\vec{u}l)=u\int_L(\vec{H}\times\vec{w})\,d\vec{l}=$$
$$=u\int_A\vec{n}\cdot\mathrm{rot}(\vec{H}\times\vec{w})\,dA.$$

Thus,

$$\frac{d}{dt}\int_A\vec{H}\cdot d\vec{A}=\int_A\frac{\partial\vec{H}}{\partial t}\cdot d\vec{A}+\int_A(\vec{\nabla}\cdot\vec{H})\vec{w}\cdot d\vec{A}+\int_A\mathrm{rot}(\vec{H}\times\vec{w})\cdot d\vec{A}$$

or

$$\frac{d}{dt}\int_{\Lambda}\vec{H}\cdot d\vec{\Lambda}=\int_{\Lambda}\left[\frac{\partial\vec{H}}{\partial t}+\operatorname{rot}(\vec{H}\times\vec{w})+\vec{w}(\vec{\nabla}\cdot\vec{H})\right]\cdot\vec{n}\,d\Lambda.$$

In a medium of infinite conductivity, as can be seen from (10.4.8), $\frac{\partial\vec{H}}{\partial t}-\operatorname{rot}(\vec{H}\times\vec{w})$ vanishes. According to Eq. (10.4.30) div $\vec{H}$ = 0 and therefore $\frac{d}{dt}\int_{\Lambda}\vec{H}\cdot d\vec{\Lambda}=0$. i.e., the flux of the vector $\vec{H}$ through a surface moving together with the gas remains unchanged.

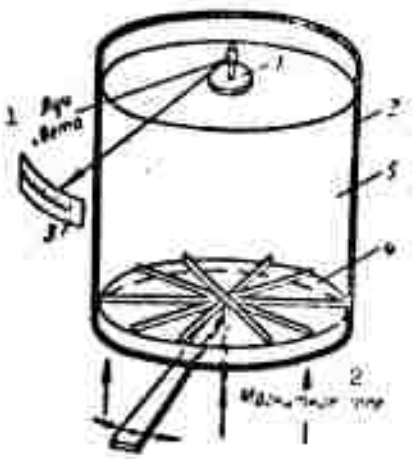


Fig. 10.4.5. In the presence of a magnetic field, the disturbances induced in mercury 5 on the bottom of the vessel 2 by vibrations of a ribbed plate 4 are immediately transferred to the surface by magnetogasdynamic disturbances. 1) Light ray; 2) magnetic field.

The lines of force are as if "frozen" in the medium. Substantial points, initially situated on any one of the magnetic lines of force remain fixed on it during the motion. This condition may be explained physically by the fact that on intersecting a contour of particles of a medium with infinite conductivity, the magnetic lines of force induce very large (infinitely large) currents and the associated electric volume forces which arise will, according to Lenz's rule, either decelerate the motion of the particles of the contour or entrain the magnetic lines of force. The substance of the gas in the transverse field of motion thus carries its magnetic lines of force along with it, i.e., they behave as if they were "glued" or "frozen" into the substance of the gas.

Alfven introduced the analogy between the magnetic lines of force and elastic filaments, assuming that the bending of magnetic lines of force during the motion of the particles of a fluid as $\sigma \to \infty$ trans-

versely to the magnetic field is accompanied by the appearance of "quasielastic" forces which tend to straighten the lines of force again.

The vibrations are thus occurring in a direction perpendicular to the undisturbed magnetic field and a sufficiently small "hump" will be displaced along the line of force with the velocity $H(\mu_e/\rho)^{1/2}$. These vibrations remind us of elastic waves along a filament. A conductive medium in a magnetic field acquires a characteristic elasticity with respect to the shear of the adjacent layers.

The existence of the Alfven waves can be demonstrated well experimentally. By way of example one of the experiments made by Lundquist and [Lehnert] may be mentioned. A cylindrical vessel 2 (Fig. 10.4.5) filled with mercury 5. On the bottom of the vessel a ribbed plate 4 which can be set in rotation, is mounted. When the plate performs periodic vibrations then, owing to the internal friction, the mercury also starts rotating. However, in view of the smallness of the frictional forces, it takes rather long time to set the surface layer of the mercury in rotation. When a magnetic field is present, however, the disturbances are immediately transferred to the surface by means of the magnetogasdynamic waves.

If the conductivity of the medium is finite, the behavior of the magnetic lines of force can be imagined, starting from the limiting case of "freezability." The magnetic lines of force are in this case entrained by the medium to some degree, but there arises an effect of relative "slipping" of field and medium. The magnetic lines of force behave as if they were going to "diffuse" in the medium. The induction Eq. (10.4.45) in a coordinate system fixed to the moving system is therefore analogous to the diffusion equation.

It can be shown [10.4.7] that the propagation rate of disturbances in a conducting medium in a magnetic field exceeds the sonic

speed.

Let us consider a one-dimensional flow in a transverse magnetic field. In this case the equation of motion may be written in the following form:

$$\frac{\partial w}{\partial t}+w\frac{\partial w}{\partial x}+\frac{1}{\rho}\frac{\partial p}{\partial x}+\frac{\mu_e}{\rho}H\frac{\partial H}{\partial x}=0. \qquad (*)$$

In the case of a steady flow of an incompressible fluid this equation can be integrated immediately:

$$\frac{w^2}{2}+\frac{1}{\rho}\left(p+\frac{\mu_e H^2}{2}\right)=\text{const}.$$

The integral obtained is analogous to Bernoulli's equation; the quantity $\mu_e H^2/2$ can be termed the "magnetic pressure."

If $Re_m \gg 1$ (e.g., for a perfectly conducting medium, $\sigma \to \infty$), then

$$\frac{H}{\rho}=\frac{H_0}{\rho_0}=\text{const}.$$

We can rewrite Eq. (*) in the following form:

$$\rho\left(\frac{\partial w}{\partial t}+w\frac{\partial w}{\partial x}\right)+\frac{\partial}{\partial x}\left(p+\frac{\mu_e}{2}H_0^2\frac{\rho^2}{\rho_0^2}\right)=0.$$

For a barotropic gas we have

$$p+\frac{\mu_e}{2}H_0^2\frac{\rho^2}{\rho_0^2}=p_c(\rho).$$

Then we obtain

$$\left(\frac{\partial w}{\partial t}+w\frac{\partial w}{\partial x}\right)+\frac{\partial p_c}{\partial x}=0.$$

It is in this form that the equation of motion is considered in classical gasdynamics, the only difference being that in the second term of the equation $p(\rho)$ is replaced by $p_c(\rho)$. It is therefore possible to treat this equation formally with the method of linearization in acoustic approximation. We then obtain (considering also the continuity equation)

$$\rho_0\frac{\partial w'}{\partial t}+\left(\frac{\partial p_c}{\partial \rho}\right)_0\frac{\partial \rho'}{\partial x}=0;$$

$$\frac{\partial \rho'}{\partial t}+\rho_0\frac{\partial w'}{\partial x}=0.$$

Inis system, as we know, leads to a wave equation, e.g., for ρ'

$$\frac{\partial^2 \rho'}{\partial t^2} = \left(\frac{d p_c}{d \rho}\right)_0 \frac{\partial^2 \rho'}{\partial x^2}.$$

The velocity at which the disturbances are propagated in the conducting medium in the magnetic field is given by

$$c_m^2 = \left(\frac{d p_c}{d \rho}\right)_0 = \left(\frac{d p}{d \rho}\right)_0 + \frac{\mu_e H_0^2}{\rho_0} = a_0^2 + c_A^2.$$

where a_0 is the sonic velocity and c_A the velocity of the Alfven waves.

We call the dimensionless ratio of gas flow velocity

$$Al = \frac{w}{H}\sqrt{\frac{\rho}{\mu_e}} \qquad (10.4.52)$$

to the velocity of the Alfven waves the Alfven number.

If $M/Al \ll 1$, then $c_m \approx a_0$; if however $M/Al \gg 1$, then the disturbances will be propagated virtually with the velocity c_A.

Let us estimate the terms which originate from the magnetogasdynamic effects in the momentum Eq. (10.4.37). By considerations analogous to (2.5) we obtain dimensionless ratios which will prove to be similarity criteria.

Thus, comparing the electric volume force per unit mass with the convective term of the equation of motion gives us the criterion

$$\frac{\mu_e^2 \sigma H^2 w}{\rho w^2 : L} = \frac{Re_m}{Al^2}. \qquad (10.4.53)$$

Comparison with the viscosity force per unit mass is analogous to multiplying this criterion by Re; this gives us

$$\frac{Re_m}{Al^2} Re = \frac{\mu_e^2 \sigma H^2 L^2}{\rho \nu} = Ha^2. \qquad (10.4.54)$$

The dimensionless combination $H\sqrt{L^2 \sigma \mu_e^2 / \nu \rho}$ is called the Hartmann number

$$Ha = H\sqrt{\frac{\mu_e}{\rho}}\sqrt{\frac{L^2 \sigma \rho_e}{\nu}}. \qquad (10.4.55)$$

The physical meaning of this criterion leads to the following. If the velocity of the Alfven waves is large enough, then in the case of

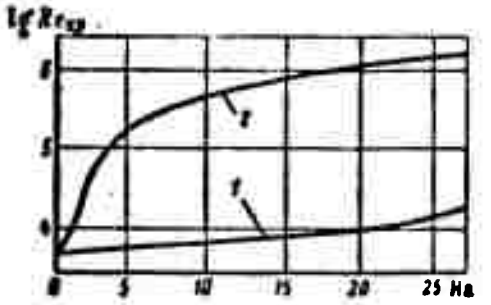


Fig. 10.4.6. Dependence of critical number Re_{kr} on the Hartmann number (Ha) in a longitudinal, 1, and a transverse magnetic field, 2.

a flow in a longitudinal magnetic field the longitudinal disturbances are the most "dangerous" [10.4.6]. These disturbances may lead to instabilities at small Reynolds numbers. In fact, experiments with a plane parallel flow in a longitudinal magnetic field at $Re_m \ll 1$ showed that the critical number Re_{kr} at which the flow becomes unsteady increases monotonically with the dimensionless parameter Ha^2/Re (curve 1 in Fig. 10.4.6). In this case of a transverse magnetic field the stabilization effect is still stronger (Curve 2 in Fig. 10.4.6), since not only the increase of the Hartmann number but also the increase in magnetic field strength distorts the velocity distribution (this will be shown in what follows), so that the effective Reynolds number is greatly decreased.

In the case of an unsteady motion, the forces then arising can be estimated by multiplying (10.4.53) by $Sh = wt/L$. Let us set up the similarity condition for this case:

$$Sh\frac{Re_m}{Al^2} = \frac{\mu_e^2 \sigma H^2 w}{\rho w : l}. \qquad (10.4.56)$$

These criteria can also be obtained from the energy Eq. (10.4.38).

Flow of an electrically conducting gas in a transverse magnetic field. When there is no electric field, i.e., when $\vec{E}=0$ and $\vec{j}=\mu_e\sigma(\vec{w}\times\vec{H})$.

we find that the sum of the first two terms of the right-hand side of Eq. (10.4.43) is zero:

$$\mu_0 \vec{w} \cdot (\vec{j} \times \vec{H}) + \frac{f}{\rho} = \vec{j} \cdot \left(\frac{\vec{I}}{\rho} - \mu_0 \vec{w} \times \vec{H} \right) = 0. \qquad (10.4.57)$$

In this case the energy equation coincides with the energy equation of classical gasdynamics. Thus, when $\vec{E} = 0$, the only effect due to magnetogasdynamics is the dynamic influence of the electric volume force.

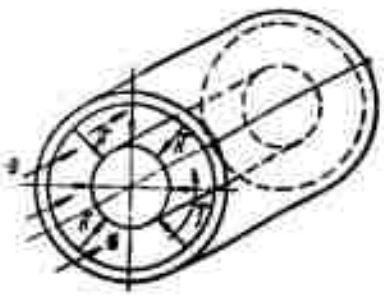


Fig. 10.4.7. In order to close the electric current in a gas it is convenient to bound the flow in an annular channel with radial magnetic field.

Let us consider the steady flow in a channel of constant cross section of an electrically conducting gas in a transverse magnetic field. To obtain a closed current in the gas we assume that the channel has an annular cross section and that the magnetic field is radially directed (Fig. 10.4.7). If the width of the ring is small compared with the diameter, the channel can be considered as being plane and the field as being homogeneous. The flow may then be considered one-dimensional. Such a flow is shown schematically in Fig. 10.4.8. The current arising in the gas because of its motion in the magnetic field creates its own magnetic field (h) which interferes with the external field (H). If we assume that $h \ll H$ the disturbance of the field by the current may be neglected.

For the case of adiabatic gas flow with friction the system of equations then has the form

$$m \frac{dw}{dt} + \frac{dp}{dx} = \mu_0 j H - \zeta \frac{mw}{2D}; \qquad (10.4.58)$$

$$\frac{d}{dx}\left(c_p T + \frac{w^2}{2} \right) = 0; \qquad (10.4.59)$$

$$\rho w = m = \text{const}; \qquad (10.4.60)$$

$$p = \rho RT; \tag{10.4.61}$$

$$j = -\mu_0 \sigma w H. \tag{10.4.62}$$

Here D = 2δ is the hydraulic radius (δ being the channel width) and $= \frac{2\Delta p}{\rho w^2}\frac{l}{D}$ is the coefficient of frictional drag.

In this statement (for the solution it is assumed that σ = const) the problem does not differ from the problem of classical gasdynamics on a flow with friction.

$$\frac{2k}{k+1}\left(\frac{2\mu_0^2\sigma H^2 D}{m} + \zeta\right)\frac{x}{D} = \chi(M_1^*) - \chi(M^*), \tag{10.4.63}$$

where

$$\chi(M^*) = \ln M^{*2} + \frac{1}{M^{*2}}.$$

As has been shown before, the first term in the parentheses of the left-hand side of Eq. (10.4.63) is the similarity criterion (10.4.53) $Re_m/A\underline{l}^2$, and the ratio of the two terms of the left-hand side is the similarity criterion (10.4.54) Ha^2. Comparing (10.4.63) with (4.4.48), we see that the qualitative influence of the magnetic field on the flow is analogous to the influence of friction: a subsonic flow is accelerated and a supersonic flow is decelerated.

In many problems both terms of the left-hand side of Eq. (10.4.63) can be equivalent. Assuming that σ = 1.0 $ohm^{-1}cm^{-1}$, H = 10^3 gauss = 10^{-5} v-sec/cm^2, ρ = 10^{-9} kg-sec^2/cm^4, w = 10^5 cm/sec, D = 10 cm and ζ = 10^{-4} we obtain

$$10{,}2\frac{2\mu_0^2\sigma H^2 D}{\zeta\rho w} = 2.$$

If reducing the density or the velocity or raising the electrical conductivity or the magnetic field strength makes the above relation become much smaller than unity, then the influence of the surface friction can be neglected. The magnetic field exerts an influence on the coefficient of friction, too. In a hypersonic flow in a magnetic

field, the surface friction may be reduced by an order of magnitude, and the total drag is determined by the magnetic pressure even in relatively weak fields [10.4.8].

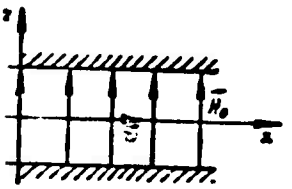


Fig. 10.4.8. In a plane channel the gas flows along the x-axis and the transverse magnetic field H acts along the z-axis.

In the case of an isothermal flow, the energy Eq. (10.4.59) is replaced by the condition that the thermodynamic flow temperature is constant (in this case the stagnation temperature varies owing to the heat exchange with the external medium). It is therefore convenient to take the Mach number M as the argument. The solution has the form

$$\left(\frac{2\mu_e^2\sigma H^2 D}{m}+\xi\right)\frac{x}{D}=2\ln\frac{M_1}{M}+\frac{1}{k}\left(\frac{1}{M_1^2}-\frac{1}{M^2}\right).$$

When friction is neglected, the solution can be written in the following form:

for an adiabatic flow

$$\frac{2\mu_e^2\sigma H^2}{\rho^*a^*}\frac{x}{D}=\frac{\rho w}{\rho^*w^*}\left[\chi(M_1)-\chi(M^*)\right]\frac{k+1}{2k};$$

for an isothermal flow

$$\frac{2\mu_e^2\sigma H^2}{\rho^*a^*}\frac{x}{D}=\frac{\rho w}{\rho^*a^*}\left[2\ln\frac{M_1}{M}+\frac{1}{k}\left(\frac{1}{M_1^2}-\frac{1}{M^2}\right)\right].$$

with

$$\frac{\rho w}{\rho^*a^*}=\left(\frac{k+1}{2}\right)^{\frac{1}{2}}M^*\left(1-\frac{k-1}{k+1}M^{*2}\right)^{\frac{1}{2(k-1)}}.$$

Figure 10.4.9 shows the critical length of a channel as dependent on the initial velocity for k = 1.4. In the range of supersonic flows the function has a maximum at $M^* \approx 1.65$ which differs considerably from the situation for a usual flow with friction. A supersonic flow with $M^* = 2.3$ can be decelerated over a given length only ten times as slowly as a supersonic flow with $M_1^* = 1.65$.

Magnetohydrodynamics of a two-dimensional flow [10.4.2]. Let us consider the steady flow of a viscous incompressible electrically conducting fluid in a channel formed by infinite plane parallel walls $z = \pm b/2$ in the presence of a homogeneous transverse magnetic field (cf. Fig. 10.4.8). If the velocity $\vec{w}$ is assumed to vary in the z-direction only, the pressure must vary in the x-direction so that the pressure gradient remains constant ($dp/dx = \text{const} = -P$). It follows from the equation $\operatorname{div} \vec{H} = 0$ that

$$H_z = \text{const} = H_0. \qquad (10.4.64)$$

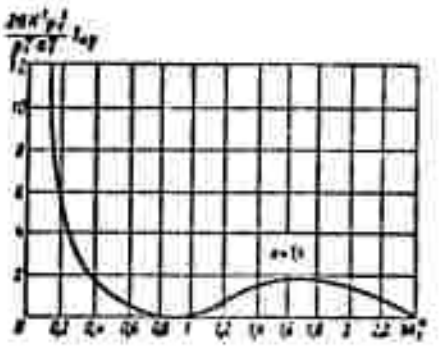


Fig. 10.4.9. Dependence of the critical length on the inlet velocity.

Analogously, for a current we have $\operatorname{div} \vec{j} = 0$, i.e., $j_z = \text{const}$. The boundary condition is furnished by the wall insulation, and therefore $j_z = 0$. The momentum equation then assumes the form

$$\mu \frac{d^2w}{dz^2} - j_y H_0 \mu_e + P = 0. \qquad (10.4.65)$$

The momentum equation with respect to the z-axis shows that $j_x = 0$, i.e., $\vec{j}$ has a component along the y-axis only (Fig. 10.4.10).

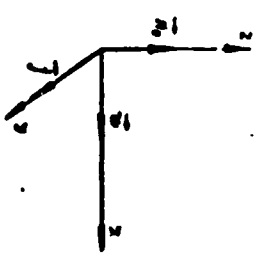


Fig. 10.4.10. The current $\vec{j}$ has a component in the y direction only.

From Ohm's law (for $\vec{E} = 0$) it follows that

$$j_y = \mu_e \sigma w H_0.$$

Substituting the value of j_y in (10.4.65) we obtain the equation

$$\mu \frac{d^2w}{dz^2} - \mu_e^2 \sigma H_0^2 w + P = 0,$$

whose solution, satisfying the boundary condition $w|_{z=\pm\frac{b}{2}} = 0$, has the form

$$w = \frac{P}{\sigma H_0^2 \mu_e^2}\left[1 - \frac{\operatorname{ch}\left(\sqrt{\frac{\sigma\mu_e^2}{\mu}} H_0 z\right)}{\operatorname{ch}\left(\sqrt{\frac{\sigma\mu_e^2}{\mu}} H_0 \frac{b}{2}\right)}\right]. \qquad (10.4.66)$$

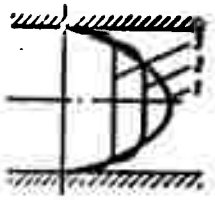


Fig. 10.4.11. As the magnetic field strength increases the values of the velocity in the core of the flow drop and the velocity distribution becomes ($H_{0_3} > H_{0_2} > H_{0_1}$).

If $\sigma \to 0$ then Formula (10.4.66) yields the familiar parabolic profile of a Poiseuille flow.

The quantity $\sqrt{\frac{\sigma\mu_e^2}{\mu}} H_0 \frac{b}{2}$ is the Hartmann (10.4.55). An increase in this quantity, which may take place particularly at the expense of an increase in H_0 leads to a flattening of the profile: the central part becomes smoother, the curvature of the profile near the walls increases, a sharp drop in velocity occurring in a very thin layer (Fig. 10.4.11). Therefore, as Ha increases, the part played by the viscosity diminishes. Moreover, for a given magnitude of the gradient the velocity

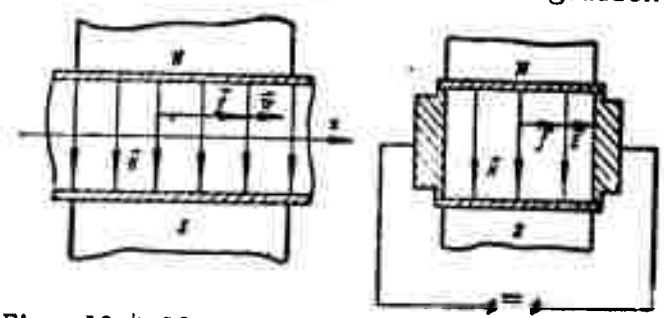


Fig. 10.4.12. Schematic diagram of acceleration of a flow by crossed electric and magnetic fields.

in the central flow drops as H_0 increases, which leads to a decrease in the Re number.

Acceleration of a flow in a channel by magnetic and electric fields [10.4.2] and [10.4.9]. Let us consider a one-dimensional steady flow along the x-axis of an electrically conducting gas in crossed electric and magnetic fields that are applied transversely to the channel (Fig. 10.4.12). The system of equations has the form

$$\rho w A = \text{const};$$

$$\rho w \frac{dw}{dx} + \frac{dp}{dx} = \sigma (E - w H \mu_e) H \mu_e;$$

$$\rho w \frac{d}{dx}\left(c_p T + \frac{w^2}{2}\right) = \sigma (E - \mu_e w H) E;$$

$$p = \rho R T.$$

Generally speaking, if A(x), E(x) and H(x) are given these equations cannot be integrated. But it is possible to calculate the derivatives dw/dx and dM/dx:

$$\frac{dw}{dx} = \frac{1}{M^2-1}\left[\frac{w}{A}\frac{dA}{dx} - \frac{\sigma H^2\mu_e^2}{\rho}\left(w - \frac{E}{H\mu_e}\right)\left(w - \frac{k-1}{k}\frac{E}{H\mu_e}\right)\right] \qquad (10.4.67)$$

$$\frac{dM}{dx} = \frac{1+\frac{k-1}{2}M^2}{M^2-1}\left[\frac{M}{A}\frac{dA}{dx} - \frac{\sigma H^2\mu_e^2}{a\rho}\left(w - \frac{E}{H\mu_e}\right)\times\right.$$
$$\left.\times\left(w - \frac{k-1}{k}\frac{E}{H\mu_e}\frac{1+kM^2}{2+(k-1)M^2}\right)\right]. \qquad (10.4.68)$$

When no magnetogasdynamic effects arise, the well-known formulas for isentropic flow in a channel are obtained.

Let us write

$$\frac{k-1}{k}\frac{E}{H\mu_e} = w_1; \quad \frac{k-1}{k}\frac{1+kM^2}{2+(k-1)M^2}\frac{E}{H\mu_e} = w_2; \quad \frac{E}{H\mu_e} = w_3.$$

These quantities are characteristic velocities. The ratio $E/H\mu_e$ may be regarded as the velocity at which the induced electric field $wH\mu_e$ becomes equal to the field applied from outside. It can be seen from the formulas that at velocities smaller than w_3 the electric volume force acts in the direction of the acceleration of the flow, and at velocities larger than w_3 in the direction of deceleration.

It is therefore possible to obtain an acceleration of a supersonic flow even in a channel of constant cross section. For this it is necessary for the velocity $\underline{w}$ to satisfy the inequality $w_3 > w > w_2$ that it is reached also under the condition $w_1 > w > w_2$. This effect is opposite to the effect of heat on the supersonic flow. If supplying heat to a supersonic flow in a channel of constant cross section causes the flow to decelerate, then supplying electromagnetic energy caused the flow to accelerate.

The presence of the factor (M^2-1) proves that a discontinuity occurs when M = 1. It is therefore practically impossible to pass through sonic velocity; even reaching it is possible only at the end

of the channel. If, however, in Eqs. (10.4.67) and (10.4.68) numerator and denominator become zero at the same time, continuous acceleration or deceleration becomes possible.

Boundary layer control. If an electric volume force occurs in the boundary layer, this will considerably influence the velocity distribution. If the electric volume force is directed along the frictional forces, i.e., is opposite to the velocity, then it causes the [illegible] change in the character of the velocity distribution as a negative pressure gradient on the profile near the point of separation [illegible]. The velocity distribution beside the wall becomes more and more [illegible] and the slope at the wall may approach to zero and even change sign (Fig. 10.4.13.a). If the e.m.f. vector is directed along the velocity, the velocity distribution is steeper (cf. Fig. 10.4.13, b). Thus, by changing the slope of the velocity distribution, the frictional drag can be reduced and also the amount of heat transferred from the body surface can be controlled since the heat transfer is likewise connected with the temperatures distribution at the walls.

Control of critical heating. In modern technology there is an important series of problems connected with the deceleration of artificial satellites or rocket-driven flying vessels on their re-entry from cosmic space into the atmosphere. If the deceleration energy is liberated in the form of heat on the vessel surface, the surface is heated, since the withdrawal of the heat from it is hampered and it therefore assumes a temperature close to the stagnation temperature. The problem would be solved to a considerable extent if some means could be found of concentrating the deceleration energy and delivering into the flying vessel where it could be easily dissipated (e.g., by transferring it to a liquid which evaporates easily).

It has been suggested [10.4.2] that the effect of ionization of

the air in the high-speed boundary layer and behind the shock wave

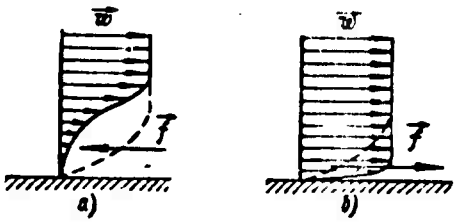


Fig. 10.4.13. Application of electric volume forces for boundary layer control.

should be used for this purpose. Two opposite parts of the surface of the vessel's nose (Fig. 10.4.14) are made of conducting material and the remainder of the surface of a dielectric, and the parts mentioned first, the electrodes, are connected via coils lying inside the vessel, then applying a transverse magnetic field to the gas flow about the body gives rise to an electric current, as is shown in Fig. 10.4.14. The initial magnetic field may be secured at the expense of the residual magnetism (should a coil be necessary, however, the electromagnet can be fed also from an outside source). The magnetic field will be amplified at the expense of the current flowing in the circuit (gas-electrode – coil of electromagnet – electrode-gas) and in turn it will amplify the current in the circuit. This will continue until saturation is reached in the core of the electromagnet.

In this case the kinetic energy is converted into electrical energy which is dissipated in the windings of the electromagnet, from which it can be removed in the form of heat by a liquid that evaporates easily. The force of drag will be applied not to the skin of the vessel but to the electromagnet. Thus, this method makes it possible to relieve the skin of the vessel of a large part of the dynamic and thermal loads.

Flow of a perfectly conducting gas about a body from the interior of which a magnetic field is excited. [10.4.13] and [10.4.14]. Let us consider a conducting gas flowing about a body with large magnetic Reynolds number ($Re_m \gg 1$).

In the space around the body there exists a magnetic field ex-

cited by the currents in the body (or "frozen" in the body). When Re_m

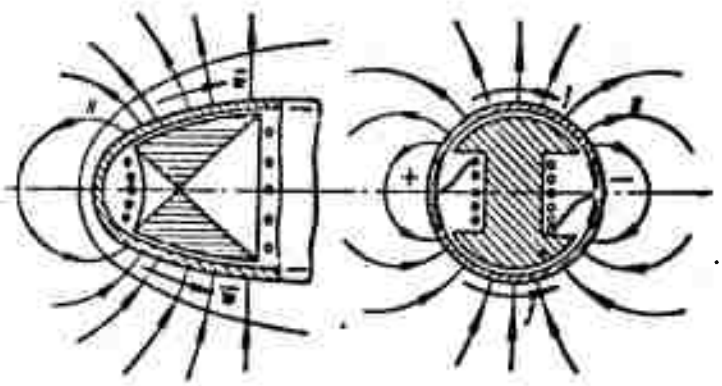


Fig. 10.4.14. Schematic diagram on the use of a magnetogasdynamic effect in order to decelerate a flying vessel entering dense layers of the atmosphere.

is sufficiently large, we obtain from the induction equation

$$\mathrm{rot}\left(\vec{w}\times\vec{H}\right)=0,$$

and since $\vec{H} = 0$ at infinity, $\vec{H} = 0$ everywhere in the flow, too. By virtue of the continuity of the normal component of the magnetic field strength vector at the boundary to the body, $H_n = \vec{H}\cdot\vec{n} = 0$ ($\vec{n}$ is the unit vector of the outer normal). If we denote by the subscript "1" the parameters at the boundary to the body and by the subscript "2" those at the boundary to the flow, then the boundary conditions can be written in the following form:

$$\vec{H}_2=0,\quad H_{n2}=0,\quad H_{\tau 2}=0,$$
$$\vec{H}_1\neq 0,\text{ and since } H_{n1}=0,\text{ we have } H_{\tau 1}\neq 0.$$

The surface of the body is therefore a tangential discontinuity surface of the magnetic field. 'Screening" of the magnetic field results from the surface currents.

When the Re_m number is not very large, the discontinuity surface evolves to a finite region across which the tangential component of

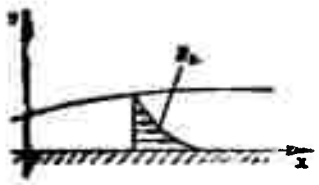


Fig. 10.4.15. The region next to the body, across which the parameters characterizing the magnetic field change rapidly, is called the magnetic boundary layer.

the magnetic field varies rapidly (Fig. 10.4.15). This region is called the magnetic boundary layer.

The width of this region is determined as in classical gasdynamics by the presence of energy dissipation, in the given case by the presence of magnetic energy losses to Joulean heat.

The thickness of the magnetic boundary layer is $\delta_m \sim \frac{l}{\sqrt{Re_m}}$ [the thickness of the gasdynamic boundary layer (6.11.2) is $\delta \sim \frac{l}{\sqrt{Re}}$].

The equation of motion of the magnetic boundary layer is written in the following form:

$$\rho\frac{\partial u_x}{\partial t}+\rho u_x\frac{\partial u_x}{\partial x}+\rho u_y\frac{\partial u_x}{\partial y}+\frac{\partial}{\partial x}\left(p+\frac{\mu_e H^2}{2}\right)=0,\quad \frac{\partial}{\partial y}\left(p+\frac{\mu_e H^2}{2}\right)=0.$$

From the second equation we find that across the magnetic field

$$p+\mu_e\frac{H^2}{2}=\text{const}. \qquad (10.4.69)$$

The gasdynamic pressure across the magnetic boundary layer may therefore change by many times, a very different situation from that encountered in the gasdynamic boundary layer.

From this condition it is possible to draw a very important conclusion: where $\frac{\mu_e H^2}{2}\Big|_{y=0} > p_\infty$, then in connection with the fact that a negative pressure in a gas is impossible, by virtue of (10.4.68) the flow will be "pressed away" from the body by the magnetic field whereupon voids ("cavities") in which $p = 0$ will be formed. Figure 10.4.16 shows the boundaries of such a cavity formed in a flow streaming about a sphere which is magnetized by means of two poles. The boundary is a surface along which electric currents flow which are subject in a magnetic field to the mechanical forces that bring about the "pressing

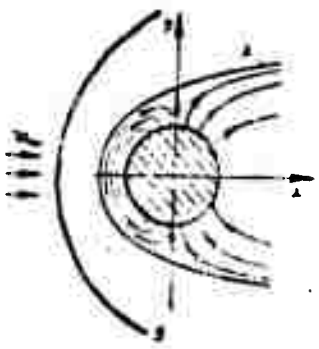


Fig. 10.4.1. Under the condition $\frac{\rho_0 H^2}{2}\Big|_{p=0} >$ [illegible] flow will be "pressed away" from the body by the magnetic field whereupon "cavities" inside which p = 0 will be produced. In this case the stream does not flow about the body but about the surface of these "cavities" (A).

away." In order to determine the shape of the cavity, the equations describing the magnetic field inside the cavity must be solved:

$$\text{curl } \vec{H} = 0 \text{ and } \text{div } \vec{H} = 0,$$

with the boundary conditions

$$\frac{\mu_0 H^2}{2}\Big|_A = p(A) \text{ and } (\vec{H}\cdot\vec{n})_A = 0.$$

Outside the surface A there is no magnetic field, and all the relations of classical gasdynamics apply. We assume for simplicity that $M_\infty \gg 1$ and then, obviously, the pressure at the surface A can be calculated with Newton's formula:

$$p = p_0 \cos^2(\vec{n}\cdot\vec{\infty}),$$

where p_0 is the stagnation pressure behind the shock wave.

The "cavities" formed around the "magnetized" body in the flow of a conducting gas at $Re_m \gg 1$ may be used to reduce the aerodynamic forces and thermal insulation at the body surface (the electromagnetic forces will act on the magnetic field sources in the body).

REFERENCES

10.4.1. Prikladnaya magnitogidrodinamika [Applied Magnetohydrodynamics], Trudy instituta fiziki AN Latv. SSSR [Trans. Phys. Inst. Acad. Sci. Latv. SSR], [illegible]a, 1956.

10.4.2. Lamb, Lin Shao-shi, Elektroprovodnost' termicheski ionizirovannogo vozdukha v udarnoy trube [Conductivity of Thermally Ionized Air in a Shock Tube], In collection entitled "Voprosy raketnoy tekhniki" [Problems of Rocket Engineering], No. 3,

IL [Foreign Literature Press], 1958.

10.4.3. Resler and Sirs, Perspektivy magnitnoy gidrodinamiki [Promise of Magnetohydrodynamics], In collection entitled "Mekhanika" [Mechanics], No. 6, IL, 1958.

10.4.4. Shi-I Pey, Uravneniye energii v magnitnoy gazovoy dinamike [The Energy Equation in Magnetogasdynamics], In collection entitled "Mekhanika" [Mechanics], No. 1, IL, 1959.

10.4.5. Zommerfel'd, A., Elektrodinamika [Electrodynamics], IL, 1958.

10.4.6. Syrovatskiy, S.I., Magnitnaya gidrodinamika [Magnetohydrodynamics], "Uspekhi fizicheskikh nauk" [Advances in the Physical Sciences], GTTI [State Technical and Theoretical Press], 1957.

10.4.7. Baum, F.A., Kaplan, S.A. and Stanyukovich, K.P., Vvedeniye v kosmicheskuyu gazodinamiku [Introduction to Cosmic Gasdynamics], Fizmatgiz [State Publishing House for Physicomathematical Literature], 1958.

10.4.8. Blewiss, Z.O., Magnetogasdynamics of Hypersonic Couette Flow, Journ. of the Aero. Space Sciences, Vol. 25, No. 10, 1958.

10.4.9. Resler and Sirs, Magnitogazodinamicheskoye techeniye v kanale [Magnetogasdynamic Flow in a Channel], ZAMP [Journal of Applied Mathematics and Physics], 1958.

10.4.10. Rossow, V., On Flow of Electrically Conducting Fluids over a Flat Plate in the Presence of a Transverse Magnetic Field, Rep. NACA, No. 1358, 1958.

10.4.11. "Magnitnaya gidrodinamika" [Magnetohydrodynamics] (Symposium Papers), Atomizdat [Publishing House of Literature on Atomic Energy], 1958.

10.4.12. Landau, L.D. and Lifshits, E.M., Elektrodinamika sploshnykh sred [Electrodynamics of Continuous Media], GTTI, 1957.

10.4.13. Kulikovskiy, A.G., Ob obtekanii namagnichennykh tel provodyashchey zhidkost'yu [Flow of Conducting Fluid Past Magnetized Bodies], DAN SSSR [Proc. Acad. Sci. USSR], Vol. 117, No. 2, 1957.

10.4.14. Zhigulev, V.N., Teoriya magnitnogo pogranichnogo sloya [Theory of the Magnetic Boundary Layer], DAN SSSR, Vol. 124, No. 5, 1959.

Appendix I

DENOTATIONS OF THE FUNDAMENTAL QUANTITIES

A area [m^2]; thermal equivalent of mechanical work [1/427 kcal/kg-m]

$\vec{B}$ magnetic induction [kg/a-sec^2, kg/a-m, v-sec/m^2]

C closed contour of integration; constant in Sutherland's formula [°K]; coefficients of forces, C_x, C_y, of moment, C_m, of pressure C_p.

D dissipation function [kgm/sec, kgm^2/sec^3]; D, displacement current [a];

E energy [kgm]; electric field strength [kg/a-sec, kgm/a-sec^3]

E electrical voltage [kgm/a-sec, kgm^2/a-sec^3, v]

F force [kg, kgm/sec^2], chiefly volume force

G weight [kg]; elastic modulus of the second kind [kg/m^2]

μG molecular weight [grams/mole]

H height [m]; magnetic field strength [a/m]

I enthalpy [kgm]; current [a, Coulomb/sec]

J mechanical equivalent of heat [427 kgm/kcal]

K compression modulus [kg/m^2]; K = (k − 1)/(k + 1); impulse pA · mw [kg];

L work [kgm]; $_1L_2$ − work on the section 1-2; body contour

M mass [kg, kg-sec^2/m]; moment of forces [kgm]; dipole moment [m^4/sec]

M Mayevskiy (Mach) number

N force along the normal to the chord of a wing [kg]; number of

molecules per unit volume [$1/m^3$]; number of turbine blades

O origin of coordinates

P force [kg], chiefly surface force

Q heat [kgm = 1/427 kcal]; $_1Q_2$ – heat supplied to section 1-2

R gas constant, per unit mass [kgm/kg-°K, m^2/sec^2-°K]; resultant of forces [kg]; drag [kg]; radius [m]

μR universal gas constant [μR = 848 kgm/kmole-°K]

S entropy [kgm/°K, 1/427/kcal/°K]

T temperature; T °K – in degrees Kelvin (abs.), T °C in degrees centigrade; force along the chord of a wing [kg]

U force potential [kgm]

V volume [m^3]

X drag [kg]

Y lift [kg]

a sonic velocity [m/sec]

b width of channel [m]; profile chord [m]; b_f position of maximum bend of the chamber line of a profile [m]; b_d position of maximum thickness of a profile [m]

c specific heat per unit mass [kgm/kg-deg, 1/427 kcal/kg-deg]; absolute particle velocity in a turbine [m/sec]; c_{sv} electromagnetic constant (equal to the velocity of light in empty space, $3 \cdot 10^8$ m/sec)

d maximum thickness of profile [m]; diameter [m]

e electric charge [k = a sec]

$\vec{f}$ stress vector of volume forces [kg/kg, m^2/sec]; maximum bend of profile [m]; relative inlet of air intake

g acceleration of terrestrial gravity [m^2/sec]

h height of roughness protuberances [m]

i enthalpy per unit mass [kgm/kg]; unit vector of x-axis

j mass flow density per second [kg/m^2-sec, kg-sec/m^3]; density of electric current [a/m^2]; unit vector of y-axis; $\vec{j}$ – unit vector of y-axis

k specific heat ratio (atomic number) $k = c_p/c_v$

$\vec{k}$ unit vector of z-axis

l length [m]

m mass flowing per unit time [kg/sec, kg-sec/m]

$\vec{n}$ unit vector of outer normal

p pressure [kg/m^2]

q heat flux density [kgm/m^2-sec, 1/427 kcal/m^2-sec]

$\vec{r}$ radius vector [m]; r_k degree of reactivity

s entropy per unit mass [kgm/kg-°K, 1/427 kcal/kg-°K]; curvilinear coordinate

t time [sec]

$\vec{\tau}$ tangent unit vector

u transport velocity [m/sec]; induced velocity [m/sec]

v specific volume, $v = 1/\rho$ volume of unit mass [m^3/kg, m^4/kg-sec^2]

w velocity [m/sec]

x axis of coordinates (abscissa)

y axis of coordinates (ordinate)

z axis of coordinates; complex number $z = x + iy$

circulation [m^2/sec]

Δ Laplace operator ($\Delta = \vec{\nabla} \cdot \vec{\nabla} = \nabla^2$)

θ angle [radian = $2\pi/360°$]; angle of curvature of profile, $\theta = \theta_1 + \theta_2$; θ_1 (θ_2)-angle of direction of leading (trailing) edge of profile

Λ aspect ratio, $\Lambda = l^2/A_{kr}$

Φ velocity potential [m^2/sec]

ψ stream function [m^2/sec]

α (rad. = $2\pi/360°$) angle of attack; angle of divergence of a channel; α_0 zero lift angle of profile; α_g geometrical angle; α_a aerodynamic angle of attack, $\alpha_a = \alpha + \alpha_0$

β Mach angle

γ specific weight [kg/m^3]

δ increment; sign characterizing a small quantity; boundary layer thickness [m]; δ^* displacement thickness, δ^{**} impulse loss thickness; δ^{***} energy loss thickness

ε dielectric constant

ζ drag coefficient

ϑ angle [rad.]

λ thermal conductivity coefficient [kgm/m-sec-deg, 1/427 kcal/m-sec-deg]

μ coefficient of viscosity [$kg\text{-}sec/m^2$]; angle between direction of velocity and direction of diagonal shock; μ_e magnetic permeability

ν kinematic viscosity [m^2/sec]; static pressure recovery coefficient; ν_0 total pressure recovery coefficient

ξ displacement on shear

ρ density [kg/m^3, $kg\text{-}sec^2/m^4$]; ρ_{sv} density of free electrons [$1/m^3$]; ρ_e resistivity [ohm-m, $kg\text{-}m^2/a\text{-}sec$]

σ normal component of stress of surface forces [kg/m^2; conductivity [1/ohm, a/b, a^2sec/kgm]; recovery coefficient

τ tangential component of stress of surface forces [kg/m^2]

τ_{xy} on a surface area normal to the x-axis in the direction of the y-axis

φ disturbance velocity potential [m^2/sec]; electrical potential [$v = kgm^2/a\text{-}sec^3$]; mass flow coefficient of air intake

χ perimeter [m]; complex potential, $\Phi + i\Psi$ [m^2/sec]

ψ stream function of disturbance [m^2/sec]

ω angular velocity of rotation [rad/sec]; angle of wedge, cone [rad.]

$\sim$ tilde ("little serpent") sign of averaging

$\rightarrow$ vector

If $c = a + ib$ then $\bar{c} = a - ib$.

Appendix 2

FORMULAS OF VECTOR ANALYSIS

I. Definitions

$$\operatorname{grad}\varphi = \lim_{\delta V \to 0} \frac{\oint_A \vec{n}\varphi \, dA}{\delta V};$$

$$\operatorname{div}\vec{a} = \lim_{\delta V \to 0} \frac{\oint_A \vec{n}\cdot\vec{a} \, dA}{\delta V};$$

$$\operatorname{rot}\vec{a} = \lim_{\delta V \to 0} \frac{\oint_A \vec{n}\times\vec{a} \, dA}{\delta V}.$$

II. Integral Formulas

1) Due to Stokes

$$\oint_C \vec{a}\cdot d\vec{l} = \int_A \vec{n}\cdot\operatorname{rot}\vec{a} \, dA$$

2) Due to Ostrogradskiy-Gauss

$$\oint_A \vec{n}\varphi \, dA = \int_V \operatorname{grad}\varphi \cdot dV; \quad \oint_A \vec{n}\cdot\vec{a} \, dA = \int_V \operatorname{div}\vec{a} \, dV;$$

$$\int_A \vec{n}\times\vec{a} \, dA = \int_V \operatorname{rot}\vec{a} \, dV$$

III. Cartesian System of Coordinates

Introducing the nabla operator

$$\vec{\nabla} = \vec{i}\frac{\partial}{\partial x} + \vec{j}\frac{\partial}{\partial y} + \vec{k}\frac{\partial}{\partial z},$$

we obtain

$$\operatorname{grad}\varphi = \vec{\nabla}\varphi = \vec{i}\frac{\partial\varphi}{\partial x} + \vec{j}\frac{\partial\varphi}{\partial y} + \vec{k}\frac{\partial\varphi}{\partial z},$$

$$\operatorname{div}\vec{a} = \vec{\nabla}\cdot\vec{a} = \frac{\partial a_x}{\partial x} + \frac{\partial a_y}{\partial y} + \frac{\partial a_z}{\partial z}.$$

$$\operatorname{rot}\vec{a}=\vec{\nabla}\times\vec{a}=\begin{vmatrix}\vec{i} & \vec{j} & \vec{k}\\ \frac{\partial}{\partial x} & \frac{\partial}{\partial y} & \frac{\partial}{\partial z}\\ a_x & a_y & a_z\end{vmatrix}=\vec{i}\left(\frac{\partial a_z}{\partial y}-\frac{\partial a_y}{\partial z}\right)+$$

$$+\vec{j}\left(\frac{\partial a_x}{\partial z}-\frac{\partial a_z}{\partial x}\right)+\vec{k}\left(\frac{\partial a_y}{\partial x}-\frac{\partial a_x}{\partial y}\right).$$

The formula of Ostrogradskiy-Gauss

$$\int_A \vec{n}(\ldots)\,dA=\int_V \vec{\nabla}(\ldots)\,dV.$$

IV. The Laplace Operator

$$\Delta\varphi=\vec{\nabla}\cdot\vec{\nabla}\varphi=\frac{\partial^2\varphi}{\partial x^2}+\frac{\partial^2\varphi}{\partial y^2}+\frac{\partial^2\varphi}{\partial z^2}.$$

V. Cylindrical Coordinates (r, ϑ, z)

$$\operatorname{grad}\varphi=\vec{e}_r\frac{\partial\varphi}{\partial r}+\vec{e}_\vartheta\frac{1}{r}\frac{\partial\varphi}{\partial\vartheta}+\vec{e}_z\frac{\partial\varphi}{\partial z},$$

$$\operatorname{div}\vec{a}=\vec{e}_r\left(\frac{1}{r}\frac{\partial a_z}{\partial\vartheta}-\frac{\partial a_\vartheta}{\partial z}\right)+\vec{e}_\vartheta\left(\frac{\partial a_r}{\partial z}-\frac{\partial a_z}{\partial r}\right)+\vec{e}_z\frac{1}{r}\left(\frac{\partial(ra_\vartheta)}{\partial r}-\frac{\partial a_r}{\partial\vartheta}\right),$$

$$\Delta\varphi=\frac{1}{r}\cdot\frac{\partial}{\partial r}\left(r\frac{\partial\varphi}{\partial r}\right)+\frac{1}{r^2}\frac{\partial^2\varphi}{\partial\vartheta^2}+\frac{\partial^2\varphi}{\partial z^2}.$$

VI. Second Order Differential Operations

$$\operatorname{rot}\operatorname{grad}\varphi=0,\quad \operatorname{div}\operatorname{rot}\vec{a}=0$$

$$\operatorname{rot}\operatorname{rot}\vec{a}=\operatorname{grad}\operatorname{div}\vec{a}-\vec{\nabla}^2\vec{a}$$

$$\operatorname{grad}(\varphi\psi)=\psi\operatorname{grad}\varphi+\varphi\operatorname{grad}\psi$$

$$\operatorname{div}\varphi\vec{a}=\varphi\operatorname{div}\vec{a}+\vec{a}\cdot\operatorname{grad}\varphi$$

$$\operatorname{rot}\varphi\vec{a}=\varphi\operatorname{rot}\vec{a}+\operatorname{grad}\varphi\times\vec{a}$$

$$\operatorname{div}(\vec{a}\times\vec{b})=\vec{b}\cdot\operatorname{rot}\vec{a}-\vec{a}\cdot\operatorname{rot}\vec{b}$$

$$\operatorname{grad}\vec{a}\cdot\vec{b}=(\vec{b}\cdot\vec{\nabla})\vec{a}+(\vec{a}\cdot\vec{\nabla})\vec{b}+\vec{b}\times\operatorname{rot}\vec{a}+\vec{a}\times\operatorname{rot}\vec{b}$$

$$\frac{1}{2}\vec{\nabla}\vec{a}^2=(\vec{a}\cdot\vec{\nabla})\vec{a}+\vec{a}\times\operatorname{rot}\vec{a}$$

$$\operatorname{rot}(\vec{a}\times\vec{b})=(\vec{b}\cdot\vec{\nabla})\vec{a}-(\vec{a}\cdot\vec{\nabla})\vec{b}+\vec{a}\cdot\operatorname{div}\vec{b}-\vec{b}\cdot\operatorname{div}\vec{a}.$$

Appendix 3

PHYSICAL CHARACTERISTICS OF SPACE NEAR THE EARTH

Molecular weight of air 28.966 g/mole. Gas constant per gram-mole $R = 8.314 \cdot 10^7$ erg/mole. Absolute gas constant $R_{abs} = 8.31 \cdot 10^3$ m^2/sec^2-deg-°K. Temperature at sea level $T_{H=0} = 288.16$ °K; pressure $p = 10.330.27$ kg/m^2; density $\rho_{H=0} = 0.12492$ kg-sec^2/m^4. Viscosity coefficient $\mu_{H=0} = 1.8286 \cdot 10^{-6}$ kg-sec^2/m^2. Sonic speed a = 340.43 m/sec.

Owing to the dissociation of the molecules of the various gases constituting the atmosphere and of the diffusional separation of molecules of different mass in the Earth's gravitational field the composition of the atmosphere begins to change at altitudes above 90 km. The main cause of the change in molecular weight at an altitude of 90 to 180 km is the dissociation of oxygen, and at a height of more than 180 km the dissociation of the nitrogen molecules and the diffusional separation of the gases.

When the nitrogen is completely dissociated, the molecular weight is 14.7 h/mole.

The change in viscosity with altitude may be determined according to Sutherland's formula $\mu_H = \mu_0 \left(\frac{T_H}{T_0}\right)^{\frac{3}{2}} \frac{T_0 + C}{T_H + C}$, with C = 120 °K. The acceleration due to the Earth's gravity varies with the altitude H according to the relation $g = g_0 \left(\frac{R}{R+H}\right)^2$, where R is the Earth's radius, equal to about 16.360 km and g_0 = 9.807 m/sec for middle latitudes.

In cosmic space at a distance of 1 a.e.* from the Sun there exist solid particles which are large compared with atomic or molecular dimensions (meteor., meteorites, dust), atomic and molecular particles

cosmic rays, electrons, electron streamas), and also electromagnetic radiation of the sun and stars.

Composition of the Air (for Altitudes from 0 to 90 km)

Газ 1	% по весу 2	Молекулярный вес 3
Азот (N) 4	78,09	28,016
Кислород (O_2) 5	20,95	32,000
Аргон A 6	0,93	39,944
Углекислота (CO_2) 7	0,03	44,010
Неон (Ne) 8	$1,8 \cdot 10^{-3}$	20,183
Гелий (He) 9	$5,24 \cdot 10^{-4}$	4,003
Криптон (Kr) 10	$1,0 \cdot 10^{-4}$	8,37
Водород (H_2) 11	$5,0 \cdot 10^{-5}$	2,016
Ксенон (Xe) 12	$8,0 \cdot 10^{-6}$	131,3
Озон (O_3) 13	$1,0 \cdot 10^{-6}$	48,000
Радон (Rd) 14	$6,0 \cdot 10^{-18}$	22

1) Gas; 2) wt%; 3) molecular weight; 4) nitrogen; 5) oxygen; 6) argon; 7) carbon dioxide; 8) neon; 9) helium; 10) krypton; 11) hydrogen; 12) xenon; 13) ozone; 14) radon.

Meteorites are relatively coarse solid bodies moving around the sun on almost circular orbits. On the average the terrestrial atmosphere is entered by one in 15 meteorites of a mean mass of 100 kg, the volume of one meteorite being $1.5 \cdot 10^3$ km^3. The density of stone meteorites amounts to 3-4, that of iron meteorites to 8. Since the former are the more frequent ones, the mean mass amounts to 4; their mean velocity relative to the Earth is 20 km/sec.

The term meteors is understood to mean solid particles of a mass from 10^4 to 10^{-4} g moving on highly elongated orbits. The meteors fall upon the Earth in the form of dust and fine particles. The mean mass of these particles is 10^{-3} g. In the course of 25 hours the Earth captures a total of $2 \cdot 10^{10}$ meteors with a total mass of $1 \cdot 10^7$ to $2 \cdot 10^7$ g.

The volume containing one meteor is equal to $2 \cdot 10^4$ km^3, the mean velocity relative to the Earth is 40 km/sec. The flux of meteorites is fairly constant. In the center of a compact meteor shower the flux may grow by a factor of between 10^3 and 10^4.

The particles of interplanetary dust have diameters from a few microns to 200-300 μ. The mean diameter of the particles is 20 μ, the density 4 and the mass 10^{-8} g. In 24 hours the Earth captures 10^9 g of interplanetary dust. The volume containing one particle amounts to $7 \cdot 10^6$ m^3. The particle velocity relative to the Earth is 30 km/sec. The dust flux is fairly constant.

Primary cosmic rays consist of rapidly moving atomic nuclei of very high energy which penetrate the whole stellar system; the volume containing one particle amounts to $7 \cdot 10^3$ m^3. The flux of cosmic rays with energies of more than 10^9 ev is 1 particle per cm^2 per second (referred to a hemisphere). The composition of cosmic rays with energies between 10^9 and 10^{13} ev is the following: protons 91%, α-particles (He nuclei) 8%, nuclei with an atomic number of 3-5, 0.1%, nuclei with an atomic number of 6-9, 0.4%, and nuclei with an atomic number of more than 9, 0.2%. The mean particle energy is $7 \cdot 10^9$ ev (or 10^{-2} erg). Particles with energies of 10^{18} and 10^{19} ev have been discovered. When the cosmic particle density was calculated, they were assumed to move at a velocity equal to that of light and the cosmic radiation was taken to be isotropic. The contribution of the sun to the total of cosmic radiation is small, except during periods of large eruptions or other disturbances.

The sun is surrounded by a cloud of electrons. At a distance of 1 a.e. from the sun the upper density limit of the cloud amounts to 10^3 electrons per cm^3, and the mean velocity to 30 km/sec.

The electron flux emerges from the disturbed regions of the sun.

The typical flux of 10^7 electrons per cm^2 per second has a velocity of 1000 km/sec between Earth and sun. These fluxes give rise to the aurea borealis and the magnetic storms in the Earth's atmosphere.

The flux of primary cosmic rays varies within the limits of a few per cent. The electron and heavy particle fluxes from the sun vary within wide limits.

The Earth receives radiation in the range of wavelengths from 10^{-8} cm (γ-rays) to radiowaves of several kilometers, mainly from the sun. The total radiation is somewhat less than 2 cal/cm^2-cm, while the mean value of the solar constant is $1.38 \cdot 10^{10}$ erg/m^2-sec. A large part of the energy emitted belongs to the visible part of the solar spectrum. The stellar radiation is far weaker than the solar radiation and amounts to 10^{-8} of the energy of solar radiation.

The solar radiation as a whole does not vary considerably but the radiation of short (10^{-5} cm) and long (10^2 cm) waves may increase by a factor of 10^2-10^3 during solar eruptions. The stellar radiation is constant.

1 Model of Atmosphere

Высота H км 2	Давление p кг/м² 3	Плотность ρ кг сек²/м⁴ 4	Температура T °K 5	Отношение $\frac{T}{\mu G}$ 6	Вероятный молекулярный вес $\mu G \frac{г}{моль}$ 7	Средняя длина свободного пробега l 8
0,500	10 959,7	1,310·10⁻¹	291,3	—	—	—
0	10 332,3	1,2497·10⁻¹	288,0	—	28,97	$8,6 \cdot 10^{-6}$
0,5	9 734,2	11 907·10⁻¹	284,8	—	—	—
1	9 164,6	1,1339·10⁻¹	281,5	—	—	—
2	8 106,2	1,0266·10⁻¹	275,0	—	—	—
3	7 149,1	9,272·10⁻²	268,5	—	—	—
4	6 285,3	8,354·10⁻²	262,0	—	—	—
5	5 508,5	7,506·10⁻²	255,5	—	—	—
6	4 811,1	6,726·10⁻²	249,0	—	—	—
7	4 187,0	6,0110·10⁻²	242,5	—	—	—
8	3 630,2	5,364·10⁻²	236,0	—	—	—
9	3 134,8	4,756·10⁻²	229,5	—	—	—
10	2 695,7	4,206·10⁻²	223,0	—	—	$2,1 \cdot 10^{-7}$
12	1 971,2	3,167·10⁻²	216,5	—	—	—

(Cont'd)

14	1438,0	$2,310 \cdot 10^{-2}$	216,5	—	—	—
16	1049,0	$1,685 \cdot 10^{-2}$	216,5	—	—	—
18	765,3	$1,229 \cdot 10^{-2}$	216,5	—	—	—
20	558,3	$8,97 \cdot 10^{-3}$	216,5	—	—	$9,7 \cdot 10^{-7}$
22	406,5	$6,54 \cdot 10^{-3}$	216,5	—	—	—
24	296,3	$4,76 \cdot 10^{-3}$	216,5	—	—	—
25	210,7	$3,48 \cdot 10^{-3}$	216,5	—	—	—
30	114,2	$1,85 \cdot 10^{-3}$	216,5	—	—	$4,8 \cdot 10^{-6}$
40	32,4	$4,3 \cdot 10^{-4}$	262,5	—	—	$2,2 \cdot 10^{-6}$
50	9,32	$1,2 \cdot 10^{-4}$	270,8	—	—	$7,8 \cdot 10^{-5}$
60	2,61	$3,6 \cdot 10^{-5}$	252,8	—	—	$2,6 \cdot 10^{-4}$
70	0,634	$1,1 \cdot 10^{-5}$	218,0	—	—	$9,3 \cdot 10^{-4}$
80	0,13	$1,75 \cdot 10^{-6}$	205,0	—	—	$4,3 \cdot 10^{-3}$
90	$2,37 \cdot 10^{-2}$	$4,2 \cdot 10^{-7}$	—	6,77	29,9	$2,1 \cdot 10^{-2}$
100	$5,62 \cdot 10^{-3}$	$7,3 \cdot 10^{-8}$	—	9,26	27,0	$9,5 \cdot 10^{-2}$
120	$8,11 \cdot 10^{-4}$	$6,72 \cdot 10^{-9}$	—	14,2	24,8	$1,3 \cdot 10^{0}$
140	$2,12 \cdot 10^{-4}$	$1,32 \cdot 10^{-9}$	—	19,3	24,4	$5,7 \cdot 10^{0}$
160	$7,89 \cdot 10^{-5}$	$3,47 \cdot 10^{-10}$	—	27,2	23,9	$3,6 \cdot 10^{1}$
180	$3,92 \cdot 10^{-5}$	$1,3 \cdot 10^{-10}$	—	36,1	23,7	$1,0 \cdot 10^{2}$
200	$2,23 \cdot 10^{-5}$	$6,42 \cdot 10^{-11}$	—	41,9	22,5	$3,0 \cdot 10^{2}$
220	$1,32 \cdot 10^{-5}$	$3,51 \cdot 10^{-11}$	—	46,7	21,3	$8,7 \cdot 10^{2}$
240	$8,75 \cdot 10^{-6}$	$2,07 \cdot 10^{-11}$	—	50,8	20,4	—
260	$5,82 \cdot 10^{-6}$	$1,28 \cdot 10^{-11}$	—	54,6	19,7	—
280	$4,00 \cdot 10^{-6}$	$8,2 \cdot 10^{-12}$	—	58,5	19,1	—
300	$2,81 \cdot 10^{-6}$	$5,41 \cdot 10^{-12}$	—	62,5	18,7	—
320	$2,24 \cdot 10^{-6}$	$3,69 \cdot 10^{-12}$	—	66,4	18,3	—
340	$1,49 \cdot 10^{-6}$	$2,60 \cdot 10^{-12}$	—	70,0	17,9	—
360	$1,16 \cdot 10^{-6}$	$1,83 \cdot 10^{-12}$	—	73,4	17,6	—
380	$8,50 \cdot 10^{-7}$	$1,35 \cdot 10^{-12}$	—	75,8	17,4	—
400	$6,50 \cdot 10^{-7}$	$1,00 \cdot 10^{-12}$	—	77,5	17,2	—
420	$5,02 \cdot 10^{-7}$	$7,60 \cdot 10^{-13}$	—	79,2	17,0	—
440	$3,90 \cdot 10^{-7}$	$5,80 \cdot 10^{-13}$	—	80,8	16,8	—
460	$3,04 \cdot 10^{-7}$	$4,50 \cdot 10^{-13}$	—	81,5	16,6	—
480	$2,38 \cdot 10^{-7}$	$3,5 \cdot 10^{-13}$	—	82,0	16,4	—
500	$1,87 \cdot 10^{-7}$	$2,70 \cdot 10^{-13}$	—	84,5	16,3	—
550	$1,05 \cdot 10^{-7}$	$1,46 \cdot 10^{-13}$	—	86,9	—	—
600	$6,07 \cdot 10^{-8}$	$8,15 \cdot 10^{-14}$	—	89,5	15,7	
650	$3,6 \cdot 10^{-8}$	$4,60 \cdot 10^{-14}$	—	94,5	15,5	15,6
700	$2,26 \cdot 10^{-8}$	$2,58 \cdot 10^{-14}$	—	105,2	15,3	15,3
750	$1,50 \cdot 10^{-8}$	$1,47 \cdot 10^{-14}$	—	122,5	15,0	15,0
800	$1,08 \cdot 10^{-8}$	$8,60 \cdot 10^{-15}$	—	150,0	14,7	—

Note: For altitudes of 40 to 80 km the data are taken from Burgess' book "To the Limits of Space". N.Y. 1957; for altitudes above 80 km mainly from an article by Kallmann "A Preliminary Model Atmosphre Based on Rocket and Satellite Data." Jour. of Geophys. Res., June 1954.

1) Model of atmosphere; 2) altitude H, km; 3) pressure p, kg/m^2; 4) density ρ, $kg\text{-}sec^2/m^4$; 5) temperature T,°K; 6) ratio; 7) probable molecular weight μG, g/mole; 8) mean free path.

Appendix 4

GASDYNAMIC FUNCTIONS

$$\frac{T}{T_0} = 1 - \frac{k-1}{k+1} M^{*2}; \quad \frac{p}{p_0} = \left(1 - \frac{k-1}{k+1} M^{*2}\right)^{\frac{k}{k-1}}; \quad \frac{\rho}{\rho_0} = \left(1 - \frac{k-1}{k+1} M^{*2}\right)^{\frac{1}{k-1}};$$

$$\frac{\rho w}{\rho^* a^*} = \frac{A^*}{A} = \left(\frac{k+1}{2}\right)^{\frac{1}{k-1}} M^* \left(1 - \frac{k-1}{k+1} M^{*2}\right)^{\frac{1}{k-1}};$$

$$y(M^*) = \left(\frac{k+1}{2}\right)^{\frac{1}{k-1}} \frac{M^*}{1 - \frac{k-1}{k+1} M^{*2}}; \quad r(M^*) = \frac{1 - \frac{k-1}{k+1} M^{*2}}{1 + M^{*2}};$$

$$\frac{1}{r(M^*)} = \frac{K}{pA}; \quad f(M^*) = (1 + M^{*2}) \left(1 - \frac{k-1}{k+1} M^{*2}\right)^{\frac{1}{k-1}}$$

1) $k = c_p/c_v = 1.4$

M^*	$\frac{T}{T_0}$	$\frac{p}{p_0}$	$\frac{\rho}{\rho_0}$	$\frac{\rho w}{\rho^* a^*} = \frac{A^*}{A}$	$y(M^*)$	$r(M^*)$	$f(M^*)$	M
0,00	1,0000	1,0000	1,0000	0,0000	0,0000	1,0000	1,0000	0,0000
0,05	0,9996	0,9986	0,9990	0,0788	0,0789	0,9971	1,0015	0,0457
0,10	0,9983	0,9942	0,9959	0,1571	0,1580	0,9885	1,0058	0,0914
0,15	0,9963	0,9870	0,9907	0,2344	0,2375	0,9744	1,0129	0,1372
0,20	0,9933	0,9768	0,9834	0,3102	0,3176	0,9551	1,0227	0,1830
0,25	0,9896	0,9640	0,9742	0,3842	0,3955	0,9314	1,0350	0,2290
0,30	0,9850	0,9485	0,9630	0,4557	0,4804	0,9037	1,0496	0,2760
0,35	0,9796	0,9303	0,9497	0,5243	0,5636	0,8727	1,0661	0,3228
0,40	0,9733	0,9097	0,9346	0,5897	0,6482	0,8391	1,0842	0,3701
0,45	0,9663	0,8868	0,9178	0,6515	0,7346	0,8035	1,1036	0,4179
0,50	0,9583	0,8616	0,8991	0,7091	0,8230	0,7666	1,1239	0,4663
0,55	0,9496	0,8344	0,8787	0,7623	0,9136	0,7290	1,1445	0,5152
0,60	0,9400	0,8053	0,8567	0,8109	1,0069	0,6912	1,1651	0,5649
0,65	0,9296	0,7745	0,8332	0,8543	1,1030	0,6535	1,1852	0,6154
0,70	0,9183	0,7422	0,8082	0,8924	1,2024	0,6163	1,2042	0,6668
0,75	0,9063	0,7086	0,7819	0,9250	1,3051	0,5800	1,2216	0,7192
0,80	0,8933	0,6738	0,7543	0,9518	1,4126	0,5447	1,2370	0,7727
0,85	0,8796	0,6382	0,7255	0,9729	1,5243	0,5107	1,2499	0,8273
0,90	0,8650	0,6019	0,6959	0,9879	1,6412	0,4779	1,2595	0,8833
0,95	0,8496	0,5653	0,6653	0,9970	1,7638	0,4466	1,2658	0,9409
1,00	0,8333	0,5283	0,6340	1,0000	1,8929	0,4167	1,2679	1,0000
1,05	0,8163	0,4913	0,6019	0,9969	2,0291	0,3882	1,2655	1,0609

1,10	0,7983	0,4546	0,5694	0,9880	2,1734	0,3613	1,2584	1,1239
1,15	0,7796	0,4184	0,5366	0,9735	2,3209	0,3357	1,2463	1,1890
1,20	0,7600	0,3827	0,5035	0,9531	2,4906	0,3115	1,2286	1,2566
1,25	0,7396	0,3479	0,4704	0,9275	2,6860	0,2886	1,2054	1,3268
1,30	0,7183	0,3142	0,4374	0,8969	2,8547	0,2670	1,1765	1,4002
1,35	0,6962	0,2818	0,4045	0,8614	3,0056	0,2467	1,1417	1,4769
1,40	0,6733	0,2505	0,3720	0,8216	3,2798	0,2278	1,1012	1,5575
1,45	0,6496	0,2209	0,3401	0,7778	3,5211	0,2094	1,0551	1,6423
1,50	0,6250	0,1930	0,3088	0,7307	3,7858	0,1923	1,0037	1,7321
1,55	0,5996	0,1669	0,2784	0,6807	4,0778	0,1762	0,9472	1,8273
1,60	0,5733	0,1427	0,2489	0,6282	4,4020	0,1611	0,8861	1,9290
1,65	0,5463	0,1205	0,2205	0,5740	4,7647	0,1467	0,8210	2,0380
1,70	0,5183	0,1003	0,1934	0,5187	5,1735	0,1333	0,7524	2,1555
1,75	0,4896	0,0821	0,1677	0,4630	5,6383	0,1205	0,6813	2,2831
1,80	0,4600	0,0660	0,1435	0,4075	6,1723	0,1085	0,6085	2,4227
1,85	0,4296	0,0520	0,1210	0,3530	6,7934	0,0971	0,5349	2,5766
1,90	0,3983	0,0399	0,1002	0,3002	7,5243	0,0864	0,4617	2,7481
1,95	0,3662	0,0297	0,0812	0,2497	8,3965	0,0763	0,3899	2,9414
2,00	0,3333	0,0211	0,0642	0,2024	9,461	0,0669	0,3203	3,1622
2,05	0,2996	0,0141	0,0491	0,1588	10,794	0,0576	0,2556	3,4190
2,10	0,2650	0,0086	0,0361	0,1198	12,509	0,0490	0,1956	3,7240
2,15	0,2296	0,0058	0,0253	0,0857	14,772	0,0408	0,1420	4,0961
2,20	0,1933	0,0032	0,0164	0,0570	17,949	0,0331	0,0960	4,5674
2,25	0,1563	0,0015	0,0097	0,0343	22,712	0,0258	0,0585	5,1958
2,30	0,1183	0,0006	0,0048	0,0175	30,058	0,0189	0,0302	6,1033
2,35	0,0796	0,0001	0,0017	0,0063	46,593	0,0122	0,0111	[illegible]
2,40	0,0400	0,00013	0,0003	0,0012	91,703	0,0059	0,0022	10,957
2,449	0	0	0	0	—	0	0	—

2) $k = c_p : c_v = 1.30$

M^*	$\frac{T}{T_0}$	$\frac{\rho}{\rho_0}$	$\frac{p}{p_0}$	$\frac{\rho w}{\rho^* a^*} = \frac{A^*}{A}$	$y(M^*)$	$r(M^*)$	$f(M^*)$	M
0,00	1,0000	1,0000	1,0000	0,000	0,000	1,0000	1,000	0,0000
0,05	0,9997	0,9990	0,999	0,0 9	0,050	0,9972	1,001	0,0466
0,10	0,9980	0,994	0,996	0,169	0,100	0,9891	1,006	0,0933
0,15	0,997	0,989	0,990	0,237	0,240	0,975	1,012	0,140
0,20	0,995	0,978	0,983	0,313	0,320	0,957	1,022	0,187
0,25	0,992	0,965	0,973	0,388	0,402	0,934	1,034	0,234
0,30	0,988	0,950	0,962	0,460	0,484	0,906	1,049	0,281
0,35	0,984	0,932	0,948	0,526	0,567	0,877	1,064	0,329
0,40	0,979	0,912	0,932	0,594	0,651	0,844	1,081	0,377
0,45	0,974	0,890	0,915	0,656	0,736	0,810	1,100	0,425
0,50	0,967	0,866	0,895	0,713	0,824	0,774	1,125	0,474
0,55	0,961	0,840	0,874	0,766	0,912	0,738	1,138	0,523
0,60	0,953	0,812	0,852	0,815	1,003	0,701	1,159	0,573
0,65	0,945	0,78	0,828	0,857	1,096	0,664	1,178	0,624
0,70	0,936	0,751	0,802	0,895	1,192	0,628	1,195	0,675
0,75	0,927	0,719	0,776	0,927	1,290	0,593	1,213	0,726
0,80	0,917	0,686	0,748	0,954	1,391	0,559	1,227	0,779
0,85	0,906	0,651	0,719	0,9[illegible]	1,495	0,526	1,238	0,833

0,90	0,894	0,616	0,689	0,989	1,603	0,494	1,247	0,888
0,95	0,882	0,581	0,659	0,997	1,716	0,464	1,254	0,443
1,00	0,870	0,546	0,628	1,000	1,832	0,435	1,256	1,000
1,05	0,856	0,510	0,596	0,997	1,954	0,407	1,253	1,058
1,10	0,842	0,475	0,564	0,988	2,08	0,381	1,246	1,118
1,15	0,828	0,440	0,532	0,975	2,21	0,357	1,236	1,178
1,20	0,812	0,406	0,500	0,956	2,35	0,333	1,220	1,242
1,25	0,796	0,372	0,468	0,932	2,50	0,311	1,199	1,306
1,30	0,780	0,340	0,436	0,903	2,66	0,290	1,173	1,373
1,35	0,762	0,309	0,405	0,871	2,82	0,270	1,143	1,442
1,40	0,744	0,278	0,374	0,834	3,00	0,251	1,107	1,513
1,45	0,726	0,249	0,344	0,794	3,18	0,234	1,067	1,587
1,50	0,707	0,222	0,314	0,751	3,38	0,218	1,021	1,664
1,55	0,687	0,196	0,286	0,706	3,60	0,202	0,973	1,744
1,60	0,666	0,172	0,258	0,658	3,83	0,187	0,918	1,828
1,65	0,645	0,150	0,232	0,610	4,08	0,173	0,864	1,916
1,70	0,623	0,129	0,207	0,560	4,35	0,160	0,805	2,008
1,75	0,601	0,111	0,183	0,510	4,64	0,148	0,743	2,105
1,80	0,578	0,093	0,160	0,460	4,97	0,136	0,678	2,208
1,85	0,554	0,077	0,139	0,411	5,32	0,125	0,615	2,318
1,90	0,529	0,063	0,120	0,363	5,72	0,115	0,553	2,436
1,95	0,504	0,051	0,102	0,317	6,16	0,105	0,490	2,561
2,00	0,478	0,041	0,086	0,273	6,66	0,0976	0,430	2,697
2,05	0,452	0,032	0,071	0,232	7,23	0,0909	0,369	2,843
2,10	0,425	0,024	0,058	0,193	7,88	0,0786	0,314	3,003
2,15	0,397	0,018	0,046	0,158	8,63	0,0706	0,259	3,181
2,20	0,369	0,013	0,036	0,126	9,50	0,0632	0,210	3,377
2,25	0,340	0,009	0,027	0,098	10,55	0,0561	0,164	3,598
2,30	0,310	0,006	0,025	0,073	11,81	0,0493	0,157	3,851
2,35	0,280	0,004	0,014	0,054	13,38	0,0429	0,091	4,140
2,40	0,249	0,002	0,010	0,037	15,36	0,0368	0,068	4,485
2,45	0,217	0,0013	0,006	0,024	17,97	0,0310	0,042	4,904
2,50	0,185	0,0007	0,004	0,014	21,5	0,0255	0,029	5,420
2,55	0,152	0,0003	0,002	0,008	26,7	0,0203	0,015	6,098
2,60	0,118	0,0001	0,001	0,003	35,0	0,0152	0,008	7,058
2,65	0,084	0,0000	0,000	0,001	50,1	0,0105	0,000	8,527
2,70	0,049	0,0000	0,000	0,0002	87,1	0,0059	0,000	12,08
2,75	0,014	0,0000	0,000	0,0000	317,5	0,0002	0,000	21,68

3) $z(M^*) = M^* + \frac{1}{M^*}$; $\chi(M^*) = \ln M^{*2} + \frac{1}{M^{*2}}$

M^*	$z(M^*)$	$\chi(M^*)$	M^*	$z(M^*)$	$\chi(M^*)$	M^*	$z(M^*)$	$\chi(M^*)$
0	∞	∞	1,00	2,0000	1,0000	2,00	2,5000	1,6363
0,05	20,050	394,0085	1,05	2,0024	1,0046	2,05	2,5378	1,6737
0,10	10,100	95,3948	1,10	2,0091	1,0170	2,10	2,5762	1,7107
0,15	6,8167	40,6501	1,15	2,0196	1,0356	2,15	2,6151	1,7472

0,20	5,2000	21,7811	1,20	2,0333	1,0590	2,20	2,6545	1,7836
0,25	4,2500	13,2274	1,25	2,0500	1,0553	2,25	2,6944	1,8194
0,30	3,6333	8,7031	1,30	2,0692	1,1164	2,30	2,7348	1,8548
0,35	3,2071	6,0636	1,35	2,0907	1,1459	2,35	2,7755	1,8900
0,40	2,9000	4,4174	1,40	2,1143	1,1831	2,40	2,8167	1,9245
0,45	2,6722	3,3414	1,45	2,1397	1,2167	2,45	2,8582	1,9588
0,50	2,5000	2,6137	1,50	2,1667	1,2553	2,50	2,9000	1,9926
0,55	2,3682	2,1102	1,55	2,1952	1,2927	2,55	2,9422	2,0360
0,60	2,2667	1,7561	1,60	2,2250	1,3306	2,60	2,9846	2,0589
0,65	2,1885	1,5057	1,65	2,2561	1,3689	2,65	3,0274	2,0915
0,70	2,1286	1,3274	1,70	2,2882	1,4110	2,70	3,0704	2,1247
0,75	2,0833	1,2024	1,75	2,3214	1,4468	2,75	3,1136	2,1554
0,80	2,0500	1,1162	1,80	2,3556	1,4842	2,80	3,1571	2,1868
0,85	2,0265	1,0591	1,85	2,3905	1,5226	2,85	3,2009	2,2178
0,90	2,0111	1,0269	1,90	2,4263	1,5607	2,90	3,2448	2,2483
0,95	2,0026	1,0054	1,95	2,4628	1,5987	2,95	3,2890	2,2786
						3,00	3,3333	2,3083

Appendix 5

TABLE OF PARAMETERS FOR NORMAL SHOCK

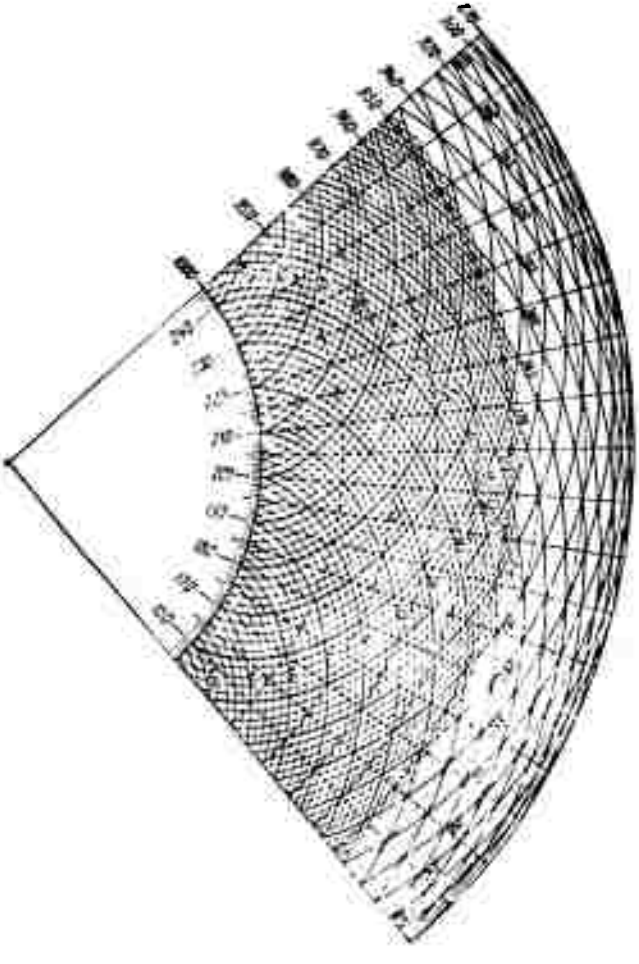
($k = 1,4$)

M_1	M_2	$\frac{p_2}{p_1}$	$\frac{w_1}{w_2} = \frac{\rho_2}{\rho_1}$	$\frac{T_2}{T_1}$	$\sigma = \frac{p_{02}}{p_{01}}$	$\frac{p_{02}}{p_1}$
1,00	1,000	1,000	1,000	1,000	1,000	1,893
1,02	0,980	1,047	1,033	1,013	1,000	1,938
1,05	0,953	1,120	1,084	1,033	1,000	2,008
1,10	0,912	1,245	1,169	1,065	0,999	2,133
1,15	0,875	1,376	1,255	1,097	0,997	2,266
1,20	0,842	1,513	1,342	1,128	0,993	2,407
1,25	0,813	1,656	1,429	1,159	0,987	2,557
1,30	0,786	1,805	1,516	1,191	0,979	2,713
1,35	0,762	1,960	1,603	1,223	0,970	2,878
1,40	0,740	2,120	1,690	1,255	0,958	3,049
1,45	0,719	2,286	1,776	1,287	0,945	3,228
1,50	0,701	2,458	1,862	1,320	0,930	3,413
1,55	0,684	2,636	1,947	1,354	0,913	3,606
1,60	0,668	2,820	2,032	1,388	0,895	3,805
1,65	0,654	3,010	2,115	1,423	0,876	4,011
1,70	0,641	3,205	2,198	1,458	0,856	4,224
1,75	0,628	3,406	2,279	1,495	0,835	4,443
1,80	0,616	3,613	2,359	1,532	0,813	4,669
1,85	0,606	3,826	2,438	1,569	0,790	4,902
1,90	0,596	4,045	2,516	1,608	0,767	5,142
1,95	0,586	4,270	2,592	1,647	0,744	5,388
2,00	0,577	4,500	2,667	1,687	0,721	5,641
2,05	0,569	4,736	2,740	1,729	0,697	5,900
2,10	0,561	4,978	2,812	1,770	0,674	6,165
2,15	0,554	5,226	2,882	1,813	0,651	6,438
2,20	0,547	5,480	2,951	1,857	0,628	6,716
2,25	0,541	5,740	3,019	1,901	0,605	7,002
2,30	0,534	6,005	3,085	1,947	0,583	7,294
2,35	0,529	6,276	3,149	1,993	0,561	7,592
2,40	0,5[illegible]	6,553	3,212	2,040	0,540	7,897
2,45	0,518	6,836	3,273	2,088	0,519	8,208
2,50	0,513	7,125	3,333	2,137	0,499	8,526
2,55	0,508	7,420	3,392	2,187	0,479	8,850
2,60	0,504	7,720	3,449	2,238	0,460	9,181
2,65	0,500	8,026	3,505	2,290	0,441	9,519
2,70	0,496	8,338	3,559	2,343	0,424	9,862
2,75	0,492	8,656	3,612	2,397	0,406	10,212
2,80	0,487	8,980	3,663	2,451	0,389	10,569
2,85	0,485	9,310	3,714	2,507	0,373	10,933
2,90	0,481	9,645	3,763	2,563	0,358	11,302

2,95	0,478	9,966	3,811	2,621	0,343	11,679
3,00	0,475	10,333	3,857	2,679	0,328	12,061
3,50	0,451	14,125	4,261	3,315	0,213	16,242
4,00	0,435	18,500	4,571	4,017	0,139	21,068
4,50	0,424	23,458	4,812	4,875	0,092	26,539
5,00	0,415	29,000	5,000	5,800	0,062	32,654
6,00	0,404	41,833	5,268	7,911	0,030	46,815
7,00	0,397	57,000	5,441	10,469	0,015	63,552
8,00	0,393	74,500	5,565	13,397	0,008	82,865
9,00	0,390	94,333	5,651	16,693	0,005	104,753
10,00	0,388	116,500	5,711	20,389	0,003	129,217
∞	0,378	∞	6,000	∞	0	∞

Appendix 6

DIAGRAM OF CHARACTERISTICS (k = 1.4)



Appendix 7

PARAMETERS OF PRANDTL-MEYER FLOW

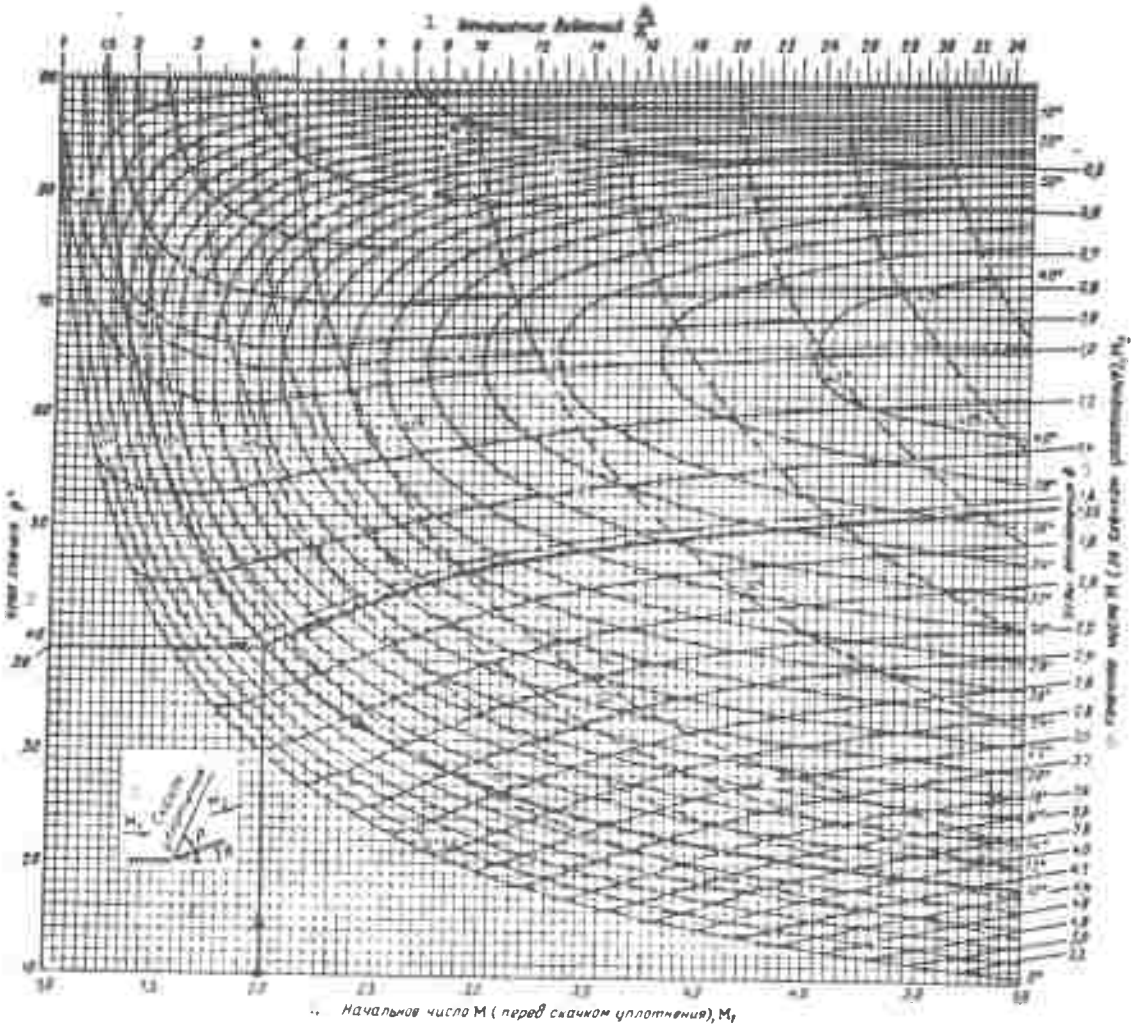
($k = 1{,}4$)

$\nu^*(M^*) = 1000 - (\varphi+\sigma)$	μ^*	θ^*	ω^*	M	M^*	$\frac{T_2}{T_0}$	$\frac{p_2}{p_0}$	$\frac{\rho_2}{\rho_0}$	$\frac{r_2}{r_0}$
1000	90°00′	0°00′	0°00′	1,000	1,000	0,833	0,528	0,634	1,000
	72°06′	0°30′	18°24′	1,051	1,042	0,819	0,497	0,607	1,049
999	67°28′	1°00′	23°32′	1,083	1,067	0,810	0,479	0,591	1,087
998	62°00′	2°00′	30°00′	1,133	1,107	0,796	0,450	0,565	1,147
997	58°06′	3°00′	34°54′	1,178	1,142	0,783	0,424	0,542	1,205
996	55°08′	4°00′	38°52′	1,219	1,172	0,771	0,402	0,522	1,262
995	52°42′	5°	42°18′	1,257	1,200	0,760	0,383	0,504	1,312
994	50°36′	6°	45°24′	1,294	1,227	0,749	0,364	0,497	1,372
993	48°42′	7°	48°18′	1,331	1,253	0,738	0,346	0,468	1,437
992	47°00′	8°	51°00′	1,367	1,277	0,728	0,330	0,452	1,498
991	45°32′	9°	53°28′	1,401	1,300	0,718	0,314	0,437	1,559
990	44°10′	10°	55°50′	1,435	1,323	0,708	0,299	0,422	1,626
988	41°40′	12°	60°20′	1,504	1,367	0,688	0,271	0,393	1,772
986	39°35′	14°	64°25′	1,569	1,408	0,670	0,246	0,367	1,923
984	37°36′	16°	68°24′	1,639	1,448	0,650	0,222	0,341	2,094
982	35°54′	18°	72°06′	1,705	1,486	0,632	0,201	0,318	2,291
980	34°18′	20°	75°42′	1,775	1,523	0,613	0,181	0,295	2,500
978	32°48′	22°	79°12′	1,846	1,559	0,595	0,162	0,273	2,735
976	31°30′	24°	82°30′	1,914	1,594	0,576	0,146	0,253	2,993
974	30°12′	26°	85°48′	1,988	1,628	0,558	0,130	0,233	3,319
972	29°00′	28°	89°00′	2,063	1,660	0,541	0,116	0,215	3,647
970	28°00′	30°	92°00′	2,130	1,691	0,523	0,1040	0,198	4,046
968	26°55′	32°	95°05′	2,209	1,722	0,506	0,0920	0,182	4,436
966	25°57′	34°	98°03′	2,285	1,752	0,488	0,0814	0,167	4,955
964	25°00′	36°	101°00′	2,366	1,782	0,471	0,0717	0,152	5,521

962	24°03′	38°	103°57′	2,454	1,810	0,454	0,0630	0,139	6,166
960	23°12′	40°	106°48′	2,539	1,838	0,437	0,0552	0,126	6,919
958	22°24′	42°	109°36′	2,624	1,865	0,420	0,0481	0,114	7,798
956	21°36′	44°	112°21′	2,717	1,891	0,404	0,0419	0,104	8,710
954	20°48′	46°	115°12′	2,816	1,918	0,387	0,0360	0,093	9,954
952	20°06′	48°	117°54′	2,910	1,943	0,371	0,0310	0,084	11,20
950	19°24′	50°	120°36′	3,010	1,967	0,355	0,0267	0,075	12,94
948	18°42′	52°	123°18′	3,119	1,990	0,340	0,0229	0,067	14,72
946	18°00′	54°	126°00′	3,236	2,014	0,324	0,0194	0,060	16,90
944	17°24′	56°	128°36′	3,344	2,036	0,309	0,0164	0,053	19,49
942	16°45′	58°	131°15′	3,470	2,058	0,294	0,0138	0,047	22,49
940	16°06′	60°	133°54′	3,606	2,080	0,279	0,0115	0,041	26,30
938	15°30′	62°	136°30′	3,742	2,100	0,265	$0,954\cdot10^{-2}$	0,036	30,55
936	14°57′	64°	139°03′	3,876	2,121	0,250	$0,784\cdot10^{-2}$	0,031	36,40
934	14°24′	66°	141°36′	4,021	2,140	0,237	$0,645\cdot10^{-2}$	0,027	43,15
932	13°48′	68°	144°12′	4,193	2,159	0,223	$0,525\cdot10^{-2}$	0,0235	51,62
930	13°18′	70°	146°42′	4,348	2,177	0,210	$0,426\cdot10^{-2}$	0,0203	62,50
928	12°48′	72°	149°12′	4,515	2,195	0,197	$0,339\cdot10^{-2}$	0,0172	75,00
926	12°18′	74°	151°42′	4,695	2,212	0,184	$0,270\cdot10^{-2}$	0,0146	91,20
924	11°45′	76°	154°15′	4,912	2,228	0,173	$0,214\cdot10^{-2}$	0,0124	111,7
922	11°15′	78°	156°45′	5,126	2,244	0,160	$0,165\cdot10^{-2}$	0,0103	143,3
920	10°45′	80°	159°15′	5,362	2,260	0,149	$0,126\cdot10^{-2}$	$0,851\cdot10^{-2}$	177,0
915	9°33′	85°	165°27′	6,028	2,296	0,122	$0,631\cdot10^{-3}$	$0,518\cdot10^{-3}$	316,2
910	8°24′	90°	171°36′	6,845	2,328	0,097	$0,285\cdot10^{-3}$	$0,294\cdot10^{-3}$	631,0
905	7°20′	95°	177°40′	7,837	2,356	0,075	$0,114\cdot10^{-3}$	$0,153\cdot10^{-3}$	1334
900	6°12′	100°	183°48′	9,259	2,380	0,055	$0,403\cdot10^{-4}$	$0,726\cdot10^{-3}$	3092
895	5°12′	105°	189°48′	11,037	2,401	0,039	$0,118\cdot10^{-4}$	$0,302\cdot10^{-3}$	9360
869,55	0°00′	130°27′	220°27′	∞	2,449	0	0	0	∞

Appendix 8

DIAGRAM OF OBLIQUE COMPRESSION SHOCKS k = 1.4



Начальное число M (перед скачком уплотнения), M_1

Appendix 8 [see page 840]

1) Pressure ratio; 2) shock angle; 3) compression shock; 4) initial Mach number (in front of the compression shock), M_1; 5) angle of deflection; 6) final Mach number M (behind the compression shock), M_2.

VELOCITIES AND THEIR POTENTIALS ON A CIRCLE IN TRANSVERSE (w_1, φ_1^*), LONGITUDINAL (w_2, φ_2^*) AND CIRCULATORY (w_3) FLOWS THROUGH A LATTICE OF UNIT CIRCLES AS A FUNCTION OF $\theta = \vartheta + \gamma$ (cf. Fig. 9.3.8)

ϑ	$\theta = 0$					$\theta = 10°$					$\theta =$					$\theta =$					$\theta = 40°$				
	$-w_1$	w_2	w_3	φ_1^*	φ_2^*	$-w_1$	w_2	w_3	φ_1^*	φ_2^*	$-w_1$	w_2	w_3	φ_1^*	φ_2^*	$-w_1$	w_2	w_3	φ_1^*	φ_2^*	$-w_1$	w_2	w_3	φ_1^*	φ_2^*
0.0	0.000	1.887	1.281	2.487	0.000	0.448	1.888	1.264	2.462	0.280	0.812	1.781													
0.25	0.000	1.552	1.469	2.350	0.000	0.421	1.523	1.427	2.288	0.288	0.830	1.534													
0.50	0.000	1.614	1.337	2.209	0.000	0.433	1.584	1.308	2.201	0.278	0.881	1.493													
0.75	0.000	1.878	1.032	2.068	0.000	0.464	1.645	1.182	2.082	0.271	0.888	1.452													
1.00	0.000	1.941	1.087	1.926	0.000	0.427	1.519	1.025	1.926	0.266	0.816	1.416													
1.25	0.000	1.510	1.777	1.785	0.000	0.479	1.478	1.735	1.779	0.261	0.945	1.378													
1.50	0.000	1.472	1.836	1.644	0.000	0.482	1.441	1.816	1.632	0.257	0.975	1.343													
1.75	0.000	1.432	1.943	1.503	0.000	0.484	1.402	1.905	1.501	0.252	1.007	1.310													
2.00	0.000	1.427	2.004	1.362	0.000	0.507	1.393	1.967	1.389	0.247	1.040	1.278													
2.25	0.000	1.404	2.065	1.220	0.000	0.516	1.384	2.025	1.264	0.243	1.073	1.249													

Appendix 9 (Cont'd)

ϑ	$\theta = 50°$					$\theta = 60°$					$\theta =$ 70°					$\theta = 80°$					$\theta = 90°$				
	$-w_1$	w_2	w_3	φ_1^*	φ_2^*	$-w_1$	w_2	w_3	φ_1^*	φ_2^*	$-w_1$	w_2	w_3	φ_1^*	φ_2^*	$-w_1$	w_2	w_3	φ_1^*	φ_2^*	$-w_1$	w_2	w_3	φ_1^*	φ_2^*
0.0	1.591	1.033	0.945	1.637	1.278	2.175	0.780	0.808	1.281	1.437	2.402	0.527	0.689	0.881	1.552	2.541	0.264	0.612	0.449	1.621	2.589	0.000	0.584	0.000	1.644
0.25	1.988	0.992	0.941	1.740	1.233	2.300	0.735	0.770	1.362	1.388	2.560	0.486	0.628	0.942	1.496	2.720	0.240	0.533	0.480	1.558	2.780	0.000	0.500	0.000	1.578
0.50	2.096	0.934	0.933	1.871	1.199	2.443	0.681	0.731	1.471	1.340	2.743	0.447	0.565	1.022	1.438	2.948	0.218	0.450	0.523	1.496	3.022	0.000	0.410	0.000	1.515
0.65	2.212	0.875	0.930	2.035	1.160	2.622	0.630	0.690	1.602	1.290	2.972	0.398	0.495	1.130	1.382	3.240	0.190	0.365	0.580	1.430	3.350	0.000	0. 22	0.000	1.445
0.70	2.452	0.815	0.908	2.258	1.122	2.850	0.570	0.651	1.804	1.243	3.283	0.346	0.427	1.266	1.327	3.657	0.158	0.281	0.655	1.366	3.795	0.000	0.230	0.000	1.379
0.75	2.520	0.760	0.894	2.570	1.087	3.140	0.512	0.603	2.082	1.196	3.720	0.292	0.260	1.452	1.270	4.240	0.125	0.212	0.760	1.304	4.450	0.000	0.147	0.000	1.314
0.80	2.730	0.696	0.876	2.983	1.052	3.505	0.452	0.550	2.462	1.152	4.360	0.227	0.292	1.754	1.214	5.098	0.085	0.146	0.926	0.239	5.411	0.000	0.079	0.000	1.244
0.85	3.000	0.635	0.850	3.610	1.021	4.020	0.380	0.491	3.032	1.108	5.290	0.165	0.225	2.220	1.157	6.510	0.050	0.086	1.195	1.176	6.920	0.000	0.035	0.000	1.180
0.90	3.330	0.576	0.817	4.803	0.990	4.725	0.303	0.428	4.107	1.067	6.734	0.106	0.150	3.116	1.101	9.119	0.020	0.029	1.733	1.110	10.367	0.000	0.006	0.000	1.112
0.95	3.752	0.516	0.770	7.564	0.958	5.811	0.233	0.348	6.745	1.022	9.520	0.054	0.081	5.437	1.045	16.166	0.004	0.005	3.259	1.049	20.343	0.000	0.000	0.000	1.049

AUXILIARY TABLES AND GRAPHS FOR CALCULATING LATTICES OF [illegible]

CHAPLYGIN PROFILE FAMILIES

TABLE 1

Values of the Angles ϑ_0 Corresponding to the Trailing Edge of the Profile ($z = 0$) and of the Velocity Potentials of a Circulation-free Flow φ (ϑ_0) About a Circle in a Lattice

$-\phi_0$

τ / q	0°	15°	30°	45°	60°	75°	90°
0,50	0°00′	19°00′	37°53′	55°32′	71°30′	83°44′	90°00′
0,55	0°00′	19°40′	39°00′	57°31′	73°46′	86°22′	90°00′
0,60	0°00′	20°07′	40°00′	59°13′	75°57′	89°04′	90°00′
0,65	0°00′	20°30′	40°54′	60°46′	78°04′	91°57′	90°00′
0,70	0°00′	21°00′	41°46′	62°12′	80°12′	95°00′	90°00′
0,75	0°00′	21°30′	42°36′	63°30′	82°16′	97°53′	90°00′
0,80	0°00′	22°00′	43°29′	64°36′	84°12′	100°44′	90°00′
0,85	0°00′	22°12′	44°12′	65°38′	86°00′	103°18′	90°00′
0,90	0°00′	22°32′	45°00′	66°34′	87°30′	105°36′	90°00′
0,95	0°00′	23°00′	45°31′	67°29′	88°30′	107°29′	90°00′

TABLE 2

τ / φ							

TABLE 3

Connection Between the Parameters ξ_0, ϑ_0 Determining the Camber $\bar{f}$ and the Thickness $\bar{d}$ of Profiles With the Density b/l and the Stagger Angle γ of the Lattice. Values of ξ_0

$\bar{d}$%	τ	+45°				+30°				0		−30°					−45°				−60°			
	$\bar{f}$%	0.5	1.0	1.5	2.0	0.5	1.0	1.5	2.0	0.5	1.0	1.5	2.0	0.5	1.0	1.5	2.0	0.5	1.0	1.5	2.0	0.5	1.0	1.5	2.0
0	0	0.000	0.000	0.000	0.000	0.000	0.000	0.000	0.000	0.000	0.000	0.000	0.000	0.000	0.000	0.000	0.000	0.000	0.000	0.000	0.000	0.000	0.000	0.000	0.000
	5	0.013	0.012	0.009	0.008	0.006	0.004	0.004	0.005	0.014	0.014	0.014	0.010	0.011	0.012	0.014	0.015	0.012	0.016	0.020	0.026	0.014	0.059	0.024	0.073
	10	0.040	0.034	0.022	0.006	0.035	0.028	0.021	0.011	0.038	0.037	0.034	0.029	0.039	0.041	0.045	0.050	0.038	0.046	0.060	0.075	0.038	0.048	0.088	—
	15	0.080	0.069	0.052	0.031	0.075	0.062	0.04	0.032	0.081	0.075	0.067	0.060	0.088	0.093	0.098	0.105	0.087	0.100	0.134	0.164	0.086	0.112	0.161	—
5	0	0.040	0.037	0.032	0.025	0.039	0.03	0.029	0.022	0.039	0.036	0.030	0.025	0.038	0.037	0.036	0.032	0.040	0.038	0.034	0.029	0.040	0.038	0.034	0.030
	5	0.050	0.042	0.032	0.020	0.042	0.035	0.030	0.026	0.046	0.041	0.038	0.035	0.049	0.046	0.044	0.045	0.051	0.050	0.050	0.048	0.052	0.053	0.056	0.060
	10	0.073	0.061	0.045	0.036	0.069	0.059	0.046	0.030	0.067	0.061	0.056	0.062	0.074	0.074	0.076	0.078	0.076	0.080	0.086	0.094	0.076	0.078	0.113	—
	15	0.113	0.096	0.074	0.048	0.105	0.099	0.075	0.094	0.110	0.102	0.090	0.078	0.116	0.117	0.118	0.120	0.118	0.126	0.146	0.176	0.110	0.128	0.180	—

(Cont'd)

10	0	0,078	0,071	0,062	0,050	0,074	0,068	0,060	0,048	0,076	0,070	0,060	0,051	0,075	0,070	0,064	0,054	0,080	0,076	0,067	0,057	0,084	0,080	0,069	0,055
	5	0,083	0,075	0,064	0,048	0,049	0,071	0,062	0,051	0,081	0,075	0,068	0,058	0,080	0,076	0,053	0,072	0,086	0,087	0,084	0,074	0,088	0,086	0,086	0,082
	10	0,106	0,094	0,076	0,054	0,102	0,090	0,076	0,060	0,104	0,096	0,086	0,073	0,108	0,106	0,192	0,100	0,113	0,115	0,114	0,11[illegible]	0,113	0,113	0,135	—
	15	0,147	0,130	0,104	0,072	0,138	0,122	0,100	0,074	0,142	0,128	0,112	0,094	0,144	0,160	0,138	0,131	0,149	0,152	0,16[illegible]	0,186	0,142	0,154	0,199	—
15	0	0,113	0,103	0,091	0,076	0,111	0,099	0,086	0,070	0,115	0,105	0,092	0,076	0,111	0,101	0,090	0,074	0,117	0,109	0,097	0,083	0,124	0,116	0,102	0,082
	5	0,121	0,110	0,091	0,070	0,116	0,104	0,090	0,07[illegible]	0,125	0,115	0,100	0,080	0,118	0,110	0,101	0,091	0,127	0,121	0,111	0,095	0,125	0,124	0,117	0,106
	10	0,140	0,124	0,102	0,074	0,134	0,120	0,100	0,078	0,136	0,124	0,101	0,092	0,142	0,135	0,126	0,114	0,116	0,112	0,14[illegible]	0,127	0,150	0,144	0,155	—
	15	0,182	0,163	0,130	0,090	0,191	0,150	0,122	0,090	0,170	0,152	0,132	0,109	0,174	0,164	0,155	0,157	0,178	0,176	0,18[illegible]	0,198	0,172	0,177	0,216	—

TABLE 4

Values of η_0

$\bar{d}$ %	$\bar{\gamma}$ % \ τ	+45°				+30°				0	
		0,5	1,0	1,5	2,0	0,5	1,0	1,5	2,0	0,5	1,0
0	0	0,000	0,000	0,000	0,000	0,000	0,000	0,000	0,000	0,000	0,000
	5	0,105	0,102	0,092	0,079	0,094	0,088	0,080	0,069	0,096	0,086
	10	0,197	0,191	0,173	0,143	0,182	0,160	0,152	0,125	0,176	0,158
	15	0,276	0,270	0,254	0,222	0,258	0,240	0,216	0,182	0,256	0,224
5	0	0,000	0,000	0,000	0,000	0,000	0,000	0,000	0,000	0,000	0,000
	5	0,099	0,095	0,086	0,073	0,090	0,083	0,074	0,062	0,091	0,082
	10	0,188	0,181	0,164	0,134	0,174	0,160	0,142	0,113	0,167	0,147
	15	0,264	0,276	0,240	0,208	0,218	0,226	0,200	0,162	0,242	0,210
10	0	0,000	0,000	0,000	0,000	0,000	0,000	0,000	0,000	0,000	0,000
	5	0,092	0,087	0,077	0,064	0,084	0,076	0,066	0,052	0,088	0,077
	10	0,175	0,168	0,152	0,124	0,166	0,150	0,130	0,102	0,160	0,138
	15	0,258	0,244	0,222	0,186	0,236	0,214	0,184	0,142	0,231	0,197
15	0	0,000	0,000	0,000	0,000	0,000	0,000	0,000	0,000	0,000	0,000
	5	0,087	0,080	0,068	0,054	0,080	0,071	0,059	0,044	0,083	0,072
	10	0,165	0,156	0,138	0,106	0,157	0,141	0,119	0,087	0,152	0,128
	15	0,236	0,224	0,200	0,159	0,226	0,204	0,170	0,120	0,219	0,182

		−30°				−45°				−60°			
		1,5	2,0	0,5	1,0	1,5	2,0	0,5	1,0	1,5	2,0	0,5	1,0	1,5	2,0
0	0	0,000	0,000	0,000	0,000	0,000	0,000	0,000	0,000	0,000	0,000	0,000	0,000	0,000	0,000
	5	0,074	0,059	0,099	0,092	0,080	0,064	0,100	0,101	0,088	0,070	0,107	0,108	0,102	0,083
	10	0,136	0,112	0,184	0,158	0,144	0,118	0,200	0,188	0,160	0,12[illegible]	0,210	0,208	0,162	0,139
	15	0,188	0,148	0,256	0,23[illegible]	0,187	0,116	0,287	0,157	0,196	0,104	0,294	0,286	0,186	—
5	0	0,000	0,000	0,000	0,000	0,000	0,000	0,000	0,000	0,000	0,000	0,000	0,000	0,000	0,000
	5	0,068	0,062	0,094	0,086	0,07[illegible]	0,057	0,100	0,094	0,079	0,06[illegible]	0,[illegible]07	0,104	0,097	0,076
	10	0,124	0,100	0,177	0,158	0,13[illegible]	0,101	0,19[illegible]	0,[illegible]20	0,[illegible]11	0,[illegible]0	0,294	0,193	0,166	0,113
	15	0,172	0,131	0,254	0,223	0,[illegible]0	0,086	0,27[illegible]	0,2[illegible]0	0,172	—	0,253	0,272	0,186	—
10	0	0,000	0,000	0,000	0,000	0,000	0,000	0,000	0,000	0,000	0,000	0,000	0,000	0,000	0,000
	5	0,063	0,048	0,090	0,080	0,06[illegible]	0,0[illegible]	0,09[illegible]	0,08[illegible]	0,070	0,04[illegible]	0,[illegible]0	0,100	0,090	0,069
	10	0,112	0,085	0,170	0,14[illegible]	0,119	0,08[illegible]	0,18[illegible]	0,16[illegible]	0,12[illegible]	0,0[illegible]	0,19[illegible]	0,188	0,152	0,094
	15	0,15[illegible]	0,108	0,[illegible]5	0,20[illegible]	0,111	0,04[illegible]	0,256	0,22[illegible]	0,150	—	0,271	0,258	0,136	—
15	0	0,000	0,000	0,000	0,000	0,000	0,000	0,000	0,000	0,000	0,000	0,000	0,000	0,000	0,000
	5	0,[illegible]5	0,040	0,085	0,075	0,060	0,041	0,09[illegible]	0,08[illegible]	0,06[illegible]	0,01[illegible]	0,[illegible]97	0,097	0,080	0,[illegible]6
	10	0,1[illegible]	[illegible]3[illegible]	0,160	0,13[illegible]	0,10[illegible]	0,06[illegible]	0,17[illegible]	0,16[illegible]	0,1[illegible]6	0,05[illegible]	0,19[illegible]	0,176	0,129	0,0[illegible]
	15	0,1[illegible]	[illegible]	0,228	0,190	0,125	—	0,240	0,20[illegible]	0,130	—	0,255	0,244	0,112	—

TABLE 5

Density $q = 2r/\underline{l}$ of a Lattice of Circles in Dependence on the Parameters $\bar{f}$, $\bar{d}$, $b/\underline{l}$ of a Lattice of Profiles. Values of q

$\bar{d}$ %	$\bar{f}$ % \ τ	+45°				+30°				0		−30°				−45°				−60°			
		0,5	1,0	1,5	2,0	0,5	1,0	1,5	2,0	0,5	1,0	1,5	2,0	0,5	1,0	1,5	2,0	0,5	1,0	1,5	2,0	0,5	1,0	1,5	2,0
0	0	0,26	0,27	0,63	0,73	0,24	0,44	0,59	0,64	0,22	0,42	0,57	0,66	0,23	0,44	0,60	0,69	0,26	0,48	0,64	0,73	0,27	0,52	0,70	0,79
	5	0,25	0,46	0,61	0,71	0,23	0,43	0,58	0,68	0,22	0,42	0,58	0,67	0,25	0,46	0,62	0,70	0,27	0,49	0,66	0,76	0,29	0,54	0,74	0,85
	10	0,25	0,46	0,61	0,71	0,23	0,43	0,58	0,68	0,23	0,43	0,59	0,68	0,26	0,48	0,65	0,75	0,28	0,53	0,71	—	0,29	0,54	0,81	—
	15	0,25	0,46	0,61	0,71	0,23	0,43	0,59	0,68	0,24	0,45	0,61	0,71	0,27	0,51	0,69	0,78	0,29	0,56	0,78	—	0,29	0,54	0,81	—
5	0	0,27	0,49	0,65	0,76	0,24	0,45	0,61	0,72	0,24	0,44	0,59	0,69	0,25	0,46	0,62	0,71	0,27	0,49	0,66	0,75	0,28	0,53	0,71	0,81
	5	0,26	0,48	0,63	0,73	0,24	0,45	0,61	0,70	0,24	0,44	0,60	0,69	0,26	0,48	0,64	0,74	0,27	0,51	0,68	0,78	0,29	0,55	0,76	—
	10	0,25	0,47	0,62	0,72	0,24	0,45	0,60	0,70	0,24	0,45	0,61	0,70	0,26	0,49	0,67	0,78	0,29	0,54	0,73	—	0,29	0,58	0,82	—
	15	0,25	0,47	0,62	0,72	0,24	0,46	0,61	0,70	0,25	0,47	0,63	0,73	0,28	0,52	0,71	0,81	0,29	0,57	0,80	—	0,30	0,58	0,81	—
10	0	0,28	0,51	0,67	0,73	0,26	0,47	0,63	0,73	0,24	0,45	0,61	0,71	0,26	0,48	0,65	0,74	0,28	0,51	0,68	0,77	0,29	0,55	0,73	0,83
	5	0,27	0,49	0,66	0,73	0,25	0,47	0,62	0,72	0,25	0,46	0,62	0,72	0,27	0,50	0,66	0,77	0,28	0,53	0,71	0,81	0,30	0,56	0,78	—
	10	0,27	0,49	0,64	0,74	0,25	0,48	0,62	0,72	0,25	0,47	[illegible]													
	15	0,27	0,49	0,64	0,74	0,25	0,48	0,62	0,72	0,26	0,49	0,65	0,76	0,28	0,54	0,73	0,84	0,30	0,58	0,82	—	0,28	0,57	0,84	—
15	[illegible]																								
	5	0,28	0,51	0,67	0,78	0,27	0,49	0,65	0,75	0,26	0,49	0,64	0,74	0,27	0,51	0,68	0,79	0,29	0,52	0,72	0,83	0,31	0,58	0,80	—
	10	0,28	0,51	0,66	0,71	0,26	0,49	0,65	0,75	0,27	0,49	0,66	0,75	0,28	0,53	0,71	0,82	0,30	0,57	0,77	—	0,32	0,58	0,80	—
	15	0,28	0,51	0,66	0,71	0,26	0,49	0,65	0,75	0,28	0,51	0,69	0,78	0,30	0,56	0,76	0,81	0,31	0,60	0,84	—	0,32	0,59	0,84	—

TABLE 6

Velocity Components on a Circle in a Lattice at a Point Corresponding to the Trailing Edge of the Profile

q	τ	0	15°	30°	45°	60°	75°	90°
0,50	$-\varpi_{10}$	0,000	0,460	0,900	1,350	1,850	2,320	2,589
	ϖ_0	1,697	1,640	1,560	1,350	1,068	0,590	0,000
	ϖ_{30}	1,387	1,365	1,310	1,155	0,968	0,727	0,584

(Cont'd)

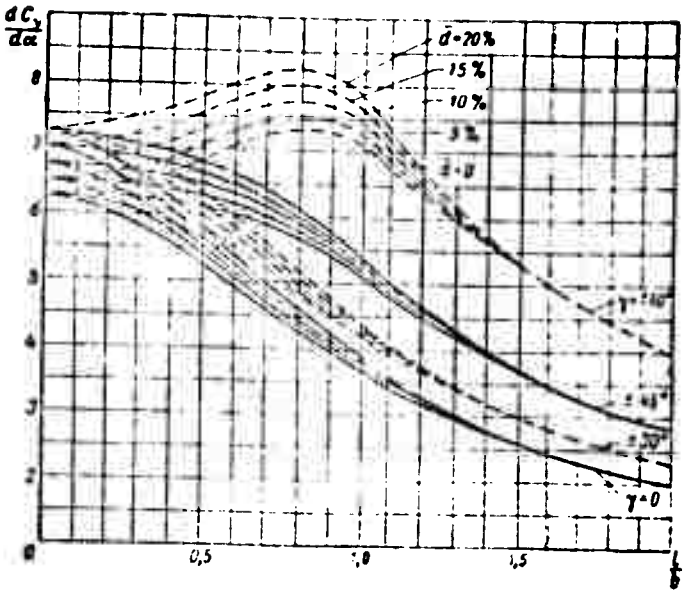
	$-\varpi_{10}$	0,000	0,430	0,870	1,340	1,860	2,400	2,780
0,55	ϖ_{20}	1,655	1,620	1,5[illegible]	1,340	1,080	0,643	0,000
	ϖ_{30}	1,460	1,425	1,353	1,215	1,000	0,710	0,500
	$-\varpi_{10}$	0,000	0,425	0,840	1,310	1,860	2,460	3,022
0,60	ϖ_{20}	1,614	1,602	1,455	1,310	1,080	0,670	0,000
	ϖ_{30}	1,537	1,500	1,415	1,280	1,040	0,712	0,410
	$-\varpi_{10}$	0,000	0,420	0,840	1,290	1,850	2,520	3,350
0,65	ϖ_{20}	1,578	1,565	1,460	1,290	1,075	0,685	0,000
	ϖ_{30}	1,615	1,575	1,490	1,350	1,090	0,725	0,322
	$-\varpi_{10}$	0,000	0,410	0,830	1,280	1,840	2,570	3,795
0,70	ϖ_{20}	1,541	1,520	1,420	1,280	1,068	0,697	0,000
	ϖ_{30}	1,697	1,662	1,570	1,427	1,115	0,770	0,230
	$-\varpi_{10}$	0,000	0,390	0,810	1,270	1,830	2,620	4,450
0,75	ϖ_{20}	1,510	1,480	1,402	1,270	1,060	0,710	0,000
	ϖ_{30}	1,777	1,740	1,650	1,510	1,240	0,825	0,147
	$-\varpi_{10}$	0,000	0,380	0,800	1,260	1,820	2,650	5,411
0,80	ϖ_{20}	1,479	1,438	1,386	1,260	1,050	0,719	0,000
	ϖ_{30}	1,859	1,632	1,735	1,585	1,325	0,900	0,079
	$-\varpi_{10}$	0,000	0,376	0,790	1,240	1,820	2,680	6,920
0,85	ϖ_{20}	1,452	1,410	1,360	1,240	1,050	0,720	0,000
	ϖ_{30}	1,940	1,910	1,815	1,670	1,400	0,965	0,035
	$-\varpi_{10}$	0,000	0,373	0,780	1,230	1,810	2,740	10,367
0,90	ϖ_{20}	1,427	1,400	1,342	1,230	1,042	0,735	0,000
	ϖ_{30}	2,018	1,990	1,903	1,745	1,476	1,030	0,006
	$-\varpi_{10}$	0,000	0,370	0,760	1,210	1,800	2,810	20,343
0,95	ϖ_{20}	1,404	1,380	1,318	1,210	1,012	0,750	0,000
	ϖ_{30}	2,095	2,065	1,975	1,800	1,540	1,120	0,0001

TABLE 7

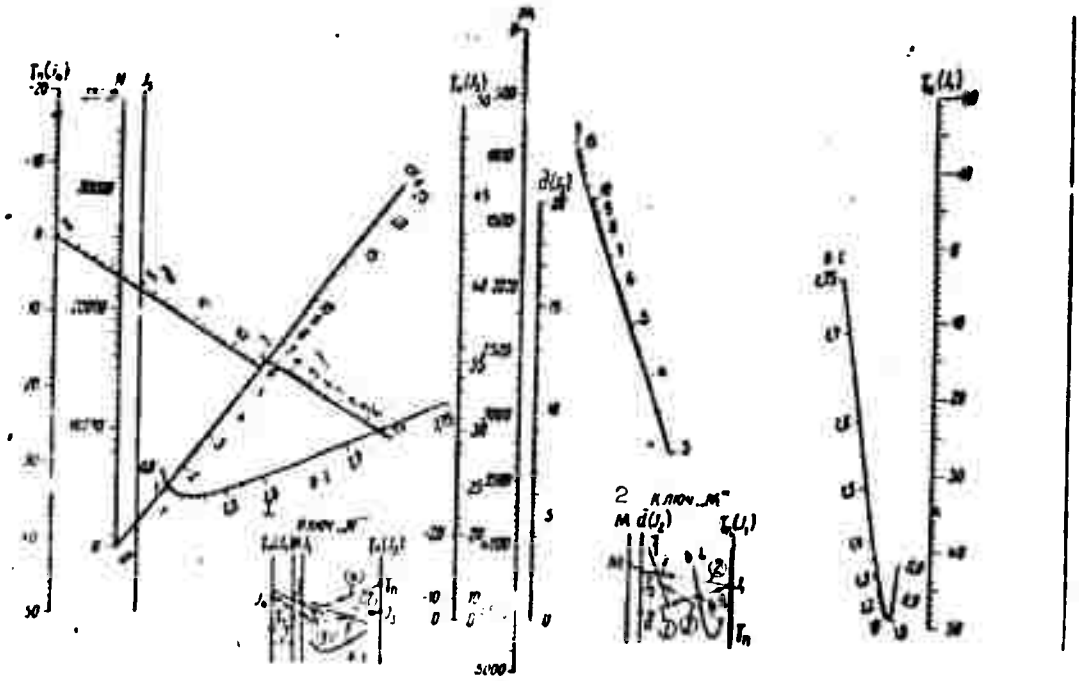
Values of the Parameter $\Gamma^* = \dfrac{\Gamma}{2\pi\varpi_\infty \sin\alpha}$

$\Gamma^*(\varphi, \gamma)$

φ \ γ	0°	15°	30°	45°	60°	75°	90°
0,5	0,612	0,625	0,688	0,825	1,104	1,655	2,216
0,55	0,567	0,581	0,645	0,780	1,075	1,730	2,760
0,60	0,525	0,551	0,650	0,723	1,031	1,790	3,690
0,65	0,489	0,515	0,565	0,679	0,981	1,806	5,202
0,70	0,454	0,473	0,524	0,636	0,925	1,730	8,250
0,75	0,425	0,441	0,490	0,597	0,855	1,643	15,130
0,80	0,398	0,406	0,461	0,565	0,791	1,530	34,250
0,85	0,375	0,382	0,431	0,530	0,750	1,440	98,800
0,90	0,354	0,361	0,407	0,490	0,709	1,379	864,000
0,95	0,335	0,345	0,385	0,475	0,675	1,300	$102 \cdot 10^3$



Graph of the values of $dc_y/d\alpha$ in dependence on the lattice density and the stagger angle.

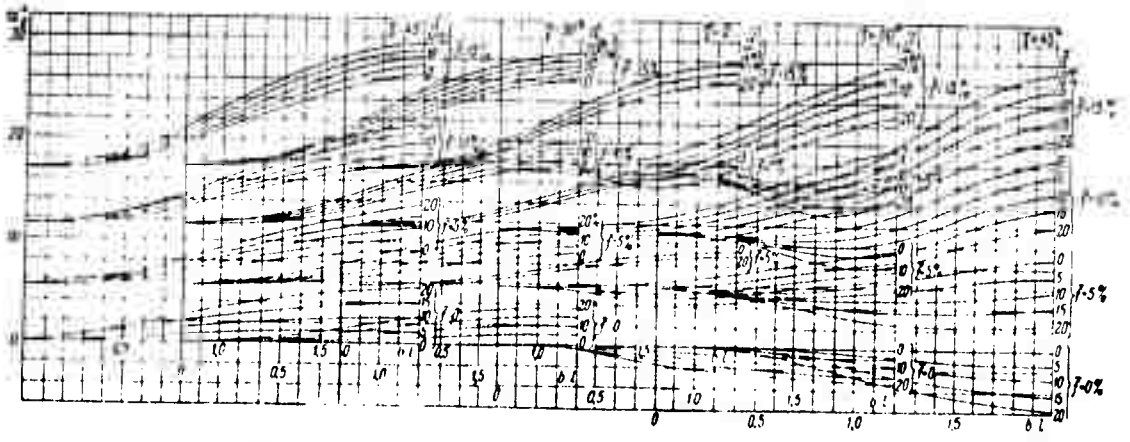


Nomogram for Calculating Two Parametric Lattices of a Family of Chaplygin Profiles

Continuining the straight line 1 which connects the points with

given values of $\bar{d}$ and $b/\underline{l}$, we find point J_1 on the "mute" scale of J_1 (coinciding with γ_p), which in turn is connected by the straight line 2 with the point of a given value of $\bar{f}$ until the intersection with the "mute" scale J_2 (coinciding with $\underline{d}$) at the point J_2. The continuation of the straight line 3, connecting the given value of the geometrical stagger γ_p with the point J_2, yields a point on the scale M which determines the number M*.

The straight line 1 connects the given values of γ_p and $\bar{f}$ which determine the "mute" point J_3; the straight line 2 connects the "mute" point J_3 with the given $\bar{d}$, thus determining the "mute" point J_4; the straight line 3 connects the mute point with a given $b/\underline{l}$ and determines the mute point J_5. The straight line 4, connecting the given point γ_p with the mute point J_5, yields N*. Connecting now the points M and N by a straight line on the α_0-scale, we can read off the value of α_0 and then find the aerodynamic stagger $\gamma = \gamma_p - \alpha_0$.



The zero lift angles α_0 in dependence on the density of the lattice and the stagger angle.

Example [9.10]

A. Calculate the coordinates of a lattice profile with the following geometrical characteristics: $\frac{b}{l} = 1.55$, $\gamma_p = 45°$; $\bar{d} = 8.8\%$; $\bar{f} = 7.2\%$.

1. Integrating according to Table 4 of Appendix 10, we find ξ_0, η_0, ϑ and from the nomogram a_0: $\xi_0=0{,}082$ $\eta_0=-0{,}095$, $\varphi=0{,}70$ $a_0=10°$, т. е. $\beta=\beta_0-a_0=35°$.

2. For $q = 0.70$ and $\beta = 35°$ we find from the table of Appendix 9 the potentials φ_1^* and φ_2^* for all selected angles ϑ, and from Tables 2 and 3 of Appendix 10 the constants $\varphi_0 = 1.88$ and $\vartheta_0 = 13°48'$.

It is suggested that the angles ϑ should be taken at intervals of 10° on the leading edge and that the angular intervals can be raised [illegible] on the remaining part of the profile.

3. Formula (6.4.3) can be used to calculate the profile coordi-

[illegible]

4. From the table of Appendix 9 we determine for given $\beta = 35°$ and [illegible] the velocities λ_1, λ_2, λ_3 for all ϑ from 0 to 90.0°.

2. From Table 4 of Appendix 1 we find the values of the velocities w_{10}, w_{20}, w_{30} at the stagnation point ($\vartheta = \vartheta_0$).

3. Using Formula (9.4.8) we calculate the value of the velocity $w_k(\vartheta)$ at the surface of a lattice of circles for the aerodynamic angle of attack $\alpha_a = a_p + a_0 = 6°20' + 10° = 16°20'$.

4. From Formulas (9.4.14) we calculate the quantities $dx/d\vartheta$ and $dy/d\vartheta$, then

$$\left|\frac{dz}{d\zeta}\right| = \sqrt{\left(\frac{dx}{d\vartheta}\right)^2 + \left(\frac{dy}{d\vartheta}\right)^2}.$$

5. The velocity $w(\vartheta)$ at the profile surface is found from Expression (9.4.13).

6. The dimensionless pressure coefficient is determined from the Bernoulli equation $p = 1 - w^2(\vartheta)$.

7. The pressure distribution curve is constructed on the profile chord, the distance from the trailing edge of the projection of the profile points onto the chord being determined by the formula $\underline{l}_k = -\sqrt{\underline{x}^2 + \underline{y}^2}\cos\left(\alpha_0 + \operatorname{arc\,tg}\frac{\underline{y}}{\underline{x}}\right)$ where $\underline{x}$ and $\underline{y}$ are the local coordinates of the profile.

The sequence of the calculations is seen from the table given on the foregoing page.

Manuscript Page No.

[Footnotes]

720 Cf. e.g., textbook of A.N. Tikhonov and A.A. Samarskiy "Equations of Mathematical Physics," GTTI, 1953.

751 G. Gred, On the kinetic theory of rarefied gases, Collection "Mechanics" No. 4-5, IL. 1952.

794 The error made is here of the order of w^2/c^2 where $\underline{c}$ is the velocity of light.

826 a.u. denotes the astronomical unit = $1.45 \cdot 10^6$ km, which is approximately equal to the distance Earth-Sun.

849 For the calculation it is insignificant to know the quantities M and N; they appear in the result of the solution of the equation which contains the approximate analytical dependence of α_0 on $b/\underline{l}$, γ, $\overline{d}$, $\overline{f}$.

DISTRIBUTION LIST

DEPARTMENT OF DEFENSE	Nr. Copies
HEADQUARTERS USAF	
ARL (ARB)	1
OTHER AGENCIES	
AEC	2
ARMY (FSTC)	3
ATD	2
CIA	1
DIA	4
NAFEC	1
NASA (ATSS-T)	1
NAVY	3
NSA	6
OAR	1
OTS	2
PWS	1
PGE (Steensen)	1
RAND	1
AFCRL (CRXLR)	1
SPECTRUM	1
FAA (SS-10)	1

MAJOR AIR COMMANDS	Nr. Copies
SAC (DISC)	1
DDC	20
AFSC	
SCFDD	1
TDBDP	2
TDBTL	5
TDGS	1
TDEPA	1
AEDC (AEY)	1
AFFTC (FTF)	1
AFWL (WLF)	1
ASD (ASFA)	2
BSD (BSF)	1
ESD (ESY)	1
SSD (SSFAR)	2